Vol. 23, No. 3, September, 2024
ISSN (Print): 0972-6268; ISSN (Online) : 2395-3454

# NATURE ENVIRONMENT & POLLUTION TECHNOLOGY

*A Multidisciplinary, International Journal on Diverse Aspects of Environment*

Technoscience Publications
website: www.neptjournal.com

Technoscience Publications
A-504, Bliss Avenue, Balewadi,
Opp. SKP Campus, Pune-411 045
Maharashtra, India

www.neptjournal.com

# Nature Environment and Pollution Technology

**(An International Quarterly Scientific Research Journal)**

## EDITORS



**Published by** : Mrs. T. P. Goel, Technoscience Publications, A-504, Bliss Avenue, Balewadi, Pune-411 045, Maharashtra, India

**E-mail** : contact@neptjournal.com; operations@neptjournal.com

## INSTRUCTIONS TO AUTHORS

### Scope of the Journal

The Journal publishes original research/review papers covering almost all aspects of environment like monitoring, control and management of air, water, soil and noise pollution; solid waste management; industrial hygiene and occupational health hazards; biomedical aspects of pollution; conservation and management of resources; environmental laws and legal aspects of pollution; toxicology; radiation and recycling etc. Reports of important events, environmental news, environmental highlights and book reviews are also published in the journal.

### Format of Manuscript

- The manuscript (mss) should be typed in double space leaving wide margins on both the sides.
- First page of mss should contain only the title of the paper, name(s) of author(s) and name and address of Organization(s) where the work has been carried out along with the affiliation of the authors.

*Continued on back inner cover...*

# Nature Environment and Pollution Technology

**Vol. 23, No. (3), September 2024**


## CONTENTS

The Journal is Currently **Abstracted and Indexed** in:

- CNKI Scholar (China National Knowledge Infrastructure)
- Scopus Cite Score (2023) 1.2
- Scopus®, SJR (2023) 0.204
- Index Copernicus (2022) = 128.35
- Indian Science Abstracts, New Delhi, India
- Chemical Abstracts, U.S.A.
- Pollution Abstracts, U.S.A.
- Elsevier Bibliographic Databases
- Paryavaran Abstract, New Delhi, India
- Zoological Records
- CAB Abstracts, U.K.
- Electronic Social and Science Citation Index (ESSCI)
- Indian Citation Index (ICI)
- CrossRef (DOI)
- EBSCO: Environment Index™
- ProQuest, U.K.
- Google Scholar
- DOAJ
- Zetoc
- J-Gate
- Environment Abstract, U.S.A.
- Centre for Research Libraries
- Elektronische Zeitschriftenbibliothek (EZB)
- CSA: Environmental Sciences and Pollution Management
- Access to Global Online Research in Agriculture (AGORA)
- Present in UGC-CARE List (Group II)
- WorldCat (OCLC)
- British Library
- Connect Journals (India)
- Indian Science
- JournalSeek
- Research Bible (Japan)
- SHERPA/RoMEO
- Directory of Science
- AGRIS (UN-FAO)
- Ulrich's (Refereed) database
- NAAS Rating 2024 = 5.33
- UDL-EDGE (Malaysia) Products like i-Journals, i-Focus and i-Future

**www.neptjournal.com**

# Nature Environment and Pollution Technology

Nature Environment and Pollution Technology
An International Quarterly Scientific Journal

p-ISSN: 0972-6268
(Print copies up to 2016)
e-ISSN: 2395-3454

Vol. 23 | No. 3 | pp. 1221-1238 | 2024

Original Research Paper

https://doi.org/10.46488/NEPT.2024.v23i03.001

Open Access Journal

# Navigating Nepal's Economic Growth and Carbon Emissions: Insights into the Environmental Kuznets Curve (EKC)

**R. Adhikari*, B. Niroula** and S. K. Singh***†**

*Tribhuvan University, Mechi Multiple Campus, Department of Economics, Nepal
**Tribhuvan University, Patan Multiple Campus, Faculty of Management, Nepal
***Department of Management, Faculty of Economics and Business, Universitas Airlangga, Surabaya, Indonesia
†Corresponding author: S. K. Singh, singhsanju@feb.unair.ac.id

**Nat. Env. & Poll. Tech.**
**Website: www.neptjournal.com**

*Received:* 13-11-2023
*Revised:* 01-01-2024
*Accepted:* 12-01-2024

**Key Words:**
Environmental Kuznets Curve
$CO_2$ emissions
Energy consumption
Electric vehicle
Sustainable employment

## ABSTRACT

This research aims to employ the Autoregressive Distributed Lag (ARDL) method within the insight into the Environmental Kuznets Curve (EKC) to verify whether EKC exists in the Nepalese economy. In this research, variables were used, such as carbon emissions per capita, GDP per capita, energy use per capita, trade volume, and urbanization from 1980 to 2021, and the ARDL method was used. The data has been taken in this research except trade volume from the World Bank and the Ministry of Finance, Nepal. The data sets are converted into the natural logarithmic form to minimize the problem of heteroskedasticity. The findings provide compelling evidence for the existence of the EKC in Nepal, that economic growth has an inverted U-shaped impact on carbon emissions. In the early stages of development, economic growth leads to rising carbon emissions, but in the later stages, economic growth becomes associated with declining emissions. Besides economic growth, per capita energy consumption and urbanization emerge as significant drivers of carbon emissions. However, the trade volume is not found to be the driving factor of carbon emissions. The findings of this study have significant policy implications for global climate change issues and Nepal's transition from an underdeveloped to a developing nation. To achieve harmonious economic growth and emissions reduction, donor countries and agencies to partner with Nepal in its ambitious endeavors. This partnership can take shape through multifaceted support as fueling socio-economic progress that aligns with Nepal's commitment to reduce carbon emissions, ensuring that development and sustainability walk together. This research recommends the government of Nepal electrify the transportation landscape by incentivizing the adoption of electric vehicles, paving the way for cleaner air and a healthier planet, empowering Nepal's natural guardians by strengthening public and private forest programs, safeguarding invaluable ecosystems and biodiversity and curbing the tide of waste mismanagement through strict regulations and robust enforcement, transforming a potential threat into a source of innovation and resourcefulness. These measures, aligned with sustainable employment generation, can pave the way for a brighter and greener future for Nepal.

## INTRODUCTION

Rapid economic growth of every country turns to developed at the same time, countries also produce high carbon emissions. Meanwhile, countries like Nepal are moving toward developing countries from least developing countries and cause carbon emissions less as compared to developed countries, thought it is one of the great challenges countries like Nepal. Carbon dioxide emissions on a worldwide scale are a worry for researchers and policymakers. The excessive use of coal, petroleum, and other fossil fuels, in addition to the mismanagement of plastic-related objects, are the number one human drivers of this problem. Along with their desire for rapid industrial development and economic success, nations' struggles for economic dominance are also to blame for the increase in global carbon emissions. According to Grossman & Krueger (1995), the environment has gotten worse resulting from the severe thrust for the fast rise in income, neglecting environmental preservation. However, the authors asserted that an increase in income can be exploited for the betterment of the environment. In the same reasoning as the initial view of Grossman & Krueger (1995), noted that $CO_2$ emissions from human activities are widely recognized as the most important sources of probable future global warming. According to studies, the impact of greenhouse gases on global ecology is not an exceptional case. To have a comprehensive understanding of the origins of greenhouse gases and their impact on global

warming, it is important to possess knowledge pertaining to the physical and ecological processes that facilitate the conversion of emissions into minimum greenhouse gas levels. Mohammed et al. (2015) identified that the tendency of increasing domestic output and the emergence of foreign direct investment are the two primary long-term economic activities driving $CO_2$ emissions.

Wang et al. (2011) claimed that emissions fueled by accelerated industrial development are found responsible for causing global warming. On the other hand, Menyah & Wolde-Rufael (2010) as cited in Khan et al. (2020) claimed that the use of traditional energy resources causes $CO_2$ emissions. Shahbaz et al. (2013) also revealed that the use of fossil fuels by households and the creation of massive smoke by industries increases $CO_2$. Jiang et al. (2018) also noticed that the matter of carbon emissions is particularly crucial since policymakers in the least developed countries (LDCs) are becoming more and more worried about increasing dependence on the imports of energy, notably fossil fuels and rising greenhouse gases.

It is also an appalling concern of the ecologists that there is an escalating worldwide warming day by day caused by $CO_2$ emissions. Human activities are solely liable for carbon emissions, which cause global warming along with increased sea levels. Not only do human activities emit carbon dioxide, but also natural sources cause carbon emissions. According to Ali et al. (2020), both natural and human activities can emit $CO_2$ emissions. One of these sources comes from the development of urbanization, and the growing population tends to rapid urbanization. Urbanization needs infrastructure for a growing population, and human beings severely exploit the environment for their needs, triggering an imbalance in the ecosystem. In the same reasoning, According to Pant (2009), the primary cause of climate change can be linked to the industrial revolution and the extensive utilization of fossil fuels. The author further argued that agriculture is also the cause of the complications through emissions of greenhouse gases. Elum & Momodu (2017) stated that carbon emissions and environmental pollution are associated with developed countries only. However, at present, attention is diverted to developing countries due to the fast industrialization and increasing economic growth in such countries. As underdeveloped countries shift into developing status, they typically experience a period of rapid economic growth. This economic growth is often accompanied by a shift from a predominantly agricultural economy to a more industrialized economy. This shift to an industrialized economy can lead to increased carbon emissions in many ways (IPCC 2022).

Although Nepal is an underdeveloped country, it is not free from the phenomenon of climate change issue. Nepal, like other countries, contributes to carbon emissions, even though its share of global emissions is negligible. According to the World Resources Institute (2017), Nepal accounts for just a mere 0.044 percent of the global aggregate of greenhouse gas emissions. Though the share of the world's emissions is very low, Nepal should also address the climate change issue. The carbon emissions, sooner or later, will become a complicated issue if it is not addressed in time. According to Piya et al. (2019), the Nepal government had not begun addressing climate change issues until the Tenth Plan (2002-2007) despite having ratified both the United Nations Framework Convention on Climate Change (UNFCCC) and the Kyoto Protocol (KP). However, the Nepal government later assured to address the climate change issue and administered the Three-Year Interim Plan (2007-2010) through the Clean Development Mechanism.

Although Nepal's per capita greenhouse gas emissions are low compared to rich industrialized nations, they have doubled in the past seven years, reaching 28,166 Gg of carbon dioxide in 2021. Nepal has submitted its second Nationally Determined Contributions (NDC) Report, third National Communication Report, and report on the technology requirements assessment two years past the deadline of 2019. As stated in the country's second NDC, the goal of Nepal is to achieve net-zero emissions by 2050 and a minimum of 55 percent decrease in carbon emissions by 2030 by reducing emissions from sectors like waste management, forestry, and power (Nepali Times 2021). Nepal, a landlocked country in South Asia, is rich in natural resources. There are eight of the world's top fourteen mountains, including Mount Everest, as well as a variety of fauna and environments. (Ministry of Forests and Soil Conservation (MoFSC 2014). However, Nepal is among the countries that are most vulnerable to the impacts of climate change and other environmental challenges on a global scale (MoFSC 2021). The Government of Nepal has made a number of commitments to address environmental issues, both domestically and internationally (Government of Nepal (GoN) (2023). Despite low current emissions, Nepal faces a unique challenge in managing future increases due to rapid economic growth as projected at 7.1% in 2023-24 by the World Bank, rising energy demand, reliance on traditional fuels like firewood, extreme climate vulnerability (MoFSC 2021), limited financial and technological resources, and complex socioeconomic and political landscapes (GoN 2023). These factors necessitate a multi-pronged approach with clean energy investments, sustainable development practices, climate resilience strategies, and international cooperation.

In 2015, Nepal ratified the Paris Agreement with the commitment to reducing carbon emissions by 23% by 2030

(Government of Nepal, Ministry of Forests and Environment (2015). The Green, Resilient, and Inclusive Development (GRID) concept was embraced by Nepal in 2021 as a national goal to steer long-term green growth and develop resilience to climate shocks (Government of Nepal, National Planning Commission, 2021). Nepal has also taken several concrete steps to implement its environmental commitments (Government of Nepal, Ministry of Forests and Environment 2022). For example, the government has invested in renewable energy, such as hydropower (Government of Nepal, Ministry of Energy, Water Resources and Irrigation 2006). It has also launched a number of programs to promote sustainable forest management and conservation (Government of Nepal, Ministry of Forests and Environment, 2019). Nepal has also been working to improve air quality and water quality in its cities (Government of Nepal, Ministry of Environment, Science and Technology, 2019, Government of Nepal, Ministry of Water Resources 2019). To implement the Paris Agreement as per the needs of the country, Nepal is committed to stepping up its climate change initiatives. Nepal aims to attain zero gas production between 2020 and 2030, followed by a period of extremely low emissions until obtaining full net-zero emissions by 2045. Nepal also wants to be acknowledged for its efforts to reduce greenhouse gas emissions. Global emissions through promoting renewable energy. The long-term strategy of Nepal strives to create a future that is inclusive, carbon-neutral, and climate-resilient through bold policy-making, social change, and technical advancement (Government of Nepal [GoN] 2021).

Global issues quickly become pressing local concerns in Nepal. Increasing temperatures are causing glaciers to melt, leading to people having to relocate and risking water sources (MoFSC 2021). Poor air quality in Kathmandu is making it difficult for people to breathe properly (MoEPE 2022). Poverty and unequal treatment of women make it especially challenging for the most vulnerable groups (Sharma & Gyawali 2012). Nepal reflects global trends but requires unique solutions to create a more positive future. Nepal's carbon footprint whispers with diverse voices, but a few shout loudest. Soaring reliance on traditional biomass (firewood) for cooking and heating dominates (MoFSC 2021), fueled by poverty and limited access to clean energy. Inefficient transport, particularly fossil-fueled vehicles, adds its rumble (GoN 2023). Industrial emissions, though modest now, could roar in future growth, demanding proactive measures (NPC 2021). Nepal's story echoes a chorus of interconnected factors requiring a conductor of sustainable solutions. Nepal, nestled amidst towering Himalayas, whispers a tale of environmental struggles. Fossil fuels roar in Kathmandu's streets**,** their fumes choking the vibrant city (MoEPE 2022). Cooking fires crackle across vast rural landscapes**,** fueled by poverty and dependence on firewood, spewing greenhouse gases into the thin mountain air (MoFSC, 2021). And in the distance, the industry's shadow looms as a potential future threat if unchecked (NPC 2021). These are the voices of Nepal's carbon conundrum, a chorus demanding sustainable solutions to ensure a vibrant future for this fragile paradise

While Nepal's current share of global emissions is minimal, its rapid economic growth and reliance on traditional energy sources raise concerns about future emissions increases. This study investigates whether Nepal can decouple its economic growth from carbon emissions and, if so, what policies and strategies are most effective. In this spirit, the present paper aims to examine the factors causing environmental deterioration in Nepal with insights into the environmental Kuznets curve (EKC) to help formulate suitable policies to minimize carbon emissions at a target level. This paper intends to answer the research query: "What is the impact of economic growth on carbon emissions in Nepal, and what are the suitable policies to minimize carbon emissions?" The research question is addressed by the verification of the Environmental Kuznets Curve (EKC) through a model based on autoregressive distributed lags (ARDL) theory. Varied studies are available in economic literature regarding the verification of EKC by ARDL models in an international context. However, the verification of EKC through this model in the Nepalese context with the latest data is not available. Hence, this study attempts to fill the methodological knowledge gap through ARDL models in EKC form with the latest data for the economy of Nepal. The survey of related literature is offered in section two, and section three talks about the research methods. The findings and discussion are presented in Section four, while the conclusions with implications are presented in Section five.

## PAST STUDIES

The EKC is a hypothesis that proposes the reversal U linkage between income growth and air pollution. It states that there is a simultaneous rise in income and pollution both in the initial phase, but later on, rising income causes pollution to decrease, giving rise to an inverse U-shaped EKC. The EKC hypothesis popularized after the 1990s is based on the Kuznets (1960) theory that posits an inverted U linkage between the growth of income and income inequality. A wide range of researchers have made contributions to the EKC's theoretical underpinnings. Several studies that elaborated and clarified the EKC hypothesis are Grossman & Krueger (1991, 1995), Stern et al. (1996), Dinda (2004), and Managi et al. (2009) among the others who attempted to enrich EKC. As argued by Agras & Chapman (1999), when the economy switches from low-income to high-income, the industrial

and manufacturing sectors tend to decline, and the service sector tends to increase. The service sector is less polluting in relation to the industrial and manufacturing sectors. As a result, the growth of the economy causes pollution to fall. Selden & Song (1994) argued that as countries grow economically, they become more aware of environmental pollution and the government enforces strict regulations regarding environmental protection. On the other hand, Jaffe & Palmer (1997) stated that countries develop cleaner technologies as they become economically prosperous. All these arguments of the researchers are sufficient bases for how environmental pollution decreases once a certain threshold is reached, giving rise to a reversal U-shaped EKC.

According to the arguments made by the researchers, environmental deterioration first rises with economic growth before declining as that growth accelerates. The researchers' arguments state that while nations first pay little attention to environmental preservation, as awareness grows and nations invest more in environmental protection, environmental deterioration gradually decreases. A reversal 'U' EKC resulted. As opined by Voumik (2005), the EKC theory has been used to observe the connection between environmental deterioration and economic development. It is believed that when economies expand, environmental contamination will first increase before declining once a certain income level is attained.

Similarly, Iwata et al. (2010) claimed that the linkage between the rise of income and environmental pollution is inverse U-shaped. The increase in income in the initial stage of economic expansion exacerbates harm to the environment and devastation of natural resources; however, these effects become less pronounced above a certain income level (Barbier 1997, Suri & Chapman 1998). According to Kijima et al. (2010), the EKC proposes an inverse U linkage between income and pollution, with emissions rising initially caused by economic growth but falling as investment increases in cleaning the environment.

The reversal of U-shaped EKC proposed by different researchers after 1990 is doubted by Babu & Datta (2013). The authors stated that the initial formulation of EKC has stimulated a large debate and the income-carbon emissions linkage produces an N-shaped pattern rather than reversal U. In the same manner, Selden & Song (1994), Panayotou (1997), Cole et al. (1997) and Dasgupta et al. (2002) also argued that there exists N-shaped EKC, in which the environment deteriorates with a rise in income initially, then improves, and subsequently worsens again. The N-shaped EKC hypothesis has several theoretical explanations. The first is that composition and technical effects have been relegated to the scale effect. The scale effect arises from increased production, leading to greater environmental pressure (Torras & Boyce 1998). The composition effect involves changes in economic activities as countries develop, shifting from agriculture to industry and services, potentially reducing environmental degradation (Bruyn et al. 1998). Technical effect indicates the development of new technologies to reduce environmental pollution (Dinda 2004).

Additionally, a shift can occur where the desire for clean and healthy outweighs the pursuit of economic growth as people become more environmentally aware (Allard et al. 2018). Amid (2015) demonstrated the connection between the formal and informal economy and the state of the environment. The author claimed that the informal economy plays a significant role in Tunisia, despite there being no direct connection between the formal and informal economies and the environmental weakening. The author argued that environmental contamination, which is largely caused by industrial and agro-food processing activities and is exacerbated by population growth, can be attributed to rising air pollution.

Palamalai et al. (2015) observed the linkage between emissions, trade, income, and several energy consumption sources, including coal, natural gases, crude oil, and renewable energy in India. The authors found a long-run link between the variables, as reported by the Gregory-Hansen cointegrating test and the error correction model. The findings validated the EKC hypothesis that growing economic activity raises energy use, which in turn causes a worsening of the environment. Saboori et al. (2014) investigated the connection among income, greenhouse gases, and energy use of the road transportation sector in the OECD. Their findings unveiled a clear association between the growth of income and pollution emissions, with the use of energy in the road transport sector demonstrating a more rapid response to changes in $CO_2$ emissions than to emission increments. The study recommended the implementation of enduring strategies focusing on energy efficiency and the transition to nuclear, renewable, and biofuel sources to significantly mitigate greenhouse gas emissions.

Alam & Adil (2019) found EKC to be invalid in India when the authors used the data of the concerned variables over the period 1991-2016. However, they identified a substantial direct link between energy supply and carbon emissions, suggesting an urgent need for India to expedite the expansion of clean and renewable energy production to curtail carbon emissions. Conversely, Shahbaz (2019) substantiated the EKC in Next-11 countries by investigating the link between air pollution and globalization through bounds testing. Zhu et al. (2016) detected the influence of foreign direct investment, economic growth, and energy use

on pollution in ASEAN-5 member nations. The authors used a panel quantile regression model and detected that FDI had a favorable effect on emissions, while energy consumption had increased emissions. On the other hand, income and population size could reduce pollution in high-emission nations. The study also suggested that trade openness could mitigate air pollution, especially in low and high-emission nations.

Environmental pollution is also caused by the openness of an economy, as claimed by Davis & Calderia (2010). The authors opined that trade openness could lead to a process known as "outsourcing emissions," in which carbon-intensive goods are produced in nations with tax laws rather than in nations with strict environmental rules. However, a study by Thuy & Nguyen (2022) demonstrated that liberalization in trade in developing nations does not worsen ecological conditions. Their results provided strong evidence for two strategies to reduce carbon dioxide emissions, which are the major factors impacting the environment in addition to foreign trade, financial transparency, and the sources of renewable energy. Udeagha & Ngepah (2022), in contrast to Thuy and Nguyen, revealed that trade openness, while initially beneficial to the environment, ultimately degrades environmental quality. This study demonstrated that the scale effect pushes up carbon emissions while the technique effect helps to lessen them, supporting the occurrence of EKC.

Varied works have examined the EKC hypothesis, and the findings have usually been in favor of the theory. For example, from 1972 to 2008, Pakistan's foreign trade, GDP, use of energy, and carbon emissions were examined by Nasir & Rehman (2011). The results demonstrated that energy use and international trade directly impacted greenhouse gases and validated the EKC hypothesis. However, short-term data disproved EKC's validation in Nasir and Rehman's study. Policymakers should consider environmental issues, develop policies to support sustainable trade practices and reduce energy consumption, forecast future energy demand using different growth scenarios, and purchase the least expensive energy, according to this study. In a similar vein, Pata's (2017) study on Turkey demonstrated a reversal of the U connection between income and greenhouse gases, both in the short and long periods, over the 1974-2013 study period. It was observed that per-head energy use, GDP per head, industrialization, and financial development were the factors causing per-head carbon emissions. Conversely, it was detected that urbanization had no impact on environmental pollution.

Saboori et al. (2014) investigated the interlink among income, greenhouse gases, and energy use of the road transportation sector in the OECD. Their findings unveiled a clear association between the growth of income and pollutant emissions, with the use of energy in the road transport sector demonstrating a more rapid response to changes in $CO_2$ emissions than to emission increments. The study recommended the implementation of enduring strategies focusing on energy efficiency and the transition to nuclear, renewable, and biofuel sources to significantly mitigate greenhouse gas emissions. On the other hand, Amid (2015) demonstrated the connection between the formal and informal economy and the state of the environment. The author claimed that the informal economy plays a significant role in Tunisia, despite there being no direct connection between the formal and informal economies and the environmental weakening. The author argued that environmental contamination, which is largely caused by industrial and agro-food processing activities and is exacerbated by population growth, can be attributed to rising air pollution.

Alam & Adil (2019) found EKC to be invalid in India when the authors used the data of the concerned variables over the period 1991-2016. However, they identified a substantial direct link between energy supply and carbon emissions, suggesting an urgent need for India to expedite the expansion of clean and renewable energy production to curtail carbon emissions. Conversely, Shahbaz (2019) substantiated the EKC in Next-11 countries by investigating the link between air pollution and globalization through bounds testing. Zhu et al. (2016) detected the influence of foreign direct investment, economic growth, and energy use on pollution in ASEAN-5 member nations. The authors used a panel quantile regression model and detected that FDI had a favorable effect on emissions, while energy consumption had increased emissions. On the other hand, income and population size could reduce pollution in high-emission nations. The study also suggested that trade openness could mitigate air pollution, especially in low and high-emission nations.

Lazar et al. (2019) found that income is generally associated with higher environmental deterioration, except for a few Central and Eastern European countries that saw faster growth without a decline in environmental quality between 1996 and 2015. Rahman et al. (2022) reported that consumption of the household sector accounted for above 62.39 percent of emissions in the SAARC area. India topped the list of countries with household emissions, which varied from 37.27% to 0.61%. According to a study by Sharma et al. (2019), Nepal's rising carbon emissions were mostly caused by remittances and increased GDP.

The consumption of energy and greenhouse gases in Pakistan are causally related in both directions, according

to Aftab et al. (2021). Nemeth-Durko (2021) found that the primary drivers of carbon emissions in Hungary were urbanization and power use, with environmental degradation being a further consequence of growth in the economy. According to Gonzalez-Sanchez and Martin-Ortega (2020), the primary factors influencing the rise in carbon emissions are GDP and final energy intensity. The primary drivers of this trend are the rise in energy efficiency and the shift to a service-oriented economy. The authors further argued that the rise in carbon emissions over the study period is not primarily attributable to rising gas prices. They also mentioned that countries have different levels of variability in the factors affecting carbon emissions, and the carbon emissions in Europe can be reduced through the development of renewable energy. Ali et al. (2020), however, held a different viewpoint. The building industry is one of the primary drivers of global emissions, according to the authors' findings. The majority of the energy used in building and operation comes from fossil fuels. Enforcing rules and policies and introducing low-carbon technologies are two ways the building industry can lessen its effect.

Ngarava (2021) investigated the relationship between South Africa's economic diversification and environmental deterioration. By using the ARDL-ECM approach with annual data, the author found that economic diversification and emissions had a one-way causal relationship, but there was no long-term association between the variables under study. GDP, population, foreign direct investment, and trade balance were the independent variables. However, when Sharma et al. (2019) employed ARDL models for the Nepalese economy, they found the surprising result that foreign aid was driving carbon emissions to decrease. According to the authors, increasing foreign aid can effectively reduce Nepal's carbon emissions. Khan et al. (2021) conducted an analysis spanning from 1985 to 2020 and employing a dynamic-stimulated ARDL. The authors found a direct link between GDP and environmental pollution both in the short-run and long-run. However, they detected an inverse association between GDP square and ai-pollution. The study found the presence of EKC in the US economy. The authors advocated the importance of institutional quality to improve environmental quality. The authors also underscored the need for a comprehensive national energy policy for cleaning the environment.

Examining the period from 1971 to 2016 in India, Kareldla et al. (2021) investigated the impact of the manufacturing industry, international trade, and income growth on $CO_2$ emissions using the ARDL bounds test approach. Their findings disclosed a sustained positive correlation between carbon emissions and all three explanatory variables. While international trade was identified as reducing $CO_2$ emissions, the manufacturing industry and GDP exhibited a significant positive long-term impact. Conversely, Destek & Sinha (2020) challenged the validity of the EKC within OECD nations. They argued that non-renewable energy exacerbates environmental degradation, while renewable energy serves to alleviate ecological damage. Their advocacy urged governments to prioritize the adoption of renewable energy to mitigate environmental deterioration.

Tenaw & Beyene (2021) applied a sustainability-focused EKC framework to scrutinize the link between environmental quality and development in 20 Sub-Saharan African countries from 1990 to 2015. While supporting a modified EKC hypothesis, the study emphasized the importance of natural resource endowment. Long-term detrimental consequences on the environment were attributed to trade openness and energy use, prompting the recommendation that environmental sustainability policies align with economic development goals. Similar insights were provided by Khan & Amhad (2021), who, using econometric techniques, underscored the positive impact of FDI and international trade on environmental pollution in emerging countries while highlighting the negative impact of renewable energy use on the environment in both developed and developing nations. The authors advised careful regulation of FDI and international trade in developing nations and the promotion of renewable energy use globally.

Hongxing et al. (2021) explored the impact of international trade, urbanization, energy use, and pollution on income growth in Belt and Road Initiative (BRI) economic corridors. Establishing a two-way causality between growth of income and consumption of energy, the study recommended government interventions, such as tax incentives, to foster clean energy technology and infrastructure. Numan et al. (2022) explored the connection between pollution and economic complexity, challenging the N-shaped EKC theory. While findings did not support the theory for all income categories in Model 1, while Model 2 suggested an N-shaped EKC, emphasizing an inverse link between the use of renewable energy and ecological footprint. This study advocated for ecologically sound energy sources to combat global warming. Voumik et al. (2022) focused on Bangladesh, utilizing population growth, use of energy, and growth of income to assess the EKC hypothesis validity from 1971 to 2020. This study supports the EKC theory, emphasizing the need for Bangladesh to shift away from nonrenewable energy sources for environmental and economic benefits.

Huang & Guo (2022) investigated the influence of fiscal improvement on decoupling carbon from GDP growth across six regions from 1995 to 2020. While effects varied by region. Population growth consistently contributes to

carbon emissions. The authors urged the development of a green financial system in regions with successful decoupling and a swift transition to new economic development models in other areas. Jiang et al. (2022) proposed that reducing the political risk index and increasing the budget for environment-related research and development significantly lowered the pollutions arising from consumption in the G7 nations. Export promotion, lower political risk, increased research and development budgets, and discouraging imports were recommended as measures to minimize $CO_2$. However, Chen et al. (2022) identified a reversal U association between urbanization and pollutions, with urbanization increasing emissions and government effectiveness positively contributing. The authors suggest promoting urbanization and improving government efficiency to combat carbon emissions and global warming.

Pena et al. (2022) established a persistent connection between pollution, GDP, FDI, and renewable energy in Philippines. Despite challenging EKC hypothesis, the research proposed legislative measures to diminish $CO_2$ emissions and accomplish sustainable development objectives. The prioritization of renewable energy utilization and the attraction of FDI were suggested strategies in alignment with sustainable development goals. Examining China's data from 1990 to 2019, Ozkan et al. (2023) scrutinized the EKC theory, "pollution haven theory," and "pollution halo theories." Their findings revealed a decline in environmental quality concurrent with a rise in real GDP, supporting the "pollution haven theory's," the adverse impacts of FDI. Trade openness and energy efficiency were linked to both long- and short-term enhancements in environmental quality, underscoring the critical importance of incorporating environmental considerations into policy decisions, particularly in light of China's 2050 climate objectives.

Shen et al. (2023) used a VAR model for carbon emissions and a Tapio decoupling score to scrutinize the decoupling between income growth and air pollutions in China from 1997 to 2019. The authors observed that different economic regions had varying degrees of decoupling, with the eastern and western regions having a more optimal state of decoupling than the center and north-eastern regions. It was found that the renewable energy consumption slowed the rise in carbon emission intensity across the board, with the western region seeing the biggest reductions. The authors came to the conclusion that while sustaining steady economic growth, achieving carbon neutrality can be facilitated by increasing each region's share of renewable energy consumption. Using moments quantile regression as a methodology, Razzaq et al. (2023) revealed that while tourist expansion had an asymmetric impact on air pollution, but it caused a positive influence on growth for the top ten GDP economies between 1995 and 2018. While tourism had a relatively higher negative environmental impact on less developed countries, it had a relatively greater positive influence on growth of developed countries. Conversely, green innovation has been found to be reducing the air pollution and promote growth, particularly in developed countries.

Utilizing the Dynamic Ordinary Least Squares (DOLS) method, Raihan et al. (2023) explored the impacts of the growth of income, tourism, agriculture output, and energy consumption (both from fossil fuels and renewable sources) on air pollution in Egypt during 1990-2019. It was observed that tourism, income growth, and the use of fossil fuels caused pollution. In contrast, the renewable energy and increased agricultural goods were identified as mitigating factors, reducing air pollution and improving environmental quality. To promote environmental sustainability in Egypt, the researchers recommended the adoption of a low-carbon economy, increased use of renewable energy, adoption of eco-friendly travel practices, and implementation of climate-smart agriculture. In a separate study, Jiao et al. (2023) employed STIRPAT and scenario analysis to investigate air pollution in Guizhou, China, from 1990 to 2020. The findings indicated a growth in coal-related emissions, which are now exhibiting signs of decoupling from economic expansion. The authors suggested that significant reductions in emissions could be achieved through decreased energy use, enhanced efficiency, and greater reliance on renewable energy sources.

Mitic et al. (2023) explored the link between air pollution, income growth, easily accessible energy, and employment in Southeast European nations using data from 1995 to 2019. They identified a substantial link between employment and accessible energy, along with a short-term two-way causal association between pollutions and employment. This study highlights a coherent directionality among GDP, employment, and energy accessibility, emphasizing the critical roles of employment and energy consumption in driving economic development. The findings underscored the presence of a short-term direct feedback loop between pollutions and economic growth. As per Ali et al. (2023), the consumption of nonrenewable energy negatively impacted the environment, while renewable energy positively influenced the growth in developing Asian nations. The evidence supporting a reciprocal link between renewable energy and economic growth aligned with the feedback hypothesis. This underscored the viability of enhancing REC as a feasible strategy to mitigate carbon emissions, enhance energy security, and expedite economic growth in these nations. In the context of Vietnam, Raihan (2023),

employing ARDL and VECM, identified a link between GDP growth, energy use, and pollution. Conversely, an increase in agricultural productivity demonstrated a less worsening of the environment. These promising findings underscore the potential of sustainable agriculture to reduce missions, offering policy recommendations to address Vietnam's $CO_2$ emissions through avenues such as low-carbon economic development, promotion of renewable energy, and implementation of sustainable agriculture practices.

Itoo & Ali (2023) employed ARDL, FMOLS, DOLS, and CRR approaches to analyze the long-term effects on air pollution in India. The authors found that the depletion of natural resources, industrial output, and remittance inflow had a small, negative influence, while energy consumption, national income, and population increase had a favorable and significant influence. This study detected reversal U-shaped EKC was not valid for India. To mitigate pollution in India, policymakers are appealed to prioritize slowing down population growth, national income growth, and energy demand, while discouraging the depletion of natural resources, industrial output, and remittance inflows. Bao & Lu (2023) utilized panel data analysis with fixed effects to investigate the likelihood of reversal U linkage between GDP and the generation of building waste in 27 European economies from 2000 to 2020. The study suggested that building waste management could be evaluated using the EKC. The authors argued that achieving sustainable development goals requires policymakers to simultaneously focus on promoting both economic growth and environmental conservation.

Thus, most studies have reached the consensus that income growth is the primary driver of air pollution. This comes as a result of the countries' unquenchable thirst for rapid economic growth. As a result, they give economic growth more importance than environmental protection. Instead of emphasizing sustainable development, they prioritize development. In addition, it has been concluded that a heavy reliance on fossil fuels, electricity, and urbanization all contribute to carbon emissions.

## MATERIALS AND METHODS

### Models and Variables

Grossman & Krueger (1991, 1995) asserted that there is a linkage between environmental deterioration and income per head. Early economic growth is linked with rising pollutant emissions and falling environmental quality. However, above a certain per capita income threshold, this tendency reverses, with economic growth being followed by improving environmental conditions, resulting in an inverted U-shaped EKC (Arouri et al. 2013). Equation (1), which represents the EKC function, was presented as:

$$C_t = f(Y_t, Y_t^2, E_t, T_t, U_t) \quad \ldots (1)$$

The non-linear algebraic form of the EKC is represented through the equation (1), where $C_t$ is the carbon emissions per head treated as explained variable and $Y_t$ the GDP per head, $Y_t^2$ square of GDP per head, $E_t$ energy use per head, $T_t$ the volume of trade and $U_t$ The rate of urbanization as an explanatory variable.

Datta & De (2021) proposed a random effect model based on the Hausman test to observe the behavior of EKC. Compared to Arouri et al. 2013 the model put forward by Datta and De differs slightly. Equation (2) presents the model as:

$$C_{it} = \gamma_i + \theta_1 Y_{it} + \theta_2 Y_{it}^2 + \theta_3 Y_{it}^3 + \theta_4 P_{it} + \theta_5 T_{it} + \varepsilon_{it} \quad \ldots (2)$$

where, where the notations have the same meaning as in equation (1), and $\mathcal{E}_{it}$ stands for residuals.

Equation (2) implies that carbon emissions are caused by the growth of GDP, urbanization, and volume of trade, also known as the openness of the economy. Rich countries are more likely than poor countries to suffer environmental damage, according to the cross-country study of Datta and De, as suggested by the Hausman test. Natural resources were thought to be utilized far more quickly in rich countries because of the massive production and consumption, which accelerates the degradation of their environments.

The present study employs secondary data on per-capita carbon emissions (in tons), Gross Domestic Product (GDP) per head (in US dollars), square of the GDP per head, energy use per head in terawatt-hours, trade volume as percentage of GDP and percentage of urban population over the period 1980-2021. The reason behind choosing the starting year 1980 for the data is that firstly all are unavailable from before 1980. Secondly, the 1980s witnessed the acceleration of globalization, opening up new trade opportunities for Nepal and facilitating access to foreign markets (Adhikari 2010). The required data on the variables are taken from the World Bank, World Resource Institute for carbon emissions, World Bank National Account Data for GDP per capita, World Bank, IEA Statistics for energy consumption per head, World Bank, United Nations Population Division for urbanization and Economic Survey of Nepal, Ministry of Finance for trade volume. The data are transformed into the natural logarithmic form with the help of Eviews software to minimize the problem of heteroskedasticity. The data sets after logarithmic transformation are denoted by $LnCE_t$ for carbon emissions per head, $LnY_t$ for GDP per head, $LnY_t^2$ for

Table 1: Detailed information regarding the data.

| Data Sets | Measurement | Nature | Source | Notation | Logarithmic Form |
|---|---|---|---|---|---|
| Carbon emissions per Capita | Tons | Secondary | WB, WRI | $EC_t$ | $LnEC_t$ |
| GDP Per capita | US Dollar | Secondary | WB National Account | $Y_t$ | $LnY_t$ |
| Energy use per capita | Terawatt-hrs | Secondary | WB, IEA Statistics | $EC_t$ | $LnEC_t$ |
| Urbanization | Percentage of urban population | Secondary | WB, United Nations Population Division | $U_t$ | $LnU_t$ |
| Trade volume | Percentage of GDP | Secondary | Ministry of Finance, Nepal | $TV$ | $LnTV$ |

the square of GDP per head, $LnEC_t$ for energy consumption per head, $LnTV$ for trade volume, and $LnU_t$ for a percentage of the urban population (a proxy for urbanization).

Table 1 presents detailed information regarding the nature and source of data and cleaning the data through log transformation.

The present study takes into consideration the Environmental Kuznets Curve (EKC) function as:

$$LnCE_t = f(LnY_t, LnY_t^2, LnEC_t, LnTV\ LnU_t) \quad \ldots (3)$$

Equation (3) represents the non-linear function form of EKC with $LnCE_t$ as the dependent variable and $LnY_t, LnY_t^2, LnEC_t, LnTV$ and $LnU_t$ as explanatory variables. Equation (3) can be expressed in algebraic non-linear form as:

$$LnEC_t = \gamma_i + \delta_i LnY_{it} + \theta_i LnY_{it}^2 + \mu_i LnEC_{it} + \sigma_i LnTV + \rho_i LnU_{it} + \varepsilon_{it} \quad \ldots (4)$$

For stability of the EKC function, the coefficient of $LnY_{it}$ is expected to be positive, whereas the coefficient of $LnY_{it}^2$ to be negative. Likewise, the coefficient of $LnEC_t$,$LnTV$ and $LnU_t$ should also be positive. The positive coefficients imply that increases in GDP, energy use, and urbanization are responsible factors causing air pollution. Positive coefficient of $LnY_{it}$ results in the part of EKC, which is monotonically increasing. Conversely, the negative coefficient of $LnY_{it}^2$ gives rise to a monotonically decreasing part of the EKC, and in general, the EKC is inverted U-shaped.

According to Sinha & Datta (2013), various types of environmental-economic relationships can be tested using equation (2). The following are the four possibilities for the income-carbon link.

a) The income-carbon link is linear and monotonically increasing as $\theta_1 > 0$ and $\theta_2 = \theta_3 = 0$, which indicates that rising incomes are the cause of increasing carbon emissions.

b) It demonstrates a monotonically declining linear income-carbon link as $\theta_1 > 0$ and $\theta_2 = \theta_3 = 0$.

c) The income-carbon link is shown to be quadratic as $\theta_1 > 0$ and $\theta_2 > 0$ and $\theta_3 > 0$. It gives an inverted U-shaped EKC. When the derivative of equation (2) is set to zero, it reveals the turning point of EKC. Now, equation (2) is converted as: $Y_t = -\frac{\theta_1}{2\theta_2}$

d) It reveals the N-shaped figure as a cubic polynomial when $\theta_1 > 0$ and $\theta_2 > 0$ and $\theta_3 > 0$..

**Econometric Methods**

The present study employs econometric methods to verify whether GDP is responsible for causing carbon emissions in Nepal. This study utilizes ARDL models, an econometric model, to examine whether EKC is valid. But before employing ARDL models, the present study checks the stationarity to identify whether the concerned variables are integrated of order one, zero, or a mixture of both order one and zero through the unit root test.

**Phillips-Perron (PP) Unit Root Test**

The unit root test known as Phillips-Perron (PP) was first introduced by Phillips & Perron (1988). It is a non-parametric statistical test that can be used to check the stationarity of the data sets under study. With the help of this test, the data sets under study can be checked as stationary or non-stationary, and their order of integration as $I(1)$ or $I(0)$ can be identified.

The Dickey-Fuller test equation without augmentation is estimated by the PP test:

$$\Delta y_t = \beta y_{t-1} + x_t'\gamma + \varepsilon_t \quad \ldots (5)$$

Where, $\Delta y_t$ is the first-order difference of the variable whose unit root is to be tested $y_{t-1}$, is the lagged regressor, $x_t$ is an exogenous explanatory variable, typically consisting of a constant and/or a trend, $\gamma$ is the coefficient of exogenous variables, and $\varepsilon_t$ is the white noise error term.

The assumption of the null is: "variable has a unit root," i.e., $\beta$=1. The assumption of null is not rejected, and hence, the variable is non-stationary. But, if the value of $\beta$ is less than 1, the variable will be stationary. More precisely, when the value of the test statistic in absolute form is larger than

the critical value in absolute form, then the assumption of the null is not accepted, and hence, the variable becomes stationary. Otherwise, the null is accepted, and the variable becomes non-stationary, having a unit root.

### Autoregressive Distributed Lags (ARDL) Models

There are different techniques for observing the long-run relationship between and among the variables. For this purpose, different types of cointegration tests like those suggested by Johansen (1988, 1991) and Johansen-Juselius (1990), the Engle-Granger test (1987), and the modified OLS technique by Phillips and Hansen (1990) are frequently employed. These methods suffer from minimal sample quality and have limited power because they need first-order integration of the variables. Consequently, because of their effectiveness-particularly when handling variables with varying integration orders, the Autoregressive Distributed Lag (ARDL) models have become more popular.

Pesaran et al. (1999) and Pesaran & Shin (1995) introduced the ARDL cointegration approach. This method facilitates the identification of long-term linkage among variables with different integration orders, such as *I*(0), *I*(1), or a combination thereof. According to Nkoro & Uko (2016), the ARDL technique determines cointegrating vectors that signify the enduring associations between underlying variables. Subsequently, the ARDL model can be transformed into ECM, illustrating how variables adjust to their long-term equilibrium in the short period. Kripfganz & Schneider (2018) stated that autoregressive distributed (ARDL) models have become more and more common as a means of analyzing their relationships over both the short and long term. The ARDL models, under a single equation framework, are influential techniques for comprehending how time series variables interact dynamically. It is reasonable for the current value of the explanatory variables to depend on their past values in addition to the previous values of the regressors. Stationary, non-stationary, or a mix of the two kinds of data will be included in the single equation framework. With the use of error-correcting procedures, we may use ARDL models to explore the impacts in the short-run and long-run. ARDL models can be used to examine cointegration, the term used to observe links between the variables in the long term.

Here, the ARDL econometric models, specifically the ARDL bound testing process, are predominantly employed to apply the EKC function. These models assess whether economic growth and additional factors (such as energy use, urbanization, and openness) cause environmental pollution in the Nepalese economy. Equation (6) outlines the ARDL model used in this work, based on the methodologies of Pesaran & Shin (1995), Pesaran & Shin (1997), Pesaran & Shin (1998), Pesaran et al. (1999), Pesaran & Shin (2001) and Pesaran et al. (2001).

We have is the dependent variable, and $LnY_t, LnY_t^2, LnEC_t, LnTV$ and $LnU_t$ are the explanatory variables. The $ARDL(p,q,r,s,m,n)$ model can be expressed as:

$$LnCE_t = \beta_0 + \sum_{i=1}^{p} \alpha_i LnCE_{t-i} + \sum_{j=1}^{q} \gamma_j LnY_{t-j} + \sum_{k=1}^{r} \delta_k LnY_{t-k}^2 + \sum_{l=1}^{s} \rho_l LnEC_{(t-l)} + \sum_{m=1}^{u} \sigma_u LnTV_{t-u} + \sum_{n=1}^{v} \theta_n dLnU_{t-n} + \varepsilon_t \quad \ldots(6)$$

where, *p*, *q*, *r* ... *n* are the lags of regressand $LnCE_t$ and regressors $LnY_t, LnY_t^2, LnEC_t, LnTV$ and $LnU_t$ respectively. The parameters $\alpha_i s, \gamma_j s, \delta_k s \ldots \theta_l s$ are the coefficients of regressors, and $e_t$ is a disturbance.

Equation (6) in error correction term can be recast as:

$$dLnCE_t = \alpha Z_{t-1} + \beta dLnY_t + \sum_{j=1}^{q} \gamma_j dLnY_{t-j} + \pi dLnY_t^2 + \sum_{k=1}^{r} \delta_k dLnY_{t-k}^2 + \sigma dLnEC_t + \sum_{l=1}^{s} \rho_l dLnEC_{(t-l)} + \sigma dLnTV + \sum_{m=1}^{u} \sigma_u dLnTV_{t-u} + \varphi dLnU_t + \sum_{n=1}^{v} \theta_m dLnU_{t-m} + \varepsilon_t \quad \ldots(7)$$

According to Shrestha & Bhatta (2018), the lagged variable coefficients of the ARDL model (equation 7) reflect short-run dynamics, but the unlagged variable coefficients of the same equation indicate the long-run link among the variables. The assumption that the null is: $\beta + \pi + \rho + \sigma + \varphi = 0$. It indicates that the variables do not cointegrate. According to Pesaran et al. (2001), the bound test is employed to observe the cointegrating link among the variables using (1) or *I*(0) variables.

## RESULTS AND DISCUSSIONS

### Covariance and Correlation Analysis

Table 2 presents the covariance and correlation matrix with corresponding t-statistic and probability values.

### Descriptive Statistics

Table 3 presents descriptive statistics of the variables under study.

### Phillips-Perron (PP) Unit Root Test

The PP unit root test results are portrayed in Table 4.

Based on Table 2, almost all variables except $LnU_t$ are found to be insignificant at 0.05 level, and hence, these are non-stationary at level forms, and they are significant at first differences representing stationary

Table 2: Covariance and correlation matrix with t-statistic and probability values.

| Covariance<br>Correlation<br>t-Statistic<br>Probability | $LnCE_t$ | $LNY_t$ | $LnEC_t$ | $LnY_t^2$ | $LnTV$ | $LnU_t$ |
|---|---|---|---|---|---|---|
| $LnCE_t$ | 0.576230 | | | | | |
| | 1.000000 | | | | | |
| | - | | | | | |
| | - | | | | | |
| $LNY_t$ | 0.521040 | 0.544616 | | | | |
| | 0.930096 | 1.000000 | | | | |
| | 16.01466 | - | | | | |
| | 0.0000 | - | | | | |
| $LnEC_t$ | 0.543688 | 0.500451 | 0.536501 | | | |
| | 0.977836 | 0.925829 | 1.000000 | | | |
| | 29.53769 | 15.49300 | - | | | |
| | 0.0000 | 0.0000 | - | | | |
| $LnY_t^2$ | 6.231673 | 6.529172 | 5.941515 | 78.40887 | | |
| | 0.927094 | 0.999149 | 0.916071 | 1.000000 | | |
| | 15.64308 | 153.1837 | 14.44769 | - | | |
| | 0.0000 | 0.0000 | 0.0000 | - | | |
| $LnTV$ | 0.082279 | 0.041501 | 0.081595 | 0.462368 | 0.042952 | |
| | 0.522993 | 0.271346 | 0.537506 | 0.251949 | 1.000000 | |
| | 3.880743 | 1.783036 | 4.031367 | 1.646581 | - | |
| | 0.0004 | 0.0822 | 0.0002 | 0.1075 | - | |
| $LnU_t$ | 0.268100 | 0.247970 | 0.270263 | 2.925738 | 0.045268 | 0.140151 |
| | 0.943409 | 0.897544 | 0.985605 | 0.882580 | 0.583450 | 1.000000 |
| | 17.99179 | 12.87425 | 36.87034 | 11.87234 | 4.543575 | - |
| | 0.0000 | 0.0000 | 0.0000 | 0.0000 | 0.0001 | - |

variables. The variables except for $LnU_t$ are I(1), and $LnU_t$ is stationary at the level and is $I(0)$. Now, the mixture of $I(1)$and $I(0)$ variables are suitable for carrying out the ARDL model as a representation of the linkage between the variables with the integration of different orders.

Table 3: Descriptive statistics of the variables.

| | $LnCE_t$ | $LnY_t$ | $LnEC_t$ | $LnY_t^2$ | $LnTV_t$ | $LnU_t$ |
|---|---|---|---|---|---|---|
| Mean | 4.775905 | 5.766938 | 6.260464 | 33.80219 | 3.744311 | 2.516472 |
| Median | 4.743986 | 5.443121 | 6.414101 | 29.62864 | 3.793570 | 2.615148 |
| Maximum | 6.234411 | 7.114277 | 7.469654 | 50.61293 | 4.159508 | 3.044999 |
| Minimum | 3.688879 | 4.826189 | 4.927254 | 23.29210 | 3.404525 | 1.806812 |
| Std. Dev. | 0.768300 | 0.746927 | 0.741341 | 8.962214 | 0.209761 | 0.378906 |
| Skewness | 0.298046 | 0.616132 | -0.078791 | 0.698375 | -0.079685 | -0.364943 |
| Kurtosis | 2.172809 | 1.829480 | 1.983804 | 1.924163 | 2.028316 | 1.813816 |
| Jarque-Bera | 1.819249 | 5.055034 | 1.850600 | 5.439585 | 1.696744 | 3.394589 |
| Probability | 0.402675 | 0.079857 | 0.396412 | 0.065888 | 0.428111 | 0.183178 |
| Sum | 200.5880 | 242.2114 | 262.9395 | 1419.692 | 157.2611 | 105.6918 |
| Sum Sq. Dev. | 24.20168 | 22.87389 | 22.53305 | 3293.172 | 1.803992 | 5.886359 |
| Observations | 42 | 42 | 42 | 42 | 42 | 42 |

Table 4: Phillips-Perron unit root test.

| Variables | t-statistics | Critical statistics at 5% Level | Probability Value |
|---|---|---|---|
| $LnCE_t$ | 0.1456 | -2.9350 | 0.9655 |
| $dLnCE_t$ | -7.4824 | -2.9369 | 0.0000 |
| $LnY_t$ | 0.9131 | -2.9350 | 0.9947 |
| $dLnY_t$ | -5.4730 | -2.9369 | 0.0000 |
| $LnY_t^2$ | 1.2492 | -2.9350 | 0.9980 |
| $dLnY_t^2$ | -5.0585 | -2.9369 | 0.0001 |
| $LnEC_t$ | -1.6223 | -2.9350 | 0.4623 |
| $dLnEC_t$ | -8.4145 | -2.9369 | 0.0000 |
| $LnTV$ | -1.8533 | -2.9350 | 0.3504 |
| $dLnTV$ | -5.5347 | -2.9369 | 0.0000 |
| $LnU_t$ | -4.1029 | -2.9350 | 0.0026 |

## Optimal Selection of Lags for ARDL Models

It is necessary to include optimal lag/s in both dependent and independent variables for the execution of suitable *ARDL* models. We select the appropriate lags that must be included in the variables under consideration using the Akaike information criterion (Pesaran & Shin 1999, Pesaran et al. 2001, Lutkepohl 2005, Narayan 2005). Fig.1 shows the optimal lags that must be included in the variables based on equations (6). The figure suggests *ARDL*(1,3,3,2,0,3) model as a suitable model for the autoregressive distributed lags as reported by the minimum value under the Akaike information criterion.

## ARDL Results

The results of the ARDL (1,3,3,2,0,3) approach are presented in Table 5, showcasing the coefficients of $LnY_t$ at a lag of two, which stands at 6.8731. This result holds significance at the 5 percent level, suggesting that as GDP per head was raised by 1 percent two years back, it caused the release of the carbons by 6.87 percent in the current period. The relationship between economic growth and carbon emissions in the present study supports Panayotou (1993), Selden & Song (1994), Grossman & Krueger (1995), Pesaran & Shin (1999), Lutkepohl (2005) and Narayan (2005). This signals that the growth of GDP is one of the drivers of carbons in Nepal. Conversely, the coefficient of  at a lag of two is -0.5713, which is significant at 0.05 level. As reported by this negative coefficient, it can be concluded that the EKC turns down when it reaches the maximum point. The positive and negative coefficient of and  respectively provide sufficient evidence supporting the prevalence of the EKC in Nepal. The findings of the reversal U-shaped EKC support Panayotou (1993), Grossman & Krueger (1994), Stern (2004) and Wang et al. (2016).

Examining the coefficient of $LnEC_t$ At a lag of zero, it stands at 0.7430 and is also significant at less than the 1%

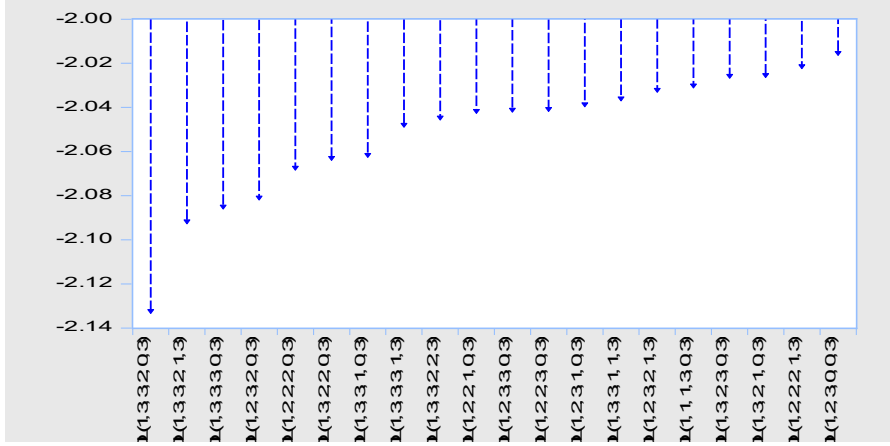


Fig. 1: Selection of optimal lag(s) by Akaike information criterion.

level. This implies a one percent rise in energy use leads to a 0.7430 percent rise in carbon emissions. Consequently, energy use is identified as another contributor to carbon emissions. The result from the present study regarding energy use and carbon emissions supports Nasir & Rehman (2011), Saboori et al. (2014), Pata (2017), Alam & Adil (2019), Gonzalez-Sanchez & Martin-Ortega (2020), Raihan et al. (2023) and Mitic et al. (2023). However, the coefficient of $LnTV_t$ is not significant, exhibiting that Nepalese openness does not influence environmental contamination. However, the coefficients of $LnU_t$ At lags zero and two are positive and also significant at 0.05 level, suggesting that an expansion of urbanization results in an adverse effect on the environment in Nepal. The impact of urbanization on carbon emissions of the present study supports Wu et al. (2016), Musah et al. (2020), Adebayo et al. (2021) and Wang et al. (2021).

It is evident given the positive and negative coefficient of $LnY_t$ and $LnY_t^2$ that the reversal u-shaped EKC is prevalence in Nepal. This suggests that increasing carbon emissions are primarily driven by GDP, while a subsequent rise in GDP becomes a secondary factor contributing to decreasing carbon emissions. Consequently, besides income growth, variables such as energy use and the rate of urbanization emerge as significant factors causing environmental pollution in the Nepalese economy.

Table 5: ARDL (1, 3, 3, 2, 0, 3) model with dependent variable $dLnCE_t$

| Regressors | Parameters | SE | t-Statistic | Probability |
|---|---|---|---|---|
| $LnEC_t(-1)$ | 0.3925 | 0.1833 | 2.1412 | 0.0441 |
| $LnY_t$ | 0.4837 | 2.0410 | 0.2370 | 0.8149 |
| $LnY_t(-1)$ | -7.4549 | 2.2512 | -3.3114 | 0.0033 |
| $LnY_t(-2)$ | 6.8731 | 2.2612 | 3.0395 | 0.0062 |
| $LnY_t(-3)$ | -2.5693 | 1.7043 | -1.5075 | 0.1466 |
| $LnY_t^2$ | -0.0207 | 0.1701 | -0.1218 | 0.9042 |
| $LnY_t^2(-1)$ | 0.5937 | 0.1912 | 3.1048 | 0.0054 |
| $LnY_t^2(-2)$ | -0.5713 | 0.1904 | -2.9999 | 0.0068 |
| $LnY_t^2(-3)$ | 0.2344 | 0.1428 | 1.6412 | 0.1156 |
| $LnEC_t$ | 0.7430 | 0.1814 | 4.0942 | 0.0005 |
| $LnEC_t(-1)$ | -0.2823 | 0.2477 | -1.1394 | 0.2674 |
| $LnEC_t(-2)$ | -0.3556 | 0.2153 | -1.6513 | 0.1135 |
| $LnTV_t$ | -0.1025 | 0.1882 | -0.5450 | 0.5915 |
| $LnU_t$ | 12.9240 | 5.2835 | 2.4460 | 0.0233 |
| $LnU_t(-1)$ | -21.6748 | 9.2087 | -2.3537 | 0.0284 |
| $LnU_t(-2)$ | 20.0657 | 8.1889 | 2.4503 | 0.0231 |
| $LnU_t(-3)$ | -10.1895 | 4.1309 | -2.4666 | 0.0223 |
| $\beta_0$ | 6.8043 | 6.7467 | 1.0085 | 0.3247 |

In 1990, Nepal transitioned to a multiparty democracy and adopted economic liberalization policies. This led to a surge in FDI and foreign aid, along with a dramatic increase in trade. The resulting economic growth and rapid industrialization ushered in a new era of urbanization, which in turn drove up carbon emissions. Hence, Nepal's carbon emissions increased substantially after the 1990s due to the rise of urbanization.

Once the ARDL model is applied, this study employs the bound tests and ECM to observe the long-run link among the variables. The findings from the ARDL bound test are outlined in Table 3, whereas Table 6 presents the results of ECM within the framework of ARDL (1, 3, 3, 2, 0, 3).

In Table 6, the ARDL bounds test adheres to an F-statistic which is 3.3960, and it exceeds the critical value of F-distribution 3.38 as proposed by Pesaran & Timmermann (2005) at a 0.05 significant level for both I(0) and $I(1)$. Consequently, the assumption of null "no cointegration," is rejected, representing a cointegration among the variables. As indicated by the bound test results, there exists a long-run link among the variables. In simpler terms, the variables, namely, $dLnCE_t, dLnY_t, dLnY_t^2, dLnEC_t\ LnTV_t$ and $LnU_t$ exhibit a linkage among them eventually. This result for the Nepalese economy supports the study by Raihan & Tuspekova (2022).

The ECM is the component of ARD, which is employed to observe the dynamics of the variables (Pesaran & Shin 1999, Pesaran et al. 2001, Narayan 2005, Narayan & Smyth 2005). Through this model, this study has explored the linkage among a set of variables $dLnCE_t, dLnY_t, dLnY_t^2, dLnEC_t\ LnTV_t$ and $LnU_t$. This test also focuses on how the variables impact the dynamics of the EKC hypothesis. The test results are portrayed in Table 7. The significance of the coefficients for $dLnY_t$ and $dLnY_t^2$ at lag of two for each is confirmed at the 0.05 level, with opposing signs: positive and negative, respectively. This observed pattern strongly suggests the presence of a reversal EKC in the Nepalese economy. Specifically, it implies that when the economy initially grows, environmental degradation increases. However, above a certain point, a further rise in income results in a decreased environmental impact on the economy of Nepal.

Table 6: Results from ARDL (1, 3, 3, 2, 0, 3) bound to test for cointegration.

| | Value | Level of Significance | | |
|---|---|---|---|---|
| F-statistic | 3.3960 | 10% | 2.08 | 3.00 |
| $k$ | 5 | 5% | 2.39 | 3.38 |
| | | 2.5% | 2.7 | 3.73 |
| | | 1% | 3.06 | 4.15 |

Moreover, the coefficients of $dLnEC_t$ At lags zero and one are both positive, and these are also observed to be statistically significant, underscoring the role of energy consumption as a driving factor behind carbon emissions in Nepal. In the same manner, the coefficients of $LnU_t$ Lag zero and lag two also exhibit statistical significance at least at 0.05 level, indicating that urbanization is a key contributor to carbon emissions. The variables $dLnY_t, dLnY_t^2, dLnEC_t$ and $LnU_t$ Demonstrate short-run negative impacts on the environment, suggesting their potential to influence environmental policy and sustainability efforts in Nepal.

It is implied that short-run disturbances have a considerable impact on the long-term equilibrium link among the variables by the *ECT* coefficient of $Z_t$ At lag one, which is negative and highly significant. To put it simply, these short-term shocks have a substantial effect on the long-term dynamics of the variables that are being studied. The error correction term coefficient is -0.6074, signifying that approximately 60.74% of the adjustment toward equilibrium occurs within a single period. The error correction modeling results of the present study are comparable to findings by Engle & Granger (1987), Pesaran & Shin (1997), Shahbaz et al. (2013), Adebayo (2020) and Adebayo (2021). In the study of Adebayo (2020) and Adebayo (2021), the ECMs' coefficients are negative and statistically significant, illustrating that prior periods' errors can be corrected by subsequent periods.

This finding indicates that the system experiences rapid correction when deviations from the long-run growth path arise from short-term perturbations. In other words, short-run fluctuations cause the dependent variable to deviate from its long-run trajectory, and approximately 60 percent of this deviation is adjusted in the succeeding period.

Table 7: Error correction modeling under ARDL (1, 3, 3, 2, 0, 3).

| Regressors | Parameters | SE | t-Statistic | Probability |
|---|---|---|---|---|
| $dLnY_t$ | 0.483798 | 1.222331 | 0.395800 | 0.6962 |
| $dLnY_t$ (–1) | -4.303802 | 1.231139 | -3.495788 | 0.0022 |
| $dLnY_t$ (–2) | 2.569356 | 1.089471 | 2.358351 | 0.0281 |
| $dLnY_t^2$ | -0.020734 | 0.101044 | -0.205203 | 0.8394 |
| $dLnY_t^2$ (–1) | 0.336823 | 0.102104 | 3.298825 | 0.0034 |
| $dLnY_t^2$ (–2) | -0.234496 | 0.090047 | -2.604147 | 0.0166 |
| $dLnEC_t$ | 0.743091 | 0.124315 | 5.977467 | 0.0000 |
| $dLnEC_t$ (–1) | 0.355689 | 0.129867 | 2.738864 | 0.0123 |
| $dLnU_t$ | 12.92401 | 3.184740 | 4.058105 | 0.0006 |
| $dLnU_t$ (–1) | -9.876227 | 4.488939 | -2.200125 | 0.0391 |
| $dLnU_t$ (–2) | 10.18952 | 3.174901 | 3.209398 | 0.0042 |
| $Z_t$ (–1) | -0.607487 | 0.109883 | -5.528484 | 0.0000 |

In conclusion, the error correction modeling results presented in Table 7 give a significant revelation into the dynamics of environmental factors in the Nepalese economy. These findings have implications for understanding the association among income, energy use, urbanization, and pollution. The identification of an EKC pattern highlights the potential for policy interventions to promote sustainability and mitigate environmental impact.

### Diagnostics and Stability Tests

The fitted ARDL models require an assessment of residual stability and diagnostic properties through serial correlation and heteroskedasticity tests. The serial correlation is examined using the Breusch-Godfrey (BG) approach (Evans & Patterson 1985), while heteroskedasticity is tested using the Breusch-Pagan-Godfrey (BPG) approach (Dufour et al. 2004). Additionally, Ramsay's RESET test (Ramsey 1969) is employed to gauge the stability of the estimated models. The results of the tests are portrayed in Table 8.

The serial correlation LM test under the BG method consists of the F-statistic $(T \times R^2)$ value, and the $\chi^2$ value, all of which are insignificant. The assumption of null, "no serial correlation," is accepted, indicating that the residuals in the ARDL models do not exhibit serial correlation. Similarly, the F-statistic, $(T \times R^2)$ value, and the $\chi^2$ value under the BPG method is also insignificant. The assumption of the null "no heteroskedasticity" is not rejected, affirming that the residuals do not exhibit heteroskedasticity. Ramsey's RESET test yields a non-significant F-statistic as well. Consequently, the fitted ARDL model is deemed robust and demonstrates linearity, as suggested by Ramsey's RESET test.

## CONCLUSIONS

As per the findings derived from ARDL models in this study, the main driving factors for air pollution in Nepal are identified as increased urbanization, escalating energy use, and growth of income. The models suggest the presence of a reversal U Environmental Kuznets Curve in Nepal during the study period. The environmental deteriorations in Nepal

Table 8: Results of serial correlation, heteroskedasticity, and Ramsey's RESET test for ARDL models.

| Description | B-G Serial Correlation | B-P-G Heteroskedasticity | Ramsey's RESET |
|---|---|---|---|
| F-statistic | 0.1703 | 0.8582 | 0.3309 |
| DF | (2,19) | (17, 21) | (1, 20) |
| Probability | 0.8447 | 0.6216 | 0.5715 |
| $T \times R^2$ | 0.6868 | 15.9876 | |
| $\chi^2$(Probability) | 0.7093 | 0.5247 | |

are found to have been caused by the country's desire for rapid economic growth. The ARDL models reveal that environmental pollutions are found to be increasing with the rise in GDP in the initial phase when the level of GDP growth is low. The economy is concentrated on achieving high and higher economic growth, giving less attention to environmental protection. But when certain maximum growth is achieved after a rise in economic growth causes carbon emissions to decrease. It is because the country has pressure from everywhere to minimize carbon emissions and protect the environment.

Consequently, the government opts the measures to minimize carbon emissions. So, along with an increase in economic growth, carbon emissions start decreasing through government commitments at the international level as well as the awareness of the government itself for cleaning the environment. Thus, carbon emissions decrease with the rise of GDP growth in the later stage. Nepal is more serious about environmental issues in the later years. Various efforts have been made on the part of the government to reduce carbon emissions. The common people are more environmentally conscious, and they are also contributing to reducing carbon emissions through afforestation and garbage management.

Nepal, an underdeveloped country, seeks to accelerate economic growth to graduate from its current status and join the League of Developing Nations. However, this economic growth must be harmonized with the need to reduce carbon emissions and protect the environment. In this context, Nepal should shift its focus towards prioritizing a green GDP over GDP, placing environmental sustainability at the forefront of its development agenda. To ensure a holistic and inclusive approach, it is paramount to discourage rural-to-urban migration, concentrating efforts on rural infrastructure development and employment generation. This transition necessitates a concerted effort on multiple fronts, where three layers of government take a leading role. Nepal should increase hydropower exports to reduce the trade deficit through the completion of ongoing hydro-projects very soon. Nepal should pivot towards electric vehicles, incentivizing the shift with reduced customs duties and subsidies while phasing out older gasoline vehicles. To encourage electric vehicles, the government should facilitate the establishment of charging stations sufficiently.

Additionally, Nepal should strengthen its public and private forest programs and enact strict regulations regarding well management of waste. The government should introduce waste management policies that create employment opportunities. Lastly, the creation of green cities and the promotion of organic farming will be pivotal in driving sustainable development while ensuring a brighter and greener future for Nepal. To achieve harmonious economic growth and emissions reduction, we also urge donor countries and agencies to partner with Nepal in its ambitious endeavors. This partnership can take shape through multifaceted support as fueling socio-economic progress that aligns with Nepal's commitment to reduce carbon emissions, ensuring that development and sustainability walk hand-in-hand.

## REFERENCES

Adebayo, T. S. 2020. Revisiting the EKC hypothesis in an emerging market: an application of ARDL-based bounds and wavelet coherence approaches. SN Appl. Sci., 2(12), 1-15. https://doi.org/10.1007/s42452-020-03705-y

Adebayo, T. S. 2021. Testing the EKC Hypothesis in Indonesia: Empirical evidence from the ARDL-based bounds and wavelet coherence approach. Appl. Econ. J., 28(1): 78-100. http://dx.doi.org/10.22004/ag.econ.334394

Adebayo, T. S., Awosusi, A. A., Odugbesan, J. A., Akinsola, G. D., Wong, W. and Rjoub, H. 2021. Sustainability of energy-induced growth nexus in Brazil: Do carbon emissions and urbanization matter? Sustainability, 5: 1-21.

Agras, J. and Chapman, D. 1999. A dynamic approach to the environmental Kuznets curve hypothesis. Ecol. Econ., 28(2): 267-277.

Akif, M. and Sinha, A. 2020. Renewable, non-renewable energy consumption, economic growth, trade openness and ecological footprint: Evidence from organisation for economic Co-operation and development countries. J. Clean. Prod., 242: 118537-118548. https://doi.org/10.1016/j.jclepro.2019.118537

Alam, R. and Adil, M. H. 2019. Validating environmental Kuznets curve in India: ARDL bounds testing framework. OPEC Energy Rev., 11: 1-24. https://doi.org/10.1111/opec.12156

Ali, A., Radulescu, M. and Balsalobre-Lorente, D. 2023. A dynamic relationship between renewable energy consumption, nonrenewable energy consumption, economic growth, and carbon dioxide emissions: Evidence from Asian emerging economies. Energy Environ., 15: 684. https://doi.org/10.1177/0958305X231151684

Ali, K. A., Ahmad, M. I. and Yusup, Y. 2020. Issues, impacts, and mitigations of carbon dioxide emissions in the building sector. Sustainability (Switz.), 12(18): 427. https://doi.org/10.3390/SU12187427

Allard, A., Takman, J., Uddin, G.S. and Ahmed, A. 2018. The N-shaped environmental Kuznets curve: an empirical evaluation using a panel quantile regression approach. Environmental Science and Pollution Research, 25: 5848-5861.

Ang, J. B. 2007. $CO_2$ emissions, energy consumption, and output in France. Energy Policy, 35: 4772-4778. https://doi.org/10.1016/j.enpol.2007.03.032

Arouri, M., Shahbaz, M., Onchang, R. and Teulon, F. 2013. Environmental Kuznets curve in Thailand: Cointegration and causality analysis. J. Energy Dev., 39(1): 900. https://www.jstor.org/stable/24812900

Babu, S. S. and Datta, S. K. 2013. The relevance of environmental Kuznets curve (EKC) in a framework of broad-based environmental degradation and modified measure of growth-a pooled data analysis. Int. J. Sustain. Dev. World Ecol., 20(4): 309-316. https://doi.org/10.1080/13504509.2013.795505

Bao, Z. and Lu, W. 2023. Applicability of the environmental Kuznets curve to construction waste management: A panel analysis of 27 European economies. Resour. Conserv. Recycl., 188: 106667. https://doi.org/10.1016/j.resconrec.2022.106667

Barbier, E. B. 1997. Development Economics: Introduction to the environmental Kuznets curve special issue. Environ. Dev. Econ., 2: 369-381. https://doi.org/10.1017/S1355770X97000193

Bruyn, S. M. De, Bergh, J. C. J. M. VanDen, & Opschoor, J. B. 1998. Economic growth and emissions: reconsidering the empirical basis of environmental Kuznets curves. Ecol. Econ., 25: 161-175. https://doi.org/10.1016/S0921-8009(97)00178-X

Chen, F., Liu, A., Lu, X., Zhe, R., Tong, J. and Akram, R. 2022. Evaluation of the effects of urbanization on carbon emissions: the transformative role of government effectiveness. Front. Energy Res., 10: 1-12. https://doi.org/10.3389/fenrg.2022.848800

Cole, M.A., Rayner, A.J. and Bates, J.M. 1997. The environmental Kuznets curve: an empirical analysis. Environment and Development Economics, 2(4): 401-416.

Dasgupta, S., Laplante, B., Wang, H. and Wheeler, D. 2002. Confronting the environmental Kuznets curve. Journal of Economic Perspectives, 16(1): 147-168.

Davis, S.J. and Caldeira, K. 2010. Consumption-based accounting of CO2 emissions. Proceedings of the National Academy of Sciences, 107(12): 5687-5692.

Dufour, J., Khalaf, L., Bernard, J. and Genest, I. 2004. Simulation-based finite-sample tests for heteroskedasticity and ARCH effects. J. Econom., 122: 317-347. https://doi.org/10.1016/j.jeconom.2003.10.024

Elum, Z. A. and Momodu, A. S. 2017. Climate change mitigation and renewable energy for sustainable development in Nigeria: A discourse approach. Renew. Sustain. Energy Rev., 76: 72-80. DOI: 10.1016/j.rser.2017.03.040

Engle, R. F. and Granger, C. W. J. 1987. Cointegration and Error Correction Representation, Estimation and Testing. Econometrica, 55: 251-276. http://dx.doi.org/10.2307/1913236

Evans, G. and Patterson, K. D. 1985. In the presence of linear restrictions. Econ. Lett., 17: 237-241. https://doi.org/10.1016/0165-1765(85)90209-5

Gonzalez-Sanchez, M. and Martin-Ortega, J. L. 2020. Greenhouse gas emissions growth in Europe: A comparative analysis of determinants. Sustainability, 12(3): 1012. https://doi.org/10.3390/su12031012

Government of Nepal (GoN). 2021. Nepal's long-term strategy for net-zero emissions. https://unfccc.int/sites/default/files/resource/NepalLTLEDS.pdf

Government of Nepal (GoN). 2023. Government of Nepal, National Planning Commission, Thirteenth Five-Year Plan (2023-2028)

Government of Nepal (GoN). 2023. National Planning Commission. https://npc.gov.np/en/

Grossman, G. M. and Krueger, A. B. 1991. Environmental impacts of a North American Free Trade Agreement. Working Paper No. 3914. National Bureau of Economic Research, Cambridge (MA).

Grossman, G. M. and Krueger, A. B. 1995. Economic growth and the environment. Q. J. Econ., 110(2): 353-377.

Halicioglu, F. 2009. An econometric study of $CO_2$ emissions, energy consumption, income and foreign trade in Turkey. Energy Policy, 37:1156-1164. https://doi.org/10.1016/j.enpol.2008.11.012

Huang, J. and Guo, L. 2022. Research on the impact of financial development in different regions on the decoupling of carbon emissions from economic growth. Energy Environ., 34(6): 2007-2030. https://doi.org/10.1177/0958305X221107341

Inmaculada, M. Z. and Antonello, M. 2011. The impact of urbanization on $CO_2$ emissions: Evidence from developing countries. Ecol. Econ., 70: 1344-1353.

IPCC (Intergovernmental Panel on Climate Change). (2022). Climate Change 2022: Mitigation of Climate Change. Intergovernmental Panel on Climate Change.

Itoo, H. H. and Ali, N. 2023. Analyzing the causal nexus between CO emissions and its determinants in India: evidence from ARDL and EKC approach. Manag. Environ. Qual. Int. J., 34(1): 192-213. https://doi.org/10.1108/MEQ-01-2022-0014

Iwata, H., Okada, K. and Samreth, S. 2010. Empirical study on the environmental Kuznets curve for CO2 in France: the role of nuclear energy. Energy Policy, 38(8): 4057-4063.

Jaffe, A. B. and Palmer, K. 1997. Environmental regulation and innovation: A panel data study. Rev. Econ. Stat., 79(4): 610-619. DOI: https://doi.org/10.1162/003465397557196

Jiang, S., Chishti, M. Z., Rjoub, H. and Rahim, S. 2022. Environmental R&D and trade-adjusted carbon emissions: evaluating the role of international trade. Environ. Sci. Pollut. Res., 29(42): 63155-63170. https://doi.org/10.1007/s11356-022-20003-9

Jiang, X. T., Su, M. and Li, R. 2018. Investigating the factors influencing the decoupling of transport-related carbon emissions from turnover volume in China. Sustainability, 10(9): 3034.

Jiao, L., Yang, R., Chen, B. and Zhang, Y. 2023. Variation, determinants, and prediction of carbon emissions in Guizhou: A new economic growth pole in southwest China. J. Clean. Prod., 417: 138049. https://doi.org/10.1016/j.jclepro.2023.138049

Johansen, S. 1988. Statistical analysis of cointegration vectors. J. Econ. Dyn. Control, 12: 231-254. https://doi.org/10.1016/0165-1889(88)90041-3

Johansen, S. 1991. Estimation and hypothesis testing of cointegration vectors in Gaussian vector autoregressive models. Econometrica, 59(6): 1551-1580. http://dx.doi.org/10.2307/2938278

Johansen, S. and Juselius, K. 1990. Maximum likelihood estimation and inference on cointegration with application to the demand for money. Oxford Bull. Econ. Stat., 52: 169-210. http://dx.doi.org/10.1111/j.1468-0084.1990.mp52002003.x

Karedla, Y., Mishra, R. and Patel, N. 2021. The impact of economic growth, trade openness and manufacturing on $CO_2$ emissions in India: an autoregressive distributive lag (ARDL) bounds test approach. J. Econ. Finance Admin. Sci., 26(52): 376-389. https://doi.org/10.1108/JEFAS-05-2021-0057

Khan, M. I., Khan, M. K., Dagar, V., Oryani, B., Akbar, S. S., Salem, S. and Dildar, S. M. 2021. Testing environmental Kuznets curve in the USA: what role institutional quality, globalization, energy consumption, financial development, and remittances can play? New evidence from dynamic ARDL simulations approach. Front. Environ. Sci., 9: 1-15. https://doi.org/10.3389/fenvs.2021.789715

Khan, Y. A. and Ahmad, M. 2021. Investigating the impact of renewable energy, international trade, tourism, and foreign direct investment on carbon emission in developing as well as developed countries. Environ. Sci. Pollut. Res., 28(24): 31246-31255. https://doi.org/10.1007/s11356-021-12937-3

Kijima, M., Nishide, K. and Ohyama, A. 2010. Economic models for the environmental Kuznets curve: A survey. J. Econ. Dyn. Control, 34(7): 1187-1201. https://doi.org/10.1016/j.jedc.2010.03.010

Kripfganz, S. and Schneider, D. C. 2018. ARDL: Estimating autoregressive distributed lag and equilibrium correction models. Lond. Stat. Conf., 7: 1-44.

Lazar, D., Minea, A. and Purcel, A. A. 2019. Pollution and economic growth: evidence from Central and Eastern European countries. Energy Econ., 81: 1121-1131. https://doi.org/10.1057/s41599-023-02197-6

Lütkepohl, H. 2005. The New Introduction to Multiple Time Series Analysis. Springer Science and Business Media, Cham.

Menyah, K. and Wolde-Rufael, Y. 2010. Energy consumption, pollutant emissions, and economic growth in South Africa. Energy Econ., 32(6): 1374-1382. http://dx.doi.org/10.1016/j.eneco.2010.08.002

Ministry of Energy, Water Resources and Irrigation (MoEST). 2006. Renewable Energy Policy, 2006. https://www.iea.org/policies/6228-renewable-energy-subsidy-policy-of-nepal

Ministry of Environment, Science and Technology (MoEST). 2019. National Air Quality Strategy, 2019. https://thehimalayantimes.com/kathmandu/government-unveils-action-plan-to-control-air-pollution

Ministry of Forests and Environment (MoFE). 2015. Intended nationally determined contributions (INDCs), 2015. https://www4.unfccc.int/sites/submissions/INDC/Published%20Documents/Nepal/1/Nepal_INDC_08Feb_2016.pdf

Ministry of Forests and Environment (MoFE). 2019. National Forest Policy, 2019. https://dnpwc.gov.np/en/policy-and-directives/

Ministry of Forests and Environment (MoFE). 2022. Nepal's Second Biennial Update Report to the UNFCCC, 2022. https://climatepromise.undp.org/what-we-do/where-we-work/nepal

Ministry of Forests and Soil Conservation (MoFSC). 2014. National Biodiversity Strategy And Government Of Nepal. July 2014.

Ministry of Forests and Soil Conservation (MoFSC). 2021. Intergovernmental Panel on Climate Change, Sixth Assessment Report, 2021. https://www.ipcc.ch/assessment-report/ar6/

Ministry of Forests and Soil Conservation (MoFSC). 2021. State of the environment in Nepal 2020. Kathmandu: Government of Nepal.

Ministry of Water Resources (MoWR). 2019. National Water Quality Management Strategy, 2019. https://climate.mohp.gov.np/downloads/National_Drinking_Water_Quality_Standards_2005.pdf

Mitic, P., Fedajev, A., Radulescu, M. and Rehman, A. 2023. The relationship between $CO_2$ emissions, economic growth, available energy, and employment in SEE countries. Environ. Sci. Pollut. Res., 30: 16140-16155. https://doi.org/10.1007/s11356-022-23356-3

Mohammed, S., Mosté, B. and Mohammed, G. 2015. Causal interactions between FDI and economic growth: evidence from dynamic panel co-integration. 23: 276-290. https://doi.org/10.1016/S2212-5671(15)00541-9

Musah, M., Kong, Y., Adjei, I., Kwadwo, S. and Mary, A. 2020. The connection between urbanization and carbon emissions: panel evidence from West Africa United States of America. Environ. Dev. Sustain., 0123456789. https://doi.org/10.1007/s10668-020-01124-y

Narayan, P. K. 2005. The saving and investment nexus for China: Evidence from cointegration tests. Appl. Econ., 37(17): 1979-1990.

Narayan, P. K. and Smyth, R. 2005. Electricity consumption, employment, and real income in Australia: Evidence from multivariate Granger causality tests. Energy Policy, 33(9): 1109-1116.

Nasir, M. and Rehman, F. U. 2011. Environmental Kuznets Curve for carbon emissions in Pakistan: An empirical investigation. Energy Policy, 39: 1857-1864. https://doi.org/10.1016/j.enpol.2011.01.025

National Planning Commission (NPC). 2021. Green, Resilient and Inclusive Development (GRID) Strategy, 2021. https://www.worldbank.org/en/events/2022/06/13/green-resilient-inclusive-development-grid-in-action-a-high-level-dialogue-for-nepal

Nemeth-Durko, E. 2021. Determinants of carbon emissions in a European emerging country: evidence from ARDL cointegration and Granger causality analysis. Int. J. Sustain. Dev. World Ecol., 28(5): 417-428. https://doi.org/10.1080/13504509.2020.1839808

Nepali Times. (2021, August 27). Nepal doubles its carbon footprint. https://www.nepalitimes.com/latest/nepal-doubles-its-carbon-footprint/

Nkoro, E. and Uko, A.K. 2016. Autoregressive Distributed Lag (ARDL) cointegration technique: application and interpretation. Journal of Statistical and Econometric Methods, 5(4): 63-91.

Numan, U., Ma, B., Meo, M. S. and Bedru, H. D. 2022. Revisiting the N-shaped environmental Kuznets curve for economic complexity and ecological footprint. J. Cleaner Prod., 365. https://doi.org/10.1016/j.jclepro.2022.132642

Ozkan, O., Necati, M., Iormom, C., Iortile, B. and Usman, O. 2023. Reconsidering the environmental Kuznets curve, pollution haven, and pollution halo hypotheses with carbon efficiency in China: A dynamic ARDL simulations approach. Environ. Sci. Pollut. Res., 30: 68163-68176. https://doi.org/10.1007/s11356-023-26671-5

Palamalai, S., Ravindra, I. S. and Prakasam, K. 2015. Relationship between energy consumption, $CO_2$ emissions, economic growth and trade in India. J. Econ. & Finan. Stud., 3(2): 93. https://doi.org/10.18533/jefs.v3i02.93

Pant, K. P. 2009. Effects of agriculture on climate change: a cross country study of factors affecting carbon emissions. J. Agric. & Environ., 10: 72-88.

Pata, U. K. 2017. The effect of urbanization and industrialization on carbon emissions in Turkey: evidence from ARDL bounds testing procedure. Environ. Sci. Pollut. Res., 10: 88-94. https://doi.org/10.1007/s11356-017-1088-6

Pena, E. M. S., Reyes, J. S. G. and Gonzalez, A. N. 2022. Assessment on the Applicability of Environmental Kuznets Curve Hypothesis on the Macroeconomic Factors Driving Carbon Dioxide Emissions in the Philippines. J. Econ. Finance Acc. Stud., 4(1): 76-92. https://doi.org/10.32996/jefas

Pesaran, M. H. and Shin, Y. 1995. Autoregressive distributed lag modelling approach to cointegration analysis. DAE Working Paper Series No. 9514, Department of Economics, University of Cambridge, Cambridge.

Pesaran, M. H. and Shin, Y. 1997. Autoregressive distributed modeling approach to cointegration analysis. Cambridge University Press, Cambridge.

Pesaran, M. H. and Shin, Y. 1998. An autoregressive distributed-lag modelling approach to cointegration analysis. In S. Strom (Ed.), Econometrics and Economic Theory in the 20th Century: The Ragnar Frisch Centennial Symposium, Cambridge University Press, Cambridge, pp. 371-413.

Pesaran, M. H. and Shin, Y. 1999. An autoregressive distributed lag modelling approach to cointegration analysis. Cambridge University Press, Cambridge.

Pesaran, M. H. and Timmermann, A. 2005. Small sample properties of forecasts from autoregressive models under structural breaks. 129, 183-217. https://doi.org/10.1016/j.jeconom.2004.09.007

Pesaran, M. H., Shin, Y. and Smith, R. J. 1999. Bounds Testing Approaches to the Analysis of Long-Run Relationships. Cambridge University Press, Cambridge.

Pesaran, M. H., Shin, Y. and Smith, R. J. 2001. Bounds testing approaches to the analysis of level relationships. J. Appl. Economet., 16(3): 289-326. https://doi.org/10.1002/jae.616

Phillips, P. and Hansen, B. 1990. Statistical Inference in Instrumental Variables Regression with I(1) Processes. Rev. Econ. Stud., 57: 99-125. http://dx.doi.org/10.2307/2297545

Phillips, P. C. B. and Perron, P. 1988. Testing for a unit root in time series regression. Biometrika, 75: 335-46. http://dx.doi.org/10.1017/S0266466698142032

Piya, L., Maharjan, K. L. and Joshi, N. P. 2019. Climate change in Nepal: Policy and programs. In Socio-economic Issues of Climate Change. Springer, Singapore. https://doi.org/10.1007/978-981-13-5784-8

Rahman, M. M., Anan, N., Mashud, A. H. M., Hasan, M. and Tseng, M. L. 2022. Consumption-based $CO_2$ emissions accounting and scenario simulation in Asia and the Pacific region. Environ. Sci. Pollut. Res., 29(23): 34607-34623. https://doi.org/10.1007/s11356-021-18265-w

Raihan, A. and Tuspekova, A. 2022. Nexus between economic growth, energy use, agricultural productivity, and carbon dioxide emissions: new evidence from Nepal. Energy Nexus, 7(April), 100113. https://doi.org/10.1016/j.nexus.2022.100113

Raihan, A., Ibrahim, S. and Ahmed, D. 2023. World Development Sustainability Dynamic impacts of economic growth, energy use, tourism, and agricultural productivity on carbon dioxide emissions in Egypt. World Development Sustainability, 2: 100059-100074. https://doi.org/10.1016/j.wds.2023.100059

Ramsey, J. B. 1969. Tests for specification errors in classical linear least-squares regression analysis. J. Royal Stat. Soc., 31(2): 350-371. https://sci-hub.hkvisa.net/10.2307/2984219

Razzaq, A., Fatima, T. and Murshed, M. 2023. Asymmetric effects of tourism development and green innovation on economic growth and carbon emissions in top 10 GDP countries. J. Environ. Plann. Manage., 66(3): 471-500. https://doi.org/10.1080/09640568.2021.1990029

Saboori, B., Sapri, M. and Baba, M. 2014. Economic growth, energy consumption and $CO_2$ emissions in OECD (Organization for Economic Co-operation and Development) countries' transport sector: A fully

modified bi-directional relationship approach. Energy, 30: 1-12. https://doi.org/10.1016/j.energy.2013.12.048

Selden, T. M. and Song, D. S. 1994. Environmental quality and development: Is there a Kuznets curve for air pollution emissions? J. Environ. Econ. Manage., 27: 147-162. http://dx.doi.org/10.1006/jeem.1994.1031

Shahbaz, M., Solarin, S. A., Mahmood, H. and Arouri, M. 2013. Does financial development reduce $CO_2$ emissions in Malaysian economy? A time series analysis. Econ. Model., 35: 145-152.

Sharma, K., Bhattarai, B. and Ahmed, S. 2019. Aid, growth, remittances and carbon emissions in Nepal. Energy J., 40: 129-141. https://doi.org/10.5547/01956574.40.1.ksha

Shrestha, M. B. and Bhatta, G. R. 2018. Selecting appropriate methodological framework for time series data analysis. J. Finance Data Sci., 4(2): 71-89. https://doi.org/10.1016/j.jfds.2017.11.001

Sinha Babu, S. and Datta, S. K. 2013. The relevance of environmental Kuznets curve (EKC) in a framework of broad-based environmental degradation and modified measure of growth- a pooled data analysis. J. Sustainable Dev. World Ecol., 20(4): 309-316. https://doi.org/10.1080/13504509.2013.795505

Suri, V. and Chapman, D. 1998. Economic growth, trade, and energy: implications for the environmental Kuznets curve. Ecol. Econ., 25: 195-208. http://dx.doi.org/10.1016/S0921-8009(97)00180-8

Tenaw, D. and Beyene, A. D. 2021. Environmental sustainability and economic development in sub-Saharan Africa: A modified EKC hypothesis. Renew. Sustainable Energy Rev., 143 (February): 1-10. https://doi.org/10.1016/j.rser.2021.110897

Thuy, D. P. and Nguyen, H. T. 2022. Effects of trade openness on environmental quality: Evidence from developing countries. Res. Square, 14: 1-27. https://doi.org/10.21203/rs.3.rs-1479740/v1

Tiwari, A. K. 2012. On the dynamics of energy consumption, $CO_2$ emissions, and economic growth: Evidence from India. Indian Econ. Rev., 47(1): 57-87. https://www.jstor.org/stable/41969718

Udeagha, M.C. and Ngepah, N. 2022. Does trade openness mitigate the environmental degradation in South Africa?. Environmental Science and Pollution Research, 29(13): 19352-19377.

Voumik, L. C., Rahman, M. H. and M. S. H. 2022. Investigating the subsistence of Environmental Kuznets Curve in the midst of economic development, population, and energy consumption in Bangladesh: Imminent of ARDL model. Heliyon, 8: e10357. https://doi.org/10.1016/j.heliyon.2022.e10357

Wang, W., Liu, L., Liao, H. and Wei, Y. 2021. Impacts of urbanization on carbon emissions: An empirical analysis from OECD countries. Energy Policy, 151: 112171. https://doi.org/10.1016/j.enpol.2021.112171

Wang, W., Wang, S., Ma, X. and Gong, J. 2011. Recent advances in catalytic hydrogenation of carbon dioxide. Chem. Soc. Rev., 40(7): 3703-3727. https://doi.org/10.1039/C1CS15008A

Wang, Y., Han, R. and Kubota, J. 2016. Is there an Environmental Kuznets Curve for $SO_2$ emissions? A semi-parametric panel data analysis for China. Renew. Sustain. Energy Rev., 54: 1182-1188. https://doi.org/10.1016/j.rser.2015.10.143

World Resources Institute (WRI). 2017. CAIT-historical emissions date (Countries, U.S. States, UNFCCC). World Resources Institute, Washington, DC.

Wu, Y., Shen, J., Zhang, X., Skitmore, M. and Lu, W. 2016. The impact of urbanization on carbon emissions in developing countries: a Chinese study based on the U-Kaya method. J. Clean. Prod., 135: 589-603. https://doi.org/10.1016/j.jclepro.2016.06.121

Zhang, X. P. and Cheng, X. M. 2009. Energy consumption, carbon emissions, and economic growth in China. Ecol. Econ., 68(18): 2706-2712.

## ORCID DETAILS OF THE AUTHORS

R. Adhikari: https://orcid.org/0000-0002-1365-4543
B. Niroula: https://orcid.org/0000-0001-8320-5156
S. K. Singh: https://orcid.org/0000-0001-6412-2101

Nature Environment and Pollution Technology
An International Quarterly Scientific Journal

p-ISSN: 0972-6268
(Print copies up to 2016)
e-ISSN: 2395-3454

Vol. 23 | No. 3 | pp. 1239-1259 | 2024

Original Review Paper

https://doi.org/10.46488/NEPT.2024.v23i03.002

Open Access Journal

# Advanced Waste-to-Energy Technologies: A Review on Pathway to Sustainable Energy Recovery in a Circular Economy

**C. G. Achi†, J. Snyman, J. M. Ndambuki and W. K. Kupolati**

Department of Civil Engineering, Faculty of the Built Environment, Tshwane University of Technology, Pretoria West, South Africa

†Corresponding author: C. G. Achi; achicg@tut.ac.za; achicgjr@gmail.com

**Nat. Env. & Poll. Tech.**
**Website: www.neptjournal.com**

*Received:* 18-10-2023
*Revised:* 08-12-2023
*Accepted:* 17-12-2023

**Key Words:**
Environmental sustainability
Advanced thermal technology
Biochemical conversion
Energy efficiency

## ABSTRACT

In the face of the rapid rise in global waste production and the pressing need to shift towards sustainable energy options, advanced Waste-to-Energy (WtE) technologies have emerged as a highly promising solution. These innovative technologies effectively utilize waste as a valuable resource, presenting a viable pathway for sustainable energy recovery and making a substantial contribution to the principles of the circular economy paradigm. This review provides a comprehensive overview of advanced WtE technologies, including thermal, biological, and chemical methods, such as gasification, pyrolysis, plasma arc gasification, anaerobic digestion, fermentation, transesterification, and hydrothermal carbonization. The efficiency of these technologies is evaluated based on their energy recovery potential, environmental impact, and economic feasibility. Case studies on successful implementations of advanced WtE technologies are analyzed to highlight their practicality and effectiveness. Finally, the paper addresses technical, regulatory, and policy challenges in this field and provides future perspectives. The objective is to underscore the role of advanced WtE technologies in achieving a sustainable and resource-efficient circular economy.

## INTRODUCTION

The consistent and rapid increase in global waste generation and the pressing need to shift towards sustainable energy sources present significant challenges for society. According to the World Bank, global waste generation could increase by 70% from 2016 levels to 3.40 billion tonnes per year by 2050, driven by rapid urbanization and growing populations (Kaza et al. 2018). Simultaneously, the growing impacts of climate change and the depletion of finite fossil fuel reserves demand a transition towards renewable and sustainable energy sources. In this context, waste-to-energy (WtE) technologies, particularly advanced systems, have emerged as a promising solution based on the need to adopt policies that will enhance the affordability, reliability, and sustainability of energy (IEA 2022). These WtE technologies have the potential to transform vast amounts of waste into valuable energy resources, such as heat and electricity, thereby providing a pathway toward sustainable energy recovery. By converting waste into energy, these technologies not only help manage waste but also contribute to the diversification of energy sources and the reduction of greenhouse gas emissions.

Additionally, WtE technologies align with the principles of a circular economy, an economic system aimed at eliminating waste through the continual use of resources (Boloy et al. 2021). In a circular economy, waste is viewed not as a problem but as a resource that can be harnessed for value creation (Hari Bhakta et al. 2021). Advanced WtE technologies exemplify this strategy by converting waste into energy, thereby contributing to a more sustainable and resource-efficient economy. This convergence of waste management, energy recovery, and circular economy principles presents a compelling rationale for a deeper examination of advanced WtE technologies. Understanding their potential, efficiency, and the challenges they face is crucial for their successful implementation and for realizing a sustainable circular economy.

### Research Questions, Objectives, and Scope of the Review

These research questions guided this study

(a) How does the principle of circular economy intersect with waste management and energy recovery?

(b) What criteria should be adopted in evaluating advanced waste-to-energy technologies in conformity with the principles of sustainability within the circular economy model?

(c) What are the technical, regulatory, and policy challenges faced by these advanced WtE technologies?

Following these research questions, the primary objective of this review is to provide a comprehensive understanding of advanced Waste-to-Energy (WtE) technologies and their role within the context of a circular economy. We aim to analyze the potential and viability of these technologies as solutions for sustainable energy recovery and waste management and evaluate their alignment with circular economy principles. In accordance with the preceding discussion, the specific objectives of the review were to (i) Explore the principles of a circular economy and how it intersects with waste management and energy recovery (ii) Provide an in-depth understanding of various thermal, biological, and chemical WtE technologies such as gasification, pyrolysis, plasma arc gasification, anaerobic digestion, fermentation, transesterification, and hydrothermal carbonization (iii) Summarize the important criteria for evaluating the efficiency of Advanced WtE technologies based on the principles compatible with the circular economy model and (iv) Present Case Studies, highlighting practical examples of successful implementations of advanced WtE technologies around the world, providing insights into their practicality and effectiveness.

The scope of the review is global, considering advanced WtE technologies and their implementations across various countries and regions. However, the specific context of each case may vary, given the influence of local factors, such as waste composition, regulatory frameworks, and socio-economic conditions.

## MATERIALS AND METHODS

### Methodology and Structure of the Paper

Based on a comprehensive literature review, this review paper draws on both theoretical and empirical sources to critically explore the subject of advanced Waste-to-Energy (WtE) technologies and their role in a circular economy. The literature review involved critical searches of several academic databases, including Google Scholar, Scopus, Web of Science, JSTOR, and Science Direct, using a combination of keywords such as "waste-to-energy," "advanced waste-to-energy technologies," "circular economy," and "sustainable energy recovery."

The paper is organized into seven main sections: Section 1 provides the background, rationale, objectives, and scope of the review, including the methodology and structure of the paper. Section 2 introduces the concept of a circular economy, discussing its principles, benefits, and how it intersects with waste management and energy recovery. Section 3 Gives an in-depth description of various thermal, biological, and chemical WtE technologies, while Section 4 Evaluates the Efficiency of Advanced WtE Technologies. Section 5 Presents Case Studies of Successful Implementations. Section 6 Discusses the technical, regulatory, and policy challenges faced by advanced WtE technologies, as well as future trends and research directions in this field. And finally Section 7: Summarizes the key findings of the review, discussing their implications for research and practice in the field of advanced WtE technologies and circular economy.

### The Concept of a Circular Economy

The concept of Circular Economy (CE) is currently being promoted by the European Union (EU), as well as by several national governments, including Japan, France, China, the United Kingdom, Canada, the Netherlands, Sweden, and Finland. Additionally, several businesses around the world are also promoting the concept of a Circular Economy (EMAF, 2012, EMAF 2013, Jouni et al. 2018). The CE is a model of production and consumption that involves sharing, leasing, reusing, repairing, refurbishing, and recycling existing materials and products as long as possible. In this way, the life cycle of products is extended, waste generation is minimized, and the value of products and materials is maintained. This is a significant shift away from the traditional linear economy, which follows a 'take-make-dispose' model of production (EMAF 2013, WEF 2014, Gustavo et al. 2017).

### Principles of a Circular Economy

The circular economy operates on the foundation of three fundamental principles: the elimination of waste and pollution through design, the continuous utilization of products and materials, and the restoration of natural systems (EMAF 2013, Velenturf & Purnell 2021). Fig. 1 summarises these key principles.

**Design out waste and pollution**: Design plays a pivotal role in shaping production methods, consumption patterns, and disposal systems, with early decisions in product, service, and system development having a significant impact on both environmental and social outcomes (EEA 2016, Reichel et al. 2016). In a circular economy, products are designed and optimized for a cycle of disassembly and reuse, which significantly reduces waste and pollution. This principle involves rethinking product design to eliminate waste, considering the entire lifecycle of a product, and using materials that can be reused or safely returned to the environment. In recent years, various studies have focused on designs that focus on eliminating waste. To sustain principles of CE where there is high potential for


Fig 1: Principles of circular economy.

circularity, the European Union action plan focuses on those sectors that use the most resources, such as electronics and ICT, batteries and vehicles, packaging, plastics, textile construction and buildings, food, water, and nutrients. Tayebi-Khorami et al. (2019) identified various integrative approaches for rethinking mining wastes framed around the circular economy, which includes social dimensions, geo-environmental aspects, geo-metallurgy specifications, economic drivers, and legal implications. For instance, in textile production, (Zhang et al. 2018) focused on improving the design for the textile production process based on life cycle assessment. Similarly (Othman & Elsawaf 2021) applied the principle of "design out waste" in Public House Projects as a strategy to achieve sustainability. Bofylatos (2022) exemplified the principle of designing out waste" by the use of simple materials such as plywood, Plexiglas, and other local materials in an iterative research-through-design process that combines experiential and tacit knowledge from local case studies. The principle of designing out waste and pollution is at the heart of a circular economy. This principle entails rethinking and redesigning products and processes to prevent waste and pollution from being created in the first place.

The key strategies for implementing the principle of 'Design out Waste and Pollution" are Eco-Design, Business Models, Industrial Symbiosis, and Regulations and Standards.

**Eco-Design**: This involves designing products to reduce their environmental impact throughout their lifecycle, from raw material extraction to end-of-life disposal. This could include using less material, choosing renewable or recyclable materials, designing for easy disassembly, and minimizing energy use during production and use. Eco-design, as defined in ISO 14062 (ISO/TR 14062, 2002), is "*a design approach aiming to reduce the environmental impacts of products and services throughout the whole life cycle while assuring similar or improved services to the end customer*." More recently, the concept of eco-design has been applied to the manufacture of nanomaterials (Ilaria et al. 2023) and in the design of polymer matrix composite. (Lazar et al. 2023) with composite materials with a polymer matrix increasingly being used in various components of modern automobiles, including the body, seats, upholstery, electrical and electronic components, and many others (Lazar et al. 2023). In general, eco-design as a key strategy for "designing out waste" contributes to environmental and human health protection, as well as efficient resource utilization.

**Business models**: Businesses can adopt models that reduce waste and pollution. For example, product-as-a-service models allow companies to retain ownership of a product while customers pay for the service it provides. This incentivizes companies to design durable, reusable, and recyclable products, as they retain the responsibility for the product at the end of its service life (Miying et al. 2018, Salwin et al. 2022).

**Industrial symbiosis**: This involves sharing resources among different industries to minimize waste. For example, the waste product from one process can be used as a raw material in another process. This not only reduces waste but also reduces the need for virgin raw materials. Industrial symbiosis has proved to be a strong ally for the achievement of environmental, economic, and social objectives (Angela et al. 2020).

**Regulations and standards**: Governments have the power to establish regulations and standards mandating waste and pollution reduction in corporate practices. One such example is the implementation of extended producer responsibility (EPR) regulations, which compel producers to manage the disposal of their products at the end of their lifecycle (Ramasubramanian et al. 2023, Jenkins et al. 2023, Leclerc & Badami 2023). By proactively addressing waste and pollution in design, the circular economy not only mitigates the

environmental consequences of production and consumption but also fosters economic prospects. Companies can reduce expenses by conserving materials and energy, while novel business prospects can emerge in sectors like recycling and product refurbishment.

**Keep Products and Materials in Use**

This principle centers on establishing a closed-loop system for all products, ensuring that resources are not discarded but are instead recycled repeatedly. It encompasses a range of strategies, including repair, remanufacturing, refurbishing, product sharing, leasing, and recycling, all aimed at maintaining these items within the economic cycle. The second core principle of the circular economy emphasizes the prolongation of product and material lifecycles to their fullest extent. The goal is to optimize the value of products and materials, decrease the need for fresh raw materials, and minimize waste generation. Here are some examples of how this principle has been put into practice:

**Repair and maintenance**: Regular repair and maintenance can extend the lifespan of products, delaying the point at which they become waste. This can involve traditional repair services, as well as innovative models like repair cafés, where community members can learn to fix their own items. The principles of repair and maintenance have been applied in many sectors, such as automobile, electrical, and more recently in healthcare equipment. Samenjo et al. (2023) extensively discussed various strategies and the extent to which the circular economy principle of repair and maintenance has been applied in the design of medical equipment for low-resource settings in Sub-Saharan Africa.

**Reuse and redistribution**: Products that are no longer needed by one person can often be used by others. This can be facilitated through second-hand markets, swapping platforms, and charitable donations.

**Remanufacturing and refurbishing**: Products can often be brought back to like-new condition through remanufacturing or refurbishing. This involves disassembling the product, repairing or replacing worn-out components, and then reassembling it. This can significantly extend the product's lifespan and reduce the need for new products to be manufactured (Ijomah 2010, Soloman et al. 2020, Coker et al. 2021, Oturu et al. 2021).

**Recycling**: When a product can no longer be repaired, reused, or remanufactured, the materials it is made from can often be recycled. This involves breaking down the product into its constituent materials, which can then be used to manufacture new products.

**Product-as-a-service models**: In these models, customers pay to use a product without owning it outright. This encourages manufacturers to design durable products and offer services to maintain and upgrade them, as they retain ownership of the product throughout its lifecycle.

By keeping products and materials in use, a circular economy can significantly reduce environmental impacts, create new business opportunities, and generate cost savings for consumers and businesses…

**Regenerate Natural Systems**

The circular economy promotes the use of renewable energy and materials and encourages systems that regenerate and restore. This means moving away from practices that harm the environment and depleting resources towards systems that improve the quality of the environment and increase resource security. (EMAF 2018, Geissdoerfer et al. 2017) These principles differentiate a circular economy from the traditional linear 'take-make-dispose' model. Instead of viewing the production process as a one-way street, the circular economy sees it as a loop that reuses and recycles materials minimizes waste, and creates sustainable patterns of consumption and production. The principle of regenerating natural systems is the third principle of a circular economy, focusing on enhancing and supporting the natural world. The idea is to go beyond just reducing harm and strive to create systems that have a positive impact on the environment. This principle is implemented through a variety of methods:

**Use of renewable resources**: Prioritizing the use of renewable resources, such as wind, solar, and geothermal energy, helps reduce dependence on finite, non-renewable resources and minimizes environmental degradation.

**Restorative practices**: Implementing practices that restore natural environments, such as reforestation and regenerative agriculture, can help rebuild ecosystems, increase biodiversity, and sequester carbon.

**Biomimicry**: This approach involves learning from and emulating nature's time-tested patterns and strategies to create sustainable solutions. For example, designing products or systems that mimic natural processes can help reduce waste and energy use. The nuances and relationship between biomimicry and sustainability were discussed extensively by (Ilieva et al. 2022), with biomimicry playing a critical role as a sustainable design methodology with a great potential to cultivate more sustainable human-nature relations (Taylor Buck et al. 2017, Lebdioui 2022).

**Biodegradability**: Using materials that can safely decompose back into the environment at the end of their life can help reduce waste and pollution and contribute to the nutrient cycle.

**Carbon sequestration**: Implementing methods to capture

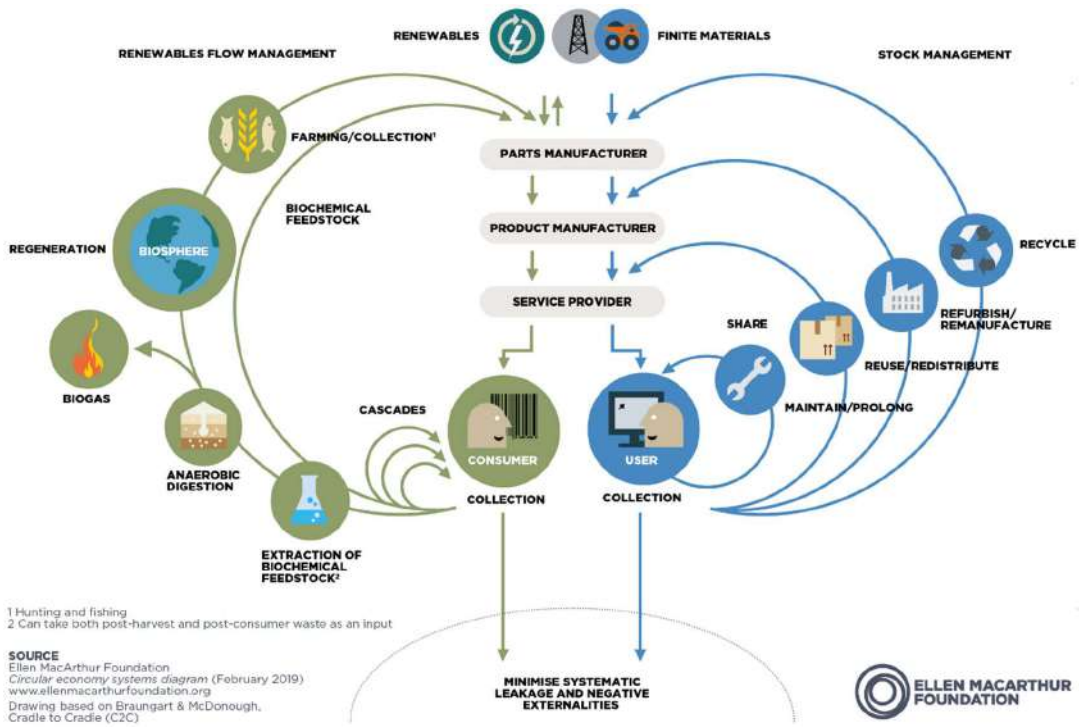


Fig. 2: Material flow in a circular economy source Ellen MacArthur Foundation (EMAF 2019).

and store carbon dioxide can help reduce greenhouse gas emissions and mitigate climate change. This can involve natural processes, such as reforestation, or technological solutions, such as carbon capture and storage.

Through the revitalization of natural systems, a circular economy supports the long-term well-being of our planet, safeguarding its capacity to provide the resources essential for human survival. This perspective acknowledges that the economy is intricately interconnected with the environment. It underscores the imperative for human society to collaborate harmoniously with nature, striving for a sustainable future instead of working at odds with it.

## Circular Economy and Waste Management

Within the framework of a circular economy, waste is not regarded as a problem but as a valuable resource that can be harnessed. The overarching concept is to 'close the loop' within product lifecycles, achieved through enhanced recycling and re-manufacturing processes that curtail waste production. This approach is universally applicable, spanning diverse waste streams such as solid municipal waste, industrial by-products, agricultural residues, and more. Given the escalating volumes of waste generated by our expanding population and consumption patterns, waste management has emerged as a formidable global challenge. A circular economy presents a holistic strategy for addressing this issue, converting waste from a terminal outcome within a linear system into a precious resource within a circular system. The significance of a circular economy in waste management can be elucidated in multiple ways. Find below in Fig. 2 the diagrammatic representation of material flow within a circular economy according to the Ellen and MacArthur Foundation (EMAF).

## Waste Reduction

By extending the utilization of materials and incorporating waste reduction measures from the inception, a circular economy can substantially curtail the volume of waste produced. This not only eases the burden on waste management systems but also mitigates the environmental repercussions tied to waste disposal, including the emission of greenhouse gases from landfill sites. Waste reduction, alternately referred to as waste prevention or waste minimization, entails the systematic reduction of waste generation by individuals, enterprises, or communities. It stands as a pivotal element within the waste management hierarchy and constitutes a fundamental tenet of a circular economy. The pursuit of waste reduction can be realized through a diverse array of strategies, such as (EMAF 2019)

- **Source Reduction**: This entails the reduction of waste

at its origin by designing products that require fewer materials in manufacturing, have extended lifespans, and are easy and straightforward to repair, remanufacture, or recycle (Guo et al. 2021, Hajam et al. 2023).

- **Reuse**: Rather than disposing of items after use, there is an opportunity for their reuse. This might involve basic practices like opting for refillable water bottles and reusable shopping bags, or it might entail businesses engineering products with reusability in mind, such as refillable packaging.
- **Recycling and composting**: Recycling involves converting waste materials into new products, reducing the demand for virgin materials. Composting is a form of recycling where organic waste is broken down into a nutrient-rich soil conditioner.

Waste reduction has numerous environmental, economic, and social benefits. Environmental benefits include conserving materials and resources, reducing the demand for raw materials, decreasing pollution and greenhouse gas emissions associated with waste disposal, and the production of new goods. Economic benefits include preventing the costs associated with waste disposal and the purchase of new goods. Social benefits include reducing pollution and health impacts associated with raw material extraction (EMAF 2019). An established policy promoting the transition to a circular economy is the European Union's five-step waste hierarchy, introduced in the 2008 EU Waste Framework Directive, with a primary focus on waste generation prevention. EU Member States were mandated to implement waste prevention programs by December 2013, with numerous countries incorporating measures to encourage innovative business models, repair, reuse, and eco-design in their programs. (EEA 2016). In many African countries, with high levels of unemployment, poverty and inequality, with high demand for energy and resources, the principle of circular economy has been applied in many informal sectors. End-of-life products and equipment are often repaired, recycled, and reused. In South Africa, with high energy demands (DOE 2019a) and water scarcity challenges, grey water has been recycled and reused for decades, with returns of about 13% of South Africa's available water supply (Godfrey 2021).

Similarly, in the energy sector, with the increasing energy crisis, various forms of renewable energies have been adopted. Government policies and initiatives play a crucial role in promoting and institutionalizing the vision of a circular economy (Wills et al. 2016).

## Value Creation

Value creation is a fundamental concept in economics and business, referring to the process through which goods, services, or some form of value is produced for consumers. Within the context of a circular economy, value creation takes on a broader and more sustainable perspective, going beyond economic profits to include environmental and social benefits. In a circular economy, value creation can occur at various stages:

- **Design phase**: Value can be created by designing products to be durable, repairable, reusable, and recyclable, extending their lifespan and reducing waste.
- **Production phase**: Value is created by using efficient processes that minimize waste and energy use, and by using renewable or recycled materials.
- **Use phase**: Value is created by providing services that enable consumers to use products longer, share them, or use them more efficiently.
- **End-of-life phase**: Value is created by recovering materials from products at the end of their life so they can be used to make new products, reducing the need for virgin resources.

Value creation in a circular economy has numerous benefits:

- **Economic**: It can generate new revenue streams, reduce costs, and create competitive advantages for businesses. It can also contribute to economic growth and job creation.
- **Environmental**: It can reduce resource use, waste, and emissions, contributing to environmental sustainability.
- **Social**: It can contribute to social wellbeing by creating more sustainable products and services, promoting fair labor practices, and reducing the social impacts of waste and pollution.

In a circular economy, the goal is to maximize value and minimize waste, not just in terms of economic profits but also in terms of environmental sustainability and social well-being. It's about creating a system that is good for people, the planet, and the economy. However, the potential for cost reduction plays a key role in the level of acceptability and implementation of the circular economy. Following the report on an investigation into South Africa's industrial perspective regarding circular economy models, motivating factors, and sustainability considerations, with a specific emphasis on composite waste, the study revealed that cost reduction stood out as the predominant catalyst and facilitator for composite recycling (Mativenga et al. 2017), Consequently, prioritizing avenues for cost reduction emerges as a pivotal element in motivating South African enterprises to adopt circular economy principles, underscoring its significance in shaping suitable national frameworks for guiding the transition toward a circular economy.

## Sustainability

A circular economy supports sustainability by reducing the extraction and consumption of finite natural resources, minimizing waste and pollution, and creating systems that can continue to function effectively over the long term. Sustainability is a broad concept that involves meeting our present needs without compromising the ability of future generations to meet their own needs. It encompasses three interconnected 'pillars' or 'dimensions': economic, environmental, and social sustainability - often referred to as 'profits, planet, and people.' Find below a summary of each of these aspects:

**Economic sustainability**: This involves creating long-term economic value and ensuring that economic growth and development are balanced and sustainable. It includes aspects like profitability, economic resilience, fair trade, and responsible consumption and production.

**Environmental sustainability**: This involves protecting and preserving the natural environment for future generations. It includes aspects like reducing pollution and waste, conserving natural resources, tackling climate change, and promoting biodiversity.

**Social sustainability**: This involves ensuring social wellbeing, equity, and justice for all people. It includes aspects like human rights, labor standards, community development, health and wellbeing, and social inclusion.

Sustainability is a key principle in a circular economy, which aims to decouple economic growth from environmental degradation by designing out waste, keeping products and materials in use, and regenerating natural systems. In a circular economy, sustainability is not just about reducing the harm we do to the planet but actively contributing to its restoration and regeneration. Sustainability requires systemic thinking and collaborative action across different sectors and disciplines. It's about finding a balance between economic growth, environmental health, and social well-being and creating a world that is resilient, equitable, and sustainable for all (Sachs 2012, SDG 2022, Agbedahin 2019, UNESCO 2014a, Mckeown 2002b).

## Climate Change Mitigation

Mitigating climate change and implementing a circular economy are closely linked in many ways. For instance, heat and electricity generation from renewable energy sources is an important means of reducing Greenhouse Gas emissions (GHGs) (Hans 2021). By reducing the demand for new resources and minimizing waste, a circular economy can help to mitigate climate change. Climate change mitigation refers to efforts to reduce or prevent the emission of greenhouse gases. This is because the extraction, processing, and disposal of materials contribute significantly to greenhouse gas emissions. By implementing a circular economy approach in waste management, society can transition towards a more sustainable, efficient, and resilient system that not only addresses the waste crisis but also contributes to broader economic, social, and environmental goals. The ultimate goal is to limit the future warming of the planet and avoid the worst impacts of climate change. Mitigation strategies can range from making energy consumption more efficient, to increasing the share of clean energy to removing carbon dioxide from the atmosphere. Previous studies have suggested the following key strategies:

**Energy efficiency**: Improving energy efficiency entails getting more output from each unit of energy. This is achieved through a variety of measures, such as improving insulation in buildings (Lachheb et al. 2019, Allouhi et al. 2015), increasing fuel economy in vehicles (Aguilar et al. 2021), and designing more efficient appliances and industrial processes. Lachheb demonstrated the efficiency of Spent Coffee Grounds (SCGs), with results indicating that up to 20% of the cooling and heating loads of a building can be reduced if SCG material substitutes the conventional one.

**Renewable energy**: Shifting from fossil fuels to renewable sources of energy, such as wind, solar, hydropower, and geothermal, can significantly reduce greenhouse gas (GHG) emissions. This also includes the use of bioenergy, as long as it's sourced sustainably.

**Carbon capture and storage (CCS)**: Carbon Capture and Storage involves capturing carbon dioxide emissions from power plants and industrial processes and storing them underground to prevent them from being released into the atmosphere.

**Land use and forestry**: Protecting and restoring forests, which absorb carbon dioxide, can help offset emissions. Other strategies include improving agricultural practices and managing land use to increase carbon sequestration and reduce deforestation and land degradation.

**Behavioral changes**: This involves changes in individual and societal behaviors, such as reducing energy use, choosing more sustainable transportation options, and adopting plant-based diets.

Climate change mitigation is a key aspect of sustainability and a circular economy. By designing out waste, keeping products and materials in use, and regenerating natural systems, a circular economy can help reduce greenhouse gas emissions and contribute to climate change mitigation. It's also crucial to transition to a low-carbon economy, where energy is sourced from renewable sources, and resources are used more efficiently and sustainably.

## CIRCULAR ECONOMY AND ENERGY RECOVERY

Energy recovery from waste is a key component of a circular economy. Advanced WtE technologies convert various types of waste into heat, electricity, and fuel, thereby providing a pathway toward sustainable energy recovery. (IEA 2020, Tun et al. 2020) By transforming waste into energy, these technologies not only contribute to the diversification of energy sources and the reduction of greenhouse gas emissions but also help to close the loop of material cycles in a circular economy.

### The Role of Waste-to-Energy in a Circular Economy

Waste-to-energy (WtE) technologies play a particular role in a circular economy. These technologies convert solid waste materials that would otherwise be destined for landfill into heat, electricity, or fuel. By doing so, waste-to-energy can reduce the volume of waste, generate energy, and save on traditional waste disposal costs. However, it's important to remember that in a truly circular economy, the goal is to keep materials in use as long as possible and reduce waste to a minimum. Therefore, waste-to-energy should be seen as a last resort for dealing with waste after options for reduction, reuse, repair, and recycling have been explored.

Waste-to-energy technologies can contribute to energy recovery and waste management in a circular economy, but they also have some drawbacks. For instance, they can produce greenhouse gases and other pollutants, and they often require a steady stream of waste for their operation, which can discourage waste reduction efforts. Therefore, while waste-to-energy has a role in a circular economy, it should not replace efforts to prevent waste and keep materials in circulation.

### Overview of Waste-to-Energy Technologies

Waste-to-Energy (WtE) technologies involve the process of generating energy in the form of electricity, heat, or fuel from waste materials. These technologies play a crucial role in waste management, energy creation, and resource recovery. Fig. 3 below shows the categories and types of some key waste-to-energy technologies:

### Traditional Waste-to-Energy Technologies

Traditional Waste-to-Energy (WtE) technologies involve the conversion of non-recyclable waste materials into usable heat, electricity, or fuel. These technologies can play a key role in waste management, reducing the volume of waste sent to landfills and generating energy. Here are some common traditional WtE technologies:

**Incineration**: Incineration is the most common form of WtE and involves the combustion of waste at high temperatures. The heat generated is used to produce steam, which in turn drives a turbine to generate electricity. Modern incineration plants are designed to reduce the emission of pollutants, but concerns about air quality and residual ash remain. Incineration is a waste-to-energy (WtE) method where solid waste is combusted at high temperatures to reduce its volume and convert it into energy. It's often used to manage municipal solid waste, industrial waste, and certain hazardous wastes. (Makarichi et al. 2018)

The incineration process involves burning waste materials at high temperatures, often above 850°C. The heat generated is used to produce steam, which drives a turbine connected to a generator, producing electricity. The residual ash, which is reduced to about 15 - 10% of the original waste

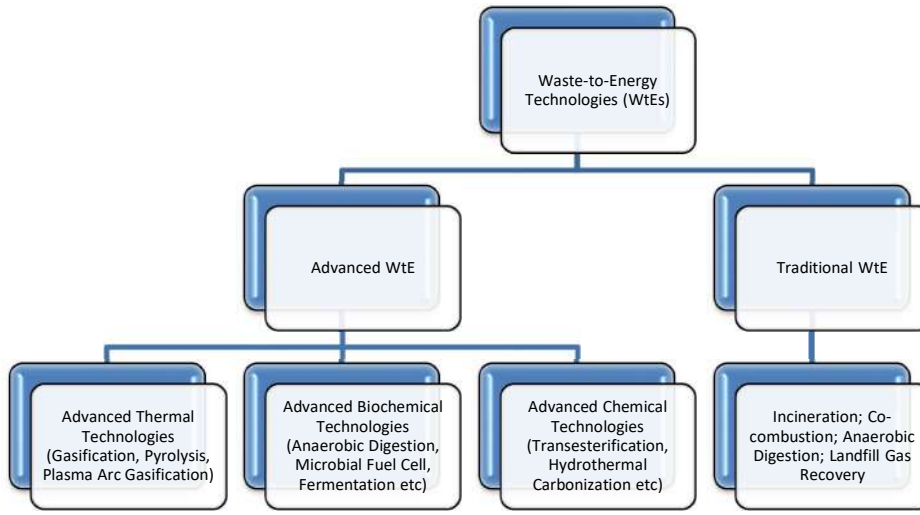


Fig. 3: Broad Categories of Waste-to-Energy Technologies.

volume, is often used in construction materials or disposed of in landfills.

**Energy production**: Incineration can generate significant amounts of energy. It's a reliable source of energy as it doesn't depend on weather conditions, unlike some renewable energy sources.

**Waste reduction**: Incineration reduces the volume of waste by about 90%, which can help save space in landfills and reduce the transportation and handling of waste (Đurđević et al. 2018, He et al. 2023).

However, there are some important considerations regarding incineration in a circular economy:

**Air pollution and greenhouse gases**: Incineration can produce pollutants like dioxins and furans, heavy metals, and particulates. Modern incinerators are equipped with pollution control equipment to reduce these emissions, but they are not eliminated. Incineration also releases carbon dioxide, a greenhouse gas, contributing to climate change.

**Waste hierarchy**: In a circular economy, the goal is to prevent waste and keep materials in use as long as possible. Therefore, incineration should only be used when waste cannot be prevented, reused, repaired, or recycled. It should not replace efforts to reduce waste and increase resource efficiency.

**Energy efficiency**: While incineration produces energy, it's less energy efficient compared to using those materials more directly. For example, recycling aluminum saves more than 90% of the energy needed to create new aluminum from raw materials, whereas incinerating aluminum waste to generate energy is far less efficient.

So, while incineration has a role in managing waste and producing energy in a circular economy, it should be used judiciously and not undermine efforts to prevent waste and recycle materials.

**Co-combustion or co-firing**: In co-combustion processes, waste materials are co-utilized with conventional fuels (such as coal) in industrial boilers or kilns, thereby contributing to a reduction in the consumption of fossil fuels and a decrease in emissions.

**Anaerobic digestion (AD)**: Conventional anaerobic digestion processes primarily target the treatment of organic waste, including sewage sludge or agricultural residues. Within these processes, microorganisms decompose the waste in an oxygen-free environment, resulting in the generation of biogas, which comprises methane and carbon dioxide. This biogas can be harnessed for electricity or heat production. Anaerobic digestion is a biological process that entails the decomposition of organic waste materials, such as food waste, manure, or sewage sludge, through the activity of microorganisms in the absence of oxygen (Angelidaki et al. 2003, Ahring 2003). This waste-to-energy technology is a crucial component of the circular economy, especially in the management of organic waste and the production of sustainable energy. In a conventional anaerobic digestion system, organic waste is deposited into an enclosed anaerobic digester, creating an oxygen-free environment. Within this digester, microorganisms break down the organic matter, resulting in the production of biogas, composed mainly of methane and carbon dioxide, along with a nutrient-rich residue known as digestate. The biogas can serve as a versatile fuel source, powering applications like combined heat and power (CHP) plants to generate both electricity and heat. Alternatively, it can undergo purification and upgrading to become biomethane, a renewable natural gas. Meanwhile, the digestate remaining after the process can be repurposed as a soil conditioner or fertilizer, replenishing soil nutrients and diminishing the reliance on synthetic fertilizers (Samoraj et al. 2022).

Anaerobic digestion offers several benefits in a circular economy, such as **Waste Management**: It provides a way to manage organic waste, reducing the amount that goes to landfills and the associated methane emissions. **Renewable Energy**: It produces a renewable source of energy, contributing to the transition away from fossil fuels. **Soil Health**: It produces a nutrient-rich residue that can improve soil health and fertility. **Greenhouse Gas Reduction**: Capturing methane (a potent greenhouse gas) from organic waste, helps to reduce greenhouse gas emissions. However, some drawbacks and challenges with anaerobic digestion have been reported, such as the need for sorting and pre-treatment of waste, managing the digestate, and ensuring the system is economically viable. It's also important to remember that in a circular economy, the priority should still be to prevent waste in the first place, and anaerobic digestion should not replace efforts to reduce food waste and other forms of organic waste. **Landfill Gas Recovery (LGR)**: As waste decomposes in landfills, it produces a gas composed largely of methane and carbon dioxide. This gas is captured and used to generate electricity or heat or processed into a transportation fuel. This process helps to reduce greenhouse gas emissions and generate energy. When organic waste decomposes in a landfill, it produces landfill gas, which is approximately 50% methane (a potent greenhouse gas), 50% carbon dioxide, and a small amount of non-methane organic compounds.

Landfill gas recovery systems involve the installation of a series of wells and pipes throughout the landfill, which collect the gas as it's produced. This gas is then either flared (burned off), used on-site for heating or power generation, or processed and sold as a commercial energy source. The recovery

and utilization of Landfill gases prevent methane, a potent greenhouse gas, from being released into the atmosphere, thereby helping to mitigate climate change. Additionally, using landfill gas as a source of energy reduces the demand for fossil fuels. Within the framework of circular economy, LGR has significant economic value as a cost-effective source of energy. By selling the gas or the electricity generated from it, landfill operators can generate additional revenue.

Additionally, the process of capturing LFG can create jobs and contribute to local economies. It can also reduce local air pollution by burning methane that would otherwise be released into the atmosphere. While landfill gas recovery is a valuable tool in waste management and energy production, it's important to remember that it's part of a broader waste management strategy. The priority should be on reducing waste, reusing materials, and recycling wherever possible to minimize the amount of waste going to landfills in the first place.

In general, traditional Waste-to-Energy (WtE) technologies, while valuable for waste management and energy generation, should be integrated into a comprehensive waste and resource management approach where the foremost emphasis lies on source waste reduction, product reuse, and material recycling, with WtE applications reserved for materials that cannot be feasibly reused or recycled and implemented with minimal environmental impact. Advanced WtE technologies emerged as a need to improve on the progress of the traditional WtE technologies.

## ADVANCED WASTE-TO-ENERGY TECHNOLOGIES

Advanced Waste-to-Energy (WtE) technologies have evolved to provide more efficient and environmental-friendly methods for converting waste into energy. These technologies address some of the environmental concerns associated with traditional WtE methods, particularly around emissions and residues. Here are some examples:

### Advanced Thermal Technologies (Gasification, pyrolysis, Plasma Arc Gasification)

These techniques involve heating waste in a low-oxygen or oxygen-free environment to produce a gas (syngas) that can be used to generate energy. These methods generally produce fewer emissions than traditional incineration and can handle a wide variety of waste types. Waste plastic, which poses a significant problem in terms of disposal, may be converted into energy through pyrolysis. Padmanabhan et al. (2022) investigated the possibility of recovering energy from waste plastics as a potential option to meet the circular economy as a fuel source. Plastic wastes were converted to diesel fuel through pyrolysis of High-Density Polyethylene (HDPE).

Gasification and pyrolysis are two related advanced thermal treatment technologies that convert waste into energy-rich fuels. They can be used to process a variety of waste materials, including municipal solid waste, industrial waste, biomass, and even certain hazardous wastes. Several studies have reported cases of energy recovery from other forms of waste, such as garden wastes through hydrothermal gasification (Ipiales et al. 2022), energy recovery for waste printed circuit boards using microwave pyrolysis (Huang et al. 2020), from pyrolysis of municipal solid waste (Husan et al. 2021) and waste tires (Abdallah et al. 2020).

The major difference between the process of gasification and pyrolysis lies in heating and process parameters.

**Gasification:** This is a process where waste is heated at high temperatures in a controlled, low-oxygen environment. This prevents combustion and instead produces a gas known as syngas (a combination of hydrogen, carbon monoxide, and sometimes carbon dioxide). Syngas is a versatile energy carrier that can be converted into electricity, heat, or transformed into other fuels (Padmanabhan et al. 2020).

**Pyrolysis:** is a process that entails heating waste in an oxygen-deprived environment, resulting in the decomposition of waste into three primary components: syngas, bio-oil, and a solid residue referred to as char. Syngas and bio-oil are versatile, finding applications in heat and electricity generation, as well as serving as chemical feedstocks. The potential use of char as a soil amendment depends on its specific properties and the presence of contaminants (Demirbas & Arin 2002, Soltes & Elder 2018).

Gasification and pyrolysis can process a variety of waste materials, including those that are difficult to recycle. They can generate energy and other valuable products, reducing the amount of waste that goes to landfills and the demand for virgin resources. However, gasification and pyrolysis also have some important considerations in a circular economy: Both processes require significant amounts of energy to heat the waste material (Jin et al. 2017). The net energy balance and resource efficiency depend on the type of waste, the specific technology used, and how the products are used. Gasification and pyrolysis can produce emissions and residues that need to be managed carefully. For example, syngas often need to be cleaned to remove impurities, and the char from pyrolysis may contain heavy metals or other contaminants Bernardo et al. 2010.

**Plasma arc gasification:** This advanced thermal treatment technology subjects waste to extremely high temperatures,

reaching levels as elevated as 10,000 to 25,000 degrees Celsius, using a plasma torch (Pourali 2009, Yayalik et al. 2020). The intense heat triggers the transformation of waste into syngas and generates a minimal amount of solid residue known as slag, which, if uncontaminated, can be repurposed in construction projects. Plasma arc gasification is often lauded for its capacity to manage a wide array of waste types and its potential to significantly reduce waste volume.

While these thermal technologies offer a means to address waste that cannot be recycled or composted, they should be integrated into a comprehensive waste management strategy that prioritizes waste reduction, reuse, and recycling. Additionally, it's crucial to acknowledge that the energy efficiency, environmental impacts, and economic viability of these technologies can vary. Hence, adapting and optimizing them to suit local conditions and specific waste streams is of paramount importance.

### Advanced Biochemical Technologies (Anaerobic Digestion, Microbial Fuel Cell, Fermentation)

Biochemical technologies involve the use of microorganisms to convert waste into usable products, including various forms of energy. Unlike conventional anaerobic digestion and fermentation, advanced AD systems continue to explore advanced techniques and processes to address the basic challenges in conventional AD systems:

**Advanced anaerobic digestion:** The Advanced Anaerobic digestion system employs an advanced biological process in which microorganisms break down organic materials in the absence of oxygen. These processes are harnessed and optimized to yield better results in terms of biogas production, comprising higher quality methane and less carbon dioxide, as well as a nutrient-rich digestate. The produced biogas can be harnessed for heat and electricity generation, while the digestate can serve as a beneficial soil conditioner or fertilizer. Enhanced Anaerobic digestion is a versatile method used for treating various organic waste streams, encompassing food waste, agricultural residues, and sewage sludge. Various advanced processes, including co-digestion and the use of additives and nanoparticles, have been applied to advanced AD to yield better results. (Hassanein 2019). Anaerobic Digestion (AD) technology holds a pivotal role in advancing the circular bioeconomy and contributes significantly to achieving carbon neutrality. It accomplishes this by converting organic materials into valuable bioenergy and biosolids. The production and reclamation of bioenergy from organic wastes through the stages of hydrolysis, acidogenesis, acetogenesis, and methanogenesis represent a cost-effective and sustainable approach for valorizing agricultural biomasses and food waste (Chibueze et al. 2021).

**Microbial fuel cells (MFCs):** These are bio-electrochemical devices that utilize the metabolic activity of microorganisms to generate electricity by oxidizing organic matter. These innovative devices have the potential to provide sustainable power generation while simultaneously treating wastewater or organic waste (Logan & Regan 2006, Franks & Nevin 2010, Slate et al. 2019).

**Fermentation:** Fermentation is a process where microorganisms, usually yeasts or bacteria, convert organic compounds - usually sugars and starches - into alcohols and gases. In a waste-to-energy context, it's often used to convert biomass or organic waste into bioethanol, a renewable fuel that can be used in transportation. The process also produces carbon dioxide and other by-products that can be captured and used.

The implementation of these technologies is currently being optimized for different waste streams and local conditions and should take into account the energy balance, environmental impacts, and economic feasibility.

### Advanced Chemical Technologies (Transesterification, Hydrothermal Carbonization)

Chemical technologies involve reactions aimed at transforming waste into energy or other valuable products. Within the waste-to-energy (WtE) sector, two prominent technologies include transesterification and hydrothermal carbonization (Kumar & Samadder 2017).

**Transesterification:** This is a chemical process that converts fats and oils into biodiesel. It involves reacting lipids (fats and oils) with an alcohol (usually methanol or ethanol) in the presence of a catalyst (usually a strong alkali) to form esters (biodiesel) and glycerol. The biodiesel produced can be used as a fuel in diesel engines (Meher et al. 2006, Gandhi et al. 2011). Transesterification is commonly used to convert waste cooking oil and animal fats into biodiesel, providing a way to recycle these waste streams and produce renewable fuel. Recently, studies have focused on converting various plant-based materials to biodiesel through transesterification processes. Plant-based non-edible feedstock such as castor bean and jatropha were successfully converted to biodiesel (Baionie Silva et al. 2023), and using the nanocatalyst transesterification process, microalgae were converted to biodiesel (Akubude et al. 2019).

**Hydrothermal carbonization (HTC):** HTC is a process that converts organic waste into a coal-like substance known as hydrochar. The process involves treating the waste with water under high pressure and temperature (Djandja et al.

2023). The resulting hydrochar can be used as a solid fuel or as a soil amendment. HTC can be used to treat a wide variety of organic waste, including sewage sludge, food waste, and agricultural waste. While advanced WtE technologies offer promising solutions to waste management and energy production, the primary focus should always be on waste prevention, reduction, and recycling. WtE technologies should be utilized for waste that cannot be recycled or reused and implemented in ways that minimize environmental and health impacts.

## Criteria for Evaluating the Efficiency of Advanced Waste-to-Energy Technologies

Assessing the effectiveness and efficiency of advanced Waste-to-Energy (WtE) technologies involves an evaluation encompassing both their technical proficiency and their environmental, economic, and social implications. In this review, the following key criteria were highlighted from all the relevant journal papers reviewed:

**Energy efficiency:** The overall energy efficiency of a WtE technology can be evaluated by comparing the energy content of the input waste to the usable energy output. This includes the heat and electricity generated or the energy content of any fuels produced.

In thermal WtE systems, such as gasification, the energy efficiency of gasification varies based on several factors, such as type of waste (feedstock), operating conditions, and the specific gasification technology. Many studies have reported a gasification energy efficiency between 60% - 80%. Zhang et al. (2011) conducted a thermodynamic evaluation of biomass gasification with air in auto-thermal gasifiers. They reported energy and exergy efficiencies of biomass gasification in the ranges of 52.38-77.41% and 36.5-50.19%, respectively. In a recent study, which integrated solar irradiation and gasification of municipal plastic wastes both energy and exergy efficiencies were obtained as 74% and 73%, respectively (Gungor & Dincer 2021, Aikalin & Dincer 2023). A higher efficiency can be achieved with advancements in gasification systems and energy optimization. In general, the efficiency of gasification processes depends on the ability to optimize the conversion of feedstock into valuable gases (e.g., syngas) while minimizing energy wastage. Variables affecting energy efficiency encompass the management of operational parameters (temperature, pressure, residence time), feedstock composition, the design of the gasification reactor, and the harnessing of waste heat for cogeneration applications. Additionally, it should be noted that energy efficiency can also be measured in terms of the overall system efficiency, considering the subsequent utilization of the produced syngas or other products. For example, if the syngas are efficiently used for combined heat and power (CHP) generation, the overall energy efficiency of the gasification system can be further improved.

The energy efficiency of biochemical systems, such as anaerobic digestion, and the energy efficiency of different biogas systems, which included single and co-digestion of multiple feedstocks, were evaluated. Pöschl et al. (2010) assessed the process energy efficiency using energy balance as the Primary Energy Input to Output (PEIO) ratio. They showed that PEIO corresponded to 10.5-64% and 34.1-55.0% for single feedstock digestion and co-digestion, respectively. When the feedstock used was transported from a distance of more than 22 km and 425 km for cattle manure and municipal solid waste, respectively, a negative energy efficiency was recorded. The overall energy input was influenced by the type and characteristics of feedstock and all other factors and processes that will contribute to energy input, such as pre-treatment of feedstock. Whereas energy balance depends on biogas yield, feedstock utilization efficiency, and energy value of intended fossil fuel substitution.

Transesterification is a chemical waste-to-energy process that involves the conversion of triglycerides, usually found in vegetable oils or animal fats, into acid alkyl esters known as biodiesels. This is usually done through a reaction with an alcohol. There are three broad types of transesterification processes – Base-catalyzed, Acid-Catalyzed, and Enzymatic Transesterification processes. The application of Ultrasound-assisted biodiesel production from waste-cotton seed cooking is gaining attention due to a lower reaction time and high energy efficiency. Sharma et al. (2020) investigated the application of Ultrasound-assisted KOH and CaO-catalyzed transesterification for biodiesel production from waste-cotton seed. They reported that the US-assisted transesterification process using KOH catalyst condition helped to reduce the mass transfer barrier and expedite the chemical reaction between non-miscible reactants. It also contributed to reducing the activation energy by allowing transesterification to be performed at lower temperatures.

**Waste reduction:** A key measure of the efficiency of WtE technologies is the degree to which they reduce the volume and mass of waste that would otherwise need to be disposed of in landfills. For instance, utilizing organic waste as a raw material, gasification, and pyrolysis systems can generate bio-oil, syngas, and thermal energy, all the while diminishing waste volume by up to 85-95% through the transformation into valuable biosolids and biochars (Srishti et al. 2021). Similarly, the waste reduction capacity from other biochemical processes, such as anaerobic digestion, will vary based on feedstock type, operating conditions,

Table 1: Classification of Waste based on WtE Technology and Energy potential.

| Waste Category | Organic Waste | Municipal Solid Waste | Agricultural Waste | Waste Oils and Fats | Sewage Sludge |
|---|---|---|---|---|---|
| Energy Content (MJ/Kg) | 15-20 | 10-15 | 10-20 | 35-40 | 5-10 |
| WtE Technology | Anaerobic Digestion (AD), Gasification, pyrolysis | Incineration, AD, Gasification, pyrolysis | Direct Combustion, AD, gasification | Transesterification | AD, Gasification, combustion |

detention time, and level of pre-treatment before utilization (Achi et al. 2020).

**Environmental impact:** The environmental impact of WtE technologies should be evaluated across their entire lifecycle, from the collection and preparation of waste to the end use of the energy produced. This includes the emissions produced during operation, the impacts of any residues that need to be disposed of, and the potential benefits of avoiding landfill disposal or fossil fuel consumption.

**Economic feasibility:** The economic feasibility of a WtE technology depends on the costs of building and operating the facility, the revenues from selling the energy produced or any valuable by-products, and the potential cost savings from reduced landfill disposal.

**Social impact:** The social impact of WtE technologies can include job creation, impacts on local communities (such as changes in traffic or noise levels), and potential health impacts from emissions.

**Integration with waste management:** Advanced WtE technologies should be evaluated as part of an integrated waste management strategy. This means considering how they fit with waste reduction, reuse, and recycling efforts and whether they are suitable for the local waste composition and quantities.

A thorough evaluation of advanced WtE technologies should consider all these aspects and involve a wide range of stakeholders, including local communities, waste management authorities, and environmental organizations. It should ideally be supported by detailed data and analysis, using tools such as life cycle assessment and cost-benefit analysis.

## ENERGY RECOVERY POTENTIAL OF WASTE AND WTE TECHNOLOGIES

Energy recovery potential refers to the amount of usable energy that can be obtained from a waste material. This can vary greatly depending on the type of waste and the technology used to convert it into energy. Table 1 shows the energy recovery potential for different waste streams and technologies.

In all cases, the actual energy recovery will depend not only on the energy content of the waste but also on the efficiency of the conversion technology and the energy used in collecting, preparing, and processing the waste. Therefore, the overall energy balance and environmental impacts of waste-to-energy systems should be evaluated using a life cycle approach.

### Environmental Impact

Waste-to-Energy (WtE) technologies can have significant environmental impacts, both positive and negative. Some of these impacts include:

#### Positive Impacts

**Reduction in Landfill Use:** By converting waste into energy, WtE technologies can significantly reduce the amount of waste that ends up in landfills. This can significantly help conserve land resources and reduce the environmental impacts associated with landfilling, such as the emission of methane, a potent greenhouse gas.

**Renewable Energy Production:** WtE technologies can produce renewable energy in the form of heat, electricity, or fuels. This can help replace fossil fuels and reduce greenhouse gas emissions.

**Resource Recovery:** Some WtE technologies can also recover valuable resources from waste, such as metals from incinerator bottom ash or nutrients from anaerobic digestion residues. This can help save natural resources and reduce the environmental impacts of mining and fertilizer production.

#### Negative Impacts

**Air emissions:** WtE technologies can produce air pollutants, such as particulate matter, nitrogen oxides, sulfur dioxide, and heavy metals, depending on the type of technology and the composition of the waste. Modern WtE facilities are equipped with advanced air pollution control systems to reduce these emissions, but they cannot eliminate them completely.

**Greenhouse gas emissions:** While WtE technologies can reduce greenhouse gas emissions by replacing fossil fuels and preventing landfill methane emissions, they can also produce carbon dioxide emissions, especially when they process waste containing fossil-derived materials like plastics.

**Residues:** WtE technologies can produce residues that need

to be managed, such as incinerator bottom ash or residues from gas cleaning systems. These can sometimes contain contaminants that need to be treated or disposed of safely.

**Energy and material use:** The collection, preparation, and processing of waste for energy recovery can consume energy and materials, which can have additional environmental impacts.

In order to assess the overall environmental impacts of WtE technologies, a comprehensive life cycle assessment (LCA) should be conducted. This should take into account not only the operation of the WtE facility itself but also the upstream and downstream processes, such as waste collection and residue management.

### Economic Feasibility

The economic feasibility of Waste-to-Energy (WtE) technologies depends on a variety of factors, including capital costs, operational costs, revenues, and policy support. Some of the key aspects to consider are:

1. **Capital costs:** The capital costs of WtE facilities can be substantial, especially for advanced technologies like gasification and pyrolysis. These costs include the design and construction of the facility, the purchase of equipment, and the installation of pollution control systems.
2. **Operational costs:** The operational costs of WtE facilities include labor, maintenance, fuel (if required), waste disposal, and other ongoing expenses. These can vary greatly depending on the technology, the scale of operation, and local conditions.
3. **Revenue streams:** The main revenue streams for WtE facilities are the sale of energy and any valuable by-products, such as metals recovered from incinerator ash or digestate from anaerobic digestion. The value of these products can depend on energy prices, commodity markets, and local demand.
4. **Policy support:** The economic feasibility of WtE technologies can be greatly influenced by policy support, such as renewable energy incentives, landfill taxes, or feed-in tariffs. These policies can help offset the costs of WtE technologies and make them more competitive with other forms of waste disposal and energy production.
5. **Waste Supply:** A reliable and sufficient supply of waste is necessary for the economic operation of a WtE facility. The costs of waste collection and preparation can also affect the economic feasibility.
6. **Life Cycle Costs:** To fully assess the economic feasibility of a WtE technology, it's important to consider the entire life cycle costs, from initial investment to decommissioning. This should also include the costs of managing any residues and potential future liabilities, such as environmental remediation.

A comprehensive economic evaluation should be undertaken to assess the viability of Waste-to-Energy (WtE) technologies, encompassing these factors and supported by realistic assumptions regarding future circumstances. Additionally, it is crucial to account for economic risks and uncertainties, such as fluctuations in energy prices or variations in waste composition.

## CASE STUDIES OF SUCCESSFUL IMPLEMENTATION OF ADVANCED WASTE-TO-ENERGY TECHNOLOGIES

There are numerous examples of successful implementation of advanced Waste-to-Energy (WtE) technologies around the world. Here are only a few examples (Table 2):

These case studies demonstrate the feasibility of advanced WtE technologies and their potential benefits in terms of renewable energy production, waste reduction, and environmental protection. However, they also highlight the importance of careful planning, good design, and community engagement in ensuring the success of these projects.

For instance, Enerkem's facility in Edmonton, Alberta, is a prime example of advanced waste-to-energy technology in action. This facility uses gasification technology to convert municipal solid waste (MSW) into biofuels and chemicals. The Enerkem facility faced several challenges, including technical difficulties in scaling up the technology, delays in construction, and fluctuations in commodity prices. However, the project has demonstrated the technical feasibility of waste-to-biofuels technology and highlighted the importance of policy support and strong partnerships in bringing such projects to fruition. It also showcases the potential of advanced waste-to-energy technologies to contribute to a circular economy, where waste is viewed not as a problem to be disposed of but as a valuable resource.

Similarly, the Amager Bakke, also known as Copenhill, is a state-of-the-art waste-to-energy plant located in Copenhagen, Denmark. This facility is notable not only for its advanced technology but also for its creative approach to urban integration and multi-functionality. It plays a key role in Copenhagen's ambition to become a carbon-neutral city by 2025. It has been designed to be as efficient as possible, with a net energy efficiency of 107% due to its ability to utilize both heat and electricity from the waste.

In compliance with environmental policies, the plant also has a robust air pollution control system in place, ensuring that it complies with strict emission limits. Any

Table 2: Summary of case studies.

| Case Studies | Type of Advanced WtE | Feedstock | Materials/Energy Recovery | Capacity/Scale |
|---|---|---|---|---|
| Enerkem, Edmonton, Canada (Enerkem, 2023) | Gasification | Municipal Solid Waste (MSW) | Methanol and Ethanol | Converts 100,000 Metric tons per year to ≈ 38 million litres of ethanol |
| Amager Bakke, Copenhagen, Denmark (Bjarke Ingels Group, 2019) | Advanced combustion/ Incinerator | MSW | Heat and Electricity | 400,000 metric tons to provide heat for 160,000 households and electricity for 62,500 households |
| Powerhouse Energy Group, United Kingdom: (Powerhouse Energy Group (2023) | Gasification (Dual fluidized bed gasification) | Plastic waste | Synthetic Gas, hydrogen, and Electricity through combined Heat and Power systems | Large-scale |
| Ensyn, Canada and USA (Ensyn 20230) | Pyrolysis (Rapid Thermal Processing) | agricultural residues and biomasses | Bio-oil and bionased chemicals | Large Scale |
| Bristol BioEnergy Centre, UK; (Bristol Bioenergy Centre 2023) | Microbial Fuel Cells | Organic Waste | Electricity | Large scale/ Commercial |
| WasteMart, Western Cape South Africa (SA) (WasteMart 2023) | Gasification | Industrial and Municipal wastes | Syngas to Electricity and Heat | Commercial |
| Sasol, South Africa (Sasol 2023) | Plasma Gasification | Wastes | Synthetic fuels and Chemicals | Large Scale |
| EThekwini Municipality Biogas project, Durban, SA; (eThekwini Municipality 2019) | Anaerobic Digestion | Landfill Organic wastes | Biogas for electricity | 3MW of electricity |

residual ash from the incineration process is treated and, where possible, recycled as a substitute for natural aggregates in road construction. One of the most unique features of Amager Bakke is its multi-functional design. The roof of the plant has been designed to include a 400-meter-long ski slope, a climbing wall, and hiking trails. This creative approach to design not only helps integrate the facility into the urban landscape but also creates additional value for the community.

The success of Amager Bakke highlights the potential of waste-to-energy projects to contribute to urban sustainability and quality of life. It also underscores the importance of innovative design, community engagement, and political leadership in bringing such projects to fruition. The Amager Bakke case study demonstrates that waste-to-energy facilities can be more than just industrial plants. With thoughtful design and planning, they can become an integral part of the urban fabric, delivering multiple benefits and improving the quality of life in cities.

## CHALLENGES AND FUTURE PERSPECTIVES

Waste-to-Energy technologies hold significant potential for managing waste and generating renewable energy. However, they also face several challenges:

1. **Technological Challenges:** Advanced WtE technologies, such as gasification and pyrolysis, are still evolving, and there can be challenges in scaling up these technologies and ensuring their operational reliability.
2. **Economic Challenges:** The high capital and operational costs of WtE facilities can be a barrier to their implementation, especially in the absence of policy support or favorable market conditions.
3. **Environmental Impacts:** While WtE technologies can have significant environmental benefits, they can also have negative impacts, such as air emissions and residues, which need to be carefully managed.
4. **Public Acceptance:** Public acceptance can be a challenge for WtE projects, especially for incineration-based technologies, due to concerns about emissions and health impacts.

With the future in perspective, there are several key areas of focus to overcome these challenges:

**Technological Innovation:** Ongoing research and development can help improve the performance and reliability of WtE technologies and reduce their costs and environmental impacts.

**Public Engagement:** Engaging with local communities and stakeholders is crucial for gaining public acceptance and ensuring the success of WtE projects.

**Policy Support:** Greater policy support, such as renewable energy incentives or landfill taxes, can help improve the economics of WtE projects.

**Sustainability Assessment:** Conducting comprehensive sustainability assessments, including life cycle assessments and socio-economic impact assessments, can help guide the planning and implementation of WtE projects to ensure they deliver net positive impacts. Although there are challenges to be overcome, the future of WtE technologies is promising, as they offer a potential solution to the dual problems of waste management and renewable energy generation.

## Technical Challenges in Waste-to-Energy Technologies

Implementing Waste-to-Energy (WtE) technologies presents several technical challenges due to the complex nature of waste and the technologies themselves. The following key technical challenges were highlighted from the reviewed literature:

**Variability of waste:** Municipal solid waste is highly heterogeneous, with its composition varying significantly over time and geographical location. This variability can affect the operation of WtE technologies, particularly those like gasification, pyrolysis, and Anaerobic Digestion systems, which require a consistent feedstock.

**Scale-up:** Many advanced WtE technologies have been proven at a small scale, but scaling up to a commercial size can be challenging. This is due to the complex physical and chemical processes involved, which may not scale linearly.

**Emission control:** WtE technologies can generate emissions, such as particulates, heavy metals, dioxins, and furans, which need to be carefully controlled to meet environmental regulations. Developing and maintaining effective emission control systems can be technically challenging.

**Energy recovery:** Improving the efficiency of energy recovery from waste is a continual challenge. This includes optimizing the conversion process and integrating the WtE facility with other energy systems, such as district heating networks or electricity grids.

**Residue management:** WtE processes can produce residues, such as ash or char, which need to be treated and disposed of safely. Managing these residues, particularly those from incineration-based technologies can be technically challenging, especially if they contain hazardous substances.

**Plant reliability and maintenance:** Like any industrial facility, WtE plants need regular maintenance to ensure reliable operation. Given the harsh operating conditions, including high temperatures and the corrosive nature of waste, maintaining the reliability of WtE plants can be technically challenging.

Future research and development efforts will need to continue addressing these technical challenges to further improve the performance and viability of WtE technologies. This will likely involve a combination of technological innovation, process optimization, and system integration.

## Regulatory and Policy Challenges in Waste-to-Energy Technologies

Implementing Waste-to-Energy (WtE) technologies can also face significant regulatory and policy challenges. The following are some of the key issues:

**Regulatory complexity:** The WtE projects often fall under the jurisdiction of multiple regulatory authorities, covering areas such as waste management, energy generation, and environmental protection. Navigating this regulatory landscape can be complex and time-consuming, and inconsistencies or uncertainties in regulations can pose significant challenges.

**Policy support:** The WtE projects typically require significant upfront investment and may not be economically viable without policy support, such as renewable energy subsidies, feed-in tariffs, or carbon pricing. The absence of such support or uncertainty about future policy direction can be a significant barrier to the development of WtE projects.

**Waste hierarchy:** Many jurisdictions follow a waste hierarchy that prioritizes waste prevention, reduction, reuse, and recycling over energy recovery and disposal. While this hierarchy is important for promoting sustainable waste management, it can also pose challenges for WtE projects, particularly if they are perceived as competing with recycling or waste reduction efforts.

**Emission standards:** Many WtE facilities are subject to strict emission standards to protect air quality and public health. Complying with these standards can be challenging, particularly for emerging technologies that may not yet have proven emission control systems.

**Permitting and approval processes:** Obtaining the necessary permits and approvals for a WtE facility can be a complex and lengthy process involving environmental impact assessments, public consultations, and detailed technical reviews. Delays or complications in this process can pose significant challenges.

Overcoming these regulatory and policy challenges requires a combination of proactive engagement with regulators and policymakers, careful project planning and design, and ongoing efforts to demonstrate the environmental and economic benefits of WtE technologies. It also underscores the importance of a stable and supportive policy environment for advancing sustainable waste management and energy recovery solutions.

### Future Directions in Advanced Waste-to-Energy Technologies

The field of Waste-to-Energy (WtE) is subject to continuous innovation, growth, and development, with several promising trends, prospects, and directions for the future:

**Advanced thermal technologies:** While incineration remains the most common WtE technology, advanced thermal technologies like gasification and pyrolysis are gaining interest. These technologies can offer higher energy efficiency and potentially lower emissions compared to incineration, though they also come with their own challenges.

**Biochemical technologies:** The use of biochemical technologies like anaerobic digestion and fermentation for producing biogas and biofuels from organic waste is another promising area. These technologies can contribute to a circular economy by turning waste into valuable products.

**Hybrid systems:** Combining different WtE technologies in a hybrid system can offer advantages in terms of flexibility, efficiency, and environmental performance. For example, a system might use mechanical and biological treatment to pre-treat waste and extract recyclables, followed by thermal treatment for energy recovery from the residual waste.

**Integration with other systems:** There is growing interest in integrating WtE facilities with other systems, such as district heating networks or carbon capture and storage facilities, to improve overall efficiency and sustainability.

**Circular economy approaches:** The concept of a circular economy, where waste is viewed as a resource and kept in use for as long as possible, is influencing the development of WtE technologies. This includes technologies that can recover valuable materials from waste, as well as those that can convert waste into a variety of products, not just energy.

**Digitalization and automation:** The use of digital technologies, such as sensors, data analytics, and automation, can help improve the operation and maintenance of WtE facilities, enhance their efficiency, and reduce their environmental impact.

These future directions highlight the potential for continued innovation and improvement in WtE technologies. However, realizing this potential will require ongoing research and development, supportive policies, and collaboration among various stakeholders, including researchers, policymakers, industry, and communities.

## CONCLUSION

Waste-to-energy (WtE) technologies hold significant potential to address two critical global challenges: managing increasing amounts of waste and reducing reliance on fossil fuels for energy generation. By converting waste into valuable energy, these technologies contribute to a more sustainable and circular economy. The case study of the Himiko plant in Tokyo, Japan, provided a detailed view of the practical implementation and potential benefits of advanced WtE technologies. However, it also highlighted the challenges involved, including managing waste variability, maintaining high energy efficiency, and ensuring public acceptance.

Several technical, regulatory, and policy challenges must be addressed to further the adoption of WtE technologies. These include the variability of waste, the difficulty of scaling up technologies, emission control, the need for policy support, and the complexity of regulatory environments. Looking to the future, promising trends include the development of advanced thermal and biochemical technologies, the integration of WtE facilities with other systems, the application of circular economy principles, and the digitalization and automation of WtE operations. Addressing these challenges and seizing these opportunities will require concerted efforts across multiple sectors and disciplines. It will necessitate ongoing research and development, supportive policy frameworks, and proactive engagement with stakeholders, including local communities.

In conclusion, while WtE technologies face significant challenges, they also offer considerable opportunities. If these challenges can be successfully addressed, WtE technologies can play an important role in transitioning towards a more sustainable and resilient energy system while also contributing to effective waste management.

### Summary of Key Findings

Through the analysis and case study of Waste-to-Energy (WtE) technologies, several key findings emerged:

1. **Value of WtE technologies:** WtE technologies can play a significant role in sustainable waste management and renewable energy generation, contributing to a circular economy by turning waste into valuable resources.
2. **Performance of advanced WtE technologies:** Advanced WtE technologies, such as gasification, as seen in the Himiko plant, can offer high energy efficiency and low emissions. However, they also pose challenges, including managing waste variability and maintaining high energy efficiency.
3. **Importance of regulatory and policy support:** Regulatory and policy support is crucial for the implementation and operation of WtE projects. This includes clear and consistent regulations, financial

incentives for renewable energy, and supportive planning and permitting processes.

4 **Challenges in WtE implementation:** There are significant technical, regulatory, and policy challenges in implementing WtE technologies. These range from the technical challenges of handling varied waste to the regulatory challenges of navigating complex environmental regulations.

5. **Future directions in WtE:** The future of WtE includes areas like advanced thermal and biochemical technologies, hybrid systems, integration with other systems, circular economy approaches, and the use of digital technologies to improve WtE operations.

These findings underscore the potential of WtE technologies to contribute to sustainable waste management and renewable energy generation. However, they also highlight the complexity and challenges involved in implementing and operating these technologies, and the need for ongoing research, development, and policy support to advance this field.

**Implications for Policy and Practice**

The key findings of this analysis have several important implications for policy and practice in the field of Waste-to-Energy (WtE):

1. **Policy support:** Given the significant upfront costs and technical challenges associated with WtE projects, policy support is crucial. This can take various forms, including financial incentives for renewable energy, simplified permitting processes, and stable, long-term policy frameworks that provide certainty for investors.
2. **Integrated waste management:** WtE should be considered as part of an integrated waste management strategy that also includes waste prevention, reduction, reuse, and recycling. Policies and practices should aim to optimize the entire waste management system rather than focusing solely on energy recovery.
3. **Stakeholder engagement:** Given the potential environmental and health impacts of WtE facilities and the public concern these can generate, proactive and transparent engagement with local communities and other stakeholders is crucial. This can help build understanding and acceptance of WtE projects and ensure that their benefits are equitably shared.
4. **Research and development:** Ongoing research and development is needed to improve WtE technologies, address technical challenges, and develop innovative solutions. This should be supported by funding and collaboration opportunities, as well as mechanisms for sharing knowledge and best practices.
5. **Regulatory harmonization:** Efforts should be made to harmonize and streamline the regulatory frameworks that apply to WtE projects. This can help reduce the complexity and uncertainty that project developers face while maintaining robust environmental and health protections.
6. **Sustainability metrics:** The development and use of comprehensive sustainability metrics can help assess the overall performance of WtE projects, taking into account not just energy output and emissions but also factors like waste reduction, resource recovery, and social impacts.

By addressing these implications, policymakers, practitioners, and other stakeholders can help advance the development and adoption of WtE technologies and maximize their contributions to sustainable waste management and renewable energy generation.

**Areas for Further Research**

The findings of this study also highlight several areas for further research in the field of Waste-to-Energy (WtE):

1. **Advanced WtE technologies:** There is a need for more research into advanced thermal and biochemical WtE technologies, including their technical performance, environmental impacts, and economic viability. This can help address the current challenges faced by these technologies and unlock their full potential.
2. **Hybrid systems and system integration:** The potential benefits of combining different WtE technologies into hybrid systems or integrating WtE facilities with other energy systems are promising areas for further research.
3. **Sustainability assessment:** More research is needed to develop comprehensive sustainability assessment methods for WtE projects, taking into account not just energy output and emissions but also other environmental, economic, and social impacts.
4. **Waste variability:** Given the significant variability of waste, research is needed to better understand its impacts on WtE operations and how these can be managed. This may involve developing more flexible technologies or improving waste sorting and pre-processing methods.
5. **Policy analysis:** Further research is needed to understand the impacts of different policies on the development and operation of WtE projects. This can inform the design of more effective policy frameworks and support mechanisms.

6. **Public acceptance:** Understanding the factors that influence public acceptance of WtE projects and how these can be addressed is another important area for research.

By pursuing these research areas, we can deepen our understanding of WtE technologies, address their current challenges, and better harness their potential to contribute to sustainable waste management and renewable energy generation.

## REFERENCES


Abdallah, R., Juaidi, A., Assad, M., Salameh, T. and Manzano-Agugliaro, F. 2020. Energy recovery from waste tires using pyrolysis: Palestine as the case of study. Energies, 13(7): 1817.

Acikalin, G. and Dincer, I. 2023. A solar based integrated gasification system for municipal plastic wastes to produce multiple useful outputs for environmental protection. Process Saf. Environ. Prot.

Agbedahin, A. V. 2019. Sustainable development, Education for Sustainable Development, and the 2030 Agenda for Sustainable Development: Emergence, efficacy, eminence, and future. Sustain. Dev., 27: 669-680. https://doi.org/10.1002/sd.1931

Aguilar Esteva, L. C., Kasliwal, A., Kinzler, M. S., Kim, H. C. and Keoleian, G. A. 2021. Circular economy framework for automobiles: Closing energy and material loops. J. Ind. Ecol., 25: 877-889. https://doi.org/10.1111/jiec.13088

Ahring, B. K. 2003. Perspectives for anaerobic digestion. Biomethanation, 4: 1-30.

Akubude, V. C., Nwaigwe, K. N. and Dintwa, E. 2019. Production of biodiesel from microalgae via nanocatalyzed transesterification process: A review. Mater. Sci. Energy Technol., 2(2): 216-225.

Allouhi, A., El Fouih, Y., Kousksou, T., Jamil, A., Zeraouli, Y. and Mourad, Y. 2015. Energy consumption and efficiency in buildings: Current status and future trends. J. Cleaner Prod., 109: 118-130. https://doi.org/10.1016/j.jclepro.2015.05.139

Lebdioui, A. 2022. Nature-inspired innovation policy: Biomimicry as a pathway to leverage biodiversity for economic development. Ecol. Econ., 202: 107585. https://doi.org/10.1016/j.ecolecon.2022.107585

Angela, N., Radu, G., Susana G., Azevedo, J. and Matias, C. O. 2020. A comprehensive review of industrial symbiosis. J. Clean. Prod., 247: 119113. https://doi.org/10.1016/j.jclepro.2019.119113

Angelidaki, I., Ellegaard, L. and Ahring, B. K. 2003. Applications of the anaerobic digestion process. Biomethanation ii: 1-33.

Anne, P. M., Velenturf, Phil Purnell. 2021. Principles for a sustainable circular economy. Sustain. Prod. Consum., 27: 1437-1457. https://doi.org/10.1016/j.spc.2021.02.018

Baionie Silva, G., Manicardi, T., Longati, A. A., Lora, E. E. and Milessi, T. S. 2023. Parametric comparison of biodiesel transesterification processes using non‐edible feedstocks: Castor bean and jatropha oils. Biofuels Bioprod. Bioref., 17(2): 297-311.

Beaulieu, L., van Durme, G. and Arpin, M. 2015. Circular Economy: A Critical Literature Review of Concept. International Reference Centre for the Life Cycle of Products, Processes and Services (CIRAIG). ISBN 978-2-9815420-0-7.

Bernardo, M., Lapa, N., Gonçalves, M., Barbosa, R., Mendes, B., Pinto, F. and Gulyurtlu, I. 2010. Toxicity of char residues produced in the co-pyrolysis of different wastes. Waste Manage., 30(4): 628-635.

Bjarke Ingels Group. 2019. Amager Bakke Copenhill. Retrieved from https://archello.com/project/amager-bakke-copenhill (Accessed on September 17, 2023)

Bofylatos, S. 2022. Upcycling systems design, developing a methodology through design. Sustainability, 14: 600. https://doi.org/10.3390/su14020600

Boloy, R. A. M., da Cunha Reis, A. and Rios, E. M. 2021. Waste-to-energy technologies towards a circular economy: a systematic literature review and bibliometric analysis. Water Air Soil Pollut., 232: 306. https://doi.org/10.1007/s11270-021-05224-x.

Bristol Bioenergy Centre. 2023. Bristol Bioenergy Centre. Retrieved from https://www.bristolroboticslab.com/bristol-bioenergy-centre (Accessed on September 17, 2023)

Chibueze, A., Amro, H. and Stephanie, L. 2020. Enhanced biogas production of cassava wastewater using zeolite and biochar additives and manure co-digestion. Energies, 13(2): 491. https://doi.org/10.3390/en13020491

Coker, A., Achi, C., Idowu, O., Olayinka, O., Oturu, K. and Ijomah, W. 2021. Remanufacture of medical equipment: A viable, sustainable strategy for medical waste reduction. In: International Conference on Remanufacturing, 2021-03-24 - 2021-03-25, Online.

Demirbas, A. and Arin, G. 2002. An overview of biomass pyrolysis. Energy Sourc., 24(5): 471-482.

Department of Energy (DoE) 2019a. The South African Energy Sector Report 2019. DoE, Pretoria. http://www.energy.gov.za/files/media/explained/2019-South-African-Energy-Sector-Report.pdf

Djandja, O. S., Liew, R. K., Liu, C., Liang, J., Yuan, H., He, W. and Kang, S. 2023. Catalytic hydrothermal carbonization of wet organic solid waste: A review. Sci. Total Environ., 873: 162119.

Đurđević, D., Blecich, P. and Jurić, Ž. 2019. Energy recovery from sewage sludge: The case study of Croatia. Energies, 12(10): 1927.

EEA 2016. Circular Economy in Europe Developing the Knowledge Base. Available at: https://www.eea.europa.eu/publications/circular-economy-in-europe

Ellen MacArthur Foundation (EMAF) 2018. What is a Circular Economy? A framework for an economy that is restorative and regenerative by design. Circular Economy 2018.

Ellen MacArthur Foundation (EMAF) 2012. Towards the Circular Economy, Report vol. 1.

Ellen MacArthur Foundation (EMAF) 2013. Towards the Circular Economy. EMAF, London, UK.

Enerkem 2023. Process technology. Available at https://enerkem.com/process-technology Accessed on September 17, 2023

Ensyn 2023. Ensyn RTP application website. Accessed at http://www.ensyn.com/overview.html

eThekwini Municipality 2019. Strategic Roadmap for Renewable Energy (2019-2050), 31 May 2019. https://www.durban.gov.za/storage/Documents/Energy%20Office/eThekwini%20Energy%20Strategic%20Roadmap.pdf

Franks, A. E. and Nevin, K. P. 2010. Microbial fuel cells, a current review. Energies, 3(5): 899-919.

Gandhi, B. S., Chelladurai, S. S. and Kumaran, D. S. 2011. Process optimization for biodiesel synthesis from Jatropha Curcas oil. Distrib. Gener. Altern. Energy J., 26(4): 6-16. https://doi.org/10.1080/21563306.2011.10462201

Geissdoerfer, M., Savaget, P., Bocken, N. M. and Hultink, E. J. 2017. The circular economy: A new sustainability paradigm? J. Cleaner Prod., 143: 757-768. https://doi.org/10.1016/j.jclepro.2016.12.048

Godfrey, L. 2021. Unlocking the Opportunities of a Circular Economy in South Africa. In: Ghosh, S. K., Ghosh, S.K. (eds) Circular Economy: Recent Trends in Global Perspective, Springer, Singapore, p. 5. https://doi.org/10.1007/978-981-16-0913-8_5

Gungor, B. and Dincer, I. 2021. Development of a sustainable community with an integrated renewable and waste-to-energy system for multiple useful outputs. J. Cleaner Prod., 312: 127704.

Guo, W., Xi, B., Huang, C., Li, J., Tang, Z., Li, W. and Wu, W. 2021. Solid waste management in China: Policy and driving factors in 2004-2019. Resour. Conserv. Recycl., 173: 105727.

Gustavo, M.,, Renato, N., Moraes, R. N., Cunha, J. and Janaina M. H. 2017. From linear to circular economy: PSS Conducting the transition. Proc. CIRP, 64: 2-6. https://doi.org/10.1016/j.procir.2017.03.012

Hajam, Y.A., Kumar, R. and Kumar, A. 2023. Environmental Waste Management Strategies and Vermi Transformation for Sustainable Development. Environ. Challenges, 547: 100747.

Hans, W. 2021. Climate Change Mitigation in A Circular Economy. In: Hans Wiesmeth (ed), Implementing the Circular Economy for Sustainable Development, Elsevier, The Netherlands, pp. 267-276. https://doi.org/10.1016/B978-0-12-821798-6.00022-3

Hari Bhakta, S., Kumar, R., Vanapalli, B., Samal, V. R., Sankar, C. B. and Dubey, J. B. 2021. The circular economy approach in solid waste management system to achieve UN-SDGs: Solutions for post-COVID recovery. Sci. Total Environ., 800: 149605. https://doi.org/10.1016/j.scitotenv.2021.149605

Hasan, M. M., Rasul, M. G., Khan, M. M. K., Ashwath, N. and Jahirul, M. I. 2021. Energy recovery from municipal solid waste using pyrolysis technology: A review on current status and developments. Renew. Sustain. Energy Rev., 145: 111073.

Hassanein, A., Lansing, S. and Tikekar, R. V. 2019. Impact of metal nanoparticles on biogas production from poultry litter. Bioresour. Technol., 275: 200-206. https://doi.org/10.1016/j.biortech.2018.12.048

He, D., Hu, H., Jiao, F., Zuo, W., Liu, C., Xie, H. and Wang, X. 2023. Thermal separation of heavy metals from municipal solid waste incineration fly ash: A review. Chem. Eng. J., 143344.

Huang, Y. F. and Lo, S. L. 2020. Energy recovery from waste printed circuit boards using microwave pyrolysis: Product characteristics, reaction kinetics, and benefits. Environ. Sci. Pollut. Res., 27: 43274-43282.

IEA 2020. Sustainable Recovery. IEA, Paris. Available at: https://www.iea.org/reports/sustainable-recovery

Ijomah, W. 2010. The application of remanufacturing in sustainable manufacture. Proc. ICE - Waste Resour. Manage., 163(4): 157-163. ISSN 1747-6526.

Ilaria, C., Iole, V., Francesco, T. and Carlo, P. 2023. Environmental safety of nanotechnologies: The eco-design of manufactured nanomaterials for environmental remediation. Sci. Total Environ., 864: 161181. https://doi.org/10.1016/j.scitotenv.2022.161181

Ilieva, L., Ursano, I., Traista, L., Hoffmann, B. and Dahy, H. 2022. Biomimicry as a sustainable design methodology—introducing the 'biomimicry for sustainability' framework. Biomimetics, 7: 37. https://doi.org/10.3390/biomimetics7020037

IEA 2022. International Energy Agency (IEA). World Energy Outlook 2022.

Ipiales, R. P., Mohedano, A. F., Diaz, E. and de la Rubia, M. A. 2022. Energy recovery from garden and park waste by hydrothermal carbonization and anaerobic digestion. Waste Manage., 140: 100-109.

ISO/TR 14062. 2002. Environmental management, integrating environmental aspects into product design and development. ISO, Geneva.

Jenkins, S., Kuijper, M., Helferty, H., Girardin, C. and Allen, M. 2023. Extended producer responsibility for fossil fuels. Environ. Res. Lett., 18(1): 011005.

Jin, C. L., Wu, Z. M., Wang, S. W., Cai, Z. Q., Chen, T., Farahani, M. R. and Li, D. X. 2017. Economic assessment of biomass gasification and pyrolysis: A review. Energy Sources Part B: Econ. Plan. Policy, 12(11): 1030-1035.

Jouni, K., Antero, Ho. and Jyri, S. 2018. Circular economy: The concept and its limitations. Ecol. Econ., 143: 37-46. https://doi.org/10.1016/j.ecolecon.2017.06.041

Kaza, S., Yao, L. C., Bhada-Tata, P. and Van Woerden, F. 2018. What a Waste 2.0: A Global Snapshot of Solid Waste Management to 2050. Urban Dev., World Bank. http://hdl.handle.net/10986/30317

Kumar, A. and Samadder, S. R. 2017. A review of technological options of waste to energy for effective management of municipal solid waste. Waste Manage., 69: 407-422.

Lachheb, A., Allouhi, A., El Marhoune, M., Saadani, R., Kousksou, T., Jamil, A., Rahmoune, M. and Oussouaddi, O. 2019. Thermal insulation improvement in construction materials by adding spent coffee grounds: An experimental and simulation study. J. Cleaner Prod., 209: 1411-1419. https://doi.org/10.1016/j.jclepro.2018.11.140

Lazˇar, S., Dobrotˇa, D., Breaz, R. E. and Racz, S. G. 2023. Eco-design of polymer matrix composite parts: A review. Polymers, 15: 3634. https://doi.org/10.3390/polym15173634

Leclerc, S. H. and Badami, M. G. 2023. Extended producer responsibility: An empirical investigation into municipalities' contributions to and perspectives on e‐waste management. Environ. Policy Gov.

Logan, B. E. and Regan, J. M. 2006. Microbial fuel cells-challenges and applications. Environ. Sci. Technol., 40(17): 5172-5180.

Makarichi, L., Jutidamrongphan, W. and Techato, K. A. 2018. The evolution of waste-to-energy incineration: A review. Renew. Sustain. Energy Rev., 91: 812-821.

McKeown, R. 2002. Progress has been made in Education for Sustainable Development. Appl. Environ. Educ. Commun., 1(1): 21-23. https://doi.org/10.1080/15330150213983

Meher, L. C., Sagar, D. V. and Naik, S. N. 2006. Technical aspects of biodiesel production by transesterification—a review. Renew. Sustain. Energy Rev., 10(3): 248-268.

Miying, Y., Palie, S., Mukesh, K., Mark, J. and Steve, E. 2018. Product-service systems business models for circular supply chains. Prod. Plan. Contr., 29(6): 498-508. https://doi.org/10.1080/09537287.2018.1449247

Othman, A. A. E. and Elsawaf, L.A. 2021. Design out the waste framework for achieving sustainability in public housing projects in Egypt. WSEAS Trans. Environ. Dev., 17: 222-231. https://doi.org/10.37394/232015.2021.17.22

Oturu, K., Ijomah, W., Broeksmit, A., Reig, D. H., Millar, M. and Peacock, C. 2021. Investigation of remanufacturing technologies for medical equipment in the UK and context in which technology can be exported in the developing world. J. Remanufacture., 11: 227-242. https://doi.org/10.1007/s13243-021-00102-5

Paul, T. Mativenga, John Agwa-Ejon, Charles Mbohwa, Al Amin Mohamed Sultan and Norshah Aizat Shuaib 2017. Circular Economy Ownership Models: A view from South Africa Industry. Proc. MANUF., 8: 284-291. https://doi.org/10.1016/j.promfg.2017.02.036

Pöschl, M., Ward, S. and Owende, P. 2010. Evaluation of energy efficiency of various biogas production and utilization pathways. Appl. Energy, 87(11): 3305-3321.

Pourali, M. 2009. Application of plasma gasification technology in waste to energy challenges and opportunities. Sustain. Altern. Energy (SAE), 11: 1-6.

Powerhouse Energy Group. 2023. Technology Review. Accessed at https://www.powerhouseenergy.co.uk/projects/technology-review/

Ramasubramanian, B., Tan, J., Chellappan, V. and Ramakrishna, S. 2023. Recent Advances in Extended Producer Responsibility Initiatives for Plastic Waste Management in Germany and UK. Mater. Circular Economy, 5(1): 6.

Reichel, A., De Schoenmakere, M., Gillabel, J., Martin, J. and Hoogeveen, Y. 2016. Circular economy in Europe: Developing the knowledge base. Eur. Environ. Agency Rep., 2, 2016.

Sachs, J. D. 2012. From millennium development goals to sustainable development goals. Lancet, 124: 2206-2211. https://doi.org/10.1016/S0140-6736(12)60685-0

Salwin, M., Jacyna-Gołda, I., Kraslawski, A. and Waszkiewicz, A. E. 2022. The use of business model canvas in the design and classification of product-service systems design methods. Sustainability, 14: 4283. https://doi.org/10.3390/su14074283

Sambandam Padmanabhan, K., Giridharan, K., Balasubramaniam, S., Kumaran, S., Kavimani, V., Nagaprasad, N., Leta Tesfaye, J. and

Ramaswamy, K. 2022. Energy recovery of waste plastics into diesel fuel with ethanol and ethoxy ethyl acetate additives on circular economy strategy. Sci. Rep., 12: 5330. https://doi.org/10.1038/s41598-022-09148-2

Sambandam, P., Venu, H. and Narayanaperumal, B. K. 2020. Effective utilization and evaluation of waste plastic pyrolysis oil in a low heat rejection single cylinder diesel engine. Energy Sources Part A-recovery Util. Environ. Eff., 1-17.

Samenjo, K. T., Oosting, R. M., Bakker, C. and Diehl, J. C. 2023. The extent to which circular economy principles have been applied in the design of medical devices for low-resource settings in Sub-Saharan Africa: A systematic review. Front. Sustain., 107: 685. https://doi.org/10.3389/frsus.2023.1079685

Samoraj, M., Mironiuk, M., Izydorczyk, G., Witek-Krowiak, A., Szopa, D., Moustakas, K. and Chojnacka, K. 2022. The challenges and perspectives for anaerobic digestion of animal waste and fertilizer application of the digestate. Chemosphere, 295: 133799.

Sasol. 2023. Sasol. Accessed at https://www.sasol.com/

Sharma, A., Kodgire, P. and Kachhwaha, S. S. 2020. Investigation of ultrasound-assisted KOH and CaO catalyzed transesterification for biodiesel production from waste cotton-seed cooking oil: Process optimization and conversion rate evaluation. J. Clean. Prod., 259: 120982.

Slate, A. J., Whitehead, K. A., Brownson, D. A. and Banks, C. E. 2019. Microbial fuel cells: An overview of current technology. Renew. Sustain. Energy Rev., 101: 60-81.

Soloman, E., Winifred, I. and Wong, T. C. 2020. Remanufacturing: A potential sustainable solution for increasing medical equipment availability. J. Remanufactur., 10: 141-159. https://doi.org/10.1007/s13243-020-00080-0

Soltes, E. J. and Elder, T. J. 2018. Pyrolysis. CRC Press, Roca Baton, pp. 63-99

Srishti, A., Janelle, J., Ming, L., Xian, L., Abhimanyu, G., Jialing, C., Shuang, S., Carly, A., Dexiang, C., Ken, L., Song, H., Lim, S., Lee, F., Subhadip, G., Alexander, L., Harn, W., Hugh, T. W., Yanjun, T. D. and Chi-Hwa, W. 2021. Gasification biochar from horticultural waste: An exemplar of the circular economy in Singapore. Sci. Total Environ., 781: 146573. https://doi.org/10.1016/j.scitotenv.2021.146573

Tayebi-Khorami, M., Edraki, M., Corder, G. and Golev, A. 2019. Re-thinking mining waste through an integrative approach led by circular economy aspirations. Minerals, 9: 286. https://doi.org/10.3390/min9050286

Taylor Buck, N. 2017. The Art of Imitating Life: The potential contribution of biomimicry in shaping the future of our cities. Environ. Plan. B Urban Anal. City Sci., 44: 120-140.

The Sustainable Development Goals. 2022. The Political Impact of the Sustainable Development Goals: Transforming Governance Through Global Goals? Cambridge University Press, Cambridge, pp. 227-243. https://doi.org/10.1017/9781009082945.010

Tun, M. M., Palacky, P., Juchelkova, D. and Síťař, V. 2020. Renewable Waste-to-Energy in Southeast Asia: Status, Challenges, Opportunities, and Selection of Waste-to-Energy Technologies. Appl. Sci., 10: 7312. https://doi.org/10.3390/app10207312

United Nations Educational, Scientific and Cultural Organization. 2014. Shaping the Future We Want: UN Decade of Education for Sustainable Development (2005–2014) Final Report. Paris: UNESCO.

WasteMart. 2023. WasteMart Waste Management Services. Accessed at https://wastemart.co.za/

Wills, A., Tshangela, M., Bohler-Muller, N., Datta, A., Funke, N., Godfrey, L., Matomela, B., Pienaary, G., Pophiwa, N., Shaxson, L., Strydom, W. and Ke, Y. 2016. Evidence and Policy in South Africa's Department of Environmental Affairs.Department of Environmental Affairs and London: Overseas Development Institute, Pretoria.

World Economic Forum. 2014. The Global Competitiveness Report 2014-2015.

Zhang, Y., Kang, H., Hou, H., Shao, S., Sun, X., Qin, C. and Zhang, S. 2018. Improved Design for Textile Production Process Based on Life Cycle Assessment. Clean Technol. Environ. Policy, 20: 1355-1365.

Yayalık, İ., Koyun, A. and Akgün, M. 2020. Gasification of municipal solid wastes in plasma arc medium. Plasma Chem. Plasma Process., 40: 1401-1416.

Zhang, Y., Li, B., Li, H. and Liu, H. 2011. Thermodynamic Evaluation of Biomass Gasification with Air in Autothermal Gasifiers. Thermochim. Acta, 519(1-2): 65-71.

## ORCID DETAILS OF THE AUTHORS

C. G. Achi: https://orcid.org/0000-0002-9723-182X

Nature Environment and Pollution Technology
An International Quarterly Scientific Journal

p-ISSN: 0972-6268
(Print copies up to 2016)
e-ISSN: 2395-3454

Vol. 23 | No. 3 | pp. 1261-1283 | 2024

Original Research Paper

https://doi.org/10.46488/NEPT.2024.v23i03.003

Open Access Journal

# Techno-Economic Analysis of Solar, Wind, and Biomass Hybrid Renewable Energy Systems to Meet Electricity Demand of a Small Village in Bihar State of India

**Anant Arun Patil***, **Rajesh Arora*†**, **Ranjana Arora**** and **S. N. Sridhara*****
*Department of Mechanical Engineering, Amity University, Gurgaon-122413, Haryana, India
**Solar Engineering Department, Amity University, Gurgaon-122413, Haryana, India
***Hindustan Institute of Technology and Science, Chennai-603103, Tamil Nadu, India
†Corresponding author: Rajesh Arora; rajesharora1219@gmail.com

**Nat. Env. & Poll. Tech.**
**Website: www.neptjournal.com**

*Received:* 24-04-2024
*Revised:* 16-05-2024
*Accepted:* 04-06-2024

**Key Words:**
Solar energy
Biomass energy
Renewable energy
HRES
COE
NPC

## ABSTRACT

This study examines the potential use of Hybrid Renewable Energy Systems (consisting of photovoltaic, wind, bio, and diesel sources) both with and without the inclusion of battery storage in the eastern region of India. An evaluation is conducted to determine the economic viability of several system configurations, and the most efficient system is selected using HOMER software. The investigation focused on six distinct scenarios to meet the energy needs of a village community. The goal was to satisfy a daily load need of 1093.7 kWh, with a peak demand of 153.63 kW. The study examined many factors, such as system efficiency, financial viability, and ecological consequences. The primary aim of the research was to compare the power costs associated with different designs of HRES. Detailed techno-commercial assessments were carried out to examine the energy production, consumption, and financial impacts of each scenario. This research provides valuable insights for individuals and organizations seeking reliable and long-lasting energy solutions by analyzing the potential benefits and drawbacks of implementing HRES in rural areas. An evaluation is conducted to determine the energy contribution of each element within an RES, as well as the influence of HRES on energy expenses and net present value. The findings of this study reveal that the optimized hybrid system comprises 133 kW photovoltaic arrays, a 130-kW wind turbine, a 0.2 kW biogas generator, a 100-kW diesel generator, a 540-kWh battery bank with nominal capacity, and a 58-kW converter. This system has a minimum COE of 0.347$/kWh and NPC of $1.71M. The research offers useful insights for designers, scholars, and policymakers on the existing design constraints and policies of biomass-based hybrid systems.

## INTRODUCTION

Energy is getting more and more recognized as a major sector. During the past several decades, the number of sources of clean energy and related technologies has increased rapidly on a worldwide scale. Governments throughout the globe around every continent, new laws and regulations have been passed to promote the use of RET. These measures include, in addition to laws, the advancement of energy connection plans, the promotion of clean energy technology, and the increase in the efficiency of energy (Perera et al. 2013, Bandara et al. 2012, Bansal et al. 2013, Balcombe et al. 2013, Moghavvemi et al. 2013). Many storage systems, backup energy sources, and RES have been created. Since RESs are intermittent, to ensure continuous power supply, this suggests that by connecting these alternative energy sources to standard electrical infrastructure, electrical power can be supplied. This will increase the long-term stability of energy supply, especially in nations that rely on outside generators to satisfy various kinds of demand. (Meyar & Vaez 2012, Hoicka & Rowlands 2011, Ismail et al. 2013, Mekhilef et al. 2013). The combination of conventional and renewable energy sources can optimize the dependability of renewable energy sources under challenging environmental circumstances, reduce the limits associated with them, and open investment opportunities that would not otherwise be feasible (Gupta & Purohit 2013). The study of hybrid technologies and the wide range of applications they are provide currently receiving a significant amount of scientific attention. Academic research has investigated a variety of arrangements. A review of the literature on electricity in rural areas shows that one of the most crucial ways to

provide reliable, high-quality power for a variety of uses to areas without access to the electrical system is via sources of clean energy (Ma et al. 2013, Mekhilef et al. 2012, Harish et al. 2014).

An essential component of any nation's industrialization, urbanization, and economic growth is electricity (Khare et al. 2013). To create electricity, a variety of standard and non-traditional power sources have been used. Two of the most common types of energy are RES, such as solar and wind power systems. Because of their versatility and environmental benefits, RES-such as wind and solar power are becoming more common (Elhadidy & Shaahid 2000). In the previous 20 years, a remarkable advancement in the field of solar wind, with a shift from standalone to integrated systems has been widely used (Nema et al. 2010). Energy from solar and wind systems operates regularly in both independent and grid-connected modes due to the stochastic nature of both power sources; however, its efficiency is reduced. Sources of clean energy are utilized to provide grid-integrated hybrid energy, which mitigates the unpredictability of nature. Conventional and renewable energy sources are integrated into a system that uses hybrid renewable energy (HRE). Additionally, two or more standalone or grid-connected RES may be included. The HRES operates in two modes: sequential and simultaneous, combining significant solar and wind resources. Even though they generate power alternately in sequential mode, both solar and wind power plants do it concurrently in simultaneous mode (Elhadidy & Shaahid 2004, Notton & Muselli 1996). The objective of the ideal simulation is to analyze a photovoltaic wind-biogas-pumped hydroelectric off-grid hybrid system for rural electrification in Sub-Saharan Africa. The researchers found that Djoundé, a remote hamlet in northern Cameroon, has implemented a comprehensive off-grid HES that relies entirely on renewable sources. This system includes wind turbines, photovoltaic arrays, and a biogas generator to meet the population's power requirements (Yimen et al. 2018). The optimal allocation of the whole load has been accomplished by harnessing wind, sun, and biomass resources. When there is very little need for energy in the local area, any extra power is sent to the national power system. According to techno-economic feasibility research, a hybrid power system can generate energy over 50 megawatts (Ahmad et al. 2018).

The Indian government concentrated on electrifying every unconnected family in the nation while slowly working towards 100% rural electrification. After analyzing in research, it was determined that the main obstacles to household electrification were the following: a lack of knowledge, the expense of establishing new connections, the complexity of the process, and other logistical challenges. The Indian government meticulously planned and implemented the Pradhan Mantri Sahaj Bijli Har Ghar Yojana, also known as Saubhagya, was launched in October 2017 with a specific focus on ensuring electricity access to all households in the country, especially those who were previously unelectrified. The Saubhagya plan is a massive endeavor aimed at achieving universal electrification, making

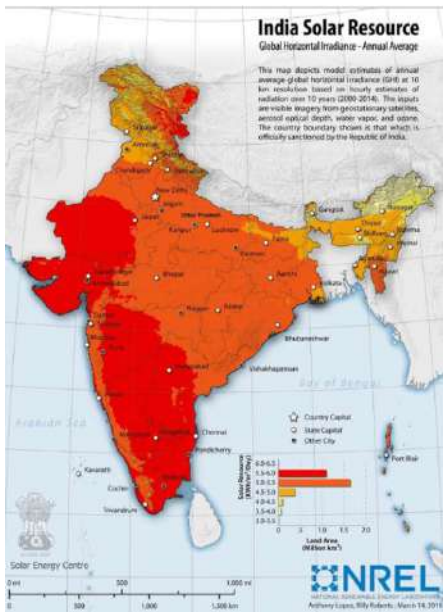


Source: (NSRDB 2024).

Fig. 1: Annual Global Horizontal Irradiation

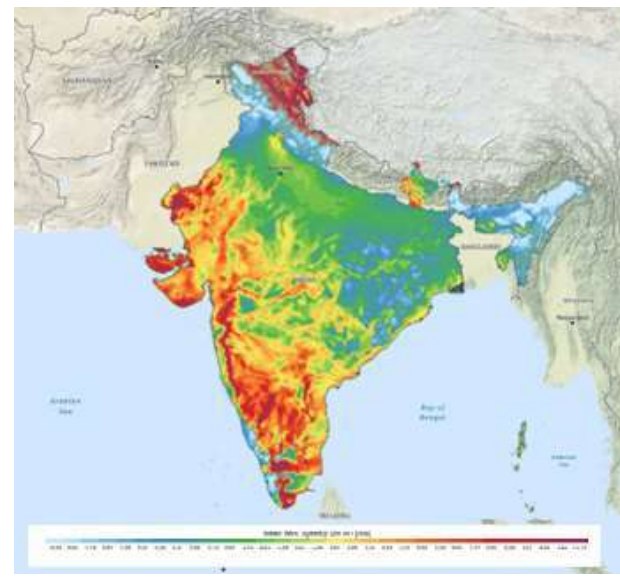

Source: (Wikipedia 2024).

Fig. 2: Mean Wind Speed

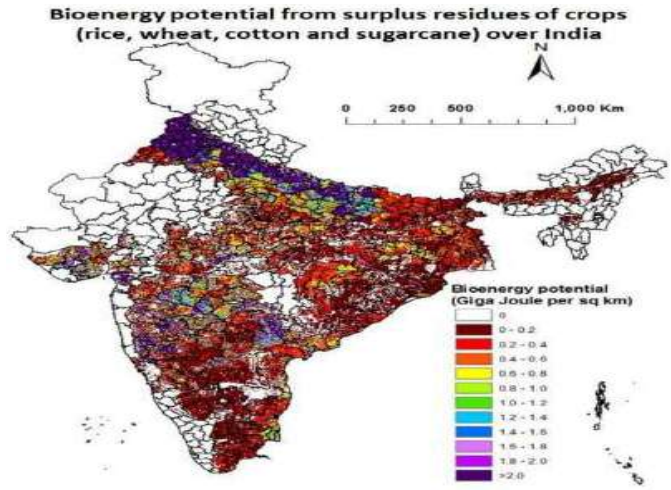


Source: (Bhuvan 2024).

Fig. 3: Bioenergy potential over India

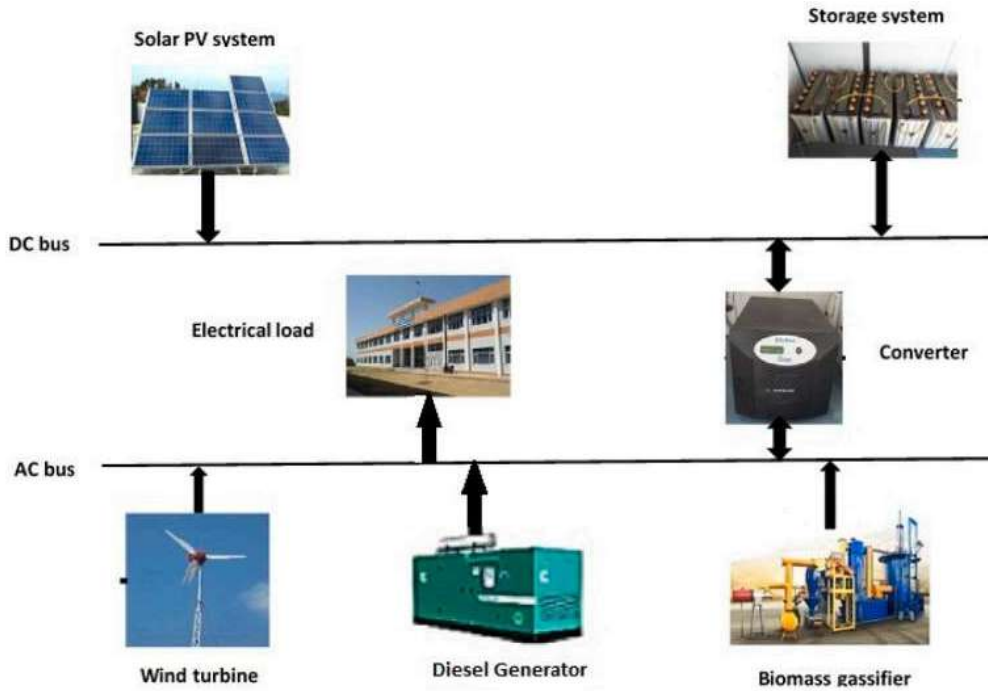


Source: (Malik et al. 2019).

Fig. 4: Hybrid Renewable Energy System.

it one of the biggest in the world. It involves the collaborative efforts of the Centre and the States (Saubhagya Dashboard 2024). Fig. 1. and Fig. 2 show annual global horizontal irradiation (NSRDB 2024) and wind speed (Wikipedia 2024).

Fig. 3 gives overall bioenergy potential in India from residues of crops rice, wheat, cotton, and sugarcane (Bhuvan 2024). The representation of HRES presented in Fig. 4 (Malik et al. 2019). Fig. 5 describes the Schematic representation of HOMER software (HOMER Pro 2024). The procedures to apply the recommended HES in HOMER are shown in Fig. 4. Finding the location's load profile and then obtaining the solar irradiation potential and wind speed potential are the two main steps in the process. Then, we model the system using various components. The component sizes are

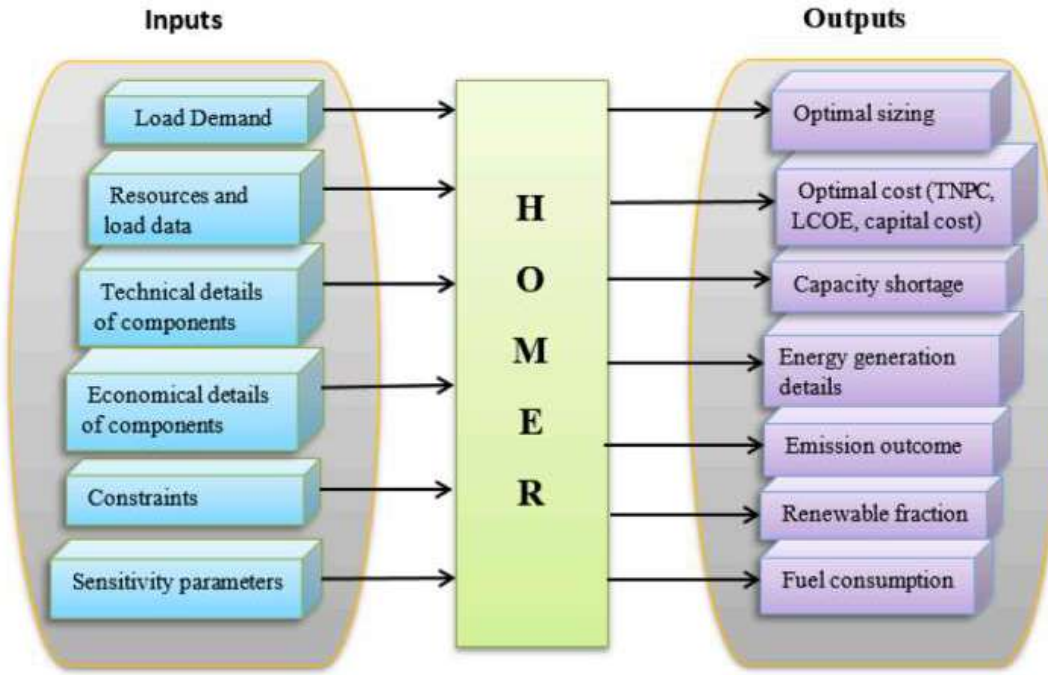


Fig. 5: Schematic representation of HOMER software (HOMER Pro 2024).

included, along with the economic characteristics. To do our model's cost optimization assessment, optimization is carried out. COE analyzes the whole simulated outcome to provide satisfying findings and determines whether the chosen outcome fulfills the study's purpose. HOMER categorizes its results according to a low-cost partnership.

This research paper presents an optimal approach for determining the appropriate dimensions and functioning of an HES that combines wind and biomass gasification. A case study is done using real-time load demand data acquired from a facility. The wind-biomass gasifier HES is also analyzed in economic research (Balamurugan et al. 2011). This study investigates the economic viability of a hybrid power system that combines biomass, photovoltaic (PV), and wind generators to fulfill the electricity requirements of isolated locations (Maherchandani et al. 2012). Conventional ways of meeting energy demand are impractical due to most of the cost involved in transportation and electrical distribution to these remote places. These days, a lot of places use hybrid electrical systems, with diesel generators serving as vital backup power sources. The primary justification for a hybrid system that uses biomass as a fuel source is the accessibility of biomass, such as goat, cow, or buffalo dung, at reasonable prices in rural regions. Biomass sources can provide electricity on overcast days and in the absence of the minimum wind requirement. The goal of the project is to determine whether combining solar PV and biomass resources can fulfill the long-term economic and technological sustainability of fulfilling the energy needs of Tola Dhumnadih Village in Banka District, Bihar. The primary aims of this study are to explore the potential of these sustainable energy sources, examine their ability to meet the village's electricity needs, evaluate the project's financial feasibility and expenses, and offer suggestions for the development of a dependable, reasonably priced, and eco-friendly energy source that could be used as a model for rural electrification in comparable areas. Ultimately, the project seeks to provide frameworks and insights into how energy from renewable sources might be used in distant areas to support long-term growth for independence from fossil fuels.

## PAST STUDIES

A hybrid electrical system generates energy from many of these sources at the same time. The biggest benefit of HES is its ability to meet energy demands. Usually, applicable in stand-alone applications for isolated areas without access to an electrical grid. Numerous research works on renewable hybrid energy sources have been published in scholarly journals. This study's review of the literature is restricted to PV-wind-biomass HRES. Anant et al. and associates evaluated the financial viability of solar, biomass, and wind turbines for generating grid power to meet the needs of rural areas (Patil et al. 2023). Meanwhile, a business has proposed HRES for Balamurugan and three Indian city-states. Making

use of an appropriate model, created by the HOMER software creators, divides the electrical power across the tasks based on significance. Researchers used a statistical approach to calculate that the price of power is US$ 0.1095 (Balamurugan et al. 2009). In Kakavayal, Kerala, India, Kumaravel and Ashok also used biomass-based HRES to electrify local villages. Using the HOMER program, they ascertained the ideal HRES configuration for biomass, solar, wind, and storage. The parametric assessment revealed that the energy cost amounted to 0.164$/kWh (Kumaravel & Ashok 2015). A study of the costs associated with implementing an ecologically friendly electricity delivery mechanism for residential usage was done for the hamlet. They modeled and optimized their wind PV hybrid system using HOMER software. They found seven distinct hybrid systems that are emulated, both with and without battery storage. The HES consisting of photovoltaic cells, biomass energy producer, and batteries is determined to be the best design, resulting in the lowest energy cost per kWh at an anticipated TNPC of $76080, with 41% PV and 59% biomass part (Malik et al. 2021, Malik et al. 2019). Sustainable application is significantly hampered by the intermittent presence of renewable resources in the settlements. Combining two or more green energies might be the best way to tackle the irregularity of those assets, the expenditures associated with producing energy, and the general efficacy of the system, including power dependability (Neves et al. 2014, Chandel et al. 2016).

Several researchers have examined the assessment and analysis of the practicality and effectiveness of off-grid HES infrastructure in India and other nations to provide rural power supply. For instance, Karki et al. evaluated the HRES feasibility for a small island in India to assess the effects of dispersed source utilization on net current cost, energy expenses, and $CO_2$ emissions (Karki et al. 2008). The technical-economic assessment of various HRES achievements for the country's rural areas was investigated (Chambon et al. 2020). In five states in India without power, including Uttarakhand, Bhatt et al. Explored the capabilities of a disengaged HRES. The optimal COE generation, assuming a 94% renewables share, was found to be 0.197 $/kWh (Bhatt et al. 2016). A framework for optimization was developed by Chauhan and colleagues for HRES based on the electric load needs of 48 non-electrified country small towns in the Chamoli district of the Indian state of Uttarakhand (Chauhan & Saini 2016). To satisfy the increasing demand, Malik et al. suggested incorporating a plant-based gasifier with the present PV/WT hybrid system (Malik et al. 2020). Li et al. After studying the viability of merging systems that utilize different battery types, utilizing energy generators rather than lithium-i along with battery packs with lead acid, zinc-bromine form batteries are more cost-effective to employ (Li et al. 2020). An investigation was conducted to assess the practicality of using HRES to meet the energy needs of a remote hamlet in Iran. by Rad et al. The results indicated that an integrated HRES with PV, WT, and BG is the optimum choice. Although the total cost will still increase by 33-37%, adding fuel cell technology would increase system flexibility further (Rad et al. 2020). Vendoti et al. conducted a comprehensive examination of HRES from both a technical and economic perspective to determine which options would best satisfy the load demands of the country's communities. Based on the study, PV-WT-BG-FC-Battery-based HRES was shown to be the most efficient design with the lowest COE of 0.214 $/kWh (Vendoti et al. 2021). Malik et al. provided a comprehensive analysis. It found that bioenergy integrated systems offer a cheap and environmentally friendly solution to powering rural areas (Malik et al. 2021). Salehin et al. proposed establishing an HRES to deliver energy to Bangladesh's isolated island of Adarsha Char (Salehin et al. 2014). Sigarchian et al. completed the sensitivity analysis and optimization of HRES for Kenyan villages that lack power. An analysis of the literature suggests that the major focus of research is on hybrid electrical systems enabling rural electrification using solar and wind power. However, research on biomass-based hybrid buildings for hilly terrain has been severely lacking (Sigarchian et al. 2015).

Taele et al. found that constructing small-scale solar energy systems in Lesotho communities reduced electricity loss, removed huge fuel storage, and prevented multiple breakdowns (Taele et al. 2012). Patil et al. conducted a study in Uttarakhand, India, to explore the incorporation of four distinct renewable energy sources (Kanase et al. 2010). This was done to address the requirements for cooking and electricity in seven communities. Baghdadi et al. conducted a study on the efficiency of a hybrid PV-wind diesel battery in the Adrar region of southern Algeria (Baghdadi et al. 2015).

Based on the calculations, the most realistic approach to satisfy the load demand is to combine a 3-kW hydrogen fuel cell with 5 kW of solar output with the least amount of non-permanent current (NPC) and zero% electricity shortage. According to Lau et al., combining batteries with diesel and solar power sources might drastically reduce dependency on the finite fuel supply (Lau et al. 2010). Yilmaz and Selim looked at many concepts for turning biomass into electricity and combining it with different renewable energy sources (Yılmaz & Selim 2013). The study shows that load demand may be efficiently satisfied with the appropriate mix of renewable energy sources and technological advancements. Rahman et al. examined the technological and economical

optimization of hybrid bioenergy & solar systems to replace traditional facilities, it is necessary to satisfy both thermal (cooking) and electric requirements (Rahman et al. 2014). Ozden's capacity in Ankara, Turkey, Tari studied the energy output exertion using a combination of solar-hydrogen technology. The total efficacy of this hybrid approach is 6.21%, while the performance of the hydrogen-generating cycle is 40.06 percent, according to the data. The researchers

Table 1: The results of some HES that were installed to electrify rural areas.

| Ref | Location | HRE technologies | | | | | | Energy consumption | COE | Findings |
|---|---|---|---|---|---|---|---|---|---|---|
| | | PV | WT | DG | BG | B | C | | | |
| (Ajlan et al. 2017). | Shafar, Yemen | √ | √ | √ | | √ | √ | 886 kWh/day | 0.137 $/kWh | The current and future feasibility of hybrid PV/WT/diesel systems over 100% RE and diesel systems. |
| (Dawoud et al. 2015). | Hurghada, Egypt | √ | √ | √ | | √ | √ | 1153 kWh/day | 0.139 $/kWh | HRES implementation over diesel-only load demand electrification has economic and environmental benefits. |
| (Sawle et al. 2018). | India | √ | √ | | √ | √ | √ | 10.6 kWh/day | 0.195 $/kWh | Different optimization strategies were used to tackle the problem. According to the findings, TLBO is an effective instrument for dealing with any issue objectives and providing an appropriate solution. |
| (Shahzad et al. 2017). | Layyah, Pakistan | √ | | | | √ | √ | 168.36 kWh/day | 5.51 Rs/kWh | Evaluated the hybrid system's techno-economic viability for use in agriculture. |
| (Gan et al. 2015). | Bishopton, Scotland | √ | √ | √ | | √ | √ | 15 kWh/day | 0.677 £/kWh | Create an optimal HRES modelling and scaling tool. Compare battery and diesel sizes and choose the one with the lowest life-cycle cost. |
| (Mandal et al. 2018). | Chorasariadho, Bangladesh | √ | √ | √ | | √ | √ | 242.56 kWh/day | 0.37 $/kWh | In contrast to grid-connected and solar home systems, an optimized off-grid HRE was exhibited. Different perspectives on hybridized energy systems' technical, economic, environmental, and social performance were explored. |
| (Shaahid & El-Amin 2009). | Rafha, KSA | √ | | √ | | √ | √ | 44 kWh/day | 0.170 $/kWh | Compared COE, fuel operating minutes, and carbon dioxide emissions with different PV/battery capacities. |
| (Akinyele 2017). | Gwagwalada Nigeria | √ | √ | √ | | √ | √ | 12.51 kWh/day | 0.3145 $/kWh | Different hybrid system designs with increasing load needs are tested for battery performance and reliability. |
| (Khan et al. 2017). | Amritsar, India | √ | √ | √ | | √ | √ | 1.3 kWh/day | 0.164 $/kWh | Show the hybrid system as the best practical alternative for serving the load with the lowest COE and highest power generation. |
| (Padrón et al. 2019). | Lanzarote, Canary Islands. | √ | | √ | | √ | √ | 250 kW KWh/day | 0.404 $/kWh | From a technological and economic standpoint, a standard HRES was proposed and assessed to ensure the power needs of an autonomous desalination system. |
| | Present Cases Study | √ | √ | √ | √ | √ | √ | 1093.75 kWh/day | 0.343 $/kWh | Of the six different cases of HRES (PV+WT+BGG+DG+B) comes with the Lowest NPC and COE. |

Table 2: Summary of Hybrid Renewable Energy System (HRES) Configuration and Results.

| Ref | Location | HRE technologies | | | | | | Energy consumption | COE | Findings |
|---|---|---|---|---|---|---|---|---|---|---|
| | | PV | WT | DG | BG | B | C | | | |
| Present Study Case 1 | Tola Dhumnadih, Bihar | √ | √ | | | √ | √ | 1093.75 kWh/day | 0.467 $/kWh | HRES developed for the lowest COE to meet load requirements using Solar PV (415 KW) + Wind (183 no's) + Battery (2820 no's) + Converter (141KW). |
| Present Study Case 2 | Tola Dhumnadih, Bihar | √ | √ | | √ | √ | √ | 1093.75 kWh/day | 0.461 $/kWh | HRES developed for the lowest COE to meet load requirements using Solar PV (427 KW) + Wind (186 no's) + Biogas Generator (0.4 KW) + Battery (2700 no's) + Converter (154KW). |
| Present Study Case 3 | Tola Dhumnadih, Bihar | √ | √ | √ | √ | √ | √ | 1093.75 kWh/day | 0.347 $/kWh | HRES developed for the lowest COE to meet load requirements using Solar PV (131 KW) + Wind (130 no's) + Biogas Generator (0.2 KW) + Diesel Generator (100 KW) + Battery (540 no's) + Converter (58.0 KW). |
| Present Study Case 4 | Tola Dhumnadih, Bihar | √ | √ | √ | √ | | √ | 1093.75 kWh/day | 0.594 $/kWh | HRES developed for the lowest COE to meet load requirements using Solar PV (283KW) + Wind (235 no's) + Biogas Generator (2 KW) + Diesel Generator (150 KW) + Converter (46.9 KW). |
| Present Study Case 5 | Tola Dhumnadih, Bihar | √ | √ | √ | | √ | √ | 1093.75 kWh/day | 0.348 $/kWh | HRES developed for the lowest COE to meet load requirements using Solar PV (133 KW) + Wind (125 no's) + Diesel Generator (100 KW) + Battery (530 no's) + Converter (55.7 KW). |
| Present Study Case 6 | Tola Dhumnadih, Bihar | √ | √ | √ | | | √ | 1093.75 kWh/day | 0.598 $/kWh | HRES developed for the lowest COE to meet load requirements using Solar PV (282 KW) + Wind (238 no's) + Diesel Generator (150 KW) + Converter (39.6 KW). |

also suggested that hybrid PV-hydrogen systems outperform PV-battery solutions in terms of performance (Ozden & Tari 2016). Shi et al. created an HRE using an inspired evolutionary algorithm. System optimization includes decreasing fuel usage, the system's yearly cost, and the chance of an outage (Shi et al. 2015). Forough and Roshandel employ multiple goals shrinking vista techniques to find the optimal electric-car timetable. Two objective functions were evaluated: the price of diesel fuel as batteries depleted (Forough & Roshandel 2017). Castellanos et al. investigated several combinations of PV cells, biogas the digester, and a single power & warming unit in a tiny community in West Bengal, India, using micro-grid modeling simulation. The outcome indicates the integration of an inverter rectifier energy system (IRES) with photovoltaic (PV) technology, an anaerobic digester, and a compact turbine. have reduced the total capital and electrical expenses of the project (Castellanos et al. 2015).

The most efficient design of the HRES may have been determined by the research employing a variety of optimization approaches in conjunction with the HOMER software. Sensitivity analysis may be used to analyze changes in variables such as load demand fluctuations, resource availability, or technology improvements to help enhance comprehension of the system's performance in different scenarios. Consider dynamic variables such as meteorological trends, fluctuations tied to different seasons, and the uncertain behavior of renewable energy sources. By including fluctuations in the accessibility of solar and biomass, the HOMER model may be enhanced by the integration of real-time data and forecasting methods. By addressing these research deficiencies, the study would enhance its comprehensiveness and accuracy, providing a more precise assessment of the economic viability, efficiency, and sustainability of the hybrid green energy source that Tola Dhumnadih Village in the Banka District of Bihar intends to use. The results of some HES that were installed to electrify rural areas are shown in Table 1 which gives insights into the location and the technology used for electrification. Table 2 gives the summary of the Hybrid Renewable Energy System (HRES) configuration and results.

## MATERIALS AND METHODS

A comprehensive examination was carried out at the location

in Tola Dhumnadih Village, located in the Banka District of Bihar, India. These investigations were carried out to collect information on the socioeconomic makeup of the community, the climate in the area, the quantity of land available for infrastructure, and the usage habits of energy. The gathering and examination of meteorological data, such as temperature, solar and wind radiation, biomass, and electric consumption, was necessary for accurate modeling. Utilizing a variety of energy systems to electrify a complete town utilizing solar, wind, bioenergy, diesel generators, and battery banks, six alternative energy models were developed and simulated using the HOMER software. The objective is to build a battery-powered HES that includes wind turbines, generators, converters, solar PV panels, and other components while taking into consideration the energy requirements and environmental characteristics of Tola Dhumnadih Village.

**Site Selection and Data Collection**

Tola Dhumnadih Village, a town in Banka, Bihar, was chosen as the main subject of the feasibility study due to its advantageous socioeconomic, physical, and energy-related attributes. Information on the topography and climate of Tola Dhumnadih, including elevation, weather patterns, latitude, and longitude of the place, and so on gathering historical as well as current data on things like the sun's average monthly irradiance, wind speed, and the area's biomass resources. Fig. 6. shows the flow diagram of the methodology for the calculation of biomass from the Bhuvan spatial information system of biomass potential from crop residues (Bhuvan 2024).

**Case Study and Description**

India has a predominantly rural population, with about 600,000 villages accounting for 72.2% of its people's resources. Rural regions consume around 40% of total energy, with the home sector accounting for 55-60% of energy usage. A few of the most important problems are these having direct and indirect implications on energy supply for rural areas. There is a shortage of both commercial and traditional energy and there is more space between supply and demand. Growing populations constantly put more strain on conventional energy sources like wood. Ecological issues are being brought on by urbanization and the deforestation that follows. Since fossil fuels are running out, and the resulting contamination of the environment, a heavy reliance on commercial fuels like coal and oil as a temporary solution to fulfill rising demand is concerning. Remote rural locations that receive energy supplies are linked to substantial transmission and transportation losses of around 22.4%. Therefore, focus should be placed on energy audits in a way that guarantees accessible, sustainable, and

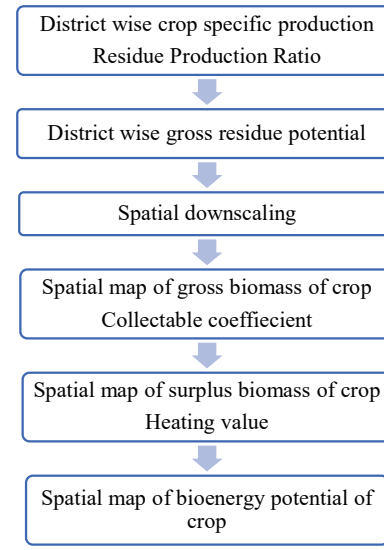


Fig. 6: Flow-Diagram of the Methodology (Bhuvan 2024).

clean energy.

The primary location for the case study is the Chanan Taluka, specifically the little village of Chanan. The town has 1890 residents, 999 of whom are males and 891 of them are women. There are 350 homes in the neighborhood. 389 children make up the whole population. The entire land area of the settlement is around 252.05 acres or 102 hectares. The information supplied provides a demographic overview of the hamlet and provides a breakdown of those living there by gender, number of children, and houses. A deep understanding of these demographics is required to achieve a range of planning, administrative, and construction goals, including resource distribution, social assistance planning, facility building, and other community-specific efforts (Census 2011 India, Indian Village Directory 2024).

Fig. 7 represents the Google Earth and Google Map location of Tola Dhumnadih with latitude 24°46′54.97″N and longitude 86°30'20.77"E region in Banka, Bihar (Google Maps 2024).

The main goal is to assess the viability from a financial standpoint of several alternative power sources. by contrasting the costs of biomass generators, PV systems, wind turbines, and batteries. In addition, one of the objectives of the study is to estimate the hourly values of the monthly electric load for the designated region.

**Energy Feasibility Studies for Solar, Wind and Biomass**

The energy feasibility study conducted in the Tola Dhumnadih region of Banka, Bihar, thoroughly investigates the utilization of biomass, solar, and wind energy sources for electricity production. This research aims to evaluate


Fig. 7: Tola Dhumnadih region in Banka, Bihar (Google Maps 2024).

the viability and achievability of different renewable energy sources in meeting the energy requirements of the region. Comprehensive evaluations of wind, solar, biomass, and battery energy are included in the research. A variety of aspects are considered, such as resource availability, economic viability, technological feasibility, and environmental effects.

The research evaluates solar radiation levels, solar PV system availability, and the viability of installing them in the Tola Dhumnadih area. Land availability, sun insolation levels, and the financial sustainability of solar power-producing technologies are all taken into account. To assess the wind speed and energy potential of the Tola Dhumnadih area, wind patterns, wind speeds, and topographical concerns must be determined.

The objective of the research is to examine the feasibility of wind-generating projects from both a technical and financial perspective to determine if it is viable to generate energy using wind turbines. The research investigates the feasibility of using local biomass resources to create power. This comprises examining the many forms of biomass that are readily available, their potential for energy generation through processes such as gasification or biogas production, and the economic viability of implementing biomass-based energy systems.

### Daily Load Analysis

The daily average connected load for different times of the day is shown in Fig. 8 and observed that the maximum requirement of connected load in the evening timing from 5

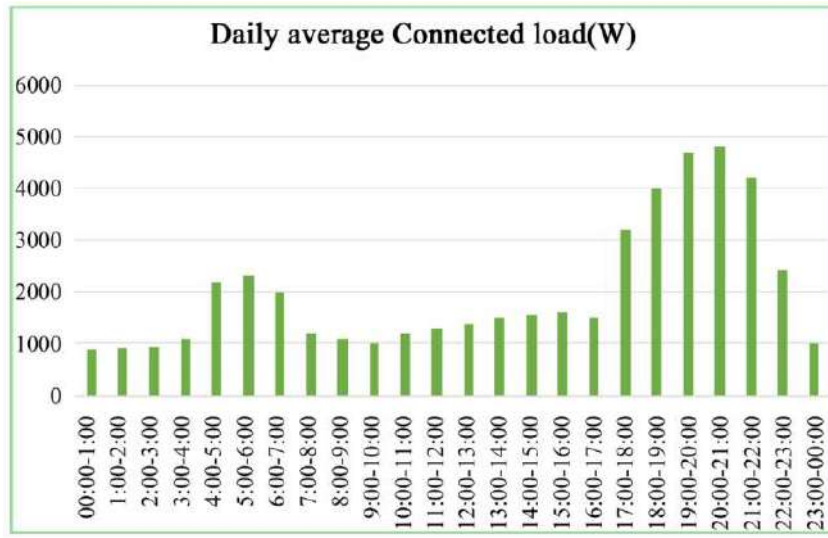


Fig. 8: Comparison of time and average daily connected load, Community 2 (Verma et al. 2015).

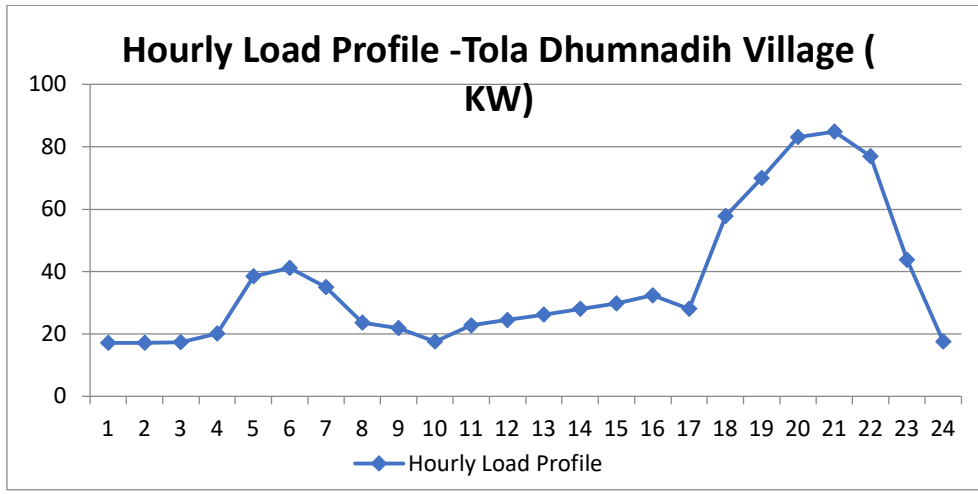


Fig. 9: Hourly Load Profile -Tola Dhumnadih Village.

pm to 10 pm (Verma et al. 2015). Similarly, Fig. 9. Hourly Load Profile calculated for Tola Dhumnadih Village.

**Monthly Load Analysis**

Using HOMER software, the monthly load study for the Tola Dhumnadih area in Banka, Bihar, comprises a detailed assessment of energy demand patterns. Options include using a generator and battery that runs on diesel in addition to utilizing 100% energy from renewable sources. To meet the neighborhood's power demands, this research will analyze how feasible it is to provide the best possible layout with an energy system based on renewable sources. The HOMER program is used to simulate and model the process of replacing the current electricity supply system with purely sustainable RES.

To have a better understanding of the fluctuating energy demand, load profiles at different times of day and seasons are analyzed. This entails figuring out if employing these resources to effectively meet the specified load profiles is viable. The study assesses the extent to which a diesel generator contributes to the integration of renewable energy sources in the energy system. The HOMER project facilitates the more efficient use of diesel generators and batteries, especially as a backup or in situations when demand may be partially satisfied by renewable energy sources, or as an additional resource to deliver a consistent power supply. The examination includes technical factors like optimizing the diesel generator's well and how big the green energy parts are. Economic assessments are also conducted to find the most economically viable energy option and to assess the cost-effectiveness of the recommended system. In Table 3 the cost of each component explains each component required for HRE generation (Verma et al. 2015, Malik et al. 2021).

The information gathered for an annual load includes all the information on the amount of power consumed or required at a certain location over a full year. These data are required to evaluate the overall energy requirements of a given area and the patterns in those requirements. When creating more energy-efficient technologies, it's critical to consider the variations in electricity use that happen overnight as well as the projected 25% growth in population and level of life. When peak and off-peak hours are identified

Table 3: Cost of each Component.

| Components | Capacity | Cost of capital [$] | Replacement Cost [$] | O & M [$/yr] | Duration [yrs/hrs] |
|---|---|---|---|---|---|
| PV (Malik et al. 2021) | 1 kW | 741.00 | 741.00 | 25 | 25 yrs |
| Wind Turbines (Sawle et al. 2021) | 1 kW | 1,200 | 850 | 20 | 20 yrs |
| Diesel Generators (Malik et al. 2021) | 1 kW | 500 | 500 | 0.030 | 15,000 hrs |
| Batteries (Malik et al. 2021) | 12V | 273 | 211 | 5.96 | 10 yrs |
| Converter (Malik et al. 2021) | 1 kW | 116 | 116 | 3 | 10 yrs |
| Biomass Generators (Malik et al. 2021) | 1 kW | 1162 | 872 | 0.010 | 15,000 hrs |

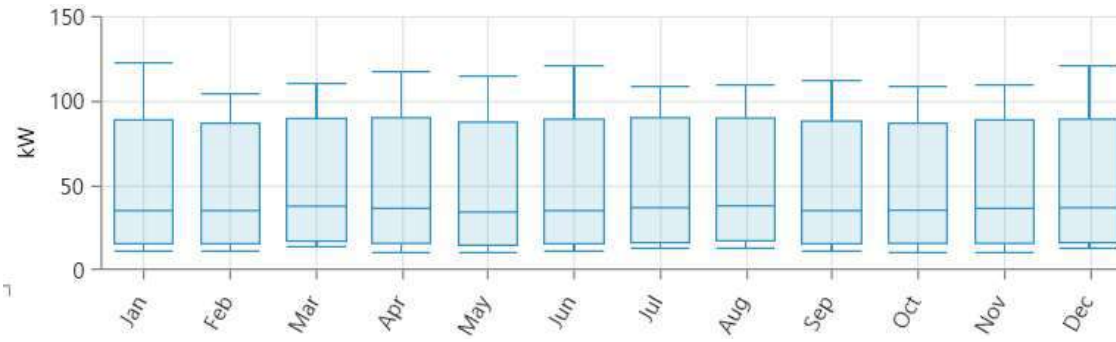


Fig. 10: Yearly Load Data (HOMER Pro 2024).

Table 4: Random variability.

| Random Variability | |
|---|---|
| Day-to-Day [%] | 10 |
| Timestep [%] | 10 |

using hourly data, utilities may improve the processes involved in generating electricity and supplying that energy. In Fig. 10 yearly Load Data given for each month of the year (HOMER Pro 2024).

Here are detailed instructions for Yearly Load Data:

Using Daily or Hourly Data:

Data Collection: Gather daily or hourly energy use data for the full year.

To find the total yearly consumption, add up how much energy is used each day or hour of the year.

a. For daily data, total energy uses from January 1st to December 31st of each year.
b. For Hourly Data: Add up the energy usage for each hour of the year, which amounts to 8760 hours in a non-leap year.

These parameters represent the extent to which the variables or conditions of the simulated system are permitted to change freely both inside the modeled scenario and daily. 10% variability indicates a significant amount of uncertainty in the model, which might be used to imitate real-world situations or explain the unpredictable nature of the system. Table 4 explains the random variability parameters considered for the HOMER simulation model also in Fig. 11 load details are shown with respect to peak load and average load.

This is the total amount of solar radiation collected by a certain area per unit of time, commonly represented in kWh/$m^2$/day. Monthly average solar irradiance measurements are essential in determining the quantity of daylight that impacts a specific location, a characteristic that directly determines solar panels' ability to create electricity. In Fig. 12 the maximum solar radiation observed in April was 6.34 kWh/$m^2$/day, and the minimum came in December at 4 kWh/$m^2$/day. The average solar radiation available at Tola Dhumnadih village is 4.89 kWh/$m^2$/day (HOMER Pro 2024).

Monthly average wind speed data is critical for assessing a region's ability to generate wind energy. This data is crucial for computing average monthly wind conditions, which can impact the economics and performance of wind energy schemes. The mean wind speed for a given month is measured in meters per second. It depicts the present weather conditions for the given period. The typical monthly value

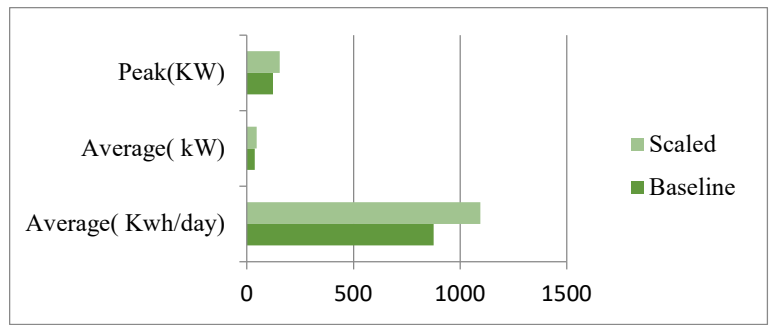


Fig. 11: Load details.

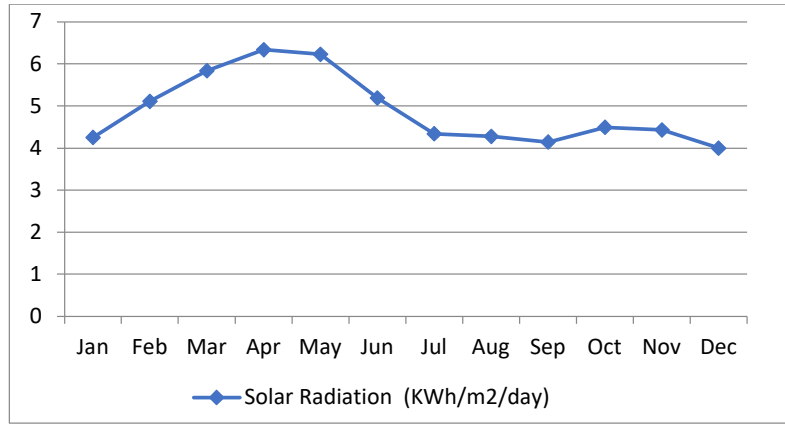


Fig. 12: Monthly average solar global horizontal irradiance data.

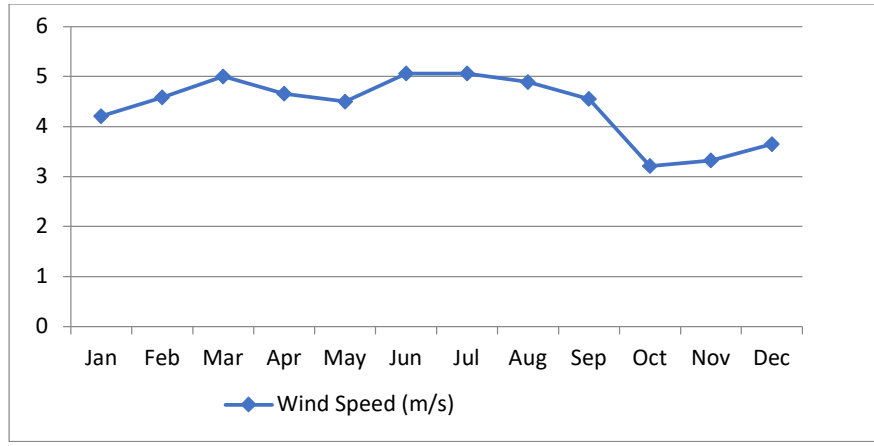


Fig. 13: Monthly average wind speed data.

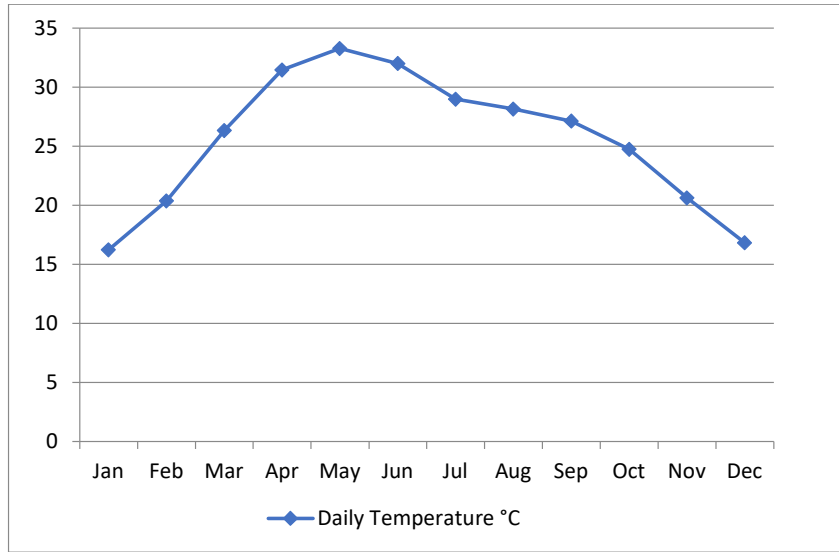


Fig. 14: Daily average temperature data.

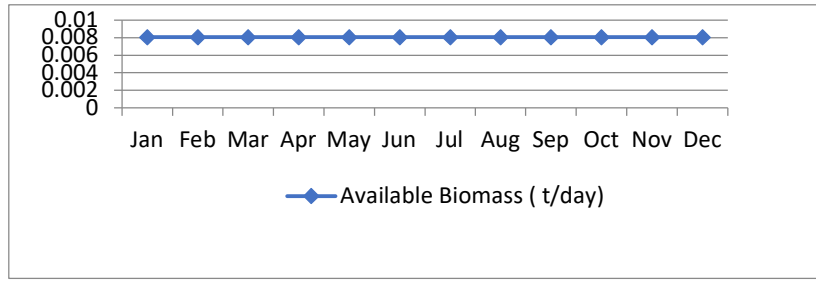


Fig. 15: Daily average available biomass data.

of the wind speed, incorporating temperature data, refers to the projected mean temperatures observed at a certain geographical place for every month of the year.

Fig. 13 and Fig. 14 show the computed wind velocity and temperature for the specified village area on a monthly and annual basis. The greatest wind speed at Tola Dhumnadih village in July was 5.060 m/s, while the minimum was 3.32 m/s in November, for a yearly average of 4.39 m/s. Similarly, the highest temperature in May is 33.23 degrees Celsius, while the lowest temp in January is 16.23 (HOMER Pro 2024).

The daily average available biomass statistics show the average amount of natural issues, or biomass that can be found or might be found in an area or region every month of the year shown in Fig 15 (Patil et al. 2023). This data is very important for finding out how helpful and readily available organic materials are for many things, including producing energy, agriculture, and studying the environment.

Here are detailed Calculation for Biomass Data:

Acers = 252.04 acres

Total Surplus Biomass [kg] = 7900000 kg

Biomass in the village [kg/year] = 2666.79

Biomass in the village [ton/day] = 0.008

## RESULTS AND DISCUSSION

This research assesses alternative energy sources using storage cells, alongside traditional energy sources as a contingency, to identify a viable solution that can fulfill the local power demand while simultaneously reducing emissions and cost considerations such as the COE, NPC, and operation and maintenance expenses (O & M). At times, a diesel generator must be used when storage cells are insufficient to meet the high demand, especially in cases when non-conventional resources are being utilized.

### A. Techno-economic and Optimal Energy Flow Research Cases

The initial optimization criteria for the study consist of a scaled average daily electric demand for a load of 1093.75 kWh per year. The average annual wind potential is 4.39 meters per second, the yearly average solar potential is 4.89 kilowatt-hours per square meter per day, the annual average biomass is 0.008 metric tonnes per day, the nominal rate of discount is 12.5%, and the inflation rate is 5.75%. The project's lifetime is 25 years. This research examines alternative energy sources that use storage cells to provide an appropriate solution that may satisfy local energy demand while simultaneously reducing cost considerations (such as cost of energy, net present cost, and operations and maintenance) and emissions. Diesel generators are seldom used until unconventional supplies, supported by storage cells, are unable to meet peak demand. HOMER conducts many simulations in this research to get the best outcomes for High Renewable Energy Systems (HRES).

### Optimization Result

After giving the essential input parameters outlined in earlier portions of the study, all six HRES setups with and without battery storage and a diesel generator are simulated based on demand load and locally available RES. The following parameters are used to compare the simulated optimum configurations: NPC, LCOE, capacity shortfall, surplus electricity generation, $CO_2$ emissions, renewable portion, operational cost, fuel consumption, and initial capital cost, with a focus on LCOE.

Table 5 displays the overall optimized HRES configuration and simulation findings for every stated situation.

The LCOE, NPC, initial capital cost (ICC), and operating cost (OC) of all the cases with and without storage are shown in Figs. 7 and 8.

### Net Present Cost

The net present cost (or life-cycle cost) of a Component is the present value of all the costs of installing and operating the Component over the project lifetime, minus the present value of all the revenues that it earns over the project lifetime.

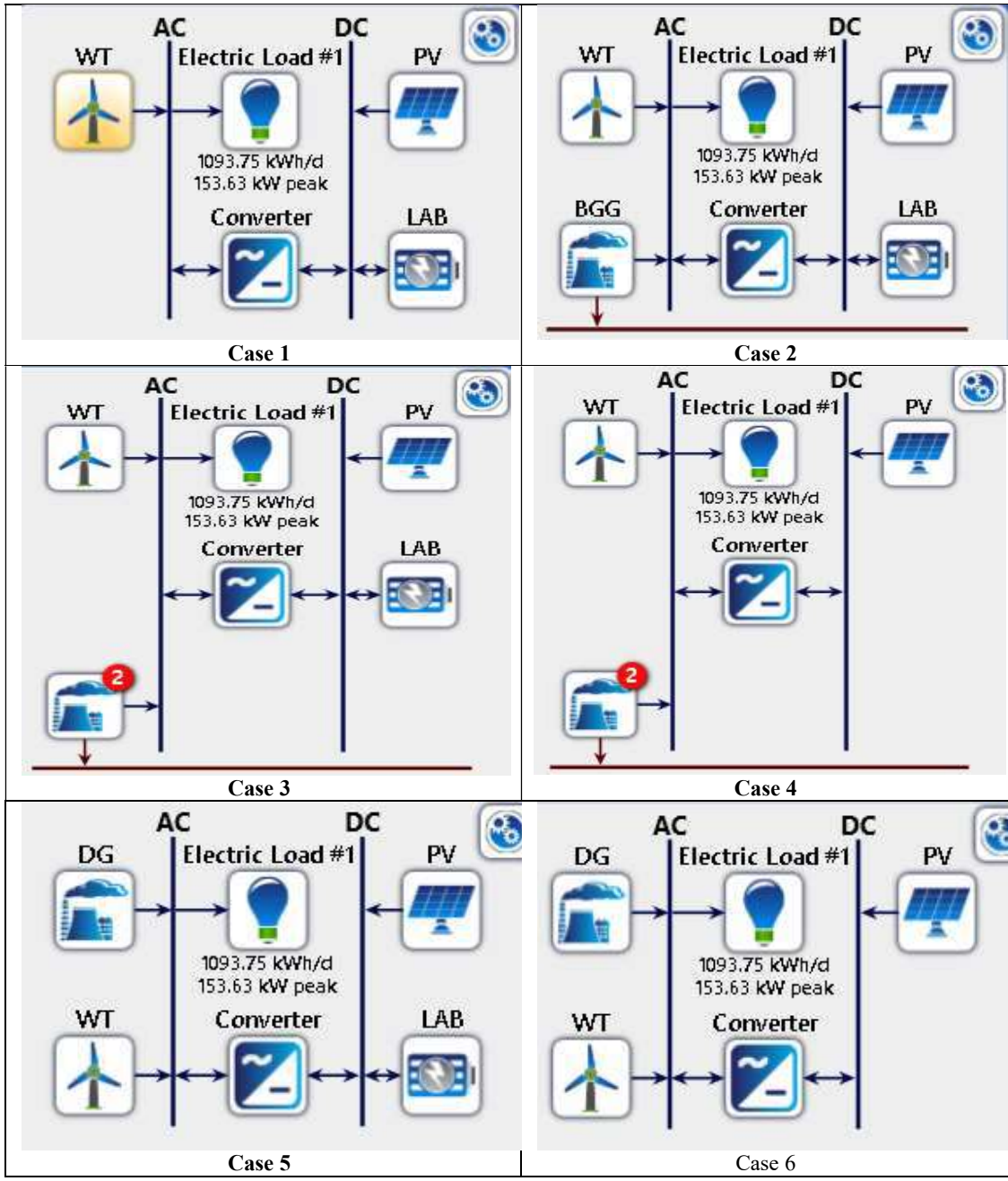


Fig. 16: Homer design model configuration.

**Levelized Cost of Energy**

LCOE measures lifetime costs divided by energy production, which also determines the present value of a power plant's total operating costs over an expected lifetime and compares diverse technologies, such as wind, solar, and bioenergy, with varying life periods, project sizes, capital costs, risk, return, and capacity.

$$LCOE = \frac{\sum_{t=1}^{n} \frac{I_t + M_t + F_t}{(1+r)^t}}{\sum_{t=1}^{n} \frac{E_t}{(1+r)^t}}$$

$I_t$ = Investment expenditures in year t

$M_t$ = Operations and maintenance expenditures in year t

Table 5: Cost of each component.

| Tola Dhumnadih Village Techno -Commercial Evaluation for Different HRES | | | | | | | |
|---|---|---|---|---|---|---|---|
| Case | | Case 1 | Case 2 | Case 3 | Case 4 | Case 5 | Case 6 |
| HRES Configuration | Units | PV - WT - LAB | PV - WT - BGG - LAB | PV - WT - BGG - DG - LAB | PV - WT - BGG -DG | PV - WT- DG - LAB | PV-WT-DG |
| Results | | | | | | | |
| PV | (KW) | 415 | 427 | 131 | 283 | 133 | 282 |
| WT | (Qty) | 183 | 186 | 130 | 235 | 125 | 238 |
| DG | (KW) | - | - | 100 | 150 | 100 | 150 |
| BGG | (KW) | - | 0.4 | 0.2 | 2 | - | - |
| Converter | (KW) | 141 | 154 | 58.0 | 46.9 | 55.7 | 39.6 |
| Battery | (Qty) | 2820 | 2700 | 540 | - | 530 | - |
| NPC | ($) | 2.30M | 2.27M | 1.71M | 2.92M | 1.71M | 2.94M |
| COE | ($) | 0.467 | 0.461 | 0.347 | 0.594 | 0.348 | 0.598 |
| Operating Cost | ($/yr) | 80002 | 78933 | 101332 | 190435 | 102259 | 192074 |
| Initial Capital | ($) | 1.31M | 1.30M | 457223 | 574475 | 449470 | 573878 |
| Renewable Fraction | (%) | 100 | 100 | 62.0 | 32.6 | 60.7 | 32 |
| Emission Carbon Dioxide | (kg/yr) | - | 5.38 | 118214 | 243424 | 122032 | 245597 |

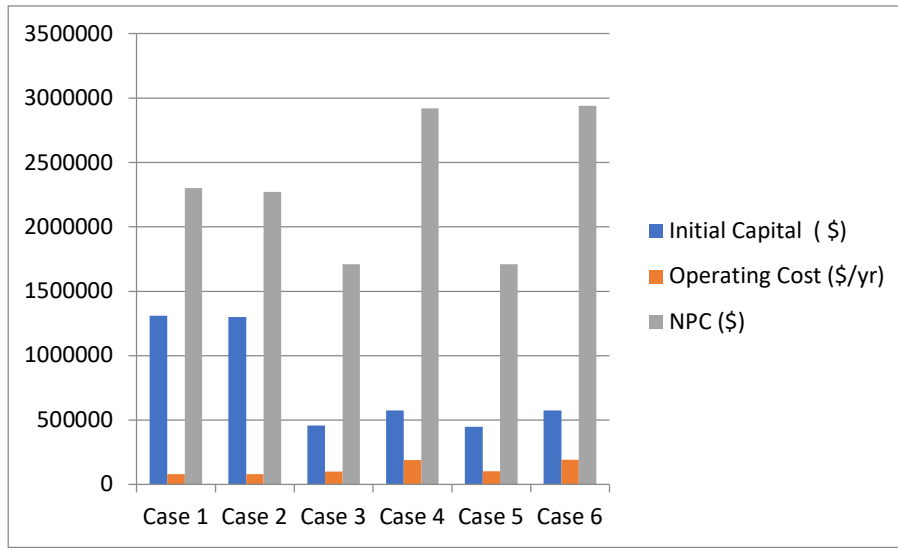


Fig. 17: Net present cost of all HRES cases.

$F_t$ = Fuel expenditures in year t

$E_t$ = Electricity generation in year t

$r$ = Discount rate

$n$ = Life of the system

The cost analysis for each scenario including initial capital cost (ICC), operating cost (OC), and net current cost is displayed in Fig. 17. The HRES setup with solar, wind, diesel generator, and battery in Case 5 has the lowest ICC of $449470, whereas Case 1 has the highest ICC of $1310000. Similar calculations are made for the operating costs of each scenario; scenario 6 of the HRES design, which includes a diesel generator, solar panel, and wind turbine, has the highest operating cost (OC). $/yr 192074 lowest OC in case 2 solar, wind, biomass generator and battery $/yr 78933. The NPC of all the instances presented in Fig. 17. and the lowest net present cost (NPC) observed were $1710000 in case 3 of the HRES configuration of solar, wind, biomass generator, diesel generator, and battery, and the highest net present cost was $2940000 in case 6 of the HRES configuration of solar, wind, and diesel generator.

The COE for each instance is displayed in Fig. 18. Case 3 of the HRES configuration, which consists of a solar, wind, biomass generator, diesel generator, and battery, had

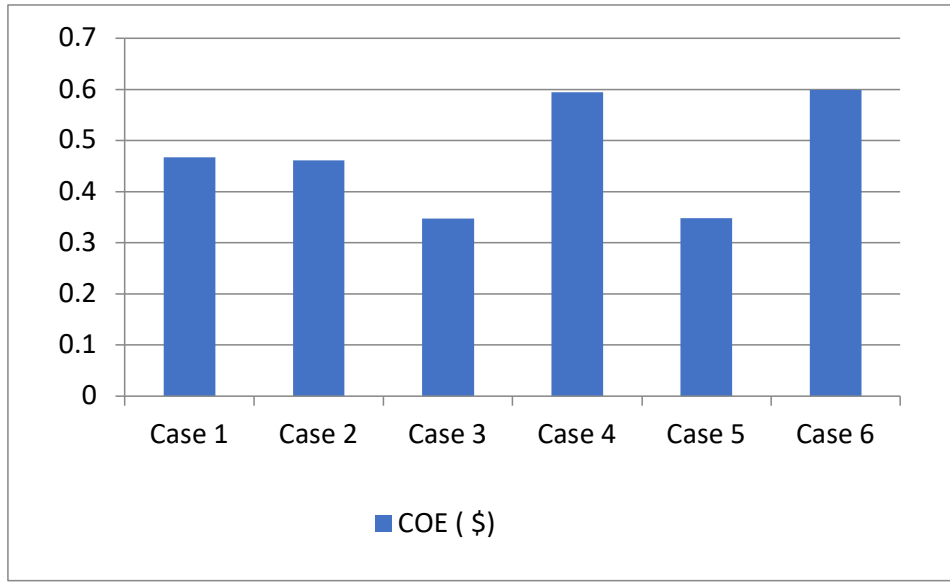


Fig. 18: COE all HRES cases.

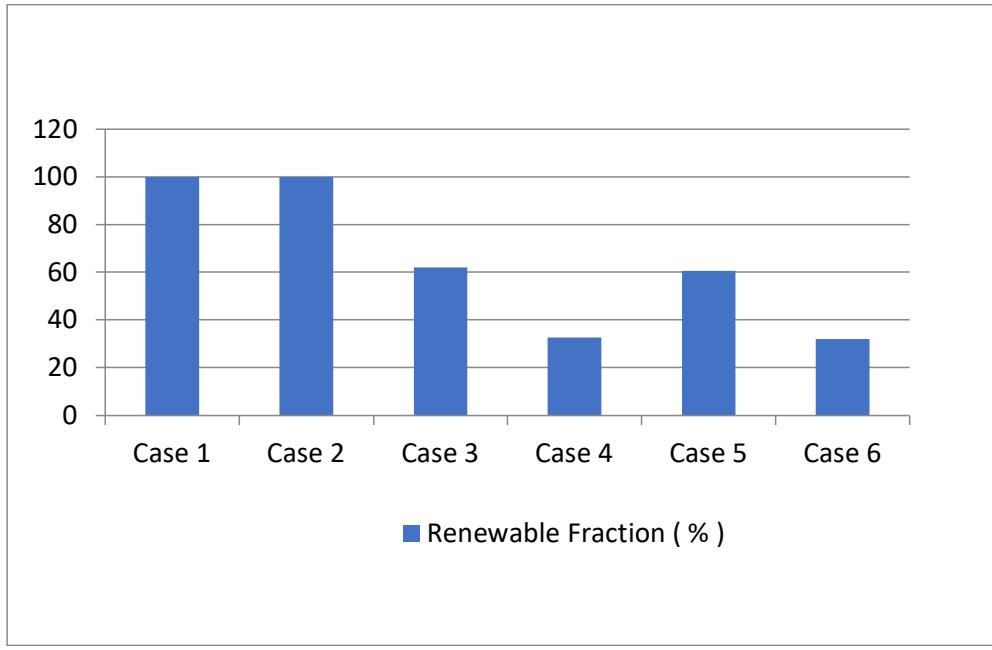


Fig. 19: Renewable fraction.

the lowest COE ($0.347). In contrast, Case 6 of the HRES configuration, which consists of a solar, wind, and diesel generator, had the highest COE ($0.598).

The renewable fraction is the proportion of the energy given to the load that came from renewable energy sources. The RF for each case is shown in Fig. 19 is displayed and observed that the integrated system's total supply power from renewable sources supplied 100% of the electricity generated from solar power, wind power, and bioenergy. In contrast, wherever we used the diesel generator at that moment, renewable energy penetration decreased.

### Monthly Electric Production from all the sources of Electricity Generation

The monthly power output from all case arrangements is given in Fig. 20-25, which demonstrates that solar PV generation

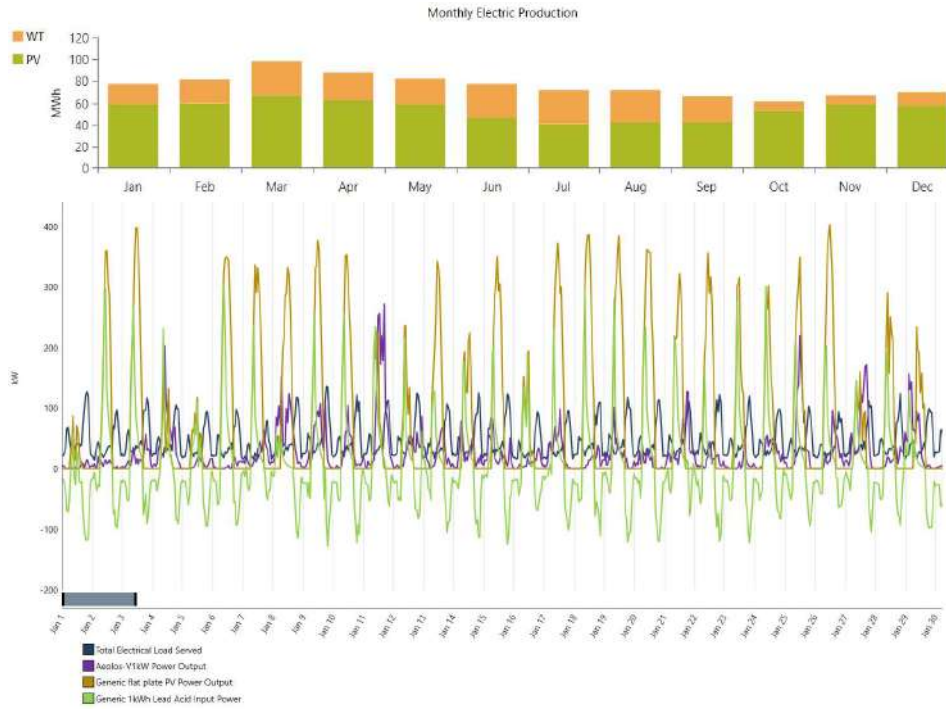


Fig. 20: Case 1 - The monthly energy generation & Electricity generation Pattern from different components of the optimized hybrid system with battery (PV/WT).

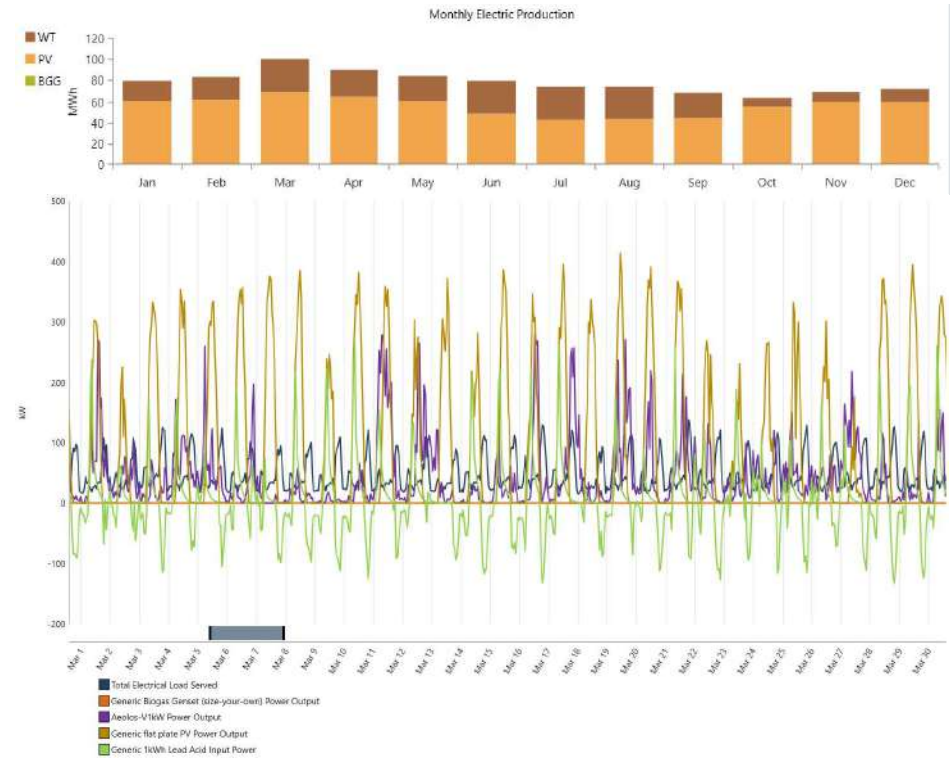


Fig. 21: Case 2 - The monthly energy generation from different components of the optimized hybrid system with battery (PV/WT/BGG).

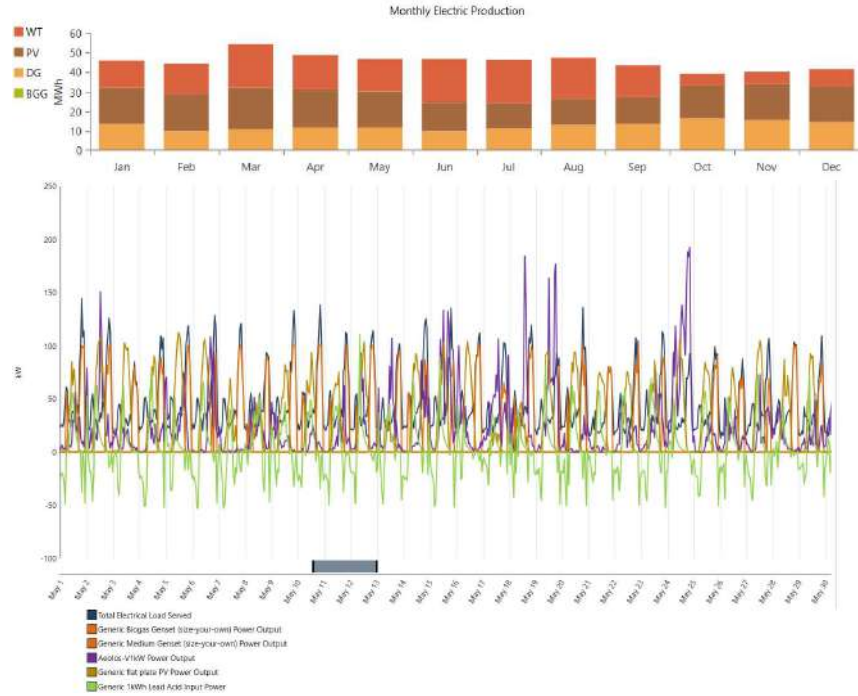


Fig. 22: Case 3 - The monthly energy generation from different components of the optimized hybrid system with battery (PV/WT/BGG/DG).

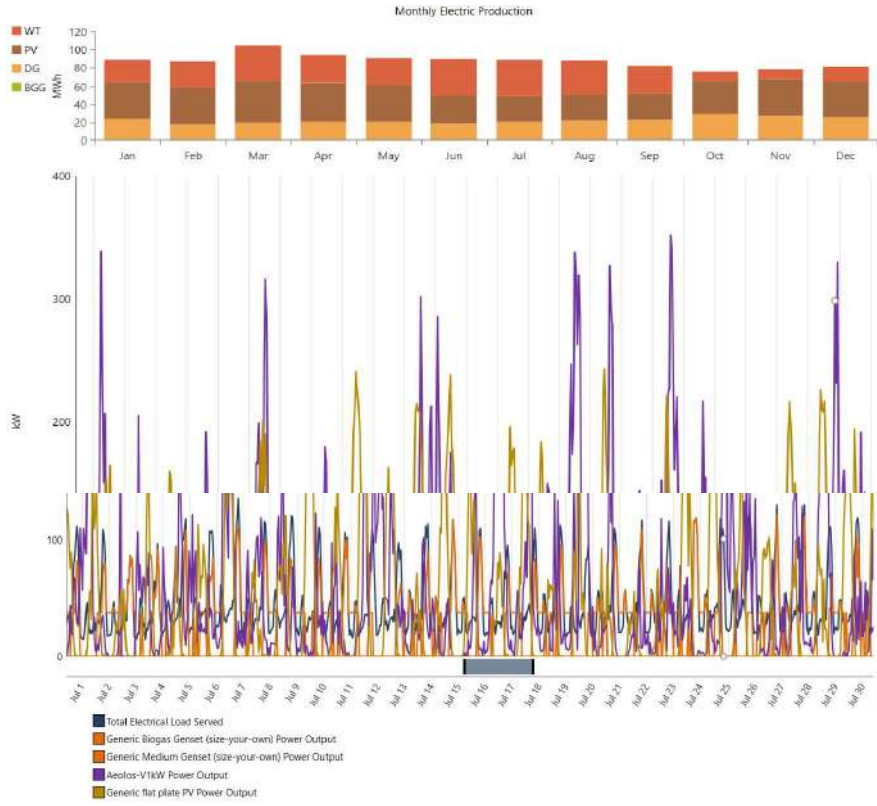


Fig. 23: Case 4 - The monthly energy generation from different components of the optimized hybrid system without battery (PV/WT/BGG/DG).

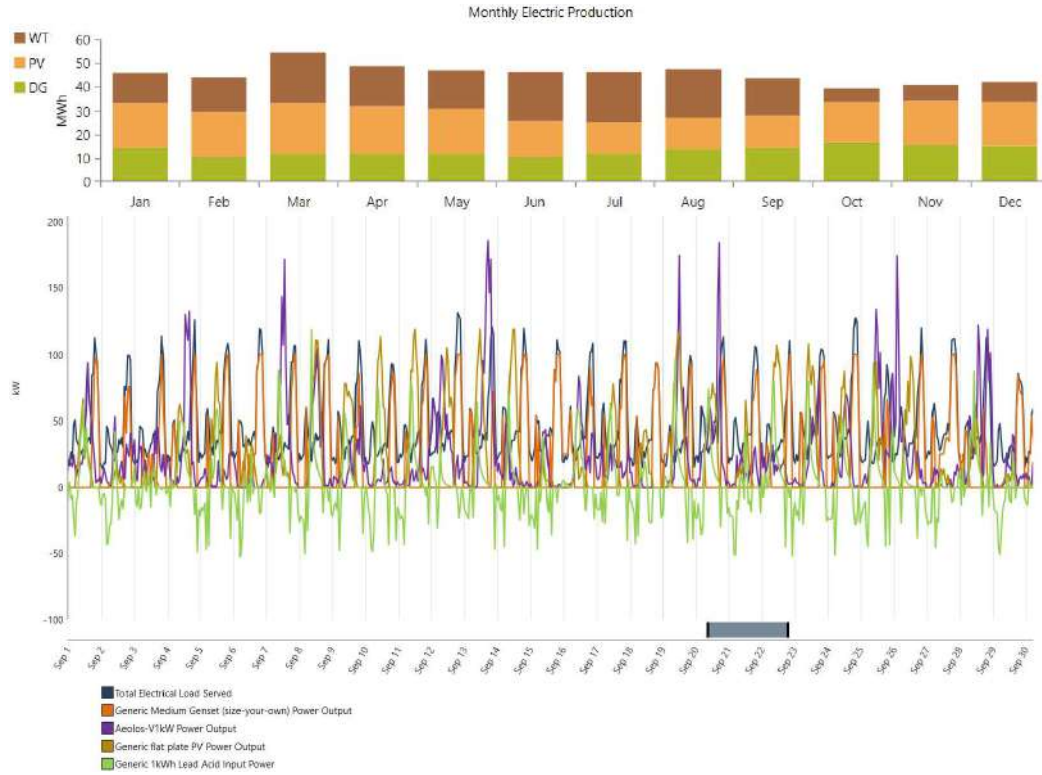


Fig. 24: Case 5 - The monthly energy generation from different components of the optimized hybrid system with battery (PV/WT/DG).

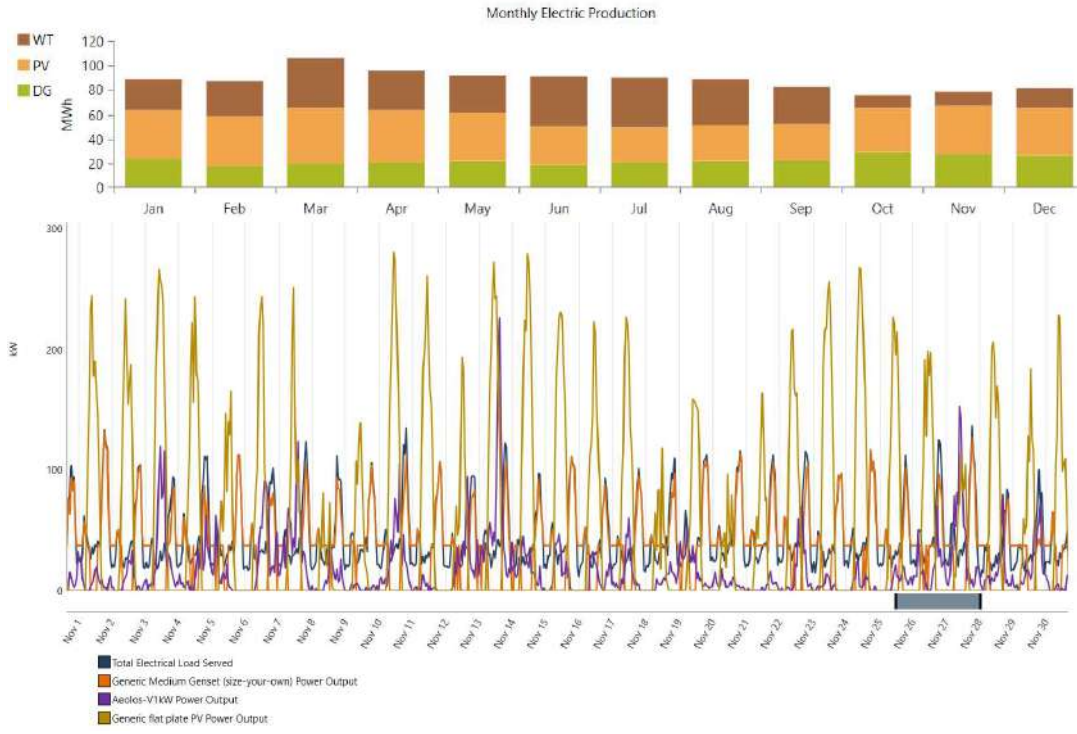


Fig. 25: Case 6 - The monthly energy generation from different components of the optimized hybrid system without battery (PV/WT/DG).

occurs at least in July owing to wet seasons, overcast circumstances, low solar radiation, greater temperatures, and so on. The maximum occurred in November because of favorable sun radiation and low temperatures. Also, wind generation was highest in July and minimum in November due to the climate in India. Furthermore, the creation of excess biomass generators is based on the availability of biomass in the individual village, as well as the usage of diesel generators to determine the best ideal option. Case1 Fig. 20. Solar PV accounts for 71% of electric output, with wind accounting for 29%, unmet electric load at 0.02%, and capacity shortfall at 0.0982%. Fig. 21 depicts an electric production contribution of 71.2% from solar PV, 28.7% from wind, 0.1% from biomass, an unmet electric load of 0.05% and a capacity shortfall of 0.1%. Fig. 22 depicts electric production with a solar PV contribution of 37.4%, wind at 34.5%, diesel generator at 27.9%, biomass at 0.17%, unmet electric load at 0.017%, and capacity shortfall at 0.05%. Fig. 23 depicts electric output with a 42% contribution from solar PV, 32.3% from wind, and 25.6% from diesel generators, with no unmet electric load and a capacity shortfall. Fig. 24 depicts solar PV's 38% contribution to electric output, wind's 33.2%, diesel generator's 28.8%, unmet electric load's 0.026%, and a capacity shortfall of 0.07%. Fig. 25 depicts an electric output contribution of 41.6% from solar PV, 32.6% from wind, and 25.7% from diesel generators, with no unmet electric load and a capacity shortfall.

## CONCLUSION AND FUTURE SCOPE

This study examined six distinct examples of HRES with and without batteries and diesel-based power sources in Tola Dhumnadih village, Kishanganj district, Bihar, India. The study's conclusions are consistent with the techno-economic analysis.

- The location in which all the resources are available to configure hybrid renewable energy with a yearly average solar radiation of 4.89 kWh/m2/day, an average monthly wind speed of 4.39 m/s at 10m height, and surplus available biomass potential in a specific village area of 8.12 kg/day with an annual average temperature of 25.52°C.
- After calculation of several combinations of different cases, it is found that the PV-WT - BGG - DG – LAB is the optimal option in terms of cost with a capacity of solar PV (131 KW), wind (130 no's), biomass generator (0.2 KW), diesel generator (100 KW), battery (540 no's), and converter (58.0 KW).
- The best cost-effective option of Case 3 is that the COE is $0.347 per kWh with a net present cost of $1710000, which is 72% less than Case 6 of the PV-WT- BGG –DG HRES configuration.
- Cases 1 and 2 with 100% renewable penetration do not have any carbon dioxide emissions, whereas the energy produced by diesel generators has significant emissions. The winning case 3 emission was more than half carbon monoxide compared with case 6.

The suggested hybrid system has proven technical and economic feasibility for electrifying rural communities in Bihar. The practical application of underutilized resources to accomplish India's renewable energy objective while also providing jobs for local populations. Furthermore, such studies include broad recommendations for best practices or proposals for future biomass-based study plans/projects in Bihar. Further simulations can be performed with sensitivity scenarios to determine the cost variance concerning the inflation rate of all the components.

## NOMENCLATURE

| | |
|---|---|
| HOMER | Hybrid Optimization Model for Electric Renewable |
| IRENA | International Renewable Energy Agency |
| HRES | Hybrid Renewable Energy System |
| NEPRA | National Electric Power Regulatory Authority |
| NPC | Net Present Cost |
| SWERA | Solar and Wind Energy Resource Assessment |
| MSW | Municipal Solid Waste |
| COE | Cost of Electricity |
| SIF | Solar Irradiance Factor |
| PV | Photo Voltaic |
| WT | Wind Turbine |
| DG | Diesel Generator |
| BGG | Biogas/ Biomass Generator |
| LAB | Battery |
| C | Converter |
| RET | Renewable Energy Technology |
| RES | Renewable Energy Sources |
| HES | Hybrid Energy System |
| TNPC | Total Net Present Cost |
| RF | Renewable Fraction |

## REFERENCES

Ahmad, J., Imran, M., Khalid, A., Iqbal, W., Ashraf, S. R., Adnan, M. and Khokhar, K. S. 2018. Techno economic analysis of a wind-photovoltaic-biomass hybrid renewable energy system for rural electrification: A case study of Kallar Kahar. Energy, 148: 208-234. doi: 10.1016/j.energy.2018.01.133.

Ajlan, A., Tan, C. W. and Abdilahi, A. M. 2017. Assessment of environmental and economic perspectives for renewable-based

hybrid power system in Yemen. Renewable and Sustainable Energy Reviews, 75: 559-570. doi: 10.1016/j.rser.2016.11.024.

Akinyele, D. 2017. Techno-economic design and performance analysis of nanogrid systems for households in energy-poor villages. Sustainable Cities and Society, 34: 335-357. doi: 10.1016/j.scs.2017.07.004.

Baghdadi, F., Mohammedi, K., Diaf, S. and Behar, O. 2015. Feasibility study and energy conversion analysis of stand-alone hybrid renewable energy system. Energy Conversion and Management, 105: 471-479.

Balamurugan, P., Ashok, S. and Jose, T. L. 2009. Optimal operation of biomass/wind/PV hybrid energy system for rural areas. International Journal of Green Energy, 6(1): 104-116. doi: 10.1080/15435070802701892.

Balamurugan, P., Ashok, S. and Jose, T. L. 2011. An optimal hybrid wind-biomass gasifier system for rural areas. Energy Sources, Part A: Recovery, Utilization, and Environmental Effects, 33(9): 823-832. oi: 10.1080/15567030903117646.

Balcombe, P., Rigby, D. and Azapagic, A. 2013. Motivations and barriers associated with adopting microgeneration energy technologies in the UK. Renewable and Sustainable Energy Reviews, 22: 655-666. doi: 10.1016/j.rser.2013.02.012.

Bandara, K., Sweet, T. and Ekanayake, J. 2012. Photovoltaic applications for off-grid electrification using novel multi-level inverter technology with energy storage. Renewable Energy, 37(1): 82-88. doi: 10.1016/j.renene.2011.05.036.

Bansal, M., Saini, R. P. and Khatod, D. K. 2013. Development of cooking sector in rural areas in India-A review. Renewable and Sustainable Energy Reviews, 17: 44-53. doi: 10.1016/j.renene.2011.05.036.

Bhatt, A., Sharma, M. P. and Saini, R. P. 2016. Feasibility and sensitivity analysis of an off-grid micro hydro–photovoltaic–biomass and biogas–diesel–battery hybrid energy system for a remote area in Uttarakhand state, India. Renewable and Sustainable Energy Reviews, 61: 53-69. doi: 10.1016/j.rser.2016.03.030.

Bhuvan 2024. Gateway to Indian Earth Observation. Accessed: Jan. 20, 2024. [Online]. Available: https://bhuvan-app1.nrsc.gov.in/bioenergy/home/

Castellanos, J. G., Walker, M., Poggio, D., Pourkashanian, M. and Nimmo, W. 2015. Modelling an off-grid integrated renewable energy system for rural electrification in India using photovoltaics and anaerobic digestion. Renewable Energy, 74: 390-398. doi: 10.1016/j.renene.2014.08.055.

Census 2011 India. Accessed: Jan. 20, 2024. [Online]. Available: https://www.census2011.co.in/

Chambon, C. L., Karia, T., Sandwell, P. and Hallett, J. P. 2020. Techno-economic assessment of biomass gasification-based mini-grids for productive energy applications: The case of rural India. Renewable Energy, 154: 432-444. doi: 10.1016/j.renene.2020.03.002.

Chandel, S. S., Shrivastva, R., Sharma, V. and Ramasamy, P. 2016. Overview of the initiatives in renewable energy sector under the national action plan on climate change in India. Renewable and Sustainable Energy Reviews, 54: 866-873. doi: 10.1016/j.rser.2015.10.057.

Chauhan, A. and Saini, R. P. 2016. Discrete harmony search based size optimization of Integrated Renewable Energy System for remote rural areas of Uttarakhand state in India. Renewable Energy, 94: 587-604. doi: 10.1016/j.renene.2016.03.079.

Dawoud, S. M., Lin, X. N., Sun, J. W., Okba, M. I., Khalid, M. S. and Waqar, A. 2015. Feasibility study of isolated PV-wind hybrid system in Egypt. Advanced Materials Research, 1092: 145-151. doi: 10.4028/www.scientific.net/AMR.1092-1093.145.

Elhadidy, M. A. and Shaahid, S. M. 2000. Parametric study of hybrid (wind+ solar+ diesel) power generating systems. Renewable energy, 21(2): 129-139.

Elhadidy, M. A. and Shaahid, S. M. 2004. Promoting applications of hybrid (wind+ photovoltaic+ diesel+ battery) power systems in hot regions. Renewable Energy, 29(4): 517-528.

Forough, A. B. and Roshandel, R. 2017. Multi objective receding horizon optimization for optimal scheduling of hybrid renewable energy system. Energy and Buildings, 150: 583-597. doi: 10.1016/j.enbuild.2017.06.031.

Gan, L. K., Shek, J. K. and Mueller, M. A. 2015. Hybrid wind–photovoltaic–diesel–battery system sizing tool development using empirical approach, life-cycle cost and performance analysis: A case study in Scotland. Energy Conversion and Management, 106: 479-494. doi: 10.1016/j.enconman.2015.09.029.

Google Maps 2024. Tola Dhumnadih - Google Maps. Accessed: Jan. 21, 2024. [Online]. Available: https://maps.app.goo.gl/PcdaZjLD4Sbb5VQE9

Gupta, S. K. and Purohit, P. 2013. Renewable energy certificate mechanism in India: A preliminary assessment. Renewable and Sustainable Energy Reviews, 22: 380-392. doi: 10.1016/j.rser.2013.01.044.

Harish, V. S. K. V. and Kumar, A. 2014. Demand side management in India: action plan, policies and regulations. Renewable and Sustainable Energy Reviews, 33: 613-624. doi: 10.1016/j.rser.2014.02.021.

Hoicka, C. E. and Rowlands, I. H. 2011. Solar and wind resource complementarity: Advancing options for renewable electricity integration in Ontario, Canada. Renewable energy, 36(1): 97-107. doi: 10.1016/j.renene.2010.06.004.

HOMER Pro - Microgrid Software for Designing Optimized Hybrid Microgrids. Accessed: Jan. 21, 2024. [Online]. Available: https://www.homerenergy.com/products/pro/index.html

Indian Village Directory 2024. Indian Village Directory. Accessed: Jan. 21, 2024. [Online]. Available: https://villageinfo.in/

Ismail, M. S., Moghavvemi, M. and Mahlia, T. M. I. 2013. Energy trends in Palestinian territories of West Bank and Gaza Strip: Possibilities for reducing the reliance on external energy sources. Renewable and Sustainable Energy Reviews, 28: 117-129. doi: 10.1016/j.rser.2013.07.047.

Kanase-Patil, A. B., Saini, R. P. and Sharma, M. P. 2010. Integrated renewable energy systems for off grid rural electrification of remote area. Renewable Energy, 35(6): 1342-1349. doi: 10.1016/j.renene.2009.10.005.

Karki, S., Mann, M. D. and Salehfar, H. 2008. Environmental implications of renewable distributed generation technologies in rural electrification. Energy Sources, Part B, 3(2): 186-195. doi: 10.1080/15567240601057057.

Khan, M. J., Yadav, A. K. and Mathew, L. 2017. Techno economic feasibility analysis of different combinations of PV-Wind-Diesel-Battery hybrid system for telecommunication applications in different cities of Punjab, India. Renewable and Sustainable Energy Reviews, 76: 577-607.

Khare, V., Nema, S. and Baredar, P. 2013. Status of solar wind renewable energy in India. Renewable and Sustainable Energy Reviews, 27: 1-10. doi: 10.1016/j.rser.2013.06.018.

Kumaravel, S. and Ashok, S. 2015. Optimal power management controller for a stand-alone solar PV/wind/battery hybrid energy system. Energy Sources, Part A: Recovery, Utilization, and Environmental Effects, 37(4): 407-415. doi: 10.1080/15567036.2011.576414.

Lau, K. Y., Yousof, M. F. M., Arshad, S. N. M., Anwari, M. and Yatim, A. H. M. 2010. Performance analysis of hybrid photovoltaic/diesel energy system under Malaysian conditions. Energy, 35(8): 3245-3255. doi: 10.1016/j.energy.2010.04.008.

Li, C., Zhou, D., Wang, H., Lu, Y. and Li, D. 2020. Techno-economic performance study of stand-alone wind/diesel/battery hybrid system with different battery technologies in the cold region of China. Energy, 192: 116702. doi: 10.1016/j.energy.2019.116702.

Ma, T., Yang, H. and Lu, L. 2013. Performance evaluation of a stand-alone photovoltaic system on an isolated island in Hong Kong. Applied Energy, 112: 663-672. doi: 10.1016/j.apenergy.2012.12.004.

Maherchandani, J. K., Agarwal, C. and Sahi, M. 2012. Economic feasibility of hybrid biomass/PV/wind system for remote villages using HOMER. International Journal of Advanced Research in Electrical, Electronics and Instrumentation Engineering, 1(2): 49-53.

Malik, P., Awasthi, M. and Sinha, S. 2019. Analysis of sensitive parameters influencing a SPV/WT/Biomass/Battery based hybrid system. In 2019 8th International Conference on Power Systems

Malik, P., Awasthi, M. and Sinha, S. 2020. Study on an existing PV/wind hybrid system using biomass gasifier for energy generation. Pollution, 6(2): 325-336. doi: 10.22059/poll.2020.293034.719.

Malik, P., Awasthi, M. and Sinha, S. 2021. Biomass based gaseous fuel for hybrid renewable energy systems: An overview and future research opportunities. International Journal of Energy Research, 45(3): 3464-3494. doi: 10.1002/er.6061.

Malik, P., Awasthi, M. and Sinha, S. 2021. Techno-economic and environmental analysis of biomass-based hybrid energy systems: A case study of a Western Himalayan state in India. Sustainable Energy Technologies and Assessments, 45: 101189.

Mandal, S., Das, B. K. and Hoque, N. 2018. Optimum sizing of a stand-alone hybrid energy system for rural electrification in Bangladesh. Journal of Cleaner Production, 200: 12-27. doi: 10.1016/j.jclepro.2018.07.257.

Mekhilef, S., Faramarzi, S. Z., Saidur, R. and Salam, Z. 2013. The application of solar technologies for sustainable development of agricultural sector. Renewable and sustainable energy reviews, 18: 583-594. doi: 10.1016/j.rser.2012.10.049.

Mekhilef, S., Saidur, R. and Kamalisarvestani, M. 2012. Effect of dust, humidity and air velocity on efficiency of photovoltaic cells. Renewable and sustainable energy reviews, 16(5): 2920-2925. doi: 10.1016/j.rser.2012.02.012.

Meyar-Naimi, H. and Vaez-Zadeh, S. 2012. Sustainable development-based energy policy making frameworks, a critical review. Energy Policy, 43: 351-361. doi: 10.1016/j.enpol.2012.01.012.

Moghavvemi, M., Ismail, M. S., Murali, B., Yang, S. S., Attaran, A. and Moghavvemi, S. 2013. Development and optimization of a PV/diesel hybrid supply system for remote controlled commercial large scale FM transmitters. Energy Conversion and Management, 75: 542-551. doi: 10.1016/j.enconman.2013.07.011.

Nema, S., Nema, R. K. and Agnihotri, G. 2010. Matlab/simulink based study of photovoltaic cells/modules/array and their experimental verification. International journal of Energy and Environment, 1(3): 487-500.

Neves, D., Silva, C. A. and Connors, S. 2014. Design and implementation of hybrid renewable energy systems on micro-communities: A review on case studies. Renewable and Sustainable Energy. doi: 10.1016/j.rser.2013.12.047.

Notton, G., Muselli, M. and Louche, A. 1996. Autonomous hybrid photovoltaic power plant using a back-up generator: a case study in a Mediterranean Island. Renewable Energy, 7(4): 371-391.

NSRDB 2024. NSRDB. Accessed: Jan. 20, 2024. [Online]. Available: https://nsrdb.nrel.gov/

Ozden, E. and Tari, I. 2016. Energy-exergy and economic analyses of a hybrid solar–hydrogen renewable energy system in Ankara, Turkey. Applied Thermal Engineering, 99: 169-178.

Padrón, I., Avila, D., Marichal, G. N. and Rodríguez, J. A. 2019. Assessment of Hybrid Renewable Energy Systems to supplied energy to Autonomous Desalination Systems in two islands of the Canary Archipelago. Renewable and Sustainable Energy Reviews, 101: 221-230. doi: 10.1016/j.rser.2018.11.009.

Patil, A. A., Arora, R., Arora, R. and Sridhara, S. N. 2023. Performance analysis of hybrid renewable energy using homer software. Tuijin Jishu/Journal Propuls. Technol., 44(3): 2832-2853.

Perera, A. T. D., Attalage, R. A., Perera, K. K. C. K. and Dassanayake, V. P. C. 2013. Designing standalone hybrid energy systems minimizing initial investment, life cycle cost and pollutant emission. Energy, 54: 220-230. doi: 10.1016/j.energy.2013.03.028

Rad, M. A. V., Ghasempour, R., Rahdan, P., Mousavi, S. and Arastounia, M. 2020. Techno-economic analysis of a hybrid power system based on the cost-effective hydrogen production method for rural electrification, a case study in Iran. Energy, 190: 116421. doi: 10.1016/j.energy.2019.116421.

Rahman, M. M., Hasan, M. M., Paatero, J. V. and Lahdelma, R. 2014. Hybrid application of biogas and solar resources to fulfill household energy needs: A potentially viable option in rural areas of developing countries. Renewable Energy, 68: 35-45.

Salehin, S., Islam, A. S., Hoque, R., Rahman, M., Hoque, A. and Manna, E. 2014. Optimized model of a solar PV-biogas-diesel hybrid energy system for Adorsho Char Island, Bangladesh. In 2014 3rd International Conference on the Developments in Renewable Energy Technology (ICDRET) (1-6). IEEE.

Saubhagya Dashboard. Accessed: Jan. 20, 2024. [Online]. Available: https://saubhagya.gov.in/

Sawle, Y., Gupta, S. C. and Bohre, A. K. 2018. Socio-techno-economic design of hybrid renewable energy system using optimization techniques. Renewable energy, 119: 459-472. doi: 10.1016/j.renene.2017.11.058.

Sawle, Y., Jain, S., Babu, S., Nair, A. R. and Khan, B. 2021. Prefeasibility economic and sensitivity assessment of hybrid renewable energy system. Ieee Access, 9: 28260-28271. doi: 10.1109/ACCESS.2021.3058517

Shaahid, S. M. and El-Amin, I. 2009. Techno-economic evaluation of off-grid hybrid photovoltaic-diesel-battery power systems for rural electrification in Saudi Arabia-A way forward for sustainable development. Renewable and sustainable energy reviews, 13(3): 625-633. doi: 10.1016/j.rser.2007.11.017.

Shahzad, M. K., Zahid, A., ur Rashid, T., Rehan, M. A., Ali, M. and Ahmad, M. 2017. Techno-economic feasibility analysis of a solar-biomass off grid system for the electrification of remote rural areas in Pakistan using HOMER software. Renewable energy, 106: 264-273. doi: 10.1016/j.renene.2017.01.033.

Shi, Z., Wang, R. and Zhang, T. 2015. Multi-objective optimal design of hybrid renewable energy systems using preference-inspired coevolutionary approach. Solar energy, 118: 96-106. doi: 10.1016/j.solener.2015.03.052.

Sigarchian, S. G., Paleta, R., Malmquist, A. and Pina, A. 2015. Feasibility study of using a biogas engine as backup in a decentralzed hybrid (PV/wind/battery) power generation system-Case study Kenya. Energy, 90: 1830-1841. doii: 10.1016/j.energy.2015.07.008.

Taele, B. M., Mokhutšoane, L., Hapazari, I., Tlali, S. B. and Senatla, M. 2012. Grid electrification challenges, photovoltaic electrification progress and energy sustainability in Lesotho. Renewable and Sustainable Energy Reviews, 16(1): 973-980. doi: 10.1016/j.rser.2011.09.019.

Vendoti, S., Muralidhar, M. and Kiranmayi, R. 2021. Techno-economic analysis of off-grid solar/wind/biogas/biomass/fuel cell/battery system for electrification in a cluster of villages by HOMER software. Environment, Development and Sustainability, 23(1): 351-372. doi: 10.1007/s10668-019-00583-2.

Verma, A., Biswas, S. and Ahmad, S. Y. 2015. Techno-financial analysis of energy access through hybrid system with solar PV under the various rural community models for State of Uttarakhand, India. Smart Grid and Renewable Energy, 6(4): 75-94.

Wikipedia 2024. File:Mean Wind Speed Map India.png - Wikipedia. Accessed: Jan. 20, 2024. [Online]. Available: https://en.m.wikipedia.org/wiki/File:Mean_Wind_Speed_Map_India.png

Yılmaz, S. and Selim, H. 2013. A review on the methods for biomass to energy conversion systems design. Renewable and Sustainable Energy Reviews, 25: 420-430. doi: 10.1016/j.rser.2013.05.015.

Yimen, N., Hamandjoda, O., Meva'a, L., Ndzana, B. and Nganhou, J. 2018. Analyzing of a photovoltaic/wind/biogas/pumped-hydro off-grid hybrid system for rural electrification in Sub-Saharan Africa—Case study of Djoundé in Northern Cameroon. Energies, 11(10): 2644. doi: 10.3390/en11102644.

## ORCID DETAILS OF THE AUTHORS

Anant Arun Patil https://orcid.org/0009-0004-2339-736X
Rajesh Arora https://orcid.org/0000-0001-9234-4115
Ranjana Arora https://orcid.org/0000-0002-8912-9067
S. N. Sridhara https://orcid.org/0000-0002-4393-6314

Nature Environment and Pollution Technology
An International Quarterly Scientific Journal

p-ISSN: 0972-6268
(Print copies up to 2016)
e-ISSN: 2395-3454

Vol. 23 | No. 3 | pp. 1285-1299 | 2024

Original Research Paper

https://doi.org/10.46488/NEPT.2024.v23i03.004

Open Access Journal

# Energy Intervention Model in Public Education Institutions that Contribute to Sustainable Development

**J. Velez-Ramos*†, D. Mayorga** and F. Gonzalez****

*CORCiEM Corporation, Monteria, Colombia, Faculty of Engineering University of Cartagena, Cartagena, Colombia

**EMA Corporation, Bogotá, Colombia

†Corresponding author: J. Velez-Ramos; jeimy.velez.ramos@gmail.com

**Nat. Env. & Poll. Tech.**
**Website: www.neptjournal.com**

*Received:* 16-12-2023
*Revised:* 29-01-2024
*Accepted:* 01-02-2024

**Key Words:**
Energy efficient city
Renewable energy
Photovoltaic energy
Sustainable development

## ABSTRACT

Sustainable development is a global policy that requires the collective effort of the actors present in each territory. In this sense, an energy renewal intervention model is presented at the Juan XXIII Educational Institution in the city of Monteria, Córdoba, Colombia, which results from alliances between international, national, and regional actors, becoming a reference that could serve as a basis. To be replicated in other institutions with characteristics similar to those described in this case. The model generally describes the entire process carried out in the intervention and focuses on the benefits generated for the educational community. Among the main results, the increase in thermal, lighting, and acoustic comfort of the educational community stands out, according to a survey and semi-structured interviews carried out. A fact that could be attributed to the perception of increased comfort in the community is the increase in the student population in 2022, going from 1,478 in 2019 to 1,909 in 2022, with a growth of approximately 29%. Energy renovation also resulted in the improvement of the indoor climate of the classrooms (from 35°C to 27°C), the improvement in the physical infrastructure of the institution, the integration of photovoltaic solar energy, and the subsequent reduction of energy cost.

## INTRODUCTION

In the city of Monteria, a city located in the Department of Córdoba in Colombia, temperatures in classrooms are higher than 35 degrees Celsius during the day. In addition, the percentage of humidity can vary between 60 and 80. The conditions of confinement due to the use of poorly ventilated classrooms result in a lack of fresh air and high concentrations of $CO_2$. According to the study done in Australia by Rajagopalan et al. 2022, Children under 15 years of age spend more than six hours a day in school buildings. They are particularly vulnerable to the effects of poor indoor air quality (IAQ). As expressed by Bogdanovica et al. (2020), indoor air quality (IAQ) can be characterized by several metrics, such as the level of pollutants, humidity, temperature, etc. Indoor carbon dioxide concentration is one of the most important indices of IAQ due to its ability to affect the human body. Carbon dioxide concentrations in the air at 1000 ppm can cause poisoning and have been shown to affect the human thought process. Likewise, Johnson et al. (2018) mention that associations have been demonstrated between poor indoor air quality (IAQ) in the classroom and the risk of asthma in schoolchildren, increased absenteeism, and poor performance on standardized tests. According to Bartyzel et al. (2020), intensive ventilation is the only way to remove excess $CO_2$ from indoors.

As expressed by Almeida et al. (2017), knowing that children spend much of their time inside school buildings, and they are more susceptible than adults to the adverse effects of indoor pollutants of their relationship with the volume of air breathed. The weight is greater and their tissues and organs are still growing. The construction and rehabilitation of school buildings must be properly planned to ensure that users have the appropriate conditions to do their work. As noted by Andamon et al. (2023), inadequate ventilation and occupant density in school classrooms result in indoor air quality exceeding the criteria of current standards. According to Chen et al. (2022), Adequate classroom air quality is vital to student health and learning outcomes.

Internal thermal comfort in hot and humid climates is extremely important for schools since inadequate comfort conditions make it difficult for students to concentrate and perform at school. Many Educational Institutions (EI) have an energy-inefficient infrastructure and Juan XXIII was no exception. An example of this was the lack of thermal insulation and airtightness, as well as the installation of inefficient lighting fixtures. This EI, like others, also

suffered from high energy costs. According to Elnabawi & Saber (2022), the high amount of energy used, in addition to its quality, is putting greater pressure on the surrounding environment by increasing the intensity of carbon emissions ($CO_2$) from the construction sector, which increases indoor and outdoor air pollution levels, generating an impact on health risk, energy insecurity, and climate change.

Since the United Nations (UN) declaration of the objectives of sustainable development, territorial dynamics have been generated at all levels aimed at the implementation of actions to achieve sustainability. As Matthey-Junod et al. (2022 ) point out, sustainable energy access interventions are often associated with both economic growth and social development. Affordable, sustainable, reliable, and modern energy, the focus of Sustainable Development Goal 7 (SDG 7), can act as an "engine" to directly influence productivity, income, and health and can promote gender equality, education, and access to other infrastructure services. One of these actions took place in the city of Monteria in response to the problems described in the city's public education institutions and was implemented at the Juan XXIII EI. The entire process arose from the approach of the "Energy Efficient City" management tool of Swiss origin, with a history of 25 years. The Initiative originated in 2018 and to date presents results at a social, environmental, and economic level. To achieve the results and as part of the "Energy Efficient City" approach, the articulation of actions of international entities was necessary, such as the Embassy of Switzerland-State Secretariat for Economic Affairs (SECO); national entities, such as the Mining-Energy Planning Unit (UPME), an entity attached to the Ministry of Mines and Energy of Colombia and the Corporation for Energy and the Environment - CORPOEMA – as well as regional institutions, such as Monteria Mayor's Office.

The Energy Efficient City tool involves municipalities in a continuous process of local energy planning, management, and monitoring aimed at a progressive improvement of local energy performance. This process involves the municipality, its administration, and its elected representatives, as well as a multitude of local partners, including the public, private, academic, and association sectors. The objective is to promote concrete actions and provide local governments and their partners with the means to carry out an integrated, participatory, and sustainable energy policy.

As noted by Rosbach et al. (2013), classroom ventilation was already recognized as an important determinant of indoor air quality at the beginning of the 20th century. According to Dovjak et al. (2020), air pollution in closed spaces can have an impact on the health of students. Likewise, Liébana (2021) mentioned the impact of the real estate stock on energy consumption and environmental pollution in Europe, leading to the development of an instrument that allows classifying the buildings of educational institutions. Thus, analyzing the current state and planning an energy renewal. As expressed by (Mombeuil, 2020) modern societies have realized that their strong dependence on conventional energies has resulted in serious environmental problems, being pollution, climate change, and deforestation being the most cited examples. Additionally, Cabello et al. (2019) evaluated the energy potential of the Colombian Caribbean Coast, corroborating the viability of renewable energy projects in the reconditioning of buildings in cities with warm climates like the city of Monteria.

Based on what was stated in previous studies, energy renewal processes in educational institutions are relevant since the conditions of the spaces in which training activities are carried out have an impact on the health and performance of the community, which suggests a responsibility of the competent authorities regarding variables associated with the comfort of individuals in these spaces. On the other hand, as expressed by Ferrer-Estévez & Chalmeta (2021), humanity is beginning to become aware of the limits of the planet and the unsustainability of its development, which has led to the current state of global emergency. The conditions of the buildings also affect environmental pollution, generating economic and environmental extra costs that can be considerably reduced by carrying out renovation processes in the buildings. Finally, there are many territories that, as in the case of Monteria, have privileged energy potentials to be used that can contribute not only to the health and performance of the educational community but also to the reduction of the impact on the environment and the economy of the institutions.

The scenario described served as a platform for the convergence of actors with common interests in sustainable development, specific according to their mission and vision. This allowed the transfer of knowledge of the actors and the development of the project entitled "*Energy renovation of the Juan xxiii educational institution, in the municipality of Montería, department of Córdoba*". This work presents the methodology that guided the development of the project and the main findings resulting from measurements of conditions in the spaces of the intervention and the perceptions of those who benefited from it. The project itself is presented as a model of energy efficiency intervention in territories and institutions with similar characteristics, which allows for the transfer of knowledge and the improvement of the methodology based on the lessons learned.

## MATERIALS AND METHODS

The development of the project was carried out with a

mixed approach with an exploratory and descriptive scope. The population was the educational community of the Juan XXIII EI with the participation of administrative staff, teachers, students, and parents. As measurement instruments, specialized equipment was used to take readings of the intervened comfort variables, perception surveys, and semi-structured interviews with administrative staff, teachers, and students. For the development of the intervention, as previously mentioned, the Energy Efficient Cities approach was followed; in this way, the entire process is presented below from the perspective of a model for energy management supported by the total quality cycle known as PHVA (Spanish for Plan, Do, Validate, and Act). This cycle allows an energy renewal project to be seen as a management process, in which we start from an initial state and generate actions to advance over time towards environmentally friendly systems that benefit not only health but also the environment and the economy of the EI. Fig. 1 shows the phases followed in the intervention.

Regarding the development of the quantitative study, pieces of equipment were installed to measure temperature, relative humidity (RH), and carbon dioxide that was present in three different places in the EI, which correspond to the three types of interventions implemented. The measurements were taken before and after the interventions at different time ranges.

In addition, the EI's Academic Coordinator carried out a perception survey with parents, teachers, administrators, and students through the communication channels enabled for the educational community during the pandemic. The survey investigated the perception of community members regarding thermal, lighting, and acoustic comfort. Interviews were also conducted with students, teachers, and administrators to collect information related to positive aspects of the intervention and aspects that should be improved.

## RESULTS AND DISCUSSION

After implementing the strategies proposed by the methodology in this study, it was possible to obtain three types of results. The first of them constitutes a model for the energy renewal of the EI, the model is established by phases that adjust to the PHVA cycle for continuous improvement. The second result corresponds to the contrast between before-and-after variables such as temperature to establish the differences gained from the intervention. The third result is the perception of comfort obtained from the opinions of the community regarding comfort variables, positive aspects, and improvements in EI after the intervention is completed.

### Model for Energy Renewal in an EI With a Hot Humid Climate

The model is made up of 4 stages that mark the beginning and continuation of a project that seeks the energy renewal of an institution and plans its operation by the incorporation of renewable energies.

#### *Planning Stage*

**Commit to the SGEn:** As a product of a collaboration

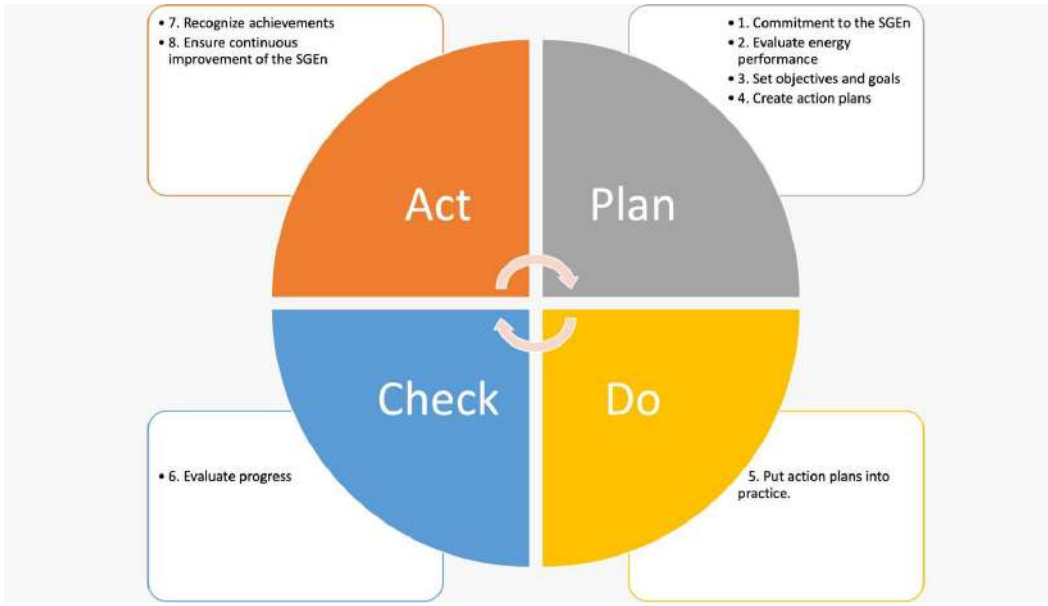


Fig. 1: Phases of the energy intervention model at the Juan XXIII Educational Institution under the approach of Energy Efficient Cities.

between the Embassy of Switzerland-State Secretariat for Economic Affairs (SECO), the Mining-Energy Planning Unit (UPME), the Corporation for Energy and the Environment - CORPOEMA- and the mayor's office of Monteria, and given the interest in the benefits of implementing the plan, the Energy Efficient City Initiative was created (www.ciudadenergetica.co).

The Initiative had a pilot phase for 3 years, with Monteria being one of the pilot cities. The energy renovation of the Juan XXIII Educational Institution is one of the flagship projects of the Local Energy Strategy that was developed for Monteria within the framework of a multi-actor participatory process. This project was born as a response to the poor living conditions in the classrooms, associated with the high concentration of students, the harshness of the subtropical climate, and a design without basic concepts of bioclimatic architecture. The challenge was to improve the conditions of the indoor environment where the students worked through the implementation of active and passive measures, with a controlled increase in the school's operational expenses. On the other hand, it is known that school performance can improve when adequate temperature conditions exist (Wargocki & Wyon 2006).

**Evaluate energy performance:** In this phase, the conditions of the EI are evaluated to establish goals and objectives. Table 1 presents some general aspects of the EI.

From the characterization of the EI, it was possible to identify problems that could be improved; these are presented in Table 2.

**Establish goals and objectives:** In the case of Juan XXIII school, three types of intervention strategies were defined to improve the quality of the interior environment of the classrooms. The objective was to reduce the budget and be able to compare different models. The goals were established based on the desired comfort situation (See Table 2)

Table 1: General parameters of the project.

| Characteristic | Initial state |
|---|---|
| Age of buildings | Between 10 and 20 years |
| Constructed area | 1.840 $m^2$ |
| Land area | 3.806 $m^2$ |
| Number of students | 1.023 |
| Educational stages | Primary and secondary |
| Number of classrooms | 14 out of 23 are not air-conditioned |
| Wall material | Cement bricks |
| Roof material | Zinc sheets |
| Windows | Flat glass in air-conditioned rooms<br>Cement brick or metallic grid in non-air-conditioned rooms |
| Air conditioning systems | Split Systems |
| Lightning | T8 Fluorescent Tube<br>T10 Fluorescent Tube<br>Compact fluorescent lightbulbs |

**Create action plans:** Based on the identified problems and the defined objective, progress was made toward specifying the actions that could be carried out to address them (Table 3).

**Doing stage:** Once the goals and objectives of the project were established, the bidding and contracting process of the companies in charge of implementing the project and the corresponding auditing began. The company SERVICIOS Y OPERACIONES S.A.S ("Contractor") had the purpose of "ENERGY RENOVATION OF THE JUAN XXIII EDUCATIONAL INSTITUTION IN THE MUNICIPALITY OF MONTERÍA, DEPARTMENT OF CÓRDOBA" and N&S CONSTRUCCIONES S.A.S acted as auditor of the project.

**Implement the action plans:** Following the proposed lines, the action plan included three types of interventions:

- **Type 1: Complete intervention.** It was applied in those areas where the worst environmental conditions existed inside. This solution is the one that allows better thermal comfort but may have higher investment and operation costs.
- **Type 2: Medium intervention.** It was mainly applied in classrooms located on the first floors since, unlike the second floors, they do not have a roof surface directly exposed to the sun. It is possible to adapt later into a complete intervention.
- **Type 3: Insulation only.** It was applied exclusively in a building that had an architectural design suitable for warm areas. It had enough roof height, allowing better natural ventilation.

Table 4 presents the measures applied and the type of intervention carried out.

### *Evaluating Stage*

**Evaluate progress:** To evaluate progress, a detailed schedule was established by stages with activities and results to be verified. The entire process was carried out by the auditor who supervised the progress of the works defined in the project. Table 5 shows the main results that were used as a basis for the evaluation of the results. Likewise, in the results part, the evidence obtained from the application of the evaluation instruments will be provided.

### *Acting Stage*

**Recognize achievements:** The benefits of the interventions have an impact on the three pillars of sustainability: society, the environment, and the economy. Among the main benefits

Table 2: Description of main issues.

| Problem | EI situation<br>2. Energy performance evaluation | Expected situation: students' comfort and safety.<br>3. Goals and objectives |
|---|---|---|
| (1) High temperatures inside the classrooms | Between 34 and 38ºC (*Measurements taken in a room with two air conditioners and several ceiling fans*) | Between 25 and 27ºC |
| (2) High temperatures outside the building | Roof temperature: 70°C Outer wall temperature: 40°C (*Measurements taken with thermal imaging camera*) | Reduction of solar radiation on walls and roofs.<br>Lower the temperature of walls and roofs.<br>Reduction of heat radiation from walls and roofs into the classroom |
| (3) High levels of relative humidity in the classrooms | Between 60% and 80% (*Monitoring carried out for several days in a classroom with air conditioning equipment and ceiling fans*) | Between 40% and 60%, along with an adequate temperature |
| (4) Very poor air quality | The $CO_2$ concentration of the air inside the classrooms: up to 3'000 parts per million (ppm)<br>Outdoor air reference: between 350 and 400 ppm<br>(*Measurements taken in an air-conditioned room*) | The $CO_2$ concentration of the air inside the classrooms below 1'000 ppm<br>(According to international recommendations of ASHRAE 62.1, with ventilation of 13 $m^{-3}.h^{-1}$ per student in each classroom) |
| (5) High energy consumption and associated costs | Rise of energy consumption after the installation of air conditioning equipment and ceiling fans (*monthly electricity bill: ~6MM COP*) | Reduction of the monthly electricity bill: at least 20% |
| (6) Lack of knowledge of the school's energy behavior | There is no energy monitoring, and the behavior of the different energy-consuming systems is not known.<br>The school neither receives electricity bills nor does it pay them directly (the Secretary of Education does so).<br>There is not enough information for taking measurements to reduce energy consumption. | There is monitoring of the main energy-consuming equipment.<br>Consequence: misuse or malfunctions can be identified, and energy consumption controlled. |
| (7) Poor lightning | Curtains, cloths, or plastic on the windows<br>Artificial lighting in classrooms is below the values recommended by Colombian regulations.<br>Dark spaces that are not suitable for studying | Control of direct solar radiation by construction elements<br>Artificial lighting according to the Technical Regulations for Lighting and Public Lighting RETILAP<br>Standardized lighting levels |
| (8) Recreation áreas barely used | Recreation areas (e.g., courts, patios, etc.) are exposed to high levels of solar radiation.<br>Little use of the courts.<br>Concrete or cement slabs emitting heat due to incident radiation | Shaded recreation areas.<br>Use of courts during regular school days and off school hours (by students and community) |
| (9) Malfunction of air conditioning equipment | The equipment works using air at 16ºC and the maximum air speed without being able to sufficiently lower the temperatures in the classrooms. | Air conditioning is configured to maintain classrooms at an ambient temperature between 25 and 27°C. |
| (10) Uneven distribution of temperatures within classrooms | Very cold high-velocity stream near air conditioning equipment<br>Students located far from air conditioning do not perceive the sensation of cooling.<br>Direct solar radiation to students located near the window | Air conditioning equipment with better temperature distribution inside the classroom<br>Control of direct solar radiation by constructive elements |
| (11) Non-compliance with electrical regulations | Non-compliance with the Technical Regulations for Electrical Installations (RETIE) due to the age of the facilities.<br>The modifications to the electrical system over time were carried out according to standards, and consent for the construction improvement was recorded.<br>Risk situation for users<br>Impossibility of modifying the school's electrical system (e.g., the installation of photovoltaic panels) without complying with the regulations | Rise and improvement of security conditions for users |
| (12) Non-compliance with structural roof regulations | Non-compliance with the regulations of some structural elements due to age<br>Safety risks for those who will work on the construction site.<br>Risk of damaging roofs during work | Structural reinforcements when necessary to allow the development of roofing work.<br>Compliance with regulations on roofs<br>Compliance with the manufacturer's recommendations for installing tiles |

identified in the intervention of the Juan XXIII EI and that have a high level of replicability in other EI, we can mention:

**Social:** Improvement of environmental comfort and health of students. With the energy renovation of the school, the temperature and humidity of the classrooms are controlled and maintained within comfort limits. This has a direct impact on overall school performance.

Improvement of school performance. An appropriate

Table 4: Matrix of measures applied to each type of intervention.

| Applied measures | Type 1: complete intervention | Type 2: semi-complete intervention | Type 3: insulation only |
|---|---|---|---|
| Outer walls insulation | x | x | x |
| Roof and ceiling insulation | x | | x |
| Removal of ceilings in rooms without air conditioning | | x | |
| Window eaves | | x | x |
| Improvement of the quality of windows and the airtightness of the enclosure | x | x | |
| Efficient air conditioning with centralized control | x | | |
| Mechanic ventilation | x | | |
| Efficient ceiling fans | | x | |
| LED lighting | x | | x |
| Ceiling ventilation | x | | |
| Photovoltaic system | x | x | x |
| Outdoor shaded areas | x | x | x |
| Vegetation areas | x | x | x |

Table 5: Planification stages and expected results.

| Stage | Phase | Activities | Results |
|---|---|---|---|
| Planning | Initial studies | • Definition of goals:<br>• Objectives, scope, and project management<br>• Participatory Consultation / Workshop<br>• Elaboration of the energy renewal concept:<br>• Preliminary data collection and analysis<br>• Definition of the current state of the building (energy consumption, operating costs, structural and electrical status, etc.) | √ General objectives and scope of the project<br>√ Team organization chart with assigned responsibilities<br>√ First project calendar<br>√ Basic status report of the school (structure, electrical system)<br>√ Energy renewal concept |
| | Engineering | • Elaboration of the energy renewal concept or basic engineering, including the measure. Elements and the action plan proposed.<br>• Validation of the budget and the measures to be implemented.<br>• Engineering details design with plans<br>• Definition of the bidding type | √ Basic engineering plans and calculations<br>√ Feasibility study with approximate costs and prioritization of measurements<br>√ Definition of parameters to be monitored.<br>√ Selection of measurements to be implemented.<br>√ Updated project calendar<br>√ Detailed engineering, including plans and calculation reports of the measurements being implemented |
| | Bidding | • Writing the technical and administrative specifications, defining the minimum requirements for selecting the company<br>• Work schedule<br>• License and permit processing<br>• Bidding publication<br>• Field trip with candidates<br>• Drafting and signing of the contract<br>• Writing and signing of the contract<br>• Bidding and hiring of the auditing company | √ Detailed engineering plans<br>√ Bidding documents (including work schedule)<br>√ Final Budget assignment (and reserve budget)<br>√ Construction license<br>√ Electrical permits<br>√ Signed contract of the construction company<br>√ Auditing company with a signed contract |

Table Cont....

| Stage | Phase | Activities | Results |
|---|---|---|---|
| Execution | Construction and approval | • Monitoring of the execution of the project and quality control<br>• Adaptation of the measurements for possible unforeseen events that may arise on-site.<br>• Implementation and trials/testing to ensure proper functioning and execution of the measurements (including any corrective actions) | √ Work monitoring reports (including quality control)<br>√ Start-up report with the measurements carried out, their results, the corrective measures to be taken, responsible staff, and the execution date.<br>√ Operation and maintenance booklets of the intervened aspects<br>√ Signed maintenance contracts.<br>√ Monitoring criterion defined.<br>√ Work reception form<br>√ Opening ceremony |
| Operation | Maintenance | • Adjustment of optimal parameters for operating and maintenance<br>• Training and education of responsible staff for operation, maintenance, data collecting, and information monitoring.<br>• Optimization and repairment of flaws prior to final delivery<br>• Frequent control and maintenance according to the booklet. | √ Building working under normal conditions<br>√ Annual monitoring reports<br>√ Maintenance reports |

work environment (controlled temperature, humidity, and noise) allows students to use their attention span and retention capacity to the fullest.

It becomes a pivotal place for the community. Once renovated and equipped, the EI has been used for community meetings, fostering the link between the community and the EI. This is particularly important in vulnerable or low-income neighborhoods.

**Environmental:** Environmental education program. Students can take advantage of the measures implemented to study the avoided environmental impacts and understand processes based on renewable energy or see how energy efficiency measures impact. These themes could be tangible for them.

Use of local renewable resources. An energy renewal project can incorporate an energy generation component based on renewable resources; typically, photovoltaic systems are connected to the grid for the generation of electrical energy. In this way, they will participate in the diversification of the country's energy matrix and increase its supply security.

Reduction of greenhouse gas emissions. The measures implemented for energy efficiency and the use of clean energy, in addition to improving the comfort of students, are interventions that contribute to the reduction of greenhouse gas emissions. This reduction in emissions is estimated at 59 $tCO_2$ per year in the case of the Juan XXIII EI. The cost of avoiding the emission of one $tCO_2$ is estimated at 28 USD. A positive outcome is compliance with international climate change mitigation goals from Colombia.

**Economic:** Reduction of operating costs. By prioritizing passive solutions (e.g., improving the enclosure, roofed patios, green areas, etc.) to improve the environment in classrooms, the use of air conditioning equipment can be reduced and optimized. This had a reduction effect on electricity costs for the school.

Improving the reputation of the school. Schools, where energy renovations are implemented, demonstrate a willingness to innovate and are in sync with the environmental and educational concerns of the moment. This is a component that contributes to its institutional image as an educational establishment. This caused an approximate increase of 29% in the demand for openings in 2022.

**Infrastructure:** Increase in structural safety. This is a non-quantifiable benefit but corresponds to the improvement of the building's infrastructure to receive the energy interventions. In the case of the intervention of Juan XXIII EI, it included the improvement in the roof of the support straps of the tiles, the placement of columns in the perimeter walls to provide greater stability, and the placement of reinforcements in some walls that presented cracks or other structural problems.

Increase in electrical safety: For the installation of photovoltaic and air conditioning systems, as well as all general electrical installations, it was required to comply with current electrical regulations. This compliance cost does not present an economic return, but it must be considered when executing this type of project since, in general, the EI does not have a safe electrical infrastructure, and the safety of the entire community is put at risk.

**Ensure continuous improvement of the SGEn:** To ensure the continuous improvement of the project, certain conditions must be met from the beginning at the level of the process, financing, communication, and community participation. Additionally, actions necessary for the correct use, maintenance, and improvement of the infrastructure and conditions generated as a product of energy renewal must be explicitly and under the responsibility of local actors. Likewise, the participation of the scientific community in the processes of project impact evaluation and its systematization as a case for future interventions should be promoted. Below, aspects to be considered at the beginning and closing of the project are detailed as lessons learned.

Process: The "soft factors" play a fundamental role in the selection of a pilot project: The implementation phase of the renovation of the Juan XXIII EI in Monteria was completed successfully, thanks to the support of the school management and the Mayor's Office. Therefore, when selecting a pilot project, it is important to ensure that local stakeholders identify 100% with the project. To continue with continuous improvement, actions must be planned after the completion of the intervention so that resources can be available for the required maintenance and empowerment of the community.

Public procedures have their own logic, characteristics, and speed of decision: They must be selected through public or private bidding in accordance with the laws for design consultancy, hiring for the construction of projects, and auditing for monitoring the consulting and construction.

Planning stages should not be omitted: The diagnosis and initial studies allow a rapid evaluation of the optimal measures and the identification of existing risks/problems (state of the structures, the electrical system, projected calculations of energy demand). These must be executed by entities completely independent of those that will execute the project and must explicitly establish agreements with local entities that guarantee the care and maintenance of the investment.

The designs and detailed engineering must be included in the bidding documents and must have been prepared by a company independent of the one that will carry out the job. It is important that the bidding documents include detailed engineering and that the company is carefully selected. This ensures the following of clear guidelines and allows control over the project budget. In addition, it will allow the demand for a certain level of quality from the construction company.

Guarantee the presence of independent technical experts to ensure quality control, especially during construction: The supervision of the work on site must be ensured by a technical expert on a regular basis to identify possible failures on time and be able to correct them. The expert must be independent from the construction company. In this way, the auditing choices can be guaranteed in accordance with the requirements of the specifications in terms of quality and national and international regulations.

Ensure the presence of local experts and entrepreneurs who participate in the planning and execution of the project. They must participate in the project team and must be trained so the local knowledge and characteristics can be integrated into the planning and execution of the project. Local companies can be trained for this work (including maintenance).

Use of a first block as a pilot: In the case of Juan XXIII EI, it was very useful to carry out a block as a first stage and evaluate and discuss the result intensively. This gives the companies and specialists carrying out the project very specific advice to avoid errors and optimize the rest of the work.

Organize monitoring from the beginning: To demonstrate the effectiveness of the energy renovation, it is very useful to have photos and/or videos from the same points of view; and, thus, compare the before and after. It is also necessary to have suitable monitoring that supports the impact that the quality of the indoor environment has on academic performance. Monitoring criteria should have been selected at an early stage to have baseline measurements. Likewise, these must continue with some regularity after the completion of the intervention, this is where local actors at a technical, scientific, and financial level play an important role and are the fundamental piece for the continuous improvement of the intervention.

Include an operation and maintenance plan: An operation and maintenance plan must be prepared to ensure that the quality of the interventions is maintained over time. This must be included in the project schedule and delivered by the construction company. Evaluate the cost-benefit of air conditioning systems that become a bottleneck due to the maintenance and care they require if there is no continuous monitoring process after the intervention is operationally delivered.

Communication participation: Public EIs are excellent platforms for the implementation of pilot projects: Public EI energy renovations not only raise awareness among students and teachers but also among parents. The Monteria pilot project aroused great political interest in the Municipality.

Political actors, both at the level of the Municipality and the state government, should participate in the pilot projects. For the projects to be carried out successfully, those responsible at the community level (mayor) as well as at the national level (Ministry of Energy and Mines, etc.) must be informed and included in the pilot projects. This must also involve subsequent commitments for continuous improvement and implementation in other settings, taking

into account the relevance of the project to the environment, health, and progress of the country.

Organize the participation of beneficiaries in a participatory process from the beginning of the project: Key actors for the project must be consulted and informed from the beginning of the project. It is beneficial to consult students and teachers about the planned measures to involve them in the process. They may have new ideas or see aspects related to the use that were not taken into account. It also helps if they are patient during the execution and take care of the building afterward because it is also "their" project. This also implies participation and agreement with the beneficiaries in subsequent stages to guarantee the transfer of knowledge and the adoption of good habits to care for the investment made.

Expectations must be managed: The information communicated must be controlled, and there must be a clear direction for this. Indeed, it is difficult to react to unmet expectations afterward. A case that was presented in the EI was the belief that there would be no power outages because there was energy available.

Communicate regularly about the progress of the project: From the planning stage, it is possible to communicate about the project using local media. This increases its political

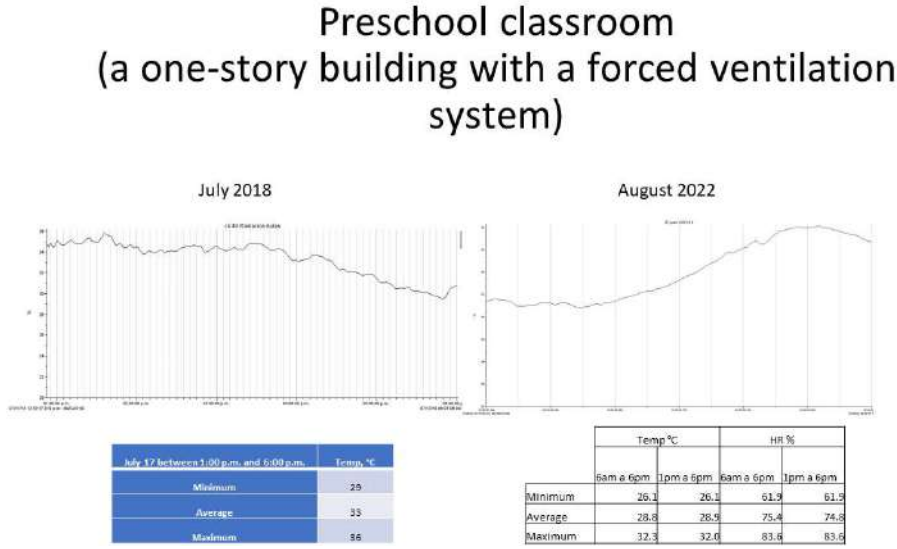


Fig. 2: Measurements before and after energy renovation in a Preschool Classroom (a one-story building with a forced ventilation system).

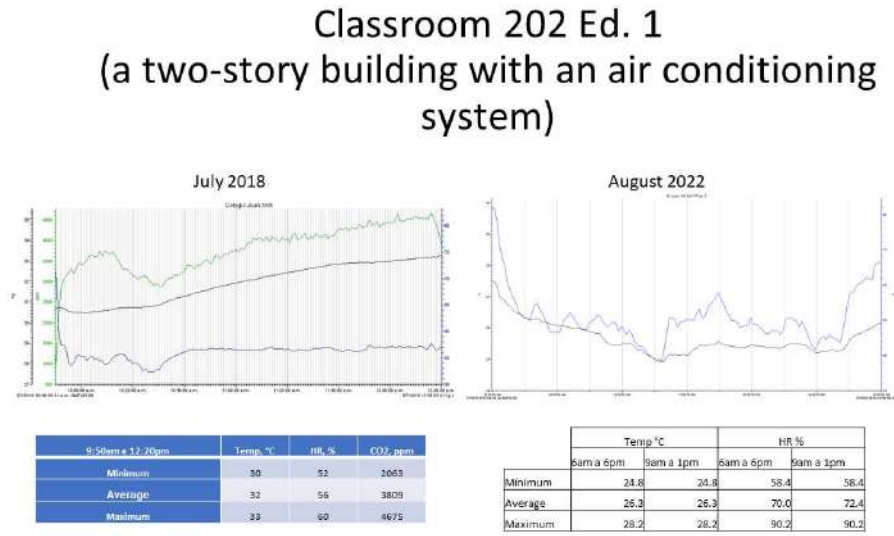


Fig. 3: Classroom 202 Ed. 1 (a two-story building with an air conditioning system).

weight and can motivate other actors to participate in the project. Furthermore, your project can inspire others at the local level and, thus, participate in a virtuous chain for improving students' comfort with reduced impact on the environment. Taking photos and/or videos from the same points of view during each stage allows you to compare the before and after, justify the work, and demonstrate the results, in addition to motivating others. A public presentation of the results at the end of the construction project is very beneficial. Subsequent meetings must also be established to evaluate the impact and to propose improvement actions according to the evolution of the products and results obtained.

**Variations in relation to temperature, relative humidity, and $CO_2$ before and after renovation:** From the baseline taken before carrying out the energy renewal process at the Juan XXIII EI, it was possible to establish differences between the variables Temperature, Relative Humidity (RH), and $CO_2$ in the three types of interventions carried out. Below are the results of the comparison between the measurements carried out.

Fig. 2 shows the measurements carried out during 2018 and 2022 in a Preschool Classroom (a one-story building with a forced ventilation system). A decrease in average temperatures is marked.

Fig. 3 shows the measurements carried out during 2018 and 2022 in classroom 202 Ed. 1. A decrease in average temperatures is also observed. In this case, a greater difference is marked since air conditioners were used.

Fig. 4 shows the measurements carried out during 2018 and 2022 in classroom 202, Ed. 2 (a two-story building with

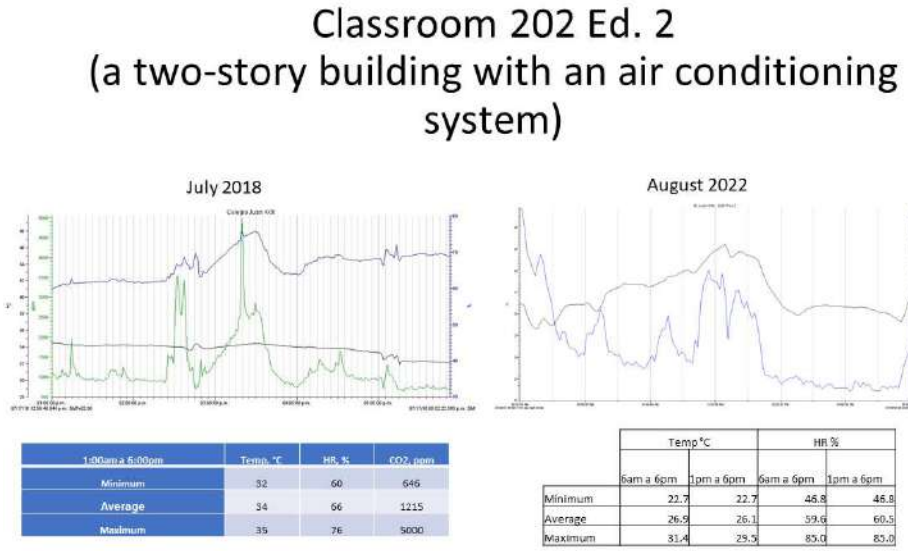


Fig. 4: Classroom 202 Ed. 2 (a two-story building with an air conditioning system).

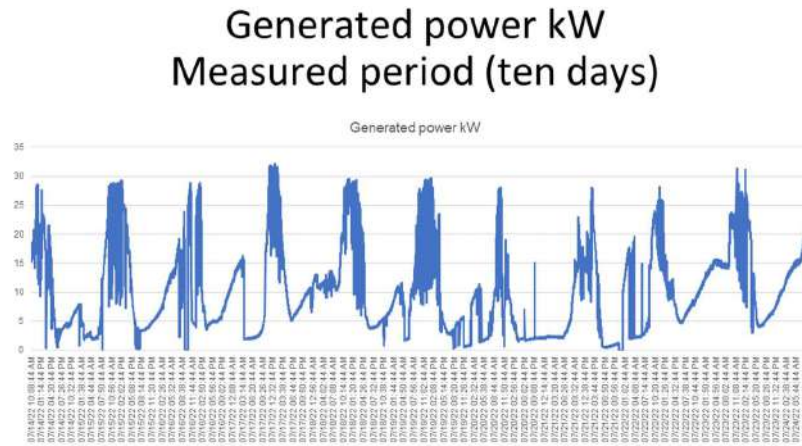


Fig. 5: Generated power in kW for 10 days.

an air conditioning system). The consistency is observed between the measurements in Figs. 3 and 4. For both rooms, air conditioners were used.

Fig. 5 shows the measurements made of the power generated in 10 days, presenting the generation of photovoltaic energy due to the energy renovation carried out.

**Perception of the educational community of the resulting comfort conditions after the intervention:** One of the most evident results was the increase in the demand for new student openings in Juan XXIII EI in 2022 after the intervention was completed. The increase was around 29% compared to 2019. This could be interpreted as the community's perception of an EI with better capacity, comfort, and/or quality based on changes in infrastructure (Fig. 6).

According to Figs. 7, 8, and 9, the community of the educational institution that participated in the survey stated that thermal comfort had improved and that they felt satisfied with the current temperatures.

According to Figs. 10, 11, and 12, the community of the educational institution that participated in the survey stated that lighting comfort had improved and that they felt satisfied with the current conditions.

According to Figs. 13, 14, and 15, the community of the educational institution that participated in the survey stated that acoustic comfort had improved and that they felt satisfied with the current conditions.

## CONCLUSIONS

The experience with the development of this project allowed

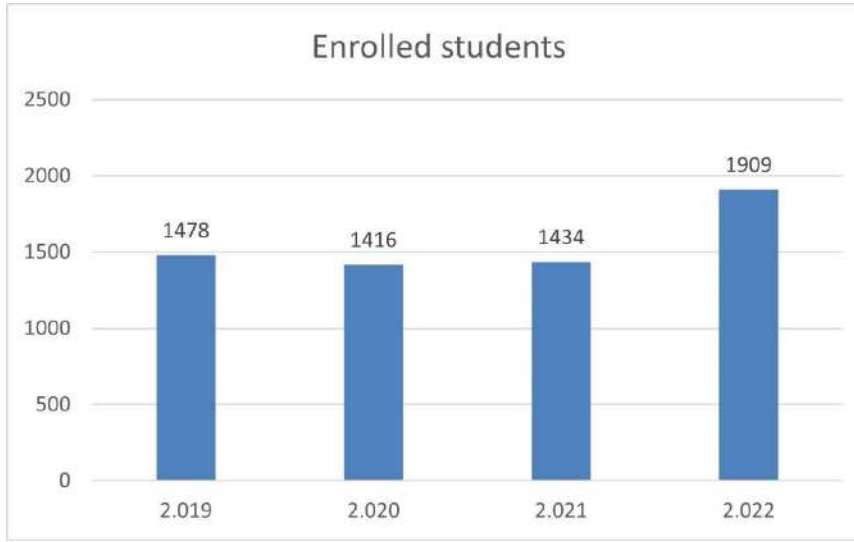


Fig. 6: Number of students enrolled per year.

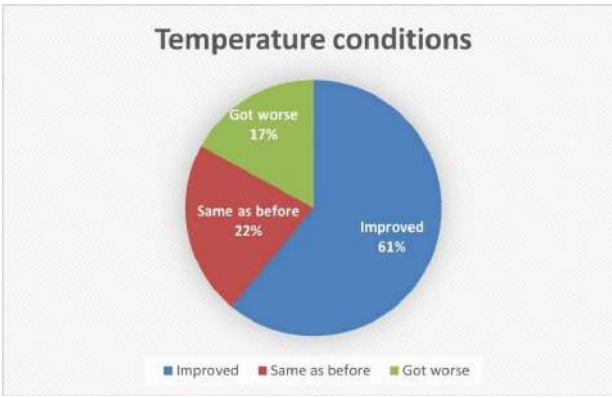


Fig. 7: Temperature conditions.

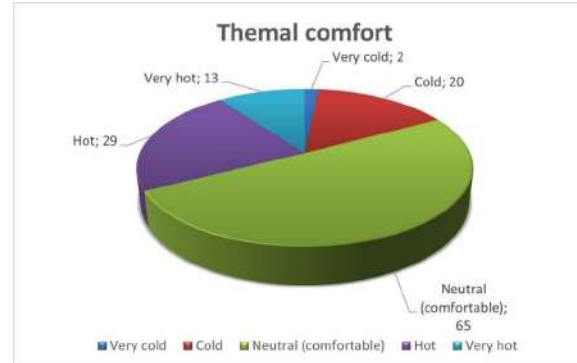


Fig. 8: Thermal comfort.

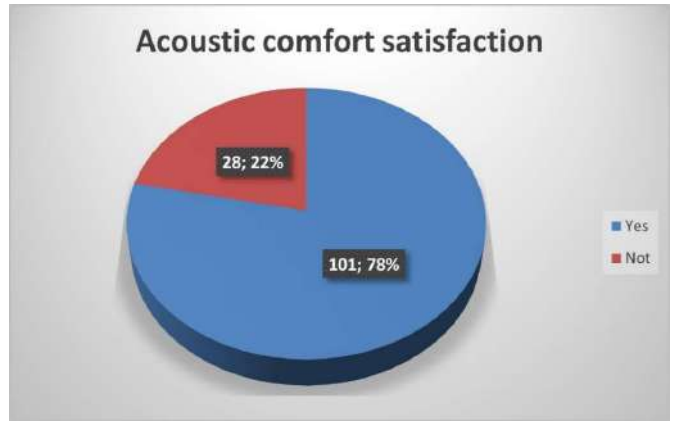


Fig. 9: Results for the questions related to thermal comfort.

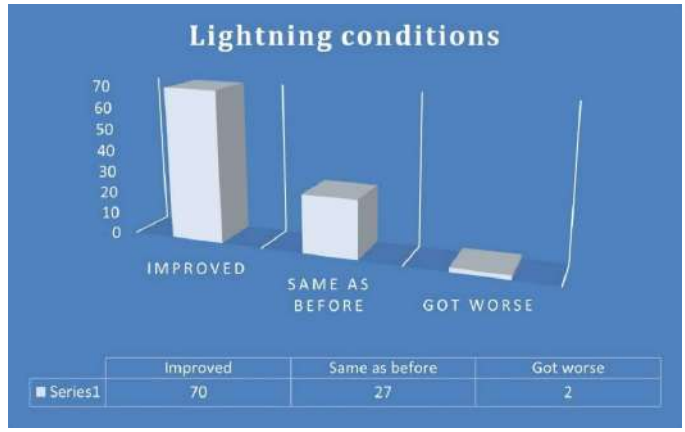


Fig. 10: Lightning conditions.

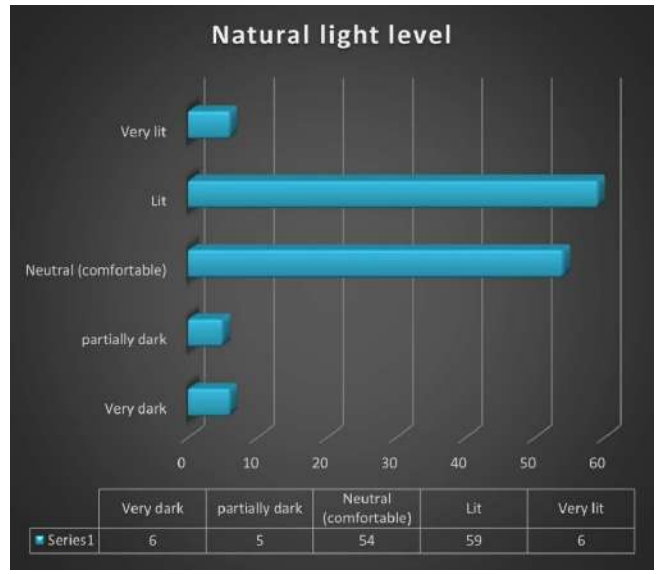


Fig. 11: Natural light level.

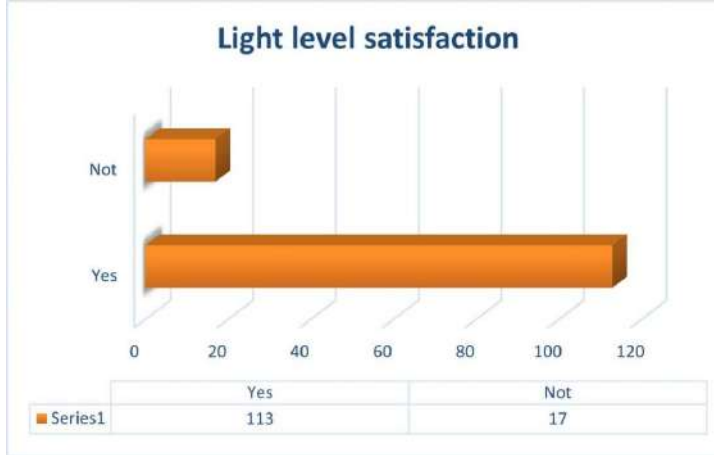


Fig. 12: Results for the questions related to lighting comfort.

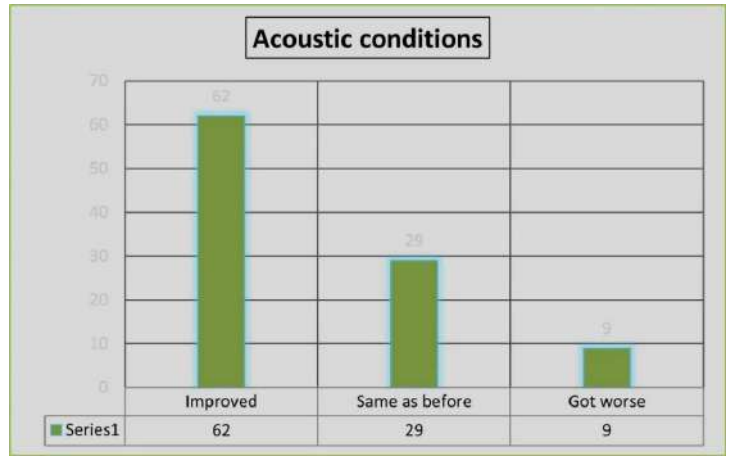


Fig. 13: Acoustic conditions.

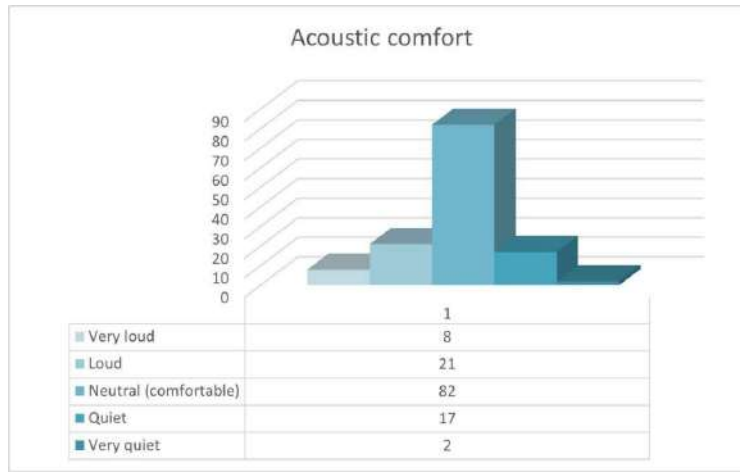


Fig. 14: Acoustic comfort.


Fig. 15: Results for the questions related to acoustic comfort.

us to identify important success factors and desirable conditions for the development of these types of projects, which are detailed in Chapter 8 of the technical report (Booklet for energy renovation of schools in hot, humid climates of Colombia 2021).

These factors generally support these four major aspects to highlight:

- Energy renovation in schools in warm climates is essential to improve the thermal comfort conditions of the educational community. It can be achieved with simple but substantial measures, such as pergolas, new windows, and efficient air conditioning and ventilation systems. Furthermore, this improves the reputation of the school, causing collateral benefits such as what happened at the Educational Institution where there was an increase of openings by approximately 29% in the number of students. Additionally, Educational Institutions where energy renovations are implemented demonstrate a willingness to innovate and are in sync with the environmental and educational concerns of the moment. This is a component that contributes to the institutional image as an educational establishment.
- Energy renewal in Educational Institutions offers significant savings in operating costs and greenhouse gas emissions. This reduction in emissions is estimated at 59 $tCO_2$ per year in the case of the Juan XXIII EI. The cost of avoiding the emission of one $tCO_2$ is estimated at 28 USD. A positive outcome is the support of Colombia's compliance with international climate change mitigation goals and the reduction of energy service costs.
- Energy renovation in Educational Institutions indirectly leads to the renovation of important structural and architectural elements; therefore, the investment costs are reflected in the longer useful times of the building and an improvement in its quality in the long term.
- The experience of renovating a building such as an Educational Institution is an excellent way to raise awareness among new generations about the benefits of energy efficiency and the use of renewable energy. The EI has a room where students are taught in a didactic way the benefits that were achieved in their school and how they contribute to sustainability.

**Financing**

Guarantee financing for the entire project: In the case of Juan XXIII EI, financing for all stages of the project was assured through the Energy Efficient City Initiative. It is important to ensure not only the financing of the execution but also the planning, consulting, review, and quality control of the project. Additionally, a later margin of time to make up for shortcomings in local action must be considered, and commitment by national and international actors must be generated before the final closure of the intervention.

Implementation Budget: As a planning element, it is important to consider an analysis of technical specifications, quantities, and prices prior to construction and/or intervention that ensures compliance with the objectives defined in the planning and design stage.

Have a reserve: It is necessary to reserve a larger budget than estimated from the beginning to be able to face unforeseen events. 10% of the gross value is recommended as a reserve. This value could also be used for the post-intervention phase.

Consider operating costs: Measures that can reduce or keep the operating costs of the EI low must be considered in the project. This will facilitate the administration of the school. Local governments must commit the necessary financing for the correct operation and proper maintenance of the systems.

## REFERENCES


Almeida, R. M. S. F., Pinto, M., Pinho, P. G. and de Lemos, L. T. 2017. Natural ventilation and indoor air quality in educational buildings: Experimental assessment and improvement strategies. Energy Efficiency, 10(4): 839-854. doi:10.1007/s12053-016-9485

Andamon, M. M., Rajagopalan, P. and Woo, J. 2023. Evaluation of ventilation in Australian school classrooms using long-term indoor $CO_2$ concentration measurements. Build. Environ., 237: 110313. doi: 10.1016/j.buildenv.2023.110313

Bartyzel, J., Zieba, D., Necki, J. and Zimnoch, M. 2020. Assessment of ventilation efficiency in school classrooms based on indoor-outdoor particulate matter and carbon dioxide measurements. Sustainability (Switzerland), 12(14): 600. doi:10.3390/su12145600

Bogdanovica, S., Zemitis, J. and Bogdanovics, R. 2020. The effect of $CO_2$ concentration on children's well-being during the process of learning. Energies, 13(22): 6099. doi:10.3390/en13226099

Cabello Eras, J., Balbis Morejón, M., Sagastume Gutiérrez, A., Pardo García, A., Cabello Ulloa, M., Rey Martínez, F. and Rueda Bayona, J. 2019. A look at the electricity generation from non-conventional renewable energy sources in Colombia. Int. J. Energy Econ., 9(1): 15-25. https://doi.org/10.32479/ijeep.7108

Chen, Y., Tu, Y., Sung, S., Weng, W., Huang, H. and Tsai, Y.I. 2022. A comprehensive analysis of the intervention of a fresh air ventilation system on indoor air quality in classrooms. Atmos. Pollut. Res., 13(4): 101373. doi: 10.1016/j.apr.2022.101373

Dovjak, M., Slobodnik, J. and Krainer, A. 2020. Consequences of energy renovation on indoor air quality in kindergartens. Build. Simul., 13: 691-708. https://doi.org/10.1007/s12273-020-0613-6

Elnabawi, M. H. and Saber, E. 2022. Reducing carbon footprint and cooling demand in arid climates using an integrated hybrid ventilation and photovoltaic approach. Environ. Dev. Sustain., 24(3): 3396-3418. doi:10.1007/s10668-021-01571-1

Ferrer-Estévez, M. and Chalmeta, R. 2021. Integrating sustainable development goals in educational institutions. Int. J. Manag. Educ., 19(2): 494. doi: 10.1016/j.ijme.2021.100494

Johnson, D. L., Lynch, R. A., Floyd, E. L., Wang, J. and Bartels, J. N. 2018. Indoor air quality in classrooms: Environmental measures and effective ventilation rate modeling in urban elementary schools. Build. Environ., 136: 185-197. doi: 10.1016/j.buildenv.2018.03.040

Liébana, M. 2021. Propuesta de clasificación tipológica de colegios con criterios de eficiencia energética. Tesis de doctorado. Univ. Politecnica of Valencia https://riunet.upv.es/handle/10251/175193

Matthey-Junod, A., Sandwell, P., Makohliso, S. and Schönenberger, K. 2022. Leaving no aspect of sustainability behind: A framework for designing sustainable energy interventions applied to refugee camps. Energy Res. Soc. Sci., 90: 2636. doi: 10.1016/j.erss.2022.102636

Mombeuil, C. 2020. Institutional conditions, sustainable energy, and the UN sustainable development discourse: A focus on Haití. J. Clean. Prod., 254 doi: 10.1016/j.jclepro.2020.120153

Rajagopalan, P., Andamon, M. M. and Woo, J. 2022. Year-long monitoring of indoor air quality and ventilation in school classrooms in Victoria, Australia. Archit. Sci. Rev., 65(1): 1-13. doi:10.1080/00038628.2021.1988892

Rosbach, J. T., Vonk, M., Duijm, F., Van Ginkel, J. T., Gehring, U. and Brunekreef, B. 2013. A ventilation intervention study in classrooms to improve indoor air quality: The FRESH study. Environ. Health, 12(1): 110. doi:10.1186/1476-069X-12-110

Wargocki, P. and Wyon, D. 2006. Effects of HVAC on student performance. ASHRAE J., 48(10): 22-28.


### ORCID DETAILS OF THE AUTHORS

J. Velez-Ramos: https://orcid.org/0000-0003-1187-6799

Nature Environment and Pollution Technology
An International Quarterly Scientific Journal

p-ISSN: 0972-6268
(Print copies up to 2016)
e-ISSN: 2395-3454

Vol. 23 | No. 3 | pp. 1301-1317 | 2024

Original Research Paper

https://doi.org/10.46488/NEPT.2024.v23i03.005

Open Access Journal

# Characterization of the Bacterial Microbiome Structure and Identification of the Beneficial Genera in the Leaf Litter Compost for its Potential Application as a Bioorganic Fertilizer

**Sophayo Mahongnao*, Pooja Sharma*, Arif Ahamad**, Neeraj Dohare*, Neeru Dhamija*, Anita Garg Mangla* and Sarita Nanda**†**

*Department of Biochemistry, Daulat Ram College, University of Delhi, Delhi-110007, India
**Department of Environmental Science, Jamia Millia Islamia University, New Delhi-110025, India
†Corresponding author: Sarita Nanda; saritananda123@gmail.com

**Nat. Env. & Poll. Tech.**
**Website: www.neptjournal.com**

*Received:* 07-12-2023
*Revised:* 05-02-2024
*Accepted:* 10-02-2024

**Key Words:**
Bio-organic fertilizer
16S rRNA metagenomics
Microbial diversity
Organic waste compost

## ABSTRACT

This study investigates the potential of leaf and various organic waste composts as bio-organic fertilizers using 16S rRNA metagenomics. The microbial richness and diversity analysis, employing alpha and beta diversity indices, reveal substantial variations influenced by organic substrates during composting. The leaf compost had a high total OTU (70,554) but low microbial diversity (Chao 1 index = 272.27). The kitchen waste compost had the highest microbial diversity (Chao 1 index = 429.18). Positive correlations between microbial biomass, diversity, and compost quality highlighted the pivotal role of microbial activity. The beneficial genera identified across all the bio-composts were *Lactobacillus, Leuconostoc, Sphingobacterium, Paenibacillus, Pseudomonas,* and *Clostridium*. Some pathogenic genera were also detected in all the composts analyzed, viz. *Prevotella, Agrobacterium, Fusobacterium,* and *Streptococcus*. Nonetheless, the ratio of beneficial to the pathogenic genera was generally high in all compost, highlighting the enrichment with beneficial microorganisms. The leaf compost demonstrated the highest proportion of beneficial genera, about 92%, indicating significant bio-fertilizing potential, with a low % level of pathogenic genera of about 3%. Thus, the leaf compost has excellent potential to be used as a bio-organic fertilizer. Understanding the microbial composition of organic waste composts is crucial for its application as bio-fertilizer for promoting sustainable agriculture.

## INTRODUCTION

Composting is a widely recognized sustainable method for managing organic waste, producing valuable soil amendments, and reducing the need for synthetic fertilizers in agriculture and horticulture (Bustamante et al. 2021, Fertiplus et al. 2019). Alternative means to chemical fertilizer for sustainable productivity have become paramount since the disproportionate use of chemical fertilizer has caused extensive environmental contamination (Chauhan 2016, Zhang et al. 2018). Composts produced from organic wastes could be an excellent alternative to chemical fertilizers for soil health and sustainable productivity. Ravindran (2022) noted that composting can help reduce greenhouse gas emissions and improve soil health. Various composting processes are available, each with unique advantages and disadvantages. Leaf litter can be a good substrate source for composting to produce valuable compost. Application of the composts generated from a different substrate, such as kitchen waste, organic fraction of the municipal solid waste (OFMSW), and vermicompost, as soil amendments have been shown to improve soil quality and increase plant growth (Eifediyi et al. 2015, Gupta et al. 2014, Horz & Conrads 2010, Machado et al. 2021, Pathak et al. 2020). However, the leaf compost produced from the leaf litter has yet to be studied comprehensively. It is essential to check the total microbiota, beneficial, and pathogenic microorganisms present in the leaf compost to understand the bio-fertilizing potential of the leaf-based compost compared to other organic waste composts.

The microbial communities present in different composts can vary depending on the type of feedstock and composting process used (Siles et al. 2021, Vishan et al. 2014). It has been reported that *Firmicutes, Proteobacteria, Actinobacteria,* and *Bacteroidetes* were the most abundant phyla in various organic waste composts such as green waste compost, food waste compost, manure compost, and vermicompost of multiple substrates such as cow manure and kitchen waste (Aguilar-Paredes et al. 2023, Wang et al. 2022). A study by Wan (2021) also reported that *Proteobacteria* and

*Chloroflexi* were the major phyla in sheep and cattle manure composts, and *Firmicutes* dominated pig and chicken manure composts. The phyla were detected in varied proportions in different organic waste composts. Still, a comprehensive analysis of the total microbiota and beneficial and pathogenic microorganisms in different organic waste composts has yet to be done and reported.

Recent advances in metagenomics have revolutionized the study of microbial communities in various environments, including organic waste composts (Horz & Conrads 2010). The16S rRNA metagenomic profiling has emerged as a powerful tool to study microbial communities in environmental samples such as composts. Using this technique, it is possible to identify the bacterial and archaeal taxa present with their relative abundance in different composts. Understanding the microbial ecology of organic waste composts can help identify the beneficial and pathogenic microorganisms in different composts. It could help us realize the potential benefits of composts and their suitability for application as bio-organic fertilizer for soil health and plant growth (Zhang et al. 2019).

The present study was designed to use 16S rRNA metagenomics to investigate the bacterial communities present in the leaf compost to identify the microbiome richness and presence of beneficial and pathogenic microbes in the compost. The fertility index and clean index, which indicate the fertilizing potential and level of potentially toxic elements, have been reported to be high for the leaf litter compost (Mahongnao et al. 2023). We further hypothesized that the leaf-based bio-compost is rich in beneficial microorganisms and can be used as a bio-organic fertilizer. Deciphering the intricate interplay between bacteria and their environment is paramount in unraveling the microbial dynamics inherent to leaf litter and diverse organic waste composts (Faust et al. 2015). This comprehension is pivotal for leveraging the intrinsic benefits of compost in bolstering soil health, promoting plant growth, and suppressing pathogens (Mahapatra et al. 2022, Wang et al. 2022). Against the backdrop of escalating concerns regarding sustainable waste management and an acknowledgment of the integral role bacteria play in ecosystem functionality. Our study seeks to furnish a comprehensive elucidation of bacterial microbiome structures within leaf litter and a spectrum of organic waste composts. These encompass cow dung manure, kitchen waste compost, municipal organic waste compost, vermicompost, and neem cake compost, with our methodology leveraging 16S metagenomic profiling.

This investigation also delved into the formulation of innovative approaches for leaf litter composts with the potential to function as biofertilizers, thereby enhancing plant health and soil quality. Our study systematically scrutinizes diverse formulations of leaf litter composts, encompassing variations in composting inoculum, initial leaf litter substrate, and including neem and castor leaves.

Beyond the meticulous evaluation of bacterial diversity and composition, our research adopts a holistic approach by integrating temporal monitoring of bacterial communities at different maturation time points during the composting processes of leaf litter. This comprehensive methodology elucidates dynamic changes in bacterial populations as compost maturation and transformation unfold. By shedding light on these critical facets, our work aspires to yield valuable insights capable of optimizing leaf litter composting protocols, thereby fostering more sustainable and ecologically responsible organic waste management practices, ultimately producing high-quality organic compost.

We also conducted a comprehensive assessment of bacterial microbiome richness and diversity within matured leaf litter compost, juxtaposed with analogous matured organic waste composts, namely kitchen waste compost, cow dung manure, municipal organic waste compost, vermicompost, and neem cake compost. Our investigation extended to discerning the presence of both beneficial and pathogenic fungal genera in these organic composts. This comparative analysis serves as a valuable tool in comprehending the aptness of these composts for utilization as bio-organic fertilizers (De Corato 2020, González-González et al. 2021).

## MATERIALS AND METHODS

### Samples Collection and Preparation

Leaf litter from trees such as Indian beech (*Pongamia pinnata*), Krishna kadamb (*Mitragyna parviflora* (Roxb.) Korth), mulberry (*Morus alba*), scholar tree (*Alstonia spp*.), frangipani (*Plumeria rubra*), and fig (*Ficus* spp.) was systematically collected within the premises of the institutional campus and subjected to shredding for composting.

During the autumnal season, a monthly accumulation of approximately 450 kg, equating to 15 kg per day, of leaf litter waste was thoroughly gathered. Mechanical shredders were employed to shred the leaf waste. Subsequently, composting was done within experimental-scale bins measuring 3 feet × 1.5 feet × 0.5 feet (length × breadth × height) at ambient environmental conditions, employing the Effective Microorganisms (EM) method (Mahongnao et al. 2023). Four sets of leaf litter composting were set up in parallel with different inoculums. Each bin was initially loaded with 4 kg (dry weight) of shredded leaf waste and subjected

to a composting duration of twelve weeks, with periodic mixing occurring every 3 to 4 days. Sampling events were conducted at three and twelve weeks into the composting duration to assess the progression of the composting process. Specifically, the leaf compost sample denoted as DRCC20 underwent a three-week composting cycle employing water as the sole inoculum. DRCTI10 was subjected to a three-week composting regimen utilizing a waste decomposer. This particular decomposer is a consortium of microorganisms extracted from cow dung developed by the National Centre of Organic Farming, Government of India.

In contrast, DRCTI140D underwent a more extended twelve-week composting cycle using the same waste decomposer developed by the National Centre of Organic Farming. Another batch, DRCTB10, was composted for three weeks, employing a stimulated sludge derived from landfill soil collected from a landfill site in New Delhi. The final compost sample, DRCLC36W, underwent a three-week composting process utilizing a combination of microorganisms extracted from fresh cow dung. Additionally, neem and castor leaves were incorporated into the composting material at a ratio of approximately 20% (w/w).

In addition to the experimental compost samples, various matured organic waste composts, including kitchen compost (DRCK), municipal organic waste compost (DRCM), cow dung manure (DRCCD), vermicompost (DRVM), and neem cake compost (DRCNM), were sourced from local producers in the Delhi-National Capital Region, India, for comparative analysis.

### DNA Extraction and PCR Amplification of V3-V4 Region of 16S gene

DNA extraction was done using the suitable method for the sample type from commercially available kits such as QIAGEN (Qiagen India Pvt Ltd**,** Delhi India), ZYMO RESEARCH (California, USA), and Thermo-Fisher (Massachusetts, USA). DNA extraction was done as per the manufacturer's recommendation. Extracted DNA from the samples was subjected to NanoDrop and gel Check before being taken for PCR amplification: The NanoDrop readings of 260/280 at a value of 1.8 to 2 were used to determine the DNA's quality (Devi et al. 2015, García-Alegría et al. 2020).

For the metagenomic analysis, the extracted DNA was amplified and sequenced to obtain the DNA sequence of the V3-V4 region of the 16S rRNA bacterial gene. The amplification was performed using a PCR mix containing High-Fidelity DNA Polymerase, 0.5mM dNTPs, 3.2mM $MgCl_2$, and PCR Enzyme Buffer. The primers used were 16sF 5' AGAGTTTGATGMTGGCTCAG 3' and 16sR 5' TTACCGCGGCMGCSGGCAC 3'. The conditions for the polymerase chain reaction (PCR) amplification were that 40ng of Extracted DNA was used for amplification along with 10 pM of each primer. The initial denaturation was set at 95°C. The 25 Cycles were set with the following conditions: denaturation at 95°C for 15 seconds, annealing at 60°C for 15 seconds, elongation at 72°C for 2 minutes, and final extension at 72°C for 10 minutes, and hold at 4°C. The amplified 16s PCR Product is purified and subjected to gel check and Nanodrop Quality Control. The NanoDrop readings of 260/280 at a value of 1.8 to 2 were used to determine the DNA's quality (Martins et al. 2013).

### Overview of Sequencing and Bioinformatics Protocol

The amplicons from each sample were purified with Ampure beads to remove unused primers, and an additional 8 cycles of PCR were performed using Illumina barcoded adapters to prepare the sequencing libraries. Libraries were purified using Ampure beads and quantitated using a Qubit dsDNA High Sensitivity assay kit (Invitrogen, California, USA). Sequencing was performed using Illumina Miseq with a 2x300PE v3 sequencing kit (Illumina, Portland, USA). Raw data quality control (QC) was done using FASTQC and MULTIQC, followed by trimming of adapters and low-quality reads by TRIMGALORE. The trimmed reads are further taken for processing, including merging of paired-end reads, chimera removal, and OTU abundance calculation and estimation correction.

The binary base call (BCL) data acquired from the sequencer underwent demultiplexing, resulting in the generation of Fastq raw data. After this, the demultiplexed data quality was evaluated using Fastqc (Version 0.11.9) and Multiqc (Version 1.10.1) tools. Samples that successfully passed the quality control assessment were deemed eligible for further analysis. Our proprietary metagenomics pipeline, the Biokart Pipeline, designed for 16S, was employed for subsequent analysis. Following the completion of the sequencing run, the final raw Operational Taxonomic Unit (OTU) table was obtained, serving as the foundational dataset for subsequent analytical visualization. This was achieved using QIIME/MOTHUR/KRAKEN/BRACKEN workflows (Ramírez-Guzmán et al. 2004).

The Table 1 shows the code of each sample, their description, and the International Nucleotide Sequence Database Collaboration (INSDC) accession number.

The construction of abundance feature tables outlining the prevalence of organisms in each sample was executed utilizing Microsoft Excel (2021). Additional analyses, such as Heatmap generation, identification of the core microbiome, Dendrogram construction, Alpha diversity assessment, Beta diversity analysis, Principal Coordinates Analysis (PCOA)

Table 1: Compost sample code and description.

| Sample code | Initial Substrate | Inoculum used in composting | Maturity time | The International Nucleotide Sequence Database Collaboration (INSDC) accession number. |
|---|---|---|---|---|
| DRCC20 | Leaf litter | Water | 3 Weeks | ERS15510559 |
| DRCTI10 | Leaf litter | Waste decomposer | 3 Weeks | ERS15529905 |
| DRCTB10 | Leaf litter | Sludge of landfill soil | 3 Weeks | ERS15529906 |
| DRCLC36W | Leaf litter with neem and castor leaves | Waste decomposer | 3 Weeks | ERS15542713 |
| DRCTI140D | Leaf litter | Waste decomposer | 12 weeks | ERS15542763 |
| DRCCD | Cow dung | Waste decomposer | 14 weeks | ERS15529931 |
| DRCK | Kitchen organic waste | Waste decomposer | 10 weeks | ERS15529907 |
| DRCM | Municipal organic waste | Waste decomposer | 10 weeks | ERS15529930 |
| DRCV | Cow dung manure | Waste decomposer | 10 Weeks | ERS15529908 |
| DRCNM | Neem cake | Waste decomposer | 10 weeks | ERS15529940 |

plot generation, and Rarefaction curve assessment, were conducted through the utilization of Microbiomeanalyst, an online tool accessible at https://www.microbiomeanalyst.ca.

This workflow enables highly accurate investigations at the genus level. The microbial diversity of different biocomposts was analyzed through Alpha and Beta diversity indices. The databases used were SILVA/ GREENGENES/ NCBI. Each read was classified based on % coverage and identity. The 16S workflow helps identify pathogens in a mixed sample or understand microbial community composition (Mbareche et al. 2017).

The raw data of the Illumina Miseq sequencing of all the samples were deposited at the Indian Nucleotide Data Archive (INDA) of the Indian Biological Data Centre with the referenced INDA (Study/Bioproject) Accession number INRP000063. The International Nucleotide Sequence Database Collaboration (INSDC) Bioproject has the accession number of this study as PRJEB62440 (Table 1).

### Statistical Analysis

A systematic categorization into three groups was undertaken to conduct an in-depth analysis of metagenomic data, including assessments of alpha and beta diversity, as well as the statistical evaluation of microbiome levels across distinct compost samples. Group 2 comprised leaf litter compost samples, namely DRC20, DRCTI10, and DRCTB10. Group 3 encompassed other organic waste compost samples, specifically DRCCD, DRCK, DRCM, DRCV, and DRCNM. Group 8 included leaf compost samples DRCTI140D and DTCLC36W. Subsequently, data pertaining to these sample groups underwent filtration, and alpha diversity was quantified utilizing four methods, Shannon-Weiner, Fisher, and Simpson, accompanied by statistical analyses employing T-test/ANOVA methodology (Willis 2019). Furthermore, beta diversity, constructed at the Genus taxonomic level, employed the Bray-Curti's index distance method, with statistical significance determined through the Permutational MANOVA (PERMANOVA) approach (Maziarz et al. 2018).

## RESULTS AND DISCUSSION

### The Microbiome Richness and Diversity

The number of reads for each compost type provides an estimate of the amount of microbial DNA present in the sample. The leaf compost sample DRC-C20 had the highest read count at 0.8 million and total OTU (253,373), followed by the treatment leaf compost samples DRC-TI10 (reads, 0.4 million, OTU, 70,554) and DRC-TB10 (reads, 0.2 million, OTU, 96,328). The leaf compost sample LC36W had the lowest read count of 0.2 million and OTU of 9,057 (Fig. 1).

Leaf waste compost, DRCC20, had the largest library size, followed by cow dung manure (DRCCD)

Among the other organic waste composts analyzed, the cow dung manure, DRCCD, had the highest reads at 0.8 million and OTU of 230,466. Whereas the neem cake compost, DRCNM, had the lowest reads and OTU at 0.05 million reads and 18,133. Interestingly, despite having fewer reads than some of the other composts, vermicompost, and kitchen-waste compost had a relatively higher total number of OTUs of 86328 and 75708, respectively.

### Alpha and Beta Diversity

All the compost samples were rarefied or normalized to even sequencing depth based on the lowest sequencing depth sample. The analysis was plotted with the filtered data source. The rarefaction curve indicated that the kitchen

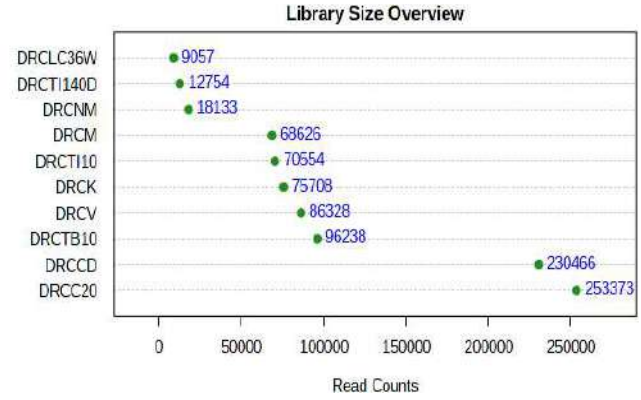


Fig. 1: Library-size overview of the leaf composts and the other organic waste composts.

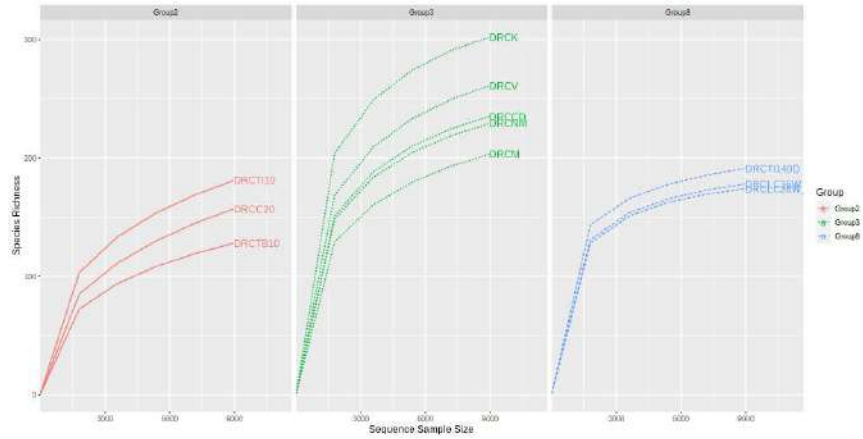


Fig. 2: Rarefaction curve of the leaf composts and the other organic waste composts.

waste compost had the highest species richness, followed by vermicompost, cow dung manure, neem cake compost, and municipal organic waste compost. The leaf compost had relatively lower species richness than the other composts analyzed in this study (Fig. 2).

The results of the alpha diversity analysis measured through diversity indices of Chao 1, Shannon, Fisher, and Simpson revealed that leaf composts and other organic waste composts had varied microbial richness and diversity (Table 2). The kitchen waste compost, DRCK, had the highest alpha diversity indices (Chao 1 index = 429.184, Shannon index = 4.452, Fisher index = 72.994, Simpson index = 0.976). Generally, the leaf composts had relatively lower alpha diversity indices than the compost produced from other organic waste substrates. Among all the samples analyzed, the leaf compost sample, DRCTB10, had the lowest alpha diversity indices (Chao 1 index = 272.276, Shannon index = 2.924, Fisher index = 35.886, Simpson index = 0.888). The *p-values* in Chao1, Shannon, Fisher, and Simpson's alpha diversity were measured to be 0.045858, 0.00055648, 0.015549, and 0.0058932, with the ANOVA *F*-value of 4.9435, 26.281, 8.0009, and 11.674, respectively (Fig. 3).

Table 2 shows the Alpha diversity indices of different bio-composts, which reveal that the different bio-composts have varying levels of bio-diversity.

Beta diversity was used to evaluate the sample diversity across the bio-compost samples. The beta diversity was constructed at the Genus taxonomic level with the Bray-Curtis index distance method based on Permutational MANOVA (PERMANOVA) statistical method. The *p*-value was < 0.002 with the PERMANOVA *F*-value of 4.8217. As expected, all the leaf composts clustered together, signifying the presence of common microorganisms. The other bio-composts spread out from leaf compost and each other, representing a different microbial diversity (Fig. 4).

## Heat Mapping

The heat map was constructed at the Genus taxonomic level. The samples are clustered using the Ward cluster algorithm

Table 2: Alpha diversity indices of the bacterial microbiome in the leaf and other organic waste composts.

| Samples | Chao 1 index | Shannon index | Fisher index | Simpson index |
|---|---|---|---|---|
| DRCC20 | 235.17 ± 31.79 | 2.92 | 27.25 | 0.887 |
| DRCTI10 | 272.27 ± 26.76 | 2.92 | 35.88 | 0.888 |
| DRCTB10 | 193.71 ± 29.27 | 2.83 | 21.25 | 0.898 |
| DRCTI140D | 232.71 ± 12.06 | 4.20 | 39.92 | 0.969 |
| DRCLC36W | 205.9 ± 9.42 | 3.96 | 35.42 | 0.959 |
| DRCV | 294.37 ± 14.19 | 4.08 | 52.08 | 0.965 |
| DRCCD | 306.78 ± 18.88 | 3.91 | 50.54 | 0.959 |
| DRCM | 298.19 ± 22.96 | 3.79 | 45.03 | 0.955 |
| DRCK | 429.18 ± 27.72 | 4.45 | 72.99 | 0.975 |
| DRCNM | 298.57 ± 17.17 | 3.75 | 50.29 | 0.909 |

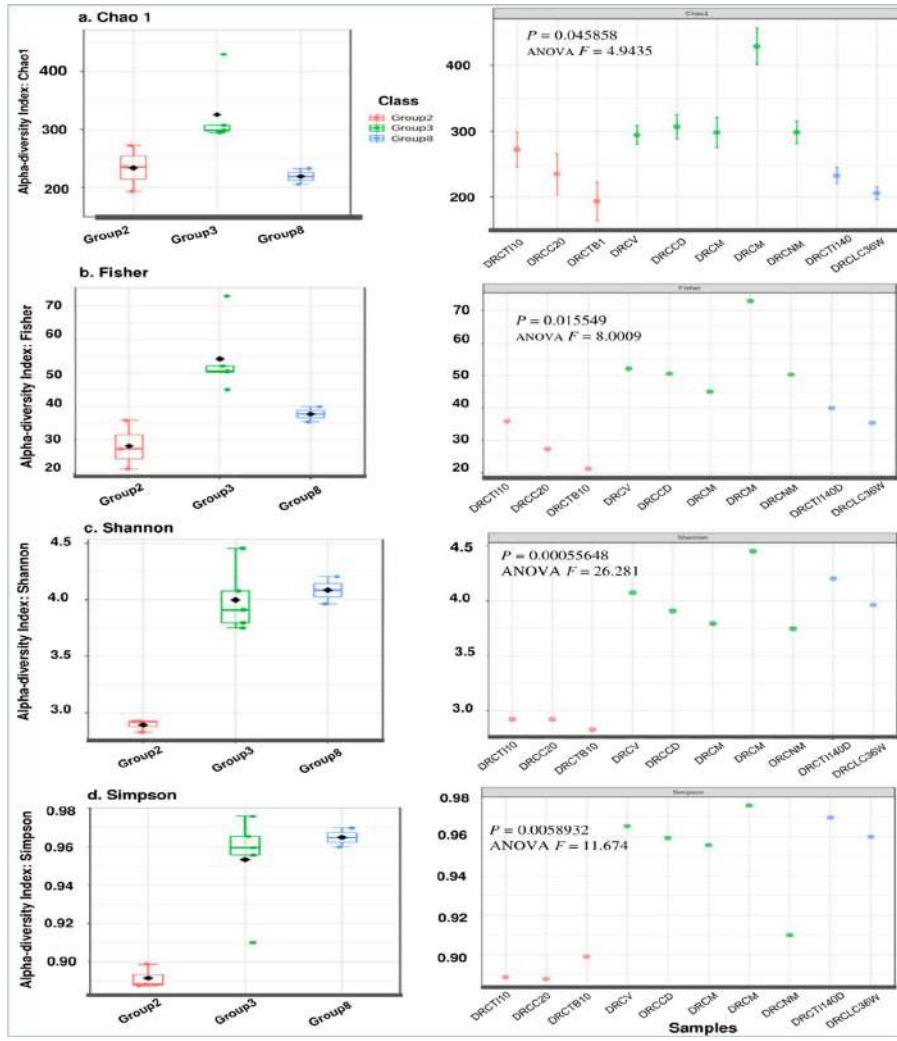


Fig. 3: Alpha diversity analysis of the leaf composts and the other organic waste composts.

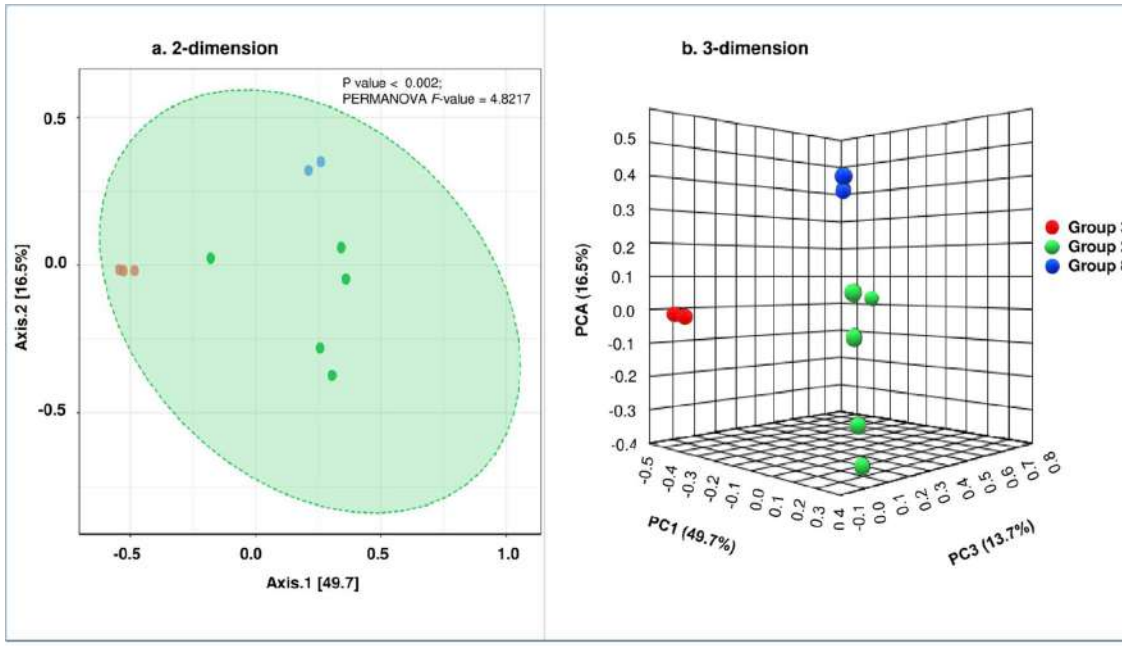


Fig. 4: Beta diversity analysis of the leaf composts and the other organic waste composts.

based on the Euclidean distance measure. About 30 bacterial genera could be classified as the core microbiome, a set of taxa detected in a high fraction of the population above a given abundance threshold. The genera detected across different composts varied according to the nature of the compost, which includes *Lactobacillus, Leuconostoc, Sphingobacterium, Paenibacillus, Pseudomonas, Clostridium, Planctomyces, Achromobacter, Stenotrophomonas,* and others. After three weeks of composting using different inoculums, namely DRDC20 and DRCTI10, the leaf composts showed changes in the bacterial community.

At the same time, there were some similarities in the bacterial community between the leaf composts, DRCC20 and DRCTB10. The heat map also showed that cow dung manure (DRCCD) and vermicompost (DRCV) had some common bacteria. The neem cake compost, DRCNM, had high amounts of bacteria genera such as Prevotella, Pseudomonas, Bacillus, and Lactococcus. At the same time, some bacterial communities in the neem cake compost were similar to the leaf litter compost. The municipal (DRCM) and kitchen waste compost (DRCK) had some common bacteria, which are present in high amounts (Fig. 5).

## Taxonomic Classification, Identification of Beneficial and Pathogenic Microbes

**Phylum level:** The microbial composition of compost samples was characterized, revealing the presence of twenty-one phyla, with the top ten species accounting for 98-99% coverage. Predominant phyla included *Proteobacteria, Firmicutes, Chloroflexi, Actinobacteria,* and *Bacteroidetes,* exhibiting divergent proportions in leaf and other organic waste composts**.** Notably, *Proteobacteria* levels were higher in leaf compost DRCC20 compared to other leaf compost treatments (DRCTI10 and DRCTB10) and comparable to cow dung manure (DRCCD), neem cake compost (DRCNM), and vermicompost (DRCV). *Firmicutes* were consistently abundant, particularly in leaf composts, with DRCC2 having higher levels. *Chloroflexi*, *Actinobacteria,* and *Acidobacteria* were present in all composts, with leaf compost showing elevated levels. *Bacteroidetes* levels were relatively lower in leaf composts than in other organic waste composts. *Planctomycetes* and *Verrucomicrobia* were more abundant in different organic waste composts such as cow dung manure, kitchen compost, and vermicompost than leaf compost. *Euryarchaeota* and *Cyanobacteria* were present in various composts, notably with higher abundance in the leaf compost than the other organic waste compost analyzed. Pathogenic phyla such as *Spirochaetes, Fusobacteria,* and *Chlamydiae* were identified across composts but had lower OTU counts than non-pathogenic phyla. *Spirochaetes* were relatively higher in municipal organic waste compost (DRCM), kitchen waste compost (DRCK), and cow dung manure (DRCCD). *Fusobacteria* were elevated in neem cake compost (DRCNM) and leaf compost DRCLC36W. *Chlamydiae* was higher in cow dung manure (DRCCD), vermicompost (DRCV), and kitchen waste compost (DRCK).

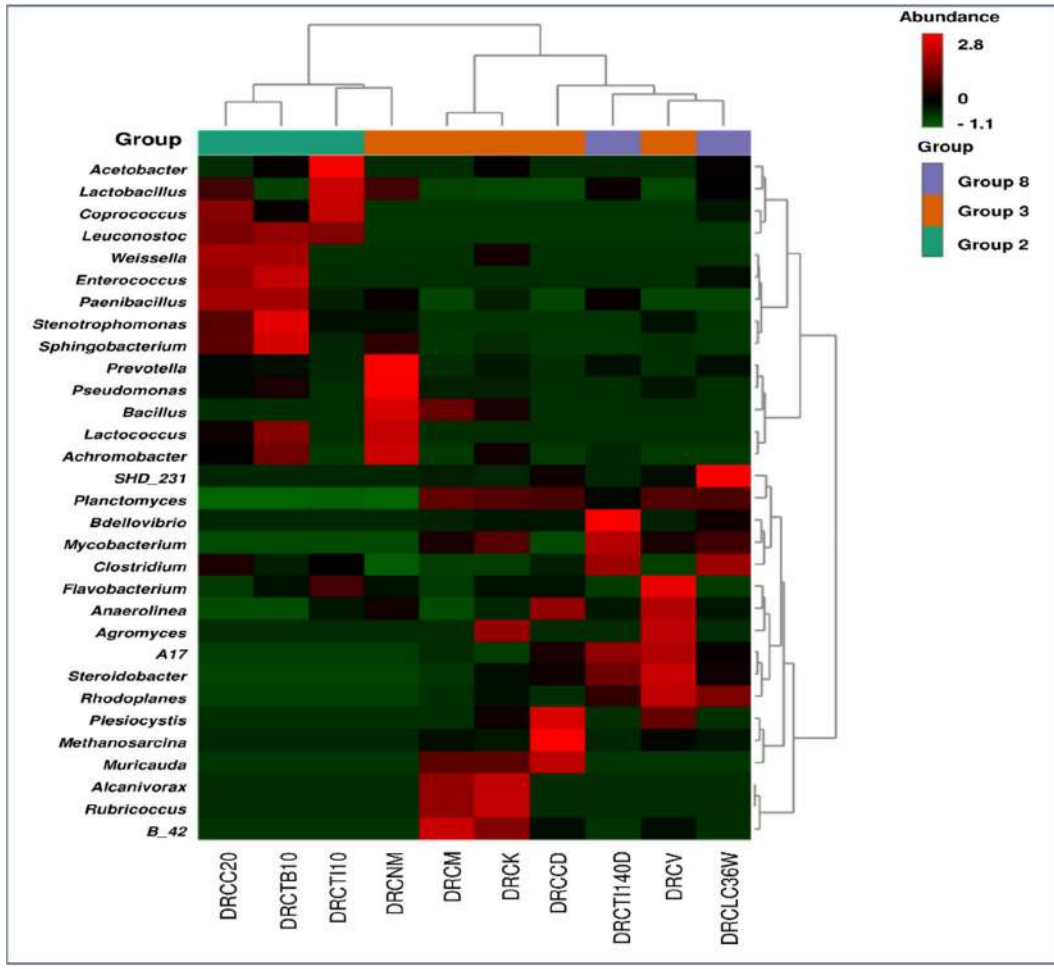


Fig. 5: Heat map of the core microbiome detected in the leaf and other organic waste composts.

These findings provide valuable insights into the microbial dynamics of diverse compost samples at the phylum level.

**Genus and species level:** Some bacterial genera identified were shared in different composts, while others were unique to each type of compost analyzed. The bacterial genera detected across the leaf litter composts and other different organic waste composts varied according to the nature of the substrate used to produce the compost. The primary beneficial bacterial genera identified across all the composts include *Lactobacillus, Leuconostoc, Sphingobacterium, Pseudomonas, Clostridium, Flavobacterium, Planctomyces, Stenotrophomonas, Achromobacter, Coprococcus, Paenibacillus, Weissella,* and *Acetobacter.*

*Lactobacillus* counts were much higher in the leaf compost than in the other organic waste composts. Among the leaf composts, the sample DRCC20 had a higher count of *Lactobacillus* than the treatment samples like DRCTI10 and DRCTB10. At the same time, the presence of *Lactobacillus* was drastically reduced in the leaf compost samples, DRCTI140D and DRCLC36W. Lactobacillus counts were relatively low in the other composts analyzed, though high only in the neem cake compost sample, DRCNM. *Leuconostoc* and *Sphingobacterium* were detected with relatively higher levels in the leaf composts than in the other organic waste composts. Among the leaf compost, the sample DRCC20 had a higher genera count than the other treatments. Remarkably, *Leuconostoc* and *Sphingobacterium* were not detected in the leaf compost samples, DRCTI140D and DRCLC36W. In the additional organic waste composts analyzed, the levels of *Leuconostoc* and *Sphingobacterium* were relatively deficient. The vermicompost (DRCV) had the lowest count of these genera among all the organic waste composts analyzed.

*Pseudomonas* was found across all the composts analyzed. The leaf compost had a higher richness of *Pseudomonas* than other organic waste composts analyzed,

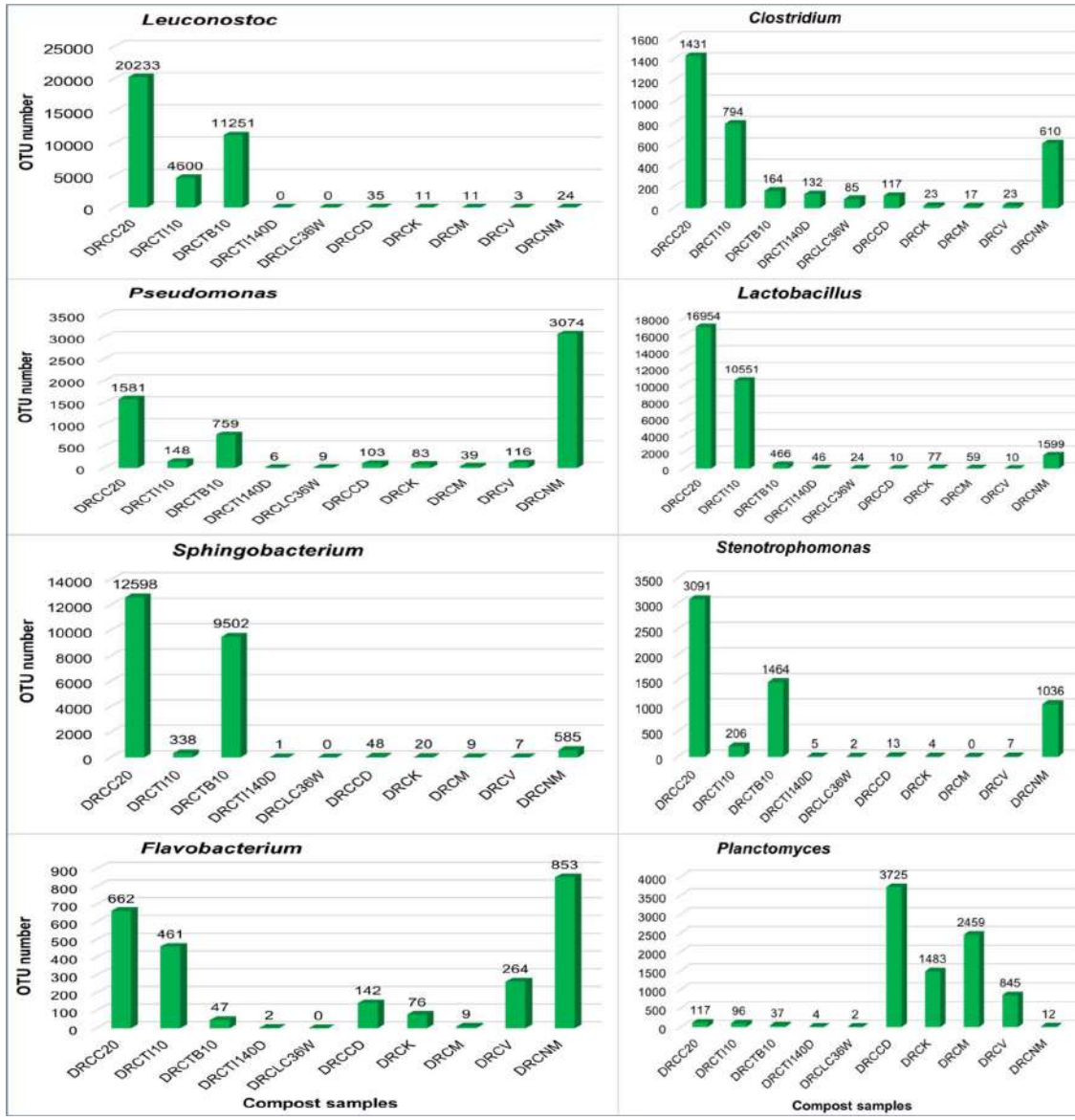


Fig. 6: The prominent beneficial bacterial genera identified in the leaf litter compost and other organic waste composts.

though lower than neem cake compost (DRCNM). Among the leaf composts, the sample DRCC20 had a higher count of *Pseudomonas* than the other treatments. Meanwhile, the municipal organic waste compost (DRCM) had the lowest count of *Pseudomonas* among all the organic waste composts analyzed. *Clostridium* enrichment was found in all the composts analyzed in this study, with relatively higher counts in leaf and neem cake composts. The counts of *Clostridium* were relatively low in the kitchen waste compost (DRCK) and vermicompost (DRCV). The municipal organic waste compost (DRCM) had the lowest level of *Clostridium* among all the composts analyzed (Fig. 6).

*Planctomyces* were also detected in all the composts but with a relatively lower level in the leaf composts. The enrichment of *Planctomyces* was highest in cow dung manure (DRCCD), followed by municipal organic waste compost (DRCM). The kitchen waste compost and vermicompost were also seen with high enrichment of *Planctomyces*. Conversely, the neem cake compost (DRCNM) had a very low level of *Planctomyces* enrichment, the lowest among all the composts. The levels of *Flavobacterium* were relatively higher in the neem cake compost, leaf compost, and vermicompost. While their counts were low in the municipal organic and kitchen waste compost

The richness of *Paenibacillus* was low in all the composts but relatively higher in the leaf composts and the neem cake compost. The cow dung manure (DRCCD) and vermicompost (DRCV) had the lowest count of *Paenibacillus* among all the organic waste composts. *Achromobacter* was also present in all the composts, with a relatively higher abundance in the leaf and neem cake composts. The level of *Achromobacter* was relatively low in the cow dung manure, municipal organic waste compost, and vermicompost. The bacterial genera such as *Stenotrophomonas, Acetobacter,* and *Enterococcus* were relatively high only in the leaf and neem cake compost.

Some bacterial genera, such as *Coprococcus, Gluconobacter, Haloarcula,* and *Haloferax*, were found to be exclusively high in leaf compost. Such bacterial genera were either very low or absent in the other organic waste composts analyzed in this study. *Methanosarcina,* a methane-producing bacterial genus, was found in high abundance in cow dung manure (DRCCD). At the same time, its presence was very low in other composts and completely absent in the leaf compost and neem cake compost. *Rhodoplanes* were also found with higher abundance in the cow dung manure and vermicompost. *Bacillus*, a biological pest control agent, was found to be present in all the composts but with low abundance in all the composts except in the neem cake compost. The neem cake compost was seen to be highly enriched with *Bacillus*.

Some bacterial genera that can be detrimental to soil and pathogenic to humans and plants were also found in different composts analyzed in this study. However, their level of counts was much lower than the beneficial genera. Such bacterial genera identified were *Agrobacterium, Fusobacterium, Prevotella, Steroidobacter, Streptococcus, Neisseria,* and *Mycobacterium*. The level of counts of each genus varied depending on the types of composts. The neem cake and leaf compost had a relatively higher count of *Prevotella*. The cow dung manure had the highest count of *Steroidobacter* among all the composts. The vermicompost

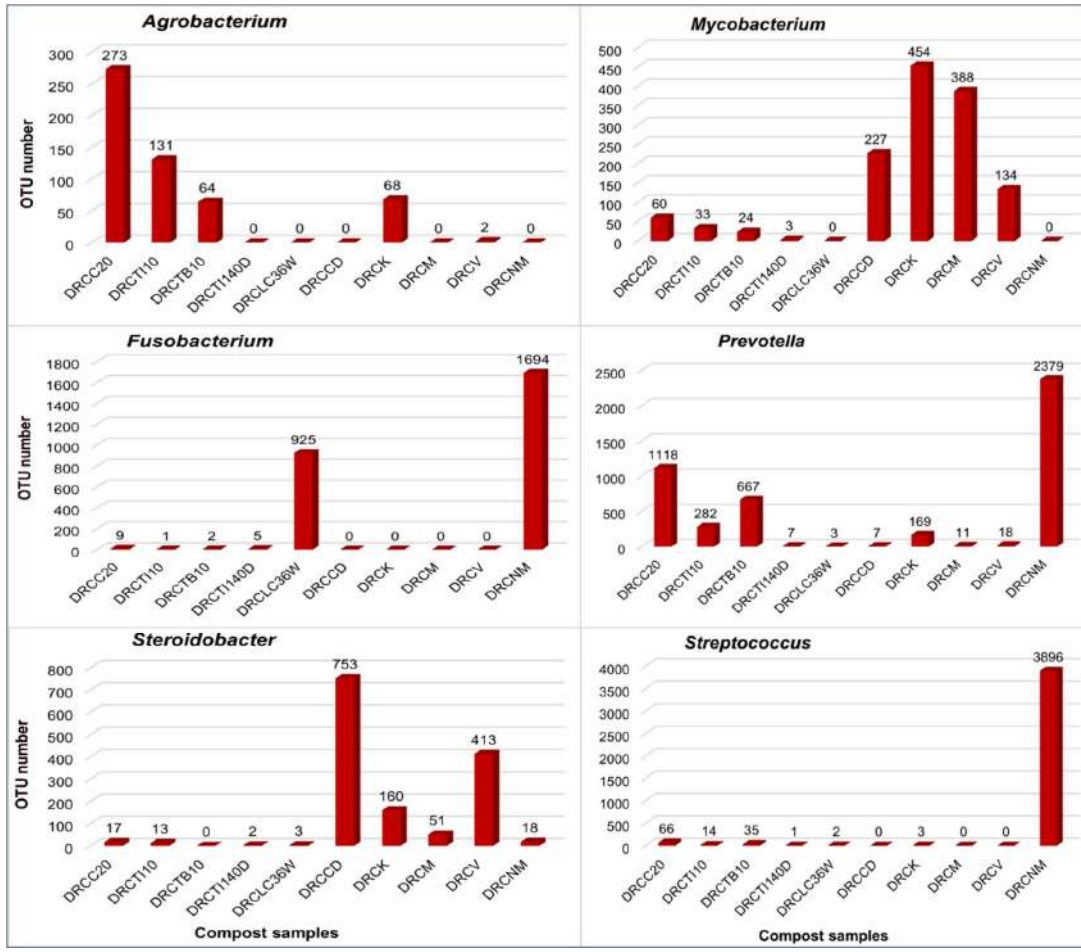


Fig. 7: The prominent bacterial pathogenic genera detected in the leaf litter compost and other organic waste composts.

and kitchen waste compost also had a relatively high level of *Steroidobacter*. A plant pathogenic genus, *Agrobacterium,* was detected only in leaf and kitchen waste compost but with relatively low abundance. The neem cake compost had a higher level of *Streptococcus, Neisseria,* and *Fusobacterium*. Such bacterial genera were either very low or absent in the other composts analyzed. *Mycobacterium, a* common human pathogen, was found with a relatively high level in kitchen waste compost, municipal organic waste compost, cow dung manure, and vermicompost. *Mycobacterium* was also detected in the leaf compost but with very low counts, and it was completely absent in the neem cake compost (Fig. 7).

The resolution of the metagenomic analysis through 16S rRNA profiling at the species level could have been better**.** However, we could identify some beneficial and pathogenic bacterial species across all the compost samples**.** The leaf compost was high in bacterial species such as *Sphingobacterium zeae, Lactobacillus intestinalis, Sphingobacterium multivorum,* and *Prevetolla copri*. Their contents were higher in the sample DCRC20 than the other treatment samples like DRCTI10 and RDCTB10. The bacterial species such as *Kuenenia stuttgartiensis, Flavobacterium defluvii, Sorangium cellulosum,* and *Ignavibacterium album* were high in the leaf compost samples, DRCTI140D and DRCLC36W. The presence of various bacterial species in different composts was also detected. The bacterial species were present in varied proportions in different bio-composts. Cow dung manure (DRCCD) was high in bacterial species such as *Sphingobacterium multivorum, Sorangium cellulosum, Legionella pneumophila*, and *Bdellovibrio bacteriovorus*. Kitchen waste compost (DRCK) had a high content of *Nocardia vinacea, Methylocystis hirsuta, Prevetolla copri, Acholeplasma ladlawii*, and *Brevundimonas diminuta*. The municipal organic waste compost (DRCM) also had an increased range of *Nocardia vinacea* and *Acholeplasma Acholeplasma ladlawii,* along with other species such as *Bacillus thermoamylovorans, Bacillus rugosus*, and *Corynebacterium stationis*. Vermicompost (DRCV) was also seen high of *Cladosporium fulvum, Nocardia vinacea, Myconacterium arupense, Prevetolla copri*, and *Halomonas campisalis*. The neem cake compost (DRCNM) had a high content of different species, such as *Streptococcus mutans, Bifidobacterium animalis, Treponema denticola, Fusobacterium nucleatum*, and *Rothia mucilaginosa*.

**The Proportion of Beneficial and Pathogenic Microbiome**

The leaf compost has an aptly high proportion of beneficial genera both in the control and the experimental samples. The proportion of beneficial and pathogenic genera varied from sample to sample, depending on the nature of the compost. The leaf compost, DRCTI10, had the highest proportion of the beneficial genera, followed by cow dung manure (DRCCD). The leaf composts had a proportion of about 92% to 95% beneficial genera. The neem cake compost, DRCNM, had the lowest percentage of the beneficial genera at 13%. The kitchen waste compost (DRCK) and municipal organic waste compost (DRCM) also had a relatively lower proportion of the beneficial genera at 21% and 24%, respectively. The cow dung manure (DRCCD) and vermicompost (DRCV) had a relatively high proportion of beneficial genera at 54% and 37%, respectively.

Table 3 shows the percentage of beneficial and pathogenic microbes in different bio-composts. The leaf waste compost and cow dung manure had a high proportion of beneficial microbes with low pathogenic microbes.

The proportion of the pathogenic genera in the leaf compost DRCTI10 was low, about 3%. The municipal organic waste and cow dung manure had a comparatively similar fraction of the pathogenic genera with that of the leaf waste compost, at 3% and 4%, respectively. The neem cake compost, municipal organic waste compost, and kitchen waste compost had a relatively higher fraction of pathogens with respect to the leaf waste compost, at about 13%, 9 %, and 6%, respectively. The leaf compost and cow dung manure had the best ratio of beneficial to pathogenic genera at 34.61 and 14.97. The neem cake compost, kitchen waste compost,

Table 3: Percentage of beneficial and pathogenic microbes in leaf compost and other organic waste composts.

| | DRC C20 | DRC TI10 | DRC TB10 | DRC TI140D | DRC LC36W | DRC CD | DRCK | DRCM | DRCV | DRCNM |
|---|---|---|---|---|---|---|---|---|---|---|
| Total OTU of all the bacterial genera | 84458 | 22084 | 38200 | 5044 | 4495 | 27653 | 15134 | 15071 | 6426 | 97541 |
| Total OTU of beneficial genera | 79761 | 20422 | 36167 | 3572 | 2540 | 15026 | 3169 | 3669 | 2392 | 12332 |
| **Percentage of beneficial genera** | **94%** | **92%** | **95%** | **71%** | **57%** | **54%** | **21%** | **24%** | **37%** | **13%** |
| Total OTU of pathogenic genera | 9664 | 590 | 5928 | 18 | 974 | 1004 | 855 | 450 | 568 | 12216 |
| **Percentage of pathogenic genera** | **11%** | **3%** | **16%** | **0.35%** | **22%** | **4%** | **6%** | **3%** | **9%** | **13%** |
| Ratio of beneficial and pathogenic genera | 8.25 | 34.61 | 6.10 | 198.44 | 2.61 | 14.97 | 3.71 | 8.15 | 4.21 | 1.01 |

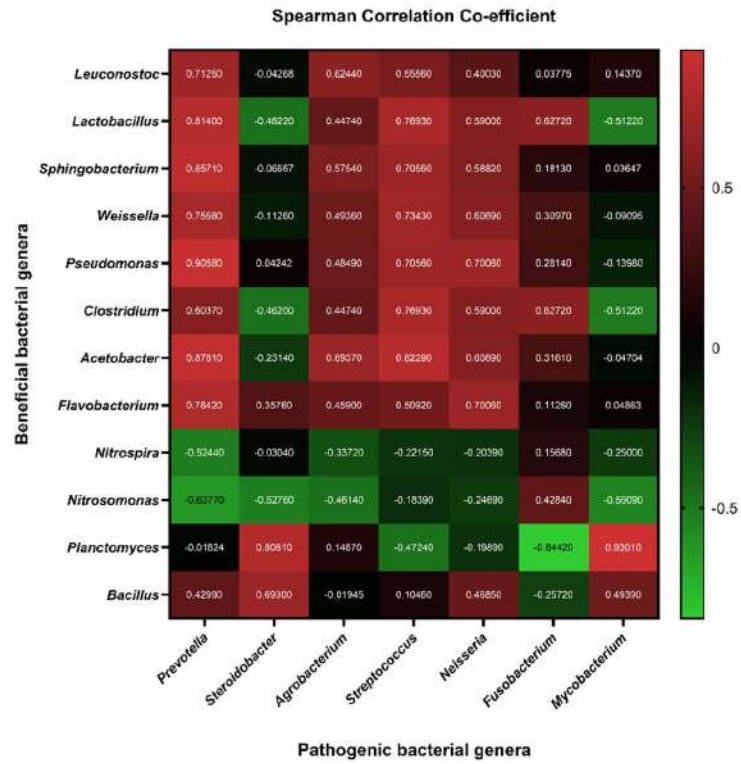


Fig. 8: The Spearman correlation coefficient between the beneficial and pathogenic bacterial genera detected in the composts.

vermicompost, and municipal organic waste compost had a lower ratio of beneficial to pathogenic genera than the leaf compost (Table 3).

The Spearman correlation coefficients revealed associations between various bacterial genera. Notably, Leuconostoc exhibited strong positive correlations with several genera, including *Lactobacillus, Sphingobacterium, Weissella, Pseudomonas, Clostridium, Acetobacter,* and *Flavobacterium*, while showing negative correlations with *Nitrospira* and *Nitrosomonas*. *Steroidobacter* demonstrated positive correlations with *Planctomyces* and *Bacillus* and negative correlations with multiple genera. *Agrobacterium* was positively correlated with numerous genera but negatively correlated with *Nitrospira* and *Nitrosomonas*. *Streptococcus* and *Neisseria* exhibited positive correlations with various genera and negative correlations with *Nitrospira* and *Nitrosomonas*. *Fusobacterium* displayed positive correlations with multiple genera and negative correlations with *Nitrospira* and *Nitrosomonas*. *Mycobacterium* was positively correlated with *Planctomyces, Bacillus,* and *Nitrosomonas*, with negative correlations observed with several other genera. These findings highlighted microbial communities' interconnectedness and potential ecological relationships, providing insights into co-occurrence patterns among different bacterial genera (Fig. 8).

## Bacterial Microbiome Diversity of Leaf and Other Organic Waste Composts

This study was conducted to understand the potential of leaf and different organic waste composts as bio-organic fertilizers through the 16S rRNA profiling method. This method is one of the most adopted approaches to analyze the whole bacterial and archaeal communities present in environmental samples like compost since it is a low-cost method with high computational and analytical speed, having a curated and extensive reference database with well-established bioinformatic analytical pipelines (Callahan et al. 2016, Quast et al. 2013, Marcelino et al. 2020). The investigation into microbial richness and diversity within these diverse compost types yielded substantive insights into the intricacies of composting processes and the resultant quality of matured compost. Notably, the enumeration of reads and operational taxonomic units (OTUs) serves as proxy indicators for microbial biomass and diversity, respectively (Mysara et al. 2017). The observed variations in microbial diversity, as discerned through alpha diversity indices (Chao 1, Shannon, Fisher, and Simpson), underscore the profound influence of organic substrates on microbial communities during composting. This phenomenon finds corroboration in existing literature, elucidating the substantive role of substrate composition in shaping

microbial consortia during composting (Franke-Whittle et al. 2014, Matheri et al. 2023, Wang et al. 2022, Willis 2019). Moreover, the inferred positive correlation between microbial biomass, as reflected by read counts, and compost quality aligns with precedent studies, substantiating the pivotal role of microbial activity in the composting process (Tiquia 2005). The alpha diversity indices, encapsulating richness and evenness, signify implications for compost quality and maturity.

Furthermore, the beta diversity analysis, conducted at the taxonomic genus level using the Bray-Curtis index distance method, affords insights into the unique microbial communities characterizing distinct compost types. The collective clustering of leaf litter composts and the discernible dispersion of other types of organic waste composts underline the divergence in microbial diversity and highlight the potential avenues for optimizing composting processes. Integrating these outcomes with other studies that elucidated the augmenting influence of diverse organic materials on microbial diversity and composting acceleration unveils prospective strategies for refining compost production practices (Chandna et al. 2013, Wang et al. 2023). The refined understanding of microbial dynamics within various compost types offers a scientific basis for adapting feedstock selection and management protocols, thereby contributing to the realization of targeted objectives of compost quality production. However, it is imperative to acknowledge the study's limitations and advocate for future research endeavors exploring the relationship between compost microbial diversity and specific indicators of plant growth and soil health. In consolidation, this investigation advances our scientific understanding of composting intricacies and their implications, laying a basis for refined practices in sustainable compost production.

**Bacterial Microorganisms in Composts Could Have Potential Benefits for Soil Health and Plant Growth**

Different organic-waste composts were seen to be enriched with various beneficial microbes that could play important roles in soil fertility and plant growth. Beneficial phyla identified in different composts include *Firmicutes, Proteobacteria, Cyanobacteria, Actinobacteria, Euryarchaeota,* and others. *Firmicutes* are known to be probiotics, which can degrade carbohydrates. It has also been reported that they could facilitate the bioremediation of contaminated soil (Gupta et al. 2018, Li et al. 2020, Wieczorek et al. 2019). Their presence was detected in all the composts analyzed, with relatively high in the leaf compost and neem cake compost. *Proteobacteria* is another phyla of interest present in all the composts studied with relatively high amounts since they have the potential for nitrogen fixation. However, some species can cause opportunistic infection in humans (Delmont et al. 2018). *Cyanobacteria* is a photosynthetic bacterium with the potential to fix nitrogen and promote plant growth (Rai et al. 2018, Singh et al. 2016). *Cyanobacteria* were detected in all the analyzed composts, with relatively higher counts in kitchen waste and leaf compost, indicating their presence in foliage compost. *Actinobacteria* are decomposers that could play an important role in the nitrogen cycle and phosphate solubilization, promoting plant growth (Vargas Hoyos et al. 2021, Zhang et al. 2019). *Actinobacteria* were detected in all the composts analyzed. Their content was high in the cow dung manure and neem cake compost while relatively poorer in the leaf compost. *Euryarchaeota*, which is a methanogenic halophile and thermophilic decomposer (Castro-Fernandez et al. 2017, Horz & Conrads 2010), was also detected in higher concentration in the cow dung manure as compared to the leaf compost and other organic-waste composts analyzed. The other phyla that could benefit soil fertility and plant growth were also detected, viz. *Planctomycetes, Chloroflexi, Acidobacteria, Verrucomicrobia, Fibrobacteres, Chlorobi, Gemmatimonadota,* and *Nitrospirae*. However, such phyla were detected in the leaf compost with a relatively lower concentration than the other composts analyzed. The presence of such phyla can render beneficial potential to the bio-composts like organic matter decomposition, nitrification, and plant growth promotion.

The prominent beneficial bacterial genera identified in different composts were *Leuconostoc*, *Lactobacillus, Sphingobacterium, Coprococcus, Clostridium, Acetobacter, Gluconobacter,* and *Haloarcula*. These genera were detected at a relatively higher level in the leaf compost than in the other organic waste composts. Such genera could impart bio-fertilizing and bio-control potential to the compost since such genera are known to be plant growth promoters, nitrogen-fixing, nutrients solubilizing, toxins degrading, salt tolerant, anti-oxidant, and anti-microbial (Horz & Conrads 2010, Mohamed & Abd-el salam 2021, Tóth et al. 2021, Vaishnav et al. 2020).

Biological pest control agents such as *Pseudomonas* and *Bacillus* were relatively higher in the neem cake compost than in the leaf compost and other composts. Methane-producing bacteria, *Methanosarcina*, was identified in cow dung manure with much abundance compared to others, and their presence was almost absent in the leaf compost. *Planctomyces*, an anammox metabolizing bacteria, were detected relatively higher in abundance in cow dung manure, municipal organic waste compost, kitchen waste compost, and vermicompost but were almost absent in the leaf and neem cake compost. Another nitrogen-fixing bacteria, *Rhodoplanes*, was identified in higher concentrations in

cow dung manure and vermicompost. While their content was almost negligible in the leaf compost and kitchen-waste compost.

At the species level, the resolution of 16s rRNA profiling of bacterial microbiome becomes very ambiguous since numerous OTUs could not be classified. However, the presence of some beneficial and pathogenic bacterial species was detected. The beneficial species detected across samples include *Sphingobacterium zeae, Prevetolla copri,* Pseudomonas *geniculata, Faecalibacterium prausnitzii, Stenotrophomonas acidaminiphila, Bdellovibrio bacteriovorus, Pseudomonas stutzeri, Flavobacterium defluvii, Lactobacillus intestinalis*, and *Blastococcus endophyticus*. These species can render beneficial characteristics to soil fertility and plant health since they can solubilize nutrients, fix nitrogen in the soil, promote plant growth, and bioremediate toxins (Gopalakrishnan et al. 2015, Lalucat et al. 2006, Yeoh et al. 2022).

**Bacterial Microorganisms in the Composts Could Pose Potential Risks to Soil Health and Plant Growth**

The presence of some pathogenic species was detected in low amounts in all the composts analyzed, with the lowest counts in the leaf compost. Some pathogenic phyla identified were *Spirochaetes, Fusobacteria,* and *Chlamydiae*. *Spirochaetes*, which is a human pathogen, was detected relatively higher in cow dung manure, kitchen waste compost, and municipal organic waste compost. *Fusobacteria*, which is also a human pathogen, was detected relatively higher in the neem cake compost and the leaf compost that was composted long with neem and castor leaves. Another human pathogenic species, *Chlamydiae*, was detected with a relatively higher content in cow dung manure, vermicompost, and kitchen waste compost than leaf compost.

Some pathogenic genera were also detected with dissimilar proportions in different composts analyzed, although their presence was very low compared to the beneficial genera. The pathogenic genera identified across the samples include *Prevotella, Agrobacterium, Streptococcus, Neisseria, Fusobacterium, and Mycobacterium*. *Prevotella,* a human pathogen (Tett et al. 2021), was detected relatively high in the neem cake compost. Its presence was also comparatively high in the leaf and kitchen waste compost with respect to vermicompost, municipal organic waste compost, and cow dung manure. *Agrobacterium*, a common plant pathogen, was detected in trace amounts in the leaf compost, kitchen waste compost, and vermicompost. However, its presence could not be detected in other bio-compost analyses. *Streptococcus*, a human pathogen, and *Neisseria*, a human pathogen and denitrifying bacteria, were detected with relatively higher abundance in the neem cake compost. Their presence was almost absent in the other composts analyzed. *Mycobacterium*, a potential human pathogenic bacterial genus, was identified in the kitchen waste compost, municipal organic waste compost, cow dung manure, and vermicompost with higher abundance than the leaf compost. *Steroiderbacter*, a denitrifying bacteria that can cause loss of nutrients in the soil (Fahrbach et al. 2008), was another non-beneficial genus detected with higher abundance in the cow dung manure, vermicompost, and kitchen waste compost.

Non-beneficial and pathogenic bacterial species identified across the samples were *Enterococcus faecium, Clostridioides difficile, Legionella pneumophila, Halomonas campisalis, Mycobacterium arupense,* and *Treponema denticola*. Many of them are pathogenic to humans, whereas some species, such as *Halomonas campisalis,* can cause de-nitrification in the soil (Elsayed & Zhan 2004, Zhou et al. 2020). However, the level of such species was relatively low compared to the beneficial species identified across the bio-composts.

**The Bio-Fertilizing Potential of Leaf and Other Organic Waste Composts**

The ratio of the beneficial genera to the pathogenic genera and total microbiome can give some insights into the bio-fertilizing potential of the compost. The results revealed that leaf compost has a high proportion of beneficial genera, making it a potentially valuable bio-fertilizer. The high percentage of beneficial genera, ranging from 92% to 95%, indicates that the leaf compost is rich in microorganisms that could contribute to the enhancement of soil fertility and plant growth (Ho et al. 2022, Ventorino et al. 2019). The relatively low proportion of pathogenic genera in the leaf compost, around 3%, is promising for its bio-fertilizing potential. A low presence of pathogenic microorganisms suggests that the compost is less likely to cause harm to plants or the soil ecosystem. This is crucial for bio-fertilizers, as they should ideally promote plant health without introducing harmful pathogens (Ahmed et al. 2023, Daniel et al. 2022). Comparatively, cow dung manure also demonstrated a high proportion of beneficial genera at 54%, making it another promising source of bio-fertilizer. The low percentage of pathogenic genera (4%) in cow dung manure further supports its potential as a beneficial soil amendment (Tagele et al. 2023).

On the other hand, neem cake compost exhibited a low percentage of beneficial genera (13%) and a relatively higher fraction of pathogenic genera (13%). This suggests that while neem cake compost may still have some bio-fertilizing potential, its effectiveness might be limited compared to

leaf compost or cow dung manure. Neem cake is known for its pesticidal properties, and its use in composting may impact the microbial composition (Del Serrone & Nicolett 2013). Kitchen waste compost and municipal organic waste compost showed lower proportions of beneficial genera (21% and 24%, respectively) and a higher fraction of pathogenic genera (6% and 9%, respectively). These composts may still contribute to soil fertility, but their bio-fertilizing potential might be somewhat compromised due to the higher presence of potentially harmful microorganisms unless well-segregated organic sources are used in composting. Vermicompost had a moderate proportion of beneficial genera (37%) and a relatively low percentage of pathogenic genera, suggesting it could be a reasonably effective bio-fertilizer, although not as high as leaf compost or cow dung manure.

In general, the leaf compost, especially DRCTI10 and cow dung manure, appear to be promising bio-fertilizers due to their high proportion of beneficial genera and low presence of pathogens. These findings emphasize the importance of understanding the microbial composition of composts to optimize their bio-fertilizing potential and promote sustainable agriculture practices (Ahmed et al. 2023, Kumar et al. 2022). The leaf litter compost was also reported to have high nutrients and low potentially toxic elements (Mahongnao et al. 2023). Thus, with these results that leaf compost has a high nutrient level and a high proportion of beneficial microorganisms with low pathogenic microorganisms and potentially toxic elements, we recommend that leaf litter compost could be suitably used as bio-organic fertilizer for sustainable agricultural productivity.

## CONCLUSION

We can conclude that leaf-based composts and other types of composts produced from different organic wastes have varied microbiome richness and diversity. Various beneficial microorganisms viz. *Lactobacillus, Leuconostoc, Sphingobacterium, Paenibacillus, Pseudomonas,* and *Clostridium* were present in divergent proportions in the leaf compost and other organic waste composts. All the composts analyzed have a high proportion of beneficial and low pathogenic organisms. The best proportion of the beneficial to the pathogenic genera was found in the leaf litter compost. Thus, it could be used as a valuable bio-organic fertilizer in agricultural systems for promoting soil health and plant growth.

## ACKNOWLEDGMENT

The Authors are thankful to Prof. Savita Roy, Principal of the Daulat Ram College, University of Delhi, for providing the logistics support for this research. We are also grateful to the Department of Biochemistry, Daulat Ram College, University of Delhi, for providing this research's working space and equipment. We also acknowledged the University Grant Commission, Govt. of India, for granting a research fellowship to the first author, bearing the award letter no. 598/CSIR-UGC NET JUNE 2018.

## REFERENCES

Aguilar-Paredes, A., Valdés, G., Araneda, N., Valdebenito, E., Hansen, F. and Nuti, M. 2023. Microbial community in the composting process and its positive impact on the soil biota in sustainable agriculture. Agronomy, 13: 542. https://doi.org/https://doi.org/10.3390/agronomy13020542

Ahmed, T., Noman, M., Qi, Y., Shahid, M., Hussain, S., Masood, H. A., Xu, L., Ali, H. M., Negm, S., El-Kott, A. F., Yao, Y., Qi, X. and Li, B. 2023. Fertilization of Microbial Composts: A Technology for Improving Stress Resilience in Plants. Plants, 12: 1-31. https://doi.org/10.3390/plants12203550

Bustamante, M. A., Gomis, M. P., Pérez-Murcia, M. D., Gangi, D., Ceglie, F. G., Paredes, C., Pérez-Espinosa, A., Bernal, M. P. and Moral, R. 2021. Use of livestock waste composts as nursery growing media: Effect of a washing pre-treatment. Sci. Hortic., 10: 281. https://doi.org/10.1016/j.scienta.2021.109954

Callahan, B. J., McMurdie, P. J., Rosen, M. J., Han, A. W., Johnson, A. J. A. and Holmes, S. P. 2016. DADA2: High-resolution sample inference from Illumina amplicon data. Nat. Methods, 13: 581-583. https://doi.org/10.1038/nmeth.3869

Castro-Fernandez, V., Zamora, R., Morande, A. H., Vallejos, G., Gonzalez Ordenes, F. and Guixé, V. 2017. Evolution, metabolism, and molecular mechanisms underlying extreme adaptation of Euryarchaeota and its biotechnological potential. Archaea. Pharm. Var. Biotechnol. Appl., 10: 77. https://doi.org/10.5772/intechopen.69943

Chandna, P., Nain, L., Singh, S. and Kuhad, R. C. 2013. Assessment of bacterial diversity during composting of agricultural byproducts. BMC Microbiol., 13. [Online]. Available: https://doi.org/10.1186/1471-2180-13-99

Chauhan, N. B. and P. S. 2016. Excessive and Disproportionate Use of Chemicals Cause Soil Contamination and Nutritional Stress. Intech, 11, 13.

Daniel, A. I., Fadaka, A. O., Gokul, A., Bakare, O. O., Aina, O., Fisher, S., Burt, A. F., Mavumengwana, V., Keyster, M. and Klein, A. 2022. Biofertilizer: The Future of Food Security and Food Safety. Microorganisms, 10. [Online]. Available: https://doi.org/10.3390/microorganisms10061220

De Corato, U. 2020. Disease-suppressive compost enhances natural soil suppressiveness against soil-borne plant pathogens: A critical review. Rhizosphere, 13: 100192. [Online]. Available: https://doi.org/10.1016/j.rhisph.2020.100192

Del Serrone, P. and Nicoletti, M. 2013. Antimicrobial activity of a neem cake extract in a broth model meat system. Int. J. Environ. Res. Public Health, 10: 3282-3295. https://doi.org/10.3390/ijerph10083282

Delmont, T. O., Quince, C., Shaiber, A., Esen, Ö. C., Lee, S. T., Rappé, M. S., MacLellan, S. L., Lücker, S. and Eren, A. M. 2018. Nitrogen-fixing populations of Planctomycetes and Proteobacteria are abundant in surface ocean metagenomes. Nat. Microbiol., 3: 804-813. https://doi.org/https://doi.org/10.1038/s41564-018-0176-9

Devi, S. G., Fathima, A. A., Radha, S., Arunraj, R., Curtis, W. R. and Ramya, M. 2015. A rapid and economical method for efficient DNA extraction from diverse soils suitable for metagenomic applications. PLoS One, 10: 1-16. https://doi.org/https://doi.org/10.1371/journal.pone.0132441

Eifediyi, E., Ahamefule, H. and Remison, S. 2015. Effects of neem seed cake on the growth and yield of okra (Abelmoschus esculentus (L.)

Moench) in Ilorin, north-central Nigeria. Agro-Science, 12: 20. https://doi.org/10.4314/as.v12i2.3

Elsayed, S. and Zhang, K. 2004. Bacteremia caused by Clostridium symbiosum. J. Clin. Microbiol., 42: 4390-4392. https://doi.org/10.1128/JCM.42.9.4390-4392.2004

Fahrbach, M., Kuever, J., Remesch, M., Huber, B. E., Kämpfer, P., Dott, W. and Hollender, J. 2008. Steroidobacter denitrificans gen. nov., sp. nov., a steroidal hormone-degrading gammaproteobacterium. Int. J. Syst. Evol. Microbiol., 58: 2215-2223. https://doi.org/10.1099/ijs.0.65342-0

Faust, K., Lahti, L., Gonze, D., de Vos, W. M. and Raes, J. 2015. Metagenomics meets time series analysis: Unraveling microbial community dynamics. Curr. Opin. Microbiol., 25: 56-66. https://doi.org/10.1016/j.mib.2015.04.004

Fertiplus, P., Vandecasteele, B., Hose, T. D., Guadalupe, L., Mart, C., Kuikman, P. J., Sinicco, T. and Mondini, C. 2019. Agronomic evaluation of biochar, compost and biochar-blended compost across different cropping systems: Perspective from the European. Agronomy, 9. https://doi.org/doi:10.3390/agronomy9050225

Franke-Whittle, I.H., Confalonieri, A., Insam, H., Schlegelmilch, M. and Körner, I. 2014. Changes in the microbial communities during co-composting of digestates. Waste Manag., 641-632 :34. https://doi.org/10.1016/j.wasman.2013.12.009

García-Alegría, A. M. anduro-Corona, I., Pérez-Martínez, C. J., Corella-Madueño, M. A. G., Rascón-Durán, M. L. and Astiazaran-Garcia, H. 2020. Quantification of DNA through the nanodrop spectrophotometer: Methodological validation using standard reference material and Sprague Dawley rat and human DNA. Int. J. Anal. Chem., 2020. https://doi.org/https://doi.org/10.1155/2020/8896738

González-González, S., Astorga-Eló, M., Campos, M., Wick, L. Y., Acuña, J. J. and Jorquera, M. A. 2021. Compost fungi allow for the effective dispersal of putative PGP bacteria. Agronomy, 11: 1-18. https://doi.org/10.3390/agronomy11081567

Gopalakrishnan, S., Srinivas, V., Prakash, B., Sathya, A. and Vijayabharathi, R. 2015. Plant growth-promoting traits of *Pseudomonas geniculata* isolated from chickpea nodules. 3 Biotech, 5: 653-661. https://doi.org/10.1007/s13205-014-0263-4

Ho, T. T. K., Tra, V. T., Le, T. H., Nguyen, N. K. Q., Tran, C. S., Nguyen, P. T., Vo, T. D. H., Thai, V. N. and Bui, X. T. 2022. Compost to improve sustainable soil cultivation and crop productivity. Case Stud. Chem. Environ. Eng., 6: 100211. https://doi.org/10.1016/j.cscee.2022.100211

Horz, H. P. and Conrads, G. 2010. The discussion goes on: What is the role of Euryarchaeota in humans? Archaea, 2010. https://doi.org/10.1155/2010/967271

Kumar, S., Diksha, Sindhu, S. S. and Kumar, R. 2022. Biofertilizers: An eco-friendly technology for nutrient recycling and environmental sustainability. Curr. Res. Microb. Sci., 3: 100094. https://doi.org/10.1016/j.crmicr.2021.100094

Lalucat, J., Bennasar, A., Bosch, R., García-Valdés, E. and Palleroni, N.J. 2006. Biology of Pseudomonas stutzeri. Microbiol. Mol. Biol. Rev., 70: 510-547. https://doi.org/10.1128/mmbr.00047-05

Li, W., Zhang, Y., Mao, W., Wang, C. and Yin, S. 2020. Functional potential differences between firmicutes and proteobacteria in response to manure amendment in a reclaimed soil. Can. J. Microbiol., 66: 689-697. https://doi.org/10.1139/cjm-2020-0143

Machado, R. M. A., Alves-Pereira, I., Robalo, M. and Ferreira, R. 2021. Effects of municipal solid waste compost supplemented with inorganic nitrogen on physicochemical soil characteristics, plant growth, nitrate content, and antioxidant activity in Spinach. Horticulturae, 7. https://doi.org/10.3390/horticulturae7030053

Mahapatra, S., Yadav, R. and Ramakrishna, W. 2022. Bacillus subtilis impact on plant growth, soil health, and environment: Dr. Jekyll and Mr. Hyde. J. Appl. Microbiol., 132: 3543-3562. https://doi.org/10.1111/jam.15480

Mahongnao, S., Sharma, P., Singh, D., Ahamad, A., Kumar, P. V., Kumar P. and Nanda S. 2023. Formation and characterization of leaf waste into organic compost. Environ. Sci. Pollut. Res. https://doi.org/https://doi.org/10.1007/s11356-023-27768-7

Martins, L. F., Antunes, L. P., Pascon, R. C., de Oliveira, J. C. F., Digiampietri, L. A., Barbosa, D., Peixoto, B. M., Vallim, M. A., Viana-Niero, C., Ostroski, E. H., Telles, G. P., Dias, Z., da Cruz, J. B., Juliano, L., Verjovski-Almeida, S., da Silva, A. M. and Setubal, J. C. 2013. Metagenomic analysis of a tropical composting operation at the São Paulo zoo park reveals diversity of biomass degradation functions and organisms. PLoS One, 8. https://doi.org/10.1371/journal.pone.0061928

Matheri, F., Kambura, A. K., Mwangi, M., Ongeso, N., Karanja, E., Adamtey, N., Mwangi, E. K., Mwangi, E., Tanga, C., Musyoka, M. W. and Runo, S. 2023. Composition, structure, and functional shifts of prokaryotic communities in response to co-composting of various nitrogenous green feedstocks. BMC Microbiol., 23: 1-18. https://doi.org/10.1186/s12866-023-02798-w

Maziarz, M., Pfeiffer, R. M., Wan, Y. and Gail, M. H. 2018. Using standard microbiome reference groups to simplify beta-diversity analyses and facilitate independent validation. Bioinformatics, 34: 3249-3257. https://doi.org/10.1093/bioinformatics/bty297

Mbareche, H., Veillette, M., Bonifait, L., Dubuis, M. E., Benard, Y., Marchand, G., Bilodeau, G. J. and Duchaine, C. 2017. A next-generation sequencing approach with a suitable bioinformatics workflow to study fungal diversity in bioaerosols released from two different types of composting plants. Sci. Total Environ., 601-602: 1306-1314. https://doi.org/10.1016/j.scitotenv.2017.05.235

Mysara, M., Vandamme, P., Props, R., Kerckhof, F.M., Leys, N., Boon, N., Raes, J. and Monsieurs, P. 2017. Reconciliation between operational taxonomic units and species boundaries. *FEMS Microbiology Ecology*, *93*(4): fix029.

Pathak, P., Singh, C., Chaudhary, N. and Vyas, D. 2020. Application of Biochar, Leaf Compost, and Spent Mushroom Compost for Tomato Growth in Alternative to Chemical Fertilizer. Res. J. Agric. Sci., 11: 1362-1366. DOI: 10.4324/9780203762264-15

Quast, C., Pruesse, E., Yilmaz, P., Gerken, J., Schweer, T., Yarza, P., Peplies, J. and Glöckner, F.O. 2013. The SILVA ribosomal RNA gene database project: Improved data processing and web-based tools. Nucleic Acids Res., 41: 1-7. DOI: 10.1093/nar/gks1219

Marcelino, V. R., Holmes, E. C. and Sorrell, T. C. 2020. The use of taxon-specific reference databases compromises metagenomic classification. BMC Genomics, 21L 1-5. DOI: 10.1186/s12864-020-6592-2

Rai, A. N., Singh, A. K. and Syiem, M. B. 2018. Plant Growth-Promoting Abilities in Cyanobacteria, Cyanobacteria: From Basic Science to Applications. Elsevier Inc., The Netherlands, pp. 23-24

Ramírez-Guzmán, A., Taran, Y. and Armienta, M. A. 2004. Geochemistry and origin of high-pH thermal springs in the Pacific coast of Guerrero, Mexico. Geofis. Int., 43: 415-425. DOI: 10.22201/igeof.00167169p.2004.43.3.967

Ravindran, B., Awasthi, M. K. and Karmegam, N. G. 2022. Co-composting of food waste and swine manure augmenting biochar and salts: Nutrient dynamics, gaseous emissions, and microbial activity. Bioresour. Technol., 344: 126300. DOI: 10.1016/j.biortech.2021.126300

Siles, J. A., García-Sánchez, M. and Gómez-Brandón, M. 2021. Studying microbial communities through co-occurrence network analyses during processes of waste treatment and in organically amended soils: A review. Microorganisms, 18-1 :9. DOI: 10.3390/microorganisms9061165

Singh, J. S., Kumar, A., Rai, A. N. and Singh, D. P. 2016. Cyanobacteria: A precious bio-resource in agriculture, ecosystem, and environmental sustainability. Front. Microbiol., 7: 1-19. DOI: 10.3389/fmicb.2016.00529

Tagele, S. B., Kim, R. H., Jeong, M., Lim, K., Jung, D. R., Lee, D., Kim, W. and Shin, J. H. 2023. Soil amendment with cow dung modifies the soil nutrition and microbiota to reduce the ginseng replanting problem. Front. Plant Sci., 14: 1-14. DOI: 10.3389/fpls.2023.1072216

Tett, A., Pasolli, E., Masetti, G., Ercolini, D. and Segata, N. 2021. Prevotella diversity, niches, and interactions with the human host. Nat. Rev. Microbiol., 19: 585-599. DOI: 10.1038/s41579-021-00559-y

Tiquia, S.M. 2005. Microbiological parameters as indicators of compost maturity. J. Appl. Microbiol., 99: 816-828. DOI: 10.1111/j.1365-2672.2005.02673.x

Tóth, Á., Bata-Vidács, I., Kosztik, J., Máté, R., Kutasi, J., Tóth, E., Bóka, K., Táncsics, A., Nagy, I., Kovács, G. and Kukolya, J. 2021. Sphingobacterium pedocola sp. nov. is a novel halotolerant bacterium isolated from agricultural soil. Antonie van Leeuwenhoek, Int. J. Gen. Mol. Microbiol., 114: 1575-1584. DOI: 10.1007/s10482-021-01623-6

Vaishnav, A., Singh, J., Singh, P., Rajput, R. S. and Singh, H.B. 2020. Sphingobacterium sp. BHU-AV3 induces salt tolerance in tomatoes by enhancing antioxidant activities and energy metabolism. Front. Microbiol., 11: 1–13. DOI: 10.3389/fmicb.2020.00443

Vargas Hoyos, H. A., Chiaramonte, J. B., Barbosa-Casteliani, A. G., Fernandez Morais, J., Perez-Jaramillo, J. E., Nobre Santos, S., Nascimento Queiroz, S. C. and Soares Melo, I. 2021. An actinobacterium strain from the soil of Cerrado promotes phosphorus solubilization and plant growth in soybean plants. Front. Bioeng. Biotechnol., 9: 1-13. DOI: 10.3389/fbioe.2021.579906

Ventorino, V., Pascale, A., Fagnano, M., Adamo, P., Faraco, V., Rocco, C., Fiorentino, N. and Pepe, O. 2019. Soil tillage and compost amendment promote bioremediation and biofertility of polluted areas. J. Clean. Prod., 239: 118087. DOI: 10.1016/j.jclepro.2019.118087

Vishan, I., Kanekar, H. and Kalamdhad, A. 2014. Microbial population, stability, and maturity analysis of rotary drum composting of water hyacinth. Biol., 69: 1303-1313. DOI: 10.2478/s11756-014-0450-0

Wan, J., Wang, X., Yang, T., Wei, Z., Banerjee, S., Friman, V. P., Mei, X., Xu, Y. and Shen, Q. 2021. Livestock manure type affects microbial community composition and assembly during composting. Front. Microbiol., 12: 1-11. DOI: 10.3389/fmicb.2021.621126

Wang, C., Jia, Y., Li, J., Li, P., Wang, Y., Yan, F., Wu, M., Fang, W., Xu, F. and Qiu, Z. 2023. Influence of microbial augmentation on contaminated manure composting: metal immobilization, matter transformation, and bacterial response. J. Hazard. Mater. 441, 129762. DOI: 10.1016/j.jhazmat.2022.129762

Wang, T., Ahmad, S., Yang, L., Yan, X., Zhang, Y., Zhang, S., Wang, L. and Luo, Y. 2022. Preparation, biocontrol activity, and growth promotion of biofertilizer containing *Streptomyces aureoverticillatus* HN6. Front. Plant Sci., 13: 1-14. https://doi.org/10.3389/fpls.2022.1090689

Wang, X., He, X. and Liang, J., 2022. Succession of microbial community during the co-composting of food waste digestate and garden waste. Int. J. Environ. Res. Public Health, 19: https://doi.org/10.3390/ijerph19169945

Wieczorek, A.S., Schmidt, O., Chatzinotas, A., Von Bergen, M., Gorissen, A. and Kolb, S. 2019. Ecological functions of agricultural soil bacteria and microeukaryotes in chitin degradation: A case study. Front. Microbiol., 10: 1293. https://doi.org/10.3389/fmicb.2019.01293

Willis, A.D. 2019. Rarefaction, alpha diversity, and statistics. Front. Microbiol. 10. https://doi.org/10.3389/fmicb.2019.02407

Yeoh, Y. K., Sun, Y., Ip, L.Y.T., Wang, L., Chan, F. K. L., Miao, Y. and Ng, S. C. 2022. Prevotella species in the human gut is primarily comprised of *Prevotella copri, Prevotella stercorea*, and related lineages. Sci. Rep. 12: 1-9. https://doi.org/10.1038/s41598-022-12721-4

Zhang, B., Wu, X., Tai, X., Sun, L., Wu, M., Zhang, W., Chen, X., Zhang, G., Chen, T., Liu, G. and Dyson, P. 2019. Variation in actinobacterial community composition and potential function in different soil ecosystems belonging to the arid Heihe River Basin of Northwest China. Front. Microbiol., 10: 1-11. https://doi.org/10.3389/fmicb.2019.02209

Zhang, L., Yan, C., Guo, Q., Zhang, J. and Ruiz-Menjivar, J. 2018. The impact of agricultural chemical inputs on the environment: Global evidence from informetrics analysis and visualization. Int. J. Low-Carbon Technol., 13: 338-352. https://doi.org/10.1093/ijlct/cty039

Zhang, X., Li, L., Butcher, J., Stintzi, A. and Figeys, D. 2019. Advancing functional and translational microbiome research using meta-omics approaches. Microbiome, 7: 1-12. https://doi.org/10.1186/s40168-019-0767-6

Zhou, X., Willems, R. J. L., Friedrich, A. W., Rossen, J. W. A. and Bathoorn, E. 2020. *Enterococcus faecium*: From microbiological insights to practical recommendations for infection control and diagnostics. Antimicrob. Resist. Infect. Contr., 9: 1-13. https://doi.org/10.1186/s13756-020-00770-1

## ORCID DETAILS OF THE AUTHORS

Sophayo Mahongnao: https://orcid.org/0000-0001-7222-5987
Sarita Nanda: https://orcid.org/0000-0003-3684-606X

Nature Environment and Pollution Technology
An International Quarterly Scientific Journal

p-ISSN: 0972-6268
(Print copies up to 2016)
e-ISSN: 2395-3454

Vol. 23 | No. 3 | pp. 1319-1332 | 2024

Original Research Paper

https://doi.org/10.46488/NEPT.2024.v23i03.006

Open Access Journal

# Saccharification of Different Delignified Sawdust Masses from Various Trees Along the Lagos Lagoon in Nigeria

**N. A. Ndukwe*, J. B. M. Seeletse** and J. P. H. van Wyk**†**

*Department of Chemical Sciences, College of Basic and Applied Sciences, Mountain Top University, Magoki, Ogun State, Nigeria

**Department of Pharmacology and Therapeutics, Sefako Makgatho Health Sciences University, South Africa

†Corresponding author: J. P. H. van Wyk: bioenergy.res@gmail.com

**Nat. Env. & Poll. Tech.**
**Website: www.neptjournal.com**

*Received:* 13-01-2024
*Revised:* 26-02-2024
*Accepted:* 10-03-2024

**Key Words:**
Sawdust
Cellulose
Cellulase
Delignification
Saccharification

## ABSTRACT

Sawdust, a major waste product of the forestry industry, is accumulating along the Lagos Lagoon in Lagos, Nigeria, without it being effectively managed. Besides its use in manufacturing sound-absorbing boards to reinforce concrete beams and for energy purposes, its potential as a renewable energy source and feedstock for bio-product development has not yet been realized. Cellulose, a glucose biopolymer and structural component of cellulose can be hydrolyzed by a hydrolytic enzyme known as cellulase. During the process, the enzyme breaks the B-1,4-glucosidic bond, which keeps the glucose units together, and by acting on this bond, numerous glucose units are released. As part of sawdust, the cellulose molecule is not freely available for the degradation action of the cellulase enzyme as it is strongly associated with lignin, which acts as bio-glue, keeping cellulose and hemicellulose together. Delignification is an effective technique that was used to make the sawdust from ten different trees along the Lagos Lagoon in Nigeria more susceptible to saccharification by cellulase isolated from the fungus *Aspergillus niger*. Delignified and non-delignified sawdust masses between 2 mg and 10 mg were incubated with the *A. niger* cellulase solution (2 $mg.mL^{-1}$), whereafter, the amount of sugar produced by the cellulase action was determined. The percentage saccharification of each sawdust material was also linked with the amount of sugar produced during cellulase action. From these investigations was concluded that delignification increased sugar production when almost all the masses of different sawdust materials were degraded. It was also observed that the ratio of sawdust mass to enzyme concentration is an important variable that influences the effectiveness of the saccharification process. The percentage saccharification of the various sawdust materials was also determined, and it indicated that the highest percentage of saccharification was not obtained when the highest amount of sawdust was degraded, producing the highest amount of sugar. The saccharification of sawdust could contribute to the development of renewable energy sources and feedstock for bioproduct development. The process is, however, not that straightforward as variables such as the type of cellulase enzyme, pretreatment of the cellulose substrate, and optimizing of cellulase to cellulose ratio are a few that need to be optimized for the process to be effective in terms of glucose production.

## INTRODUCTION

Environmental pollution is increasing at an alarming rate as a result of rapid population growth and industrialization with the production of solid waste, the most visualized form of waste. This type of waste is not only present in cities and towns because of human activities but is also a major pollutant in the forestry industry, where numerous volumes of sawdust are produced daily. Such is the case in Nigeria along the Lagos Lagoon, where thousands of trees are felled annually (Akhator et al. 2017). Simultaneously is the production of sawdust, which not only occupies land but has a negative effect on the water quality of the Lagos Lagoon and has also been identified as a major pollutant of air, causing a threat to the quality life of many people living along the Lagoon (Martin et al. 2020). Another concerning reality of these huge volumes of sawdust is its flammability, and due to the small particle size of this material, the spread of fire will be quick and unstoppable (Przybysz et al. 2023).

Also of environmental concern is the process of fossil fuel consumption not only as a source of energy but also as feedstock for the synthesis of many chemical-related

substances (Kapsalyamova & Paltsev 2020). The search for alternative and renewable energy resources that could also be developed as a feedstock for the biosynthesis of chemicals, biochemicals, and chemical substances with medicinal properties is topical, as many research efforts are focused on this approach (Mishra et al. 2021). Many cities are already using solid waste, especially organic parts such as kitchen waste, garden waste, and agriculture waste, as a resource to produce electricity by burning these materials, and the development of this type of waste as a resource for chemical synthetic procedures is well researched (Phiri et al. 2024). Biomass, including wood waste such as sawdust, has been identified as a renewable substance with a good potential to be developed as a resource for the synthesis of many bioproducts such as organic acids, polyhydroxyalkanoates, and bioplastics (Ashokkumar et al. 2022). The chemical substance in wood which makes sawdust attractive as a resource for bioproduct development is cellulose, a structural component, and glucose-based bio-polymer (Wan et al. 2010), also described as a complex chemical substance with the glucose units linked through B-1,4-glucosidic bonds (Andberg et al. 2015) to form chains which are interacting with each other through hydrogen bonds (Wang et al. 2023a).

When resolved into individual glucose units, the released glucose, which is a fermentable sugar, can be bio-converted into an environmentally friendly fuel known as bio-ethanol (Liu & Bao 2019), and the degradation of cellulose into glucose can be done employing acid or alkaline hydrolysis (Abeer et al. 2010). This process of degrading cellulose is not environmentally benign due to the negative effect of these acids and alkaline substances on the environment when regarded as a waste product after performing the hydrolysis process. Alternative to acidic and alkaline degradation of cellulose into glucose is a process that is catalyzed by cellulase, a multi-component enzyme system, and which is environmentally friendly (Wang et al. 2023b). This enzyme originates mostly from bacterial (Ali et al. 2013) and fungal (Yang et al. 2023) sources and has been described in the saccharification of many cellulose-containing substances such as bagasse (Hemansi & Saini 2023), wood rice straw (Pal et al. 2022) and wastepaper (Ndlovu & Van Wyk 2023). Besides the environmental benefit of using cellulase to degrade cellulose into fermentable sugars is the fact that the enzyme has components that can act specifically on the two structural sections of cellulose, namely the amorphous (Ciolacu et al. 2011) and crystalline (Cheng et al. 2011) sections which are essential for the effective degradation of cellulose. These sections show different susceptibilities towards the cellulase enzymes and need specific components of the cellulase complex to be degraded into sugars.

The saccharification of cellulose into fermentable sugars by the cellulase enzyme is a complicated process and many variables of the process need to be optimized for the process to be effective in terms of sugar production. A major stumbling block in the bioconversion process is the presence of lignin in the wood material. This bio-polymer acts as a biological glue, keeping cellulose and hemicellulose strongly together, and destroying this interaction will make cellulose more susceptible to cellulase-catalyzed degradation. Many variables regarding the saccharification of cellulose, such as cellulase concentration (Kaschuk et al. 2019), incubation temperature (Bhati et al. 2019), incubation pH (Bellaouchi et al. 2021), and product inhibition (Zou et al. 2021), could influence the outcome of this glucose producing process.

The current investigation reveals information regarding the *Aspergillus niger* cellulase-catalyzed saccharification of sawdust from different trees along the Lagos Lagoon in Nigeria. To increase the susceptibility of the cellulose to cellulase action, the various sawdust materials have been delignified with the Kraft process (Gustafson et al. 1983) as well as hydrogen peroxide treatment (Ndukwe et al. 2009). This investigation focused on the effect which different masses of the non-delignified and delignified sawdust materials will have on the saccharification thereof by the *A. niger* cellulase enzyme.

## MATERIALS AND METHODS

### Sawdust Substrate and Cellulase Enzyme

Non-delignified and delignified sawdust samples from ten different trees were transferred in triplicate into test tubes. Names of these sawdust samples are *Erythropleum suaveolens, Symphona globulifera, Ricindendron heudelotii, Pterygota macrocarpa, Milicia excels, Ipomoeu asarifolia, Hallelea ciliate, Sacoglottis gabonensis, Pycnanthus angolensis,* and *Terminalia superb*. Commercially obtained *Aspergillus niger* cellulase enzyme (0.1g) was dissolved in 0.005 mol.dm$^{-3}$ pH 5.0 tris buffer resulting in an enzyme solution concentration of 2.0 mg.mL$^{-1}$.

### Delignification of Sawdust- Kraft Pulping and Hydrogen Peroxide Treatment of the Wood Sawdust

To ensure a maximum cellulose exposure to the cellulase enzyme, the various sawdust materials were delignified by subjecting 2kg of each of the different sawdust materials (2.8-5.0 mm particle size) to 350g of NaOH and 140g $NaS_2$ during the Kraft pulping process. The Kraft pulping chemicals were dissolved in 8 L water. The delignification of the lignocellulosic materials (sawdust) was carried out in a rotary steel digester at 170°C and a pressure of 200 kPa for

1 h 45 min at cooking liquor to the wood ratio of 4:1. After the Kraft pretreatment, the extracted cellulose fibers were washed in turns with deionized water until they were free of the Kraft reagents (Ndukwe et al. 2009).

To remove residual lignin from these Kraft-treated cellulose, all these sawdust materials (10 g) were treated with 30% hydrogen peroxide (60 mL) at 40°C for 25-30 min.

### Cellulase Incubation and Sugar Analyses

The delignified and non-delignified sawdust materials (2 mg, 4 mg, 6 mg, 8 mg, and 10 mg) were transferred in triplicate in test tubes and incubated with the *A. niger* cellulase enzyme solution (200 uL) and Tris buffer solution pH 5.0 (800 uL) for 2h at an incubation temperature of 50°C. The concentration of sugars released from the sawdust materials during cellulase-catalyzed degradation was determined from a standard glucose calibration curve constructed with glucose standard solutions at concentrations of 0.50 $mg.mL^{-1}$, 2.00 $mg.mL^{-1}$, 4.00 $mg.mL^{-1}$, 6.00 $mg.mL^{-1}$ and 8.00 $mg.mL^{-1}$. The DNS method, as described by Miller (1959), was used to calculate the concentration of the sugar produced during *A. niger* action on the waste sawdust.

### Calculation of Resultant Amount of Sugar Produced and Percentage Saccharification

The resultant amount of sugar produced from the delignified and non-delignified sawdust was calculated by subtracting the amount of sugar released from each type of sawdust in the absence of cellulase action from the amount of sugar released when the sawdust was treated with the cellulase enzyme. This amount of sugar, known as the resultant amount of sugar, was released because of the cellulase action on each type of sawdust material.

The percentage saccharification of each sawdust material was calculated by dividing the resultant mass of sugars produced through cellulase action by the total mass of the sawdust incubated multiplied by a hundred. These values indicate to what extent the sawdust was bioconverted into sugars and can also be used to conclude the relative saccharification of the various sawdust materials.

### Statistical Analysis

All the experimental analyses were performed in triplicate, and the mean values with standard deviations were determined with Microsoft Excel.

## RESULTS AND DISCUSSION

The physical interaction between an enzyme and a substrate is an important prerequisite for the action of the bio-catalyst in converting the substrates into products. In the case of cellulase technology, the cellulase enzyme attacks a cellulose molecule, and during the interaction, the reaction product, glucose, is produced. During the cellulolytic action, the cellulase enzyme performs an adsorption-desorption action on the cellulose materials while degrading cellulose into either shorter cellulose chains or in glucose (Wang et al. 2020). One of the factors which control the rate and magnitude of cellulose hydrolysis is the availability and accessibility of cellulose to the cellulase enzyme which will determine the adsorption of the enzyme onto the cellulose surface. The interaction and binding of cellulase to cellulose is a mandatory step for cellulose degradation (Kim et al. 2005). The three-dimensional structure, size, and shape of the substrate determine the enzyme accessibility to the substrate, which has more ordered internal and less ordered external surfaces (Chang et al. 1981). The adsorption has also been attributed to other features including the irreversibility of the cellulase adsorption (Palonen et al. 1999), interaction among the adsorbing components of enzyme in high concentrations (Jeon et al. 2002), multiple adsorbing sites for a single cellulase molecule (Linder & Teeri 1997, Carrard & Linder 1999), enzymes being entrapped by cellulose pores (Lee et al. 1988) and adsorption of multiple components having different constants (Beldman et al. 1987).

Described above are all variables that could affect the outcome of the cellulase-catalyzed saccharification reaction of cellulose, and during this investigation, the mass of various insoluble sawdust samples was increased while treated with a fixed amount (concentration) of the *A. niger* cellulase enzyme. Delignified as well as non-delignified sawdust samples with masses varied between 2 mg to 10 mg were treated with the cellulase enzyme, and the amount of sugar produced from each material, as well as the percentage saccharification of each sawdust material, were determined. The sugar-producing and saccharification profiles are illustrated on various graphs and illustrated the increase in the sugar concentration produced from the delignified sawdust and the non-delignified sawdust when degraded by the cellulase enzyme.

The sugar production profiles, as well as percentage saccharification and the resultant amount of sugar produced from the different non-delignified and delignified sawdust samples from *E. suaveolens,* are represented in Fig. 1. The bioconversion of non-delignified sawdust from *E. suaveolens* by *A. niger* cellulase resulted in an increased amount of sugar produced that varied between a concentration of 0.78 $mg.mL^{-1}$ when 2 mg of the sawdust was degraded to a concentration of 1.12 $mg.mL^{-1}$ during the degradation of the highest masses of 8 mg and 10 mg. These results showed

a 143% increase in sugar production from the lowest mass of sawdust to the highest mass of sawdust at an increasing rate of 0.034 mg sugar produced for a 1 mg increase in sawdust degraded. When the delignified sawdust was degraded, the relative amount of sugar produced from all the masses exposed to the cellulase enzyme was higher than the sugar produced from the corresponding non-delignified sawdust masses. The sugar concentration produced from delignified sawdust increased from 1.16 $mg.mL^{-1}$ when 2 mg was degraded to a concentration of 2.26 $mg.mL^{-1}$ during degradation of the highest mass of 10 mg. This degradation pattern shows an increase of 195% in sugar formation from the lowest mass to the highest mass bioconverted by the cellulase enzyme.

The difference in sugar production between the non-delignified and delignified sawdust materials at different masses showed an increase in difference, which varied from 0.38 $mg.mL^{-1}$ when 2 mg of the material was degraded to 1.14 $mg.mL^{-1}$ when the highest mass of 10 mg was degraded. The rate of sugar production when the delignified sawdust was degraded was calculated at 0.11 mg sugar produced for an increase of 1 mg delignified sawdust degraded. The general trend of saccharification for both the non-delignified as well as delignified sawdust showed a decrease in percentage saccharification as the mass degraded is increased. In the case of the non-delignified sawdust, the percentage of saccharification decreased from 39% when the lowest mass was degraded to 12% when the highest mass of 10 mg was degraded. The degradation of the delignified sawdust resulted in a 58% degradation when the lowest mass of 2 mg was saccharified. At the same time, a 22% saccharification was obtained when the highest mass of 10 mg was bioconverted into sugars.

The sugar production profiles, as well as percentage saccharification and the resultant amount of sugar produced from the different non-delignified and delignified sawdust samples from *S. globulifera*, are represented in Fig. 2. The bioconversion of non-delignified sawdust from *S. globulifera* by *A. niger* cellulase resulted in an increased amount of sugar produced that varied between a concentration of 1.21 $mg.mL^{-1}$ when 2 mg of the sawdust was degraded to a concentration of 1.95 $mg.mL^{-1}$ during the degradation of the highest masses of 10 mg. These results showed a 161% increase in sugar production from the lowest mass of sawdust to the highest mass of sawdust at an increasing rate of 0.074 mg sugar produced for a 1 mg increase in sawdust degraded. When the delignified sawdust was degraded, the relative amount of sugar produced from all the masses exposed to the cellulase enzyme was higher than the sugar produced from the corresponding non-delignified sawdust masses. The sugar concentration produced from delignified sawdust increased from 1.21 $mg.mL^{-1}$ when 2 mg was degraded to a concentration of 2.18 $mg.mL^{-1}$ during degradation of the highest mass of 10 mg. This degradation pattern shows an increase of 180% in sugar formation from the lowest mass to the highest mass bioconverted by the cellulase enzyme.

The difference in sugar production between the non-delignified and delignified sawdust materials at different

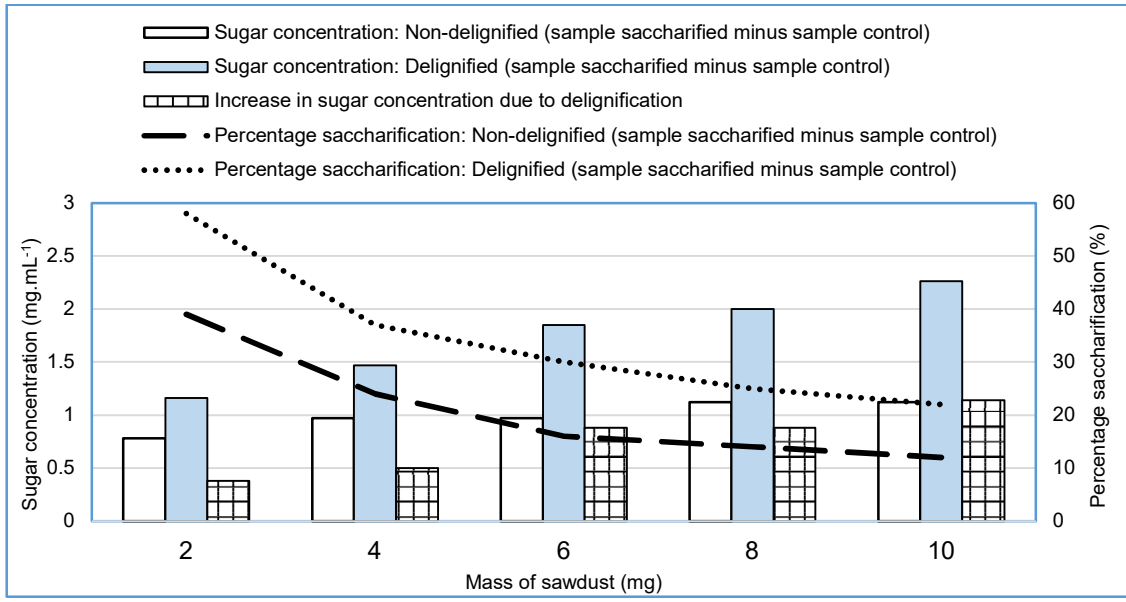


Fig. 1: *A. niger* cellulase catalyzed degradation of delignified as well as non-delignified sawdust from *Erythropleum suaveolens*.

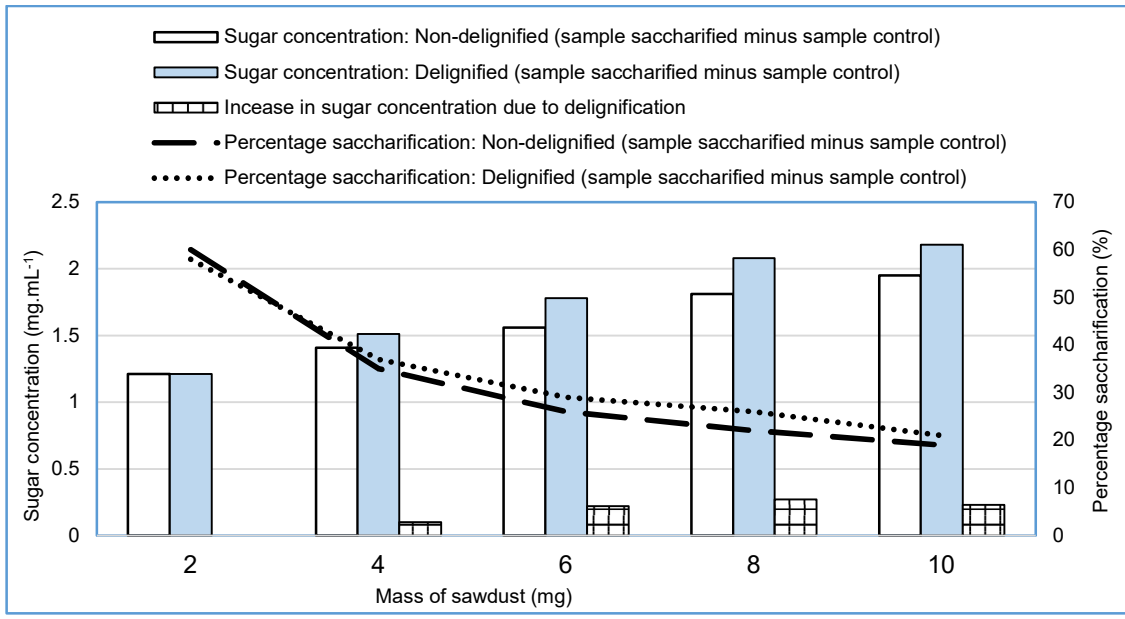


Fig. 2: *A. niger* cellulase catalyzed degradation of delignified as well as non-delignified sawdust from *Symphonia globulifera*.

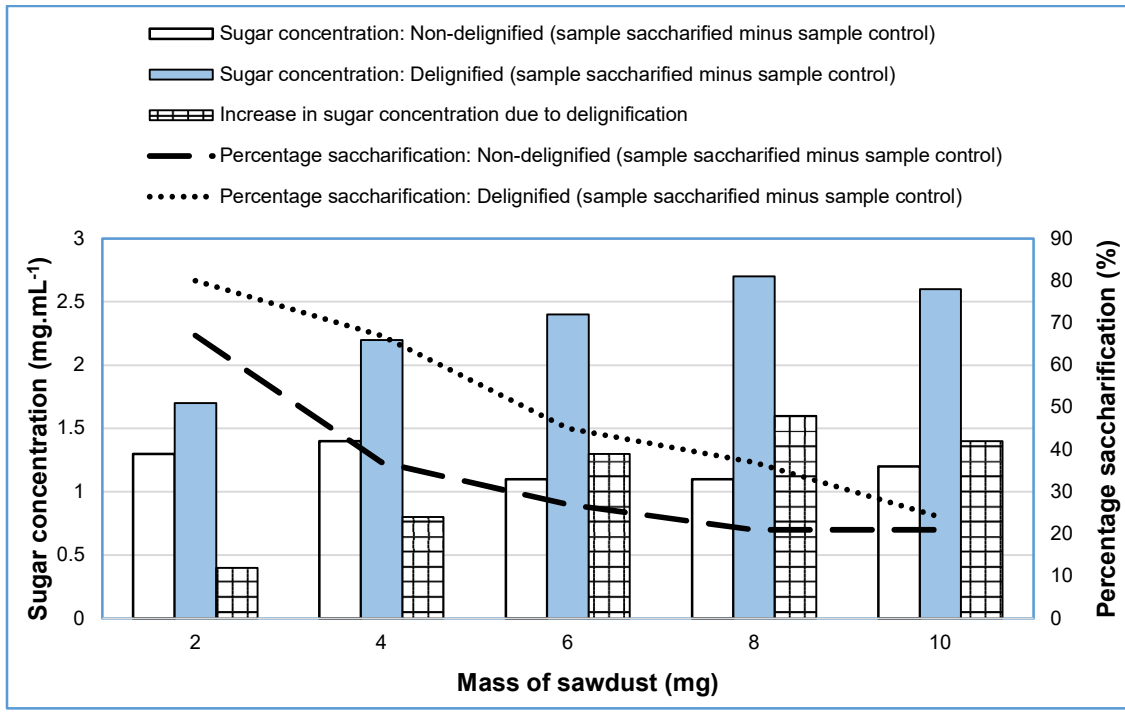


Fig. 3: *A. niger* cellulase catalyzed degradation of delignified as well as non-delignified sawdust from *Ricindendron heudelotti*.

masses showed an increase in difference, which varied from 0.00 $mg.mL^{-1}$ when 2 mg of the material was degraded to 0.23 $mg.mL^{-1}$ when the highest mass of 10 mg was degraded. The rate of sugar production when the delignified sawdust was degraded was calculated at 0.097 mg sugar produced for an increase of 1 mg delignified sawdust degraded. The general trend of saccharification for both the non-delignified as well as delignified sawdust showed a decrease in percentage saccharification as the mass degraded is increased. In the case of the non-delignified sawdust, the

percentage of saccharification decreased from 60% when the lowest mass was degraded to 19% when the highest mass of 10 mg was degraded. The degradation of the delignified sawdust resulted in a 58% degradation when the lowest mass of 2 mg was saccharified, while a 21% saccharification was obtained when the highest mass of 10 mg was bioconverted into sugars.

The sugar production profiles, as well as percentage saccharification and the resultant amount of sugar produced from the different non-delignified and delignified sawdust samples from *R. heudelotti,* are represented in Fig. 3. The bioconversion of non-delignified sawdust from *R. heudelotti* by *A. niger* cellulase resulted in an amount of sugar produced that varied between a concentration of 1.1 mg.mL$^{-1}$ and 1.4 mg.mL$^{-1}$ during the degradation of the masses starting from 2 mg and 10 mg. These results showed a 161% increase in sugar production from the lowest mass of sawdust to the highest mass of sawdust at an increasing rate of 0.074 mg sugar produced for a 1 mg increase in sawdust degraded. When the delignified sawdust was degraded, the relative amount of sugar produced from all the masses exposed to the cellulase enzyme was higher than the sugar produced from the corresponding non-delignified sawdust masses. The sugar concentration produced from delignified sawdust increased from 1.7 mg.mL$^{-1}$ when 2 mg was degraded to a concentration of 2.7 mg.mL$^{-1}$ and 2.6 mg.mL$^{-1}$ during degradation of the highest mass of 8 mg and 10 mg. This degradation pattern shows an increase of 158% in sugar formation from the lowest mass to the highest mass bioconverted by the cellulase enzyme.

The difference in sugar production between the non-delignified and delignified sawdust materials at different masses showed an increase in difference, which varied from 0.4 mg.mL$^{-1}$ when 2 mg of the material was degraded to 1.4 mg.mL$^{-1}$ when the highest mass of 10 mg was degraded. The rate of sugar production when the delignified sawdust was degraded was calculated at 0.1 mg sugar produced for an increase of 1 mg delignified sawdust degraded. The general trend of saccharification for both the non-delignified as well as delignified sawdust showed a decrease in percentage saccharification as the mass degraded is increased. In the case of the non-delignified sawdust, the percentage of saccharification decreased from 80% when the lowest mass was degraded to 24% when the highest mass of 10 mg was degraded. The degradation of the delignified sawdust resulted in a 67% degradation when the lowest mass of 2 mg was saccharified. At the same time, a 21% saccharification was obtained when the highest mass of 10 mg was bioconverted into sugars.

The sugar production profiles, as well as percentage saccharification and the resultant amount of sugar produced from the different non-delignified and delignified sawdust samples from *P. macrocarpa,* are represented in Fig. 4. The bioconversion of non-delignified sawdust from *P. macrocarpa* by *A. niger* cellulase resulted in an increased amount of sugar produced that varied between a concentration

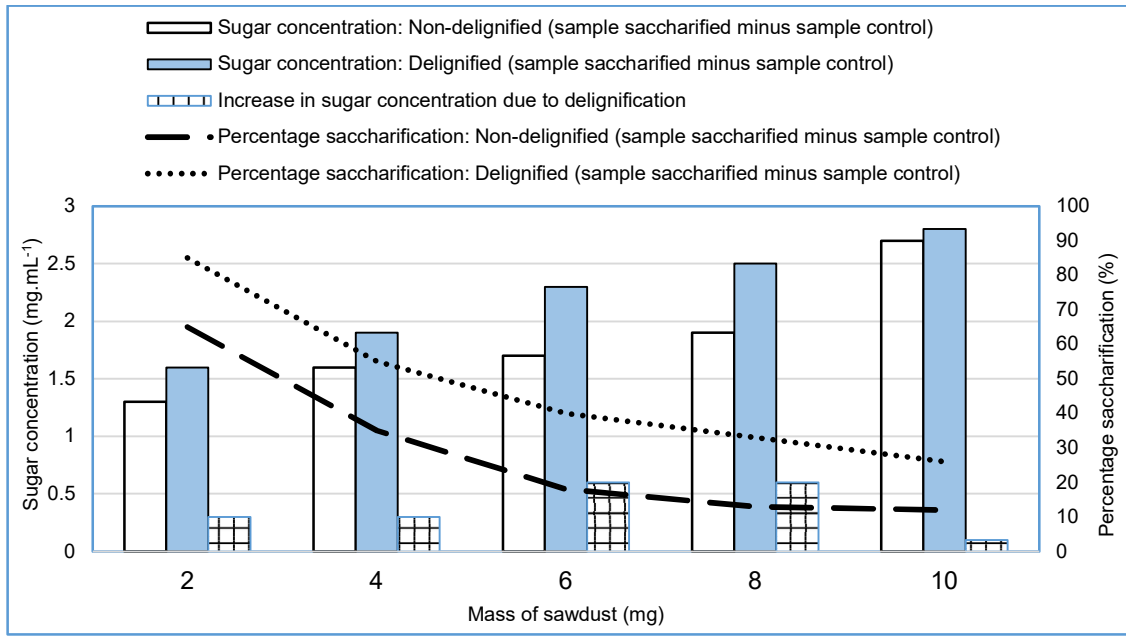


Fig. 4: *A. niger* cellulase catalyzed degradation of delignified as well as non-delignified sawdust from *Pterygota macrocarpa*.

of 1.3 mg.mL$^{-1}$ when 2 mg of the sawdust was degraded to a concentration of 2.7 mg.mL$^{-1}$ during the degradation of the highest masses of 10 mg. These results showed a 140% increase in sugar production from the lowest mass of sawdust to the highest mass of sawdust at an increasing rate of 0.14 mg sugar produces for a 1 mg increase in sawdust degraded. When the delignified sawdust was degraded, the relative amount of sugar produced from all the masses exposed to the cellulase enzyme was higher than the sugar produced from the corresponding non-delignified sawdust masses. The sugar concentration produced from delignified sawdust increased from 1.6 mg.mL$^{-1}$ when 2 mg was degraded to a concentration of 2.8 mg.mL$^{-1}$ during degradation of the highest mass of 10 mg. This degradation pattern shows an increase of 175% in sugar formation from the lowest mass to the highest mass bioconverted by the cellulase enzyme.

The difference in sugar production between the non-delignified and delignified sawdust materials at different masses showed an increase in difference, which varied from 0.3 mg.mL$^{-1}$ when 2 mg of the material was degraded to 0.1 mg.mL$^{-1}$ when the highest mass of 10 mg was degraded. The rate of sugar production when the delignified sawdust was degraded was calculated at 0.12 mg sugar produced for an increase of 1 mg delignified sawdust degraded. The general trend of saccharification for both the non-delignified as well as delignified sawdust showed a decrease in percentage saccharification as the mass degraded is increased. In the case of the non-delignified sawdust, the percentage of saccharification decreased from 65% when the lowest mass was degraded to 12% when the highest mass of 10 mg was degraded. The degradation of the delignified sawdust resulted in an 85% degradation when the lowest mass of 2 mg was saccharified, while a 26% saccharification was obtained when the highest mass of 10 mg was bioconverted into sugars.

The sugar production profiles, as well as percentage saccharification and the resultant amount of sugar produced from the different non-delignified and delignified sawdust samples from *M. Excels,* are represented in Fig. 5. The bioconversion of non-delignified sawdust from *M. excels* by *A. niger* cellulase resulted in an increased amount of sugar produced that varied between a concentration of 1.34 mg.mL$^{-1}$ when 2 mg of the sawdust was degraded to a concentration of 2.17 mg.mL$^{-1}$ during the degradation of

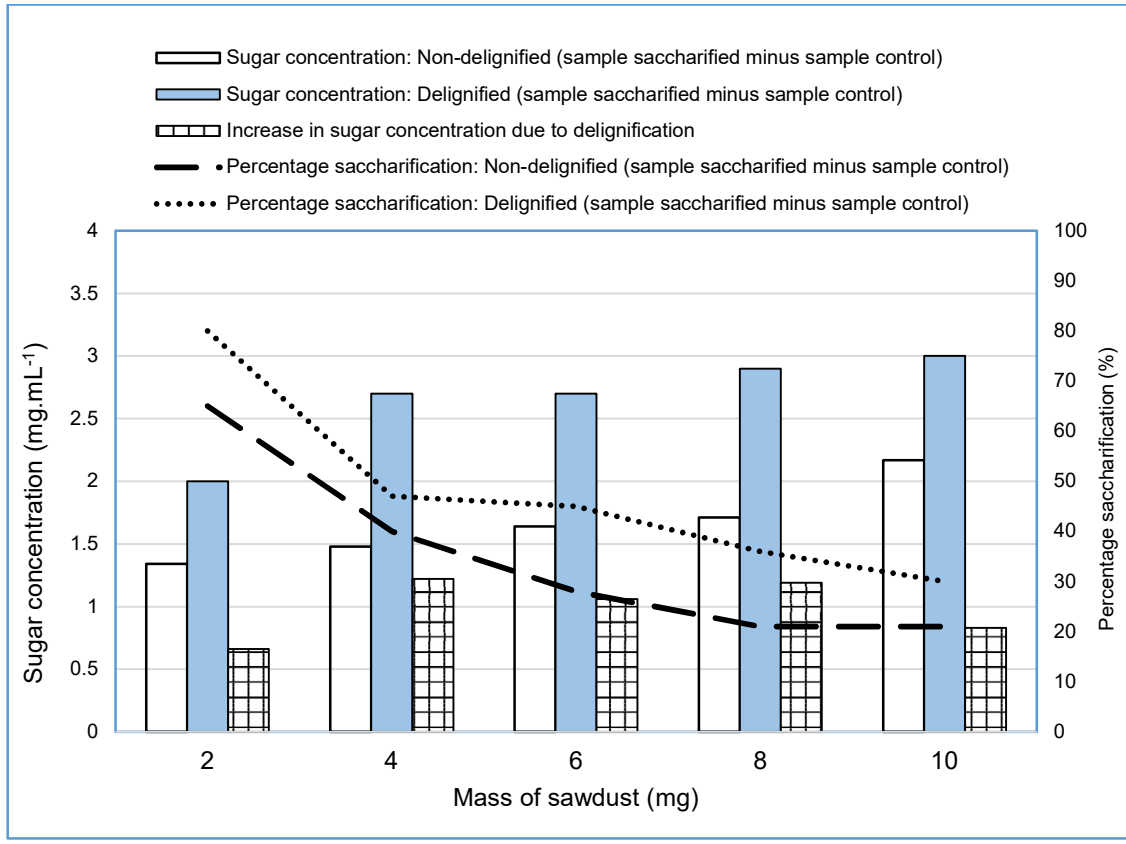


Fig. 5: *A. niger* cellulase catalyzed degradation of delignified as well as non-delignified sawdust from *Milicia excels*.

the highest masses of 10 mg. These results showed a 161% increase in sugar production from the lowest mass of sawdust to the highest mass of sawdust at an increasing rate of 0.083 mg sugar produced for a 1 mg increase in sawdust degraded. When the delignified sawdust was degraded, the relative amount of sugar produced from all the masses exposed to the cellulase enzyme was higher than the sugar produced from the corresponding non-delignified sawdust masses. The sugar concentration produced from delignified sawdust increased from 1.16 $mg.mL^{-1}$ when 2 mg was degraded to a concentration of 2.26 $mg.mL^{-1}$ during degradation of the highest mass of 10 mg. This degradation pattern shows an increase of 195% in sugar formation from the lowest mass to the highest mass bioconverted by the cellulase enzyme.

The difference in sugar production between the non-delignified and delignified sawdust materials at different masses showed an increase in difference, which varied from 0.66 $mg.mL^{-1}$ when 2 mg of the material was degraded to 1.22 $mg.mL^{-1}$ when the mass of 4 mg was degraded. The rate of sugar production when the delignified sawdust was degraded was calculated at 0.1 mg sugar produced for an increase of 1 mg delignified sawdust degraded. The general trend of saccharification for both the non-delignified as well as delignified sawdust showed a decrease in percentage saccharification as the mass degraded is increased. In the case of the non-delignified sawdust, the percentage of saccharification decreased from 65% when the lowest mass was degraded to 21% when the highest mass of 10 mg was degraded. The degradation of the delignified sawdust resulted in 80% degradation when the lowest mass of 2 mg was saccharified, while a 30% saccharification was obtained when the highest mass of 10 mg was bioconverted into sugars.

The sugar production profiles, as well as percentage saccharification and resultant amount of sugar produced from the different non-delignified and delignified sawdust samples from *I. asarifolia*, are represented in Fig. 6. The bioconversion of non-delignified sawdust from *I. asarifolia* by *A. niger* cellulase resulted in an increased amount of sugar produced that varied between a concentration of 0.85 mgmL when 2 mg of the sawdust was degraded to a concentration of 1.49 $mg.mL^{-1}$ during the degradation of the highest masses of 10 mg. These results showed a 175% increase in sugar production from the lowest mass of sawdust to the highest mass of sawdust at an increasing rate of 0.064 mg sugar produced for a 1 mg increase in sawdust degraded. When the delignified sawdust was degraded, the relative amount of sugar produced from all the masses exposed to the cellulase enzyme was higher than the sugar produced from the corresponding non-delignified sawdust masses. The sugar concentration produced from delignified sawdust increased from 0.83 $mg.mL^{-1}$ when 2 mg was degraded to a concentration of 1.75 $mg.mL^{-1}$ during degradation of the highest mass of 10 mg. This degradation pattern shows an increase of 210% sugar formation from the lowest mass to the highest mass bioconverted by the cellulase enzyme.

The difference in sugar production between the non-delignified and delignified sawdust materials at different masses showed an increase in difference, which varied from 0.67 $mg.mL^{-1}$ when 2 mg of the material was degraded to 0.35 $mg.mL^{-1}$ when the highest mass of 10 mg was degraded. The rate of sugar production when the delignified sawdust

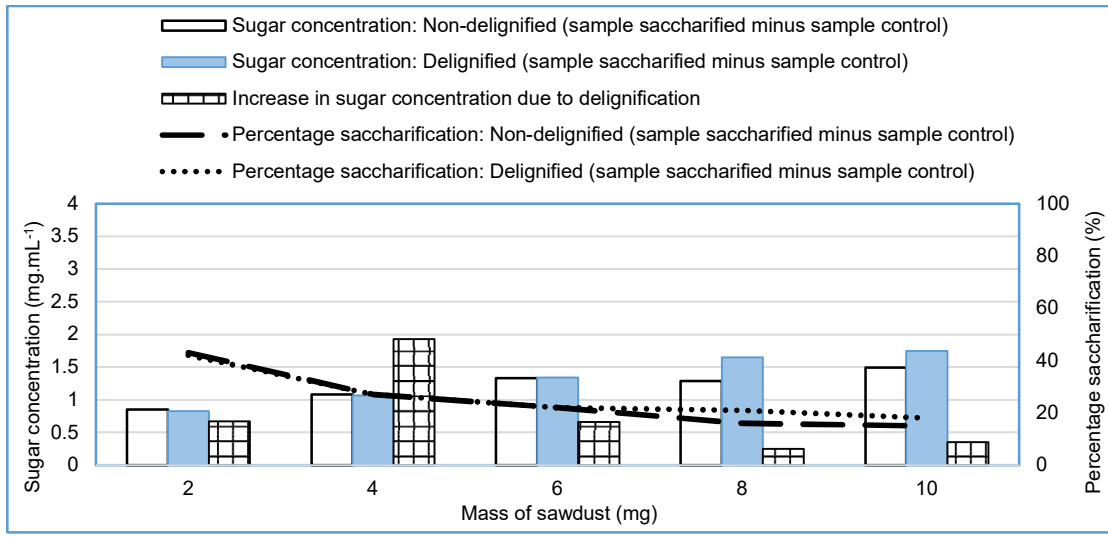


Fig. 6: *A. niger* cellulase catalyzed degradation of delignified as well as non-delignified sawdust from *Ipomoea asarifolia*.

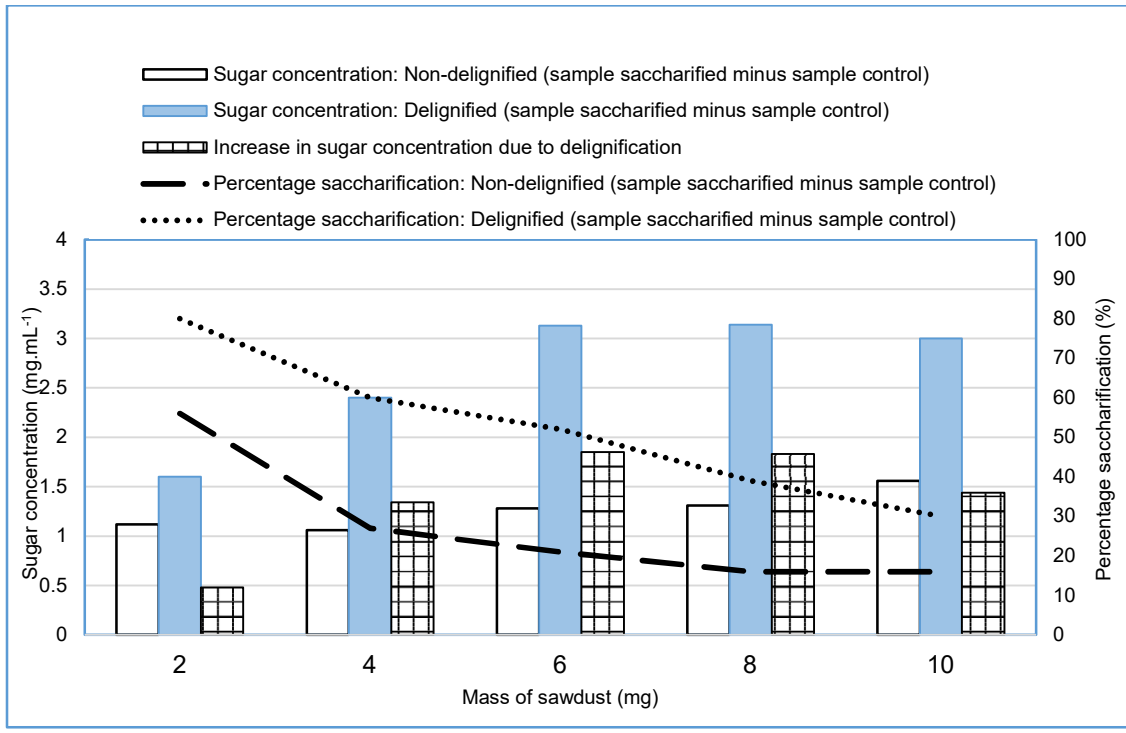


Fig. 7: *A. niger* cellulase catalyzed degradation of delignified as well as non-delignified sawdust from *Hallelea ciliate*.

was degraded was calculated at 0.092 mg sugar produced for an increase of 1 mg delignified sawdust degraded. The general trend of saccharification for both the non-delignified as well as delignified sawdust showed a decrease in percentage saccharification as the mass degraded is increased. In the case of the non-delignified sawdust, the percentage of saccharification decreased from 43% when the lowest mass was degraded to 15% when the highest mass of 10 mg was degraded. The degradation of the delignified sawdust resulted in 42% degradation when the lowest mass of 2 mg was saccharified, while an 18% saccharification was obtained when the highest mass of 10 mg was bioconverted into sugars.

The sugar production profiles, as well as percentage saccharification and the resultant amount of sugar produced from the different non-delignified and delignified sawdust samples from *H. ciliate*, are represented in Fig. 7. The bioconversion of non-delignified sawdust from *H. ciliate* by *A. niger* cellulase resulted in an increased amount of sugar produced that varied between a concentration of 1.12 $mg.mL^{-1}$ when 2 mg of the sawdust was degraded to a concentration of 1.56 $mg.mL^{-1}$ during the degradation of the highest mass of 10 mg. These results showed a 139% increase in sugar production from the lowest mass of sawdust to the highest mass of sawdust at an increasing rate of 0.044 mg sugar produced for a 1 mg increase in sawdust degraded. When the delignified sawdust was degraded, the relative amount of sugar produced from all the masses exposed to the cellulase enzyme was higher than the sugar produced from the corresponding non-delignified sawdust masses. The sugar concentration produced from delignified sawdust increased from 1.6 $mg.mL^{-1}$ when 2 mg was degraded to a concentration of 3.13 $mg.mL^{-1}$, 3.14 $mg.mL^{-1}$, and 3.0 $mg.mL^{-1}$ during degradation of the high masses of 6 mg, 8 mg, and 10 mg. This degradation pattern shows an increase of 196% in sugar formation from the lowest mass to the highest mass bioconverted by the cellulase enzyme.

The difference in sugar production between the non-delignified and delignified sawdust materials at different masses showed an increase in difference, which varied from 0.48 $mg.mL^{-1}$ when 2 mg of the material was degraded to 1.44 $mg.mL^{-1}$ when the highest mass of 10 mg was degraded. The rate of sugar production when the delignified sawdust was degraded was calculated at 0.154 mg of sugar produced for an increase of 1 mg delignified sawdust degraded. The general trend of saccharification for both the non-delignified as well as delignified sawdust showed a decrease in percentage saccharification as the mass degraded is increased. In the case of the non-delignified sawdust, the percentage of saccharification decreased from

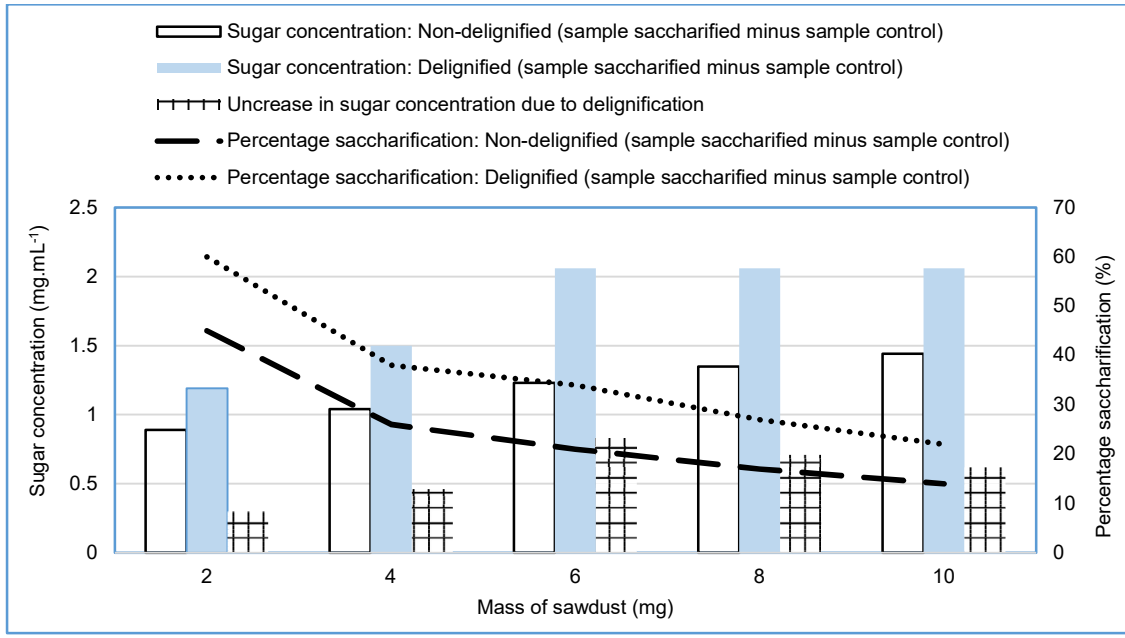


Fig. 8: *A. niger* cellulase catalyzed degradation of delignified as well as non-delignified sawdust from *Sacoglottis gabonensis*.

56% when the lowest mass was degraded to 16% when the highest mass of 10 mg was degraded. The degradation of the delignified sawdust resulted in an 80% degradation when the lowest mass of 2 mg was saccharified, while a 30% saccharification was obtained when the highest mass of 10 mg was bioconverted into sugars.

The sugar production profiles, as well as percentage saccharification and resultant amount of sugar produced from the different non-delignified and delignified sawdust samples from *S. gabonensis*, are represented in Fig. 8. The bioconversion of non-delignified sawdust from *S. gabonensis* by *A. niger* cellulase resulted in an increased amount of sugar produced that varied between a concentration of 0.89 mg.mL$^{-1}$ when 2 mg of the sawdust was degraded to a concentration of 1.44 mg.mL$^{-1}$ during the degradation of the highest masses of 10 mg. These results showed a 161% increase in sugar production from the lowest mass of sawdust to the highest mass of sawdust at an increasing rate of 0.055 mg sugar produced for a 1 mg increase in sawdust degraded. When the delignified sawdust was degraded, the relative amount of sugar produced from all the masses exposed to the cellulase enzyme was higher than the sugar produced from the corresponding non-delignified sawdust masses. The sugar concentration produced from delignified sawdust increased from 1.19 mg.mL$^{-1}$ when 2 mg was degraded to a concentration of 2.06 mg.mL$^{-1}$ during degradation of the masses 6 mg, 8 mg, and 10 mg. This degradation pattern shows an increase of 231% in sugar formation from the lowest mass to the highest mass bioconverted by the cellulase enzyme.

The difference in sugar production between the non-delignified and delignified sawdust materials at different masses showed an increase, varying from 0.3 mg.mL$^{-1}$ when 2 mg of the material was degraded to 0.62 mg/mL when the highest mass of 10 mg was degraded. The rate of sugar production for the delignified sawdust was calculated at 0.087 mg of sugar produced per 1 mg increase in degraded delignified sawdust. The general trend of saccharification for both non-delignified and delignified sawdust showed a decrease in percentage saccharification as the mass degradation increased. For the non-delignified sawdust, the percentage of saccharification decreased from 45% at the lowest mass to 14% at the highest mass of 10 mg. The degradation of the delignified sawdust resulted in 60% saccharification at the lowest mass of 2 mg, while 22% saccharification was obtained at the highest mass of 10 mg.

The sugar production profile, as well as percentage saccharification and resultant amount of sugar produced from the different non-delignified and delignified sawdust samples from *P. angolensis*, are represented in Fig. 9. The bioconversion of non-delignified sawdust from *P. angolensis* by *A. niger* cellulase resulted in an increased amount of sugar produced that varied between a concentration of 0.52 mg.mL$^{-1}$ when 2 mg of the sawdust was degraded to a concentration of 1.15 mg.mL$^{-1}$ during the degradation of the highest masses of 10 mg. These results showed a 221%

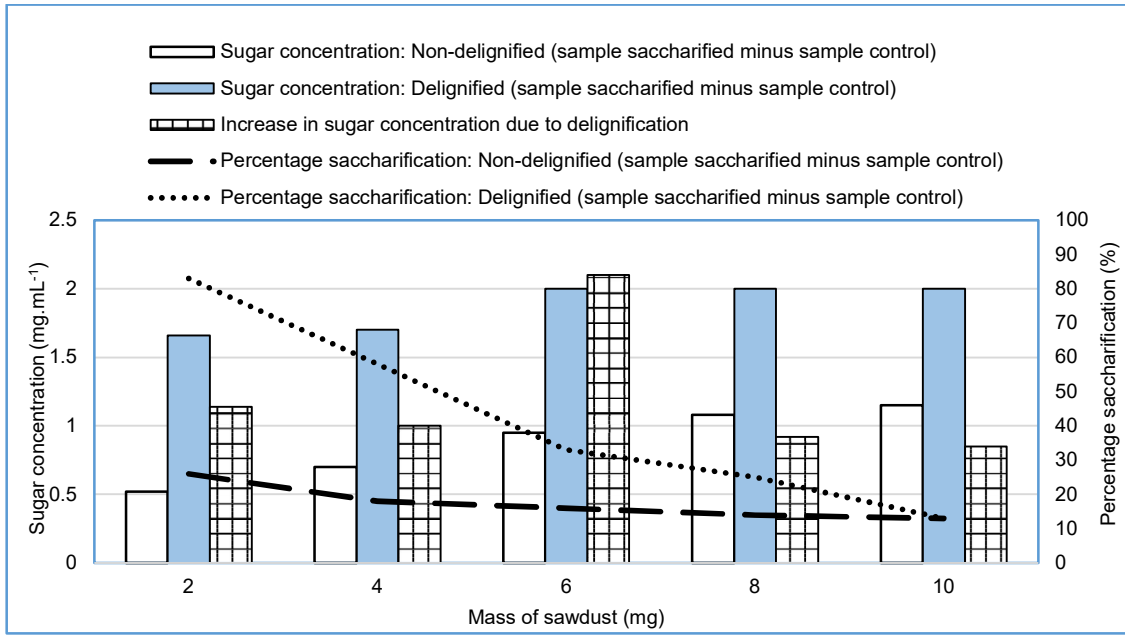


Fig. 9: *A. niger* cellulase catalyzed degradation of delignified as well as non-delignified sawdust from *Pycnanthus angolensis*.

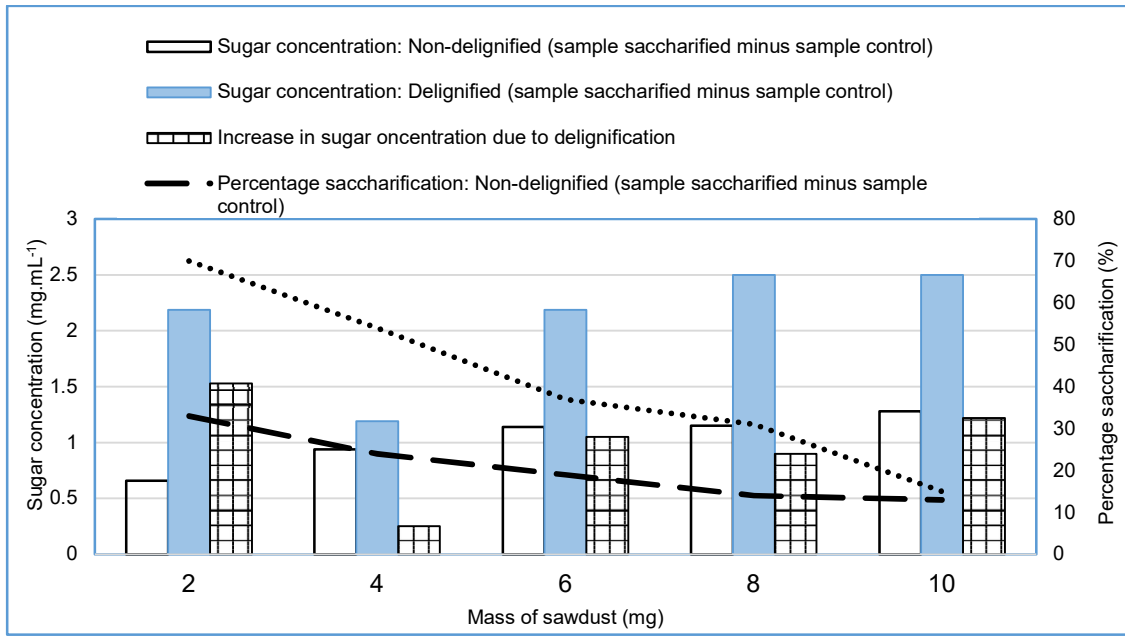


Fig. 10: *A. niger* cellulase catalyzed degradation of delignified as well as non-delignified sawdust from *Terminalia superb*.

increase in sugar production from the lowest mass of sawdust to the highest mass of sawdust at an increasing rate of 0.063 mg sugar produced for a 1 mg increase in sawdust degraded. When the delignified sawdust was degraded, the relative amount of sugar produced from all the masses exposed to the cellulase enzyme was higher than the sugar produced from the corresponding non-delignified sawdust masses. The sugar concentration produced from delignified sawdust increased from 1.66 $mg.mL^{-1}$ when 2 mg was degraded to a concentration of 2.0 $mg.mL^{-1}$ during degradation of the masses of 6 mg, 8 mg, and 10 mg. This degradation pattern shows an increase of 120% in sugar formation from

the lowest mass to the highest mass bioconverted by the cellulase enzyme.

The rate of sugar production when the delignified sawdust was degraded was calculated at 0.034 mg sugar produced for an increase of 1 mg delignified sawdust degraded. The general trend of saccharification for both the non-delignified as well as delignified sawdust showed a decrease in percentage saccharification as the mass degraded is increased. In the case of the non-delignified sawdust, the percentage of saccharification decreased from 26% when the lowest mass was degraded to 13% when the highest mass of 10 mg was degraded. The degradation of the delignified sawdust resulted in an 83% degradation when the lowest mass of 2 mg was saccharified, while a 13% saccharification was obtained when the highest mass of 10 mg was bioconverted into sugars.

The sugar production profiles, as well as percentage saccharification and the resultant amount of sugar produced from the different non-delignified and delignified sawdust samples from *T. superb,* are represented in Fig. 10. The bioconversion of non-delignified sawdust from *T. superb* in *A. niger* cellulase resulted in an increased amount of sugar produced that varied between a concentration of 0.66 $mg.mL^{-1}$ when 2 mg of the sawdust was degraded to a concentration of 1.28 $mg.mL^{-1}$ during the degradation of the highest masses of 10 mg. These results showed a 193% increase in sugar production from the lowest mass of sawdust to the highest mass of sawdust at an increasing rate of 0.062 mg sugar produced for a 1 mg increase in sawdust degraded. When the delignified sawdust was degraded, the relative amount of sugar produced from all the masses exposed to the cellulase enzyme was higher than that produced from the corresponding non-delignified sawdust masses. The sugar concentration produced from delignified sawdust increased from 2.19 $mg.mL^{-1}$ when 2 mg was degraded to 2.5 mg/mL during the degradation of the highest mass of 10 mg. This degradation pattern shows an 86% increase in sugar formation from the lowest mass to the highest mass bioconverted by the cellulase enzyme.

The difference in sugar production between the non-delignified and delignified sawdust materials at different masses showed an increase in variance, ranging from 1.53 $mg.mL^{-1}$ when 2 mg of the material was degraded to 1.22 $mg.mL^{-1}$ when the highest mass of 10 mg was degraded. The rate of sugar production for the delignified sawdust was calculated at 0.031 mg sugar produced per 1 mg increase in degraded delignified sawdust. The general trend of saccharification for both non-delignified and delignified sawdust showed a decrease in percentage saccharification as the mass degradation increased. For the non-delignified sawdust, the percentage of saccharification decreased from 33% at the lowest mass to 13% at the highest mass of 10 mg. The degradation of the delignified sawdust resulted in 70% saccharification at the lowest mass of 2 mg, while a 15% saccharification was obtained at the highest mass of 10 mg.

The development of alternative and renewable energy resources would become a crucial phenomenon as the use of petrochemical-derived substances results in the intensification of climate change and global warming. What is also of immense importance is to introduce procedures for the effective management of solid waste which negative effects on the environment are visible and realized. Biomass has already been proven to fulfill the requirements of a clean resource for the energy industries and feedstock for chemical-related industries (Long et al. 2013). An effective dual action would be to consider organic solid waste such as sawdust as a potential resource for bio-energy as well as bio-product development. Such an action would not only limit the amount of solid waste, but it could also decrease the global dependence on fossil fuels for energy and feedstock purposes. Certain pretreatment procedures, such as delignification before cellulase-catalyzed degradation, should be a standard procedure as it increases the bioconversion of cellulose into fermentable sugars such as glucose (Soleimanzadeh et al. 2023). It should also be advisable to grow cellulase systems that are more active on the cellulose structure by focusing on the production of cellulase systems with more active endoglucanase, exoglucanase, and B-glucosidase enzyme components (Ejaz et al. 2021). Sawdust is not the only organic waste material that is susceptible to saccharification by the cellulase enzyme system, as other materials like wastepaper, kitchen waste, and garden waste are also potential resources due to their relatively high cellulose content.

## CONCLUSIONS

Cellulose, one of the structural components of organic waste materials such as sawdust, has the potential to be developed as a resource for alternative and renewable fuel production and bioproduct synthesis. Glucose, the major saccharification product produced during cellulase-catalyzed degradation of cellulose, is a fermentable sugar with a huge potential as a renewable feedstock for many synthetic procedures. Concluded from this study is not only that cellulose from different trees has different susceptibilities for a specific cellulase enzyme system, such as that from *A. niger*, but that delignification resulted in an increase in saccharification compared to the amount of sugar released from nom-pretreated sawdust. The positive effect of increasing masses of the non-delignified and lignified materials on the sugar-

releasing ability of the cellulase enzyme acting on cellulose is also well concluded. Delignification proved to be an effective pretreatment procedure, resulting in an increase in the degradation of sawdust compared to the non-delignified material.

## REFERENCES


Abeer, I., Adel, M., Zeinab, H., El–Wahab, A., Ibrahim, A. A. and Al-Shemy, M. T. 2010. Characterization of microcrystalline cellulose prepared from lignocellulosic materials. Part I. Acid-catalyzed hydrolysis. Biores. Technol., 101(12): 4446-4455.

Akhator, P., Obanor, M. and Ugege, A. 2017. Nigerian wood waste: A potential resource for economic development. J. Appl. Sci. Environ. Manag., 21: 246. 10.4314/jasem.v21i2.4

Ali, S. S., Jiao, H., El-Sapagh, S. and Sun, J. 2023. Biodegradation of willow sawdust by a novel cellulase-producing bacterial consortium from wood-feeding termites for enhancing methane production. Biores. Technol., 383: 129232.

Andberg, M., Penttilä, M. and Saloheimo, M. 2015. Swollen in from *Trichoderma reesei* exhibits hydrolytic activity against cellulosic substrates with features of both endoglucanases and cellobiohydrolases. Biores. Technol., 181: 105-113.

Ashokkumar, V., Venkatkarthick, R, Jayashree, S., Chuetor, S, Dharmaraj, S., Kumar, G., Chen, W. and Ngamcharussrivichai, C. 2022. Recent advances in lignocellulosic biomass for biofuels and value-added bioproducts: A critical review. Biores. Technol., 344: 126195.

Beldman, G., Voragen, A. G., Rombouts, F. M., Searle-van Leeuwen, M. F. and Pilnik, W. 1987. Adsorption and kinetic behavior of purified endoglucanases and exoglucanases from *Trichoderma viride*. Biotechnol. Bioeng., 30(2): 251-257. doi:10.1002/bit.260300215.

Bellaouchi, R., Abouloifa, H. and Rokni, Y. 2021. Characterization and optimization of extracellular enzyme production by *Aspergillus niger* strains isolated from date by-products. J. Genet. Eng., Biotechnol., 50 :19. https://doi.org/10.1186/s-00145-021-43141y

Carrard, G. and Linder, M. 1999. Widely different off rates of two closely related cellulose-binding domains from *Trichoderma reesei*. Eur. J. Biochem., 262(3): 637-643.

Chang, M., Chou, T. C. and Tsao, G. 1981. Structure, pretreatment, and hydrolysis of cellulose. In: Fiechter A (ed) Bioenergy, Adv. Biochem. Springer, Berlin Heidelberg, 20: 15-42. doi:10.1007/3-540-11018-6_2.

Cheng, G., Varanasi, P., Li, C., Liu, H., Melnichenko, Y. B., Simmons, B. A., Kent, M. S. and Singh, S. 2011. Transition of cellulose crystalline structure and surface morphology of biomass as a function of ionic liquid pretreatment and its relation to enzymatic hydrolysis. Biomacromolecules, 12(4): 933-941.

Ciolacu, D. E., Ciolacu, F. and Popa, V. I. 2011. Amorphous cellulose-Structure and characterization. Cellul. Chem. Technol., 45(1): 13-21.

Ejaz, U., Sohail, M. and Ghanemi, A. 2021. Cellulases: From bioactivity to a variety of industrial Applications. Biomimetics, 6(3): 44.

Gustafson, R. R., Sleicher, C. A., McKean, W. T. and Finlayson, B. A. 1983. A theoretical model of the Krafting pulping process. Ind. Eng. Chem. Process. Des. Dev., 22(1): 87 -96.

Hemansi, H. and Saini, J. K. 2023. Enhanced cellulosic ethanol production via fed-batch simultaneous saccharification and fermentation of sequential dilute acid-alkali pretreated sugarcane bagasse. Biores. Technol., 372: 128671.

Jeon, S. D., Yu, K. O., Kim, S. W. and Han, S. O. 2012. The processive endoglucanase is active in crystalline cellulose degradation as a cellulosomal subunit of *Clostridium cellulovorans*. New Biotechnol., 29(3): 365-371.

Kapsalyamova, Z. and Paltsev, S. 2020. Use of natural gas and oil as a source of feedstocks. Energy Econ., 92: 104984.

Kaschuk, J. J., Lacerda, T. M. and Frollin, E. 2019. Investigating effects of high cellulase concentration on the enzymatic hydrolysis of the sisal cellulosic pulp. Int. J. Biol. Macromol., 138: 919-926.

Kim, Y. J., Kim, D. O., Chun, O. K,. Shin, D. H., Jung, H., Lee, C.Y. and Wilson, D. B. 2005. Phenolic extraction from apple peel by cellulases from *Thermobifida fusca*. J. Agric. Food Chem., 53(24): 9560-9565.

Lee, N. E., Lima, M. and Woodward, J. 1988. Hydrolysis of cellulose by a mixture of *Trichoderma reesei* cellobiohydrolase and *Aspergillus niger* endoglucanase. Biochim. Biophys. Acta., 440-437 :(3)967.

Linder, M. and Teeri, T. T. 1996. The cellulose-binding domain of the major cellobiohydrolase of *Trichoderma reesei* exhibits true reversibility and a high exchange rate on crystalline cellulose. Proc. Natl. Acad. Sci. USA, 12255-12251 :(22)93.

Liu, G. and Bao, J. 2019. Constructing super large-scale cellulosic ethanol plant by decentralizing dry acid pretreatment technology into biomass collection depots. Biores. Biotechnol., 275: 338-344.

Long, H., Li, X., Wang, H. and Jia, J. 2013. Biomass resources and their bioenergy potential estimation: A review. Renew. Sustain. Energy, 26: 344-352.

Martin, G., Boehmer, H. and Olenick, S. M. 2020. Correction to thermally-induced failure of smoke alarms. Fire Technol., 56(2): 673-692. 10.1007/s10694-019-00898-6.

Miller, G. L. 1959. Use of dinitrosalicylic acid reagent for determination of reducing sugar. Anal. Chem., 31: 426-428.

Mishra, M., Sharma, M., Dubey, R., Kumari, P. Ranjan, V. and Pandey, J. 2021. Green synthesis interventions of pharmaceutical industries for sustainable development. Curr. Res. Green Sustain. Chem., 4: 100174.

Ndlovu, T. M. and Van Wyk, J. P. H. 2023. Saccharification of various wastepaper materials by cellulase from brown garden snail (*Cornu aspersum*) at different incubation pH-values. Nat. Environ. Pollut. Technol., 22(4): 2153-2162.

Ndukwe, N. A., Jenmi, W. O., Okiei, W. O. and Alo B. I. 2009. Comparative study of percentage yield of pulp from various Nigerian wood species using the kraft process. AJEST, 3(1): 21-25.

Pal, P., Li, H. and Saravanamurugan, S. 2022. Removal of lignin and silica from rice straw for enhanced accessibility of holocellulose for the production of high-value chemicals. Biores. Technol., 361: 127661.

Palonen, H., Tenkanen, M. and Linder, M. 1999. Dynamic interaction of *Trichoderma reesei* cellobiohydrolases Cel6A and Cel7A and cellulose at equilibrium and during hydrolysis. Appl. Environ. Microbiol., 5233-5229 :(12)65.

Phiri, R., Rangappa, S. M. and Siengchin, S. 2024. Agro-waste for renewable and sustainable green production: A review. J. Clean. Prod., 434: 139989.

Przybysz, J., Celiński, M., Kozikowski, P., Mizera, K., Borucka, M. and Gajek, A. 2023. Flammability and explosion characteristics of hardwood dust. J. Fire Sci., 41(3): 89-101. doi:10.1177/07349041231168554.

Soleimanzadeh, H., Salari, D., Olad, A. and Ostadrahimi, A. 2023. Optimization of delignification and cellulose isolation process from natural cotton and preparation of its nanofibers with choline-lactic acid eutectic solvents. Biomass Conver. Bioener., https://doi.org/10.1007/s13399-023-04141-9

Wan, J., Wang, Y. and Xiao, Q. 2010. Effects of hemicellulose removal on cellulose fiber structure and recycling characteristics of eucalyptus pulp. Biores. Biotechnol., 101(12): 4577-4583.

Wang, H., Qi, X., Gao, S., Zhang, Y. and An, Y. 2023b. Biochemical characterization of an engineered bifunctional xylanase/feruloyl esterase and its synergistic effects with cellulase on lignocellulose hydrolysis. Biores. Biotech., 355: 127244.

Wang, J., Wang, J., Zhoumin, L. and Zhang, J. 2020. Adsorption and desorption of cellulase on/from enzymatic residual

lignin after alkali pretreatment. Indus. Crops Prod., 155: 112811.

Wang, W., Xu, Y., Zhu, B., Ge, H., Wang, S. Li, B. and Xu, H. 2023a. Exploration of the interaction mechanism of lignocellulosic hybrid systems based on deep eutectic solvents. Biores. Biotechnol., 385: 129401.

Yang, J., Yue, H. R., Pan, L. Y., Feng, J. X., Zhao, S., Suwannarangsee, S., Champreda, V., Liu, C. G. and Zhao, X. Q. 2023. Fungal strain improvement for efficient cellulase production and lignocellulosic biorefinery: Current status and prospects. Biores. Biotech., 385: 129449.

Zou, G., Bao, D., Wang, Y., Zhou, S., Xiao, M., Yang, Z., Wang, Y. and Zhou, Z. 2021. Alleviating product inhibition of *Trichoderma reesei* cellulase complex with a product-activated mushroom endoglucanase. Biores. Biotech., 319: 124119.

## ORCID DETAILS OF THE AUTHORS

J. P. H. van Wyk: https://orcid.org/0000-0003-3067-6231

Nature Environment and Pollution Technology
An International Quarterly Scientific Journal

p-ISSN: 0972-6268
(Print copies up to 2016)
e-ISSN: 2395-3454

Vol. 23 | No. 3 | pp. 1333-1344 | 2024

Original Research Paper

https://doi.org/10.46488/NEPT.2024.v23i03.007

Open Access Journal

# Emerging Issues in Energy Sustainability: A Systematic Review and Research Agenda

**Aqsa Anjum*†, Jahangir Chauhan*, Marghoob Enam** and Irfan Ali*****
*Department of Commerce, Aligarh Muslim University, Aligarh, U.P., India
**Department of Management, Indian Institute of Technology, Dhanbad, Jharkhand, India
***Department of Statistics, Aligarh Muslim University, Aligarh, U.P., India
†Corresponding author: Aqsa Anjum; aqsaanjum23@gmail.com

**Nat. Env. & Poll. Tech.**
**Website: www.neptjournal.com**

*Received:* 22-11-2023
*Revised:* 10-01-2024
*Accepted:* 21-01-2024

**Key Words:**
Energy generation technologies
Renewable energy
Social impacts
Sustainable development
External cost

## ABSTRACT

This research paper seeks to investigate and categorize previous studies to understand better the role of energy generation technology in promoting sustainable development of a country country. The primary aim of this review is to identify and emphasize key issues related to energy sustainability. The study employs a systematic review approach, drawing on academic publications from the Web of Science and Scopus database. The analysis reveals five key issues: the nexus between energy generation and greenhouse gas emissions, energy generation and employment, the impact of energy generation and land use intensity, the association between energy generation and water footprint, and the nexus between energy generation and human health. This study delves into the theoretical dimensions of research concerning the interplay between energy sustainability and various aspects of energy generation technologies. Furthermore, it contributes to the existing body of knowledge concerning Sustainable Development Goal 7, with the overarching goal of enhancing both human well-being and economic prosperity through advancements in energy generation technologies. The study comprehensively explores the subject matter, offering an in-depth analysis of energy sustainability. Its unique contribution lies in its extensive examination of multiple facets of energy sustainability, making it a significant addition to the field of research.

## INTRODUCTION

The nexus between energy utilization and its environmental consequences underscores the significance of comprehending the full spectrum of impacts associated with diverse energy sources. Globally, the escalating trajectory of energy generation poses significant ecological challenges. Achieving the Sustainable Development Goals (SDGs) by 2030 involves transitioning toward a low-carbon economy, a pivotal strategy highlighted in Goal 7. In the Indian context, the energy sector contributed 68.7 percent of greenhouse gas emissions (GHGs) in 2021. Addressing carbon emissions demands more incremental adjustments, necessitating a comprehensive reconfiguration in energy production, transportation, and consumption. The fifteenth goal of the SDGs accentuates the need to avert land degradation arising from the rising energy supply and consumption. One of India's SDG targets (Goal 6) also addresses the judicious management and prevention of water contamination. This involves providing affordable energy services, catering to immediate and future basic needs, aligning with environmental sustainability, and garnering societal and individual acceptance. Renewable energy technologies emerge as a salient avenue for addressing the exigency of energy scarcity (Ray 2019). The substitution of renewable resources for fossil fuels in the energy sector holds promise for diminishing $CO_2$ emissions and mitigating other pollutants. Delving into India's energy landscape, statistics for 2022 revealed a consumption of 12,75,534 Million Units (MU) and a supply of 12,70,663 Million Units (Ministry of Power 2022). In contemporary society, electricity distribution is pivotal in facilitating a consistent, sufficient, and economically viable energy supply that underpins many human activities. Coal, constituting over 60% of total energy generation, is India's predominant electricity source, as shown in Fig. 1. Projections by Energy Statistics (2022) indicated a trajectory of 772 million metric tons of coal consumption in the country by 2040.

Beyond the pressing need of meeting electricity requirement, the ramifications of fossil-based power generation extend to climate change and public health. The

ramifications of power generation technologies go beyond their direct environmental effects, affecting public health, ecosystems, and climate change. Fossil fuel-based approaches are associated with air pollution, resource exhaustion, and sustained ecological disturbances. Fig. 2 illustrates the externalities associated with energy generation technologies. Decarbonizing the electricity generation landscape emerges as a strategic lever in curtailing the adverse climate and health effects of extant technologies. The inception of solar photovoltaic (PV) technology for electricity generation in India in the early 2000s marked a shift from the predominant reliance on coal. The global impetus towards sustainable energy production, aligned with sustainable development goals, prompted India to pioneer the Ministry of New and

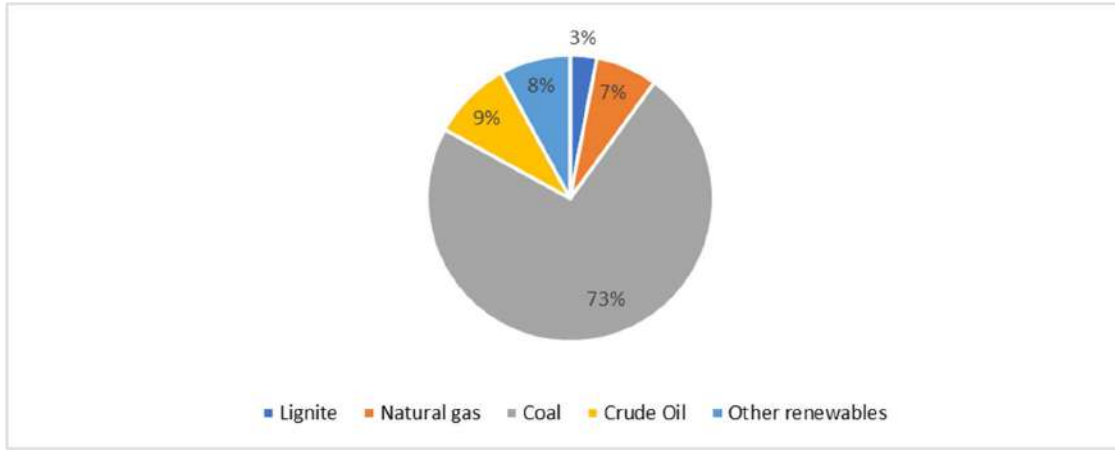


Fig. 1: Net electricity generation by fuel in India. (Energy Statistics 2022)

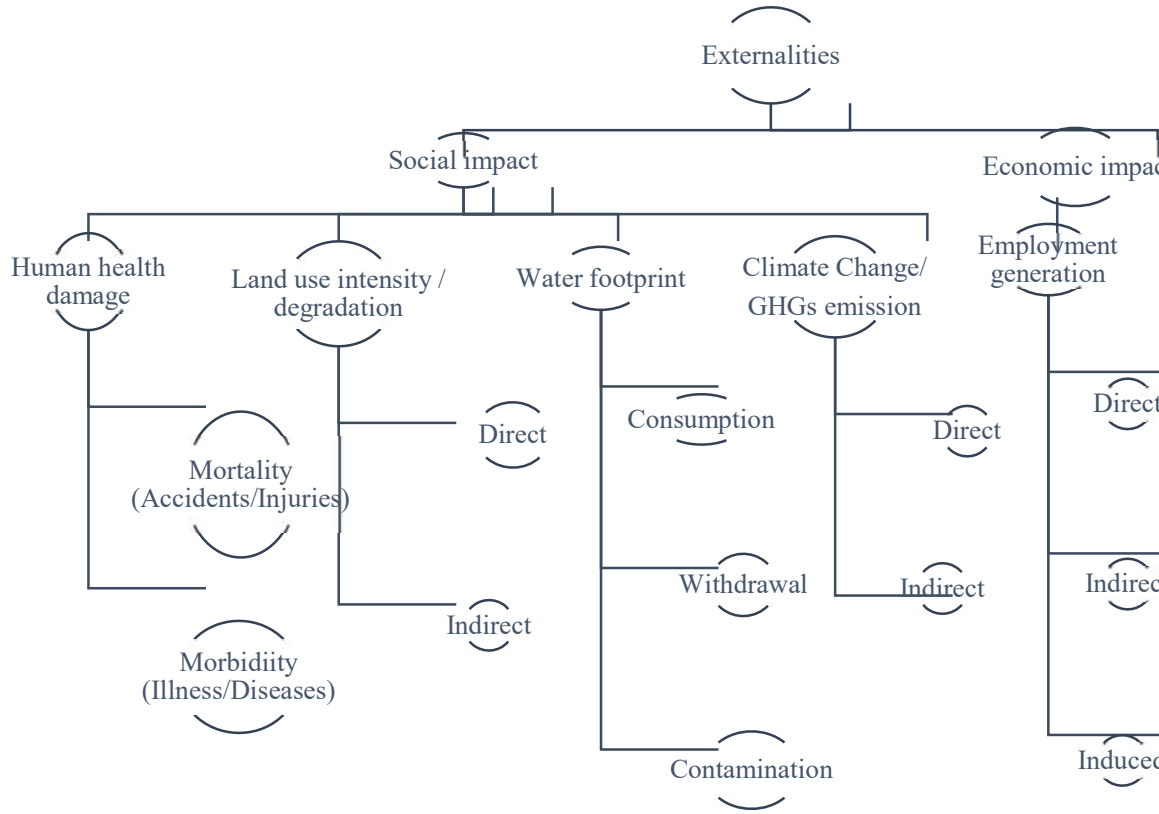


Fig. 2: Externalities of power generation technologies.

Renewable Energy (MNRE) establishment in the 1980s (MNRE). This institutional commitment positions India as a trailblazer in leveraging sustainable technologies, with a pronounced ambition of achieving a net-zero target by 2070.

The study of energy generation technology and sustainability, or energy sustainability, has been a popular research area since 1990. However, after 2009, there was an unprecedented expansion and popularization of energy-related literature. Initially, literature concentrated solely on the economic side of energy. With the expansion of the literature, the field experienced a drastic transition from formerly economic-focused studies to more probing studies of energy sustainability. The increasing interest in energy and sustainability may be seen in the growth of research articles over the last decade, worldwide conferences on sustainability and green energy reports. Energy sustainability has been critically analyzed in several scholarly works. Various aspects of energy generation, such as energy generation and air pollution, have been discussed by many researchers. However, research on energy sustainability is still ongoing, and there is much to be discovered on it. To highlight the key research advances and identify gaps in the various aspects of energy generation, this study attempts to thoroughly review the literature on energy generation and its connected issues. To accomplish this, the study focused on five key issues in the field of energy generation to uncover understudied sections of this field and its connections to various consequences to advance the academic study of energy generation. The study is organized according to a conventional structure. The following section presents a thorough literature analysis of pertinent studies on five distinct energy-generating concepts to support its links with the highlighted issues. The research approach is then described, followed by the discussion and conclusion. In the last, research implications, limitations, and direction for future research are presented.

## MATERIALS AND METHODS

This systematic literature review (SLR) compiles and assesses several research papers to give a thorough overview of all the available literature pertinent to a particular research question. The main goal of the study is to find new issues in the energy generation field. The following research questions were chosen: 1. What are the emerging issues in energy sustainability? 2. What are the important research and study

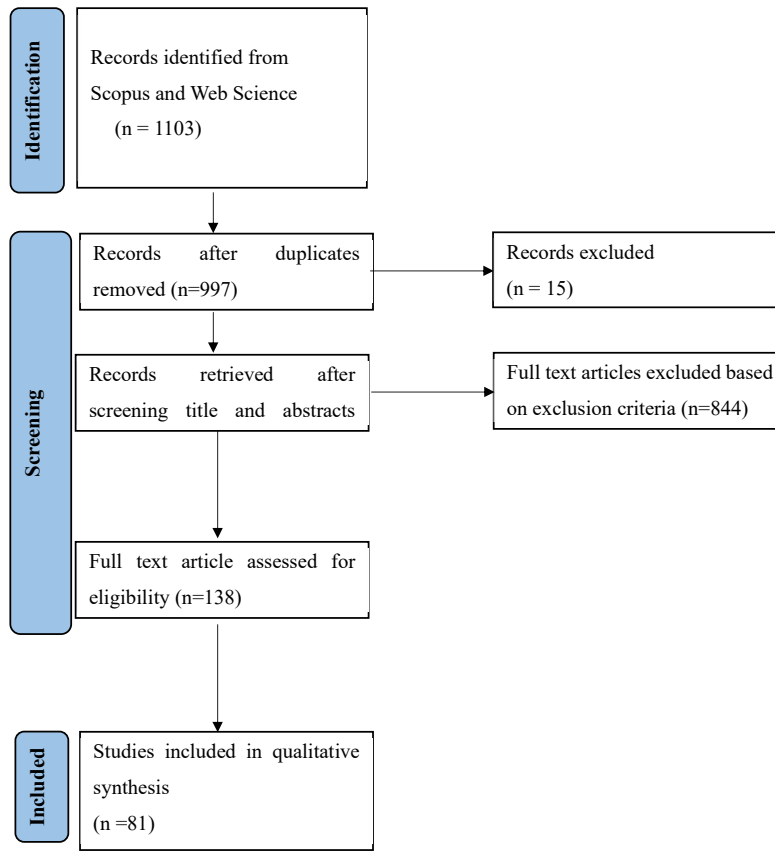


Fig. 3: Literature review workflow (PRISMA).

loops in energy generation sustainability that have been noted for each theme? 3. What fresh avenues of inquiry are recommended by the body of existing research?

The study followed the PRISMA standards when searching the literature. The PRISMA (Preferred Reporting Items for Systematic Reviews and Meta-Analyses) approach is frequently employed in systematic literature reviews because it provides a structured and transparent method for documenting the review procedure, improving quality and reliability (Sarkis-Onofre et al. 2021). It has become the industry standard for disclosing meta-analyses and systematic reviews in various disciplines. This approach enhances transparency and trustworthiness, improving the validity and applicability of the review results (Page 2017). The PRISMA method has several advantages over other alternative techniques for systematic literature reviews, including enhanced reproducibility, decreased bias risk, better presentation, and widespread acceptance. Two prominent research databases, Scopus and Web of Science, were used to locate relevant literature since they contain high-impact, peer-reviewed journal articles. Systematic reviews incorporate peer-reviewed journal articles, the quality and accuracy of the output gets increase (Mickan et al. 2013, Uttley et al. 2023).

The search combined the title, abstract, and keywords with the Boolean operators 'OR' and 'AND' to ensure that all potential articles were retrieved. The terms used in the search were 'Energy generation impacts' AND 'Coal energy generation' AND 'Cost of solar energy' AND 'Wind energy impact' OR 'Thermal plants' OR 'energy generation' OR 'Social cost of energy generation' OR 'Solar energy impact' OR 'Coal energy impacts' OR 'Energy generation impacts' OR 'Energy externalities.' This study considered studies published in peer-reviewed journals, written in English, and terms mentioned in the title, authors' keywords, or abstract. The study excludes book chapters, editorials, conference proceedings, and editorial notices. The data for this study was limited to 2009-2022. Fig. 3 depicts a full description of the approach used in this study.

## RESULTS

### Energy Generation and Water Footprint

The intricate connection between water consumption and energy technologies highlights their vital interdependence in modern life. Water plays a crucial role in various energy generation processes, creating a symbiotic relationship that requires careful consideration for sustainable energy solutions (Okadera et al. 2014, Jin et al.2019). As our reliance on diverse energy is increasing, there is a growing demand for water resources, necessitating strategies to optimize water usage and enhance energy efficiency while minimizing environmental impacts. Recognizing the reciprocal relationship between water and energy, from generation to distribution and consumption, underscores the need for holistic approaches to resource management. Population growth and increased water consumption in industrial sectors are predicted to reduce the average per capita water supply. The Indian energy sector drew over 20 billion cubic meters of water and consumed over 3 billion cubic meters in 2019. Almost 35% of coal energy plants use freshwater for cooling, primarily in water-stressed parts of India. Coal power plants are the largest consumers of fresh water since they require water during coal extraction and processing (Kenny et al. 2009, Pan et al. 2012, Qin et al. 2015). A study by (Meldrum et al. 2013) estimated water consumption and withdrawal in the operation and maintenance of coal plants and found that around 76 percent and 83 percent are utilized in these processes, respectively, leading to water source contamination. Even if the contaminated water is recycled, only eight percent of the wastewater released by coal plants can be used for cooling purposes (International Energy Agency (IEA) 2021). The transition towards renewables is required to reduce this consumption and contamination of the water. The most efficient way to lower the water consumption intensity of energy sector is to increase the use of renewable energy sources (Mekonnen et al. 2015, Ding et al. 2018). Groesbeck and Pearce (2018) revealed that wind turbines and solar PV panels need very little water to generate electricity, whereas water required to cool thermal energy plants ranges from 85% to 95%. Even if the water contamination issue of coal energy plants is resolved through desalination (quality improvement), it would not be an effective solution; the only alternative is renewable sources that supply energy without impacting the environment. Research findings by (Al-Karaghouli & Kazmerski 2012, Feria-Diaz et al. 2021) affirmed that adopting renewable energy sources can lessen the burden on freshwater resources. Conversely, Meldrum et al. (2013) highlighted that renewables cause water contamination in their operation and maintenance; around 20 gal.MWh$^{-1}$ of water is used to maintain the solar panels. Although solar photovoltaic utilities consume and withdraw less water than coal power plants, they consume more water during construction (Klise et al. 2013).

Table 1 shows the water footprint of different electricity generation technologies during their lifecycle. Maximum water footprint occurs in operating thermal power plants and constructing solar power plants. Findings of studies confirmed that solar energy technology could significantly cut water usage, withdrawals, and contamination (Tawalbeh et al. 2021, Jin et al. 2019). Various subjects showed a

link between energy generation and conceptions of water use intensity. Few studies have thoroughly examined the intensity of water use in energy generation and other sectors. However, there is a need for more research investigating energy generation resources and their water use intensity, particularly in underdeveloped or developing countries. Furthermore, more research needs to be conducted on the multifaceted element of water utilization in energy generation. Such research would attract regulators, legislators, and manufacturers, particularly those with resources that must be made aware of sustainability.

## Energy Generation and Greenhouse Gases (GHG) Emissions

The rising energy and fuel energy demand considerably add to greenhouse gas emissions and global climate change. According to the Ministry of Environment, Forest and Climate Change (2021), greenhouse gas emissions from the energy sector increased from 55.95 percent in 2011 to 56.66 percent in 2016. Chakravarty and Somanathan (2021) revealed that the mortality rate due to air pollution was 2.03 cents/kWh by coal energy generation in 2018. Their finding aligns with the findings of (Cropper et al. 2021, Sahu et al. 2021). Wiser et al. (2016) projected the ecosystem and human health benefits of renewable sources, inferring that solar energy is viable even without subsidies in the coming years. Bernal-Agustin and Dufo-Lopez (2006) investigated that investment in grid-connected PV systems is profitable from an economic and environmental perspective. However, the high payback period may deter investors; still, solar PV can save between 0.08 and 0.38 Euros per kWh, which calls for the substitution of coal power plants.

All types of PV systems are a potential method of electricity generation for reducing $CO_2$ emissions and conserving energy resources (Sherwani & Usmani 2010).

Table 1: Average consumptive water footprint per unit of electricity.

| Technology | Construction ($m^3$ $TJe^{-1}$) | Operation ($m^3$ $TJe^{-1}$) | Fuel Supply ($m^3$ $TJe^{-1}$) |
|---|---|---|---|
| Coal and lignite | 1.1 | 440 | 54 |
| Natural gas | 1.1 | 240 | 6 |
| Hydro energy | 0.3 | 15100 | 0 |
| Nuclear | 0.3 | 610 | 68 |
| Oil | 1.1 | 440 | 55 |
| Wind | 1.1 | 0.2 | 0 |
| Firewood | 0.4 | 400 | 156000 |
| Geothermal | 2.1 | 340 | 0 |
| Solar (PV + CSP) | 90 | 50 | 0 |

Source: Martin (2012)

Likewise, many researchers supported renewable sources' positive implications for mitigating greenhouse gas emissions. Samadi (2017) inferred that renewable energy generation technologies exhibit fewer externalities than coal-based technologies. Wu et al. (2017) indicated that one megawatt solar PV plant would provide yearly $2.08 \times 10^9$ g $CO_2$ equivalent greenhouse gas emission savings. On the contrary, Desideri (2012) evaluated a hypothetical PV plant and inferred that even solar plants are not environmentally friendly as they produce 44.7 $g.kWh^{-1}$ emissions. Their finding corresponds to the study of Nugent et al. (2014), which revealed that both solar and wind systems cause GHG emissions during their lifecycle; they are not emissions-free technologies.

Despite a few disadvantages, solar energy technology is the most viable energy source for future global energy needs, followed by biomass and geothermal (Kabir et al. 2018). Emissions from thermal energy plants are extremely harmful; only 3.6 percent of solar PV is necessary to counteract life loss due to coal pollution (Ftehnakis et al. 2008). Energy generation through solar PV can save 69-100 million tonnes of $CO_2$, 69000-98000 tonnes of NOx, and 126000-184000 tonnes of $SO_2$ by 2030 (Shahsavari & Akbari 2018). Among energy technologies, hydro-energy emits only 0.011 tCO2/MWh, but it affects the aquatic habitat (Table 2). The next best alternative is nuclear energy, which emits less emissions but produces radioactive waste (Harris et al. 2013). Wind energy emits only 0.0295 $tCO2.MWh^{-1}$ but has wildlife-related risks because wind turbines kill Avian (Sanchez-Zapata et al. 2016, Teff-Seker et al. 2022). Solar photovoltaic energy is efficient in combating greenhouse gases without creating additional issues. It was determined that increased energy generation from fossil-fuel-based industries is connected with higher GHG emissions, and solar PV has the potential to reduce emissions drastically (Amponsah et al. 2014, Hardisty et al. 2012). Greenhouse gas emissions (GHGs) could not be utilized as a single metric to depict a technology's environmental sustainability (Georgakellos & Didaskalou 2014). Climate change must be prioritized among the impacts of energy generation systems, followed by land footprint (Turney & Fthenakis 2011).

Despite the global recognition of Sustainable Development Goals (SDGs), there is a significant gap in research addressing sustainability in energy generation technologies. Limited scholarly publications have explored energy generation systems through the lens of multi-dimensional sustainability, necessitating further examination. Moreover, sustainable energy generation technologies may sometimes involve extra costs for utilities. Consequently, empirical investigations are crucial to offer improved solutions and

Table 2: Total lifetime global warming potential (MT $CO_2$eq) for technologies.

| Technology (5.5 TWh) | $CO_2$(×$10^6$) | $CH_4$ (×$10^4$ ) | $N_2O$ (×$10^4$ ) | GWE (×$10^6$) |
|---|---|---|---|---|
| Hydroelectric | 0.51 | 0.084 | 0.85 | 0.51 |
| Photovoltaic | 1.1 | 0.78 | 8.7 | 1.1 |
| Wind Farm | 0.82 | 0.054 | 0.65 | 0.83 |
| Coal | 86 | 35 | 220 | 86 |
| Natural Gas | 51 | 50 | 220 | 54 |

Source: Bergerson & Lave (2002)

ascertain the willingness to incur these additional expenses for environmental betterment.

## Energy Generation and Health Impacts

Health impacts include the effects of air pollution on human health, crop production, and buildings, leading to occupational diseases, injuries, and accidents at the workplace. The magnitude of the health impact is primarily connected to the population density and environmental conditions in the exposed areas. According to AirClim (2013), over 19 million people in India suffered from respiratory ailments, and 80,100 to 1,14900 premature deaths occurred due to harmful emissions from thermal energy plants in 2012. The environmental impact and health damage costs of thermal energy plants are approx. 39.3 cents per kWh (Nkambule & Blignaut 2012). According to Guttikunda and Jawahar (2014), if the emission control measures were not adopted, respiratory diseases would increase to 42.7 million by 2030, resulting in 23000 crore health care costs per year. Nonetheless, deaths from coal energy generation were significantly higher than those from solar energy generation in 2014 (Fig. 4). Major accidents occur due to operational errors in solar photovoltaic production and coal mining (Prehoda & Pearce 2017). However, operational errors in solar PV are minimal. In 2015, 0-202 per 100000 people were killed by PM2.5 emissions from coal energy plants, while the deaths due to NO2 ranged from 0-72 per 100000; this rate is anticipated to increase 2-3 times by 2030 (Khomenko et al. 2021). With the release of PM2.5 from coal-fired energy plants, the mortality rate would be 6 per 10000 by 2025 (Chio et al. 2019). Around 112000 deaths occur annually in India due to coal-fired energy plant emissions (Cropper et al. 2021). Coal and oil plants have impacted respiratory diseases and the fertility rate among people. Studies have considered the effects of early retirement of coal plants and the effects of the transition to renewable (Maamoun et al. 2020, 2022).

Fertility rates per 1000 women (15-44 yrs) increased by eight births within 5 km and two deliveries within 5-10 km near energy plants per year after the exit of thermal plants (Casey et al. 2018). One gigawatt hour (GWh) of solar energy reduces hospitalizations due to respiratory problems by 52 percent in cities near the displaced plants (~13 percent decline on average) (Rivera et al. 2021). The reductions in cardiovascular and pulmonary ailments were primarily evident in newborns, children (ages 6-14), and seniors due to the shift from thermal energy plants to solar energy generation. Between 2005 and 2016, the retirement of coal-based energy plant units saved 26,600 lives in the United States (Burney 2020). The value assessments from various studies discovered that switching to solar PV is not entirely viable, yet it saves lives and money (Breyer et al. 2015, Jenniches & Worrell 2019, Jager-Waldau et al. 2020). Understanding the origins and quantities of emissions produced by energy-producing systems is critical. Despite the energy sector's prominent position in public health damage, research on measuring health damage caused by energy-producing technologies is limited. Research on long-term solutions for managing and mitigating health damage, morbidity, and mortality caused by energy-producing technology is scarce. Furthermore, while there has been much research on health effect mitigation techniques in the energy industry in developed nations (Masnadi et al. 2018, Yeh et al. 2010), little work has been done in underdeveloped countries.

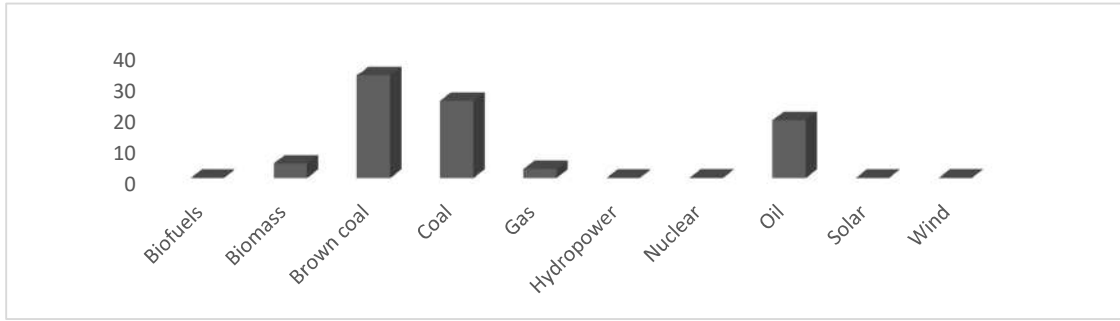


Source: Sovacoolet al. (2016), Markandya & Wilkinson (2007)

Fig. 4: Death rates from energy sources (per TWh).

**Energy Generation and Employment Generation**

Energy generation technologies significantly impact the nation's employment rate (Bryan et al. 2017, Nagatomo et al. 2021). Even without considering the type of energy technology, the employment rate varies during different phases, like upstream and downstream processing of generation technology (Odeh & Cockerill 2008).

Coal energy employs more unskilled people in mining and transportation to obtain raw materials. In case ofrenewables, the rate of indirect and induced employment is higher than the rate of direct employment. However, the renewable energy sector engages skilled workers, such as skilled labor, in manufacturing modules and equipment and installing solar PV plants (Wei et al. 2010). Multiple studies supported adopting a renewable system for dealing with the unemployment problem globally. Ali et al. (2021) proposed enhancing reliance on renewable energy and reducing the usage of fossil fuels to ramp up the employment rate up to 2030. According to Natarajan and Nalini (2015), solar PV would generate 0.152 million jobs and 0.225 million on-grid and off-grid by 2022. The employment rate in the coal energy sector will decrease by 52% by 2040, owing to decarbonization. Solar Photovoltaic contributed to 3.98 million jobs among renewables in 2020. According to the International Renewable Energy Agency (IRENA 2021), on-grid solar employment generated 93,900 jobs, while off-grid solar employment generated 69,600 jobs in India. Moreover, a study by Stanford University stated that renewable technology might generate twenty-eight million jobs globally in the future. Employment by renewable plants would be five times more than that of fossil fuel plants.

Similarly, Garett-Peltier (2017) stated that every million USD spent on renewable energy creates 7.5 full-time equivalent jobs across the economy. Studies confirmed that green technologies benefit the energy generation industry and the overall economy, analyzing the impacts of technologies. More academic scholars from many nations are exploring the issue of 'employment generation' in the energy sectors. Future studies should prioritize a more comprehensive multidisciplinary examination of various aspects of employment in the energy generation sector. Fig. 5 depicts global employment due to energy generation technologies in which the share of solar photovoltaics is high. Assessing the effects on employment would assist policymakers in formulating transformation strategies influenced by climatic and environmental challenges and social factors.

**Energy Generation and Land Use Intensity**

The most apparent effect of land use is the quantity of land taken at the price of the natural ecosystem, leading to land and soil deterioration. One of the objectives of SDG 15 is to prevent land degradation induced by energy supply and consumption. Studies have considered land use differently: land occupation and transformation, direct land use, and indirect land use. Land use intensity, health damage, greenhouse gas emissions, energy cost, and energy security should be considered in energy system planning (Lovering et al. 2022). Coal energy plants cover the land for mining, storage, and evacuation of sites for raw coal. The installation of coal energy plants negatively impacts the environment because of the pollutants produced during extraction, construction, and energy generation. This makes the land unusable for irrigation and rehabilitation; as a result,

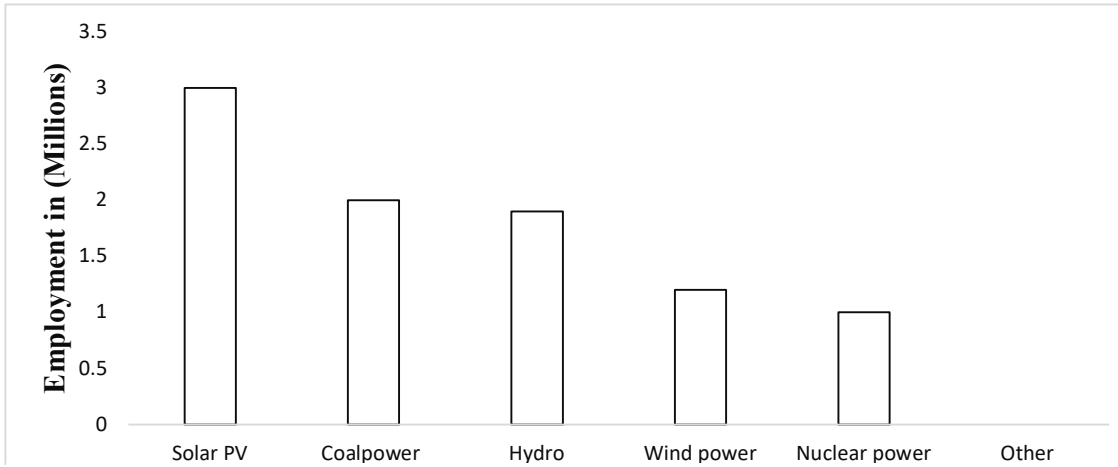


Source: IEA, 2022

Fig. 5: Global employment in energy generation technologies.

the people living there are forced to move. Multiple studies have studied the land use intensity of generation technologies and come up with different conclusions. Rej and Nag (2020) analyzed that the transition to a low-carbon economy by 2030 is associated with a massive land demand. Correspondingly, Kiesecker et al. (2019) estimated a 55000 to 125000 $km^2$ land requirement to build the projected energy capacity by 2022. In addition, they pointed out that there is more than enough land area (more than ten times) in India to achieve the target for solar and wind energy by 2022. Moreover, Fthenakis and Kim (2009) made a comparative analysis and revealed that the direct land use by solar PV is less than that needed for coal-fired and natural gas plants.

In case of coal, indirect land usage (more than 55%) for coal is greater than direct land use, indicating that the PV plants cause less land disturbance than others. Ong et al. (2013) assessed the land needed for solar PV. They estimated that around 2.1 -12.3 acres per MWac of direct land use is required for a solar PV installation, with an average overall land use of 3.6 acres per $GWh.Yr^{-1}$. Mohan (2017) analyzed that nuclear energy requires only six percent of the total land area of solar PV and around 1/5th of the land area for wind energy per GWh of electricity generated. Turney and Fthenakis made a similar comparison in 2011; they found that the land transformation rate of solar plants was lower than that of coal plants for more than 27 years. The utilization of land by hydropower projects varies greatly. Deepwater dams have a lower footprint than shallow dams because energy generation depends on hydraulic pressure and water flow rate (Fthenakis & Kim 2009).

Selecting energy technology based solely on land use impact is inadequate to support policy decisions fully, yet it is a crucial factor to consider (Mohan 2017). Locating solar systems (agrivoltaic systems) and wind systems alongside agriculture has been proposed as a strategy to reduce the land footprint of renewable energy systems (Dinesh & Pearce 2016, Ravi et al. 2016, Moretti & Marucci 2019). Table 3 shows that the land use intensity of all energy systems differs depending on the source, ranging from 0.1 to 500 $m^2.MWh^{-1}$. While estimating global warming potential is well advanced, many other indicators are still in the early stages of development. As the transition to more renewable-based systems occurs, these measurements will demand the same attention as those related to climate change. Otherwise, they may pose unexpected challenges to the energy transition.

Table 3: Land use intensity in electricity generation.

| Energy sources | Land use Intensity [$m^2.MWh^{-1}$] |
|---|---|
| Nuclear | 1 |
| Natural gas | 0.1 |
| Coal (Underground) | 0.2 |
| Surface (open-cast) | 0.4 |
| Wind | 0.7 |
| Geothermal | 2.5 |
| HydroEnergy (large dams) | 3.5 |
| Solar photovoltaic | 8.7 |
| Solar – concentrated solar Energy | 7.8 |
| Biomass (from Crops) | 450 |

Source: IINAS (2017)

## DISCUSSION AND CONCLUSION

This study examined the literature on the social cost of energy generation using the Web of Science and Scopus databases. Articles emerging from the search were read, evaluated, and grouped in categories linked to the impacts of electricity generation for creating the systematic literature review. A reading procedure of articles was done to make the literature summary of existing studies in this area. Most studies focused on coal-based energy production technologies, while others focused on renewable energy generation technologies. Numerous studies found that the external costs of coal-based energy generation were high. Studies in this area were based on qualitative and quantitative approaches (maximum studies were quantitative). Very limited studies were based on primary research in this area, mostly based on secondary sources. Solar photovoltaic was analyzed as the most efficient renewable energy generation technology in land utilization efficiency, outperforming coal plants and other technologies. Wind was found to be the most efficient technology regarding water footprint, followed by solar PV, while coal plants were the least significant option. Solar photovoltaic technology was the leading option in job creation, while the coal energy sector was on the reverse side due to severe health impacts and job fall due to decarbonization. Saving lives by switching from coal-fired electricity to solar energy is proven viable in the existing literature, and this transition would create significant health and environmental benefits. According to studies, the externality of coal-fired energy is increasing, and coal is still the dominant source of energy generation. Replacing coal energy with solar energy benefits humans, the environment, and the economy. This transition would help ensure our planet's sustainability. It has been concluded that renewable energy technologies are the best solutions, even after considering the storage and dumping of waste after the end of their lifecycle.

### Implications

#### Theoretical Implications

The significance of every study is determined by its

contribution to research theory, technique, and knowledge advancement. This study adds to the literature on energy sustainability by expanding theoretical support on the connection between energy generation technologies and other factors by covering the issues under five themes. In addition to these factors, the study has identified gaps in each theme, directing academics to work on low-investigated aspects and associated issues. Research based on qualitative techniques must be expanded to significantly advance theoretical understanding in this field of study.

### Practical Implications

This study has major implications for enterprises that provide sustainable products or services based on several qualities that foster sustainability, regional growth, economic development, and technical innovation. Sustainability issue can be found everywhere, notably in the energy sector, whether at the household, commercial, or industrial level. Understanding these five issues will allow developers to devise more efficient techniques for boosting green energy generation and meeting the energy demand. To be more precise, this review emphasizes the need to accept sustainable energy and how it may be shown as a crucial element of the community. This gives insight to business executives about the importance of focusing solely on green energy technology.

### Limitation and Future Scope

This study contains limitations that pave the path for future research. To begin with, this analysis entirely uses theoretical data; subsequent research may use survey responses or interviews to objectively evaluate these relationships between energy generation and other factors. The review section summarizes each connected aspect to touch upon as many energy generation topics as is practical; further research could provide a more in-depth assessment of various factors related to energy sustainability. Future research should focus on issues like how energy creation affects waste disposal and how to encourage recycling of waste created by electricity generation technology. Finally, this analysis only included openly available research; future analyses can integrate more studies by subscription to various journals to reach works that are not publicly accessible and add to the body of existing knowledge.

### Declaration of Competing Interest

The authors declare that they have no known competing financial interests or personal relationships that could have appeared to influence the work reported in this paper.

## REFERENCES


Airclem. 2013. Air Pollution and Climate Secretariat. Coal pollution kills Indians. https://www.airclim.org/acidnews/coal-pollution-kills-indians. Accessed December 30, 2022.

Ahmad, S., Iraj, M., Abbas, M. and Mahdi, A. 2016. Analysis of occupational accidents induced human injuries: a case study in construction industries and sites. J. Civ. Eng. Constr. Technol., 7(1): 1-7. https://doi.org/10.5897/JCECT2015.0379.

Ali, I., Modibbo, U.M., Chauhan, J. and Meraj, M. 2021. An integrated multi-objective optimization modelling for sustainable development goals of India. Environ. Dev. Sustain., 23:3811-3831. https://doi.org/10.1007/s10668-020-00745-7.

Al-Karaghouli, A. and Kazmerski, L.L. 2013. Energy consumption and water production cost of conventional and renewable-energy-powered desalination processes. Renew. Sustain. Energy Rev., 24:343-356. https://doi.org/10.1016/j.rser.2012.12.064.

Amponsah, N.Y., Troldborg, M., Kington, B., Aalders, I. and Hough, R.L. 2014. Greenhouse gas emissions from renewable energy sources: A review of lifecycle considerations. Renew. Sustain. Energy Rev., 39: 461-475. https://doi.org/10.1016/j.rser.2014.07.087.

Bernal-Agustín, J.L. and Dufo-Lopez, R. 2006. Economical and environmental analysis of grid connected photovoltaic systems in Spain. Renew. Energy, 31(8): 1107-1128. https://doi.org/10.1016/j.renene.2005.06.004.

Bielecki, A., Ernst, S., Skrodzka, W. and Wojnicki, I. 2020. The externalities of energy production in the context of development of clean energy generation. Environ. Sci. Pollut. Res., 27: 11506-11530. https://doi.org/10.1007/s11356-020-07625-7.

Breyer, C., Koskinen, O. and Blechinger, P. 2015. Profitable climate change mitigation: The case of greenhouse gas emission reduction benefits enabled by solar photovoltaic systems. Renew. Sustain. Energy Rev., 49: 610-628. https://doi.org/10.1016/j.rser.2015.04.061.

Bryan, J., Evans, N., Jones, C. and Munday, M. 2017. Regional electricity generation and employment in UK regions. Reg. Stud., 51(3): 414-425. https://doi.org/10.1080/00343404.2015.1101516.

Burney, J.A. 2020. The downstream air pollution impacts of the transition from coal to natural gas in the United States. Nat. Sustain., 3(2): 152-160. https://doi.org/10.1038/s41893-019-0453-5.

Casey, J.A., Gemmill, A., Karasek, D., Ogburn, E.L., Goin, D.E. and Morello-Frosch, R. 2018. Increase in fertility following coal and oil energy plant retirements in California. Environ. Health, 17:1-10. https://doi.org/10.1186/s12940-018-0388-8.

Cerny, M., Bruckner, M., Weinzettel, J., Wiebe, K., Kimmich, C., Kerschner, C. and Hubacek, K. 2021. Employment effects of the renewable energy transition in the electricity sector: An input-output approach. ETUI Res. Pap.-Work. Pap. https://dx.doi.org/10.2139/ssrn.4013339.

Chakravarty, S. and Somanathan, E. 2021. There is no economic case for new coal plants in India. World Dev. Perspect., 24:100373. https://doi.org/10.1016/j.wdp.2021.100373.

Chio, C. P., Lo, W. C., Tsuang, B.J., Hu, C.C., Ku, K.C., Chen, Y.J., Lin, H.H. and Chan, C.C. 2019. Health impact assessment of PM2.5 from a planned coal-fired energy plant in Taiwan. J. Formos. Med. Assoc., 118(11): 1494-1503. https://doi.org/10.1016/j.jfma.2019.08.016.

Cropper, M., Cui, R., Guttikunda, S., Hultman, N., Jawahar, P., Park, Y., Yao, X. and Song, X.P. 2021. The mortality impacts of current and planned coal-fired energy plants in India. Proc. Natl. Acad. Sci., 118(5): 2017936118. https://doi.org/10.1073/pnas.2017936118.

Cruz-Benito, J. 2016. Systematic literature review and mapping. https://doi.org/10.5281/zenodo.

Ray, P. 2019. Renewable energy and sustainability. Clean Technol. Environ. Policy, 21: 1517-1533. https://doi.org/10.1007/s10098-019-01739-4.

Desideri, U., Zepparelli, F., Morettini, V. and Garroni, E. 2013. Comparative analysis of concentrating solar power and photovoltaic technologies:

Technical and environmental evaluations. Appl. Energy, 102: 765-784. https://doi.org/10.1016/j.apenergy.2012.08.033.

Dinesh, H. and Pearce, J.M. 2016. The potential of agrivoltaic systems. Renew. Sustain. Energy Rev., 54: 299-308. https://doi.org/10.1016/j.rser.2015.10.024.

Ding, N., Liu, J., Yang, J. and Lu, B. 2018. Water footprints of energy sources in China: exploring options to improve water efficiency. J. Clean. Prod., 174:1021-1031. https://doi.org/10.1016/j.jclepro.2017.10.273.

Energy Statistics. 2022. Electricity Generation Fuel-Wise in India, Ministry of Statistics and Programme Implementation. India, New Delhi. Retrieved from https://www.mospi.gov.in (accessed March 15, 2023).

Feria-Diaz, J.J., Lopez-Méndez, M.C., Rodríguez-Miranda, J.P., Sandoval-Herazo, L.C. and Correa-Mahecha, F. 2021. Commercial thermal technologies for desalination of water from renewable energies: A state of the art review. Processes, 9(2): 262. https://doi.org/10.3390/pr9020262.

Fthenakis, V.M., Kim, H.C. and Alsema, E. 2008. Emissions from photovoltaic life cycles. Environ. Sci. Technol., 42(6): 2168-2174. https://doi.org/10.1021/es071763q.

Fthenakis, V. and Kim, H.C. 2009. Land use and electricity generation: A lifecycle analysis. Renew. Sustain. Energy Rev., 13(6-7): 1465-1474. https://doi.org/10.1016/j.rser.2008.09.017.

Garrett-Peltier, H. 2017. Green versus brown: Comparing the employment impacts of energy efficiency, renewable energy, and fossil fuels using an input-output model. Econ. Model., 61: 439-447. https://doi.org/10.1016/j.econmod.2016.11.012.

Georgakellos, D.A. and Didaskalou, E.A. 2014. Life cycle external cost of green electricity: The case of Greek energy plants. Recent Adv. Environ. Sci. Geosci., 38.

Groesbeck, J.G. and Pearce, J. M. 2018. Coal with carbon capture and sequestration is not as land use efficient as solar photovoltaic technology for climate neutral electricity production. Sci. Rep., 8(1): 13476. https://doi.org/10.1038/s41598-018-31505-3.

Gupta, A. and Spears, D. 2015. Health externalities of India's expansion of coal plants: Suggestive evidence from a national panel of 40,000 households. https://doi.org/10.1016/j.jeem.2017.04.007.

Guttikunda, S.K. and Jawahar, P. 2014. Atmospheric emissions and pollution from the coal-fired thermal energy plants in India. Atmos. Environ., 92:449-460. https://doi.org/10.1016/j.atmosenv.2014.04.057.

Hardisty, P.E., Clark, T.S. and Hynes, R.G. 2012. Life cycle greenhouse gas emissions from electricity generation: a comparative analysis of Australian energy sources. Energies, 5(4): 872-897. https://doi.org/10.3390/en5040872.

Harris, G., Heptonstall, P., Gross, R. and Handley, D. 2013. Cost estimates for nuclear energy in the UK. Energy Policy, 62:431-442. https://doi.org/10.1016/j.enpol.2013.07.116.

Hope, C. 2011. The social cost of $CO_2$ from the PAGE09 model. Econ. Disc. Pap., 39: 863. https://dx.doi.org/10.2139/ssrn.1973863.

IEA. 2021. India Energy Outlook 2021. https://iea.s/1de6d91e-e23f-4e02-b1fb-51fdd6283b22/India_Energy_Outlook_2021.pdf.

IINAS. 2017. Selected Results from GEMIS 4.95: Electricity Generation. Retrieved from http://iinas.org (accessed November 29, 2022).

IRENA. 2021. Sector-Wise Jobs in the Renewable. Retrieved from https://www.irena.org (accessed November 31, 2022)

Jager-Waldau, A., Kougias, I., Taylor, N. and Thiel, C. 2020. How photovoltaics can contribute to GHG emission reductions of 55% in the EU by 2030. Renew. Sustain. Energy Rev., 126: 109836. https://doi.org/10.1016/j.rser.2020.109836.

Jaramillo, P. and Muller, N.Z. 2016. Air pollution emissions and damages from energy production in the US: 2002-2011. Energy Policy, 90: 202-211. https://doi.org/10.1016/j.enpol.2015.12.035.

Jenniches, S. and Worrell, E. 2019. Regional economic and environmental impacts of renewable energy developments: Solar PV in the Aachen Region. Energy Sustain. Dev., 48: 11-24. https://doi.org/10.1016/j.esd.2018.10.004.

Jin, Y., Behrens, P., Tukker, A. and Scherer, L. 2019. Water use of electricity technologies: A global meta-analysis. Renew. Sustain. Energy Rev., 115: 109391. https://doi.org/10.1016/j.energy.2014.03.113.

Kabir, E., Kumar, P., Kumar, S., Adelodun, A.A. and Kim, K.H. 2018. Solar energy: Potential and future prospects. Renew. Sustain. Energy Rev., 82: 894-900. https://doi.org/10.1016/j.rser.2017.09.094.

Kapp, K.W. 1970. Environmental disruption and social costs: A challenge to economics. Kyklos, 23(4): 833-848. https://doi.org/10.1111/j.1467-6435.1970.tb01047.x.

Kenny, J.F., Barber, N.L., Hutson, S.S., Linsey, K.S., Lovelace, J.K. and Maupin, M.A. 2009. Estimated use of water in the United States in 2005 (No.1344). U.S. Geol. Surv., 13: 134 https://doi.org/10.3133/cir1344.

Khomenko, S., Cirach, M., Pereira-Barboza, E., Mueller, N., Barrera-Gómez, J., Rojas-Rueda, D., de Hoogh, K., Hoek, G. and Nieuwenhuijsen, M. 2021. Premature mortality due to air pollution in European cities: a health impact assessment. Lancet Planet. Health, 5(3): 272. https://doi.org/10.1016/S2542-5196(20)30272-2.

Kiesecker, J., Baruch-Mordo, S., Heiner, M., Negandhi, D., Oakleaf, J., Kennedy, C. and Chauhan, P. 2019. Renewable energy and land use in India: a vision to facilitate sustainable development. Sustainability, 12(1): 281. https://doi.org/10.3390/su12010281.

Klise, G.T., Tidwell, V.C., Reno, M.D., Moreland, B.D., Zemlick, K.M. and Macknick, J. 2013. Water use and supply concerns for utility-scale solar projects in the Southwestern United States. Natl. Renew. Energy Lab., 21: 206. https://doi.org/10.2172/1090206.

Lovering, J., Swain, M., Blomqvist, L. and Hernandez, R.R. 2022. Land-use intensity of electricity production and tomorrow's energy landscape. PLoS One, 17(7): 155. https://doi.org/10.1371/journal.pone.0270155.

Maamoun, N., Chitkara, P., Yang, J., Shrimali, G., Busby, J., Shidore, S., Jin, Y. and Urpelainen, J. 2022. Identifying coal plants for early retirement in India: A multidimensional analysis of technical, economic, and environmental factors. Appl. Energy, 312: 118644.

Maamoun, N., Kennedy, R., Jin, X. and Urpelainen, J. 2020. Identifying coal-fired power plants for early retirement. Renew. Sustain. Energy Rev., 126: 109833. https://doi.org/10.1016/j.rser.2020.109833.

Markandya, A. and Wilkinson, P. 2007. Electricity generation and health. Lancet, 370(9591): 979-990. https://doi.org/10.1016/S0140-6736(07)61253-7.

Masnadi, M.S., El-Houjeiri, H.M., Schunack, D., Li, Y., Englander, J.G., Badahdah, A., Monfort, J.C. anderson, J.E., Wallington, T.J., Bergerson, J.A. and Gordon, D. 2018. Global carbon intensity of crude oil production. Science, 361(6405): 851-853. https://doi.org/10.1126/science.aar6859.

Mekonnen, M.M., Gerbens-Leenes, P.W. and Hoekstra, A.Y. 2015. The consumptive water footprint of electricity and heat: a global assessment. Environ. Sci.: Water Res. Technol., 1(3): 285-297. https://doi.org/10.1039/C5EW00026B.

Meldrum, J., Nettles-Anderson, S., Heath, G. and Macknick, J. 2013. Life cycle water use for electricity generation: a review and harmonization of literature estimates. Environ. Res. Lett., 8(1): 015031. https://doi.org/10.1088/1748-9326/8/1/015031.

Mickan, S., Tilson, J.K., Atherton, H., Roberts, N.W. and Heneghan, C. 2013. Evidence of effectiveness of health care professionals using handheld computers: a scoping review of systematic reviews. J. Med. Internet Res., 15(10). https://doi.org/10.2196/jmir.2530.

Ministry of Power (MoP). ANNUAL REPORT (2021-22). https://powermin.gov.in/sites/default/files/uploads/MOP_Annual_Report_Eng_2021-22.pdf.

Ministry of New and Renewable Energy. Introduction. https://mnre.gov.in/about-department/introduction/

Mohan, A. 2017. Whose land is it anyway? Energy futures & land use in India. Energy Policy, 110:257-262. https://doi.org/10.1016/j.enpol.2017.08.025.

Moretti, S. and Marucci, A. 2019. A photovoltaic greenhouse with variable

shading for the optimization of agricultural and energy production. Energies, 12(13): 2589. https://doi.org/10.3390/en12132589.

MOSPI. 2011. All-India Projected Water Demand in India by Different Uses (2010, 2025 and 2050), Government of India. Retrieved December 21, 2022, from https://www.nabard.org.

Mu, Y., Cai, W., Evans, S., Wang, C. and Roland-Holst, D. 2018. Employment impacts of renewable energy policies in China: A decomposition analysis based on a CGE modeling framework. Appl. Energy, 210:256-267. https://doi.org/10.1016/j.apenergy.2017.10.086.

Nagatomo, Y., Ozawa, A., Kudoh, Y. and Hondo, H. 2021. Impacts of employment in energy generation on renewable-based energy systems in Japan-Analysis using an energy system model. Energy, 226:120350. https://doi.org/10.1016/j.energy.2021.120350.

Natarajan, P. and Nalini, G.S. 2015. Social cost-benefit analysis of solar energy projects. Prabandhan: Indian J. Manage., 8(5): 36-42. https://www.researchgate.net.

NITI Ayog. 2018. Water Index report, Ministry of Jal Shakti. Retrieved November 30, 2022, from https://www.niti.gov.in/sites/default/files/2019-08/CWMI-2.0-latest.pdf.

Nkambule, N.P. and Blignaut, J.N. 2012. The external costs of coal mining: the case of collieries supplying Kusile Energy station. J. Energy Southern Africa, 23(4): 85-93. Retrieved December 22, 2022, from http://www.scielo.org.za.

Nordhaus, W.D. 2011. Estimates of the social cost of carbon: background and results from the RICE-2011 model (No. w17540). Natl. Bur. Econ. Res. https://doi.org/10.3386/w17540.

Nugent, D. and Sovacool, B.K. 2014. Assessing the lifecycle greenhouse gas emissions from solar PV and wind energy: A critical meta-survey. Energy Policy, 65:229-244. https://doi.org/10.1016/j.enpol.2013.10.048.

Odeh, N.A. and Cockerill, T.T. 2008. Life cycle analysis of UK coal-fired power plants. Energy Convers. Manage., 49(2): 212-220. https://doi.org/10.1016/j.enconman.2007.06.014.

Okadera, T., Chontanawat, J. and Gheewala, S.H. 2014. Water footprint for energy production and supply in Thailand. Energy, 77:49-56. https://doi.org/10.1016/j.energy.2014.03.113.

Ong, S., Campbell, C., Denholm, P., Margolis, R. and Heath, G. 2013. Land-use requirements for solar energy plants in the United States (No. NREL/TP-6A20-56290). Natl. Renew. Energy Lab. (NREL), Golden, CO (United States). https://doi.org/10.2172/1086349.

Page, M.J. and Moher, D. 2017. Evaluations of the uptake and impact of the preferred reporting items for systematic reviews and meta-analyses (PRISMA) statement and extensions: a scoping review. Syst. Rev., 6(1): 1-14. https://doi.org/10.1186/s13643-017-0663-8.

Pan, L., Liu, P., Ma, L. and Li, Z. 2012. A supply chain-based assessment of water issues in the coal industry in China. Energy Policy, 48:93-102. https://doi.org/10.1016/j.enpol.2012.03.063.

Pasaoglu, G., Garcia, N.P. and Zubi, G. 2018. A multi-criteria and multi-expert decision aid approach to evaluate the future Turkish energy plant portfolio. Energy Policy, 119:654-665. https://doi.org/10.1016/j.enpol.2018.04.044.

Prehoda, E.W. and Pearce, J.M. 2017. Potential lives saved by replacing coal with solar photovoltaic electricity production in the US. Renew. Sustain. Energy Rev., 80:710-715. https://doi.org/10.1016/j.rser.2017.05.119.

Qin, Y., Curmi, E., Kopec, G.M., Allwood, J.M. and Richards, K.S. 2015. China's energy-water nexus–assessment of the energy sector's compliance with the "3 Red Lines" industrial water policy. Energy Policy, 82:131-143. https://doi.org/10.1016/j.enpol.2015.03.013.

Ravi, S., Macknick, J., Lobell, D., Field, C., Ganesan, K., Jain, R., Elchinger, M. and Stoltenberg, B. 2016. Colocation opportunities for large solar infrastructures and agriculture in drylands. Appl. Energy, 165:383-392. https://doi.org/10.1016/j.apenergy.2015.12.078.

Reddy, V.S., Kaushik, S.C. and Panwar, N.L. 2013. Review on energy generation scenario of India. Renew. Sustain. Energy Rev., 18:43-48. https://doi.org/10.1016/j.rser.2012.10.005.

Rej, S. and Nag, B. 2021. Land and clean energy trade-off: estimating India's future land requirement to fulfill INDC commitment. Int. J. Energy Sect. Manage., 15(6): 1104-1121. https://doi.org/10.1108/IJESM-12-2020-0006.

Rentizelas, A. and Georgakellos, D. 2014. Incorporating life cycle external cost in optimization of the electricity generation mix. Energy Policy, 65: 134-149. https://doi.org/10.1016/j.enpol.2013.10.023.

Rivera, N.M., Ruiz-Tagle, C. and Spiller, E. 2021. The health benefits of solar energy generation: Evidence from Chile. Environ. Def. Fund Econ. Disc. Pap. Ser., EDF EDP, 21-02. https://dx.doi.org/10.2139/ssrn.3789139.

Roth, S., Hirschberg, S., Bauer, C., Burgherr, P., Dones, R., Heck, T. and Schenler, W. 2009. Sustainability of electricity supply technology portfolio. Annals of Nuclear Energy, 36(3): 409-416. https://doi.org/10.1016/j.anucene.2008.11.029.

Sahu, S.K., Zhu, S., Guo, H., Chen, K., Liu, S., Xing, J., Kota, S.H. and Zhang, H. 2021. Contributions of power generation to air pollution and associated health risks in India: Current status and control scenarios. Journal of Cleaner Production, 288: 125587. https://doi.org/10.1016/j.jclepro.2020.125587.

Samadi, S. 2017. The social costs of electricity generation—Categorising different types of costs and evaluating their respective relevance. Energies, 10(3): 356. https://doi.org/10.3390/en10030356.

Sánchez-Zapata, J.A., Clavero, M., Carrete, M., DeVault, T.L., Hermoso, V., Losada, M.A., Polo, M.J., Sanchez-Navarro, S., Perez-Garcia, J.M., Botella, F., Ibanez, C. and Donázar, J.A. 2016. Effects of renewable energy production and infrastructure on wildlife. In: Mateo, R., Arroyo, B., Garcia, J. (eds) Current Trends in Wildlife Research. Wildlife Research Monographs, vol 1. Springer, Cham. https://doi.org/10.1007/978-3-319-27912-1_5.

Sarkis-Onofre, R., Catala-Lopez, F., Aromataris, E. and Lockwood, C. 2021. How to properly use the PRISMA statement. Systematic Reviews, 10(1): 1-3. https://doi.org/10.1186/s13643-021-01671-z.

Shahsavari, A. and Akbari, M. 2018. The potential of solar energy in developing countries for reducing energy-related emissions. Renewable and Sustainable Energy Reviews, 90: 275-291. https://doi.org/10.1016/j.rser.2018.03.065.

Shearer, C., Fofrich, R. and Davis, S.J. 2017. Future $CO_2$ emissions and electricity generation from proposed coal-fired energy plants in India. Earth's Future, 5(4): 408-416. https://doi.org/10.1002/2017EF000542.

Sherwani, A.F. and Usmani, J.A. 2010. Life cycle assessment of solar PV based electricity generation systems: A review. Renewable and Sustainable Energy Reviews, 14(1): 540-544. https://doi.org/10.1016/j.rser.2009.08.003.

Shindell, D.T. 2015. The social cost of atmospheric release. Climatic Change, 130:313-326. https://doi.org/10.1007/s10584-015-1343-0.

Shrimali, G. 2020. Making India's energy system clean: Retirement of expensive coal plants. Energy Policy, 139:111305. https://doi.org/10.1016/j.enpol.2020.111305.

Sovacool, B.K. andersen, R., Sorensen, S., Sorensen, K., Tienda, V., Vainorius, A., Schirach, O.M. and Bjorn-Thygesen, F. 2016. Balancing safety with sustainability: assessing the risk of accidents for modern low-carbon energy systems. Journal of Cleaner Production, 112:3952-3965. https://doi.org/10.1016/j.jclepro.2015.07.059.

Statista. 2021. Greenhouse gas emissions from the energy sector. Retrieved December 25, 2022, from https://www.statista.com/topics/8881/emissions-in-india/.

Tawalbeh, M., Al-Othman, A., Kafiah, F., Abdelsalam, E., Almomani, F. and Alkasrawi, M. 2021. Environmental impacts of solar photovoltaic systems: A critical review of recent progress and future outlook. Science of The Total Environment, 759:143528. https://doi.org/10.1016/j.scitotenv.2020.143528.

Teff-Seker, Y., Berger-Tal, O., Lehnardt, Y. and Teschner, N. 2022. Noise pollution from wind turbines and its effects on wildlife: A cross-national

analysis of current policies and planning regulations. Renewable and Sustainable Energy Reviews, 168:112801. https://doi.org/10.1016/j.rser.2022.112801.

Tourkolias, C. and Mirasgedis, S. 2011. Quantification and monetization of employment benefits associated with renewable energy technologies in Greece. Renewable and Sustainable Energy Reviews, 15(6): 2876-2886. https://doi.org/10.1016/j.rser.2011.02.027.

Treyer, K., Bauer, C. and Simons, A. 2014. Human health impacts in the life cycle of future European electricity generation. Energy Policy, 7: 34. . https://doi.org/10.1016/j.enpol.2014.03.034.

Turconi, R., Boldrin, A. and Astrup, T. 2013. Life cycle assessment (LCA) of electricity generation technologies: Overview, comparability, and limitations. Renewable and Sustainable Energy Reviews, 28:555-565. https://doi.org/10.1016/j.rser.2013.08.013.

Turney, D. and Fthenakis, V. 2011. Environmental impacts from the installation and operation of large-scale solar energy plants. Renewable and Sustainable Energy Reviews, 15(6): 3261-3270. https://doi.org/10.1016/j.rser.2011.04.023.

Uttley, L., Quintana, D.S., Montgomery, P., Carroll, C., Page, M.J., Falzon, L., Sutton, A. and Moher, D. 2023. The problems with systematic reviews: a living systematic review. Journal of Clinical Epidemiology. https://doi.org/10.1016/j.jclinepi.2023.01.011.

Volkart, K., Bauer, C., Burgherr, P., Hirschberg, S., Schenler, W. and Spada, M. 2016. Interdisciplinary assessment of renewable, nuclear, and fossil energy generation with and without carbon capture and storage in view of the new Swiss energy policy. International Journal of Greenhouse Gas Control, 54:1-14. https://doi.org/10.1016/j.ijggc.2016.08.023.

Wang, J., Wang, R., Zhu, Y. and Li, J. 2018. Life cycle assessment and environmental cost accounting of coal-fired energy generation in China. Energy Policy, 115:374-384. https://doi.org/10.1016/j.enpol.2018.01.040.

Wiser, R., Millstein, D., Mai, T., Macknick, J., Carpenter, A., Cohen, S., Cole, W., Frew, B. and Heath, G. 2016. The environmental and public health benefits of achieving high penetrations of solar energy in the United States. Energy, 113:472-486. https://doi.org/10.1016/j.energy.2016.07.068.

Wei, M., Patadia, S. and Kammen, D.M. 2010. Putting renewables and energy efficiency to work: How many jobs can the clean energy industry generate in the US? Energy Policy, 38(2): 919-931. https://doi.org/10.1016/j.enpol.2009.10.044.

Wolfram, P., Wiedmann, T. and Diesendorf, M. 2016. Carbon footprint scenarios for renewable electricity in Australia. Journal of Cleaner Production, 124:236-245. https://doi.org/10.1016/j.jclepro.2016.02.080.

Wu, X.D. and Chen, G.Q. 2017. Energy and water nexus in energy generation: The surprisingly high amount of industrial water use induced by solar energy infrastructure in China. Applied Energy, 195:125-136. https://doi.org/10.1016/j.apenergy.2017.03.029.

Yeh, S., Jordaan, S.M., Brandt, A.R., Turetsky, M.R., Spatari, S. and Keith, D.W. 2010. Land use greenhouse gas emissions from conventional oil production and oil sands. Environmental Science & Technology, 44(22): 8766-8772. https://doi.org/10.1021/es1013278.

## ORCID DETAILS OF THE AUTHORS

Aqsa Anjum: https://orcid.org/0000-0002-2442-185X

Nature Environment and Pollution Technology
An International Quarterly Scientific Journal

p-ISSN: 0972-6268
(Print copies up to 2016)
e-ISSN: 2395-3454

Vol. 23 | No. 3 | pp. 1345-1362 | 2024

Original Research Paper

https://doi.org/10.46488/NEPT.2024.v23i03.008

Open Access Journal

# Microbial Fuel Cell: Optimizing Graphene-Sponge Anode Thickness and Chamber pH Using Taguchi Experimental Method

**Emilio Steven C. Navarro*† and Melissa May M. Boado****

*Engineering Program, School of Advanced Studies, Saint Louis University, Lower Bonifacio St., Baguio City, 2600, Philippines

**Department of Chemical and Mining Engineering, School of Engineering and Architecture, Saint Louis University, Lower Bonifacio St., Baguio City, 2600, Philippines

†Corresponding author: Emilio Steven C. Navarro; ecnavarro1@alum.up.edu.ph

**Nat. Env. & Poll. Tech.**
**Website: www.neptjournal.com**

*Received:* 12-12-2023
*Revised:* 29-01-2024
*Accepted:* 01-02-2024

**Key Words:**
Microbial fuel cell
Graphene-sponge anode
Taguchi method
Optimization

## ABSTRACT

The rapid consumption of fossil fuels has led to calls to switch from non-renewable to renewable energy sources. Microbial fuel cells are a promising technology that simultaneously treats wastewater and produces power. This study used the Taguchi Experimental method to optimize anode thickness and pH to obtain the maximum power density of an air-cathode microbial fuel cell (ACMFC). The graphene-sponge (G-S) anode thickness and chamber pH were selected as operating parameters, with their corresponding levels. The $L_9$ orthogonal array was chosen for the experimental design. According to the Taguchi Method, the optimum G-S anode thickness and chamber pH were determined to be 1.0 cm and 8.0, respectively. A confirmatory run was performed under these optimum conditions, and the maximum power density observed was 707.75 $mW \cdot m^{-3}$. Analysis of variance (ANOVA) was conducted to identify the percentage contributions of the operating parameters to the process, which were found to be 30.66% for pH and 69.34% for anode thickness.

## INTRODUCTION

The rapid depletion of fossil fuel resources and elevated greenhouse gas levels are intensifying the call to switch to less environmentally damaging alternative fuels with the same efficiencies as conventional fuels (Chandrasekar et al. 2022). Microbial fuel cells (MFCs) provide a clean energy alternative due to their capability to treat organic and inorganic waste while simultaneously generating power (Tan et al. 2021, Kumar et al. 2015, Dewan et al. 2008). MFCs directly transform chemical energy into electrical energy by incorporating microbial and electrochemical cycles to oxidize organic matter into simpler fragments that are precursors to form water (Prathiba et al. 2022, Zhang et al. 2016).

The different mechanisms occurring within a single-chamber MFC are depicted in Fig. 1. In the anode section, respiratory bacteria attach to the electrode surface, feed on, and oxidize the organic compounds to produce electrons and protons ($H^+$). The electrons pass through an external circuit, and the protons travel through a proton exchange membrane (PEM) towards the cathode section, where oxygen reduction reaction (ORR) occurs, subsequently producing water (Yaqoob et al. 2020). The typical ORR in an air-cathode microbial fuel cell (ACMFC) follows a four-electron pathway (Bajracharya et al. 2016), expressed as:

$$O_2 + 4H^+ + 4e^- \rightarrow 2H_2O \quad E^{\circ\prime} = 0.82V \quad vs. \quad SHE \; at \; pH \; 7 \qquad \ldots(1)$$

The reduction of overpotential boosts the performance of MFCs. One way to achieve a lower overpotential is through an optimized selection of materials and configurations, which can provide more microbial enrichment and efficient electron transfer sites (Huang et al. 2021, Ji et al. 2020). Carbon-based electrodes, non-toxic by nature, offer significantly higher specific surface area and adsorption characteristics, which are important for biocompatibility and biocatalyst immobilization (Chen et al. 2020, Herkendell 2021, Logan et al. 2019, Taskan & Hasar, 2015). Several modern carbon-based electrodes, such as 3D-printed porous carbon anodes (Bian et al. 2018) and electrospun carbon fibers (Sanchez et al. 2021), have been proven to replace traditional graphite rods in wastewater-based electricity generation. The use of nanomaterials can significantly improve the electrochemical performance of MFCs by enhancing biofilm adhesion and facilitating fast direct electron transfer (Liu et al. 2020, Wei et al. 2011). Due to their promising capabilities, MFCs with nanomaterial-based electrodes have become popular

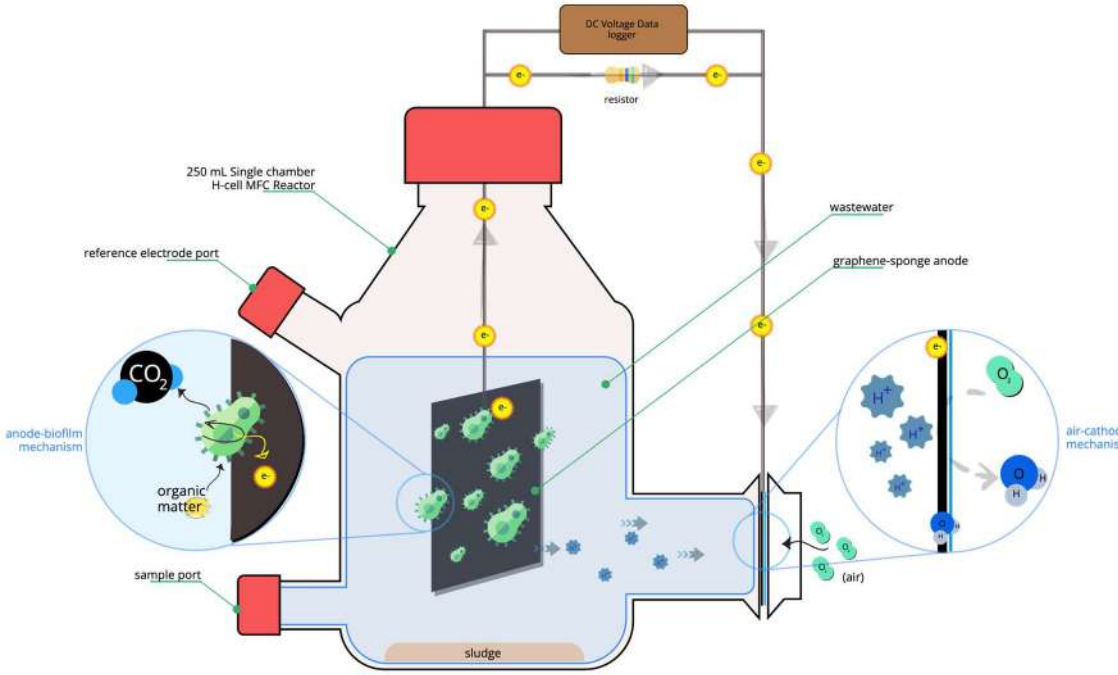


Fig. 1: Graphical illustration of the overall mechanism of a typical ACMFC.

in bioelectrochemical research. Among the pioneer studies, Nimje et al. (2011) have found that carbon materials with layered architecture and small-fiber diameter promote biofilm growth with high cell density. Mink & Hussain (2013) use multi-walled carbon nanotubes (MWCNTs) as an MFC, comparing gold and nickel as anode materials. Results show that MWCNTs produced current and power density at 880 $mA \cdot m^{-2}$ and 19 $mW \cdot m^{-2}$, respectively, outperforming gold and nickel anodes by 6 to 20 times. To increase the extracellular electron transfer efficiency, Zhao et al. (2019) used the chemical vapor deposition method to grow carbon nanotubes on carbon fibers and employed pyrrole via in situ polymerization on the exterior and interior of the carbon nanotubes. The study obtained a maximum power density of 1876.62 $mW \cdot m^{-2}$, which is 2.63 times higher than a traditional carbon brush anode.

The modification mentioned above is limited to a small scale due to high production costs. One of the most promising techniques to address economic constraints to date is using macroporous sponges coated with carbon-based nanomaterials. This technique offers an easy-to-synthesize method, a continuous three-dimensional carbon nanotube surface, controllable and tunable pore size, and excellent mechanical properties. The same approach has been employed in a study by Xie et al. (2012), which holds the highest maximum volumetric power density (182 $W \cdot m^{-3}$). The authors found that voltage drop and power losses are insignificant in a graphene-sponge-stainless steel (G-S-SS) anode up to 1 m conduction length, with 0.015 m graphene-sponge (G-S) thickness and 0.01 m stainless steel (SS) thickness.

Anode material and its configuration are key factors in reducing losses such as activation, concentration, and ohmic losses. To further enhance the electrode performance, determining the optimum chamber pH in ACMFC operation is essential in minimizing power losses by providing a favorable environment for microbial communities and electron transfer sites. Appropriate pH condition favors the proliferation of exoenergens on the anode surface, reducing the activation losses. Maintaining pH in the electrode environment is necessary for proton transfer from the anode to the cathode via a membrane to reduce concentration losses. With a constant pH in the chamber, hydrogen ions ($H^+$) being produced from anoxygenic conditions can freely travel from the anode to the cathode, preventing the accumulation of protons (Kim et al. 2007, Kumar & Mungray 2017). Puig et al. (2010) reported that continuous MFC operation at pH level 9.5 for 30 days improved the power generation up to 1.8 $W \cdot m^{-3}$. The same study has also concluded a 70% removal rate of organic matter.

Meanwhile, Martin et al. (2010) demonstrated promising ACMFC performance with a maximum power density of 9.8 $W \cdot m^{-3}$ at an anolyte pH of 6.5 and organic matter reduction efficiency at 91.2% COD removal rate. In an optimization

study for a membrane-less MFC, Azmi et al. (2021) found that pH 8.0 is the most suitable pH condition for *Bacillus subtilis* to proliferate alongside a voltage generation of 807 mV, biomass concentration of 15.45 $mg.L^{-1}$, and power density of 373.3 $mW{\cdot}m^{-2}$. To date, mixed culture microorganisms in an MFC can produce a decent amount of power at pH 10.0 (He et al. 2008).

Most studies on MFC focus on individual components of a microbial fuel cell which mostly are processes associated with it. Only a few studies involve a simultaneous variation of two or more components (Carmona-Martínez et al. 2021, Kumar & Mungray 2017). With this, the researcher has sought to conduct a study involving engineering design (Graphene-sponge Anode Thickness) and operational conditions (chamber pH). A simulation study by Xie et al. (2012) shows no significant voltage drop in the G-S anode having a thickness of up to 0.015 m. However, Xie et al. (2012) did not compare the performance of G-S experimentally at different thickness levels to confirm the extent of the effect of G-S thickness on the overall performance of the microbial fuel cell.

Varying operational pH could also alter the performance of anode materials. Several studies have observed favorable electricity generation and wastewater treatment performances at pH ranging from 6.5 to 9.5. However, no studies combining G-S anode thickness and pH of anolyte show results without significant voltage drop. This predicament of researchers may be due to studies that involve multidisciplinary approaches requiring too many experiments to develop reliable results. Hence, Genichi Taguchi developed the Taguchi Experimental Method to address experimental engineering problems by addressing factor biases and proposing less time-consuming and costly experimental runs compared to a normal full factorial design of the experiment. Besides its economic benefits, the Taguchi method has been widely used in applied industries for its uniform, decentralized, orderly, and contrasted orthogonal experiments (Cheng et al. 2010).

This study aims to optimize the system's design (anode thickness) and operating condition (pH) to get a suitable response. This response indicates the ACMFC chamber's performance in terms of power density and wastewater treatment efficiency expressed as percentage removal of the chemical oxygen demand (COD). By varying the G-S anode thickness (0.5, 1.0, 1.5 in cm) and the pH (6.5, 8.0, 9.5) of the chamber simultaneously, power density and COD removal will be determined in every parameter combination. As per Taguchi Method, the $L_9$ orthogonal array is suitable when two (2) factors in three (3) levels are to be analyzed. The relation between factors and response from the signal-to-noise (S/N) ratio is determined, and accordingly, optimum parameters are deduced from the data. The results are also analyzed to find out which of the parameters greatly affects the response. Finally, a confirmatory run is performed on the experimental MFC set-up to check the optimized condition.

Several studies focusing on cell configuration (Estrada-Arriaga et al. 2017), electrode materials and design (Dong et al. 2012, Logan et al. 2007), enhanced operational conditions (Erable et al. 2009, He et al. 2008, Patil et al. 2011), microbial exoelectrogenic communities (Butler et al. 2010, Islam et al. 2017), etc., have been conducted to improve power density generated in MFCs. This technology can potentially treat wastewater on a large scale while generating power. However, its viability as an independent external power source is yet to be achieved (Jadhav et al. 2021a, 2021b). It is essential to conduct thorough research on the individual and synergism of different factors to gain a deeper understanding of scaling up the technology and achieving optimum power production and wastewater treatment capability at a minimal cost (D'Angelo et al. 2017, Wang et al. 2018).

The main framework of the study stems from treating wastewater while producing energy. The study commenced with a preliminary experiment to confirm and/or determine the different levels of independent variables: G-S anode thickness and chamber pH. In contrast, the dependent variables, namely power generation and percentage COD removal rate, were recorded simultaneously using a DC voltage data logger (Extech SD910) and a colorimeter (HACH). The data generated from the experiment were processed using experimental design software, which is expected to identify the optimum combination of anode thickness and chamber pH to maximize power production and COD reduction.

## MATERIALS AND METHODS

### Materials and Data Gathering Tools

**Graphene-sponge with stainless steel current collector (Anode)**: A synthetic polyurethane (PU) sponge purchased from a local grocery store was used as the main material for the fabrication of the graphene-sponge anode electrode. The PU sponge was cut into three smaller sponges, each with the same width and length (3 cm by 5 cm) but with different thicknesses (0.5 cm, 1 cm, and 1.5 cm). These sponges were then cut in half to form a graphene sponge with stainless steel as a current collector placed between the halved sponges.

Graphene sponges were fabricated by preparing the sponge, graphene oxide (GO) solution, and L-Ascorbic Acid (LLA) reducing agent. From the concentrated solution, 10 mL of 10% GO dispersion (rGO 1% dispersion, William Blythe Ltd.) was dispensed using a pipette and diluted to

1 mg·mL$^{-1}$ by adding distilled water to form the soaking solution. The diluted solution was mixed thoroughly using a stirring rod. Afterward, 100 mg of LLA-reducing agent was added and dissolved in the 100 mL diluted GO solution for 15 min to ensure a homogeneous mixture. Subsequently, the precut PU sponges were submerged in the graphene oxide-ascorbic acid solution. Fig. 2 illustrates the step-by-step fabrication process of the graphene-sponge anode using the hydrothermal reaction method.

The sponges were soaked for 15 min and simultaneously pressed about five times to ensure that all the sponge strands were wetted with the solution. The sponges submerged in the GO solution were ultrasonicated for 15 min to further ensure the graphene oxide adhered to the scaffold surfaces of the sponge. Afterward, the sponges soaked in the GO solution were transferred to a sealed media bottle for a hydrothermal reaction at 95°C for 3 h. The hydrothermal reaction initiates and completes the conversion of graphene oxide to form a reduced graphene oxide-sponge (rGO) composite (Hu et al. 2010). The graphene-coated sponges were washed with an ethanol-water solution and then dried at 40°C for 24 h. The composite's durability was assessed using adhesive tape and water flashing to check whether the graphene had sufficiently adhered to the sponge. Stainless steel (SS) wire mesh, serving as a current collector, was placed and assembled between two graphene sponges (G-S) using carbon conductive glue (Ted Pella Inc.). Fig. 3 shows both the schematic of the G-S anode composite and how the stainless steel mesh aids the transfer of electrons from the G-S sponge to the other side of the MFC.

**Air-cathode electrode**: The air-cathode electrode consists of a conductive gas diffusion layer (CGDL) and a catalyst layer (CL). The CGDL comprises 60% carbon black and 40% polytetrafluoroethylene (PTFE), while the CL comprises 60% activated carbon (AC) and 40% PTFE. In addition, an updated fabrication technique by Dong et al. (2012) was also adopted for the catalyst layer by not subjecting it to heat treatment under the furnace to further improve the performance of the air-cathode electrode.

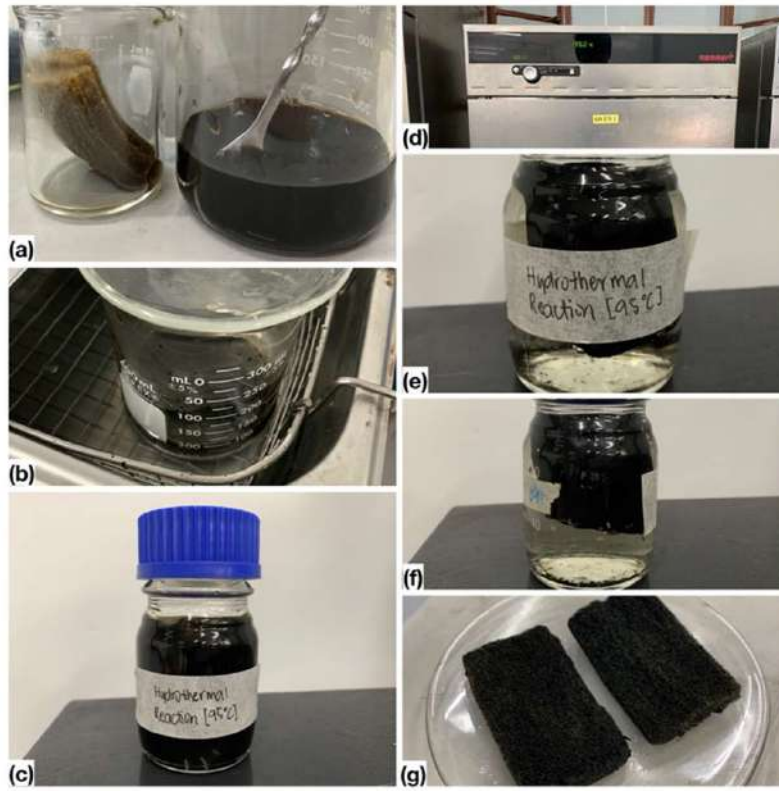


*Note*. (a) soaking and pressing of sponge in the GO solution, (b) sonication of sponge in the GO solution for 15 min, (c) sealed media bottle with the sponge soaked in GO solution, (d) hydrothermal reaction in an oven at 95°C for 3 h, (e) and (f) post-hydrothermal reaction: reduced graphene oxide clumped on the surface of the sponge, (g) dried graphene-sponge

Fig. 2: Step-by-step fabrication of graphene-sponge anode via hydrothermal reaction.

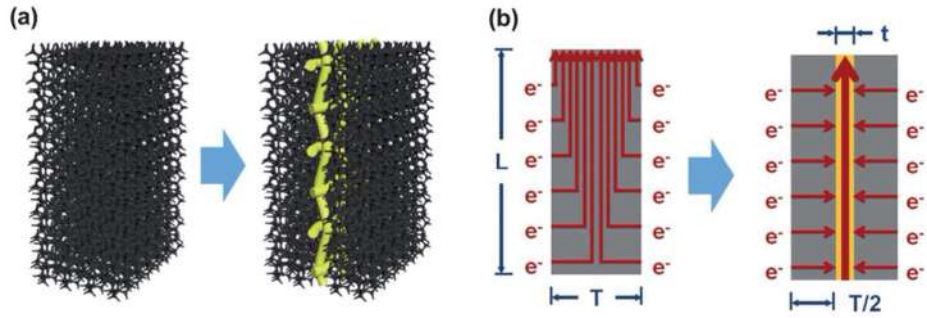


*Note.* Fig. 3 shows a G-S with a stainless steel (SS) collector (G-S-SS). (a) Schematic of the G-S-SS composite electrode (right) vs. the G-S composite electrode (left). (b) Schematic showing the electron pathways in the G-S electrode with (right) and without (left) SS current collector (Xie et al. 2012).

Fig. 3: Schematic of anode composite and electron transfer.

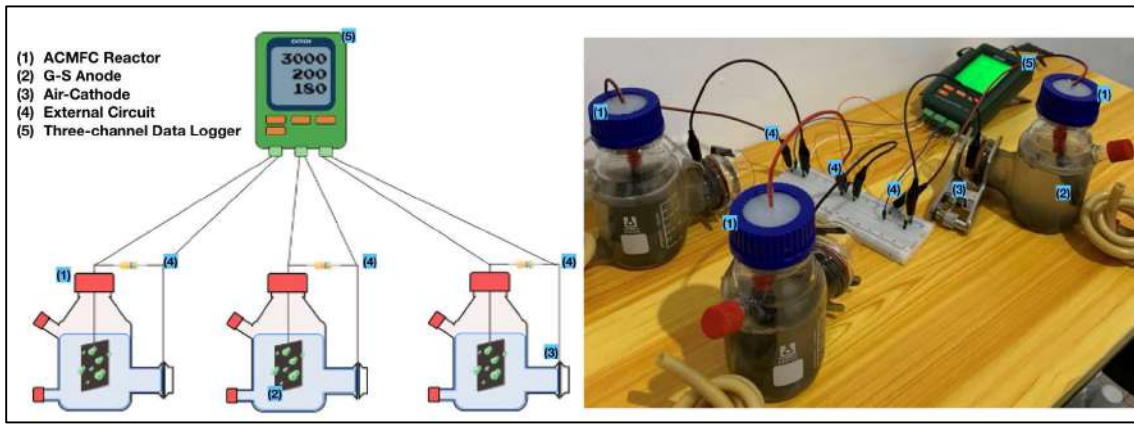


*Note*. Fig. 4 shows the (left) graphical representation of the experimental setup and (right) actual experimental setup in the study.

Fig. 4: Experimental set-up for optimization of graphene-sponge thickness and chamber pH of ACMFC.

**Experimental Set-Up:** Experimental runs with duplicates were performed simultaneously within 24 h. Only duplicate reactors were used in the study, as noted by Logan (2012), as having two trials for a single run is sufficient as long as the results are in good agreement. The second trial was performed 24 h after the first trial. Based on the data, the generated currents are relatively similar to each other.

The prefabricated ACMFC reactor with a total working volume of 250 mL was purchased from Laborxing (China). G-S as the anode, is used in the ACMFC reactor. The external electric voltage was monitored and recorded every 10 min for 24 h using a DC voltage data logger (Extech SD910). Chemical oxygen demand (COD) in influents and effluents was measured using a HACH COD digestion reactor and HACH Colorimeter. COD Digestion Vials were purchased from Dynalab. Percentage COD removal (%) is calculated as:

$$Percentage\ COD\ removal = [(COD_0 - COD_t)\ /\ COD_0\ ] \times 100 \quad \ldots(2)$$

Where $COD_0$ is the influent COD concentration (mg $L^{-1}$), $COD_t$ is the effluent COD concentration (mg $L^{-1}$), and t is time (h)

A digital handheld pH meter (HM Digital PH200) was used to measure the pH of the wastewater during adjustment and variation of the initial substrate pH (Eaton & Franson 2006).

Voltage and current were measured using a DC voltage data logger (Extech SD910) and an analog multimeter, respectively. The current measurements were varied by changing the external resistance from 10,000 Ω to 23 Ω (Logan et al. 2007) at all pH conditions. Moreover, voltage and current were measured every 10 min to stabilize the cells from being interrupted due to the effect of the measuring devices. This was done to minimize errors and to approximate the actual values of measured values. Every 24 h, current density, and power density were calculated using Equations 3 and 4, respectively (Logan et al. 2006a).

$$Current\ Density = \frac{I}{V_{wastewater}} \quad \ldots(3)$$

Where the current density is in milliamperes per volume of the wastewater in cubic meters ($m^3$)

$$Power\ Density = Voltage \times Current\ Density \quad \ldots(4)$$

where voltage is in millivolts, and power density is in milliwatts per cubic meter

**Activities and procedures**: The wastewater used in the entire experiment was collected from the Baguio Sewerage Treatment Plant (BSTP) (Fig. 5). This wastewater served as a source of microorganisms and substrate during the operation of the ACMFC reactor. It was assumed that the wastewater contains naturally occurring exoenergetic microorganisms. The three anodes with varying thicknesses were assembled in their respective reactors, and the desired pH of the electrolytes was set by gradually adding 0.5 M NaOH and 0.5 M HCl solutions, depending on the target pH. Anode inoculation may take up to two weeks. In this study, it took eight days to achieve stable voltage generation and another two days to stabilize. Hence, ten days were allotted to acclimate the ACMFC reactors in preparation for the actual experimental runs.

For every experimental run, the pH of the wastewater feed was adjusted by dropping appropriate amounts of acid and base and measured using a handheld pH meter (HM Digital PH200). Pretreated wastewater was transferred into the ACMFC reactor using a syringe. The preliminary experiment was repeated thrice for a period of 24 hours to determine the expected stabilization duration of the biofilm. The COD, open circuit voltage (OCV), and current were measured after the completion of a single experimental run.

## Treatment and Analysis of Data

**Taguchi method:** The experimental parameters and their levels were determined from studies conducted by Kumar & Mungray (2017) and Xie et al. (2012). Preliminary experiments were done to confirm these value levels. Based on the rules of the Taguchi Method, the $L_9$ orthogonal array (9 experimental runs) is acceptable as a basis for the experimental procedure for two parameters of three levels each. The performance of the ACMFC could be influenced by several factors, such as controllable (thickness of anode and pH of the chamber) and uncontrollable (noise), which can be evaluated through its performance in terms of power density and COD removal rate. In the engineering system, the S/N ratio is defined as the ratio of the expected output to the unexpected output or variabilities around the mean. The S/N equation is used to optimize the system where a higher S/N ratio is desired. The two outputs are both desirable at a higher value. Hence, they fit into the larger-the-better characteristics described by Equation 5.

$$\frac{S}{N}(\eta) = -10 \times log_{10}\left[\frac{1}{r}\sum_{i=1}^{r}\frac{1}{y_i{}^2}\right] \quad \ldots(5)$$

where $r$ denotes the number of tests in a trial (number of repetitions regardless of noise levels), $y_i$ indicates the measurement results, and subscript $i$ points out the number of simulation design factors arranged in the experiments of the orthogonal array (OA) table. The S/N response Table and response graph are constructed by the S/N ratio, which then enables the robust design effect of the factor to be applied.

The data generated from the experiment were processed using the Minitab experimental design software, which located the optimum combination of the thickness of the

*Note*. Images of the (left) Primary clarifier and (right) sampling station in BSTP

Fig. 5: BSTP Facility located in Sanitary Camp, Baguio City, Benguet.

*Note*. This photo of Hitachi TM4000Plus was taken inside the Testing Laboratory at the Philippine Science High School Ilocos Region Campus.

Fig. 6: Table-top Scanning Electron Microscope.

anode and chamber pH with the optimum amount of power produced.

**Analysis of Means (ANOM)**: ANOM is used to identify the optimal combination of the design factors. It is important to determine the effects of each factor after calculating the S/N ratios in keeping with experimental results. The effect of a factor level signifies the difference it causes to the overall mean. The effects of each factor can illustrate the influence rank of every factor on quality parameters and locate the optimum combination of the factor levels from the response table to the response graph.

**Analysis of Variance (ANOVA):** The design and process parameters, which greatly influence the performance of ACMFC in terms of power density and COD removal, were determined using ANOVA. Minitab software is used to analyze the data collected. ANOVA is used as an aid in determining the effect of parameters and their contributions to the performance of the ACMFC (Gandhi et al. 2012, Douglas Montogomery 2005).

**Morphology and characteristics of the submicron-structured anode:** To determine the submicron structure of the graphene-sponge anode, the morphology is investigated using a scanning electron microscope (Hitachi TM4000Plus) (Fig. 6), and results are compared to other literature for reference.

## RESULTS AND DISCUSSION

### General Observations

The wastewater sample from the BSTP had an initial pH of 6.8, which is slightly acidic. This observation conforms to the study conducted by Odjadjare & Okoh (2010), in which the pH in municipal wastewater ranges from 6 to 8.

The inoculation period lasted for eight (8) days, with an additional two (2) days allotted to ensure maximum and stable voltage generation (e.g., 650 mV for all reactors) was observed. Among the reactors, the chamber with a G-S anode thickness of 1.0 cm has the fastest rate (reached 600 mV on Day 6) of attaining its high and stable voltage. The other two set-ups, with 0.5cm and 1.5cm anode thicknesses, had slower rates (reached 600 mV on Day 9) compared to the earlier one and almost had the same behavior in the early days in terms of voltage generation.

From the results, polarization curves and power curves have been constructed and are shown in Fig. 7, 8, and 9. The Figures depict a typical fuel cell behavior where an increase in external resistance corresponds to a decrease in the current generation.

Fig. 7a, 8a, and 9a present the changes in voltage produced in the ACMFC. Across all combinations of parameters, the voltage drop was abrupt when external resistance was very minimal while stable at a higher resistance. Moreover, Fig. 7a, 8a, and 9a show a slightly sharper voltage drop in all pH conditions at very low resistances (initial stages of the graphs) that can be attributed to activation overpotential. After a sharp fall, a straight line with a lesser slope is noticeable in every graph, which is due to the combined effects of mass transport efficiency and ohmic losses, collectively known as internal resistances in ACMFC.

Table 1 presents the comparison of the performances (current and power densities) of ACMFC based on different G-S anode thicknesses and chamber pH. The internal resistances were calculated using Equation 6 (Logan et al. 2006b), as shown in the 5th column.

$$E_{cell} = OCV - IR_{int} \quad \ldots(6)$$

Where $E_{cell}$ is the actual voltage measurement in

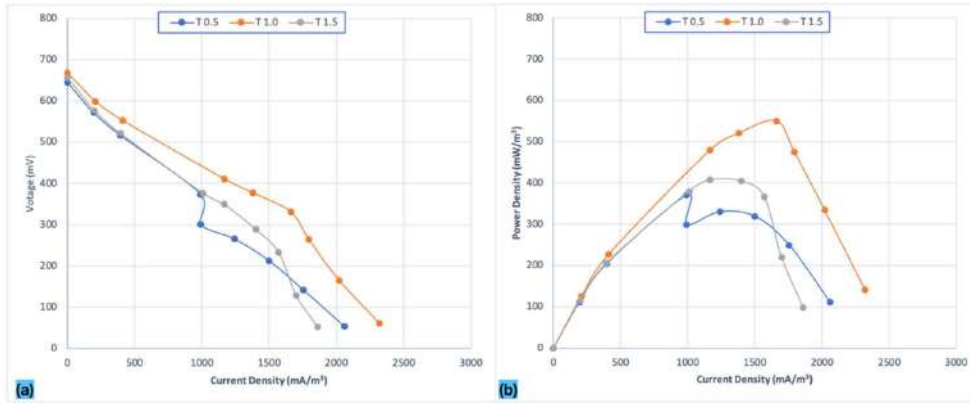


*Note*. Polarization curves generated at pH level 6.5 with respect to the change of current density depicting (a) the behavior of voltage output and (b) the behavior of power density output (right).

Fig. 7: Polarization curves at pH level 6.5.

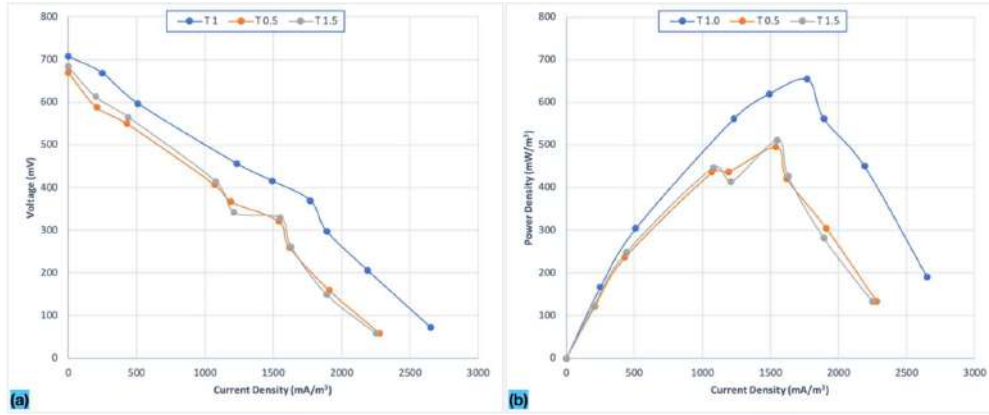


*Note*. Polarization curves generated at pH level 8 with respect to the change of current density depicting (a) the behavior of voltage output and (b) the behavior of power density output.

Fig. 8. Polarization curves at pH level 8.0.

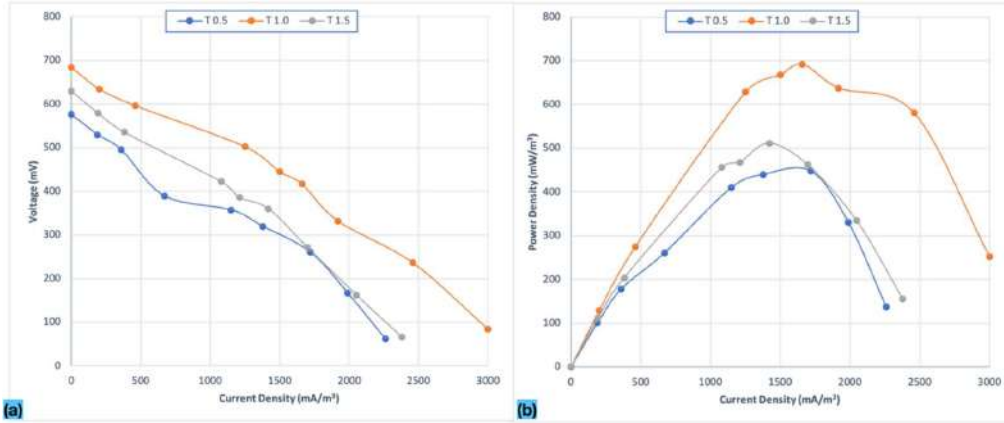


*Note*. Polarization curves generated at pH level 9.5 with respect to the change of current density depicting (a) the behavior of voltage output and (b) the behavior of power density output.

Fig. 9. Polarization curves at pH level 9.5.

Table 1: Internal resistance in $L_9$ orthogonal experiment.

| Chamber pH | G-S Thickness [cm] | Current Density [mA·m$^{-3}$] | Power Density [mW·m$^{-3}$] | Internal Resistance [Ω] |
|---|---|---|---|---|
| 6.5 | 0.5 | 2060 | 370.51 | 1096.77 |
| 6.5 | 1 | 2320 | 550.29 | 809.64 |
| 6.5 | 1.5 | 1860 | 407.52 | 1053.17 |
| 8 | 0.5 | 2280 | 495.11 | 906.49 |
| 8 | 1 | 2650 | 654.02 | 763.84 |
| 8 | 1.5 | 2250 | 510.73 | 914.84 |
| 9.5 | 0.5 | 2260 | 448.06 | 733.72 |
| 9.5 | 1 | 3000 | 692.22 | 644.58 |
| 9.5 | 1.5 | 2380 | 511.20 | 760.56 |

millivolts, *OCV* is in millivolts, *I* is the current flowing at a certain external resistance, and $R_{int}$ is the internal resistance.

### Effect of Chamber pH on Polarization Curves

Bacteria react with varying internal and external pH by adapting the activity and synthesis of proteins accompanying various processes such as proton translocation, amino acid degradation, adjusting to acidic or basic conditions, and virulence. Electrolyte pH has a significant contribution to power generation. Researchers have found that acidic electrolyte lowers power output (Hernández-Fernández et al. 2015, Jung & Pandit 2019) by inhibiting the growth of both methanogens and electrons on the anode, while slightly alkaline electrolyte promotes microbial metabolism and leads to a more negative anode potential, hence improving MFC performance (Kumar & Mungray 2017). Meanwhile, highly alkaline conditions in the cathodic portion could reduce $O_2$ potential (Munoz-Cupa et al. 2021).

In the experimental runs, it was noticed that all reactors almost had the same OCV values initially but more evident differences at higher pH values. There was a noticeable increase in voltage generation and a faster stabilization rate when pH levels were adjusted to 8.0. Meanwhile, the difference in maximum voltage was most evident when pH was adjusted to 9.5. Furthermore, increasing pH levels caused a decrease in internal resistances across all G-S anode thicknesses. Polarization curves showed that power density initially increases up to a certain resistance and then begins to decrease after the internal resistance value approaches the external resistance value (where maximum power density is approximated).

Chamber pH at 9.5 gave the highest current density and power density, mainly due to relatively low internal resistance, as shown in Table 1. Meanwhile, pH 8.0 exhibited the highest OCV at 707.5 mV, however, it produced a lesser power density and current density than that of pH 9.5, probably due to higher internal resistance. In addition, performances observed in pH 6.5 were consistently lower than the other two (2) pH levels, which only peaked at 667 mV, 2320 mA·m$^{-3}$, and 550 mW·m$^{-3}$ for OCV, current density, and power density, respectively. The lowest performance was observed at pH 6.5, manifested by having the highest internal resistances across all G-S anode thickness levels.

Several studies show similar results as the present study, in which differences in performances are attributed to the effect of pH on microbial activity and kinetics, and electrochemical resistances. Behera et al. (2010) conducted a MFC study on rice mill wastewater treatment using a proton exchange membrane and earthen pot. They varied the operational pH and found that maximum power densities generated from Earthen pot and PEM MFCs were observed in reactors that were fed with wastewater at pH 8.0. They attributed their findings to the fact that extracellular electron transfer in alkaline conditions is more effective, and electrogenic bacterial growth is favored in this pH microenvironment. The morphological characterization of the anode done by Margaria et al. (2017) presented a more diverse microbial morphology in alkaline MFCs than in neutral MFCs. Moreover, the microbial community attached to the electrodes from the alkaline MFCs was more compact and tightly connected. This may be attributed to exopolymeric substances that thrive when the pH increases.

Meanwhile, Ge et al. (2013) reported that at pH 5.48 ± 0.43, the current generation significantly dropped. The acidophilic condition, a condition that is attributed to concurrent reactions from the acidification process and proton accumulation, was observed after a buffer-less experiment. This inversely affected the growth of electrochemically active bacteria. In a study conducted by Zhang et al. (2011) on the influence of initial pH on the performance of anodic microbes, an increase in turbidity during MFC operation at pH 4.0 and 5.0 was observed, which was noted as a result of detached anodic biofilms. Detached biofilms are an indication of weakened or even dead microorganisms. The negative charges on the exopolysaccharide, an important component in biofilm formation, were neutralized at high $H^+$ concentrations due to acidification. The neutralization reaction destroyed the electrostatic actions, resulting in reduced biomass and biofilm thickness. Hence, maintaining an alkaline condition near the anode, which means having an elevated $OH^-$, is of great importance to counter the accumulation of $H^+$ ions.

To understand the electrochemical properties of two-chamber MFCs at varying pH conditions, Yuan et al. (2011)

analyzed the anode impedances using electrochemical impedance spectroscopy at different pH levels (9.0, 7.0, and 5.0). Their measurements showed slightly different ohmic resistances (7.8 Ω, 12.9 Ω, and 11.4 Ω for pH levels 5.0, 7.0, and 9.0, respectively) across pH levels but significantly variated in charge transfer resistances (256.2 Ω, 82.1 Ω and 9.1 Ω for pH levels 5.0, 7.0, 9.0 respectively). Karthikeyan et al. (2009) and Park et al. (2009) analyzed the electrochemical kinetics of biofilm using the Tafel plots in terms of exchange current density ($i_o$) and anodic Tafel slope (*b*a). The better anodic reaction is facilitated when *b*a is minimized, and $i_o$ is maximized. Results of their studies revealed pH 9.0 had the lowest *b*a (200 mV/decade) and highest $i_o$ (4.4 μA $m^{-2}$), which means anodic reactions are most favorable in such microenvironment pH conditions.

The results of this study also agreed with other works (Margaria et al. 2017, Zhang et al. 2011) that pH can be considered a limiting agent in a single-chamber MFC since acidification and alkalinization could severely affect both the electrodes of an ACMFC. Hence, proper identification of pH improves the performance of ACMFC. Some studies, however, claim that high alkaline (pH level beyond 8.0) condition slows down bacterial activity but can still favor an effective extracellular electron transfer (Cui et al. 2019). This phenomenon could explain why almost the same power output of pH levels 8.0 and 9.5 have been observed while having different percentages of COD removal (pH 8.0 has a higher percentage of COD removal than pH 9.5).

### Effect of Graphene-Sponge Anode Thickness on Polarization Curves

During the 8-day biofilm inoculation period, all G-S anode thicknesses have almost the same maximum OCV generated. However, they differed mainly in the rate at which their maximum voltage was reached. The reactor with a G-S anode thickness of 1.0 cm was the first to reach its maximum voltage after the refill of wastewater. Meanwhile, reactors with anode thicknesses of 0.5 cm and 1.5 cm had almost the same performance as an anode thickness of 1.0. This observation may be attributed to the time it took for biofilms to form on the surface area of the G-S sponges. Lesser biofilm may be formed at 0.5 cm and slower to form at 1.5 cm.

The experimental runs with a pH level of 6.5 showed relatively identical OCV across all G-S anode thicknesses. Among the three thickness levels, G-S anode thickness of 1.0 cm consistently showed to have the highest OCV, current density, and power density at 707.5 mV, 3000 $mA \cdot m^{-3}$, and 692.22 $mW \cdot m^{-3}$, respectively, and the lowest internal resistances across all pH levels.

Generally, increasing anode thickness also increases power generation which is in agreement with the result of this study comparing the power generation between the G-S thicknesses 0.5 cm and 1.0 cm. This can be associated with graphene-sponge anodes providing high surface area favorable for microbial immobilization (e.g., *E. coli*) and high porosity for more efficient mass transport suitable for biocatalyst proliferation (Chou et al. 2014). The high porosity of graphene-based anode is due to the tendency of graphene to form layer-like structures, which are caused by $\pi-\pi$ stacking between graphene sheets (Zhao et al. 2021). Hence, the thicker the sponge anode, the thicker biofilms are formed and the microorganisms consume the more organic compounds.

In addition, the G-S electrode's inherent biocompatibility can facilitate the direct electron transfer rate and growth of electroactive bacteria. A study on the electrochemical behavior of graphene-induced carbon cloth anode by Liu et al. (2012) reported high peak current and lower peak separation. Furthermore, their study revealed that graphene-induced carbon cloth has a stronger impact on direct electron transfer than the mediated electron process, which is indicative of graphene's excellent enhancing property on the interfacial electron transfer rate for electrochemical reactions.

On the contrary, Cai et al. (2020) noted that current and power density, to some extent, decreases with increasing electrode thickness due to the blockage of biofilm from microbial propagation to the pore-like structure. This report was also observed in the current study where the G-S anode with a thickness of 1.5 cm has lesser power generated than with a thickness of 1.0 cm. Chou et al. (2014) reported that microbial growth not only within the porous area blocks the sponge but also contributes to the weakening of electron transfer due to the inherent insulating property of biofouling caused by a build-up of waste from secretions and metabolism. In effect, biofilm may be inactivated. Chen et al. (2012) also had similar claims on anode thickness, in spite of reticulated carbon foam from pomelo peel (RCF-PP) being a promising anode material, MFCs having porous-based anodes suffered mass transfer limitations, which increase as the electrode thickness also increases.

Increasing electrode thickness is also a primary consideration that affects the transport of waste and nutrients within the porous anode. An insufficient nutrient delivery negatively affects the growth of electrogenic bacteria, which may have happened in this study with the G-S anode sponge of 1.5 cm thickness. This phenomenon may lead to dormancy. Dormancy (lag time) is generally induced when bacterial colonies are subjected to stresses such as starvation, osmotic pressure, and temperature fluctuation. In this state,

bacteria tend to consume fewer organic compounds. Hence, microorganisms under this condition may inadequately act as biocatalysts for electrochemical oxidation (Chou et al. 2014).

The current study revealed a noteworthy trend in the performance of MFC when varying the anode thickness. Specifically, it was observed that increasing the anode thickness from 0.5 cm to 1.0 cm resulted in a significant improvement in MFC performance. However, further increasing the thickness to 1.5 cm led to a decline in performance. These findings align with a simulation study conducted by Xie et al. (2012), which demonstrated a similar graphical representation in Fig. 10. In their study, they observed that, at a fixed SS current collector thickness, the voltage drop and power loss exhibited an exponential increase with greater G-S thickness when the conduction length was less than 1 m.

Based on the results, it can be inferred that increasing the anode thickness from 0.5 cm to 1.0 cm creates a favorable electrochemical environment for both voltage and power generation, with losses not being dominant in this particular configuration. However, surpassing the thickness of 1.5 cm may have resulted in excessive energy overpotentials, thereby decreasing the overall performance of the MFC compared to the earlier anode thicknesses.

The power density achieved by Xie et al. (2012) was considerably higher at 392 $W.m^{-3}$, as compared to the power density generated in the current study. This significant difference may be attributed to the variations in other components of the MFC, such as the carbon cloth electrode coated with Pt catalyst as the cathode, in contrast to the simpler construction of the Nafion- and Platinum-free carbon black-activated carbon air cathode used in this study.

### Effect of pH and G-S Anode Thickness on Percentage COD Removal

Table 2 shows the COD removal efficiency based on the chamber pH and corresponding G-S anode thickness. From the table, it can be seen that the peak percentage of COD removal was achieved at pH 8.0. On the other hand, the percentage of COD removal did not significantly change across all G-S anode thicknesses used. Both pH levels 6.5 and 9.5 have noticeably lower COD removal efficiency than pH 8.0, this might be due to reduced bacterial activity at highly acidic and alkaline conditions. Lower COD consumption levels (35% in acidic MFCs and 10% in pH greater than 10) were also observed by Margaria et al. (2017) while determining the effects of pH variation on anodic marine consortia in a dual chamber MFC. Hence, COD consumption might not be directly associated with electrochemical performance. As observed by Nimje et al. (2011), COD degradation could be for the direct growth and sustenance of bacteria.

At high solution pH, the sorption rate is reduced due to electrostatic repulsion between deprotonated acid functional groups, which may lead to lower organic removal (N. Cai et al. 2015). Whereas, at neutral to slightly alkaline conditions, microbial metabolism and methanogenesis coexist, which have an additive impact on the degradation of organic compounds, hence, high COD removal (Martin et al. 2010).

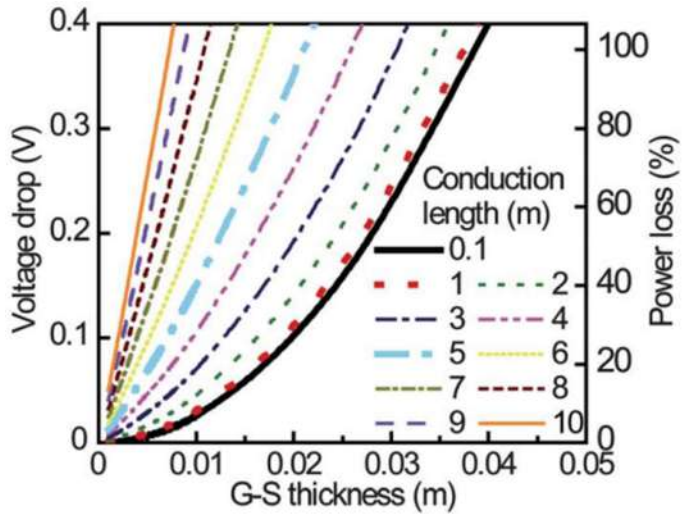


*Note:* Fig. 10 shows the simulation results for G-S electrodes in large-scale applications for voltage drop and power loss in different G-S thicknesses. Graphenesponges as high-performance, low-cost anodes for microbial fuel cells Xie et al. (2012).

Fig. 10: Voltage drop and Power loss v.s. G-S thickness.

Graphene-based materials have a high surface area, making them a popular adsorbing material for various chemicals such as oil (Wang et al. 2019) and toxic organic pollutants (Baig et al. 2019). Based on Table 2, the change in percentage COD removal with respect to varying G-S sponge anode thickness is statistically insignificant, with a P-value (0.4001) greater than 0.05. It can be inferred that graphene provides a sufficient effective surface area in which even the lowest anode thickness removes the same amount of COD concentration from wastewater as the thicker ones by adsorption. The same results were observed by di Lorenzo et al. (2010) using packed beds of irregular graphite granules, which are known to have a high surface area, as anode material. Varying layers of granules (e.g., 0.3 cm and 1 cm) were observed. However, the study showed no significant difference in percentage COD removal between 0.3 cm layer and 1 cm layer (35% and 41%, respectively.).

In addition, the large surface area of the graphene material may have been inhabited by both non-isoenergetic bacteria, which can also contribute to COD removal. Katuri et al. (2011) had similar observations where COD removal did not correlate with coulombic efficiency, which is attributed to different microbial communities coinhabited in the anode surface area, dominated by non-electrogenic microorganisms.

In this study, it can be said that pH (with a *P*-value less than 0.05) is the percentage COD removal limiting factor. Whereas varying anode thickness did not significantly contribute to the wastewater treatment performance, as supported by ANOVA in Table 3.

## Optimization Study

In MFC studies, the higher the power density produced, the better. Hence, larger-the-better performance characteristics were used for calculating the S/N ratio using the Taguchi Experimental Method. Table 4 gives the average power density and internal resistance values of the first and second runs at the same operating conditions. In addition, Table 5 presents the response table of the S/N ratio. In this table, the total variation in the S/N ratio is calculated using Equation 7.

$$S_T = \left[\sum_{i=1}^{n} \left(\frac{S}{N}\right)_t^2\right] - \left[\frac{\sum_{i=1}^{n}\left(\frac{S}{N}\right)_i}{n}\right]^2 \quad \ldots(7)$$

where $n$ is the total number of experiments, $t$ is the total sum of the S/N ratio, and $i$ is the S/N ratio at a particular pH and thickness condition

Fig. 11 is a graph to show the impact of the parameters on the performance characteristics using the data presented in Table 4. The optimum values of parameters for obtaining the maximum power density are selected corresponding to the highest S/N ratio value calculated using Equation 5 (Table 3). Meanwhile, the best conditions can be observed in the graphical representation, e.g., Fig. 11, by locating the peak points in both graphs.

Based on the $L_9$ experimental analysis, the G-S anode thickness of 1.0 and pH 9.5 produced a maximum power density among all nine experiments. Nonetheless, the Taguchi method selects the conditions with the highest values of mean S/N ratios, which happened to be G-S anode

Table 2: Percentage COD Removal.

| | Chamber pH | | |
|---|---|---|---|
| Anode Thickness | 6.5 | 8.0 | 9.5 |
| 0.5 | 35.99 | 76.43 | 54.81 |
| 1.0 | 58.68 | 72.93 | 59.85 |
| 1.5 | 44.82 | 74.73 | 62.26 |

*Note*. The table shows the different percentages of COD removal of the different combinations of parametric conditions.

Table 3: ANOVA on the effect of varying Chamber pH and anode thickness on Percentage COD Removal.

| | Degree of Freedom | Sum of square | *F*-value | *P*-value* |
|---|---|---|---|---|
| pH | 2 | 27.6213 | 8.9374 | 0.0334 |
| Thickness | 2 | 3.5906 | 1.1618 | 0.4001 |

*$p < 0.05$ indicates the parameter significantly contributes to the output

Table 4: $L_9$ orthogonal array, power density, and S/N ratio for thickness and pH effects.

| Exp. No. | Chamber pH | G-S Thickness | Power Density | S/N |
|---|---|---|---|---|
| 1 | 6.5 | 0.5 | 370.51 | 51.38 |
| 2 | 6.5 | 1.0 | 550.29 | 54.81 |
| 3 | 6.5 | 1.5 | 407.52 | 52.20 |
| 4 | 8.0 | 0.5 | 495.11 | 53.89 |
| 5 | 8.0 | 1.0 | 654.02 | 56.31 |
| 6 | 8.0 | 1.5 | 510.73 | 54.16 |
| 7 | 9.5 | 0.5 | 448.06 | 53.03 |
| 8 | 9.5 | 1.0 | 692.22 | 56.80 |
| 9 | 9.5 | 1.5 | 511.20 | 54.17 |

*Note*. The table was generated using the Minitab software.

Table 5: Response table for S/N ratio according to the larger-the-better condition of Taguchi Experimental Method.

| Level | Chamber pH, A | G-S Thickness, B |
|---|---|---|
| 1 | 52.80 | 52.77 |
| 2 | 54.79 | 55.98 |
| 3 | 54.67 | 53.51 |
| Delta | 1.99 | 3.21 |

*Note*. The table was generated using the Minitab software.

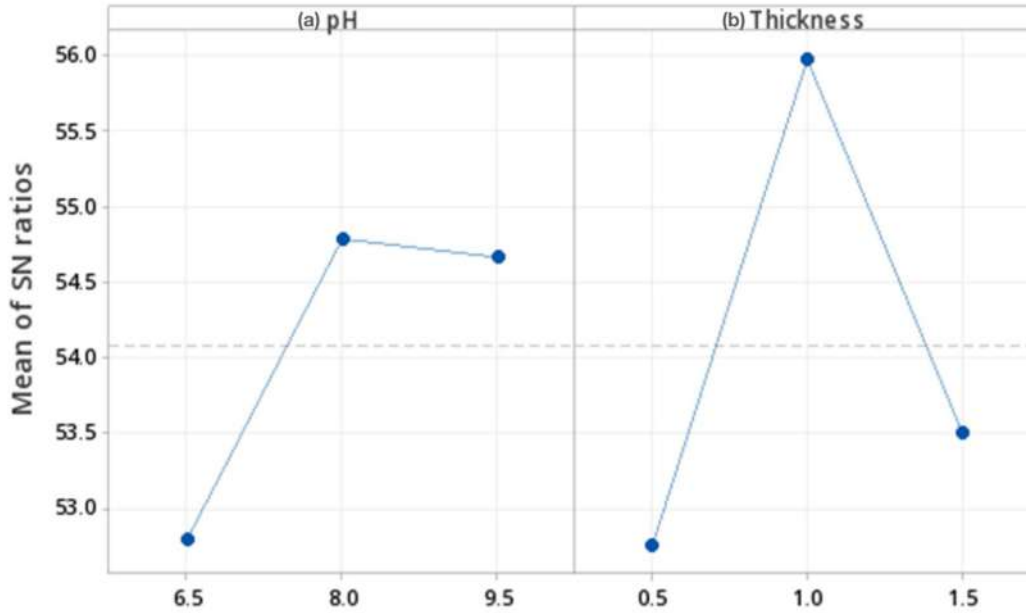


*Note*. The highest peaks of the graphs correspond to the optimum value of both (a) chamber pH and (b) anode thickness

Fig. 11: Optimization of parameters using the main effects plot for S/N ratios.

thickness 1.0 and pH 8.0 as the optimized condition. These optimum values are illustrated on the peak points both in pH and thickness in Fig. 11.

### Analysis of Variance

The *F*-value for both anode thickness and chamber pH is defined as the ratio of the mean of the square error. The larger the *F*-value of a parameter, the greater its impact in producing maximum power density. The optimal combination of anode thickness and chamber pH can be approximated using performance characteristics and ANOVA. The results of the ANOVA for the experiments are presented in Table 6.

The degree of freedom for the factors is calculated by the number of levels (k) minus 1. Meanwhile, the *P*-value is calculated to either accept or reject the null hypothesis at 95% confidence. If the P-value is less than 0.05, then the null hypothesis can be rejected, and it can be concluded that the G-S thickness and chamber pH bear a significant impact on the process. As presented in Table 6, both the parameters have *P*-values less than 0.05, however, have different percentage contributions to the maximum power density of the experiment. G-S anode thickness has a larger percentage contribution, which means that it has a larger impact on the production of maximum power density. Meanwhile, chamber pH although it bears a smaller impact, still contributes a significant effect on the response.

### Confirmatory Experiment

Based on the optimized conditions, i.e., G-S thickness of 1.0 and chamber pH of 8, the researcher conducted a confirmatory experiment with two (2) trials. The reactors were fed with wastewater with an adjusted pH of 8 and left to stabilize for three (3) days for better acclimatization. Optimal pH was maintained for the same number of days. The mean values of the two trials were plotted in Fig. 12, which gave similar results from the previous experiment with a high-power density of up

Table 6: ANOVA for the maximum power density value of the experiment.

| | Degree of Freedom | Sum of square | Average of squares | *F*-value | *P*-value* | Percentage contribution |
|---|---|---|---|---|---|---|
| pH | 2 | 7.4868 | 3.7434 | 29.10 | 0.004 | 30.66 |
| Thickness | 2 | 16.9340 | 8.4670 | 65.82 | 0.001 | 69.34 |
| Residual Error | 4 | 0.5145 | 0.1286 | | | |
| Total | 8 | 24.9353 | | 94.92 | | |

*$p < 0.05$ indicates the parameter significantly contributes to the output

[a] not provided by Minitab, calculated separately.

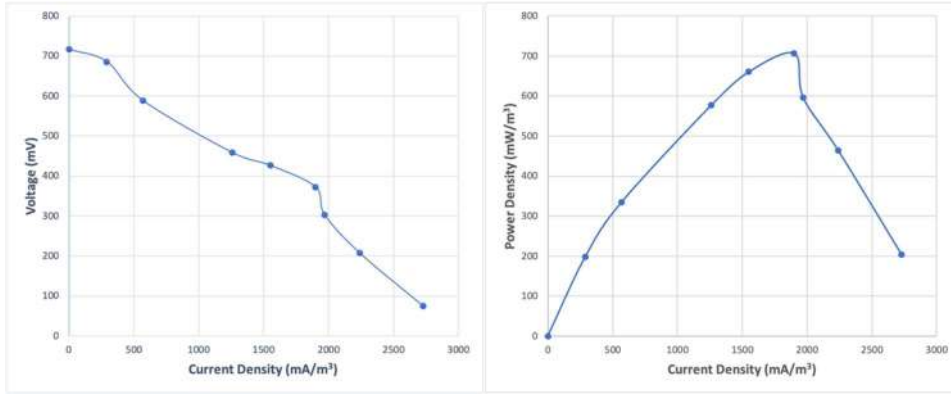


*Note*. Polarization curves generated from the confirmatory experiment at optimized conditions resulting from the Taguchi Experimental Method.

Fig. 12: Polarization Curves for the optimal levels of G-S anode thickness and chamber pH.

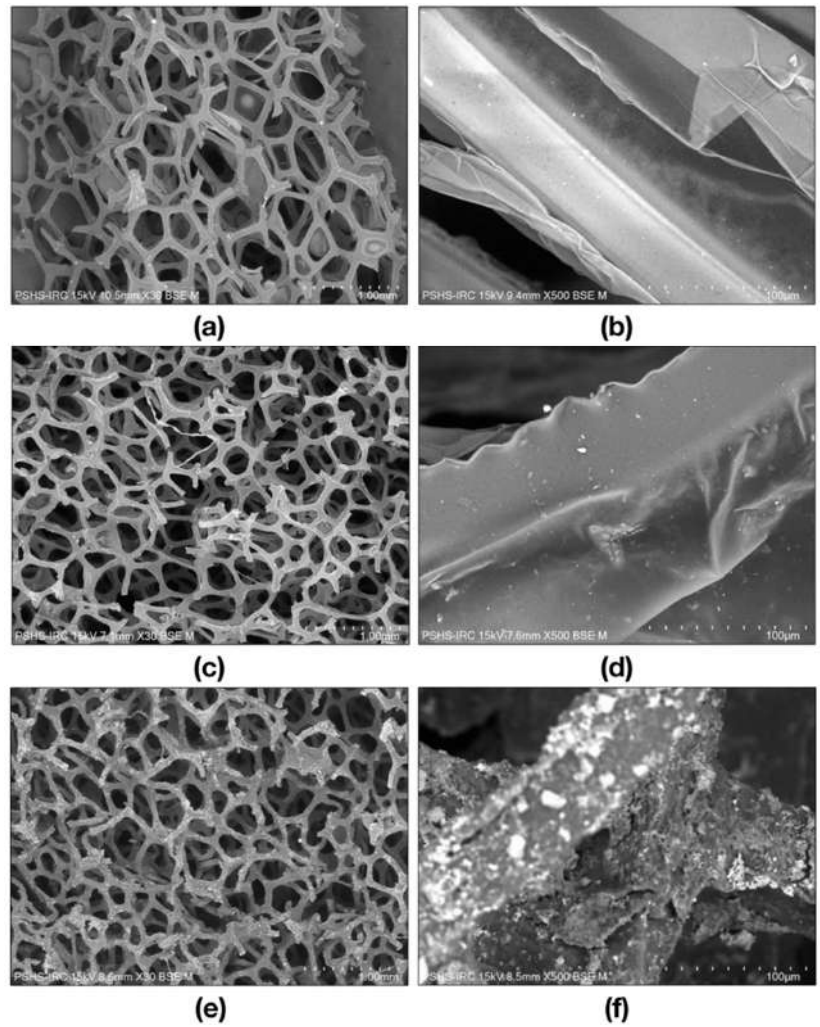


*Note*. SEM images at x30 and x 500 magnification of (a, b) plain polyurethane sponge, (c, d) G-S anode without biofilm, and (e, f) G-S with biofilm after experimental runs.

Fig. 13: Sub-microstructure images of different sponges generated under a SEM.

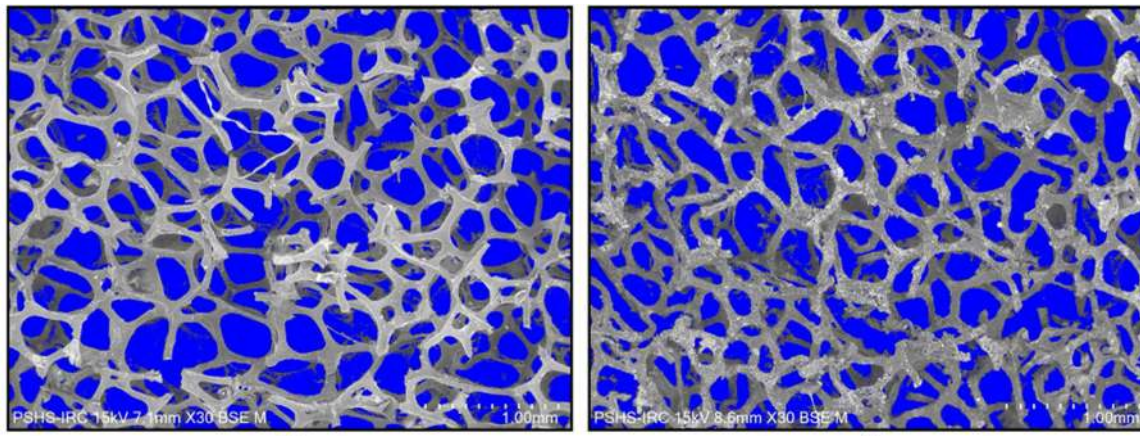


*Note*. Comparison of pore size area (in $mm^2$) of (a) biofilm-less GS and (b) biofilm-rich GS

Fig. 14: Estimation of pore size using ImageJ software.

to 707.75 $mW \cdot m^{-3}$. The slightly higher power generation is due to the acclimatization time, which promotes better biofilm performance and proper proton transfer from the anode to the cathode (Kumar & Mungray 2017).

### Morphological Characterization using Scanning Electron Microscopy

The SEM images of different forms in different magnifications (x30 and x500) are shown in Fig. 13, which clearly shows the intensity of shades among different conditions. Fig. 14a and 14b are images of a plain polyurethane sponge. It can be seen that compared to the latter images, plain polyurethane is less distinct and lighter. Meanwhile, Fig. 14c and 14d are images of the G-S anode that are more distinct than the plain polyurethane sponge with the presence of graphene. It is also evident that graphene conductive coating conforms to the morphology of the plain sponge without blocking the open porous structure. This conformity and stability of graphene wrapping around the sponge fibers are attributed to the flexibility of its 2D structure and strong van der Waals forces (Xie et al. 2012). The strong intermolecular forces are manifested by the anode's excellent performance during the scotch tape test and water flushing, where the graphene was neither removed nor flushed away.

Fig. 13e and 13f illustrate the condition of the G-S anode after several experimental runs. In Fig. 13f, it is very clear that thick biofilms have attached to the surfaces of the anode, which can be due to the excellent biocompatibility of the fabrication process and the synthesized material itself.

Furthermore, the ImageJ software was used to analyze the size of the pores. Fig. 14 illustrates a comparison of the average pore size, measured in terms of area (in $mm^2$), between the biofilm-rich and biofilm-less GS. The results indicate that the mean pore size in biofilm-rich GS is slightly smaller (131.319 $mm^2$) than in biofilm-less GS (140.479 $mm^2$). Although there is a difference in the average pore size, the presence of biofilm did not significantly obstruct microbial growth between the scaffolds of the GS. However, the study did not provide a detailed characterization of the graphene structure, which could have helped to further investigate the growth of biofilm within the graphene structures.

## CONCLUSIONS

Improving the engineering design and operating conditions of emerging technologies is crucial. The Taguchi method offers a cost-effective experimental design and reliable results through the $L_9$ orthogonal array. It is suitable for optimizing G-S anode thickness and chamber pH to maximize power density. ANOM and ANOVA were employed to evaluate the parameters, assess their impact on the output response, and determine their significance. The summarized results are as follows:

1. The optimal parameter values for G-S anode thickness and chamber pH are 1.0 cm and 8.0, respectively. A verification experiment using these values yielded a power density of 707.75 $mW \cdot m^{-3}$.
2. Both G-S anode thickness and chamber pH significantly contribute to the power generation of ACMFCs, as indicated by ANOVA. ANOM analysis further confirmed that anode thickness has a greater impact on the output.
3. Chamber pH plays a significant role in wastewater treatment capability, whereas varying anode thickness did not lead to significant differences in COD removal.

Anode thickness plays a vital role in power generation. Increasing the thickness provides a larger surface area for biofilm formation, resulting in higher current density. However, thicker biofilms can lead to pore blockage due to waste accumulation from microbial activity, affecting mass transport efficiency and electron transfer.

Chamber pH influences the internal resistance of the system. Slightly alkaline pH reduces internal resistance, thereby enhancing MFC performance in terms of power generation. This is attributed to the promotion of exopolymeric substances, which support extracellular electron transport. Conversely, pH acts as a limiting factor for COD removal since it affects bacterial growth kinetics. Lower pH slows down microbial activity, as evident in ACMFC chambers with a pH of 6.5, leading to lower current density output. It's important to note that good electrochemical performance does not necessarily translate to high COD removal, as the microbial degradation of compounds is influenced by pH, which depends on the specific microbial culture present in the wastewater.

### Recommendations

To enhance the study, it would be beneficial to increase the level of parameter variation. By including other parameters, the findings of this study could apply to larger-scale MFC operations. Additionally, identifying the specific bacteria present could provide further insights into the optimal conditions for their growth and culture kinetics.

Future studies could explore other aspects of MFC operation as well. Investigating techniques such as continuous operation and wastewater recirculation using a G-S anode could help mitigate mass transfer limitations.

Furthermore, in the fabrication process of the G-S anode, a significant amount of excess reduced graphene oxide (rGO) is typically disposed of after the hydrothermal reaction. To minimize costs, it would be advisable to optimize the amount of graphene oxide (GO) solution used in relation to the volume of the sponge that needs to be coated. This optimization process could help reduce waste and improve cost-efficiency.

## ACKNOWLEDGMENTS

Special thanks to the Department of Science and Technology - Science Education Institute (DOST-SEI) Science and Technology Regional Alliance of Universities for National Development (STRAND) Scholarship Program for granting the Student Research Support Fund (SRSF) in addition to the outright thesis allowance. The authors would like to express their gratitude to the SLU School of Advanced Studies and the School of Engineering and Architecture for their unwavering support throughout the conduct of this study. The authors would also like to thank Engr. Roy Domalanta, Engr. Ramde Gonzales and Dr. Aizza Corpuz for their valuable input and expertise in reviewing the paper as thesis panel members.

## REFERENCES

Azmi, N. M., Anandita, N., Tajarudin, H. A., Shoparwe, N. F. and Makhtar, M. M. Z. 2021. Membrane-less microbial fuel cell: effect of pH on the electricity generation powered by municipal food waste. J. Phys.: Conf. Ser., 2129(1): 012095. https://doi.org/10.1088/1742-6596/2129/1/012095

Baig, N., Ihsanullah, Sajid, M. and Saleh, T. A. 2019. Graphene-based adsorbents for the removal of toxic organic pollutants: A review. J. Environ. Manag., 244: 370-382. https://doi.org/10.1016/j.jenvman.2019.05.047

Bajracharya, S., ElMekawy, A., Srikanth, S. and Pant, D. 2016. Cathodes for Microbial Fuel Cells. Elsevier, The Netherlands, pp. 179-213. https://doi.org/10.1016/B978-1-78242-375-1.00006-X

Behera, M., Jana, P. S., More, T. T. and Ghangrekar, M. M. 2010. Rice mill wastewater treatment in microbial fuel cells fabricated using proton exchange membrane and earthen pot at different pH. Bioelectrochemistry, 79(2): 228-233. https://doi.org/10.1016/j.bioelechem.2010.06.002

Bian, B., Shi, D., Cai, X., Hu, M., Guo, Q., Zhang, C., Wang, Q., Sun, A. X. and Yang, J. 2018. 3D printed porous carbon anode for enhanced power generation in a microbial fuel cell. Nano Energy, 44: 174-180. https://doi.org/10.1016/j.nanoen.2017.11.070

Butler, J. E., Young, N. D. and Lovley, D. R. 2010. Evolution of electron transfer out of the cell: comparative genomics of six Geobacter genomes. BMC Genomics, 11(1): 40. https://doi.org/10.1186/1471-2164-11-40

Cai, N., Peak, D. and Larese-Casanova, P. 2015. Factors influencing natural organic matter sorption onto commercial graphene oxides. Chem. Eng. J., 273: 568-579. https://doi.org/10.1016/j.cej.2015.03.108

Cai, T., Meng, L., Chen, G., Xi, Y., Jiang, N., Song, J., Zheng, S., Liu, Y., Zhen, G. and Huang, M. 2020. Application of advanced anodes in microbial fuel cells for power generation: A review. Chemosphere, 248: 125985. https://doi.org/10.1016/j.chemosphere.2020.125985

Chandrasekar, K., Sudhakar, S., Rajappan, R., Senthil, S. and Balu, P. 2022. Present developments and the reach of alternative fuel: A review. Mater. Today: Proc., 51: 74–83. https://doi.org/10.1016/j.matpr.2021.04.505

Chen, H., Simoska, O., Lim, K., Grattieri, M., Yuan, M., Dong, F., Lee, Y. S., Beaver, K., Weliwatte, S., Gaffney, E. M. and Minteer, S. D. 2020. Fundamentals, applications, and future directions of bioelectrocatalysis. Chem. Rev., 120(23): 12903-12993. https://doi.org/10.1021/acs.chemrev.0c00472

Chen, S., Liu, Q., He, G., Zhou, Y., Hanif, M., Peng, X., Wang, S. and Hou, H. 2012. Reticulated carbon foam derived from a sponge-like natural product as a high-performance anode in microbial fuel cells. J. Mater. Chem., 22(35): 18609. https://doi.org/10.1039/c2jm33733a

Chou, H. T., Lee, H. J., Lee, C. Y., Tai, N. H. and Chang, H. Y. 2014. Highly durable anodes of microbial fuel cells using a reduced graphene oxide/carbon nanotube-coated scaffold. Bioresour. Technol., 169: 532-536. https://doi.org/10.1016/j.biortech.2014.07.027

Cui, W., Liu, G., Zeng, C., Lu, Y., Luo, H. and Zhang, R. 2019. Improved hydrogen production in the single-chamber microbial electrolysis cell with inhibition of methanogenesis under alkaline conditions. RSC Adv., 9(52): 30207-30215. https://doi.org/10.1039/C9RA05483A

D'Angelo, A., Mateo, S., Scialdone, O., Cañizares, P., Fernandez-Morales, F. J. and Rodrigo, M. A. 2017. Optimization of the performance of an air-cathode MFC by changing solid retention time. J. Chem. Technol. Biotechnol., 92(7): 1746-1755. https://doi.org/10.1002/jctb.5175

Dewan, A., Beyenal, H. and Lewandowski, Z. 2008. Scaling up Microbial Fuel Cells. Environ. Sci. Technol., 42(20): 7643-7648. https://doi.org/10.1021/es800775d

Di Lorenzo, M., Scott, K., Curtis, T. P. and Head, I. M. 2010. Effect of increasing anode surface area on the performance of a single chamber microbial fuel cell. Chem. Eng. J., 156(1): 40-48. https://doi.org/10.1016/j.cej.2009.09.031

Dong, H., Yu, H., Wang, X., Zhou, Q. and Feng, J. 2012. A novel structure of scalable air-cathode without Nafion and Pt by rolling activated carbon and PTFE as catalyst layer in microbial fuel cells. Water Res., 46(17): 5777-5787. https://doi.org/10.1016/j.watres.2012.08.005

Douglas Montogomery, C. 2005. Design and Analysis of Experiments: Response Surface Method and Designs. New Jersey: John Wiley and Sons, Inc.

Erable, B., Etcheverry, L. and Bergel, A. 2009. Increased power from a two-chamber microbial fuel cell with a low-pH air-cathode compartment. Electrochem. Commun., 11(3): 619-622. https://doi.org/10.1016/j.elecom.2008.12.058

Estrada-Arriaga, E. B., Guillen-Alonso, Y., Morales-Morales, C., García-Sánchez, L., Bahena-Bahena, E. O., Guadarrama-Pérez, O. and Loyola-Morales, F. 2017. Performance of air-cathode stacked microbial fuel cell systems for wastewater treatment and electricity production. Water Sci. Technol., 76(3): 683-693. https://doi.org/10.2166/wst.2017.253

Gandhi, P. J., Murthy, Z. V. P. and Pati, R. K. 2012. Optimization of process parameters by Taguchi robust design method for the development of nano-crystals of sirolimus using sonication-based crystallization. Cryst. Res. Technol., 47(1): 53-72. https://doi.org/10.1002/crat.201100329

Ge, Z., Zhang, F., Grimaud, J., Hurst, J. and He, Z. 2013. Long-term investigation of microbial fuel cells treating primary sludge or digested sludge. Bioresour. Technol., 136: 509-514. https://doi.org/10.1016/j.biortech.2013.03.016

He, Z., Huang, Y., Manohar, A. K. and Mansfeld, F. 2008. Effect of electrolyte pH on the rate of the anodic and cathodic reactions in an air-cathode microbial fuel cell. Bioelectrochemistry, 74(1): 78-82. https://doi.org/10.1016/j.bioelechem.2008.07.007

Herkendell, K. 2021. Status Update on Bioelectrochemical Systems: Prospects for Carbon Electrode Design and Scale-Up. Catalysts, 11(2): 278. https://doi.org/10.3390/catal11020278

Hernández-Fernández, F. J., Pérez de los Ríos, A., Salar-García, M. J., Ortiz-Martínez, V. M., Lozano-Blanco, L. J., Godínez, C., Tomás-Alonso, F. and Quesada-Medina, J. 2015. Recent progress and perspectives in microbial fuel cells for bioenergy generation and wastewater treatment. Fuel Process. Technol., 138: 284-297. https://doi.org/10.1016/j.fuproc.2015.05.022

Huang, X., Duan, C., Duan, W., Sun, F., Cui, H., Zhang, S. and Chen, X. 2021. Role of electrode materials on performance and microbial characteristics in the constructed wetland coupled microbial fuel cell (CW-MFC): A review. J. Clean. Prod., 301: 126951. https://doi.org/10.1016/j.jclepro.2021.126951

Islam, M. A., Karim, A., Woon, C. W., Ethiraj, B., Cheng, C. K., Yousuf, A. and Rahman Khan, M. M. 2017. Augmentation of air cathode microbial fuel cell performance using wild-type Klebsiella variicola. RSC Adv., 7(8): 4798-4805. https://doi.org/10.1039/C6RA24835G

Jadhav, D. A., Carmona-Martínez, A. A., Chendake, A. D., Pandit, S. and Pant, D. 2021a. Modeling and optimization strategies towards performance enhancement of microbial fuel cells. Bioresour. Technol., 320: 124256. https://doi.org/10.1016/j.biortech.2020.124256

Jadhav, D. A., Mungray, A. K., Arkatkar, A. and Kumar, S. S. 2021b. Recent advancement in scaling-up applications of microbial fuel cells: From reality to practicability. Sustain. Energy Technol. Assess., 45: 101226. https://doi.org/10.1016/j.seta.2021.101226

Ji, B., Kang, P., Wei, T. and Zhao, Y. 2020. Challenges of aqueous per- and polyfluoroalkyl substances (PFASs) and their foreseeable removal strategies. Chemosphere, 250: 126316. https://doi.org/10.1016/j.chemosphere.2020.126316

Jung, S. P. and Pandit, S. 2019. Important factors influencing microbial fuel cell performance. Elsevier, The Netherlands, pp. 377-406. https://doi.org/10.1016/B978-0-444-64052-9.00015-7

Karthikeyan, R., Sathish Kumar, K., Murugesan, M., Berchmans, S. and Yegnaraman, V. 2009. Bioelectrocatalysis of *Acetobacter aceti* and *Gluconobacter roseus* for current generation. Environ. Sci. Technol., 43(22): 8684-8689. https://doi.org/10.1021/es901993y

Katuri, K. P., Scott, K., Head, I. M., Picioreanu, C. and Curtis, T. P. 2011. Microbial fuel cells meet with external resistance. Bioresour. Technol., 102(3): 2758-2766. https://doi.org/10.1016/j.biortech.2010.10.147

Kim, B. H., Chang, I. S. and Gadd, G. M. 2007. Challenges in microbial fuel cell development and operation. Appl. Microbiol. Biotechnol., 76(3): 485-494. https://doi.org/10.1007/s00253-007-1027-4

Kumar, P. and Mungray, A. K. 2017. Microbial fuel cell: optimizing pH of anolyte and catholyte by using the taguchi method. Environ. Prog. Sustainable Energy, 36(1): 120-128. https://doi.org/10.1002/ep.12459

Kumar, R., Singh, L., Wahid, Z. A. and Din, M. F. Md. 2015. Exoelectrogens in microbial fuel cells toward bioelectricity generation: a review. Int. J. Energy Res., 39(8): 1048-1067. https://doi.org/10.1002/er.3305

Liu, J., Qiao, Y., Guo, C. X., Lim, S., Song, H. and Li, C. M. 2012. Graphene/carbon cloth anode for high-performance mediatorless microbial fuel cells. Bioresour. Technol., 114: 275-280. https://doi.org/10.1016/j.biortech.2012.02.116

Liu, Y., Zhang, X., Zhang, Q. and Li, C. 2020. Microbial fuel cells: Nanomaterials based on anode and their application. Energy Technol., 8(9): 2000206. https://doi.org/10.1002/ente.202000206

Logan, B., Cheng, S., Watson, V. and Estadt, G. 2007. Graphite fiber brush anodes for increased power production in air-cathode microbial fuel cells. Environ. Sci. Technol., 41(9): 3341-3346. https://doi.org/10.1021/es062644y

Logan, B. E. 2012. Essential data and techniques for conducting microbial fuel cell and other types of bioelectrochemical system experiments. Chem. Sus. Chem., 5(6): 988-994. https://doi.org/10.1002/cssc.201100604

Logan, B. E., Hamelers, B., Rozendal, R., Schröder, U., Keller, J., Freguia, S., Aelterman, P., Verstraete, W. and Rabaey, K. 2006. Microbial Fuel Cells: Methodology and Technology. Environ. Sci. Technol., 40(17): 5181-5192. https://doi.org/10.1021/es0605016

Logan, B. E., Hamelers, B., Rozendal, R., Schröder, U., Keller, J., Freguia, S., Aelterman, P., Verstraete, W. and Rabaey, K. 2006b. Microbial Fuel Cells: Methodology and Technology. Environ. Sci. Technol., 40(17): 5181-5192. https://doi.org/10.1021/es0605016

Logan, B. E., Rossi, R., Ragab, A. and Saikaly, P. E. 2019. Electroactive microorganisms in bioelectrochemical systems. Nat. Rev. Microbiol., 17(5): 307-319. https://doi.org/10.1038/s41579-019-0173-x

Margaria, V., Tommasi, T., Pentassuglia, S., Agostino, V., Sacco, A., Armato, C., Chiodoni, A., Schilirò, T. and Quaglio, M. 2017. Effects of pH variations on anodic marine consortia in a dual chamber microbial fuel cell. Int. J. Hydrogen Energy, 42(3): 1820-1829. https://doi.org/10.1016/j.ijhydene.2016.07.250

Martin, E., Savadogo, O., Guiot, S. R. and Tartakovsky, B. 2010. The influence of operational conditions on the performance of a microbial fuel cell seeded with mesophilic anaerobic sludge. Biochem. Eng. J., 51(3): 132-139. https://doi.org/10.1016/j.bej.2010.06.006

Mink, J. E. and Hussain, M. M. 2013. Sustainable design of high-performance microsized microbial fuel cell with carbon nanotube anode and air cathode. ACS Nano, 7(8): 6921-6927. https://doi.org/10.1021/nn402103q

Munoz-Cupa, C., Hu, Y., Xu, C. and Bassi, A. 2021. An overview of microbial fuel cell usage in wastewater treatment, resource recovery, and energy production. Sci. Total Environ., 754: 142429. https://doi.org/10.1016/j.scitotenv.2020.142429

Nimje, V. R., Chen, C. Y., Chen, C. C., Tsai, J. Y., Chen, H. R., Huang, Y. M., Jean, J. S., Chang, Y. F. and Shih, R. C. 2011. The microbial fuel cell of Enterobacter cloacae: Effect of anodic pH microenvironment on current, power density, internal resistance, and electrochemical losses. Int. J. Hydrogen Energy, 36(17): 11093-11101. https://doi.org/10.1016/j.ijhydene.2011.05.159

Odjadjare, E. E. O. and Okoh, A. I. 2010. Physicochemical quality of an urban municipal wastewater effluent and its impact on the receiving environment. Environ. Monit. Assess., 170(1-4): 383-394. https://doi.org/10.1007/s10661-009-1240-y

Park, W., Ahmed, J. and Kim, S. 2009. Heterogeneous electron-transfer kinetics for PQQ covalently attached to aminoalkanethiol monolayers on gold. Colloids Surf. B Biointerfaces, 68(1): 120-124. https://doi.org/10.1016/j.colsurfb.2008.09.007

Patil, S. A., Harnisch, F., Koch, C., Hübschmann, T., Fetzer, I., Carmona-Martínez, A. A., Müller, S. and Schröder, U. 2011. Electroactive mixed culture derived biofilms in microbial bioelectrochemical systems: The role of pH on biofilm formation, performance, and composition. Bioresour. Technol., 102(20): 9683-9690. https://doi.org/10.1016/j.biortech.2011.07.087

Prathiba, S., Kumar, P. S. and Vo, D. V. N. 2022. Recent advancements in microbial fuel cells: A review on its electron transfer mechanisms, microbial community, types of substrates and design for bio-electrochemical treatment. Chemosphere, 286: 131856. https://doi.org/10.1016/j.chemosphere.2021.131856

Puig, S., Serra, M., Coma, M., Cabré, M., Balaguer, M. D. and Colprim, J. 2010. Effect of pH on nutrient dynamics and electricity production using microbial fuel cells. Bioresour. Technol., 101(24): 9594-9599. https://doi.org/10.1016/j.biortech.2010.07.082

Sanchez, J. L., Pinto, D. and Laberty-Robert, C. 2021. Electrospun carbon fibers for microbial fuel cells: A novel bioanode design applied to wastewater treatment. Electrochim. Acta, 373: 137864. https://doi.org/10.1016/j.electacta.2021.137864

Tan, W. H., Chong, S., Fang, H. W., Pan, K. L., Mohamad, M., Lim, J. W., Tiong, T. J., Chan, Y. J., Huang, C. M. and Yang, T. C. K. 2021. Microbial Fuel Cell Technology-A Critical Review on Scale-Up Issues. Processes, 9(6): 985. https://doi.org/10.3390/pr9060985

Taskan, E. and Hasar, H. 2015. Comprehensive comparison of a new tin-coated copper mesh and a graphite plate electrode as an anode material in microbial fuel cell. Appl. Biochem. Biotechnol., 175(4): 2300-2308. https://doi.org/10.1007/s12010-014-1439-4

Wang, Y., Wu, J., Yang, S., Li, H. and Li, X. 2018. Electrode modification and optimization in air-cathode single-chamber microbial fuel cells. Int. J. Environ. Res. Public Health, 15(7): 1349. https://doi.org/10.3390/ijerph15071349

Wang, Y., Zhou, L., Luo, X., Zhang, Y., Sun, J., Ning, X. and Yuan, Y. 2019. Solar-heated graphene sponge for high-efficiency clean-up of viscous crude oil spill. J. Clean. Prod., 230: 995-1002. https://doi.org/10.1016/j.jclepro.2019.05.178

Wei, J., Liang, P. and Huang, X. 2011. Recent progress in electrodes for microbial fuel cells. Bioresour. Technol., 102(20): 9335-9344. https://doi.org/10.1016/j.biortech.2011.07.019

Xie, X., Yu, G., Liu, N., Bao, Z., Criddle, C. S. and Cui, Y. 2012. Graphene–sponges as high-performance low-cost anodes for microbial fuel cells. Energy Environ. Sci., 5(5): 6862. https://doi.org/10.1039/c2ee03583a

Yaqoob, A. A., Ibrahim, M. N. M. and Rodríguez-Couto, S. 2020. Development and modification of materials to build cost-effective anodes for microbial fuel cells (MFCs): An overview. Biochem. Eng. J., 164: 107779. https://doi.org/10.1016/j.bej.2020.107779

Yuan, Y., Zhao, B., Zhou, S., Zhong, S. and Zhuang, L. 2011. Electrocatalytic activity of anodic biofilm responses to pH changes in microbial fuel cells. Bioresour. Technol., 102(13): 6887-6891. https://doi.org/10.1016/j.biortech.2011.04.008

Zhang, L., Li, C., Ding, L., Xu, K. and Ren, H. 2011. Influences of initial pH on performance and anodic microbes of fed-batch microbial fuel cells. J. Chem. Technol. Biotechnol., 86(9): 1226-1232. https://doi.org/10.1002/jctb.2641

Zhang, Q., Hu, J. and Lee, D.J. 2016. Microbial fuel cells as pollutant treatment units: Research updates. Bioresour. Technol., 217: 121-128. https://doi.org/10.1016/j.biortech.2016.02.006

Zhao, H., Chen, H., Xu, C., Li, Z., Ding, B., Dou, H. and Zhang, X. 2021. Charge Storage Mechanism of an Anthraquinone-Derived Porous Covalent Organic Framework with Multiredox Sites as Anode Material for Lithium-Ion Battery. ACS Appl. Energy Mater., 4(10): 11377-11385. https://doi.org/10.1021/acsaem.1c02200

Zhao, N., Ma, Z., Song, H., Xie, Y. and Zhang, M. 2019. Enhancement of bioelectricity generation by synergistic modification of vertical carbon nanotubes/polypyrrole for the carbon fibers anode in a microbial fuel cell. Electrochim. Acta, 296: 69-74. https://doi.org/10.1016/j.electacta.2018.11.039

## ORCID DETAILS OF THE AUTHORS

Emilio Steven C. Navarro: https://orcid.org/0000-0003-1023-2617
Melissa May M. Boado: https://orcid.org/0000-0001-9596-5574

Nature Environment and Pollution Technology
An International Quarterly Scientific Journal

p-ISSN: 0972-6268
(Print copies up to 2016)
e-ISSN: 2395-3454

Vol. 23 | No. 3 | pp. 1363-1374 | 2024

Original Research Paper

https://doi.org/10.46488/NEPT.2024.v23i03.009

Open Access Journal

# Heavy Metal Contamination of Surface Sediments-Soil Adjoining the Largest Copper Mine Waste Dump in Central India Using Multivariate Pattern Recognition Techniques and Geo-Statistical Mapping

**Anoop Kant Shukla*†, Manoj Pradhan* and Onkar Nath Tiwari****
*Mining Engineering Department, National Institute of Technology, Raipur-492010, Chhattisgarh, India
**Hindustan Copper Limited; Kolkata-700019, India
†Corresponding author: Anoop Kant Shukla; anoop5052@gmail.com

**Nat. Env. & Poll. Tech.**
**Website: www.neptjournal.com**

*Received:* 10-12-2023
*Revised:* 20-01-2024
*Accepted:* 23-01-2024

**Key Words:**
Leaching
Sediment contamination
Soil contamination
Sulphide ore mining
Hierarchal cluster analysis

## ABSTRACT

This detailed study assessed heavy metal contamination of sediments/soil near central India's largest copper mining area using 38 sampling sites within 10 km of the mine using atomic absorption spectroscopy. This study utilized multivariate pattern recognition methods, namely hierarchical clustering analysis (HCA) and principal component analysis (PCA), for source identification. Twelve parameters, i.e., copper (Cu), manganese (Mn), cobalt (Co), zinc (Zn), nickel (Ni), lead (Pb), organic matter (OM), cation exchange capacity (CEC), soil pH, distance (D), and elevation (E) were analyzed. The hierarchical cluster analysis (HCA) was used to analyze the sample sites with similar metal contamination and principal component analysis (PCA) was used to analyze the relationship between the parameters as well as to identify sources of heavy metal pollution. Three major pollution hotspots were detected by AHC and were classified as unpolluted/low pollution sites (UPS: mean concentration factor of 1.35 for Cu), highly polluted sites (HPS: mean concentration factor of 22 for Cu), and extremely polluted sites (EPS: mean concentration factor of 74 for Cu). PCA revealed three hidden factors/components, namely PC1 (explaining 38% of the variability), PC2 (18% of the variability), and PC3 (14% of the variability). Metals showed strong positive loading in PC1, explaining the highest variability. The mean content of Cu in soil/sediment samples was 502.526 mg/kg. The mean copper content was 10 times higher than the natural crustal value of 45mg/kg, indicating severe pollution in several sites around the study area. Mapping of copper contamination was conducted to reveal the spatial distribution of copper contamination using QGIS. This study exposes the heavy metal contamination level in surface sediments/soil and the effectiveness of pattern recognition techniques for the assessment of multivariate datasets in discerning spatial disparities and identifying the contamination causes.

## INTRODUCTION

The soil can store anthropogenic and natural contaminants. Under some conditions, soils can discharge hazardous compounds into the environment, contaminating groundwater food chains (Lu & Bai 2010, C. S. C. Wong et al. 2006). Heavy metals like Pb, Cu, Co, Ni, and others were found at elevated amounts in soils in numerous cities worldwide (Ajmone-Marsan & Biasioli 2010, Biasioli et al. 2006, Chen et al. 2005, Chirenje et al. 2004, Jarva et al. 2009, Lee et al. 2006). Location and concentration data alone cannot uncover hidden heavy metal linkages and distribution patterns. Univariate statistics such as mean, median, mode, etc., cannot discern spatial patterns in soil/sediment heavy metal distribution. Spatial impact studies use multivariate statistics such as Agglomerative Hierarchal Clustering (AHC) and Principal Component Analysis (PCA). These methods can be used as suitable tools to identify the sources of contamination (Facchinelli et al. 2001, Li et al. 2013, Tariq et al. 2008). Mining of minerals causes the removal of rock located beneath the earth's surface. When the mined mineral is brought to the surface, the minerals react with air and water (in the form of moisture), leading to various chemical interactions. If the rock mass contains sulfide minerals like iron pyrite ($FeS_2$), it can react with oxygen and water to produce an acidic discharge known as Acidic Mine Drainage (AMD). Large open pit porphyry copper mines produce copper sulfides (Gordon et al. 2006, Greenwood & Earnshaw 1984). Copper ore mining sites with sulfide content can, therefore, produce AMD (Shukla et al. 2018). Heavy metals in sediments, soil, and water around mining operations come from acid mine drainage (Meadows & Carpenter 1997, Swarnakar et al. 2023). This study investigates

heavy metal contamination levels in surface sediments/soil and the effectiveness of pattern recognition techniques for assessing and identifying the contamination causes around mine waste dumps.

## STUDY AREA

The study area is a large central Indian mining project. It has 40% of India's copper reserves (Pandey et al. 2007). The study area covers an open-cast mine and an ore processing plant with two sites for the disposal of waste, namely a mines waste dump (MWD) and tailing storage facility (TSF), as shown in Fig. 1. Chalcopyrite ($CuFeS_2$) with a grade of 1% copper is the main ore mined. The open pit is 2200 meters in length and 500 m in width (Tiwari et al. 2017). The study region spans latitude 21.9406920 N to 22.0836800 N and longitude 80.6567170 E to 80.7607280 E. Fig. 2 shows two perennial rivers flowing in the neighborhood of the study area known as 'Banjar' River located in the north-east quadrant of the study area and 'Son' river located in the southern quadrant of the study area with sampling sites. Digital elevation model demarcated both the river basins and revealed that there was no cross contamination as the basins showed no intersection between the two rivers.

## MATERIALS AND METHODS

### Sample Collection and Analysis

A Digital Elevation Model (DEM) was created using Shuttle Radar Topography Mission (SRTM) data files (N21E080. SRTMGL1.hgt and N22E080.SRTMGL1.hgt) obtained from NASA's Earthdata portal. This DEM was developed using QGIS software version LTR 3.10. Sampling locations for rivers and tributaries were chosen based on their natural topographic flow. Additionally, samples from the roadside or exposed soil were collected to analyze any additional pollution source present in the study area Fig. 2 & 3. In total, 38 samples were collected in duplicate at a depth of 10 cm from various river and tributary points. To prevent contamination, each sample was collected using a plastic tool and then sealed in a marked polypropylene Ziploc bag. The precise locations of these samples were recorded with GPS. Any pebbles, rock fragments, or plant matter were removed from the samples. Subsequently, the samples were pulverized using an agate mortar, finely crushed, sifted through a 200-mesh screen, and stored in polyethylene containers that had been pre-cleaned with a mixture of nitric acid and distilled water in a 3:1 ratio.

Each sample was dried to constant weight at 108°C. After drying, 1g of each sample was digested according to the technique recommended by the US EPA (Environmental Protection Agency, 1996). The leachate analysis was done using an Atomic Absorption Spectrophotometer (AAS, model AA8000 FG, Lab India). The samples were analyzed for Copper (Cu), Manganese (Mn), Cobalt (Co), Zinc (Zn), Nickel (Ni), Lead (Pb), and Iron (Fe). Soil pH, CEC, and OM were determined using standard methods (BIS 2720-22 2020, BIS 2720-24 2020, BIS 2720-26 2021).


Fig. 1: Study area (Courtesy: Google® Earth).

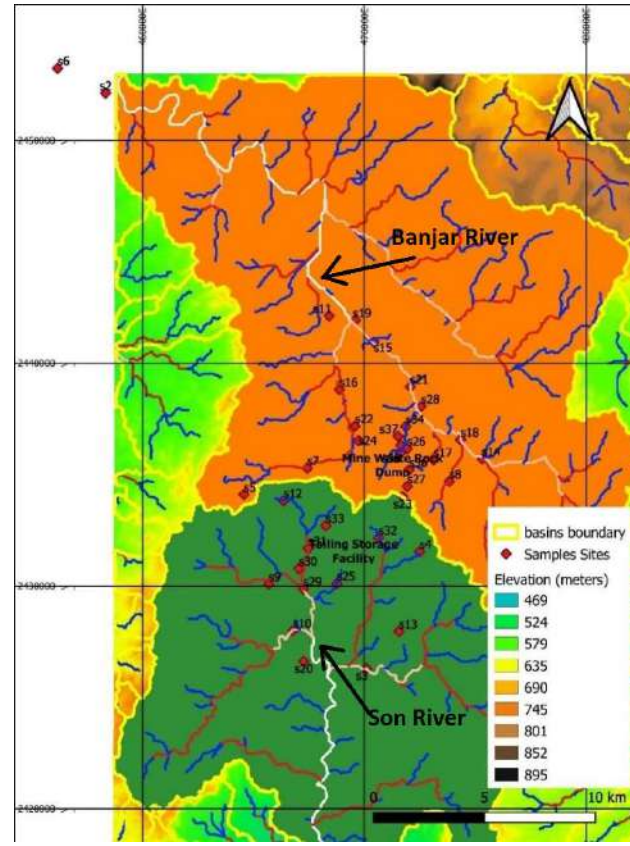


Fig. 2: SRTM digital elevation model clipped to study area and drainage channels.


Fig. 3: (a) to (d) Affected area with green-colored deposits over soil surface adjoining a mine waste dump.

**Analysis of Data Set**

The data set generated using the methodology mentioned in previous section was subjected to statistical treatment. Since different metals have different crustal abundance, therefore Contamination Factor (CF) was used instead of the actual concentration. It is defined as follows:

$$Cf_x = {C_i}/{C_{background}} \quad \ldots(1)$$

Where $C_i$ is the contamination level of the metal *'i'* under study, and $C_{background}$ is the background occurrence level of the same metal 'i'(Varol 2011). The parameters with larger concentrations heavily skewed the analysis results, and the order and range of concentrations of the several physicochemical characteristics varied significantly, suggesting that the dataset is not distributed normally. The Shapiro-Wilks (S-W) test was used to test for normality, and it was found that, except for Zn, all metals failed the S-W normality test. Therefore, the Box-Cox (B-C) transformation of the data matrix was conducted to reduce the impact of outliers, and the dataset that had been B-C transformed provided the best match for the S-W normality test (Box & Cox 1964). The S-W test revealed that, with 95% confidence, all the variables for the B-C converted data were normally distributed. Kaiser-Meyer-Olkin (KMO) and Bartlett's tests assessed data appropriateness for PCA. KMO measures sampling adequacy by estimating latent factor variance in variables. Bartlett's sphericity test determines if the correlation matrix is an identity matrix, suggesting unrelated variables. The data analysis was performed in MS Excel® with XLSTAT® (Addinsoft 2023) add-in.

**Cluster analysis:** CA's fundamental goal is to organize data sets into clusters that are related yet distinct (Razmkhah et al. 2010). AHC is a bottom-up clustering algorithm. The contamination factor dataset was analyzed using Ward's AHC approach (Ward 1963) to find multivariate commonalities between sampling sites at different sampling points. Numerous researchers have reported using the CA approach to evaluate the quality of water (Astel et al. 2007, Hussain et al. 2008, Singh et al. 2005). Similarly, numerous studies have utilized AHC on soil data as well (Dragović et al. 2008, Lamontagne & Camire 1987, Micó et al. 2006, Navas & Machín 2002, Pîrnău et al. 2020, Tume et al. 2006).

Table 1: Basic statistics of heavy metals concentration in the study area.

| | Cu [mg.kg$^{-1}$] | Mn [mg.kg$^{-1}$] | Co [mg.kg$^{-1}$] | Zn [mg.kg$^{-1}$] | Ni [mg.kg$^{-1}$] | Pb [mg.kg$^{-1}$] |
|---|---|---|---|---|---|---|
| Mean | 502.526 | 702.00 | 24.84 | 24.21 | 28.76 | 23.55 |
| Median | 83.5 | 395.00 | 23.25 | 23.00 | 24.00 | 19.50 |
| Min | 5 | 10.00 | 7.00 | 5.00 | 7.00 | 5.00 |
| Max | 3408 | 5030.00 | 55.00 | 50.00 | 99.00 | 97.00 |
| Std dev. (n-1) | 846.809 | 898.23 | 13.20 | 9.67 | 18.47 | 17.23 |

**Principal component analysis:** PCA minimizes data variability to reveal patterns in the dataset and emphasize dissimilarities and reduction in variables. The eigenvalues and eigenvectors in PCA are extracted from the covariance matrix, which also reflects the dispersion of the observed parameters. When we multiply the initially correlated variables by a vector of coefficients (loadings or scores), we produce new orthogonal variables called principal components (PCs). The original variables are combined in a weighted linear fashion by the PCs (Wunderlin et al. 2001). Projecting data onto a new axis creates a new variable from a PC and an eigenvector. Although there are numerous PCs used as original variables, PCs that provide details on the most important traits, summarize the entire data set, and enable data reduction with little information loss are selected (Helena et al. 2000).

## RESULTS AND DISCUSSION

### Agglomerative Hierarchal Clustering of Heavy Metals Dataset

The basic statistics of heavy metals contamination levels (mg.kg$^{-1}$) and their respective contamination factor (CF) are provided in Table 1 & Table 2. Copper and Manganese had a greater mean and standard deviation than the other heavy metals, whereas Zn had the lowest standard deviation. Cu's greater mean concentration and high standard deviation suggest abnormal distribution suggesting a multivariate statistical study. The background concentration for Cu, Mn, Co, Zn, Ni, and Pb is provided in Table 3.

The contamination factor data was subjected to the AHC routine available in XLSTAT®. The AHC algorithm clustered data using Euclidean distance for Dissimilarity and Ward's method for Agglomeration. This resulted in the clustering of the data set into three distinct clusters/groups (Fig. 4). A total of 38 sample locations were grouped into three clusters: 25 unpolluted/low pollution sites (UPS), 11 highly polluted sites (HPS) and 2 extreme pollution sites (EPS). CA indicates that one sampling point per cluster is sufficient to represent the soil quality of the whole cluster spatially. The central sample sites for each cluster are shown in Table 4.

Table 2: Sample-wise contamination factors in the study area.

| Samples | CF(Cu) | CF(Mn) | CF(Co) | CF(Zn) | CF(Ni) | CF(Pb) |
|---|---|---|---|---|---|---|
| s1 | 0.11 | 0.43 | 0.42 | 0.21 | 0.32 | 0.65 |
| s2 | 0.11 | 0.43 | 0.53 | 0.20 | 0.30 | 0.50 |
| s6 | 0.27 | 0.72 | 1.05 | 0.31 | 0.34 | 0.80 |
| s7 | 0.27 | 0.53 | 1.50 | 0.16 | 0.26 | 0.45 |
| s8 | 0.29 | 0.65 | 1.11 | 0.18 | 0.20 | 0.40 |
| s11 | 0.51 | 0.71 | 1.03 | 0.40 | 0.40 | 0.65 |
| s14 | 1.24 | 1.00 | 1.58 | 0.32 | 0.94 | 1.60 |
| s15 | 1.33 | 0.13 | 1.11 | 0.20 | 0.62 | 1.30 |
| s16 | 1.27 | 0.83 | 0.71 | 0.14 | 0.40 | 0.85 |
| s17 | 1.33 | 0.12 | 0.39 | 0.05 | 0.14 | 0.25 |
| s18 | 1.42 | 0.18 | 1.97 | 0.25 | 0.98 | 1.55 |
| s19 | 1.44 | 0.24 | 0.63 | 0.17 | 0.40 | 0.70 |
| s21 | 2.40 | 0.23 | 0.39 | 0.08 | 0.14 | 0.25 |
| s22 | 2.76 | 0.29 | 1.50 | 0.23 | 0.72 | 2.35 |
| s23 | 16.07 | 1.30 | 1.66 | 0.29 | 0.78 | 1.10 |
| s24 | 3.69 | 2.57 | 2.89 | 0.29 | 1.98 | 2.45 |
| s26 | 5.73 | 0.54 | 0.87 | 0.27 | 0.70 | 1.45 |
| s27 | 17.53 | 1.19 | 1.50 | 0.23 | 1.16 | 1.80 |
| s28 | 9.82 | 0.30 | 0.79 | 0.11 | 0.22 | 0.40 |
| s34 | 27.11 | 2.68 | 2.68 | 0.24 | 1.14 | 1.80 |
| s35 | 33.07 | 1.83 | 1.11 | 0.23 | 0.68 | 1.65 |
| s36 | 51.33 | 1.44 | 2.61 | 0.24 | 0.56 | 1.45 |
| s37 | 72.29 | 0.45 | 1.58 | 0.48 | 0.54 | 0.90 |
| s38 | 75.73 | 0.25 | 0.79 | 0.53 | 0.78 | 1.55 |
| s3 | 0.11 | 0.43 | 0.74 | 0.21 | 0.30 | 0.30 |
| s4 | 0.13 | 0.50 | 0.58 | 0.19 | 0.22 | 0.35 |
| s5 | 0.22 | 0.16 | 0.37 | 0.41 | 0.34 | 0.75 |
| s9 | 0.31 | 0.45 | 1.18 | 0.35 | 0.30 | 0.65 |
| s10 | 0.44 | 0.48 | 1.50 | 0.26 | 0.36 | 0.70 |
| s12 | 0.80 | 1.28 | 1.82 | 0.29 | 1.00 | 1.40 |
| s13 | 1.11 | 1.06 | 1.97 | 0.31 | 0.90 | 1.15 |
| s20 | 2.27 | 0.01 | 0.71 | 0.14 | 0.22 | 0.75 |
| s25 | 4.09 | 0.08 | 1.26 | 0.23 | 0.52 | 2.00 |
| s29 | 10.87 | 0.42 | 1.42 | 0.26 | 0.70 | 1.05 |
| s30 | 12.51 | 0.45 | 1.34 | 0.22 | 0.44 | 1.55 |
| s31 | 20.29 | 1.06 | 2.68 | 0.26 | 0.76 | 4.85 |
| s32 | 21.04 | 1.07 | 2.45 | 0.41 | 0.34 | 0.45 |
| s33 | 23.02 | 0.02 | 1.26 | 0.32 | 0.76 | 1.95 |

Table 3: Background concentration of metals in the study.

| Metal | Background concentration [mg.kg$^{-1}$] | Metal | Background concentration [mg.kg$^{-1}$] |
|---|---|---|---|
| Copper (a) | 45 | Zinc (a) | 95 |
| Manganese (a) | 850 | Nickel (b) | 50 |
| Cobalt (a) | 19 | Lead (a) | 20 |
| (a): (Turekian & Wedepohl 1961), (b) (HS1191/HS1191: Nickel Nutrition in Plants) | | | |

Table 4: Central sample for each cluster.

| Cluster | CF(Cu) | CF(Mn) | CF(Co) | CF(Zn) | CF(Ni) | CF(Pb) |
|---|---|---|---|---|---|---|
| 1 (s16) | 1.270 | 0.830 | 0.710 | 0.140 | 0.400 | 0.850 |
| 2 (s33) | 23.020 | 0.020 | 1.260 | 0.320 | 0.760 | 1.950 |
| 3 (s37) | 72.290 | 0.450 | 1.580 | 0.480 | 0.540 | 0.900 |

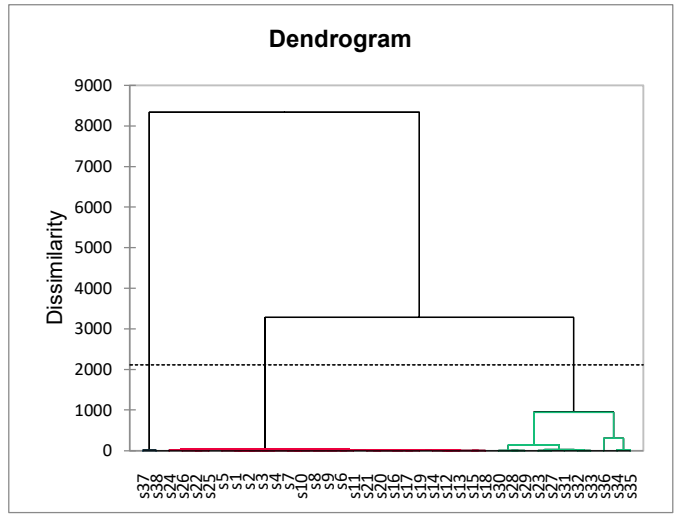


Fig. 4: Dendrogram showing spatial similarities of sampling sites.

Table 5: Basic statics of each cluster.

| | Statistic | $CF_{(Cu)}$ | $CF_{(Mn)}$ | $CF_{(Co)}$ | $CF_{(Zn)}$ | $CF_{(Ni)}$ | $CF_{(Pb)}$ |
|---|---|---|---|---|---|---|---|
| Cluster C1 (Unpolluted Sample Sites – UPS) | No. of Samples | 25 | | | | | |
| | Mean | 1.35 | 0.56 | 1.11 | 0.23 | 0.52 | 0.97 |
| | Standard deviation (n-1) | 1.44 | 0.53 | 0.62 | 0.09 | 0.40 | 0.64 |
| Cluster C2 (Highly Polluted Sample Site – HPS) | No. of Samples | 11 | | | | | |
| | Mean | 22.06 | 1.07 | 1.77 | 0.26 | 0.69 | 1.64 |
| | Standard deviation (n-1) | 11.96 | 0.77 | 0.70 | 0.07 | 0.29 | 1.19 |
| Cluster C3 (Extremely Polluted Samples Sites) | No. of Samples | 2 | | | | | |
| | Mean | 74.01 | 0.35 | 1.19 | 0.51 | 0.66 | 1.23 |
| | Standard deviation (n-1) | 2.43 | 0.14 | 0.56 | 0.04 | 0.17 | 0.46 |

Sample s16 represents cluster UPS (unpolluted sample sites with all CFs close to 1.00), Sample 33 represents cluster HPS (highly polluted sample sites with $CF_{Cu}$ of 23.02, meaning Cu concentration was 23 times the crustal abundance and Sample 37 represents cluster EPS with $CF_{Cu}$ of 72.29 indicating extremely high copper accumulation in cluster C3). The summary of each cluster is presented in Table 5.

According to spatial similarity, three clusters (Table 4 & Fig. 4) are formed with increasing order of metal contamination. The UPS cluster (s1, s2, s6, s7, s8, s11, s14, s15, s16, s17, s18, s19, s21, s22, s24, s26, s3, s4, s5, s9, s10, s12, s13, s20, s25) contains points which are unaffected by the mining waste dump activity because of distance from the mine site. The HPS cluster (s23, s27, s28, s34, s35, s36, s29, s30, s31, s32, s33) contains sample locations that are located near the mine site and receive contamination via the drainage network present in the study area. The EPS cluster contains two locations, namely, s37 and s38, with extremely high copper content because these two locations are adjacent to the mine waste dump (Fig. 2). It can be observed that AHC has segregated the spatial observations in data. The clusters HPS & EPS are polluted sites in the study area and may require attention.

## Principal Component Analysis of the Dataset

With the help of a few independent variables, PCA, a potent pattern recognition approach, can be used to explain the variation of a large dataset made up of many intercorrelated variables. (Ramadan et al. 2000). As demarcated by HCA, the effects of MWD and TSF drainages are critically evaluated through PCA. To evaluate the effects of mining waste dumps (MWD) and tailing storage facilities (TSF), respectively, PCA was used on contamination factor data sets.

Cluster HPS & Cluster EPS served as markers for polluted sites. The PCA was conducted on two data sets. The first dataset included all the clusters named as MWISP dataset (Mine Waste Including Seepage Points), and the second dataset was created by excluding the HPS and EPS clusters MWESP dataset (Mine Waste Excluding Seepage Points). Results of KMO and Bartlett's test are provided in Table 6.

**PCA-spatial impact studies on cluster MWISP (mine waste including seepage points):** PCA was applied to the MWISP dataset, which contains all the sample points collected in the study area. The scree plot indicated 3 PCs

Table 6: Results of KMO and Bartlett's test.

| | Bartlett's sphericity Test (p-Value < 0.05) | | Kaiser-Meyer-Olkin measure of sampling adequacy (adequate KMO > 0.500) |
|---|---|---|---|
| MWISP Dataset | Chi-square (Observed value) | 248.287 | KMO = 0.628 (Test Passed) |
| | Chi-square (Critical value) | 73.311 | |
| | DF | 55 | |
| | p-value (Two-tailed) | <0.0001 | |
| | alpha | 0.050 | |
| MWESP Dataset | Chi-square (Observed value) | 168.134 | KMO = 0.541 (Test Passed) |
| | Chi-square (Critical value) | 73.311 | |
| | DF | 55 | |
| | p-value (Two-tailed) | <0.0001 | |
| | alpha | 0.050 | |

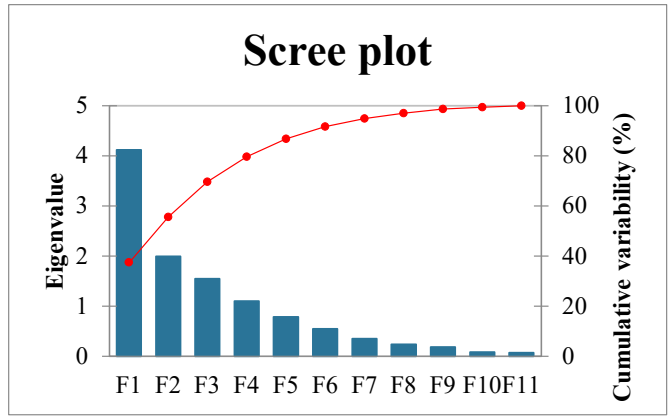


Fig. 5: Scree plot for PCA on MWISP data set.

Table 7: Factor loadings for the MWISP dataset (loadings magnitude>0.5 highlighted in bold).

| | PC1 | PC2 | PC3 |
|---|---|---|---|
| CF(Cu) | **0.773** | **-0.540** | -0.013 |
| CF(Mn) | **0.526** | 0.481 | 0.341 |
| CF(Co) | **0.779** | 0.189 | 0.313 |
| CF(Zn) | **0.527** | 0.223 | -0.499 |
| CF(Ni) | **0.864** | 0.247 | 0.130 |
| CF(Pb) | **0.837** | 0.006 | 0.068 |
| OM | -0.333 | **0.559** | **-0.637** |
| CEC | 0.147 | **0.834** | 0.003 |
| pH | -0.331 | 0.367 | **0.666** |
| distance | **-0.716** | 0.332 | 0.206 |
| elevation | 0.394 | 0.265 | -0.415 |

explaining 70% of the total variance in data, although 4 PCs had eigenvalues more than 1.0. Fig. 5 shows the scree plot of PCs generated by the PCA method on the MWISP dataset.

Table 7 & Fig. 6 provides the factor loadings for the PCA analysis on different Principal Components (PCs). In order to be classified as "strong," "moderate," and "weak," loadings must correspond to absolute loading levels of >0.75, 0.75-0.50, and 0.50-0.30, respectively, according to ((Liu et al. 2003).

The loading plots demonstrated the association between the parameters; the closer the endpoint of variables, the more strongly the values were correlated. (see Fig. 6). It can be observed from Table 7 that the loading for Cu (0.773), Co (0.779), Ni (0.864), and Pb (0.837) in PC1 (explains 37.4 % variance) was strongly positive (factors loadings > 0.75) and for Zn (0.526) and Mn (0.527) the factor loading was moderately positive. It lies between 0.50 – 0.75. The factor loading for the distance(D) parameter was moderately negative (-0.716). This can be explained by the fact that the study area is located near an eco-sensitive zone, and no other means of heavy metal pollution are present. Therefore, being the only source in the study area, the pollution decreases as the distance from the mine site increases. Also, Table 2 shows that the contamination factor is highest for copper with a mean of 11.17, whereas CF for Mn, Co, Zn, Ni, and Pb show a mean value of 0.70, 1.31, 0.25, 0.58 & 1.18, respectively. Indicating high copper contamination in the samples. Therefore, copper dominates over other elements in the polluted samples, and it may also explain the relatively lower loading for PCs of Mn and Zn, which are essential soil elements.

PC1 explains that heavy metal pollution has occurred in the study area with copper contamination to a high degree.

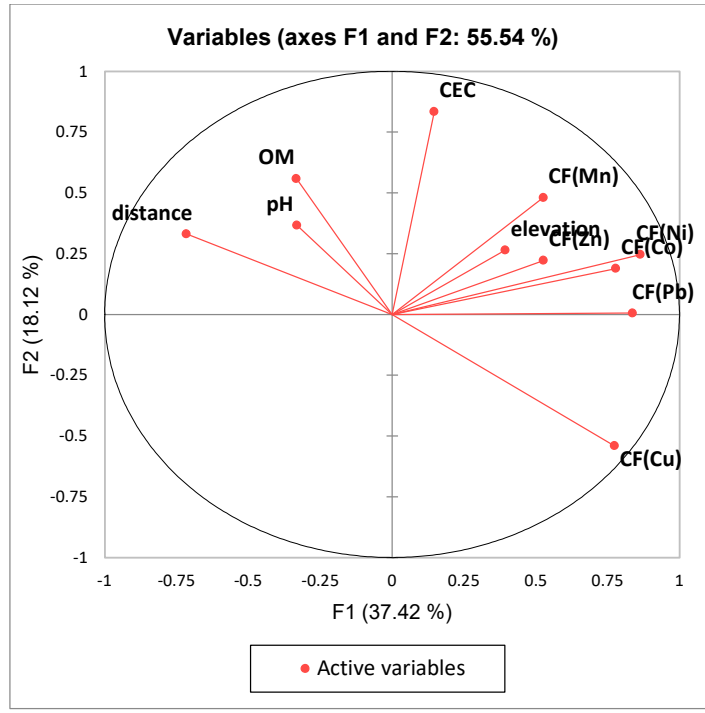


Fig. 6: Loading plot of PCA on MWISP dataset.

Soil pH is negatively correlated with the metal content indicating that the acidic discharge for mine waste dump and tailing storage facility has high metallic content. PC2 explains 18.12% of the variance in the data. It exhibits moderate negative loading of Cu (-0.540), whereas Mn (0.481), Co (0.189), Zn (0.223), Ni (0.247), and Pb (0.006) had low/weak factor loadings. OM (0.559) and CEC (0.834) have moderate and strong positive loading, respectively. The capacity of a particle to exchange positive bases in response to its surroundings is known as the CEC. From the surfaces of clay minerals and organic materials, cations can swap for another positively charged ion (Aprile & Lorandi 2012). Therefore, the presence of OM can increase the CEC of soil. In PC2, negative loading of Cu with positive loading of OM and CEC indicates that acidic discharge from the mine may deplete the OM initially present in the soil and, in turn, accumulate copper in the soil matrix.

The PCA analysis can delineate the process of soil degradation by acidic mine drainage. Initially, fertile soil with high OM is attacked by the acidic discharge consuming the OM. Thus, the pH value of the discharged solution rises, which in turn precipitates heavy metal in the soil. PC3 explains 14% of the variance in the data, with pH (0.666) and OM (-0.637) showing moderate positive and negative loadings. By releasing hydrogen ions associated with organic anions or by nitrifying in an open system, organic matter typically reduces soil pH (Porter 1980). The biplot of PC1 and PC2 with sample data and parameters provides

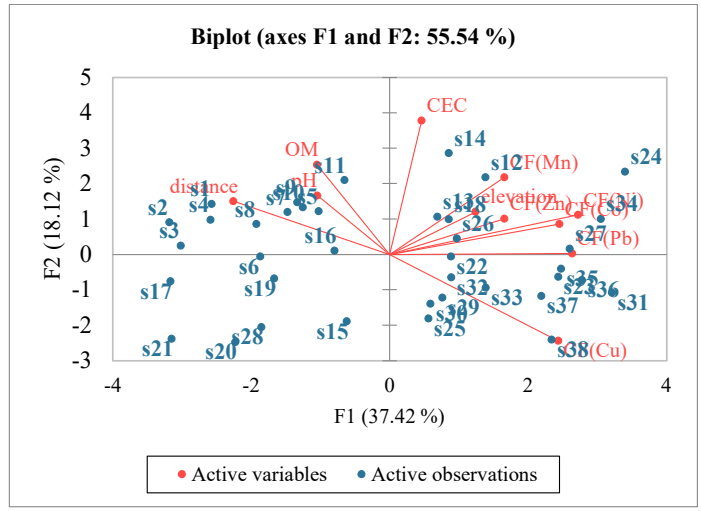


Fig. 7: Biplot of PCs with Sample Locations.

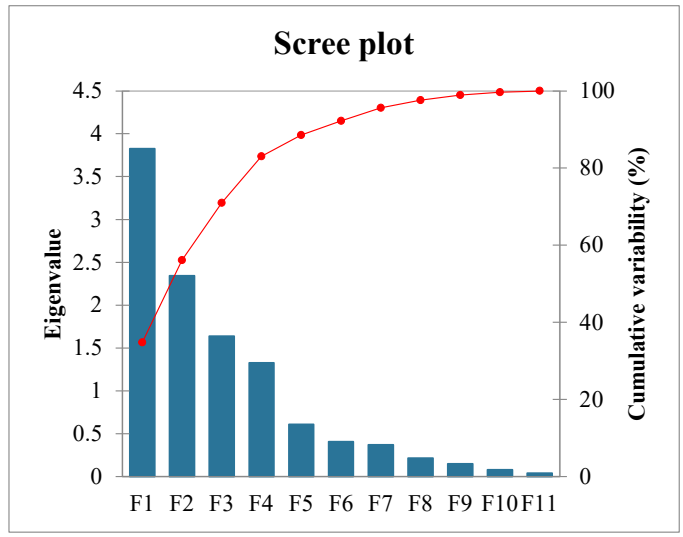


Fig. 8: Scree plot of PCs.

Table 8: Factor loadings for the MWESP dataset (loadings >0.5 highlighted in bold).

| | F1 | F2 | F3 |
|---|---|---|---|
| CF(Cu) | 0.441 | **-0.820** | 0.181 |
| CF(Mn) | **0.609** | 0.462 | -0.250 |
| CF(Co) | **0.833** | -0.066 | -0.286 |
| CF(Zn) | **0.612** | **0.505** | -0.055 |
| CF(Ni) | **0.933** | -0.114 | -0.195 |
| CF(Pb) | **0.844** | -0.321 | -0.088 |
| OM | 0.005 | **0.792** | 0.414 |
| CEC | **0.589** | 0.491 | 0.270 |
| pH | 0.070 | 0.128 | **-0.544** |
| distance | -0.360 | 0.418 | **-0.639** |
| elevation | 0.364 | 0.145 | **0.680** |

a spatial distribution of heavy metals in the study area (Fig. 7).

**PCA-spatial impact studies on MWESP (mine waste excluding seepage points):** PCA was conducted on a dataset excluding the seepage points, namely MWESP (Mine Waste Excluding Seepage Points). The scree plot indicated 3 PCs explaining 70% of the total variance in data, although 4 PCs had eigenvalues more than 1.0. Fig. 8 shows the scree plot of PCs generated by the PCA method on the MWESP dataset.

Table 8 provides the factor loadings of PCs after PCA analysis on the MWESP dataset. It can be observed that Copper had a strong positive loading of 0.773 in PC1 of the MWISP dataset, whereas it falls even below 0.5 to 0.441 in PC1 of the MWESP dataset. This indicates that sample locations directly receive AMD drainage emanating from mine waste dumps and tailing storage facilities. AMD contains Copper and these locations are affected by it. The dataset MWESP contains unpolluted or very low contamination sites; therefore, typical soil behavior is observed with CEC-linked metal content in the soil with a moderate positive loading of 0.589 in PC1.

PC2 explains 21% of the variance in the dataset, where OM is positively correlated with Zn and Mn and a strongly negative correlation with Cu. High OM loadings mean un-

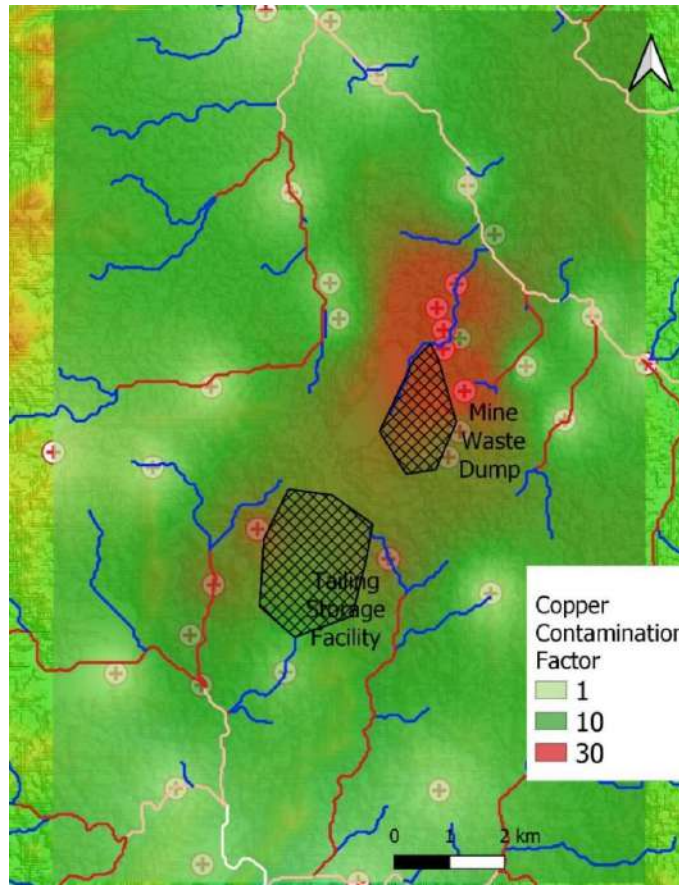


Fig. 9: Spatial map of copper contamination factor using inverse distance weighing method.

disturb soil with positive correlation with essential elements like Zn, Mn and Co. PC3 explains 14% of the variance in data with moderate negative loading of pH (-0.544), Distance (-0.639) and moderate positive loading of elevation (0.680). The negative correlation between elevation and pH is because the mining area is located at a relatively higher elevation; therefore, soil quality near the mine site is acidic due to the impact of acidic discharge by the mine waste sites.

### Spatial Mapping of Copper Contamination Using Geostatistical Inverse Distance Weighing Method

The Inverse Distance Weighting (IDW) method is a spatial analysis and geo-statistics technique primarily used for interpolation. IDW is based on the premise that spatial entities that are close to each other are more alike than those further apart (Shepard 1968). The general formula for IDW is as follows:

$$Zp = \frac{\sum_{i=1}^{i=n}\left(Z_i / d_i{}^p\right)}{\sum_{i=1}^{i=n}\left(1 / d_i{}^p\right)}$$

Here, Zp is the estimated value at point (p), $Z_i$ is the known value at the (i)-th point, ($d_i$) is the distance between the point (i) and (p), and ($p$) is a power parameter that dictates the rate at which influence decreases with distance. The distance is typically calculated using Euclidean distance, though other distance metrics can be used. IDW is employed in various fields such as meteorology, geology, agriculture, and environmental science for interpolating data like temperature, mineral concentrations, and pollution levels. The copper contamination is shown in the red-shaded region in Fig. 9.

A spatial map of copper contamination was generated using the Inverse Distance Weighing method in QGIS software. It can be observed that a significant elevation of copper content is present in the vicinity of the Mine Waste Dump and Tailing Storage Facility within 1.25 kilometers of waste sites in the study area.

## CONCLUSIONS

The study revealed that 13 out of the 38 samples (HPS & EPS Clusters) showed signs of contamination however, it is contained to flow paths. The soil samples not located on the flow paths indicated little to no contamination. The contaminated sites are situated along the drainage routes for AMD seepage emanating from the two mine waste sites (MWD & TSF), indicating that such flow paths are particularly vulnerable to Acid Mine Drainage (AMD) effects.

This study examined how mine waste dumps/storages and drainage from tailing storage facilities affected surface soil/sediments using multivariate statistical approaches. PCA and HCA were used to evaluate spatial variation in the complicated data. AHC categorization found three statistically significant soil heavy metal clusters. The PCA analysis between MWISP and MWESP datasets shows that excluding seepage spots from mining waste dumps and tailing storage facilities reduces pollution throughout the study area. PCA found several correlations: (1) Heavy metal content returns to normal with an increase in distance from the mining site. (2) Copper dominates other elements in polluted samples and lowers PC loadings of soil elements such as Mn and Zn. (3) Acidic mine discharge may deplete soil OM and increase soil matrix copper by precipitation and mechanical deposition. PCA analysis shows how acidic mine drainage degrades soil quality. The acidic discharge attacks fertile soil with high OM, consuming it and raising the pH, which precipitates heavy metals in the soil. Multivariate statistical methods helped analyze complicated data and understand their spatial variance by eliminating redundant data variables.

The TSF and MWD were identified as probable AMD sites during the field survey; therefore, mine waste is an environmental hazard and must be taken seriously. The majority of heavy metal accumulation associated with Acid Mine Drainage (AMD) in the study area was attributed to the Tailings Storage Facility (TSF) and Mine Waste Dumps (MWD). It is essential to segregate these areas from nearby drainage systems and ensure that their discharge is confined within the boundary of the mine site.

## ACKNOWLEDGEMENT

Anoop Kant Shukla, Manoj Pradhan, and Onkar Nath Tiwari conceived and designed the research work. Anoop Kant Shukla and Manoj Pradhan conducted the experiments. Anoop Kant Shukla analyzed the data and wrote the manuscript. All authors read and approved the manuscript.

## REFERENCES

Addinsoft. 2023. XLSTAT statistical and data analysis solution (XLSTAT 2022.1.1). Addinsoft, New York, USA.

Ajmone-Marsan, F. and Biasioli, M. 2010. Trace elements in soils of urban areas. Water, Air, & Soil Pollut., 213(1): 121-143. https://doi.org/10.1007/S11270-010-0372-6

Aprile, F. and Lorandi, R. 2012. Evaluation of cation exchange capacity (cec) in tropical soils using four different analytical methods. J. Agric. Sci., 4(6): p278. https://doi.org/10.5539/JAS.V4N6P278

Astel, A., Tsakovski, S., Barbieri, P. and Simeonov, V. 2007. Comparison of self-organizing maps classification approach with cluster and principal components analysis for large environmental data

sets. Water Res., 41(19): 4566-4578. https://doi.org/10.1016/J.WATRES.2007.06.030

Biasioli, M., Barberis, R. and Ajmone-Marsan, F. 2006. The influence of a large city on some soil properties and metals content. Sci. Total Environ., 356(1-3): 154-164. https://doi.org/10.1016/J.SCITOTENV.2005.04.033

BIS 2720-22. 2020. BIS 2720-22. Bureau of Indian Standards. Retrieved from https://archive.org/details/gov.in.is.2720.22.1972

BIS 2720-24. 2020. BIS 2720-24. Bureau of Indian Standards. Retrieved from https://archive.org/details/gov.in.is.2720.24.1976

BIS 2720-26. 2021. BIS 2720-26. Bureau of Indian Standards. Retrieved from https://archive.org/details/gov.in.is.2720.26.1987

Box, G.E.P. and Cox D.R. 1964. An analysis of transformations. J. R. Stat. Soc. B., 26. https://www.jstor.org/stable/2984418

Chen, T.B., Zheng, Y.M., Lei, M., Huang, Z.C., Wu, H.T., Chen, H., Fan, K.K., Yu, K., Wu, X. and Tian, Q.Z. 2005. Assessment of heavy metal pollution in surface soils of urban parks in Beijing, China. Chemosphere, 60(4): 542-551. https://doi.org/10.1016/J.CHEMOSPHERE.2004.12.072

Chirenje, T., Ma, L.Q., Reeves, M. and Szulczewski, M. 2004. Lead distribution in near-surface soils of two Florida cities: Gainesville and Miami. Geoderma, 119(1-2): 113-120. https://doi.org/10.1016/S0016-7061(03)00244-1

Dragović, S., Mihailović, N. and Gajić, B. 2008. Heavy metals in soils: distribution, relationship with soil characteristics and radionuclides and multivariate assessment of contamination sources. Chemosphere, 72(3): 491-495. https://doi.org/10.1016/j.chemosphere.2008.02.063

Environmental Protection Agency, U. 1996. Method 3050b acid digestion of sediments, sludges, and soils 1.0 scope and application. Method 3050B: Acid Digestion of Sediments, Sludges, and Soils. https://www.epa.gov/sites/default/files/2015-06/documents/epa-3050b.pdf

Facchinelli, A., Sacchi, E. and Mallen, L. 2001. Multivariate statistical and GIS-based approach to identify heavy metal sources in soils. Environ. Pollut., 114(3): 313-324. https://doi.org/10.1016/S0269-7491(00)00243-8

Gordon, R.B., Bertram, M. and Graedel, T.E. 2006. Metal stocks and sustainability. Proc. Natl. Acad. Sci. U.S.A., 103(5): 1209-1214. https://doi.org/10.1073/pnas.0509498103

Greenwood, N.N. and Earnshaw, A. 1984. Chemistry of the Elements (1st Edition), 268-327.

Helena, B., Pardo, R., Vega, M., Barrado, E., Fernandez, J.M. and Fernandez, L. 2000. Temporal evolution of groundwater composition in an alluvial aquifer (Pisuerga River, Spain) by principal component analysis. Water Res., 34(3): 807-816. https://doi.org/10.1016/S0043-1354(99)00225-0

HS1191/HS1191: Nickel Nutrition in Plants. Retrieved November 28, 2023, from https://edis.ifas.ufl.edu/publication/HS1191

Hussain, M., Ahmed, S.M. and Abderrahman, W. 2008. Cluster analysis and quality assessment of logged water at an irrigation project, eastern Saudi Arabia. J. Environ. Manage., 86(1): 297-307. https://doi.org/10.1016/J.JENVMAN.2006.12.007

Jarva, J., Tarvainen, T., Lintinen, P. and Reinikainen, J. 2009. Chemical characterization of metal-contaminated soil in two study areas in Finland. Water, Air, Soil Pollut., 198(1-4): 373-391. https://doi.org/10.1007/S11270-008-9852-3

Lamontagne, L. and Camire, C. 1987. Soil analysis and numerical classification of the Lanoraie delta, Quebec. Can. J. Soil Sci., 67(3): 417-432. https://doi.org/10.4141/cjss87-041

Lee, C.S.L., Li, X., Shi, W., Cheung, S.C.N. and Thornton, I. 2006. Metal contamination in urban, suburban, and country park soils of Hong Kong: a study based on GIS and multivariate statistics. Sci. Total Environ., 356(1-3): 45-61. https://doi.org/10.1016/J.SCITOTENV.2005.03.024

Liu, C.W., Lin, K.H. and Kuo, Y.M. 2003. Application of factor analysis in the assessment of groundwater quality in a blackfoot disease area in Taiwan. Sci. Total Environ., 313(1-3): 77–89. https://doi.org/10.1016/S0048-9697(02)00683-6

Li, X., Liu, L., Wang, Y., Luo, G., Chen, X., Yang, X., Hall, M.H.P., Guo, R., Wang, H., Cui, J. and He, X. 2013. Heavy metal contamination of urban soil in an old industrial city (Shenyang) in Northeast China. Geoderma, 192(1): 50-58. https://doi.org/10.1016/J.GEODERMA.2012.08.011

Lu, S.G. and Bai, S.Q. 2010. Contamination and potential mobility assessment of heavy metals in urban soils of Hangzhou, China: relationship with different land uses. Environ. Earth Sci., 60(7): 1481-1490. https://doi.org/10.1007/S12665-009-0283-2

Maas, S., Scheifler, R., Benslama, M., Crini, N., Lucot, E., Brahmia, Z., Benyacoub, S. and Giraudoux, P. 2010. Spatial distribution of heavy metal concentrations in urban, suburban and agricultural soils in a Mediterranean city of Algeria. Environ. Pollut. (Barking, Essex: 1987), 158(6): 2294-2301. https://doi.org/10.1016/J.ENVPOL.2010.02.001

Meadows, A.E. and Carpenter, A.A. 1997. Acid Mine Drainage and Groundwater Pollution. Groundwater Pollut. Primer, CE, 4594.

Micó, C., Recatalá, L., Peris, M. and Sánchez, J. 2006. Assessing heavy metal sources in agricultural soils of a European Mediterranean area by multivariate analysis. Chemosphere, 872-863 :(5)65. https://doi.org/10.1016/j.chemosphere.2006.03.016

Navas, A. and Machin, J. 2002. Spatial distribution of heavy metals and arsenic in soils of Aragón (northeast Spain): controlling factors and environmental implications. Appl. Geochem., 17(8): 961-973. https://doi.org/10.1016/S0883-2927(02)00006-9

Pandey, P.K., Sharma, R., Roy, M. and Pandey, M. 2007. Toxic mine drainage from Asia's biggest copper mine at Malanjkhand, India. Environ. Geochem. Health, 29(3): 237-248. https://doi.org/10.1007/s10653-006-9079-4

Pîrnău, R.G., Patriche, C.V., Roşca, B., Vasiliniuc, I., Vornicu, N. and Stanc, S. 2020. Soil spatial patterns analysis at the ancient city of Ibida (Dobrogea, SE Romania), via portable X-ray fluorescence spectrometry and multivariate statistical methods. Catena, 189: 104506. https://doi.org/10.1016/j.catena.2020.104506

Porter, W.M. 1980. Soil acidity: is it a problem in Western Australia? J. Dept. Agric. West. Australia, Ser. 4, 21(4): 126-133. https://researchlibrary.agric.wa.gov.au/journal_agriculture4/vol21/iss4/8

Ramadan, Z., Song, X.H. and Hopke, P.K. 2000. Identification of sources of Phoenix aerosol by positive matrix factorization. J. Air Waste Manag. Assoc. (1995), 50(8): 1308-1320. https://doi.org/10.1080/10473289.2000.10464173

Razmkhah, H., Abrishamchi, A. and Torkian, A. 2010. Evaluation of spatial and temporal variation in water quality by pattern recognition techniques: A case study on Jajrood River (Tehran, Iran). J. Environ. Manage., 91(4): 852-860. https://doi.org/10.1016/j.jenvman.2009.11.001

Shepard, D. 1968. A two-dimensional interpolation function for irregularly-spaced data. Proc. 1968 23rd ACM Natl. Conf. On, 517-524. https://doi.org/10.1145/800186.810616

Shukla, A.K., Pradhan, M. and Tiwari, O.N. 2018. Impact on sediments and water by release of copper from chalcopyrite bearing rock due to acidic mine drainage. AIP Conf. Proc., 1952(1): 020064. https://doi.org/10.1063/1.5032026

Singh, K.P., Malik, A. and Sinha, S. 2005. Water quality assessment and apportionment of pollution sources of Gomti River (India) using multivariate statistical techniques - A case study. Anal. Chim. Acta, 538(1-2): 355-374. https://doi.org/10.1016/J.ACA.2005.02.006

Swarnakar, A.K., Bajpai, S. and Ahmad, I. 2023. Performance evaluation of different soil media by batch-operated pilot-scale horizontal subsurface flow constructed wetlands for wastewater treatment. Pollut., 4(9): 1567-1578. https://doi.org/10.22059/POLL.2023.357480.1855

Tariq, S.R., Shah, M.H., Shaheen, N., Jaffar, M. and Khalique, A. 2008. Statistical source identification of metals in groundwater exposed to industrial contamination. Environ. Monit. Assess., 138(1-3): 159-165. https://doi.org/10.1007/S10661-007-9753-8

Tiwari, O.N., Shukla, A.K., Pradhan Manoj, and Nandy Tapas. 2017. Migration of copper to nearby adjoining surface water bodies from tailing impoundment of an open pit copper mine. Ecol., Environ. Conserv., 24(1): 306-314.

Tume, P., Bech, J., Longan, L., Tume, L., Reverter, F. and Sepulveda, B. 2006. Trace elements in natural surface soils in Sant Climent (Catalonia, Spain). Ecol. Eng., 27(2): 145-152. https://doi.org/10.1016/j.ecoleng.2006.01.004

Turekian, K.K. and Wedepohl, K.H. 1961. Distribution of the elements in some major units of the earth's crust. GSA Bull., 72(2): 175-192. https://doi.org/10.1130/0016-7606(1961)72[175]2.0.CO;2

Varol, M. 2011. Assessment of heavy metal contamination in sediments of the Tigris River (Turkey) using pollution indices and multivariate statistical techniques. J. Hazard. Mater., 195: 355-364. https://doi.org/10.1016/J.JHAZMAT.2011.08.051

Ward, J.H. 1963. Hierarchical grouping to optimize an objective function. J. Am. Stat. Assoc., 58(301): 236-244. https://doi.org/10.1080/01621459.1963.10500845

Wong, C.S.C., Li, X. and Thornton, I. 2006. Urban environmental geochemistry of trace metals. Environ. Pollut., 142(1): 1-16. https://doi.org/10.1016/J.ENVPOL.2005.09.004

Wong, S.C., Li, X.D., Zhang, G., Qi, S.H. and Min, Y.S. 2002. Heavy metals in agricultural soils of the Pearl River Delta, South China. Environ. Pollut., 119(1): 33-44. https://doi.org/10.1016/S0269-7491(01)00325-6

Wunderlin, D.A., María Del Pilar, D., María Valeria, A., Fabiana, P.S., Cecilia, H.A. and María De Los Ángeles, B. 2001. Pattern recognition techniques for the evaluation of spatial and temporal variations in water quality. A Case Study: Suquía River basin (Córdoba-Argentina). Water Res., 35(12): 2881-2894. https://doi.org/10.1016/S0043-1354(00)00592-3

## ORCID DETAILS OF THE AUTHORS

Anoop Kant Shukla: https://orcid.org/0000-0003-2135-9672

Nature Environment and Pollution Technology
An International Quarterly Scientific Journal

p-ISSN: 0972-6268
(Print copies up to 2016)
e-ISSN: 2395-3454

Vol. 23 | No. 3 | pp. 1375-1386 | 2024

Original Review Paper

https://doi.org/10.46488/NEPT.2024.v23i03.010

Open Access Journal

# A Review on Bioremediation of Tannery Effluent using Immobilized Bacteria

**J. Raveena Jayam and Priya Chokkalingam†**

Department of Biotechnology, Dr. M.G.R. Educational and Research Institute, Maduravoyal, Chennai-600095, Tamil Nadu, India

†Corresponding author: Priya Chokkalingam; priya.ibt@drmgrdu.ac.in

**Nat. Env. & Poll. Tech.**
**Website: www.neptjournal.com**

*Received:* 21-12-2023
*Revised:* 19-01-2024
*Accepted:* 23-01-2024

**Key Words:**
Tannery effluent
Bioremediation
Immobilized bacteria
Immobilizing techniques
Bioreactor

## ABSTRACT

Tannery effluent is a significant contributor to contaminants such as heavy metals within the ecosystem. Effluents generally contain heavy metals, and they also contain more bacteria that can thrive in such an environment. Bioremediation has ancestrally been performed using bacteria; in recent decades, the implementation of "immobilized" bacteria has acquired recognition as an intriguing technique due to manifold assistance. This review systematizes a humongous amount of extant literature on multifarious toxicants that can be tackled with immobilized bacteria. We further explore assorted deterministic facets using immobilized bacteria for environmental remediation with an emphasis on encapsulation in biomaterials and their role in detoxifying toxic compounds. We explore multiple techniques for immobilizing bacteria in numerous complementary arrays incorporating multiple species of bacteria, factors that influence the remediation process, such as bioreactor layouts used in pilot, lab-scale applications. Exploits and drawbacks of using immobilized bacteria in fermenters to treat tannery effluent are also described. The imperishable future aspects, recovery of significant commodities, in addition to bioremediation, represent an important incentive of the immobilized treatment process that makes more cost-effective, legitimate treatment enforcement that is also congruent with the precepts of the bioeconomy.

## INTRODUCTION

Tannery effluent is one of the paramount defilements of the world (Suman et al. 2021). For the past few decades, a few treatments and entente were accomplished but still, waste production cannot be invalidated or overturned. Effective tannery effluent treatment and recovery approaches are indispensable and expository for an eco-friendly environment. Biological treatment systems were also superior to toxic chemical forms of treatment and mechanisms (Mehrotra et al. 2021). The Tannery sector has had a crucial impact in several countries, such as China, India, and Brazil. Fairly comprehensive tannery effluent trammels established a significant contribution greatly to economic development.

Moreover, inadequate disposal of tannery effluent poses global hazards, and intensifying emphasis has been placed on mitigating tannery effluent harmful emissions (Zhao et al. 2022). The outflow of tannery effluents without adequate treatment resulted in much greater levels of sources or areas of land (Maheshwari et al. 2017). Tannery effluent undergoes several processes that deodorize the effluent before it is extravasated into the environment. Tannery effluents include substantial quantities of contamination samples due to the comportment of colored and deleterious substances (Shaheen Fathima et al. 2020).

Heavy metals are substantial in manufacturing use and are the most massive environmental toxins (Haso et al. 2022). Heavy metal contamination of the environment poses a significant risk to living organisms that comprise an ecology. Due to various bioaccumulations and nonbiodegradability in origins, heavy metal contamination is a major threat to the environment. Pollutants like lead (Pb), cadmium (Cd), and mercury (Hg) have no process and are hazardous to microbes that live (Haso et al. 2022, Igiri et al. 2018). The Tannery industry is renowned for its high water usage and large discharge of effluent (Zhao et al. 2022). Biodegradation of effluents is a non-toxic, environmentally sustainable, ideal substitute. Current technological innovations in developments in biotechnology presently permit the adjustment of microbes such that one rudimentary method is streamlined, debases more multifaceted substances, and disposes of quantities (Maheshwari et al. 2017). Hence, these organisms (microbial consortia) have been isolated, identified, and used for treating the same (Suman et al. 2021, Maheshwari et al. 2017, Yusif et al. 2016).

Immobilized microbes have been utilized in an array of scientific and industrial initiatives since they were demonstrated to be extraordinarily beneficial in environmental remediation (Mehrotra et al. 2021). Immobilized microbes are utilized in organic compounds,

diagnostic and contaminant analysis, food processing, pharmaceutics, and industrial remediation. The progression of bioengineering and anticipated advancements has incentivized repercussions to immobilize bacteria for attributed reasons. Immobilization of organic material inside determines the components that provide tangible assistance, optimum size, tensile stability, resistance, and highly permeable properties of the biomolecules (Maheshwari et al. 2017). Numerous developments of debilitated bacteria have surfaced, including tannery effluent, which has prompted more findings into core aspects of rendered immobile systems, particularly of immobilization on bacterial consortium in legion frameworks (Mehrotra et al. 2021).

In this review, we provide an overview of the present state of expertise about the use of immobilized bacteria for environmental bioremediation possibilities. We also cover various support matrices, immobilized bacterial cultures and communities, immobilization techniques, nutrients for immobilized bacteria, contaminants treated by immobilized microbes, transfer of mass factors (salinity, pH, and contaminants' toxic effects), and factors that affect the remediation process when using immobilized cells. We wrap up with a quick talk about the difficulties, most recent advancements, and potential future directions**.**

## CATEGORIES OF CARRIERS OR SUPPORT MATERIALS

Inorganic materials, natural organic composites, and synthetic organic composites are three main types of carrier materials used for immobilization (Berillo et al. 2021) (Fig. 1). Ceramic materials, cellulosic, and polymer blends are prevalent as sustaining arrays for microbes or polymers in function (Mehrotra et al. 2021) (Berillo et al. 2021). Furthermore, the discovered bacteria are immobilized on the matrix. Multiple biological variations are induced to enable adjunct and cell expansion inside the rendered immobile lattice (Tuson & Weibel 2013). Multiple synthetic, natural organic substances were examined to determine their capacity to intervene as an impactful provider or layer for the stabilization of bacteria for environmental bioremediation.

Natural organic carriers have been readily accessible, reasonably priced, bio-based, innocuous, the residence of manifold unembellished on apparently biological pattern subsidiary to the assimilated scope. Materials constructed from naturally occurring polymers, including guar gum, pectate, agar, silica gel, chitin, charcoal, lignin, dextrose, hyaluronic, cellulose, and alginate (Fig. 1), have been made by gel formation (Mehrotra et al. 2021) of bioavailable composites mixture with different particle. During the immobilization process, xanthan gum-incapacitated bacteria will not experience rapid physical and chemical variations, and the gel is pliable and consistent (Mehrotra et al. 2021). Chitin is favorable long-term support because it provides presumably defensive peptide structural features that can optimize bacteria association to the identified areas that require it (Labus et al. 2016, Suhag et al. 2015).

Polyvinyl alcohol (PVA), polyacrylamide (PAM), polycarbamoyl sulfonate (PCS), and polyethylene glycol are widely used emulsifiers. Polyethylene (PE), polyurethane (PU), polypropylene (PP), polyacrylonitrile (PAN), and polyvinyl chloride (Fig. 1) are examples of well-known plastic substances (Mehrotra et al. 2020). Biomaterials, already renowned as hydrophilic polyimide emulsions, are increasing in popularity as sustainable formulations for cellular immobilization. Nanogels are just not coherent as a result of their configuration and interplaying structure. The polyimide distinction ascertains the demand for complex

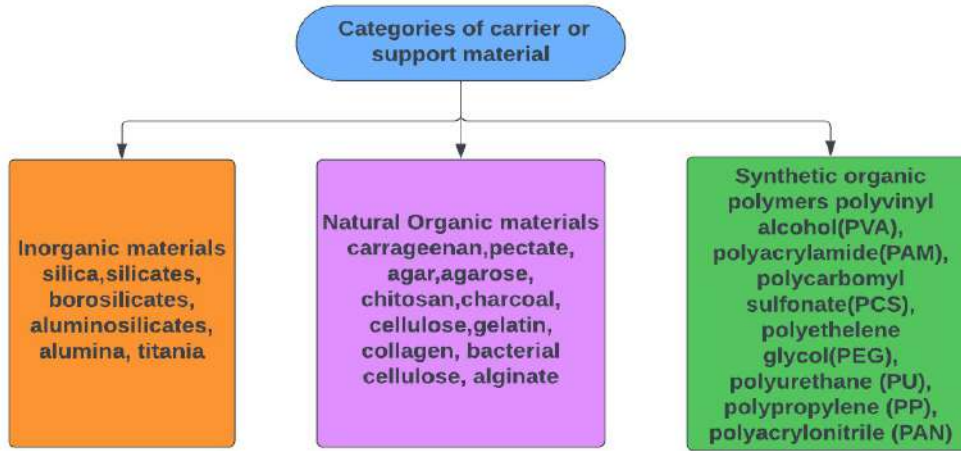


Fig. 1: Support materials.

intermediaries. As a consequence, biomaterials containing paralyzed bacteria are a palatable innovation for remediation implementation (Mehrotra et al. 2020).

## IMMOBILIZED BACTERIA

Immobilization of a culture or an experimental microbial consortium is simpler as well as more effective for an intended area than stabilization of leguminous microbes retrieved from a sophisticated polluted site having various recognized and unidentified bacteria (enteric pathogens to one another). *Agrobacterium radiobacter* J14a, plain atrazine denigrating custom, as well as an instinctual combination of resources of bacteria alienated from an atrazine-polluted particular crop, for instance, were adsorbed utilizing hydroxylation alcohol aerogel (Siripattanakul et al. 2008). A synthesized pathogenic bacteria alliance (comprising 17 isolates) immobilized in chitin beads was researched in yet another investigation for the rehabilitation of a hydrocarbon marshland. In fifteen days, the experimentally pathogenic syndicate healed the pollutant (Angelim et al. 2013, Dong et al. 2017).

Microbes from the rapidly increasing society have been cultivated, and the produced microbes were commodified. The mixture and de-ionized water were evaluated in a conical flask with a volume of 250 milliliters in a 20:80 ratio and emulsified to verify consistency. 3.063 g of sodium alginate was evaluated in the intensive organisms (Maheshwari et al. 2017). The concoction was once implanted using a disinfected hypodermic needle and syringe into a glass beaker of 70 mL of 0.12 M calcium chloride. Gelation appeared at ambient temperature as eventually, the molecular- droplets emerged into close interaction with the calcium solvent. Entire precipitation formed circular droplets with an average diameter of 3-4 mm. At 1-2 h, the granules are empowered to firm up totally and utterly. The micelles were cleaned with a complete calcium cross-integration remedy (Maheshwari et al. 2017). In another survey, Sergio and Bustos identified that sorbent entrapped in calcium-alginate particles was efficacious in ammonia bioremediation in effluent. Integrating transgenic bacteria has emerged as a subsequent mainstream thing to enhance biochips and biocontrol by adjusting the organisms' extant alleles to diagnose and deteriorate specific residues.

### Benefits for Immobilized Bacteria

Nitrogen, carbon dioxide, and micronutrients are vital to the development, prevalence, and feature of various microorganisms (yet if liberated or entrapped). Throughout remediation employing incapacitated bacteria, attain these substances predominantly from either the effluent that is usually embellished in these supplements in addition to the multiverse in which they have been adsorbed. Saez et al. investigated Streptomyces strains to devalue lindane with immobilized bacteria in various matrices. The strains, both free and incapacitated, seemed to be capable of evolving in varying concentrations with contaminants that they utilized as both sources of energy and carbon (Saez et al. 2012). Lindane (Fig. 2) exclusion was reported to be greater in biomolecules than it is in suspended cells. The largest increase of Pseudomonas species. A2, A5, but rather A11 might have been ascertained in a polycrystalline capsule substrate surface, which may have contributed to sufficient permeation of oxygen and precursors proffered by the conduit (Saez et al. 2012). Prolonged access to nitrogen and carbon is compelled throughout wastewater, but permeation and allocation of such supplements should be appropriate and unhindered (Suzana et al. 2013). Table 1 shows the immobilization matrix and pollutant removal performance of various baterias.

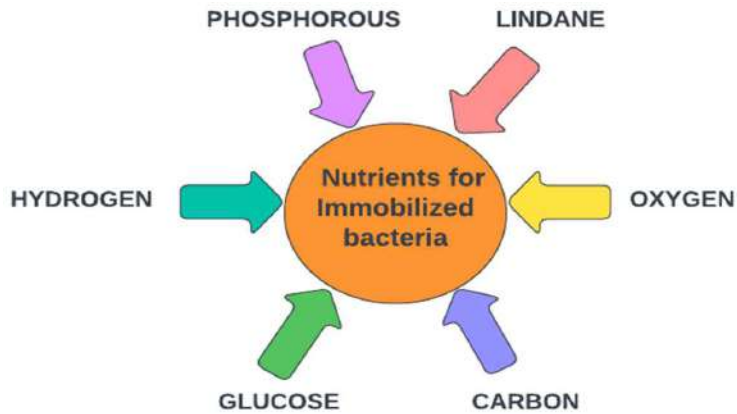


Fig. 2: Nutrients for immobilized bacteria.

Table 1: Immobilization on copious matrix and performances for removal.

| Bacteria | Immobilizing matrix | Methods | Pollutants | Performance | References |
|---|---|---|---|---|---|
| *Klebsiella variicola* strain SKV2, *Sphingomonas* sp. | Polyurethane Calcium-alginate | Entrapment | polycyclic aromatic hydrocarbons Chlorpyrifos | 44.3%,71.8% | (Dai et al. 2020; Santillan et al. 2020) |
| *Bacillus pseudomycoides* | PVA-Glutaraldehyde | Entrapment | BOD<br>COD | 86%<br>71% | (Mehrotra et al. 2020) |
| *Pseudomonas putida*<br>*Bacillus cereus* | Sodium Alginate, | Entrapment | BOD, COD | 79% ,84%, 16-65% | (Maheshwari et al. 2017) |
| | Calcium Chloride | | BOD, COD<br>Cr | 83%,89%<br>86%,91% | |
| *Pseudomonas putida* YNS1 | Alginate | Encapsulation | Phenol<br>Cadmium<br>copper | 92%<br>99%<br>97% | (Namane et al. 2020) |
| *Arsenic oxidizing* bacteria | PVA | Entrapment | Arsenic | ~ 80% | (Labus et al. 2016) |
| *Selenastrum capricornutum* | Alginate | Entrapment | Copper, cadmium, nickel, zinc | 99% | (Partovinia & Rasekh 2018) |
| *Bacillus* sp., *Serratia* sp. | Alginate, Polyacrylamide | Entrapment | Chromium, mercury, nickel | - | (Suhag et al. 2015) |
| *E. coli* MG1655 | Agar and alginate | Entrapment and Encapsulation | Arsenic | - | (Qiu et al. 2022) |
| *Arthrobacter chlorophenolicus* A6 | Calcium Alginate | Entrapment | 4-chlorophenol | 98.6% | (Sahoo & Panigrahy 2018) |
| *Bacillus licheniformis* | Iron oxide magnetic | Biosorbent | Pb (II) | 98% | (Wen et al. 2018) |
| *Saccharomyces cerevisiae* | Synthesized titania | Optimization and Modeling by Response Surface | Cr (VI) | 99.92% | (Choudhury et al. 2017) |
| *Fusarium verticillioides*, *Pencillium funiculosum* | Nanosilica | Biosorption | Cr (III)<br>Cr (VI) | 128.26, 138.66<br>336.24, 332.77 | (Mahmoud et al. 2015) |
| *Arthrospira platensis* | Alginate, Silica gel, Agarose | Biosorption | Pb (II) | 65.85 $mg.g^{-1}$, 2.58 $mg.g^{-1}$ | (Duda-Chodak et al. 2013) |
| *Bacillus cereus* RC-1 | Biochar derived from sewage sludge | Biosorption | Cd (II) | 158.77$mg.g^{-1}$ 127.71 $mg.g^{-1}$ | (Huang et al. 2020) |
| *Sulfate-reducing* bacteria | Sodium alginate | Entrapment | Fe<br>Zn<br>Cd<br>Pb<br>Ni | 85–95%<br>85–95%<br>85–95%<br>85–95%<br>75-95% | (Gopi Kiran et al. 2018) |
| *Pseudomonas putida* | Agar beads | Entrapment | Cu (II)<br>Zn (II) | 0.28 $mg.g^{-1}$<br>0.25 $mg.g^{-1}$ | (Meringer et al. 2021) |
| *Escherichia coli*, | Kaolin | Biosorption | Cr<br>Zn | 89 $mg.g^{-1}$<br>68 $mg.g^{-1}$ | (Quiton et al. 2018) |
| *Staphylococcus epidermidis* | | | Cr<br>Zn | 46 $mg.g^{-1}$<br>48 $mg.g^{-1}$ | |
| *Chlorella sorokiniana* | Loofa sponge | Biosorption | Cr | 69.26 $mg.g^{-1}$ | (Nasreen et al. 2008) |
| *Saccharomyces cerevisiae* Sr(II) | chitosan beads | Biosorption | Sr (II)<br>Co (II)<br>s(I) | 34.96 $mg.g^{-1}$<br>28.90 $mg.g^{-1}$<br>17.62 $mg.g^{-1}$ | (Yin et al. 2017) |
| *Bacillus drentensis* | Bio-carrier Beads | Biosorption | Pb<br>Cu | 0.3332 $mg.g^{-1}$, 0.5598 $mg.g^{-1}$ | (Seo et al. 2013) |

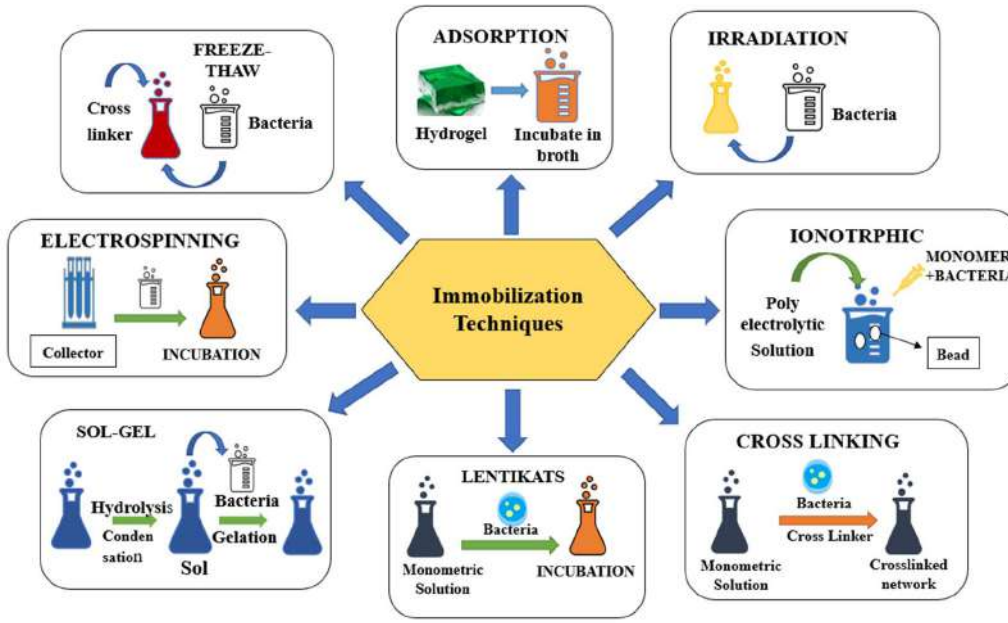


Fig. 3: Numerous methods and support materials used in the bacterial immobilization process.

## BACTERIAL IMMOBILIZATION METHODS

A lot of changes over the decades: a numerous approach for isolating bacteria in biopolymers were created over time (Fig. 3). Several myriad processes evolved for inactivating bacteria in biopolymers (Mehrotra et al. 2021). Ligand binding and polymeric bond formation on solid substrates are among the most prevalent and significant procedures. Cross-linking among biomolecules/biocatalysts/bacteria and the viscoelastic insurer is another tactic, as is virtualization by vesicles and entanglement in a composite membrane (Mehrotra et al. 2020).

### Adsorption

Ligand binding of molecules on alginate for biotechnological implementations constitutes a basic, reduced, ubiquitously utilized insertion method. It is premised on the transient intimate contact of bacteria with the transmission exterior via low intermolecular influences (Suzana et al. 2013). Even though feeble conversations are embroiled in the adsorbents, there's a strong probability of bacterial attachment oozing away from endorsements further into the ecosystem; thereby, this substrate procedure has specific applicability (Dzionek et al. 2016).

### Covalent Bonding

Covalent binding symbiosis, on the reverse side, is potent for peroxidase confinement and yet is seldom often used for disorienting bacteria. The organic solvents in use for intermolecular are broadly highly toxic, minimizing bacteria and survivability and subsequently causing cells to perish (Dzionek et al. 2016).

### Cross Linking

Cross-linking is an illustration strategy of cell disruption that requires the establishment of chemical bonding between the stimulated biodynamic assist and bacteria employing functionalized homologous recombination entities, including solvent, hexyl, diphenyl, and many others. Mehrotra et al. previously entrapped an untrodden type of bacteria, *Bacillus pseudomycoides*, in an Extracellular matrix and agglomerated to fumaric acid for the biotreatment of tannery effluents and revealed not only majestic biological membranes for about 2 months and also impactful disinfectants of effluents without bioleaching (Mehrotra et al. 2020) Bai et al. observed alloying of Polyvinyl alcohol biomaterials in the mere existence of acetic anhydride as a merge intermediary to inactivate nitrifying bacteria in the hopes of evaluating the matrix's capacity to maintain bacteria productivity. Based on the report's positive findings, the technique might be employed in a diverse selection of bioactivities (Bai et al. 2010). Another additional benefit of this technique is that it makes it possible for synchronous polycondensation without the necessity for a compatibilizer or innovator (Bai et al. 2010). Singh et al. previously reviewed 5 bacteria isolated on beta alginate for physicochemical expulsion of heavy metals; 62-71 percent of total rehabilitation of 10 $g.mL^{-1}$ strontium has been demonstrated out of conduit (Singh

et al. 2020). Some cross micelles can also be complexed utilizing radio waves, individuals that have been indicated to be using ultra-violet (UV) irradiation-induced pictures of oxidative damage. Hsueh et al. presented Ultraviolet light glycerine immobilized bacteria, a technique that augmented the brewing process in the biomedicine, pharmacological, and industrial products (Hsueh et al. 2017).

### Ionotropic Gelation Method

Ion channel phase transition accumulation of bacterium in granules employing varied chelating and polyatomic cations must have observed substantial application to the innovation of incapacitating colony forming units. The biggest drawback of calmodulin emulsions is their own destruction and successive volatilization by oxalate, leading to decreased intensity and tensile stability. The problem was conquered across polymer chains copolymerization and emulsifier transplantation with polymeric materials including Composite, along with additional rehabilitation to polyethylene and dimerization. Bhabha Atomic Research Centre (BARC) in Bombay, the beta copolymer, has been employed to sustain hydrocolloid particles to oxalate catalysts (Mehrotra et al. 2021). In addition to their greater recompression and $o_2$ propagation prospects, barium-alginate particles are additionally indicated as nitrogen fixation under hypoxic conditions.

### Sol-gel Method

Sol-gel implementation including whole bacteria, has served as a traditional procedure for over a half century. Nevertheless, there are certain boundaries to this approach, including the requirement for excessive pH conditions as well as the initiation of liquor during the transesterification reaction - both are detrimental towards the immobilized bacteria but instead impede biological conflict, and pathogenic cells were siphoning out from a dimensional analog. This seems to have a substantial influence on profitability (Eleftheriou et al. 2013). The curing scheme (vapor or defrost), retained hydraulic conductivity and extension of nanofiller (e.g., porcelain fibrils), and risk factors for the development of papule ingredients (e.g., xylitol), or even the amalgamation of liquid composites also including propylene glycol which can significantly affect such considerations (Eleftheriou et al. 2013).Utilizing porcelain granules, particulate Silicon dioxide, and the bicomponent in an amorphous form approach to create 'biocers' (biological ceramic composites), which are highly permeable, flexural copolymers of almost zero deformation (Pannier et al. 2012).

### LentiKats Technology

The cryo technique was applied to the gelatinization of widely utilized polymer matrix, including Copolymer, which resulted in the development of bonds, more durable, harder biopolymers. Numerous different techniques for Polyaniline hydrogel were evolved, like polypropylene establishment to oxalic acid, however, the materials seemed to be fragile and precarious (Mehrotra et al. 2021). LentiKats® technique is feasible despite the destructive substances. The delicate phase transition strategy for use by LentiKats® technology (optics carriers) has been previously amplified to production usages. That has been sufficiently integrated to resist heavy temperatures of upwards of 50 with a diverse variety of ionic strengths but also merge the economic advantages between both big and tiny beads. The Polyvinyl alcohol LentiKats® procedure of elevated chemical and physical predictability permits the incapacitation of bacteria in their own initial dimensions and form. Because of the enhanced durability and resistance of the LentiKats®, diverse effluent could be depicted (Mehrotra et al. 2021).

### Electrospinning Method

Bacterial implementation normally happens in arrays that seem to be many times heavier than nanomaterials, creating supplements. Still, instead, retentate complicated to deflect through into a range of immobilized bacteria, decreasing overall productivity. Utilizing a mixture that includes the bacteria of intrigue, an electromagnetic mandate will be employed to turn and emit adhesive strands. The above technique is simple, cost-effective, and versatile, with promising prospects for inactivating sustainable bacterial species (Zamel et al. 2019). Nevertheless, due to polyvinyl alcohol and the bond being water-based in the environment, they couldn't operate precisely for tannery effluent. In order the purpose of eliminating the blue-colored pigment substance cetyl/poly monomer (ethylene oxide) microfibers were electrospun alongside DMSO (dimethyl sulfoxide) as a carrier fluid to inhibit acceptable *Bacillus mycoides* (Zamel et al. 2019). Hardick et al. showed an electrically spinning framework that includes cellulose acetate, a polymer (that is recyclable, bioabsorbable, ethyl-insoluble, and extremely penetrable) for bacteria suspension, produces the development of nanofibers with immobilize many different bacteria for productive biological remediation. The structure might serve commercial uses because of numerous benefits involving simple interaction with affordability and its potential to be repurposed multitudinous (Aliheidari et al. 2019).

## ASPECTS THAT INFLUENCE REMEDIATION USING IMMOBILIZED BACTERIA

### Mass Transfer Limitation

Bacteria immobilized in water-based gel possess an enhanced

resistance for hazardous substances owing to their defensive encasing, yet also exhibit an extended transmission of development advertising components (such as oxygen and dietary supplements) in part due to the additional weight that serves as a conveyance challenge. In one instance, investigations on the biological breakdown of gasoline through bound organisms demonstrated that their tiny permeability and brittle arrangement of calcium chloride beads impeded matter transfer (nutrient, diesel). This issue was eliminated through the mixture of fiber with a substance called sodium alginate, leading to straw-alginate beads (Xue et al. 2019, 2020). This might promote retention throughout cells that function. The multiple functions of the substrate (carrier and adsorbent) in embedded *Bacillus* cells adsorbed ions of Cd (II) were researched (Huang et al. 2020).

**Toxicity of Pollutants**

For the breakdown of chlorophenol, three distinct polyvinyl confined systems utilizing activated sludge have been examined (cryogel strands alongside biomass production merely, cryogel beads about PAC with edges and material, and cryogel beads with pulverized PAC and propyl (Xue et al. 2020). The most recent research on the consequences and breakdown of sulfamethoxazole (SMX) throughout analogously eliminated emphasize (ADC) rehabilitation in a photobioreactor contrasted three distinct types of microalgal-bacterial consortium: at ease levity, CA immobile fragments, and CA bound pieces alongside a powdered form of activated carbon (Xue et al. 2020).

**Salinity**

A variety of halophilic bacteria to endure salt is crucial for fluid breakdown in elevated humidity effluent, and efficiency is usually compromised over a particular threshold. A continuous breakdown utilizing cell debris demonstrated that input concentrations of TDS above 145,000 $mg.L^{-1}$ substantially decreased the proliferation of bacteria. In another investigation, the shell of walnuts (WS) was utilized to inhibit halophilic bacteria for use in the biological processing of tannery effluent (Pendashteh et al. 2018). While the effluent contaminants were more than 90,000 $mg.L^{-1}$, it was determined which WS enhanced the system's susceptibility to salt content astonishment as well as exacerbated its biological importing pace. In a large-scale experiment, bacteria trapped on the polypropylene material surpassed independent cells by four to seven instances at the finest water content assessed (180 $g.L^{-1}$) (Hasanzadeh et al. 2020).

**Co-Contaminants**

Immobilization has additionally been demonstrated to defend cells that exist compared to harmful impacts of materials beyond the desired pollutants. Heavy metals, for instance, have been experimentally illustrated to impede nitrification bacteria. In a recent research investigation, the impacts of multiple frameworks upon encapsulation of a Pseudomonas fatigue that shields denitrification species from the hazardous effects of Cr (VI) were evaluated (Yu et al. 2020). Free cells eliminated only 4% of the nitrogen oxides -N, but tissue trapped removed 86%, 88%, and 100%, correspondingly. Immobilization alongside retention transporters (biochar activated carbon, ceramsite) proved to have been inadequate. The initial amount of the substances may be elevated to 800 $mg.L^{-1}$ utilizing CA immobilized bacteria removed from effluent, though the appropriate fatal dosage over cell liberation was just 400 $mg.L^{-1}$. However, there have been situations during which substance amount hasn't been considered to be the most crucial aspect. Ji and Wang implemented a *Shigella fergusonii* demand immobilized over CA blend beads to eliminate Se (VI) within PBR (Ji & Wang 2020). The reactor levels and HRT have been demonstrated to regulate the process's elimination efficacy, and the influential Se level did not impact these.

**pH**

In biosorption procedure and metabolism, the acidity of the environment contributes to the magnetic attraction among bacteria as well as substances through determining substance differentiation as well as the physical and chemical characteristics (e.g., zeta) that impact the variety of receptors on the bacteria. For instance, ecological remediation of Cr (VI) employing CA-anchored yeast used for baking has been investigated by ranging the acidity level of the mixture from 1.5 to 7.5, at pH 3.5, suffering its greatest consumption abilities (Mahmoud & Mohamed 2017). Further investigations demonstrate an analogous degree of addiction (Dhanarani et al. 2016). The pH level of the substrate affects the functioning of enzymes and the development of bacteria evaluated throughout decomposition. The ideal pH value for biological remediation in a specific biomass reactor might be established with an empirical procedure. Usually, bound cells revealed a broad desirable pH examined by defending the organic matter about detrimental conditions for growth. As an instance, at pH 3, a *Sphingomonas* strain's phenol breakdown capacity proved entirely impeded, though poly vinyl ethyl-alginate-kaolin confined cells retained 95% effectiveness in elimination (Zhang et al. 2017). In extremely alkaline circumstances, like pH 10 and 12, independent cells solely eradicated 70% and 50% of the phenol, which is, accordingly, while bound cells currently ditched 95% of the phenol, despite at a slightly slower pace. Another investigation gazed into the way temperatures and pH levels impacted the ecological restoration of polluted soil by deploying imprinted bacteria.

## DESIGN OF BIOFILTRATION SYSTEMS BY IMMOBILIZED BACTERIA

The implementation of immobilized bacteria in the bioretention of tannery effluent (Pathak et al. 2020, Li et al. 2016, Tong et al. 2013) varied in commercial and residential sources, like quarrying (Ma et al. 2020), petroleum (Dev et al. 2017), pharmacological, fabric, paper and pulp industries, livestock production, and sludges, has received considerable interest. Diverse fermenter kinds, along with packed-bed bioprocesses, fluidized bed bioreactors, hybrid fermentation, anaerobic membrane processes, and continuously stirred tank bioreactors, had also investigated the potential that use of paralyzed bacteria in particles for wastewater treatment from diverse sources (Table 2).

### Packed-bed Bioreactor (PBR)

The PBR usually consists of a hollow tube filled with bacteria-immobilized water-based gels, which can function using an up-flow or down-flow arrangement. PBR with *Bacillus cereus* confined is employed for disinfecting wastewater produced by the industry (Banerjee & Ghoshal 2017). The researchers indicated that over ninety percent of COD, 96% of TOC, 100% of phenol compounds, 49% of ammonia nitrogen, and 42.6% of phosphates had been eliminated from wastewater. A further investigation indicated a complete elimination of the phenol about a water-based solution utilizing *Bacillus cereus* bound in CA beads (Banerjee & Ghoshal 2016). Another investigation utilized a variety of cultures retained in Ca-alginate beads to disinfect artificial metal-polluted effluent in an identical way (Gopi et al. 2018).

### Fluidized Bed Bioreactor (FBR)

The FBR is composed of bound bacteria in hydrophilic gels, which are embedded in a tube that is inflated by the upflow of polluted water at an appropriate acceleration that encourages effective blending. A pure culture for *Bacillus cereus* imprisoned in CA was implemented to purify polluted water generated by hydrocarbons (Banerjee & Ghoshal 2017, 2016). Researchers disclosed eliminating over ninety-five percent of COD and phenol compounds in petroleum refineries, the effluent *Rhodococcus* rubber and *Rhodococcus* opacus had been suspended for the purification of 72-98% volatile organic compounds from artificially lined up fluids in an identical investigation. The FBR arrangement permits immediate mass movement to the paralyzed bacteria gel/beads, leading to an immediate proliferation of biomass and elevated pollutant rate of elimination throughout the disinfection of effluent (Bello et al. 2017).

### Hybrid Bioreactor (HBR)

To enhance biological reactor effectiveness, the hybrid reactor encompasses either a halted or connected bed for the growth of bacteria. HBR implemented metabolic bacteria debris immobilized in PVA to process artificial effluent. This recently disclosed that this HBR system, which is comprised of anaerobic waste immobilized in polyvinyl alcohol beads, dissolved material, and biofilm transport resources, eradicates 80% of nitrogen and 72-90% (Wu et al. 2018). A separate investigation discovered that HBR performed from biological reactors compacted with PVA eliminated 89% COD from effluent wastewater within 72 hours of the process (Pandey & Sarkar 2017). The HBR arrangement might shield immobilized bacteria from being exposed directly to particular impurities yet improve the treatment process (Grandclément et al. 2017)

Table 2: Immobilized bacteria in various bioreactor types for the treatment of tannery effluent.

| Bioreactors | Immobilizing matrix | Bacteria | HRT (h) | Performance | Reference |
|---|---|---|---|---|---|
| FBR | Ca- alginate | *Bacillus cereus* | - | > 95%, COD | (Banerjee & Ghoshal 2016) |
| | | *Rhodococcus ruber*, | | 100% removal of alkanes. | |
| | PVA-cryogel | *Rhodococcus opacus* | - | 65–72% removal of PAH | (Bello et al. 2017) |
| HBR | PVA | Sludge from tannery effluent | - | 67–80% inorganic nitrogen | (Wu et al. 2018) |
| | PVA | Anaerobic microbe from upflow bioreactor | 72 | 89% COD removal | (Pandey & Sarkar 2017) |
| MBR | | Mixed microbial | 24 | 84.7% COD removal | (Juntawang et al. 2017) |
| | PVA | community from anaerobic | | 78% COD removal | (Ng et al. 2016) |
| | triacetate | Microbial community from marine sediment | 40 | 22% removal. | |
| CSTR | PEG | *Afipia* sp. | 16 | 2–99% dioxane removal | (Isaka et al. 2016) |

**Anaerobic Membrane Bioreactor (AnMBR)**

The AnMRB consists of a barrier immobilized upon fluids over the process of treatment of pollutants pursuant to anaerobic circumstances using an up-flow or down-flow arrangement in Anaerobic debris immobilized in polyvinyl alcohol was demonstrated to eliminate 84.7% COD compared to electronically lined up domestic wastewater throughout AnMBR execution at 24 h HRT (Juntawang et al. 2017). In further investigation, the community of bacteria that originated in marine debris proved imprisoned in the material triacetate for the purification of effluent(Ng et al. 2016). The interaction among immobilized beads, as well as their membrane exterior, diminishes the development of cakes on the barrier of the substrate and enhances MBR effectiveness for tannery effluent (Juntawang et al. 2017)

**Continuously Stirred Tank Bioreactor (CSTR)**

To overcome the conveyance of mass constraints, the CSTR incorporates bacteria-immobilized water-based gels, which are precisely transformed with pollutants employing constant swirling and ventilation. At a duration of sixteen hours (Isaka et al. 2016), HRT, an intact culture of *Afipia* sp., encased polyethylene glycol (administered in CSTR to eradicate 85-91% dioxin about the water-based solution. Anammox debris immobilized in polyvinyl alcohol was initially applied by CSTR for the disinfection of the wastewater treatment facility, disregarding fluid. The researchers indicated that functioning the CSTR at 3 h HRT in nitrate deletion of 88-92% ( Hsieh et al. 2015). A further investigation adopting sewage effluent immobilized in polyethylene glycol conveyed a total nitrogen reduction of 92% throughout the conduct at 1.5 h HRT.

## FUTURE PERSPECTIVES AND POSSIBILITIES

The progress made in immobilizing bacterial cells with different polymers, untested bacterial strains, and novel cell immobilization methods for the bioremediation of environmental pollutants is covered in this review. As this article discusses, the use of immobilized bacteria in the bioremediation of industrial wastes has demonstrated promising performance in the removal of contaminants; however, the majority of existing work has been primarily restricted to laboratory-scale studies. The complexity of operations, matrix stability, characteristics, presence of multiple contaminants, mass transfer limitation of substrates into immobilized cells, build-up of toxic metabolic products around the cells due to low dispersion level, which may prevent microbiological growth, and thick biofilm formation, which may obstruct the beads' pores and prevent the transfer of substrate from the bulk liquid to the immobilized cells. Despite these obstacles, this field of study keeps developing to better understand and develop these procedures.

The study of various composite materials, such as biodegradable sponge-polycaprolactone, water-soluble sponge-NaCl-PEG, and Pb-contaminated water, respectively, is one of the most recent advancements in the field of immobilized bacteria for bioremediation. Furthermore, the process of immobilizing bacteria on matrices has been shown to aid in the remediation of contaminated sites by increasing the rate at which pollutants can be biodegraded, enhancing the durability of the immobilized strains, increasing their tolerance to high pollutant loads, and increasing bacterial enzyme activity.

The production of suitable substrates to immobilize affordable bacteria, have stable physical and chemical properties, have high porosity and surface area, and are non-toxic should be one of the main topics of future research. Future studies could also look into the proper ratios of biological biomass and immobilizing substance applied to stop cell overcrowding, which is the cause of high biofilm formation and pore-clogging. To prevent pore clogging, another tactic to slough off the mature and overgrown biofilms is to optimize the flow rate through the bioreactor. The immobilized cell-based treatment process could be made more sustainable by recovering value-added products through simultaneous bioremediation processes, such as recovering the metals during the biological treatment of wastewater that is high in metals. Ultimately, immobilized microbes could become a common bioremediation tool with the standardization of bead-formation techniques and the development of basic, theory-based engineering design principles, governing equations, and recommendations. All things considered, the idea of immobilizing microbes is fascinating and keeps drawing attention from researchers looking to remediate a wide range of contaminants using reusable matrix materials and next-generation smart materials. In the upcoming decades, we predict that research in this field will continue to expand quickly and that there will be more instances of this technology being used in the field and on a commercial scale.

## ACKNOWLEDGEMENT

I express my earnest and deep sense of gratitude to Dr M.G.R Educational and Research Institute, Maduravoyal, who has always been a moral support.

## REFERENCES

Aliheidari, N., Nojan, A., Mangilal, A. and Hamid, D. 2019. Electrospun nanofibers for label-free sensor applications. Sensors, 19(16): 44-48.

Angelim, A. L., Costa, S. P., Farias, B. C. S., Aquino, L. F. and Melo, V. M. M. 2013. An innovative bioremediation strategy using a bacterial consortium entrapped in chitosan beads. J. Environ. Manag., 127: 10-17. doi: 10.1016/j.jenvman.2013.04.014.

Bai, X., Ye, Z. F., Li, Y. F., Zhou, L. C. and Yang, L. Q. 2010. Preparation of crosslinked macroporous PVA foam carrier for immobilization of microorganisms. Process Biochem., 45(1): 60-66. doi: 10.1016/j.procbio.2009.08.003.

Banerjee, A. and Ghoshal, A. K. 2016. Biodegradation of real petroleum wastewater by immobilized hyper phenol-tolerant strains of Bacillus cereus in a fluidized bed bioreactor. 3 Biotech, 6(2): 447. doi: 10.1007/s13205-016-0447-1.

Banerjee, A. and Ghoshal, A. K. 2017. Biodegradation of an actual petroleum wastewater in a packed bed reactor by an immobilized biomass of Bacillus cereus. J. Environ. Chem. Eng., 5(2): 1696-1702. doi: 10.1016/j.jece.2017.03.008.

Bello, M. M., Raman, A. A. A. and Purushothaman, M. 2017. Applications of fluidized bed reactors in wastewater treatment – A review of the major design and operational parameters. J. Cleaner Prod., 141: 1492-1514.

Berillo, D., Al-Jwaid, A. and Caplin, J. 2021. Polymeric materials used for immobilisation of bacteria for the bioremediation of contaminants in water. Polymers, 13(15): 466. doi: 10.3390/polym13152466.

Choudhury, P. R., Bhattacharya, P., Ghosh, S., Majumdar, S., Saha, S. and Sahoo, G. C. 2017. Removal of Cr (VI) by synthesized titania embedded dead yeast nanocomposite: Optimization and modeling by response surface methodology. J. Environ. Chem. Eng., 5(1): 214-221. doi: 10.1016/j.jece.2016.11.041.

Dai, X., Lv, J., Yan, G., Chen, C., Guo, S. and Fu, P. 2020. Bioremediation of intertidal zones polluted by heavy oil spilling using immobilized laccase-bacteria consortium. Bioresour. Technol., 309: 123305. doi: 10.1016/j.biortech.2020.123305.

Dev, S., Roy, S. and Bhattacharya, J. 2017. Optimization of the operation of packed bed bioreactor to improve the sulfate and metal removal from acid mine drainage. J. Environ. Manage., 200: 135-144. doi: 10.1016/j.jenvman.2017.04.102.

Dhanarani, S., Viswanathan, E., Piruthiviraj, P., Arivalagan, P. and Kaliannan, T. 2016. Comparative study on the biosorption of aluminum by free and immobilized cells of bacillus safensis KTSMBNL 26 isolated from explosive contaminated soil. J. Taiwan Inst. Chem. Eng., 69: 61-67. doi: 10.1016/j.jtice.2016.09.032.

Dong, H., Wang, W., Song, Z., Dong, H., Wang, J., Sun, S., Zhang, Z., Ke, M., Zhang, Z., Wu, W. M., Zhang, G. and Ma, J. 2017. A high-efficiency denitrification bioreactor for the treatment of acrylonitrile wastewater using waterborne polyurethane immobilized activated sludge. Bioresource Technol., 239: 472-481. doi: 10.1016/j.biortech.2017.05.015.

Duda-Chodak, A., Wajda, Ł. and Tarko, T. 2013. The immobilization of arthrospira platensis biomass in different matrices - A practical application for lead biosorption. j. environ. sci. health - Part A Toxic/Hazard. Subst. Environ. Eng., 48(5): 509-17. doi: 10.1080/10934529.2013.730425.

Dzionek, A., Wojcieszyńska, D. and Guzik, U. 2016. Natural carriers in bioremediation: A review. Electron. J. Biotechnol., 23: 28-36.

Eleftheriou, N. M., Ge, X., Kolesnik, J., Falconer, S. B., Harris, R. J., Khursigara, C., Brown, E. D. and Brennan, J. D. 2013. Entrapment of living bacterial cells in low-concentration silica materials preserves cell division and promoter regulation. Chem. Mater., 25(23): 4798-4805. doi: 10.1021/cm403198z.

Gopi Kiran, M., Pakshirajan, K. and Das, G. 2018. Heavy metal removal from aqueous solution using sodium alginate immobilized sulfate reducing bacteria: Mechanism and process optimization. J. Environ. Manage., 218: 486-496. doi: 10.1016/j.jenvman.2018.03.020.

Grandclément, C., Seyssiecq, I., Piram, A., Wong-Wah-Chung, P., Vanot, G., Tiliacos, N., Roche, N. and Doumenq, P. 2017. From the conventional biological wastewater treatment to hybrid processes, the evaluation of organic micropollutant removal: A review. Water Res., 111: 297-317.

Hasanzadeh, R., Souraki, B. A., Pendashteh, A., Khayati, G. and Ahmadun, F. R. 2020. Application of isolated halophilic microorganisms suspended and immobilized on walnut shell as biocarrier for treatment of oilfield produced water. J. Hazard. Mater., 400: 21397. doi: 10.1016/j.jhazmat.2020.123197.

Haso, H. W., Dubale, A. A., Chimdesa, M. A. and Atlabachew, M. 2022. High performance copper based metal organic framework for removal of heavy metals from wastewater. Front. Mater., 9: 16-25. doi: 10.3389/fmats.2022.840806.

Hsieh, Y. L., Tseng, S. K. and Chang, Y. J. 2015. Nitrogen removal from wastewater using a double-biofilm reactor with a continuous-flow method. Senors, 11: 54-69.

Hsueh, Y. H., Liaw, W. C., Kuo, J. M., Deng, C. S. and Wu, C. H. 2017. Hydrogel film-immobilized Lactobacillus Brevis RK03 for γ-aminobutyric acid production. Int. J. Mol. Sci., 18(11): 2324. doi: 10.3390/ijms18112324.

Huang, F., Li, K., Wu, R. R., Yan, Y. J. and Xiao, R. B. 2020. Insight into the $Cd^{2+}$ biosorption by viable Bacillus cereus RC-1 immobilized on different biochars: Roles of bacterial cell and biochar matrix. J. Clean. Prod., 272: 2743. doi: 10.1016/j.jclepro.2020.122743.

Igiri, B.E., Okoduwa, S.I.R., Idoko, G.O., Akabuogu, E.P., Adeyi, A.O. and Ejiogu, I.K. 2018. Toxicity and bioremediation of heavy metals contaminated ecosystem from tannery wastewater: A review. J. Toxicol., 54: 1145-1153.

Isaka, K., Udagawa, M., Kimura, Y., Sei, K. and Ike, M. 2016. Biological wastewater treatment of 1,4-dioxane using polyethylene glycol gel carriers entrapping Afipia sp. D1. J. Bioosci. Bioeng., 121(2): 203-208. doi: 10.1016/j.jbiosc.2015.06.006.

Ji, Y. and Wang, Y. T. 2020. Se(VI) reduction by continuous-flow reactors packed with Shigella fergusonii strain TB42616 immobilized by Ca2+-alginate gel beads. Process Biochem., 91: 46-56. doi: 10.1016/j.procbio.2019.11.031.

Juntawang, C., Rongsayamanont, C. and Khan, E. 2017. Entrapped cells-based-anaerobic membrane bioreactor treating domestic wastewater: Performances, fouling, and bacterial community structure. Chemosphere, 187: 147-155. doi: 10.1016/j.chemosphere.2017.08.113.

Labus, K., Drozd, A. and Trusek-Holownia, A. 2016. Preparation and characterisation of gelatine hydrogels predisposed to use as matrices for effective immobilisation of biocatalysts. Chem. Papers, 70(5): 523-530. doi: 10.1515/chempap-2015-0235.

Li, C., Wang, S., Du, X., Cheng, X., Fu, M., Hou, N. and Li, D. 2016. Immobilization of iron- and manganese-oxidizing bacteria with a biofilm-forming bacterium for the effective removal of iron and manganese from groundwater. Bioresour. Technol., 220: 76-84. doi: 10.1016/j.biortech.2016.08.020.

Ma, H., Wei, M., Wang, Z., Hou, S., Li, X. and Xu, H. 2020. Bioremediation of cadmium polluted soil using a novel cadmium immobilizing plant growth promotion strain Bacillus sp. TZ5 loaded on biochar. J. Hazard. Mater., 12: 388. doi: 10.1016/j.jhazmat.2020.122065.

Maheshwari, U., Ali, A. J. and Jain, M. K. 2017. Bioremediation by free and immobilized bacteria isolated from tannery effluent, 5: 75-90.

Mahmoud, M. S. and Mohamed, S. A. 2017. Calcium alginate as an eco-friendly supporting material for baker's yeast strain in chromium bioremediation. HBRC J., 13(3): 245-254. doi: 10.1016/j.hbrcj.2015.06.003.

Mahmoud, M. E., Yakout, A. A., Abdel-Aal, H. and Osman, M. M. 2015. Speciation and selective biosorption of Cr(III) and Cr(VI) using nanosilica immobilized-fungi biosorbents. J. Environ. Eng., 141(4): 899. doi: 10.1061/(asce)ee.1943-7870.0000899.

Mehrotra, T., Dev, S., Banerjee, A., Chatterjee, A., Singh, R. and Aggarwal, S. 2021. Use of immobilized bacteria for environmental bioremediation: A review. J. Environ. Chem. Eng., 9(5): 121-136.

Mehrotra, T., Zaman, M. N., Prasad, B. B., Shukla, A., Aggarwal, S. and Singh, R. 2020. Rapid immobilization of viable Bacillus pseudomycoides in polyvinyl alcohol/glutaraldehyde hydrogel for biological treatment of municipal wastewater. Environ. Sci. Pollut. Res., 27(9): 9167-9180. doi: 10.1007/s11356-019-07296-z.

Meringer, A., Liffourrena, A. S., Heredia, R. M., Lucchesi, G. I. and Boeris, P. S. 2021. Removal of copper and/or zinc ions from synthetic solutions by immobilized, non-viable bacterial biomass: Batch and fixed-bed column lab-scale study. J. Biotechnol., 328: 87-94. doi: 10.1016/j.jbiotec.2021.01.011.

Namane, A., Amrouche, F., Arrar, J., Ali, O. and Hellal, A. 2020. Bacterial behaviour in the biodegradation of phenol by indigenous bacteria immobilized in Ca-alginate beads. Environ. Technol. (United Kingdom), 41(14): 1829-836. doi: 10.1080/09593330.2018.1551427.

Nasreen, A., Muhammad, I., Iqbal, Z. S. and Javed, I. 2008. Biosorption characteristics of unicellular green alga Chlorella sorokiniana immobilized in loofa sponge for removal of Cr(III). J. Clean. Prod., 20: 616.

Ng, K. K., Shi, X., Ong, S. L., Lin, C. F. and Ng, H. Y. 2016. An innovative of aerobic bio-entrapped salt marsh sediment membrane reactor for the treatment of high-saline pharmaceutical wastewater. Chem. Eng. J., 295: 317-25. doi: 10.1016/j.cej.2016.03.046.

Pandey, S. and Sarkar, S. 2017. Anaerobic treatment of wastewater using a two-stage packed-bed reactor containing polyvinyl alcohol gel beads as biofilm carrier. J. Environ. Chem. Eng., 5(2): 1575- 1585. doi: 10.1016/j.jece.2017.02.013.

Pannier, A., Mkandawire, M., Soltmann, U., Pompe, W. and Böttcher, H. 2012. Biological activity and mechanical stability of sol-gel-based biofilters using the freeze-gelation technique for immobilization of Rhodococcus ruber. Appl. Microbiol. Biotechnol., 93(4): 1755-1767. doi: 10.1007/s00253-011-3489-7.

Partovinia, A. and Rasekh, B. 2018. Review of the immobilized microbial cell systems for bioremediation of petroleum hydrocarbons polluted environments. Crit. Rev. Environ. Sci. Technol., 48(1): 1-38.

Pathak, U., Banerjee, A., Roy, T., Das, S. K., Das, P., Kumar, T. and Mandal, T. 2020. Evaluation of mass transfer effect and response surface optimization for abatement of phenol and cyanide using immobilized carbon alginate beads in a fixed bio-column reactor. Asia-Pac. J. Chem. Eng., 15(2). doi: 10.1002/apj.2405.

Pendashteh, A. R., Chaibakhsh, N. and Ahmadun, F. R. 2018. Biological treatment of high salinity produced water by microbial consortia in a batch stirred tank reactor: Modelling and kinetics study. Chem. Eng. Commun., 205(3): 387-401. doi: 10.1080/00986445.2017.1398742.

Qiu, Y., Yu, S. and Li, L. 2022. Research progress in fluorescent probes for arsenic species. Molecules, 27(23): 25-36.

Quiton, K. G., Doma, B., Futalan, C. M. and Wan, M. W. 2018. Removal of chromium(VI) and zinc(II) from aqueous solution using kaolin-supported bacterial biofilms of gram-negative E. coli and gram-positive Staphylococcus epidermidis. Sustain. Environ. Res., 28(5): 206-213. doi: 10.1016/j.serj.2018.04.002.

Saez, J. M., Benimeli, C. S. and Amoroso, M. J. 2012. Lindane removal by pure and mixed cultures of immobilized actinobacteria. Chemosphere, 89(8): 982-987. doi: 10.1016/j.chemosphere.2012.06.057.

Sahoo, N. K. and Panigrahy, N. 2018. Biodegradation and kinetic study of 4-chlorophenol in bioreactor packed with stabilized bacteria entrapped in calcium alginate beads system. Environ. Processes, 5(2): 287-302. doi: 10.1007/s40710-018-0294-7.

Santillan, J. Y., Rojas, N. L., Ghiringhelli, P. D., Nóbile, M. L., Lewkowicz, E. S. and Iribarren, A. M. 2020. Organophosphorus compounds biodegradation by novel bacterial isolates and their potential application in bioremediation of contaminated water. Bioresour. Technol., 12: 317. doi: 10.1016/j.biortech.2020.124003.

Seo, H., Lee, M. and Wang, S. 2013. Equilibrium and kinetic studies of the biosorption of dissolved metals on Bacillus drentensis immobilized in biocarrier beads. Environ. Eng. Res., 18(1): 45-53. doi: 10.4491/eer.2013.18.1.045.

Shaheen Fathima, A., Bhuvaneswari, R. and Jeyanthi, J. 2020. Characterization of tannery effluent and synthesis of natural coagulant. AIP Conf. Proc., 312: 2270.

Singh, R., Shitiz, K. and Singh, A. 2020. Immobilization of bacterial cells in hydrogels prepared by gamma irradiation for bioremoval of strontium ions. Water, Air, Soil Pollut., 231(1): 4374. doi: 10.1007/s11270-019-4374-8.

Siripattanakul, S., Wirojanagud, W., McEvoy, J. and Khan, E. 2008. Effect of cell-to-matrix ratio in polyvinyl alcohol immobilized pure and mixed cultures on atrazine degradation. Water, Air, Soil Pollut. Focus, 8(3–4): 257-266. doi: 10.1007/s11267-007-9158-2.

Suhag, D., Bhatia, R., Das, S., Shakeel, A., Ghosh, A., Singh, A., Sinha, O.P., Chakrabarti, S. and Mukherjee, M. 2015. Physically cross-linked pH-responsive hydrogels with tunable formulations for controlled drug delivery. RSC Adv., 5(66): 53963-53972. doi: 10.1039/c5ra07424j.

Suman, H., Sangal, V.K. and Vashishtha, M. 2021. Treatment of tannery industry effluent by electrochemical methods: A review. Mater. Today: Proc., 47: 1112.

Suzana, C. S. M., Claudia, M., Martins, M. C., Fiuza, L. G. and Santaella, T. 2013a. Immobilization of microbial cells: A promising tool for treatment of toxic pollutants in industrial wastewater. Afr. J. Biotechnol., 12(28): 4412-18. doi: 10.5897/ajb12.2677.

Tong, K., Zhang, Y., Liu, G., Ye, Z. and Chu, P. K. 2013. Treatment of heavy oil wastewater by a conventional activated sludge process coupled with an immobilized biological filter. Int. Biodeterior. Biodegrad., 84: 65-71. doi: 10.1016/j.ibiod.2013.06.002.

Tuson, H. H. and Weibel, D. B. 2013. Bacteria-surface interactions. Soft Matter, 9(17): 4368-80.

Wen, X., Du, C., Zeng, G., Huang, D., Zhang, J., Yin, L., Tan, S., Huang, L., Chen, H., Yu, G., Hu, X., Lai, C., Xu, P. and Wan, J. 2018. A novel biosorbent prepared by immobilized Bacillus licheniformis for lead removal from wastewater. Chemosphere, 200: 173-79. doi: 10.1016/j.chemosphere.2018.02.078.

Wu, N., Zeng, M., Zhu, B., Zhang, W., Liu, H., Yang, L. and Wang, L. 2018. Impacts of different morphologies of anammox bacteria on nitrogen removal performance of a hybrid bioreactor: Suspended sludge, biofilm and gel beads. Chemosphere, 208: 460-468. doi: 10.1016/j.chemosphere.2018.06.012.

Xue, J., Wu, Y., Fu, X., Li, N., Sun, J. and Qiao, Y. 2020. Study on degradation characteristics and bacterial community structure changes of immobilized cells in straw-alginate beads in marine environment. Bioresour. Technol. Rep., 10: 402. doi: 10.1016/j.biteb.2020.100402.

Xue, J., Wu, Y., Shi, K., Xiao, X., Gao, Y., Li, L. and Qiao, Y. 2019. Study on the degradation performance and kinetics of immobilized cells in straw-alginate beads in marine environment. Bioresour. Technol., 280: 88-94. doi: 10.1016/j.biortech.2019.02.019.

Yin, Y., Hu, J. and Wang, J. 2017. Removal of Sr2+, Co2+, and Cs+ from aqueous solution by immobilized Saccharomyces cerevisiae with magnetic chitosan beads. Environ. Prog. Sustainable Energy, 36(4): 989-996. doi: 10.1002/ep.12531.

Yu, X., Shi, J., Khan, A., Yun, H., Zhang, P., Zhang, P., Kakade, A., Tian, Y., Pei, Y., Jiang, Y., Huang, H., Wu, K. and Li, X. 2020. Immobilized-microbial bioaugmentation protects aerobic denitrification from heavy metal shock in an activated-sludge reactor. Bioresour. Technol., 307: 12738. doi: 10.1016/j.biortech.2020.123185.

Yusif, B. B., Bichi, K. A., Oyekunle, O. A., Girei, A. I., Garba, P. Y. and Garba, F. H. 2016. A review of tannery effluent treatment. J. Clean. Prod., 2: 29.

Zamel, D., Hassanin, A. H., Ellethy, R., Singer, G. and Abdelmoneim, A. 2019. Novel bacteria-immobilized cellulose acetate/poly(ethylene oxide) nanofibrous membrane for wastewater treatment. Sci. Rep., 9(1): 5265. doi: 10.1038/s41598-019-55265-w.

Zhang, K., Liu, Y., Luo, H., Chen, Q., Zhu, Z., Chen, W., Chen, J., Ji, L. and Mo, Y. 2017. Bacterial community dynamics and enhanced degradation of di-n-octyl phthalate (DOP) by corncob-sodium alginate immobilized bacteria. Geoderma, 305: 264-74. doi: 10.1016/j.geoderma.2017.06.009.

Zhao, J., Wu, Q., Tang, Y., Zhou, J. and Guo, H. 2022. Tannery wastewater treatment: Conventional and promising processes, an updated 20-year review. J. Leather Sci. Eng., 4(1): 72.

## ORCID DETAILS OF THE AUTHORS

Priya Chokkalingam: https://orcid.org/0000-0002-5705-7871

Nature Environment and Pollution Technology
An International Quarterly Scientific Journal

p-ISSN: 0972-6268
(Print copies up to 2016)
e-ISSN: 2395-3454

Vol. 23 | No. 3 | pp. 1387-1405 | 2024

Original Research Paper

https://doi.org/10.46488/NEPT.2024.v23i03.011

Open Access Journal

# Survey and Characterization of Edible Fruit and Ethnomedicinal Trees in the Forest Landscape of Apayao Province

**Hannie T. Martin†, Olivia C. Tomas, Ryan W. Gabit, Maria Christina Z. Manicad and David A. Rodolfo**
Apayao State College, Conner, Apayao, Phlippines
†Corresponding author: Hannie T. Martin; hanmarzan@yahoo.com

**Nat. Env. & Poll. Tech.**
**Website: www.neptjournal.com**

*Received:* 15-11-2023
*Revised:* 08-01-2024
*Accepted:* 15-01-2024

**Key Words:**
Edible trees
Ethnomedicinal trees
DNA barcoding
Phytochemical analyses

## ABSTRACT

This study was conducted in the six municipalities of Apayao Province, namely, Luna, Pudtol, Flora, Conner, Kabugao, and Calanasan. This aimed to survey and characterize the edible fruit and ethnomedicinal trees in the forest landscape of Apayao province. It determined the geographical location, morphological characteristics, ecological status, DNA sequencing, phytochemical contents, uses, and threats of the edible and ethnomedicinal trees in the forests of Apayao. The methods used were qualitative and quantitative research. Fifteen (15) edible and 10 ethnomedicinal trees were surveyed with sixteen (16) families were identified. Out of 25 edible and ethnomedicinal trees, the conservation status is endangered, threatened, rare, vulnerable, and least concerned. Out of 25 edible and ethnomedicinal fruit trees, most are with identity results that range from 93 to 100% identity. Flavonoids, tannins, and sapotin compounds are mostly present in edible and ethnomedicinal trees. The community members are using 15 different ethnomedicinal trees to address 32 health-related conditions. The results of the phytochemical analyses provide support evidence to support the traditional uses of ethnomedicinal trees. All surveyed trees are susceptible to pests, diseases, and destruction brought by natural phenomena such as the effect of climate change. A policy recommendation for the conservation and protection of edible and ethnomedicinal trees is then proposed.

## INTRODUCTION

Apayao province, as the last frontier of the watershed in the north, lies in the northernmost part of Luzon mainland. It is landlocked by the province of Cagayan in the northeast, bounded on the northwest by Ilocos Norte and Abra, and on the south by Kalinga province. The elevation of Apayao ranges from 70 to 1,644 meters above sea level, whereas Mount Sulo, the highest registered mountain peak in Apayao, lies at an elevation of 1,503 masl. Low elevations are mostly found in Lower Apayao, particularly in Luna and Sta. Marcela. The province is composed of seven municipalities and 134 barangays. These are geographically subdivided into two separate regions: Upper Apayao, which is composed of the upland municipalities of Calanasan, Conner, and Kabugao, while Lower Apayao is composed of the lowland municipalities of Flora, Luna, Pudtol, and Sta Marcela. Of the six (6) provinces in the Cordillera Administrative, Apayao has the lowest population but has the widest land area of 5,113 sq. km, which is about one-fourth of the region's total land area. The municipality of Kabugao remains the capital town provided under RA 7878. However, the municipality of Luna acts as the newly designated provincial government center (Apayao Tourism Development Plan 2014-2019).

The province's water resources account for 24 rivers, draining 75% of its area. The Apayao river is the longest stretching a distance of 181 kilometers, traversing through all of the province's municipalities except Conner. It has 18 tributaries and is presently used for irrigation, power generation, and communal fishing ground. Other important rivers in the province include the Matalag River in Conner, Maton and Nagan Rivers in Pudtol, and the Zumigui-Ziwanan River in Calanasan.

The forest landscape of the province is home to many flora and fauna. Vegetation compositions are largely grouped into two, namely timber and non-timber resources. Timber resources are predominantly of Dipterocarp species such as red lauan (*Shorea negrosensis*), mayapis (*Shorea palosapis*), tanguile (*Shorea polysperma*), yakal (*Hopea acuminata*), guijo (*Shorea guiso*) and many other premium species which are considered endangered. The diversity of non-timber resources that are observed in the province are palms, herbs, vines, ferns, orchids, bamboo, and others.

As one of the provinces that still possesses rich floral resources, there might be species in its forests that still need to be discovered to science or some of these species may already have been described but with insufficient data.There is also the big possibility of the presence of other species that were not recorded, and some of these may have already become extinct over the years. The floral species thriving in the forest landscape of the province have specific human use and important roles in the natural ecosystem. The diverseness of the floral composition of the forest landscape of the province is exposed to threats such as conversion of land use, habitat loss, degradation, invasive species, and anthropogenic climate change. These threats may contribute to the loss of biodiversity in the province. Conservation of edible fruit trees and ethnomedicinal important tree species in the province requires initial basic steps that should be given attention and importance such as survey and characterization in terms of their morphological and chemical attributes. With this basic information, approaches in conservation could be determined whether through propagation with the use of seeds or asexual in nature. In addition, this project may contribute to floral species that may need genetic conservation.

This study will have a demonstrable contribution to the significant advances in understanding the methods, theory, and application in the identification, collection, characterization, storage, and DNA barcoding of floral species. Also, knowing the ecological status will be the basis for developing protocols in ex-situ conservation, thus contributing to biodiversity conservation and protection to sustain ecological services for the present and future generations. Hence, this study.

### Objectives/Statement of the Problem

General objective: To study the morphological and chemical characteristics and document the edible fruit and ethnomedicinal trees as the basis for conservation in terms of propagation and policy recommendations.

Specifically, this study aimed to:

a. Survey and map using GIS as a tool of the edible and ethnomedicinal trees in the Apayao forest landscape,
b. Characterize morphologically of the edible fruit and ethnomedicinal trees,
   b.1. Determine the conservation status of identified species
   b.2. Conduct DNA barcoding of edible fruit and ethnomedicinal trees,
c. Conduct Phytochemical Analysis of edible and ethnomedicinal trees,
   c.1. Determine the uses and preparation of the ethnomedicinal trees.
   c.2. Assess the utilization of native fruit and ethnomedicinal trees vis a vis the result of phytochemical analyses

## MATERIALS AND METHODS

### Location

This research paper was conducted in the forest landscape of Apayao province, particularly in the municipalities of

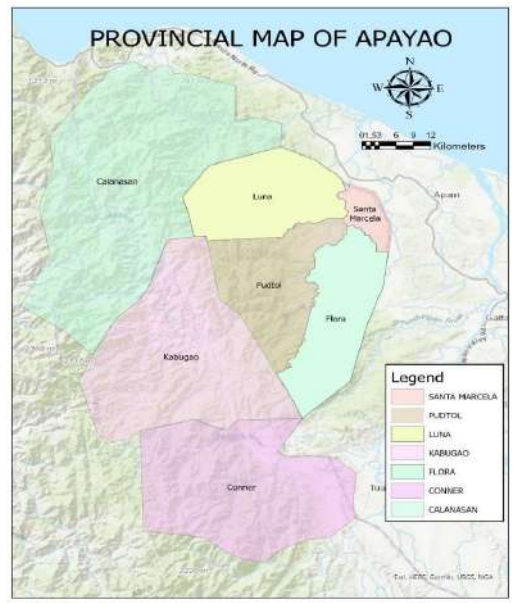


Fig. 1: Map of Apayao.

Pudtol Luna, Flora, Kabugao, Conner, and Calanasan (Fig. 1).

### Data Gathering Procedure and Sources

#### *Survey of Edible Fruit and Ethnomedicinal Trees in the Apayao Forest Landscape*

The survey of edible fruit and ethnomedicinal trees in the forest landscape of the municipalities of Conner, Kabugao, Pudtol, Luna, Flora, and Calanasan was conducted through fieldwork and focus group discussions with the community. Before the field survey, a consent letter was given to the office of the Governor of the Apayao Province and cascaded to the different Mayors' offices and the selected barangays. The focus group discussion was conducted to identify the edible fruit and ethnomedicinal trees located in the locality. The coordinates of the edible and ethnomedicinal trees were recorded through the Global Positioning System (GPS) and used to generate maps. The overlay of the location of native fruit and ethnomedicinal trees was developed using Arc GIS 10.8.

#### *Characterization of the Edible Fruit Trees and Ethnomedicinal Trees*

Selected edible fruit trees and ethnomedicinal trees were characterized based on their morphological features, such as roots, leaves, stems, bark, flowers, and fruits. The faculty of the Forestry Department of ASC Luna Campus did morphological characterization.

#### *Conservation Status of Edible Fruit and Ethnomedicinal Trees*

The conservation status of the edible fruit and ethnomedicinal trees was determined through the data from the International Union for Conservation of Nature (IUCN) and validated by the data from the Department of Environment and Natural Resources (DENR) Administrative Order No. (DAO) 2007-01 and Administrative Order (DAO) 2007 s.11.

#### *DNA Barcoding of Edible Fruit and Ethnomedicinal Trees*

Collection of the identified specimens (leaves) was done at different Barangay of six (6) municipalities of Apayao: Luna (Barangay Marag, Dagupan, and San Gregorio), Pudtol (Barangay Lydia and Upper Maton), Flora (Barangay Balasi, San Jose, and Tamalunog), Kabugao (Barangay Badduat, Cabeyatan, and Poblacion), Conner (Calafug, Karikitan, Malama, and Mawegui), Calanasan (Barangay Lubong, Sabangan, and Eliazar). The specimens (leaves) were air-dried for three (3) days and packed using Ziplock with silica gel to avoid the occurrence of moisture. The specimen was then sent to the Philippine Genome Center, University of Philippines, Los Baños for DNA Barcoding. In DNA Barcoding, BLAST was used to initially identify each edible fruit based on the proportion of individuals assigned to the correct species, genus, or family and the percentage identity of each taxon identified. The primer used was maturase K (*matK*).

#### *Phytochemical Analysis of Edible Fruit and Ethnomedicinal Trees*

In the phytochemical analysis, 3-5 kilograms of leaves of each of the 44 edible fruit and ethnomedicinal trees were collected from identified locations. The collected leaves were chopped into small pieces, and approximately 100 g of chopped leaves were used for each specimen. They were then preserved in jars treated with sufficient 90% methyl alcohol to submerge the material completely. The material was soaked for 48 hours. After 48 hours, the soaked materials were extracted using a blender. The collected plant extract was then boiled for about 1 hour and 30 minutes to obtain the concentrated plant extract. After extraction, the leaf extract was stored at a cold temperature of about 0-5 °C and was transported to DOST Tuguegarao. DOST Tuguegarao used the Guevara et al. (2005) method to screen the chemical compounds found in the identified species.

#### *Uses and Preparation of the Ethnomedicinal Trees*

Focus group discussion was conducted in the selected municipalities with the communities that are active users of the identified ethnomedicinal trees. The parts of plant use and mode of preparation were then demonstrated to the researchers.

### Data Analysis

Data analysis was done through quantitative and qualitative analysis. Quantitative research was used to generate maps and perform DNA Barcoding. A qualitative method was used for morphological and phytochemical characterization and description of uses and threats.

## RESULTS AND DISCUSSION

### Surveyed Edible Fruit and Ethnomedicinal Trees

The actual identification of the location and local names or vernacular names of edible fruit and ethnomedicinal trees was conducted through field walks with the assistance of the local communities. Table 1 presents the surveyed edible fruit and ethnomedicinal trees. Fifteen (15) edible fruit trees and ten (10) ethnomedicinal trees were surveyed. The Municipality of Calanasan had nine (9) species identified,

and the Municipality of Luna had eight (8) species identified. Four (4) species were found in the municipality of Conner, two (2) in the municipality of Flora, and one (1) each in the municipalities of Kabugao and Pudtol.

In addition, six (6) maps were generated using Arc GIS 10.8. The map shows the location of the 15 identified edible fruit trees and 10 ethnomedicinal trees in the respective barangays of Municipality Luna, Pudtol, Flora, Kabugao, Conner, and Calanasan. Fig. 2-7 presents the location of trees under study.

Thus, ethnomedicinal and edible fruit trees exist throughout the municipalities of Apayao. Understanding the locations of the Apayao forest's edible fruit and ethnomedicinal trees is crucial for conservation and preservation initiatives. According to Franklin & Miller (2009), mapping tree species is a crucial activity that yields the data required for sustainable forest management. Data on the distribution of tree species is also a valuable source of information for a range of applications, including habitat characterization and susceptibility to insect infestation or range expansion.

## Morphological Characteristics of Edible Fruit and Ethnomedicinal Trees

The fifteen (15) surveyed edible fruit trees and ten (10) ethnomedicinal trees were characterized based on their

Table 1: List of surveyed edible fruit and ethnomedicinal trees.

| Local Name | Common Name | Scientific Name | Family Name | Location |
|---|---|---|---|---|
| Native Fruit Trees | | | | |
| Ada | Lipote | *Syzygium polycephaloides* (C.B.Rob.) Merr. | Myrtaceae | Sabangan, Calanasan, Apayao |
| Baluko | Binukau | *Garcinia binucao* (Blanco) Choisy | Clusiaceae | San Gregorio, Luna, Apayao |
| Chesa | Tiesa | *Pouteria rivicoa* (Gaertn.f.) Ducke | Sapotaceae | Mawegui, Conner, Apayao |
| Gratis | Balimbing | *Averrhoa carambola* Linn | Oxalidaceae | Marag Valley, Luna, Apayao |
| Kamagong | Mabolo | *Diplodiscus blancoi* A.DC | Ebenaceae | Calafug, Conner, Apayao |
| Kandulce | Black musk heart | *Alangium polyosmoides* (F.Muell.) W.J.de Wilde & Duuyfjes) | Cornaceae | San Gregorio, Luna, Apayao |
| Kuribeng/Kusibeng | Katap | *Trigostemon philippinesis* Stapf. | Euphorbiaceae | Dagupan, Luna, Apayao |
| Malubeg | Lubeg | *Syzygium lineatum* (Roxb.) Merr. & Perry | Myrtaceae | Malama, Conner, Apayao |
| Makopa | Makopa | *Syzygium samarangense* (Blume) Merr. & Perry | Myrtaceae | Karikitan, Conner, Apayao |
| Maladalaga | Bitok | *Ochrocarpos ramiflorus* Merr. | Guttiferae | Eleazar, Calanasan, Apayao |
| Malatibig | Pakiling | *Ficus odorata* (Blanco) Merr. | Moraceae | Dagupan, Luna, Apayao |
| Miscellanous | Balakat-gubat | *Balakata luzonica* (Vidal) Esser | Euphorbiaceae | Lubong, Calanasan, Apayao |
| Matabual | Korthal gisihan | *Aglaia korthalsii* Miq. | Meliaceae | Eleazar, Calanasan, Apayao |
| Namut | Amuyong | *Gonothalamus amuyon* (Blanco) Merr. | Annonaceae | San Gregorio, Luna, Apayao |
| Umila | Subiang | *Bridelia insulana* Hance | Euphorbiaceae | Lubong, Calanasan, Apayao |
| Ethnomedicinal Trees | | | | |
| Addil | Matang-hipon | *Breynia vitis-idaea* (Burm.f.) C.E.C. Fisch | Euphorbiaceae | Eleazar, Calanasan, Apayao |
| Aplas | Hauili | *Ficus septica* Burm.f. | Moraceae | San Jose, Flora, Apayao |
| Apatot | Noni | *Morinda citrifolia* L. | Rubiaceae | Tamalunog, Flora, Apayao |
| Arintudog | Horsebush | *Dendrolobium umbellatum* (L.) Benth. | Leguminosae | Badduat, Kabugao, Apayao |
| Bagbag | Rarang | *Erythrina subumbrans* (Hassk) Merr. | Fabaceae | Marag Valley, Luna, Apayao |
| Binuran | Tangisang-bayawak | *Ficus variegata* Blume | Moraceae | Eleazar, Calanasan, Apayao |
| Kakling | Lunas | *Lunas amara* Blanco var. *amara* | Rutaceae | Upper Maton, Pudtol, Apayao |
| Lumpanginay | Halimumog | *Ehretia philippinensis* A. DC. | Boraginaceae | Eleazar, Calanasan, Apayao |
| Lusit | Talisai-gubat | *Terminalia foetidissima* Griff. | Combretaceae | Eleazar, Calanasan, Apayao |
| Sablot | Bagna | *Glochidion triandrum* (Blanco) C.B.Rob. | Euphorbiaceae | Marag Valley, Luna, Apayao |

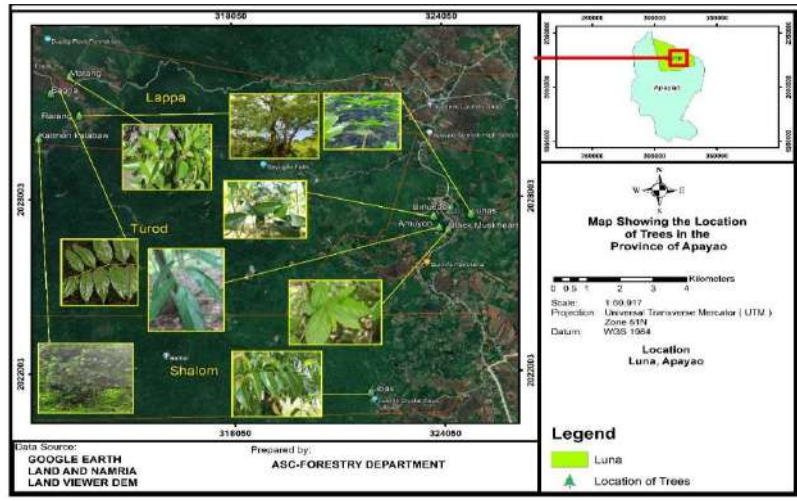


Fig. 2: Map of the location of the identified species at the Municipality of

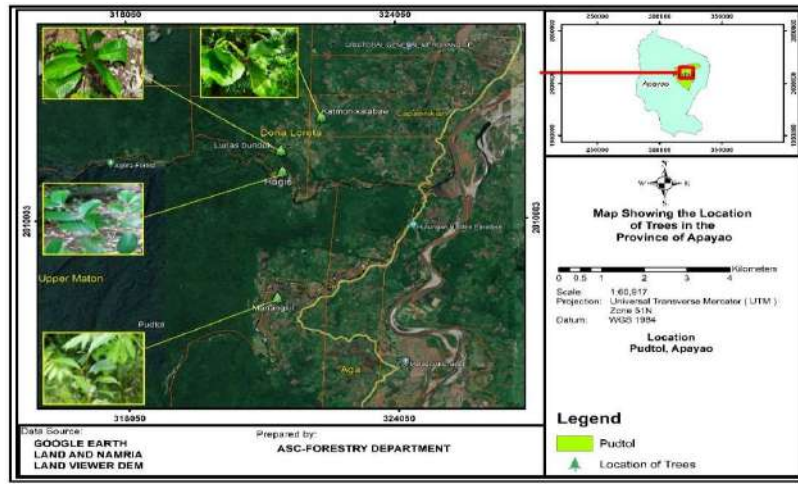


Fig. 3: Map of the location of the identified species at the Municipality of Pudtol.

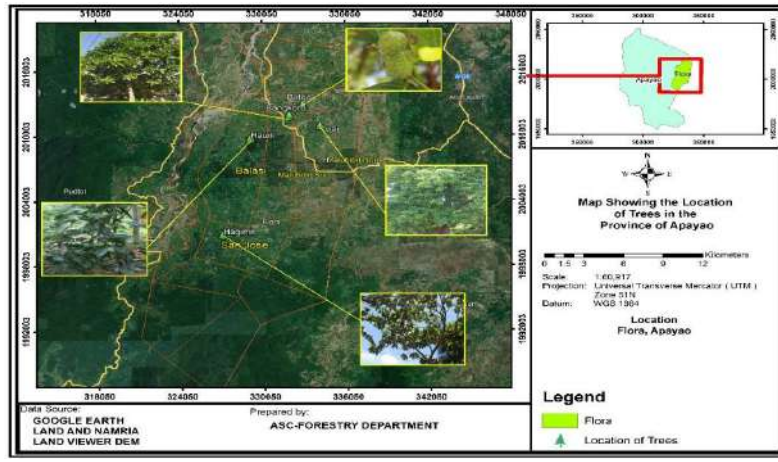


Fig. 4: Map of the location of the identified species at the Municipality of Flora.

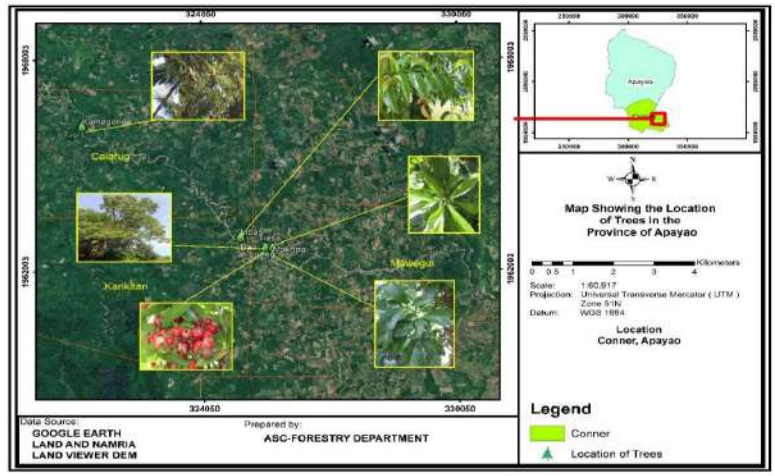


Fig. 5: Map of the location of the identified species at the Municipality of Conner.

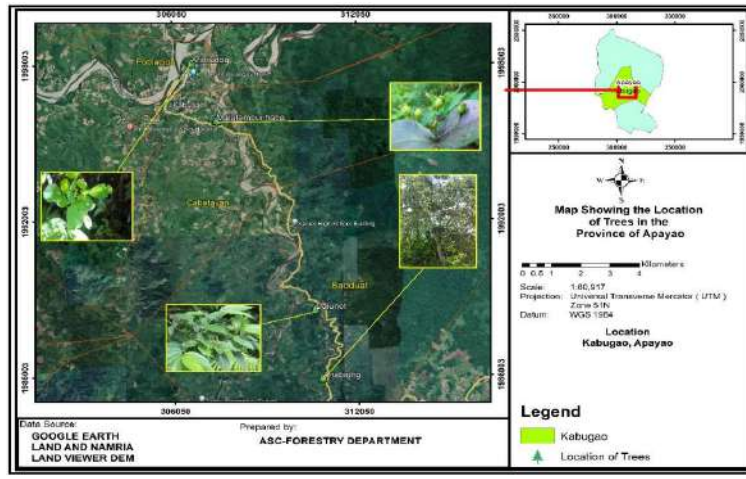


Fig. 6: Map of the location of the identified species at the Municipality of Kabugao.

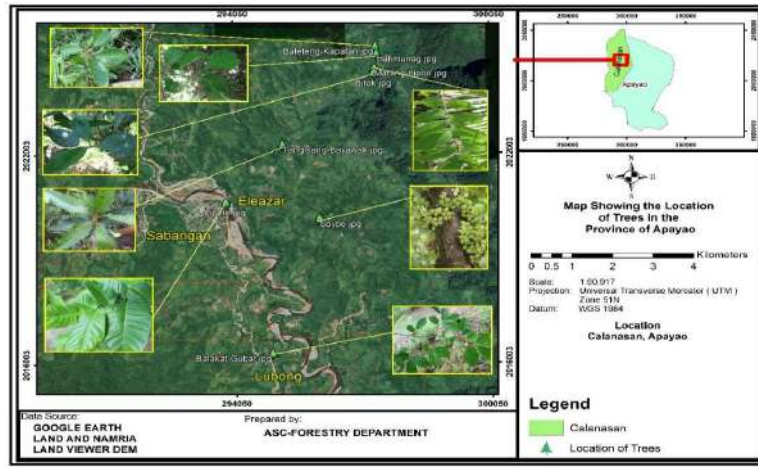


Fig. 7: Map of the location of the identified species at the Municipality of Calanasan.

morphological characteristics, such as leaves, fruit, flower, bark, seed, and size of the trees. Out of the twenty-five (25),

Fig. 8: Lipote **[Local Name:** Ada, **Common Name:** Lipote**, Scientific Name:** *Syzygium polycephaloides* (C.B.Rob.) Merr.**, Family Name:** Myrtaceae, **Location:** Sabangan, Calanasan, Apayao, **Description:** Lipote is an evergreen fruit tree, small to medium-sized tree growing up to 15 meters tall. The bark is purplish gray. Leaves are alternate, oblong-lanceolate, or obovate. Flowers are white, numerous, and in panicles. **Habitat:** In primary forests at low and medium altitudes. Reported in Sulawesi and Lesser Sunda Island. **Phenology:** Flowering season is from June to July., **Propagation:** By seed, **Timber Classification:** Lesser Used, **Conservation Status:** Endangered (IUCN Red List of Threatened Species)]

Fig. 9: Binukau **[Local Name:** Baluko, **Common Name:** Binukau, **Scientific Name:** *Garcinia binucao* (Blanco) Choisy, **Family Name:** Clusiaceae, **Location:** San Gregorio, Luna, Apayao, **Description:** Binucao is a tree reaching a height of about 25 m and a diameter of 40 cm. Leaves are opposite, shiny, and smooth. The newly emerged leaves often exhibit a reddish color. It has a smooth bark. The color is black, spotted with white color. Fruits are green in color and can be eaten, somewhat rounded. **Habitat:** Binucao is common and widely distributed throughout Luzon and Visayan Island. They are found scattered and are second-story trees of primary lowland and secondary forests. **Phenology:** Flowering season is from February to September. **Propagation:** Through seed, **Timber Classification:** Lesser Used Species, **Conservation Status:** Least Concern Species (IUCN Red List of Threatened Species)]

Fig. 10: Tiesa [**Local Name:** Chesa, **Common Name:** Tiesa, **Scientific Name:** *Pouteria rivicoa* (Gaertn.f.) Ducke, **Family Name:** Sapotaceae, **Location:** Mawegui, Conner, Apayao, **Description:** Tiesa is a slender, erect tree with a spreading form. The color of its bark is brown containing white gummy latex. Leaves are mostly grouped at branch tips, it is thin, glossy, and petiolate. Flowers are small clusters borne at leaf axils or leaflet nodes. Fruits are variable in shape, from nearly round to somewhat ovoid, oval, or spindle-shaped, with or without a pointed apex or curved break. **Habitat:** In the Philippines, Tiesa adapts well from sea level to medium altitudes in areas with a short to long rainy season. **Phenology:** Fruits are best harvested from August to January when the fruits are fully matured and ripened. In general, plant establishment to plant maturity takes about 1 to 3 years. **Propagation:** Propagation may be done through seeds with fifty-day germination or cleft grafting. **Timber Classification:** Lesser-used Species, **Conservation Status:** Least Concern Species (IUCN Red List of Threatened Species]

Fig. 11: Balimbing [**Local Name:** Granatis, **Common Name:** Balimbing, **Scientific Name:** *Averrhoa carambola* Linn, **Family Name:** Oxalidaceae, **Location:** Marag Valley, Luna, Apayao, **Description:** It is a small tree growing to a height of 5 meters or less. Leaves are pinnate. The petals of its flower are purple to bright purple. Fruit is fleshy, green to greenish-yellow, sharp, and angular lobes. **Habitat:** In cultivated and semi-cultivated areas throughout the Philippines, **Phenology:** Carambola flowering seasons, which are generally from July to August, and fruiting seasons from October to January. **Propagation:** Commonly used when propagating starfruit trees, they are seed propagation, air layering and grafting. **Timber Classification:** Lesser used species, **Conservation Status:** Least Concern Species (IUCN Red List of Threatened Species)]

ten (10) species were identified as large-sized trees, followed by the nine (9) species were identified as small while the six (6) species considered as small-sized trees. The morphological characteristics of these species are shown in Figs. 8-22 (Edible fruit) and Figs. 23-32 (Ethnomedicinal Trees).

Fig. 12: Mabolo [**Local Name:** Kamagong, **Common Name:** Mabolo, **Scientific Name:** *Diplodiscus paniculatus* Turez. **Family Name:** Ebenaceae, **Location:** Calafug, Conner, Apayao, **Description:** Mabolo is a straight tree up to 60 ft tall and above, which has a drooping branch. It has black bark. Leaves are alternate, oblong, and pointed at the apex. It is dark green in color, smooth and glossy on the upper surface, and silver hairy underneath. The fruits are brown, smooth, to somewhat circular. **Habitat:** In forests, at low and medium altitudes. **Phenology:** Flowering season: June to September, but occasional fruits may be found on the tree at almost any time of the year. **Propagation:** The tree is generally grown from seeds. Shield-budding has been successfully practiced in the Philippines and is the preferred means of perpetuating superior types. **Timber Classification:** Premium species, **Conservation Status:** Critically Endangered Species (DAO No.2007-01)]

Fig. 13: Blackmuskheart [**Local Name:** Kandulce, **Common Name:** Black Muskheart, **Scientific Name:** *Alangium polyosmoides (F.Muell.) W.J.de Wilde & Duuyffjes,* **Family Name:** Cornaceae, **Location:** San Gregorio, Luna, Apayao, **Description:** A small to medium tree up to 20 meters in height. The bark is marked by lenticels, scales and corky bumps and irregularities, greyish in color. Leaves are alternate on the stem with a long point. The flowers are pale yellow in color from the leaf axis, while the fruit is green when not ripe and reddish when it is ripe. **Habitat:** Grows in coastal subtropical and dry rainforest. **Phenology,** The flowering seasons are from October to April. The fruit ripened from September to February. **Propagation:** Seed, **Timber Classification:** Lesser Used Species, **Conservation Status:** Least Concern Species (IUCN Red List of Threatened Species)]

## Conservation Status

Ten (10) edible fruit trees were classified as Least Concern, while two (2) species were classified as Critically Endangered. One per species was classified as Near

Fig. 14: Katap [**Local Name:** Kuribeng/Kusibeng, **Common Name:** Katap, **Scientific Name,** *Trigostemon philippinesis* Stapf. **Family Name:** Euphorbiaceae, **Location:** Dagupan, Luna, Apayao, **Description:** Katap is a medium-sized tree reaching up to 20 meters tall. The bark is brownish to greyish in color. Leaves are petiole terete, glabrous, or slightly pubescent. Fruits are green when unripe while reddish to dark purple when ripe. **Habitat:** Lowland evergreen to deciduous forests, sometimes on limestone hills, near rivers, growing on red to yellow calcareous soils to granite bedrocks. **Phenology:** Flowering and fruiting: all year round, **Propagation:** Seed and stem cutting, **Timber Classification:** Lesser Used Species, **Conservation Status:** Least Concern Species (IUCN Red List Threatened Species ver. 3.1. 2021)]

Fig. 15: Lubeg [**Local Name:** Malubeg, **Common Name:** Lubeg, **Scientific Name:** *Syzygium lineatum* (Roxb.) Merr. & Perry, **Family Name:** Myrtaceae, **Location:** Mawegui, Conner, Apayao, **Description:** It is a tree reaching up to five meters in height. Its bark is flaky, corky, and grayish to brown. Leaves are oppositely arranged, ovoid to elliptical. Flowers have an inferior ovary, regular and complete, while the fruits are in clusters and turn red to purple when ripe. **Habitat:** Disturbed forests and regrowth, also in the undisturbed swamp, mixed dipterocarp, and sub-montane forests at elevations to 2,000 meters. Usually on alluvial, swampy sites by rivers and streams, as well as on hillsides and ridges. **Phenology:** Flowering and Fruiting Season: July-August, **Propagation:** By seeds, cuttings, and grafting, **Timber Classification:** Lesser-used Species, **Conservation Status:** Least Concern Species (IUCN Red List of Threatened Species)]

Fig. 16: Makopa [**Local Name:** Makopa, **Common Name:** Makopa, **Scientific Name:** *Syzygium samarangense* (Blume) Merr. & Perry, **Family Name:** Myrtaceae, **Location:** Karikitian, Conner, Apayao, **Description:** Is a shrub or small tree with a small crown reaching a height of up to 10 meters? The bark is pinkish-gray in color. The leaves are elliptical but rounded at the base. The flowers are white to yellowish-white, while the fruit is bell-shaped, with colors ranging from white, pale green, or green to red, purple, or even black when it's ripe. **Habitat:** Seasonal rainforest, monsoon forest and gallery forest, usually at elevations below 100 meters. **Phenology:** Flowering Season: March-April, **Propagation:** Seeds lose their viability quickly and should be sown fresh from the fruit. Air layering is a simple method of propagation. **Budding**: The buds do not always continue to grow successfully. **Timber Classification:** Lesser-used species, **Conservation Status:** Least Concerned Species (IUCN Red List of Threatened Species ver. 3.1)]

Fig. 17: Bitok [**Local Name:** Maladalaga, **Common Name:** Bitok, **Scientific Name:** *Ochrocarpos ramiflorus* Merr., **Family Name:** Guttiferae, **Location:** Calanasan, Apayao, **Description:** Bitok is a tree with very pretty and glossy foliage. Tiny flowers are borne in clusters on the tree trunk and mature branches. Flowers have a very pleasant scent, which lasts even when the flowers dry up. The flowers appear in hot weather, and the fruits ripen during the rainy season. **Local Name:** Maladalaga, **Common Name:** Bitok, **Scientific Name:** *Ochrocarpos ramiflorus* Merr, **Family Name:** Guttiferae, **Location:** Calanasan, Apayao, **Description:** Bitok is a tree with very pretty and glossy foliage. Tiny flowers are borne in clusters on the tree trunk and mature branches. Flowers have a very pleasant scent, which lasts even when the flowers dry up. The flowers appear in hot weather, and the fruits ripen during the rainy season. **Habitat:** A mid-canopy tree in undisturbed mixed dipterocarp to sub-montane forests at elevations up to 1,400 meters. Usually on alluvial sites, but also common on hillsides and ridges. On sandy to clay soils, but also common on or near limestone. **Phenology:** Flower period is from June to September and fruiting period is from October to January. **Propagation:** By seed, **Timber Classification:** Lesser Used Species, **Conservation Status:** Least Concern Species (IUCN Red List of Threatened Species ver. 3.1)]

Fig. 18: Pakiling. [**Local Name:** Malatibig, **Common Name:** Pakiling, **Scientific Name:** *Ficus odorata* (Blanco) Merr., **Family Name:** Moraceae, **Location:** Dagupan, Luna, Apayao, **Description:** Pakiling is a small tree reaching a height of up to 9 meters. Leaves are simple, alternate, oblong, or broadly ovate and rounded. Fruits are attached to the trunk and branches, green to reddish in color; they are clustered in form. **Habitat:** It can be found in lowland primary and secondary forests at 250 to 500 meters. **Phenology:** The complete fruiting season is from February to August. **Propagation:** By seeds and can be asexually propagated by cuttings. **Timber Classification:** Lesser Used species, **Conservation Status:** Least Concerned Species (IUCN Red List of Threatened Species ver. 3.1)]

Fig. 19: Balakat-gubat [**Common Name:** Balakat-gubat, **Scientific Name:** *Balakata luzonica* (Vidal) Esser, **Family Name:** Euphorbiaceae, **Location:** Lubong, Calanasan, Apayao, **Description:** A tree grows up to 25m and has a diameter of about 100cm. The bark is brown and scaly. Leaves are shiny, alternate, ovately elliptic to oblong in shape, 7-14cm long to 6cm wide. Fruits are ovoid to obovoid and 1-seed. **Habitat:** Found in humid forests of Luzon, Visayas, Davao (Mindanao), **Propagation:** By seed, **Timber Classification:** Lesser Used Species. **Conservation Status:** Vulnerable (DAO No. 2007 s.01)]

Threatened, Vulnerable, and Endangered based on the combined data acquired in the Administrative Orders of the Department of Environment and Natural Resource and the International Union for Conservation of Nature (IUCN). Eight of the ten (10) identified species in Ethnomedicinal Trees were classified as Least Concern, and one species was classified as No Data and Not Threatened.

Fig. 20: Korthal gisihan **[Local Name:** Matabual, **Common Name:** Korthal gisihan, **Scientific Name:** *Aglaia korthalsii* Miq. **Family Name:** Meliaceae, **Location:** Eleazar, Calanasan, Apayao, **Description:** It is an evergreen tree growing to 26 m tall and above. Leaves are compounds. The bark is pale to dark reddish-brown. The fruit is globose, orange-red when ripe. **Habitat:** A mid-canopy tree in undisturbed mixed dipterocarp to sub-montane forests at elevations up to 1,400 meters. Usually on alluvial sites, but also common on hillsides and ridges. It is on sandy to clay soils, but it is also common on or near limestone. **Phenology:** Flower seasoning is from March to June and fruiting season is from June to August. **Propagation:** By seed, **Timber Classification:** Lesser Used Species, **Conservation Status:** Near Threatened (IUCN Red List of Threatened Species ver. 3.1)]

Fig. 21: Amuyong **[Local Name:** Namut, **Common Name:** Amuyong, **Scientific Name:** *Gonothalamus amuyon* (Blanco) Merr. **Family Name:** Annonaceae, **Location:** San Gregorio, Luna, Apayao, **Description:** Amuyon is a small tree. Leaves are smooth and oblong. Flowers are yellowish green, borne on sides on the or at the axils of the leaves. Fruit is smooth, cylindrically elongated, or sausage-like, green when unripe, and yellow when ripe. **Habitat:** Found in forests at low and medium altitudes, **Phenology:** Flowering seasons in May and June. **Propagation:** Seed, **Timber Classification:** Furniture/ Construction Hardwood, **Conservation Status:** Critically Endangered (IUCN Red List of Threatened Species)]

Fig. 22: Subiang **[Local Name:** Umila, **Common Name:** Subiang, **Scientific Name:** *Bridelia insulana* Hance, **Family Name:** Euphorbiaceae, **Location:** Lubong, Calanasan, Apayao, **Description:** An evergreen tree reaching a height of up to 10 meters. It has a straight bole and is cylindrical, and the bark is smooth with visible lenticels. Leaves are simple, alternate, and elliptically oblong. **Habitat:** In primary forest at low altitudes. **Phenology:** For observation, **Propagation:** By seed, **Timber Classification:** Lesser Used Species, **Conservation Status:** Least Concern Species (IUCN Red List of Threatened Species ver. 3.1)]

Fig. 23: Matang-hipon **[Local Name:** Addil, **Common Name:** atang-hipon, **Scientific Name:** *Breynia vitis-idaea* (Burm.f.) C.E.C. Fisch, **Family Name:** Euphorbiaceae, **Location:** Eleazar, Calanasan, Apayao, **Description:** A large shrub reaches 3-4 m high. The bark is yellowish-gray. Leaves are elliptic to elliptic-ovate. **Habitat:** Semi-evergreen and moist deciduous forests, also in the plains. Open areas, forest edges, **Propagation:** Seed, **Timber Classification:** Lesser Used Species, **Conservation Status:** Least Concern Species (IUCN Red List of Threatened Species)]

## DNA Barcoding

Using a brief, standardized DNA sequence from a particular area of an organism's genome, DNA barcoding is a technique for classifying species. The process entails identifying the species by analyzing an unknown specimen's DNA and comparing it to a reference database of known DNA sequences. It has been applied to the identification of

Fig. 24: Hauili [**Local Name:** Aplas, **Common Name:** Hauili, **Scientific Name:** *Ficus septica* Burm.f., **Family Name:** Moraceae, **Location:** San Jose, Flora, Apayao, **Description:** Hauili is an erect, small tree that grows 3 to 8 meters high, is smooth, and has more or less hairy young shoots. Leaves are smooth and shining, not all roughened, oblong-ovate to elliptic-ovate. **Habitat:** Ficus septica trees live up to 1800m in montane forests or secondary-growth environments. It can be seen often along rivers. **Phenology:** Fruiting and flowering season is observed from January to February. **Propagation:** Seed and cuttings, **Timber Classification:** Lesser Used Species, **Conservation Status:** Least Concern Species (IUCN Red List of Threatened Species)]

Fig. 25: Noni [**Local Name:** Apatot, **Common Name:** Noni, **Scientific Name:** *Morinda citrifolia* L., **Family Name:** Rubiaceae, **Location:** Tamalunog, Flora, Apayao, **Description:** Is a deciduous tree reaching a height of 10 meters above. Leaves are smooth and shining with tapering pointed tips. They are opposite, pinnately veined. Flowers are borne on inflorescences that grow on the stems of trees, and small white flowers grow around a half in across. Fruits are drupe and pale green in color. **Habitat:** Common in thickets and forests at low and medium altitudes throughout the Philippines. **Phenology:** Flowering and fruiting season is throughout the year. **Propagation:** Seed and cuttings, **Timber Classification,** Lesser Used Species, **Conservation Status:** No data]

species in many different settings, such as mixed samples, small or damaged specimens, and environmental samples. Additionally, DNA barcoding has been used to track changes in biodiversity over time and evaluate how human activity affects ecosystems (Hebert et al. 2003).

Fig. 26: Horsebush [**Local Name:** Arintudog, **Common Name:** Horsebush, **Scientific Name:** *Dendrolobium umbellatum* (L.) Benth, **Family Name:** Leguminosae, **Location:** Badduat, Kabugao, Apayao, **Description:** The species is a small tree. The leaves are trifoliate. The flowers are small and arranged in an umbel, while the fruit pods are beaded. **Habitat:** It grows on rocky or sandy seashores or tidal mud, monsoon forest edges, riverbanks, rocky cliffs, savanna, and secondary forests from sea level up to 180 m altitude. **Propagation:** By seed, **Timber Classification:** Lesser Used Species, **Conservation Status:** Least Concern Species (IUCN Red List of Threatened Species)]

Fig. 27: Rarang [**Local Name:** Bagbag, **Common Name:** Rarang, **Scientific Name:** *Erythrina subumbrans (Hassk) Merr,* **Family Name:** Fabaceae, **Location:** Marag Valley, Luna, Apayao, **Description:** A deciduous tree with a trunk and branches with spines, Bark is grey or grey-green, smooth, and soft, often with spine on twigs and trunk. Leaves are trifoliate, with 3 primary basal veins. Leaflets are broadly ovate, pointed, base rounded, margin entire, Flowers are large, pea-flower-shaped, and orange-color. **Habitat:** Moist valleys, near streams, in open locations, and secondary forests at low and medium elevations. **Phenology:** Flowering season is on May. **Propagation:** Seed and cuttings, **Timber Classification:** Lesser Used Species, **Conservation Status:** Not threatened]

The BLAST (NCBI-GenBank) was utilized to determine the homology of the plant samples. Table 2 presents the maximum identity of edible fruit and ethnomedicinal species with identical species provided by the Philippine Genome Center using *matK* Primer. One (1) species had a

Fig. 28: Tangisang bayawak [**Local Name:** Binuran, **Common Name:** Tangisang-bayawak, **Scientific Name:** *Ficus variegata* Blume, **Family Name:** Moraceae, **Location:** Eleazar, Calanasan, Apayao, **Description:** It is a large tree that may reach 40 meters in height. The bark is smooth and greyish in color. Young leaves are dentate, while old leaves have a wavy edge. Fruit is directly attached to the trunk or the branches. It is yellow-green. **Habitat:** Valleys at low to medium elevations. A mid-canopy tree in regrowth, forest gardens, and disturbed or open sites in mixed dipterocarp forests at elevations up to 500 meters. Along rivers and streams or on alluvial sites. **Phenology:** Fruiting season is from April to June. **Propagation:** Seed - germinates best at a temperature around 20°c. Air layering and tip cuttings around 4 - 12cm long, taken from lateral branches. **Timber Classification:** Lesser Used Species, **Conservation Status:** Least Concern Species (IUCN Red List of Threatened Species)]

Fig. 29: Lunas **[Local Name:** Kakling, Palitan and Lunas Bundok, **Common Name:** Lunas, **Scientific Name:** *Lunas amara* Blanco var. *amara,* **Family Name:** Rutaceae, **Location:** Upper Maton, Pudtol, Apayao, **Description:** Lunas is an erect shrub growing to a height of 3 meters. Twigs are smooth, and the young tips olivaceous lepidote. Leaves are alternately crowded, obovate-oblong, centimeters wide, often pointed at both ends. Bark are smooth. The outer bark color is grey, while the inner bark is green in color. **Habitat:** In thickets and forests and low and medium altitudes. **Phenology:** Flowering and bearing fruits all year round. **Propagation:** Plantation and seed propagation, **Timber Classification:** Lesser Used Species, **Conservation Status:** Least Concern Species (IUCN Red List of Threatened Species)]

Fig. 30: Halimunog **[Local Name:** Lumpanginay, **Common Name:** Halimumog, **Scientific Name:** *Ehretia philippinensis* A. DC. **Family Name:** Boraginaceae, **Location:** Eleazar, Calanasan, Apayao, **Description:** This small tree is up to 10 meters high with light brown bark. Leaves are alternate or opposite and usually entire. Fruit is schizocarp. **Habitat:** Dune bush and coastal forest, and inland in woodland and on forest margins. **Propagation:** By seed, **Timber Classification:** Lesser Used Species, **Conservation Status:** Least Concern Species (IUCN Red List of Threatened Species)]

Fig. 31: Talisai-gubat **[Local Name:** Lusit, **Common Name:** Talisai-gubat, **Scientific Name:** *Terminalia foetidissima* Griff. **Family Name:** Combretaceae, **Location:** Eleazar, Calanasan, Apayao, **Description:** It is a tree, up to 30m tall. The leaves are spirally arranged and tend to cluster near the tips of the branches. The leaves have an attractive cream-green mottled pattern. Flowers are small and occur on a spike. Fruit are hard, ellipsoid. **Habitat:** An upper canopy tree in dense primary forests, growing on alluvial and dry sites (hillsides and ridges) on clayey to sandy soils at elevations up to 200 meters. **Propagation:** By seed, **Timber Classification:** Furniture and Construction hardwood, **Conservation Status:** Least Concern Species (IUCN Red List of Threatened Species)]

maximum identity of 100% while fourteen (14) species had a maximum identity of 99%, like *Trigostemon philippinesis* Stapf. and *Alangium polyosmoides* (F.Muell.) W.J.de Wilde & Duuyfjes. The rest of the species comprised 98%, 97%,

Fig. 32: Bagna [**Local Name:** Sablot, **Common Name:** Bagna, **Scientific Name:** *Glochidion triandrum* (Blanco) C.B.Rob., **Family Name:** Euphorbiaceae, **Location:** Marag Valley, Luna, Apayao, **Description:** It is a tree reaching a height of 10 meters and above. The bark is light black to grayish. Leaves are deciduous, simple, and lanceolate, **Habitat:** In thickets and secondary forests at low and medium altitudes, **Phenology:** For observation, **Propagation:** Seed, **Timber Classification:** Lesser Used Species, **Conservation Status:** Least Concerned Species (IUCN Red List of Threatened Species)]

93%, 91%, and 90% maximum identity. The results show that matK produced a high amplification rate and, thus, higher universality.

This implies that the percentage of the sequence identified for each species was directly proportional to the accuracy of the identification. The higher the percentages, the more accurate the identification.

## Phytochemical Analysis

The use of herbal medicines and phytonutrients or nutraceuticals continues to expand rapidly across the world, with many people now resorting to these products for treatment of various health challenges in different national healthcare settings (WHO 2004). In addition, this past decade has obviously witnessed a tremendous surge in acceptance and public interest in natural therapies both in developing and developed countries, with these herbal remedies being available not only in drug stores, but also in food stores and

Table 2: BLAST analysis with the percentage of maximum identity (Max.Id.) for each sample collected.

| A. Edible fruit trees | | | | |
|---|---|---|---|---|
| No. | Common Name | Scientific Name | matK | Max. Id. % |
| 1 | Lipote | *Syzygium polycephaloides* (C.B.Rob.) Merr. | *Syzygium tenuiflorum* | 93.21 |
| 2 | Binukau | *Garcinia binucao* (Blanco) Choisy | *Ficus tikoua* | 90.81 |
| 3 | Tiesa | *Pouteria rivicoa* (Gaertn.f.) Ducke | *Lucuma campechiana* | 99.88 |
| 4 | Balimbing | *Averrhoa carambola* Linn | *Averrhoa carambola* | 100 |
| 5 | Mabolo | *Diplodiscus blancoi* A.DC. | *Ficus sagittata* | 93.18 |
| 6 | Black musk heart | *Alangium polyosmoides* (F.Muell.) W.J.de Wilde & Duuyfjes | *Alangium salviifolium* | 99.1 |
| 7 | Katap | *Trigostemon philippinesis* Stapf. | *Elaeocarpus floribundus* | 99.01 |
| 8 | Lubeg | *Syzygium lineatum* (Roxb.) Merr. & Perry | *Lucuma campechiana* | 99.88 |
| 9 | Makopa | *Syzygium samarangense* (Blume) Merr. & Perry | *Diospyros blancoi* | 99.88 |
| 10 | Bitok | *Ochrocarpos ramiflorus* Merr. | *Ficus hispida* | 97.96 |
| 11 | Pakiling | *Ficus odorata* (Blanco) Merr. | *Averrhoa carambola* | 98.93 |
| 12 | Balakat gubat | *Balakata luzonica* (Vidal) Esser | *Artocarpus lacucha* | 99.61 |
| 13 | Korthal Gisihan | *Aglaia korthalsii* Miq. | *Canarium album* | 99.2 |
| 14 | Amuyong | *Gonothalamus amuyon* (Blanco) Merr. | *Microcos blattifolia* | 99.61 |
| 15 | Subiang | *Bridelia insulana* Hance | *Brackenridgea australiana* | 98.45 |

| B. Ethnomedicinal Trees | | | | |
|---|---|---|---|---|
| No. | Common Name | Scientific Name | matK | Max. Id. % |
| 1 | Matang-hipon | *Breynia vitis-idaea* (Burmf.) C.E.E. Fisch | *Phyllanthus sieboldianus* | 99.76 |
| 2 | Hauili | *Ficus septica* Burm.f. | *Ficus tuphapensis* | 91.42 |
| 3 | Noni | *Morinda citrifolia* L. | *Ficus sarmentosa* | 96.76 |
| 4 | Horsebush | *Dendrolobium umbellatum* (L) Benth. | *Grona heterocarpos* | 97.72 |
| 5 | Rarang | *Erythrina subumbrans* (Hassk) Merr. | *Erythrina numerosa* | 99.62 |
| 6 | Tangisang Bayawak | *Ficus variegate* Blume | *Parashorea cf. tomentella* | 91.37 |
| 7 | Lunas | *Lunasia amara* Blanco *var.amara* | *Pouteria obovoidea* | 99.48 |
| 8 | Halimumog | *Ehretia philippinensis* A. DC. | *Maesa japonica* | 97.31 |
| 9 | Talisai-gubat | *Terminalia foetidissima* Griff | *Alseodaphne huanglianshanensis* | 99.63 |
| 10 | Bagna | *Glochidion triandrum* (Blanco) C.B.Rob. | *Litsea firma* | 99.51 |

supermarkets. Tables 3 and 4 provide the phytochemical analysis of the 25 surveyed tree species. Out of 15 edible fruit trees, only the Amuyong tree has no flavonoid content, only the Lubeg tree has no tannins, and Binukau, Tiesa, Lubeg, and Amuyong trees have no saponin compounds. For ethnomedicinal trees, out of ten (10), only Hauili and Talisai-gubat have no flavonoids, only Hauili and Rarang trees have no tannins, and Tangisang-bayawak, Talisai-gubat, and Lunas tress are lack of saponin metabolite.

Wadood et al. (2013) stated that the phytochemical study of plants is particularly significant in the pharmaceutical industry's quest to produce novel medications that may cure a wide range of illnesses. Secondary metabolites are organic chemicals produced by any life form, such as bacteria, fungi, animals, or plants, that are not directly engaged in the regular growth, development, or reproduction of the organism. They are sometimes referred to as specialized metabolites, toxins, secondary products, or natural products. It frequently has a significant impact on other interspecies defenses as well as plant defenses against herbivory. Humans use secondary metabolites as recreational drugs, flavorings, medications, and pigments.

In this study, the secondary metabolites that were considered are flavonoids, tannins, and saponins. Flavanoids consist of a large group of polyphenol compounds with a benzoyl-y-pyrone structure and are ubiquitously present in plants. The phenylpropanoid pathway synthesizes them. Available reports tend to show that secondary metabolites of a phenolic nature, including flavonoids, are responsible for a variety of pharmacological activities (Pandey et al. 2007). Flavonoids are hydroxylated phenolic substances and are known to be synthesized by plants in response to microbial infection (Dixon et al. 1983). The term tannin is widely applied to a large complex biomolecule of a polyphenol nature that has sufficient hydroxyls and other suitable groups such as carboxyl, to form strong complexes with various macromolecules (Navarrete 2013). Tannins are generally used in the tanning process and as healing agents in inflammation, burns, piles, and gonorrhea. Lastly, Saponins are an important group of plant secondary metabolites that are widespread throughout the plant kingdom. Saponins are basically phytochemicals that are found in most vegetables, beans, and herbs (Francis et al. 2002)

**Uses and Threats of Ethnomedicinal Trees**

Table 4 provides the identified ethnomedicinal trees from different barangays of six (6) municipalities of Apayao, including information on the utilization of cures for illnesses as claimed by community members. Ten (10) different ethnomedicinal trees are being used by the community members that address 32 health-related conditions. The most frequently used plant parts for the preparation of the remedy were leaves, followed by bark, roots, and sap.

Table 4 provides information on the uses of the identified ethnomedicinal species. Ten different ethnomedicinal trees were used to address 32 diseases or health-related conditions in this study. The most frequently used plant parts for the preparation of the remedy were leaves, followed by bark, roots, and sap. There were fourteen different ways to prepare the ethnomedicinal trees, and the most common forms were mashed or crushed, followed by boiling and decoction. Smoking, drinking, chewing, grinding, and directly applying to the skin were also practiced. The plant parts used and the mode of preparation of the ethnomedicinal trees depend on the ailments to be addressed and to whom they will be administered.

Most of the ethnomedicinal tree modes of preparations recorded were administered externally or by applying plant parts directly on the body parts, rubbing plant extracts and drops, and bathing or soaking. The rest were taken orally by drinking decoction, using it as a mouthwash, and chewing.

In this study, the identified ethnomedicinal trees belonged to the following families: Combretaceae, Euphorbiaceae, Moraceae, Boraginaceae, Leguminasae, Fabaceae, Rutaceae, and Rubiaceae.

The study conducted by Dapar (2020) on the Ethnomedicinal Importance and Conservation Status of Medicinal Trees among Indigenous Communities in Esperanza, Agusan del Sur, Philippines, supports some identified families of the study, such as the Moraceae (fig family) has proven for their potential biological and pharmacological activities. This family possesses a wide variety of bioactive compounds with biomedicinal properties that were formerly investigated in *Ficus racemose* L., *Ficus carica, and Ficus benjamina*. The Rutaceae family is comprised of aromatic deciduous shrubs and trees that have been used in gastronomy and traditional medicine. For instance, secondary metabolites of Zanthoxylum *limonella* were isolated from the stems, barks, and fruits which were reported to cure several health problems like stomachache, diarrhea, dental carries, and rheumatism.

In addition, threats to the survival of these trees were also determined, such as the effect of extreme weather events, forest fires caused by lightning, conversion of forest land into agricultural land, the occurrence of pests and diseases, and illegal logging.

**Assessment of the Utilization of Edible and Ethnomedicinal Trees Vis A Vis the Result of Phytochemical Analyses.**

The results of the phytochemical analyses provide support

Table 3: Compounds that are present in the identified species.

| A. Edible Fruit Trees | | | | |
|---|---|---|---|---|
| No. | Common Name | Parameter (Phytochemical Screening) | Result | Method Used |
| 1 | Lipote | Flavanoids | Present | Guevara et al. (2005) |
| | | Tannins | Present | |
| | | Saponins | Present | |
| 2 | Binukau | Flavanoids | Present | Guevara et al. (2005) |
| | | Tannins | Present | |
| | | Saponins | Absent | |
| 3 | Tiesa | Flavanoids | Present | Guevara et al. (2005) |
| | | Tannins | Present | |
| | | Saponins | Absent | |
| 4 | Balimbing | Flavanoids | Present | Guevara et al. (2005) |
| | | Tannins | Present | |
| | | Saponins | Present | |
| 5 | Mabolo | Flavanoids | Present | Guevara et al. (2005) |
| | | Tannins | Present | |
| | | Saponins | Present | |
| 6 | Black muskheart | Flavanoids | Present | Guevara et al. (2005) |
| | | Tannins | Present | |
| | | Saponins | Present | |
| 7 | Katap | Flavanoids | Present | Guevara et al. (2005) |
| | | Tannins | Present | |
| | | Saponins | Absent | |
| 8 | Lubeg | Flavanoids | Present | Guevara et al. (2005) |
| | | Tannins | Absent | |
| | | Saponins | Absent | |
| 9 | Makopa | Flavanoids | Present | Guevara et al. (2005) |
| | | Tannins | Present | |
| | | Saponins | Present | |
| 10 | Bitok | Flavanoids | Present | Guevara et al. (2005) |
| | | Tannins | Present | |
| | | Saponins | Present | |
| 11 | Pakiling | Flavanoids | Present | Guevara et al. (2005) |
| | | Tannins | Present | |
| | | Saponins | Present | |
| 12 | Balakat gubat | Flavanoids | Present | Guevara et al. (2005) |
| | | Tannins | Present | |
| | | Saponins | Present | |
| 13 | Korthal gisihan | Flavanoids | Present | Guevara et al. (2005) |
| | | Tannins | Present | |
| | | Saponins | Present | |
| 14 | Amuyong | Flavanoids | Absent | Guevara et al. (2005) |
| | | Tannins | Present | |
| | | Saponins | Absent | |
| 15 | Subiang | Flavanoids | Present | Guevara et al. (2005) |
| | | Tannins | Present | |
| | | Saponins | Present | |

Table Cont....

| B. Ethnomedicinal Trees | | | | |
|---|---|---|---|---|
| No. | Common Name | Parameter (Phytochemical Screening) | Result | Method Used |
| 1 | Matang-hipon | Flavanoids | Present | Guevara et al. (2005) |
| | | Tannins | Present | |
| | | Saponins | Present | |
| 2 | Hauili | Flavanoids | Absent | Guevara et al. (2005) |
| | | Tannins | Absent | |
| | | Saponins | Present | |
| 3 | Noni | Flavanoids | Present | Guevara et al. (2005) |
| | | Tannins | Present | |
| | | Saponins | Present | |
| 4 | Horsebush | Flavanoids | Present | Guevara et al. (2005) |
| | | Tannins | Present | |
| | | Saponins | Present | |
| 5 | Rarang | Flavanoids | Present | Guevara et al. (2005) |
| | | Tannins | Absent | |
| | | Saponins | Present | |
| 6 | Tangisang bayawak | Flavanoids | Present | Guevara et al. (2005) |
| | | Tannins | Present | |
| | | Saponins | Absent | |
| 7 | Lunas | Flavanoids | Present | Guevara et al. (2005) |
| | | Tannins | Present | |
| | | Saponins | Absent | |
| 8 | Halimumog | Flavanoids | Present | Guevara et al. (2005) |
| | | Tannins | Present | |
| | | Saponins | Present | |
| 9 | Talisai-gubat | Flavanoids | Absent | Guevara et al. (2005) |
| | | Tannins | Present | |
| | | Saponins | Absent | |
| 10 | Bagna | Flavanoids | Present | Guevara et al. (2005) |
| | | Tannins | Present | |
| | | Saponins | Present | |

evidence to support the traditional use of ethnomedicinal trees.

For example, Matang hipon leaves and bark have been used in the traditional medicine of the communities to treat a variety of diseases, including fever, tonsilitis, and after childbirth. Phytochemical analyses of matang-hipon have revealed the presence of active compounds, including flavonoids, tannins, and saponins. Flavanoids were stated to show anti-cancer properties, and plants containing high amounts of flavonoids could be useful as anti-bacterial; tannins are also known as healing agents for inflammation, burns, piles, and gonorrhea, and saponins are for lowering cholesterol levels, reducing blood sugar levels, and boosting the immune system, anti-inflammatory, antiviral, and anti-cancer properties (Sharma et al. 2020)

However, in the study of Guinto & Bautista (2020), they mention that saponins have a detrimental effect on one's health because they can cause sneezing and can irritate the mucous membrane. They can also destroy red blood corpuscles by hemolysis or the liberation of hemoglobin. In tannin compounds, they also mentioned that it is beneficial in the treatment of burns because they can precipitate the protein of the exposed tissue and will provide an antiseptic protective coat, thus preventing external infection, which is similar to the claim of the communities in Rarang (*Erythrina*

Table 4: Uses of ethnomedicinal trees.

| Parts used | Uses | Preparation |
|---|---|---|
| **1. Matang-hipon** | | |
| Leaves | Fever | Infusion of leaves in warm water, then drink 3-4 times daily. |
| | Tonsilitis | Smoked the dried leaves like tobacco. |
| Bark | After Childbirth | The processed bark is used as a stringent to prevent hemorrhages. |
| **2. Hauli** | | |
| Leaves | Headaches | Heat the leaves to the fire and put it directly on the forehead. |
| | Stomachache | Crushed/smashed the leaves, then put them to the stomach. |
| Roots | Diuretic | Decoction of roots. |
| | Boils | Grind the roots until they produce juice/sap, turn them into a paste, and add water or a certain oil. Collect the paste into a waterproof cloth and tie it off then place it directly on the affected surface skin. |
| | Asthma | Extract the liquid/juice/sap and add menthol to the juice, then can be inhaled. |
| Sap | Herpes | Extract the sap from the plant and directly apply to the affected area. |
| **3. Noni** | | |
| Leaves | Cough | Boil the leaves into the water or use the decoction process. |
| | Sprain | Poultice from the leaves applied to the affected sprained foot. |
| Roots | Painful body parts | Extract the sap/juice from the roots, add oil, and then apply it to the body parts. |
| | Wounds, Cuts, and sores | Follow the decoction process and apply it to the wounds, cuts, and sores. |
| Bark | Dermatitis | Chopped bark is boiled to the water. The decoction is used to wash the affected areas twice a day. |
| **4. Horsebush** | | |
| Leaves | Not able to sleep | Leaves were put at the back of the body as a remedy for sleeping. |
| | Malaria | Crushed the leaves and shoot and massaged to an enlarged spleen. |
| | General Tonic | Follow the decoction process, then drink. |
| | Fever | Used to bathe the body to prevent slight chill. |
| Bark | Fever | Used to bathe the body to prevent slight chill. |
| Roots | Vitamin | Boiled the roots, then drank. |
| **5. Rarang** | | |
| Leaves | Sores Eyes | Mashed and squeeze the leaves until the juice is extracted, and then drop them to the eyes. |
| | Wounds | Crush the leaves, then apply on the surface of the skin. |
| | Coldness to the Body | Crush the leaves and add oil, apply it to the back of the body. |
| Bark | Coldness to the Body | Decoction/Extract the liquid from the bark, then apply to the back of the body |
| **6. Tangisang bayawak** | | |
| Leaves | Boils | Mashed/crushed the leaves, then applied them to the affected skin. |
| Bark | Boils/Skin infection | Paste prepared from the sap/juice is mixed with milk and then applied to the affected skin. |
| | Dysentery | Directly chewed the bark. Another process is decoction or boiling the bark and then drinking. |
| **7. Lunas** | | |
| Leaves | Stomachache | Extract the juice/sap from the leaves, add oil, and use it as an ointment for the stomach. |
| | Ulcers | Boil the leaves |
| Bark | Snake Bites | Crush/mash the bark until the sap/juice is extracted and put into the affected area for first aid. |
| | Sore Eyes | The sap of the bark is used as the eye drops for the affected/irritated eyes. |

Table Cont....

| Parts used | Uses | Preparation |
|---|---|---|
| **8. Halimumog** | | |
| Leaves | Bruises and swelling joints | Mash/crush the leaves, then apply them to the affected skin or use the poultice preparation. |
| | Cellulitis | Mash/crush the leaves, then apply them to the affected skin or use the poultice preparation. |
| Bark and roots | Toothache | Boil the bark in the water and use it as a mouthwash |
| | Diarrhea and Dysentery | Boil the chopped bark or roots, not too many, and then wait until it becomes warm, then drink. |
| **9. Talisa-gubat** | | |
| Leaves | Heart failure and chest pain | Boil the leaves, and then drink the boiled water to prevent heart failure and chest pain. |
| Bark | Diabetes and High Cholesterol | Boil the bark in the water then drink. |
| **10. Bagna** | | |
| Leaves | Bruises | Crush the leaves, then apply them to the skin. |
| | Sprained Foot | Boil the leaves, then soak the sprained foot. |
| Bark | Rheumatic joints | Boil the bark, then soak the feet. |

*subumbrans*), Botgo (*Ficus caulocarpa*) species wherein they contain tannins. The leaves of the Rarang and Botgo species are used to treat wounds. However, prolonged utilization of tannin-rich plants, such as ordinary tea, is hazardous due to its carcinogenic potential.

## CONCLUSIONS

In this study, there are 25 edible and ethnomedicinal trees thriving in the forest of Apayao with the ecological status of critically endangered, vulnerable, rare, nearly threatened, least concerned, and data deficient. This serves as baseline information on native and medicinal trees as critical genetic resources in Apayao province.

Using DNA barcoding provides useful baseline data in selected edible and medicinal trees to distinguish genuine edible from non-edible fruit trees and medicinal tree species from non-medicinal ones. The primer matK is thought to be effective. The practical and precise verification of edible and medicinal plants using this DNA barcode may help to avoid the use of substitutes.

The phytochemical results of this study revealed that most of the edible fruit and ethnomedicinal trees contain flavonoids, saponins, and tannins compounds. The phytochemical results of this study revealed that most of the plants contain flavonoids, saponins, and tannins compounds. These phytochemicals have been shown to have a variety of biological activities, including antibacterial, antiviral, anti-inflammatory, and anti-cancer properties, which also support the claim of the communities on their traditional uses of ethnomedicinal trees as first aid in illnesses such as toothache, bruises, and rheumatic joints. All surveyed trees are susceptible to pests, diseases, and destruction brought about by natural phenomena such as the effect of climate change.

### Recommendations

1. Further study on the abundance of edible fruit trees and ethnomedicinal trees,
2. Further research on quantitative chemical analysis of the edible fruit and ethnomedicinal trees,
3. Further study on the causal organism on pests and diseases of the edible fruit and ethnomedicinal trees,
4. Conduct Information Dissemination and Communication (IEC) activity to communities to raise awareness on the importance, conservation, and protection of edible fruit and ethnomedicinal trees and
5. A policy recommendation for conservation and protection of the edible and ethnomedicinal trees.

## ACKNOWLEDGEMENT

The authors are conveying their sincerest gratitude to the Department of Environment and Natural Resources (DENR) through the Foreign-Assisted and Special Projects Service (FASPS) for providing funds for this study and to the Apayao State College for the unwavering support in the conduct of this study.

## REFERENCES

Dapar, M. 2020. Ethnomedicinal importance and conservation status of medicinal trees among indigenous communities in Esperanza, Agusan del Sur, Philippines. J. Compl. Med. Res., 11(1): 591.

Dixon, R. A., Dey, P. M. and Lamb, C. J. 1983. Phytoalexins: enzymology and molecular biology. Advances in Enzymology and Related Areas of Molecular Biology, 55: 1-136.

Francis, G., Kerem, Z., Makkar, H. P. and Becker, K. 2002. The biological action of saponins in animal systems: a review. British journal of Nutrition, 88(6): 587-605.

Franklin, J. and Miller, J. A. 2009. Mapping species distributions: spatial inference and prediction. Cambridge University Press.

Guevara, B. Q. 2005. A Guidebook to Plant Screening: Phytochemical and Biological. University of Santo Tomas Publishing House.

Guinto, V. M. R. and Bautista, A. S. 2020. Phytochemical analysis of black mulberry tree (Morus nigra). ASEAN Multidisciplinary Research Journal, 6.

Navarrete, P., Pizzi, A., Pasch, H., Rode, K. and Delmotte, L. 2013. Characterization of two maritime pine tannins as wood adhesives. Journal of Adhesion Science and Technology, 27(22): 2462-2479.

Pandey, K. D., Patel, A. K., Singh, M. and Kumari, A. 2021. Secondary metabolites from bacteria and viruses. Natural Bioactive Compounds, 19-40.

Wadood, A., Ghufran, M., Jamal, S. B., Naeem, M., Khan, A. and Ghaffar, R. 2013. Phytochemical analysis of medicinal plants occurring in local area of Mardan. Biochem anal biochem, 2(4): 1-4.

WHO 2004. WHO guidelines on safety monitoring of herbal medicines in pharmacovigilance systems. Geneva, Switzerland: World Health Organization

Hebert, P. D., Cywinska, A., Ball, S. L. and DeWaard, J. R. 2003. Biological identifications through DNA barcodes. Proceedings of the Royal Society of London. Series B: Biological Sciences, 270(1512): 313-321.

Sharma, T., Pandey, B., Shrestha, B. K., Koju, G. M., Thusa, R. and Karki, N. 2020. Phytochemical screening of medicinal plants and study of the effect of phytoconstituents in seed germination. Tribhuvan University Journal, 35(2): 1-11.

Nature Environment and Pollution Technology
An International Quarterly Scientific Journal

p-ISSN: 0972-6268
(Print copies up to 2016)
e-ISSN: 2395-3454

Vol. 23 | No. 3 | pp. 1407-1418 | 2024

Original Research Paper

https://doi.org/10.46488/NEPT.2024.v23i03.012

Open Access Journal

# Zinc and Boron Foliar Application Effects on Primed Mung Bean (*Vigna radiata* L.) Growth and Productivity

**Lalit Saini, Prasann Kumar and Hina Upadhyay†**

Department of Agronomy, School of Agriculture, Lovely Professional University, Phagwara-144411, Punjab, India

†Corresponding author: Hina Upadhyay; hina_bostan@yahoo.com

**Nat. Env. & Poll. Tech.**
**Website: www.neptjournal.com**

*Received:* 22-11-2023
*Revised:* 20-01-2024
*Accepted:* 23-01-2024

**Key Words:**
Gibberellic acid
Growth regulators
Micronutrients
Mung bean
Sustainable production

## ABSTRACT

Mung bean is recognized for its abundant high-quality protein content. For human consumption, it is a high-quality protein source and also serves various purposes crops, its harvested residue is used for green manuring and also used for fodder purposes. The research aimed to assess the impact of foliar micronutrient application on primed mung bean (*Vigna radiata*). The experimental procedures were executed in the sandy loam soil prevalent in the central plain region of Punjab. The investigation was conducted during the Zaid season 2022, focusing on the (SML-1827) mung bean variety. Specifically, the research assessed the impact of foliar micronutrient applications involving zinc and boron at 15 and 45 days after sowing (DAS) on primed mung bean growth characteristics. The experimental design employed a Randomized Block Design, incorporating 11 distinct treatment combinations, each replicated thrice. The investigation revealed that foliar micronutrient treatment on primed mung bean substantially influenced growth and yield parameters. Growth indicators for mung bean exhibited a positive trend when zinc and boron were jointly applied to primed seeds with gibberellic acid, followed by a decline in the control group, which experienced typical growth conditions devoid of growth regulators and micronutrients. Specifically, the highest recorded plant height was 70.1 cm in the T9 (GA(50 mg.$L^{-1}$) + $ZnSO_4$ (0.5%) + B (1%)) treatment, while the lowest height was 58 cm in the T0 (control) treatment. Similarly, the most significant fresh weight was observed in T9 (GA (50 mg.$L^{-1}$) + $ZnSO_4$ (0.5%)+ B (1%)) treatments at 136.8 g, with the lowest weight recorded in T0 (control) treatments at 86.6g. the most significant grain yield was achieved in T9 112 g.$m^{-2}$, followed by T10 (SA(150 mg.$L^{-1}$)+ $ZnSO_4$ (0.5%)+B (1%)) at 105.7 g.$m^{-2}$. This study suggests micronutrients and growth regulators can be sustainable agricultural inputs to enhance soil health and productivity.

## INTRODUCTION

Micronutrients play a pivotal role in human health, plant growth, and agricultural development, with documented significance (Ahmad et al. 2022, Haider et al. 2022). All crops require micronutrients in small quantities for optimal growth and productivity (Nasiri et al. 2010). The global issue of micronutrient deficiency is particularly acute in underdeveloped nations (FAO 2017). Analyzing the nutritional composition of mung bean seeds reveals 367 mg phosphorus and 132 mg calcium per 100 g of seeds, accompanied by 50% carbohydrates, 26% protein, 4%-5% ash, 3%-4.5% fiber, and 3% lipids (Ahmed et al. 2000). Mung bean sprouts are notably rich in vitamin C (8 mg per 100 g). They are typically cultivated in semi-arid and arid climates (Haider et al. 2021). Mung beans boast a protein content of 25%, a carbohydrate content of 59.9%, and notable levels of lysine (460 mg.$g^{-1}$) and tryptophan (60 mg.$g^{-1}$). Sprouted mung beans exhibit significant quantities of ascorbic acid, riboflavin (0.21 mg per 100 g), minerals (3.84 g per 100 g), and calcium (75 mg per 100 g). Zinc insufficiency affects approximately 2 billion individuals globally (Gibson 2012) and ranks as the fifth leading cause of mortality in underdeveloped countries and the eleventh globally (Stevens et al. 2009). In Pakistan, around 33% of children and 40% of mothers experience zinc insufficiency, primarily in rural regions. Iron deficiency is another global concern impacting approximately 2 billion people, predominantly children and women, in Latin America, South Asia, and Africa (Glahn et al. 2021). Roughly 40% of women of reproductive age in South Asia are anaemic, accounting for 37.5% of all anaemic cases worldwide. In South America, the Caribbean, and Central America, approximately 46.2%, 42.9%, and 33.9% of the population are anemic, with a higher prevalence among children under 11 months (Hummel et al. 2020). In 2018-19, India cultivated mung beans over 4.1 million hectares,

yielding 1.9 million tonnes with a productivity of 463 kg per hectare (Gowda et al. 2015). Major mung bean-producing states include Orissa, Maharashtra, Andhra Pradesh, Telangana, Madhya Pradesh, Karnataka, and Uttar Pradesh, with Orissa leading in acreage, output, and productivity, followed by Maharashtra and Andhra Pradesh in area and production. To meet the agricultural demands of the nation, the cultivation and production of agricultural seeds must be expanded (Alshikh 2019). Mung bean, classified as an annual vine with yellow blossoms and fuzzy brown pods, is further categorized into three subspecies, with *Vigna radiata* subsp. radiata being the cultivated variety. The plant ranges in height from 15 to 125 cm and boasts a robust root system characterized by numerous slender lateral roots and root nodules. The stems are densely branched, and exhibit twining at their tips, with young stems appearing purple or green and aging stems taking on a greyish-yellow or brown hue. Mung beans are predominantly self-pollinating, and their fruits are elongated cylindrical or flat cylindrical pods, typically yielding 30 to 50 pods per plant. According to Mina (2015), these pods measure 5-10 cm in length and 0.4-0.6 cm in width, containing 12-14 seeds separated by septa. Seed priming is a fundamental physiological approach for enhancing seed performance, facilitating swifter and more synchronized germination, and ultimately contributing to increased crop yield. Various methods encompass priming with chemicals, antioxidants, and hormones, guarding against cell death in the apical meristem, especially DNA damage (Hussain et al. 2016). Boron, vital for processes like cell wall construction, maintenance of biological membrane integrity, and the efficient transfer of sugar or energy to fuel plant growth (Qamar et al. 2016), becomes critical in the event of a boron deficiency. Such a deficiency hinders growth, reduces the root-to-shoot ratio, and limits essential nutrients such as phosphorus, potassium, and iron levels in plant roots and shoots (Broadley et al. 2012). Mung beans are a notable source of lysine, an amino acid often deficient in grains (Ntatsi et al. 2018). Despite the numerous advantages in crop management and nutritional value, the cultivation and production of mung beans are not expanding at the same pace as other cereals. Zinc sulfate treatment has been observed to enhance pod count per plant, seed output, and the vegetative growth of legumes (Singh et al. 2015). Gibberellic acid (GA3) has the potential to induce morphological and yield-related changes in various legume crops, including soybeans and mung beans (Sardoei et al. 2014). As a plant growth regulator, GA3 is increasingly important in agriculture for increasing production. Gibberellin seed priming is pivotal in influencing multiple aspects of plant life, including seed germination, leaf expansion, phloem loading, water, and mineral uptake, assimilate transportation, and yield index (Pasala et al. 2016). Salicylic acid may also play a crucial role in regulating plant development. Priming seeds with hormones mitigates the adverse effects of various environmental stressors, facilitating accelerated germination and improved seedling establishment. Consequently, such primed seeds exhibit increased resilience to soil-borne pests and diseases (Movaghatian et al. 2013).

## MATERIAL AND METHODS

The impact of zinc and boron foliar treatment on the growth-primed Mung bean (salicylic acid gibberellin) was studied at the farm of the Department of Agronomy, Lovely Professional University, Phagwara, Kapurthala district. A study trial was conducted in the Zaid season of 2022 in that area, which has a sub-tropical environment in the middle plains of Punjab. The study used a randomized block design (RBD) and was duplicated three times for each therapy. The crop was harvested on May 17th, 2022, after it was sown on March 9th, 2022. Each plot's dimensions were set at 5m x 3m. The farm, 252 meters above mean sea level and 20 km from Jalandhar, Punjab, is between 31.24 North latitude and 75.6909 East latitude. The soil in the region is sandy loamy to clay-textured, with a pH range of 7.8 to 8.5. The existing location is classified as part of the Trans-Gangetic Agro-climatic Zone. It receives 527.1 mm of rain per year on average.

### Plant Genetic Material

Summer mung bean cultivar SML 1827 features an upright and determinate plant type with medium size. It bears pods in clusters and matures synchronously (in approximately 62 days). Each pod contains roughly ten seeds. It is resistant to yellow mosaic disease. Grains are bright green and medium in size, with good culinary characteristics. It produces 5.0 quintals per acre on average.

### Experimental Treatments

The study comprised six hours of seed priming before planting with salicylic acid at 150 $mg.L^{-1}.kg^{-1}$ seed and gibberellin at 50 $mg.L^{-1}.kg^{-1}$ seed as a plant growth regulator. Zinc and boron foliar applications were administered 15 and 45 days after seeding. T0 is the control, T1 is the GA (50 $mg.L^{-1}$), T2 is the SA (150 $mg.L^{-1}$), T3 is the $ZnSO_4$ (0.5%), T4 is the B (1%), T5 is the GA (50 $mg.L^{-1}$) + $ZnSO_4$ (0.5%), T6 is the GA (50 $mg.L^{-1}$) + B (1%), T7 is the SA (150 $mg.L^{-1}$) + $ZnSO_4$ (0.5%), T8: SA (150 $mg.L^{-1}$) + B (1%), T9: GA (50 $mg.L^{-1}$) + $ZnSO_4$ (0.5%) + B (1%), T10: SA (150 $mg.L^{-1}$) + $ZnSO_4$ (0.5%) + B (1%). The observations were made at 30, 60, and at harvest following seeding, as well as at harvesting.

### Fertilizers

In the current study, the suggested fertilizer dose for summer moong was 5 kilograms N (11 kg urea) and 16 kg $P_2O_5$ (100 kg single superphosphate) per acre. Nitrogen is applied when planting, and a single superphosphate is utilized as a potassium supplement during sowing.

Plant height, fresh weight, dry weight, number of branches, nodule count, Chl a, Chl b, total soluble sugar, and grain yield were recorded on time.

### Data Collection

**Plant height:** In each plot, the final plant height was measured using a measuring scale, the height of three randomly selected plants was estimated at 30DAS, 60DAS, and at harvest, and observations were gathered. The mean of these three plants was calculated and analyzed using the OPSTAT and SPSS software packages.

**Number of branches:** The number of branches was counted at 30 and 60 DAS from three randomly selected plants in each plot and averaged.

**Number of nodules:** Three plants were randomly removed from the observation plot using a fork without injuring the roots at the Mung bean flowering and harvesting stages. The roots were gently cleansed to eliminate any dirt that had adhered to them, and nodules were counted.

**Fresh and dry weight:** Four Mung bean plants were picked from each batch independently for fresh and dry weight calculations. Following fresh weight measurement, the tissues were placed in a hot air oven at 50°C for two days, followed by three days at 60°C, and dried plant weight was recorded at 30 DAS, 60 DAS, and at harvest (Zhang et al. 2016).

**Chl a and Chl b:** The chlorophyll content in the leaf of mung bean was estimated by the method of Arnon DI. (1949) at 30 and 60DAS. The absorbance was measured at 645 nm and 663 nm. The amount of chlorophyll was calculated using the absorbance coefficient.

Chlorophyll 'a' (mg/g Fresh Weight) = $12.25(A663)-2.79(A645) \times \frac{V}{1000 \times W}$

Chlorophyll 'b' (mg/g Fresh Weight) = $21.50(A645)-5.10(A663) \times \frac{V}{1000 \times W}$

where V = Final volume of the extract

W = Fresh weight of the leaves

A = absorbance at a specific wavelength.

**Total soluble sugar:** The method developed by Sadasuvam & Manickam (1992) was followed. Total soluble sugar was estimated in the leaf of mung bean at 30 and 60DAS. Absorbance was measured at 620 nm with the help of a spectrophotometer.

**Grain yield:** After harvesting weight of grains was measured by weighing balance.

**Statistical analysis**: The statistical analysis of the data variance was performed using R software with Duncan 's multiple range test (DMRT) with a probability $p<0.05$. The means of all treatments were compared.

Table 1: Effect of foliar application of zinc and boron on primed mung bean Plant height and Fresh Weight during Summer 2022.

| Treatments | Plant Height | | | Fresh Weight | | |
|---|---|---|---|---|---|---|
| | 30DAS | 60DAS | At Harvest | 30DAS | 60DAS | At Harvest |
| T0 Control | $11.00^{h}\pm 0.50$ | $54.83^{g}\pm 2.25$ | $54.83^{h}\pm 3.00$ | $10.80^{f}\pm 1.51$ | $63.16^{g}\pm 2.69$ | $86.60^{i}\pm 3.65$ |
| T1 GA (50 mg.L$^{-1}$) | $11.17^{h}\pm 0.76$ | $57.67^{ef}\pm 2.25$ | $58.00^{g}\pm 1.89$ | $12.89^{de}\pm 1.58$ | $68.63^{f}\pm 12.23$ | $94.06^{h}\pm 3.80$ |
| T2 SA [150 mg.L$^{-1}$] | $11.50^{gh}\pm 0.50$ | $57.00^{f}\pm 2.00$ | $60.83^{ef}\pm 2.75$ | $11.98^{ef}1.77\pm$ | $65.96^{fg}\pm 3.55$ | $88.16^{i}\pm 3.15$ |
| T3 $ZnSO_4$ [0.5%] | $12.83^{ef}\pm 0.76$ | $58.33^{def}\pm 2.51$ | $60.33^{f}\pm 4.50$ | $14.07^{cd}\pm 1.17$ | $81.40^{e}\pm 3.15$ | $105.00^{g}\pm 4.05$ |
| T4 B [1%] | $12.17^{fgh}\pm .076$ | $57.00^{f}\pm 2.00$ | $62.67^{de}\pm 3.25$ | $12.66^{de}\pm 0.41$ | $78.50^{e}\pm 3.05$ | $103.30^{g}\pm 4.03$ |
| T5 GA [50 mg.L$^{-1}$] + $ZnSO_4$ [0.5%], | $14.83^{bc}\pm 1.04$ | $61.00^{c}\pm 2.50$ | $61.67^{def}\pm 2.25$ | $18.63^{a}\pm 2.25$ | $111.40^{b}\pm 3.61$ | $127.93^{c}\pm 5.44$ |
| T6 GA [50 mg.L$^{-1}$] + B [1%] | $13.50^{de}\pm 1.32$ | $59.17^{cde}\pm 2.02$ | $66.83^{b}\pm 3.01$ | $13.03^{de}\pm 0.30$ | $104.66^{c}\pm 4.31$ | $115.76^{e}\pm 4.10$ |
| T7 SA [150 mg.L$^{-1}$] + $ZnSO_4$ [0.5%] | $14.50^{cd}\pm 1.32$ | $60.17^{cd}\pm 1.75$ | $65.17^{bc}\pm 2.50$ | $14.86^{c}\pm 0.35$ | $90.00^{d}\pm 3.60$ | $122.00^{d}\pm 4.51$ |
| T8 SA [150 mg.L$^{-1}$] + B (1%) | $12.50^{efg}\pm 0.50$ | $58.33^{def}\pm 2.51$ | $66.00^{b}\pm 1.72$ | $14.21^{cd}\pm 1.85$ | $81.10^{e}\pm 3.70$ | $110.16^{f}\pm 3.81$ |
| T9 GA [50 mg.L$^{-1}$] + $ZnSO_4$ [0.5%] + B [1%] | $16.50^{a}\pm 0.86$ | $65.17^{a}\pm 2.25$ | $63.23^{cd}\pm 0.76$ | $17.38^{ab}\pm 2.59$ | $119.93^{a}\pm 4.85$ | $136.86^{a}\pm 6.15$ |
| T10 SA [150 mg.L$^{-1}$] + $ZnSO_4$ [0.5%] + B [1%] | $15.83^{ab}\pm 0.76$ | $63.00^{b}\pm 1.73$ | $70.17^{a}\pm 1.50$ | $16.47^{b}\pm 0.33$ | $112.66^{b}\pm 3.75$ | $131.93^{b}\pm 5.61$ |
| CD | 1.30 | 3.50 | 3.98 | 2.48 | 8.12 | 7.83 |

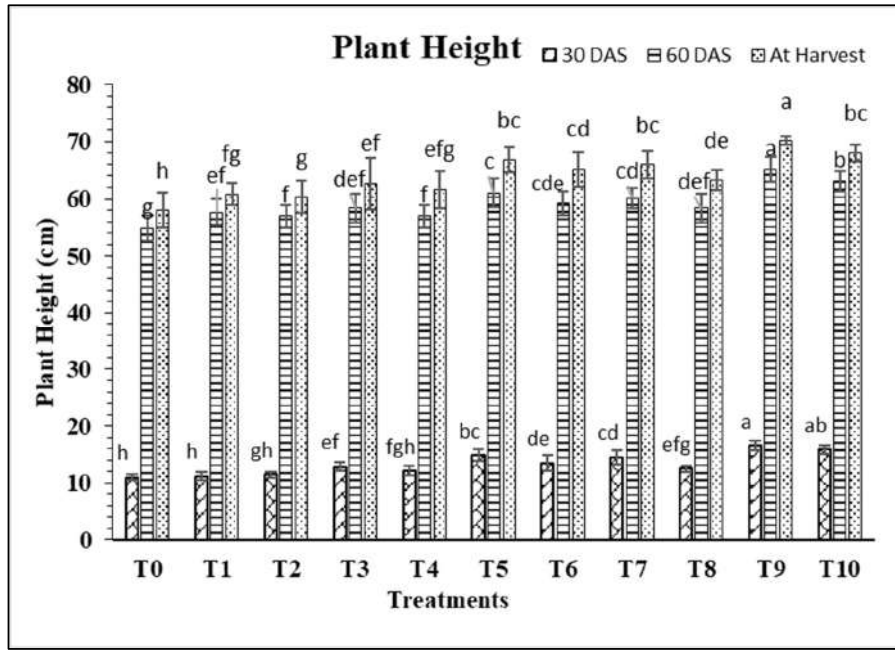


Fig. 1: Effect of foliar application of zinc and boron on primed mung bean plant height at 30, 60DAS and at harvest.

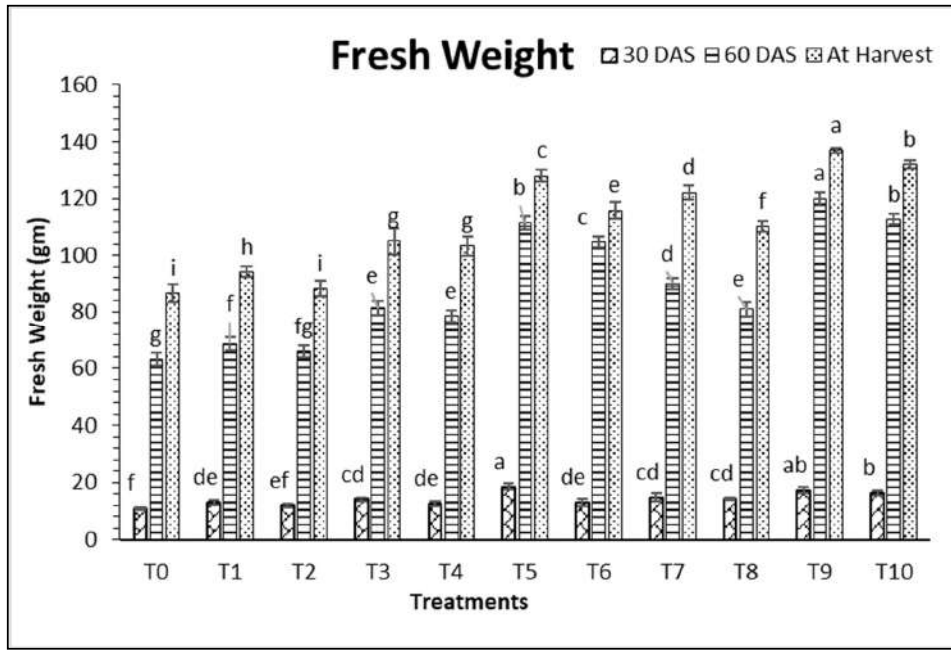


Fig. 2: Effect of foliar application of zinc and boron on primed mung bean fresh weight at 30, 60DAS and harvest.

## RESULTS AND DISCUSSION

This study investigated the impact of varying foliar spray treatments on the height of primed mung bean plants at different stages. At 30 days after sowing (30DAS), the tallest and shortest plants, measuring 16.5 cm and 11 cm, were observed in the T9 treatment (comprising GA (50 $mg.L^{-1}$), $ZnSO_4$ (0.5%), and B (1%)) and the control treatment (T0), respectively. Subsequently, at 60 days after sowing (60DAS), the tallest plant height was recorded in T9 (65.1 cm) and the control (T1) at 54.8cm shown in Table 1. At harvest, the

Table 2: Effect of foliar application of zinc and boron on primed mung bean Dry weight (gm plant$^{-1}$) and Number of Branches during Summer 2022.

| Treatments | Dry Weight | | | Number of Branches | |
|---|---|---|---|---|---|
| | 30DAS | 60DAS | At Harvest | 30DAS | 60DAS |
| T0 Control | $3.56^{d}\pm 0.20$ | $19.74^{f}\pm 0.84$ | $27.93^{h}\pm 1.18$ | $2.00^{c}\pm 0$ | $4.66^{d}\pm 0.58$ |
| T1 GA [50 mg.L$^{-1}$] | $3.96^{cd}\pm 0.15$ | $21.44^{f}\pm 3.82$ | $30.34^{g}\pm 1.22$ | $2.67^{bc}\pm 0.58$ | $5.33^{cd}\pm 0.58$ |
| T2 SA [150 mg.L$^{-1}$] | $3.93^{cd}\pm 0.15$ | $20.61^{f}\pm 1.11$ | $28.44^{h}\pm 1.01$ | $2.67^{bc}\pm 0.58$ | $5.00^{d}\pm 0$ |
| T3 $ZnSO_4$ [0.5%] | $4.40^{bc}\pm 0.29$ | $25.43^{e}\pm 0.98$ | $33.87^{f}\pm 1.30$ | $3.00^{ab}\pm 0$ | $5.66^{bcd}\pm 0.58$ |
| T4 B [1%] | $4.36^{bcd}\pm 0.30$ | $24.53^{e}\pm 0.95$ | $33.32^{f}\pm 1.30$ | $2.67^{bc}\pm 0.58$ | $5.33^{cd}\pm 0.58$ |
| T5 GA [50 mg.L$^{-1}$] + $ZnSO_4$ [0.5%], | $5.10^{ab}\pm 0.20$ | $34.81^{b}\pm 1.13$ | $41.26^{b}\pm 1.75$ | $3.33^{ab}\pm 0.58$ | $6.33^{abc}\pm 0.58$ |
| T6 GA [50 mg.L$^{-1}$] + B [1%] | $4.03^{cd}\pm 0.15$ | $32.70^{c}\pm 1.34$ | $37.34^{d}\pm 1.32$ | $3.33^{ab}\pm 0.58$ | $6.33^{abc}\pm 0.58$ |
| T7 SA [150 mg.L$^{-1}$] + $ZnSO_4$ [0.5%] | $4.43^{bc}\pm 0.35$ | $28.12^{d}\pm 1.12$ | $39.35^{c}\pm 1.45$ | $3.33^{ab}\pm 0.58$ | $6.33^{abc}\pm 0.58$ |
| T8 SA [150 mg.L$^{-1}$]+ B [1%] | $4.39^{bc}\pm 0.59$ | $25.34^{e}\pm 1.15$ | $35.53^{e}\pm 1.22$ | $3.00^{ab}\pm 0$ | $5.66^{bcd}\pm 0.58$ |
| T9 GA [50 mg.L$^{-1}$] + $ZnSO_4$ [0.5%] + B [1%] | $5.37^{a}\pm 0.55$ | $37.47^{a}\pm 1.51$ | $44.15^{a}\pm 1.98$ | $3.67^{a}\pm 0.58$ | $7.00^{a}\pm 0$ |
| T10 SA (150 mg.L$^{-1}$] + $ZnSO_4$ [0.5%] + B [1%] | $5.26^{a}\pm 0.30$ | $35.20^{b}\pm 1.17$ | $42.55^{b}\pm 1.81$ | $3.67^{a}\pm 0.58$ | $6.66^{ab}\pm 0.58$ |
| CD | 0.49 | 2.52 | 2.53 | 0.63 | 0.92 |

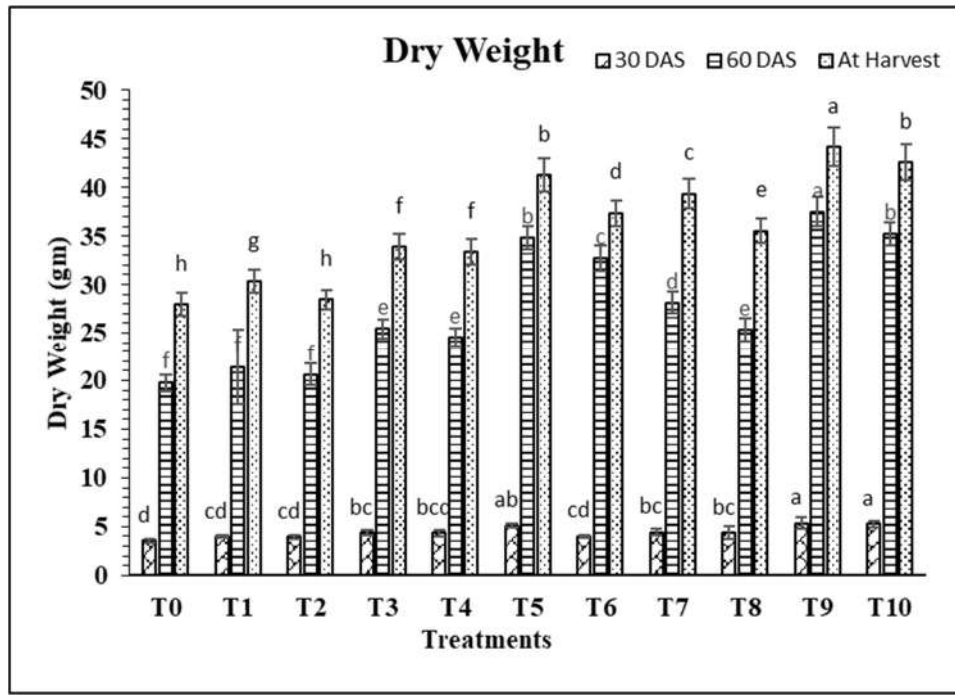


Fig. 3: Effect of foliar application of zinc and boron on primed mung bean dry weight at 30 and 60 DAS.

most significant plant height was achieved in T9 (70.1cm), followed by T10 (SA(150 mg.L$^{-1}$)+ $ZnSO_4$ (0.5%)+B (1%)) at 68cm, while T0 (control) had a height of 58 cm (Table 1 and Fig. 1). It is noteworthy that GA3 priming primarily influences the elongation of tissues with rapid growth, such as stems, petioles, and flower inflorescences (Ayala-Silva et al. 2005). Ross et al. (2003) reported that GA3 promotes stem elongation, contributing to improved plant height. Increased plant height corresponds to heightened vegetative growth, conversely. Boron plays a role in metabolism and increases photosynthetic rates, often resulting in greater mature plant height (Kaisher et al. 2010). In contrast, zinc supplementation significantly enhanced the growth and height of Mung bean plants (Gobarah et al. 2006).

In treatment T9 (comprising GA(50 mg.L$^{-1}$), $ZnSO_4$ (0.5%), and B (1%)) and the control group (T0), we observed

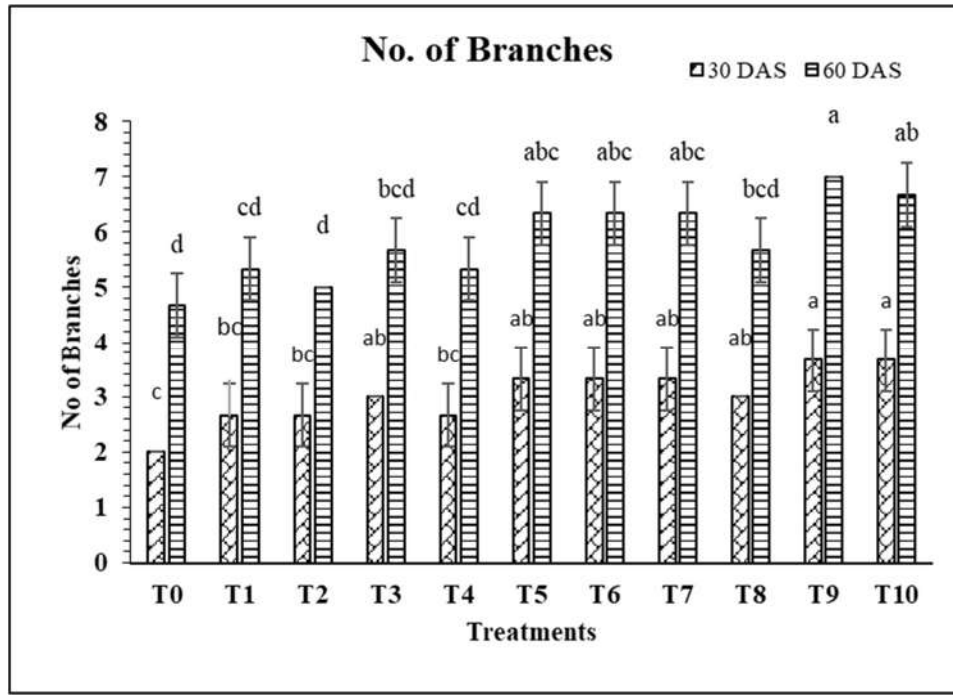


Fig. 4: Effect of foliar application of zinc and boron on primed mung bean branches at 30 and 60 DAS.

variations in the fresh weight of mung bean plants. The highest fresh weight recorded was 17.38g in T9, while the lowest was 10.8 g in the control (T0) 30 days after sowing (30DAS). At 60 days after sowing (60DAS), the maximum fresh weight reached 119.9 g in T9 and 63.1 g in T0 shown in Table 1. At harvest, the highest fresh weight was 136.8 g in T9, followed by 131.9 g in T10 (SA(150 mg.$L^{-1}$) + $ZnSO_4$ (0.5%) + B (1%)), with the lowest at 86.6g in the control (T0) (Table 1 and Fig. 2). Plant growth parameters, including stem and overall fresh weight, exhibited variability due to different foliar applications and treatment types. Rahman et al. (2018) reported that foliar application of GA3 significantly enhanced plant growth. They observed an increase in leaf area and fresh weight in *Vigna radiata*, concluding that GA3, combined with zinc or boron as foliar applications, provided substantial benefits for achieving greater leaf area, ultimately enhancing plant fresh weight.

Regarding dry weight, T9 (GA(50 mg.$L^{-1}$) + $ZnSO_4$ (0.5%)+ B (1%)) had the highest dry weight at 5.37 g, while T1 (control) had the lowest at 3.56 g, as depicted in Table 2 and Fig. 3. The maximum dry weight at harvest was 44.15 g in T9, followed by 42.52 g in T10 [SA (150 mg.$L^{-1}$) + $ZnSO_4$ (0.5%) + B (1%)] (Table 2 and Fig. 3). Salam et al. (2005) reported that micronutrients, particularly zinc and boron, significantly influenced the accumulation of dry matter, resulting in increased plant biomass, pod and seed production, and other growth-related parameters.

At 30 days after sowing (30DAS), the highest and lowest number of branches per plant were observed in T9 (GA (50 mg.$L^{-1}$) + $ZnSO_4$ (0.5%)+ B (1%)) and the control group (T0), with 3.6 and 2 branches, respectively. At 60 days after sowing (60DAS), the maximum number of branches was 7 in T9, followed by 6.6 in T10 (SA(150 mg.$L^{-1}$) + $ZnSO_4$ (0.5%)+B (1%)), and the control (T0) had 4.6 branches (Table 2 and Fig. 4). Zinc treatments have been known to enhance growth characteristics in various crops, as reported by Jain & Dahama (2007), Sharma & Abraham (2010), Dubey et al. (2013), and Khalil & Prakash (2014). In *Phaseolus vulgaris*, soil and foliar applications of zinc substantially increased plant height, branch count, radiation use efficiency, and extinction coefficient, according to studies by Necat et al. (2004) and Nasri et al. (2011).

At 30 days after sowing (30DAS), the highest and lowest numbers of nodules in mung bean roots were observed in T9 (GA(50 mg.$L^{-1}$) + $ZnSO_4$ (0.5%)+ B (1%)) and the control group (T0), with 21.3 and 13 nodules, respectively. At 60 days after sowing (60DAS), the maximum number of nodules was recorded in T9, followed by 35.6 in T10 (SA(150 mg.$L^{-1}$)+ $ZnSO_4$ (0.5%)+B (1%)), and the control (T0) had 22 nodules (Table 3 and Fig. 5). Das et al. (2012) found that combining various micronutrients resulted in increased nodulation. Inversely proportional to nitrogen fixation: as nodule number increases, nitrogen fixation decreases. There is an evident correlation between N-fixation and

Table 3: Effect of foliar application of zinc and boron on primed mung bean number of nodules and Chl a, b (mg.g$^{-1}$ FW) during Summer 2022.

| Treatments | Number of Nodules | | Chlorophyll "a" | | Chlorophyll "b" | |
|---|---|---|---|---|---|---|
| | 30DAS | 60DAS | 30DAS | 60DAS | 30DAS | 60DAS |
| T0 Control | $13^{f}\pm 1.00$ | $22^{g}\pm 3.00$ | $4.43^{e}\pm 0.70$ | $8.58^{f}\pm 0.10$ | $1.33^{c}\pm 0.24$ | $2.11^{d}\pm 0.17$ |
| T1 GA [50 mg.L$^{-1}$] | $15^{de}\pm 1.00$ | $24.66^{fg}\pm 3.51$ | $5.46^{de}\pm 0.85$ | $9.28^{def}\pm 0.29$ | $1.62^{bc}\pm 0.26$ | $2.43^{bcd}\pm 0.59$ |
| T2 SA [150 mg.L$^{-1}$] | $14^{ef}\pm 2.00$ | $25.66^{ef}\pm 3.51$ | $4.73^{de}\pm 0.08$ | $8.99^{ef}\pm 0.37$ | $1.55^{bc}\pm 0.39$ | $2.31^{cd}\pm 0.58$ |
| T3 $ZnSO_4$ [0.5%] | $17.66^{bc}2.51\pm$ | $27.33^{de}\pm 3.51$ | $5.28^{de}\pm 1.73$ | $9.49^{cdef}\pm 0.28$ | $1.94^{bc}\pm 0.16$ | $2.77^{abcd}\pm 0.25$ |
| T4 B [1%] | $16.66^{cd}\pm 2.08$ | $26.33^{def}\pm 3.51$ | $5.18^{de}\pm 1.11$ | $9.33^{def}\pm 0.20$ | $1.79^{bc}\pm 0.06$ | $2.79^{abcd}\pm 0.52$ |
| T5 GA [50 mg.L$^{-1}$] + $ZnSO_4$ [0.5%], | $17.66^{bc}\pm 1.52$ | $33.66^{b}\pm 3.05$ | $7^{bc}\pm 1.82$ | $10.71^{ab}\pm 0.28$ | $2.33^{b}\pm 0.51$ | $3.15^{abc}\pm 0.58$ |
| T6 GA [50 mg.L$^{-1}$] + B [1%] | $16.33^{cd}\pm 2.51$ | $30.66^{c}\pm 3.05$ | $5.85^{cde}\pm 0.25$ | $10.3^{abcd}\pm 0.17$ | $2.41^{b}\pm 0.35$ | $2.63^{bcd}\pm 0.35$ |
| T7 SA [150 mg.L$^{-1}$] + $ZnSO_4$ [0.5%] | $17.66^{bc}\pm 2.08$ | $30.33^{c}\pm 3.51$ | $6.1^{bcd}\pm 0.21$ | $10.44^{abc}\pm 0.44$ | $2.42^{b}\pm 0.35$ | $3.16^{abc}\pm 0.40$ |
| T8 SA [150 mg.L$^{-1}$] + B (1%) | $17^{c}\pm 2.00$ | $28.66^{cd}\pm 2.51$ | $5.59^{cde}\pm 0.84$ | $9.94^{bcde}\pm 0.49$ | $1.96^{bc}\pm 0.71$ | $2.97^{abcd}\pm 0.35$ |
| T9 GA [50 mg.L$^{-1}$] + $ZnSO_4$ [0.5%] + B [1%] | $21.33^{a}\pm 2.51$ | $37.66^{a}\pm 3.51$ | $8.76^{a}\pm 1.12$ | $11.15^{a}\pm 0.99$ | $3.28^{a}\pm 0.13$ | $3.72^{a}\pm 0.54$ |
| T10 SA [150 mg.L$^{-1}$] + $ZnSO_4$ [0.5%] + B [1%] | $19.33^{b}\pm 3.05$ | $35.66^{ab}\pm 3.05$ | $7.39^{b}\pm 0.42$ | $10.93^{ab}\pm 1.28$ | $2.3^{b}\pm 0.68$ | $3.41^{ab}\pm 0.87$ |
| CD | 2.91 | 5.72 | 1.76 | 0.93 | 0.69 | 0.78 |

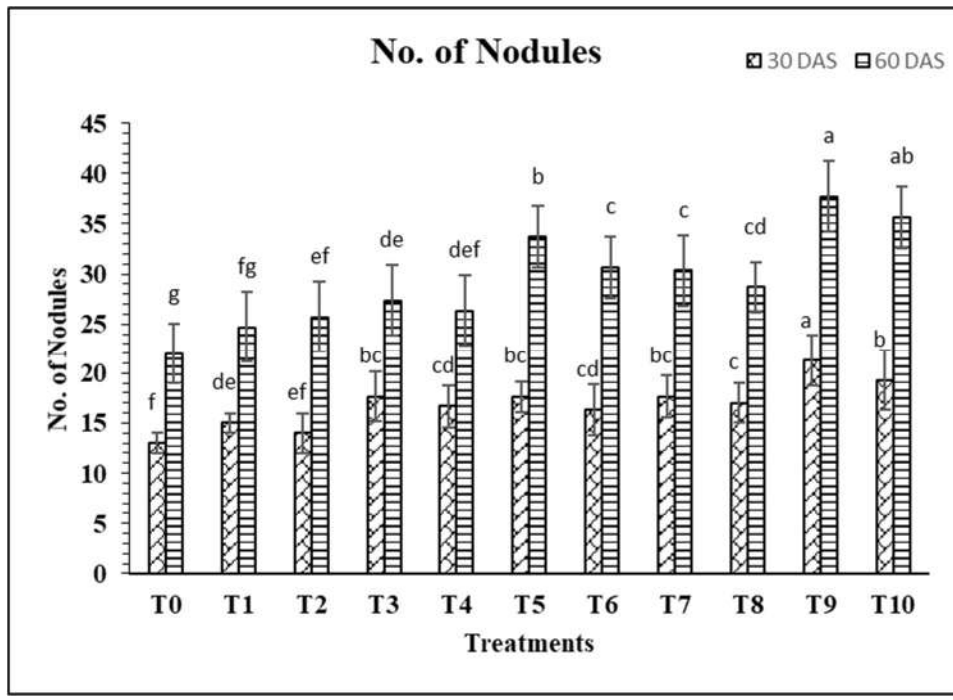


Fig. 5: Effect of foliar application of zinc and boron on primed mung bean nodules number at 30 and 60 DAS.

protein synthesis in mung bean plants. Combining B and Zn increased the rate of root nodulation and, consequently, the protein content of cereals by a substantial margin, according to the findings. Increased nodule counts and desiccated weight were observed as a consequence of micronutrient treatment (Tripathi et al. 2012).

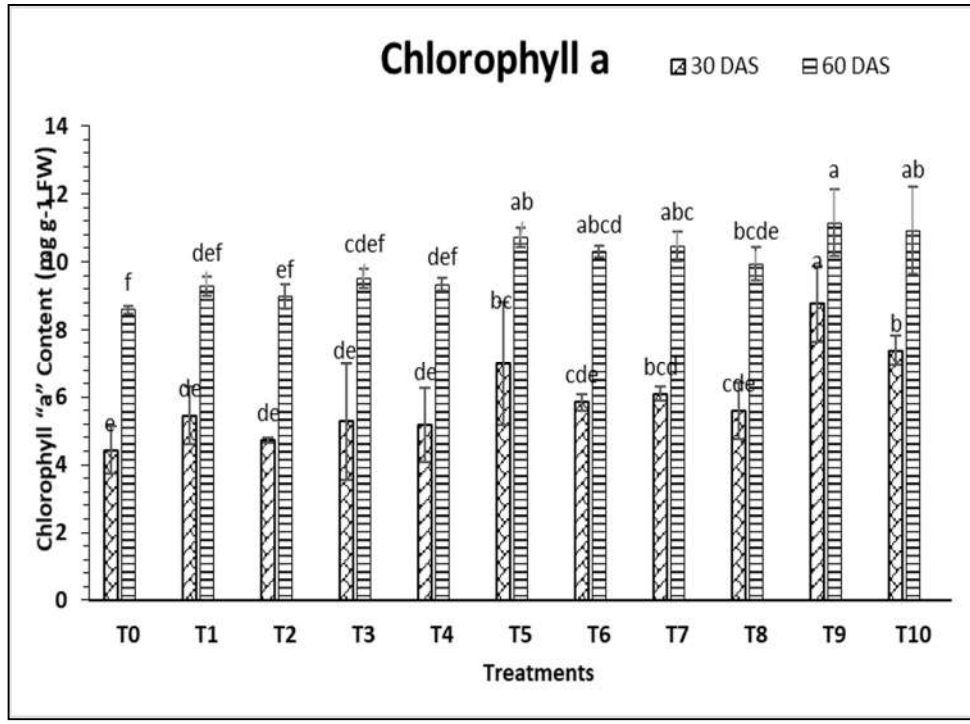


Fig. 6: Effect of foliar application of zinc and boron on primed mung bean Chlorophyll "a" mg.g$^{-1}$ FW at 30 and 60 DAS.

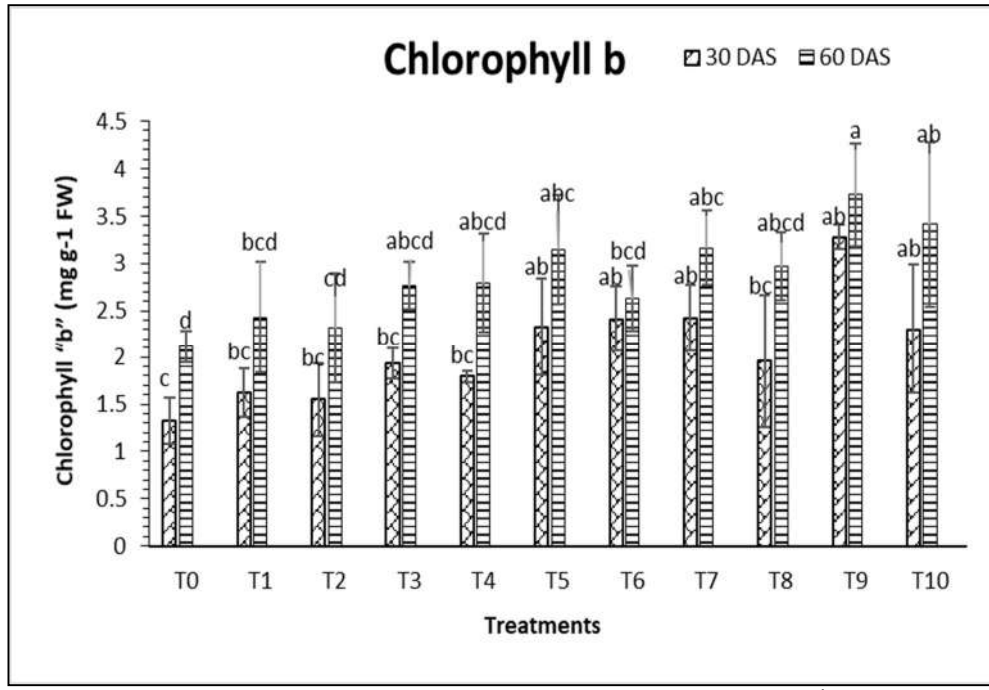


Fig. 7: Effect of foliar application of zinc and boron on primed mung bean Chlorophyll "b" mg.g$^{-1}$ FW at 30 and 60 DAS.

In the plant leaves, the content of chlorophyll a raised when the foliar application of $ZnSO_4$ (0.5%) and B (1%) in a primed seed with gibberellic acid (T9) done, then the content of chlorophyll "a" was raised by 8.7, and 11.14 mg.g$^{-1}$ FW at 30 and 60DAS in respect to controlled treatment (T0) (Table 3 and Fig. 6). At 30 days after sowing (30DAS),

Table 4: Effect of foliar application of zinc and boron on primed mung bean Total Soluble Sugar (mg.g$^{-1}$ FW) and Grain Yield (g.m$^{-2}$) during Summer 2023.

| Treatments | Total Soluble Sugar | | Grain Yield (g.m$^{-2}$) |
|---|---|---|---|
| | 30DAS | 60DAS | Harvest |
| T0 Control | $0.47^{b}$± 0.06 | $0.82^{e}$± 0.08 | $89.93^{f}$± 4.12 |
| T1 GA [50 mg.L$^{-1}$] | $0.53^{b}$± 0.03 | $1^{cde}$ ± 0.17 | $92.67^{f}$± 3.72 |
| T2 SA [150 mg.L$^{-1}$] | $0.52^{b}$± 0.04 | $0.96^{de}$± 0.06 | $90.8^{f}$± 8.95 |
| T3 $ZnSO_4$ [0.5%] | $0.59^{b}$± 0.15 | $1.24^{bcde}$ ± 0.06 | $96.13^{de}$± 3.61 |
| T4 B [1%] | $0.59^{b}$± 0.05 | $1.14^{cde}$± 0.07 | $93.07^{ef}$± 6.44 |
| T5 GA [50 mg.L$^{-1}$] + $ZnSO_4$ [0.5%], | $0.85^{ab}$± 0.09 | $1.63^{abc}$ ± 0.15 | $103.73^{bc}$± 4.84 |
| T6 GA [50 mg.L$^{-1}$] + B (1%) | $0.73^{ab}$± 0.06 | $1.38^{abcde}$ ± 0.13 | $101.2^{c}$± 6.44 |
| T7 SA [150 mg.L$^{-1}$] + $ZnSO_4$ [0.5%] | $0.82^{ab}$± 0.09 | $1.52^{abcd}$ ± 0.21 | $101.73^{c}$± 4.77 |
| T8 SA [150 mg.L$^{-1}$] + B (1%) | $0.69^{ab}$± 0.11 | $1.31^{bcde}$± 0.07 | $97.47^{d}$± 6.63 |
| T9 GA [50 mg.L$^{-1}$] + $ZnSO_4$ [0.5%] + B [1%] | $1.05^{a}$± 0.02 | $1.95^{a}$± 0.24 | $112.93^{a}$± 5.28 |
| T10 SA [150 mg.L$^{-1}$] + $ZnSO_4$ [0.5%] + B (1%) | $0.87^{ab}$± 0.06 | $1.78^{ab}$± 0.47 | $105.73^{b}$± 6.82 |
| CD | 0.13 | 0.31 | 10.09 |

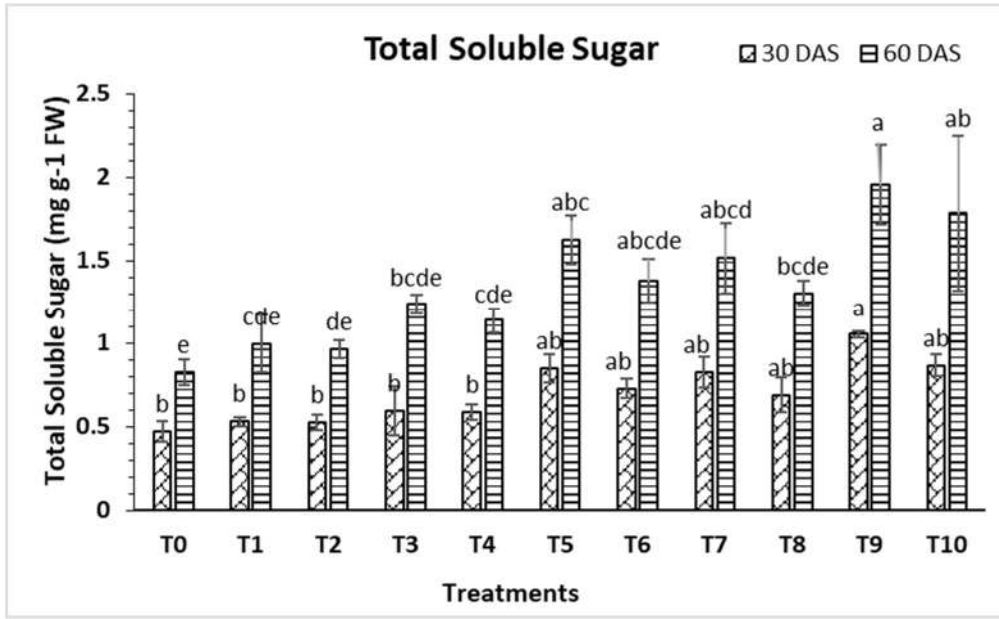


Fig. 8: Effect of foliar application of zinc and boron on primed mung bean total soluble sugar mg.g$^{-1}$ FW at 30 and 60 DAS.

The maximum content of chlorophyll "b" was observed in treatment T9, followed by 2.3 in T10 (SA(150 mg.L$^{-1}$)+ $ZnSO_4$ (0.5%)+B (1%)). The control (T0) had 1.3 mg.g$^{-1}$ (FW) (Table 3 and Fig. 7). At 60DAS highest content of chlorophyll "a" was 7 mg·g$^{-1}$ fresh leaf of mung bean plant observed in treatment T9 (GA(50 mg.L$^{-1}$)+ $ZnSO_4$ (0.5%)+ B (1%)) as compared to control treatment T0 4.67. Enhanced chlorophyll formation and plant cell division may contribute to an increase in leaf chlorophyll content. This finding is supported by Shah et al. (2012) and Khan et al. (2009). In contrast, Soheil et al. (2011) reported that zinc supplementation increased the levels of chlorophyll a, chlorophyll b, carotenoids, and protein in soybeans.

At 30 days after sowing (30DAS), the maximum total soluble sugar in mung bean plant leaves was observed in T9 (GA(50 mg.L$^{-1}$)+ $ZnSO_4$ (0.5%)+ B (1%)) and the control group (T0), with 1.05 and 0.47 mg.g$^{-1}$ FW (fresh weight) shown in Table 4, respectively. At 60 days after sowing (60DAS), the maximum total soluble sugar was 1.95 in T9, followed by 1.78 in T10 (SA(150 mg.L$^{-1}$)+ $ZnSO_4$ (0.5%)+B (1%), and the control (T0) had 0.82 mg.g$^{-1}$ FW (fresh weight) (Table 4 and Fig. 8). The result supported by Islam et al. (2021), Ahmad et al. (2021), Kaur et al. (2023). The promotion of seed germination and early

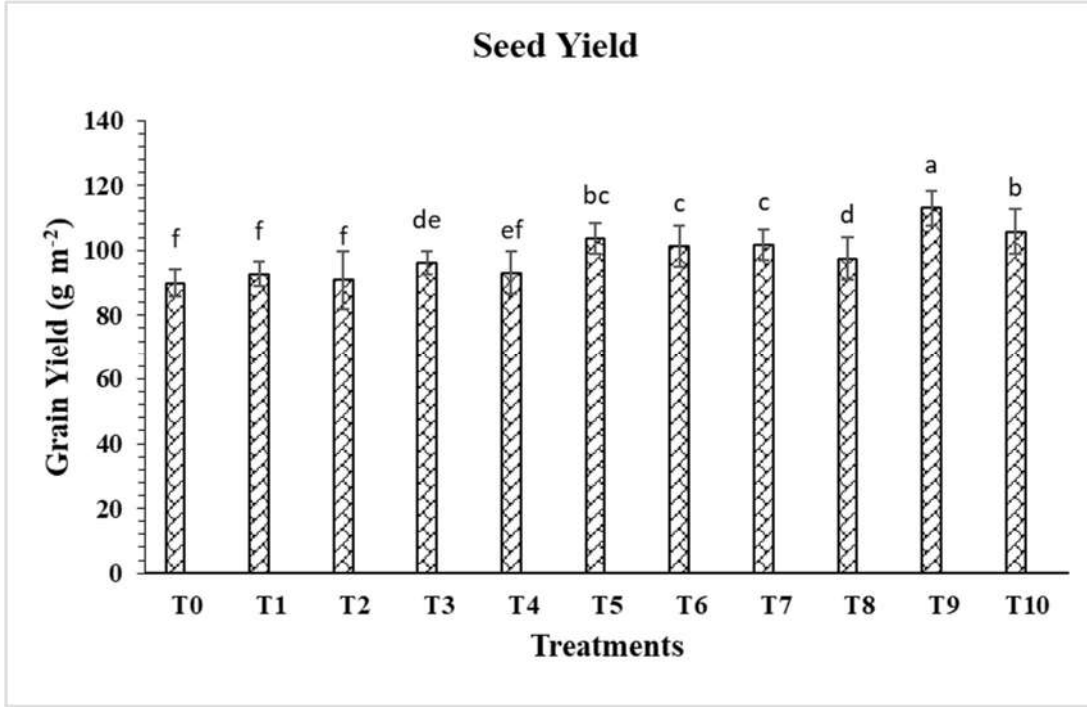


Fig. 9: Effect of foliar application of zinc and boron on primed mung bean Grain Yield ($g.m^{-2}$) at 30 and 60 DAS.

seedling development by GA priming may have contributed to an increase in photosynthetic activity. Additionally, it could potentially enhance the overall well-being of plants and safeguard the pathways involved in sucrose synthesis. Micronutrients zinc and boron, when applied foliarly, can exert a direct influence on enzymes that are implicated in the process of sucrose metabolism.

After the mung bean harvest, the most significant grain yield was achieved in T9 112 $g.m^{-2}$, followed by T10 [SA (150 $mg.L^{-1}$) + $ZnSO_4$ (0.5%) + B (1%)] at 105.7 $g.m^{-2}$, while T0 (control) had a grain yield of 89.9 $g.m^{-2}$ (Table 4 and Fig. 9). The result supported by Chen et al. (2017) the combined foliar application of Zn, B, and seed priming with gibberellic acid maximize the net photosynthetic rate in leaves and better translocation of metabolites and photosynthates. The concentration of Zn in grains increases due to an increase in source Zn concentration through the soil and foliar application of Zn. Usman et al. (2014) reported that Zn-fertilization increases biological yield and grains, enhancing the number of grains per pod in mung bean.

## CONCLUSION

In conclusion, our experimental findings underscore the significant positive impact of foliar micronutrient application and the priming of mung bean seeds using Gibberellic acid (GA) and salicylic acid (SA) on various growth and yield parameters. The treatment combining GA-primed seeds with foliar applications of zinc and boron [GA (50 $mg.L^{-1}$) + $ZnSO_4$ (0.5%) + B (1%)] produced remarkable improvements in mung bean development and yield. Notably, GA (50 $mg.L^{-1}$) + $ZnSO_4$ (0.5%) + B (1%) emerged as the most effective treatment, underscoring the preference for Gibberellic acid priming at 50 $mg.L^{-1}.kg^{-1}$ seed in conjunction with varying intervals of micronutrient foliar spraying. Additionally, treatment T10 [SA (150 $mg.L^{-1}$) + $ZnSO_4$ (0.5%) + B (1%)] yielded results comparable to those of T9 [GA (50 $mg.L^{-1}$) + $ZnSO_4$ (0.5%) + B (1%)] in terms of plant height, the number of branches, and fresh weight. Treatment T5 [GA(50 $mg.L^{-1}$) + $ZnSO_4$ (0.5%)] showed similar outcomes to T10 [SA(150 $mg.L^{-1}$) + $ZnSO_4$ (0.5%) + B (1%)] concerning nodule number and dry weight. The Seed priming with gibberellic acid and combined application of boron or Zn-fertilization increases biological yield and grains, enhancing the number of grains per pod in mung bean. The most significant grain yield was achieved in T9 112 $g.m^{-2}$, followed by T10 [SA(150 $mg.L^{-1}$)+ $ZnSO_4$ (0.5%)+B (1%)] at 105.7 $g.m^{-2}$. Conversely, the absolute control treatment (T0), devoid of growth regulators or micronutrients, demonstrated the lowest treatment efficacy. These findings underscore the efficacy of these treatments in optimizing mung bean growth and yield, providing valuable insights for agricultural practices and future research in this domain.

## ACKNOWLEDGEMENT

The authors thank the School of Agriculture at Lovely Professional University, Phagwara, Punjab for their assistance in delivering the necessary components and completing the trial.

## REFERENCES

Ahmad, F., Kamal, A., Singh, A., Ashfaque, F., Alamri, S., Siddiqui, M.H. and Khan, M.I.R. 2021. Seed priming with gibberellic acid induces high salinity tolerance in Pisum sativum through antioxidants, secondary metabolites, and up-regulation of antiporter genes. Plant Biol., 23: 113-121.

Ahmad, M., Ishaq, M., Shah, W.A., Adnan, M. and Fahad, S. 2022. Managing phosphorus availability from organic and inorganic sources for optimum wheat production in calcareous soils. Sustainability, 14: 7669. https://doi.org/10.3390/su14137669

Ahmed, F., Haraguchi, T., Hirota, O. and Rahman, M.A. 2000. Growth analysis, yield, and canopy structure in maize-Mung bean intercropping. Bull. Inst. Trop. Agric. Kyushu Univ., 23: 61-69.

Alshikh, Z.A.S. 2019. Effect of DAP fertilizer and seed rate on two varieties of mung bean as a forage crop. Doctoral dissertation, Sudan Univ. Sci. Technol.

Ayala-Silva, T., Akin, D.E., Foulk, J. and Dodd, R.B. 2005. Effect of growth regulators on yield, fiber quality, and quantity in flax (*Linum usitatissimum* L.). PGRSA Quart., 33: 90-100.

Broadley, M., Brown, P., Cakmak, I., Rengel, Z. and Zhao, F. 2012. Function of nutrients: micronutrients. In Marschner's Mineral Nutrition of Higher Plants, 3rd edn (Ed. P Marschner) pp. 191-248.

Chen, X.P., Zhang, Y.Q., Tong, Y.P., Xue, Y.F. and Liu, D.Y. 2017. Harvesting more grain zinc of wheat for human health. Sci. Rep., 7: 1-8.

Das, S., Pareek, N., Raverkar, K.P., Chandra, R. and Kaustav, A. 2012. Effectiveness of micronutrient application and Rhizobium inoculation on growth and yield of Chickpea. Int. J. Agric. Environ. Biotechnol., 5: 445-452.

Dubey, S.K., Tripathi, S.K. and Singh, B. 2013. Effect of sulfur and zinc levels on growth, yield, and quality of mustard [Brassica juncea (L.) Czern & Cross]. Agric. J. Crop Sci. Technol., 2: 2319-3395.

Food and Agriculture Organization (FAO). 2017. The State of Food Security and Nutrition Globally. Second edition. Rome, Italy.

Gibson, R.S. 2012. Zinc deficiency and human health: Etiology, health consequences, and future solutions. Plant Soil, 361: 291-299.

Glahn, R.P. and Noh, H. 2021. Redefining bean iron biofortification: A review of the evidence for moving to a high Fe bioavailability approach. Front. Sustain. Food Syst., 5: 215.

Gobarah, E., Mirvat, M.H., Mohamed, M.H. and Tawfik, M.M. 2006. Effect of phosphorus fertilizer and foliar spraying with zinc on growth, yield, and quality of groundnut under reclaimed sandy soil. J. Appl. Sci. Res., 2: 491-496.

Gowda, C.L., Chaturvedi, S.K., Gaur, P.M., Sameer Kumar, C.V. and Jukanti, A.K., 2015. Pulses research and development strategies for India. Pulses Handbook. pp. 17-33

Haider, M.U., Hussain, M., Farooq, M., Ul-Allah, S. and Ansari, M.J. 2021. Zinc biofortification potential of diverse Mung bean [*Vigna radiata* (L.) Wilczek] genotypes under field conditions. PLoS One, 16: e0253085.

Haider, M.W., Nafees, M., Ahmad, I., Ali, B. and Maryam, 2022. Postharvest dormancy-related changes of endogenous hormones in relation to different dormancy-breaking methods of potato (Solanum tuberosum L.) tubers. Front. Plant Sci., 13: 945256. https://doi.org/10.3389/fpls.2022.945256

Hummel, M., Talsma, E.F., Taleon, V., Londoño, L. and Brychkova, G. 2020. Iron, zinc and phytic acid retention of biofortified, low phytic acid, and conventional bean varieties when preparing common household recipes. Nutrients, 12: 658. https://doi.org/10.3390/nu12030658

Hussain, M., Waqas-ul-Haq, M., Farooq, S., Jabran, K. and Farroq, M., 2016. The impact of seed priming and row spacing on the productivity of different cultivars of irrigated wheat under early season drought. Experimental Agriculture, 52(3): 477-490.

Islam, M.R., Kamal, M.M., Alam, M.A., Hossain, J., Soufan, W., Skalicky, M. and Islam, M.S. 2021. Physiochemical changes of Mung bean [*Vigna radiata* (L.) R. Wilczek] in responses to varying irrigation regimes. Horticulturae, 7: 565.

Jain, N.K. and Dahama, A. K. 2007. Effect of different levels of zinc on the extractable zinc content of soil and chemical composition of rice. Asian J. Plant Sci., 1: 20-21.

Kaisher, MS., Rahman, M. A., Amin, M.H.A., Amanullah, A.S.M. and Ahsanullah, A.S.M. 2010. Effects of sulfur and boron on the seed yield and protein content of Mung bean. Bangladesh Res. Publ. J., 3: 1181-1186.

Kaur, H., Nazir, F., Hussain, S.J., Kaur, R., Rajurkar, A.B., Kumari, S. and Khan, M.I.R. 2023. Gibberellic acid alleviates cadmium-induced seed germination inhibition through modulation of carbohydrate metabolism and antioxidant capacity in mung bean seedlings. Sustainability, 15: 3790.

Khalil, K. and Prakash, V. 2014. Effect of rhizobial inoculation on growth, yield, nutrient and economics of summer urdbean (*Vigna mungo* L.) in relation to zinc and molybdenum. Int. J. Adv. Res. Chem. Chem. Eng., 1: 25.

Khan, H.A., Ayub, C. M., Pervez, M. A., Bilal, R. M., Shahid, M. A. and Ziaf, K. 2009. Effect of seed priming with NaCl on salinity tolerance of hot pepper (Capsicum annuum L.) at the seedling stage. Soil Environ., 28: 81-87.

Mina, V.A.M. 2015. Molecular analysis of evolutionary relationships of *Phaseolus dumosus* with the gene pool of common bean. Univ. Coll. Cork., 11: 121-138.

Ministry of Health. 2009. National health. In: Stepping towards better health. Ministry of Health, Islamabad, Pakistan.

Movaghatian, A. and Khorsandi, F. 2013. Effects of salicylic acid on wheat germination parameters under drought stress. Am. J. Agric. Environ. Sci., 13: 1603-1608.

Nasiri, Y., Zehtab-Salmasi, S., Nasrullahzadeh, S., Najafi, N. and Ghassemi-Golezani, K. 2010. Effects of foliar application of micronutrients (Fe and Zn) on flower yield and essential oil of chamomile (*Matricaria chamomilla* L.). J. Med. Plants Res., 4: 1733-1737.

Nasri, M., Mansoureh, K. and Hossein, A.F. 2011. Zn-foliar application influence on quality and quantity features in *Phaseolus vulgaris* under different levels of N and K fertilizers. Adv. Environ. Biol., 5: 839-846.

Necat, T., Vahdettin, C. and Yesim, T. 2004. The effects of zinc fertilization on yield and some yield components of dry bean (*Phaseolus vulgaris* L.). Asian J. Plant Sci., 3: 701-706.

Ntatsi, G., Gutiérrez-Cortines, M.E., Karapanos, I., Barros, A., Weiss, J., Balliu, A., dos Santos Rosa, E.A. and Savvas, D., 2018. The quality of leguminous vegetables as influenced by preharvest factors. Scientia Horticulturae, *232*: 191-205.

Pasala, R.K., Khan, M.I.R., Minhas, P.S., Sultana, R., Per, T.S., Deokate, P.P. and Rane, J. 2016. Can plant bioregulators minimize the crop productivity losses caused by drought, heat stress, and salinity? An integrated review. Environ. Pollu., 41: 63-78.

Petry, N., Olofin, I., Hurrell, R.F., Boy, E. and Wirth, J.P. 2016. The proportion of anemia associated with iron deficiency in low, medium, and high human development index countries: A systematic analysis of national surveys. Nutrients, 8: 693. https://doi.org/10.3390/nu8110693

Qamar, J., Rehman, A., Ali, M.A., Qamar, R., Ahmed, K. and Raza, W. 2016. Boron increases the growth and yield of Mung bean. J. Adv. Agric., 6: 3.

Rahman, A.B.M., Khan, M., Hasan, M.M., Banu, L.A. and Howlader, M.H.K. 2018. Effect of foliar application of gibberellic acid on different growth contributing characters of Mung bean. Prog. Agric. 29: 233-238. https://doi.org/10.3329/pa.v29i3.40008

Ross, J.J., O'Neill, D.P. and Rathbone, D.A. 2003. Auxin-gibberellin interactions in pea: integrating the old with the new. J. Plant Growth Regul., 22: 99-108. https://doi.org/10.1007/s00344-003-0021-z

Sadasivam, S. and Manickam, A. 1992. Biochemical Methods for Agricultural Sciences. Wiley Eastern Limited, New Delhi, India.

Salam, P.K., Rajput, R.S., Mishra, P.K. and Srivastava, A. 2005. Effect of micronutrients fertilization on productivity potential of urdbean (*Phaseolus mungo* L.). Ann. Agric. Res. 25: 329-332.

Sardoei, A.S., Shahadadi, F., Shahdadneghad, M. and Imani, A.F. 2014. The effect of benzyladenine and gibberellic acid on reducing sugars of *Spathiphyllum wallisii* plant. Int. J. Farm. Alli Sci., 3: 328-332.

Shah, H., Jalwat, T., Arif, M. and Miraj, G. 2012. Seed priming improves early seedling growth and nutrient uptake in Mung beans. J. Plant Nutr., 35: 805-816.

Sharma, V. and Abraham, T. 2010. Response of blackgram (*Phaseolus mungo*) to nitrogen, zinc, and farmyard manure. Legume Res., 33: 295-298.

Shenkin, A. 2006. Micronutrients in health and disease. Postgrad. Med. J., 82: 559-567.

Shivay, Y.S., Prasad, R. and Pal, M. 2014. Genetic variability for zinc use efficiency in chickpea as influenced by zinc fertilization. International Journal of Bio-resource and Stress Management, 5(1): 31-36.

Singh, A.K., Singh, S.S., Prakash, V.E.D., Kumar, S. and Dwivedi, S. K. 2015. Pulses production in India: Present status, bottleneck, and way forward. J. AgriSearch, 2: 75-83.

Soheil, K., Keyvan, S. and Siros, E. 2011. Soybean nodulation and chlorophyll concentration (SPAD value) are affected by some micronutrients. Ann. Biol. Res., 2: 414-422.

Stevens, G., Mascarenhas, M. and Mathers, C. 2009. Global health risks: Progress and challenges. Bull. World Health Organ., 87: 646.

Tripathi, P.K., Singh, M.K., Singh, J.P. and Singh, O.N. 2012. Effect of rhizobial strained and micronutrient nutrition on Mung bean (*Vigna radiata* L.) cultivars under dry-land agro-ecosystem of Indo-Gangetic plain. Afr. J. Agric. Res., 7: 34-42.

Usman, M., Tahir, M. and Majeed, M.A. 2014. Effect of zinc sulfate as soil application and seed treatment on green gram (*Vigna radiata* L.). Pak. J. Life Soc. Sci., 12: 87-91.

## ORCID DETAILS OF THE AUTHORS

Hina Upadhyay: https://orcid.org/0000-0002-0369-746X

Nature Environment and Pollution Technology
An International Quarterly Scientific Journal

p-ISSN: 0972-6268
(Print copies up to 2016)
e-ISSN: 2395-3454

Vol. 23 | No. 3 | pp. 1419-1431 | 2024

Review Research Paper

https://doi.org/10.46488/NEPT.2024.v23i03.013

Open Access Journal

# The Nexus Between Climate Variability and Undernutrition: A Systematic Review

**Niraj K.C.† and Kuaanan Techato**
Faculty of Environmental Management, Sustainable Energy Management, Prince of Songkhla University, Hat Yai, Thailand
†Corresponding author: Niraj K.C.; kcniraj1987@gmail.com

**Nat. Env. & Poll. Tech.**
**Website: www.neptjournal.com**

*Received:* 27-02-2024
*Revised:* 09-04-2024
*Accepted:* 20-04-2024

**Key Words:**
Undernutrition
Children
Climate variability

## ABSTRACT

Undernutrition is a confront to the health and output of the populace. It is viewed as one of the five leading contrary health impacts of climate variability and is defined as different measures of nutritional status. We aimed to assess the scientific evidence base for the impact of climate variability on childhood undernutrition (particularly wasting and underweight) in low- and middle-income countries. A systematic review was conducted to identify the peer-reviewed and gray full-text studies in English with no limits for the year of publication and study design. This review covers only published studies from four databases (PubMed, Scopus, Web of Science, and Science Direct). The risk of bias was assessed using the ROVBIS tool in individual studies. The PRISMA Statement checklist for systematic reviews was referred for this review process. A significant correlation between climate variables, temperature, rainfall, and drought, and at least one undernutrition parameter in 19 out of 22 studies was observed in this systematic review. In addition, we note that crop yield, maternal education, nutritional status of mothers, wealth status at the household level, and individual levels also play substantial roles in mediating the nutritional impacts. The findings of our analysis imply that exposure to climate variables may be linked to an increased risk of undernutrition both during and for several years following climate events. This may imply that undernutrition is never caused by temperature, precipitation, drought, or other weather-related factors alone but rather that undernutrition is triggered in children who are already at risk.

## INTRODUCTION

Children's bodies are delicate and highly susceptible to climatic changes, so any impairment they suffer during these formative years may have long-term effects (Bennett & Friel 2014). Undernutrition, defined as various measures of nutritional status, is a threat to the population's health and productivity and is considered one of the five main adverse health effects of climate variability (Phalkey et al. 2015, Madan et al. 2018). Climate change is expected to increase the current global burden of child malnutrition across climate variables, including temperature, precipitation, and humidity (Belesova et al. 2019). In the developing world, child undernutrition poses a serious health risk, impeding children's long-term growth and development (Amir et al. 2022). It is widely acknowledged that human development at the individual, societal, and global levels depends on children receiving adequate nutrition up until the age of five. It has also been shown that chronic malnutrition during early life can permanently damage a child's physical and mental development (McMahon & Gray 2021).

Undernutrition during early childhood can permanently impair an individual's well-being and socioeconomic achievement throughout their life, and it may increase children's risk of other morbidities and mortality (Pelletier et al. 1995). Here, our goal is to determine the undernutrition status in low- and middle-income countries due to climatic variables. Previous studies have not determined the undernutrition status among children under five in low- and middle-income countries. Children under the age of five who are exposed to climate variability without protection may have long-term health and social consequences (Alderman et al. 2006, Currie & Vogl 2013, Maccini & Yang 2009).

After considering these factors, we qualify our prediction that above-average temperatures and precipitation will have the greatest negative impact on childhood nutrition. Finally, we consider the strength and direction of climate effects as a research question. We examine the respective effects of temperature, precipitation, and humidity inconsistencies on child wasting and underweight across a sample from 9 different countries and sub-Saharan countries in low and middle countries. Our findings add to the emerging literature on climate and nutrition. This study focuses on the six main climate variables: temperature, precipitation, humidity,

cyclone, drought, and rainfall. Using extensive data sets, our systematic review investigated relationships between climate variability and childhood nutrition in low- and middle-income nations.

It is anticipated that variations in temperature, precipitation, humidity, and the secondary effects of similar environmental variations will have an impact on child malnutrition in several ways (Grace et al. 2012, Randell et al. 2020). Food security, availability, and accessibility in low- and middle-income communities that depend on rainfed agriculture can vary significantly between and within communities based on seasonal factors such as temperature and rainfall (Lieber et al. 2022, Niles et al. 2021). Given these circumstances, implementing healthy infant and young child feeding (IYCF) practices-such as exclusive breastfeeding and feeding beginning at 6-59 months-can be fatal for ensuring that kids receive the nutrition they need to grow and develop according to growth and development metrics (Shively 2017). Few studies have examined the effects of specific extreme climate variables on child nutrition; most of these studies have focused on low- and middle-income countries, which are the most vulnerable to climate variability. A family's ability to afford food may also be impacted by climate variability if there are differences in income that are not related to changes in crop yields or costs (Mueller et al. 2020). According to the Intergovernmental Panel on Climate Change, since 1970, average surface temperatures have risen by roughly 1.70 degrees Celsius per decade due to greenhouse gas emissions. By the year 2100, average surface temperatures worldwide are expected to have increased by $1.80^{o}$ Celsius to $4.00^{o}$ (IPCC 2007). In contrast to climate variability, which denotes naturally occurring variations in temperature and precipitation that occur over months to years, like the El Niño Southern Oscillation, climate change (McMichael & Kovats 2000, Ziervogel et al. 2006). The primary distinction between the two pertains to their temporal scales: climate variability usually transpires over periods ranging from months to years, whereas climate change transpires over decades to extended durations (Smit et al. 2000, Zhang & Huang 2012).

There is a knowledge gap and a lack of clarity regarding the relationship between climate variability and nutrition outcomes in children because the relationship between the two is not well understood and is frequently unclear (Macheka et al. 2022). Strategies for adapting to climate change should integrate nutrition security, giving special attention to those who are most at risk of undernutrition in childhood (Tirado et al. 2013, Crahay et al. 2010). By 2050, child undernutrition may increase by up to 20% as a result of decreased food production and declining nutritional quality, and 600 million more people will be hungry as a result of climate change (Field & Barros 2014).

In low- and middle-income nations with sufficient data available, we aimed to specify summary estimations of the status of underweight and wasting among children aged 6-59 months and investigate the effects of temperature, precipitation, and humidity on childhood undernutrition. The purpose of this systematic review article is to elucidate the main climatic variability that low- and middle-income countries face and how it may affect the nutrition of children. Risks resulting from temperature increases and extreme weather are taken into account. The methods currently in use to stop or lessen these effects are outlined, along with suggestions for future developments that could be crucial to enhancing the nutrition of children in low- and middle-income nations. A previous review primarily aimed at articles before the year 2015 examined the association between climate variability and childhood stunting and found variable associations (Chowdhury et al. 2020). Specially, this study found that extreme weather events and fluctuations in temperature and precipitation were associated with childhood underweight and wasting in 21 out of 22 studies.

In this paper, we evaluated published (peer-reviewed) data on database studies about climate variables in low- and middle-income countries (LMICs) regarding undernutrition among children under the age of five. The following research questions were the focus of the investigation:

What is the current status of climate variability-related undernutrition?

Which undernutrition parameters are most frequently employed in research?

What aspects of the climate variables affect the nutrition of children?

What is the relationship between undernutrition in children and climate variability?

## MATERIALS AND METHODS

### Literature Review Methodology

**Eligibility and ineligibility criteria:** Certain eligibility criteria were identified through the goal of choosing and incorporating only noteworthy studies for our topic of the systematic review acknowledged from the databases (Table 1).

**Information source and search strategy:** The systematic review took into account English language studies that were published between January 2014 and June 2023. We used Scopus, PubMed, Science Direct, and Web of Science to search the literature. In October 2023, a total of 276 publications from PubMed, 892 from Web of Science, 125 from Scopus, and 57 from Science Direct were found. These

Table 1: Eligibility and ineligibility criteria.

| Eligibility Criteria | Ineligibility Criteria |
|---|---|
| EC1: Journal Articles | IC1: Proceedings of conference papers, books, book chapters, and other nonpeer-reviewed publications. |
| EC2: The study is written in English. | IC2: The study is not written in English. |
| EC3: The study is peer-reviewed. | IC3: The study is not peer-reviewed. |
| EC4: The study is not listed in another database. | IC4: The study is listed in another database. |
| EC5: The study was conducted in low and middle-income countries. | IC5: The study was not conducted in low and middle-income countries. |
| EC6: The study is related to environmental subjects. | IC6: The study is not related to environmental subjects |
| EC7: The gray full text of the study is available. | IC7: The full text of the study is not available |
| EC8: The study includes research or descriptions of climate variables and childhood undernutrition | IC8: The study only includes opinions about climate variability and childhood undernutrition |
| EC9: The study addresses the relationship between climate variability and undernutrition | IC9: The study does not address the relationship between climate variability and undernutrition, or it mention it just briefly |
| EC10: The study focused exclusively on wasting and underweight | IC10: The study focused exclusively on stunting |

Table 2: Information source and search string with parameters.

| Information Source | Search String and Parameters |
|---|---|
| PubMed | ((((((“Climate Change”[Mesh]) AND “Malnutrition”[Mesh]) AND “Child”[Mesh])) OR “Extreme Weather”[Mesh]) AND (“Weather”[Mesh] OR “Extreme Hot Weather”[Mesh])<br>Document type: Article<br>Language: English |
| Scopus | (ALL ( “weather variability” ) OR ALL ( “climate change” ) AND TITLE-ABS-KEY ( “impact” ) AND TITLE-ABS-KEY ( “child nutrition” ) OR ALL ( “under-nutrition” ) AND NOT TITLE-ABS-KEY ( “maternal nutrition” ) ) AND PUBYEAR > 2005 AND PUBYEAR < 2024 AND ( LIMIT-TO ( DOCTYPE, “ar” ))<br>Document type: Article<br>Language: English |
| Web of Science | ((((((ALL=(“weather events”)) OR TS=(climate variability )) AND TS=(child undernutrition)) AND TS=(impact)) OR TS=(malnutrition )) NOT TS=(mother))<br>Document type: Article<br>Language: English |
| Science Direct | Term(s): “extreme weather events” OR “climate change” AND “child nutrition”;<br>Document type: Article<br>Language: English |

four databases were chosen based on their widely recognized impact indices, which include peer-reviewed, scholarly literature published globally in a variety of scientific fields and arenas (Salisbury 2009).

Using Boolean operators (AND, OR, NOT) with simple operators using parenthesis in the search string, the search strategy was based on the use of fundamental concepts related to the study’s topic and research question (Khine & Langkulsen 2023). A search string was created following testing and a fast review of the syntax needed by each database (Table 2).

### Data Collection and Selection Process

Following the initial literature searches, the titles and abstracts of each study were examined, and any potentially pertinent studies were further evaluated for eligibility. The study selection procedure is explained in great detail in the PRISMA flow diagram (Fig.1). We selected the pertinent articles based on the eligibility and ineligibility standards. Research that the titles and abstracts judged unnecessary were not included. After an independent review of the remaining studies, disputed studies were either included or excluded based on a consensus.

Twenty-two suitable journal articles from nine low- and middle-income countries, published over 9 years, were found by our search: four articles from Bangladesh, one from Brazil, three from Burkina Faso, four from Ethiopia, two from Ghana, one from Kenya, two from India, one from Nepal, two from Sub-Saharan Africa, one each from Ghana and Bangladesh, and one from Uganda. The included studies reported a total of 22 main outcomes related to undernutrition across 6 climate variables. The most common criteria used to characterize climate variability were temperature, rainfall, humidity, precipitation, cyclones, and drought. Significant undernutrition in children was found in 19 studies. Every study published results for children younger than 60 months.

### Data Items (Outcomes)

Table 3: The examined undernutrition outcomes and their measurements.

| Undernutrition Effects | Measurements | Acronym |
|---|---|---|
| Wasting | Weight-for-Height Z-scores | WHZ |
| | Mid-upper arm circumference | MUAC |
| Underweight | Weight-for-age Z-scores | WAZ |

### Synthesis Methods

Data synthesis was done by two authors (NKC and KT) by using a synthesis format arranged in Microsoft Excel. The PRISMA Statement checklist for systematic reviews was referred for the review process (Page et al. 2021). The search results were combined, and duplicates were automatically eliminated before a second manual revision. The full-text review was left for the studies whose eligibility was questionable. The 92 chosen articles underwent full-text reviews, manual data synthesis, and matrix documentation by the two independent reviewers (N.KC and K.Techato). Differences were agreed upon and accepted.

We performed narrative synthesis into a matrix format: reference, first author name, year of publication, study period, sample size, age in months, geographical focus, data source, the status of undernutrition, parameters of undernutrition, climate variability, and the association between climate variability and undernutrition included in the models (Table 4).

## RESULTS AND DISCUSSION

### Study Selection

Initially, in our study, 1350 research papers were selected for study. After eliminating twelve redundant studies, 737 studies were eliminated based on their titles, and 320 abstracts were excluded. Since the criteria did not align with the study's goals, an additional 189 studies were eliminated. Out of the 92 papers that were left for the analysis, 41 papers did not align with the findings of this investigation, 24 papers did not align with the geographical context, and 5 systematic reviews were excluded. Following the removal of 70 papers altogether, 22 papers were chosen for this analysis, as

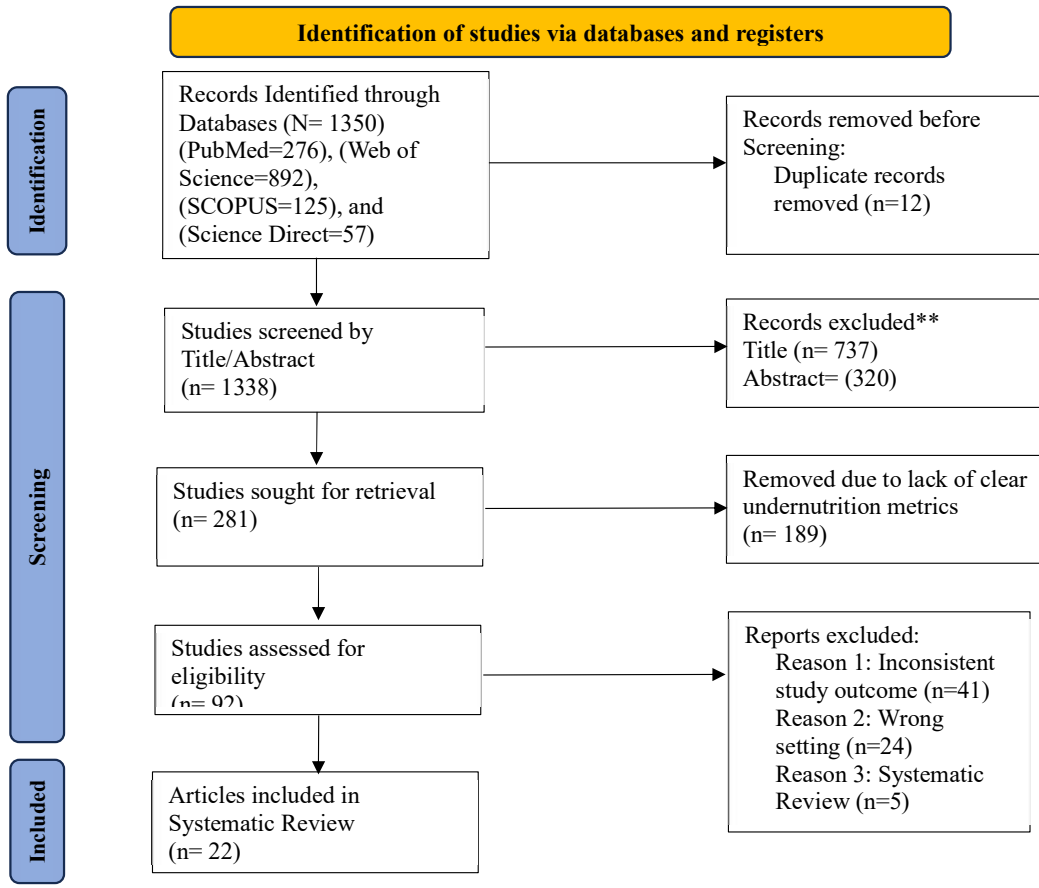


Fig. 1: PRISMA 2020 flow diagram for new systematic reviews, which included searches of databases and registers only.

depicted in Fig. 1. Four primary databases, PubMed, Scopus, Web of Science, and Science Direct, were used to finish it. The eligibility and ineligibility criteria were established before the selection of these papers.

### Study Characteristics

In each study, the age category of children under the age of five and the sample size varied greatly, ranging from 0 to 60 months and 40 to over 200000, respectively. Three studies presented primary data analysis, only one study presented both primary and secondary data analysis, and the majority of the studies used secondary data. In this study, papers published from 2014 to 2023 were analyzed. Every article in this analysis originated in a low- or middle-income nation. Of the 22 papers that made up this analysis, 4 had longitudinal study designs, and 18 had cross-sectional study designs. Table 4 provides a summary of each study's key features.

### Assessment of the Risk of Bias in Individual Studies

In individual studies, the ROVBIS tool was used to evaluate the risk of bias. We allocated the five domains according to each study's ROBVIS assessment. The bias resulting from the randomization process, deviations from intended interventions, missing outcomes, bias in outcome measurement, and bias in the selection of reported results were the five main domains (McGuinness & Higgins 2021). Every study received a score of "high," "low," or "some concerns." Each article received an inclusive ROBIS score, as suggested by the tool's guidelines. The possibility of bias in the studies' conclusions has been highlighted by an evaluation of their validity that was part of a Cochrane review.

The risk of bias in each included study has been evaluated by the Cochrane Collaboration, which has also compiled data by type of undernutrition in Fig. 2. This includes an explanation and an assessment for every entry in a "Risk of Bias," where each entry deals with a particular aspect of the research. Each entry is evaluated based on its response to the question; 'Yes' indicates a low risk of bias, 'No' indicates a high risk, and 'Unclear' indicates neither a lack of information nor some reservations about potential bias.

**What is the current status of climate variability-related child undernutrition in low and middle-income countries?:** Child undernutrition was observed in all of the selected low- and middle-income nations in this study. This study specifically addressed the undernutrition of 9 distinct low- and middle-income countries as well as Sub-Saharan low- and middle-income countries. The problem of undernutrition among children under the age of five has been observed in most countries as a result of climate variables. The rate of wasting has increased in Nepal as a result of the heavy rains. Due to the drought, the rate of waste in Kenya has increased by 20%. Long-term rainfall increased wasting by 4.5 percent in Uganda, while humidity increased underweight by 10.5 percent. According to a study conducted in Malawi, high temperatures are likely to increase the rate of wasting in children. A Brazilian longitudinal study found a 2.5 percent increase in undernutrition for every 1°C daily increase in temperature. Excessive rainfall over twelve months was associated with the problem of wasting in Ghana, whereas the same problem was observed in Bangladesh among older children. Both studies in the Sub-Saharan region confirmed that as temperatures rose, children's wasting problems worsened. Several studies on climate variables and undernutrition in Bangladesh have discovered that temperature, cyclones, humidity, and rainfall are primarily to blame for children wasting and being underweight. Malnutrition among children is a problem, according to a study conducted in many districts of India where the Climate Vulnerability Index is high. Three studies in Burkina Faso discovered that high temperatures, drought, and high rainfall

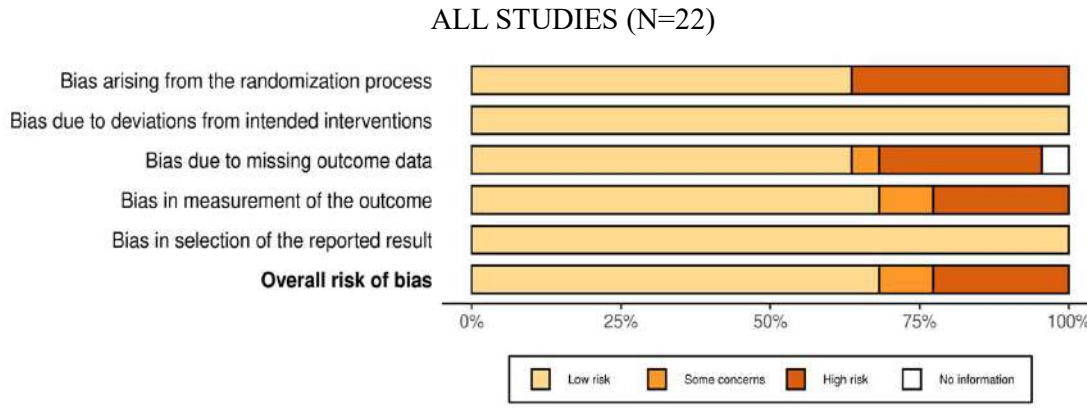


Fig. 2: The risk of bias in each included study.

Table 4: Summary of included studies

| Articles | Author and Year of Publication | Study Period | Sample Size | Age in months | Geographic focus | Data Source | Study Design | Status of Undernutrition | Parameters of Undernutrition | Climate Variability | Association between climate variability and Undernutrition |
|---|---|---|---|---|---|---|---|---|---|---|---|
| 1 | Alfred, 2020 | 2015 | 5149 | 0-59 | Malawi | Secondary | Cross-sectional | ✓ | Wasting | Rainfall, Temperature | ✓ |
| 2 | Ahsanuzzaman et al., 2020 | 2011 | 7861 | 0-59 | Bangladesh | Secondary | Cross-sectional | ✓ | Wasting | Cyclone | ✓ |
| 3 | Kristine et al., 2017 | 1992-2012 | 44616 | 0-59 | Burkina Faso | Secondary | Cross-sectional | ✓ | Underweight | Precipitation | ✓ |
| 4 | Hanson, 2021 | 2019-2020 | 40 | 0-59 | Ghana | Primary | Cross-sectional | ✓ | Underweight | Rainfall | ✓ |
| 5 | Brian et al., 2020 | 1980-2019 | 400 | 0-59 | Sub-Saharan | Secondary | Cross-sectional | ✓ | Wasting | Precipitation | ✓ |
| 6 | Shouro et al., 2020 | 1993-2010 | NA | 0-59 | Burkina Faso | Secondary | Cross-sectional | ✓ | Wasting | Temperature, Precipitation | ✓ |
| 7 | Arbinda et al., 2020 | 2015-2016 | NA | 0-59 | India | Secondary | Cross-sectional | ✓ | Wasting | Rainfall | ✓ |
| 8 | Arnout et al., 2017 | 2007-2011 | 4333 | 0-60 | Bangladesh | Secondary | Cross-sectional | ✓ | Wasting | Rainfall | ✓ |
| 9 | Matthew et al., 2019 | 2011-2015 | 4617 | 0-60 | Ghana & Bangladesh | Primary and Secondary | Cross-sectional | ✓ | Wasting | Rainfall | ✓ |
| 10 | Ahmed et al., 2022 | 2011-2020 | 19357 | 0-36 | Bangladesh | Secondary | Cross-sectional | ✓ | Wasting | Temperature, Rainfall, Humidity | ✓ |
| 11 | Jan et al., 2017 | 2009-2013 | 3302 | 0-59 | Kenya | Secondary | Cross-sectional | ✓ | Wasting | Drought | ✓ |
| 12 | Anna, 2021 | 2005-2016 | 21551 | 0-59 | Ethiopia | Secondary | Cross-sectional | ✓ | Wasting | Drought | ✗ |
| 13 | Rachel et al., 2020 | NA | 190000 | 6-59 | Sub-Saharan | Secondary | Cross-sectional | ✓ | Wasting | Temperature | ✓ |
| 14 | Ledlie et al., 2017 | 2011-2013 | 2659 | 6-59 | Ethiopia | Secondary | Cross-sectional | ✓ | Wasting | Rainfall | ✗ |
| 15 | Chris, 2023 | 2013-2016 | 976 | 0-60 | Uganda | Secondary | Longitudinal | ✓ | Underweight | Rainfall | ✓ |

Table Cont....

| Articles | Author and Year of Publication | Study Period | Sample Size | Age in months | Geographic focus | Data Source | Study Design | Status of Undernutrition | Parameters of Undernutrition | Climate Variability | Association between climate variability and Undernutrition |
|---|---|---|---|---|---|---|---|---|---|---|---|
| 16 | Bidhubhusan et al., 2021 | 2015-2016 | 243213 | 0-60 | India | Secondary | Cross-sectional | ✓ | Wasting, Underweight | Rainfall, Temperature | ✓ |
| 17 | Isabel et al., 2021 | 2017-2019 | 1439 | 0-48 | Burkina Faso | Secondary | Longitudinal | ✓ | Wasting | Rainfall | ✓ |
| 18 | Rongbin et al., 2019 | 2000-2015 | 31597 | 0-48 | Brazil | Primary | Longitudinal | ✓ | Underweight | Temperature | ✓ |
| 19 | Hirvonen et al., 2020 | 2012-2016 | 3582 | 0-59 | Ethiopia | Secondary | Cross-sectional | ✓ | Wasting | Drought | ✗ |
| 20 | Alice et al., 2023 | 2014-2015 | 1586 | 0-59 | Bangladesh | Primary | Cross-sectional | ✓ | Wasting | Rainfall | ✓ |
| 21 | Sailesh et al., 2016 | 2001-2011 | 13682 | 0-60 | Nepal | Secondary | Cross-sectional | ✓ | Wasting | Rainfall | ✓ |
| 22 | Seifu et al., 2014 | 1996-2004 | 145 | 0-59 | Ethiopia | Secondary | Longitudinal | ✓ | Wasting, Underweight | Rainfall, Temperature | ✓ |

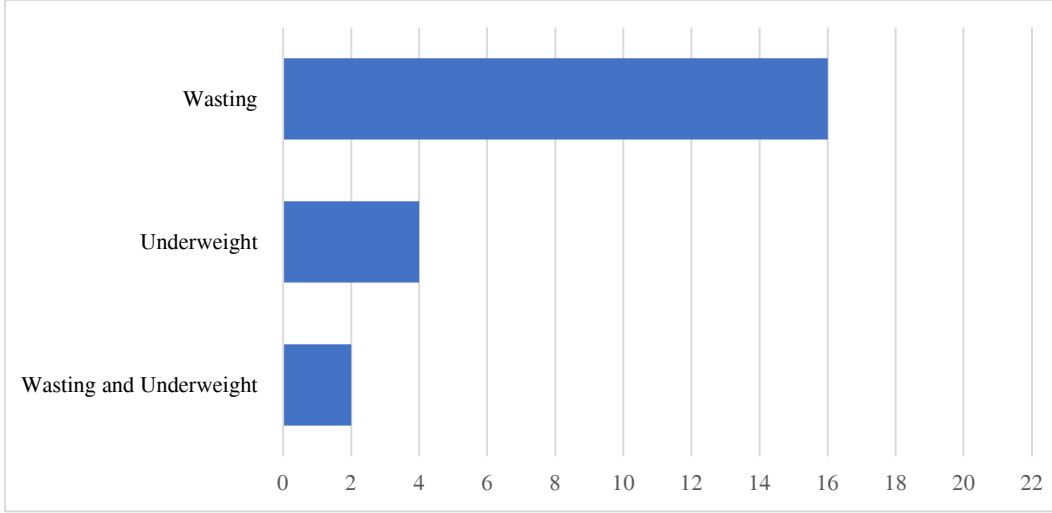


Fig. 3: Parameters of undernutrition observed in studies.

increased childhood wasting and underweight. Several cross-sectional and longitudinal studies in Ethiopia have found that high draft, high temperature, and high humidity are associated with an increased risk of childhood wasting and underweight.

**Which undernutrition parameters are most frequently employed in research?:** In this study, wasting was measured in 16 papers out of a total of 22 papers. Similarly, the problem of underweight has been measured in 4 papers, while wasting and underweight both have been observed in two papers (Fig. 3). Wasting and underweight, the main parameters of climate-related undernutrition in children, were studied from 1992 to 2019 using primary and secondary data on children aged 0 to 60 months. Although stunting is a key indicator of malnutrition, it was excluded because it did not fall within the scope of this study. In Malawi, Bangladesh, Burkina Faso, India, Ghana, Kenya, Ethiopia, Nepal, and Sub-Saharan Africa, wasting was measured. Burkina Faso, Uganda, Brazil, and Ghana all had underweight children. Both wasting and underweight were observed in Ethiopia and India.

**What aspects of the climate variables affect the nutrition of children in low- and middle-income countries?:** We identified six climate variables that specifically influence undernutrition in children under the age of five in this study. We primarily looked for temperature, rainfall, cyclone, precipitation, drought, and humidity climate variables in this study. Ghana, India, Bangladesh, Ethiopia, Uganda, Burkina Faso, and Nepal are among the nine countries where only rainfall has been studied. Similarly, rainfall and temperature were found in three different papers about the effect of two climate variables in India, Malawi, and Ethiopia. In Ethiopia and Kenya, we found 3 papers on the effects of drought on children's malnutrition. We observed in 2 papers that children from Sub-Saharan and Brazil have wasting and underweight problems due to the temperature. We noted in separate papers that the problem of wasting in children due to cyclones, wasting, and undernutrition due to precipitation has been affected in Bangladesh, Burkina Faso, and Sub-Saharan respectively. We observed the problem of wasting in children in a paper studied in the coastal region of Bangladesh by examining three climate variables; temperature, rainfall, and humidity. A study in Burkina Faso found that wasting is the major child undernutrition, using temperature and precipitation as climate impact variables.

**What is the relationship between undernutrition in children and climate variability?:** Nine studies that looked into the relationship between rainfall and undernutrition all found strong associations. It is well known that low crop production has an impact on children's nutritional status as a result of high rainfall. It showed that Bangladesh's high rainfall has led to an increase in the wasting rate (OR= 0.27, 95% CI: 0.17 - 0.44) among children between the ages of 0 and 59 months as compared with the low rainfall (OR=0.54, 95% CI: 0.35-0.83) (Wolfle & Channon 2023). Tiwari et al. (2017) confirm this result in Nepal that high rainfall (SD= 0.315, $P < 0.01$) had statistically significant impacts on wasting in comparison to normal rainfall (SD= 0.299, $P < 0.01$). Van Soesbergen et al. (2017) also discovered a significant correlation (OR= 0.27, $P < 0.05$) between rainfall and wasting, but they pointed out that the influence is caused by a collection of anomalies in the Normalized Difference Vegetation Index. A similar observation was

reported from Kenya (Bauer & Mburu 2017). Isabel et al. noted that exposure of mothers to high rainfall may contribute to a decline in the weight-for-height scores (B= 0.032, 95% CI: 0.01-0.06, P < 0.05) among under 5 years children in Burkina Faso (Mank et al. 2021). Ledlie et al. found that shocks associated with rainfall had a statistically insignificant impact on undernutrition in children (SD= 0.56, P > 0.05). They state that there was a significant correlation between wasting and other factors like maternal education (P < 0.05) and the wealth index (P < 0.05) (Ledlie et al. 2018). Arbinda et al. India had the highest likelihood of wasted children (B = -1.5, P < 0.001) but not anemic ones (B = -0.21, P > 0.05) (Acharya & Das 2015). There was a significant correlation found between Ugandan children's long-term exposure to rainfall and both underweight and wasting (Boyd 2023). Matthew et al. assessed the standardized precipitation index (SPI) for excessive rainfall over a short time window of 12 months was associated with lower weight-for-height z scores (SD= 0.00236, P < 0.05) (Cooper et al. 2019). Stressful farming season and exposure to fluctuating rainfall cause mothers to be unable to feed their children, resulting in undernutrition (Nyantakyi 2021).

In eight of the twenty-two studies, the temperature was discussed. For underweight Ethiopian children aged 0-59 months, it was highly significant (R2 = -0.26). The authors found that, in addition to temperature, other significant determinants included livestock and rainfall during the growing season. However, they were unsure if the impact was due to per capita crop (Hagos et al. 2014). Using spatial autocorrelation to measure climate vulnerability rather than ambient temperature and rainfall. Bidhubushan et al. found the strongest evidence (AOR: 1.45, 95% CI: 1.30-1.61) for underweight children (Mahapatra et al. 2021). In Malawi, children who are exposed to higher temperatures have a higher likelihood of being wasted (B = 1.220, P < 0.05). According to the author, wasting was significantly correlated with additional factors like large family size, proximity to water, mother's BMI, and diarrhea (Ngwira 2020). According to Rachel et al.'s assessment of the monthly temperature variation, children's weight-for-height was significantly (P < 0.001) impacted by rising temperatures (25–300 C) in the survey month (Baker & Anttila 2020). Rongbin et al. found a strong positive correlation (OR= 1.025, 95% CI: 1.020-1.030, P < 0.001) between undernutrition and daily mean temperature increases of 10 C. They noted that the effect was as strong in males as in females (Xu et al. 2019). When Kristine et al. examined the relationship between child survival and the annual food crop productivity index, they found a strong correlation (Hazard Ratio= 2.73, 95% CI: 2.10-3.55) between underweight (Belesova et al. 2018). According to Brian et al., the prevalence of childhood wasting in Sub-Saharan Africa was 8.1 percentage points higher than the baseline average and was temperature-dependent (Thiede & Strube 2020). Ahmed et al. observed that children born at a higher temperature were significantly associated with 2.2 mm lower MUAC measures relative to the mean. They report that humidity was also strongly associated (P= < 0.05) with children wasting (Ahmed et al. 2022). Elizabeth reported that children in Burkina Faso experienced wasting when exposed to short-term weather shocks, particularly temperatures exceeding 260 degrees (Dasgupta & Robinson 2023).

However, Hirvonen et al. did not find that Ethiopian child wasting was influenced by drought. Rather, they identified the primary contributors as the head of the household's age, the availability of electricity, the availability of toilets, and the availability of safe water (Hirvonen et al. 2020). An analogous observation revealed no proof that Ethiopia's risk of child wasting is impacted by seasonal droughts (Dimitrova 2021).

One study out of 22 examined how undernutrition children are to cyclones. For children ages 0 to 12 months, the cyclone was positively significant for underweight and wasting (P < 0.001); however, this was not the case for children older than 12 months (Ahsanuzzaman & Islam 2020).

## DISCUSSION

The results of our review confirm the hypothesis that undernutrition is caused by a complex network of interdependent and interconnected farming, environmental, socioeconomic, demographic, and health factors at the societal, family, and individual levels (Fig. 4). We observed that many of the mediating factors are sensitive to changes in climate variability. The UNICEF framework lists the following reasons for undernutrition in children: underlying causes (food insecurity, poor hygiene and sanitation practices, inadequate health and nutrition services), immediate causes (diseases and inadequate diet practices), and enabling causes (political, financial, and social actions) (UNICEF 2021).

In more than 85% of the 22 studies that made up the review, a significant correlation was found between undernutrition and one or more climate variables. To make any kind of inference, however, more or contradictory data on humidity, precipitation, drought, and cyclones were required. Rainfall and temperature were still frequently discussed factors.

Climate variables were most frequently associated with anthropometric measures (especially underweight and wasting) in children under five years old. Existing research

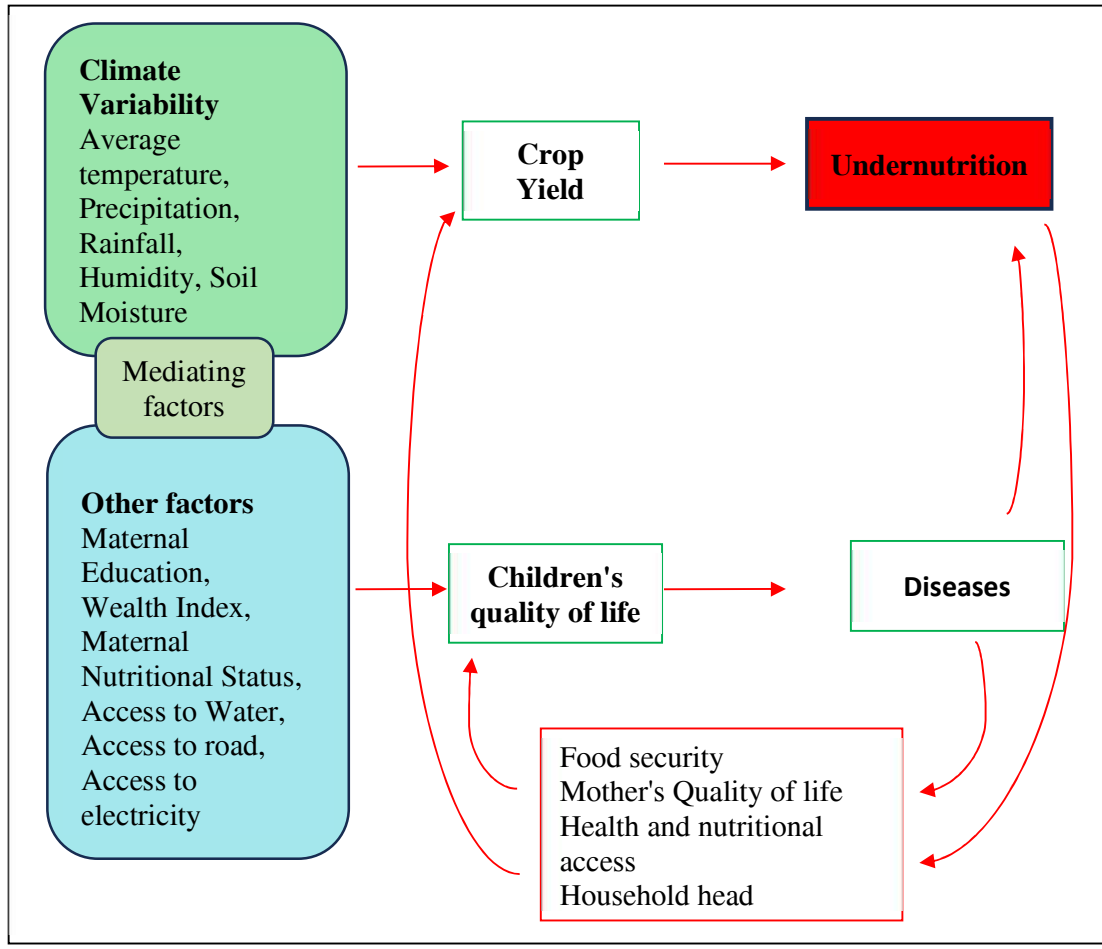


Fig. 4: Vicious pathways relating climatic factors to undernutrition. The factors connected to climate variables and their potential effects on crop yield and undernutrition.

suggests that climate factors, including household factors, are more closely associated with undernutrition (Tiwari et al. 2022, Thiede & Gray 2020, Tusting et al. 2020). This review, however, indicates that climate variability plays a similarly significant role in determining undernutrition in children.

The mechanisms linking malnutrition and climate variability are too complex for this study to fully explore. This review, however, identifies several significant mechanisms that may mediate this relationship, such as decreased crop yields and elevated incidence of other illnesses like malaria and diarrhea (Dimitrova 2020, Agostoni et al. 2023). These results highlight how crucial it is to use sustainable farming and healthcare practices as technological tools to counteract the detrimental effects of climate variability on children's nutrition. Gender was found to be an insignificant moderating factor in our studies. However, according to a study, boys are more susceptible than girls to the negative impacts of climate change on undernutrition (Lieber et al. 2022). Several factors that lessen the impact of climatic variability on undernourishment were also highlighted in this review. Among them, age is one of the most important; children are most vulnerable to changes in climate variables between the ages of 0 and 5 years. Nevertheless, this variable was not significant in the Mali study (Johnson & Brown 2014).

The majority of the study children analyzed in the papers that were reviewed were classified as vulnerable because of factors related to the climate, maternal education, children's nutritional status, and wealth status (Le & Nguyen 2022, Shively et al. 2022, Dimitrova & Bora 2020, Fenta et al. 2021, Khan et al. 2023). This may imply that undernutrition is never caused by temperature, precipitation, drought, or other weather-related factors alone but rather that undernutrition is triggered in children who are already at risk. The majority of research indicates that there is room

to improve intervention programs' efficacy, especially their preventative components. This can entail fusing long-term preventative initiatives with short-term response interventions, focusing on various pathways that mitigate the effects of climate variability and attend to additional sources of vulnerability. Although there is general agreement that nutrition and climate variables are related, this relationship is often complex and indirect. Reduced food production is a result of higher temperatures and more frequent rainfall, which affects the amount and quality of nutrients ingested (Van et al. 2022, Haile et al. 2018).

This review primarily concentrated on malnutrition in low- and middle-income countries where a significant proportion of the populace relies on subsistence farming as a means of subsistence (Fantom & Serajuddin 2016). We did not mean to exclude the relatively small number of studies that looked at the relationship between undernutrition and climate variability in high-income countries, but that was one of the selection criteria. The results of this review may, therefore, not apply to children in more developed nations where subsistence farming is not as common. However, these studies are useful in emphasizing how common undernutrition is in LMICs during the high temperature, rainfall, and drought events that are studied, covering the full range of years from 1992 to 2019. As part of the Sustainable Development Goals (SDG) agenda, the global community has set a target of eliminating all forms of malnutrition worldwide by 2030. To this end, efforts are being made to develop measures, track progress, and put policies into place (Villanueva 2022). According to the WHO, these levels demand both immediate attention and the long-term development of preventative measures. The findings of our analysis imply that exposure to climate variables may be linked to an increased risk of undernutrition both during and for several years following climate events (United Nations 2022).

## CONCLUSION

Without a doubt, determining the mechanisms by which undernutrition is impacted by climate change is a difficult task that needs to be tackled. Both the direct effects of crop yields on childhood undernutrition, particularly acute undernutrition and the influence of climate variability on crop yields have been extensively studied and recognized. There is a strong correlation between weather variables and childhood underweight and wasting, despite the limited evidence currently available. Nevertheless, a relatively small number of primary data-based studies examine the fraction of all undernourished children that can be linked to climate variability. Understanding the relationship, ideally at both the macro and micro levels, between crop yields, climate variability, and undernutrition in children is imperative. It is, therefore, important to methodically document these associations over the coming years, even "with associated uncertainties," as this could contribute to the creation of more accurate projections for the future.

According to IPCC and World Health Organization projections, undernutrition will account for the majority of morbidity and mortality caused by climate variables (WHO 2019, IPCC 2022). We provide a comprehensive literature review that connects child undernutrition and proxies for climate variability. We discovered that the nexus between climate variables and at least one undernutrition parameter in 19 out of 22 studies was found to be significant.

## ACKNOWLEDGMENTS

We express our gratitude to every author of the studies that were part of the review. A principal investigator is N. KC. Whether it was during the project's conception, screening, assessment of the final included article, data extraction, inclusion verification, or quality assurance evaluation, each author made an equal contribution to the work. Each author committed to taking responsibility for every part of the work and took part in a critical review of the completed manuscript.

## REFERENCES

Acharya, A. and Das, A. K. 2015. District-level analysis of climate vulnerability and household nutrition status among rural communities in Odisha, India. Int. J. Popul. Stud., 6(1): 41-55. https://doi.org/10.18063/ijps.v6i1.1069

Agostoni, C., Baglioni, M., La Vecchia, A., Molari, G. and Berti, C. 2023. Interlinkages between climate change and food systems: The impact on child malnutrition-narrative review. Nutrients, 15(2). https://doi.org/10.3390/nu15020416

Ahmed Hanifi, S. M. M., Menon, N. and Quisumbing, A. 2022. The impact of climate change on children's nutritional status in coastal Bangladesh. Soc. Sci. Med., 294: 114704. https://doi.org/10.1016/j.socscimed.2022.114704

Ahsanuzzaman and Islam, M. Q. 2020. Children's vulnerability to natural disasters: Evidence from natural experiments in Bangladesh. World Dev. Perspect., 19: 100228. https://doi.org/10.1016/j.wdp.2020.100228

Alderman, H., Hoddinott, J. and Kinsey, B. 2006. Long-term consequences of early childhood malnutrition. Oxf. Econ. Pap., 58(3): 450-474. https://doi.org/10.1093/oep/gpl008

Amir-Ud-Din, R., Fawad, S., Naz, L., Zafar, S., Kumar, R. and Pongpanich, S. 2022. Nutritional inequalities among under-five children: a geospatial analysis of hotspots and cold spots in 73 low- and middle-income countries. Int. J. Equity Health, 21(1): 135. https://doi.org/10.1186/s12939-022-01733-1

Baker, R. E. and Anttila-Hughes, J. 2020. Characterizing the contribution of high temperatures to child undernourishment in Sub-Saharan Africa. Sci. Rep., 10(1): 18796. https://doi.org/10.1038/s41598-020-74942-9

Bauer, J. M. and Mburu, S. 2017. Effects of drought on child health in Marsabit District, Northern Kenya. Econ. Hum. Biol., 24: 74-79. https://doi.org/10.1016/j.ehb.2016.10.010

Belesova, K., Agabiirwe, C. N., Zou, M., Phalkey, R. and Wilkinson, P. 2019. Drought exposure as a risk factor for child undernutrition in low- and middle-income countries: A systematic review and assessment of empirical evidence. Environ. Int., 131: 104973. https://doi.org/10.1016/j.envint.2019.104973

Belesova, K., Gasparrini, A., Sie, A., Sauerborn, R. and Wilkinson, P. 2018. Annual crop-yield variation, child survival, and nutrition among subsistence farmers in Burkina Faso. Am. J. Epidemiol., 187(2): 242-250. https://doi.org/10.1093/aje/kwx241

Bennett, C. M. and Friel, S. 2014. Impacts of climate change on inequities in child health. Children (Basel), 1(3): 461-473. https://doi.org/10.3390/children1030461

Boyd, C.M. 2023. Rainfall, mothers' time use, and child nutrition: evidence from rural Uganda. Popul. Environ., 45(3): 428. https://doi.org/10.1007/s11111-023-00428-1

Change, I. P. O. C. 2007. Climate change 2007: The physical science basis. Agenda, 6(07): 333. https://www.slvwd.com/sites/g/files/vyhlif1176/f/uploads/item_10b_4.pdf

Chowdhury, T. R., Chakrabarty, S., Rakib, M., Afrin, S., Saltmarsh, S. and Winn, S. 2020. Factors associated with stunting and wasting in children under 2 years in Bangladesh. Heliyon, 6(9): 484. https://doi.org/10.1016/j.heliyon.2020.e04849

Cooper, M., Brown, M. E., Azzarri, C. and Meinzen-Dick, R. 2019. Hunger, nutrition, and precipitation: evidence from Ghana and Bangladesh. Popul. Environ., 41(2): 151-208. https://doi.org/10.1007/s11111-019-00323-8

Crahay, P., Mitchell, A., Gomez, A., Israel, A. D., Salpeteur, C., Mattinen, H. and Dufour, C. 2010. The threats of climate change on undernutrition: A neglected issue that requires further analysis and urgent actions. SCN News, (38): 4-10.

Currie, J. and Vogl, T. 2013. Early-life health and adult circumstance in developing countries. Annu. Rev. Econ., 5(1): 1-36. https://www.nber.org/system/files/working_papers/w18371/w18371.pdf

Dasgupta, S. and Robinson, E. J. Z. 2023. Climate, weather, and child health in Burkina Faso. Aust. J. Agric. Resour. Econ., 67(4): 576-602. https://doi.org/10.1111/1467-8489.12530

Dimitrova, A. 2020. Impacts of droughts on undernutrition among children aged under five in Ethiopia. https://pure.iiasa.ac.at/id/eprint/16622/1/WP-20-012.pdf

Dimitrova, A. 2021. Seasonal droughts and the risk of childhood undernutrition in Ethiopia. World Dev., 141. https://doi.org/10.1016/j.worlddev.2021.105417

Dimitrova, A. and Bora, J.K. 2020. Monsoon weather and early childhood health in India. PLoS One, 15(4): e0231479. https://doi.org/10.1371/journal.pone.0231479

Fantom, N. J. and Serajuddin, U. 2016. The World Bank's classification of countries by income. World Bank Policy Res. Work. Pap., (7528). http://econ.worldbank.org

Fenta, H. M., Zewotir, T. and Muluneh, E. K. 2021. Spatial data analysis of malnutrition among children under five years in Ethiopia. BMC Med. Res. Methodol., 21(1): 232. https://doi.org/10.1186/s12874-021-01391-x

Field, B. F. and Barros, V. R. 2014. Climate Change 2014 Impacts, Adaptation, and Vulnerability Part A: Global and Sectoral Aspects. Cambridge University Press, 32(1). www.cambridge.org/9781107641655

Grace, K., Davenport, F., Funk, C. and Lerner, A. M. 2012. Child malnutrition and climate in Sub-Saharan Africa: An analysis of recent trends in Kenya. Appl. Geogr., 35(1-2): 405-413. https://doi.org/10.1016/j.apgeog.2012.06.017

Hagos, S., Lunde, T., Mariam, D. H., Woldehanna, T. and Lindtjørn, B. 2014. Climate change, crop production and child undernutrition in Ethiopia; a longitudinal panel study. BMC Public Health, 14: 1-9. http://www.biomedcentral.com/1471-2458/14/884

Haile, B., Azzarri, C., Heady, D. and You, L. 2018. Climate, climate shocks and child nutrition in Africa's diverse farming systems. Adv. Res. Nutri., 6: 5-11

Hirvonen, K., Sohnesen, T. P. and Bundervoet, T. 2020. Impact of Ethiopia's 2015 drought on child undernutrition. World Dev., 131. https://doi.org/10.1016/j.worlddev.2020.104964

Intergovernmental Panel on Climate, C. 2023. Climate Change 2022 – Impacts, Adaptation and Vulnerability. https://doi.org/10.1017/9781009325844

Johnson, K. and Brown, M. E. 2014. Environmental risk factors and child nutritional status and survival in a context of climate variability and change. Appl. Geogr., 54: 209-221. https://doi.org/10.1016/j.apgeog.2014.08.007

Khan, J. R., Bakar, K. S. and Hossain, M. S. 2023. Unveiling the link between rainfall, temperature, and childhood undernutrition in Bangladesh using spatial analysis. Environ. Res. Health, 1(3). https://doi.org/10.1088/2752-5309/ace2e0

Khine, M. M. and Langkulsen, U. 2023. The Implications of Climate Change on Health among Vulnerable Populations in South Africa: A Systematic Review. Int. J. Environ. Res. Public Health, 20(4): 425. https://doi.org/10.3390/ijerph20043425

Le, K. and Nguyen, M. 2022. Droughts and child health in Bangladesh. PLoS One, 17(3): e0265617. https://doi.org/10.1371/journal.pone.0265617

Ledlie, N. A., Alderman, H., Leroy, J. L. and You, L. 2018. Rainfall shocks are not necessarily a sensitive early indicator of changes in wasting prevalence. Eur. J. Clin. Nutr., 72(1): 177-178. https://doi.org/10.1038/ejcn.2017.144

Lieber, M., Chin-Hong, P., Kelly, K., Dandu, M. and Weiser, S. D. 2022. A systematic review and meta-analysis assessing the impact of droughts, flooding, and climate variability on malnutrition. Glob. Public Health, 17(1): 68-82. https://doi.org/10.1080/17441692.2020.1860247

Maccini, S. and Yang, D. 2009. Under the weather: Health, schooling, and economic consequences of early-life rainfall. Am. Econ. Rev., 99(3): 1006-1026. https://www.nber.org/system/files/working_papers/w14031/w14031.pdf

Macheka, L., Mudiwa, T., Chopera, P., Nyamwanza, A. and Jacobs, P. 2022. Linking climate change adaptation strategies and nutrition outcomes: A conceptual framework. Food Nutr. Bull., 43(2): 201-212. https://doi.org/10.1177/03795721221078362

Madan, E. M., Haas, J. D., Menon, P. and Gillespie, S. 2018. Seasonal variation in the proximal determinants of undernutrition during the first 1000 days of life in rural South Asia: A comprehensive review. Glob. Food Secur., 19: 11-23. https://doi.org/10.1016/j.gfs.2018.08.008

Mahapatra, B., Walia, M., Rao, C. A. R., Raju, B. M. K. and Saggurti, N. 2021. Vulnerability of agriculture to climate change increases the risk of child malnutrition: Evidence from a large-scale observational study in India. PLoS One, 16(6): e0253637. https://doi.org/10.1371/journal.pone.0253637

Mank, I., Belesova, K., Bliefernicht, J., Traore, I., Wilkinson, P., Danquah, I. and Sauerborn, R. 2021. The impact of rainfall variability on diets and undernutrition of young children in rural Burkina Faso. Front. Public Health, 9: 693281. https://doi.org/10.3389/fpubh.2021.693281

McGuinness, L. A. and Higgins, J. P. T. 2021. Risk-of-bias VISualization (robvis): An R package and Shiny web app for visualizing risk-of-bias assessments. Res. Synth. Methods, 12(1): 55-61. https://doi.org/10.1002/jrsm.1411

McMahon, K. and Gray, C. 2021. Climate change, social vulnerability, and child nutrition in South Asia. Glob. Environ. Change, 71: 102414. https://doi.org/10.1016/j.gloenvcha.2021.102414

McMichael, A. J. and Kovats, R. S. 2000. Climate change and climate variability: adaptations to reduce adverse health impacts. Environ. Monit. Assess., 61: 49-64. https://link.springer.com/content/pdf/10.1023/A:1006357800521.pdf

Mueller, V., Sheriff, G., Dou, X. and Gray, C. 2020. Temporary migration and climate variation in Eastern Africa. World Dev., 126: 104704. https://doi.org/10.1016/j.worlddev.2019.104704

Ngwira, A. 2020. Climate and location as determinants of childhood stunting, wasting, and overweight: An application of semiparametric multivariate probit model. Nutr., 70S: 100010. https://doi.org/10.1016/j.nutx.2020.100010

Niles, M. T., Emery, B. F., Wiltshire, S., Brown, M. E., Fisher, B. and Ricketts, T. H. 2021. Climate impacts associated with reduced diet diversity in children across nineteen countries. Environ. Res. Lett., 16(1): https://doi.org/10.1088/1748-9326/abd0ab

Nyantakyi-Frimpong, H. 2021. Climate change, women's workload in smallholder agriculture, and embodied political ecologies of undernutrition in northern Ghana. Health Place, 68: 102536. https://doi.org/10.1016/j.healthplace.2021.102536

Page, M. J., McKenzie, J. E., Bossuyt, P. M., Boutron, I., Hoffmann, T. C., Mulrow, C. D. and Moher, D. 2021. The PRISMA 2020 statement: an updated guideline for reporting systematic reviews. Int. J. Surg., 88: 105906. https://doi.org/10.1016/j.ijsu.2021.105906

Pelletier, D. L., Frongillo Jr, E. A., Schroeder, D. G. and Habicht, J. P. 1995. The effects of malnutrition on child mortality in developing countries. Bull. World Health Organ., 73(4): 443. https://www.ncbi.nlm.nih.gov/pmc/articles/PMC2486780/

Phalkey, R. K., Aranda-Jan, C., Marx, S., Hofle, B. and Sauerborn, R. 2015. Systematic review of current efforts to quantify the impacts of climate change on undernutrition. Proc. Natl. Acad. Sci. U.S.A., 112(33): E4522-4529. https://doi.org/10.1073/pnas.1409769112

Randell, H., Gray, C. and Grace, K. 2020. Stunted from the start: Early life weather conditions and child undernutrition in Ethiopia. Soc. Sci. Med., 261: 113234. https://doi.org/10.1016/j.socscimed.2020.113234

Salisbury, L. 2009. Web of Science and Scopus: A comparative review of content and searching capabilities. Charleston Advisor, 11(1): 5-18.

Shively, G. E. 2017. Infrastructure mitigates the sensitivity of child growth to local agriculture and rainfall in Nepal and Uganda. Proc. Natl. Acad. Sci. U.S.A., 114(5): 903-908. https://doi.org/10.1073/pnas.1524482114

Shively, G., Sununtnasuk, C. and Brown, M. 2015. Environmental variability and child growth in Nepal. Health Place, 35: 37-51. https://doi.org/10.1016/j.healthplace.2015.06.008

Smit, B., Burton, I., Klein, R. J. and Wandel, J. 2000. An Anatomy of Adaptation To Climate Change And Variability. Springer, Netherlands, pp. 223-251. https://doi.org/10.1007/978-94-017-3010-5_12

Thiede, B. C. and Gray, C. 2020. Climate exposures and child undernutrition: Evidence from Indonesia. Soc. Sci. Med., 265: 113298. https://doi.org/10.1016/j.socscimed.2020.113298

Thiede, B. C. and Strube, J. 2020. Climate variability and child nutrition: Findings from Sub-Saharan Africa. Glob. Environ. Change, 65: 102192. https://doi.org/10.1016/j.gloenvcha.2020.102192

Tirado, M. C., Crahay, P., Mahy, L., Zanev, C., Neira, M., Msangi, S. and Müller, A. 2013. Climate change and nutrition: creating a climate for nutrition security. Food Nutr. Bull., 34(4): 533-547. https://doi.org/10.1177/156482651303400415

Tiwari, I., Tilstra, M., Campbell, S. M., Nielsen, C. C. and et al. 2022. Climate change impacts on the health of South Asian children and women subpopulations - A scoping review. Heliyon, 8(10): e10811. https://doi.org/10.1016/j.heliyon.2022.e10811

Tiwari, S., Jacoby, H. G. and Skoufias, E. 2017. Monsoon babies: Rainfall shocks and child nutrition in Nepal. Econ. Dev. Cult. Change, 65(2): 167-188. http://www.journals.uchicago.edu/t-and-c

Tusting, L. S., Bradley, J., Bhatt, S., Gibson, H. S., Weiss, D. J., Shenton, F. C. and Lindsay, S. W. 2020. Environmental temperature and growth faltering in African children: a cross-sectional study. Lancet Planet Health, 4(3): e116-e123. https://doi.org/10.1016/S2542-5196(20)30037-1

UNICEF. 2021. UNICEF conceptual framework on maternal and child nutrition. Retrieved from https://www.unicef.org/media/113291/file/UNICEF%20Conceptual%20Framework.pdf (Accessed on May 18, 2022.)

United Nations. Department of Economic and Social Affairs. 2022. The Sustainable Development Goals: Report 2022. https://unstats.un.org/sdgs/report/2022/

Van der Merwe, E., Clance, M. and Yitbarek, E. 2022. Climate change and child malnutrition: A Nigerian perspective. Food Policy, 113: 102281. https://doi.org/10.1016/j.foodpol.2022.102281

Van Soesbergen, A., Nilsen, K., Burgess, N.D., Szabo, S. and Matthews, Z. 2017. Food and nutrition security trends and challenges in the Ganges Brahmaputra Meghna (GBM) delta. Elem. Sci. Anth., 5: 56. https://doi.org/10.1525/elementa.153

Villanueva, M. 2022. The Impact of Climate Shocks and Women's Empowerment on Child Undernutrition in Mozambique. https://escholarship.org/uc/item/75s3g91b

Wolfle, A. and Channon, A.A. 2023. The effect of the local environment on child nutritional outcomes: how does seasonality relate to wasting amongst children under 5 in southwest coastal Bangladesh? Popul. Environ., 45(3): 434-437. https://doi.org/10.1007/s11111-023-00434-3

World Health Organization. 2019. Technical Series on Adapting to Climate Sensitive Health Impacts: Undernutrition. WHO, Geneva

Xu, R., Zhao, Q., Coelho, M., Saldiva, P. H. N., Abramson, M. J., Li, S. and Guo, Y. 2019. The association between heat exposure and hospitalization for undernutrition in Brazil during 2000-2015: A nationwide case-crossover study. PLoS Med., 16(10): e1002950. https://doi.org/10.1371/journal.pmed.1002950

Zhang, T. and Huang, Y. 2012. Impacts of climate change and inter-annual variability on cereal crops in China from 1980 to 2008. J. Sci. Food Agric., 92(8): 1643-1652. https://doi.org/10.1002/jsfa.5523

Ziervogel, G., Nyong, A., Osman, B., Conde, C., Cortés, S. and Downing, T. 2006. Climate Variability and Change. Washington, DC, USA.

## ORCID DETAILS OF THE AUTHORS

Niraj K.C.: https://orcid.org/0000-0003-3460-8949
Kuaanan Techato: https://orcid.org/0000-0002-9178-8416

Nature Environment and Pollution Technology
An International Quarterly Scientific Journal

p-ISSN: 0972-6268
(Print copies up to 2016)
e-ISSN: 2395-3454

Vol. 23 | No. 3 | pp. 1433-1447 | 2024

Original Research Paper

https://doi.org/10.46488/NEPT.2024.v23i03.014

Open Access Journal

# GIS-Based Mapping of the Water Quality and Geochemical Assessment of the Ionic Behavior in the Groundwater Aquifers of Middle Ganga Basin, Patna, India

**Mohammad Masroor Zafar, Mohammed Aasif Sulaiman and Anupma Kumari†**
Environmental Biology Laboratory, Department of Zoology, Patna University, Patna-800005, Bihar, India
†Corresponding author: Anupma Kumari, anupma-zoology@patnauniversity.ac.in

**Nat. Env. & Poll. Tech.**
**Website: www.neptjournal.com**

*Received:* 25-12-2023
*Revised:* 14-02-2024
*Accepted:* 15-03-2024

**Key Words:**
Groundwater
GIS
Water quality index
Hydrogeochemical assessment

## ABSTRACT

The study implemented Geographic Information System (GIS) techniques and multivariate hydrogeochemical analysis to evaluate the spatial-temporal and seasonal variation in the groundwater quality of Patna, India. For this purpose, sixty groundwater samples were collected and analyzed for major anions and cations during the pre-monsoon, monsoon, and post-monsoon seasons of 2019-2020. The physicochemical parameters such as pH, EC (Electrical Conductivity), TDS (Total Dissolved Solids), TH (Total Hardness), $Ca^{2+}$, $Mg^{2+}$, $Na^{+}$, $K^{+}$, $HCO_3^{-}$, $Cl^{-}$, $SO_4^{2-}$ were considered to evaluate the water quality index. The result revealed degradation in groundwater quality from pre-monsoon (49.21) to post-monsoon (74.48). EC, TDS, TH, $Mg^{2+}$, $Na^{+}$, $Ca^{2+}$, $K^{+}$, and $HCO_3^{-}$ ions were found accountable for high WQI values at various sampling sites during different seasons. Spatial maps showed that 45 % of the sampling stations exhibited poor quality in all three seasons, where the eastern part of the studied region was revealed to be the most affected area. The application of multivariate statistical methods and hydrogeochemical investigation has clearly defined the dominant role of the weathering process, and reverse ion exchange mechanism in controlling the aquifer's ionic chemistry. Moreover, poor seepage system, and waste leachate from the surface have been found as the main cause of high levels of $Na^{+}$, $K^{+}$, and $Cl^{-}$ in the eastern part of Patna.

## INTRODUCTION

Groundwater is one of the most critical natural resources as it meets the domestic, agricultural, and industrial necessities and has an impact on the economic development of countries across the world (Li et al. 2018, Wu et al. 2020), especially in the arid and semi-arid regions (Li et al. 2018, Zhang et al. 2018, Adimalla et al. 2020). Nearly one-third of the global population relies on groundwater for drinking and domestic purposes, whereas it supplies 42% of the agricultural and 27% of the industrial demand worldwide (Nickson et al. 2005, Verma et al. 2020). However, the increasing demand for groundwater due to population explosion, coupled with the predicted water shortages, raises concerns about the sustainability of groundwater resources in meeting the future water needs of the world's population. By 2025, it is estimated that more than half of the world's population will be vulnerable to water shortages, while certain developing countries are projected to experience a shortfall of over 50% in water supply by 2030. In India, groundwater meets 85% of rural water supply, 62% of irrigational needs, and 45% of urban water consumption (Saha & Ray 2018, Verma et al. 2020). Increasing Population density, rapid urbanization, industrialization, and rising living standards have contributed to a continuous increase in water demands, which eventually led to unjudicial exploitation and deterioration in groundwater quality (Bodrud-Doza et al. 2020, Jha et al. 2020, Khan et al. 2020, Divya et al. 2023). Moreover, consumption of contaminated groundwater poses health risks associated with mortality and morbidity to humans and other living organisms (Bodrud-Doza et al. 2019, Kadam et al. 2019, Li & Wu 2019, Mgbenu & Egbueri 2019, Zhu et al. 2019, Bulut et al. 2020, Sulaiman et al. 2023a, Sulaiman et al. 2024). In 2017, contaminated water caused 1.2 million fatalities worldwide, with 569,679 deaths reported in India (Ritchie & Roser 2019). Bihar had a disproportionately high share of these deaths, accounting for 11.97% compared to the national average of 7.65%. (The Times of India 2018).

Patna, the state capital and largest city of Bihar has also experienced a drop in groundwater quality because of the city's uncontrolled growth, an antiquated and unrepaired water supply network, a poor drainage system, and overexploitation of groundwater sources (CDP PATNA 2010, UDHD 2016). According to the report published in Block-wise Ground Water Resources Assessment (2017),

50% of the blocks of Patna agglomeration are categorized as critical, 25% are overexploited, and only 25% are safe. Several researchers reported that groundwater quality is deteriorating at an alarming rate (Egbueri 2018, Egbueri & Unigwe 2019). Therefore, groundwater quality assessment is essential for knowing its suitability for domestic uses. Physico-chemical parameters are useful indicators of water quality, as they provide information on various physical and chemical characteristics of water, such as pH, EC, TDS, cations, anions, and levels of nutrients. However, these parameters alone may not provide a complete picture of water quality, as acceptable limits for each may vary. Water quality index (WQI) is a tool that combines multiple parameters into a single value to assess overall water quality. It takes into account the concentrations of different parameters and provides an easy-to-understand rating system for water quality (Horton 1965, Liou et al. 2004, Boyacioglu 2007). Numerous studies based on WQI approaches have been conducted globally (Boateng et al. 2016, Khosravi et al. 2017, Kawo & Karuppannan 2018, Khan & Rehman 2018, Karakuş 2019, Molekoa et al. 2019) and in India (Khan & Jhariya 2017, Acharya et al. 2018, Deepa & Venkateswaran 2018, Prasad Chourasia 2018, Gaikwad et al. 2020) validating its effectiveness in water quality assessment.

Moreover, combining the knowledge of traditional index systems with geospatial and hydrogeochemical mapping will certainly enhance the quality of assessment. GIS, or Geographic Information System, is a powerful tool used for analyzing, visualizing, and managing spatial data. It provides a platform for storing and retrieving huge amounts of data, which can be spatially linked to generate the necessary output for spatial analysis and integration. This feature of GIS makes it an important tool for solving water resource concerns, evaluating water quality, and assessing groundwater vulnerability. Besides, hydrogeological study can provide us information about the origin of the contaminants, or any spatial-temporal change in the chemical composition. Many authors have combined WQI with Geographic Information System (GIS) for assessing and depicting groundwater quality (Tiwari et al. 2017, 2018, Chakraborty et al. 2021, Chaurasia et al. 2021, Makki et al. 2021), but no previous work in such context has been conducted for Patna. Kumar et al. (2023a) and Sulaiman et al. (2023b) conducted a study to determine the geochemical processes controlling groundwater quality using multivariate approaches at Patna but did not put any emphasis on the water quality, its spatial and seasonal variation in their studies. Other studies conducted in Patna were based on physico-chemical analysis and WQI assessment and irrigation suitability but did not mention the root cause of the deterioration of groundwater quality (Zafar et al. 2022, Praveen & Roy 2021, Sukumaran et al. 2015). Therefore, the present study aims to fill this knowledge gap by employing a combined approach of WQI, GIS, and hydrogeology to provide a detailed account of groundwater status in Patna, which can provide valuable insights for developing effective conservation strategies and sustainable management practices for groundwater resources in Patna.

## MATERIALS AND METHODS

### Study Area

The present study is carried out in and around Patna, situated in South Bihar alluvial plains (latitude 25º13'and 25º45'N, longitude 84º43' and 86º44' E) with an area of 3172 Sq.km (Fig. 1). It is defined by the heavy deposition of Tertiary and Quaternary alluvial sediment, sourced from the Himalaya (Valdiya 2016). This district experiences a subtropical climate with hot summer and cold winter, and temperatures vary from 30°C to 43°C during summer and 5°C to 21.4°C during winter. The mean annual rainfall is around 1076 mm, and relative humidity reaches approximately 100 % during summer (Sulaiman et al. 2021). The groundwater aquifer at Patna is under semi-confined conditions (Singh & Mishra 2012). A total of 85 deep tube wells dug by Patna Municipal Corporation and many shallow tube wells drilled by households extract groundwater daily from these aquifers (UDHD 2016). The current water demand for the Patna Planning area is 961 MLD (Million Liter Per Day), projected to increase by 452 MLD by 2031 (UDHD 2016). Groundwater resources have been preferred over surface water resources for a long time at Patna as the water of both River Ganga and Sone is unfit for drinking and requires extensive treatment before use.

### Sample Collection and Analysis

In the present study, 60 borewell samples were collected seasonally in the month of March-April (pre-monsoon), August-September (monsoon), and October-November (post-monsoon) from 20 different sampling sites during 2019-2020. Sampling was done following the procedure prescribed by (APHA, AWWA, WEF 2012). Physico-chemical parameters like pH, EC, TDS, TH, $Ca^{2+}$, $Mg^{2+}$, $Na^{+}$, $K^{+}$, $HCO_3^{-}$, $Cl^{-}$, and $SO_4^{2-}$ were analyzed following standard methods (APHA, AWWA, WEF 2012) and compared with (BIS 2012) standards. This study's statistical analysis is performed using SPSS version 22.0, XL STAT, and MS Excel 2019. A graphical representative of the dominant geochemical process and hydrogeochemical facie has been constructed using Grapher 14.0 software. ArcGIS 10.5 software is used to restrict the boundaries of Patna and all spatial distribution maps of WQI using the inverse distance weighted (IDW) interpolation technique.

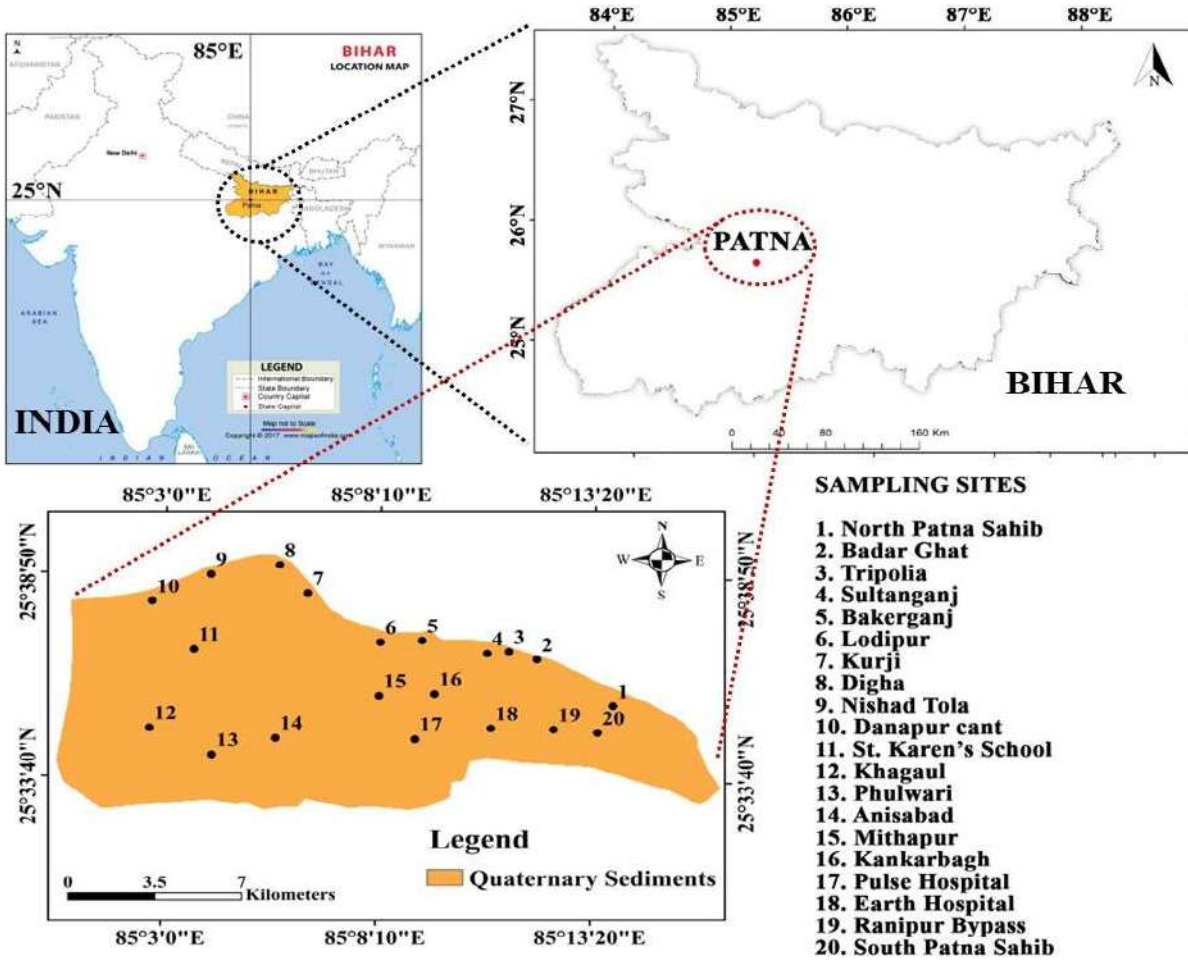


Fig. 1: Map showing the study area with 20 sampling locations.

**Evaluation of the Water Quality Index**

WQI is an effective tool that appraises water quality by combining the effect of different Physicochemical parameters into a single numeric value (Abtahi et al. 2015, Li et al. 2016, Iticescu et al. 2019). pH, EC, TDS, TH, $Ca^{2+}$, $Mg^{2+}$, $Na^{+}$, $K^{+}$, TA, $Cl^{-}$, $SO_4^{2-}$ were considered along with (BIS 2012) standards to evaluate the water quality index. In the current study, WQI was estimated by the Weighted Arithmetic Index method (WAWQI) using the equation (1) developed by (Tiwari & Mishra 1985):

$$WQI = \frac{\Sigma W_n \times Q_n}{\Sigma W_n} \quad \ldots(1)$$

Where $W_n$ is the relative unit weight of the $n^{th}$ water quality parameter, and $Q_n$ is the quality rating of the $n^{th}$ water quality parameter. The relative unit weight ($W_n$) and quality rating ($Q_n$) for each parameter can be calculated using the following expression given as equations (2) and (3), respectively.

$$W_n = \frac{K}{V_s} \quad \ldots(2)$$

Where K is the constant of proportionality, and it is calculated using the equation $K = 1/\sum 1/V_s$.

$$Q_n = \left[\frac{(V_n - V_i)}{(V_s - V_i)}\right] \times 100 \quad \ldots(3)$$

Where $V_n$ is the value of the respective physico-chemical parameter obtained after analysis, $V_i$ is the ideal parameter value, and $V_i = 0$ for all other parameters except for pH ($V_i = 7$). $V_s$ is the standard permissible value for the $n^{th}$ water quality parameter. The computation of relative weight and WQI for S1 during PRM is summarized in Table 1.

**Multivariate Statistical Analysis**

Two of the most used statistical methods, Principal component analysis (PCA) and Hierarchical cluster analysis (HCA) have been performed using SPSS version 22.0. The

Table 1: Calculation of WQI value for S1 sampling site during Pre-monsoon.

| Chemical Parameters | $V_s$ | $1/V_S$ | $W_n$ | $V_n$ | $Q_n$ | $W_n X Q_n$ |
|---|---|---|---|---|---|---|
| pH | 8.5 | 0.117647 | 0.427838 | 7.7 | 46.66 | 19.96292 |
| EC | 750 | 0.001333 | 0.004849 | 600 | 80 | 0.387906 |
| TH | 200 | 0.005 | 0.018183 | 245 | 122.5 | 2.227432 |
| $Ca^{2+}$ | 75 | 0.013333 | 0.048488 | 61 | 81.333333 | 3.943716 |
| $Mg^{2+}$ | 30 | 0.033333 | 0.121221 | 22 | 73.333333 | 8.889523 |
| $HCO_3^-$ | 200 | 0.005 | 0.018183 | 296 | 148 | 2.691101 |
| TDS | 500 | 0.002 | 0.007273 | 326 | 65.2 | 0.474216 |
| $Na^+$ | 200 | 0.005 | 0.018183 | 98 | 49 | 0.890973 |
| $K^+$ | 12 | 0.083333 | 0.303052 | 10.4 | 86.666667 | 26.2645 |
| $Cl^-$ | 250 | 0.004 | 0.014546 | 28 | 11.2 | 0.162921 |
| $SO_4^{2-}$ | 200 | 0.005 | 0.018183 | 20 | 10 | 0.181831 |
| | $\sum 1/V_s =$ | 0.27498 | | | $\sum W_n X Q_n =$ | 66.07704 |
| | K= | 3.636623 | | | | |

Note: Unit in mg/L, Except EC (µS/cm) and pH.

principal component analysis is a form of factor analysis that reduces the dimensionality of large inter-correlated variables and attempts to explain the association and variance between them (Marghadhe et al. 2015, Barzegar et al. 2017). The outcome of the PCA is a simplified data set extracted from the linear combination of the variables from the original matrix as a new set of composite variables or Principal components (PC). Eigenvalue > 1 has been selected widely as a criterion for selecting representative Principal factors (Kaiser 1958). The study uses the varimax method for the orthogonal rotation of the original variables, which maximizes the variance of the rotated axes (Al-Qudah et al. 2011, Kaur et al. 2019). Factor loading of individual parameters is expressed as a numeric score that specifies the contribution of each variable along that principal axis. Factor loading of variables having a value >0.5 was considered significant for result interpretation. Further, validation of factor analysis was done using Hierarchical cluster analysis, which group data sets with underlying similarities. The study uses the widely accepted Ward's method, in combination with squared Euclidean distance for clustering variables, as it tends to maximize the homogeneity between two variables in such a way that the distance between them represents the difference between their observed value (Bhuiyan et al. 2011, Kumar 2019).

### GIS Mapping

The IDW interpolation technique was employed in conducting a spatial analysis of the Water Quality Index (WQI) using ArcGIS version 10.5. Inverse Distance Weighting (IDW) is an interpolation technique commonly used in Geographic Information Systems (GIS) to estimate values of a variable at unsampled locations based on known values at surrounding sample locations (Gunarathna et al. 2016). The technique assumes that the surrounding sample locations influence the values at unsampled locations, and the influence decreases with distance from each sample location (Gnanachandrasamy et al. 2015). IDW is widely used due to its user-friendliness, computational efficiency, and ability to accommodate outliers, resulting in highly accurate results (Zafar et al. 2022).

## RESULTS AND DISCUSSION

### Analytical Results

Table 2 represents the physicochemical characteristics and comparative analysis range with Bureau of Indian Standards limits (BIS 2012). The values of pH, $Cl^-$, and $SO_4^{2-}$ were within the desirable limits. The concentration of EC and TDS ranges from 300 to 1700 µS/cm and 236 to 1195 mg/L, and 31.66% have high EC and TDS exceeding BIS standard guidelines. More dissolved salts caused the elevated EC level in the water (Panghal & Bhateria 2020, Sarker et al. 2020, Narasaiah & Rao 2021). Several researchers reported that a high concentration of EC and TDS might be due to soil mineralization and increasing ionic activity in groundwater aquifers (Adimalla 2019, Chegbeleh et al. 2020). $HCO_3^-$ is the most dominant among the anions, followed by $Cl^-$ >

Table 2: Summary of the physico-chemical parameters and its comparison with (BIS 2012) Standard during 2019-2020.

| Parameters | PRM (Range) | MON (Range) | POM (RangE) | Annual Avg. ± STD | BIS (2012) Acceptable Limit | % Sample Exceeding BIS standards |
|---|---|---|---|---|---|---|
| pH | 7.3-8.1 | 7.1-7.8 | 7.1-7.7 | 7.39 ± 0.18 | 8.5 | 0 |
| EC (µS/cm) | 300-1300 | 400-1400 | 500-1700 | 722.5 ± 277.79 | 750 | 30 |
| TH [mg.L$^{-1}$] | 207-575 | 158-418 | 204-554 | 287.45 ± 79.10 | 200 | 100 |
| $Ca^{2+}$[mg.L$^{-1}$] | 61-149 | 17.63-72.48 | 34.46-165.93 | 66.59 ± 19.88 | 75 | 25 |
| $Mg^{2+}$[mg.L$^{-1}$] | 3-44 | 14.12-81.81 | 16.07-66.23 | 29.15 ± 11.79 | 30 | 30 |
| TDS [mg.L$^{-1}$] | 236-995 | 262-1188 | 279-1195 | 462.70 ± 223.65 | 200 | 35 |
| $Na^{+}$ [mg.L$^{-1}$] | 43-125 | 43.1-102.4 | 43.3-236 | 69.99 ± 20.74 | 500 | 0 |
| $K^{+}$ [mg.L$^{-1}$] | 3-10.4 | 4.6-79 | 5.8-126 | 10.6 ± 9.86 | 200 | 15 |
| $HCO_3^{-}$ [mg.L$^{-1}$] | 260-388 | 250-456 | 228-426 | 307.15 ± 40.38 | 12 | 100 |
| $Cl^{-}$ [mg.L$^{-1}$] | 8-167 | 7-161 | 11-169 | 50.53 ± 44.05 | 250 | 0 |
| $SO_4^{2-}$ [mg.L$^{-1}$] | 3-69 | 1-92.2 | 10.2-113.8 | 35.29 ± 28.11 | 200 | 0 |

$SO_4^{2-}$, and all the samples have $HCO_3^{-}$ above BIS guidelines. Increased bicarbonate ion concentration is attributed to the carbonate and silicate weathering process (Alaya et al. 2014, Narsimha & Sudarshan 2017, Roy et al. 2018, Srivastava & Parimal 2020, Divya et al. 2023). (He et al. 2021) reported that a high concentration of $HCO_3^{-}$ in groundwater might be due to the water-soil interactions and degradation of organic matter. The cations concentration is found as $Ca^{2+}$> $Na^{+}$ >$Mg^{2+}$>$K^{+}$ during pre-monsoon and post-monsoon whereas $Mg^{2+}$ $Na^{+}$> $Ca^{2+}$>$K^{+}$ in monsoon season. In total, 36.66% and 25% of groundwater samples have high $Mg^{2+}$ and $Ca^{2+}$. A high concentration of $Mg^{2+}$ and $Ca^{2+}$ with $HCO_3^{-}$ determines the hardness of groundwater. The total hardness value in 88.33% of collected samples exceeds the BIS guidelines for drinking. Increased TH levels could be related to calcite and dolomite minerals and their subsequent leaching into the groundwater (Sharma et al. 2017, Adimalla & Venkatayogi 2018, Sampson et al. 2020).

## Water Quality Index

WQI was calculated seasonally using the Weighted Arithmetic Water Quality Index method (Horton 1965) for all sampling locations during 2019-2020. Classification of groundwater based on WQI values is shown in (Table 3, Fig. 3). Averaged WQI varied from 49.21 in pre-monsoon, 51.54 in monsoon, and 74.48 during post-monsoon seasons, revealing a decline in water quality from pre-monsoon to post-monsoon. A deteriorated WQI value during post-monsoon in the study area is due to an elevated EC, TDS, $Mg^{2+}$, $Na^{+,}$ and $K^{+}$ ion (Krishna Kumar et al. 2015, Chaudhry & Sachdeva 2020, Mahmud et al. 2020). Similar trends were reported from some other regions of the Indo-Gangetic Plains (Verma et al. 2018, Palmajumder et al. 2021). A study conducted by (Balamurugan et al. 2020) in Tamil Nadu also revealed the deterioration of WQI value during the post-monsoon period. Groundwater quality degradation during the monsoon and post-monsoon season can be attributed to increased solute concentration in the groundwater as water seeps down through the vadose zone (Subba Rao 2008, Manikandan et al. 2020). Shukla & Saxena (2020) reported contrasting results from the Raebareli district of the neighboring state of Uttar Pradesh, where 57% of samples fall in the poor category during pre-monsoon whereas 43% during monsoon and post-monsoon. The spatial variation map of WQI showed that water quality was poor in most of the eastern (S1, S2, S3, S4, S6, S16, S20) and south-western portion of the study area (S11, S12, S13) during the pre-monsoon (Fig 2. a) whereas during monsoon majority of study area falls in poor category except small patches of northern (S5, S7, S8, S9, S10) and central (S15, S18) regions (Fig 2. b). During post-monsoon, a major portion of the study area falls in poor water quality, where S10 and S19 fall in good, S3 is very poor, and S20 is in the unsuitable category (Fig 2. c). Similar trends were reported from some other regions of the Indo-Gangetic Plains (Verma et al. 2018, Palmajumder et al. 2021). Shukla & Saxena (2020) reported contrasting results from the Raebareli district of the neighboring state of Uttar Pradesh, where 57% of samples fall in the poor category during pre-monsoon whereas 43% during monsoon and post-monsoon. Another study conducted by (Balamurugan et al. 2020) in Tamil Nadu also revealed the deterioration of WQI value during the post-monsoon period. Groundwater quality degradation during the monsoon and post-monsoon season can be attributed to increased solute concentration in the groundwater as water seeps down through the vadose zone (Subba Rao 2008, Manikandan et al. 2020). Fig. 3 represents a line graph that summarizes the overall WQI

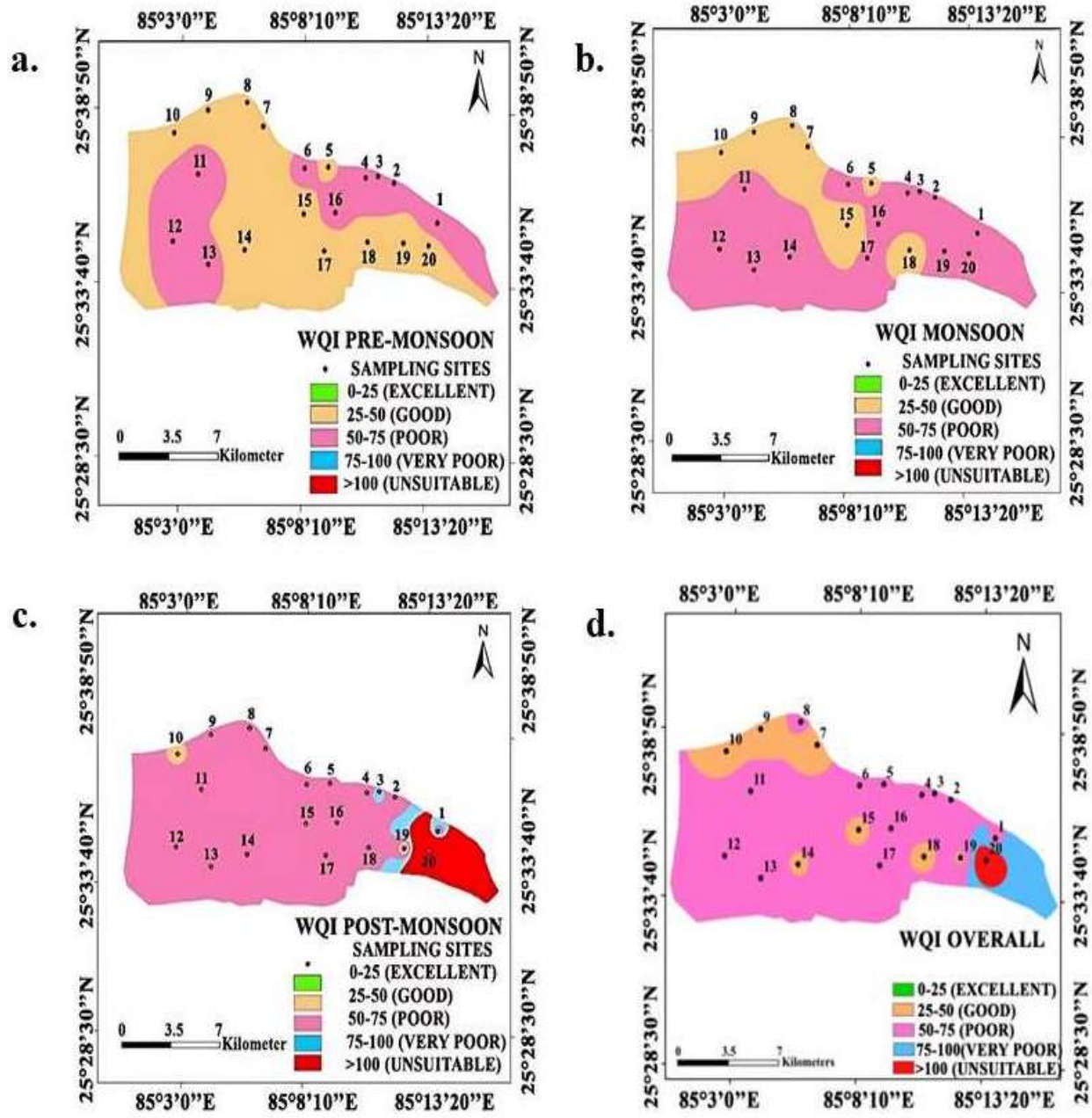


Fig. 2: Spatial maps showing variation in WQI values during (a) pre-monsoon, (b) monsoon, (c) post-monsoon.

of the sampling sites. Line graph showed that S1, S2, S3, S4, S5, S6, S8, S11, S12, S13, S16, S17 fall in poor water quality whereas S7, S9, S10, S14, S15, S18, S19 falls in good water category and S20 falls in unsuitable for drinking purposes.

## Hydro-Geochemical Investigation for the Quality Deterioration

**Water type and weathering process:** The lithological framework, solute kinetics, and flow pattern through the groundwater aquifer are combinedly described as a function of hydrogeochemical facie. It is used to elucidate information about the water type and hydrogeochemical process controlling the ionic composition of the study area (Ali & Ali 2018, Singh et al. 2020). Durov (1948) proposed a diagram with one central rectangular plot at the base of two separate ternary plots. The point in the rectangular plot falling in a particular grid represents the intersection of cationic and anionic values from their respective ternary plots (Chadha 1999). Nearly 20% of samples plotted in field 5 denote water

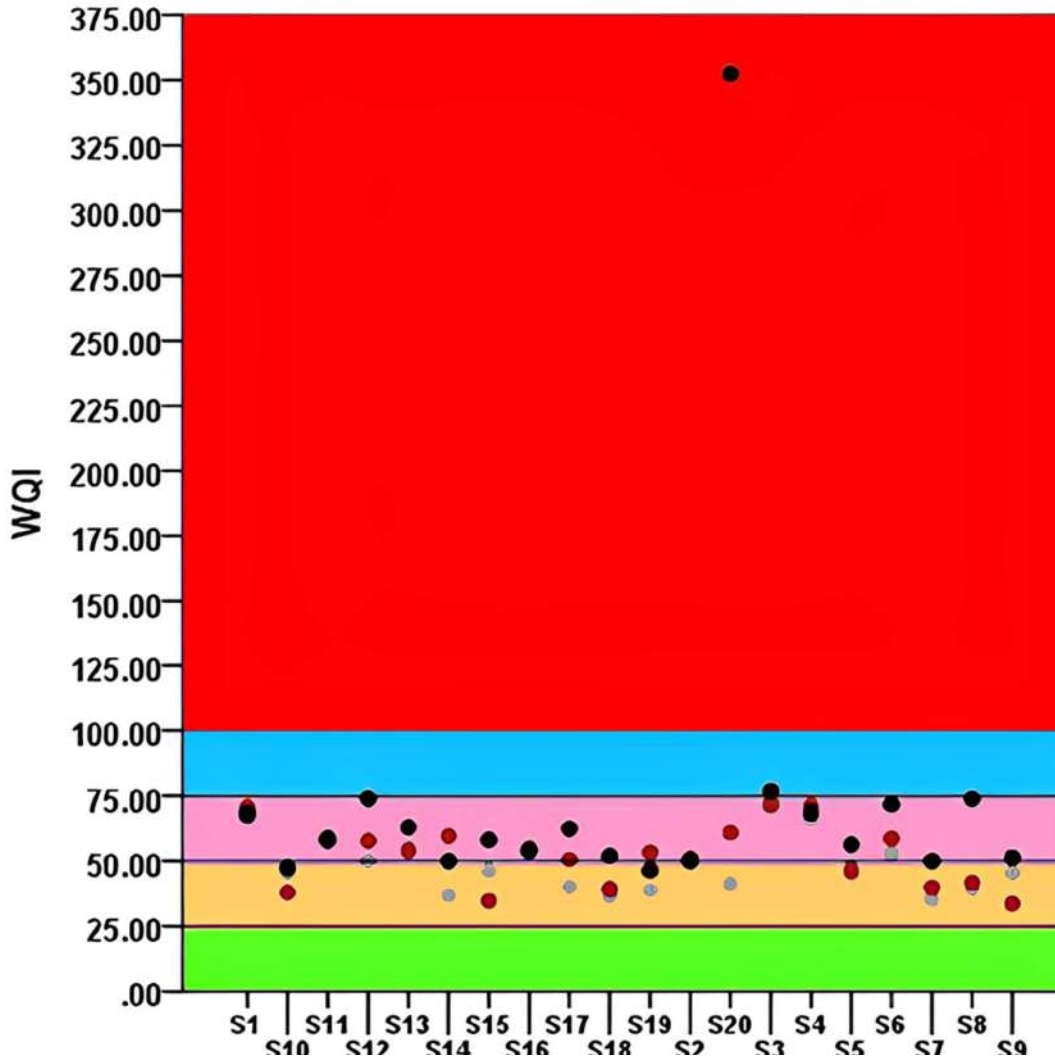


Fig. 3: Scatter plot of WQI value during different seasons in the study area.

with no dominant cations and anions. The samples that were plotted in field 5 include S3, S4, S19, and S20, which in the above discussions have marked with a higher value of total dissolved solids. Several studies have concluded similar findings and suggested infiltration of recent freshwater has caused the simple dissolution of these ions in the studied area (Singh et al. 2020, Das et al. 2021, Kumar et al. 2019). The dominant hydrogeochemical facie in the groundwater of the study area was revealed to be Mg-$HCO_3$ water type, with ~80% of samples falling in field 6 (Fig. 4). The influence of silicate weathering might be the reason behind the surplus of $HCO_3^-$ ion. In contrast, mineral dissolution of carbonate rocks and reverse ion exchange processes caused an elevation in the level of $Mg^{2+}$ ions in the study area (Saha 2019). The outcome of the Durov diagram further explains the geogenic input of divalent ions has contributed to an increase in the conductivity and hardness of the groundwater samples, whereas anthropogenic source has led to a remarkable rise in $Na^+$ and $K^+$ levels in the eastern side of the study area.

The rock water interaction, weathering process, climatic conditions, and residence time of groundwater in the aquifer of the catchment area primarily control the geo-chemistry of groundwater. The ionic composition of the groundwater is dependent on the types of minerals and rocks that it has encountered during this percolation process. Many researchers have employed bivariate ion scatter plots to investigate the dominant rock weathering process, and any deviation from the general trend might signify the presence of anthropogenic disturbances (Kumar et al. 2022, Sulaiman et al. 2023c, Kumar et al. 2023b). The position of a groundwater sample in a $Ca^{2+} + Mg^{2+}$ versus $HCO_3 + SO_4^{2-}$ plot provides

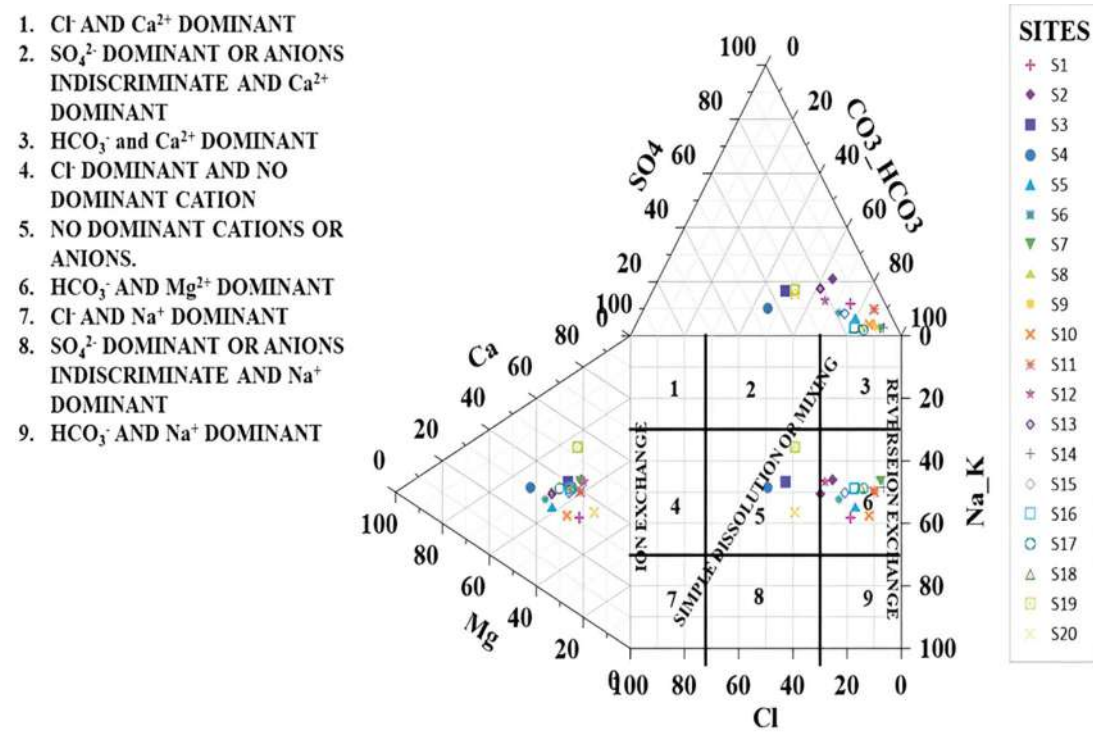


Fig. 4: Durov diagram denoting major hydrogeochemical facie and process controlling the solute chemistry in the groundwater of Patna.

insights into the weathering processes in the studied region. Groundwater samples falling above the euiline (1:1) in the plot suggest high concentrations of $Ca^{2+}$ and $Mg^{2+}$ ions, which are associated with the dissolution of carbonate rocks, and the prevalence of reverse ion exchange processes.

In contrast, samples located below the euiline (1:1) are characterized by lower concentrations of $Ca^{2+}$ and $Mg^{2+}$ ions, where the input of $HCO^3$ is associated with silicate weathering and ion exchange processes. Most of the groundwater samples lay near or below the 1:1 equiline, suggesting the prevalence of silicate weathering, with substantial input from carbonate rocks to the groundwater aquifer (Fig. 5a). Thereafter, the samples in the $Ca^{2+} + Mg^{2+}$ versus total cation ($TZ^+$) scatter plot were situated around $0.5TZ^+$ equiline, validates the involvement of silicate rocks, or cal-silicate minerals (amphiboles, pyroxene, plagioclase) in making the ionic composition of the studied area (Fig. 5b). The bivariate plot of $Na^+ + K^+$ against total cations ($TZ^+$), deciphers the input of $Na^+ + K^+$ ion in the groundwater aquifer. The samples plotted near or above the 0.5 $TZ^+$ marked the role of silicate weathering in contributing the monovalent ions to the groundwater, whereas deviation from the $0.5TZ^+$ equiline suggests some anthropogenic agricultural or seepage leaching. The results further affirm the involvement of the silicate weathering process as the majority of the studied region has spread near the $0.5TZ^+$ equiline (Fig. 5c). However, sites S3, S4, S19 showed a notable deviation from the $0.5TZ^+$ equiline, which signifies the presence of reverse ion exchange process that has elevated the level of divalent ion in these sites.

Interestingly, site 20 was noted with the highest cationic budget, where excess of $Na^+ + K^+$, might be a consequence of some anthropogenic activities. As there are no such agricultural activities marked on the sites, abrupt increases in $Na^+$ and $K^+$ might be due to poor seepage systems and sewage infiltrations. The same has been investigated by plotting Cl/($HCO_3$+$SO_4$) against $Na^+ + K^+$ (Fig. 5d). In the absence of any geogenic source, a high value of Cl-indicates the sewage, domestic, and animal waste infiltration (Zafar et al. 2022). The result revealed a good correlation of $r^2$=0.524 between the two variables of interest, suggesting the role of mineral dissolution in contributing $Cl^-$ and $Na^+$ to the groundwater. A higher value of $Cl^-$ ion was noted at sites S3, S4, S19, and S20, where increasing value $Na^+ + K^+$ at S20, S3, and S4 suggests a similar source of these ions, such as poor seepage system and waste leachate from the cattle corralled in the household in the groundwater at the respective sites.

**Principal component analysis:** The KMO (Kaiser-Meyer-Olkin) value was found to be 0.641, which suggests the data set is relevant for factor analysis (Eyduran et al. 2010). A substantially greater value of Bartlett's sphericity test ($\chi^2$=388.383) than the critical value ($\chi^2$=85.965) at 'degree

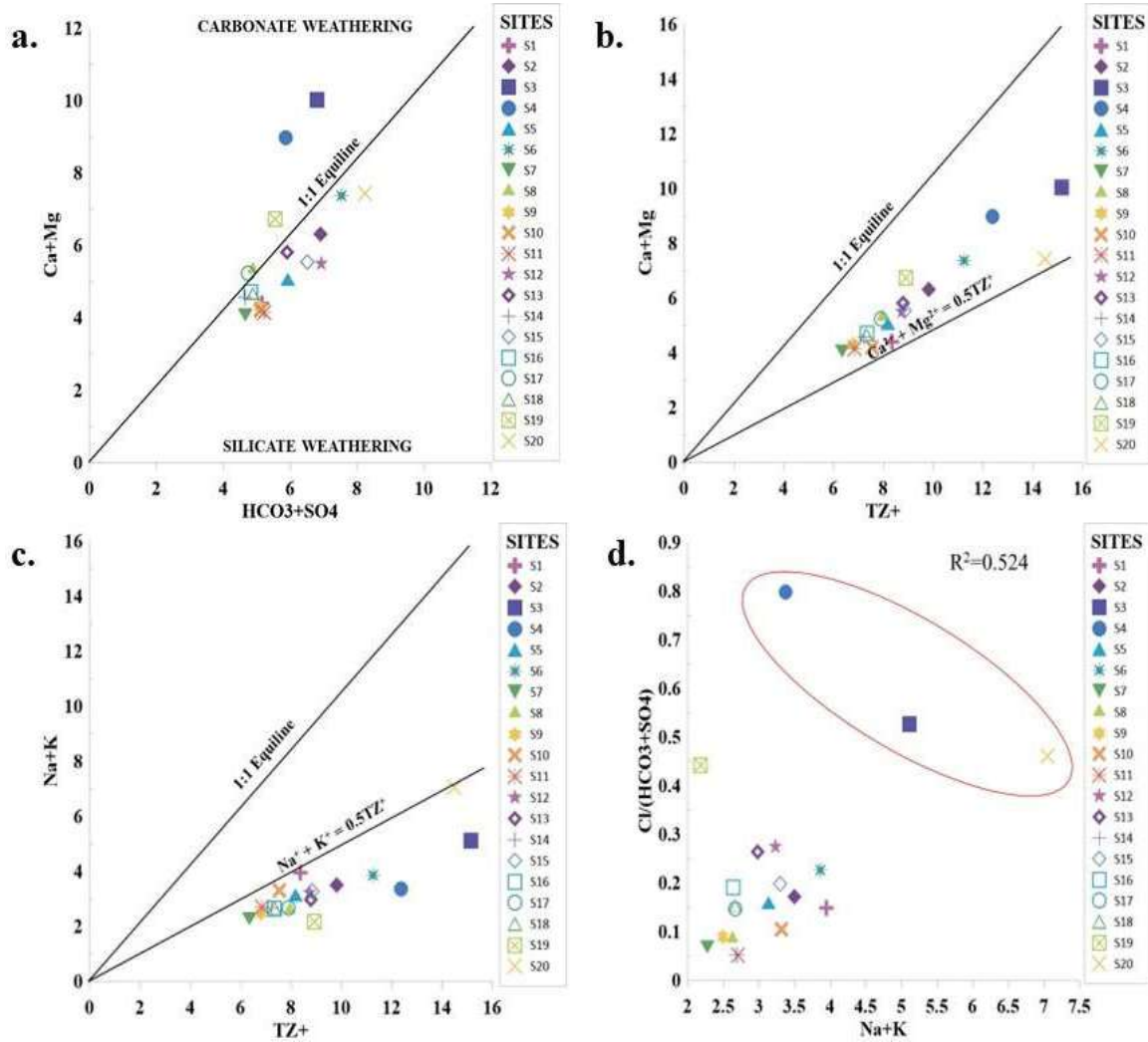


Fig. 5: Bivariate ion scatter plots identifying ionic relationships between different variables.

of freedom' 66 and significance level 0.05 revealed that the test has significantly reduced the dimensionality of the original data (Kumar et al. 2018, Kumar et al. 2019). After that, PCA was performed for the obtained data set using varimax rotation in XL-STAT to evaluate the effect of each WQV on their respective principal factor in a PCA. The two principal factors having eigenvalue >1 that cover the cumulative variance of 78.25% were considered significant for further interpretation (Kim & Mueller 1978) (Fig. 6a). According to (Liu et al. 2003), loading values >0.75 signifies "strong," between 0.5 - 0.75 considered as "moderate" and "weak" when lies between 0.3 to 0.5. The water quality variable with high factor loading along Principal Factor 1 include TH (0.962), TDS (0.897), EC (0.869), $Cl^-$ (0.887), $Mg^{2+}$ (0.842) and $Ca^{2+}$ (0.745) (Table. 3). The high value of EC, TDS, and TH in the first factor might be due to the high loading of $Ca^{2+}$, $Mg^{2+}$, and $Cl^-$ leading to increased hardness and conductivity (Kaur et al. 2019). The dominance of $Ca^{2+}$ and $Mg^{2+}$ (cations), along with principal factor 1, also indicates the presence of rock weathering or reverse ion exchange process (Subramani et al. 2010). A low factor loading of WQI in component 1 is attributable to the high factor loading of the mentioned variable. It signifies that any decrease in the value of those variables in the first factor tends to increase the factor loading of WQI (Mohammadpour et al. 2016), which is evident in the Principal Factor 2 matrix. Principal Factor 2 was observed to have a % variance of 15.03 and is characterized by a high factor loading of monovalent cation $K^+$ (.958) and $Na^+$ (.809), suggesting the presence of anthropogenic influence (Singh et al. 2019, Kaur et al. 2019) (Table 3). The result obtained for principal factor 2 suggests the influence of the silicate weathering process and

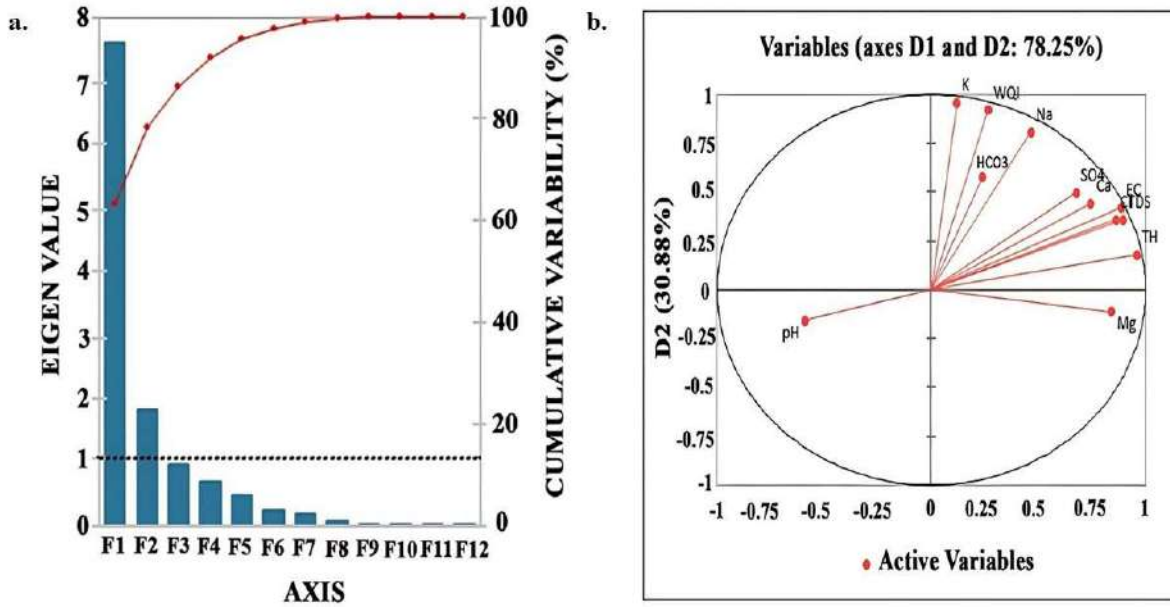


Fig. 6a: Scree plot showing principal factors and their eigenvalue together with cumulative variability **b.** Score plot showing positive and negative factor loading in groundwater at Patna.

reverse ion exchange process in the study area playing a significant role in lowering the concentration of $Mg^{2+}$ (-0.113) and $Ca^{2+}$ (.441) (Srinivasamoorthy et al. 2014) and thereby increasing the factor loading of WQI (0.920) in Principal factor 2.

**Hierarchical cluster analysis (HCA):** Hierarchical Cluster Analysis has been performed to categorize the primary group of water quality variables, which are alike and most probably originated from similar sources. The hierarchical tree of water parameters exhibited two distinct clusters, as shown in Fig. 7. Cluster 1 showed a very strong association between electrical conductivity (EC), total hardness (TH), and total dissolved solids (TDS). The ions that contribute to a relatively high value of hardness and TDS include $Cl^-$, $Ca^{2+}$, $SO_4^{2-}$, and $Mg^{2+}$. Moreover, the clustering of these variables together suggests the geogenic dissolution of rocks into the groundwater aquifer. A similar observation is also seen in the case of factor analysis discussed above. A strong association between $K^+$ and WQI shows a significant contribution of $K^+$ ions in deteriorating water quality, followed by $Na^+$, as depicted in cluster 2. A close association of $Na^+$ with $HCO_3^-$ in cluster 2 marked the role of the silicate weathering process in the higher concentration of $HCO_3$ ion in the groundwater. The two separate clusters suggest each parameter's role in determining the water quality of the study area.

Table 3: Factor loading after Varimax rotation.

| | D1 | D2 |
|---|---|---|
| pH | -0.59 | -0.158 |
| EC | **0.887** | 0.422 |
| TH | **0.962** | 0.181 |
| $Ca^{2+}$ | **0.745** | 0.441 |
| $Mg^{2+}$ | **0.842** | -0.113 |
| TDS | **0.897** | 0.359 |
| Na | 0.465 | **0.809** |
| K | 0.118 | **0.958** |
| $HCO_3^-$ | 0.24 | 0.581 |
| $Cl^-$ | **0.861** | 0.359 |
| $SO_4^{2-}$ | **0.677** | 0.498 |
| WQI | 0.265 | **0.92** |

## CONCLUSION

The present study investigated the current groundwater status of Patna, Bihar, for domestic purposes using traditional WQI methods (WAWQI) as well as modern (Geographical Information System and multivariate geochemical investigations) methods. The study area was marked with similar ionic composition throughout the sampling stations and seasons, where Mg-$HCO_3$ water type and reverse ion exchange process dominated the water chemistry. The seasonal impact was very evident with the deterioration of water quality in the post-monsoon season. The spatial analysis revealed comparatively higher WQI values in the northeastern region of Patna in nearly all seasons. The operative application of

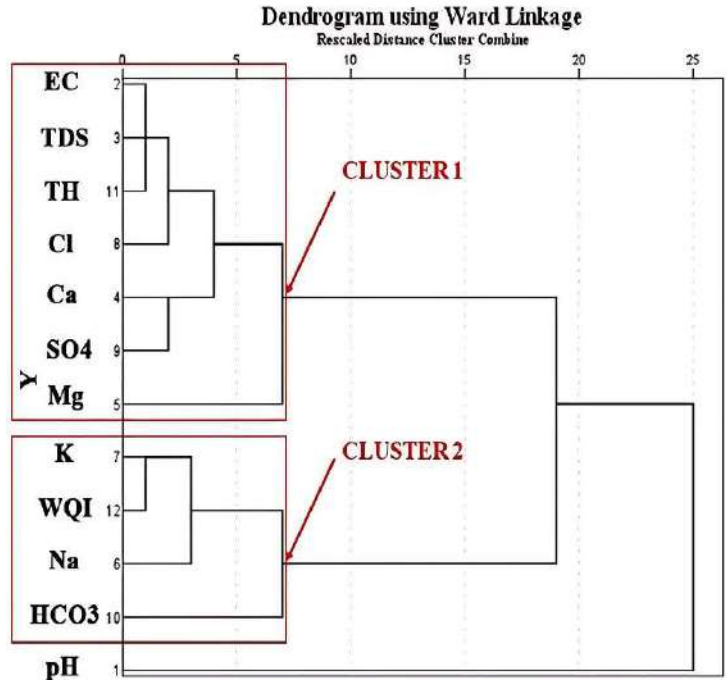


Fig. 7: Dendrogram showing homogeneity between different water quality variables of the groundwater in Patna.

multivariate techniques in the source identification of ionic constituents is further documented in the study. It discusses the role of $Na^+$ and $K^+$ in water quality deterioration in the northeastern part, which revealed high factor loading of (0.809), (0.958), $Na^{+,}$ and $K^+$ in the principal factor 2. The study provides a very pioneer and comprehensive insight into the water quality status in areas where such work has not been documented before, which assesses the water quality index using the GIS approach and multivariate techniques. Moreover, the future perspectives for assessing water quality index using the GIS approach and multivariate techniques are promising, and this approach is likely to become an essential tool for water resources management and decision-making. By providing a more comprehensive understanding of the spatial and temporal variations of water quality, it can help support sustainable water use, protect public health, and preserve groundwater.

## ACKNOWLEDGMENT

The authors are thankful to members of the Environmental Biology Laboratory.

## REFERENCES

Abtahi, M., Golchinpour, N. and Yaghmaeian, K. 2015. A modified drinking water quality index (DWQI) for assessing drinking source water quality in rural communities of Khuzestan Province, Iran. Ecol. Indic., 52: 165-173. DOI: 10.1016/j.ecolind.2015.02.009

Acharya, S., Sharma, S. K. and Khandegar, V. 2018. Assessment of groundwater quality by water quality indices for irrigation and drinking in South West Delhi, India. Data Br., 18: 1071-1078. DOI: 10.1016/j.dib.2018.04.120

Adimalla, N. 2019. Groundwater quality for drinking and irrigation purposes and potential health risks assessment: A Case Study from Semi-Arid Region of South India. Expo. Heal., 11(2): 125-143. DOI: 10.1007/s12403-018-0288-8

Adimalla, N., Dhakate, R., Kasarla, A. and Taloor, A. K. 2020. Appraisal of groundwater quality for drinking and irrigation purposes in Central Telangana, India. Groundw. Sustain. Dev., 11: 100334. DOI: 10.1016/j.gsd.2020.100334

Adimalla, N. and Venkatayogi, S. 2018. Geochemical characterization and evaluation of groundwater suitability for domestic and agricultural utility in a semi-arid region of Basara, Telangana State, South India. Appl. Water Sci., 8(6): 177. DOI: 10.1007/s13201-018-0682-1

Alaya, M.B., Saidi, S., Zemni, T. and Zargouni, F. 2014. Suitability assessment of deep groundwater for drinking and irrigation use in the Djeffara aquifers (Northern Gabes, south-eastern Tunisia). Environ. Earth Sci., 71(4): 1637-1650. DOI: 10.1007/s12665-013-2729-9

Ali, S. A. and Ali, U. 2018. Hydrochemical characteristics and spatial analysis of groundwater quality in parts of Bundelkhand Massif, India. Appl. Water Sci., 8(1): 1-15.

Al-Qudah, O., Woocay, A. and Walton, J. 2011. Identification of probable groundwater paths in the Amargosa Desert vicinity. Appl. Geochem., 26(4): 565-574.

APHA. 2012. Standard Methods for Examination of Water and Wastewater. American Public. Health Association, Washington DC.

Babbar, R. and Babbar, S. 2017. Predicting river water quality index using data mining techniques. Environ. Earth Sci., 76: 52. DOI: 10.1007/s12665-017-6845-9

Balamurugan, P., Shunmugapriya, G. and Vanitha, R. 2020. GIS-based assessment of groundwater for domestic and irrigation purposes

in Vazhapadi Taluk, Salem, Tamil Nadu, India. Taiwan Water Conservancy, 68(2): 1-10.

Barzegar, R., Moghaddam, A. A., Tziritis, E., Fakhri, M. S. and Soltani, S. 2017. Identification of hydrogeochemical processes and pollution sources of groundwater resources in the Marand Plain, northwest of Iran. Environ. Earth Sci., 76(7): 259.

Bhuiyan, M. A. H., Bodrud-Doza, M., Islam, A. R. M., Rakib, M. A., Rahman, M. S. and Ramanathan, A. L. 2016. Assessment of groundwater quality of Lakshimpur district of Bangladesh using water quality indices, geostatistical methods, and multivariate analysis. Environ. Earth Sci., 75(12): 1-23.

BIS 2012. Indian Standards Drinking Water Specifications IS 10500:2012. Bur Indian Stand Indian Stand Drink Water Specification, New Delhi

Bhateja, V., Satapathy, S. C., Zhang, Y. D. and Aradhya, V. M. 2019. Intelligent computing and communication proceedings of 3rd ICICC 2019, Bangalore, p. 18. DOI: 10.1007/978-981-15-1084-7.

Blockwise Ground Water Resources Assessment. 2017. Central Ground Water Board, Ministry of Water Resources, RD &GR Government of India, New Delhi.

Boateng, T. K., Opoku, F., Acquaah, S. O. and Akoto, O. 2016. Groundwater quality assessment using statistical approach and water quality index in Ejisu-Juaben Municipality, Ghana. Environ. Earth Sci., 75: 1. DOI: 10.1007/s12665-015-5105-0.

Bodrud-Doza, M., Islam, S. M. D. U. and Hasan, M. T. 2019. Groundwater pollution by trace metals and human health risk assessment in the central west part of Bangladesh. Groundw. Sustain. Dev., 9: 100219 DOI: 10.1016/j.gsd.2019.100219.

Bodrud-Doza, M., Islam, S. M. D. U. and Rume, T. 2020. Groundwater quality and human health risk assessment for safe and sustainable water supply of Dhaka City dwellers in Bangladesh. Groundw. Sustain. Dev., 10: 100374. DOI: 10.1016/j.gsd.2020.100374.

Boyacioglu, H. 2007. Development of a water quality index based on a European classification scheme. Water SA, 33(1). DOI: 10.4314/wsa.v33i1.47882.

Bulut, O.F., Duru, B., Çakmak, Ö., Günhan, Ö., Dilek, F.B. and Yetis, U. 2020. Determination of groundwater threshold values: A methodological approach. Journal of Cleaner Production, 253: 120001. Prod. DOI: 10.1016/j.jclepro.2020.120001.

Chakraborty, B., Roy, S. and Bera, A. 2021. Geospatial Assessment of Groundwater Quality for Drinking through Water Quality Index and Human Health Risk Index in an Upland Area of Chota Nagpur Plateau of West Bengal, India.

Chaudhry, A.K. and Sachdeva, P. 2020. Groundwater quality and non-carcinogenic health risk assessment of nitrate in the semi-arid region of Punjab, India. Journal of Water and Health, 18(6): 1073-1083. DOI: 10.2166/wh.2020.121.

Chaurasia, A.K., Pandey, H.K., Tiwari, S.K., Pandey, P. and Ram, A. 2021. Groundwater vulnerability assessment using water quality index (WQI) under geographic information system (GIS) framework in parts of Uttar Pradesh, India. Sustainable Water Resources Management, 7(3): 40. DOI: 10.1007/s40899-021-00513-z.

Chadha, D. K. 1999. A proposed new diagram for geochemical classification of natural waters and interpretation of chemical data. Hydrol. J., 7(5): 431-439.

Chegbeleh, L. P., Akurugu, B. A. and Yidana, S. M. 2020. Assessment of groundwater quality in the Talensi District, Northern Ghana. Sci. World J., 2020: 8450860, 1-13. DOI: 10.1155/2020/8450860.

Chen, Y., Song, L. and Liu, Y. 2020. A review of the artificial neural network models for water quality prediction. Appl. Sci., 10: 75776, 1-15. DOI: 10.3390/app10175776.

Chen, W. B. and Liu, W. C. 2015. Water quality modeling in reservoirs using multivariate linear regression and two neural network models. Adv. Artif. Neural Syst., 2015: 6-6.

City Development Plan (2010-30) Patna, Urban Development and Housing Department Government of Bihar. Retrieved from-https://nagarseva.bihar.gov.in/udhd/cache/SHOW_DOCS/Final%20CDP%20Patna.pdf.

Das, B., Panigrahi, K. and Patel, B. 2021. Analysis of ground water quality using spatial techniques in Naya Raipur Atal Nagar, Chhattisgarh, India. SAMRIDDHI J. Phys. Sci. Eng. Technol., 13(02): 109-117.

Dadhich, A.P., Goyal, R. and Dadhich, P.N. 2021. Assessment and prediction of groundwater using geospatial and ANN modeling. Water Resources Management, 35(9): 2879-2893. DOI: 10.1007/s11269-021-02874-8.

Deepa, S. and Venkateswaran, S.J.M.E.S. 2018. Appraisal of groundwater quality in upper Manimuktha sub basin, Vellar river, Tamil Nadu, India by using Water Quality Index (WQI) and multivariate statistical techniques. Modeling Earth Systems and Environment, 4: 1165-1180. DOI: 10.1007/s40808-018-0468-3.

Divya, Sulaiman, M. A., Zafar, M. M. and Kumari, A. 2023. Assessing the fluoride toxicity and the source contributors to the major ionic constituents in the groundwater aquifer of Middle Ganga River Basin, Rohtas, India. Int. J. Energy Water Resour., 2023: 1-15. DOI: 10.1007/s42108-023-00245-0.

Durov, S. A. 1948. Natural waters and graphic representation of their composition. DoklAkadNauk SSSR, 59(3): 87-90.

Egbueri, J. C. 2018. Assessment of the quality of groundwaters proximal to dumpsites in Awka and Nnewi metropolises: a comparative approach. Int. J. Energy Water Resour., 18: 1-15. DOI: 10.1007/s42108-018-0004-1.

Egbueri, J. C. and Unigwe, C. O. 2019. An integrated indexical investigation of selected heavy metals in drinking water resources from a coastal plain aquifer in Nigeria. SN Appl. Sci., 4: 1489. DOI: 10.1007/s42452-019-1489-x.

El Bilali, A., Taleb, A. and Brouziyne, Y. 2021. Comparing four machine learning model performances in forecasting the alluvial aquifer level in a semi-arid region. J. Afr. Earth. Sci., 181: 104244, 1-10. DOI: 10.1016/j.jafrearsci.2021.104244.

Eyduran, E., Topal, M. and Sonmez, A. Y. 2010. Use of factor scores in multiple regression analysis for estimation of body weight by several body measurements in brown trouts (Salmo trutta fario). Int. J. Agric. Biol., 10: 1-5

Gaikwad, S. K., Kadam, A. K. and Ramgir, R. R. 2020. Assessment of the groundwater geochemistry from a part of the west coast of India using statistical methods and water quality index. Hydro. Res., 20: 1-14. DOI: 10.1016/j.hydres.2020.04.001.

He, X., Li, P. and Wu, J. 2021. Poor groundwater quality and high potential health risks in the Datong Basin, northern China: research from published data. Environ. Geochem. Health, 20: 527. DOI: 10.1007/s10653-020-00520-7.

Horton, R. K. 1965. Horton, R.K. 1965. An index number system for rating water quality. J Water Pollut. Control Fed., 37(3): 300-306.

Husna, N. E. A., Bari, S. H., Hussain, M. M., Ur-Rahman M. T. and Rahman, M. 2016. Groundwater level prediction using artificial neural network. Int. J. Hydrology Sci. Technol., 6(4): 371-381.

Ighalo, J. O., Adeniyi, A. G. and Marques G. 2021. Artificial intelligence for surface water quality monitoring and assessment: a systematic literature analysis. Model. Earth Syst. Environ., 10: 441. DOI: 10.1007/s40808-020-01041-z.

Iticescu, C., Georgescu, L. P. and Murariu, G. 2019. Lower Danube water quality was quantified through WQI and multivariate analysis. Water (Switzerland), 11: 1-15.

Jha, M. K., Shekhar, A. and Jenifer, M. A. 2020. Assessing groundwater quality for drinking water supply using hybrid fuzzy-GIS-based water quality index. Water Res., 11: 586. DOI: 10.1016/j.watres.2020.115867.

Joseph, R.M., Manjaly, A.D., Unni, S., Able, E.C. and Sharon, V., 2021. Prediction of Groundwater Quality Using Artificial Neural Network. AIJR Proceedings, pp. 213-221.

Kadam, A. K., Wagh, V. M. and Muley, A. A. 2019. Prediction of water quality index using artificial neural network and multiple linear regression modeling approach in Shivganga River basin, India. Model. Earth Syst. Environ., 5: 951-962. DOI: 10.1007/s40808-019-00581-3.

Karakuş, C. B. 2019. Evaluation of groundwater quality in Sivas province (Turkey) using water quality index and GIS-based analytic hierarchy process. Int. J. Environ. Health Res., 29: 500-519. DOI: 10.1080/09603123.2018.1551521.

Kassem, Y., Gökçekuş, H. and Maliha, M.R. 2021. Identifying most influencing input parameters for predicting chloride concentration in groundwater using an ANN approach. Environmental Earth Sciences, 80(7): 248. DOI: 10.1007/s12665-021-09541-6.

Kaur, L., Rishi, M. S. and Sharma, S. 2019. Hydrogeochemical characterization of groundwater in alluvial plains of River Yamuna in Northern India: An insight of controlling processes. J. King Saud Univ. Sci., 1: 5. DOI: 10.1016/J.JKSUS.2019.01.005.

Kawo, N. S. and Karuppannan, S. 2018. Groundwater quality assessment using water quality index and GIS technique in Modjo River Basin, central Ethiopia. J African Earth Sci., 147: 300-311. https://doi.org/10.1016/j.jafrearsci.2018.06.034

Khalil, B. M., Ayman, G. A., Hussein, K. and Ashraf, E. S. 2012. Application of artificial neural networks for the prediction of water quality variables in the Nile Delta. Journal of Water Resource and Protection, 2012.

Khan, A. and Rehman, Y. 2018. Groundwater Quality Assessment using Water Quality Index (WQI) in Liaquatabad Town, Karachi, Pakistan. Int. J. Gr. Sediment Water, 07: 2373-2989.

Khan, M.J., Shah, B.A. and Nasir, B. 2020. Groundwater quality assessment for drinking purpose: a case study from Sindh Industrial Trading Estate, Karachi, Pakistan. Modeling Earth Systems and Environment, 6(1): 263-272. https://doi.org/10.1007/s40808-019-00676-x.

Khan, R. and Jhariya, D. C. 2017. Groundwater quality assessment for drinking purposes in Raipur city, Chhattisgarh using water quality index and geographic information system. J. Geol. Soc. India, 90: 69-76. https://doi.org/10.1007/s12594-017-0665-0.

Khosravi, R., Eslami, H. and Almodaresi, S. A. 2017. Use of geographic information system and water quality index to assess groundwater quality for drinking purpose in Birjand city, Iran. Desalin. Water Treat., 67: 74-83. https://doi.org/10.5004/dwt.2017.20458.

Kim, J. O. and Mueller, C. W. 1978. Factor Analysis: Statistical Methods and Practical Issues, Springer, Cham.

Kouadri, S., Elbeltagi, A., Islam, A. R. M. and Kateb, S. 2021. Performance of machine learning methods in predicting water quality index based on irregular data set: application on Illizi region (Algerian southeast). Appl. Water Sci., 21: 528-539. https://doi.org/10.1007/s13201-021-01528-9.

Krishnakumar, S., Logeshkumaran, A. and Magesh, N. S. 2015. Hydro-geochemistry and application of water quality index (WQI) for groundwater quality assessment, Anna Nagar, part of Chennai City, Tamil Nadu, India. Appl. Water Sci., 14: 196. https://doi.org/10.1007/s13201-014-0196-4.

Kumar, R., Kumar, R., Singh, A., Singh, S., Bhardwaj, A., Kumari, A. and Gupta, A. 2019. Hydro-geochemical analysis of meltwater draining from Bilare Banga glacier, Western Himalaya. Acta Geophys., 67: 651.

Kumar, R., Kumari, A., Kumar, R., Sulaiman, M. A., Zafar, M. M., Singh, A. and Pippal, P. S. 2023a. Assessing the geochemical processes controlling groundwater quality and their possible effect on human health in Patna, Bihar. Environ. Sci. Pollut. Res., 12: 1-20.

Kumar, R., Kumar, R., Singh, A., Arif, M., Kumar, P. and Kumari, A. 2022. Chemometric approach to evaluate the chemical behavior of rainwater at high altitude in Shaune Garang catchment, Western Himalaya. Sci. Rep., 12(1): 12774.

Kumar, R., Kumar, R., Singh, S., Singh, A., Bhardwaj, A., Kumari, A., Randhawa, S. S. and Saha, A. 2018. Dynamics of suspended sediment load with respect to summer discharge and temperatures in Shaune Garang glacierized catchment, Western Himalaya. Acta Geophys., 16: 454.

Kumar, R., Kumar, R., Bhardwaj, A., Singh, A., Singh, S., Kumari, A. and Sinha, R. K. 2023b. Multivariate statistical analysis and Geospatial approach for evaluating Hydro-geochemical characteristics of meltwater from Shaune Garang Glacier, Himachal Pradesh, India. Acta Geophys., 71(1): 323-339.

Kumari, K. and Yadav, S. 2018. Linear Regression Analysis Study. J. Pract. Cardiovasc. Sci., 4: 33-36.

Li, L., Jiang, P., Xu, H. and Xiang, G. 2019. Water quality prediction based on recurrent neural network and improved evidence theory: a case study of Qiantang River, China. Environ. Sci. Pollut. Res., 19: 511. https://doi.org/10.1007/s11356-019-05116-y.

Li, P., He, S., Yang, N. and Xiang, G. 2018. Groundwater quality assessment for domestic and agricultural purposes in Yan'an City, northwest China: implications to sustainable groundwater quality management on the Loess Plateau. Environ. Earth Sci., 7: 7968. https://doi.org/10.1007/s12665-018-7968-3.

Li, P. and Wu, J. 2019. Drinking water quality and public health. Expo. Heal., 24: 299. https://doi.org/10.1007/s12403-019-00299-8.

Li, P., Wu, J. and Qian, H. 2016. Hydrochemical appraisal of groundwater quality for drinking and irrigation purposes and the major influencing factors: a case study in and around Hua County, China. Arab. J. Geosci., 15: 2059. https://doi.org/10.1007/s12517-015-2059-1.

Liou, S. M., Lo, S. L. and Wang, S. H. 20 04. A generalized water quality index for Taiwan. Environ. Monit. Assess., 64: 115-129. https://doi.org/10.1023/B:EMAS.0000031715.83752.a1.

Liu, C. W., Lin, K. H. and Kuo, Y. M. 2003. Application of factor analysis in the assessment of groundwater quality in a blackfoot disease area in Taiwan. Sci. Total Environ., 313 (1-3): 77-89.

Manikandan, E., Rajmohan, N. and Anbazhagan, S. 2020. Monsoon impact on groundwater chemistry and geochemical processes in the shallow hard rock aquifer. Catena, 6: 341. https://doi.org/10.1016/j.catena.2020.104766.

Marghade, D., Malpe, D. B. and Subba Rao, N. 2015. Identification of controlling processes of groundwater quality in a developing urban area using principal component analysis. Environ. Earth Sci., 74: 5919-5933. https://doi.org/10.1007/s12665-015-4616-z.

Mahmud, A., Sikder, S. and Joardar, J. C. 2020. Assessment of groundwater quality in Khulna city of Bangladesh in terms of water quality index for drinking purposes. Appl. Water Sci., 51: 1142-149. https://doi.org/10.1007/s13201-020-01314-z.

Makki, Z. F., Zuhaira, A. A. and Al-Jubouri, S. M. 2021. GIS-based assessment of groundwater quality for drinking and irrigation purposes in central Iraq. Environ. Monit. Assess., 21: 885. https://doi.org/10.1007/s10661-021-08858-w.

Meenakshi, P. and Ambiga, K. 2022. Prediction of the Water Quality Index Using ANFIS Modelling. J. Pharm. Negat. Results, 132: 1289-1298. https://doi.org/10.47750/pnr.2022.13.S03.202.

Mehdi, M. and Sharma, B. 2022. Prediction of water quality index of groundwater using the artificial neural network and genetic algorithm. Int. J. Adv, Comp. Intell., 19: 332.

Mgbenu, C.N. and Egbueri, J.C. 2019. The hydrogeochemical signatures, quality indices and health risk assessment of water resources in Umunya district, southeast Nigeria. Applied water science, 9(1): 22. https://doi.org/10.1007/s13201-019-0900-5.

Mohammadpour, R., Shaharuddin, S., Zakaria, N. A. and Gokcekus, H. 2016. Prediction of water quality index in free surface constructed wetlands. Environ. Earth Sci., 75: 1-12. https://doi.org/10.1007/s12665-015-4905-6.

Molekoa, M. D., Avtar, R. and Kumar, P. 2019. Hydrogeochemical assessment of groundwater quality of Mokopane area, Limpopo, South Africa using statistical approach. Water (Switzerland), 33: 90-99. https://doi.org/10.3390/w11091891.

Narasaiah, V. and Rao, B. V. 2021. Groundwater quality of an hard rock aquifer in the Subledu Basin of Khammam district, India. Appl. Water Sci., 13: 221. https://doi.org/10.1007/s13201-021-01424-2.

Narsimha, A. and Sudarshan, V. 2017. Contamination of fluoride in groundwater and its effect on human health: a case study in hard rock aquifers of Siddipet, Telangana State, India. Appl. Water Sci. 16: 441. https://doi.org/10.1007/s13201-016-0441-0.

Nickson, R. T., McArthur, J. M. and Shrestha, B. 2005. Arsenic and other drinking water quality issues, Muzaffargarh District, Pakistan. Appl. Geochem., 1: 56 https://doi.org/10.1016/j.apgeochem.2004.06.004.

Palmajumder, M., Chaudhuri, S., Das, V. K. and Nag, S. K. 2021. An appraisal of geohydrological status and assessment of groundwater quality of Indpur Block, Bankura District, West Bengal, India. Appl. Water Sci., 21: 1389. https://doi.org/10.1007/s13201-021-01389-2.

Palani, S., Liong, S. Y. and Tkalich, P. 2008. An ANN application for water quality forecasting. Mar. Pollut. Bull., 56(9): 1586-1597. https://doi.org/10.1016/j.marpolbul.2008.05.021.

Pandey, K., Kumar, S., Malik, A. and Kuriqi, A. 2020. Artificial neural network optimized with a genetic algorithm for seasonal groundwater table depth prediction in Uttar Pradesh, India. Sustainability, 12: 893. https://doi.org/10.3390/su12218932.

Panghal, V. and Bhateria, R. 2020. A multivariate statistical approach for monitoring of groundwater quality: a case study of Beri block, Haryana, India. Environ. Geochem. Health, 20: 654. https://doi.org/10.1007/s10653-020-00654-8

UDHD 2016. Patna Master Plan 2031. Urban Development & Housing Department, Government of Bihar.

Prasad Chourasia, L. 2018. Assessment of groundwater quality using water quality index in and Around Korba City, Chhattisgarh, India. Am. J. Softw. Eng. Appl., 7: 12. https://doi.org/10.11648/j.ajsea.20180701.12

Ritchie, H. and Roser, M. 2019. Clean Water. Retrieved from https://ourworldindata.org/water-access (accessed 06.07.2021)

Roy, A. Keesari, T. and Mohokar, H. 2018. Assessment of groundwater quality in hard rock aquifer of central Telangana state for drinking and agriculture purposes. Appl. Water Sci., 14: 234. https://doi.org/10.1007/s13201-018-0761-3

Saha, D. and Ray, R. K. 2018. Groundwater resources of India: Potential, challenges and management. Groundw. Dev. Manag. Issues Chall., 11: 19-42. https://doi.org/10.1007/978-3-319-75115-3_2

Saha, S. Reza, A. S. and Roy, M. K. 2019. Hydrochemical evaluation of groundwater quality of the Tista floodplain, Rangpur, Bangladesh. Appl. Water Sci., 9(8): 1-12.

Sampson, L. M. Bassey, U. L. Njoku, P. C. Essien, E. S. and Anyanwu, J. C. 2020. Physicochemical analysis of selected groundwater sources in Ikot Abasi Urban, Akwa Ibom state. Water, 51(1): 12-12.

Sarker, P. Nahar, S. and Begum, R. 2020. Physicochemical and microbial groundwater quality assessment and evaluation in Noakhali Region, Bangladesh. J. Appl. Life Sci. Int., 23: 149 https://doi.org/10.9734/jalsi/2020/v23i330149

Sarkar, A. and Pandey, P. 2015. River water quality modeling using artificial neural network technique. Aquatic procedia, 4: 1070-1077. https://doi.org/10.1016/j.aqpro.2015.02.135

Sharma, D. A. Rishi, M. S and Keesari, T. 2017. Evaluation of groundwater quality and suitability for irrigation and drinking purposes in southwest Punjab, India, using a hydrochemical approach. Appl. Water Sci., 16: 456. https://doi.org/10.1007/s13201-016-0456-6

Sharma, V., Rai, S. and Dev, A. 2012. A comprehensive study of artificial neural networks. Int. J. Adv. Res. Comput. Sci. Softw. Eng, 2: 278-284.

Singh, B. Sihag, P. Parsaie, A. and Angelaki, A. 2021. Comparative analysis of artificial intelligence techniques for the prediction of infiltration process. Geol. Ecol. Landsc., 5(2): 109-118. https://doi.org/10.1080/24749508.2020.1833641

Singh, G. Rishi, M. S. Herojeet, R. Kaur, L. and Priyanka, Sharma, K. 2020. Multivariate analysis and geochemical signatures of groundwater in the agricultural-dominated taluks of Jalandhar district, Punjab, India. J. Geochem. Explor., 208: 106395.

Singh, K. K. and Mishra, B. K. 2012. Evaluation of deep aquifer resources in lower Ganga Plain of Patna Urban Agglomerate, Bihar. Bhujal News Quart. J., 6: 5-14.

Singha, S. Pasupuleti, S. Singha, S. S. Singh, R. and Kumar, S. 2021. Prediction of groundwater quality using efficient machine learning technique. Chemosphere, 12: 35-41. https://doi.org/10.1016/j.chemosphere.2021.130265

Shiri, N. Shiri, J. and Yaseen, Z. M. 2021. Development of artificial intelligence models for well groundwater quality simulation: Different modeling scenarios. PLoS One, 25: 510. https://doi.org/10.1371/journal.pone.0251510

Shukla, S. and Saxena, A. 2020. Water quality index assessment of groundwater in the Central Ganga Plain with reference to Raebareli district, Uttar Pradesh, India. Current Science, 119(8): 1308-1315.

Srinivasamoorthy, K., Gopinath, M. and Chidambaram, S. 2014. Hydrochemical characterization and quality appraisal of groundwater from Pungar sub basin, Tamilnadu, India. J. King Saud Univ. Sci., 26: 37-52. https://doi.org/10.1016/j.jksus.2013.08.001.

Srivastava, A. K. and Parimal, P. S. 2020. Source rock weathering and groundwater suitability for irrigation in Purna alluvial basin, Maharashtra, central India. J. Earth Syst. Sci., 10: 1312. https://doi.org/10.1007/s12040-019-1312-5.

Subba Rao, N. 2008. Factors controlling the salinity in groundwater in parts of Guntur district, Andhra Pradesh, India. Environmental Monitoring and Assessment, 138(1): 327-341. https://doi.org/10.1007/s10661-007-9801-4.

Subramani, T., Rajmohan, N. and Elango, L. 2010. Groundwater geochemistry and identification of hydrogeochemical processes in a hard rock region, Southern India. Environ. Monit. Assess., 9: 781. https://doi.org/10.1007/s10661-009-0781-4.

Sulaiman, M. A., Divya, Zafar, M. M., Anjum, S. and Kumari, A. 2023a. Groundwater contamination by fluoride and mitigation measures for sustainable management of groundwater in the Indo-Gangetic Plains of India. In Groundwater in Arid and Semi-Arid Areas: Monitoring, Assessment, Modelling, and Management (pp. 289-314). Cham: Springer Nature Switzerland.

Sulaiman, M. A., Zafar, M. M., Prabhakar, R., Kumar, R., Sinha, R. K. and Kumari, A. 2023b. A multivariate statistical approach to evaluate the hydro-geochemistry of groundwater quality in the middle Ganga-river basin, Patna, India. Acta Geophys., 7: 1-14.

Sulaiman, M. A., Zafar, M. M., Divya, Prabhakar, R. and Kumari, A. 2023c. Evaluation of ionic composition and hydrogeochemical processes of the groundwater in Muzaffarpur district (Bihar), India. Indian J. Environ. Prot., 43(3): 263-269. https://www.e-ijep.co.in/43-3-263-269/.

Sulaiman, M. A., Zafar, M. M., Divya, Gaurav, K. and Kumari, A. 2024. Fluoride contamination in groundwater of the middle Gangetic plains of India: A comparative geochemical and health risk assessment. Groundw. Sustain. Dev., 2142: 101112.

Sunayana, Kalawapudi, K., Dube, O. and Sharma, R. 2020. Use of neural networks and spatial interpolation to predict groundwater quality. Environ. Dev. Sustain., 9: 319. https://doi.org/10.1007/s10668-019-00319-2.

Times of India. 2018. Pollution-related deaths in Bihar alarming: Study. Retrieved from http://timesofindia.indiatimes.com/articleshow/64900399.cms?utm_source=contentofinterest&utm_medium=text&utm_campaign=cppst (accessed 06.07.2021).

Tiwari, A. K., Ghione, R., De Maio, M. and Lavy, M. 2017. Evaluation of hydrogeochemical processes and groundwater quality for suitability

of drinking and irrigation purposes: a case study in the Aosta Valley region, Italy. Arab. J. Geosci., 54: 1425. https://doi.org/10.1007/s12517-017-3031-z.

Tiwari, A. K., Singh, A. K. and Mahato, M. K. 2018. Assessment of groundwater quality of Pratapgarh district in India for suitability of drinking purpose using water quality index (WQI) and GIS technique. Sustain. Water Resour., 21: 1-16. Manag. https://doi.org/10.1007/s40899-017-0144-1.

Tiwari, T. N. and Mishra, M. 1985. A preliminary assignment of water quality index to major Indian rivers. Indian J. Environ. Prot., 5: 246-252.

Tiyasha, Tung, T. M. and Yaseen, Z. M. 2020. A survey on river water quality modelling using artificial intelligence models: 2000-2020. J. Hydrol., 585: 124670. https://doi.org/10.1016/j.jhydrol.2020.124670.

Verma, D. K., Bhunia, G. S., Shit, P. K. and Tiwari, A. K. 2018. Assessment of groundwater quality of the central Gangetic Plain Area of India Using Geospatial and WQI Techniques. J. Geol. Soc. India. 11: 27-36. https://doi.org/10.1007/s12594-018-1097-1.

Verma, P., Singh, P. K., Sinha, R. R. and Tiwari, A. K. 2020. Assessment of groundwater quality status by using water quality index (WQI) and geographic information system (GIS) approaches: A case study of the Bokaro district, India. Appl. Water Sci., 119: 1088. https://doi.org/10.1007/s13201-019-1088-4.

Wang, J., Zhai, Y., Yao, P., Ma, M. and Wang, H. 2020. Established prediction models of thermal conductivity of hybrid nanofluids based on artificial neural network (ANN) models in waste heat system. Int. Commun. Heat Mass Transf., 110: 104444. https://doi.org/10.1016/j.icheatmasstransfer.2019.104444.

Wu, J., Zhang, Y. and Zhou, H. 2020. Groundwater chemistry and groundwater quality index incorporating health risk weighting in Dingbian County, Ordos basin of northwest China. Chemie der Erde., 12: 5607. https://doi.org/10.1016/j.chemer.2020.125607.

Zafar, M. M., Sulaiman, M. A., Prabhakar, R. and Kumari, A. 2022. Evaluation of the suitability of groundwater for irrigational purposes using irrigation water quality indices and geographical information systems (GIS) at Patna (Bihar), India. Int. J. Energy Water Resour., 22: 193. https://doi.org/10.1007/s42108-022-00193-1.

Zhang, Y., Wu, J. and Xu, B. 2018. Human health risk assessment of groundwater nitrogen pollution in Jinghui canal irrigation area of the loess region, northwest China. Environ. Earth Sci., 18: 7456. https://doi.org/10.1007/s12665-018-7456-9.

Zhu, L., Yang, M., Chen, X. and Liu, J. 2019. Health risk assessment and risk control: drinking groundwater in Yinchuan Plain, China. Expo. Heal., 7: 266. https://doi.org/10.1007/s12403-017-0266-6.

Nature Environment and Pollution Technology
An International Quarterly Scientific Journal

p-ISSN: 0972-6268
(Print copies up to 2016)
e-ISSN: 2395-3454

Vol. 23 | No. 3 | pp. 1449-1459 | 2024

Original Research Paper

https://doi.org/10.46488/NEPT.2024.v23i03.015

Open Access Journal

# The Effect of Mycorrhiza and Plant Growth-Promoting Rhizobacteria Supplementation on *Zea mays saccharata* Sturt. Growth and Productivity Grown on Low Nutrients Soil

**T. Nurhidayati*†, L. N. Sari*, A. R. Anggraeni*, A. Luqman*, M. Shovitri*, N. D. Kuswytasari*, T. B. Saputro* and H. D Rizki****

*Department of Biology, Faculty of Science and Data Analytics, Institut Teknologi Sepuluh Nopember, Surabaya, Indonesia
**Department of Chemistry, Faculty of Science and Data Analytics, Institut Teknologi Sepuluh Nopember, Surabaya, Indonesia
†Corresponding author: Tutik Nurhidayati; tutiknur0972@gmail.com

**Nat. Env. & Poll. Tech.**
**Website: www.neptjournal.com**

*Received:* 13-12-2023
*Revised:* 07-02-2024
*Accepted:* 07-03-2024

**Key Words:**
Sweet corn
Mycorrhizae
Productivity
NPK
Soil fertility

## ABSTRACT

Marginal land has low nutrient content (nitrogen, phosphorus, potassium). Addressing nutrient deficiencies on marginal land requires a strategic approach. Biological fertilizers like Arbuscular Mycorrhizal Fungi (AMF) and plant growth-promoting rhizobacteria (PGPR) enhance nutrient availability through symbiotic interactions. In addition, organic fertilizers such as compost could provide organic matter and improve soil structure to increase plant growth and productivity. Combining these three fertilizers with the addition of low doses of NPK fertilizer can increase the growth and productivity of maize crops on sub-marginal land. This study aims to determine the effect of AMF, consortium of PGPR, and a low dose of NPK on the growth and productivity of maize and soil nutrients on sub-marginal land by measuring plant growth up to 8 WAP (week after planting) (parameters: plant height, stem diameter, number of leaves, leaf area, chlorophyll content, stomatal density) and productivity (parameters: cob length, cob weight with husk, fresh weight, dry weight) and levels of N, P, and K elements at 8 WAP in the soil after planting. All treatments showed an increase in the level of N and K elements, while the P element showed a decrease compared to the control (soil without treatment). Moreover, each parameter did not show a significant difference, but the P2 (Compost + PGPR consortium + AMF + 50% of NPK) treatment showed the best growth and productivity. Overall, the data showed the utilization of PGPR and AMF combination was able to reduce the usage of chemical fertilizer by 50%.

## INTRODUCTION

Maize is the second staple commodity in Indonesia, with increasing demand over the years. However, due to over-farming, the low nutrient of soil becomes a problem, which leads to a decrease in maize productivity (Ng et al. 2022, Sprunger et al. 2019). The overuse of pesticides and non-organic fertilizers such as NPK ((Nitrogen Phosphorus Potassium) causes land and soil degradation and eventually lowers land productivity (Nunes et al. 2020).

Utilizing organic fertilizer and biofertilizer becomes an alternative to recover the nutrients in the soil and increase crop productivity. One example is compost, an organic fertilizer that provides organic matter and improves soil amendments (Assefa & Tadesse 2019). Biofertilizer is also reported to be able to improve soil nutrients by mobilizing and increasing the nutrient availability in soil (Mitter et al. 2021). Mycorrhiza is often combined with the Plant Growth-Promoting Rhizobacteria (PGPR) to be used as a biofertilizer. The symbiosis between them improves the growth and productivity of crops (Raklami et al. 2019).

As soil degradation becomes more frequent while the demand for maize keeps increasing, exploiting the symbiosis of mycorrhiza and PGPR as a biofertilizer on maize can be an alternative. In this study, we investigated the effects of mycorrhiza and PGPR supplementation together with compost on maize's (*Zea mays* Saccharate Sturt.) growth and productivity.

## MATERIALS AND METHODS

### Preparation of Mycorrhizae Propagule

The tools and materials are hoes, shovels, scales, hoses, plant shears, soil, compost, arbuscular mycorrhizal fungi (AMF), water, polybags, and sweet corn seeds. Then, soil and Dewi Fortuna Compost were prepared to be mixed in a ratio of 1:1, which was then placed in 100 polybags measuring 40 cm. Before planting corn, conventional AMF

MycoVir (Bogor) was first sprinkled with AMF Genera *Acaulospora, Gigaspora, Glomus,* and *Scutellasporra*, with sterile sand and vermiculite as much as 50 grams/polybag. Sweet corn is planted in polybags containing a mixture of soil and compost and a sprinkling of mycorrhizae. Watering was carried out once a day until the plants were 14 DAP (days after planting). At the age of 15 DAP, maize plants were given stress treatment by cutting the plant crown and not watering for 14 days. At the age of 29 DAP, the plants were watered again once a day until the age of 60 DAP. Harvesting was carried out at 61 DAP by cutting the base of the stem and taking the root part for further chopping ± 1 cm. The chopped results are put in a plastic bag.

**Purification and Rejuvenation of Bacteria Isolate**

PGPR bacterial isolates in K1, P1, and P2 treatment from the collection of the Microbiology and Biotechnology Laboratory, Department of Biology, Sepuluh Nopember Institute of Technology, were purified on a Nutrient Agar (NA) medium (Shovitri et al. 2021). The isolates were rejuvenated on NA medium using the streak plate method with 16 streaks to obtain a single colony, then incubated for 24 h at room temperature. After that, the pure colonies were re-cultured in NA agar slant and stored at 4°C.

**Preparation of Application Inoculum**

A consortium of three bacterial isolates with codes K1, P1, and P2 was used in this study. Each bacterial isolate was inoculated into Nutrient Broth (NB) medium and then incubated for 24 hours at room temperature. A 25 mL sample of previously prepared NB media was suspended in sterile distilled water after the inoculation. Using a rotary shaker, three 25 mL Erlenmeyer bottles with bacteria K1, P1, and P2 were cultured for 24 hours. Following cultivation in 25 mL Erlenmeyer, 225 mL of sterile distilled water is prepared previously and poured into 500 mL Erlenmeyer. Using a rotary shaker at room temperature, the consortium's results were recultivated for 24 hours.

**Preparation of Maize Media**

The application inoculum (bacteria consortium suspension) contained 1.5% molasses, 82.5% tap water, and 16% bacterial consortium with a total volume of 5000 mL. 1.5% molasses (75 mL), 82.5% well water (4175 mL), and a consortium of 16% bacteria (750 mL) were poured into a 25 L jerry can. After the three were mixed, they were allowed to stand for 90 minutes before being applied to plants.

**Preparation of Experiment Plant**

The soil was taken from citrus Batu, East Java, which was used for planting and was taken 300 g first for initial NPK testing. Then, soil and conventional compost (Dewi Fortuna) were mixed in a ratio of 1:1, which was then put into 45 cm × 45 cm (10 kg) polybags and watered with 300 mL of suspension of the rhizosphere bacteria P1, P2, and K1 consortium (biological fertilizer). The consortium watering was carried out for two consecutive days and allowed to stand for three days. Next, the soil pH is measured, and when the soil pH is around 7, it can be continued in the next stage. If the soil is acidic, dolomite is given with a sowing system of 66 grams/polybag, then left for 3 days. Soil that has been in a neutral pH state is ready to plant sweet corn. Then, the corn seeds are soaked in distilled water for about 3 h and selected, which are submerged and then drained. The planting media for sowing is 1 kg of soil and 1 kg of compost, which is then prepared on a tray. The selected seeds are sown at a depth of approximately 1 cm from the top surface of the soil.

Furthermore, it was grown until the age of 9 DAS (Days After Seedling) until growing 2 leaves. Seedlings were transferred to polybag planting media as deep as 3 cm from the soil surface. After the transfer, watering, weeding, and pest control are carried out. Water the plant every day using water with a small discharge. Weeding is done manually by pulling weeds that grow around the plants. Pest control is done by giving insecticide sow, which is sprinkled around the plants (5 grams/polybag). After 7 DAP, the plants were ready to be given treatment.

**Application of Mycorrhizae, PGPR, and NPK to Sweet Corn**

The application of rhizobacterial consortium biofertilizers and NPK fertilizers was carried out at 5 and 26 DAP. The suspension of the rhizobacteria consortium was sprinkled on the plants as much as 300 mL per polybag. NPK fertilizer was sprinkled according to the dose of each treatment (K2 = 4.8 g, P1 = 1.2 g, P2 = 2.4 g). The PGPR consortium was applied at 3 DAP (days after planting), 7 DAP, 21 DAP, 35 DAP, and 49 DAP. Mycorrhizae were applied at 0 DAP. The NPK application was carried out at the age of 5 DAP and 26 DAP.

**Measuring Growth and Productivity of Plant**

During the planting period, measurements were done once per week, with the Observation of research results, including plant height, stem diameter, number of leaves, and leaf area index. After harvesting, sweet corn plants (65 DAP) in all treatments that had been harvested were removed, and their roots were cleaned from the soil. Corn plants are cut between the base of the stem and the roots. Wet weight was measured from the base of the stem to the top of the plant. Measuring

of wet and dry weight was carried out after the plants were 65 DAP. Plants that have been taken in each treatment are cleaned of dirt and soil. The next step is measuring the dry weight, which is done by first chopping it into smaller pieces and putting it in a paper wrapper. Wrapping paper containing chopped sweet corn is put in the oven, then baked for 6 h at 121°C. If the weight is constant, it can be weighed three times. Constant weight data can be retrieved and recorded. Corn cobs, cob height, and cob weight were weighed at the age of 8 WAP.

**Measurement of N, P, K Level in The Soil After Planting**

The test for the nutrient level content of N, P, and K of the planting soil was carried out at the Surabaya Industrial Standardization and Research Office. The soil was tested with parameters: nitrogen (N) content using the Kjeldahl method, phosphate (P) using the Spectrophotometric method, and potassium (K) using the Atomic Absorption Spectroscopy (AAS) method.

**Chlorophyll Content**

After harvesting, the leaves on each treatment plant were taken. Corn leaves were cut (0.1 grams). The leaf samples were then crushed in a mortar using a pestle with 80% acetone (10 mL) until all the colors were separated from the tissue. The result in the form of the extract is first filtered using filter paper and put into a centrifuge. The surface of the cuvette is cleaned, then the results of the centrifuge are transferred to the cuvette to be inserted into the spectrophotometer. Measurements with a spectrophotometer used absorbance chlorophyll solution at wavelengths of 663 nm and 645 nm (Cao et al. 2020). The concentration results are calculated by the following formula (Harborne 1987):

$$\text{Total chlorophyll (mg/L)} = (17.3 \times A645) + (7.18 \times A663)$$

**Stomatal Density**

Stomatal density was measured on the 6th leaf from the base of the stem using the imprint method. The leaves are first cleaned of dirt using tissue. Then, prepare transparent nail polish. Transparent nail polish was applied to the abaxial part of the 6th leaf of the corn plant, 1 cm wide, then waited for it to dry. Next, a transparent adhesive is glued to be affixed to the dry nail polish and peeled off the replica leaves, and the replica is affixed to the slide. The results on the object glass were observed using a microscope with a magnification of 400 x with a field of view of 0.025 $mm^2$. Stomatal density was calculated using the formula according to (Maylani et al. 2020).

Stomatal density = Number of stomata/field of view

**Percentage of Mycorrhizae Infection**

Mycorrhizae infection in root tissue can be done by observing the percentage of infection in root tissue. First, the roots of the corn plant were cleaned and then cut into pieces of about 1 cm, then heated in 10% KOH at 90°C for about 10 minutes. Furthermore, the soaked roots were drained and washed with distilled water. Then, the roots were put back into 0.1 N HCl drained again, and then washed with distilled water. Staining was carried out using Lactophenol Trypan Blue 0.05% for a while and added to lactoglycerol. The results on the object glass were observed using a microscope with a magnification of 400 x with a field of view of 0.025 $mm^2$. The percentage of mycorrhizal infection in the roots was calculated using the formula (Nurhidayati et al. 2010):

$$\text{Mycorrhizae infection (\%)} = \frac{Number\ of\ infected\ root}{Number\ of\ roots\ observed} \times 100\%$$

**Data Analysis**

This research is an experimental study to know the effect of the combination of compost, mycorrhizae, PGPR consortium, and low-dose NPK variation on the growth of sweet corn. This study used a completely randomized design with 5 replications. The data that has been obtained will be tested for normality using the Shapiro-Wilk test. If the treatment has a significant effect, the p-value is more than 0.05 or has a significant effect, and the data is normally distributed, a follow-up test will be carried out using Way Analysis of Variance (ANOVA), and if it is not normally distributed, a non-parametric test will be used. (Kruskal-Wallis). Data analysis visualization was performed on RStudio.

## RESULTS AND DISCUSSION

In this study, we treated the maize with different supplementation combinations of mycorrhiza, PGPR consortium, and different doses of NPK. To avoid the redundancy of the treatment groups explanation, the treatment grouping is as follows:

K1: Control (no supplementation)

K2: 100% dose of NPK fertilizer (4.8 gram/polybag)

K3: Mycorrhizal (100 g of AMF per polybag)

P0: PGPR consortium + mycorrhiza

P1: PGPR consortium + mycorrhiza + 25% dose of NPK (1.2 gram/polybag)

P2: PGPR consortium + mycorrhiza + 50% dose of NPK (2.4 gram/polybag)

Note :

NPK dose (25% = 1.2 g, 50% = 2.4 g, 100% = 4.8 g)

Mycorrhizae (100% = 100 gr/polybag)

### The Effect of Mycorrhiza and PGPR Supplementation on the Growth of Maize

Growth parameters (height, stem diameter, number of leaves, and total leaf area) were observed weekly for 8 weeks in maize with various combinations between mycorrhiza, a consortium of PGPR, and different doses of NPK. In week 8th, the P2 treatment group, which is maize supplemented with PGPR consortium, mycorrhiza, and 50% dose of NPK, showed the highest score overall except for the leaf number. The maize in the P2 treatment group reached 97.8 ± 8.70 cm as the mean height, 1.29 ± 0.11 cm as the mean of the stem diameter, 9.6 ± 0.89 as the mean number of the leaf, and 359.25 ±32.83 $cm^2$ as the mean of total leaf area. Whereas the K3 treatment group, where we supplemented the maize with the mycorrhiza only, showed the overall lowest score except for the stem diameter. The maize in the K3 treatment group reached only 78 ± 26.05 cm as the mean height, 1.11 ± 0.33 cm as the mean of the stem diameter, 8.4 ± 1.52 as the mean number of the leaf, and 285.05 ± 72.64 $cm^2$ as the mean of total leaf area. For the increase of the overall growth parameters, the maize from the P2 treatment group showed the highest growth from week 1 to week 8 (Fig. 1).

### The Effect of Mycorrhiza and PGPR Supplementation on the Maize's Productivity

At 65 days after planting (DAP), we harvested the cob and measured the length and the weight, as well as the maize fresh and dry weight. All treatment groups showed almost similar cob lengths (20.68 – 21.58 cm) except the K3 treatment group, which showed to have the shortest cob with a mean cob length is 16.06 ± 9.38 cm (Fig. 2A). K3 treatment group exhibited the lowest cob weight as well (40.3 ± 9.38 gram), and the P2 treatment group had the highest cob weight (60.712 ± 1.85 gram) (Fig. 2B). Both fresh weight (p-value > 0.05) and dry weight (p-value > 0.05) there was no significant difference among treatments. The average fresh weight and dry weight of all treatments are presented in Fig. 2C. P2 treatment showed the highest fresh weight compared to all treatments.

### The Effect of Mycorrhiza and PGPR Supplementation on the Chlorophyll Content and Stomatal Density

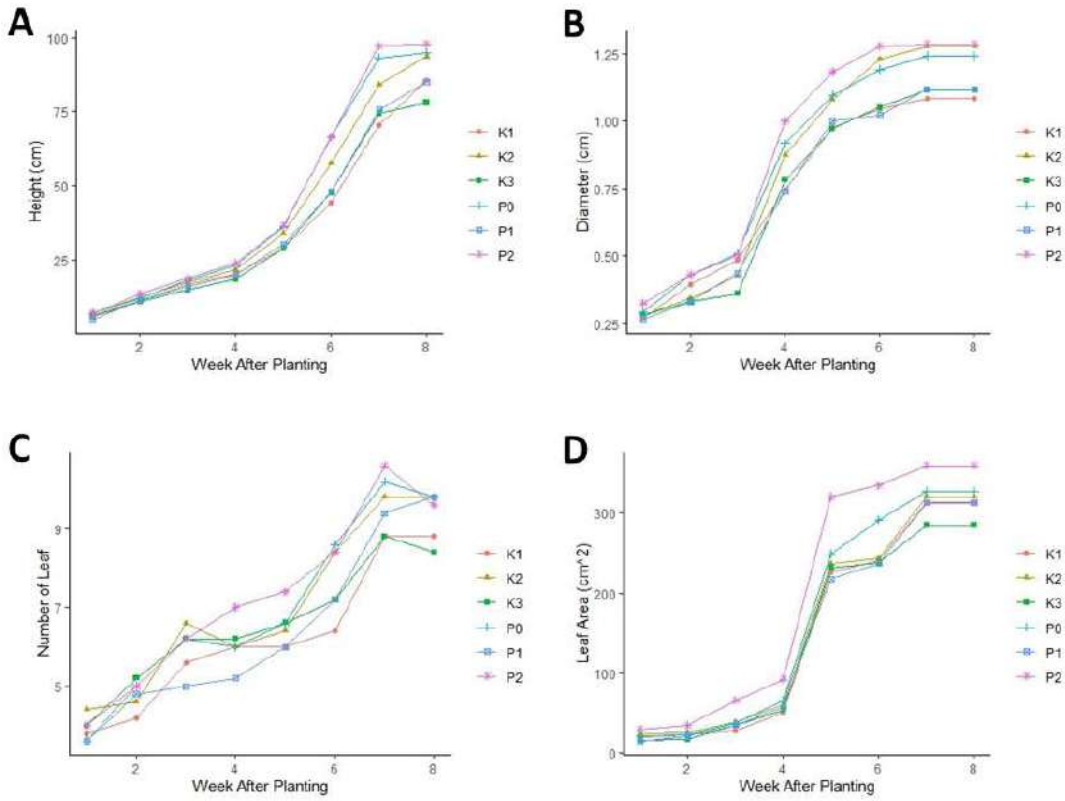


Fig. 1: The effect of mycorrhiza, PGPR consortium, and NPK fertilizer on maize's growth parameters: (A) height, (B) stem diameter, (C) leaf number, and (D) leaf area. The graphs represent the mean of the value (n=5).

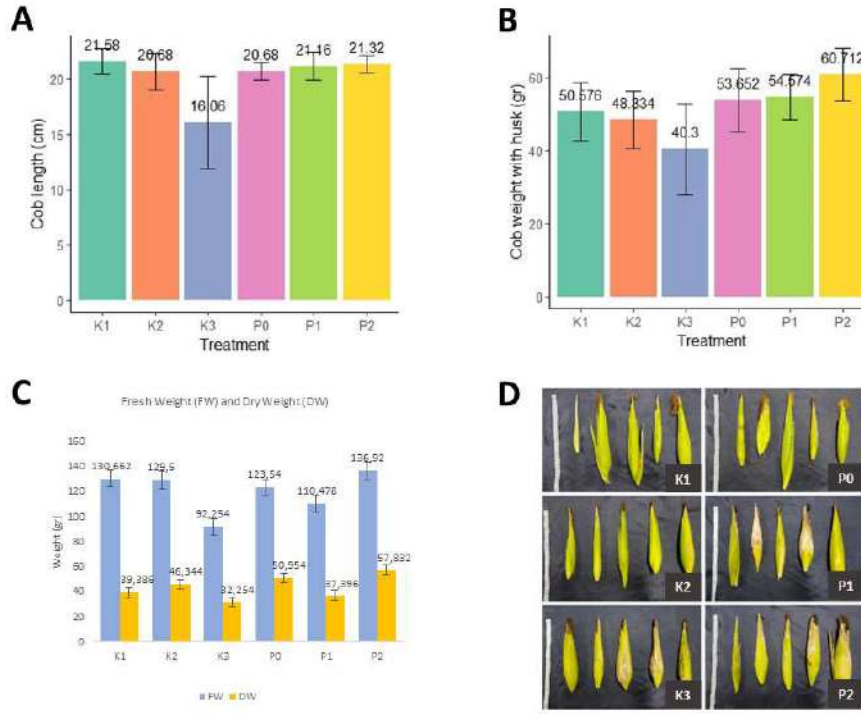


Fig. 2: The effect of mycorrhiza and PGPR supplementation on the maize's productivity (A) Cob length (B) Cob weight (C) Fresh and dry weight (D) Cob in each treatment.

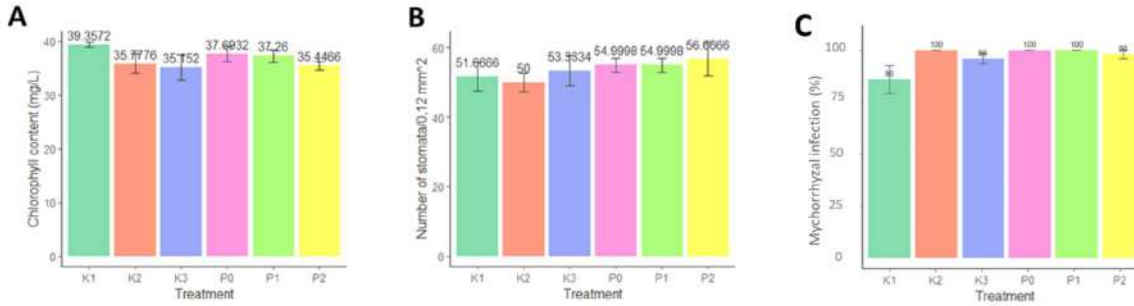


Fig. 3: The effect of mycorrhiza, PGPR consortium, and NPK fertilizer on chlorophyll content and stomata density (A) chlorophyll content (B) stomata density.

Besides measuring the productivity parameters, we also measured the chlorophyll content and stomatal density post-harvesting. We observed there was no significant difference for these parameters with different treatments. Based on the results of the ANOVA test, chlorophyll levels were not affected by the treatment given (p-value > 0.05). The average chlorophyll content in all treatments is presented in Fig.3.

Based on Fig. 3A, the highest chlorophyll content was in the K1 treatment with compost fertilizer. Stomatal density is defined as the number of stomata in one field of view. Stomatal density can be indicated as the plant transpiration rate, where the more stomata, the higher the plant transpiration rate (Maylani et al. 2020). Stomata regulate gas exchange between plants and the environment and control water loss (Man et al. 2015). The process of transpiration in plants is influenced by several factors, one of which is the number of stomata (Jiaying et al. 2022). Based on the results of statistical tests that showed that the stomatal density was not normally distributed, then Kruskal-Walli's test was performed with a p-value >0.05 or no significant effect from each treatment. The results of the average stomatal density in each treatment are shown in Fig. 3B.

Based on the research results presented in Fig. 3C, all treatments show infection percentages ranging from 75 – 100%, indicating high infection levels (Padri et al. 2015). The planting media provided with mycorrhiza are

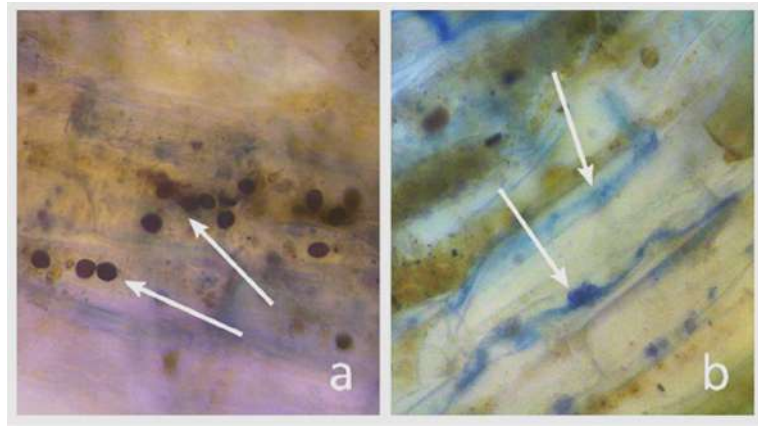


Fig. 4: Mycorrhizal infection on the root of maize (M= 400x). a) Spores of Mycorrhizae,b) Hifa of Mycorrhizae.

treatments K3, P0, P1, and P2. The occurrence of infection demonstrates the ability of both Indigenous (native spores of mycorrhyza in planting medium) and exogenous mycorrhiza (spores of mycorrhyza added to the planting medium) to form a mutualistic symbiosis with the host plant, maize (Fig. 4). PGPR positively influences this symbiosis through various mechanisms, such as enhancing spore germination and hyphal permeability in plant roots (Ramasamy et al. 2011). Similarly, treatments K1 and K2, which were not supplemented with mycorrhiza, were also capable of infecting maize plants. This suggests the involvement of indigenous mycorrhiza present in the planting media. The presence of Indigenous spores is greatly influenced by biotic factors (such as humans and animals, propagules, and mycorrhiza dispersal) and abiotic factors (wind, soil pH and temperature, crop rotation, fertilizers and organic matter content, soil moisture, pesticides, heavy metals, and salinity) (Bueno & Moora 2019, Vikas et al. 2016). Therefore, the presence of native mycorrhiza in treatments K1 and K2 is presumed to be due to favorable abiotic and biotic conditions.

The effect of mycorrhiza, PGPR consortium, and NPK fertilizer on maize growth is shown in Fig. 1. The highest height of P2 treatment has been influenced by the treatment of these fertilizers. The 50% NPK dose in the P2 treatment was suspected of helping plant height growth because there were elements of N, P, and K. Nitrogen is regarded as an essential macronutrient for the growth of plants. It involves the morphological and physical development of plants. N is a crucial component in building the structural integrity of plant proteins. Furthermore, the N function controls a variety of plant enzymatic processes (Ghorai & Ghosh 2022). Additionally, this substance (nitrogen) can promote plant height, root branching, shoot branching, flowering, and fruiting (de Bang et al. 2021).

The addition of biological fertilizers, such as AMF and the PGPR consortium, in the P2 treatment, also helps the height growth of corn plants. Compost provides organic matter that is degraded by microorganisms so that the nutrients contained in compost can be used for plant growth (de Bang et al. 2021). Thus, the presence of AMF and PGPR in P2 treatment could help plants by degrading compost and increasing plant height. The results of P2 treatment are in line with research by (de Bang et al. 2021), which showed that the highest plants were found in the PGPR application and the *Glomus mosseae* application, which was also a combination of AMF (*G. mosseae*) and the PGPR consortium. AMF functions in increasing root growth and uptake of water and nutrients by hyphae growth, which increases plant height. PGPR can also increase plant height by producing phytohormones that stimulate root growth and enrich nutrient uptake areas by fixing nitrogen from the atmosphere, dissolving P, and producing plant growth hormones (de Bang et al. 2021).

The P2 treatment, which consisted of a plant with full treatment, including compost, AMF, PGPR consortia, and 50% dose of NPK, had the largest stem diameter. The content of the applied complete fertilizer has an impact on the production of stem diameter. The NPK fertilizer application to the P2 treatment had a higher dose than P0 and P1. These findings are consistent with those of Sayara et al. (2020), who found that the more NPK fertilizer is applied to plants, the more nutrients (N, P, and K) are made available to them. These nutrients are then used by plants for metabolism, growth, and development, one of which is the increase in stem diameter. The availability of nitrogen can boost photosynthesis results to be converted into protein and create protoplasm, which impacts the expansion of stems. The N element released from NPK fertilizer affects the growth of stem diameter, which plays a role in the

enlargement of organs such as stems (Khalediyan et al. 2021, Kuila et al. 2020). It was also believed that the addition of AMF and PGPR to the P2 treatment would have supported the growth in stem diameter. By causing the release of IAA and GA hormones, which might impact cell elongation, the administration of PGPR to plants helps to promote growth (Gusta & Same 2022, Marler 2022). One consequence is the lateral lengthening of stem cells, which increases stem diameter.

Additionally, the N, P, Ca, K, and Na content of plants can be improved by combining PGPR and AMF (Cao et al. 2020). When plants are infected with AMF, the presence of PGPR raises the nitrogen capacity of leaves. In addition to the element N, PGPR bacteria can also support AMF symbiosis by increasing the available bio phosphate because P will be dissolved by organic acids produced by plants and bacteria to increase absorption by plant root hairs. In addition, AMF microorganisms applied to plants can help plants scavenge P outside the rhizosphere region and make P available to plants (Marler 2022). Therefore, P2 plants are thought to be able to increase stem diameter with the help of AMF and the PGPR consortium.

The P2 plants with the complete composition of fertilizer, which included compost, AMF, PGPR, and NPK 50%, aged 7 WAP, had the highest number of leaves, where this composition was thought to affect the growth of plant leaves. The presence of nitrogen perhaps affected the number of leaves in the P2 treatment. Nitrogen nutrients will be translocated to the vegetative part of the plant, such as the leaf (Adekiya et al. 2020). In addition, the increase in the number of leaves in the P2 treatment was thought to have a role from the AMF and the PGPR consortium. AMF and PGPR are able to help provide nutrients, including phosphorus and nitrogen, which plants use for the growth of organs such as leaves (Adekiya et al. 2020). This is supported by the opinion of Cao et al. (2020), who states that the addition of PGPR combined with AMF can increase the content of N, P, Ca, K, and Na in plants.

Furthermore, the addition of NPK in P2 treatment with a dose of 50%, which was the highest dose between P0 and P1, was thought to affect the increase in the number of plant leaves. NPK fertilizer contains elements needed for plant growth, such as elements of N, P, and K (Umami et al. 2019). Therefore, the P2 treatment got a nutrient supply from NPK fertilizer, which was used to increase the number of leaves.

The P2 treatment with a full composition of compost, AMF, PGPR consortium, and 50% dose of NPK produced the highest Leaf Area Index (LAI) from 1 to 8 WAP, as well as the highest yields in plant height, stem diameter, and number of leaves. It is believed that the type of fertilizer used to feed plants can influence how much leaf area grows. The P2 treatment had the most leaf area because it had an adequate supply of N and P. It was believed that N and P in the P2 treatment came from NPK fertilizer. The nutrients in NPK, particularly nitrogen and phosphorus, aid in cell division and elongation, which increases the size, length, and rate of development of leaves (Johnson 2010, Sokoto et al. 2012). The results of the P2 treatment are in line with the study by Kuila et al. (2020), which showed higher leaf area yields in the combination of AMF and PGPR, compared to the leaf area yields of single microorganisms. The presence of PGPR allows for the growth of leaf area by dissolving P and nitrogen fixation that plants can use to expand leaves (Johnson 2010, Sokoto et al. 2012). The results of plant growth, stem diameter, number of leaves, and leaf area had the same relative highest yield in P2 treatment. This is thought to be closely related to the final yield of N levels in plants. In the post-harvest soil of P2 plants, it is known that P2 plants have the lowest levels of N and P. This is thought to be due to the harvest. The soil will lose N and/or P after harvesting because it is taken up by plants (Liu et al. 2021, Wang & Ning 2019).

Based on Fig. 2, it is shown the effect of mycorrhiza, PGPR, and NPK supplementation on the maize's productivity. The highest cob weight results were found in the P2 treatment. NPK fertilizer is thought to be able to provide nutrients for N, P, and K elements that can be absorbed by plants, thereby enriching plant nutrients that can provide higher yields (Hu et al. 2020). NPK given in the P2 treatment is thought to also help increase the weight of the seeds. According to Xu et al. (2020), P affects seed filling because P in vegetative organs is reused to support the growth of developing grains.

Furthermore, the aging leaves (senescence) transfer at least 50% of the P content to the grain. Then, the element K which was also found in NPK fertilizer, which was applied to the P2 treatment, also increased the weight of the cobs. Elemental K can increase productivity by being involved in plant physiological processes such as assisting the activation of more than 60 enzymes that catalyze the uptake and transport of metabolite and nitrate products from the roots to the top of the plant where this process also affects plant productivity and adds weight to the ear (Senbayram et al. 2015). The P2 treatment was also given biological fertilizers, namely AMF and the PGPR consortium, which were suspected to be involved in the weight gain of the cobs. This is thought to be due to the symbiotic relationship between the two, which is able to enrich nutrients for plants, thus affecting the weight of the cobs. The combination of AMF and PGPR is known to increase the uptake of N and P elements in the soil, which can be utilized by plants for growth and productivity (Tulung et al. 2021). Thus, AMF and

PGPR help plants utilize the available N and P to increase the weight of the cobs.

The results of fresh and dry weight, which are shown in Fig. 2C, indicate that the application of 50% compost, AMF, PGPR, and NPK to P2 produces the highest fresh weight. In comparison to all plants, it was believed that the largest fresh weight, P2, would accumulate water and produce the maximum photosynthetic yields. The P2 treatment, which had the largest dose of NPK fertilizer relative to P0 and P1, was then assumed to also contribute to the increase in fresh weight. According to Friede et al. (2016), a larger dose of NPK fertilizer will enhance crop yields. Crop yields are derived from N and P components, and the higher the amount of nutrients taken by the plant, the higher the plant growth, which in turn affects the fresh weight.

Additionally, P2 treatment has inoculated PGPR, which also has an impact on the fresh weight. By delivering N fixed from the environment, PGPR had a function as diazotroph bacteria engaged in biological N2 fixation (BNF), which may have a direct impact on the plant's N budget (Okonwu & Mensah 2012). AMF is believed to have an impact on the wet weight of P2 treatments in addition to PGPR since it can supply nutrients (N, P, and K) to the soil to promote growth (Chapin 2003). Fresh weight and growth parameters are positively correlated because fresh weight is an accumulation of photosynthetic products during the growth process (Liu et al. 2021). Therefore, the growth yield of P2 treatment was positively correlated with the fresh weight yield.

The dry weight (DW) parameter was in line with the yield of plant height and LAI, where the P2 treatment plants had the highest result. Dry weight is supported by the presence of nutrients in the soil. The results of the P2 treatment are in accordance with the research of Barin et al. (2022), where the application of NPK can increase plant growth, such as height, leaf area, and dry weight. The photosynthetic process is assumed to produce the dry weight at P2, with nutrients coming from the complete composition of fertilizers (compost, AMF, PGPR consortium, and 50% NPK) being applied. Dry weight is the result of the formation (95%) of various organic compounds from the photosynthesis process (the use of light energy to reduce carbon dioxide into sugar) (Ma et al. 2021). Dry weight accumulation is influenced by the process of photosynthesis in leaves (Anwar et al. 2020). One of the factors that affect the process of photosynthesis is the content of nutrients, such as N. Application of NPK can increase the process of photosynthesis (Anwar et al. 2020). Therefore, the application of NPK will affect the photosynthetic process which has an impact on the accumulation of plant dry weight. Thus, it can be said that the presence of NPK fertilizer may influence the dry weight of the P2 treatment. The higher the dose of NPK given, the higher the N element obtained by the plant used for photosynthesis, which affects the dry weight of the plant. The highest dose of NPK fertilizer (50%), compost, and a combination of AMF and PGPR are thought to help the accumulation of dry weight in P2 treatment. The presence of microorganisms like AMF and PGPR was also believed to have contributed to the elevation in dry weight in the P2 treatment. A study showed consistent results that an increase in plant dry weight occurred when *Glomus intraradices* (included in AMF) was applied alone or in combination with *Pseudomonas fluorescens*, which is one of the phosphate solubilizing bacteria, where phosphate can increase the dry weight (Li et al. 2020, Song et al. 2019).

In line with the fresh weight yield, the lowest dry weight was found in the K3 treatment with the fertilizer composition consisting of compost and AMF. When compared to P2, the lack of K3 nutrient sources is also suspected to be the cause of the low dry weight because it affects the photosynthesis process. After all, when compared to P2, which is the treatment with the highest dry weight, it has a complete fertilizer composition. The results of the lowest mean dry weight of K3 treatment were also thought to be because the application of AMF to plants was not very effective. The cause of the ineffectiveness of AMF in the plant growth process that correlated with dry weight was the absence of symbiosis of AMF with PGPR and the interaction of parasitism between AMF and host plants (He et al. 2019, Raklami et al. 2019).

The high chlorophyll content in the K1 treatment was thought to be due to the high content of K elements. The high content of K elements in plants will affect plant metabolic activities, such as playing a role in activating protein synthesis enzymes, sugar transport, N and C metabolism, and photosynthesis (Andriani et al. 2017). The influence of N in chlorophyll synthesis will affect the chlorophyll content in leaves. Therefore, the chlorophyll content in K1 increases, assisted by the K element in the soil. Morphologically, the control K1 showed greener leaves than all treatments. In addition, the results of this high chlorophyll content were thought to influence the productivity of maize treated with K1, which also showed the highest average cob length. Chlorophyll in plants can affect growth because photosynthetic products are used by plants, one of which is to increase growth (Campbell et al. 2021). The lowest chlorophyll content was found in the K3 treatment, which was treated with compost and AMF. In addition to chlorophyll content, K3 treatment also showed the lowest growth in plant height and leaf area. Chlorophyll is a photosynthetic pigment that involves photosynthetic

capacity and affects plant growth (Li et al. 2018, Maylani et al. 2020, Wankmüller & Carminati 2022). The small leaf area in the K3 treatment was thought to affect the chlorophyll because the leaf area index (LAI) is a biophysical parameter that has a strong correlation with chlorophyll that indicates photosynthetic capacity for plant yields (Jo & Shin 2021). Campbell et al. (2021) and Li et al. (2018) said that plants use chlorophyll for photosynthesis and produce sucrose, which is used to increase growth.

The highest stomatal density was found in the P2 treatment with the composition of fertilizers, compost, AMF, PGPR consortium, and 50% NPK (highest dose), which was in line with the yield of plant height, stem diameter, number of leaves, and leaf area which also showed the highest yields. Stomatal density and soil fertility, which support the availability of nutrients, are correlated with the photosynthetic process of plants. AMF and PGPR, which were applied to the P2 treatment, were thought to affect the stomatal density of the leaves. Sakoda et al. (2020) said that one of the factors that influence stomatal density is soil fertility. Soil fertility can be increased by adding compost, AMF, PGPR consortium, and NPK to provide nutrients in the form of N, P, K, Ca, Mg, and S (Ashari et al. 2017, Khalediyan et al. 2021, Raklami et al. 2019, Xue et al. 2020). The elements N, P, and K correlated with an increase in the photosynthetic product on the dry weight. Stomatal density in P2 treatment was thought to play a role in the accumulation of plant dry weight. The dry weight of plants is one of the results of photosynthesis, which requires $CO_2$ through stomata from the environment (Jiaying et al. 2022, Sun et al. 2020). The process of photosynthesis is influenced by elements such as N, P, and K because they can increase photosynthetic capacity (Ashari et al. 2017). These elements and the exchange of $CO_2$ through the stomata will help increase the photosynthetic yield (dry weight). Therefore, the high dry weight in the P2 treatment correlated with the stomatal density and the higher the nutrients NPed by the P2 treatment plants.

The lowest stomatal density was found in K2 treatment with 100% NPK fertilizer and compost. Compost fertilizer and 100% NPK were thought to be ineffective in increasing the number of stomata. The low density of stomata is thought to be influenced by the fertilizer applied. One study said that chemical fertilizers can significantly reduce soil pH, which is closely related to a decrease in bacterial diversity and a significant change in the composition of the bacterial community (Wang et al. 2021). Therefore, the presence of microorganisms in K2 plants may be affected because the presence of NPK is at most at a dose of 100% or 4.8 grams, which causes the innate microorganisms in the soil to be disturbed and cannot help regulate hormones and water, which affects the number of stomata in leaves. In addition, this result is also in line with Sashinta's research (Ashari et al. 2017), where a mixture of organic fertilizer and NPK fertilizer does not have a significant effect on plants, presumably because stomatal density is more influenced by factors of temperature, sunlight, and plant adaptation to the environment. Low water supply will negatively affect the formation of stomata, so plants reduce the number of stomata to avoid water deficit.

## CONCLUSION

In all treatment groups, nitrogen (N) and potassium (K) levels increased, whereas phosphorus (P) levels decreased compared to the control group (soil without treatment). However, there were no notable differences observed for each parameter except in the P2 treatment that comprised compost, PGPR consortium, AMF, and 50% of NPK, which displayed the most favorable growth and productivity outcomes. In addition, all treatment shows a high percentage of mycorrhizal infection. In summary, the findings suggest that the combination of PGPR and AMF effectively halved the use of chemical fertilizers.

## ACKNOWLEDGEMENT

This research was supported by "The Research Magister of the Ministry of Education, Culture, Research and Technology, Indonesia." Project No. 2017/PKS/ITS/2023 And Agreement/contract No. 112/E5/PG.02.00.PL/2023. We all thank all members of Plant Biosains and Technology Laboratory for their valuable help in supporting to experiment.

## REFERENCES

Adekiya, A. O., Ejue, W. S., Olayanju, A., Dunsin, O., Aboyeji, C. M., Aremu, C., Adegbite, K. and Akinpelu, O. 2020. Different organic manure sources and NPK fertilizer on soil chemical properties, growth, yield, and quality of okra. Sci. Rep., 10(1): 291. https://doi.org/10.1038/S41598-020-73291-X

Andriani, A. A. S. P. R., Suaria, I. N., Yudiana, I. W., Parlindungan Situmeang, Y., Mayun Wirajaya, A. A. N. and Bagus Udayana, I. G. 2017. Application of fertilization time and nitrogen dosage on peanut plant Arachis hypogaea L.. SEAS. Sustain. Environ. Agric. Sci., 1(1): 27. https://doi.org/10.22225/seas.1.1.437.27-31

Anwar, A., Yu, X. and Li, Y. 2020. Seed priming as a promising technique to improve growth, chlorophyll, photosynthesis and nutrient contents in cucumber seedlings. Not. Bot. Horti Agrobot. Cluj., 48(1): 116-127. https://doi.org/10.15835/NBHA48111806

Ashari, D. S., Sudradjat, M. and Sugiyanta, L. 2017. The roles of bio organic and NPK compound fertilizer to growth and production of four year old oil palm. Asian J. Appl. Sci., 5(5): 937-943. www.ajouronline.com

Assefa, S. and Tadesse, S. 2019. The principal role of organic fertilizer on soil properties and agricultural productivity: A review. Agric. Res. Technol. Open Access J., 22(2): 1-5. https://doi.org/10.19080/ARTOAJ.2019.22.556192

Barin, M., Asadzadeh, F., Hosseini, M., Hammer, E. C., Vetukuri, R. R. and Vahedi, R. 2022. Optimization of biofertilizer formulation for phosphorus solubilizing by pseudomonas fluorescens Ur21 via response surface methodology. Processes, 10(4): 650. https://doi.org/10.3390/PR10040650

Bueno, C. G. and Moora, M. 2019. How do arbuscular mycorrhizal fungi travel? New Phytol., 222(2): 645-647.

Campbell, N. A., Urry, L. A., Cain, M. L., Wasserman, S. A., Minorsky, P. V. and Orr, R. B. 2021. Campbell Biology. Twelfth edition. Pearson Educ., Inc., NJ

Cao, Y., Jiang, K., Wu, J., Yu, F., Du, W. and Xu, T. 2020. Inversion modeling of japonica rice canopy chlorophyll content with UAV hyperspectral remote sensing. PloS One, 15(9): 530. https://doi.org/10.1371/JOURNAL.PONE.0238530

Chapin III, F. S. 2003. Biogeochemistry Biogeochemistry of terrestrial net primary production. Treatise on Geochem., 47: 215-247.

de Bang, T. C., Husted, S., Laursen, K. H., Persson, D. P. and Schjoerring, J. K. 2021. The molecular-physiological functions of mineral macronutrients and their consequences for deficiency symptoms in plants. New Phytol., 229(5): 2446-2469. https://doi.org/10.1111/NPH.17074

Friede, M., Unger, S., Hellmann, C. and Beyschlag, W. 2016. Conditions promoting mycorrhizal parasitism are of minor importance for competitive interactions in two differentially mycotrophic species. Front. Plant Sci., 7: 1465 https://doi.org/10.3389/fpls.2016.01465

Ghorai, P. and Ghosh, D. 2022. Ameliorating the performance of NPK biofertilizers to attain sustainable agriculture with special emphasis on bioengineering. Bioresour. Technol. Rep., 19: 101117. https://doi.org/https://doi.org/10.1016/j.biteb.2022.101117

Gusta, A. R. and Same, M. 2022. The Effect of Organic Fertilizer and NPK on the Growth of the Master Pepper Plants. IOP Conf. Ser.: Earth Environ. Sci., 1012(1): 012028. https://doi.org/10.1088/1755-1315/1012/1/012028

Harborne, J. B. 1987. Phytochemical Methods Guide Modern Ways to Analyze Plants. ITB Press, NY.

He, L., Chen, J. M., Liu, J., Zheng, T., Wang, R., Joiner, J., Chou, S., Chen, B., Liu, Y., Liu, R. and Rogers, C. 2019. Diverse photosynthetic capacity of global ecosystems mapped by satellite chlorophyll fluorescence measurements. Remote Sens. Environ., 232: 111344: https://doi.org/10.1016/J.RSE.2019.111344

Hu, W., Lu, Z., Meng, F., Li, X., Cong, R., Ren, T., Sharkey, T. D. and Lu, J. 2020. The reduction in leaf area precedes that in photosynthesis under potassium deficiency: the importance of leaf anatomy. New Phytol., 227(6): 1749-1763. https://doi.org/10.1111/NPH.16644

Jiaying, M., Tingting, C., Jie, L., Weimeng, F., Baohua, F., Guangyan, L., Hubo, L., Juncai, L., Zhihai, W., Longxing, T. and Guanfu, F. 2022. Functions of Nitrogen, Phosphorus, and Potassium in Energy Status and Their Influences on Rice Growth and Development. Sci. Direct, 29(2): 166-178. https://doi.org/10.1016/j.rsci.2022.01.005

Jo, W. J. and Shin, J. H. 2021. Development of a transpiration model for precise tomato (Solanum lycopersicum L.) irrigation control under various environmental conditions in a greenhouse. Plant Physiol. Biochem., 162: 388-394. https://doi.org/10.1016/J.PLAPHY.2021.03.005

Johnson, N. C. 2010. Resource stoichiometry elucidates the structure and function of arbuscular mycorrhizas across scales. New Phytol., 185(3): 631-647. https://doi.org/10.1111/J.1469-8137.2009.03110.X

Khalediyan, N., Weisany, W. and Schenk, P. M. 2021. Arbuscular mycorrhizae and rhizobacteria improve growth, nutritional status, and essential oil production in Ocimum basilicum and Satureja hortensis. Ind. Crops Prod., 160: https://doi.org/10.1016/J.INDCROP.2020.113163

Kuila, D., Mal, B., Mondal, S., Ghosh, S. and Biswas, G. 2020. Effect of an Indigenous AM and PGPR combination on chili growth and productivity in lateritic soil. Biotecnol. Veg., 20(3): 177-188.

Li, J., Zhang, Y., Gu, L., Li, Z., Li, J., Zhang, Q., Zhang, Z. and Song, L. 2020. Seasonal variations in the relationship between sun-induced chlorophyll fluorescence and photosynthetic capacity from the leaf to canopy level in a rice crop. J. Exp. Bot., 71(22): 7179-7197. https://doi.org/10.1093/JXB/ERAA408

Li, Y., He, N., Hou, J., Xu, L., Liu, C., Zhang, J., Wang, Q., Zhang, X. and Wu, X. 2018. Factors influencing leaf chlorophyll content in natural forests at the biome scale. Front. Ecol. Evol., 6: 324791. https://doi.org/10.3389/FEVO.2018.00064/BIBTEX

Liu, J., Chen, W., Wang, H., Peng, F., Chen, M., Liu, S. and Chu, G. 2021. Effects of NPK fertilization on photosynthetic characteristics and nutrients of pecan at the seedling stage. J. Soil Sci. Plant Nutr., 21(3): 2425-2435. https://doi.org/10.1007/S42729-021-00533-W/TABLES/6

Ma, X., Geng, Q., Zhang, H., Bian, C., Chen, H. Y. H., Jiang, D. and Xu, X. 2021. Global negative effects of nutrient enrichment on arbuscular mycorrhizal fungi, plant diversity, and ecosystem multifunctionality. New Phytol., 229(5): 2957-2969. https://doi.org/10.1111/NPH.17077

Man, J., Shi, Y., Yu, Z. and Zhang, Y. 2015. Dry matter production, photosynthesis of flag leaves and water use in winter wheat are affected by supplemental irrigation in the Huang-Huai-Hai Plain of China. PLoS ONE, 10(9): 137274. https://doi.org/10.1371/journal.pone.0137274

Marler, T. E. 2022. NPK Fertilization of serianthes plants influences growth and stoichiometry of leaf nutrients. Horticulturae, 8(8): 717. https://doi.org/10.3390/HORTICULTURAE8080717

Maylani, E. D., Yuniati, R. and Wardhana, W. 2020. The effect of leaf surface character on the ability of water hyacinth, Eichhornia crassipes (Mart.) Solms. To transpire water. IOP Conf. Ser.: Mater. Sci. Eng., 902(1): 12070. https://doi.org/10.1088/1757-899X/902/1/z12070

Mitter, E. K., Tosi, M., Obregón, D., Dunfield, K. E. and Germida, J. J. 2021. Rethinking crop nutrition in times of modern microbiology: innovative biofertilizer technologies. Front. Sustain. Food Syst., 5: 606815. https://doi.org/10.3389/fsufs.2021.606815

Ng, J. F., Ahmed, O. H., Jalloh, M. B., Omar, L., Kwan, Y. M., Musah, A. A. and Poong, K. H. 2022. Soil Nutrient retention and pH buffering capacity are enhanced by calciprill and sodium silicate. Agronomy, 12(1): 1-24. https://doi.org/10.3390/agronomy12010219

Nunes, F. C., de Jesus Alves, L., de Carvalho, C. C. N., Gross, E., de Marchi Soares, T. and Prasad, M. N. V. 2020. Soil as a complex ecological system for meeting food and nutritional security. In Climate Change and Soil Interactions. LTD. https://doi.org/10.1016/b978-0-12-818032-7.00009-6

Nurhidayati, T., Indah Purwani, K. and Dini Ermavitalini Jurusan Biologi Fakultas Matematika dan Ilmu Pengetahuan Alam, dan. 2010. Isolasi Mikoriza Vesikular-Arbuskular Pada Lahan Kering Di Jawa Timur. Berk. Penel. Hayati Edisi Khusus, 1970: 2010.

Okonwu, K. and Mensah, S. I. 2012. Effects of NPK (15:15:15) fertilizer on some growth indices of pumpkin. Asian J. Agric. Res., 6(3): 137-143. https://doi.org/10.3923/ajar.2012.137.143

Padri, M. H., Baharuddin, M. and Herawatiningsih, R. 2015. The presence of arbuscular mycorrhizal fungi in white jabon in peatlands. J. Hutan Lestari, 3(3): 401-410.

Ramasamy, K., Joe, M. M., Kim, K. Y., Lee, S. M., Shagol, C., Rangasamy, A., Chung, J. B., Islam, Md. R. and Sa, T. M. 2011. Synergistic effects of arbuscular mycorrhizal fungi and plant growth promoting rhizobacteria for sustainable agricultural production. Korean J. Soil Sci., 44(4): 637-649.

Raklami, A., Bechtaoui, N., Tahiri, A. I., Anli, M., Meddich, A. and Oufdou, K. 2019. Use of rhizobacteria and mycorrhizae consortium in the open field as a strategy for improving crop nutrition, productivity and soil fertility. Front. Microbiol., 10(MAY): 1-11. https://doi.org/10.3389/fmicb.2019.01106

Sakoda, K., Yamori, W., Shimada, T., Sugano, S. S., Hara-Nishimura, I. and Tanaka, Y. 2020. Higher stomatal density improves photosynthetic induction and biomass production in arabidopsis under fluctuating

light. Front. Plant Sci., 11: 589603. https://doi.org/10.3389/FPLS.2020.589603/BIBTEX

Sayara, T., Basheer-Salimia, R., Hawamde, F. and Sánchez, A. 2020. Recycling of organic wastes through composting: Process performance and compost application in agriculture. Agronomy, 11)10): 838. https://doi.org/10.3390/agronomy10111838

Senbayram, M., Gransee, A., Wahle, V. and Thiel, H. 2015. Role of magnesium fertilisers in agriculture: Plant-soil continuum. Crop Pasture Sci., 66(12): 1219-1229. https://doi.org/10.1071/CP15104

Shovitri, M., Sugianto, S. K., Kuswytasari, N. D. and Alami, N. H., Zulaika, E. 2021. Application of rhizobacteria and NPK for growth and productivity of sweet corn (Zea mays L.). Adv. Biol. Sci. Res., 22: 111-117.

Sokoto, M. B., Abubakar, I. U. and Dikko, A. U. 2012. Correlation analysis of some growth, yield, yield components and grain quality of wheat (Triticum aestivum L.). Niger. J. Basic Appl. Sci., 20(4): 349-356. http://www.ajol.info/index.php/njbas/index

Song, X., Zhou, G., Ma, B. L., Wu, W., Ahmad, I., Zhu, G., Yan, W. and Jiao, X. 2019. Nitrogen application improved photosynthetic productivity, chlorophyll fluorescence, yield and yield components of two oat genotypes under saline conditions. Agronomy, 9(3): 115. https://doi.org/10.3390/agronomy9030115

Sprunger, C. D., Culman, S. W., Palm, C. A., Thuita, M. and Vanlauwe, B. 2019. Long-term application of low C residues enhances maize yield and soil nutrient pools across Kenya. Nutr. Cycl. Agroecosyst., 114(3): 261-276. https://doi.org/10.1007/s10705-019-10005-4

Sun, M., Yuan, D., Hu, X., Zhang, D. and Li, Y. 2020. Effects of mycorrhizal fungi on plant growth, nutrient absorption and phytohormones levels in tea under shading condition. Not. Bot. Horti Agrobot. Cluj-Napoca, 48(4): 2006-2020. https://doi.org/10.15835/48412082

Tulung, L. E. A., Amin, M. and Manoppo, C. N. 2021. Response of growth and production of potato plants to the application of NPK fertilizer. E3S Web Conf., 306, 1-6. https://doi.org/10.1051/e3sconf/202130601018

Umami, N., Abdiyansah, A. and Agus, A. 2019. Effects of different doses of NPK fertilization on growth and productivity of Cichorium intybus. IOP Conf. Ser. Earth Environ. Sci., 387(1): 012097. https://doi.org/10.1088/1755-1315/387/1/012097

Vikas, K., Kirth, S. G. and Poulose, L. 2016. Types, importance and factors affecting mycorrhiza production for sustainable plant growth. Van Sangyan, 2(10): 25-29.

Wang, C. and Ning, P. 2019. Post-silking phosphorus recycling and carbon partitioning in maize under low to high phosphorus inputs and their effects on grain yield. Front. Plant Sci., 10. https://doi.org/10.3389/FPLS.2019.00784/FULL

Wang, J. L., Liu, K. L., Zhao, X. Q., Zhang, H. Q., Li, D., Li, J. J. and Shen, R.F. 2021. Balanced fertilization over four decades has sustained soil microbial communities and improved soil fertility and rice productivity in red paddy soil. Sci. Total Environ., 793: 148664. https://doi.org/10.1016/j.scitotenv.2021.148664

Wankmüller, F. J. P. and Carminati, A. 2022. Stomatal regulation prevents plants from critical water potentials during drought: Result of a model linking soil–plant hydraulics to abscisic acid dynamics. Ecohydrology, 15(5): e2386. https://doi.org/10.1002/ECO.2386

Xu, X., Du, X., Wang, F., Sha, J., Chen, Q., Tian, G., Zhu, Z., Ge, S. and Jiang, Y. 2020. Effects of potassium levels on plant growth, accumulation and distribution of carbon, and nitrate metabolism in apple dwarf rootstock seedlings. Front. Plant Sci., 11: 1-13. https://doi.org/10.3389/fpls.2020.00904

Xue, Z., Asante-Badu, B., Appiah-Badu, M. O., Kgorutla, L. E. and Qiang, G. 2020. Maize (Zea mays L.) response to potassium application and K+ uptake in the soil: A review. Agric. Rev., 41(03): 527. https://doi.org/10.18805/ag.a-527

Nature Environment and Pollution Technology
An International Quarterly Scientific Journal

p-ISSN: 0972-6268
(Print copies up to 2016)
e-ISSN: 2395-3454

Vol. 23 | No. 3 | pp.1461-1470 | 2024

Original Research Paper

https://doi.org/10.46488/NEPT.2024.v23i03.016

Open Access Journal

# Reuse and Recovery of Water from Industrial Textile Dyeing Effluent Using High-Performance Electrodes Continuous Flow Electrocoagulation Reactor

**P. Jegathambal†, Brunoc*, Shobina*, C. Mayilswamy* and K. Parameswari****
*Water Institute, Karunya Institute of Technology and Sciences, Coimbatore, T.N., India
**Department of Chemistry, Karunya Institute of Technology and Sciences, Coimbatore, T.N., India
†Corresponding author: P. Jegathambal; esther.jegatha2011@gmail.com

**Nat. Env. & Poll. Tech.**
**Website: www.neptjournal.com**

*Received:* 22-06-2023
*Revised:* 26-10-2023
*Accepted:* 03-11-2023

**Key Words:**
Electrocoagulation
Color removal efficiency
Sludge settling rate
Characterization
Water recovery

## ABSTRACT

The dye effluents released from the textile and printing industries contain strong colorants, inorganic salts, and other toxic compounds. The conventional coagulation technique of dye effluent treatment is plagued with issues of low removal rate of color, generation of large quantities of sludge, and toxic end-products. Recently electrocoagulation technique gained immense attention due to its high efficiency. This technique involves the dissolution of the sacrificial anodes to provide an active metal hydroxide as a strong coagulant that destabilizes the pollutants and removes them by precipitation or flocculation. This study is about the efficiency of the electrocoagulation process using titanium coated - aluminum and mild steel electrodes to treat industrial dye wastewater. Effects of parameters such as current density & initial dye concentration were investigated. It was observed that, for the same current density, electrode consumption was higher with $TiO_2$/Al electrode than with mild steel electrode, resulting in more color removal efficiency (CRE) using $TiO_2$/Al electrode. The settling rate of the flocs was higher in the rector having $TiO_2$/Al electrode at the 100 mL with current density (2.5 $mL.min^{-1}$ to 5.3 $mL.min^{-1}$), while in the reactor with mild steel electrode, the settling rate was very less. The results showed that dye removal was 95.11% and 92.1% for mild steel and titanium-coated electrodes, respectively. It was observed that 50 % of Aluminum was removed from the treated effluent after the final stage of filtration. Based on the multicriteria analysis to identify the optimum operational parameters to be applied at the field level, it was observed that maximum CRE may be obtained with $TiO_2$/Al electrode and the applied current of 1 Amps with a flow rate of 100 $mL.min^{-1}$. It can be concluded that electrocoagulation is a highly efficient and the fastest method to treat dye effluents from industries.

## INTRODUCTION

In recent days, synthetic dyes have been widely used in leather, textile, paper, food, cosmetics, and pharma industries. Wastewater, which is the outcome of dyeing and washing processes from textile industries, is of special concern due to the wide range of chemicals used in the corresponding process and its related toxic effects. It is estimated that about 15% of the dyestuff is left unused and is discharged as waste.

Due to the expansion of industrial activities and increased population growth, environmental degradation is intensified, as visually seen by the deterioration of land and water ecosystems. Nature, which was once tamed by anthropogenic activities, has started rebounding its action by posing a great challenge in the treatment of water and wastewater to researchers, engineers, and scientists. It is reported that 2,500 textile weaving factories and 4,135 textile finishing factories are functioning in India. Out of 60% of total dye production for various applications, 10-15% of unspent dyes are let out into water bodies which makes the water polluted with a concentration range of 10-200 ppm. Though conventional methods like reverse osmosis, ion exchange, membrane filtration, adsorption, electrocoagulation, and chemical precipitation are widely used, adsorption is an attractive, efficient, and cost-effective method with less maintenance cost that is commonly applied to remove Total Dissolved Solids (TDS), organic, inorganic and heavy metals.

In the physical treatment method, the dyestuffs in wastewater are removed by using naturally occurring forces, such as gravity, electrical attraction, and van der Waal forces, as well as by the use of physical barriers. Physical treatment methods include adsorption, membrane filtration, and coagulation. On the other hand, chemical treatment processes include, oxidative process, ozonation, chemical coagulation, etc. In the chemical coagulation process, coagulants with

charges opposite to those of the suspended solids are added to wastewater to neutralize the negative charges on dispersed non-settable solids such as organic substances. When the charge is neutralized, the small suspended particles stick together to form flocs that settle down over time. The major disadvantage of the chemical coagulation method is that it transfers toxic compounds into the sample, which has to be treated subsequently, and it involves high costs and is time-consuming. Because of these reasons, another alternate method that overlays these disadvantages has to be developed. The conventional methods of wastewater treatment demand more area, consume more time, cause sludge disposal problems, energy-intensive and demand-based.

**Electrochemical Methods**

Electrochemical methods gained attention during the second part of the 20$^{th}$ century. Though the investment and current consumption were high at the time of the introduction of the electrochemical method, after extensive research on electrochemical methods, the cost of electrochemical methods is comparable with other wastewater treatment techniques (Vik 1984, Stuart 1946, Bonilla 1947). In specific applications, the electrochemical methods are more efficient than conventional methods of treatment. The main disadvantage of using the chemical coagulation method is, due to the addition of chemicals like alum and ferric chloride, additional anions get into the effluents by which the TDS increases in concentration more than that of the electrochemical method where the pure metal electrodes (Al, Fe, Ti, etc.) are used as sacrificial anodes. Electrocoagulation is a water treatment technique recently discovered that is used to remove the total suspended solids (TSS), heavy metals (Mn, Cu, Zn, Ni, Al, Fe, Co..), emulsified oils, bacteria, and other contaminants from the wastewater (Heidmann et al. 2010, Abdelwahab et al. 2009). Electrocoagulation consists of a pair of metal sheets called electrodes. In this process, the electro-dissolution of sacrificial anodes, usually made of aluminum or iron, to the wastewater leads to the formation of hydrolysis products (hydroxo-metal species) that are effective in the destabilization of pollutants. The hydroxo-metal species forms flocs that trap the pollutants in the wastewater (Zongo et al. 2009, Balasubramaniam et al. 2009, Azarian et al. 2007).

**Electrocoagulation**

In electrocoagulation, the coagulant/metal ions/destabilizing agents are generated in situ through electrolytic redox reactions at the anode and cathode in the electrochemical reactor that neutralize the charged colloids in the solution. The sacrificial anodes get corroded due to the oxidation process. The generated electrons move towards the cathode that dissociates water into hydrogen gas and hydroxide ions. The metal ions generated from the anode get hydrolyzed in the solution to form various monomeric hydroxide species based on the pH of the solution. In the case of Al electrodes, in the alkaline environment (at pH>9), the final pH of the treated effluent is reduced because of the formation of aluminate ($Al(OH)_4^-$) which consumes alkalinity. When the metal ions with high charge are released from anodes, polyvalent poly-hydroxide complexes (Al-O-Al-OH)/gelatinous charged hydroxy cationic complexes with high adsorption capacity are formed that will adsorb the colloids/pollutants. In the case of Fe electrodes, the $Fe(OH)_n$ species in the gelatinous form remove the colloids/pollutants either through electrostatic force of attraction or through complexation (in which the colloids/pollutants act as a Ligand to bind the hydroxyl ion. In an acidic environment and the presence of oxygen, Ferric ions are formed that lead to the generation of amorphous $Fe(OH)_3$ species with large surface area, which are beneficial in the adsorption of organic and inorganic pollutants. At higher pH, the higher forms of hydroxide species $Fe(OH)_4^-$ and $Fe(OH)_6^-$ are formed. During the electrocoagulation process, simultaneous generation of $O_2$ at the anode and $H_2$ at the cathode are released due to the decomposition of water. In addition to that, highly reactive $OH^-$and $HO_2$ radicals are formed (Morena et al. 2007, Picard et al. 2000)

Electrocoagulation is a cost-effective and efficient technology that has been widely applied in the area of textile dye removal, treating wastewater containing organic compounds like fats, oils, detergents, heavy meals, microorganisms, other anions and cations, etc.

The type of electrochemical reactions and the type of actions released into the solution depends on the type of electrode materials used. In the case of Al electrodes, the metal ions are released in the form of $Al^{3+,}$ and Fe gets dissolved in the form of Fe (II) and Fe (III). The performance of Fe (III) ions is better in the removal of pollutants because of the higher positive charge and lower solubility of hydroxides (Linares et al. 2009, Krishna et al. 2010, Katal et al. 2011). Based on the type of pollutants to be removed and the size of the cations, the performance of Al and Fe electrodes differ. The size of $Fe^{3+}$ ions (10-30 micrometer) is bigger than $Al^{3+}$ ions (0.01-1 micrometer). The bigger the size of the metal ions, the higher the removal of colloids/pollutants. From past works, it was observed that the Fe electrodes are more efficient in odor removal. In most of the studies, Fe, Stainless steel, Al, Cu, and Ni electrodes have been used as the sacrificial electrodes (Alil et al. 2012, Marconato et al. 1998, Secula et al. 2012).

In this study, the $TiO_2$/Al electrodes are used as an anode and cathode for the *in situ* generation of $Ti^{4+}$ metal ions, which have a tetravalent charge with better dye removal efficiency than $Al^{3+}$ or $Fe^{3+}$ ions. The $Ti^{4+}$ ions will be released till the coating/ thermally deposited $Ti^{4+}$ gets dissolved into the solution. Then, after, $Al^{3+}$ ions may start getting dissolved. This type of nano-composite electrode takes advantage of both metal ions in removing the dye from the effluent. The main reactions occurring in the reactor are: when the potential is applied to the metallic anode, the metal ions ($Ti^{4+}$, $Al^{3+}$) get dissolved into the solution, while an equivalent number of electrons pass through the circuit and dissociate water into $H_2$ (g) and $OH^-$ ions at the cathode. The hydrogen gas is released at the cathode, while oxygen is released at the anode. In the presence of supporting electrolyte and with slow stirring, the electro-driven coagulants and hydroxyl ions come into contact to form both monomeric, polymeric metal hydroxides and poly-hydroxy metallic flocs like $Al_{13}(OH)_{34}^{5+}$, $Al_6(OH)_{15}^{3+}$, $Al_8(OH)_{20}^{4+}$, $Al_{13}O_4(OH)_{24}^{7+}$, $Al_7(OH)_{17}^{4+}$, which finally get transformed to $Al(OH)_3$ based on precipitation kinetics, that adsorb/entrap the dye/ pollutants from the waste stream. Due to the formation of $OH^-$ (aq) and consumption of protons at low initial pH, Al ions get dissolved from the cathode to form aluminate ($Al(OH)_4^-$) which increases the pH of the effluent in the reactor. Capacitive Deionization is one of the efficient electro-adsorption techniques for removing salt from aqueous solutions. When the electrodes are charged, the oppositely charged ions get adsorbed into the electrical double layer region on the surface of the respective electrodes (anions to anode and cations to cathode), thereby the concentration of anions and cations contributing to the increase in TDS gets removed. Then, during depolarization, due to a reduction in the cell voltage, the adsorbed ions get released into a waste stream (Mahvi et al. 2009, Canizares et al. 2009, Ahmed et al., 2016).

The generated hydroxyl species and generated metal ions affect the conductivity of the solution. When the initial pH of the wastewater to be treated is in the acidic medium, during electrocoagulation, due to the interaction between metal ions and other anions present in the wastewater as well as the formation of hydroxyl species near the anode. Also, the evolution of $H_2$ gas at the cathode increases the pH of the solution. But when the initial pH of the wastewater is around 2, then there will not be a significant increase in the pH of the solution (Abhinesh Kumar et al. 2016). At pH>4, the alkalinity of the medium gradually rises.

The current intensity greatly influences the voltage between the anode and the cathode. The economics and amount of in-situ generation of metal ions from the anode depend on the power consumption/current density (Danis et

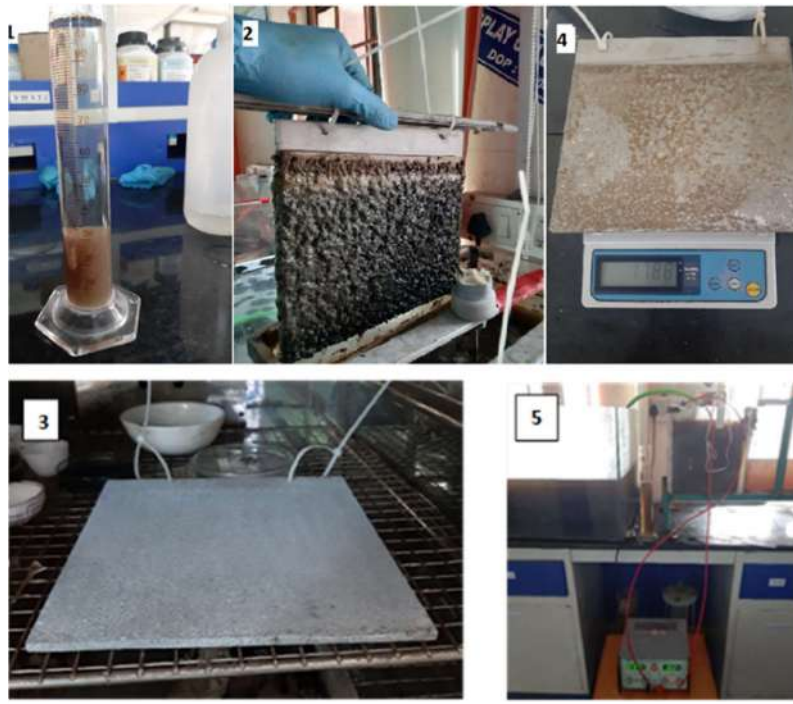


Fig. 1. Settling of sludge 2. Anode scrap 3. Weight measurement of the electrode 4. Weight measurement of cathode 5. Continuous flow reactor.

al. 2017, MohdKhairu et al. 2016). The actual dissolution of the metal ions from the anode for the applied current is compared with the calculation using Faraday's law. In an acidic or neutral medium, the dissolution from Al and Fe electrodes is primary, whereas in the alkaline medium, the actual rate of dissolution of Fe is less than the theoretical value (calculated through Faraday's law). The applied current greatly affects the size of the reactor and also the efficiency. At higher currents, the reactor size may be small. But when a high current (more than optimum) is applied, the performance is poor since most of the electrical energy is converted into heat energy, which raises the temperature of the treated effluent (Ming et al. 2012, Honore et al. 2017, Chafi et al. 2011).

## MATERIALS AND METHODS

### Continuous Flow Studies

The electrocoagulation reaction tank was initially filled with the dye effluent to be treated. The electrodes were labeled and kept inside the reaction tank. A DC power supply meter is used to pass current onto the electrodes. The TDS of the solution was kept at 2000-2500 $mg.L^{-1}$ concentration.

Initially, 1 Amp (25 $A.m^{-2}$) of current was applied to the electrodes to achieve the formation of the floc. Later, the experiment was run by varying the current and the inflow rate of the dye effluent from the storage tank to the reaction tank. Once the flocs were formed, the settling rate of the flocs was measured. When the dense flocs are formed, the continuous flow is maintained from the inlet tank. The quality of the effluent from the reaction tank, settling tank, and filter tank for every one-hour interval. The collected samples were first filtered using filter paper, and the filtrate was used for further analysis (Fig. 1 & Fig. 2).

The samples were tested for pH, EC, TDS, COD, absorbance, and settling rate. The flow rate and current were changed for every 4th or 5th hour. Before varying the flow rate and current, the sludge deposited on the electrode was scrapped and kept in the oven for drying. The electrode plates were then washed and dried before placing it in the reaction tank. This was repeated every time the flow rate and current were changed. The experiment was run with different flow rates, currents, and electrolyte concentrations to find the optimum experimental condition to attain maximum color removal efficiency.

## RESULTS AND DISCUSSION

The samples collected from the reaction tank, settling tank, and filter tank were analyzed for pH, EC, TDS, Colour removal efficiency (CRE), and settling rate of the flocs.

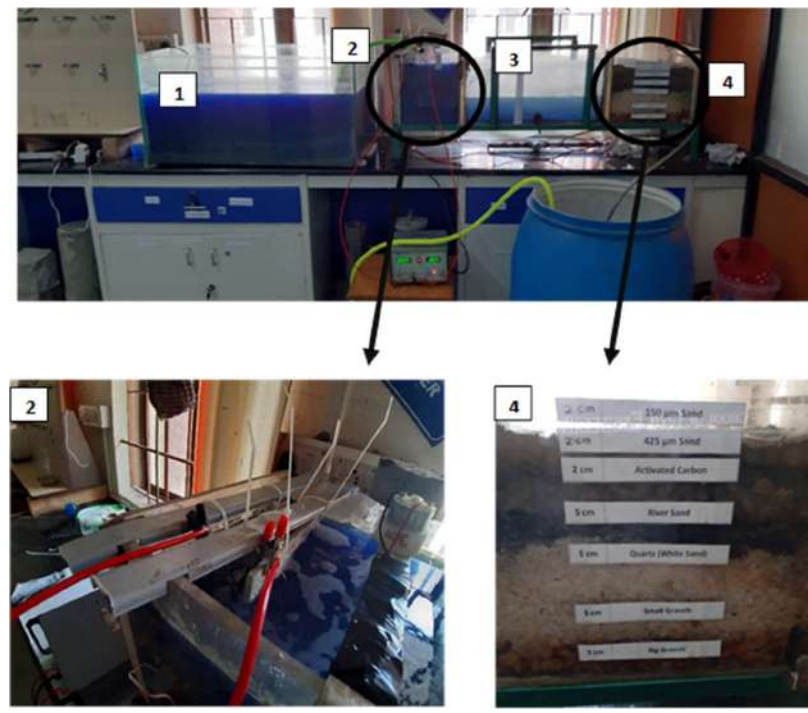


Fig. 2: Continuous Flow Reactor, Settling Tank, and Filtration.

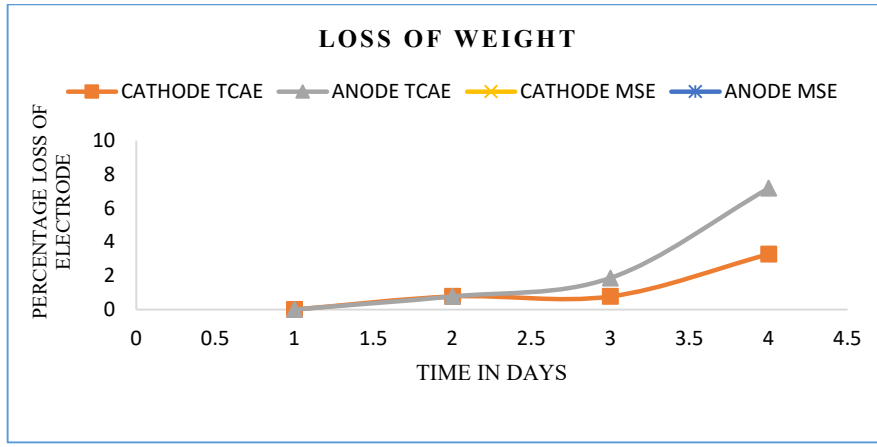


Fig. 3: Loss in weight of anode and cathode after treatment.

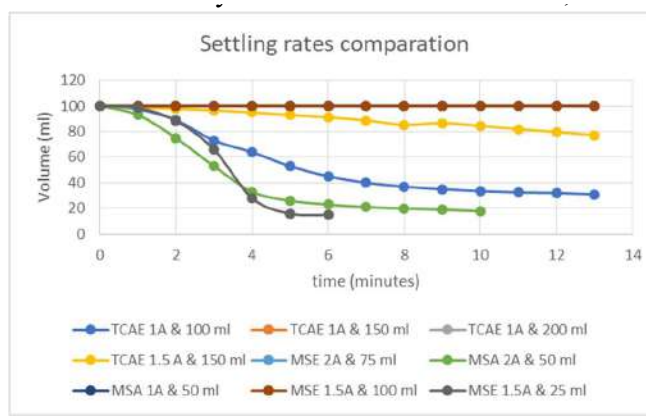


Fig. 4: Comparison of Settling rate with Ti and Mild Steel electrodes.

**Electrode Consumption**

The weight of the electrodes was measured before starting the experiment. Based on the t difference in weight of the electrodes of different materials, the consumption of the electrode was determined. Based on the results (Fig. 3), it was observed that, for the same applied current, the consumption of the mild steel electrode was less when compared to the titanium-coated aluminum electrode. The less consumption of the electrode led to the decreased color removal efficiency in mild steel electrodes (Fig. 3).

**Settling Rates**

In the case of TCAE, when the flow rate was maintained at 100 mL with a current density was 45 $A.m^{-2}$, the settling rate of the flocs was high within 13 min (2.5 $mL.min^{-1}$ to 5.3 $mL.min^{-1}$). When the flow rate was increased to 150 $mL.min^{-1}$ with the same current density, the flocs were apart, and no settling was observed. Similar is the case at the flow rate of 200 $mL.min^{-1}$. However, when the current density was increased to 67 $A.m^{-2}$, the setting was observed, but at a slower rate (1 $mL.min^{-1}$ to 1.75 $mL.min^{-1}$). In the case of MSE, when the flow rate varied from 50 to 100 mL, there was no settling observed with the varying current from 45$A.m^{-2}$ to 89 $A.m^{-2}$. This is due to the lack of formation of hydroxide flocs because of the slow oxidation of anode which, in turn, less metal ions are being released to form the flocs. However, when the flow is reduced to 25 $mL.min^{-1}$, the flocs are formed due to the release of metal ions that can interact with hydroxyl ions to form the flocs. This has induced the fast settling of sludge at a rate varying from 2.5 $mL.min^{-1}$ to 14.2 $mL.min^{-1}$. After this, the compression settling occurred. Also, at the flow rate of 50 $mL.min^{-1}$, with the current density of 89 $A.m^{-2}$, the settling rate was almost constant (7 $mL.min^{-1}$ to 7.2 $mL.min^{-1}$).

The graphical plot represents the settling volume of the sludge at every minute when the reactor was operated at different current densities and flow rates. Mild steel

electrodes operated at 100 mL.min$^{-1}$ flow rate with 1.5 Amp potential showed higher settling rates. However, the necessity to apply high potential for fewer flow rates makes mild steel undesirable over the titanium-coated aluminum electrode (Fig. 4 ).

**Color Removal Efficiency (CRE)**

The color removal efficiency (CRE) of the electrodes used was determined by the absorbance value measured at 325.5nm and 520nm wavelengths using a UV-spectrophotometer. The absorbance of the filter tank samples is also influenced by the packing materials that are used in the filter tank as also they contribute to the removal of the pollutants from the effluent. In the case of mild steel electrodes, a higher removal efficiency of about 95.11% was observed with 50 mL.min$^{-1}$. The flow rate of the effluent and 1.5 Amps of potential applied. In the case of titanium-coated Aluminum Electrodes (TCAE), better removal of about 92.1% was observed with 150 mL.min$^{-1}$ and 1.5 Amps potential being applied (Fig. 5).

The absorbance of the samples collected from the filter tank, settling tank, and reaction tank indicates that the current applied to the electrodes plays a major role in the removal of the pollutants present in the effluent sample. It is observed that both electrodes showed better results when high potential was applied with minimum flow rates. The increase in flow rates has also influenced the removal efficiency, as the active flocs that are formed during the reaction time were being utilized over time.

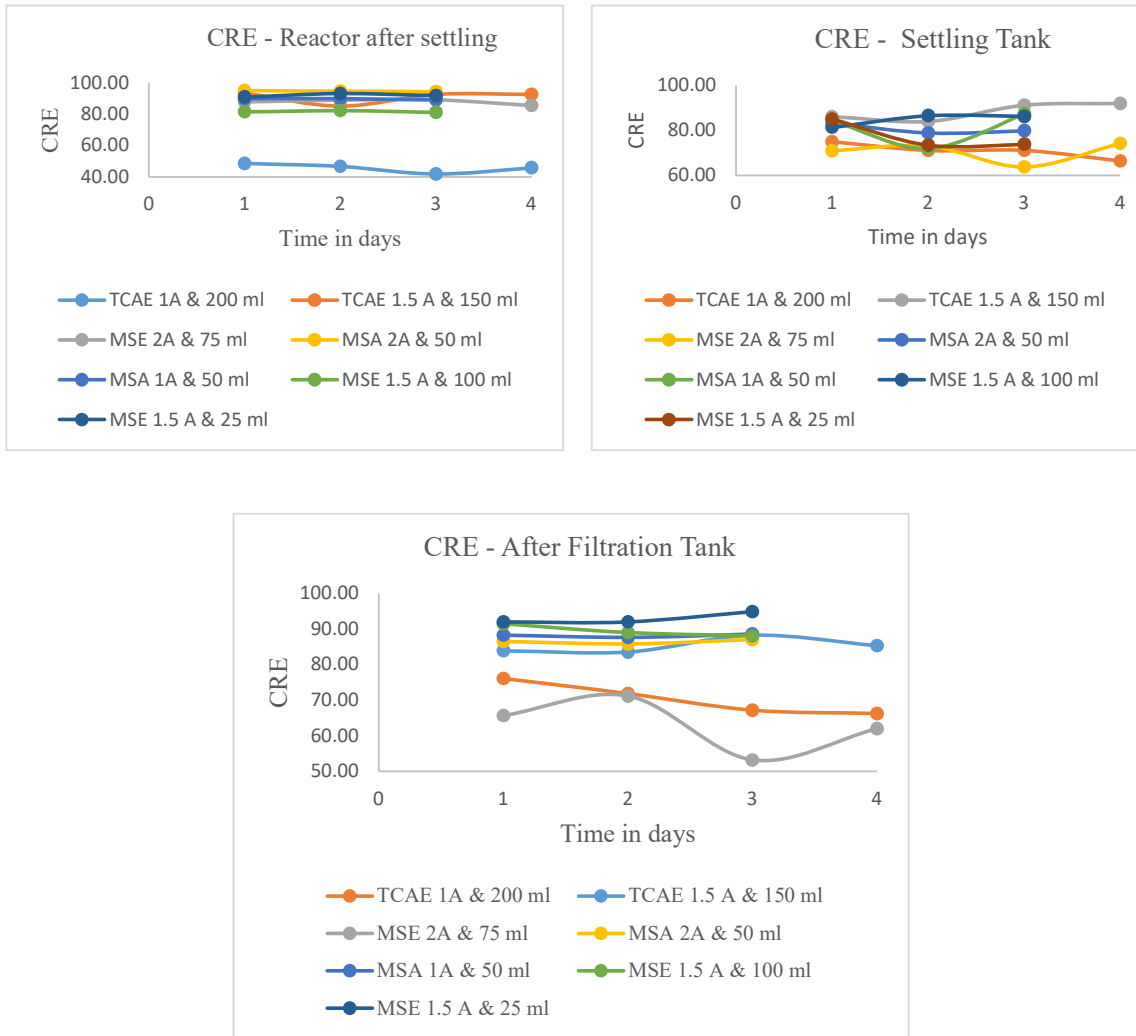


Fig. 5: Comparison of settling rate with Ti and mild steel electrodes at different flow rates.

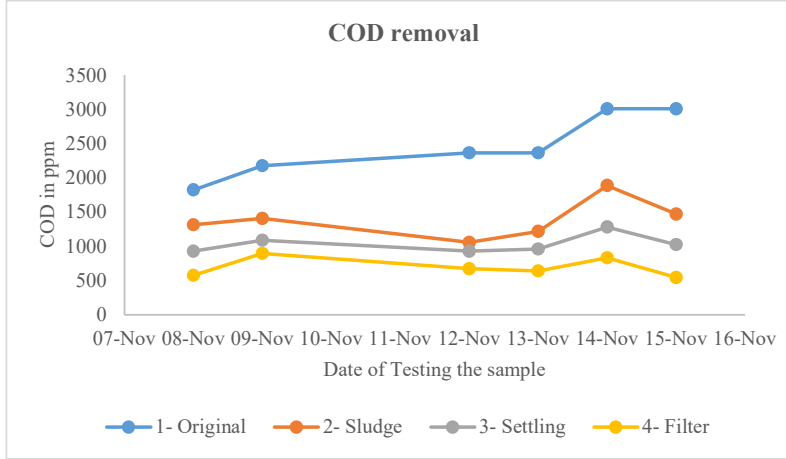


Fig. 6: Comparison of EC with Ti and mild steel electrodes at different flow rates in the reactor.

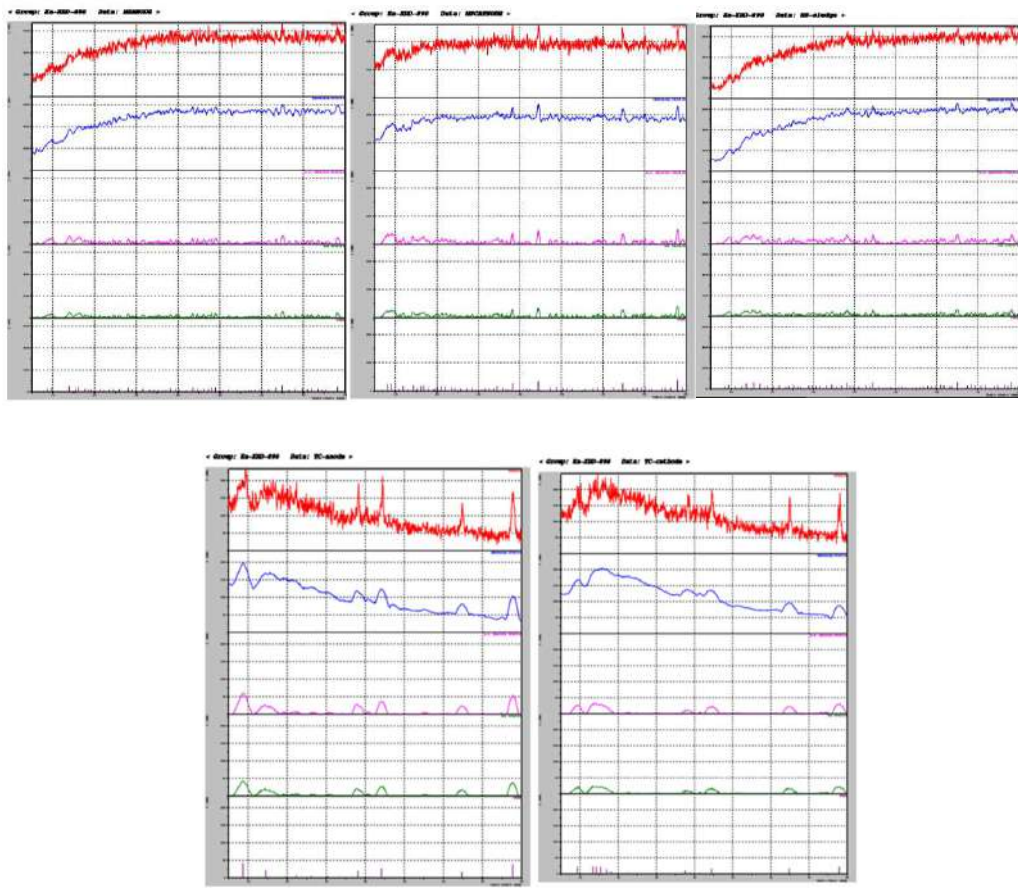

Fig. 7: XRD analysis of anodes and cathodes of Titanium coated Aluminum Electrodes (TCAE) and mild steel electrodes.

### Chemical Oxygen Demand (COD)

Reduced levels of Chemical Oxygen Demand is an indicator of better treatment of the wastewater by the method adopted. In comparison with both the electrodes, the COD levels are greatly reduced in the case of the TCAE than the MSE (Fig. 6).

### XRD

In the case of TCAE (scrap and sludge), the XRD pattern of Titanium shows a high intensity, strong diffraction peak at 2θ=26,1º, which corresponds to an interlayer distance (d) of 3.401 Å. This confirms the presence of Titanium. The strongest peak at 2θ=77.7º with an interlayer distance

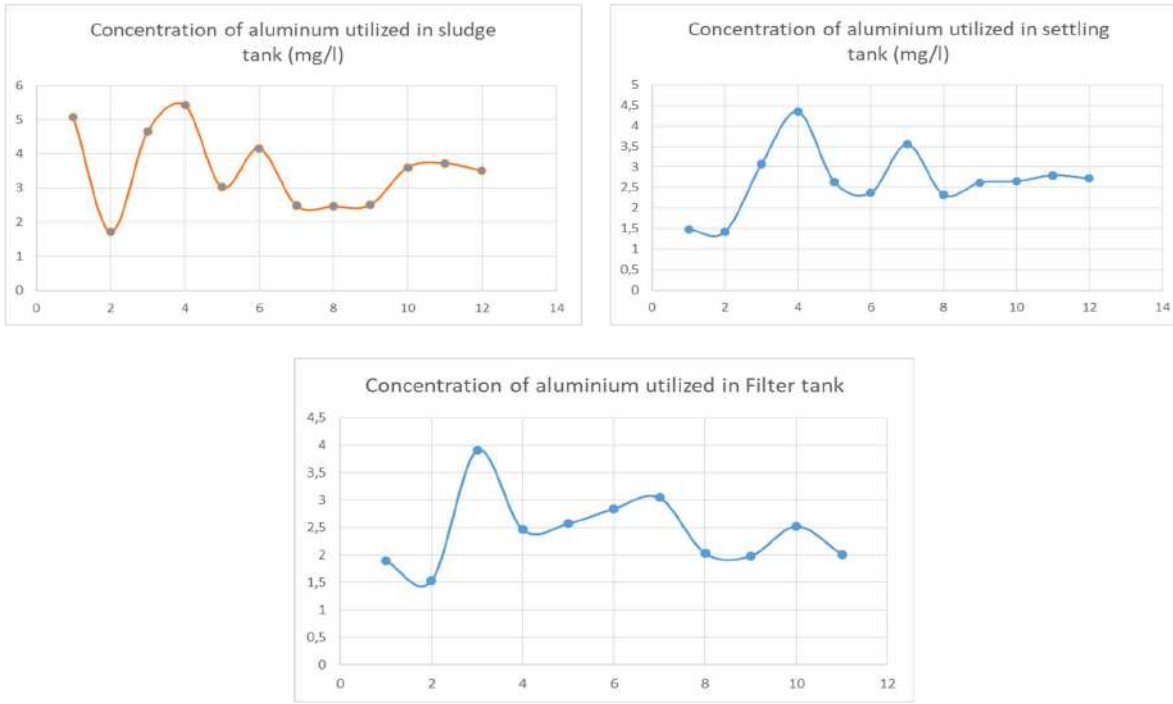


Fig. 8: Concentration of Aluminum in the reactor, settling tank and filtration.

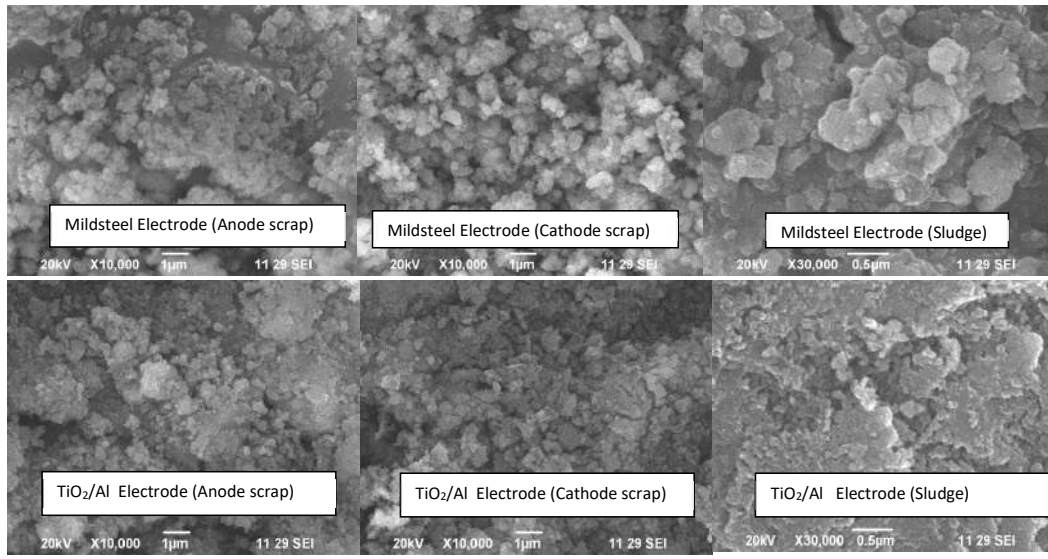


Fig. 9: SEM images of the sludge and the scrap from anode and cathode.

Table 1: Multicriteria analysis for optimization of operational parameters.

| | TCAE 1A & 100 mL | TCAE 1A & 150 mL | TCAE 1A & 200 mL | TCAE 1.5A & 150 mL | MSA 2A & 75 mL | MSA 2A &50 mL | MSA 1A &50 mL | MSA 1.5A & 100 mL | MSA 1.5A & 25 mL |
|---|---|---|---|---|---|---|---|---|---|
| Lose of weight | 8 | 8 | 8 | 8 | 5 | 5 | 5 | 5 | 5 |
| Setting rate | 14 | 0 | 0 | 5 | 0 | 17 | 0 | 0 | 17 |
| % colour removal | 16 | 13 | 9 | 16 | 5 | 16 | 14 | 20 | 22 |
| pH | 7 | 8 | 7 | 8 | 8 | 8 | 8 | 8 | 8 |
| EC | 10 | 6 | 10 | 2 | 8 | 7 | 6 | 5 | 4 |
| TDS | 10 | 6 | 10 | 2 | 8 | 7 | 6 | 5 | 4 |
| COD | 16 | 16 | 16 | 16 | 10 | 10 | 10 | 10 | 10 |
| Total | 81 | 57 | 60 | 57 | 44 | 70 | 49 | 53 | 70 |

(d) of 1.227 Å confirms the presence of aluminum. The crystalline or grain size of titanium was calculated using the Scherrer formula: $D = \frac{K * \lambda}{\beta * \cos(\theta)}$. Using this formula, the crystalline size of aluminum and titanium is found to be 5.48 nm and 54.56 nm, respectively. In the case of MSE (scrap and sludge), the XRD diffraction peaks at 42.9, 65.3,44.5, and 38.3 indicated the presence of Fe (Fig. 7).

### Concentration of Aluminum

The above graph of AAS analysis indicates the concentration of aluminum in the filter samples collected from the reaction, settling, and filter tank (Fig. 8).

### SEM Images

From the SEM images (Fig. 9), it was observed that the sludge obtained using $TiO_2$/Al electrodes is flaky, while the sludge obtained using mild steel electrodes is amorphous. The scrap obtained from both anode and cathodes from both types of electrodes are dense flocs, which are amorphous.

### Multicriteria Analysis for Optimization of Operational Parameters

The most common way to obtain the best possible result is using a multicriteria analysis; in this method, the values are represented in percentages of any parameter. The comparison study run by using TCAE and MSE was mainly focused on analyzing the optimum experimental condition in terms of flow rate, current applied, electrolyte concentration, and reaction time.

From the multicriteria table analysis (Table 1), it is found that the TCAE operated at 1 Amp current with a 100 mL flowrate of effluent gave better results. From this study, it is found that the TCAE is efficient even at low potential applied with maximum flow rate. Whereas in the case of MSE electrodes, it required high potential to be applied with minimum flow rates for better results. Thus, among the two electrodes used TCAE was more desirable to be used for industry-scale treatment methods.

## CONCLUSIONS

The continuous flow treatment of industrial textile dyeing effluent from a small-scale textile dyeing unit was carried out using a prototype model in the laboratory in which titanium-coated aluminum plates and mild Steel plates were used as anodes and cathodes. The influence of different operational parameters, sludge settling studies, characterization of the sludge, and the water quality parameters were studied. From the experimental investigations, it was observed that the range of CRE varies from 92 to 96 % at the varying flow rate from 25 to 200 mL.min$^{-1}$. About 70% removal of COD was noticed in the treated effluent in addition to the dye removal. The characterization studies confirmed the removal of dye and organic content. The crystalline size of the sludge/flocs formed using the treatment using $TiO_2$/Al electrodes in the reactor and characterized through XRD was 10 times larger than the flocs formed using mild steel electrodes, leading to the faster settling rate and high CRE. The multicriteria analysis used to identify the optimum operational parameters for the efficient removal of dye also confirmed the same. It is concluded that $TiO_2$/Al can be effectively used in small-scale textile dyeing units with high CRE, COD, and less settling time and current density.

## ACKNOWLEDGMENT

This is to acknowledge that this work was carried out as a part of the project from the Department of Science and Technology, GoI.

## REFERENCES


Abdelwahab, O., Amin, N. and Ashtoukhy, E. 2009. Electrochemical removal of phenol from oil refinery wastewater. J. Hazard. Mater., 163: 711-716.

Sleptsov, G., Gladkii, A., Sokol, E. and Novikova S. 1987. Electrocoagulation treatment of oil emulsion wastewaters of industrial enterprises. Elektron. Obrab. Mater., 6: 69-72.

Naje, A.S., Chelliapan, S., Zakaria, Z. and Abbas, S.A. 2016. Electrocoagulation using a rotated anode: A novel reactor design for textile wastewater treatment. J. Environ. Manage., 176.

Alill, I., Gupta, V., Khan, T. and Asim, M. 2012. Removal of arsenate from aqueous solution by electrocoagulation method using Al-Fe electrodes. Int. J. Electrochem. Sci., 7: 1898-1907.

Azarian, G., Mesdaghinia, A., Vaezi, F., Nabizadeh, R. and Nematollahi, D. 2007. Algae removal by electrocoagulation process; application for treatment of the effluent from an industrial wastewater treatment plant. Iran. J. Public Health, 36(4): 57-64.

Bonilla, C. 1947. Possibilities of the electronic coagulator for water treatment. Water Sewage, 85: 21-22.

Balasubramanian, N., Kojima, T., Basha, C. and Srinivasakannan, C. 2009. Removal of arsenic from aqueous solution using electrocoagulation. J. Hazard. Mater., 167(1): 966-969.

Chafi, M., Gourich, B., Essadki A.H., Vial, C. and Fabregat, A. 2011. Comparison of electrocoagulation using iron and aluminium electrodes with chemical coagulation for the removal of a highly soluble acid dye. Desalination, 281: 285-292.

Cañizares, P., Jiménez, C., Martínez, F., Rodrigo, M. and Sáez, C. 2009. The pH as a key parameter in the choice between coagulation and electrocoagulation for the treatment of wastewaters. J. Hazard. Mater., 164-158 :163.

Kartikaningsih, D., Huang, Y.-H. and Shih, Y.-J. 2017. Electro-oxidation and characterization of nickel foam electrode for removing boron. Chemosphere, 166: 184-191.

Heidmann, I. and Calmano, W. 2010. Removal of Ni, Cu, and Cr from galvanic wastewater in an electrocoagulation system with Fe and Al electrodes. Sep. Purif. Technol., 71: 308-314.

Bassalaa, H.D., Dedzoa, G.K., Bemembaa, C.B.N., Seumoa, P.M.T., Daziea, J.D., Nanseu-Njikia, C.P. and Ngameni, E. 2017. Investigation of the efficiency of a designed electrocoagulation reactor: Application for dairy effluent treatment. Process Saf. Environ. Prot., 111: 122-128.

Katal, R. and Pahlavanzadeh, H. 2011. Influence of a different combination of aluminum and iron electrode on electrocoagulation efficiency: application to the treatment of paper mill wastewater. Desalination, 265: 199-205.

Krishna, B., Murthy, U., Kumar, B.M. and Lokesh, L. 2010. Study of the electrochemical process for distillery wastewater treatment. J. Environ. Res. Dev., 5(1): 134-140.

Linares-Hermandez, I., Barrera-Diaz, C., Roa-Morales, G., Bilyeu, B. and Urena-Ninez, F. 2009. Influence of the anodic material on electrocoagulation performance. Chem. Eng. J., 148: 97-105.

Moreno, H., Cocke, D., Gomes, J., Morkovsky, P., Parga, J., Peterson, E. and Garcia, C. 2007. Electrochemistry behind electrocoagulation using iron electrodes. ECS Trans., 6(9): 1-15.

Marconato, J., Bidola, E. and Rochia-Filho, R. 1998. Electrolytic treatment of wastewater from a fowl slaughter house using cast-iron electrodes. Bull. Electrochem., 14: 228-230.

Mahvi, A., Mansoorian, H. and Rajabizadeh, A. 2009. Performance evaluation of electrocoagulation process for removal of sulfate from aqueous environments using plate aluminum electrodes. World Appl. Sci., 7(12): 1526-1533.

Mollah, M., Morkovsky, P., Gomes, J., Prajapati, A.K., Chaudhari, P.K., DharmPalb, C., Chandrakarc, A. and Choudhary, R. 2016. Electrocoagulation treatment of rice grain-based distillery effluent using copper electrode. J. Water Process Eng., 11: 1-7.

Wei, M.C., Wang, K.S., Huang, C.L., Chiang, C.W., Chang, T.J., Lee, S.S. and Chang, S.H. 2012. Improvement of textile dye removal by electrocoagulation with low-cost steel wool cathode reactor. Chem. Eng. J., 192: 37-44.

Mahmad, M.K.N., M.A.Z., M.R.R., Abustan, I. and Baharuna, N. 2016. Electrocoagulation process by using aluminum and stainless steel electrodes to treat total chromium, color, and turbidity. Procedia Chem., 19: 681-686.

Picard, T., Cathalifaud-Feuillade, G., Mazet, M. and Vandensteendam, C. 2000. Cathodic dissolution in the electrocoagulation process using aluminum electrodes. J. Environ. Monit., 2: 77-80.

Stuart, F. 1946. Electronic water purification; progress report on the electronic coagulator, a new device that gives promise of unusually speedy and effective results. Water Sewage, 84: 24-26.

Secula, M., Cretescu, I. and Petrescu, S. 2012. Electrocoagulation treatment of sulfide wastewater in a batch reactor: effect of electrode material on electrical operating costs. Environ. Eng. Manage. J., 11: 1485-1491.

Trompette, J. and Vergnes, H. 2009. On the crucial influence of some supporting electrolytes during electrocoagulation in the presence of aluminum electrodes. J. Hazard. Mater., 163: 1282-1288.

Vik, E., Carlson, D.A., Eikun, E. and Gjessing, E. 1984. Electrocoagulation of portable water. Water Res., 18(11): 1355-1361.

Zongo, I., Leclerc, J.P., Maiga, H. and Lapicque, F. 2009. Removal of hexavalent chromium from industrial wastewater by electrocoagulation: a comprehensive comparison of aluminum and iron electrode. Sep. Purif. Technol., 66: 159-166.

Nature Environment and Pollution Technology
An International Quarterly Scientific Journal

p-ISSN: 0972-6268
(Print copies up to 2016)
e-ISSN: 2395-3454

Vol. 23 | No. 3 | pp. 1471-1482 | 2024

Original Research Paper

https://doi.org/10.46488/NEPT.2024.v23i03.017

Open Access Journal

# Nitrogen Nutrition-Induced Changes in Macronutrient Content and Their Indirect Effect on N-Metabolism Via an Impact on Key N-Assimilating Enzymes in Bread Wheat (*Triticum aestivum* L.)

**Vandna*, Vasundhara Sharma**, Kalidindi Usha****, Dalveer Singh***, Ranjan Gupta*, V. K. Gupta* and Bhupinder Singh****†**

*Department of Biochemistry, Kurukshetra University, Kurukshetra, Haryana, India
**Department of Plant Physiology, ICAR-National Research Centre on Seed Spices (NRCSS), Ajmer, Rajasthan, India
***Division of Plant Physiology, ICAR-Indian Agricultural Research Institute (IARI), New Delhi, India
****Division of Environment Science, ICAR-Indian Agricultural Research Institute (IARI), New Delhi, India
†Corresponding author: Bhupinder Singh; bhupindersinghiari@yahoo.com

**Nat. Env. & Poll. Tech.**
**Website: www.neptjournal.com**

*Received:* 22-12-2023
*Revised:* 02-02-2024
*Accepted:* 14-02-2024

**Key Words:**
Nitrogen deficiency
N-metabolism
N-Assimilating enzymes
*Triticum aestivum* L.

## ABSTRACT

Judicious application of nitrogen (N) fertilizers in crop production is critical for reducing the nitrate pollution of groundwater and greenhouse gas emissions. It is, thus, important to improve the nitrogen use efficiency under the reduced application of nitrogen. A genotypic variation in N-uptake and N-use efficiency particularly under low N-input conditions exists across crops that can be deciphered and exploited for environmentally sustainable farming without any significant penalty of yield and quality. The present research conducted under the nutrient solution culture aimed to explore the inherent variability in the growth response of ten genetically diverse wheat varieties to low fertilizer N-application (N-, 10 µM N) in comparison to N sufficient control (N+, 8.5 mM N) viz., a viz., the activity of various key N-assimilating enzymes and to delineate the indirect effect of low N on uptake and partitioning of other major macronutrients viz., P, K, S, which may indirectly regulate the N-use efficiency. A notable increase in sulfur, potassium, and phosphorus content was observed under nitrogen-deficient conditions. Varieties such as Carnamah and HD 2824 exhibit a significant increase in shoot phosphorus content, emphasizing their potential to optimize phosphorus acquisition and utilization efficiency under nutrient-limited conditions. The findings highlight the complex interplay between nutrient availability and plant responses, showcasing varietal-specific adaptations to nitrogen limitations.

## INTRODUCTION

Wheat, a cornerstone of global agriculture, is more than just a cereal crop; it's a primary source of sustenance, providing over 20% of the world's consumed calories (Giraldo et al. 2019). As we stand on the cusp of a global population surge, with projections soaring beyond 9 billion by 2050 (Dutia 2014), the demand for food is primed for a substantial upswing. To meet this burgeoning need, wheat production must surge by approximately 20% annually, an imperative recognized long ago, yet historical trends have shown a mere 0.9% annual increase (Ramadas et al. 2020). Nitrogen (N), a linchpin of plant physiology, is an elemental cornerstone found in an array of secondary metabolites within plants, including coenzymes, nucleic acids, amino acids, and proteins. Its multifaceted role extends beyond mere sustenance, as it orchestrates the very essence of growth and development in all plant species. Within the world of wheat, nitrogen takes center stage, profoundly influencing crop growth, yield, and nutritional composition. Effective nitrogen utilization is not only crucial for agricultural economics but also a matter of paramount importance, given that nitrogen ranks among the scarcest of plant nutrients in numerous agricultural regions worldwide. The dynamic nature of nitrogen, coupled with its propensity to escape through intricate plant-soil interactions, presents challenges in its effective regulation (Ladha et al. 2022). The insufficiency of essential nutrients in the soils of agricultural lands impedes optimal plant yield (Sandhu et al. 2021). Fertilizer application rates, notably nitrogen, directly impact crop production pace, yet excessive inputs may lead to poor nutrient use efficiency due to runoff water, where fertilizer inputs exceed crop requirements (Singh & Craswell 2021, Govindasamy et al. 2023). Paradoxically, certain agricultural fields grapple

with severe nutrient deficiencies, which detrimentally affect agricultural productivity (Hirel et al. 2011a).

In the Indian context, nitrogen assumes paramount importance as the most deficient macronutrient in soil, prompting farmers to apply elevated doses of external nitrogen to maximize crop productivity. This practice, while aiming to augment yield and returns, also precipitates environmental pollution, underscoring the need for judicious nitrogen fertilizer application (Paramesh et al. 2023). Historically, crop genetic improvement has yielded substantial increases in crop yields, contributing 50% to 60% of the overall growth. Simultaneously, the deployment of synthetic nitrogen (N), phosphorus (P), and potassium (K) fertilizers has substantially boosted yields. In crops like maize, high fertilizer usage has coincided with the selection of high-yielding genotypes tolerant of high seed density and receptive to increased N fertilizer inputs (Yin et al. 2018, Asibi et al. 2019, Gheith et al. 2022). However, the unbridled escalation of applied nitrogen may not necessarily result in enhanced yields. Instead, it raises concerns about environmental repercussions, including water pollution, greenhouse gas emissions, and soil degradation (Zhang et al. 2012, Nair 2021, Wang et al. 2021, Yadav et al. 2023). Consequently, the need to simultaneously elevate yields while moderating, or ideally decreasing, applied nitrogen becomes apparent, to optimize Nitrogen Use Efficiency (NUE) (Anas et al. 2020, Yan et al. 2020). The pivotal role of nitrogen in wheat goes beyond its direct influence on growth and yield; it is intricately woven into the biochemical processes that govern nutrient uptake and utilization. In wheat plants, nitrogen uptake typically occurs in the form of nitrate, subsequently reduced to nitrite by nitrate reductase (NR), further transformed into ammonium by nitrite reductase (NiR), and eventually converted into glutamine through the catalysis of glutamine synthetase/glutamate synthase (GS/GOGAT) and glutamate dehydrogenase (GDH). These biochemical reactions lay the foundation for amino acid production, an essential aspect of nitrogen metabolism. The activity of these enzymes is highly sensitive to nitrogen availability, with low nitrogen stress exerting a profound influence.

Within this intricate nitrogen assimilation network, glutamine synthetase (GS) emerges as a central player (Habash et al. 2001) and may be used as a marker for selecting genotypes with heightened NUE (Sharma et al. 2023). Similarly, glutamate synthase (GOGAT), with its two isoforms (NADH-GOGAT and Fd-GOGAT), assumes a vital role in photosynthetic tissues, recapturing ammonia released during photorespiration or senescence processes (Zhou et al. 2018, Sharma et al. 2023). The role of glutamate dehydrogenase (GDH), while still debated, remains pivotal in either ammonia assimilation or carbon recycling (Cooper 2012). It is worth mentioning here that nitrogen assimilation and yield often hinge not on the level and activity of NR/NiR enzymes, but rather on GS, which occupies the intersection of carbon and nitrogen metabolic pathways. Nutritional and biochemical factors that directly or indirectly induce or regulate the GS activity may, thus, hold promise for potentially enhancing the NUE by fostering efficient nutrient recycling (Foulkes et al. 2009, Cooper 2012). NUE as such cannot be increased by adding more N-fertilizer and the continued careless application of N fertilizer shall have ecological repercussions, including water pollution, greenhouse gas emission, and soil degradation. It is, thus, important to understand the N-nutrition-mediated regulation of mineral nutrient status and decipher their direct and indirect effect on the activity of key N-assimilating enzymes in order to determine the principle regulators of NUE under low N availability conditions of crop growth. The present research endeavor, thus, aimed to unravel the complex nexus between nitrogen, the growth attributes of wheat, and the realm of macro-nutrient management, seeking sustainable practices that reconcile the dual objectives of crop productivity and environmental stewardship. By scrutinizing the impact of nitrogen deficiency on wheat at multiple levels - from macronutrient dynamics to the underlying biochemical processes - we aim to contribute vital insights for a more resilient and sustainable future in wheat agriculture.

## MATERIALS AND METHODS

### Planting Material and Experimental Conditions

Bread wheat varieties viz., Ajantha, Atilla-12, C 306, Carnamah, HD 2824, KYPO 328, PBW 502, Stilleto, Turaco, and UP 2338 were procured from the Division of Genetics, ICAR-Indian Agricultural Research Institute, New Delhi and were raised under hydroponic condition, according to Sathee et al. (2018). For this, the wheat grains were rinsed twice with distilled water before being surface sterilized for 5 minutes with 0.1% mercuric chloride ($HgCl_2$). Grains were properly washed five to six times with double distilled water to eliminate any trace of $HgCl_2$. After 5-6 days of germination in petri plates lined with moist germination paper, uniform healthy wheat seedlings were selected and transplanted into plastic tanks containing 15 L Hoagland solution(Hoagland & Arnon 1950), at two levels of nitrogen (N) i.e., sufficient nitrogen control (SN, 8.5mM N) and N deficiency (LN, 10 µM N) under continuous aeration. To maintain a balanced nutrient availability during the growth period, the nutrient solution was replaced every 3 days up to 25 days after the transfer of seedlings to the nutrient solution culture, after which the experiment was terminated and observations

were taken. For each treatment, three independent biological replications were maintained, and all observations were recorded in triplicate.

### Variation in Growth Response of Wheat Varieties to Sufficient (SN) and Low N (LN) Input Condition

**Shoot and root biomass:** Shoot and root biomass (g dw plant$^{-1}$) was determined at 25 days after germination (DAG), after dissecting the respective N-treatment seedlings into the root and shoot tissues and drying them in hot air over for a few days until constant weights were obtained.

### Variation in Macronutrient Acquisition in Wheat Varieties under Sufficient (SN) and Low N (LN) Input Condition

**Shoot and root nitrogen (N):** Total nitrogen (N) in the plant samples was determined using Kjeldahl's method (Jones et al. 1987). The method involved the digestion of pre-weighed shoot and root samples to convert organic and inorganic nitrogen compounds into ammonium ions which are subsequently quantified through titration.

**Shoot and root phosphorus (P), potassium (K) and sulfur (S):** A 100 mg dried shoot and root samples were digested in a 50 mL volumetric flask using 10 mL of di-acid mixture i.e., concentrated nitric acid and concentrated perchloric acid (10:3) pre-digested overnight. The pre-digested mixture was further digested on a hot plate, maintained at a temperature of 200-250°C for a minimum of 2 hours. The transition of the mixture from opaque to clear indicated the complete digestion of the organic matter. Subsequently, the mixture was allowed to cool to room temperature and was then adjusted to a final volume of 50 mL using double distilled water. The solution was then filtered using quantitative ashless filter paper (Whatman no. 42) and preserved for subsequent analysis. This resulting solution was suitable for a variety of analytical techniques. Phosphorus (P) levels in the samples were assessed using the ascorbic acid method (Murphy & Riley 1962) on a UV-Vis spectrophotometer (ECIL, India), while K was analyzed using a microcontroller based Flame photometer (Systronics India Ltd, India). The sulfur content was determined using the turbidity method described by Skwierawska et al. (2016).

### Variation in Activity of Key Enzymes of N-Assimilating Pathway in Wheat Varieties under Sufficient (SN) and Low N (LN) Input Condition

**Enzyme extraction:** Extraction of enzymes and assays of GS, GOGAT, and GDH were done following the method of Mohanty & Fletcher (1980). Leaf samples were extracted in Tris-HCl buffer, which contained 100 mM Tris-HCl, 100 mM sucrose, 10 mM EDTA and 10 mM $MgCl_2$. Tissue samples were ground in a chilled pestle and mortar with an extraction buffer. Ground samples were centrifuged at 5,000 rpm for 10 min at 4°C. The supernatant was collected and re-centrifuged at 12,000 rpm for 15 min at 40°C. The supernatant was collected in separate Eppendorf tubes and used for the estimation of GS and GOGAT. The pellet was dissolved in 1 mL of 50 mM phosphate buffer with 2.14 g.100 mL$^{-1}$ sucrose with pH 7.5 and was used for estimation of GDH.

**Leaf nitrate reductase (NR) activity:** Estimation of *in vivo* nitrate reductase activity was done by estimating nitrite formed by the enzyme action, which was then diazotized using sulphanilamide in an acidic medium and NEDD using the method of Klepper et al. (1971) and modified by Nair & Abrol (1973). Nitrite was estimated by the method of Evans & Nason (1953), Xu et al. (2000) and Sun et al. (2003). The leaves and roots were cut into 2 mm pieces and after thorough mixing of the leaf samples, 0.3 g was weighed and added to ice cold incubation medium containing 3 mL each of phosphate buffer (0.2 M, pH 7.5) and potassium nitrate solution (0.4 M). To it, 0.2 mL of n-propanol was added. The leaf samples were infiltrated with the solution using a vacuum pump and then incubated in a water bath at 30°C for 30 minutes under dark conditions. At the end of the incubation period, tubes were placed in a water bath (70-80°C) for 3-4 minutes to stop the enzyme activity and for the complete leaching of the nitrite into the medium. The nitrite was then estimated by taking an adequate amount of aliquot in a test tube followed by the addition of 1 mL of sulphanilamide (1% in 1 N HCl). After mixing, 1 mL NEDD (0.02%) was added and again mixed well. The pink colour was formed immediately and after 20 minutes the total volume was made up to 3 mL with double distilled water. Absorbance was measured using a UV-visible spectrophotometer (model Specord Bio-200, Analytik Jena, Germany) at 540 nm. The calibration curve was prepared using a standard sodium nitrite solution. The enzyme activity was expressed as μmol nitrite formed g$^{-1}$ DW h$^{-1}$.

**Leaf glutamine synthetase (GS) activity:** Estimation of GS activity was done by measuring the γ-glutamylhydroxamate formed. All the reagents viz., 0.35 mL of 200 mM Tris buffer, 0.25 mL of 200 mM $MgSO_4$, 0.1 mL of 50 mM cysteine, 0.25 mL of 500 mM α-glutamate, 0.1 mL of 50mM ATP, and 0.25 mL of 40 mM hydroxylamine were pipetted out along with 0.2 mL of aliquot and kept at 37°C for 30 min. To stop the reaction 0.5 mL $FeCl_3$ reagent was added and then centrifuged (sigma 3K30) at 1500-2000 rpm for 10 min. Absorbance was measured using a UV-visible spectrophotometer (Specord Bio-200, Analytik Jena, Germany). The

enzyme activity was expressed as γ-glutamylhydroxamate formed $g^{-1}$ protein $h^{-1}$.

**Leaf glutamate synthase (GOGAT) activity:** Estimation of GOGAT activity was done by measuring the NADH oxidization. All the reagents viz., 1 mL of 75 mM Tris-HCl, 0.2 mL of 50 mM α-ketoglutaric acid, and 0.2 mL of 200 mM L-glutamine were pipetted out with 0.1 mL of aliquot and volume made to 2.8 mL with double distilled water. To it, 0.2 mL of 1.5 mM of NADH was added into a cuvette with a reaction mixture just before taking absorbance reading mixed well and absorbance was measured using a UV-visible spectrophotometer (Specord Bio-200, AnalytikJena, Germany) at 340 nm for 60 second. The enzyme activity was expressed as µmol NADH oxidized $g^{-1}$ protein $h^{-1}$.

**Leaf glutamate dehydrogenase (GDH) activity:** All the reagents viz., 1 mL of 75 mM phosphate buffer, 0.2 mL of 100 mM α-ketoglutaric acid, and 0.4 mL of 750 mM $NH_4Cl$ were pipetted out with 0.2 mL of aliquot and volume made to 2.8 mL with double distilled water. To it, 0.1 mL of 1.5 mM of NADH was added into a cuvette with a reaction mixture just before taking absorbance reading mixed well and absorbance was measured using a UV-visible spectrophotometer (Specord Bio-200, AnalytikJena, Germany) at 340 nm for 60 second. The enzyme activity was expressed as µmol NADH oxidized $g^{-1}$ protein $h^{-1}$.

**Leaf alanine aminotransferase (AlaAT) activity:** AlaAT activities were determined using the spectrophotometric method based on the procedure outlined by De Sousa & Sodek 2003. For AlaAT activity, the assay was conducted in the direction of alanine to pyruvate conversion, coupled with the oxidation of NADH by lactate dehydrogenase. The reaction mixture (1.5 mL) contained 0.1 M Tris–HCl buffer at pH 7.5, 0.5 M L-alanine, 15 mM 2-oxoglutaric acid, 0.18 mM NADH, 5 units of lactate dehydrogenase, and the enzyme extract. The reactions were carried out at 30°C, and the oxidation of NADH was continuously monitored at 340 nm. The activities of AlaAT were calculated using the absorption coefficient for NADH (e = 6.22 $mM^{-1}$ $cm^{-1}$) and expressed in units, with each unit representing the amount of enzyme capable of catalyzing the formation of 1 nmol of product per minute.

**Statistical analysis:** Statistical analysis and graphical representation were carried out utilizing SPSS V26 and GraphPad Prism version 9.1 (La Jolla, California, USA) respectively. The statistical analysis involved the execution of a one-way analysis of variance (ANOVA) to compute adjusted P values, thereby establishing the significance level. To discern differences in means, Tukey's multiple comparisons test was applied.

## RESULTS AND DISCUSSION

### Growth Response of Wheat Varieties to Low Nitrogen Stress

**Shoot and root biomass:** Significantly higher shoot biomass was observed under sufficient nitrogen (SN) than low nitrogen (LN) conditions, while a reverse trend was observed for the root biomass which was distinctly higher under LN than SN treatment across all the ten experimental bread wheat varieties (Fig. 1, Table 1). The range of variation for the shoot, and root biomass under the SN and LN treatment was 0.18-0.29, 0.08-0.13, and 0.12-0.15, 0.18-0.28 g.$plant^{-1}$ respectively with an average value of 0.242, 0.123 and 0.15, 0.232 g $plant^{-1}$ under SN and LN treatments. The results reveal that LN is being perceived as a nutrient stress which gets reflected in the higher root growth across the varieties under N stress than N-sufficient control.

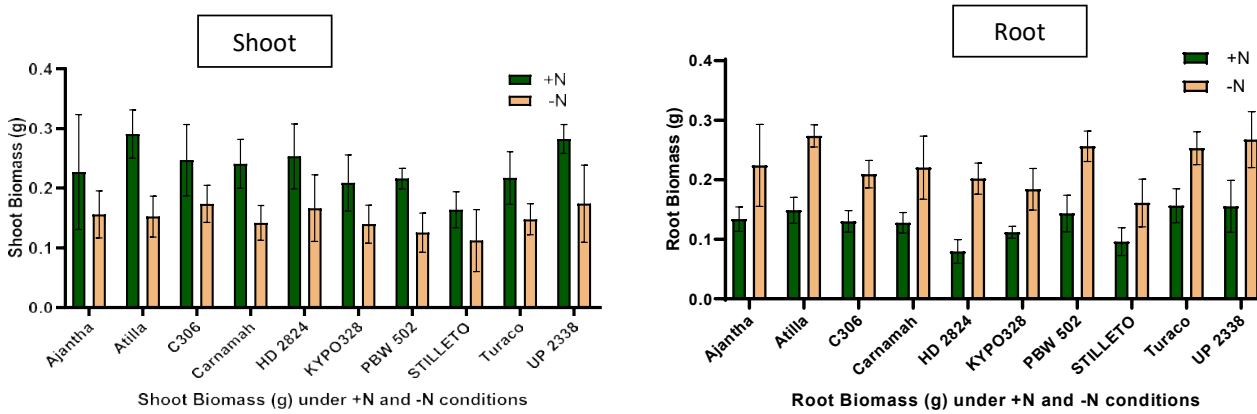


Fig. 1: Shoot and Root biomass of 25 days old seedlings of bread wheat varieties raised under sufficient (N+) and low N (N-) conditions in nutrient solution culture.

Table 1: Shoot and Root biomass of 25 days old seedlings of bread wheat varieties raised under sufficient (N+) and low N (N-) conditions in nutrient solution culture (SN: Sufficient Nitrogen; LN: Low Nitrogen).

| Varieties | Shoot Biomass | | Root Biomass | | Total Biomass | |
|---|---|---|---|---|---|---|
| | SN | LN | SN | LN | SN | LN |
| Ajantha | 0.227 | 0.156 | 0.122 | 0.224 | 0.349 | 0.38 |
| Atilla | 0.290 | 0.153 | 0.149 | 0.273 | 0.439 | 0.426 |
| C306 | 0.247 | 0.174 | 0.130 | 0.209 | 0.377 | 0.383 |
| Carnamah | 0.241 | 0.142 | 0.128 | 0.221 | 0.369 | 0.363 |
| HD 2824 | 0.253 | 0.166 | 0.079 | 0.202 | 0.332 | 0.368 |
| KYPO 328 | 0.209 | 0.139 | 0.112 | 0.184 | 0.321 | 0.323 |
| PBW 502 | 0.216 | 0.125 | 0.143 | 0.246 | 0.359 | 0.371 |
| Stilleto | 0.164 | 0.112 | 0.096 | 0.161 | 0.26 | 0.273 |
| Turaco | 0.223 | 0.151 | 0.160 | 0.256 | 0.383 | 0.407 |
| UP 2338 | 0.282 | 0.174 | 0.156 | 0.301 | 0.438 | 0.475 |

## Macronutrient Profile of Bread Wheat Varieties under Low N Stress

**Shoot and root nitrogen:** In general, under nitrogen deficiency (LN, N-), wheat varieties exhibited a significant decline in the shoot nitrogen content, with a few exceptions (Fig. 2). Bread wheat variety Ajantha showed a 34.6% increase in leaf N under N- than N+ treatment. The inhibitory effect of low N availability on root growth was more pronounced than that observed for the shoot growth when compared with the sufficient N control (N+). Shoot N, in general, varied from 2.87 to 6.37%, while the root N content ranged from 1.55 to 4.46% under the N-sufficient (SN, N+) condition. On the other hand, under low nitrogen (LN, N-) conditions, both shoot and root nitrogen decreased significantly over N+ treatment, with a range of 2.63 to 4.42% for shoot N and 0.89 to 2.56%. The mean N content of shoot, and root under SN and LN treatments, averaged over the experimental bread wheat varieties was 4.28, 3.07, and 3.45, 1.64% respectively. In bread wheat var. Ajantha, in contrast to the observed low N mediated shoot growth induction, almost 70.5% decline in root growth was measured, when compared with N+ treatment. The results indicate the low N stress tolerance and an efficient N-uptake and N-translocation characteristic of var. Ajantha than the other experimental varieties.

Indeed, N deficiency typically triggers various adaptive mechanisms in plants, including enhanced uptake of other essential nutrients like P, K, and S, as observed in our study. This upregulation helps maintain cellular homeostasis and metabolic functions under stress (Amtmann & Hermans 2006, Hawkesford et al. 2012). However, the observation of higher leaf N content in Ajantha and UP 2338 under N-deficient conditions (Fig 2) can be due to the following reasons:

**Enhanced N acquisition efficiency:** These genotypes might possess a more efficient system for N uptake and utilization, even under N deficiency. This could involve improved root architecture, enhanced transporter activity, or better internal N mobilization mechanisms (Garnett et al. 2009, Sinclair & Gorissen 2009). For example, studies have shown that wheat genotypes with longer and denser root systems exhibit higher N uptake efficiency under limited N availability (Balemi et al. 2019).

**Differential N allocation:** While overall N uptake might be similar, these genotypes might prioritize allocation to leaves, maintaining higher N content for critical metabolic processes even under stress. This could involve altered signaling pathways or regulatory mechanisms governing N distribution within the plant (Xu et al. 2012, Hirel et al. 2011b). For instance, research suggests that certain wheat varieties preferentially allocate N to leaves under N deficiency to maintain photosynthetic capacity, potentially contributing to improved stress tolerance (Zheng et al. 2020).

**Alternative N sources:** Exploring potential contributions from atmospheric N fixation or N scavenging from organic matter in the soil could provide additional insights into the observed discrepancy. While not as common in wheat as in legumes, some genotypes exhibit inducible atmospheric N fixation capabilities under N stress (Kennedy & Roughley 2000). Additionally, efficient utilization of soil organic N through enhanced mineralization or root-microbial interactions could contribute to higher leaf N content (He et al. 2020).

**Shoot and root phosphorus (P):** The phosphorous content of shoot and root, under sufficient nitrogen (N+) conditions (Fig. 3), ranged from 1.22 to 3.53 ppm, and 1.71 to 4.66 ppm. However, under the low nitrogen (N-) condition, a significant increase in both shoot and root P was observed across the

experimental wheat varieties. The range of variation in shoot and root P under N- treatment was 4.72 to 15.20 ppm and 6.52 ppm to 10.57 ppm. The mean P content of shoot, and root under SN and LN treatments, averaged over the experimental bread wheat varieties was 2.02, 2.99, and 9.86, 7.86 ppm respectively. A similar synergistic effect of P availability on N-metabolism of wheat including the expression of the N transport genes and enhanced activity of key N-assimilating enzymes (NR, GS, GDH, and GOGAT) has been recently reported by Li et al. (2023).

**Shoot and root potassium (K):** When subjected to nitrogen deficiency (LN, N-), a significant increase in the shoot K content of the wheat varieties was evidenced (Fig. 3). Under sufficient nitrogen (SN, N+) conditions, the shoot K ranged from 19.28 to 56.87 ppm, while the root K varied between 7.33 to 15.32 ppm. However, under low nitrogen (LN, N-) conditions, both shoot and root K increased significantly exhibiting a range variation of 79.99 to 115.88 ppm and 24.53 to 45.83 ppm respectively in the shoot and the root tissues of N-stressed (N-) plants. An increase in K application was reported to facilitate the uptake and transport of nitrate and also enhance the activity of N- assimilating enzymes in Spinach (Anjana & Iqbal 2009), while a reduced K was shown to impair the N- metabolism in sweet potato (Liu et al. 2022).

**Shoot and root sulfur (S):** In general, the shoot S content was significantly higher than root S under both N+ and N- conditions across the wheat varieties (Fig. 3). When compared between the N treatments, the tissue S content was found to be significantly higher under the N- than N+ condition of growth. The mean sulfur content across varieties varied significantly in a range from 18.78 to 33.85 ppm under sufficient nitrogen (SN, N+), while under N- treatment, the range of variation for shoot S was 26.46 to 49.65 ppm. In the case of root, the sulfur content under N+ and N- treatment varied between 4.93 to 14.93 ppm and 8.28 to 22.89 ppm respectively. The average shoot S content, across varieties, showed a significant increase from 27.34 under sufficient N to 38.65 ppm under low N stress. A similar pattern of increase in root S between N+ (10.25 ppm) and N- (15.66 ppm) was also recorded. Further, under nitrogen deficiency (N-), wheat varieties viz., Ajantha, Atilla, and Carnamah, demonstrated a heightened sulfur (S) uptake response in the shoot tissues. The above varieties, in general, also showed an increase in root S under low N (N-) than sufficient N (N+) treatment (Fig. 3). A lower content of S in the root than the shoot under N- over N+ treatment indicates a surge in root to shoot S-translocation, which may be a low N stress adaptation strategy. The findings highlight the nuanced changes in the sulfur content of wheat plants by nitrogen and thus, indicate an intricate interplay and influence of N and S metabolism on each other. Significant interaction between N and S on growth nutritional components and secondary metabolites (Jian et al. 2021) has been reported.

## Activity of N-Assimilating Enzymes under Low N Stress

This study focused on evaluating the activity of key N-assimilating enzymes viz., glutamine synthetase (GS), glutamate synthase (GOGAT), nitrate reductase

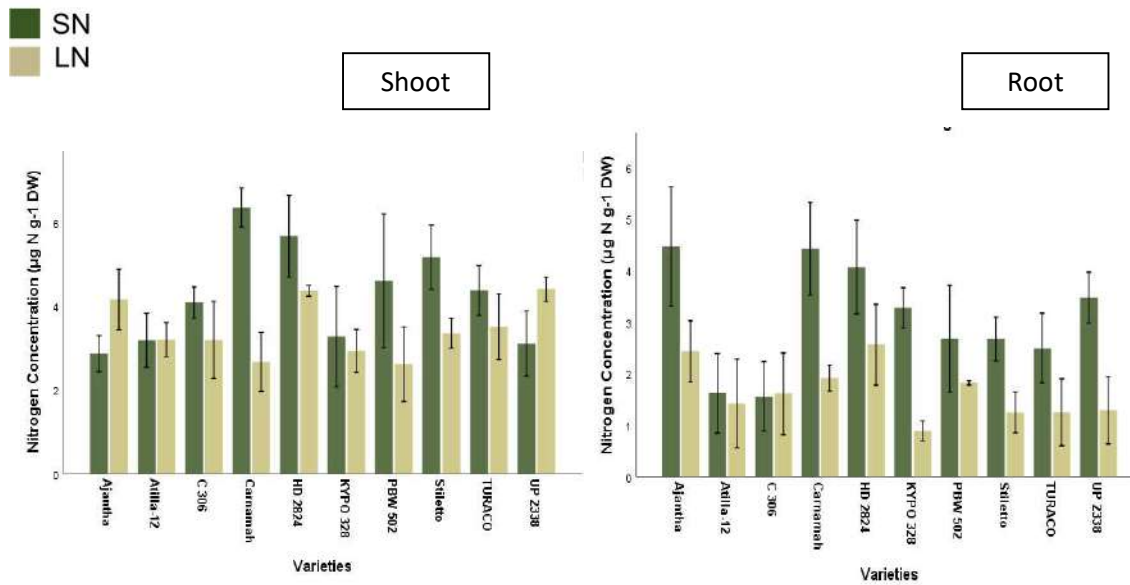


Fig. 2: Shoot and root nitrogen content of diverse wheat varieties under N-sufficient and N-deficient conditions of growth in nutrient solution culture.

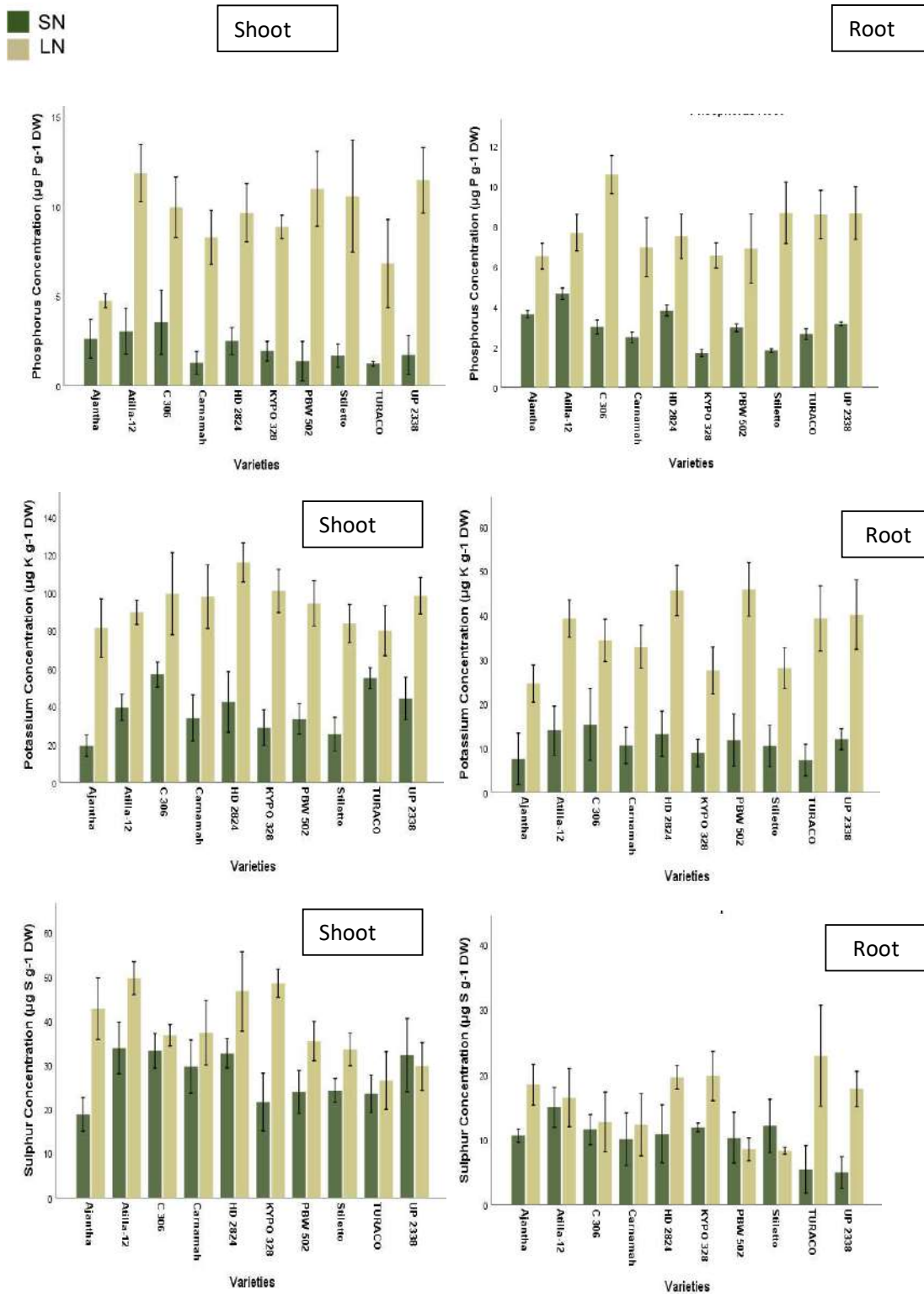


Fig. 3: Shoot and root phosphorus, potassium, and sulfur content of diverse wheat varieties under N-sufficient (SN) and N-deficient (LN) conditions of growth in nutrient solution culture.

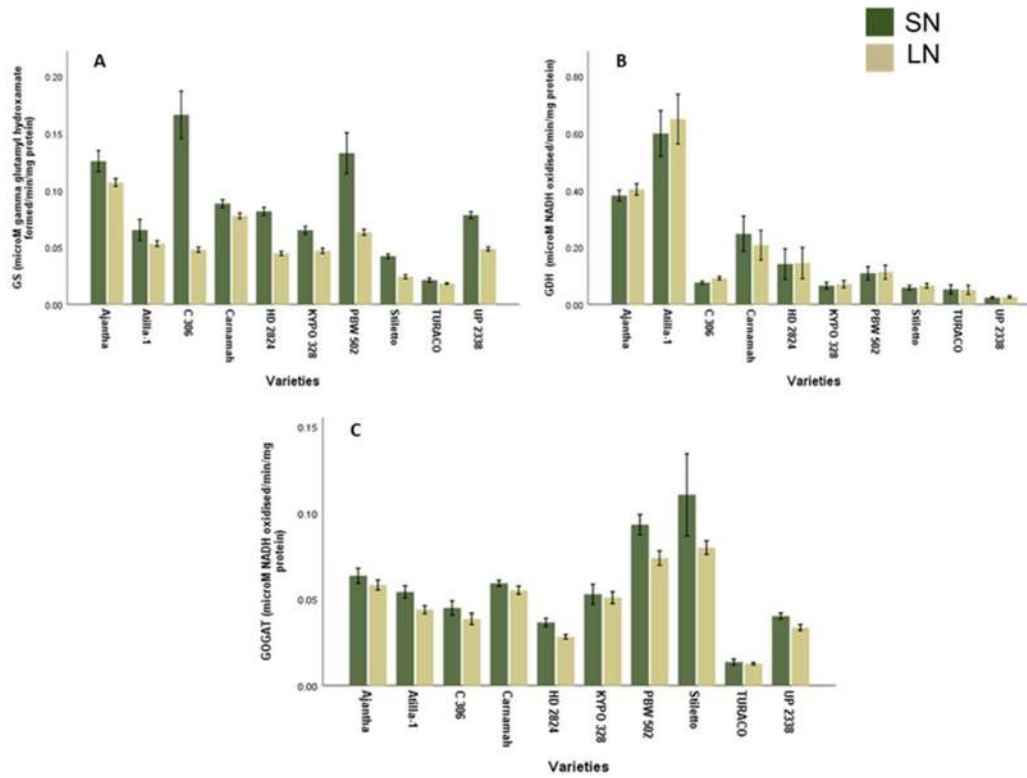


Fig. 4: Effect of N-stress on the activity of key N-assimilating enzymes viz., A) Glutamine synthetase (GS); B) Glutamate dehydrogenase (GDH); and C) Glutamate synthase (GOGAT) in wheat.

(NR), glutamate dehydrogenase (GDH), and alanine aminotransferase (AlaAT) as affected by nitrogen availability in bread wheat.

**Glutamine synthetase (GS) activity:** The glutamine synthetase (GS) activity varied between 0.021 to 0.166 and 0.018 to 0.107 µmol γ-glutamylhydroxamate formed per gram of protein per hour respectively under N+ and N- treatments. A decline in GS activity was recorded under N- over N+ condition (Fig. 4A). Mean GS activity averaged over the experimental wheat varieties, decreased significantly from 0.087 to 0.053 µmol γ-glutamylhydroxamate formed per gram of protein per hour under low nitrogen (N-) than N+ condition of growth. In general, three varieties i.e., Ajantha, Carnamah, and UP 2338 showed a relatively lesser decline in GS activity, also the bread wheat var. Turaco showed the least GS activity under the N- treatment.

**Glutamate dehydrogenase (GDH) activity:** In general, the GDH activity was not profusely affected by the N availability condition (Fig. 4B). In contrast to GOGAT, an increase in the GDH activity was recorded under the N-stress (0.183 µmol NADH oxidized per gram of protein per hour) when compared the N+ (0.176 µmol NADH oxidized per gram of protein per hour) treatment. The mean GDH activity, across the wheat varieties, varied from 0.024 to 0.600 and 0.026 to 0.650 µmol NADH oxidized per gram of protein per hour under the N+ and the N- treatment respectively. Bread wheat variety Atilla followed by Ajantha showed higher GDH activities, while the least activities across the N-treatments were observed for var., UP 2338.

**Glutamate synthase (GOGAT) activity:** A general decline in GOGAT activity under N- than N+ treatment was recorded (Fig. 4C). The GOGAT activity for the wheat varieties ranged between 0.014 to 0.111 and 0.013 to 0.080 µmol NADH oxidized per gram of protein per hour, respectively under the N+ and the N- treatment. For GOGAT, the average activity decreased from 0.057 to 0.048 µmol NADH oxidized per gram of protein per hour under N-stress. Another variety Turaco though showed the least GOGAT activity under the N-sufficient (N+) treatment, it did not decline under the low N (N-) input condition.

**Nitrate reductase (NR) activity:** A significant reduction in NR activity under the N- than compared with the N+ treatment was observed (Fig. 5A). The nitrate reductase (NR) activity, varied between 16.12 to 32.29 and 1.46 to 15.84 µmol nitrite formed per gram dw per hour respectively under the N+ and the N- condition of growth. A relatively

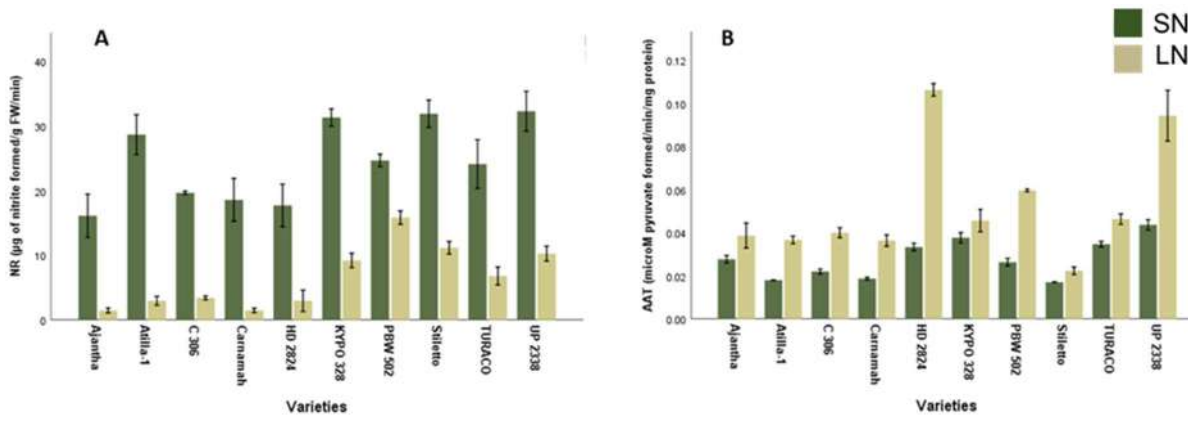


Fig. 5: Effect of N-stress on the activity of A) Nitrate reductase (NR) and B) Alanine aminotransferase (AlaAT) in wheat.

lower decline in the NR activity under the N- over the N+ treatment was recorded for var., PBW 502. Mean NR activity, averaged over the experimental varieties, under the N+ and the N- treatments was 24.51 and 6.55 µmol nitrite formed per gram dw per hour respectively.

**Alanine aminotransferase (AlaAT) activity:** Contrary to NR activity, the AlaAT activity across the bread wheat varieties was significantly induced under the N- than N+ treatment. Alanine Aminotransferase (AlaAT) activity, across varieties, varied from 0.017 to 0.044 and 0.022 to 0.106 µmol pyruvate formed per minute per mg protein under the N+ and the N- treatments respectively (Fig. 5B). Mean AlaAT activity, averaged over experimental varieties, increased from 0.028 (N+) to 0.053 µmol pyruvate formed per minute per mg protein under the N stress condition. A significantly higher N-stress-induced increase in AlaAT activity was recorded for var. HD 2824 and UP 2338 when compared to their respective enzyme activities under the N+ treatment.

Several studies have established the crucial role of macronutrients in influencing nitrogen (N) assimilation, particularly under N-deficient conditions. Anjana & Iqbal (2009) observed a significant decrease in glutamine synthetase (GS) activity, a key N-assimilating enzyme, in wheat experiencing combined S and N deficiency. Similarly, Jian et al. (2021) reported that co-limiting S and P in wheat significantly reduced both GS and glutamate dehydrogenase (GDH) activity, hindering N assimilation. Further emphasizing the interconnectedness of macronutrients, Liu et al. (2022) found that K deficiency under low N conditions further exacerbated the decrease in GS and GDH activity, highlighting the importance of balanced macronutrient availability for optimal N metabolism.

This current study builds upon this knowledge by demonstrating that supplementing S, P, and K under low N input (N-) can indirectly regulate N metabolism in wheat. Notably, this study observed an increase in the activity of N-assimilating enzymes in wheat plants receiving increased S, P, and K nutrition under N-deficient conditions. This enhanced enzyme activity is potentially linked to improved low N stress tolerance, as evidenced by Table 2.

Delving deeper into the mechanisms underlying this dependence holds immense potential for improving crop performance under N-limited conditions. Future research should focus on elucidating the specific roles of these macronutrients in enzyme synthesis, stability, and activity regulation. Additionally, investigating the species-specificity of these dependencies and exploring breeding strategies for enhanced N-assimilation efficiency and low N stress tolerance across various crops can significantly contribute to sustainable agriculture. Optimizing N use efficiency through balanced macronutrient management not only improves crop productivity but also minimizes environmental pollution associated with excessive N fertilizer application.

Table 2: Summary table showing an interactive effect of N-nutrition on macronutrients and activity of key N-assimilating enzymes in wheat. Upward and downward arrows indicate an increased and decreased activity for the observed parameter.

| Nutrient | Shoot | Root |
|---|---|---|
| Nitrogen | Low ↓ | Low ↓ |
| Sulfur | High ↑ | High ↑ |
| Potassium | High ↑ | High ↑ |
| Phosphorus | High ↑ | High ↑ |
| N-assimilating enzymes | Shoot | |
| Glutamine synthetase | Low ↓ | |
| Glutamate synthase | Low ↓ | |
| Glutamate dehydrogenase | Low ↓ | |
| Nitrate reductase | Low ↓ | |
| Alanine aminotransferase | High ↑ | |

Table 3: Relationship between the macronutrient content of wheat with the activities of key N-assimilating enzymes under the low N input condition (N-).

| Parameter | GS | GOGAT | GDH | AlaAT | NR | Nitrogen | Phosphorus | Potassium | Sulfur |
|---|---|---|---|---|---|---|---|---|---|
| GS | 1 | 0.331 | 0.483** | -0.083 | -0.385* | 0.320 | -0.535** | -0.162 | 0.226 |
| GOGAT | | 1 | 0.088 | -0.460* | 0.389* | -0.271 | -0.184 | -0.318 | -0.296 |
| GDH | | | 1 | -0.280 | -0.514** | 0.133 | -0.166 | -0.200 | 0.502** |
| AlaAT | | | | 1 | 0.101 | 0.550** | 0.498** | 0.767** | 0.180 |
| NR | | | | | 1 | -0.407* | 0.149 | 0.060 | -0.476** |
| Nitrogen | | | | | | 1 | 0.136 | 0.217 | 0.265 |
| Phosphorus | | | | | | | 1 | 0.673** | -0.058 |
| Potassium | | | | | | | | 1 | 0.177 |
| Sulfur | | | | | | | | | 1 |

*Correlation is significant at the 0.05 level (2-tailed). **Correlation is significant at the 0.01 level (2-tailed).

Further, the Pearson correlation analysis was performed to study the association between different macronutrients (N, P, K, and S) and nitrogen-related enzymes (GS, GOGAT, GDH, AlaAT and NR) under nitrogen deficit (N-) conditions. A significant positive correlation of AlaAT activity with nitrogen (r=0.550**) phosphorus (r=0.498**) and potassium (r=0.767**) nutrition of wheat was recorded (Table 3). Further, a significant positive correlation between the GS and the GDH activity (r=0.483**), but a negative correlation between the NR and the GDH activity (r=0.514**) and between S and GDH (r=0.502**) were observed. NR activity showed a significant negative correlation with sulfur (r=0.476*).

The observed variations in sulfur, phosphorus, potassium, and nitrogen content in both shoot and root tissues shed light on the complex interplay between nutrient availability and plant responses. The significant increase in sulfur content in the shoot tissues under nitrogen-deficient conditions aligns with previous studies emphasizing the role of sulfur in enhancing plant tolerance to abiotic stresses (Hasanuzzaman et al. 2018). A coordinated mediation between sulfur and nitrogen metabolism under salt stress has been reported (Jahan et al. 2021). The notable increase in shoot and root potassium content under nitrogen-deficient conditions is in agreement with previous research highlighting the role of potassium in enhancing plant osmoregulation and stress tolerance (Nieves-Cordones et al. 2016, Shabala 2017). The observed genotypic variation in macronutrients may be attributed to differences in nutrient uptake and utilization efficiency (Wang et al. 2015). The substantial increase in shoot phosphorus content in response to nitrogen deficiency, as exemplified by var. Carnamah and HD 2824, reflect the significance of phosphorus in enhancing plant metabolic processes and stress adaptation.

## CONCLUSION

The observed variations in the activity of key enzymes such as glutamine synthetase (GS), nitrate reductase (NR), alanine aminotransferase (AlaAT), glutamate synthetase (GOGAT), and glutamate dehydrogenase (GDH) under nitrogen deficiency highlight the intricate regulation of nitrogen assimilation and amino acid metabolism in wheat. The ability of var. Turaco to maintain a similar level of GS activity under both the sufficient (N+) and the deficient N (N-) input/availability condition of growth, reflects upon its ability to tolerate low N stress. The trait can be introgressed into the high-yielding wheat varieties to improve their resilience against abiotic stresses. The findings further emphasize the importance of understanding the nuanced interplay between nitrogen availability, macronutrient uptake, and N-metabolism in wheat, and provide a foundation for targeted breeding and agronomic interventions aimed at enhancing the nutrient uptake efficiency and crop resilience in the face of changing environmental conditions. Understanding the nutrient interactions in controlled environments will further our knowledge and pave the way for developing more effective stress mitigation strategies for fortifying our quest for sustainable agriculture.

## ABBREVIATIONS

GS: Glutamine synthetase
GOGAT: Glutamate synthase
GDH: Glutamate dehydrogenase
AlaAT: alanine aminotransferase
NR: Nitrate reductase

## REFERENCES

Anjana, S. U. and Iqbal, M. 2009. Effect of applied potassium in increasing the potential for N assimilation in spinach (*Spinacea oleracea L.*). Electron. Int. Fertil. Corresp., 20: 8-10.

Anas, M., Liao, F., Verma, K. K., Sarwar, M. A., Mahmood, A., Chen, Z.-L., Li, Q., Zeng, X.-P., Liu, Y. and Li, Y. R. 2020. Fate of nitrogen in agriculture and environment: Agronomic, eco-physiological and molecular approaches to improve nitrogen use efficiency. Biol. Res., 53(1): 47. https://doi.org/10.1186/s40659-020-00312-4

Amtmann, A. and Hermans, C. 2006. Coping with manganese toxicity in plants: physiological and molecular mechanisms. Annu. Rev. Plant Biol., 57(1): 361-385.

Asibi, A. E., Chai, Q. and Coulter, J. A. 2019. Mechanisms of nitrogen use in maize. Agronomy, 9(12): 775. https://doi.org/10.3390/agronomy9120775

Balemi, T. H., Ghafourizadeh, S. and Sohrabi, Y. 2019. Root traits contributing to nitrogen use efficiency in wheat genotypes under water stress. J. Plant Physiol., 233: 154-162.

Cooper, A. J. L. 2012. The role of glutamine synthetase and glutamate dehydrogenase in cerebral ammonia homeostasis. Neurochem. Res., 37(11): 2439-2455. https://doi.org/10.1007/s11064-012-0803-4

De Sousa, C. A. F. and Sodek, L. 2003. Alanine metabolism and alanine aminotransferase activity in soybean (Glycine max) during hypoxia of the root system and subsequent return to normoxia. Environ. Exp. Bot., 50(1): 1-8. https://doi.org/10.1016/S0098-8472(02)00108-9

Dutia, S. 2014. AgTech: Challenges and opportunities for sustainable growth. SSRN Electron. J. https://doi.org/10.2139/ssrn.2431316

Evans, H. J. and Nason, A. 1953. Pyridine nucleotide-nitrate reductase from extracts of higher plants. Plant Physiol., 28(2): 233. https://doi.org/10.1104%2Fpp.28.2.233

Foulkes, M. J., Hawkesford, M. J., Barraclough, P. B., Holdsworth, M. J., Kerr, S., Kightley, S. and Shewry, P. R. 2009. Identifying traits to improve the nitrogen economy of wheat: Recent advances and future prospects. Field Crops Res., 114(3): 329-342.

Garnett, T. P., Brundle, M. J. and Kniemeyer, A. 2009. Enhanced root shoot communication in nitrogen starved plants. Plant Cell Environ., 32(4): 382-395.

Gheith, E. M. S., El-Badry, O. Z., Lamlom, S. F., Ali, H. M., Siddiqui, M. H., Ghareeb, R. Y., El-Sheikh, M. H., Jebril, J., Abdelsalam, N. R. and Kandil, E. E. 2022. Maize (*Zea mays* L.) productivity and nitrogen use efficiency in response to nitrogen application levels and time. Front. Plant Sci., 13, 941343. https://doi.org/10.3389/fpls.2022.941343

Giraldo, P., Benavente, E., Manzano-Agugliaro, F. and Gimenez, E. 2019. Worldwide research trends on wheat and barley: A bibliometric comparative analysis. Agronomy, 9(7): 352. https://doi.org/10.3390/agronomy9070352

Govindasamy, P., Muthusamy, S. K., Bagavathiannan, M., Mowrer, J., Jagannadham, P. T. K., Maity, A., Halli, H. M., G. K., S., Vadivel, R., T. K., D., Raj, R., Pooniya, V., Babu, S., Rathore, S. S., L., M. and Tiwari, G. 2023. Nitrogen use efficiency-A key to enhance crop productivity under a changing climate. Front. Plant Sci., 14, 1121073. https://doi.org/10.3389/fpls.2023.1121073

Habash, D. Z., Massiah, A. J., Rong, H. L., Wallsgrove, R. M. and Leigh, R. A. 2001. The role of cytosolic glutamine synthetase in wheat. Ann. Appl. Biol., 138(1): 83-89. https://doi.org/10.1111/j.1744-7348.2001.tb00087.x

Hasanuzzaman, M., Bhuyan, M. H. M. B., Mahmud, J. A., Nahar, K., Mohsin, S. M., Parvin, K. and Fujita, M. 2018. Interaction of sulfur with phytohormones and signaling molecules in conferring abiotic stress tolerance to plants. Plant Signal. Behav., 13(5), e1477905. https://doi.org/10.1080/15592324.2018.1477905

He, J.Z., Wang, Z.L., Zhang, X.M., Li, X.L., Christie, P. and Li, F.S. 2020. Wheat genotypes differ in their rhizosphere priming effect and its regulation by nitrogen availability. Soil Biol. Biochem., 143, 107680.

Hirel, B., Piques, M. and Gouesnard, B. 2011a. Sustainability of crop production: how to reduce dependence on mineral nitrogen fertilization? Agric. Ecosyst. Environ., 144(1): 226-245.

Hirel, B., Tétu, T., Lea, P. J. and Dubois, F. 2011b. Improving nitrogen use efficiency in crops for sustainable agriculture. Sustainability, 3(9): 1452-1485. https://doi.org/10.3390/su3091452

Hoagland and Arnon, D. I. 1950. The water-culture method for growing plants without soil. Circular. Calif. Agric. Exp. Station 1950 Vol.347 pp.32 pp. https://www.cabdirect.org/cabdirect/abstract/19500302257

Jahan, B., Rasheed, F., Sehar, Z., Fatma, M., Iqbal, N., Masood, A., Anjum, N. A. and Khan, N. A. 2021. Coordinated role of nitric oxide, ethylene, nitrogen, and sulfur in plant salt stress tolerance. Stresses, 1(3): 181-199. https://doi.org/10.3390/stresses1030014

Jian, S. F., Huang, X. J., Yang, X. N., Zhong, C. and Miao, J. H. 2021. Sulfur regulates the trade-off between growth and andrographolide accumulation via nitrogen metabolism in Andrographis paniculata. Front. Plant Sci., 12: 687954, https://doi.org/10.3389/fpls.2021.687954

Jones Jr, J. B. 1987. Nitrogen: Kjeldahl nitrogen determination what's in a name. J. Plant Nutr., 10(9-16): 1675-1682. https://doi.org/10.1080/01904168709363706

Kennedy, I.R. and Roughley, R.J. 2000. Nitrogen fixation in non-leguminous plants: an untapped resource for sustainable agriculture? Plant Soil, 228(2): 351-366.

Klepper, L., Flesher, D. and Hageman, R. H. 1971. Generation of reduced nicotinamide adenine dinucleotide for nitrate reduction in green leaves. Plant Physiol., 48(5): 580-590. https://doi.org/10.1104/pp.48.5.580.

Ladha, J. K., Peoples, M. B., Reddy, P. M., Biswas, J. C., Bennett, A., Jat, M. L. and Krupnik, T. J. 2022. Biological nitrogen fixation and prospects for ecological intensification in cereal-based cropping systems. Field Crops Research, 283: 108541. https://doi.org/10.1016/j.fcr.2022.108541

Li, Y., Wang, Y., Chen, S., Gao, Y. and Shi, Y. 2023. Effects of different nitrogen and phosphorus synergistic fertilizer on enzymes and genes related to nitrogen metabolism in wheat. Phyton (0031-9457), 92(7).

Liu, J., Xia, H., Gao, Y., Pan, D., Sun, J., Liu, M. and Li, Z. 2022. Potassium deficiency causes more nitrate nitrogen to be stored in leaves for low-K sensitive sweet potato genotypes. Frontiers in Plant Science, 13: 1069181. https://doi.org/10.3389/fpls.2022.1069181

Murphy, J. A. M. E. S. and Riley, J. P. 1962. A modified single solution method for the determination of phosphate in natural waters. Analytica chimica acta, 27: 31-36. https://doi.org/10.1016/S0003-2670(00)88444-5

Mohanty, B. and Fletcher, J. S. 1980. Ammonium influence on nitrogen assimilating enzymes and protein accumulation in suspension cultures of Paul's Scarlet rose. Physiologia Plantarum, 48(3): 453-459. https://doi.org/10.1111/j.1399-3054.1980.tb03285.x

Nair, K. P. 2021. Concluding comments and future imperatives. In K. P. Nair, Thermodynamics Of Soil Nutrient Bioavailability, (pp. 61-88). Springer International Publishing. https://doi.org/10.1007/978-3-030-76817-1_6

Nair, T. V. R. and Y. P. Abrol. 1973. Nitrate reductase activity in developing wheat ears. Experientia, 29.12: 1480-1481. https://doi.org/10.1007/BF01943867

Nieves-Cordones, M., Al Shiblawi, F. R. and Sentenac, H. 2016. Roles and transport of sodium and potassium in plants. The alkali metal ions: Their role for life, 291-324. https://doi.org/10.1007/978-3-319-21756-7_9

Paramesh, V., Mohan Kumar, R., Rajanna, G. A., Gowda, S., Nath, A. J., Madival, Y., Jinger, D., Bhat, S. and Toraskar, S. 2023. Integrated nutrient management for improving crop yields, soil properties, and reducing greenhouse gas emissions. Frontiers in Sustainable Food Systems, 7: 1173258. https://doi.org/10.3389/fsufs.2023.1173258

Ramadas, S., Kiran Kumar, T. M. and Pratap Singh, G. 2020. Wheat Production in India: Trends and Prospects. In F. Shah, Z. Khan, A. Iqbal, M. Turan, & M. Olgun (Eds.), Recent Advances in Grain Crops Research. IntechOpen. https://doi.org/10.5772/intechopen.86341

Sandhu, N., Sethi, M., Kumar, A., Dang, D., Singh, J. and Chhuneja, P. 2021. Biochemical and genetic approaches improving nitrogen use efficiency in cereal crops: A review. Frontiers in Plant Science, 12: 657629. https://doi.org/10.3389/fpls.2021.657629

Sathee, L., Adavi, S. B., Jain, V., Pandey, R., Khetarpal, S., Meena, H. S. and Kumar, A. 2018. influence of elevated $CO_2$ on kinetics and expression of high affinity nitrate transport systems in wheat. Indian Journal of Plant Physiology, 23(1): 111-117. https://doi.org/10.1007/s40502-018-0355-y

Shabala, S. (Ed.). 2017. Plant stress physiology. Cabi Publication, ISBN: 9781780647296

Sharma, S., Kumar, T., Foulkes, M. J., Orford, S., Singh, A. M., Wingen, L. U., Karnam, V., Nair, L. S., Mandal, P. K., Griffiths, S., Hawkesford, M. J., Shewry, P. R., Bentley, A. R. and Pandey, R. 2023. Nitrogen uptake and remobilization from pre- and post-anthesis stages contribute towards grain yield and grain protein concentration in wheat grown in limited nitrogen conditions. CABI Agriculture and Bioscience, 4(1): 12. https://doi.org/10.1186/s43170-023-00153-7

Sinclair, T.R. and Gorissen, A. 2009. Wheat responses to agronomic nutrients and their efficiency in use. Soil Use and Management, 25(2): 196-209.

Singh, B. and Craswell, E. 2021. Fertilizers and nitrate pollution of surface and ground water: An increasingly pervasive global problem. SN Applied Sciences, 3(4): 518. https://doi.org/10.1007/s42452-021-04521-8

Skwierawska, M., Skwierawska, M., Skwierawski, A., Benedycka, Z. and Jankowski, K. 2016. Sulfur as a fertiliser component determining crop yield and quality. Journal of Elementology, 2/2016. https://doi.org/10.5601/jelem.2015.20.3.992

Sun, J., Zhang, X., Broderick, M. and Fein, H. 2003. Measurement of nitric oxide production in biological systems by using Griess reaction assay. Sensors, 3(8): 276-284. https://doi.org/10.3390/s30800276

Wang, Y. and Wu, W. H. 2015. Genetic approaches for improvement of the crop potassium acquisition and utilization efficiency. Current Opinion in Plant Biology, 25: 46-52.

Wang, X., Bai, J., Xie, T., Wang, W., Zhang, G., Yin, S. and Wang, D. 2021. Effects of biological nitrification inhibitors on nitrogen use efficiency and greenhouse gas emissions in agricultural soils: A review. Ecotoxicology and Environmental Safety, 220: 112338. https://doi.org/10.1016/j.ecoenv.2021.112338

Xu, J., Xu, X. and Verstraete, W. 2000. Adaptation of E. coli cell method for micro-scale nitrate measurement with the Griess reaction in culture media. Journal of Microbiological Methods, 41(1): 23-33. https://doi.org/10.1016/S0167-7012(00)00141-X

Xu, G., Fan, X. and He, H. 2012. Plant nitrogen assimilation and allocation under salt stress. Plant, Cell & Environment, 35(6): 1620-1635.

Yadav, M. R., Kumar, S., Lal, M. K., Kumar, D., Kumar, R., Yadav, R. K., Kumar, S., Nanda, G., Singh, J., Udawat, P., Meena, N. K., Jha, P. K., Minkina, T., Glinushkin, A. P., Kalinitchenko, V. P. and Rajput, V. D. 2023. Mechanistic understanding of leakage and consequences and recent technological advances in improving nitrogen use efficiency in cereals. Agronomy, 13(2): 527. https://doi.org/10.3390/agronomy13020527

Yan, S., Wu, Y., Fan, J., Zhang, F., Zheng, J., Qiang, S., Guo, J., Xiang, Y., Zou, H. and Wu, L. 2020. Dynamic change and accumulation of grain macronutrient (N, P and K) concentrations in winter wheat under different drip fertigation regimes. Field Crops Research, 250: 107767. https://doi.org/10.1016/j.fcr.2020.107767

Yin, Z., Guo, W., Xiao, H., Liang, J., Hao, X., Dong, N., Leng, T., Wang, Y., Wang, Q. and Yin, F. 2018. Nitrogen, phosphorus, and potassium fertilization to achieve expected yield and improve yield components of mung bean. PLOS ONE, 13(10): e0206285. https://doi.org/10.1371/journal.pone.0206285

Zhang, A., Liu, Y., Pan, G., Hussain, Q., Li, L., Zheng, J. and Zhang, X. 2012. Effect of biochar amendment on maize yield and greenhouse gas emissions from a soil organic carbon poor calcareous loamy soil from Central China Plain. Plant and soil, 351: 263-275. https://doi.org/10.1007/s11104-011-0957-x

Zheng, Z., Liu, M., Li, P., Li, J., Li, X. and Jing, Q. 2020. Wheat genotypes with different nitrogen use efficiency exhibit contrasting responses to nitrogen deficiency in terms of root architecture and root exudation. Journal of Agronomy and Crop Science, 206(2): 260-272.

Zhou, B., Serret, M. D., Pie, J. B., Shah, S. S. and Li, Z. 2018. Relative contribution of nitrogen absorption, remobilization, and partitioning to the ear during grain filling in Chinese winter wheat. Frontiers in Plant Science, 9: 1351. https://doi.org/10.3389/fpls.2018.01351

Nature Environment and Pollution Technology
An International Quarterly Scientific Journal

p-ISSN: 0972-6268
(Print copies up to 2016)
e-ISSN: 2395-3454

Vol. 23 | No. 3 | pp. 1483-1494 | 2024

Original Research Paper

https://doi.org/10.46488/NEPT.2024.v23i03.018

Open Access Journal

# Urban Nature Reserves Waste Challenges from Neighboring Informal Settlements: Western Cape, South Africa

**X. S. Grangxabe*, T. Maphanga*† and B. S. Chidi****

*Department of Occupational and Environmental Studies, Cape Peninsula University of Technology, Keizergracht, Cape Town 7925, South Africa

**Bioresource Engineering Research Group (BioERG), Department of Biotechnology and Consumer Science, Faculty of Applied Sciences, Cape Peninsula University of Technology, Zonnebloem, Cape Town 8000, South Africa

†Corresponding author: T. Maphanga; maphangat@cput.ac.za

**Nat. Env. & Poll. Tech.**
**Website: www.neptjournal.com**

*Received:* 29-04-2023
*Revised:* 06-06-2023
*Accepted:* 10-06-2023

**Key Words:**
Illegal dumping
Waste management
Conservation efforts
Community participation
Partnerships

## ABSTRACT

Nature reserves have played a crucial role in biodiversity conservation for decades. Rapid urban sprawl has increased the amount of solid waste created by littering and illegal dumping in metropolitan nature reserves. This paper examines how two nature reserves, Wolfgat Nature Reserve and Witzands Aquifer Nature Reserves, can combine community conservation with waste management. To determine aspects such as the socioeconomic impact of the nature reserves on the surrounding communities, questionnaires with a specific focus on the topic were distributed to the surrounding communities and subsequently administered. Data was collected using semi-structured interviews with key informants from the nature reserve staff and observational methods, and SPSS was used to analyze the data. Consistent with previous research, this study revealed that ignoring local populations frequently results in people disobeying the appropriate regulations in these protected areas and that education does not guarantee conservation support. Despite this, the survey revealed an absence of community participation; conservators were more reactive than proactive. In this study, the level of education, which in some studies is always associated with knowledge, was contradicted; those with post-secondary education knew little about these areas, and the vast majority of participants were unaware of the protected areas just a few kilometers away from their communities.

## INTRODUCTION

Rapid population growth in emerging nations, particularly in large cities, is driving a strong demand for space. As a result, residential areas are being constructed close to protected areas, leading to increased human engagement with the natural environment. In the past, humans and nature were considered different entities, resulting in nature being viewed as an infinite supply of raw materials and an infinite dumpsite for garbage. Later, it became apparent that the exclusion strategy had caused conflict between protected zones and the surrounding communities (Simelane et al. 2006). Community-based conservation (CBC) is utilized globally to engage local people in the protection of natural areas and the preservation of nature and its animals. It is also utilized to better develop a connection between community people, the environment, and conservationists. Although tourists and members of the neighboring community are now permitted in select protected areas. Even though protected areas are intended to conserve natural resources and limit human effects. According to De Witt & Van der Merwe (2015), the fast population growth in protected regions has led to a rise in environmental issues including trash pollution since it degrades the aesthetic quality of the ecosystem, irresponsible rubbish disposal has been one of the most evident forms of deterioration in protected areas for many years (de los Angele Somarriba-Chang 2012). Moreover, inefficient waste management is rapidly affecting crucial environmental and human health factors. According to research by Kadafa et al. (2014) and Przydatek (2019), the rising volume of solid waste is a significant problem for many nations, particularly emerging nations where education and environmental awareness are inadequate. Illegal dumping is a widespread concern for natural protected areas (Jakiel et al. 2019), as is the ignorance or lack of understanding of tourists who continue to trash in these protected areas; protected spaces are thus not an exception.

This research addresses unlawful garbage disposal and investigates community engagement options that

might successfully solve waste issues in protected areas. Communities around nature reserves have a propensity to dispose of rubbish illegally in protected areas, as these locations are frequently perceived as open spaces that harbor criminals due to their dense vegetation (Mcdonald et al. 2009, City of Cape Town 2019). This is especially prevalent in informal communities, which lack dependable garbage collection services. However, although some dispose of their trash in open fields, high winds and rains force it directly into protected areas, creating waste management issues. Thousands of protected places are currently badly impacted by metropolitan areas, and many more will be in the future (Mcdonald et al. 2009). According to Pryzdatek (2019), countries handle protected areas differently. Nature reserves are declared according to section 23 of the National Environmental Management: Protected Areas Act 57 of 2003 whereby the legislation safeguards and preserves environmentally valuable places (Hatton 2002). Therefore, the National Environmental Management: Trash Act (No. 59 of 2008), which limits the discharge of waste into or onto land, guides and regulates waste management in protected areas. In addition, protected areas were governed by the Environmental Conservation Act of 1989, Section 73, which forbids trash in any manner. Despite these restrictions, littering is a chronic problem in many urban protected areas; trash from outside the reserve, primarily from surrounding towns, and garbage created by visitors pose a danger to the protected areas' integrity. The expansion of new complexes and the persistent demand for homes in the region further jeopardize conservation initiatives.

## MATERIALS AND METHODS

### Study Region

Wolfgat Nature Reserve is a coastal nature reserve located in Mitchells Plain and Khayelitsha, between the resorts of Mnandi and Monwabisi (Fig. 1). Wolfgat encompasses 248 hectares and was designated a nature reserve by the City of Cape Town in 1986. It preserves more than 150 plant species and is home to the endangered Strandveld flora of the Cape Flats dune (City of Cape Town (CoCT) 2008). The reserve's proximity to disadvantaged communities makes it susceptible to criminal activities. Khayelitsha, a notoriously high-crime area with a population of 391.749 (Stats SA 2011), and Mitchell's Plain, a large, spreading colored township with a population of 310.485 are home to more than half of Cape Town's jobless (Stats SA 2011). Mitchells Plain is one of fifteen high-priority areas for anti-crime

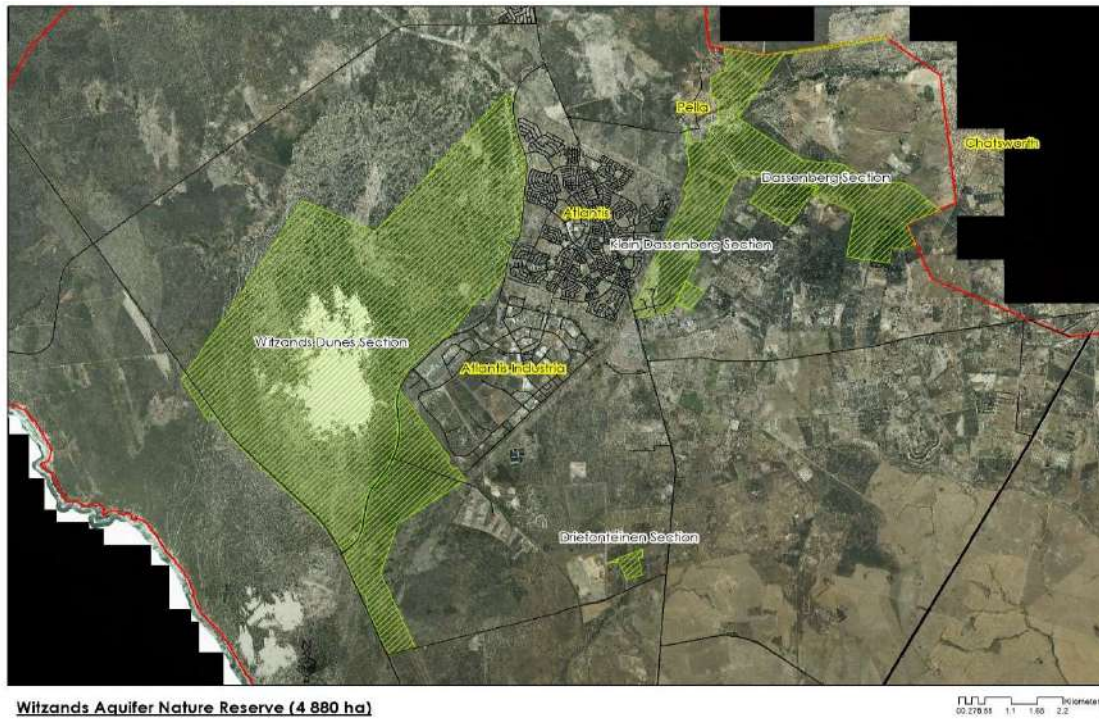


(Source: Jacques van der Merwe)

Fig. 1: Map of Atlantis Aquifer Nature Reserve and other satellite sites highlighted in green.

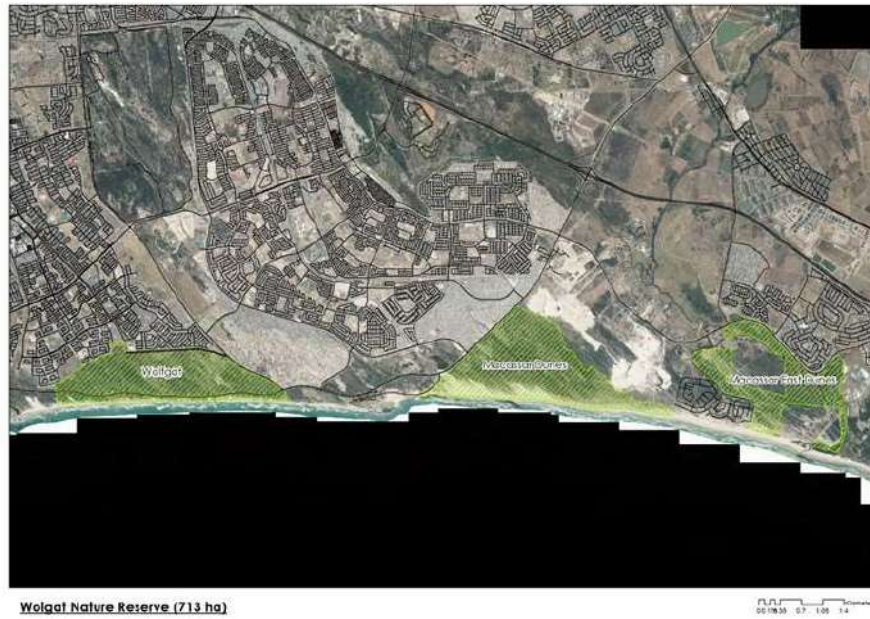


(Source: Jacques van der Merwe)

Fig. 2: Wolfgat Nature Reserve aerial map.

and anti-drug addiction initiatives (Eksteen 2012, Stats SA 2011).

The 1,750-hectare Atlantis Dune area is included in the Witzands Aquifer Nature Reserve. According to (CoCT 2008), the reserve is home to two distinct types of flora: the severely endangered Cape Flats dune Strandveld, which is the dominating vegetation in the reserve, and the critically endangered Atlantis sand Fynbos. The nature reserve is notable for its non-vegetated movable dunes and rocky outcrops (CoCT 2008), the dunes are commonly used for recreational activities, which increase the number of visitors to the region. The reserve borders residential and industrial areas such as Atlantis, Mamre, and the informal settlement of Witzands and Pella communities. Except for the informal settlement of Witzands, these villages depend largely on the reserve for water, the reserve natural aquifer supplies water that is harvested and purified for human use (Eksteen 2012). The residential neighborhoods are dominated by persons of color and range in income from poor to middle class (Stats SA 2011). Atlantis has a population of 67,491 and an unemployment rate of 37% (CoCT 2006, Stats SA 2011). Mamre has a population of 9,048 people, whereas Pella has just 1,681 individuals. (Stats SA 2011). Fig. 2 shows the aerial map of the Wolfgat Nature Reserve.

## Sampling Method

Questionnaires, interviews, and observational procedures were used to collect data as part of qualitative and quantitative research techniques. The questionnaire was sent to villages surrounding the reserve to collect data on garbage generation in the protected regions. There were both open-ended and closed-ended questions on the surveys. A qualitative interview, according to Oakley (1998), is a framework in which practices and standards are not only documented, but also achieved, challenged, and reinforced. This study employed unstructured interviews because they are frequently employed in long-term fieldwork and permit respondents to express themselves in their own way and at their own pace, with few restrictions on their responses. Ethnographers pioneered the use of unstructured interviews with local key informants, as well as the collection of data via observation and field notes, and the involvement of study participants (Gray 2021). To be more precise, an unstructured interview more closely resembles a conversation than an interview and is always assumed to be a "controlled conversation" skewed towards the interviewer's interests (Gray 2021).

This study included three distinct non-probability sampling strategies, namely purposive, snowball, and convenience sampling. These methods were used to obtain information from all participants (managers, community members, community partners, etc.) (Marshall 1996). The non-probability sampling approach of purposive sampling was employed to interview individuals who were presumed to comprehend the study and have relevant responses (Taherdoost 2016). In this area, the major actors were the

managers and community partners. The convenience sampling approach was implemented in public areas close to the nature reserve, where participants/residents volunteered to take part in the study, and the snowball technique was utilized, in which current study subjects recruited or discovered potential research participants. The reserve managers were interviewed in the form of unstructured interviews regarding awareness and interactions with the neighboring community while the closed-ended questionnaires were used for the residents and reserve partners. In addition, the approach of observational assessment was employed to observe people's behavioral patterns and interactions with the natural environment.

### Sampling Size

Using sampling approaches based on probability, the researcher selected a representative sample of the investigated population. To get a probability sample for the investigation, a simple random and stratified sampling method was employed. Stratified sampling requires the researcher to split a population into homogenous subpopulations, or strata, depending on certain criteria (e.g., race, gender, location, etc.). Then, each stratum was sampled using a second form of probability sampling, simple random sampling. The researcher utilized a basic random sampling approach to randomly choose a subset of a population. In this sampling technique, all potential biases were eliminated, and each person in the population had an equal chance of being picked to participate in the research.

These methods were used to obtain information from all participants (managers, community members, community partners, etc.). Used to interview individuals who were considered to comprehend the study and had the relevant responses. In this area, the major actors were the managers and community partners. As of the 2011 Census, Atlantis has 67491 residents (Stats SA 2011). Slovin's formula was used to compute the sample size, where (n) is the sample size, (N) is the known population size and (e) is the margin of error. The definition of the margin of error is "the range of values below and above the sample statistic in a confidence interval". It is computed as, $n = \frac{N}{1 + Ne^2}$ with a 95% confidence interval, therefore the margin of error is 0.05%.

### Data Analysis

The researcher read all of the administered surveys and had the interview recordings transcribed to have an overall understanding of the data supplied and the material to be analyzed. Using IBM Statistical Package for the Social Sciences (SPSS) version 26, a program used for editing and analyzing data (Verma 2012) that assures the meaningful and symbolic value of qualitative data, the demographic information from the questionnaires was analyzed. The significance of the major statements and phrases about the examined phenomena developed into significant statements.

Thematic analysis is defined as the important systematic method for identifying, organizing, and presenting patterns of themes across a data set (Clarke 2015). In essence, thematic analyses are a meaningful method for identifying common themes in a way that enhances the exploration of the key elements that focus on the discussed topic and provide answers to the research questions. Given this context, the present study employed thematic analysis to identify the common concern that emerged from the questionnaire survey which formed part of the unstructured interview with the nature reserves managers.

## RESULTS AND DISCUSSION

There were a few parallels and variances among participants from Atlantis and Khayelitsha (Fig. 3). In terms of demographic statistics, minimal distinctions were detected, such as the employment rate, dominating population group, and level of education; nonetheless, it was noted that both places had weak economic growth, and the areas are sprawling with informal settlements and low-cost housing. According to research, the most significant component of an effective society is not income or a high level of education, but rather social capital, which consists of deeply ingrained ties of trust and vision (Pitt & Boulle 2010). According to Eksteen (2012) people's relationships with the environment vary with individuals but not only does people's profession influence their perception but also their history and encounters with the environment. Therefore, how people interact with the natural environment is not entirely based on their level of education there are various influencing factors such as where they were raised. Fig. 3 illustrates Atlantis and Khayelitsha communities' level of education. Based on the results for both areas, the majority of people had formal education; however, they had little to no knowledge about nature reserves. Furthermore, other studies contradict Fig. 3 by stating that a positive attitude toward the natural environment tends to increase with respondents' level of education and knowledge about conservation issues (Bajracharya et al. 2007, Brown et al. 2010). However, based on the majority of the results of people with formal education they have never been to a nature reserve before. Therefore, the participant's level of education cannot be used as an indicator of knowledge regarding a specific area.

The findings reveal that both study areas had a majority representative population of people in their youth (35-44) and the communities were dominated by middle-aged

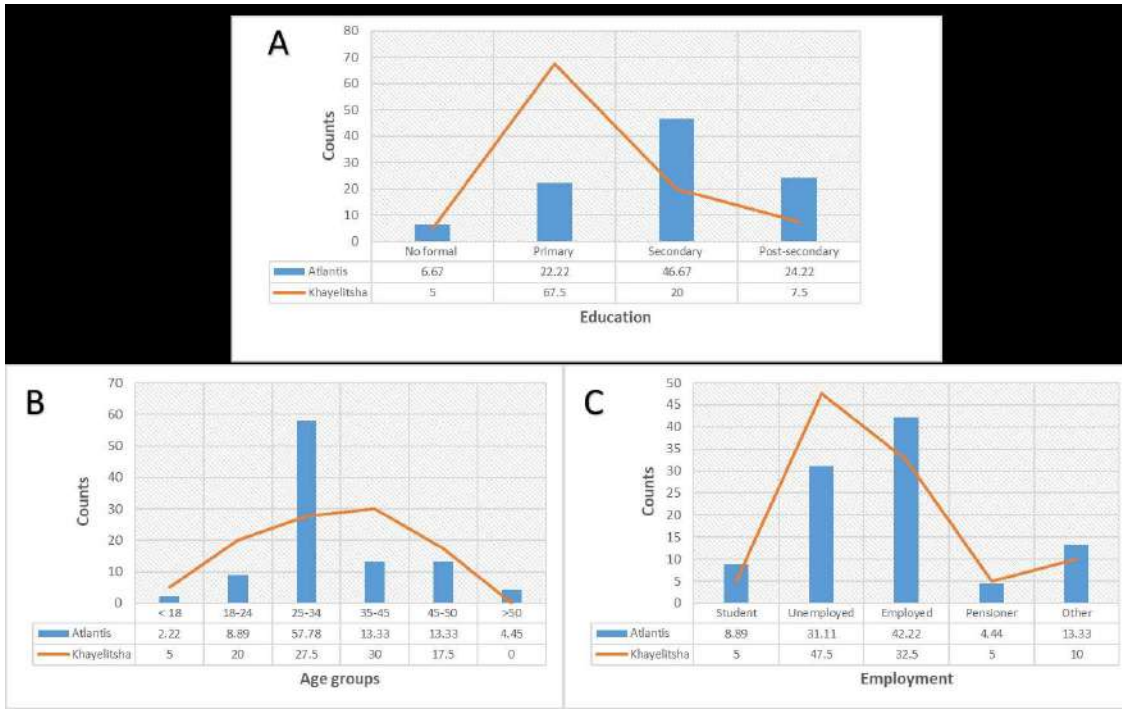


Fig. 3: Summary of the demographics for Atlantis and Khayelitsha.

people (Fig. 3) and fewer teenagers for both sites, few youth representatives (18-24). The age pyramid of Atlantis, on the other hand, contradicts the aforementioned findings, indicating that there are a greater number of young, both males and women, between the ages of 20 and 30 (Census 2011). According to research by Saadat et al. (2022), states that the COVID-19 pandemic has also changed people's lifestyles; caused extensive job losses, and threatened the sustenance of millions of people, as businesses have shut down to control the spread of the virus. This has caused employment losses among populations that have historically been susceptible, such as the less educated, young, and people of color (Wessels et al. 2021). The Atlantis and Khayelitsha neighborhoods are characterized by a low-to-middle-income margin, Atlantis with having a 37% unemployment rate (Stats SA 2011). Although, most people were harmed by job loss owing to Covid-19 the chosen group had a majority of employed people in Atlantis than in Khayelitsha (Fig. 3). According to the literature both areas are still impoverished, with many individuals jobless or underemployed. Stats SA (2021) just released its latest Quarterly Force Labor Survey, which shows that the Western Cape currently has the lowest unemployment rate in the country, at 27.9%.

Through literature and observation by the author, litter is known to have hazardous consequences on biodiversity and humans therefore protected areas such as nature reserves have strict visitor management measures put in place to minimize the impact of litter and there are frequent patrols and clean ups in these areas. However, illegal dumping and littering have economic repercussions as well as environmental and social ones (Table 1). Conservation problems have arisen, especially in urban nature reserves, Table 1 illustrates the cost of disposing of waste in a landfill, however, the cost does not include the labor, hiring of the special machine (digger loader), and the fuel used to transport the waste. Illegal dumping is a complex issue that affects more than one aspect. Education and environmental information, which is seen as an effective means to raise community awareness may be working for some groups. However, it does not work as a waste management tool to prevent littering. According to Simelane et al. (2006) community involvement and liaising have more impact and can influence change in people's behavior in natural areas.

Fig. 4 is the illustration of the participants' responses when they were questioned about their role in tackling illegal dumping in their communities. 20% of those individuals who were unfamiliar with illegal dumping knew their role in dealing with illegal dumping. 12.50% indicated that their role as community members is to clean the litter, while 25% of the participants advised that it should be disposed of correctly through the use of wheelie bins, 12.50% said it was none of their business and 37.50% were unclear followed

Table 1: Waste removals, delivered to False Bay Coastal Park landfill from July to September 2021.

| DATE 2021 | FROM | WEIGHT (KG) | COST (R) R1 ($0,061) |
|---|---|---|---|
| JULY | | | |
| 05 Jul | Wolfgat Nature Reserve | 5240 | 3360.61 |
| 05-Jul | Wolfgat Nature Reserve | 11040 | 7201.2 |
| 05-Jul | Wolfgat Nature Reserve | 8520 | 336061 |
| 06-Jul | Wolfgat Nature Reserve | 9000 | 5760.9 |
| 07-Jul | Wolfgat Nature Reserve | 9660 | 6241.2 |
| 07-Jul | Wolfgat Nature Reserve | 7460 | 4800.9 |
| 08-Jul | Wolfgat Nature Reserve | 6980 | 185.5 |
| 08-Jul | Wolfgat Nature Reserve | 6480 | 185.5 |
| 08-Jul | Wolfgat Nature Reserve | 4380 | 2880.6 |
| 08-Jul | Wolfgat Nature Reserve | 9740 | 6241.2 |
| 09-Jul | Wolfgat Nature Reserve | 5960 | 159 |
| 15-Jul | Wolfgat Nature Reserve | 6980 | 185.5 |
| 15-Jul | Wolfgat Nature Reserve | 8660 | 5601.1 |
| 16-Jul | Wolfgat Nature Reserve | 7620 | 4961 |
| 16-Jul | Wolfgat Nature Reserve | 7000 | 4480.7 |
| 26-Jul | Wolfgat Nature Reserve | 7680 | 4961 |
| 27-Jul | Wolfgat Nature Reserve | 7640 | 4961 |
| 27-Jul | Wolfgat Nature Reserve | 6820 | 4480.7 |
| 27-Jul | Wolfgat Nature Reserve | 2240 | 1440.3 |
| 28-Jul | Wolfgat Nature Reserve | 2240 | 1440.3 |
| 29-Jul | Wolfgat Nature Reserve | 2340 | 1600.4 |
| **21 Days** | **TOTAL** | **136 000 Kg** | **R 407 189,61** |
| AUGUST | | | |
| 11-Aug | Wolfgat Nature Reserve | 480 | 3600 |
| 12-Aug | Wolfgat Nature Reserve | 480 | 3600 |
| 20-Aug | Wolfgat Nature Reserve | 3140 | 2080.4 |
| 23-Aug | Wolfgat Nature Reserve | 2020 | 1440.3 |
| 23-Aug | Wolfgat Nature Reserve | 3160 | 2080.4 |
| 23-Aug | Wolfgat Nature Reserve | 1400 | 960.3 |
| 25-Aug | Wolfgat Nature Reserve | 5760 | 3840.6 |
| 25-Aug | Wolfgat Nature Reserve | 7680 | 212 |
| 25-Aug | Wolfgat Nature Reserve | 5260 | 3520.71 |
| 30-Aug | Wolfgat Nature Reserve | 3300 | 2240.5 |
| **8 Days** | **TOTAL** | 32 680 Kg | R 23 575,21 |

Source: Zandisile Biko

by 12.50% of participants who said it should be reported to the local authorities. Out of the 17.5% that disagreed that illegal dumping impacts the reserve, 57.14% of respondents responded with "I do not know" while 42.87% was equally split amongst those who say it should be cleaned, not their business and those who say the community should prohibit dumping and protect the environment. A maximum of 28% of those who agreed that illegal dumping affects the reserve indicated that the communities' role is to report it, 20% stated that people should stop dumping, 16% said clean it, the lowest number of people said the community's role is deal with littering challenges (4%).

Due to their reduced reliance on natural resources, urbanites are the most disconnected from nature. According

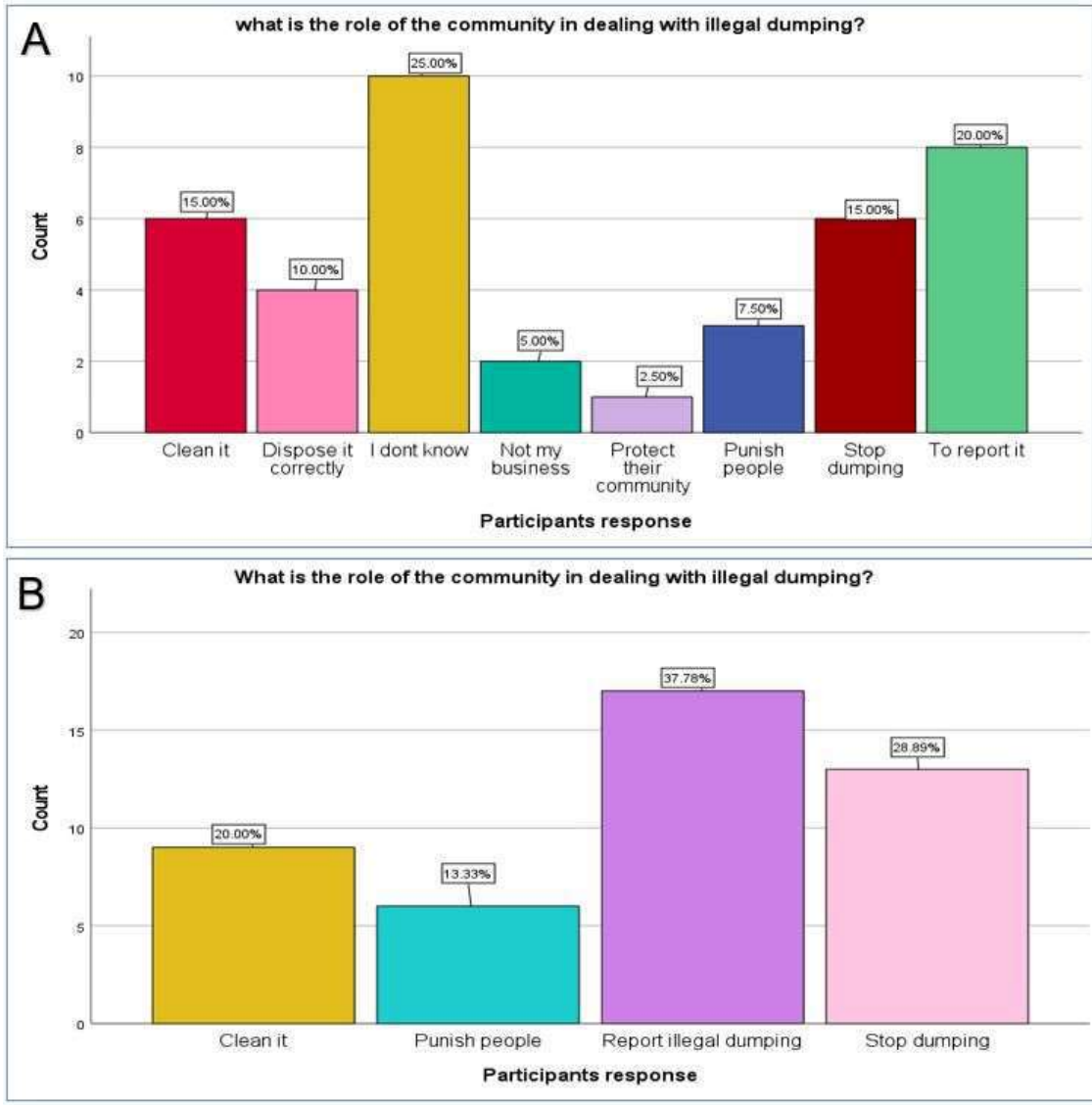


Fig. 4: Response of Atlantis (A) and Khayelitsha (B) residents on how to deal with illegal dumping.

to Eksteen (2012), there has been a steady transition from living in rural, natural regions to living in urban, urbanized regions. Fig. 3 demonstrates that poor people are aware of their impact on the environment but lack the time to care due to a variety of adverse social and economic consequences. In addition, other research confirms the findings, indicating that some individuals are aware of their impact on the environment and wish to act in a way that minimizes the damage they cause (Eksteen 2012, Wells & McShane 2004). As evidenced by the diagram, everyone was aware of their responsibilities regarding illegal dumping. Since laws and regulations do not guarantee compliance and the government cannot enforce them perfectly, it is essential to involve communities in conservation (Agrawal & Gibson 1999). According to a study by Matsumoto & Takeuchi (2011), illegal dumping is more prevalent in communities with a high unemployment rate. The results of Fig. 4b were interpreted and the relationship observed. The figure demonstrates that, of all the study participants, 71.11% agreed that illegal dumping affects the nature reserve, while 8.88% disagreed and the remaining participants were unsure. About 71.11% of the participants were aware of the impact of litter on the nature reserve, and 21.88% stated that their role in addressing dumping is to clean it up, while 9.38% stated that litterbugs should be punished. 43.75% of respondents indicated that, as members of the community, they should report it, while

25% recommended that people stop dumping. Approximately 20% of respondents indicated that litter has an impact on the nature reserve, with 11.1% indicating that it should be cleaned, 22.22% preferred the community to punish litterers and 22.22% insisted that it should they should report illegal dumping, while the majority of 44.44% indicated that it is the community's responsibility to stop dumping. Communities should not be regarded in isolation from the environment, and according to Agrawal & Gibson (1999), one actor should not be isolated from the other. Environmental protection must be prioritized, and local people must be educated and empowered to monitor their environment and manage their trash at levels that are acceptable to them (Joseph 2006). According to research (Joseph 2006, Przydatek 2019), communities and cultures may fight unlawful dumping by empowering themselves since individuals who engage in illegal dumping operations do so deliberately.

**Possible Ways of Dealing with the Illegal Dumping**

Rapid urbanization has wreaked havoc on developing countries' ecosystems and will continue to do so unless urgent action is taken (Pitt & Boulle 2010). A growing body of evidence suggests that the best hope for protecting our endangered resource is for the majority of humans to become instinctive and passionate conservationists, which can only be accomplished by making people truly aware of our interdependence with nature by involving communities and making them critical stakeholders. Several studies have found that individuals in these villages have a terrible relationship with their neighboring protected areas (Kaltenborn et al. 2008). Kruger National Park is a good example, as neighboring communities continue to struggle with park authorities. Despite confrontations between local populations and conservators, Andrade & Rhodes (2012) demonstrated that most local communities are still prepared to help biodiversity conservation and management by collaborating with conservators. A large number of studies have also revealed that communities have a limited understanding of the resources occurring within their neighboring protected areas (Andrade & Rhodes 2012, Angwenyi et al. 2021, Western & Henry 1979) because many protected areas followed the traditional and exclusionary approach in which people were denied access to the areas. This is a tendency that has been recognized and implemented widely for many years (Andrade & Rhodes 2012). Furthermore, Simelane et al. (2006) stated that the lack of awareness of natural resources in South Africa is comprehensible because most conservation areas were privately fenced after communities were evicted without sufficient explanations.

Neglecting local communities may result in negative social consequences. As a result, such effects may lead to hostility against conservation efforts, undermining protection

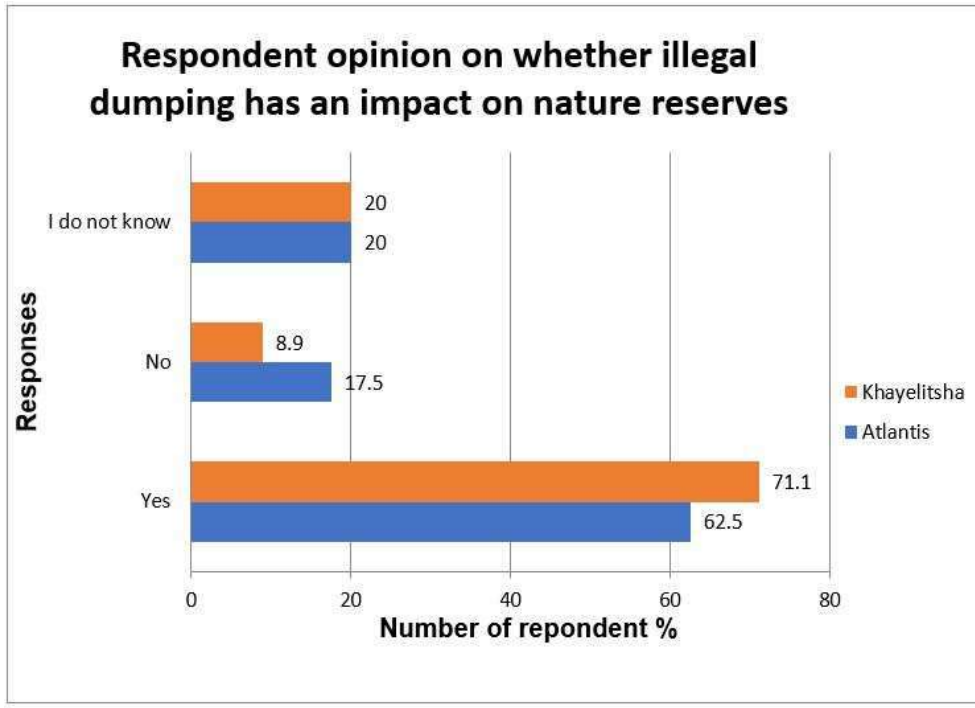


Fig. 5: Participants' response to illegal dumping.

regulations and reducing the use of protected areas for biodiversity. According to Simelane et al. (2006), to maximize local community participation and avoid conflict between conservationists and local communities, a comprehensive understanding of environmental concerns as well as the role of a community in that specific conservation area must be prioritized. On the other hand, a lack of connectivity between local communities and regions of biological importance can jeopardize the future and viability of protected areas such as South Africa's Kruger National Park (Simelane et al. 2006). In other words, conservation area management must always adapt and respond quickly to conservation-related difficulties by using tactics that encourage community support for protected areas. Regardless of the fencing and other strategies in place, illegal dumping continues to be a huge threat to the existence of these areas; therefore, the far most effective strategy is to work with communities and make them the fence of these areas, allowing them to defend these areas from any environmental degradation; it has been demonstrated that local residents can contribute significantly to the reduction of illegal dumping. To combat the environmental issue of illegal dumping and littering, nature reserves must employ a people-centered approach and garner public support by incorporating the public in important decision-making and management plans.

The study found that residents living near the reserve are aware of the effects of illegal dumping on the reserve and are aware of their role as community members (Fig. 5). However, the value of the areas was unknown to the majority of the participants; they indicated that the areas are important for income generation, but only a few respondents valued the areas for their ecological importance. An increasing collection of evidence indicates that no barrier is strong enough to withstand the indifference of an indifferent population (Pitt & Boulle 2010, Wessels et al. 2021). Poorly managed garbage from neighboring residences and unlawful dumping are the principal threats in most protected areas; dumping of waste ranging from household debris, building rubble, tires, and hazardous waste such as asbestos occurs unabated (Wessels et al. 2021).

Fig. 5 shows that, out of all the people that participated in the study in Atlantis, 62,50% agreed that illegal dumping has an impact on the nature reserve while 17,50% disagreed that illegal dumping has an effect and 20% did not have knowledge on the subject matter. According to a study conducted by Wessels et al. (2021), improper waste management in protected areas is frequently ascribed to the actions of residents and insufficient service from the municipality. Illegal dumping is recognized to have significant environmental, health, and economic consequences; there is adequate evidence that excessive dumping poses a fire hazard risk; and hazardous items can contaminate soil and groundwater and harm plants and wildlife (Carlon et al. 2003). Illegal dumping also harms tourism and can be a financial burden on governments (see Table 1). According to Brandt (2017), unlawful dump sites are difficult to rehabilitate; for example, in 2010, Australian local governments spent $10 million (approx. R 162, 739, 500) removing and disposing of illegally discarded pollutants (Crofts et al. 2010). In the United States, the costs of illegal dumping site rehabilitation can consume up to 30% of municipal government budgets (Glanville & Chang 2015).

**Unstructured Interview Responses from Key Informants**

1. City of Cape Town participants on the nature reserve's relationship with the surrounding community:

"The relationship is going well but in terms of the social standards there are challenges here and there" (Reserve Supervisor, Wolfgat Nature Reserve)

"It's a work in progress but there's always changing community leadership; it's a constantly moving relationship" (Functional Operational Manager) "The relationship is not as positive but we still do environmental awareness" (Reserve Supervisor, Witzands Aquifer Nature Reserve)

The above findings indicate that the community's relationship with nature reserves is relatively poor; the majority of those who took part in the study had never visited a nature reserve or been a part of a community-based project. This reveals a shortage of marketing and community participation efforts targeted at raising awareness and fostering relationships. Socioeconomic considerations are critical since a hungry person will be apathetic to the protected territory if his or her immediate needs are not satisfied. Additionally, conservators are aware of this dysfunctional connection, although one interviewee asserts that the tie is developed via education. Indeed, Graham & Ernston (2012) found that cooperation should not just be theoretical, but also practical.

2. The nature reserve's strategies for ensuring sustainable yield, promoting compliance with applicable laws, integrating biodiversity issues with waste management, and promoting sustainable eco-tourism. What are these techniques?

"Due to visitors leaving their litter on the reserve unattended, we have adapted to new policies; some of our reserves are now" Bin Free" reserves and regular patrols are being done to monitor illegal dumping, in terms of promoting eco-tourism we allow harvesting of alien plants (wood species) through permit systems" (Functional Operational Manager).

"We have methods in terms of compliance; we have coordinated with the law enforcement and field rangers to conduct patrols. Jerome September integrates biodiversity concerns with waste management through working with local people such as Sangomas, Khoisan, etc. through education" (Reserve Supervisor, Wolfgat Nature Reserve).

The local communities from both nature reserves have indicated that the municipality provides them with Waste Management Services; however, illegal dumping is still an environmental issue for nature reserves regardless of the methods and laws that have been implemented. Well-known conservation agencies such as SANParks have adopted a proactive strategy to ensure community support, and this includes the establishment of various community development projects. A study by Dube (2018) states that local communities should be one of the important stakeholders in protected area management as they have valuable information to share about the area.

3. What environmental challenges does the nature reserve face, and is the current waste management system effective, according to participants from the City of Cape Town?

"The nature reserve is currently confronted with many challenges, but illegal dumping, particularly near the fence separating the nature reserve from the houses, is a major issue. Yes, we do have a waste management system in place, and so far it has been effective" (Reserve Supervisor, Wolfgat Nature Reserve)

The Witzands Aquifer Nature Reserve is not significantly affected by illegal dumping, but remote sites are. Witzands Aquifer Nature Reserve is a bin-free nature reserve; visitors bring their own bags and leave with their trash; thus far, this has been effective" (Witzands Aquifer Nature Reserve Supervisor)"

According to the conservators' semi-interviews, illegal dumping and litter brought in from neighboring communities were identified as the primary environmental issues for both nature reserves, despite respondents' assertions that their reserves' waste management plans were efficient. The communities surrounding both areas indicated that they had witnessed illegal dumping and were aware of their role as community members. Even though people are aware of the problem and nature reserves are protected by specific laws and regulations, they continue to experience waste problems. According to Joseph (2006), to make real progress in waste management, local communities must be involved, but collaborative approaches have led to attitude shifts without corresponding behavioral cooperation.

4. A compilation of quotations regarding the nature reserve's strategies for ensuring sustainable yield, promoting compliance with applicable laws, integrating biodiversity concerns with waste management, and promoting sustainable ecotourism. What are these strategies?

"Due to visitors leaving their trash unattended on the reserve, we have adopted new policies; some of our reserves are now "Bin Free" reserves, and regular patrols are conducted to monitor illegal dumping in the interest of promoting ecotourism. Through permit systems, we permit the harvesting of alien plants (wood species) for tourism" (Functional Operational Manager).

"We have methods for ensuring compliance; we have coordinated patrols with law enforcement and field rangers." Jerome September integrates concerns about biodiversity with waste management by educating local people such as Sangomas, Khoisan, etc. (Superintendent of the Wolfgat Nature Reserve)

The local communities of both nature reserves have indicated that the municipality provides them with Waste Management Services; despite the methods and laws that have been implemented, illegal dumping remains an environmental concern for nature reserves. Notable conservation organizations, such as SANParks, have adopted a proactive strategy to ensure community support, which includes the establishment of numerous community development projects. Local communities should be one of the key stakeholders in protected area management, according to a study by Dube (2018), because they have valuable information to share about the area.

## CONCLUSION

There is growing evidence that higher incomes and education do not necessarily translate to greater environmental awareness. As a result, nature reserves must empower individuals with skills and vision to develop their communities. According to literature, the majority of the world's population is migrating to urban areas for economic reasons as urbanization increases; however, such migration frequently leads to unlawful land occupation without proper dumping and sanitation facilities, which puts a strain on natural resources and threatens urban conservation spaces. The relationship between conservationists and communities is the starting point for making conservation relevant to local communities, according to the literature. The conservation-community relationship contributes to the long-term security and sustainability of ecosystems that are severely threatened. Through the study, the researcher investigated the relationship between conservationists and communities in greater depth by administering a questionnaire to communities who reside near the reserves and not just community partners. According

to the study, conservationists have a variety of relationships with local communities that range from poor to excellent. As a result of changes in community leaders and socioeconomic conditions, the conservator stated that the relationship is constantly changing. By providing temporary jobs and environmental education programs, significant progress has been made in trying to improve these relationships. The importance of these relationships to people is not to serve biodiversity, but rather to serve some of their social needs. Although the majority of respondents from both sites have never visited a nature reserve or participated in a community conservation project, they have a good understanding of the environmental impact of waste on the nature reserve. Despite their knowledge, communities lacked a sense of ownership and belonging as a result of exclusionary decision-making in conservation-related activities. They were more concerned with issues such as inequality, marginalization, and poverty.

## ACKNOWLEDGEMENTS

The authors wish to thank Cape Peninsula University of Technology for its encouragement and contribution to the writing of this article. Their families are also thanked for their support and encouragement.

## REFERENCES

Agrawal, A. and Gibson, C. C. 1999. Enchantment and disenchantment: the role of community in natural resource conservation. World Development, 27(4): 629-649.

Andrade, G. S. and Rhodes, J. R. 2012. Protected areas and local communities: an inevitable partnership toward successful conservation strategies? Ecology and Society, 17(4).

Angwenyi, D., Potgieter, M. and Gambiza, J. 2021. Community perceptions towards nature conservation in the Eastern Cape Province, South Africa. Nature Conservation, 43: 41.

Bajracharya, S. B., Gurung, G. B. and Basnet, K. 2007. Learning from community participation in conservation area management. Journal of Forest and Livelihood, 6(2): 54-66.

Brandt, A. 2017. Illegal dumping as an indicator for community social disorganization and crime. Doctoral dissertation, San José State University.

Brown, T. J., Ham, S. H. and Hughes, M. 2010. Picking up litter: An application of theory-based communication to influence tourist behaviour in protected areas. Journal of Sustainable Tourism, 18(7): 879-900.

Clarke, R. 2015. Beyond landscape designation: innovative funding, delivery and governance and the UK protected area system. Management of Environmental Quality: An International Journal, 26(2): 172-194.

Creswell, J. W. and Tashakkori, A. 2007. Differing perspectives on mixed methods research, 1(4): 303-308.

Critto, A., Carlon, C. and Marcomini, A. 2003. Characterization of contaminated soil and groundwater surrounding an illegal landfill (S. Giuliano, Venice, Italy) by principal component analysis and kriging. Environmental Pollution, 122(2): 235-244.

Crofts, P., Morris, T., Wells, K. and Powell, A. 2010. Illegal dumping and crime prevention: A case study of Ash Road, Liverpool Council. Pub. Space: JL and Soc. Just., 5(1).

de los Angeles Somarriba-Chang, M and Gunnarsdotter, Y. 2012. Local community participation in ecotourism and conservation issues in two nature reserves in Nicaragua. Journal of Sustainable Tourism, 20(8): 1025-43.

De Witt, L. and Van der Merwe, P. 2015. Key environmental management factors in protected areas an eco-tourist perspective, 4(2). Available at: http://www.aarcherinc.com/files/2011/11/environmental-policy.jpg

Dube, C.N. 2018. Community participation in the management of South Africa's protected areas. African Journal of Hospitality, Tourism and Leisure, 7(2): 1-18.

Eksteen, L. 2012. Relationships between conservators, community partners, and urban conservation areas: a case study of nature reserves on the Cape Flats. Unpublished Magister Artium thesis, University of the Western Cape, Cape Town.

Glanville, K. and Chang, H. C. 2015. Remote sensing analysis techniques and sensor requirements to support the mapping of illegal domestic waste disposal sites in Queensland, Australia. Remote Sensing, 7(10): 13053-13069.

Graham, M. and Ernstson, H. 2012. Comanagement at the fringes: examining stakeholder perspectives at Macassar Dunes, Cape Town, South Africa at the intersection of high biodiversity, urban poverty, and inequality. Ecology and Society, 17(3).

Jakiel, M., Bernatek-Jakiel, A., Gajda, A., Filiks, M. and Pufelska, M. 2019. Spatial and temporal distribution of illegal dumping sites in the nature protected area: The Ojców National Park, Poland. Journal of Environmental Planning and Management, 62(2): 286-305.

Kadafa, A. A., Latifah, A. M., Abdullah, H. S. and Sulaiman, W. N. A. 2013. Current Status of Municipal Solid Waste Management Practice in FCT Abuja. Research Journal of Environmental and Earth Sciences, 5(6): 295-304.

Kaltenborn, B. P., Nyahongo, J. W., Kidegesho, J. R. and Haaland, H. 2008. Serengeti National Park and its neighbours–Do they interact? Journal for Nature Conservation, 16(2): 96-108.

Marshall, M. N. 1996. Sampling for qualitative research. Family Practice, 13(6): 522-526.

Matsumoto, S. and Takeuchi, K. 2011. The effect of community characteristics on the frequency of illegal dumping. Environmental Economics and Policy Studies, 13(3): 177-193.

Oakley, A. 1998. Gender, methodology and people's ways of knowing: Some problems with feminism and the paradigm debate in social science. Sociology, 32(4): 707-731.

Pitt, B. and Boulle, T. 2010. Thinking and Practice of Urban Nature Conservators.

Przydatek, G. 2019. Waste Management in Selected National Parks–A Review. Journal of Ecological Engineering, 20(4): 14-22.

Sadat al Sajib, S. M., Islam, S. Z. and Sohad, M. K. N. 2022. Rohingya influx and socio-environmental crisis in southeastern Bangladesh. The International Journal of Community and Social Development, 4(1): 89-103.

Simelane, T. S., Kerley, G. I. H. and Knight, M. H. 2006. Reflections on the relationships between communities and conservation areas of South Africa: The case of five South African national parks. Koedoe, 49(2): 85-102.

Statistics South Africa (StatsSA). 2011. Census Data. http://www.resource.capetown.gov.za/documentcentre. [20 November 2021]

Taherdoost, H. 2016. Sampling methods in research methodology; how to choose a sampling technique for research. How to choose a sampling technique for research (April 10, 2016), (IJARM), 5.

The City of Cape Town. 2008. Nature Reserves: A network of amazing biodiversity. https://www.capetown.gov.za/environment [18 November 2021]

Verma, J. P. 2012. Data analysis in management with SPSS software. New Delhi: Springer Science and Business Media.

Wells, M. P. and McShane, T. O. 2004. Integrating protected area management with local needs and aspirations. AMBIO: A Journal of the Human Environment, 33(8): 513-519.

Wessels, N., Sitas, N., Esler, K. J. and O'Farrell, P. 2021. Understanding community perceptions of a natural open space system for urban conservation and stewardship in a metropolitan city in Africa. Environmental Conservation, 1-11.

Western, D. and Henry, W. 1979. Economics and conservation in third world national parks. BioScience, 29(7): 414-418.

## ORCID DETAILS OF THE AUTHORS

X. S. Grangxabe: https://orcid.org/0000-0001-6189-7147
T. Maphanga: https://orcid.org/0000-0002-8714-1185
B. S. Chidi: https://orcid.org/0000-0001-8497-7596

Nature Environment and Pollution Technology
An International Quarterly Scientific Journal

p-ISSN: 0972-6268
(Print copies up to 2016)
e-ISSN: 2395-3454

Vol. 23 | No. 3 | pp. 1495-1505 | 2024

Original Research Paper

https://doi.org/10.46488/NEPT.2024.v23i03.019

Open Access Journal

# Seasonal Variation of (Benzo[a]Pyrene) in Ambient Air of Urban to Peri-urban Areas of Panvel Municipal Corporation, Raigad with Reference to Particulate Matter

**Namrata Kislay*, Harshala V. Kasalkar*, Nilesh D. Wagh** and Geeta Malbhage*†**
*Amity School of Applied Sciences, Amity University, Mumbai-410206, India
**SK Somaiya College, Somaiya Vidyavihar University, Mumbai 400077, India
†Corresponding author: Geeta Malbhage; gkmalbhage@mum.amity.edu

**Nat. Env. & Poll. Tech.**
**Website: www.neptjournal.com**

*Received:* 21-11-2023
*Revised:* 15-01-2024
*Accepted:* 22-01-2024

**Key Words:**
Benzo[a]pyrene
Particulate matter
Pollution
Polyaromatic hydrocarbons

## ABSTRACT

Polyaromatic Hydrocarbons (PAHs) in the environment have been linked to severe health effects. This study aims to assess the atmospheric pollutant and analyze the variation in PAHs, focussed on benzo[a]pyrene [B(a)P]. Among all PAHs, B(a)P is regarded as a marker for human carcinogenicity. This study reflects the B(a)P concentration and its correlation with the particulate matter ($PM_{10}$ and $PM_{2.5}$) in rural, peri-urban, and urban areas of Panvel Municipal Corporation, Maharashtra, India. Samples were collected during the pre & post-monsoon season for two consecutive years (Yr. 2020 and Yr. 2021). B(a)P level was determined using high-performance liquid chromatography coupled with a diode array detector. It was observed that $PM_{2.5}$ and $PM_{10}$ show a strong positive correlation (r=0.8-0.9) with B(a)P. It is observed that B(a)P concentrations were high in pre-monsoon w.r.t. post-monsoon, and this concentration increased spatially as we moved from rural to urban areas. Pre-monsoon B(a)P concentration varies somewhat by 5% between rural to urban areas as compared to post-monsoon. High levels of vehicular emissions and industry were associated with the distribution of B(a)P in urban areas, whereas a combination of local emissions and metropolitan area diffusion was responsible for the presence of B(a)P in peri-urban and rural areas. Also, this study captures the variation of B(a)P levels during the period of COVID-19. In future studies, Artificial Intelligence (AI) can augment the determination of PAHs in soil by improving the accuracy and speed of analysis using predictive modeling based on different input parameters to determine outliers in soil PAH data, building sensor networks for real-time monitoring of PAH levels, leverage robotics for automated sample preparations, and rapid testing of samples to identify hotspots.

## INTRODUCTION

Industrialization and urban development, especially in emerging countries, have increased air pollution dispersion in densely populated cities in the past few decades (Buhaug & Urdal 2013, Kermani et al. 2019). These are further augmented by industrial & manufacturing waste, traffic pollution, construction, and burning of biomass that includes Polyaromatic Hydrocarbons (PAHs), particulate matter, and other pollutants.

The PAHs are a category of persistent organic compounds and are one of the most prevalent contaminants in soil, water, and air. It originates from both natural (forest fires, volcanoes, etc.) as well as anthropogenic sources (incomplete combustion of organic matter, like carbon, coke, oil, gas, coal, biomass, vehicular emission, residential heating, asphalt production, etc.) (Wolska et al. 2012, Manoli et al. 2016). Also, the lipophilic nature of PAH makes it easily dissolved and transported by the cell membrane and makes it accumulate in the fatty tissues of living organisms.

Out of sixteen main compounds, Benzo[a]Pyrene, B(a)P is a specific compound that belongs to the group of PAHs. The World Health Organization (WHO) considers B(a)P to be one of the most potent mutagens, frequently employed as a general indicator of PAHs and a marker for carcinogenicity. The Toxic Equivalent Factor (TEF) for all PAHs was determined by comparing the cancer risk of all PAHs relative to the cancer risk of B(a)P (Yu et al. 2008). This can potentially lead to undesirable effects, including cancer, gene mutation (Zhang et al. 2009, Chen et al. 2016), and getting absorbed by fine particulate matter (Baek et al.1991).

Particulate matter (i.e., $PM_{10}$ and $PM_{2.5)}$ has a significant role as a carrier, resulting in air contamination, detrimental health consequences, and global climate changes. They can travel from one area to another for days or even weeks in the air before they gradually get deposited from the atmosphere to the soil. Over the multiple studies done on the size distribution of particulate-bounded PAHs, size is the factor that determines particle deposition, particularly in the respiratory system. Such as $PM_{2.5}$ is more damaging than $PM_{10}$ in terms of its aerodynamic diameter (Oberdorster et al. 2005, Dat & Chang 2017, Kumar et al. 2020). Hence, a significant focus on epidemiological study caters to the measurement of PAHs in $PM_{2.5}$.

In this segment of the study, there are extensive data sets available in developed countries, but the same is not true for developing countries like India. Similar to this there haven't been any studies published about the B(a)P concentrations and their likely sources in the ambient air in Panvel Municipal Corporation (PMC), Panvel (Maharashtra, Inda). PMC is a right-fit study area because it is a fast-developing industrial & residential area, and international airport construction is in progress in the vicinity.

The purpose of this research paper is to study the level of the B(a)P & its impacts on the air in the PMC and its nearby areas over pre and post-monsoon seasons. Hence, the outcome of this study will be utilized to:

(1) assess & predict B(a)P levels using the air samples collected from PMC, Panvel from urban, peri-urban to rural areas, and

(2) identify the factors resulting in seasonal variations, their likely sources of emissions, and their impacts.

In theory, the B(a)P and B(a)P equivalent concentration (BaPeq) can be used to estimate the health risks associated with PAH. The Central Pollution Control Board (CPCB) has set a target value for B(a)P of 1ng.$m^{-3}$ (National Ambient Air Quality Standards).

## MATERIALS AND METHODS

### Sampling Sites, Atmospheric Conditions, and Their Description

The study was carried out in Panvel Municipal Corporation (PMC), which is located between 18°58′N and 19°70′N latitudes and 73°2′E and 73°9′E longitudes. A node of Navi Mumbai metropolis, PMC is situated in Maharashtra's Raigad district in the Konkan division. Many factors make PMC a right-fit location for such a study, including industrial presence, urban & suburban mix, proximity to Mumbai, ecological diversity, transportation density, land-usage changes, and possible environmental policy implications at local & regional levels. The land-use pattern is mostly residential-cum-industrial, with a total population of 5.09 lakh (2011 census), and this number must have experienced reasonable growth till the year 2023. From 2016 to 2021, the built-up area increases by a factor of two.

Additionally, a tropical climate exists in the study area with an average temperature of 37°C and annual rainfall of ~3267 mm, respectively (Environmental Status Report, 2020-21). It is surrounded by offshoots of Sahyadri Ranges in the East, Thane and Dombivali in the North, JNPT port and Uran in the South, and Navi Mumbai in the West. The development in built-up areas throughout the cited areas is seen as primarily responsible for the decline in agriculture, vegetation, barren land, and other land uses. We have identified five different sites in the Panvel Municipal Corporation (PMC) area. It is one of the fully developed industrial areas with businesses engaged in a range of commercial endeavors. Chemical, food and fish processing, dairy products and cold storage, and engineering are the most prevalent industrial activities. Five separate locations were chosen based on the urban, per-urban, and rural areas, and this includes – Panvel, Taloja, Karanjade, Ulwe, and Bhatan. Table 1 and Table 2 show the location-matrix and their respective co-ordinates. Panvel is one of the most populated and advanced cities in this area. Taloja is a popular chemical industrial area created by the Maharashtra Industrial Development Corp. (MIDC). Karanjade is a growing residential area adjoining Panvel town. Ulwe is home to the upcoming Navi Mumbai International Airport (Environmental Status Report, 2020-21). Bhatan is thought

Table 1. Location-matrix view

| | Urban | Peri-Urban | Rural |
|---|---|---|---|
| Industrial | Taloja | - | - |
| Residential | Panvel | Karanjade | - |
| Agricultural | - | Ulwe | Bhatan |

Table 2. Area and co-ordinates

| Sr. No. | Area | Latitude | Longitude |
|---|---|---|---|
| 1. | Bhatan | 18.931531 | 73.163786 |
| 2. | Taloja | 19.058538 | 73.112741 |
| 3. | Ulwe | 18.982386 | 73.078349 |
| 4. | Karanjade | 18.983045 | 73.091544 |
| 5. | Panvel | 18.99340 | 73.116775 |

of as a control location. The burning of coal and biomass is the main cause of air pollution emissions. Another factor contributing to pollution is the highway network.

Atmospheric conditions are another important criterion since it has a significant impact on the formation of numerous atmospheric pollutants (Zhang 2019, Chen et al. 2020 b). Various combinations and a range of atmospheric data points were considered to perform this study, including maximum temperature, relative humidity, wind speeds, and precipitation for the pre-monsoon and post-monsoon seasons in the years 2020 and 2021. These data were acquired from Power Data Access Viewer, NASA, and the meteorological parameter is depicted in Table 3.

The above data sets constitute nearly 180 units of readings across six months ranging from pre and post-monsoon. The wind is a crucial component for the dispersion and dilution of pollutant plumes. Air pollution is more likely to disperse under high wind conditions than it is to accumulate in low

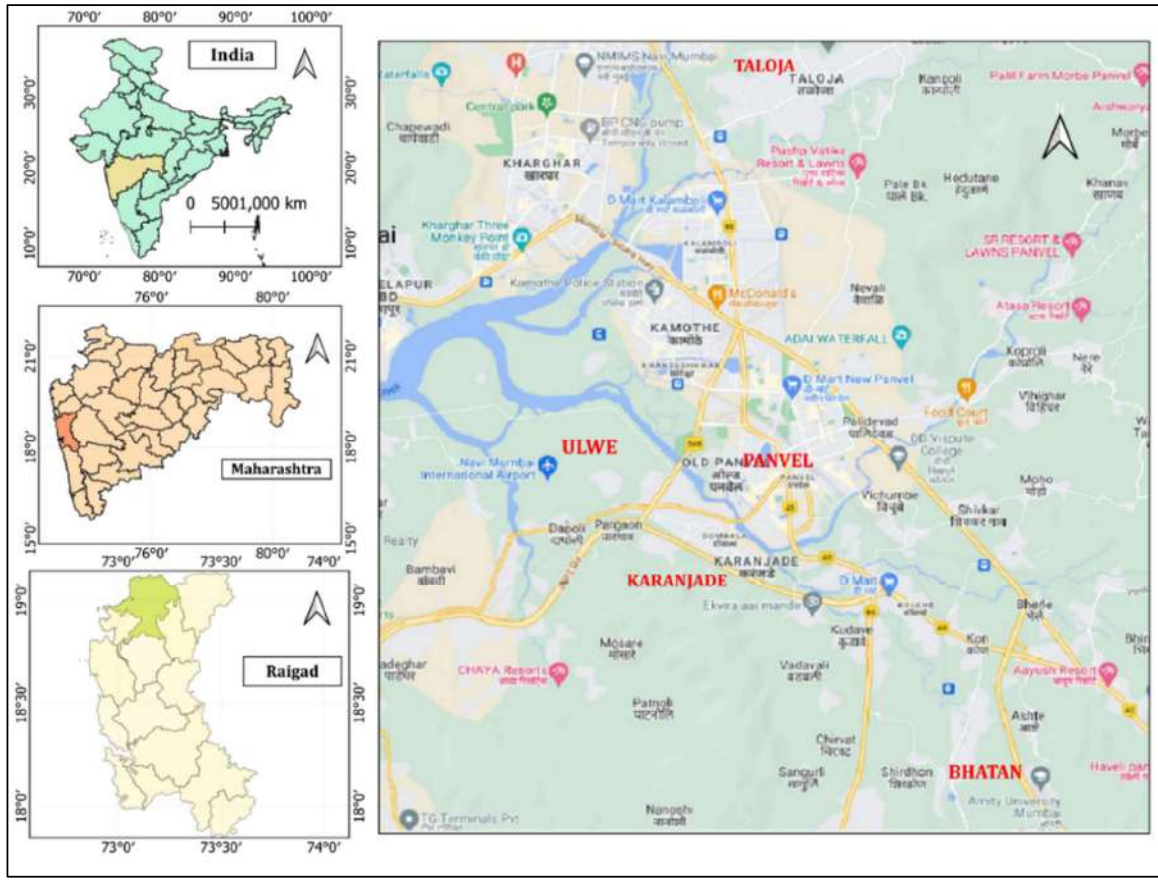


Fig. 1: The study area of the five sites located within the PMC.

Table 3: Meteorological parameters of the area

| Parameters Months | Temperature [°C] Mean ± SD | | Relative Humidity [%]Mean ± SD | | Wind speed [m.s$^{-1}$] Mean ± SD | | Precipitation [mm] | |
|---|---|---|---|---|---|---|---|---|
| | 2020 | 2021 | 2020 | 2021 | 2020 | 2021 | 2020 | 2021 |
| March | 35.83 ±3.29 | 39.12 ±1.50 | 49.34 ±11.8 | 37.32 ±9.19 | 6.41±1.12 | 7.03±0.97 | 0.13 | 0.07 |
| April | 40.40 ±1.88 | 39.14 ±1.28 | 51.15 ±5.18 | 51.03 ±5.68 | 7.25±1.03 | 6.33±0.80 | 0.171 | 0.255 |
| May | 39.42±1.56 | 35.93±3.64 | 57.28±3.47 | 65.06 ±15.25 | 6.57±0.74 | 6.87±3.72 | 0.23 | 0.26 |
| October | 30.73±1.04 | 30.79±1.06 | 82.77±7.09 | 81.40 ±5.93 | 4.87±1.44 | 5.60±1.58 | 5.81 | 2.34 |
| November | 30.89±0.78 | 39.14±1.28 | 75.99±4.44 | 78.90 ±5.87 | 7.05±1.50 | 6.94±1.50 | 0.015 | 1.66 |
| December | 29.98±0.94 | 35.93±3.64 | 69.42±7.78 | 75.30 ±5.24 | 7.23±1.96 | 6.74±1.75 | 0.39 | 2.27 |

wind conditions. Strong winds can concentrate the pollutants by directing a plume to a specific location. Like this, rain can remove particulate matter (PM) from the air. The generation and emissions of air pollutants were influenced by temperature. Also, relative humidity (RH) has a significant impact on atmospheric photochemistry, including the production of $O_3$ and OH radicals (Lu et al. 2019 b).

### Sample Equipment, Collection Frequency, and Sample Size

Sample equipment: Sampling of particulate matter and PAH was conducted during the pre-monsoon (March-April-May) and post-monsoon (October-November-December) seasons for the years 2020 and 2021. Separate samples were collected for $PM_{2.5}$ and $PM_{10.}$ Collecting samples before and after the monsoon helps with better influence assessment of PAH levels in particulate matter. Monsoon changes can have an impact on atmospheric conditions and can affect the transport, deposition, and chemical transformation of particulate matter and PAHs in the environment. Also, it enables a more comprehensive understanding of the dynamics of PAHs in the environment by providing insights into the complex interactions between meteorological conditions, emissions sources, and pollutant levels.

A total number of 350 data samples were collected for $PM_{10}$ over the year 2020 and 2021 from all the sites. For a few of the sites, sample data were collected from Maharashtra Pollution Control Board (MPCB) portals. (https://mpcb.gov.in/). While for $PM_{2.5}$ and B(a)P, 120 data samples each were collected from all the sites. In this study, $PM_{10}$ and B(a)P sampling was carried out using a High-Volume Sampler with Glass Fibre Filter paper. Glass fiber filter papers have a high collection efficiency for fine particles and are designed to effectively capturing and retaining particles, preventing them from passing through the filter and escaping into the environment during sampling. These particles are inhaled deeply into the respiratory system due to their small size and thus pose a health risk to humans. Glass fiber filters are effective at capturing particles in this size range.

Whereas $PM_{2.5}$ sampling was done using Fine Particulate Samplers with Teflon Filter paper. $PM_{2.5}$ sampling is designed to target fine particulate matter with a diameter of 2.5 micrometers or less. Teflon filters are effective at capturing particles in this size range. Teflon filters are chemically inert and do not introduce contaminants or react with the collected particles. This is crucial for accurate measurements of $PM_{2.5}$ composition.

Sample collection frequency: The sampling for particulate matter was carried out for 8 hours with a frequency of twice a week. All the sampling was carried out as per the Central Pollution Control Board (CPCB) guidelines. (https://cpcb.nic.in/).

### Sample Processing

In this sampling process, the exposed filter paper was cut into pieces and transferred to a 250 ml beaker. Ultrasonic extraction was carried out using methanol. The bottles were forcefully shaken to suspend the contents after being sealed with screw cap closures packed with polytetrafluoroethylene (PTFE)-faced silicone rubber septum. After that, the bottles were subjected to a high-performance ultrasonic bath that was microprocessor-controlled for precise temperature and time control. This process took place for 60 minutes at 50°C. The samples were periodically re-suspended by shaking and inverting the sample bottles. The supernatant from the centrifuged extraction solutions was then decanted into 4 mL amber vials and kept in the refrigerator until clean-up and analysis were complete (Oluseyi et al. 2011). Sample contaminants may be cleaned out using Solid Phase Extraction (SPE). The residue was then transferred to 1-mL vials and examined using high-performance liquid chromatography (Agilent Technologies, 1260 Infinity).

By comparing the retention times of the samples to those of B(a)P standards, the chromatographic peaks of the samples were detected. The absence of PAH chemicals in the blank samples proved that there was no sample contamination. The chromatographic setups used for the analysis are listed in Table 4.

### Data and Result Analysis

Pearson correlation was used in the form of a correlation coefficient to determine the following relationships.

- between B(a)P and particulate matters ($PM_{2.5}$ & $PM_{10}$), and
- only between particulate matters ($PM_{2.5}$ & $PM_{10}$)

Pearson correlation was used to assess and identify any statistically significant association between the concentrations of B(a)P and particulate matter. This helps determine the relationship between B(a)P and particulate matter, which is essential for understanding their potential co-occurrence and interdependence, if any.

Table 4: Conditions for B(a)P analysis in HPLC.

| Column | Poroshell C18, 4.6x 250 mm |
|---|---|
| Column temperature | 40°C |
| Eluent | Acetonitrile: water (60%:40%) |
| Detector | UV-Visible detector |
| Run time | 10 mins |
| Flow rate | 1mL.min$^{-1}$ |
| Injection volume | 10 µL |

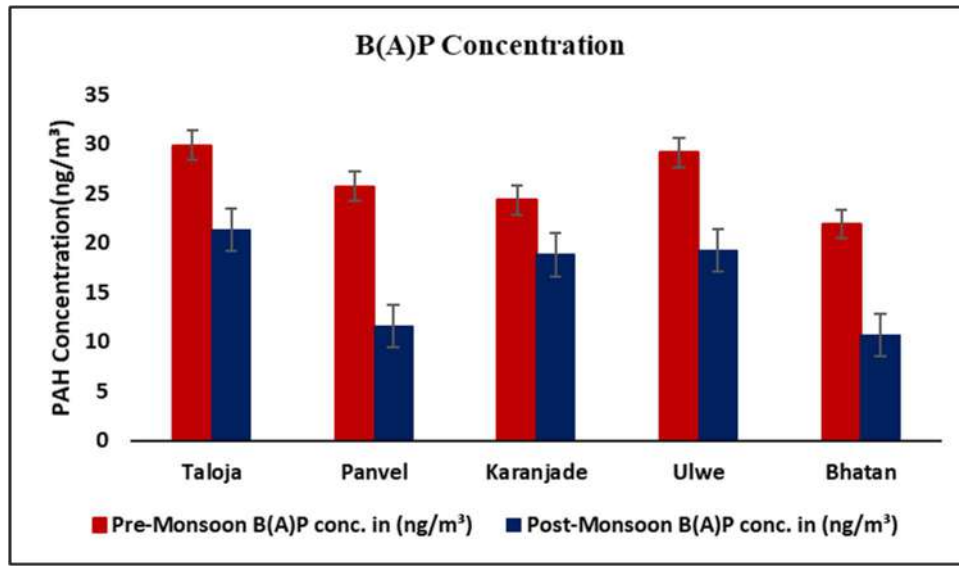


Fig. 2: B(a)P concentrations at five different locations during the pre-monsoon and post-monsoon.

A relationship or correlation analysis can provide insights into potential sources of pollution. Suppose there is a strong positive correlation between B(a)P and PM. In that case, it may indicate that B(a)P is originating from sources that also emit particulate matter, such as combustion processes. Additionally, a positive correlation between B(a)P and PM can influence regulatory decisions and policies. It may prompt stricter regulations on sources that emit pollutants to reduce overall environmental and health impacts.

## RESULTS AND DISCUSSION

### Pre-Monsoon and Post-Monsoon Variation of B(a)P at Different Sampling Sites

It was observed in the study that the concentrations of B(a) P at the urban, peri-urban, and rural sites were in the ranges of 10.41-29.90 ng.m$^{-3}$, 15.4-29.17 ng.m$^{-3,}$ and 10.69-21.93 ng.m$^{-3}$, respectively. In general, concentrations of B(a)P were observed to be on the higher side for all the sampling sites. The B(a)P levels and trends varied significantly between sampling sites and over seasons (i.e., pre-monsoon and post-monsoon).

In pre-monsoon, the concentration pattern showed the following trend (highest to lowest), i.e., Taloja > Ulwe > Panvel > Karanjade > Bhatan.

While there is slight variation observed in the post-monsoon pattern, i.e., Taloja > Ulwe > Karanjade > Panvel > Bhatan.

As per the National Ambient Air Quality Standards (NAAQS), the annual concentration of B(a)P in ambient air is 1ng.m$^{-3}$ in industrial, residential, rural, and other areas.

In general, the B(a)P was more abundant in pre-monsoon season samples. The maximum B(a)P concentration (29.90 ng.m$^{-3}$) was found at the urban site in the pre-monsoon season, and the minimum (10.69 ng.m$^{-3}$) at the rural site in the post-monsoon season. Fig. 2 shows the pre and post-monsoon concentration of the B(a)P across the five different sites within Panvel Municipal Corporation. Details of the Pre-monsoon and Post-Monsoon for the year 2021.

There are multiple reasons behind the different concentrations of B(a)P for all the sites over different seasons are highlighted below. Firstly, the urban sites (i.e., Taloja and Panvel) are located near an industrial area and may receive more pollutants from vehicular movement and other sources. Secondly, the B(a)P concentration gap between the urban and peri-urban areas has narrowed down because of growth & development activities that include new construction and a rise in vehicular ownership. Additionally, B(a)P was found in rural area samples (i.e., Bhatan) that potentially could be a result of local emissions, which include improper disposal of solid waste, burning of fossil fuels, and diffusion from metropolitan areas.

### Source-Identification and Long-Range Transport of Air-Borne Particulate Matter

During the study period, 'Backward Trajectory' computations were used to forecast the air parcel trajectories of atmospheric contaminants, B(a)P, over PMC, Panvel. This computation gives an indicative picture of the pollution brought on by airborne particles that are carried by the wind or released by local origin sources.

As part of this study, a 5-day isentropic back trajectory was calculated for a total run time of 120 Hours at an altitude of 500m using Hybrid-Single Particle Lagrangian Integrated Trajectory (HYSPLIT) model developed by the National Oceanic and Atmospheric Administration's (NOAA) Air Resources Laboratory (ARL) for the pre-monsoon and post-monsoon season for the year 2020 and 2021. The HYSPLIT model (Draxler et al. 2012, http://ready.arl.noaa.gov/HYSPLIT.php) was used in conjunction with the Global Data Assimilation System (GDAS1) metrological database as input. The backward trajectory was created as an indicative cause of PMC's elevated PAH concentration. The study was carried out at the control spot, i.e., a rural site (Bhatan), and it is similar to all the other sites because of its proximity. It is shown in Fig. 3 (a, b, c, and d) for all the possible flow combinations:

- Pre-Monsoon, Year 2020
- Post-Monsoon, Year 2020
- Pre-Monsoon, Year 2021
- Post-Monsoon, Year 2021

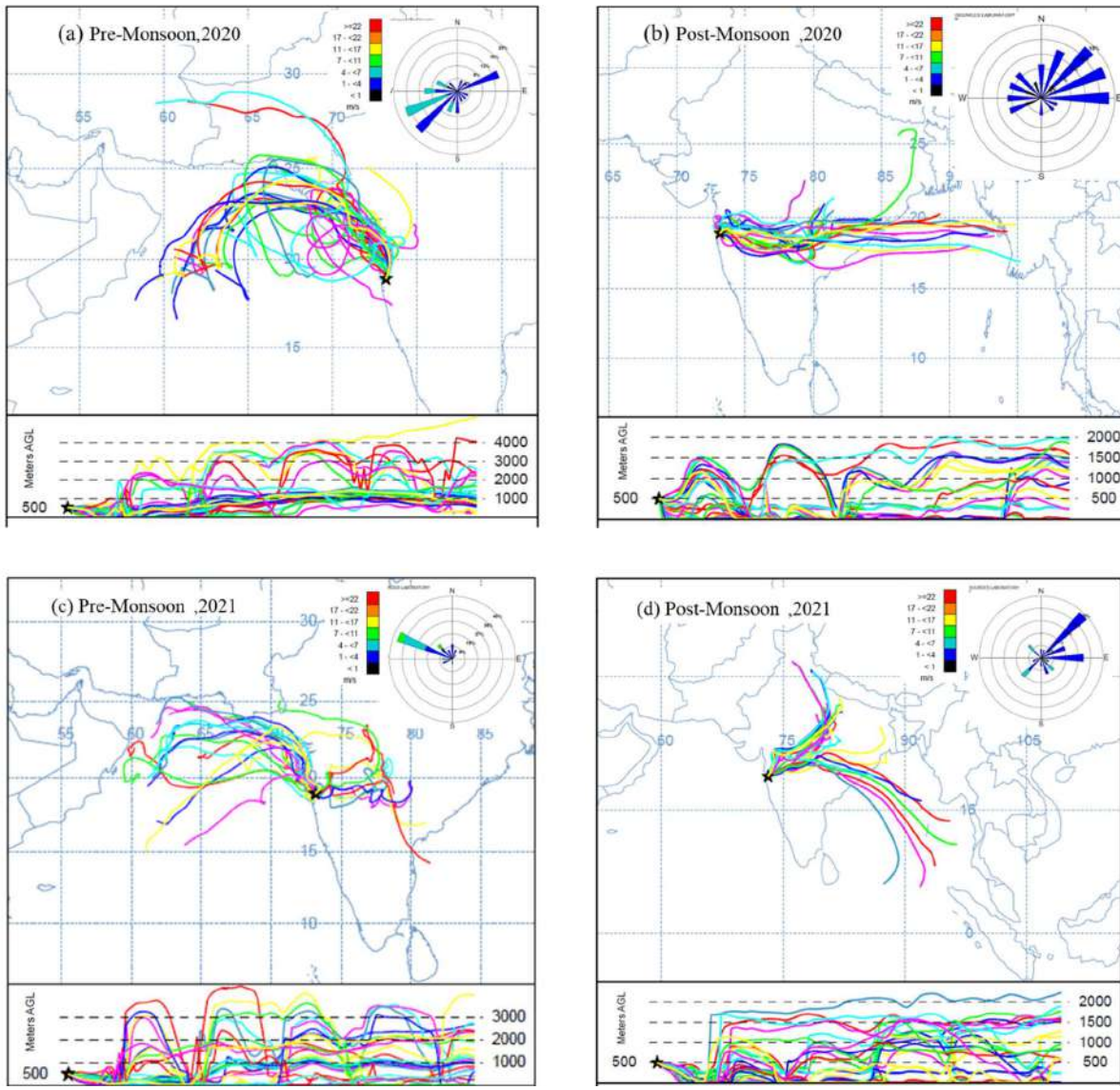


Fig. 3: (a, b, c, d and d) 5-day HYSPLIT air mass backward trajectories at 500 m AGL at PMC, Panvel for the pre and post-monsoon. The color scale represents the traveling altitude by the air mass before reaching the observation site.

The back-trajectory research study revealed that the air mass came from various sources depending on the season. Most of the back trajectories that were analyzed suggested that the air mass may have originated and transported from outside India. The trajectories during the pre-monsoon season indicate a long-distance transit of the filthy air flowing towards PMC, Panvel, over the Arab nations and continents of the Middle East. Due to frequent dust storms and relatively strong winds, the pre-monsoon season's high concentration of $PM_{2.5}$ is typically impacted by wind-blown dust (Panicker et al. 2013). In the post-monsoon, the trajectories originated from the northern and northeastern parts of India. The nearby industrial operations and agricultural activities also contributed to the large mass concentration of pollution over the research site.

## Particulate Matter Concentration in PMC, Panvel (Maharashtra, India)

This section reflects the analysis around the seasonal variation and depiction of satellite study via the Giovanni NASA portal.

Table 4: The average concentration of $PM_{10}$ and $PM_{2.5}$ of all five sampling sites over pre & post-monsoon seasons.

| | Pre-Monsoon, 2020 | | Post-Monsoon, 2020 | | Pre-Monsoon, 2021 | | Post-Monsoon, 2021 | |
|---|---|---|---|---|---|---|---|---|
| | $PM_{10}$ | $PM_{2.5}$ | $PM_{10}$ | $PM_{2.5}$ | $PM_{10}$ | $PM_{2.5}$ | $PM_{10}$ | $PM_{2.5}$ |
| Taloja | 62.66 ±11.45 | 32.8 ± 3.81 | 65.42 ± 7.85 | 39.3 ± 1.49 | 66.78 ± 4.74 | 39.81 ± 1.30 | 67.35 ± 11.21 | 41.71 ± 3.69 |
| Panvel | 40.7 ±7.02 | 32.5 ± 3.67 | 50.96 ±4.40 | 37.15 ± 1.44 | 54.08 ±5.70 | 36.5 ± 2.28 | 54.62 ±10.79 | 37.36 ± 1.02 |
| Karanjade | 47.9 8.59± | 30.8 ± 2.96 | 58.5±8.42 | 35.6 ± 1.11 | 57.33±2.65 | 37.2 ± 2.68 | 60.14±7.51 | 38.78 ± 1.63 |
| Ulwe | 41.28 6.26± | 33.1 ± 5.09 | 62±4.23 | 38.4 ± 1.33 | 65.76±3.46 | 40.67 ± 1.52 | 65.5±8.42 | 40.31 ± 1.58 |
| Bhatan | 53.4 4.79± | 27.5 ± 1.27 | 44.4±2.83 | 34.3 ± 1.08 | 48.67±3.95 | 33.41 ± 1.06 | 47.9±5.25 | 34.51 ± 2.60 |

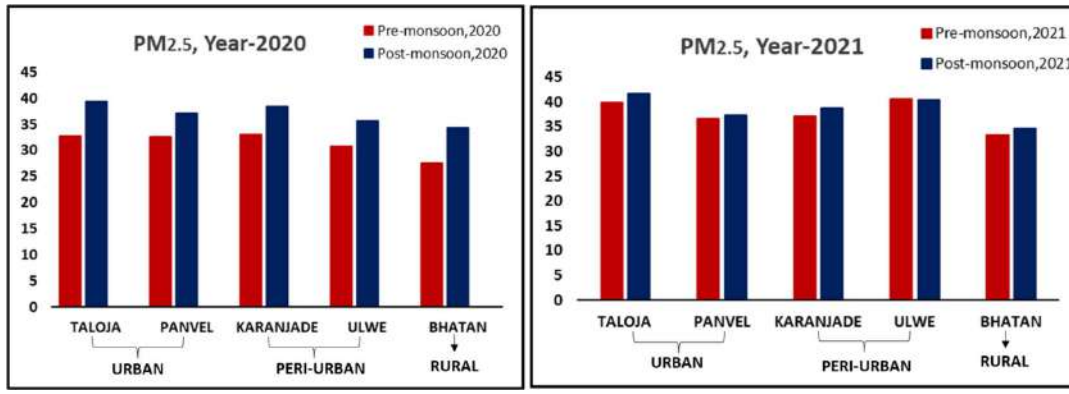


Fig. 4: $PM_{2.5}$ concentration pattern during pre-monsoon and post-monsoon.

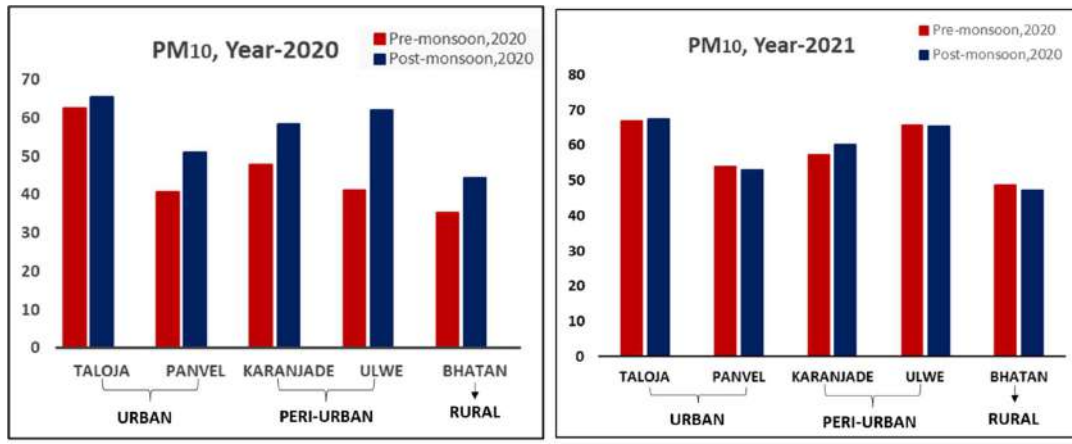


Fig. 5: $PM_{10}$ concentration pattern during pre-monsoon and post-monsoon.

**Seasonal variations of $PM_{2.5}$ and $PM_{10}$ value across pre and post-monsoon seasons:** Basis the study, seasonal variation can be observed for $PM_{2.5}$ and $PM_{10}$ values (shown in Table 4).

For $PM_{2.5}$,

- Pre-monsoon average concentrations are in the range of 27.5-33.1 $\mu g.m^{-3}$ and 33.41-40.67 $\mu g.m^{-3}$ for the years 2020 and 2021, respectively,
- Post-monsoon average concentrations are in the range of 34.3-39.3 $\mu g.m^{-3}$ and 34.51-41.71 $\mu g.m^{-3}$ for the years 2020 and 2021, respectively.

For $PM_{10}$,

- Pre-monsoon average concentrations are in the range of 40.7-62.66 $\mu g.m^{-3}$ and 48.67-66.78 $\mu g.m^{-3}$ for the years 2020 and 2021, respectively.
- Post-monsoon average concentrations are in the range of 44.4-65.42 $\mu g.m^{-3}$ and 47.9-67.35 $\mu g.m^{-3}$ for the years 2020 and 2021, respectively.

All the measured concentrations exceed the NAAQS standards of annual averages of 40 $\mu g.m^{-3}$ for $PM_{2.5}$ and 60 $mg.m^{-3}$ for $PM_{10.}$ High concentration of PM in the atmosphere can be attributed to several variables, including high

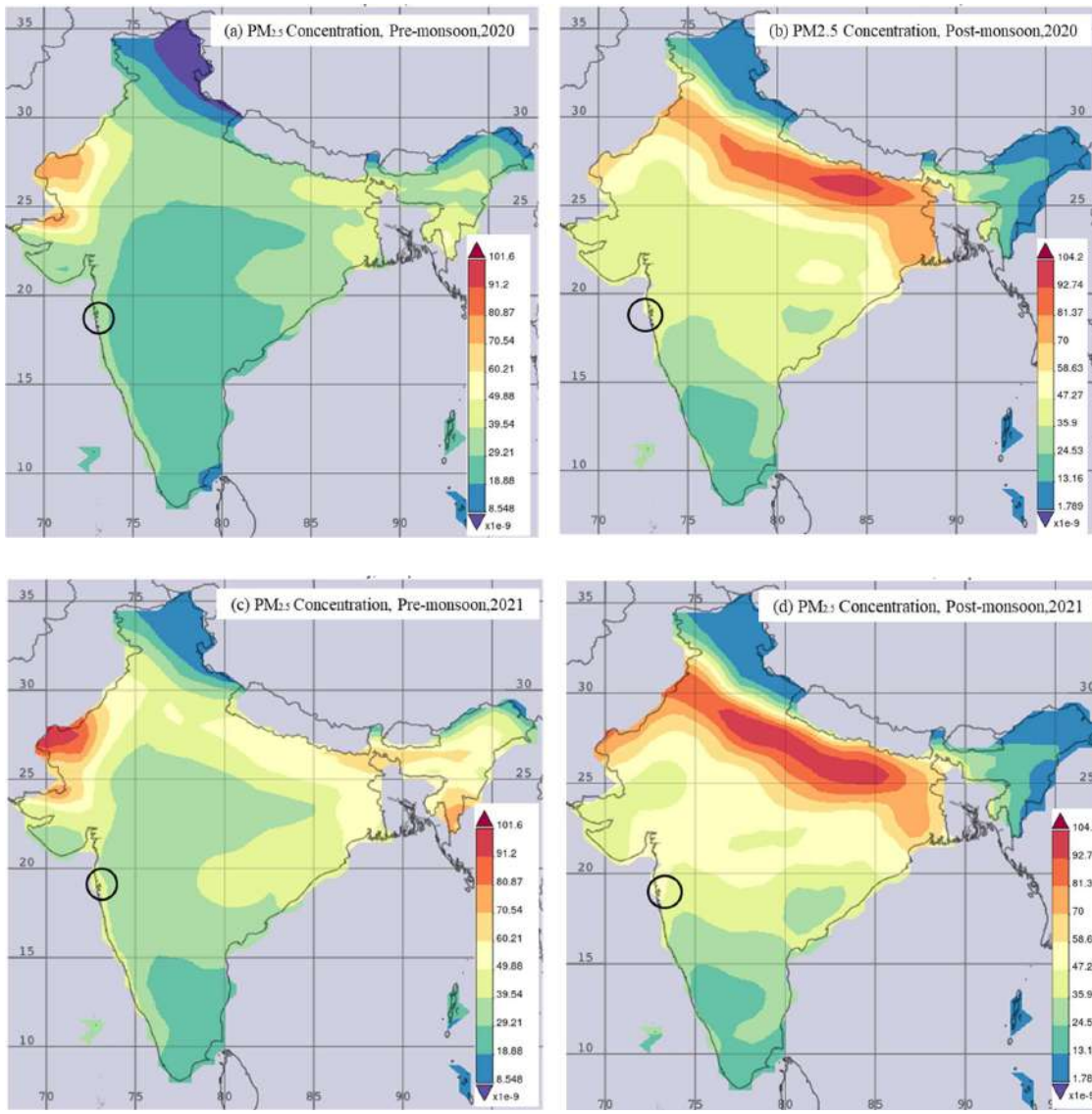


Fig. 6: (a, b, c, and d) Time average map of $PM_{2.5}$ surface mass concentration monthly 0.5 × 0.625 deg. (MERRA-2 Model M2TMNXAER v 5.12.4) $Kg.m^{-3}$ at the two different seasons (Pre-Monsoon and Post-Monsoon).

energy consumption, rapid economic growth, etc. Details of the Pre-monsoon and Post-Monsoon for the year 2020-21.

Fig. 4 and 5 illustrate the distinct seasonal fluctuations in PM levels at all 5 sampling sites. From the figures, both $PM_{10}$ and $PM_{2.5}$ are slightly higher in post-monsoon than in pre-monsoon.

All the sampling sites in Table 4 are distinguished into three functional areas: urban, peri-urban, and rural (including industrial, residential, and agricultural sites). Additionally, it was found that, as compared to rural areas, particulate concentrations are higher in urban and peri-urban areas. Differences in the kinds and intensities of emissions primarily caused the geographic variations in particulate matter between sampling locations. The study data indicates that residential firewood burning has an impact on rural areas, while automotive emissions are the main source of particulate matter in urban and peri-urban areas, with a large contribution from industries.

**$PM_{2.5}$ satellite study via the Giovanni NASA portal:** $PM_{2.5}$ measurements were also observed from the satellite study via the Giovanni NASA website for the years 2020 and 2021. This helps analyze various data sets collected by NASA's Earth-observing satellites.

The pictorial representation (Fig. 6) is the result of the time average map of $PM_{2.5}$ surface mass concentration monthly $0.5 \times 0.625$ deg. (MERRA-2 Model M2TMNXAER v 5.12.4) $Kg.m^{-3}$ at the two different monsoon seasons.

Key takeaways from the above representation include the burning of biomass, coal, waste incineration, and stubble as the major sources of particulate matter in post-monsoon. It should be noted that as biomass and coal are utilized for heating in these regions during the winter, a significant portion of the contribution from burning these fuels came from the north and north-eastern states, including Haryana, Uttar Pradesh, Bihar, and West Bengal states in India (Guo et al. 2018). This may help to partially explain the large contributions from biomass burning, which is also India's main source of particulate matter. The higher concentration of particulate matter in the study area is directly or indirectly linked with the long-range transport of pollutants from other states, as shown in the backward trajectory. However, it cannot be concluded that the particulate matter getting carried by the air is resulting in increased benzo[a]pyrene concentration. So, the gap that is identified as part of this study can be further studied in future research activities.

### B(a)P Level During the Period of COVID-19

We all experienced the effects of COVID-19 and the blackouts it resulted in. All companies, industrial complexes, educational institutions, and local marketplaces were required to shut down completely, per an order from the Indian government during the COVID-19 lockdown. It had the biggest impact in reducing traffic emissions in 2020, which may have caused the B(a)P level to fall significantly across all sites. At the same time, industrial activity was also affected by the pandemic. Even though many nations saw human casualties, on the contrary, environmental conditions improved, leading to a decrease in particulate matter, black carbon, and PAH emissions, thus resulting in an improved air quality level (Agarwal et al. 2020, Gautam 2020, Panda et al. 2020, Sharma et al. 2020, Singh & Chauhan 2020, Ambade et al. 2021). Due to this, air pollution emission sources altered substantially throughout the lockdown period.

This is to note that B(a)P was not present in a detectable amount during this period at the sites in consideration. While in the research, Phenanthrene and Pyrene were the most abundant PAH detected during the lockdown period in both pre-monsoon and post-monsoon samples. Prior research has identified some PAHs, such as pyrene and phenanthrene, as markers for different types of air pollution in metropolitan areas, such as coal combustion, incineration, and wood burning. Low molecular weight PAH, like Pyrene, is more prevalent in emissions from the burning of dried cow dung (Harrison et al. 1996, Khalili et al. 1995, Li & Kamens 1993). The concentration of pyrene in the ambient samples in Mumbai is due to the combustion of cooking fuel, i.e., animal manure, Liquid Petroleum Gas, and Kerosene (Raiyani et al. 1993).

While short-term reductions in air pollution were observed during COVID-19 lockdowns, long-term trends in B(a)P levels may require more data points and continuous monitoring. Long-term impact on B(a)P levels depends on factors, including ongoing emission reduction efforts and required future policy amendments related to air quality and environmental sustainability.

### Correlation of Particulate Matter ($PM_{2.5}$ and $PM_{10}$) and B(a)P Using Statistical Approach

The quality of the air was examined with respect to B(a)P in particle size fractions $PM_{2.5}$ and $PM_{10}$. The relationship between B(a)P and particulate matter was analyzed using Pearson correlation. The study showed a significant positive correlation between the levels of $PM_{2.5}$ and $PM_{10}$ with B(a)P in the air (i.e., r = 0.8-0.9).

The strong correlation between particulate matter and B(a)P showed that B(a)P concentrations increased effectively with increasing particulate matter mass concentrations. Table 5 shows the correlation for particulate matter. This correlation is established using 30 data sets distributed over

Table 5: Pearson correlations of particulate matter ($PM_{10}$ and $PM_{2.5}$) and B(a)P concentrations in pre-monsoon and post-monsoon period.

| Pre-monsoon period, 2021(n=30) | | | | Post-monsoon period, 2021(n=30) | | | |
|---|---|---|---|---|---|---|---|
| | $PM_{2.5}$ | $PM_{10}$ | B(a)P | | $PM_{2.5}$ | $PM_{10}$ | B(a)P |
| $PM_{2.5}$ | 1.000 | | | $PM_{2.5}$ | 1.000 | | |
| $PM_{10}$ | 0.856** | 1.000 | | $PM_{10}$ | 0.859** | 1.000 | |
| B(a)P | 0.928** | 0.900** | 1.000 | B(a)P | 0.871** | 0.949** | 1.000 |

**Correlation is significant at the 0.01 level (2-tailed).

pre-monsoon and post-monsoon samples.

Concentrations of $PM_{2.5}$ and $PM_{10}$ were also highly correlated because the primary sources of emissions are almost similar for both particulate matters. Smaller particulates typically contain more B(a)P. This is because high-temperature sources, such as combustion, mainly produce fine particulates with a high B(a)P content. They are an excellent adsorbent due to a high number of concentrations, small size, and comparatively large surface area per unit of mass (Sheu et al. 1997). These results indicated that the sources of particulate matter and B(a)P in the air were mainly comparable. Hence, reducing particulate matter levels reflects an efficient strategy to lower the B(a) P level in the air.

## CONCLUSION

This is the first study carried out on the particulate matter and B(a)P in urban, peri-urban, and rural areas of PMC in pre-monsoon and post-monsoon periods, and it has presented valuable insights. The result showed that the concentration of particulate matter and B(a)P was quite concerning when compared to NAAQS benchmarks. The B(a)P concentration was thirty times higher than the standard limit of NAAQS ($1ng.m^{-3}$).

The concentration of B(a)P and particulate matter were higher at urban sites, i.e., the maximum concentration of B(a) P was recorded in Taloja in both periods, i.e. 29.9 $ng.m^{-3}$ and 21.32 $ng.m^{-3,}$ respectively. When compared to post-monsoon, the seasonal variation pattern of B(a)P reveals a considerable increase in concentration. Thus, the increased B(a)P load in the PMC (i.e., 5 sites) is attributed to increased industrial activities, vehicular emissions, and population density. This requires proper corrective intervention to reduce the adverse effects of prolonged exposure on the surrounding population. And thus, help realize the importance of sustainable urban planning and pollution control measures to mitigate adverse health and environmental effects. The study also reflects the importance of implementing air quality management policies tailored to the larger requirements of urban, peri-urban, and rural areas. These measures should include stricter emissions controls, green infrastructure development, and public awareness campaigns.

Nonetheless, it is critical to start leveraging Artificial Intelligence (AI) in the study of particulate matter and B(a) P that significantly enhances and enables fast turnaround in research processes. AI can be used to develop predictive models for PM and B(a)P basis historical data and air circulation patterns can help devise pro-active pollution control measures. Additionally, AI combined with GIS will help create faster and more detailed maps for PM and B(a) P in areas like PMC and can be a potential next step of this research. A holistic integration of data sets – collected from satellite imagery, weather data, and ground-based sample results – can also provide a view of air quality and pollution sources. By harnessing the power of AI, institutions can work toward effective pollution control mechanisms and public health protection strategies in Panvel Municipal Corporation, Maharashtra.

## ACKNOWLEDGEMENTS

The writers share their great appreciation and heartfelt thanks to the readers for their constructive comments and valuable feedback that led to this article's development, completeness, and transparency.

## REFERENCES

Agarwal, A., Kaushik, A., Kumar, S. and Mishra, R.K. 2020. Comparative study on air quality status in Indian and Chinese cities before and during the COVID-19 lockdown period. Air Qual. Atmos. Health, 13: 1167-1178. https://doi.org/10.1007/s11869-020-00881-z

Ambade, B., Kurwadkar, S., Sankar, T.K. and Kumar, A. 2021. Emission reduction of black carbon and polycyclic aromatic hydrocarbons during COVID-19 pandemic lockdown. Air Qual. Atmos. Health, 14(7): 1081-1095. https://doi.org/10.1007/s11869-021-01004-y

Ambade, B., Sankar, T.K., Kumar, A., Gautam, A.S. and Gautam, S. 2021. COVID-19 lockdowns reduce the Black carbon and polycyclic aromatic hydrocarbons of the Asian atmosphere: source apportionment and health hazard evaluation. Environ. Dev. Sustain., 23(8): 12252-12271.

Baek, S.O., Field, R.A., Goldstone, M.E., Kirk, P.W.W., Lester, J.N. and Perry, R., 1991. A review of atmospheric polycyclic aromatic hydrocarbons: sources, fate, and behavior. Water Air Soil Pollut., 60: 279-299. https://doi.org/10.1007/BF00282628

Buhaug, H. and Urdal, H. 2013. An urbanization bombs. Population growth and social disorder in cities. Glob. Environ. Change, 23: 1-10. https://doi.org/10.1016/j.gloenvcha.2012.10.016

Chen, L., Zhu, J., Liao, H., Yang, Y. and Yue, X. 2020b. Meteorological influences on PM2.5 and O3 trends and associated health burden since

China's clean air actions. Sci. Total Environ., 744: 140837. https://doi.org/10.1016/j.scitotenv.2020.140837

Chen, Y.C., Chiang, H.C., Hsu, C.Y., Yang, T.T., Lin, T.Y., Chen, M.J., Chen, N.T. and Wu, Y.S. 2016. Ambient PM2.5-bound polycyclic aromatic hydrocarbons (PAHs) in Changhua County, central Taiwan: Seasonal variation, source apportionment and cancer risk assessment. Environ. Pollut., 218: 372-382. https://doi.org/10.1016/j.envpol.2016.07.01

Dat, N.D. and Chang, M.B. 2017. Review of characteristics of PAHs in the atmosphere, anthropogenic sources, and control technologies. Sci. Total Environ., 609: 682-693. https://doi.org/10.1016/j.scitotenv.2017.07.204

Draxler, R., Stunder, B., Rolph, G., Stein, A., Taylor, A., Zinn, S., Loughner, C. and Crawford, A. 2012. HYSPLIT4 User's Guide, Version 4, Report. NOAA, Silver Spring, Md www.arl.noaa.gov/documents/reports/hysplit_user_guide.pdf.

Environmental Status Report 2020-2021. Panvel Municipal Corporation, https://www.panvelcorporation.com/myfinalimg/1655554824.pdf

Gautam, S. 2020. COVID-19: air pollution remains low as people stay at home. Air Qual. Atmos. Health, 13: 853–857. https://doi.org/10.1007/s11869-020-00842-6

Guo, H., Kota, S.H., Chen, K., Sahu, S. K., Hu, J., Ying, Q., Wang, Y. and Zhang, H. 2018. Source contributions and potential reductions to health effects of particulate matter in India. Atmos. Chem. Phys., 18: 15219–15229.https://doi.org/10.5194/acp-18-15219

Harrison, R.M., Smith, D.T.J. and Luhana, L., 1996. Source apportionment of atmospheric polycyclic aromatic hydrocarbons collected from an urban location in Birmingham, UK. Environ. Pollut., 21: 950. https://doi.org/10.1021/es950252d

Kermani, M., Asadgol, Z. and Arfaeinia, H. 2018. A study of polycyclic aromatic hydrocarbons (PAHs) and trace elements in ambient air PM2.5 in an urban site of Tehran, Iran. J. Health Saf. Environ., 5: 947-956.

Khalili, N.R., Scheff, P.A. and Holsen, T.M., 1995. PAH source fingerprints for coke ovens, diesel and gasoline engines, highway tunnels, and wood combustion emissions. Atmos. Environ., 29: 533-542. https://doi.org/10.1016/1352-2310(94)00275-P

Kumar, A., Sankar, T.K., Sethi, S.S. and Ambade, B. 2020b. Characteristics, toxicity, source identification and seasonal variation of atmospheric polycyclic aromatic hydrocarbons over East India. Environ. Sci. Pollut. Res., 27: 678-690. https://doi.org/10.1007/s11356-019-06882-5

Li, C.K. and Kamens, R.M. 1993. The use of polycyclic aromatic hydrocarbons as source signatures in receptor modeling. Atmos. Environ., 27A: 523-529. https://doi.org/10.1016/0960-1686(93)90209-H

Lu, X., Zhang, L. and Shen, L. 2019b. Meteorology and climate influences on tropospheric ozone: A review of natural sources, chemistry, and transport patterns. Curr. Pollut. Rep., 5: 238-260. https://doi.org/10.1007/s40726-019-00118-3

Manoli, E., Kouras, A., Karagkiozidou, O., Argyropoulos, G., Voutsa, D. and Samara, C. 2016. Polycyclic aromatic hydrocarbons (PAHs) at traffic and urban background sites of northern Greece: source apportionment of ambient PAH levels and PAH-induced lung cancer risk. Environ. Sci. Pollut. Res., 23: 3556-3568. https://doi.org/10.1007/s11356-015-5573-5

Oberdorster, G., Oberdorster, E. and Oberdorster, J. 2005. Nanotoxicology: an emerging discipline evolving from studies of ultrafine particles. Environ. Health Perspect., 113: 823-839. https://doi.org/10.1289/ehp.7339

Oluseyi, T., Olayinka, K., Alo, B. and Smith, R.M. 2011. Comparison of extraction and clean-up techniques for the determination of polycyclic aromatic hydrocarbons in contaminated soil samples. Afr. J. Environ. Sci. Technol., 5(7): 482-493. https://doi.org/10.5897/AJEST10.307

Panda, S., Mallik, C., Nath, J., Das, T. and Ramasamy, B. 2020. A study on the variation of atmospheric pollutants over Bhubaneswar during the imposition of nationwide lockdown in India for the COVID-19 pandemic. Air Qual. Atmos. Health, 14: 97-108. https://doi.org/10.1007/s11869-020-00916-5

Panicker, A.S., Lee, D.I., Kumkar, Y.V., Kim, D., Maki, M. and Uyeda, H. 2013. Decadal climatological trends of aerosol optical parameters over three different environments in South Korea. Int. J. Climatol., 33: 1909-81916. https://doi.org/10.1002/joc.3557

Raiyani, C.V., Shah, S.H., Desai, N.M., Venkaiah, K., Patel, J.S., Parikh, D.J. and Kashyap, S.K., 1993. Characterization and problems of indoor pollution due to cooking PLOS, 1: 227. https://doi.org/10.1016/0960-1686(93)90227-P

Rolph, G., Stein, A. and Stunder, B. 2017. Real-time environmental applications and display system: READY. Environ. Model. Softw., 95: 210-228. https://doi.org/10.1016/j.envsoft.2017.06.025

Sharma, M., Jain, S. and Lamba, B.Y. 2020. Epigrammatic study on the effect of lockdown amid Covid-19 pandemic on air quality of most polluted cities of Rajasthan (India). Air Qual. Atmos. Health, 13: 1157-1165. https://doi.org/10.1007/s11869-020-00879-7

Sheu, H.L., Lee, W.J., Lin, S.J., Fang, G.C., Chang, H.C. and You, W.C., 1997. Particle-bound PAH content in ambient air. Environ. Pollut., 96: 369-382. https://doi.org/10.1016/S0269-7491(97)00044-4

Singh, R.P. and Chauhan, A. 2020. Impact of lockdown on air quality in India during COVID-19 pandemic. Air Qual. Atmos. Health, 13: 921-928. https://doi.org/10.1007/s11869-020-00863-1

Stein, A.F., Draxler, R.R., Rolph, G.D., Stunder, B.J.B., Cohen, M.D. and Ngan, F. 2015. NOAA's HYSPLIT atmospheric transport and dispersion modeling system. Bull. Am. Meteorol. Soc., 96: 2059-2077. http://dx.doi.org/10.1175/BAMS-D-14-00110.1

Wolska, L., Mechlińska, A., Rogowska, J. and Namieśnik, J. 2012. Sources and fate of PAHs and PCBs in the marine environment. Crit. Rev. Environ. Sci. Technol., 42: 1172-1189. https://doi.org/10.1080/10643389.2011.556546

Yu, Y., Guo, H., Liu, Y., Huang, K., Wang, Z. and Zhan, X. 2008. Mixed uncertainty analysis of polycyclic aromatic hydrocarbon inhalation and risk assessment in ambient air of Beijing. J. Environ. Sci., 20: 505-512. https://doi.org/10.1016/S1001-0742(08)62087-2

Zhang, P., Song, J. and Yuan, H. 2009. Persistent organic pollutant residues in the sediments and mollusks from the Bohai Sea coastal areas, North China: an overview. Environ. Int., 35: 632-646. https://doi.org/10.1016/j.envint.2008.09.014

Zhang. Y. 2019. Dynamic effect analysis of meteorological conditions on air pollution: a case study from Beijing. Sci. Total Environ., 684: 178-185. https://doi.org/10.1016/j.scitotenv.2019.05.360

Nature Environment and Pollution Technology
An International Quarterly Scientific Journal

p-ISSN: 0972-6268
(Print copies up to 2016)
e-ISSN: 2395-3454

Vol. 23 | No. 3 | pp. 1507-1516 | 2024

Original Research Paper

https://doi.org/10.46488/NEPT.2024.v23i03.020

Open Access Journal

# Bioaccumulation of Lead (Pb) and Cadmium (Cd) in *Padina Australis* Hauck at Palang Beach, Tuban, East Java, Indonesia

**F. Rachmadiarti*†, Winarsih*, H. Fitrihidajati*, T. Purnomo*, S. Kuntjoro*, F. A. Nafidiastri**, R. Yolanda***, R. Ambarwati***, D. Anggorowati***, W. Budijastuti****, U. Faizah***, D. Putriarti* and N. F. Rosyidah***

*Lab of Ecology, Universitas Negeri Surabaya, Surabaya, Indonesia
**Lab of Microbiology, Universitas Negeri Surabaya, Surabaya, Indonesia
***Lab of Taxonomy, Universitas Negeri Surabaya, Surabaya, Indonesia
****Lab of Structure, Universitas Negeri Surabaya, Surabaya, Indonesia
†Corresponding author: Fida Rachmadiarti; fidarachmadiarti@unesa.ac.id

**Nat. Env. & Poll. Tech.**
**Website: www.neptjournal.com**

*Received:* 19-11-2023
*Revised:* 19-01-2024
*Accepted:* 31-01-2024

**Key Words:**
Heavy metals
Macroalgae
Phytoremediation
*Padina australis*

## ABSTRACT

Waters polluted with Pb and Cd have a negative impact on the environment. *Padina australis* grows abundantly on the coast of Palang Subdistrict, Tuban, and the local community consumes it. Macroalgae as food must be free of metal contamination. This study aims to determine the impact of Pb and Cd bioaccumulation on *P. australis*. Sampling was conducted at two stations, including Station I, Panyuran Village, and Station II, Glodog Village. Analysis of Pb and Cd metal levels using Atomic Absorption Spectrophotometry (AAS). Analysis of protein content using the Kjeldahl method. The data obtained was analyzed with Principle Component Analysis (PCA). The results of the analysis of Pb and Cd levels in P. australis at station II, which are 0.200 ± 0.028 and 0.021 ± 0.004 $mg.kg^{-1}$ higher than station I, which are 0.194 ± 0.015 and 0.010 ± 0.001 $mg.kg^{-1}$. The protein content of P. australis at station I was 4.713 ± 0.508 $mg.kg^{-1}$, and at station II was 5.900 ± 0.928 $mg.kg^{-1}$. This shows that *P. australis* is still considered good for consumption even though it has been polluted and contains Pb and Cd metals. P. australis can tolerate and does not experience severe physiological damage so it has the potential as a heavy metal phytoremediator.

## INTRODUCTION

Indonesia is a maritime country because it has a larger ocean area than a land area, with a coastline of ±95,000 $km^2$ (Sukamto 2017). Indonesian waters are rich in natural resources, including aquatic biological resources such as seaweed. Seaweed is widely used as a biomonitor for metal contamination levels. Some types of seaweed are known to have a high ability to accumulate metals so that they can be used as indicators of heavy metals in water (Sohrab & Alireza 2011). Macroalgae have a very important role in human life, both economically and ecologically. Macroalgae can be used as vegetables, traditional medicines, organic fertilizers, and animal feed (Ramdhan & Ratnasari 2021).

*Padina australis* is included in brown seaweed (Phaeophyta), which is widely found in Indonesian waters. In terms of nutrition, *P. australis* contains protein, fat, carbohydrates, water, ash (Maharany et al. 2017), and minerals such as calcium, magnesium, potassium, sodium, copper, zinc, and iron (Ramdhan & Ratnasari 2021). *P. australis* also contains various active compounds, such as steroids, terpenoids, flavonoids, tannins, and saponins (Hudaifah et al. 2020), which can be utilized as medicine (Priamanatha 2023). Kustantinah et al. (2022) revealed that *P. australis* from Kelapa Beach, Tuban Regency, has the potential to be utilized as animal feed, especially as a soluble carbohydrate and organic mineral source. Mantiri et al. (2019) in their research analyzed that *P. australis* can remain alive even though heavy metals have been found in its talus cell wall. The presence of heavy metal contents of As, Cu, Zn, and Mg in *P. australis* indicates that this macroalgae can be used as a heavy metal phytoremediator. According to Paz et al. (2019), Pb and Cd are listed as the most toxic metals found in edible seaweeds in Asia. *P. australis* can absorb $Cd^{2+}$ ions in 3 h with an absorption presentation of 74.54% (Bijang et al. 2018). This is because the surface of its cell wall consists of functional groups, such as amino, hydroxyl, carboxyl sulfate imidazole, and sulfonate, that can bind to metal ions (Firdaus 2019).

Marine pollution is a global problem faced by countries located in coastal areas. Increased residential, agricultural,

and industrial development produces discharges or wastes containing pollutants. One of the main pollutants is heavy metals, such as lead (Pb) and copper (Cu). Heavy metals are toxic if they enter the water in quantities exceeding the maximum limit that has been set (Nurhayati & Putri 2019). Heavy metals have high toxicity to the aquatic environment because they easily settle in sediments and marine biota for a long time (Nurfadhilla et al. 2020). These metals enter the bodies of marine organisms through the respiratory tract, are then absorbed by the digestive system, and accumulate in the liver and kidneys because they cannot be decomposed (Astuti et al. 2016). The entry of heavy metals into water bodies can cause a decrease in water quality both physically and biophysically.

Marine waters in Palang, Tuban Regency, are suspected to be polluted. According to Ummi et al. (2017), the average Pb level in seawater in Palang, Tuban Regency, was 0.18 ± 0.13 mg.$L^{-1}$, and Cd levels ranged from 0.008 to 0.04 on the North Tuban coast. This condition has exceeded the quality standard threshold based on the Decree of the Minister of Environment No. 51 Year 2004. Some seafood products from the Palang Sub-district of Tuban Regency, such as salted fish and shrimp paste, were also found to be positive for lead, with levels exceeding the threshold set by BSN. The lead level in shrimp paste was 8.84 ± 0.12 mg.$kg^{-1}$, and the lead level in salted fish was 6.72 ± 0.11 mg.$kg^{-1}$. Ummi et al. (2017) also found that tuna from the sea of Palang Subdistrict, Tuban Regency, was found to contain heavy metal lead (Pb) of 0.61 mg.$kg^{-1}$. Marine pollution in Palang, Tuban Regency, also occurs due to the offshore oil industry. This industrial waste is suspected to contain heavy metal compounds that are toxic and harmful to marine ecosystems and living organisms. Meanwhile, the possibility of Pb and Cd heavy metal contamination in macroalgae, including *P. australis,* is not yet known. *P. australis,* as a food ingredient, must meet food safety requirements. According to BPOM Regulation No. 21 of 2021, food safety is a condition and effort needed to prevent food from possible biological, chemical, and other contaminants that can interfere with and endanger human health, ensuring it is safe for consumption. One of the requirements for macroalgae food safety is to be free from heavy metal chemical contamination. The feasibility and food safety of macroalgae must be known and compared with the required quality standards.

Based on this background, it is necessary to analyze the levels of Pb and Cd metals in water, sediment, and *P. australis*, as well as protein levels in *P. australis* at Palang Subdistrict Beach, Tuban Regency, considering the consumption of *P. australis* by the local community and the absence of previous studies so that the potential of *P. australis* in accumulating heavy metals Pb and Cd and its food safety status is important to study.

## MATERIALS AND METHODS

### Study Site

This research was conducted from September to November 2023 at Palang Beach, Palang Subdistrict, Tuban Regency. Observations were made at two stations, namely Panyuran Village (Station I) and Glodog Village (Station II) (Fig. 1). Research samples included water, sediment, and P. australis, along with the measurement of physico-chemical parameters

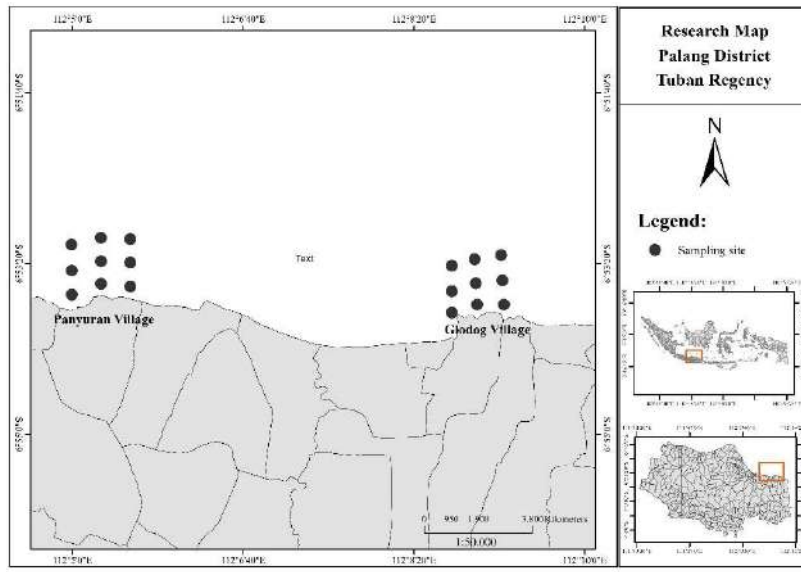


Fig. 1: Sampling location.

in the waters. Analysis of heavy metal levels of Pb, Cd, and protein levels was carried out at the Airlangga University Nutrition Laboratory.

### Fieldwork

The equipment used to measure water quality included a Gea S-006 rod thermometer, a Milwaukee pH meter, an Atago S-28 refractometer, and an MW-600 Milwaukee DO meter. Materials needed in this study included macroalgae P. australis, seawater, marine sediments, clean water, distilled water, aquabides, $Na_2SO_4$-HgO (catalyst), ethanol 96%, $HNO_3$ 65%, $H_2O_2$, HCl 0.2 N, NaOH 1%, $H_3BO_4$ 4%, and $H_2SO_4$ 98%.

Sampling of *P. australis* macroalgae for Pb and Cd metal content tests was conducted at two observation stations with two repetitions. The macroalgae samples taken had the same color and size. Samples of *P. australis* were stored in a cool box at a temperature of 2-4°C and then brought to the laboratory for analysis

### Analysis of Lead and Cadmium Content

This analysis was carried out at the Nutrition Laboratory Airlangga University using the dry destruction method. 3.5-gram samples were weighed using an analytical balance, then placed in a porcelain dish, labeled, and incubated for 3 h at 800°C. The sample that has been kilned is put into a beaker glass and added 1 mL of concentrated $HNO_3$ and 10 mL of aquademin. Next, the sample was stirred until well mixed and filtered using filter paper. Furthermore, the sample is ready to be analyzed using the AAS method.

### Analysis of Protein Content

In each treatment, 0.2 grams of *P. australis* was then mashed. After that, put it into a 30 mL Kjeldahl flask, then add $Na_2SO_4$-HgO (2:1) and 2 mL $H_2SO_4$. Boil the sample for 2.5 h until the liquid becomes clear. After the cold sample is added with 15 mL of distilled water, 10 mL of NaOH is added into the distillation tube, 10 mL of $H_2BO_4$ is added into Erlenmeyer, and then placed under the condenser. The sample was distilled until 15 mL of greenish distillate was collected in the Erlenmeyer. Next, titrate using 0.2 N HCL until the color changes to pink. Then do the blank determination and calculate the total N and protein percentage with the following formula.

$$\% \text{ N} = \frac{ml\ HCl\ x\ N\ HCl \times 14.008}{Biomass\ (mg)} \times\ 100\%$$

$$\% \text{ Protein} = \% \text{ N} \times 6.25$$

### Data Analysis

Water quality data from the measurement of physico-chemical parameters, including seawater Pb and Cd metal levels, were analyzed descriptively with reference to the quality standards of marine waters based on Government Regulation No. 22 of 2021 concerning the Implementation of Environmental Protection and Management. Data on sediment Pb and Cd metal levels were analyzed descriptively with reference to quality standards based on the 2002 Candian Council of Ministers for the Environment (CCME) Guidelines for Aquatic Sediment Quality. Data on macro algae Pb and Cd metal levels were analyzed descriptively with reference to quality standards based on the Decree of the Director General of Food and Drug Control No. 5 of 2018 50 concerning Maximum Thresholds for Pb and Cd Metal Contaminants in Food Ingredients. Protein content data were analyzed descriptively with reference to the Indonesian Food Composition Table (TKPI) of the Indonesian Ministry of Health 2017. The relationship between water quality, Pb and Cd levels of water, sediment, *P. australis*, and protein levels of *P. australis* were analyzed using Principal Component Analysis (PCA) using XLSTAT software for Excel.

## RESULTS AND DISCUSSION

### Physical and Chemical Water Quality

The physical and chemical conditions of the water also influence metal absorption. Based on the results of PCA analysis, station I is characterized by high pH and temperature, while station II is characterized by high salinity, dissolved oxygen, and current velocity. Pb metal levels are actually low at station I, which is known to have a higher temperature than station II (Table 1).

Based on the results of PCA analysis, it was known that temperature is negatively correlated with seawater Pb levels, sediment Pb levels, and Pb levels of *P. australis* (Fig. 2). This result is in accordance with the research of Paramita et al. (2017) which states that an increase in water temperature can reduce the adsorption of particulate heavy metal compounds, while a decrease in water temperature will increase the adsorption of heavy metals to particulates to settle to the bottom of the waters, these particulates will potentially become a secondary source of heavy metal pollution in the waters.

The pH at both stations is classified as alkaline because it is more than 7. According to Melsasail et al. (2018), macroalgae require an alkaline condition for their life so macroalgae tend to be found in alkaline waters. The high pH is due to the sampling time at the beginning of the rainy season. Yulis (2018) states that an increase in pH causes the

Table 1: Measurement results of physico-chemical parameters of water quality at Palang Beach, Tuban.

| Parameter | Station | Average ± SD | Quality Standards (*) |
|---|---|---|---|
| Temperature (°C) | I | 29,933 ± 1,576 | 28-30°C |
| | II | 28,700 ± 1,236 | |
| pH | I | 7,993 ± 0,012 | 7-8,5 |
| | II | 7,867 ± 0,082 | |
| Salinity ($‰_o$) | I | 31,667 ± 0,471 | 33-34$‰_o$ |
| | II | 33,333 ± 0,471 | |
| Dissolved Oxygen [mg.L$^{-1}$] | I | 5,167 ± 0,590 | >5 mg.L$^{-1}$ |
| | II | 5,473 ± 0,271 | |
| Flow Velocity [m.s$^{-1}$] | I | 0,263 ± 0,127 | Low = 0,5 m.s$^{-1}$<br>Medium = 0,5 m.s$^{-1}$<br>High = >0,5 m.s$^{-1}$<br>(**) |
| | II | 0,653 ± 0,052 | |

Note: (*) Government Regulation No. 22 Year 2021 (**) Yusuf et al. 2012. Bolded values are not in accordance with quality standards.

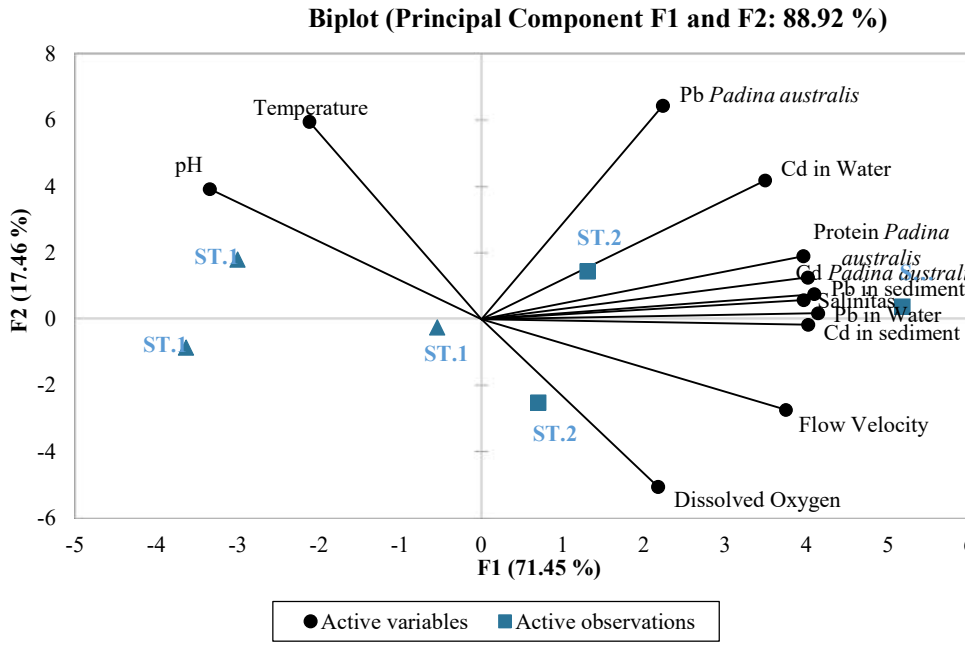


Fig. 2: PCA relationship of water physico-chemical parameters, Pb and Cd levels water, Pb and Cd levels sediments, *P. australis* Pb and Cd levels, *P. australis* protein levels at both stations.

solubility of heavy metals to decrease due to a change in the stability of the form of carbonate compounds to hydroxide compounds. The results of this study are similar to (George & Abowei 2018), who found that pH is strongly negatively correlated with water Pb levels (Fig. 2).

Salinity at station II is quite high but still meets the quality standards, while salinity at station I does not meet the quality standards based on Government Regulation No. 22 of 2021 (Table 1). Melsasail et al. (2018) in their research found that *P. australis* was able to survive in waters with a salinity of 26.3‰. A similar study (George & Abowei, 2018) also found salinity to be positively correlated with water Pb levels (Fig. 2). High salinity is associated with high electrical conductivity ions in the water that can increase the concentration of heavy metals in the water. According to Saraswati & Rachmadiarti (2021), decreasing salinity can lead to increased accumulation of heavy metals. This occurs due to the process of dilution and hydrodynamics that occur naturally in waters.

The current velocity at station II was higher than at station I (Table 1). Current speed is a parameter that influences the rate of metal sedimentation. Based on the results of PCA analysis, current velocity was most strongly positively correlated with seawater Pb levels, sediment Cd levels, and

*P. australis* Cd levels (Fig. 2). Current velocity causes stirring of particles in water, including metal ions. High current velocity causes metal ions to remain in the water body. Station II has a shallow water depth, so the water current tends to be stronger than station I, which has a deeper water depth. This is in line with Melsasail et al. (2018) which states that high current speed is influenced by water depth and the presence or absence of seagrass. The presence of seagrasses and sufficient water depth prevent strong currents.

Dissolved oxygen is classified as good at both stations because it meets the quality standards based on Government Regulation No. 22 of 2021 (Table 1). The influence of high current velocity can cause good dissolved oxygen at both stations. Based on the results of PCA analysis, dissolved oxygen is strongly positively correlated with current velocity (Fig. 2). According to Nurjanah et al. (2021), current speed increases water dissolved oxygen levels through oxygen exchange with the water surface. Sufficient oxygen in the waters can support maximum macroalgae growth. Metal levels with dissolved oxygen are most strongly positively correlated with sediment Pb (Fig. 2). Increased deposition of heavy metals in sediments causes a decrease in heavy metal levels in water bodies, so dissolved oxygen in the waters increases. According to WHO (1985), dissolved oxygen can affect the solubility and availability of nutrients that can be released from sediments in low dissolved oxygen conditions.

**Pb and Cd levels**

Based on the results of the analysis, seawater at Station I Panyuran Village and Station II Glodog Village has been polluted with Pb and Cd metals, where the levels have exceeded the maximum threshold of quality standards based on Indonesian Government Regulation No. 22 of 2021 (Table 2). The quality standard for Pb in seawater is 0.008 $mg.L^{-1}$. The quality standard for Cd metal levels is 0.001 $mg.L^{-1}$. The level of heavy metal Pb in seawater in this study is lower when compared to Ummi et al. (2017), who found the average Pb content of seawater in Palang Subdistrict, Tuban Regency was 0.18 ± 0.13 $mg.L^{-1}$. However, it is higher when compared to Azizah et al. (2018) in the Awur Bay Waters of Jepara, which found an average seawater Pb level of 0.003 $mg.L^{-1}$. This can be caused by differences in sampling location and time, as well as the physical and chemical conditions of the waters. Pb metal that enters the water has the potential to be deposited in sediments. Metal ions in waters are less stable, so they easily bind to organic substances and potentially settle in sediments.

Metal levels in sediments are contributed by water pollution. Based on the hydrological cycle, less than 0.1% of metals are dissolved in water, and more than 99.9% are stored in sediments (Pradit et al. 2013). Sediment is a good medium for heavy metal deposition. Metals in sediments continue to increase along with the increase in water metal levels and will persist for a long period. Based on the results of the analysis, the levels of Pb and Cd metals in the sediments of Palang District Beach still meet the quality standards based on the Candian Council of Ministers for the Environment (CCME) 2002 (Table 2). The quality standard for Pb in sediment is 30.2 $mg.kg^{-1}$. The quality standard for sediment Cd metal content is 0.7 $mg.kg^{-1}$. When viewed from the type of sediment, the two stations have different sediment characteristics. Station I is composed of sediments in the form of coarse sand, and there are few coral rocks, while station II is composed of sediments in the form of fine sandy clay, and there are quite a lot of coral rocks. This causes sediment metal levels at station II to be higher than at station I. According to Wardani et al. (2014), sediment type affects the absorption of heavy metals with the category that clay sediments more easily absorb heavy metals> sandy clay > sand.

Table 2: Pb and Cd levels in water, sediment, and *P. australis* in Palang Beach, Tuban.

| Station | Heavy Metals | Seawater [$mg.L^{-1}$] | Sediment [$mg.kg^{-1}$] | *P. australis* [$mg.kg^{-1}$] |
|---|---|---|---|---|
| Station I | Pb | 0,026 ± 0,004 | 2,235 ± 0,047 | 0,194 ± 0,015 |
| | Cd | 0,010 ± 0,003 | 0,052 ± 0,003 | 0,010 ± 0,001 |
| Station II | Pb | 0,040 ± 0,005 | 2,352 ± 0,073 | 0,200 ± 0,028 |
| | Cd | 0,015 ± 0,005 | 0,08 ± 0,007 | 0,021 ± 0,004 |

The results of this study show that although the water metal levels do not meet the quality standards, the sediment metal levels still meet the quality standards. This indicates that heavy metal pollutants entering the water are more in the water phase than settling into the sediment. This occurrence is caused by changes in the physical and chemical conditions of waters, such as pH, temperature, salinity, and organic substances that can allow the decomposition of metals from the solid phase, decomposition and degradation of organic matter in an oxidized state (Rumhayati & Retnaningdyah 2018), the influence of current velocity, dilution of heavy metals in waters due to rain, and the characteristics of the sediment fraction itself. The Pb and Cd levels of Palang Subdistrict Beach sediments are known to be lower when compared to the results of Syaifullah et al. (2018), which found the Pb metal content of Tuban Sea sediments to be 2.944 ± 0.360 $mg.kg^{-1}$ and the Cd metal content to be 2.978 ± 0.224 $mg.kg^{-1}$. Metals contained in sediments can be absorbed by organisms that live attached to sediments, one of which is *Padina australis* seaweed.

*P. australis* at both stations is known to contain metals Pb and Cd. *P. australis* lives submerged in water and attached to the sediment so that it can absorb Pb and Cd metals. Based on the analysis results, the Cd level of *P. australis* at both stations is still below the quality standard threshold according to the Decree of the Directorate General of Food and Drug Control (BPOM) No. 5 of 2018, which is 0.05 $mg.kg^{-1}$, while the Pb level of *P. australis* at both stations has approached the quality standard threshold, which is 0.20 $mg.kg^{-1}$ (Table 2). The Pb and Cd levels of *P. australis* at the Palang sub-district beach were higher than those of *P. australis* in South Sumatra, which contained Pb metals of 0.0496 - 0.1050 ppm to 0.0964 - 0.1388 ppm (Supardi & Nugroho 2019). However, it is lower than *P. australis* in Sanur Beach Bali, which contains a Pb metal of 0.368 $mg.L^{-1}$ and Cd of 0.212 $mg.L^{-1}$ (Rosiana et al. 2022). Based on the levels of heavy metals contained (Naw et al. 2020), *P. australis* from Palang District Beach is not too toxic and can be recommended to be applied and utilized by the food and medicine industries. In addition, the utilization of *P. australis* for animal feed is also highly recommended. However, the utilization of *P. australis* must still pay attention to the levels of heavy metals contained.

Seawater, sediment, and *P. australis* at station II (Glodog Village) had higher levels of heavy metals Pb and Cd than station I (Panyuran Village) (Table 2). Station II of Glodog Village is an anchorage for fishing boats located close to the Palang Fish Auction Place (TPI). The loading and unloading activities at the TPI and the traffic of fishing boats contribute Pb and Cd heavy metal pollutants to the waters. In addition, station II is a residential area that is also close to the river estuary that carries contaminants from the settlement. Tosepu & Effendy (2016) mentioned that ship traffic and ship corrosion, organic insecticides, pesticides, and agricultural fertilizers are sources of metal pollution in waters. Lee et al. (2021) added that residential areas directly affect metal concentrations in water, sediments, and organisms. This is worrying for local people who consume marine organisms because Cd and Pb are highly toxic and harmful to the body. Meanwhile, station I is a residential area located far from TPI Palang but quite close to the river mouth. This shows that TPI Palang is the biggest source of pollution.

Based on the type of heavy metal, the Pb metal level in Palang Subdistrict Beach, Tuban Regency, is higher than the Cd metal level. This is because there are more sources of Pb metal in Palang Beach than Cd metal. According to Mamboya (2007), the availability of heavy metals in water affects the bioavailability of the heavy metals themselves. Pb heavy metal is widely used by industry and is contained in many industrial products, so its pollution in the environment is found to be quite high. Syaifullah et al. (2018) mentioned that the source of damage and pollution of the Tuban Sea comes from the waste of residents in the fishing village area along Tuban Beach. Based on its ability to precipitate, Pb can precipitate better than Cd. According to Hutagalung (1991), the ability of some heavy metals to settle in sediments in order is Hg > Cu > Ni > Pb > Co > Cd. Bayu et al. (2022) explained that the accumulation and solubility of heavy metals are also related to the characteristics of each heavy metal. The relative density/atomic weight of each heavy metal can affect its solubility in waters and sediments. The higher the atomic weight, the easier it is to precipitate.

The results of this study showed that an increase in seawater metal levels was followed by an increase in

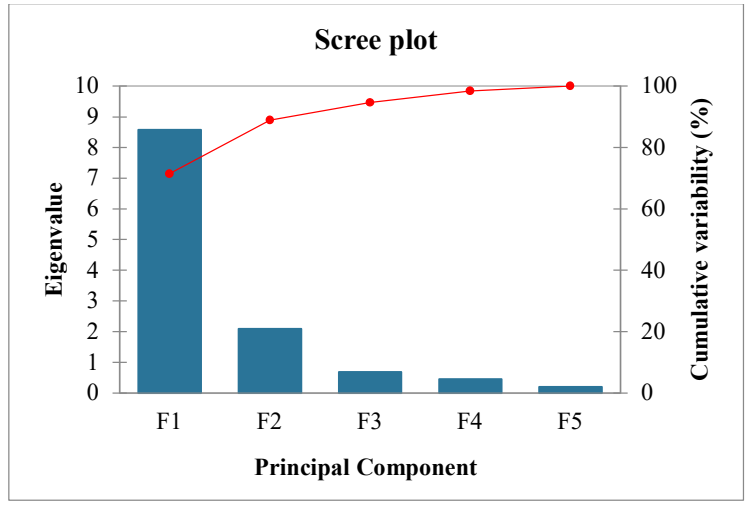


Fig. 3: Scree plot Principal Component Analysis (PCA) and Cumulative variability.

(a) (b)

Fig. 4: *P. australis* in Palang sub-district beach, Tuban Regency. (a) Morphology of *P. australis*. (b) *P. australis* grows attached to the coral sediment (Personal Documentation).

sediment metal levels and *P. australis* metal levels. Based on the results of PCA analysis, all three were positively correlated, meaning that an increase in one variable was followed by an increase in the other (Fig. 3). Pb and Cd metal levels in the sediment correlated more strongly with *P. australis* metal levels than with seawater metal levels. This is because the roots attached to the sediment can absorb metals, spreading metals from the roots to other organs (Sholikah & Rachmadiarti 2019). Plants can localize metals in a particular organ, for example, in the roots themselves (Irhamni 2017). In addition, the deposition and solidification of metal ions in sediments causes metal ions that have solidified in sediments to be difficult to release, so sediments will continue to contain heavy metals even though the waters are not polluted with metals. Metal levels in sediments will increase when there is metal pollution in the waters. This affects the roots of *P. australis* which will absorb metals from the sediment all the time. According to Amini et al. (2013), the positive correlation between sediment metal content and algae indicates that this algae species can absorb metals from sediments and can be used as an object of biomonitoring pollution.

**Protein Content of *P. Australis***

Based on the observation of *P. australis* samples morphologically from Palang Subdistrict Beach, it has brown talus with sizes varying from small to large that live attached to the coral substrate (Fig. 4). *P. australis* is a phytoremediator that can be used as a bioindicator of metal pollution (Al-Awlaqi et al. 2019) because it includes brown seaweed as a source of alginate. Alginate is a polysaccharide organic polymer composed of 2 monomeric units of D-sour guluronate and L-sour manuronate or alternating both. Carboxyl and hydroxyl groups are the active parts of alginate that absorb metals. Heavy metals accumulated in the talus of *P. australis* can cause morphological and physiological disorders.

In this study, the crude protein content of *P. australis* containing heavy metals Pb and Cd was analyzed to determine the effect of heavy metals on the physiology of *P. australis* and to determine the safety of utilizing *P. australis* for industrial applications. Physiologically, heavy metals affect the process of photosynthesis and protein in algae (Zamani-Ahmadmahmoodi et al. 2020). Brown seaweed has the lowest protein content of about 15% of dry weight when compared to red and green seaweed protein (Sahri 2023). Based on the results of the analysis (Table 3), it is known that the protein content of *P. australis* at station I amounted to $4.713 \pm 0.508$ mg.kg$^{-1}$ and at station II amounted to $5.900 \pm 0.928$ mg.kg$^{-1}$. The protein content of *P. australis* from both stations has exceeded the minimum quality standard of commercial protein content of 2.80% (Murdinah 2009). *P. australis* from Palang Sub-district Beach is classified as good and has the potential to be a commercially valuable protein source for industry use. However, the utilization of *P. australis* from Palang District Beach must consider the levels of heavy metals it contains. The protein content of *P. australis* from Palang Subdistrict Beach, Tuban, is higher than that of *P. australis* from Karimun Jawa, with 3.9% protein (Siahaan et al. 2018). However, it is lower than that of *P. australis* from Pantai Kelapa Tuban, which has a crude protein level

Table 3: Protein content in *P. australis*.

| Station | Protein Content [mg.kg$^{-1}$] | Quality Standards [mg.kg$^{-1}$]* |
|---|---|---|
| Station I (Panyuran Village) | $4.713 \pm 0.508$ | 2.8 |
| Station II (Glodog Village) | $5.900 \pm 0.928$ | 2.8 |

Note: (*) Murdinah 2009.

of 12.57% (Hidayah et al. 2022), and P. australis from Pantai Kelapa Lima Teluk Kupang, with a crude protein level of 13.89%. This difference can be attributed to variations in the age of *P. australis*, weather conditions, and habitat (Salosso et al. 2020). In this study, the age of *P. australis* was unknown, but only those with talus of relatively similar size and color were selected. Sampling coincided with the beginning of the rainy season. According to Denis et al. (2010), the protein content of *P. australis* varies and is influenced by the season. The highest concentration of seaweed protein occurs during early spring and winter, while the minimum concentration is during early fall and summer.

The results of this study indicate that the protein content of *P. australis* is still relatively good even though *P. australis* has been contaminated with metals. These results differ from some previous studies that metal levels in seaweed were negatively correlated with protein levels. *P. australis* seaweed containing heavy metals has low protein levels. Anggreani & Rachmadiarti (2021) in Sendang Biru Beach Malang found that *P. australis* with an average Cd metal content of $0.019 \pm 0.001$ mg.kg$^{-1}$ to $0.027 \pm 0.001$ mg.kg$^{-1}$ contains protein levels of 0.0002 mg.L$^{-1}$ to 0.0004 mg.L$^{-1}$. The Cd metal content and protein levels are the same. Cd metal levels and protein levels are negatively correlated, which means that the higher the levels of Cd metal, the lower the protein content in seaweed *P. australis*. Based on the results of Pearson correlation analysis in this study, it is known that the levels of Cd metal *P. australis* and protein levels *P. australis* have a very strong positive correlation (0.890) (Fig. 3). The higher the Cd metal content of *P. australis*, the higher the protein content of *P. australis*. The correlation between Pb metal and protein content of *P. australis* was strong and lower than Cd. The higher the Pb metal content of *P. australis*, the higher the protein content of *P. australis*. The correlation between the two was not significant. The results of this study are similar to Carfagna et al. (2013) who found that the effect of Cd metal on *Chlorella sorokiniana* microalgae was greater than Pb metal. This may be because Cd has greater toxicity than Pb. The difference between this study and Carfagna et al. (2013) is that in the experimental study, Carfagna et al. (2013) found that Cd and Pb metals had a negative impact on microalgae. Microalgae exposed to Cd for 24 h had very low total protein levels, which were only 48 and 35% of the control cells. These protein levels were lower than microalgae exposed to Pb at the same time. According to research by Bavi et al. (2011), protein synthesis is strongly influenced by cadmium. The higher the cadmium concentration, the greater the decrease in protein levels. The reduction in protein levels can be caused by a decrease in protein synthesis or an increase in the rate of protein degradation (Balestrasse et al. 2003). Cadmium will react with SH groups and result in protein denaturation (Fuhrer 1982). Cadmium causes the production of reactive oxygen species (ROS) in plant cells (Haider et al. 2021). Cd metal that enters the body of organisms can interfere with photosynthesis and growth (Vo et al. 2020).

*P. australis* has a high tolerance to Pb and Cd metals, so in this study, the metal levels contained in *P. australis* can still be tolerated and do not cause significant physiological damage. Algae have various binding groups such as $COO^-$, $SH^-$, $OH^-$, $RNH_2^-$, $RS^-$, and $RO^-$ for biosorption of metal ions. These binding groups exist on the cell surface and in the cytoplasm, especially within the vacuole (Salama et al. 2019). Carboxyl functional groups ($COO^-$) are the most abundant acidic functional groups in the brown cell walls of algae. Excretion and exclusion of metals from cells, production of proteins such as proline and other binding compounds such as metallothioneins (MTs) and glutathione (GSH) are among the mechanisms used by algae to prevent metal-induced damage (Aude-Garcia et al. 2016). If a plant experiences abiotic stress, protein is used to meet energy needs (Wang et al. 2004). An increase in total protein content indicates an increase in antioxidant enzyme levels (Kovtun et al. 2000). Antioxidant enzymes present in cells scavenge reactive oxygen species and eliminate oxidative stress. Superoxide dismutase is essential in converting more reactive and harmful oxygen radicals into less reactive hydrogen peroxide (Foyer 2018).

## CONCLUSION

This study showed that the physico-chemical quality of seawater at Palang Subdistrict Beach, Tuban Regency, influenced the levels of Pb and Cd in water and sediment. The increase in metal levels in seawater was followed by an increase in sediment metal levels and metal levels in *P. australis*. Pb and Cd levels at station I, which amounted to $0.194 \pm 0.015$ and $0.010 \pm 0.001$ mg.kg$^{-1}$, while at station II, which is $0.200 \pm 0.028$ and $0.021 \pm 0.004$ mg.kg$^{-1}$. Pb metal levels in Palang Subdistrict Beach, Tuban, are higher than Cd metal levels because there are more Pb metal pollutant sources than Cd metal pollutant sources. Station II (Glodog Village) has higher levels of heavy metals Pb and Cd than station I (Panyuran Village) because station II is close to the fish auction and residential areas that cause higher levels of pollution. Protein levels of *P. australis* at stations I and II, namely $4{,}713 \pm 0.508$ and $5{,}900 \pm 0.928$ mg.kg$^{-1}$. This shows that heavy metal levels in *P. australis* affect the protein content of *P. australis*. The protein content of *P. australis* is still classified as good according to quality standards even though *P. australis* has been polluted and contains Pb and Cd metals, so it is still safe for consumption. In addition,

*P. australis* can tolerate heavy metals because it does not experience significant physiological damage so it can be used as a bioindicator of Pb and Cd heavy metal pollution in seawater.

## ACKNOWLEDGEMENT

Authors are grateful to Universitas Negeri Surabaya, which has funded this research in 2023 through a competitive basic research scheme.

## REFERENCES

Al-awlaqi, N. A., Shazili, N. A. M. and Nurulnadia, M. Y. 2019. Spatial and seasonal variation of metal accumulation in brown seaweed, Padina sp. on the South China Sea coast of Terengganu, Peninsular Malaysia. Bioflux, 12(5): 1592-1605.

Amini, F., Riahi, H. and Zolgharnain, H. 2013. Metal concentrations in Padina species and associated sediment from Nayband Bay and Bostaneh Port, Northern Coast of the Persian Gulf, Iran. J. Persian Gulf (Mar. Sci.), 4(11): 17-24.

Anggreani, N. and Rachmadiarti, F. 2021. Content of the heavy metal cadmium (Cd) in Padina Australis at Sendang Biru Beach, Malang. LenteraBio, 10(1): 115-124.

Astuti, I., Karina, S. and Dewiyanti, I. 2016. Analysis of the heavy metal pb content in Crassostrea cucullata oysters on the Krueng Raya Coast, Aceh Besar. Unsyiah Marine Fish. Stud. Sci. J., 1(1): 104-113.

Aude-Garcia, C., Villiers, F., Faure, V. C., Pernet-Gallay, K., Jouneau, P. H., Sorieul, S., Mure, G., Gerdil, A., Herlin-Boime, N., Carriere, M. and Rabilloud, T. 2016. Different in vitro exposure regimens of murine primary macrophages to silver nanoparticles induce different fates of nanoparticles and different toxicological and functional consequences. Nanotoxicology, 10(5): 586-596.

Azizah, R., Malau, R., Susanto, A. B., Santosa, G. W., Hartati, R. and Irwani, S. 2018. Lead content in water, sediment, and seaweed Sargassum sp. in Jepara Waters, Indonesia. J. Kelaut. Tropis, 21(2): 155-166.

Badan Pengawas Obat dan Makanan (BPOM). 2018. Food and Drug Supervisory Agency Regulation Number 21 of 2021 concerning the Implementation of a Processed Food Quality Safety Guarantee System in Distribution Facilities. Jakarta, BPOM.

Badan Pengawas Obat dan Makanan (BPOM). 2021. Food and Drug Supervisory Agency Regulation Number 21 of 2021 concerning the Implementation of a Processed Food Quality Safety Guarantee System in Distribution Facilities. Jakarta, BPOM.

Balestrasse, K. B., Benavides, M. P., Gallego, S. M. and Tomaro, M. L. 2003. Effect of cadmium stress on nitrogen metabolism in nodules and roots of soybean plants. Funct. Plant Biol., 30: 57-64.

Bavi, K., Kholdebarin, B. and Moradshahi, A. 2011. Effect of cadmium on growth, protein content, and peroxidase activity in pea plants. Pak. J. Bot., 43(3): 1467-1470.

Bayu. 2022. Analisis Kandungan Logam Berat (Pb, Cd dan As) pada Rumput Laut (Eucheuma cottonii) (Studi Kasus: Perairan Laut Wongsorejo, Banyuwangi). J. Grouper, 13(2): 168-176.

Bijang, C. M., Tehubijuluw, H. and Kaihatu, T. G. 2018. Biosorpsi Ion Logam Kadmium ($Cd^{2+}$) Pada Biosorben Rumput Laut Coklat (Padina australis) Asal Pantai Liti Pulau Kisar. Indones. J. Chem. Res., 6(1): 51-58.

Canadian Council of Ministers for The Environment (CCME). 2002. Sediment Quality Guidelines for The Protection of Aquatic Life Summary Table. CCME: Winnipeg.

Carfagna, S., Lanza, N., Salbitani, G., Basile, A., Sorbo, S. and Vona, V. 2013. Physiological and morphological responses of Lead or Cadmium exposed Chlorella sorokiniana 211-8K (Chlorophyceae). SpringerPlus, 2(1): 1-7.

Denis, C., Morançais, M., Li, M., Deniaud, E., Gaudin, P., Wielgosz-Collin, G., Barnathan, G., Jaouen, P. and Fleurence, J. 2010. Study of the chemical composition of edible red macroalgae Grateloupia turuturu from Brittany (France). Food Chem., 119(3): 913-917.

Firdaus, M. 2019. Seaweed Pigments and Their Health Benefits. University Brawijaya Press, Malang.

Foyer, C. H. 2018. Reactive oxygen species, oxidative signaling, and the regulation of photosynthesis. Environ. Exp. Bot., 154: 134-142.

Fuhrer, J. 1982. Early effects of excess cadmium uptake in Phaseolus vulgaris. Plant Cell Environ., 5: 263-270.

George, A. D. I. and Abowei, J. F. N. 2018. Physical and chemical parameters and some heavy metal for three rainy season months in water and sediments of upper new Calabar River, Niger Delta, Nigeria. Open Access Libr. J., 5(5): 1-4.

Haider, F. U., Liqun, C., Coulter, J. A., Cheema, S. A., Wu, J., Zhang, R., Wenjun, M. and Farooq, M. 2021. Cadmium toxicity in plants: Impacts and remediation strategies. Ecotoxicol. Environ. Saf., 211: 111887.

Hidayah, N., Noviandi, C., Astuti, A. and Kustantinah. 2022. Chemical composition of brown and red algae from Kelapa Beach, Tuban, East Java and their potential as ruminant feed. Earth Environ. Sci., 1114: 012003.

Hudaifah, I., Mutamimah, D. and Utami, A. U. 2020. Bioactive components from Euchema cottonii, Ulva lactuca, Halimeda opuntia, and Padina australis. J. Lemuru, 2(2): 63-70.

Hutagalung, H. P. 1991. Marine Pollution by Heavy Metals in Some Waters. Indonesia. Puslitbang. Hlm 45–59. Oseanologi LIPI, Jakarta.

Irhamni, S., Purba, E. and Hasan, W. 2017. Absorption of essential and non-essential heavy metals in Banda Aceh City landfill leachate in realizing sustainable development. J. Serambi Eng., 2(3): 134-140.

Kovtun, Y., Chiu, W. L., Tena, G. and Sheen, J. 2000. Functional analysis of oxidative stress-activated mitogen-activated protein kinase cascade in plants. Science, 97(6): 2940-2945.

Kustantinah, H. N., Noviandi, C. T., Astuti, A. and Paradhipta, D. H. V. 2022. Nutrient content of four tropical seaweed species from Kelapa Beach, Tuban, Indonesia, and their potential as ruminant feed. Biodiversitas, 23(12): 6191-6197.

Lee, A. C., Idrus, F. A. and Aziz, F. 2021. Cadmium and lead concentrations in water, sediment, fish and prawn as indicators of ecological and human health risk in Santubong Estuary, Malaysia. Jordan J. Biol. Sci., 14(2): 317-325.

Maharany, F., Nurjanah, S. R., Anwar, E. and Hidayat, T. 2017. The content of bioactive compounds in seaweed Padina australis and Eucheuma cottonii as raw materials for sunscreen cream. J. Pengolahan Hasil Perikanan Indones., 20(1): 10-17.

Mamboya, F. A. 2007. Heavy Metals Contamination and Toxicity: Studies of Mucroalgae from Tanzanian Coast. Stockholm University, Sweden, pp. 1–48.

Mantiri, D. M. H., Kepel, R. C., Manoppo, H., Paulus, J. J. H., Paransa, S. S. and Nasprianto. 2019. Metals in seawater, sediment, and Padina australis (Hauck, 1887) algae in the waters of North Sulawesi. Bioflux, 12(3): 840-851.

Melsasail, K., Awan, A. and Papilaya, P. M. 2018. Analysis of environmental physical-chemical factors and macroalga species in the coastal water of Nusa Laut, Central Maluku – Indonesia. Sriwijaya J. Environ., 3(1): 31-36.

Murdinah. 2009. Effect of Extracting and Aging Agents on the Quality of Carrageenan from Seaweed Eucheuma Cottonii. UGM Fisheries and Marine Affairs with the Research Center for Marine and Fisheries Product Processing and Biotechnology, Indonesia.

Naw, S. W., Zaw, N. D. K., Aminah, N. S., Alamsjah, M. A., Kristanti, A. N., Nege, A. S. and Aung, H. T. 2020. Bioactivities, heavy metal contents, and toxicity effect of macroalgae from two sites in Madura, Indonesia. J. Saudi Soc. Agric. Sci., 19(8): 528-537.

Nurfadhilla, N., Nurruhwati, I., Suranrdi, and Zahidah, M. 2020. Level of heavy metal lead (Pb) contamination in Tutut (Filopaludina javanica) in Cirata Reservoir, West Java. J. Akuatika Indones., 5(2): 61-70.

Nurhayati, D. and Putri, D. 2019. Bioaccumulation of heavy metals in green mussels (Perna viridis) in Cirebon waters based on different seasons. J. Akuatika Indones., 4(1): 6-10.

Nurjanah, A., Supriharyono, M. and Yulianto, B. 2021. Relationship between lead (Pb) in Sediment, Seaweed, and Brackish Water Ponds in Tegal City. Ecol. Environ. Conserv. J., 2(3): 1119-1130.

Paramita, R. W., Wardhani, E. and Pharmawati, K. 2017. Content of heavy metals cadmium (Cd) and chromium (Cr) in surface water and sediment: Case study of Saguling Reservoir, West Java. J. Online Inst. Teknol. Nas., 2(5): 1-12.

Paz, S., Rubio, C., Frias, I., Gutierrez, A. J., Gonzalez-Weller, D., Martin, V., Revert, C. and Hardisson, A. 2019. Toxic metals (Al, Cd, Pb, and Hg) in the most consumed edible seaweeds in Europe. Chemosphere, 218: 879-884.

Pemerintah Republik Indonesia. 2021. Law Number 22 of 2021 Concerning Implementation of Environmental Protection and Management, Appendix VIII. State Secretariat, Jakarta.

Pradit, S., Pattarathomrong, M. S. and Panutrakul, S. 2013. Arsenic cadmium and lead concentrations in sediment and biota from Songkhla Lake: A review. Procedia - Soc. Behav. Sci., 91: 573-580.

Priamanatha, D. D. 2023. Phytochemistry and Potential of Sargassum binderi, *Sargassum cinereum, Padina australis*, and *Turbinaria conoides* from the Thousand Islands as Medicinal Ingredients. Doctoral dissertation, University National, Jakarta, Indonesia.

Ramdhan, B. and Ratnasari, J. 2021. Utilization of macroalgae by the Binuangeun Lebak Banten community. J. Trop. Ethnobiol., 47-51.

Rumhayati, B. and Retnaningdyah, C. 2018. Integrative assessment of Pb and Cd pollution in Porong estuaries using sediment chemistry, bioavailability, and bioconcentration factor. Indones. J. Chem., 18(3): 464-471.

Rosiana, I. W., Wiradana, P. A., Permatasari, A. A. A. P., Pelupessy, Y. A. E. G., Dame, M. V. O., Soegianto, A., Yulianto, B. and Widhiantara, I. G. 2022. Concentrations of heavy metals in three brown seaweed (Phaeophyta: Phaeophyceae) collected from tourism areas in Sanur Beach, Coast of Denpasar, Bali, and Public Health Risk Assessment. J. Ilmiah Perikanan Kelautan, 14(2): 327-339.

Sahri, A. 2023. Getting to know the potential of seaweed: a study of the use of seaweed resources from industrial and health aspects. Maj. Ilmiah Sultan Agung, 44(118): 95-116.

Salama, E. S., Roh, H. S., Dev, S., Khan, M. A., Abou-Shanab, R. A. I., Chang, S. W. and Jeon, B. H. 2019. Algae as a green technology for heavy metals removal from various wastewater. World J. Microbiol. Biotechnol., 35(5): 1-19.

Salosso, Y., Aisiah, S., Toruan, L. N. L. and Pasaribu, W. 2020. Nutrient content, active compound, and antibacterial activity of *Padina australis* against *Aeromonas hydropillar*. Pharmacogn. J., 12(4): 771-776.

Saraswati, A. R. and Rachmadiarti, F. 2021. Heavy metal lead (Pb) content in *Padina australis* at Sendang Biru Beach, Malang. LenteraBio, 10(1): 67-76.

Sholikah, M. and Rachmadiarti, F. 2019. The ability of *Ludwigia adscendens* plants to absorb the heavy metal cadmium (Cd) at various concentrations. LenteraBio, 8(3): 150-155.

Siahaan, E. A., Asaduzzaman, A. K. M. and Pangestuti, R. 2018. Chemical compositions of two brown seaweed species from Karimun Jawa, Indonesia. Mar. Res. Indones., 43(2): 71-78.

Sohrab, A. D. and Alireza, N. 2011. Environmental monitoring of heavy metals in seaweed and associated sediment from the Strait of Hormuz, I.R. Iran. World J. Fish Mar. Sci., 3(6): 576-589.

Sukamto. 2017. Management of Indonesian maritime potential in the spirit of Islamic economics. MALIA: J. Ekon. Islam, 9(1): 35-61.

Supardi, W. and Nugroho, A. P. 2019. Bioaccumulation of lead (Pb) in the Macroalga *Padina australis* Hauck in marine waters in Makassar City, South Sulawesi. Bioma: Berkala Ilmiah Biol., 21(1): 9-15.

Syaifullah, M., Candra, Y. A., Soegianto, A. and Irawan, B. 2018. Content of non-essential metals (Pb, Cd, and Hg) and essential metals (Cu, Cr, and Zn) in sediments in the waters of Tuban, Gresik, and Sampang, East Java. J. Kelautan, 11(1): 69-74.

Tosepu, R. and Effendy, D. S. 2016. Coastal Community Health. YCAB Public, Southeast Sulawesi.

Ummi, F., Mahmudati, N. and Waluyo, L. 2017. Test for lead (Pb) content in shrimp paste and salted fish in Palang, Tuban Regency. University of Muhammadiyah Malang, Indonesia.

Vo, M. T., Nguyen, V. T., Vo, T. M. C., Bui, T. N. P. and Dao, T. S. 2020. Responses of green algae and diatom upon exposure to chromium and cadmium. Vietnam J. Sci. Technol. Eng., 62(1): 69-73.

Wang, W., Vinocur, B., Shoseyov, O. and Altman, A. 2004. Role of plant heat-shock proteins and molecular chaperones in the abiotic stress response. Trends Plant Sci., 9(5): 244-252.

Wardani, D. A. K., Dewi, N. K. and Utami, N. R. 2014. Accumulation of lead, heavy metal (Pb) in green shellfish (Perna viridis) at Muara Sungai Banjir Kanal Barat Semarang]. Unnes J. Life Sci., 3(1): 1-8.

WHO. 1985. Guidelines for Drinking Water Quality. Vol. 2: Health Criteria and Supporting Information. Vol. 1: Recommendations. 130. WHO, Geneva.

Yulis, P. A. R. 2018. Analysis of mercury (Hg) and (Ph) metal levels in Kuantan River water affected by gold mining without a permit (PETI). Orbital: J. Pendidik. Kim., 2(1): 28-36.

Yusuf, M., Handoyo, G., Muslim., Wulandari, S. Y. and Setiyono, H. 2012. Characteristics of current patterns in relation to water quality conditions and phytoplankton abundance in the waters of the Karimunjaw Marine National Park Area. Bul. Oseanogr. Mar., 1: 63-74.

Zamani-Ahmadmahmoodi, R., Malekabadi, M. B., Rahimi, R. and Johari, S. A. 2020. Aquatic pollution caused by mercury, lead, and cadmium affects cell growth and pigment content of marine microalgae Nannochloropsis oculata. Environ. Monit. Assess., 192(6): 330.

## ORCID DETAILS OF THE AUTHORS

Fida Rachmadiarti: https://orcid.org/0000-0002-0802-124X

Nature Environment and Pollution Technology
An International Quarterly Scientific Journal

p-ISSN: 0972-6268
(Print copies up to 2016)
e-ISSN: 2395-3454

Vol. 23 | No. 3 | pp.1517-1526 | 2024

Original Research Paper

https://doi.org/10.46488/NEPT.2024.v23i03.021

Open Access Journal

# Enhanced Phenanthrene Biodegradation by *Bacillus brevis* Using Response Surface Methodology

**Kiran Bishnoi*(**)†, Pushpa Rani* and Narsi R. Bishnoi*****

*Department of Environmental Science & Engineering, Guru Jambheshwar University of Science & Technology, Hisar-125001, Haryana, India

**Department of Environmental Studies, Govt. College for Women, Hisar-125001, Haryana, India

***Guru Jambheshwar University of Science & Technology, Hisar-125001, Haryana, India

†Corresponding author: Kiran Bishnoi; kiranbishnoi@gmail.com

**Nat. Env. & Poll. Tech.**
**Website: www.neptjournal.com**

*Received:* 22-11-2023
*Revised:* 10-01-2024
*Accepted:* 21-01-2024

**Key Words:**
Polycyclic aromatic hydrocarbons
Phenanthrene
Response surface methodology
Box-Behnken design
Biodegradation

## ABSTRACT

The current investigation assessed the capability of a well-adapted and enriched bacterial strain known as *Bacillus brevis* for the biodegradation of phenanthrene. To enhance the removal efficiency of phenanthrene, employed Response Surface Methodology (RSM) in conjunction with a Box-Behnken design (BBD) model. The experiments were designed to explore the impact of pH (6.0 to 9.0), temperature (20 to 40°C), initial phenanthrene concentration (50 and 100 ppm), and incubation time (7 to 21 days) on biodegradation of phenanthrene. The highest level of phenanthrene biodegradation, approximately 55.0%, was achieved by *Bacillus brevis* when the optimal conditions were met as pH of 7.0, temperature 30°C, and initial phenanthrene concentration (70 ppm) after 21 days of incubation time. This study underscores the significance of employing statistical tools like RSM to enhance the microbial degradation of contaminants.

## INTRODUCTION

Polycyclic aromatic hydrocarbons (PAHs) represent a class of chemical compounds characterized by the fusion of at least two aromatic rings, and they are classified as persistent organic pollutants. PAHs are ubiquitous organic contaminants with a natural presence in fossil fuels like petroleum and coal. They come into contact with the environment through incomplete combustion of organic materials such as waste incineration, the combustion of wood and vegetation, petroleum refining, volcanic eruptions, and forest fires (Barbosa et al. 2023, Cao et al. 2023). In 1983, the United States Environmental Protection Agency (USEPA) designated 16 PAHs as priority pollutants due to their prevalence in high concentrations, increased exposure levels, persistent characteristics, and toxicity (Dai et al. 2022). Because of their stubborn characteristics, environmentalists are greatly concerned about their long-term persistence (Urana et al. 2021). Prolonged exposure to PAHs via the consumption of contaminated food and inhalation of polluted air can have detrimental impacts on human health (Domingo et al. 2020, Marquès et al. 2020). The level of contamination and the current environmental circumstances will determine how the PAH decontamination strategy is implemented. Bioremediation employs a wide variety of microorganisms, and their selection depends on biotic and abiotic variables (Patel et al. 2020).

Phenanthrene (Phe) stands out among PAHs as a subject of frequent research interest. This is due to its possession of both K and bay regions, recognized as fundamental structures associated with carcinogenicity and mutagenicity in many high molecular weight PAHs (Gu et al. 2023). Its pronounced hydrophilic nature and excellent water solubility render it easily detectable in aqueous environments (Ghosal et al. 2016). So, Phe stands out as the ideal choice as a model for laboratory research on PAHs.

Historically, researchers employed a one-factor-at-a-time approach to optimize multi-variate systems, which proved inadequate in revealing the interplay of factors and their effects (Swati et al. 2019). To circumvent this issue, we utilized Response Surface Methodology (RSM), a widely recognized statistical multivariable experimental approach. RSM serves as a potent tool for the Design of Experiments (DOE) aimed at optimizing processes through modeling techniques. This methodology comprises a set of statistical

and mathematical techniques employed to establish a series of experimental designs, enabling the determination of optimal conditions based on input variables to predict the corresponding output variables (Massoudinejad et al. 2016, Khuri 2017). This study involved the selection of four key factors (pH, temperature, initial Phe concentration, and incubation time) to optimize a single response, which is the percentage degradation of Phe by using the Box-Behnken design.

## MATERIALS AND METHODS

### Chemicals and Solvents

From Sigma Aldrich Chemicals in Germany, all PAHs (phenanthrene, acenaphthene, anthracene, fluoranthene, and pyrene) with 99.0% purity analytical standard were purchased. All chemicals were used without further purification.

### Enrichment of Bacterial Strain and Biodegradation Study

The nutrient broth (NB) medium containing ($g.L^{-1}$) glucose10.0, peptone 5.0, yeast extract 3.0, and NaCl 5.0 were used for the proliferation and culturing of Phe degrading microorganisms. Bacterial strain (*Bacillus brevis*) was taken from the laboratory and acclimatized with the same enrichment media, which was used for further study. 1 mL bacterial inoculum was inoculated into a 250 mL conical flask containing 100 mL sterilized Nutrient broth (NB) media amended with 0.01% Phe. It was shaken for five days at 28°C and 120 rpm in a shaker cum-incubator. After five days, enrichment was made by serially subculturing in the same medium using 10% inoculum from the previous culture. The enrichment action was repeated for 3 months and the next three months with a 0.01% mixture of five PAHs (phenanthrene, acenaphthene, anthracene, fluoranthene, and pyrene). The Phe biodegradation study was carried out in 100 mL sterilized nutrient broth (NB) in 250 ml Erlenmeyer flasks. Variables were incubated at 120 rpm as given by the model.

### Process Optimization for Phenanthrene Degradation

The optimization process for achieving maximum Phe degradation, a dependent response, involved selecting various independent variables such as pH, temperature, initial Phe concentration, and incubation time. This optimization was carried out using the Box-Behnken design (BBD) within the Stat-Ease Design Expert software. The BBD serves as an excellent design tool for assessing the presence of a lack of fit when a sufficient number of experimental values are available. The experimental region extended from –1 to +1 in terms of coded variables (Table 1). Four variables studied were pH (6.0-9.0), temperature (20-40°C), initial Phe concentration (50-100 ppm), and incubation time (7-21 days) to obtain the response, i.e., biodegradation (*Y*). The experimental design was implemented following the determination of the range for each variable (maximum and minimum), and the model designed a total of twenty-nine experiments. The experimental results yielded quantitative data, which was utilized to establish a regression model equation and identify the optimal operational parameters for achieving the highest desired response. RSM enables the quantitative representation of individual process parameters in Eq. (1):

$$Y = b_0 + \sum b_i X_i + \sum b_{ii} X_i^2 + \sum b_{ij} X_i X_j \quad \ldots(1)$$

where *Y* represents the predicted response, while $b_0$ stands for the response function, $X_i$ and $X_j$ denote the coded experimental variables, respectively. A second-order polynomial regression model was employed to fit experimental data and derive the Phe biodegradation equation. This model included four linear ($X_i$), four quadratic ($X^2_i$), six interaction ($X_iX_j$), and a constant ($b_0$). Utilizing the software, an Analysis of Variance (ANOVA) was performed ($p < 0.05$), and the coefficient of regression (R) was determined to assess the significance and goodness of fit of the model (Al Farraj et al. 2019). The quadratic equation Eq. (2) was used to assess the second-order polynomial mathematical connection between the response variable *Y* and four factors, i.e., pH, temperature, initial Phe concentration, and incubation period.

Table 1: Experimental factors and their levels used in the BBD design.

| Coded factor | Actual factor | Units | Actual level | | | Coded level | | |
|---|---|---|---|---|---|---|---|---|
| | | | Low | Middle | High | Low | Middle | High |
| A | pH | | 6 | 7.5 | 9 | -1 | 0 | 1 |
| B | Temperature | °C | 20 | 30 | 40 | -1 | 0 | 1 |
| C | Initial Phe concentration | Ppm | 50 | 75 | 100 | -1 | 0 | 1 |
| D | Incubation time | days | 7 | 14 | 21 | -1 | 0 | 1 |

$$Y = b_0 + b_1X_1 + b_2X_2 + b_3X_3 + b_4X_4 + b_{11}X_1^2 + b_{22}X_2^2 + b_{33}X_3^2 + b_{44}X_4^2 + b_{12}X_1X_2 + b_{13}X_1X_3 + b_{14}X_1X_4 + b_{23}X_2X_3 + b_{24}X_2X_4 + b_{34}X_3X_4 \quad \ldots(2)$$

### Extraction and Quantification

The ultrasonic extraction method was used for quantification of PAHs. The cleanup process involved the use of a chromatographic column (35.5 × 1.5cm) by using hexane as an elution solvent, and glass wool was fixed at the tip of the column. The samples were concentrated on a rotary evaporator (JSGW) twice with hexane and filtrated through 0.45 µm syringe filters. High-performance liquid chromatography (HPLC Water 600) equipped with a UV detector at 254 nm was used for the analysis of the samples. The PAH concentration was determined by assessing the peak areas of the sample chromatogram and comparing them to the peak area of the standard chromatogram. Biodegradation efficiency was calculated as:

$$\text{Biodegradation efficiency (\%)} = \frac{(C_0 - C_e)}{C_0} \times 100 \quad \ldots(3)$$

$C_0$ is the initial concentration of Phe (ppm); $C_e$ is the final/residual concentration of Phe.

## RESULTS AND DISCUSSION

### Regression Model and Statistical Analysis

Table 2 shows the experimental design and results for Phe degradation in each run. ANOVA was conducted to assess the model's significance and adequacy (Table 3). When Prob > F is less than 0.05, it indicates that the model terms hold significance. The lack of fit displaying a non-significant value confirms the validity of the quadratic model for Phe removal by the bacterial strain *B. brevis*, and these models

Table 2: Box-Behnken design matrix for experimental design along with actual and predicted response.

| Std | Coded value of variables | | | | Response | |
|---|---|---|---|---|---|---|
| | pH (A) | Temperature ($^oC$) (B) | Phenanthrene conc. (ppm) (C) | Incubation time (days) (D) | Actual | Predicted |
| 1 | -1 | -1 | 0 | 0 | 34.02 | 33.80 |
| 2 | +1 | -1 | 0 | 0 | 26.54 | 27.35 |
| 3 | -1 | +1 | 0 | 0 | 35.97 | 35.65 |
| 4 | +1 | +1 | 0 | 0 | 32.96 | 33.67 |
| 5 | 0 | 0 | -1 | -1 | 29.92 | 31.62 |
| 6 | 0 | 0 | +1 | -1 | 28.99 | 29.81 |
| 7 | 0 | 0 | -1 | +1 | 52.18 | 51.85 |
| 8 | 0 | 0 | +1 | +1 | 44.93 | 43.71 |
| 9 | -1 | 0 | 0 | -1 | 32.18 | 32.46 |
| 10 | +1 | 0 | 0 | -1 | 27.24 | 26.97 |
| 11 | -1 | 0 | 0 | +1 | 47.4 | 48.25 |
| 12 | +1 | 0 | 0 | +1 | 45.01 | 45.31 |
| 13 | 0 | -1 | -1 | 0 | 32.96 | 33.17 |
| 14 | 0 | +1 | -1 | 0 | 38.36 | 39.09 |
| 15 | 0 | -1 | +1 | 0 | 30.04 | 29.96 |
| 16 | 0 | +1 | +1 | 0 | 31.91 | 32.29 |
| 17 | -1 | 0 | -1 | 0 | 39.97 | 39.09 |
| 18 | +1 | 0 | -1 | 0 | 35.13 | 33.77 |
| 19 | -1 | 0 | +1 | 0 | 32.72 | 33.01 |
| 20 | +1 | 0 | +1 | 0 | 30.09 | 29.90 |
| 21 | 0 | -1 | 0 | -1 | 28.13 | 27.04 |
| 22 | 0 | +1 | 0 | -1 | 33.18 | 31.74 |
| 23 | 0 | -1 | 0 | +1 | 44.34 | 44.71 |
| 24* | 0 | +1 | 0 | +1 | 48.17 | 48.19 |
| 25* | 0 | 0 | 0 | 0 | 50.15 | 50.71 |
| 26* | 0 | 0 | 0 | 0 | 50.23 | 50.71 |
| 27* | 0 | 0 | 0 | 0 | 51.25 | 50.71 |
| 28* | 0 | 0 | 0 | 0 | 50.91 | 50.71 |
| 29* | 0 | 0 | 0 | 0 | 51.02 | 50.71 |

Std = Standard run order, * Central value

align well with the measured data. The second-order model exhibited strong statistical significance ($p < 0.05$) in the context of Phe degradation, demonstrating the actual relationship between variables and the response. Eq. (4) below represents the model for Phe degradation.

% biodegradation ($Y^2$) = +50.71 -2.11*A +2.04*B -2.49*C +8.53*D -8.88*$A^2$ -9.21*$B^2$ -7.89*$C^2$ -3.58*$D^2$ +1.12*A*B +0.55*A*C +0.64*A*D -0.88*B*C -0.31*B*D -1.58 *C*D …(4)

The data exhibited the most favorable fit when described by a second-order polynomial equation, as evidenced by the strong correspondence between the experimental data and the

Table 3: Analysis of variance (ANOVA) for variables.

| Source | Sum of Squares | DF | Mean Square | F-Value | Prob > F | |
|---|---|---|---|---|---|---|
| Model | 2139.31 | 14 | 152.81 | 140.72 | 0.0001*** | Significant |
| A | 53.30 | 1 | 53.30 | 49.08 | 0.0001*** | |
| B | 50.10 | 1 | 50.10 | 46.14 | 0.0001*** | |
| C | 74.20 | 1 | 74.20 | 68.33 | 0.0001*** | |
| D | 873.64 | 1 | 873.64 | 804.51 | 0.0001*** | |
| $A^2$ | 511.84 | 1 | 511.84 | 471.34 | 0.0001*** | |
| $B^2$ | 550.73 | 1 | 550.73 | 507.15 | 0.0001*** | |
| $C^2$ | 403.47 | 1 | 403.47 | 371.54 | 0.0001*** | |
| $D^2$ | 83.04 | 1 | 83.04 | 76.47 | 0.0001*** | |
| AB | 5.00 | 1 | 5.00 | 4.60 | 0.05 $^{NS}$ | |
| AC | 1.22 | 1 | 1.22 | 1.12 | 0.3069 $^{NS}$ | |
| AD | 1.63 | 1 | 1.63 | 1.50 | 0.2413 $^{NS}$ | |
| BC | 3.12 | 1 | 3.12 | 2.87 | 0.1124 $^{NS}$ | |
| BD | 0.37 | 1 | 0.37 | 0.34 | 0.5676 $^{NS}$ | |
| CD | 9.99 | 1 | 9.99 | 9.20 | 0.009*** | |
| Residual | 15.20 | 14 | 1.09 | | | |
| Lack of Fit | 14.23 | 10 | 1.42 | 5.86 | 0.0516 | Not significant |
| Pure Error | 0.97 | 4 | 0.24 | | | |
| Cor total | 2154.51 | 28 | | | | |
| $R^2$ | 0.9929 | | | | | |
| $R^2_{adj}$ | 0.9859 | | | | | |
| CV | 2.71 | | | | | |
| Std dev | 1.04 | | | | | |

Std dev = Standard deviation, * Significance (P< 0.001), NS = Not significant, DF = Degree of freedom, CV = Coefficient of variation

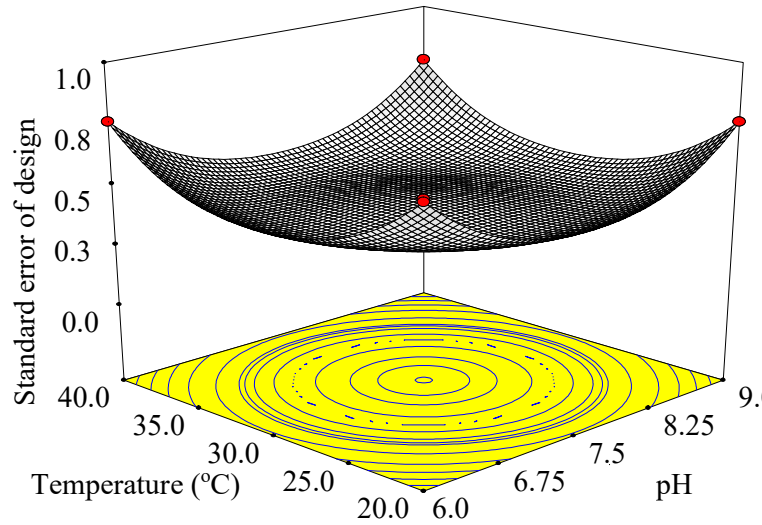


Fig. 1: 3D graph of the standard error design of the model with temperature and pH for biodegradation of Phenanthrene.

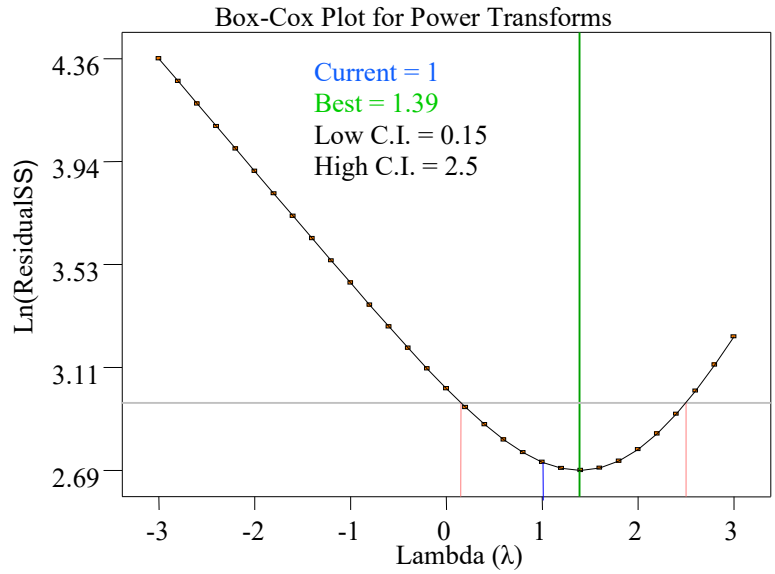


Fig. 2: Box-Cox plot of model transformation for biodegradation of Phenanthrene.

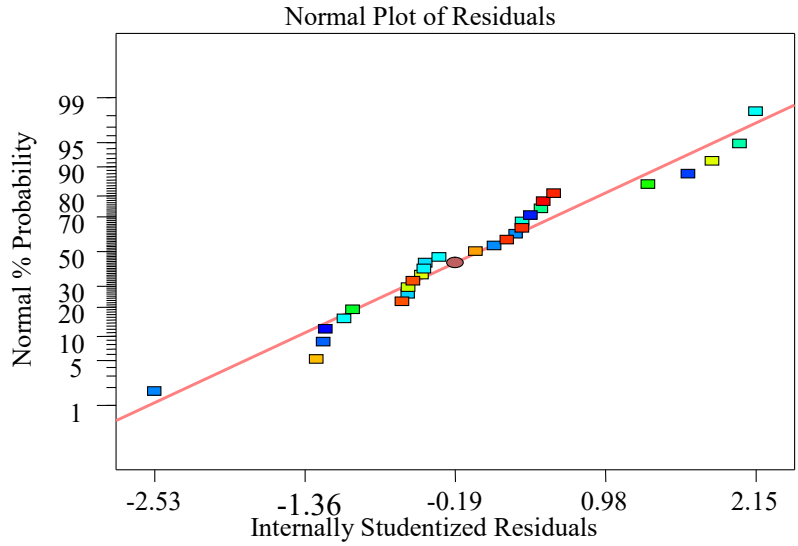


Fig. 3: Normal plot of studentized residuals versus normal percentage probability for biodegradation of Phenanthrene.

model's predictions. The correlation coefficient ($R^2$) values stood at 0.9929, implying that the data displayed limited variation and a high degree of uniformity and homogeneity. The adjusted $R^2$ of 0.9859 was in reasonable concordance with the $R^2$ value, which approached 1.0, signifying the model's superior fitness to the experimental data. An $R^2$ value near 1.0 is desirable, and it is essential for the adjusted $R^2$ to exhibit reasonable agreement (Dalvand & Ghiasvand 2019).

The standard error has a minimum value of 0.422207 around the centroid, and the maximum prediction variance is 0.578 at the design points. These observations suggest that the current model is suitable for exploring the design space in the present study (Fig. 1). The model exhibits a minimum confidence interval value of 0.15 and a maximum value of 2.5. When examining the natural logarithm (Ln) of the residual sum of squares (SS) against λ is one, it reveals a minimum within a steeply declining region, indicating an optimal value of 1.39 (Fig. 2). The diagnostic details articulated by Design-Expert can best be digested by viewing plots of normal probability versus studentized residual. The complete set of data points for the normal probability and studentized residual is almost linear and clustered around the

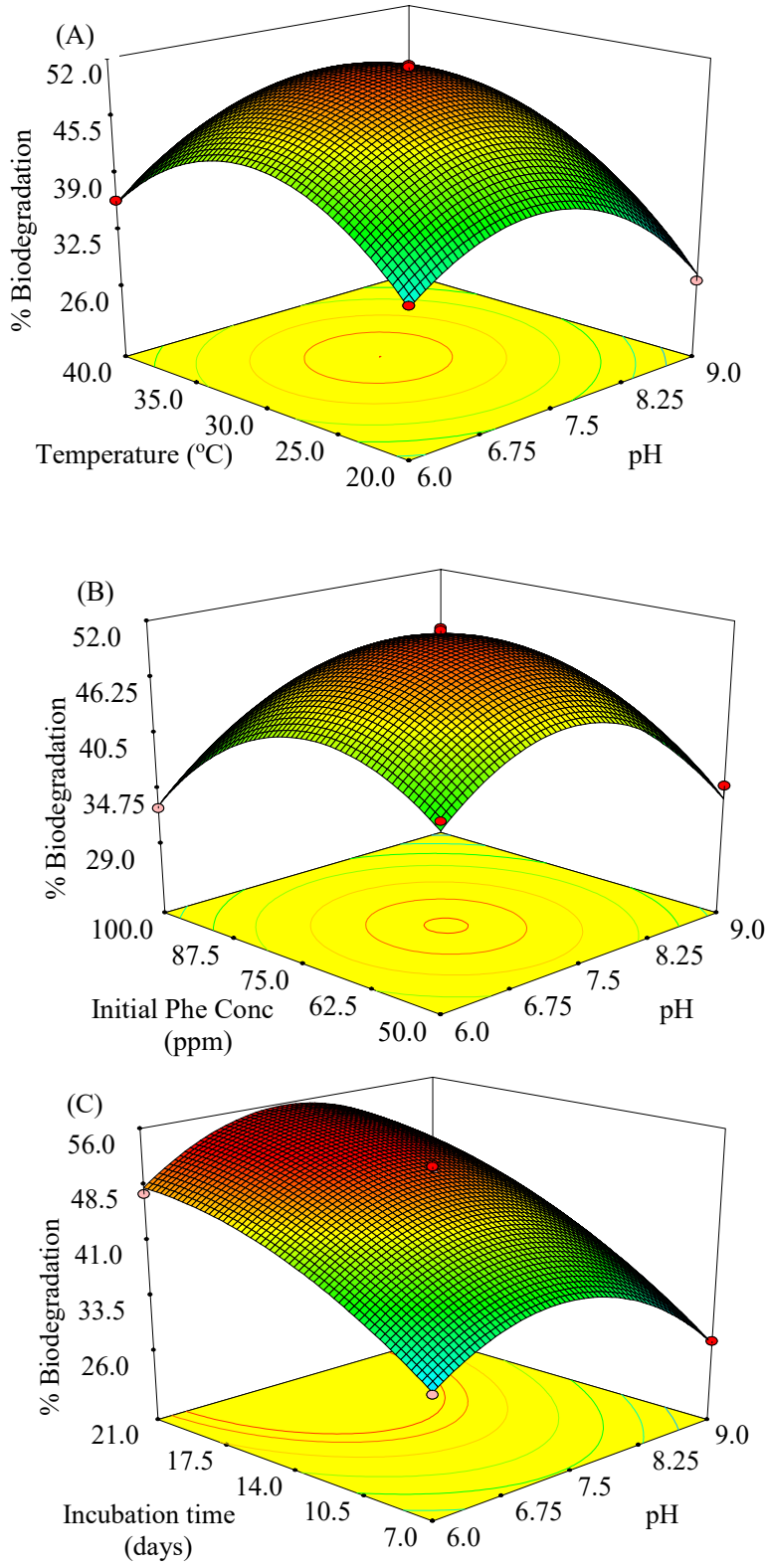


Figure Cont....

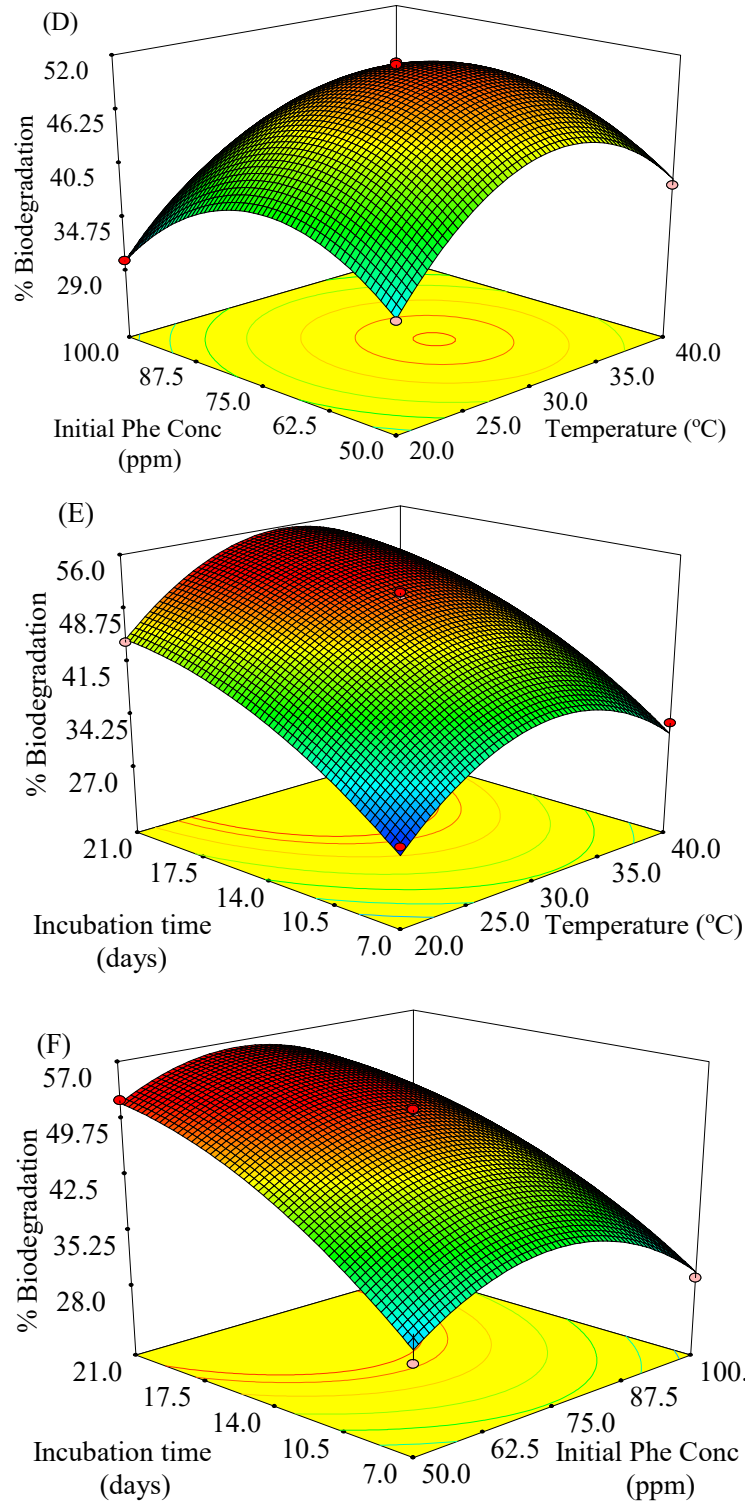


Fig. 4: 3D-surface plot showing the interactive of (A) pH and temperature (B) of pH and initial Phenanthrene Conc (C) incubation time and pH (D) temperature and initial Phenanthrene Conc (E) incubation time and temperature (F) incubation time and initial Phenanthrene Conc on biodegradation of Phenanthrene.

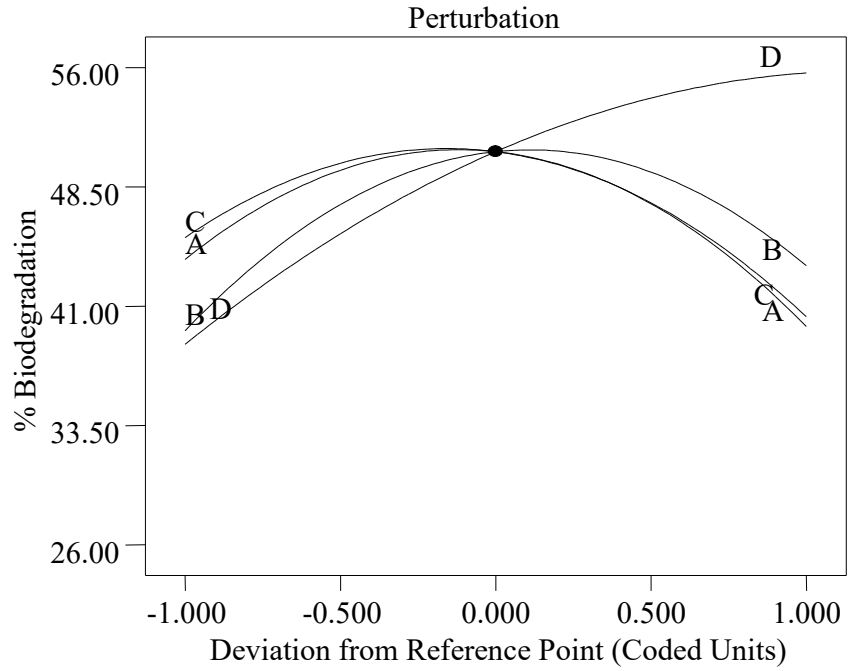


Fig. 5: Perturbation plots representing the individual variable effect on biodegradation of Phenanthrene.

zero line, which represents the model's suitability and shows no signs of any problems in our data (Fig. 3).

The statistical analysis of the positive linear coefficient for incubation time was observed to be the paramount factor impacting biological degradation significantly (Eq. 5). Up to a point, the negative quadratic coefficient for each variable showed the existence of maxima. Beyond that, the variable as a whole had an inhibiting effect on response. Out of the total of 14 effects, 9 (A, B, C, D, $A^2$, $B^2$, $C^2$, $D^2$, and CD) were significant. In the current investigation, the remaining five factors exhibited no significant influence on the response. Nevertheless, none of these factors displayed a noteworthy impact on the ultimate biodegradation percentage, as indicated by probability (p) values exceeding 0.05 for all five effects (Table 3).

**Effects of Variables on Biodegradation of Phenanthrene**

To ascertain the optimal levels of each variable for achieving maximum results, we generated 3D plots by graphing the response. Based on the interaction between two variables and the fixed level of another variable for Phe biodegradation, the response surface was selected.

Fig. 4 illustrates the quadratic surface response. The interactive effects of pH and temperature, with another variable being at the fixed level on biodegradation of Phe by *B. brevis,* is reported in Fig. 4A. Initially increase in pH resulted in the enhancement of biodegradation to values in the vicinity of 7.0. Still, beyond that, a decreasing trend was observed. The level of biodegradation observed was 33.8%, 50.7%, and 27.35% at the lowest (pH 6 and 20°C), middle (pH 7.5 and 30°C), and higher levels (pH 9 and 40°C) of variables by *B. brevis*. The Phe removal rates varied with pH, with the highest recorded at 88.33% when the pH was 7.0 and the lowest observed at 82.07% when the pH was 4.0, as reported by Liu et al. (2019). The optimum temperature observed for biodegradation of Phe was 30°C for *B. brevis* holding Phe concentration at 75ppm and 14 days of incubation time. Fig. 4B shows the interactive effects of pH and initial Phe concentration. The increase in initial Phe concentration from 50 to 70 ppm resulted in increased biodegradation, i.e., 39.09 to 51.03% by *B. brevis* with a change in pH 6 to 7.3. Beyond these, the reduction in the rate of biodegradation was observed with an increase in both variables. Phe biodegradation dropped above 100 $mgL^{-1}$ and was less than 10% at 400 $mgL^{-1}$(Mai et al. 2021). At higher PAH concentrations, the substrate functions as the limiting factor because of their toxicity to microbes and slower biodegradation rate (Yuan et al. 2002). Fig. 4C depicts the interactive effects of incubation time and pH on the biodegradation of Phe by *B. brevis,* keeping the temperature (30°C) and initial Phe concentration (75 ppm). The negative value of the quadratic coefficient (Eq 5) and three-dimensional plots indicated that an increase in duration beyond optimum did not affect the

biodegradation significantly as the Phe degradation became slower or nearly constant. The similar response curvature for lower and higher ranges of temperature and initial Phe concentration for biodegradation showed the same effects (Fig. 4D). An increase in biodegradation with the increase in temperature from 20°C to 30°C and a decrease with an increase in temperature from 30°C to 40°C was observed. As the temperature rose, the solubility of Phe increased, leading to enhanced Phe bioavailability. However, excessively high temperatures could hinder microbial activity, consequently reducing Phe degradation (Liu et al. 2019). Fig. 4E shows the interactive effects of temperature and incubation time. The 3D figure clearly showed that the biodegradation rate was initially high, but after 18 days of incubation, biodegradation did not increase proportionally with increasing incubation period. The increase in duration to 18 days and temperature (30°C) increased the degradation efficiency to 55.7% after that, the degradation is about constant. Fig. 4F shows the interactive effects of the incubation time and initial Phe concentration. The strains presumably degraded Phe at slower rates during the initial incubation time. At the end of the incubation period, the degradation trend reversed, with the highest Phe degradation observed at 53% on the 18th day of incubation.

The interactive effects of the four process variables on the biodegradation of Phe are presented in (Fig. 5). The perturbation plots of biodegradation potential versus all four tested variables suggest that the variable contributed to the biodegradation activity, representing outline views of the response surface. The parabolic curves of pH (A), temperature (B), and initial Phe concentration (C) reflected that the initial rate of biodegradation increased with an increase in variables, and beyond, an optimum reduction in degradation was observed with further increases in the variables.

## CONCLUSION

By RSM using Box-Behnken design, this study showed the significant effects of pH, temperature, initial Phe concentration, and incubation time on the biodegradation of Phe by *B. brevis*. A "Prob>F" value below 0.05 signifies that model terms substantially influence Phe's biodegradation. The model explains that the determination coefficient value $R^2 = 0.9929$ indicates that the data is more uniform and less variable in the experimental data. Maximum biodegradation of Phe was observed at almost 55.0% by *B. brevis*at pH 7.0, temperature 30°C, and initial Phe concentration (70 ppm) after 21 days of incubation time. The mathematical evaluation, significant model, and RSM approach proved advantageous.

## REFERENCES

Al Farraj, D.A., Hadibarata, T., Yuniarto, A., Syafiuddin, A., Surtikanti, H.K., Elshikh, M.S., Al Khulaifi, M.M. and Al-Kufaidy, R. 2019. Characterization of pyrene and chrysene degradation by halophilic *Hortaea* sp. B15. Bioprocess Biosyst. Eng., 42: 963–969. https:// doi.org/10.1007/s00449-019-02096-8.

Barbosa, F., Rocha, B.A., Souza, M.C., Bocato, M.Z., Azevedo, L.F., Adeyemi, J.A., Santana, A. and Campiglia, A.D. 2023. Polycyclic aromatic hydrocarbons (PAHs): updated aspects of their determination, kinetics in the human body, and toxicity. J. Toxicol. Environ. Health B Crit. Rev., 26: 28-65. https://doi.org/10.1080/10937404.2022.2164390.

Cao, W., Yuan, J., Geng, S., Zou, J., Dou, J. and Fan, F. 2023. Oxygenated and nitrated polycyclic aromatic hydrocarbons: sources, quantification, incidence, toxicity, and fate in soil: A review study. Processes, 11: 52. https://doi.org/10.3390/pr11010052.

Dai, Q., Wang, Y., Chen, L., Li, P., Xia, S. and Huang, Q. 2022b. Contamination of 16 priority polycyclic aromatic hydrocarbons (PAHs) in urban source water at the tidal reach of the Yangtze River. Environ. Sci. Pollut. Control Ser., 29: 61222–61235. Doi: 10.1007/s11356-022-20052-0.

Dalvand, K. and Ghiasvand A. 2019. Simultaneous analysis of PAHs and BTEX in soil by a needle trap device coupled with GC-FID and using response surface methodology involving Box-Behnken design. Anal. Chim. Acta, 1083: 119-129. https://doi.org/10.1016/j.aca.2019.07.063.

Domingo, J. L., Marquès, M., Nadal, M. and Schuhmacher, M. 2020. Health risks for the population living near petrochemical industrial complexes. 1. Cancer risks: A review of the scientific literature. Environ. Res., 186: 109495. https://doi.org/10.1016/ j.envres.2020.109495.

Ghosal, D., Ghosh, S., Dutta, T. K. and Ahn, Y. 2016. Current state of knowledge in microbial degradation of polycyclic aromatic hydrocarbons (PAHs): A review. Fron. Microb., 7: 1369. https://doi.org/10.3389/ fmicb.2016.01369.

Gu, H., Yan, J., Liu, Y., Yu, X., Feng, Y., Yang, X., Lam, S. S., Naushad, M., Li, C. and Sonne, C. 2023. Autochthonous bioaugmentation accelerates phenanthrene degradation in acclimated soil. Environ. Research, 224: 115543. https://doi.org/10.1016/j.envres.2023.115543.

Khuri, A. I. 2017. A General Overview of Response Surface Methodology. Biometrics Biostat. Int. J., 5: 87-93. DOI: 10.15406/bbij.2017.05.00133

Liu, S.H., Zeng, Z.T., Niu, Q.Y., Xiao, R., Zeng, G. M., Liu, Y., Cheng, M., Hu, K., Jiang, L. H., Tan, X. F. and Tao, J. J. 2019. Influence of immobilization on phenanthrene degradation by Bacillus sp. P1 in the presence of Cd(II). Sci. Total Environ., 655: 1279-1287. https://doi.org/10.1016/j.scitotenv.2018.11.272

Mai, Z., Wang, L., Li, Q., Sun, Y. and Zhang, S. 2021.Biodegradation and metabolic pathway of phenanthrene by a newly isolated bacterium Gordonia sp. SCSIO19801. Biochem. Biophys. Res. Commun., 585: 42-47. https://doi.org/10.1016/j.bbrc.2021.10.069

Marquès, M., Domingo, J. L., Nadal, M. and Schuhmacher, M. 2020. Health risks for the population living near petrochemical industrial complexes. 2. Adverse health outcomes other than cancer. Sci. Total Environ., 730: 139122. https://doi.org/ 10.1016/j.scitotenv.2020.139122

Massoudinejad, M., Ghaderpoori, M., Shahsavani, A. and Amini, M. M. 2016. Adsorption of fluoride over a metal-organic framework Uio-66 functionalized with amine groups and optimization with response surface methodology. J. Mol. Liq., 221: 279-86. https://doi.org/10.1016/j.molliq.2016.05.087

Patel, A.B., Shaikh, S., Jain, K.R., Desai, C. and Madamwar, D. 2020. Polycyclic aromatic hydrocarbons: Sources, toxicity and remediation approaches. Fron. Microb., 11: 562813. https://doi.org/10.3389/fmicb.2020.562813.

Swati, B., Ghosh, P. and Thakura, I. S. 2019. Biodegradation of pyrene by Pseudomonas sp. ISTPY2 isolated from landfill soil: Process

optimisation using Box-Behnken design model. Bioresour. Technol. Rep., 8: 100329. https://doi.org/10.1016/j.biteb.2019.100329

Urana, R., Dahiya, A., Sharma, P. and Singh, N. 2021. Effects of plant growth promoting rhizobacteria on phytoremediation of phenanthrene contaminated sodic soil. Polycycl. Aromat. Compd., 41: 1020-1029. https://doi.org/10.1080/10406638.2019.1639063.

Yuan, S.Y., Shiung, L.C. and Chang, B.V. 2002. Biodegradation of polycyclic aromatic hydrocarbons by inoculated microorganisms in soil. Bull. Environ. Contam. Toxicol., 69: 66-73. https://doi.org/10.1007/s00128-002-0011-z

Nature Environment and Pollution Technology
An International Quarterly Scientific Journal

p-ISSN: 0972-6268
(Print copies up to 2016)
e-ISSN: 2395-3454

Vol. 23 | No. 3 | pp. 1527-1535 | 2024

Original Research Paper

https://doi.org/10.46488/NEPT.2024.v23i03.022

Open Access Journal

# Combined Application of Biochar and Silicon Fertilizer for Improved Soil Properties and Maize Growth

**Muhammad Wasil Bin Abu Bakar*, M. K. Uddin†*, Susilawati Kasim*, Syaharudin Zaibon*, S. M. Shamsuzzaman**, A. N. A. Haque* and A. Reza***

*Soil Science Faculty of Agriculture, University Putra Malaysia, 43300, Seri Kembangan, Selangor, Malaysia
**Soil Resources Development Institute, Dhaka, Bangladesh
Corresponding author: M. K. Uddin; mkuddin@upm.edu.my

**Nat. Env. & Poll. Tech.**
**Website: www.neptjournal.com**

*Received:* 31-05-2023
*Revised:* 19-07-2023
*Accepted:* 02-08-2023

**Key Words:**
Acid soil
Biochar
Silicon fertilizer
Soil properties
Maize growth

## ABSTRACT

Biochar can be a good soil amendment to reduce the soil pH, increase crop growth rate, and improve the efficient use of fertilizer. Other than that, silicon fertilizer also would promote photosynthetic ability on plant development that would help to produce high yield. In this work, a series of experiments was conducted to observe the effect of rice husk biochar and silicon fertilizer on the maize growth rate and soil pH. A 45-day pot experiment in the greenhouse with three replicates of 9 experimental treatment combinations of RHB at two rates (5 and 2.5 $t.ha^{-1}$) with silicon fertilizer at three rates (125%, 100%, 75%), sole biochar (10 t.ha $t.ha^{-1}$), sole silicon fertilizer (100%) and control (NPK) to observe the best rate and combination to improve growth rate and change in soil chemical in acid soil. The result showed that the co-application of sole biochar and biochar with Silicon significantly improved growth development, increased photosynthesis rate, altered soil pH, and reduced Fe concentration compared to control. The plant height increased 88.35% from T4 (5 $t.ha^{-1}$ RHB + 100% Si) compared to the control and the conductance was higher in T4 (0.53) followed by T8 (0.438) while T1 (0.071) recorded the lowest conductance. The shoot fresh weight was higher in T4 (127.83 g) followed by T8 (57.14 g). However, the weight increased by 343.7% at T4 followed by T8 (2.5 $t.ha^{-1}$ RHB + 75% Si) at 98.33%. The highest pH increment of 1.24 units (T1 = 5.53, T4 = 6.77) of soil pH was noted from T4 (5 $t.ha^{-1}$ RHB + 100% Si) compared to control (NPK), and the highest total Fe in soil was observed from T1 (442.30 $mg.kg^{-1}$). The current study results showed that T4 (50% RHB + 100% Silicon) was the best treatment over the other rates of RHB and silicon increased plant height, photosynthetic rate, and biomass.

## INTRODUCTION

The maize plant (*Zea mays*) is a common type of crop that is being cultivated in many countries as the staple food for humans and the source of animal feed (Urassa 2015). Countries with a large population of people without a sufficient supply of rice declare maize as an important source of crop in the country such as Ghana, Bangladesh, and Pakistan (Shashi et al. 2018, Abukari 2014, Khan et al. 2017). Other than that, it is also widely used as a feed mill and thus can be classified as the major supply of energy for poultry (Dei & Herbert 2017). Unfortunately, the soil acidity has caused many problems with the cultivation of maize and also other crops (Shetty & Prakash 2020, Mosharrof et al. 2021).

One study records that the production of biochar has started to rise in Asia. In 2011, Malaysia recorded around 592,477 tons of rice husk and 32,000 tons of rice husk biochar produced from paddy plant waste (Manickam et al. 2015). The productivity of biochar depends on the type of organic residue used and the condition of pyrolysis applied and it is also high content of carbon (Oni et al. 2019). It has also been proven that high application of biochar as a soil amendment would bring a better impact on the crop (Shashi et al. 2018) increase soil organic carbon, nitrogen, and sulfur, and decrease soil bulk density to a favorable level (Islam et al. 2018).

On the other hand, silicon gives benefits to plant growth and plants promote the development of plants by increasing plant resistance and tolerance to various biotic and abiotic stresses (Kostic et al. 2017, Yongchao et al. 2015). Moreover, silicon is listed as the fourth most important element after nitrogen (N), phosphorus (P), and potassium (K) by the International Soil Classification system (Swe et al. 2021). It also can be used to stimulate photosynthesis, enhance tissue strength, and reduce the plant transpiration rate (Xie et al. 2014).

Increasing the rate of application of rice husk biochar would also increase the crop morphology growth and

biomass of plants (Shetty & Prakash 2020, Islam et al. 2018). Furthermore, the nitrogen and total organic have been observed to increase with the presence of biochar (Abukari 2014). Moreover, various mineral stresses should be reduced in plants to support growth in acidic conditions (Pontigo et al. 2015). The required pH can be maintained through basic cation additions and $H^+$ consumption (Mosharrof et al. 2021) and it was found that biochar can reduce the acidity of the soil through this mechanism (Islam et al. 2018). Rahman et al. (2022) state that the pH can be increased to reduce the acidity on a large scale (6.5 to 8.8) which takes around a 26% increase. The micronutrient concentration in the plant was not affected by the application of biochar but affected the macronutrient (NPK) (Ullah et al. 2018). The addition of fertilizer such as silicon would affect the mass and the height of the crop (Younas et al. 2021). The efficient nutrient management will respond to the crop cycle and its productivity (Gandahi et al. 2015).

Limited sources of good soil have reduced the possibility of cultivating maize on a large scale. Biochar is now being considered as an application to improve the soil properties together with the growth rate. Singh et al. (2018) reported that biochar could contribute to the enhancement of soil nutrients and improve crop productivity. It also plays a vital role in improving the soil structure, nutrient uptake, and root elongation. Biochar single application or with compost can enhance soil quality and improve maize yield (Mensah & Frimpong 2018). On the other hand, silicon would stimulate plant growth under acid-growth considerations (Pitann et al. 2021). The application of biochar and silicon fertilizer helps to reduce soil acidity and improve maize growth and nutrient uptake. Limited research has reported on the effect of biochar and silicon on maize production in acidic soil especially in Malaysia. Hence the main objective of the study was to evaluate the effect of Biochar and silicon on the growth, and nutrient uptake of maize plants in acidic soil.

## MATERIALS AND METHODS

### Experimental Site

A pot experiment was conducted for 45 days (May to June 2022) in the greenhouse UPM at 2°98′36.6″ N (north) latitude and 101°73′81.9″ E (east) longitudes with an elevation of 56.8 m from sea level at the west coast of Peninsular Malaysia.

### Experimental Design and Treatments

The pot experiment was laid out in a completely randomized design (CRD) with three replications having a pot size of 38 cm (height) and 32 cm (diameter). The Bungor (Typic Paleudult; Order: Ultisol) soil series was collected in depth from 0-20 cm from Taman Pertanian, UPM, Puchong, Selangor (2°58′59.7″ N latitude; 101°38′47.5″ E longitude). It was air-dried and sieved through a 2 mm before chemical analysis. For the greenhouse experiment, the soil was sieved to 4 mm and applied in all of the pots at a rate of 20 kg of soil $pot^{-1}$. The biochar treatment was applied to the soil based on the dose required with a recommended rate of 10 $t.ha^{-1}$ and mixed well and left for about one week before adding silicon 150 $kg.ha^{-1}$ recommended as the optimal amount for maize by (Xie et al. 2014) (Table 1). Additional NPK based on MARDI recommendation fertilizer: 120 kg N/Ha in the form of urea, 80 kg Phosphorus in the form of triple superphosphate, and 100 kg Potassium in the form of Muriate of potash was applied. In this experiment, the $F_1$ Hybrid Sweet Corn variety was collected from a local market as a test crop and it is also a common variety used by Malaysian farmers. The maize seedling was put and watered regularly to maintain a soil moisture content of 60-70% of water holding capacity during the growth period, and just they were about to be destructively harvested 45 days after planting.

### Physicochemical Properties of Initial Soil

The soil textural class was determined using the pipette method (Teh & Talib 2006). Soil pH was determined in water at a soil-to-solution ratio of 1:10 (TAN 1995). Leco CHNS Analyzer (LECO Truspec Micro Elemental Analyzer CHNS, New York) was used to determine the total Carbon and Nitrogen. Available phosphorus in soil was determined by the method described by (Olsen et al. 1954). Exchangeable cation was extracted using ammonium acetate (Schollengberger & Simon 1945) and the concentration of K, Ca and Mg in the solutions was determined by using inductively coupled plasma-atomic emission spectrometry (ICP). Determination of total Mn and Iron of soil was carried out using the aqua-regia extraction method (Zarcinas et al. 1987, McGrath & Cunliffe 1985). Table 2 shows the initial soil properties.

Table 1: Treatments for conducting the experiment.

| No | Treatment |
|---|---|
| 1. | Control (NPK) |
| 2. | 100% RHB |
| 3. | 100% Si |
| 4. | 50% RHB + 100% Si |
| 5. | 50% RHB + 75% Si |
| 6. | 50% RHB + 125% Si |
| 7. | 25% RHB + 100% Si |
| 8. | 25% RHB + 75% Si |
| 9. | 25% RHB + 125% Si |

Table 2: Physicochemical properties of initial soil.

| Parameter | Value |
|---|---|
| Texture | Sand- 69.27%, Silt- 2.28%, Clay-28.44% (Sandy clay loam) |
| Moisture % | 6.94 ± 1.14 |
| pH | 4.22±0.063 |
| Available P (mg $kg^{-1}$) | 0.5±0.222 |
| Total C % | 1.03±0.016 |
| Total N % | 0.03±0.02 |
| Total S % | 0.01±0.013 |
| Exc K (cmol.$kg^{-1}$) | 0.38±0.007 |
| Exc Ca (cmol.$kg^{-1}$) | 3.2±0.068 |
| Exc Mg (cmol.$kg^{-1}$) | 0.46±0.024 |
| Exc Al (cmol.$kg^{-1}$) | 0.104±0.02 |
| Total Mn (mg.$kg^{-1}$) | 0.5±0.023 |
| Total Fe (mg.$kg^{-1}$) | 422.6±8.3 |

## Physicochemical Properties of Rice Husk Biochar (RHB)

The pH of biochar was determined in water at a ratio of 1:10 of biochar to solution (TAN 1995). Leco CHNS Analyzer (LECO Truspec Micro Elemental Analyzer CHNS, New York) was used to determine the total Carbon and Nitrogen. Total phosphorus in biochar was determined by the dry ash method followed by ICP-OES (Cottenie 1980). Exchangeable cation was extracted using ammonium acetate (Schollengberger & Simon 1945) and the concentration of K, Ca & Mg in the solutions was determined by using inductively coupled plasma-atomic emission spectrometry (ICP). Table 3 shows the Rice Husk Biochar properties.

## Plant Material Analysis

**Number of leaves and plant height analysis:** The number of open leaves was counted at (15 DAS, 30 DAS and 45DAS) and the plant height was determined using a measuring tape at harvest (15 DAS, 30 DAS and 45DAS) from the base to the tip of the longest leaf (Lai 2019).

Table 3: Physicochemical properties of Rice Husk Biochar (RHB).

| Properties | RHB |
|---|---|
| Moisture | 2.93 |
| pH | 7.77 |
| Total c % | 24.86 |
| Total n % | 1.13 |
| Total s % | 0.15 |
| Exc K (cmol.$kg^{-1}$) | 17.45 |
| Exc Ca (cmol.$kg^{-1}$) | 19.46 |
| Exc Mg (cmol.$kg^{-1}$) | 13.96 |
| Total P (mg.$kg^{-1}$) | 3098.4 |

**Leave chlorophyll and conductance:** The leaf chlorophyll content was measured using a portable chlorophyll meter (SPAD-502 Konica Minolta, Inc., Tokyo, Japan). The Chlorophyll reading was taken from the middle part of the largest leave of each plant using a meter (SPAD--502, Konica Minolta, Osaka, Japan) (Alarefee et al. 2021) and the conductance reading was recorded at the same time.

**Shoot Fresh weight and biomass (g):** After harvest, the shoot (stem and leaves) were washed and dammed with tissue paper before each shoot was weighed and then it was placed into envelopes and dried in an oven at 60 °C for 72 h and weighed again for the biomass (Mosharrof et al. 2021)

**Shoot nutrient Uptake (ppm):** The dried shoot was blended and again dried in a crucible in an oven and then put in a glass desiccator before 0.25 g was taken to extract the macro element of the shoot by using the drying ashing method (Yuan et al. 2016). The concentration of P, K, Ca and Mg were determined using inductively coupled plasma-atomic emission spectrometry (ICP) The result was then converted into (ppm)

$$\text{Nutrient concentration (ppm)} = \text{Mean (mg/L)} \times \left(\frac{\text{mark up volume(50ml)}}{\text{weight(0.25g)}}\right)$$

The maize nutrient uptake was later calculated by multiplying the respective dry weight oven-dry weight of the plant part with the nutrient content (Alarefee et al. 2021) as the formula below

$$\text{Nutrient Uptake} = \text{Nutrient Content (ppm)} \times \text{Biomass (g)}$$

## Post-Harvest Soil Analysis

**Acidity (pH):** Soil pH was determined in water at a soil-to-solution ratio of 1:10 (TAN 1995). 1 g oven-dried soil sample was placed into a vial and 10 Ml Distilled water was added to it. It was shaken thoroughly for 5 minutes and allowed to stand for 2 hours and the pH of the suspension was then measured using a pH meter for soil samples respectively.

**Determination of total carbon and nitrogen:** Leco CHNS Analyzer (LECO Truspec Micro Elemental Analyzer CHNS, New York) was used to determine the C and N of soil that were air-dried and sieved through a 2 mm mesh

**Exchangeable cation (magnesium, potassium and calcium):** Exchangeable cation was extracted using 100 mL of 1N ammonium acetate (Schollengberger & Simon 1945). Ashless cotton was put down at the hole of the leaching tube to prevent the soil from passing through the tube and covered with filter paper of small size before putting the 10 g soil

sample. Another filter paper was put on the soil sample to prevent the soil from being inverted when the solution was poured. The leaching valve was adjusted to make sure that the ammonium acetate flowed through the soil sample slowly with the speed of one drop to another drop around 6 to 8 seconds. The concentration of K, Ca and Mg in the solutions was determined by the inductively coupled plasma-atomic emission spectrometry (ICP).

**Total soil micronutrient (iron and manganese):** Determination of macronutrients and micronutrients of soil was carried out using the aqua-regia extraction method with the mix of concentrated hydrochloric acid HCl and nitric acid $HNO_3$in the ratio of 3:1 (Zarcinas et al. 1987, McGrath & Cunliffe 1985). 1 g soil sample was put into the digestor tube. 1 mL 1.2% nitric acid and 3 mL concentrated hydrochloric acid were added to the soil and handshake gently. The digestor block was prepared to heat at 110 degrees before the tube was put in and the mixture heated until a white precipitate formed. The supernatant was then left to cool down. After that around 20 mL of distilled water was added and heated in a digestor block at 80 degrees Celsius for 30 minutes and all of the mixture was clear and transferred to a 50 mL beaker to mark up it. The concentration of iron and manganese in the solutions was determined by inductively coupled plasma-atomic emission spectrometry (ICP).

### Soil Available P

0.5M sodium bicarbonate, $NaHCO_3$, was prepared (21g of sodium bicarbonate was dissolved in about 450 mL distilled water and was adjusted to 8.5 pH with 1N NaOH and marked up to volume). 1 g of soil sample was weighed into the plastic vial, and 20 mL of the 0.5M sodium bicarbonate was added. It was shaken for 30 minutes, filtered by filter paper No. 2 and sent to ICP for phosphorus analysis (Olsen et al.1954).

### Soil Exchangeable Aluminum

1N KCL solution was prepared. Then 5 g of soil in plastic vial, added with 50 mL KCL solution, the cap was closed and the solution was shaken for 30 minutes. After that, the supernatant was slowly passed through the Whatman no 42 filter paper and sent to ICP for aluminum analysis.

### Percent Relative Data

The relative data of the value were expressed as percentages, relative to control for each element by the following formula proposed by (Ashraf & Waheed 1990):

$$\text{Relative data (\%)} = \left(\frac{\text{Treatment value} - \text{control value}}{\text{control value}}\right) \times 100$$

where the treatment value was the biochar and silicon amended treatment, and the control value was treatment with only NPK.

### Statistical Analysis

Analysis of Variance (ANOVA) procedure was used to analyze all of the data, and Tukey's Honestly Significant Difference (HSD) test was used to separate the means. Repeated measures analyses were performed on all parameters using John's Macintosh Project (JMP) Analysis Software, ($p \leq 0.05$).

## Result and Discussion

**The effect of biochar and silicon on the plant height and leaf number of maize on three different days after sowing (15 DAS, 30 DAS & 45 DAS):** Table 4 demonstrated

Table 4: Maize growth development.

| Treatment | Leaf number | | | Plant Height | | |
|---|---|---|---|---|---|---|
| | 15 DAYS | 30 DAYS | 45 DAYS | 15DAY | 30 DAYS | 45 DAYS |
| T1 | 4±0.333ab | 5±0.33a | 6±0.33b | 7.30±0.21e | 8.03±0.88c | 27.17±0.14d |
| T2 | 3±0.33b | 5±0.33a | 6±0.33b | 7.57±0.09de | 8.90±0.86bc | 28.57±0.73d |
| T3 | 4±0.33ab | 6±0.58a | 8±1ab | 10.80±0.35bc | 12.70±2.10abc | 31.57±1.23d |
| T4 | 4ab | 6±0.33a | 10±0.68a | 9.75±0.72cde | 15.70±2.05abc | 54.30±0.52a |
| T5 | 5±0.33a | 7±0.67a | 9±0.33a | 13.70±1.04a | 20.83±3.47a | 37.27±1.3c |
| T6 | 4ab | 6±0.33a | 9±0.33ab | 11.50±0.06abc | 15.53±1.87abc | 46.10±1.46b |
| T7 | 4±0.33ab | 6±0.58a | 9±0.58a | 10.03±0.58cd | 16.53±1.97abc | 38.37±1.13c |
| T8 | 5a | 6±0.67a | 10±0.33a | 12.80±0.44ab | 17.47±0.61ab | 51.43±0.6a |
| T9 | 5±0.33a | 6±0.33a | 9a | 11.70±0.4abc | 18.13±0.90a | 42.13±1.24cd |

Means within the same column followed by the different letters are significantly different at $p \leq 0.05$; (Tukey's HSD test). The column represents the mean values ± standard error. T1 = Recommended rate of NPK ($t.ha^{-1}$), T2=10 $t.ha^{-1}$ RHB, T3= 150 $kg.ha^{-1}$ Si, T4= 50 %RHB + 100 % Si, T5= 50 % RHB + 75 % Si, T6= 50 %RHB + 125 % Si, T7= 25 % RHB + 100 % Si, T8= 25 % RHB + 75 % Si, T9= 25 % RHB + 125 % Si.

Table 5: Plant morphological and physiological parameters.

| Treatment | Shoot fresh weight (g) | Biomass (g) | Photosynthesis rate | Conductance |
|---|---|---|---|---|
| T1 | 28.81±0.49c | 2.37±0.26e | 23.65±1.91c | 0.071±0.01e |
| T2 | 39.03±0.09bc | 3.94±0.1de | 25.03±2.03c | 0.148±0.002d |
| T3 | 40.30±0.4bc | 4.12±0.46 | 29.63±1.79bc | 0.264±0.01c |
| T4 | 127.83±5.62a | 12.04±0.55a | 45.5±3.68a | 0.53±0.02a |
| T5 | 56.12±2.37b | 5.92±0.51cd | 40.87±2.6a | 0.438±0.02b |
| T6 | 48.16±3.85bc | 4.36±0.16de | 38.47±1.04ab | 0.416±0.02b |
| T7 | 46.34±2.85bc | 7.77±0.47bc | 38.1±2.52ab | 0.4089±0.002b |
| T8 | 57.14±4.35b | 8.72±0.57b | 41.2±2.57a | 0.464±0.01ab |
| T9 | 47.31±6.41bc | 7.45±0.71bc | 36.53±0.59ab | 0.423±0.01b |

Means within the same column followed by the different letters are significantly different at $p \leq 0.05$; (Tukey's HSD test). The column represents the mean values ± standard error. T1 = Recommended rate of NPK ($t.ha^{-1}$), T2=10 $t.ha^{-1}$ RHB, T3= 150$kg.ha^{-1}$ Si, T4= 50 %RHB + 100 % Si, T5= 50 %RHB + 75 % Si, T6= 50 %RHB + 125 % Si, T7= 25 %RHB + 100 % Si, T8= 25 %RHB + 75% Si, T9= 25 %RHB + 125 % Si.

the effect of different treatments on leaves of maize plant recorded in three different phases 15 DAS, 30 DAS and 45 DAS. The leaf number of maize in 15 DAS is significantly affected by the different doses of biochar and silicon. The highest number was shown by T5, T8 and T9 (5) followed by other treatments with four leaves and the lowest showed by T2 (3). Biochar and silicon did not significantly affect the leaf number at 30 DAS of the maize plant. While at 45 DAS of the maize plant, the number of leaves was significantly affected by the treatment application. The highest leaves were shown by T4 & T8 (10) and followed by other treatments ranging from 8 to 9 and the low was shown by T1 & T2 (6).

Table 4 shows the Plant height (cm) of the maize measured at 15 DAS, 30 DAS and 45 DAS. The plant height varied significantly among different amounts of biochar and silicon. In general, the heights were measured higher at 45 DAS compared with 15 and 30 DAS. At 15 DAS T1 showed the shortest high (7.30 cm) compared to other treatments. All the remaining treatments result in higher heights ranging from 7.57 cm to 13.70 cm. At the 30 DAS tallest height was recorded in T5 (20.83 cm) identically followed by T8 (18.13 cm). T1 resulted in the shortest height (8.03 cm) closely followed by T2 (8.90 cm). The remaining treatments resulted in intermediate height ranging from 12.70 cm to 17.47 cm. For the height measure at 45 DAS, the tallest was recorded by T4 (54.30) followed by t8 (51.43 cm). While t1 (27.17 cm) showed the shortest height. T4 showed a 99.85% increase compared to the control. This finding was the same as to result obtained by Shashi et al. (2018) with the highest RHB dose (20 $t.ha^{-1}$) producing the tallest height (44.83 cm) and Alarefee et al. (2021) also recorded an increase in height with the application of biochar compare to control and NPK application. The height increases together with the increase of biochar may be caused by the high content of phosphorus in biochar that helps the development of the plant cell (Mosharrof et al. 2021) and high silicon dose increases the development and growth of plants by increasing the plant resistance to various abiotic and biotic stresses (Kostic et al. 2017).

**The effect of biochar and silicon on the shoot fresh weight, shoot dry weight, photosynthesis rate and conductance of maize:** In this study, it was noticed that shoot fresh weight was significantly affected by biochar and silicon application ($p<0.05$) (Table 5). The shoot fresh weight was higher in $T_4$ (127.83 g) followed by $T_8$ (57.14 g) while $T_1$ (28.81 g) recorded the lowest weight. However, the weight increased by 343.7% at T4 followed by T8 at 98.33%. The treatment also significantly affected the plant biomass of maize ($p<0.05$) (Table 5). The maize biomass (g) for treatment was ranging from 2.37 to 12.04 g. T1 has the lowest weight (2.37 g) followed by T2 (3.94 g). The highest weight was recorded by T4 (12.04 g) followed by T7 (7.77 g). T4 showed a 40.8% increase compared to the control. This finding was quite same with one study concluding that the application of 80 kg $ha^{-1}$ Si with chitosan shows the highest weight of dry shoot compared to the control and single silicon application (Younas et al. 2021). On the other hand, Amin et al. 2018 agree that silicon application on maize plants would increase their growth rate by improving the photosynthetic rate and lowering transpiration. Thus, biochar applied together with silicon seemed to increase nutrient availability, help the development of the tissue and increase plant Biomass (Xie et al. 2014, Shetty & Prakash 2020).

The maize photosynthesis rate was significantly affected by the application of biochar and silicon fertilizer ($p<0.05$) (Table 5) The highest photosynthesis rate was recorded by T8 (41.2) and the lowest was T1 (23.65). The highest T8

Table 6: CNS concentration and CN ratio.

| Treatment | C (%) | N (%) | CN | S (%) |
|---|---|---|---|---|
| T1 | 0.609±0.01g | 0.029±0.001b | 20.75±0.38d | 0.016±0.002a |
| T2 | 0.635±0.05g | 0.013±0.002d | 49.29±1.08c | 0.016±0.002a |
| T3 | 3.969±0.06a | 0.046±0.005a | 86.92±4.54b | 0.015±0.003a |
| T4 | 2.409±0.4b | 0.03±0.00008b | 79.51±1.27b | 0.019±0.002a |
| T5 | 1.187±0.04f | 0.008±0.001d | 143.22±6.29a | 0.013±0.001a |
| T6 | 1.539±0.015e | 0.022±0.001c | 71.17±1.6b | 0.019±0.001a |
| T7 | 1.830±0.01d | 0.025±0.002bc | 72.17±3.53b | 0.019±0.002a |
| T8 | 2.184±0.05c | 0.028±0.0003b | 78.43±2.09b | 0.014±0.001a |
| T9 | 2.039±0.002c | 0.046±0.005a | 44.85±2.97c | 0.013±0.001a |

Means within the same column followed by the different letters are significantly different at $p \leq 0.05$; (Tukey's HSD test). The column represents the mean values ± standard error. T1 = Recommended rate of NPK ($t.ha^{-1}$), T2=10 $t.ha^{-1}$ RHB, T3= 150 $kg.ha^{-1}$ Si, T4= 50%RHB + 100% Si, T5= 50%RHB + 75% Si, T6= 50%RHB + 125% Si, T7= 25%RHB + 100% Si, T8= 25%RHB + 75% Si, T9= 25%RHB + 125% Si.

relatively increased double compared to the control. All of the treatment shows more than 30 photosynthesis rates except for the control (T1), single silicon (T2) and single biochar (T3) applications. This shows that the biochar and silicon together can increase the rate of photosynthesis rate in the leaf. While Mosharrof et al. (2022) showed a rise in photosynthesis rate with the combining of biochar with lime. On the other hand, Xie et al. (2014) showed that Silicon can be used to stimulate the photosynthesis rate by rise up the chlorophyll content and biochar would help with carbon sequestration and increase carbon storage that would support the photosynthesis process in plants (Mensah & Frimpong 2018).

In this study, it was noticed that conductance (gl) from maize leaf was significantly affected by biochar and silicon application ($p<0.05$) (Table 5). The conductance was higher in $T_4$ (0.53) followed by $T_8$ (0.438) while $T_1$ (0.071) recorded the lowest conductance. However, the conductance increased by 64.6% at T4 followed by T8 51.7%. This finding was also against Gao et al. (2006) who concluded that the Si application significantly lowered the conductance and transpiration rate from the leaf. The control in this experiment was the lowest conductance caused by the stress of the plant. While the silicon has potential to reduce stress and cause the stomata to open larger at the same time increase plant activity (Yongchao et al. 2015) at the same time biochar helps to maintain the soil water content and reduce the stress causing the increase of conductance (Rogovska et al. 2014).

**The effect of biochar and silicon on soil carbon, nitrogen, sulfur content and CN ratio:** It was noticed that C and N content from post-harvest soil were significantly affected by biochar and silicon application ($p<0.05$) (Table 6). The highest content was recorded by T3 C (3.969%) and N (0.046%). Followed by T4 for C (2.409%) and T9 for N (0.046%) while the lowest C (0.609%) was recorded by T1 and the lowest N was recorded by T2 (0.013%). Both control and sole Silicon showed low C & N content. A few studies have proved that biochar application would raise the soil's organic carbon and nitrogen (Islam et al. 2018, Abukari 2014).

The treatment significantly affected the CN ratio of post-harvest soil. The CN ratio range for treatment was 20.75 to 143.22. T1 has the lowest ratio (20.75). The highest ratio was recorded by T5 (143.22) followed by T3 (86.93). T5 showed 59.02% and T3 showed a 31.89% increase compared to the control. The S% content was not significant.

**The effect of biochar and silicon on pH available P, macro-nutrient exchangeable (K, Ca & Mg) and total micro-nutrients (Mn & Fe) & exchangeable Al:** The soil pH was significantly affected by the application of biochar and silicon fertilizer. The highest pH was recorded by $T_4$ (6.77) followed by $T_5$ (6.73) while $T_1$ (5.53) recorded the lowest pH. Thus, the pH increased by 21.69% at T4 and followed by T8 by 21.7%. Islam et al. (2018) also found that biochar is potentially strong enough to change the soil from acidic to slightly acidic. This low pH may be caused by the reduced levels of Fe in the soil by the release of carbon and cation activity by the biochar (Galindo et al. 2021, Sheng et al. 2016).

It was noticed that available P ($mg.kg^{-1}$) from post-harvest soil was significantly affected by biochar and silicon application ($p<0.05$) (Table 7). The available P ($mg.kg^{-1}$) was higher in $T_3$ (13.75) followed by $T_5$ (8.8) while $T_1$ (0.15) recorded the lowest available P ($mg.kg^{-1}$). However, the available P increased by 90.67% at T3 followed by T5 at 57.67%. One pot experiment proved that the highest P available in 45 days (16.43 $mg.kg^{-1}$) with 10 $t.ha^{-1}$ RHB

Table 7: Post-harvest soil properties.

| Treatment | pH | P ($mg.kg^{-1}$) | K ($cmol.kg^{-1}$) | Ca ($cmol.kg^{-1}$) | Mg ($cmol.kg^{-1}$) | Mn ($mg.kg^{-1}$) | Fe ($mg.kg^{-1}$) | Al ($cmol.kg^{-1}$) |
|---|---|---|---|---|---|---|---|---|
| T1 | 5.53±0.07c | 0.15±0.03c | 0.84±0.02f | 2.35±0.02f | 3.24±0.12d | 0.481±0.02a | 442.30±1.23a | 0.028±0.002b |
| T2 | 6.4±0.00ab | 0.157±0.03c | 0.69±0.03f | 2.89±0.01d | 4.36±0.2c | 0.491±0.05a | 334.47±2.02f | 0.056±0.002a |
| T3 | 6.63±0.03a | 13.75±0.26a | 6.24±0.02a | 3.24±0.06b | 7.83±0.19a | 0.59±0.06a | 305.13±1.77g | 0.074±0.006a |
| T4 | 6.77±0.09a | 4.25±1.07bc | 3.60±0.02b | 3.42±0.01a | 7.36±0.14a | 0.606±0.01a | 313.97±0.88g | 0.061±0.002a |
| T5 | 6.73±0.07a | 8.8±0.46b | 1.25±0.01e | 2.75±0.03e | 5.40±0.13b | 0.549±0.04a | 408.73±0.26b | 0.016±0.00bcd |
| T6 | 6.43±0.17ab | 7.15±2.57b | 3.70±0.03b | 2.94±0.02d | 7.58±0.20a | 0.570±0.04a | 338.27±4.28f | 0.007±0.003cd |
| T7 | 6.1±0.15b | 7.35±1.41b | 1.92±0.01d | 2.65±0.01e | 5.72±0.09b | 0.596±0.05a | 364.97±2.14e | 0.004±0.001d |
| T8 | 6.13±0.07b | 5.9±1.96bc | 1.41±0.06e | 3.14±0.01bc | 5.66±0.14b | 0.529±0.05a | 396.73±1.95c | 0.016±0.014bcd |
| T9 | 6.33±0.07ab | 7.85±0.55b | 3.21±0.07c | 3.09±0.01c | 7.56±0.11a | 0.487±0.04a | 381.53±0.39d | 0.027±0.014bc |

Means within the same column followed by the different letters are significantly different at $p \leq 0.05$; (Tukey's HSD test). The column represents the mean values ± standard error. T1 = Recommended rate of NPK ($t.ha^{-1}$), T2=10 $t.ha^{-1}$ RHB, T3= 150 $kg.ha^{-1}$ Si, T4= 50 %RHB + 100 % Si, T5= 50 %RHB + 75 % Si, T6= 50 %RHB + 125 % Si, T7= 25 %RHB + 100 % Si, T8= 25 %RHB + 75 % Si, T9= 25 %RHB + 125 % Si.

Table 8: Plant nutrient uptake.

| | P ($g.Plant^{-1}$) | K ($g.Plant^{-1}$) | Ca ($g.Plant^{-1}$) | Mg ($g.Plant^{-1}$) | Si ($g.Plant^{-1}$) |
|---|---|---|---|---|---|
| T1 | 0.798±0.09d | 9.57±1.153e | 0.894±0.12d | 0.407±0.06f | 0.145±0.02a |
| T2 | 0.808±0.01d | 12.266±0.39e | 1.474**±0.05**cd | 0.604±0.02ef | 0.163±0.01a |
| T3 | 1.936±0.34cd | 19.153±2.19de | 1.378±0.14d | 0.740±0.08def | 0.227±0.02a |
| T4 | 7.164±0.10a | 49.169±1.18a | 3.676±0.07a | 1.723±0.04ab | 0.603±0.02a |
| T5 | 3.226±0.23bc | 31.519±2.54bc | 2.246±0.23bc | 1.339±0.11bc | 0.332±0.06a |
| T6 | 2.241±0.15c | 21.114±1.90cde | 1.654±0.13cd | 0.916±0.06cde | 0.873±0.6a |
| T7 | 4.540±0.50b | 40.72±4.99ab | 2.825±0.24b | 1.697±0.16ab | 0.351±0.02a |
| T8 | 6.003±0.41a | 39.20±2.75ab | 2.905±0.21ab | 2.007±0.14a | 0.357±0.03a |
| T9 | 2.256±0.13c | 24.61±1.36cd | 2.616±0.18b | 1.191±0.07cd | 0.335±0.03a |

Means within the same column followed by the different letters are significantly different at $p \leq 0.05$; (Tukey's HSD test). The column represents the mean values ± standard error. T1 = Recommended rate of NPK ($t.ha^{-1}$), T2=10 $t.ha^{-1}$ RHB, T3= 150 $kg.ha^{-1}$ Si, T4= 50 %RHB + 100 % Si, T5= 50 %RHB + 75 % Si, T6= 50 %RHB + 125 % Si, T7= 25 %RHB + 100 % Si, T8= 25 %RHB + 75 % Si, T9= 25 %RHB + 125 % Si.

application (Mosharrof et al. 2021). The Reduction of Fe and Al activity and, the increase of cation and pH cause the P availability to rise (Mensah & Frimpong 2018).

The application of biochar and silicon fertilizer significantly affected the exchangeable cation of the soil (ca,k, mg). The highest exchangeable Ca was recorded by $T_4$ (3.42 $cmol.kg^{-1}$) and the lowest was recorded by $T_1$ (3.42 $cmol.kg^{-1}$). The highest exchangeable K & Mg was recorded by sole biochar $T_3$ (6.24 $cmol.kg^{-1}$) & (7.83 $cmol.kg^{-1}$) and the lowest was $T_1$ (0.84 $cmol.kg^{-1}$) & (3.24 $cmol.kg^{-1}$). The increase of the three cations ($Ca^{2+}$, $K^+$, and $Mg^{2+}$) causes the decreasing concentration of exchangeable $H^+$ and Fe with the increase in pH (Zhang et al. 2018).

The highest total Fe in soil was observed from $T_1$ (442.30 mg/kg) and the lowest was recorded by sole biochar $T_3$ (305.15 $mg.kg^{-1}$). Mosharrof et al. (2021) reported that the application of rice husk biochar decreases the extractable of Fe in soil compared to the control and soil-applied NPK and (Xu et al. 2022) also found a similar thing but the application of rice straw biochar as a potential to reduce soil Fe bioavailability.

**The effect of biochar and silicon on plant nutrient uptake by maize:** There was a significant difference in plant nutrient uptake of maize, represented in Table 8.

With T1, T2 and T3 the concentration and total uptake of P, K, Ca, and Mg taken up by the maize plant were statistically lower than those of biochar and silicon-amended treatments (T4 to T9). The highest uptake of P (6.003 $g.plant^{-1}$) and Mg (2.007 $g.plant^{-1}$) was obtained from T8 (25%RHB + 75% Si); the highest K (49.169 $g.plant^{-1}$) was noted from T4 (50%RHB + 100% Si); but the treatment does not give a significant different on the Silicon uptake of the plant. Mosharrof et al. (2021) found that the application of biochar and dolomitic limestone was higher compared to

the control and recommended NPK application. The effect of silicon and rice husk on the phosphorus available reduces the effect of acidity that increases the base's cation and raises the nutrient uptake (Frank et al. 2021).

## CONCLUSION

The current study results showed that $T_4$ (50% RHB + 100% Silicon) was the best treatment over the other rates of RHB and Silicon increased plant height, photosynthetic rate and Biomass.

We found that biochar with silicon increased soil pH, exchangeable K, Ca and Mg, and decreased total Fe. Thus $T_4$ (50% RHB + 100% Silicon) was continued to implement together with various rates of TSP (50%,75% & 100%) together with $T_7$ (25% RHB + 100% Silicon).

## ACKNOWLEDGMENTS

Conceptualization, M.K.U. and S.K., literature collection, A.N.A.H. and S.M.S., writing-original draft preparation, A.N.A.H. and M.K.U., writing-review and editing, M.K.U., S.K., S.M.S. and S.N.A.H. All authors have read and agreed to the published version of the manuscript. This work was supported under research grant FRGS 5540305. The authors thank the Ministry of Higher Education Malaysia (MOHE) and Universiti Putra Malaysia for sponsoring the research work.

## REFERENCES

Abukari, A. 2014. Effect of rice husk biochar on maize productivity in the guinea savannah zone of Ghana (Doctoral Dissertation).

Alarefee Ahmed, H., Ishak, C. F., Karam, D. S. and Othman, R. 2021. The efficiency of rice husk biochar with poultry litter co-composts in oxisols for improving soil physico-chemical properties and enhancing maize performance. Agronomy, 11(12): 2409.

Amin, M., Ahmad, R., Ali, A., Hussain, I., Mahmood, R., Aslam, M. and Lee, D. J. 2018. Influence of silicon fertilization on maize performance under limited water supply. Silicon, 10(2): 177-183.

Ashraf, M. and Waheed, A. 1990. Screening of local/exotic accessions of lentils (Lens culinaris Medic.) for salt tolerance at two growth stages. Plant Soil, 128: 167-176.

Cottenie, A. 1980. Soil and plant testing as a basis of fertilizer recommendations. FAO Soil Bulletin 38/2. Food and Agriculture Organization of the United Nations, Rome.

Dei, H. K. 2017. Assessment of maize (Zea mays L.) as a feed resource for poultry. Poultry Science, 1-32.

Frank Stephano, M., Geng, Y., Cao, G., Wang, L., Meng, W. and Meiling, Z. 2021. Effect of silicon fertilizer and straw return on the maize yield and phosphorus efficiency in Northeast China. Communications in Soil Science and Plant Analysis, 52(2): 116-127.

Galindo, F. S., Pagliari, P. H., Rodrigues, W. L., Fernandes, G. C., Boleta, E. H. M., Santini, J. M. K. and Teixeira Filho, M. C. M. 2021. Silicon amendment enhances agronomic efficiency of nitrogen fertilization in maize and wheat crops under tropical conditions. Plants, 10(7): 1329.

Gandahi, A. W., Baloch, S. F., Sarki, M. S., Gandahi, R. and Lashari, M. S. 2015. Impact of rice husk biochar and macronutrient fertilizer on fodder maize and soil properties. International Journal of Biosciences, 7(4): 12-21.

Gao, X., Zou, C., Wang, L. and Zhang, F. 2006. Silicon decreases transpiration rate and conductance from stomata of maize plants. Journal of Plant Nutrition, 29(9): 1637-1647.

Islam, S. J. M., Mannan, M. A., Khaliq, Q. A. and Rahman, M. M. 2018. Growth and yield response of maize to rice husk biochar. Australian Journal of Crop Science, 12(12): 1813-1819.

Khan, W. U. D., Aziz, T., Hussain, I., Ramzani, P. M. A. and Reichenauer, T. G. 2017. Silicon: a beneficial nutrient for maize crop to enhance photochemical efficiency of photosystem II under salt stress. Archives of Agronomy and Soil Science, 63(5): 599-611.

Kostic, L., Nikolic, N., Bosnic, D., Samardzic, J. and Nikolic, M. 2017. Silicon increases phosphorus (P) uptake by wheat under low P acid soil conditions. Plant and Soil, 419(1): 447-455.

Lai, L. 2019. Utilization of rice straw biochar and urea to mitigate greenhouse gases emission in sustainable rice production. Ph.D. Thesis, University Putra Malaysia, Selangor, Malaysia.

Manickam, T., Cornelissen, G., Bachmann, R. T., Ibrahim, I. Z., Mulder, J. and Hale, S. E. 2015. Biochar application in Malaysian sandy and acid sulfate soils: Soil amelioration effects and improved crop production over two cropping seasons. Sustainability, 7(12): 16756-16770.

McGrath, S. P. and Cunliffe, C. H. 1985. A Simplified method for the extraction of the metals Fe, Zn, Cu, Ni, Cd, Pb, Cr, Co and Mn from soils and sewage sludge. Journal of the Science of Food and Agriculture, 36: 794-798. http://dx.doi.org/10.1002/jsfa.2740360906

Mensah, A. K. and Frimpong, K. A. 2018. Biochar and/or compost applications improve soil properties, growth, and yield of maize grown in acidic rainforest and coastal savannah soils in Ghana. International Journal of Agronomy, 1)2018), p.6837404.

Mosharrof, M., Uddin, M. K., Mia, S., Sulaiman, M. F., Shamsuzzaman, S. M. and Haque, A. N. A. 2022. Influence of rice husk biochar and lime to reduce phosphorus application rate in acid soil: A field trial with maize. Sustainability, 14, x.

Mosharrof, M., Uddin, M. K., Sulaiman, M. F., Mia, S., Shamsuzzaman, S. M. and Haque, A. N. A. 2021. Combined application of rice husk biochar and lime increases phosphorus availability and maize yield in an acidic soil. Agriculture, 11(8): 793.

Olsen, S. R. 1954. Estimation of available phosphorus in soils by extraction with sodium bicarbonate (No. 939). US Department of Agriculture.

Oni, B. A., Oziegbe, O. and Olawole, O. O. 2019. Significance of biochar application to the environment and economy. Annals of Agricultural Sciences, 64(2): 222-236.

Pitann, B., Bakhat, H. F., Fatima, A., Hanstein, S. and Schubert, S. 2021. Silicon-mediated growth promotion in maize (Zea mays L.) occurs via a mechanism that does not involve activation of the plasma membrane H+-ATPase. Plant Physiology and Biochemistry, 166: 1121-1130.

Pontigo, S., Ribera, A., Gianfreda, L., de la Luz Mora, M., Nikolic, M. and Cartes, P. 2015. Silicon in vascular plants: uptake, transport and its influence on mineral stress under acidic conditions. Planta, 242(1): 23-37.

Rahman, M. A., Kader, M. A., Jahiruddin, M., Islam, M. R. and Solaiman, Z. M. 2022. Carbon mineralization in subtropical alluvial arable soils amended with sugarcane bagasse and rice husk biochars. Pedosphere, 32(3): 475-486.

Rogovska, N., Laird, D. A., Rathke, S. J. and Karlen, D. L. 2014. Biochar impact on Midwestern Mollisols and maize nutrient availability. Geoderma, 230: 340-347.

Schollenberger, C. J. and Simon, R. H. 1945. Determination of exchange capacity and exchangeable bases in soil-ammonium acetate method. Soil Science, 59: 13-24.

Shashi, M. A., Mannan, M. A., Islam, M. M. and Rahman, M. M. 2018. Impact of rice husk biochar on growth, water relations and yield of maize (Zea mays L.) under drought condition. The Agriculturists, 16(02): 93-101.

Sheng, Y., Zhan, Y. and Zhu, L. 2016. Reduced carbon sequestration potential of biochar in acidic soil. Science of the Total Environment, 572: 129-137.

Shetty, R. and Prakash, N. B. 2020. Effect of different biochars on acid soil and growth parameters of rice plants under aluminium toxicity. Scientific Reports, 10(1): 1-10.

Singh, C., Tiwari, S., Gupta, V. K. and Singh, J. S. 2018. The effect of rice husk biochar on soil nutrient status, microbial biomass and paddy productivity of nutrient poor agriculture soils. Catena, 171: 485-493.

Swe, M. M., Mar, S. S., Naing, T. T., Zar, T. and Ngwe, K. 2021. Effect of silicon application on growth, yield and uptake of rice (Oryza sativa L.) in two different soils. Open Access Library Journal, 8(10): 1-15.

Tan, K. H. 1995. Soil Sampling, Preparation, and Analysis. CRC press.

Teh, C. B. S. and Talib, J. 2006. Soil Physics Analyses. Vol. 1, Universiti Putra Malaysia Press.

Ullah, Z., Akmal, M. S., Ahmed, M., Ali, M., Khan, A. Z. and Ziad, T. 2018. Effect of biochar on maize yield and yield components in rainfed conditions. International Journal of Agronomy and Agricultural Research (IJAAR), 12: 46-51.

Urassa, J. K. 2015. Factors influencing maize crop production at household levels: A case of Rukwa Region in the southern highlands of Tanzania. African Journal of Agricultural Research, 10(10): 1097-1106.

Xie, Z., Song, F., Xu, H., Shao, H. and Song, R. 2014. Effects of silicon on photosynthetic characteristics of maize (*Zea mays* L.) on alluvial soil. The Scientific World Journal, 2014(1): p.718716.

Xu, Q., Xu, Q., Zhu, H., Li, H., Yin, W., Feng, K. and Wang, X. 2022. Does biochar application in heavy metal-contaminated soils affect soil micronutrient dynamics? Chemosphere, 290: 133349.

Yongchao Liang, Miroslav Nikolic, Richard Bélanger, Haijun Gong, Alin Song, 2015. Silicon in agriculture: From theory to practice, Springer, Dordrecht Heidelberg New York, London, Biljni lekar, 43(5): 472-473.

Younas, H. S., Abid, M., Shaaban, M. and Ashraf, M. 2021. Influence of silicon and chitosan on growth and physiological attributes of maize in a saline field. Physiology and Molecular Biology of Plants, 27(2): 387-397.

Yuan, Z., Cao, Q., Zhang, K., Ata-Ul-Karim, S. T., Tian, Y., Zhu, Y., Cao, W. and Liu, X. 2016. Optimal leaf positions for SPAD meter measurement in rice. Frontiers in Plant Science, 7: 719.

Zarcinas, B. A., Cartwright, B. and Spouncer, L. R. 1987. Nitric acid digestion and multi-element analysis of plant material by inductively coupled plasma spectrometry. Commun. Soil Sci. Plant Anal., 18: 131-146.

Zhang, Q., Yi, W., Li, Z., Wang, L. and Cai, H. 2018. Mechanical properties of rice husk biochar reinforced high density polyethylene composites. Polymers, 10(3): 286.

Nature Environment and Pollution Technology
An International Quarterly Scientific Journal

p-ISSN: 0972-6268
(Print copies up to 2016)
e-ISSN: 2395-3454

Vol. 23 | No. 3 | pp. 1537-1545 | 2024

Original Research Paper

https://doi.org/10.46488/NEPT.2024.v23i03.023

Open Access Journal

# Experimental Investigation on Photocatalytic Degradation of Refractory Organics in Biologically Treated Tannery Effluent Using Photocatalysis

**S. Hema*† and S. Kavya****

*Department of Civil Engineering, Sri Ramakrishna Engineering College, Coimbatore-641022, Tamil Nadu, India
**Department of Civil Engineering, Sri Krishna College of Technology, Coimbatore-641042, Tamil Nadu, India
†Corresponding Author: Hema Sudhakar; hema.s@srec.ac.in

**Nat. Env. & Poll. Tech.**
**Website: www.neptjournal.com**

*Received:* 28-12-2023
*Revised:* 24-01-2024
*Accepted:* 25-01-2024

**Key Words:**
Photocatalysis
Refractory organics
Tannery effluent
Advanced oxidation process

## ABSTRACT

There is a pressing demand for the introduction of environmentally safe technologies for the industries that supply the basic needs of industrialized societies. Advanced Oxidation Processes may become one of the answers to these uprising pollution management problems in the near future. The present investigation aimed to reduce the refractory organics present in the biologically treated (Activated Sludge Process) tannery effluent using Photocatalysis. The optimum time, pH, dosage of $H_2O_2$, and mass of NPAC required for the effective treatment using photocatalysis were found to be 60 mins, 8, 0.2 mg.$L^{-1}$, and 1g. 100 $mL^{-1}$, respectively. Although the efficiency of homogeneous photocatalysis was found to be higher than that of heterogeneous photocatalysis, the biodegradability was higher in the latter, with a value of 0.26. The experimental results have proved that photocatalysis could be a promising technology to reduce the refractory organics present in the tannery effluent.

## INTRODUCTION

Industrialization has taken up a rapid pace of growth in recent times due to the growing needs of the population, urbanization, and technological advancements. The leather processing industry is one of the major economic shareholders, with an approximated annual worldwide leather production of 1.67 billion $m^2$ amidst a total trade value of around seventy million Dollars per year. South Asia is one of the major contributors to this production, satisfying approximately 20% of the world's demand in total (Rao et al. 2003). It is understood that, unlike other industries, leather processing is said to be highly water intensive and also the major contributor to water pollution (Subramani & Haribalaji 2012, Haydar et al. 2007, Mannucci et al. 2010), producing 30-35 $m^3$ of wastewater per tonne of raw hide on average. However, the quantity and quality of wastewater are highly variable based on the characteristics of raw materials used in the process (Tunay et al. 1995). The processing of leather in tanneries generates an enormous amount of organic and inorganic waste materials, namely phenolic compounds, metals, dyes, etc., as effluents. The effluent from tanneries has been thus identified as the main factor for environmental degradation affecting aquatic life, flora, and fauna. It also causes severe illnesses in human beings (Shakir et al. 2012), such as hepatocellular cancer, sperm damage, feto-maternal death, etc., Due to these towering problems, the treatment of tannery effluent has gained more emphasis than ever before. Apart from serious environmental and health issues, the presence of recalcitrant organic substances in these effluents renders their treatment incomplete and poses a serious ecological issue when it is continuously let into the water and soil environment.

Recalcitrant organic is a general term that represents all organic substances that are resistant to bio-degradation. The biological treatment processes were found ineffective in the complete removal of residual organics, whereas the membrane treatment processes show drawbacks of membrane fouling and failure due to the dye molecules and other impurities present in the tannery effluent. The development of an economical method for the removal of low-concentration refractory organics in industrial wastewater is a difficult environmental challenge (Ran et al. 2021). In particular, for the treatment of wastewater's refractory organic constituents, scientific treatment approaches should be matched with the demands of the wastewater treatment technology. In other words, only via the scientific treatment of refractory compounds in wastewater, can the quality of wastewater treatment be improved (Runzhe 2019). Such treatment requires sustainable methods to minimize environmental impact through resource recovery, recycling, and reuse. One of the sustainable new technologies for treating refractory organic pollutants found in various

industrial wastewaters, such as those from paper and pulp, pharmaceuticals, petrochemicals, refineries, and textiles is the advanced oxidation process (AOP) (Manna & Sen 2022). AOP has gained attention in the past few years for the effective treatment of tannery effluents. The process involves complete mineralization of both organic as well as inorganic compounds. Owing to this reason, AOP is preferred to be used in conjunction with biological treatment. Combined tertiary processes like ozonation and activated carbon adsorption have drawbacks, including the potential for the generation of oxidation intermediates and ineffective disinfection (Giusy et al. 2019). On the other hand, membrane separations (Koltuniewicz 2010) have proven to be a viable integration option (Suthanthararajan et al. 2004) to have a more robust treatment process using both the AOPs and membrane separations since they have demonstrated better performances than the standard treatment methods and produce fewer byproducts. However, further effort is required to improve these membrane's efficiency, anti-fouling capabilities, and large-scale module design (Mirzaa et al. 2020).

The following two steps of oxidation are involved in AOPs: a) the production of potent oxidants (such as hydroxyl radicals) and b) the interaction of these oxidants with organic pollutants in water. But the phrase "advanced oxidation process" especially refers to procedures where organic pollutants are oxidized largely through interactions with hydroxyl radicals (Xu et al. 2010, Glaze et al. 1987, Wang & Xu 2012, Hengtao et al. 2021). AOPs often relate to a certain group of procedures that use $O_3$, $H_2O_2$, and/or UV radiation in water treatment applications. All of these procedures have the potential to generate hydroxyl radicals, which can chemically react and eliminate a variety of organic pollutants. Although some of the processes mentioned above might have additional methods for eliminating organic pollutants, an AOP's efficiency is often inversely correlated with its capacity to produce hydroxyl radicals. The possibility of post-treating a toxic as well as non-biodegradable effluent with AOP using optimum chemical and energy consumption and producing an output that is completely and rapidly biodegradable (Ticiane et al. 2006, Manna et al. 2022), has been extensively reviewed and published in many research works. There is now a chance for comprehensive and inexpensive elimination of refractory organics in the tannery effluent (Ambaye et al. 2020). Thus, the present study focuses on the degradation of refractory organics using photocatalysis with a view to the application of the same in industrial sectors on a large scale, offering an effective treatment. The second objective is to evaluate the effectiveness of bio-degradability of biologically treated tannery effluent through Ultraviolet radiation, thereby assessing the compatibility of Nanoporous Activated Carbon and hydrogen peroxide when used as catalysts in the process.

## MATERIALS AND METHODS

Ultraviolet radiation is one of the most effective advanced oxidation processes. It involves the dissociation of water molecules by the incident ultraviolet radiation into hydroxyl radical species. Hydroxyl radicals are proven to be the most powerful oxidants which readily attack the organic as well as inorganic contaminants until they are reduced to simple inorganic molecules such as carbon dioxide and water. The most frequent and efficient electron acceptor in photocatalytic oxidation is oxygen, which works to further impede the electron-hole recombination action. Hydrogen peroxide has been the subject of several researches to examine its potential as an alternative electron acceptor (Burlacu et al. 2020) because of the potential for $H_2O_2$ reduction (0.72 V) to be higher than that of oxygen (−0.13 V) reduction. Hydrogen peroxide can present beneficial (Pillai et al. 2009, Poulios et al. 2003) or detrimental effects (Bandala et al. 2002, Dillert et al. 1996) on the photocatalytic degradation of organic contaminants. However, the majority of past photocatalytic research on the impact of hydrogen peroxide has noted that the ideal catalyst concentration depends on the properties of the wastewater. Hydrogen peroxide and nano-porous activated carbon corresponding to a mean pore size of 3.6 nm were used as catalysts in the ultraviolet radiation experiment. A multi-lamp photoreactor (Heber scientific model No HML-SW-MW-LW-888) was used for the study. The multi-lamp photoreactor (Paul et al. 2013) consists of six UV lamps arranged circularly, with six vials each of 100 mL capacity. It can produce UV light sources of intensities 254 nm, 312 nm, and 365 nm, respectively. The effluent sample was collected from the outlet of the secondary clarifier after the biological treatment from Pallavaram Common Effluent Treatment Plant, Chennai, Tamilnadu.

The collected samples were immediately stored at 20°C to maintain the humidity and temperature at constant values. The samples were analyzed for the physico-chemical characteristics in the laboratory according to the standard procedures (Chun & Park 1994, APHA 1990), and the results are presented in Table 1. The COD value is 656 $mg.L^{-1}$ with a standard deviation of 54 $mg.L^{-1}$. The BOD value of secondary treated tannery effluent is a range of 20 - 35 $mg.L^{-1}$, and the average TOC value is 212 ppm. The very low BOD/COD ratio in secondary-treated tannery effluent illustrates the presence of very poor biodegradable refractive organics in secondary-treated tannery wastewater.

## RESULTS AND DISCUSSION

An experimental investigation was performed to reduce the refractory organics present in the biologically treated (Activated Sludge Process) tannery effluent using

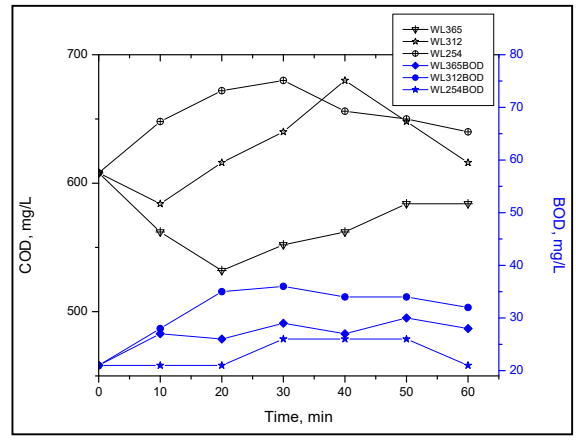


Fig. 1: Effect of wavelength on COD and BOD characteristics.

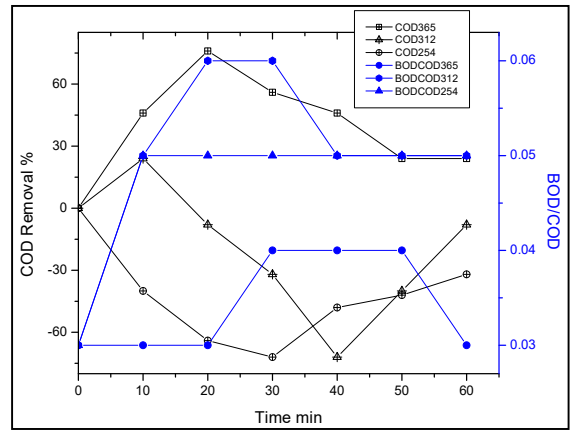


Fig. 2: Effect of wavelength on degradation and biodegradability index.

Photocatalysis. Furthermore, the process parameters such as time, pH and catalysts were analyzed in the oxidation process.

## Effect of Wavelength in Photolysis of Organics

The photodegradation of wastewater mainly depends on the light absorption properties of its constituents. The light-absorbing properties of STTE could be studied by investigating the degradability of organics under different wavelengths. The effect of wavelength in the photodegradation of organic constituents of STTE in terms of the COD and BOD of STTE is shown in Fig.1. The characteristic organic constituents of the secondary treated wastewater after UV photodegradation at natural pH showed the refractoriness of organics towards photolysis. The biodegradability pattern over the study time is presented in Fig. 2. The biodegradability, i.e., the BOD/COD ratio, doesn't seem to have shown improvement after photodegradation. The COD content of the STTE was found to increase after the treatment, which may be due to the oxidation of inert organic material into an active state.

Table 1: Characteristics of secondary treated tannery effluent.

| S.No. | Parameters | Mean ± SD |
|---|---|---|
| 1. | pH | 7 ± 0.273 |
| 2. | COD, mg.L$^{-1}$ | 656 ± 54 |
| 3. | BOD, mg.L$^{-1}$ | 35 ± 10 |
| 4. | TDS, mg.L$^{-1}$ | 4500 ± 530 |
| 5. | TOC, ppm | 213 ± 46 |
| 6. | BOD/COD | 0.08 ± 0.012 |

## Effect of pH in Photolysis of Organics

The pH is one of the most important parameters that influence the photodegradation of organic pollutants. Therefore, the degradation of STTE was studied at different pH values namely, 5.5,6,8 and 8.5, using 254 nm, 312 nm, and 354 nm

UV light, respectively. The results are represented in Figs. (3-6). The photodegradation of STTE at pH 5.5 with UV light of 254nm, 312 nm, and 365 nm (Fig. 3) was observed to produce COD removal efficiency of 13%, 13%, and 17%, respectively. The BOD value reached a maximum of 108 mg.L$^{-1}$ after degradation under 312 nm, whereas the biodegradability of the wastewater increased from 0.03 to 0.19. Although the COD removal efficiency was maximum at 365 nm, the biodegradability of the wastewater showed marginal improvement from 0.03 to 0.10, suggesting that the higher degradation percentage may correspond to the oxidation of volatile organics rather than the target refractory organics.

The photodegradation of STTE at pH 6 showed comparatively lesser efficiency in terms of degradation. The UV range of 312 nm and 365 nm was efficient by 21% and 18% in terms of COD reduction, whereas under 254 nm light, it showed an initial decrease to 532 mg.L$^{-1}$, and then it raised the COD level to 688 mg.L$^{-1}$. However, the biodegradability of STTE showed a decrease from 50 min of reaction time, suggesting lesser scope for further degradation. This may be attributed to the non-availability of compounds absorbing 254 nm light. The light absorption spectra of the STTE (Fig. 4) also showed light-absorbing compounds only in 200- 230 nm and 290-310 nm. This also supports the mode of light absorption. The photodegradation of STTE at pH 8 with UV light of 312 nm (Fig. 5) showed COD removal efficiency of 18%, and the biodegradability index was 0.16 after 60 min of degradation time. The BOD reached a maximum value of 97 mg.L$^{-1}$ after degradation with light of 254 nm, showing the further increase in reaction time for photolysis of STTE of pH value 8 would positively

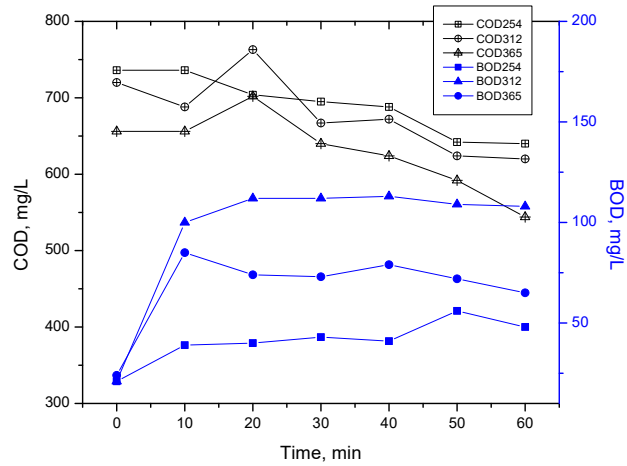


Fig. 3: Photodegradation of STTE: COD and BOD characteristics at pH 5.5.

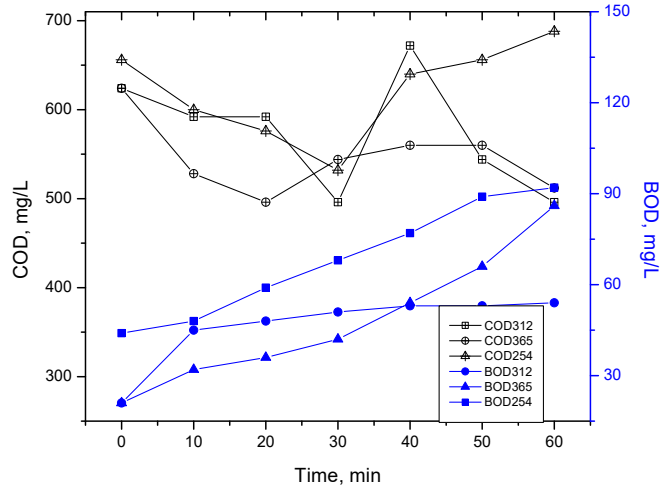


Fig. 4: Photodegradation of STTE: COD and BOD characteristics of STTE at pH 6.

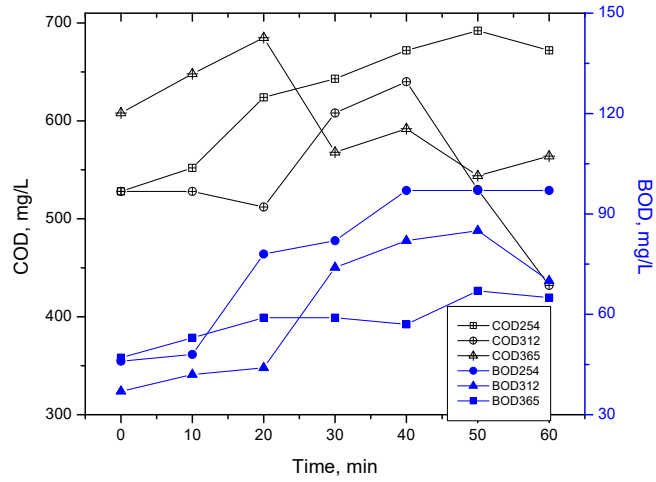


Fig. 5: Photodegradation of STTE: COD and BOD characteristics at pH 8.

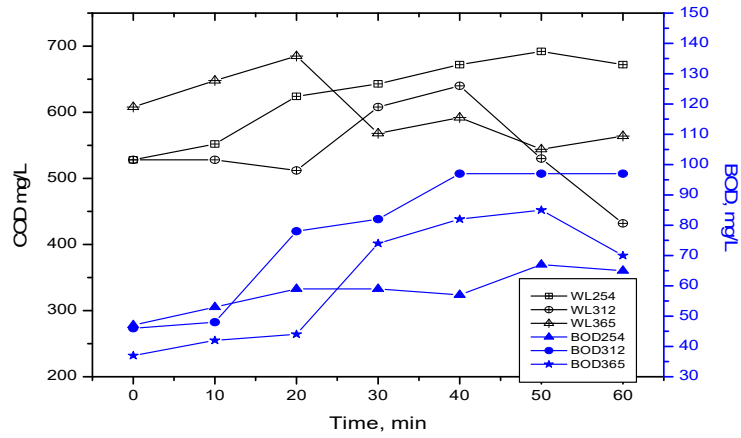


Fig. 6: Photodegradation of STTE: COD and BOD characteristics at pH 8.5.

influence in degradation of organics in wastewater (Fig. 6).

Numerous investigations have shown that the electrical excitation of the organic substrate takes place during the photolysis of organic materials (Giri et al. 2019, Hao et al. 2019, Sanzone et al. 2018, Xiong et al. 2016). The excitation causes the transfer of an electron from the excited state of the substrate to the ground state of molecular oxygen. It could also be caused by the hemolysis of substrate to form organic radicals, which later react with oxygen (Feng et al. 2013). Hence, the present study shows that the degradation of the contaminants by direct UV photolysis depends largely on the target compound under investigation (Kim & Tanaka 2009).

### Effect of Catalyst in Photolysis of Organics

The key factors influencing UV photolysis are the medium's absorption properties, the photon flow rate at the excitation wavelength, and the amount of dissolved molecular oxygen present (De la Cruz et al. 2012). The wastewater samples were found to be rich in dissolved organic matter, thus showing reduced possibilities for direct UV photolysis treatment since, after subsequent biological treatment, the remaining colloidal organics may cause the photo-chemically active light to be filtered and screened. It is clear that the UV/$H_2O_2$ process implies the cleavage of $H_2O_2$ molecules by UV light into hydroxyl radicals (Jain et al. 2018), and the OH radical has high oxidation potential. The NPAC produced from the rice husk is capable of OH radical generation in the presence of oxygen (Karthikeyana et al. 2014). Hence, a detailed investigation was performed for the photocatalytic oxidation of STTE with $H_2O_2$ and NPAC as catalysts, respectively.

The characteristics of NPAC samples are important for enumerating their ability to enhance the efficiency

of oxidation. In NPAC, which belongs to the extrinsic semiconductor range, the energy gap (Eg) of 1.55 eV correlates with the highest reflectance at a wavelength equivalent to 800 nm. Due to its ideal surface area, pore diameter volume, and free electron density properties, NPAC was chosen as a heterogeneous catalyst for the oxidation process (Table 2). The Photocatalytic oxidation of STTE with $H_2O_2$ as the catalyst, as a function of time (Fig. 7), shows a maximum efficiency of 30% COD removal. However, the biodegradability was not much enhanced, and the

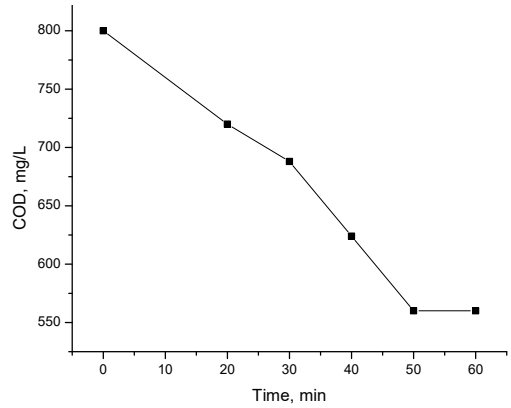


Fig. 7: Photocatalytic oxidation of STTE with $H_2O_2$ as catalyst.

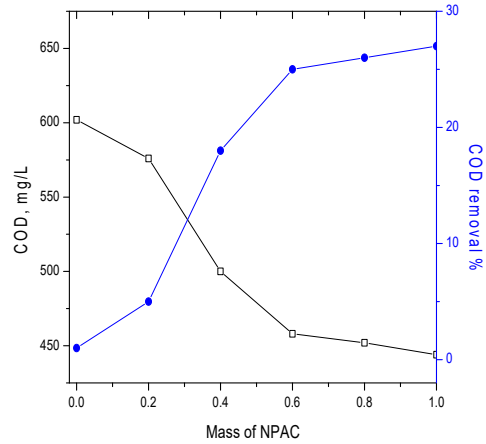


Fig. 8.a: Effect of mass of NPAC on degradation of organics-COD.

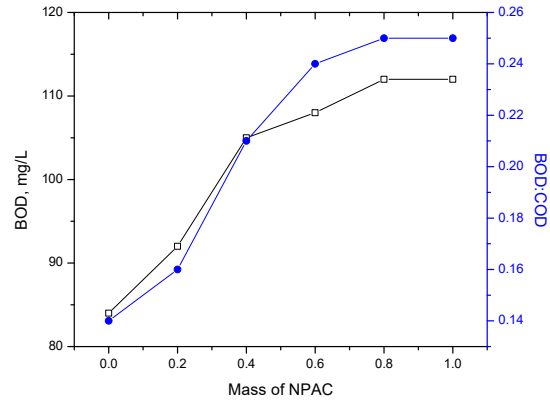


Fig. 8.b: Effect of mass of NPAC on degradation of organics – BOD, biodegradability.

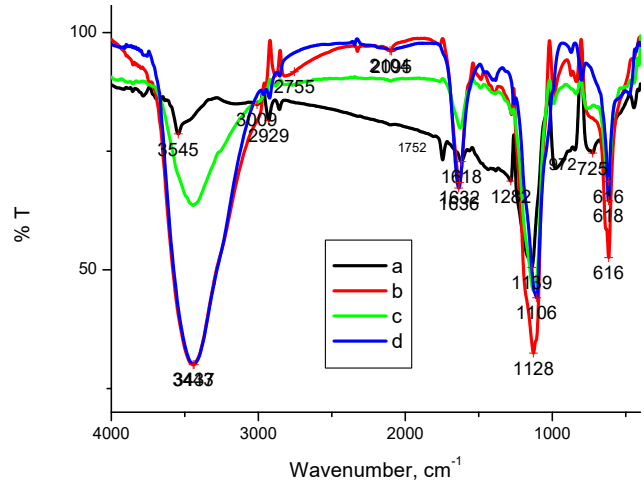


Fig. 9: FTIR spectrum of photodegradation of organics in secondary treated tannery effluent.
a. Initial, b. Photolysis at 312 nm for 60 min, c. Photocatalytic Oxidation with NPAC as Catalyst, and d. Photocatalytic Oxidation with Hydrogen Peroxide as Catalyst.

Table 2: Characteristics of nano-porous activated carbon.

| S.No. | Parameters | Values |
|---|---|---|
| 1. | Surface Area [$m^2.g^{-1}$] | 379 |
| 2. | Average pore diameter [Å] | 39.36 |
| 3. | Carbon [%] | 41.58 |
| 4. | Hydrogen [%] | 2.85 |
| 5. | Nitrogen [%] | 0.75 |
| 6. | Free electron density [spins.$g^{-1}$] | 16.05 x$10^{21}$ |
| 7. | Energy gap [eV] | 1.55 |
| 8. | Ash Content [%] | 41.60 |

biodegradable index of wastewater after the photocatalytic oxidation of STTE with $H_2O_2$ was found to be only 0.13. Fig. 8 (a & b) shows the effective treatability of refractory organics by photocatalytic oxidation with NPAC as the catalyst. Among all the oxidation reactions carried out, the photocatalytic oxidation of refractory organics with NPAC as a catalyst showed a maximum efficiency of 27%, and the biodegradability also increased to 0.25, further improving the content of biodegradable materials in the wastewater. This is also supported by the FTIR instrumental evidence, as shown in Fig. 9.

The variation in the region 1600-1200 $cm^{-1}$ depicts the formation of a new compound after photon interaction in all the studies. There occurred elimination of many bands after the photocatalytic oxidation with NPAC as a catalyst. 2929 $cm^{-1}$ in the raw wastewater sample may correspond to the presence of the methoxy group, which was then eliminated after degradation. The weak band at 3545 $cm^{-1}$ may be attributed to p-CN or p-$NO_2$ group presence, which later got eliminated after the photo interaction of organics

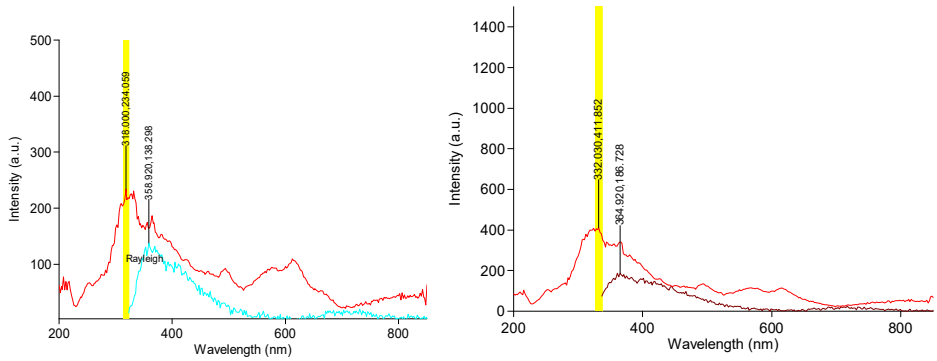


Fig. 10: Fluorescence spectrum of wastewater (a) before and (b) after degradation.

in wastewater. The medium band corresponds to hydroxyl absorption, and the elimination of the band at 1752 $cm^{-1}$ may correspond to cyclic lactam. The UV visible spectrum and the fluorescence spectrum of wastewater before and after degradation also confirm the effective photocatalytic oxidation of refractory organics (Fig. 10). The shift in excitation wavelength from 318 to 332 nm and the increase in absorption intensity of the 332 nm peak suggests the formation of degraded products of less complexity after photocatalytic oxidation.

## CONCLUSIONS

The Advanced Oxidation Process, especially UV photocatalysis, is a very useful method for the treatment of water consisting of aromatic compounds, which are highly bio-refractory and toxic. The optimum time, PH, dosage of $H_2O_2$, and mass of NPAC required for the effective treatment of the synthetic wastewater using photocatalysis were found to be 60 min, 8, 0.2 $mg.L^{-1}$, and 1g.100 $mL^{-1}$, respectively. It was found that the heterogeneous photocatalysis improves the biodegradability of refractory organics. The efficiencies of photolysis, homogeneous photocatalysis, and heterogeneous photocatalysis were found to be 18%, 30%, and 27%, respectively. Although the efficiency of homogeneous photocatalysis was found to be higher than that of heterogeneous photocatalysis, the biodegradability was higher in the latter, with a value of 0.26. The biodegradability of the former was found to be 0.13. Thus, heterogeneous photocatalysis assures a promising scope for future work. Further analysis in this study with prolonged time and higher mass of carbon may increase the efficiency of this process. Further research is needed to assess the suitability of photocatalysis in industrial sectors.

## ACKNOWLEDGMENT

The authors wish to acknowledge the support given by CSIR-CLRI, Chennai, for giving necessary permission to carry out the analytical studies.

## REFERENCES

Ambaye, T. G. and Hagos, K. 2020. Photocatalytic and biological oxidation treatment of real textile wastewater. Nanotechnol. Environ. Engineering, 5**:** 28.

APHA 1990. Standard Methods for the Examination of Water and Wastewater, Water Environment Federation: American Water Works Association, Washington DC.

Bandala, E. R., Gelover, S., Leal, M. T., Arancibia-Bulnes, A., Jimenez, A. and Estrada, C. A. 2002. Solar photocatalytic degradation of aldrin. Catal. Today., 76: 189-199.

Burlacu, F., Favier, L., Matei, E., Predescu, C. and Deák, G. 2020. Photocatalytic degradation of a refractory water pollutant using nano-sized catalysts. J. Environ. Protect. Ecol., 21**:** 571.

Chun, H. D. and Park, J. K. 1994. Photocatalytic oxidation of chlorinated organic compounds over $tio_2$ membrane coated on glass tube hazard. Wastes Hazard. Mater., 11: 501-510.

De la Cruz, N., Giménez, J., Esplugas, S., Grandjean, D., de Alencastro, L.F. and Pulgarín, C. 2012. Degradation of 32 emergent contaminants by UV and neutral photo-fenton in domestic wastewater effluent previously treated by activated sludge. Water Res., 46: 1947-1957.

Dillert, R., Fornefett, I., Siebers, U. and Bahnemann, D. 1996. Photocatalytic degradation of trinitrotoluene and trinitrobenzene: Influence of hydrogen peroxide. J. Photochem. Photobiol A Chem., 94: 231-236.

Feng, L., Van Hullebusch, E. D., Rodrigo, M. A., Esposito, G. and Oturan, M. A. 2013. Removal of residual anti-inflammatory and analgesic pharmaceuticals from aqueous systems by electrochemical advanced oxidation processes- A review. Chem. Eng. J., 228: 944-964.

Giri, A. S. and Golder, A. K. 2019. Ciprofloxacin degradation in photo-Fenton and photo-catalytic processes: Degradation mechanisms and iron chelation. J. Environ. Sci., 80: 82-92.

Giusy, C., Melina, A., Roccamante, I. O., Sixto, M. and Luigi, R. 2019. Contaminants of emerging concern removal from real wastewater by UV/free chlorine process: A comparison with solar/free chlorine and UV/$H_2O_2$ at pilot scale. Chemosphere, 236**:** 124354.

Glaze, W.H., Kang, J.W. and Chapin, D.W. 1987. The chemistry of water-treatment processes involving ozone, hydrogen peroxide, and ultraviolet radiation. Ozone Sci. Eng., 9: 335.

Hao, H., Shi, J.L., Xu, H., Li, X. and Lang, X. 2019. N-hydroxyphthalimide-TiO2 complex visible light photocatalysis. Appl. Catal. B Environ., 246: 149-155.

Haydar, S., Aziz, J. A. and Ahmad, M. S. 2007. Biological treatment of tannery wastewater using activated sludge process. Pak. J. Eng. Appl. Sci., 1: 61-66.

Hengtao, X., Zhe, H., Weihua, F., Ting, W. and Yao, L. 2021. Mechanism of photodegradation of organic pollutants in seawater by $TiO_2$-based photocatalysts and improvement in their performance. ACS Omega, 6(45): 30698.

Jain, B., Kumar, A., Hyunook, S., Eric, K. and Virender, L. 2018. Treatment of organic pollutants by homogeneous and heterogeneous Fenton reaction processes. Environ. Chem. Lett., 16: 947-967.

Karthikeyana, S., Bavas Ahamedb, R., Velanb, M. and Sekarana, G. 2014. Synthesis characterization of Co-NPAC and in-situ hydroxyl radical generation for oxidation of dye-laden wastewater from the leather industry. RSC Adv., 4: 63354-63366.

Kim, I. and Tanaka, H. 2009. Photodegradation characteristics of PPCPs in water with UV treatment. Environ. Int., 35: 793.

Koltuniewicz, A. (ed.) 2010. Integrated membrane operations in various industrial sectors: comprehensive membrane science and engineering. Elsevier, The Netherlands, pp.109-164.

Manna, M. and Sen, S. 2022. Advanced oxidation process: a sustainable technology for treating refractory organic compounds present in industrial wastewater. Environ. Sci. Pollut. Res., 30(10): 25477.

Mannucci, A., Munz, G., Mori, G. and Lubello, C. 2010. Anaerobic treatment of vegetable tannery wastewaters: a review. Desalination, 264: 1-8.

Mirzaa, N. R., Huanga R., Dub E., Du, E., Peng, M., Pan, Z., Ding, H., Shan, G., Ling, L. and Xie, Z. 2020. A review of the textile wastewater treatment technologies with a special focus on advanced oxidation processes (AOPs), membrane separation, and integrated AOP-membrane processes. Desal. Water Treat., 206: 83-107.

Paul, H., Nicos, L., Robert, A., Sorin, F. and John, R. 2013. The importance of double bond position and cis-trans isomerization in diesel combustion and emissions. Fuel, 105: 477-489.

Pillai, K. C., Kwon, T. O. and Moon, I. S. 2009. Degradation of wastewater from terephthalic acid manufacturing process by ozonation catalyzed with $Fe^{2+}$, $H_2O_2$ and UV light: direct versus indirect ozonation reactions. Appl. Catal. B Environ., 91: 319.

Poulios, E., Micropoulou, R. and Panou, E., Kostopoulou. 2003. Photo-oxidation of eosin Y in the presence of semiconducting oxides. Appl. Catal. B Environ., 41: 345-355.

Ran, D., Dandan, Z., Yingxin, G., Xing, C. and Min, Y. 2021. Characteristics of refractory organics in industrial wastewater treated using a Fenton-coagulation process. Environ. Technol., 3440-3432 :(22)42.

Rao, J. R., Chandrababu, N. K., Muralidharan, C., Nair, B. U., Rao, P. G. and Ramasami,T. 2003. Recouping the wastewater: A way forward for cleaner leather processing. J. Clean. Prod., 11: 591-599.

Runzhe, S. 2019. Advanced oxidation technology for refractory organic compounds in wastewater. IOP Conf. Ser.: Earth Environ. Sci., 384:12051.

Sanzone, G., Zimbone, M., Cacciato, G., Ruffino, F., Carles, R., Privitera, V. and Grimaldi, M.G. 2018. Ag/$TiO_2$ nanocomposite for visible light-driven photocatalysis. Superlattices Microstruct., 123: 394-402.

Shakir, L., Ejaz, S., Ashraf, M., Ahmad, N. and Javeed, A. 2012. Characterization of tannery effluent wastewater by proton-induced X-ray emission (PIXE) analysis to investigate their role in water pollution. Environ. Sci. Pollut. Res. Int., 19: 492-501.

Subramani, T. and Haribalaji, D. 2012. Biodegradation of tannery effluent and designing the reactor clarifier and activated sludge Process. International Journal of Modern Engineering Research, 2(3): 774-781.

Suthanthararajan, R., Ravindranath, E., Chits, K., Umamaheswari, B., Ramesh, T. and Rajamam, S. 2004. Membrane application for recovery and reuse of water from treated tannery wastewater, Desalination, 164:151-156.

Ticiane. P. S., Leonardo, C., André, L. B. O., Humberto, J. J. and Regina, D. F. P. 2006. Advanced oxidation processes applied to tannery wastewater containing Direct Black 38-Elimination and degradation kinetics. J. Hazard. Mater., 135: 1-3.

Tunay, O., Kabdasli, I., Orhon, D. and Ates, E. 1995. Characterization and pollution profile of leather tanning industry in Turkey. Water Sci. Technol., 32: 1-9.

Wang, J. L. and Xu, L. J. 2012. Advanced oxidation processes for wastewater treatment: Formation of hydroxyl radical and application. Crit. Rev. Environ. Sci. Technology., 42 (3): 251-325.

Xiong, X. and Xu, Y. 2016. Synergetic effect of Pt and borate on the $TiO_2$ -Photocatalyzed Degradation of Phenol in Water. J. Phys. Chem. C., 120: 3906-3912.

Xu, A., Shao, K., Wu, W., Fan, J., Cui, J. and Yin, G. 2010. Oxidative degradation of organic pollutants catalyzed by trace manganese (II) ions in sodium bicarbonate solution. Chin. J. Catal., 31(8): 1031-1036.

## ORCID DETAILS OF THE AUTHORS

S. Hema: https://orcid.org/0000-0002-8769-7044

Nature Environment and Pollution Technology
An International Quarterly Scientific Journal

p-ISSN: 0972-6268
(Print copies up to 2016)
e-ISSN: 2395-3454

Vol. 23 | No. 3 | pp.1547-1557 | 2024

Original Research Paper

https://doi.org/10.46488/NEPT.2024.v23i03.024

Open Access Journal

# Potential of Heavy Metals and Microplastics Contamination in River Mpanga, Fort Portal, Kabarole District, Uganda

**C. Nyakoojo*, W. Kabiswa*, E. Najjuma*†, P. Matovu* and H. Ocaya****
*Department of Biological Sciences, Faculty of Science, Technology and Innovation, Mountains of the Moon University, Fort Portal, Uganda
**National Fisheries Resources Research Institute, Jinja, Uganda
†Corresponding author: E. Najjuma; efrance.najjuma@mmu.ac.ug

**Nat. Env. & Poll. Tech.**
**Website: www.neptjournal.com**

*Received:* 19-11-2023
*Revised:* 13-02-2024
*Accepted:* 07-03-2024

**Key Words:**
Microplastics
Heavy metals
Contamination
River Mpanga

## ABSTRACT

Anthropogenic environmental pollution is a major development challenge in Ugandan rivers and lakes, the key drivers being industrialization, agriculture, and urbanization. The aim of the study was to assess the potential of heavy metal and microplastic contamination in River Mpanga, Fort Portal, Uganda. Triplicate water and sediment samples were collected from three sampling sites, preserved, and analyzed at the Chemistry Department, Makerere University for heavy metals, while microplastics analysis was conducted at NaFIRRI, Jinja. Sediment heavy metal contamination was assessed from the geoaccumulation index, while microplastic characterization and quantification were determined from stereomicroscopy and morphological features. Arsenic was the most prevalent metal with a mean concentration of 13.2 ppm thus higher than permissible maximum limits of WHO. The mean concentrations (ppm) of copper, lead, and cadmium were 0.01, 0.01, and 0.001 respectively, and below the permissible maximum. Sediment samples revealed very strong arsenic contamination, strong contamination for copper, moderate to strong contamination for lead, and a potential lack of contamination for cadmium. The higher concentrations of the heavy metals in the sediments compared to water could be attributed to bioaccumulation, as evidenced by the high geoaccumulation values. Microplastics occurred throughout the river and included fragments, filaments, film, pellets, form, and fibers. The presence of heavy metals and microplastics was attributed to anthropogenic activities within the river vicinity, which discharged heavy metal-laden waste into River Mpanga. High arsenic concentrations and sediment accumulation of contaminants pose serious potential public health threats to the local communities.

## INTRODUCTION

Environmental pollution is a major development challenge in Uganda. The recent advances in economic growth, industrialization, farming, and urbanization have been key drivers of water, air, and land pollution (Pierre & Karani 2016). In Uganda, the rate of urbanization has been reported at 4.5% per annum (Yusuf et al. 2019). The majority of the urban areas in Uganda are slums, characterized by unplanned urban centers and urban settlements. These have limited access to clean water, sanitation infrastructure, and facilities for waste disposal (Jonas & Kirungyi 2020). They tend to generate a lot of waste, exerting pressure on the already inadequate municipal and local authority waste management schemes (Aryampa et al. 2019).

Sustainable municipal solid waste (MSW) management is a major concern for all African cities (Aryampa et al. 2019). Poor disposal of solid waste and wastewater exposes underground and surface water systems to physical, biological, and chemical contamination (Vasanthi et al. 2008). Industrial and urban wastes resulting from anthropogenic activities are usually discharged into aquatic ecosystems, leading to heavy metal, microbial, and plastic contamination (Bentum et al. 2011).

### The Mpanga Catchment

In Uganda, lakes and rivers are the main sources of water for domestic and commercial purposes. The Mpanga catchment in Western Uganda covers an area of 4,700 km² (Businge et al. 2021). Mpanga River begins in the foothills of the Rwenzori Mountains in Kabarole District. It starts as a small river but increases in size as a diverse range of streams and rivers join it. The river flows through forested, highly populated, and cultivated areas in the districts of Kabarole, Kyenjojo, and Kamwenge before discharging its water into Lake George (Businge et al. 2021, Onyutha et al. 2021).

River Mpanga catchment has four major sub-catchments, including Upper Mpanga, Middle Mpanga, Lower Mpanga, and Rushango, with drainage areas equal to 384, 1174, 477, and 3170 $km^{2,}$ respectively (Onyutha et al. 2021). It is the main source of water in several urban areas in the western part of Uganda including Fort Portal, Kamwenge, and Ibanda.

Despite its economic importance, recent reports indicate deterioration in the water quality of River Mpanga, posing contamination risks not only to communities that depend on its waters but also to its flora, fauna, and the water quality of Lake George. For example, Businge et al. (2021) reported fecal coliform contamination in the river. Coliform contamination also indicates the presence of other microbial contaminants, including *Salmonella*, rotaviruses, hepatitis E virus, and *E. coli* (Korajkic et al. 2018). Besides microbial contamination, other potential forms of water pollution accruing from anthropogenic sources include heavy metal and microplastic contamination (Baguma et al. 2022, Basooma et al. 2021).

## Effect of Heavy Metal Contamination

Heavy metals are chemical elements with high molecular weights and a specific gravity at least five times greater than that of water and are toxic at concentrations that exceed their threshold values. Heavy metals are used in domestic, industrial, agricultural, medical, and technological applications, which have led to their uncontrollable distribution in the environment. Their physicochemical nature makes them persistent, toxic, and bio-accumulative. Owing to their high degree of toxicity, As, Cd, Cr, Pb, and Hg are listed as priority heavy metals that are of public health significance (Singh et al. 2022). Humans get exposed to heavy metals through three main pathways, namely, ingestion, inhalation, and skin absorption (Kumar et al. 2020).

Heavy metals react with biological systems by losing one or more electrons and forming cations that can ably bind with the nucleophilic sites of the vital macromolecules. Their toxicity is caused by the disruption of cellular activities such as growth, differentiation, damage-repairing processes, and apoptosis (Baguma et al. 2022). These may be mediated through the generation of reactive oxygen species (thus causing oxidative stress), weakening the organism's antioxidant defense system, complexation or ligand-formation with organic compounds, and the active sites of enzymes. Their toxicity is contingent on the exposure route, dose, chemical form, and the age, gender, and nutritional status of the individual in question (Balali-Mood et al. 2021).

Additionally, heavy metals, as persistent toxicants, are deposited in the ecosystem and subsequently get absorbed in food chains (Kumar & Khan 2020). Pollution of aquatic ecosystems with heavy metals can lead to environmental problems hence adverse ecological impacts. In aquatic macrophytes, growth inhibition has been observed to occur in duckweed and algae, whereas in benthic invertebrates and freshwater fingerlings, reductions in fecundity, growth, and survival of these organisms have also been reported (Vera-Candioti et al. 2011).

## Microplastics

Microplastics (MPs) are synthetic polymeric compounds on a microscopic scale (<5 mm). Microplastic contaminants originate from the breakdown of larger plastics by agents like wave action, temperature, and radiation (Li et al. 2021). Microplastic fragments even break down further to form smaller particles (< 0.1 micrometers) called nanoparticles (Danopoulos et al. 2020). More than 45 plastic compounds are in commercial use currently. These include polypropylene (PP), polyethylene (PE), polyethylene terephthalate (PET), polystyrene (PS), polyurethane (PU), polyvinyl chloride (PVC), and polycarbonate (PC) (Kannan & Vimalkumar 2021). Most of the microplastic waste ends up in soils and freshwater bodies. Their small size, coupled with resistance to microbial degradation, renders them potential contaminants to water and soil ecosystems (Issac & Kandasubramanian 2021).

Despite the occurrence of microplastics in most aquatic environments such as underground water systems, rivers, lakes, estuaries, shorelines, and domestic tap water systems, existing research on MP contamination has majorly focused on marine water systems (Danopoulos et al. 2020, Lamm et al. 2021) thus creating a knowledge gap on the potential contamination of MPs in freshwater systems. Human exposure to microplastics is mainly through contaminated drinking water, ingestion, and inhalation (Kannan & Vimalkumar 2021). Although limited knowledge has been established on the human health impacts associated with exposure to microplastics, the potential effects of microplastic exposure to aquatic biota are well documented. These include intestinal obstruction, reduced energy metabolism, and reproductive malfunction. In addition, exposure to MPs enhances the absorption of hydrophobic organic contaminants (HOCs) from the environment into living systems (Lamm et al. 2021). As a result of the widespread existence of MPs, their absorption, distribution, metabolism (along with the potential toxicity), and excretion processes in humans have drawn increasing attention (Dick-Vethaak & Legler 2021). These MPs may affect human health by interfering with metabolic processes (Vaughan et al. 2017).

Even though the effects of exposure to microplastics on human health are still not fully understood, continuous

exposure to microplastics is documented to cause inflammation in body systems (Wu et al. 2021). MP ingestion not only poses physical impacts by internal abrasions and blockages but also provides a possible pathway of exposure to the respective organisms via adsorbing organic contaminants and metals from the ambient environment (Zhao et al. 2015).

Although some studies have been conducted to assess the potential of heavy metal (Basooma et al. 2021; Egesa et al. 2020; Mbabazi et al. 2010, Sekabira 2010) and microplastic contamination (Egesa et al. 2020), knowledge of heavy metals and microplastic contamination in Ugandan river ecosystems is still scanty. Knowledge of heavy metal and microplastic concentrations in aquatic environments and commercial water systems is essential for monitoring water quality, controlling pollution, protecting aquatic ecosystems, and safeguarding human health. The study, therefore, focused on assessing the potential of microplastics and heavy metals (As, Cd, Cu, and Pb) contamination in River Mpanga. These metals have been documented as prime heavy metals of concern to human health owing to their high levels of toxicity (Balali-Mood et al. 2021).

## MATERIALS AND METHODS

### Description of the Study Area

The study was carried out on the section of River Mpanga, which is within the geographical confines of Fort Portal City, Kabarole District. River Mpanga is a lifeline for an estimated 1.2 million people in Uganda. From its origin in the Rwenzori Mountains, the river flows 250 km through the Kabarole, Kamwenge, and Kyenjojo districts before reaching Lake George. Three georeferenced locations of the river: Kazingo (36 N 185263E 72611N), Kabandaire (36 N 196628E 72699N), and Nyamigira (36 N 207662E 73601N) were selected and referred to as upstream, midstream and downstream sites (Fig. 1).

### Sample Collection

Triplicate water samples were collected from each of the three sites in the river using a 10 L sterile plastic container and filtered through a 63 µm neuston net. The final concentrates were kept in sterile glass bottles, preserved in 70% ethanol, and kept in cool boxes before analysis for four heavy metals, namely arsenic, cadmium, copper, and lead.

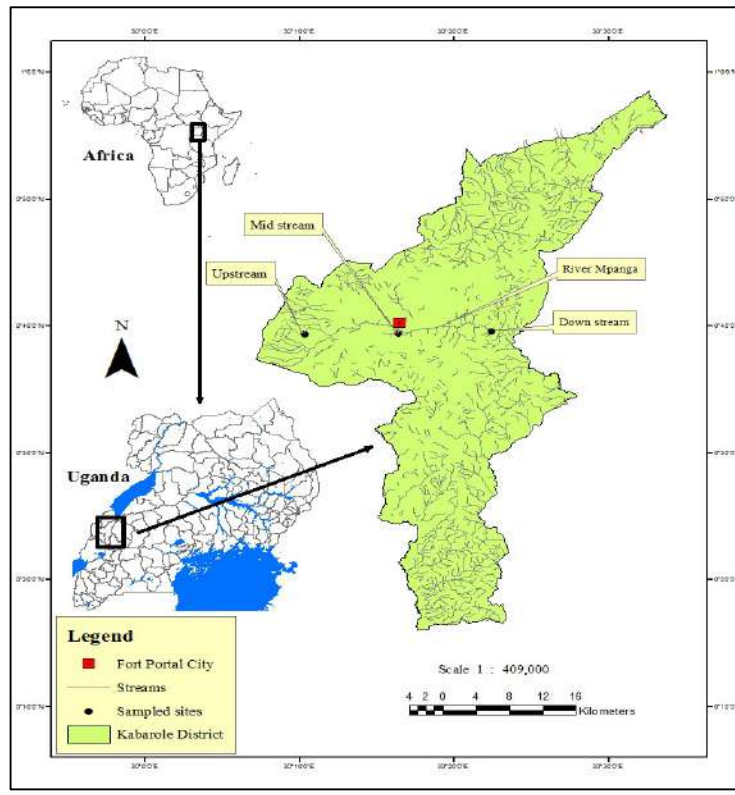


Fig. 1: Location of the study sites.

Sediment samples were collected from each of the three locations of the river using an Ekman sediment grab from which sub-samples were obtained for analyses. Sediment samples were prior kept in a cool box before delivery to the laboratory for further sample processing and analysis.

Additional information about each sampling area was also obtained, i.e., approximate width of the river, land use pattern, type of shoreline materials, river velocity and factors that affect it, topography, river use, distance from the nearest population center, any development nearby, industrial complex, wastewater discharges, and other pollution sources.

## Sample Analysis

**Water sample analysis for heavy metals:** Water samples for heavy metal analyses were subjected to hot peroxide digestion to break down any organic matter. The samples were filtered through a 0.45 µm pore size Whatman glass fiber filter paper. The filter paper was then placed into a glass petri dish and kept in a desiccator. Sample digestion and filtration were conducted following the protocols provided by Masura et al. (2015). Negative controls comprising tap and deionized water were used as quality control measures of the laboratory analysis procedures.

**Sediment sample analysis for heavy metals:** Sediment samples were oven-dried at 105$^{o}$C overnight before grinding them to fine powder, of which 1 g was mixed with 50 mL of deionized water in a conical flask. To each mixture, 3 mL of $HNO_3$ was added, and the mixture was heated slowly to concentrate the sample to 5 mL, to which 5 mL of $HNO_3$ acid was added. The conical flask was covered with a watch glass and heated. Heating was continued until a light-colored solution was realized, indicating the completion of the digestion process. This was followed by the addition of 10 mL of 1 + 1 HCl and 15 mL of deionized water per 100 mL. This was followed by an additional 15 minutes of heating to dissolve any precipitate or residues. The digested sample was cooled and filtered through a GF/C Whatman filter paper (0.45 um pore size, 47 mm diameter) to remove insoluble material that could clog the nebulizer (EPA 1996). The concentrations of the heavy metals were determined in ppm (parts per million) by using the atomic absorption spectrophotometer (AAS).

**Water sample analysis for microplastics in water:** Microplastic analyses were conducted using a stereomicroscope (×50 mag) scanning through each petri dish for physical characterization of any observed microplastic particles based on morphological and visual guidelines (Branch et al. 2022). The key morphological descriptors used were fragments for broken-off plastic pieces, foam for all particles that are easily deformed under pressure and exhibit elastic characteristics, film for all particles with smooth, angular edges, flat and flexible, pellet for particles that are harder than foam and lastly filament for particles that are long, or fibrous (Branch et al. 2022). All the observed microplastics were recorded by use of photographs, and each particle type was tallied and the counts summed up.

## Data Analysis

Data analysis involved the use of descriptive statistics to indicate proportions, distribution, and counts for microplastic data. On the other hand, means and standard deviations were used to indicate different heavy metal concentrations.

Table 1: Field information obtained during sampling of River Mpanga water and benthic sediment.

| River Properties | | Sampling points | | |
|---|---|---|---|---|
| | | Upstream | Midstream | Downstream |
| | Site location | 36 N 185263E 72622N | 36 N 196628E 72699N | 36 N 207662E 73601N |
| Catchment information | Topography | Slope | Gentle slope | Gentle slope |
| | Land use | Farming | Market, car wash, laundry | Tea plantation |
| | River use | Domestic use | Laundry & commercial car washing | Domestic use |
| River physical properties | Mean river width [m] | 1.9 | 4.4 | 7 |
| | Mean river depth [cm] | 38.7 | 46.3 | 88.7 |
| | Shoreline/benthic type (sand, gravel, clay) | Rock | Clay + sand | Rocks |
| | River bed type (sand, gravel, clay) | Gravel | Gravel | Rocks |
| | Objects affecting current | Boulders | Plastic debris & plant materials | Stones |
| River hydraulic properties | Velocity [m.sec$^{-1}$] | 0.47 | 0.68 | 1 |

Table 2: Concentrations (ppm) of heavy metals in water samples from River Mpanga.

| | Heavy metal concentration in 10 L water sample | | | |
|---|---|---|---|---|
| | Mean [PPM] | | | |
| Location along the river | As | Cu | Pb | Cd |
| River upstream (n =3) | 12.67±2.43 | 0.05±0.06 | 0.01± 0.00 | 0.00± 0.001 |
| River mid stream (n=3) | 13.13±0.58 | 0.04±0.01 | 0.03 ±0.01 | 0.002±0.00 |
| River downstream (n =3) | 13.80±3.00 | 0.03±0.02 | 0.00±0.00 | 0.001±0.00 |
| Background | 10 | 1 | 0.026 | 1 |
| Mean along the river | 13.20±0.57 | 0.04±0.01 | 0.01± 0.01 | 0.0013±0.001 |
| WHO (2017) limit | 0.05 | 1.5 | 0.05 | 0.005 |
| EPA (2018) limit | 0.01 | 1.3 | 0.015 | 0.005 |

Table 3: Concentration of heavy metals in River Mpanga bed sediment.

| | Heavy metal concentration in riverbed sediment | | | |
|---|---|---|---|---|
| | Mean [PPM] | | | |
| Location along the river | As | Cu | Pb | Cd |
| River upstream (n =3) | 1838 ±14.6 | 54.3± 7.6 | 32.3± 5.5 | 0.11± 0.02 |
| River mid stream (n=3) | 2113± 10.26 | 29.3± 7.0 | 31.3± 3.05 | ND |
| River downstream (n =3) | 2808 ±15 | 41.9± 6.4 | 27.3± 6.02 | ND |
| Mean along the river | 2253 ±499 | 41±12 | 30.3 ± 2.64 | 0.11 ± 0.02 |
| Background | 0.1 - 10 | 5 -50 | 15 - 40 | 0.01 - 1 |

Additionally, analysis of the heavy metal pollution index in the river bed sediments was established using a geoaccumulation indexing approach (Igeo index) using equation (1) (Muller 1969).

$$Igeo = \ln (Cn/1.5 \times Bn) \quad \ldots(1)$$

Where Cn = measured concentration, $mg.kg^{-1}$, and Bn = geochemical background value, mg/kg. In equation 1, average values were used and 1.5 was the factor used for lithologic variations of trace elements and the resulting findings compared to the permissible limits as provided by the World Health Organization (2018) and the Environmental Protection Agency (2017). All the analysis was conducted using SPSS version 15.0, and the results were presented in tables and figures.

## RESULTS

### Description of the River Characteristics

Samples were collected from three points with varrying gradients, that is Kazingo (sloping), Kabundaire and Nyamigira (gently sloping). The dominant land use type is agriculture, while the river water is being exploited for various domestic uses. The width of the river ranged between 1.9 to 7 m while the depth ranged from 38 to 9 cm. The riverbed was dominated by gravel, although parts of it were rocky. The velocity of the river, as expected, decreased downstream, with river flow being under the influence of variously-sized stones and foreign material (Table 1).

### Heavy Metal Concentration in Mpanga River

**Heavy metal concentration in water samples:** Analysis of heavy metal concentrations indicated varying results for the three sections of the river. The mean concentration of arsenic, 13.2 ppm, was greater than the permissible maximum concentration (0.05 ppm) as provided by WHO (2018). The highest concentration of 13.8 ppm was detected at the river downstream, whereas the lowest concentration of 12.7 ppm was detected at the river upstream (Table 2). The mean concentrations (ppm) of copper, lead, and cadmium were 0.01, 0.01, and 0.001, respectively, and within the permissible maximum limits of WHO.

**Heavy metal concentration in water sediments:** The study findings revealed varying and high concentrations of arsenic in the river bed sediment. While the background arsenic concentration is between 0.1 to 10 ppm, an average concentration of 2253 ppm was detected along the river. The highest arsenic concentration of 2808 ppm was recorded at the downstream site, while the lowest value of 1838 ppm was recorded at the upstream site. Except for the copper concentration of 54.3 ppm upstream, the overall concentrations of copper, lead, and cadmium were below the background limits (Table 3).

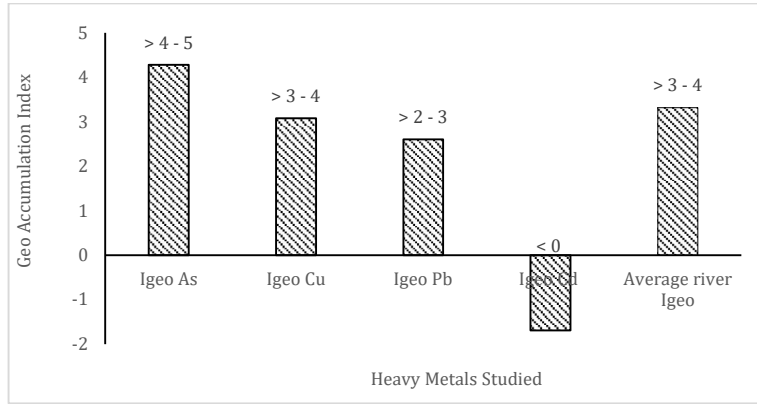


Fig. 2: Geoaccumulation index of heavy metals in River Mpanga sediment
Key: >4-5 strong to very strong contamination, >3-4 strong contamination, > 2- 3 Moderate to strong contamination, < 0 practically uncontaminated.

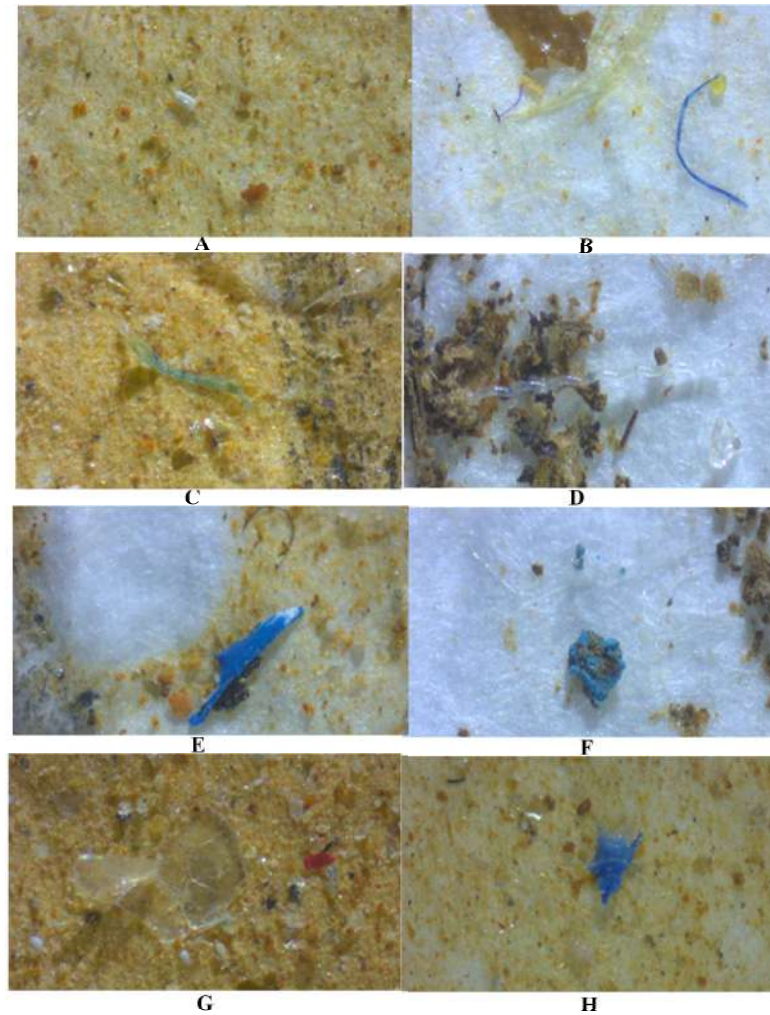


Fig. 3: Microplastics (mag ×50) in River Mpanga
A = Pellets, B - D = Filaments, E - G = Fragments, H = Film
Description: Foam = near spherical or granular particles, Pellet = resin bead, granular shape, Filament = long fibrous material, Fragment = granular, irregularly shaped hard particles, Film = sheet, flat and flexible.

**Heavy metal geoaccumulation index (Igeo) in the river bed sediment:** The heavy metal accumulation in the sediments showed varying indices. Analysis of the river Igeo (> 3-4) indicated a strong level of contamination. The order of Igeo indices for the four metals was -1.69 for cadmium, 2.6 for lead, 3.08 for copper, and 4.28 for arsenic. Compared to the Igeo classification scale, findings from the study indicate a strong to very strong arsenic contamination, strong contamination for copper, moderate to strong contamination for lead, and a potential lack of contamination for cadmium. Therefore, the average bioaccumulation index of heavy metals in the river bed sediment was in the order of As > Cu> Pb > Cd (Fig. 2).

## Characterization and Concentration of Microplastics in Water

Water analysis for microplastic contamination revealed six types of microplastics: fragment, film, pellet, form, fiber, and filament (Fig. 3).

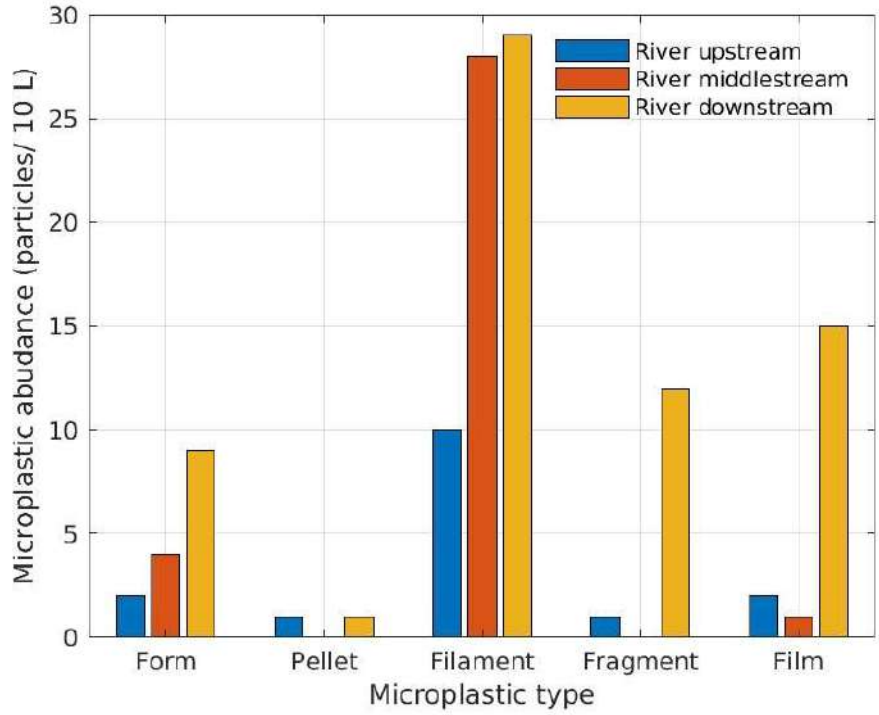


Fig. 4: Microplastic counts in the water samples.

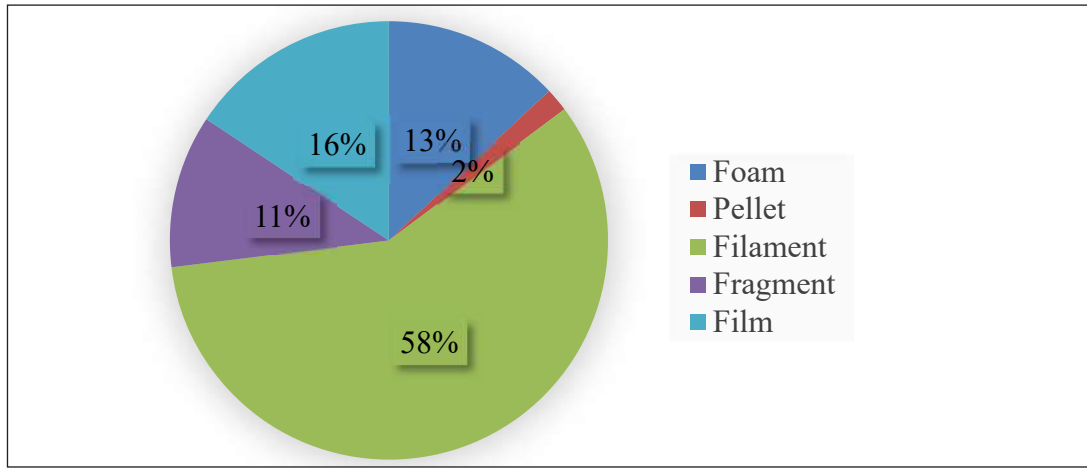


Fig. 5: Sediment microplastics characterization, composition and contribution of River Mpanga.

The study indicated a total microplastic of 115 particles per 10-L water sample in the river. Microplastic abundance increased from the upstream to the downstream section of the river. The total microplastic count was lowest at the river upstream (16), moderate at the river mid stream (33), and highest at the river downstream (66) (Fig. 3). The filament, form, and film types occurred across all sites, while the pellet and fragment foams were only recorded upstream and downstream. For all the three sites of the river studied, the most abundant microplastic was filaments (58%), followed by film (16%), foam (13%), fragments (11%), and pellets (2%). The filament type was represented more midstream and downstream (Fig. 4 & Fig. 5).

## DISCUSSION

The presence of arsenic above the maximum permissible levels by EPA and WHO poses serious potential health risks to the communities within the river vicinity. Arsenic exposures as low as 10ug/L have been linked to adverse health problems like cancer, neurological disorders, and skin lesions, whereas prolonged exposures result in genetic mutations (Lamm et al. 2021). Although arsenic has been recorded in other rivers (Liu et al. 2020) its concentrations are comparatively lower than in the River Mpanga case.

Elevated levels of arsenic could be due to deposition from agriculture through arsenic-containing agrochemicals, domestic sewage, arsenic laundry products, mining, and untreated effluent (Li et al. 2021). The activities evident in the Mpanga catchment near Fort Portal City included subsistence and commercial farming, untreated waste disposal, and commercial car washing. A higher water arsenic concentration at the river downstream site compared to the other sites could be attributed to likely contamination from adjacent tea plantations. Long-term use of agrochemicals like pesticides and fertilizers represents a significant anthropogenic factor contributing to the contamination of the environment with heavy metals (Kumari & Mishra 2021). In addition, river velocity of 0.47m/sec, 0.68 m/sec, and 1m/sec was recorded at the upstream, midstream and downstream, respectively. The relatively higher heavy metal concentration at the river downstream would be attributed to heavy metal resuspension attributed to the increasing velocity (Bao et al. 2023, Huang et al. 2012). On the other hand, the low concentration of copper and cadmium (below the permissible limit) in the water samples at all the sections of the river studied could be due to bioaccumulation in the sediments downstream.

The findings are in line with Astatkie et al. (2021), who indicated a reduction in heavy metal concentration in the Awetu watershed from upstream to downstream. This decrement of heavy metal in the downstream may be due to bioaccumulation, involving the adsorption of heavy metals into sediments and aquatic biota (Astatkie et al. 2021).

While arsenic contamination was above the background level in the river bed sediment, only the river upstream indicated copper contamination in the river sediment above the permissible level. Copper contamination in the water sediments could be attributed to the proximity of this river section to Mountain Rwenzori and the former Kilembe copper mines. Cases of environmental pollution arising from the Kilembe mines, even after its closure, have been reported widely in plants and the surrounding environment (Sarah et al. 2022). Additionally, the higher concentrations of the heavy metals in the sediments compared to water could be attributed to bioaccumulation, as evidenced by the high geoaccumulation values. River sediment contamination with arsenic has also been reported by Zhuang et al. (2018) but in lower concentrations compared to the Mpanga River.

The Igeo index of the Mpanga River sediment indicates moderate to very strong contamination with lead, copper, and arsenic. According to the classification of sediment pollution status based on the geoaccumulation index, Mpanga River falls within the scale of 3-4, which is an indicator of strong contamination and hence poor sediment quality (Goher et al. 2014, Wang et al. 2023). High accumulation of contaminants is a threat to the benthic biodiversity of the river, which may bioaccumulate and hence biomagnify them through trophic transfer and may eventually get into human food chains (Goher et al. 2014). They pose a potential health threat to the local communities because there is a likelihood of the heavy metals being reintroduced into the water column through geochemical cycles (Pierre & Karani 2016). Sediment heavy metal pollution in Ugandan rivers has also been reported by Baguma et al. (2022) and Sekabira (2010).

Overall, the contamination of the river could be attributed to the fact that the river is within the vicinity of garages, schools, markets, sewage plants, vehicle washing bays, and hospitals, which are likely to discharge heavy metal-laden waste into River Mpanga (Bentum et al. 2011, Singh et al. 2022).

Study findings indicated an accumulating trend of microplastics from the river upstream to the downstream. Like other parts of the country, Fort Portal City is characterized by heavy dependence on a diversity of plastic items. This is because plastic items, namely household utensils and packaging materials, are cheap, durable, and have good thermal and electrical insulation properties (Singh et al. 2022). Formerly a municipality, Fort Portal was elevated to a tourism city status in 2020, and this is likely to lead to increased urban contamination. Due to insufficient

solid waste management practices, a lot of plastic debris ends up in River Mpanga carried by wind, surface runoff after rain, or littering in water by the locals (Egessa et al. 2020).

Floating and deposited/trapped plastics are a common sight on the river. These macroplastics are broken down as the water moves downstream by natural processes like mechanical wear, weathering/aging, photolysis, hydrolysis, heat, and biological fragmentation into microplastics (Chen et al. 2023, Li et al. 2021). This probably accounts for the highest concentration of microplastics at the downstream Nyamigira site. The Kabundaire wastewater treatment plant could have also contributed to increased microplastic pollution because small microplastics like fibres may not be removed by treatment processes and thus end up in the effluent that enters the river (Liu et al. 2020). The microplastic load could also have formed from primary microplastics, which are manufactured intentionally for various domestic applications, like use in personal skin care products, toothpaste, etc. The foam, fibers, films, pellets, and fragments identified in this study were also reported by Singh et al. (2022). However, the foam, which is characterized by spherical or granular particles in River Mpanga, was absent in their study area.

Several studies have been conducted to assess the spatial variation, composition, and abundance of different types of MPs in different river systems (Li et al. 2021, Singh et al. 2022). The common finding is the dominant anthropogenic influence on the spatial distribution of microplastics, with higher concentrations in urban areas potentially due to factors such as poor waste management strategies. The predominance of fibers in water samples could be due to car washing and laundry (Gasperi et al. 2015). The occurrence of microplastics in all the sampling sites of the river concurs with the findings of Li et al. (2021). This poses a potential threat to the river ecosystem and the community because they are highly persistent, bioaccumulative, and toxic. Microplastic accumulation in aquatic organisms, especially fibers, has been reported in some aquatic organisms, including fish (Kumar & Khan 2020). They may ultimately enter humans through the food chain.

## CONCLUSION

Heavy metal analysis revealed alarming concentrations of arsenic in water and river sediments. For the river water samples, arsenic concentration was above the WHO and EPA permissible limits for all sections of the river studied. This poses a serious concern to health and the environment as arsenic is a known carcinogen capable of causing health problems. The overall geoaccumulation index of the river was in the range of 3-4, also classified under strong contamination of heavy metals in the river bed sediment. A couple of activities, namely plantation agriculture, laundry, and commercial car-washing, evidenced along the Mpanga River, may be contributing to heavy metal contamination in the river. Additionally, the elevation of Fort Portal to a tourism city status in 2020 is likely to lead to an increased population and number of tourists, resulting in increased waste generation and thus increased heavy metal and microplastics contamination of River Mpanga.

## RECOMMENDATIONS

Mpanga River is the main source of water for Fort Portal City. Besides its use by the National Water and Sewerage Cooperation of Fort Portal City, the river is also used directly by the communities within its vicinity without any prior treatment. This is a major concern, as the water is contaminated with heavy metals, microplastics, and other pollutants. The study recommends a stakeholder awareness campaign to educate the public about the contamination of the river water. In addition, the study recommends a thorough investigation of the possibility of the presence of heavy metals and microplastics in domestic piped water. The study also highlights the need to examine the influence of seasonality, precipitation, and flow rate on microplastic abundances.

Dumping of waste in the river is common. Activities observed on the river included commercial car wash, plantation agriculture and laundry. In addition, the river is in close proximity to Kabundaire Market, the Kabundaire Abattoir, and Buhinga Hospital, which are all likely to contribute to contaminated effluents in the river. The study recommends advocating for arsenic-free washing detergents and designating areas for commercial car wash. Additionally, the city council could put in place structures for solid and water waste management.

## ACKNOWLEDGEMENT

We appreciate the technical support of the staff at the National Fisheries Resources Research Institute for providing laboratory facilities and the technical support during laboratory analysis. Additionally, we are grateful to Mr Samuel Habimana and the entire Faculty of Science and Technology, Mountains of the Moon University staff, for the review and informative comments on the manuscript.

## REFERENCES

Aryampa, S., Maheshwari, B., Sabiiti, E., Bateganya, N. L. and Bukenya, B. 2019. Status of waste management in the East African cities: Understanding the drivers of waste generation, collection and disposal and their impacts on Kampala City's sustainability.

Sustainability (Switzerland), 11(19): 1-16. https://doi.org/10.3390/su11195523

Astatkie, H., Ambelu, A. and Mengistie, E. 2021. Contamination of stream sediment with heavy metals in the Awetu watershed of southwestern Ethiopia. Front. Earth Sci., 9: 658737.

Baguma, G., Musasizi, A., Twinomuhwezi, H., Gonzaga, A., Nakiguli, C. K., Onen, P., Angiro, C., Okwir, A., Opio, B., Otema, T., Ocira, D., Byaruhanga, I., Nirigiyimana, E. and Omara, T. 2022. Heavy Metal Contamination of Sediments from an Exoreic African Great Lakes' Shores (Port Bell, Lake Victoria), Uganda. Pollutants, 2(4): 407-421. https://doi.org/10.3390/pollutants2040027

Balali-Mood, M., Naseri, K., Tahergorabi, Z., Khazdair, M. R. and Sadeghi, M. 2021. Toxic Mechanisms of Five Heavy Metals: Mercury, Lead, Chromium, Cadmium, and Arsenic. Front. Pharmacol., 12(April): 1-19. https://doi.org/10.3389/fphar.2021.643972

Bao, T., Wang, P., Hu, B., Wang, X. and Qian, J. 2023. Mobilization of colloids during sediment resuspension and its effect on the release of heavy metals and dissolved organic matter. Sci. Total Environ., 861: 160678.

Basooma, A., Teunen, L., Semwanga, N. and Bervoets, L. 2021. Trace metal concentrations in the abiotic and biotic components of River Rwizi ecosystem in western Uganda, and the risks to human health. Heliyon, 7(11): e08327. https://doi.org/10.1016/j.heliyon.2021.e08327

Bentum, J. K., Anang, M., Boadu, K. O., Koranteng-Addo, E. J. and Owusu Antwi, E. 2011. Assessment of heavy metals pollution of sediments from Fosu lagoon in Ghana. Bull. Chem. Soc. Ethiop., 25(2): 191-196. https://doi.org/10.4314/bcse.v25i2.65869

Businge, F., Kagoya, S., Omara, T. and Angiro, C. 2021. Pollution of Mpanga River by Kabundaire Abattoir Effluents, Fort Portal Tourism City, Uganda. Asian J. Fish. Aquat. Res., 10: 34-43. https://doi.org/10.9734/ajfar/2021/v11i130195

Chen, Z., Shi, X., Zhang, J., Wu, L., Wei, W. and Ni, B. J. 2023. Nanoplastics are significantly different from microplastics in urban waters. Water Res. X, 19: 100169. https://doi.org/10.1016/j.wroa.2023.100169

Danopoulos, E., Twiddy, M. and Rotchell, J. M. 2020. Microplastic contamination of drinking water: A systematic review. PLoS ONE, 15(7): 1-23. https://doi.org/10.1371/journal.pone.0236838

Dick Vethaak, A. and Legler, J. 2021. Microplastics and human health: Knowledge gaps should be addressed to ascertain the health risks of microplastics. Science, 371(6530): 672-674.

Egessa, R., Nankabirwa, A., Ocaya, H. and Pabire, W. G. 2020. Microplastic pollution in surface water of Lake Victoria. Sci. Total Environ., 741: 140201. https://doi.org/10.1016/j.scitotenv.2020.140201

EPA, U. 1996. Method 3050B: Acid Digestion of Sediments. Sludges, and Soils.

Gasperi, J., Dris, R., Mandin, C. and Tassin, B. 2015. The first overview of microplastics in indoor and outdoor air. 15th EuCheMS International Conference on Chemistry and the Environment, 22-25 September 2015, Leipzig, Germany, The Royal Society of Chemistry, UK, pp. 2-4.

Goher, M. E., Farhat, H. I., Abdo, M. H. and Salem, S. G. 2014. Metal pollution assessment in the surface sediment of Lake Nasser, Egypt. Egypt. J. Aquat. Res., 40(3): 213-224. https://doi.org/10.1016/j.ejar.2014.09.004

Huang, J., Ge, X., Yang, X., Zheng, B. and Wang, D. 2012. Remobilization of heavy metals during the resuspension of Liangshui River sediments using an annular flume. Chin. Sci. Bull., 57(27): 3567-3572. https://doi.org/10.1007/s11434-012-5370-1

Issac, M. N. and Kandasubramanian, B. 2021. Effect of microplastics in water and aquatic systems. Environ. Sci. Pollut. Res., 28(16): 19544-19562. https://doi.org/10.1007/s11356-021-13184-2

Jonas, M. and Atukunda Kirungyi, P. 2020. Creation of new cities in Uganda. Environment, 49: 1-11.

Kannan, K. and Vimalkumar, K. 2021. A Review of Human Exposure to Microplastics and Insights Into Microplastics as Obesogens. Front. Endocrinol., 12(August): 1-19. https://doi.org/10.3389/fendo.2021.724989

Korajkic, A., McMinn, B. R. and Harwood, V. J. 2018. Relationships between microbial indicators and pathogens in recreational water settings. Int. J. Environ. Res. Public Health, 15(12): 1-39. https://doi.org/10.3390/ijerph15122842

Kumar, D. and Khan, E. A. 2020. Remediation and detection techniques for heavy metals in the environment. Environ. Impact Assess. Remed., 12: 122-130. https://doi.org/10.1016/B978-0-12-821656-9.00012-2

Kumar, P., Sharma, N., Sharma, S. and Gupta, R. 2020. Rhizosphere stochiometry, fruit yield, quality attributes and growth response to PGPR transplant amendments in strawberry (Fragaria × ananassa Duch.) growing on solarized soils. Sci. Hortic., 265(3): 109215. https://doi.org/10.1016/j.scienta.2020.109215

Kumari, S. and Mishra, A. 2021. Heavy metal Contamination. IntechOpen, UK.

Lamm, S. H., Boroje, I. J., Ferdosi, H. and Ahn, J. 2021. A review of low-dose arsenic risks and human cancers. Toxicology, 456(March): 152768. https://doi.org/10.1016/j.tox.2021.152768

Li, Y., Bi, Y., Mi, W., Xie, S. and Ji, L. 2021. Land-use change caused by anthropogenic activities increases fluoride and arsenic pollution in groundwater and human health risks. J. Hazard. Mater., 406: 124337. https://doi.org/10.1016/j.jhazmat.2020.124337

Liu, Y., Zhang, J., Cai, C., He, Y., Chen, L., Xiong, X., Huang, H., Tao, S. and Liu, W. 2020. Occurrence and characteristics of microplastics in the Haihe River: An investigation of a seagoing river flowing through a megacity in northern China. Environ. Pollut., 262: 114261. https://doi.org/10.1016/j.envpol.2020.114261

Masura, J., Baker, J., Foster, G. and Arthur, C. 2015. Laboratory methods for the analysis of microplastics in the marine environment: Synth. Part., 32: 1076

Müller, L. 1969. Fundamentals of Rock Mechanics. International Centre for Mechanical Sciences.

Onyutha, C., Turyahabwe, C. and Kaweesa, P. 2021. Impacts of climate variability and changing land use/land cover on River Mpanga flows in Uganda, East Africa. Environ. Chall., 5: 273 https://doi.org/10.1016/j.envc.2021.100273

Pierre, F. and Karani, W. S. S. 2016. Assessment of the Environment Pollution and its Impact on Economic Cooperation and Integration Initiatives of the IGAD Region, Regional The European Union's EDF Programme Eastern, Southern Africa and the Indian Ocean Framework Contract Beneficiaries 2. CONSORTIUM SAFEGE FWC-Lot6 Executive, February: 1-35. https://doi.org/10.13140/RG.2.1.2830.2480

Sarah, N., Abraham, R. M. and Esther, K. 2022. Essential and potentially toxic trace elements in selected antimalarial plants: A pilot study in Kilembe copper mine catchment, Kasese District, Uganda. Afr. J. Environ. Sci. Technol., 16(10): 355-362. https://doi.org/10.5897/ajest2022.3130

Sekabira, K., Origa, H. O., Basamba, T. A., Mutumba, G. and Kakudidi, E. 2010. Assessment of heavy metal pollution in the urban stream sediments and its tributaries. Int. J. Environ. Sci. Tech., 7: 435-446.

Singh, A., Sharma, A., Verma, R. K., Chopade, R. L., Pandit, P. P., Nagar, V., Aseri, V., Choudhary, S. K., Awasthi, G., Awasthi, K. K. and Sankhla, M. S. 2022. Heavy Metal contamination of water and their toxic effect on living organisms. Toxicity Environ. Pollut., 10: 507-515.

Vasanthi, P., Kaliappan, S. and Srinivasaraghavan, R. 2008. Impact of poor solid waste management on groundwater. Environ. Monit. Assess., 143(1-3): 227-238. https://doi.org/10.1007/s10661-007-9971-0

Vaughan, R., Turner, S. D. and Rose, N. L. 2017. Microplastics in the sediments of a UK urban lake. Environ. Pollut., 229: 10-18. https://doi.org/10.1016/j.envpol.2017.05.057

Vera Candioti, M. F., Nuñez, J. J. and Úbeda, C. 2011. Development of the nidicolous tadpoles of *Eupsophus emiliopugini* (Anura: Cycloramphidae) until metamorphosis, with comments on systematic

relationships of the species and its endotrophic developmental mode. Acta Zool., 92(1): 27-45. https://doi.org/10.1111/j.1463-6395.2010.00448.x

Wang, W., Wu, F., Yin, T., Jiang, S., and Tang, S. 2023. Distribution source and contamination assessment of heavy metals in surface sediments of the Zhifu Bay in nothern China. Marine Pollution Bulletin, 194: 115449.

Wu, W., Du, K., Kang, X. and Wei, H. 2021. The diverse roles of cytokinins in regulating leaf development. Hortic. Res., 8(1): 558. https://doi.org/10.1038/s41438-021-00558-3orld Health Organisation (WHO) 1998. Report on 33rd meeting, Joint FAO/ WHO Joint Expert Committee on Food Additives, Toxicological evaluation of certain food additives and contaminants No.24, International Programme on Chemical Safety, WHO, Geneva.

Yusuf, A. A., Peter, O., Hassan, A. S., Tunji, L. A., Oyagbola, I. A., Mustafa, M. M. and Yusuf, D. A. 2019. Municipality solid waste management system for Mukono District, Uganda. Procedia Manuf., 35: 613-622. https://doi.org/10.1016/j.promfg.2019.06.003

Zhao, S., Zhu, L. and Li, D. 2015. Microplastic in three urban estuaries, China. Environ. Pollut., 206: 597-604. https://doi.org/10.1016/j.envpol.2015.08.027

Zhuang, Q., Li, G. and Liu, Z. 2018. Distribution, source, and pollution level of heavy metals in river sediments from South China. CATENA, 170: 386-396. https://doi.org/10.1016/j.catena.2018.06.037

Nature Environment and Pollution Technology
An International Quarterly Scientific Journal

p-ISSN: 0972-6268
(Print copies up to 2016)
e-ISSN: 2395-3454

Vol. 23 | No. 3 | pp. 1559-1568 | 2024

Original Research Paper

https://doi.org/10.46488/NEPT.2024.v23i03.025

Open Access Journal

# Estimation of Surface and Groundwater Interaction by Stable Isotopic Techniques – A Case Study of Chengalpattu District, OMR Region

**Surendar Natarajan**
Sri Sivasubramaniya Nadar College of Engineering (SSN CE), Department of Civil Engineering, Kalavakkam-603110, Tamil Nadu India
†Corresponding author: Surendar Natarajan; surendarn@ssn.edu.in, surendarnatarajan86@gmail.com

**Nat. Env. & Poll. Tech.**
**Website: www.neptjournal.com**

*Received:* 10-01-2024
*Revised:* 13-02-2024
*Accepted:* 14-02-2024

**Key Words:**
Stable isotopes
OMR region
GMWL
LMWL
Surface-groundwater interaction

## ABSTRACT

Isotopes are atoms of an element having the same atomic number but different mass numbers. Isotopes in hydrology and water resources are used for identifying its occurrence, movement, residence times, recharge, and discharge process. Stable isotopes of hydrogen($\delta^2H$) and oxygen($\delta^2O$) are used for identifying the surface and groundwater interactions as they constitute hydrogen and oxygen. In this study oxygen and hydrogen stable isotopes are used to identify surface and groundwater interaction in Old Mahabalipuram Road (OMR) regions of Chengalpattu district. The precipitation, lake, surface, and groundwater were collected during pre-monsoon, monsoon, and post-monsoon seasons. The collected sample is analyzed for stable isotopic compositions of oxygen and hydrogen seasonal-wise. The measured stable isotopic compositions during pre-monsoon season of stable oxygen are -4.29 to -2.00 and stable hydrogen are -29.39 to -24.67. The isotopic compositions during monsoon season range from -4.72 to -4.00 and for hydrogen ranges from -29.39 to -23.50. During monsoon season the depletion of isotopic composition is seen and the enrichment of isotopic composition is observed during pre-monsoon season. The variation in stable isotopic composition of oxygen and hydrogen are observed. A Groundwater Water Meteoric Water Line (GMWL) is developed for the study area, and it is compared with a Local Meteoric Water Line (LMWL) for better interpretation of the results. A slight deviation is observed from that of GMWL to LMWL mostly due to isotopic depletion and evaporation effects. From the analysis, a good correlation exists between precipitation and surface water in the study area indicating about recharge mechanism existing in the study area. The groundwater recharge is observed during monsoon seasons and discharge is more towards the pre-monsoon seasons.

## INTRODUCTION

The most crucial problem these days in the world is water scarcity due to population and economic growth. So, it necessitates identifying the water resources, their origin movement, and recharge processes (Greve et al. 2018, Herrera-Franco et al. 2020). The surface and groundwater resources interactions are necessary to study the hydrological cycle and water budget in a watershed (Sophocleous 2002). Knowledge of finding water path, movement, origin, distribution, surface, and groundwater interaction will give a clear knowledge of existing water resources (Esam Ismail et al. 2022). The utilization of excess surface water and groundwater pumping will influence the surface and groundwater interaction in the form of recharge and discharge. The excessive utilization of these water resources leads to a decline in water quality (Chen et al. 2007). The extensive irrigation and industrial activities also decrease the surface and groundwater in arid and semi-arid regions spatially. This extensive use in turn affects the water resources and its effects are seen in the ecological systems. The surface and groundwater interaction not only affects the quantity but also the quality (Zhang et al. 2016).

In some places, sewage water and artificial recharge pollute the surface and groundwater. Excess water utilization, pollution, and continuous irrigation will have an impact on surface and groundwater. This excess water usage necessitates identifying new water resources for better water management. The surface and groundwater interaction can be estimated by various methods like numerical modeling (Ala-aho et al. 2015), seepage meters (Ala-aho et al. 2013), environmental tracers (Wright & Novakowski 2019) or by integrating any of these methods.

In recent times environmentally stable isotopic techniques have been used for identifying water origin, movement, climate change, surface, and groundwater interaction (Jassas & Merkel 2015, Dar et al. 2021, Krishan et al. 2022, Boosalik

et al. 2022). Stable oxygen and hydrogen are water-containing stable isotopes($\delta^{18}O$, $\delta^{2}H$) that show spatial and temporal variations due to the isotope fractionation which makes changes in the water cycle and its diffusion stages (Gibson et al. 2005). Stable isotopes use the tracing principle, which transforms the relationship between surface and groundwater. Various isotopic studies were done by researchers globally and nationally to identify the water resources. In Tianshan Mountain, the relationship between climatic conditions and water resources is studied on a large scale by stable isotopes (Fan et al. 2022). In North-Central Chile, Grande River basin the isotopic composition in surface and groundwater interactions are studied by Ricardo Oyarzún et al. 2016. The unique gradient is developed for each parameter if there exists a surface and groundwater interaction (Gardner 1999). In Northern Finland, in glaciofluvial aquifers large data sets of stable isotopes are used for determining contamination due to land use. They also found that shallow groundwaters are also susceptible to contamination (Yapiyev et al. 2023). The changes in surface and groundwater interaction by using stable isotopes of oxygen $\delta^{18}O$ and $\delta^{2}H$ hydrogen were studied in Xiong a new area by Zhu et al. 2019. The factors affecting the stable isotopes in precipitation with respect to surface and groundwater recharge process in the Shwan sub-basin northeast, Iraq were studied by adopting stable oxygen and hydrogen (Al-Gburi et al. 2022). At the Indian level, the limited isotopic studies were studied as discussed. In Yamuna River, the surface and groundwater interactions were identified by stable isotopic techniques and developed an LMWL (Krishan et al. 2017). For identifying the water resources and aquifer dynamics in Gangetic basins stable isotopes of ($\delta^{2}H$, $\delta^{18}O$) and $\delta^{13}C_{TIC}$ were the tools used (Manoj Kumar et al. 2019).

## Motivation of the Study

The excess utilization of surface and groundwater in OMR regions in Chengalpattu district threatens the existing water resources in this region. So, it necessitates to study of the surface and groundwater interaction by stable isotopic techniques. Urbanization and IT industries, cause more settlements in the OMR region making more surface and groundwater utilization. This enhances to identification of the surface and groundwater resources and their interactions in the study area for better management of existing water resources. Based upon the existing condition in the study area the objectives of the study are framed accordingly.

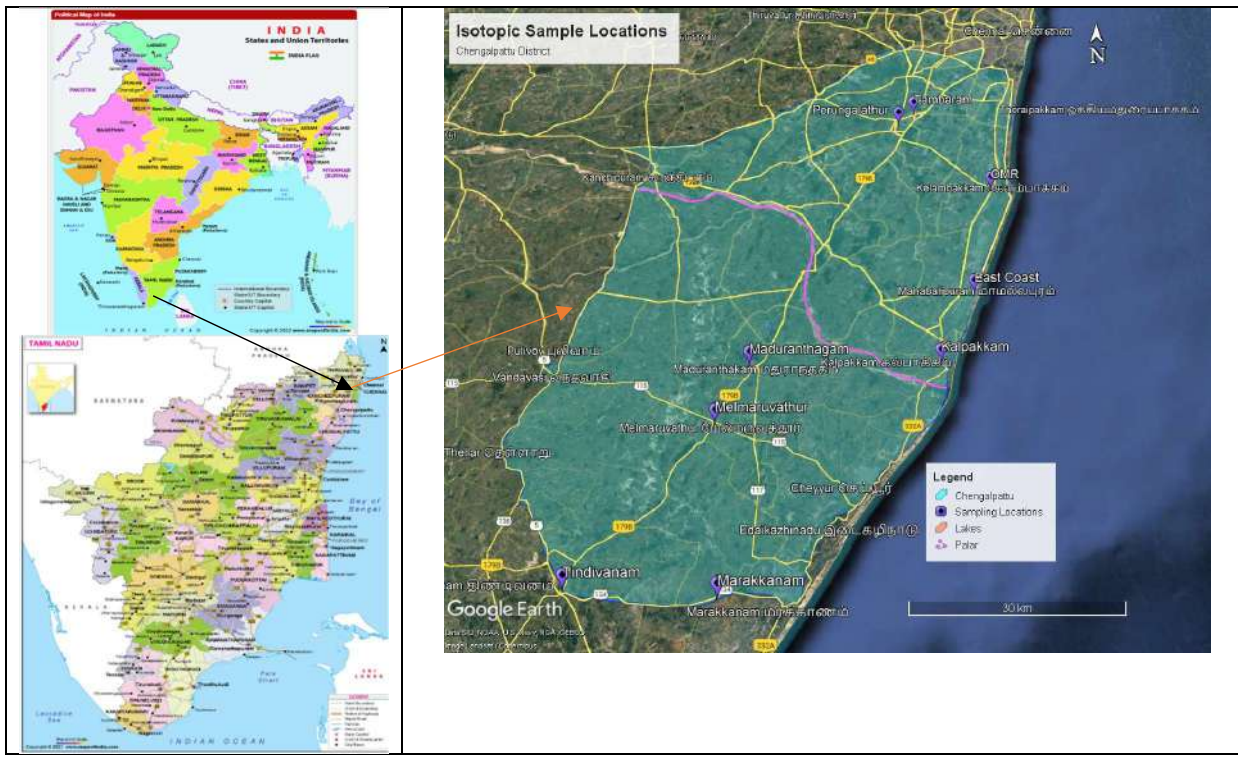


(Source -Map of India)

Fig. 1: Study area - OMR and its selected areas, India and Tamil Nadu Map.

### Objectives of the Study

- To study isotopic compositions in precipitations for various seasons in the study area.
- To identify the surface and groundwater interaction, recharge resources in the OMR region.
- To recommend suitable water harvesting structures in the study area.

## MATERIALS AND METHODS

### Study Area

Chengalpattu district is known as the lake district bounded by north to Chennai city, to the west by Kanchipuram district as shown in Fig.1

The southern part of the district is surrounded by Villupuram and Tiruvannamalai district. The northeast part of the district is surrounded by the east coast and the coastal line of the district extends up to 57 km. The study area experiences tropical wet and dry climates. The average annual rainfall of the district is 1400 mm and most of the rainfall is received during the Northeast monsoon season. In this study, the east coast part of Chengalpattu district is concentrated as most of the developmental activities are happening around the Old Mahabalipuram Road (OMR) region. The major river that flows through the district is Palar. The few residual hills like St. Thomas Mount, Thirukalukundram, and Vandalur are found in the district. The granite, gneiss, sandstone, and marine deposits are found throughout the district.

### Methodology

The methodology adopted for the present study is shown in Fig. 2. The methodology involves data collection, analysis, and discussions as explained in.

### Data Collection

The data involved in the study are a collection of spatial and temporal data. The spatial data includes the satellite images collected from the USGS website. The temporal data used are precipitation, surface water, and well water samples that are collected seasonally like pre-monsoon, monsoon, and post-

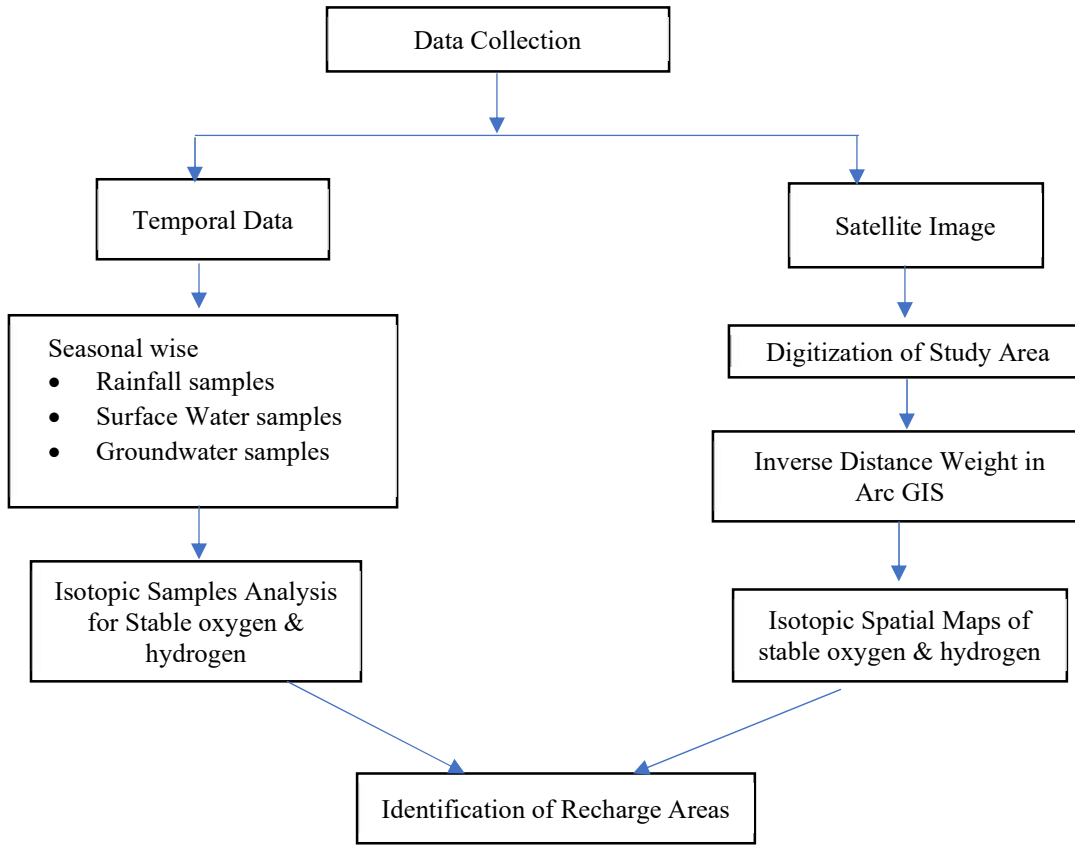


Fig. 2: Proposed methodology of the study.


Fig. 3: Collecting water samples-Thiruporur lake.

monsoon seasons. The collected water samples were analyzed in a continuous stable isotopic mass spectrometer and dual spectrometer at the Centre for Water Resources Development Management (CWRDM) Kozhikode. The limited number of precipitation and surface water samples are collected during the pre-monsoon season due to its availability.

### Stable Oxygen and Hydrogen Isotopic Analysis

The precipitation, lake water, and well water samples were collected at selected locations in the OMR region namely Kelambakkam, Thaiyur, and Illalore during the pre-monsoon, monsoon, and post-monsoon seasons as shown in Fig. 3. The water samples were collected in 60 mL High-Density Polyethylene (HDPE) bottles for identifying stable oxygen and hydrogen isotopes as shown in Fig. 3. For $\delta^2H$ analysis 1 mL of water sample was kept in equilibrium condition and mixed with hydrogen gas at 50°C with $P_t$ catalyst for 1 h. The mixed hydrogen gas was introduced into the mass spectrometer for stable hydrogen analysis. Similarly, for measuring stable oxygen 1 mL of water is kept at equilibrium condition along with carbon-di-oxide gas at 50°C for 8 hours. Then the gas kept at equilibrium condition was introduced into the mass spectrometer for stable oxygen analysis. The result analysis is reported in δ notation as the deviations are related to standard, V-SMOW (Vienna-Standard Mean Ocean Water) in units of parts per thousand (denoted as ‰). The δ values are calculated by Equation (1) given below.

$$\delta\% = \left(\frac{Rx}{Rs} - 1\right) \times 1000 \quad \ldots(1)$$

Here R denotes the ratio of heavy to light isotope. $R_x$ and $R_s$ are the ratios in the sample and standards respectively. The precision of measurement for $\delta^2H$ is ± 0.5 ‰ and $\delta^{18}O$ is ± 0.1‰.

## RESULTS AND DISCUSSION

### Stable Isotopes in Water Samples

The obtained isotopic analysis for the OMR region is shown in Table 1 which projects the latitude and longitude details as well as the volume of samples used for analyzing isotopic signatures. Limited surface and rainwater samples are collected due to lack of rainfall. The Local Meteoric Water Line (LMWL) is compared with the existing LMWL of the nearby region. The deviation of LMWL with nearby regions gives the isotopic pattern distributions. There is also a seasonal variation of isotopic compositions observed during the study period. Throughout the pre-monsoon season analysis, the average spatial isotopic signatures of oxygen and hydrogen in the lake water are from -2.9 to -21.7, and for the well water, it ranges between -2.57 to -25.8. A depletion of stable isotopes was also seen in the samples collected during the monsoon season. The oxygen and hydrogen isotopes in the well water samples during the monsoon season range from -3.5 to -25.2. Similarly, in the wells, the stable isotopic compositions of oxygen and hydrogen are between -2.6 to -22.7.

In the case of post-monsoon season, a difference in isotopic compositions is observed in the well as well as the lake water. The average isotopic composition in the

Table 1: Isotopes in water samples-pre-monsoon season.

| Sample | Latitude | Longitude | $\delta^{18}O$ | $\delta^{2}H$ | Source of sample | Volume/ quantity of sample supplied(mL/mg) |
|---|---|---|---|---|---|---|
| Taiyur Well -1 | 12.75 | 80.219 | -3.1 | -21.7 | Well water | 60 mL/mg |
| Tirupur tank Water-1 | 12.76 | 80.22 | -2.9 | -20.9 | Lake water | 60 mL/mg |
| Well, no-3 | 12.77 | 80.201 | -2.7 | -18.1 | Well water | 60 mL/mg |
| Well, no -9 | 12.78 | 80.184 | -3.3 | -20.3 | Well water | 60 mL/mg |
| Well-10 | 12.79 | 80.16 | -3 | -21.1 | Well water | 60 mL/mg |
| Well-12 | 12.80 | 80.139 | -4.3 | -25.8 | Well water | 60 mL/mg |
| Precipitation | - | - | - | - | | |

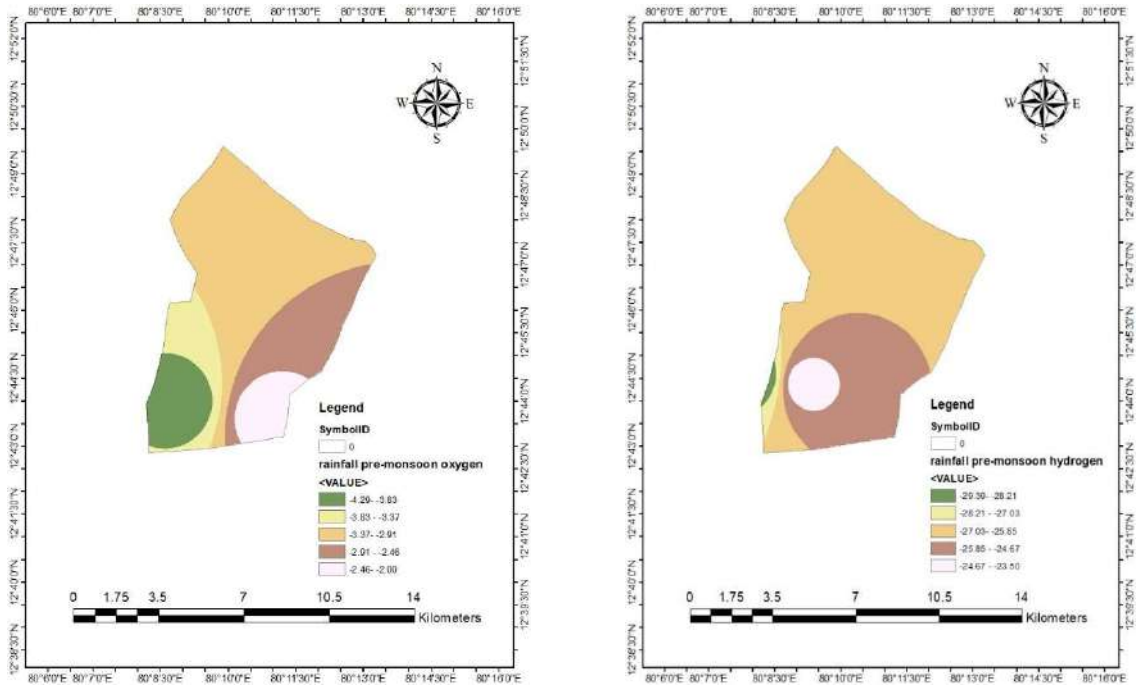


Fig. 4: Stable isotopic composition of rainfall (a) oxygen &(b) hydrogen-post-monsoon season.

well water samples ranges from -3.3 to -21.8. The spatial distribution of stable oxygen and hydrogen isotopic composition in precipitation during monsoon season is created through the Inverse Distance Weight (IDW) method in Arc-GIS as shown in Fig. 4.

The isotopic composition in any region is governed by the water vapor transport process and the moisture air masses present in the precipitation. The observed enrichment and depletion of isotopic composition is due to the coastal influence and evaporation effects that exist in the study area. From the analysis of stable oxygen and hydrogen, the LMWL is developed for the study area. A linear equation of isotopic composition is developed for the study area as given below in equation (2)

$$\delta^{2} H = 8\,\delta^{18}O + 35 \quad \ldots(2)$$

The developed LMWL is compared to the Ground Water Meteoric line and Surface Water Meteoric line. The meteoric water lines show a slighter deviation from the LMWL that indicates a fall in precipitation and has undergone slighter evaporation. The reason for the lower slope of the meteoric water line is due to variations in climatic conditions. The climatic variations can be identified through Deuterium excess which is used for characterizing the origin of water vapor from the precipitation. The developed Deuterium excess is given in equation (3). The d-excess values for the study area range from (+-5%).

$$d - excess\ (\%) = \delta^{2}H - 8xd^{18}O \quad \ldots(3)$$

If there exists a low d-excess in precipitation it reflects the slower evaporation due to high humidity that prevails in the OMR region. If less humidity means, there exists a high

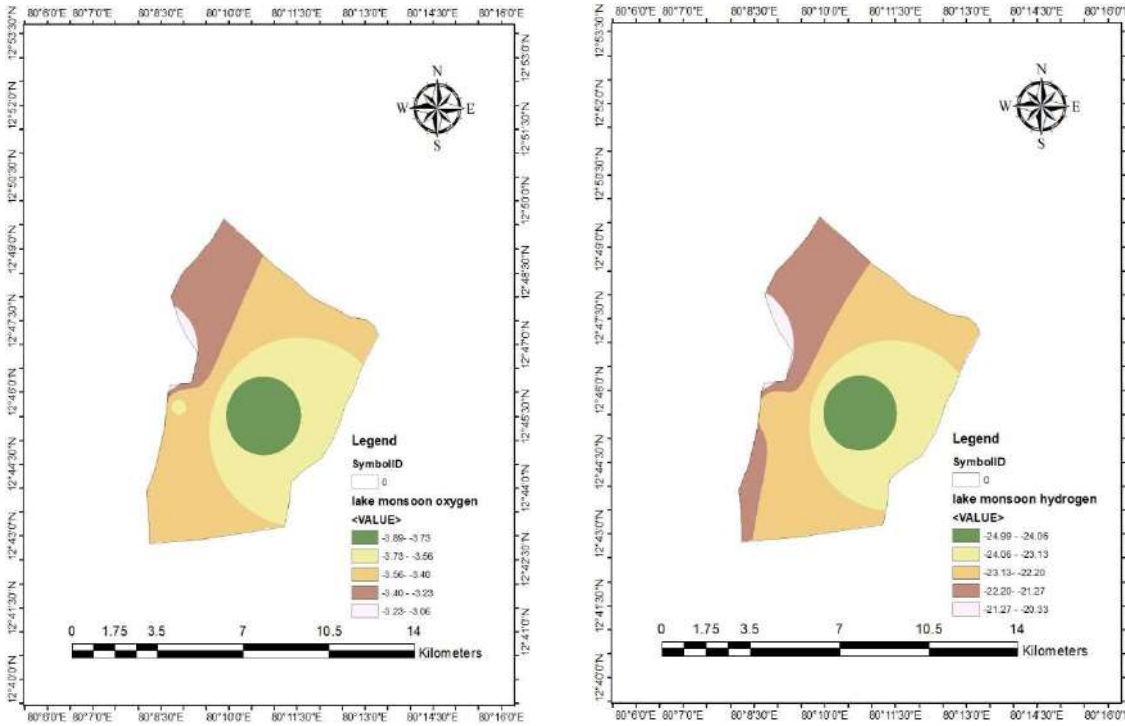


Fig. 5: Stable isotopic composition in Lake water (a) oxygen (b) hydrogen monsoon season.

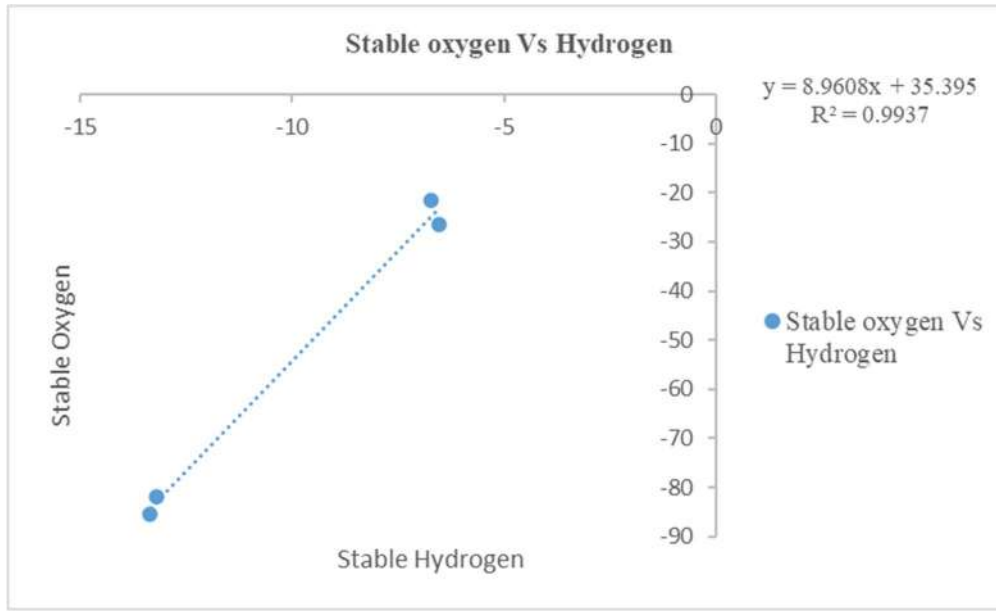


Fig. 6: Derived relation between $\delta^{18}O$ and $\delta^{2}H$ in rainfall.

evaporation. The spatial variation of isotopic composition in lake water during the various seasons is shown in Fig. 5.

The monsoon season for the OMR region usually starts from the Southwest and ends in the Northeast monsoon season. The southwest monsoon season contributes only 10% of the rainfall of annual precipitation. The remaining 90% of rainfall is received during the Northeast monsoon seasons. The source of precipitation during the Northeast Monsoon

season is from the Bay of Bengal due to cyclonic depressions. The weighted stable isotopic compositions during Northeast monsoon ranges from -2.6% to -17.6% with d excess value of 8± to 0.5±. The contribution of rainfall during the southwest monsoon is less and enrichment of isotopic composition is observed in the rainfall. Since the rainfall process of the southwest monsoon is from the Arabian Sea and the Indian Ocean.

The general reasons for stable isotope enrichment and depletion are due to the seasonal reversal of temperature and pressure gradients and its associated wind circulation patterns. If a negative correlation exists between $\delta^{18}O$ it will result in heavy rainfall, and it is termed an amount effect. The derived relationship between $\delta^{18}O$ and $\delta^{2}H$ in the rainfall is shown in Fig. 6. From the analysis it is observed that some samples show a good correlation of isotopic composition of rainfall collected during the northeast monsoon season. The best-fit line equation generated between the stable oxygen and hydrogen is given below. The average rate of depletion of stable isotopes is found to be –6 % to -80%.

**Isotopic Compositions in Surface and Groundwater**

The lake water samples collected during post-monsoon seasons show maximum enrichment of stable oxygen and hydrogen isotopes with an average of -3.5% to -22.5%. The rainfall samples of the post-monsoon season were not collected because of non-occurrence of rainfall. The mean stable oxygen and hydrogen isotopes of groundwater samples analyzed for post-monsoon season range from -3.48 % and -22.57%. The variations of stable isotopes are observed in surface and groundwater samples during the post-monsoon seasonal analysis. This shows that there is a contribution of surface water to groundwater in the post-monsoon season. The derived distribution of stable oxygen and hydrogen isotopes in the water samples is shown in Fig. 7. The best-fit line of post-monsoon seasons of isotopic samples for surface water samples is given by equation (4). From the analysis, it is observed that the meteoric water line deviates from LMWL and has a lower slope indicating an existence of evaporation in the surface water during pre-monsoon season. There is not much deviation observed in the best-fit line during the monsoon season which indicates groundwater recharge that is happening from the surface water. This shows that the lake water, groundwater, and rainfall have the same meteoric origin and isotopic composition despite the evaporation. The deviation of the slope is lesser when there occurs a mixing of surface and groundwater, and a difficult process to differentiate between these two mixing processes. For a better understanding of the recharge process between surface and groundwater, it is necessary to assess the enrichment and depletion of stable isotopes.

$$\delta^2 H = 3\,\delta^{18}O - 4 \qquad \ldots(4)$$

**Identification of Surface and Groundwater Interaction**

The mixing model is used to estimate the recharge between precipitation, surface, and groundwater. The assumptions

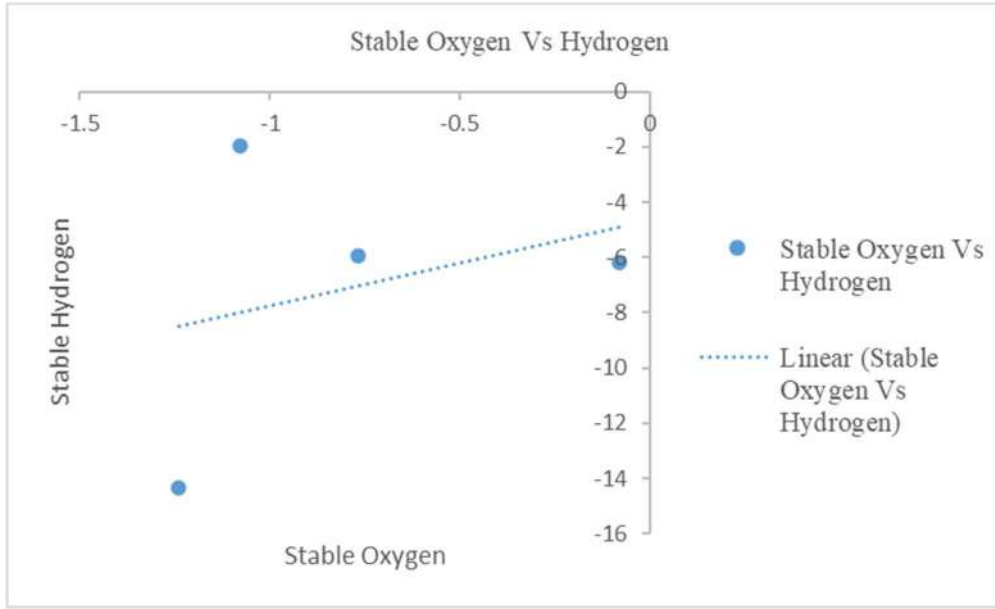


Fig. 7: Distribution of stable $\delta^{18}O$ and $\delta^{2}H$ in Lake water.

made in this model are that both surface and groundwater should have the same isotopic composition and mix conservatively. The percentage of recharge from surface to groundwater is estimated from the equation (5) and (6).

$$X\% = \frac{(\delta^{18}O_g - \delta^{18}O_p)}{(\delta^{18}O_{sl} - \delta^{18}O_p)} 100 \quad \ldots(5)$$

$$\delta^2 H = 1.6\, \delta^{18}O - 13.4 \quad \ldots(6)$$

Where $\delta^{18}O_g$, $\delta_{18}O_p$, and $\delta_{18}O_{st}$ represent $\delta_{18}O$ of groundwater, precipitation, recharged groundwater, and surface water from lake recharge water respectively. The average of $\delta_{18}O_{sl}$ for surface water and $\delta_{18}O_p$ is taken for the mixing model calculation to identify the influences of surface water on the groundwater. Slight evaporation is seen during the recharge process since more humidity is seen in the study area. The surface and groundwater relation in the form of a best-fit line is shown in Fig. 8. The surface and groundwater mixing happens in the study area as a process of recharge which is inferred through stable oxygen and hydrogen isotope variations. In some places there is less contribution from surface water to groundwater is also observed because of the higher electrical conductivity. If the groundwater is brackish then exists a higher electrical conductivity. The less electrical conductivity indicates a process of recharging.

The analysis of isotopic enrichment and depletion in the mixing model indicates there exists an interaction between rainfall, surface water, and groundwater. The percentage of recharge from surface water to groundwater is around 30%. The recharge percentage from lake to well water depends upon the distance from the lake and the existing geological conditions in OMR regions. Further enhancing the water recharging process, it is also recommended to rehabilitate the existing lakes in the study area.

## CONCLUSIONS

In this study, the environmentally stable isotopes are applied to identify the surface and groundwater recharge in OMR regions of Chengalpattu district. Initially, the isotopic characteristics in rainfall, lake water, and well water samples were analyzed season-wise. The variations of isotopic signatures were observed in collected water samples. The enrichment of stable oxygen and hydrogen isotopes is observed during the pre-monsoon season and the depletion of isotopic composition is observed during the post-monsoon season. The average enrichment of isotopic composition in surface water ranges from -3.48 to -21.92. The isotopic composition in the rainfall during the post-monsoon season shows an enrichment of isotopic composition. This is due to the southwest monsoon season as its moisture originates from the Arabian Sea and Indian Ocean. The southwest monsoon rainfall contribution from surface to groundwater recharge is less when compared to the Northeast monsoon season. The depletion of isotopic composition is observed during the monsoon season. During the Northeast monsoon season, the moisture for rainfall originates from the Bay of Bengal which brings more rainfall and depletes isotopic composition in the study area. There exists a strong correlation between stable isotopic composition of the precipitation during

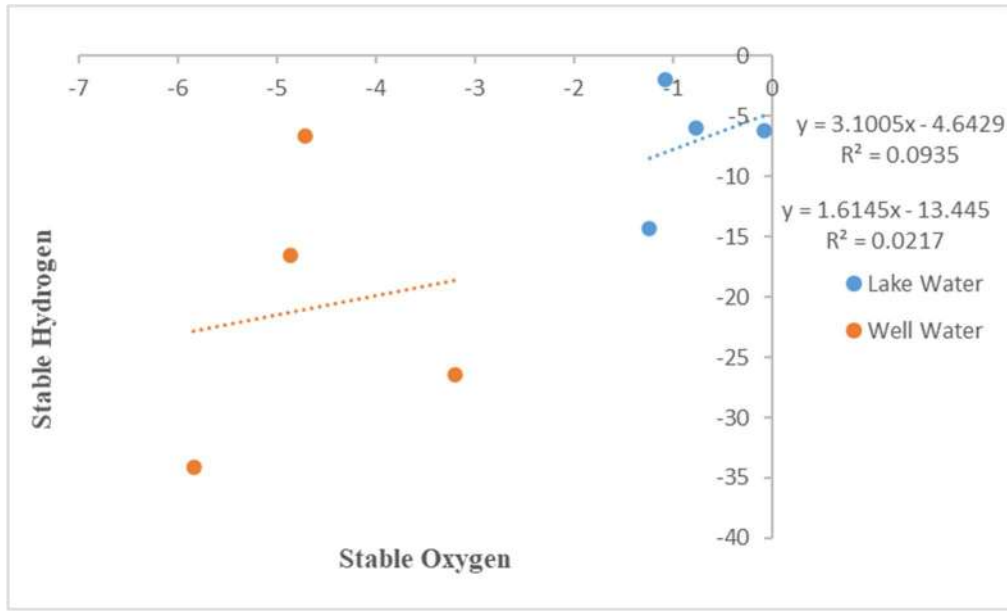


Fig. 8: Surface and groundwater interaction (a) pre-monsoon season.

Northeast monsoon season which indicates the recharge is from rainfall to groundwater. The inferences observed from the study are discussed below.

**Inferences from the Study**

- The analyzed isotopic data indicates two sources of groundwater recharge, one is directly from precipitation and the other one is from the nearby lakes.
- The observed isotopic compositions show that groundwater recharge mostly occurs during North-East monsoon season.
- The lower slope of the GWML line indicates the existence of evaporation in the study area.

**Future Scope of the Study**

- The climatic conditions during enrichment and depletions of isotopic studies should be studied.
- The origination of precipitation and its moisture content should be studied through stable isotopic composition.
- The more precipitation, surface and groundwater samples should be collected spatially for more years.
- The irrigation return flow of the study area should also be considered.
- For better estimation of surface and groundwater interaction, an integrated approach like an electrical resistivity survey should be done for identifying groundwater potential zones.

## ACKNOWLEDGMENTS

This work was done through the Internal Faculty Funded Project (IFFP-2021) sponsored by SSN Trust. The author extends thanks to CWRDM Calicut for isotopes analysis and the USGS website for providing satellite data free of cost. The author also extends thanks to the reviewers for reviewing the manuscript.

## REFERENCES

Ala-aho, P., Rossi, P. M. and Kløve, B. 2015. Estimation of temporal and spatial variations in groundwater recharge in unconfined sand aquifers using Scots pine inventories. Hydrol. Earth Syst. Sci., 19(4): 1961-1976. https://doi.org/10.5194/hess-19-1961-2015

Ala-aho, P., Rossi, P. M. and Kløve, B. 2013. Interaction of esker groundwater with headwater lakes and streams. J. Hydrol., 500: 144-156. https://doi.org/10.1016/J.JHYDROL.2013.07.014

Boosalik, Z., Jafari, H., Clark, I. D. and Bagheri, R. 2022. Chemo-isotopic tracing of the groundwater salinity in arid regions: An example of Shahrood aquifer (Iran). J. Geochem. Explor., 239: 107029.

Chen, Y., Li, J., Chen, W.-H., Chen, Y.-I., Liu, J.Z. and He, B. 2007. Ecological effect of synthesized governing in Tarim River valley. China Environ. Sci., 27: 24-28.

Dar, F. A., Jeelani, G., Perrin, J. and Ahmed, S. 2021. Groundwater recharge in semi-arid karst context using chloride and stable water isotopes. Groundw. Sustain. Dev., 14: 100634. doi:10.1016/j.gsd.2021.100634.

Ismail, E., Abdelhalim, A., Ali, A., Ahmed, M. S., Scholger, R. and Khalil, M. M. 2022. Isotopic, geophysical, and hydrogeochemical investigations of groundwater in west middle upper Egypt. ACS Omega. https://doi.org/10.1021/acsomega.2c05387

Fan, Y., Wu, Y., Wang, Y., Jiang, S., Yu, S. and Shang, H. 2022. An analysis of surface water–groundwater interactions based on isotopic data from the Kaidu River Basin, South Tianshan Mountain. Water, 14: 2259. https://doi.org/10.3390/w14142259

Gardner, K. M. 1999. The importance of surface water groundwater interactions. Issue paper; Environmental Protection Agency, Seattle.

Gibson, J. J., Edwards, T. W. D., Birks, S. J., St Amour, N. A., Buhay, W. M., McEachern, P., Wolfe, B. B. and Peters, D. L. 2005. Progress in isotope tracer hydrology in Canada. Hydrol. Process, 19: 303-327.

Krishan, G., Singh, S., Sharma, A., Sandhu, C., Kumar, S., Kumar, C. P. and Gurjar, S. 2017. Assessment of river Yamuna and groundwater interaction using isotopes in Agra and Mathura area of Uttar Pradesh, India. Int. J. Hydro., 1(3): 86-89.

Greve, P., Kahil, T., Mochizuki, J., Schinko, T., Satoh, Y., Burek, P., Fischer, G., Tramberend, S., Burtscher, R. and Langan, S. 2018. Global assessment of water challenges under uncertainty in water scarcity projections. Nat. Sustain., 1: 486-494.

Herrera-Franco, G., Carrión-Mero, P., Aguilar-Aguilar, M., Morante-Carballo, F., Jaya-Montalvo, M. and Morillo-Balsera, M. C. C. 2020. Groundwater resilience assessment in a communal coastal aquifer system. The case of Manglaralto in Santa Elena, Ecuador. Sustainability, 12: 8290.

Al-Gburi, H. F., Al-Tawash, B. S., Al–Tamimi, O. S. and Schüth, C. 2022. Stable isotope composition in precipitation and groundwater of Shwan Sub-Basin, Kirkuk governorate, northeast of Iraq. Water Supply, 22(10): 7442-7459. doi: https://doi.org/10.2166/ws.2022.327

Jassas, H. A. and Merkel, B. J. 2015. Investigating groundwater recharge by means of stable isotopes in the Al-Khazir Gomal Basin, northern Iraq. Environ. Earth Sci., 73: 8533-8546. doi:10.1007/s12665-015-4013-7.

Krishan, G., Rao, M. S., Vashisht, R., Chaudhary, A., Singh, J. and Kumar, A. 2022. Isotopic assessment of groundwater salinity: a case study of the Southwest (SW) Region of Punjab, India. Water, 14(1): 133. doi:10.3390/w14010133

Manoj Kumar, A. L., Ramanathan, A., Mukherjee, A., Sawlani, R. and Ranjan, S. 2019. Delineating sources of groundwater recharge and carbon in Holocene aquifers of the central Gangetic basin using stable isotopic signatures. Isot. Environ. Health Stud., 55(3): 254-271. doi: 10.1080/10256016.2019.1600515

Oyarzún, R., Zambra, S., Maturana, H., Oyarzún, J., Aguirre, E. and Kretschmer, N. 2016. Chemical and isotopic assessment of surface water–shallow groundwater interaction in the arid Grande river basin, North-Central Chile. Hydrol. Sci. J., 61(12): 2193-2204. doi: 10.1080/02626667.2015.1093635

Sophocleous, M. 2002. Interactions between groundwater and surface water: The state of the science. Hydrogeol. J., 10: 52-67.

Wright, S. N. and Novakowski, K. S. 2019. Groundwater recharge, flow, and stable isotope attenuation in sedimentary and crystalline fractured rocks: Spatio-temporal monitoring from multi-level wells. J. Hydrol., 571: 178-192. https://doi.org/10.1016/j.jhydrol.2019.01.028

Yapiyev, V., Rossi, P. M., Ala-Aho, P. and Marttila, H. 2023. Stable water isotopes as an indicator of surface water intrusion in shallow aquifer wells: A cold climate perspective. Water Resour. Res., 59. https://doi.org/10.1029/2022WR033056

Zhang, B., Song, X., Zhang, Y. et al. 2016. The interaction between surface water and groundwater and its effect on water quality in the Second Songhua River basin, northeast China. J. Earth Syst. Sci., 125: 1495-1507. https://doi.org/10.1007/s12040-016-0742-6

Zhu, M., Wang, S., Kong, X., Zheng, W., Feng, W., Zhang, X., Yuan, R., Song, X. and Sprenger, M. 2019. Interaction of surface water and groundwater influenced by groundwater over-extraction, wastewater discharge and water transfer in Xiong'an new area, China. Water, 11(3): 539. https://doi.org/10.3390/w11030539

## ORCID DETAILS OF THE AUTHORS

Surendar Natarajan: https://orcid.org/0000-0002-6545-8544

Nature Environment and Pollution Technology
An International Quarterly Scientific Journal

p-ISSN: 0972-6268
(Print copies up to 2016)
e-ISSN: 2395-3454

Vol. 23 | No. 3 | pp. 1569-1577 | 2024

Original Research Paper

https://doi.org/10.46488/NEPT.2024.v23i03.026

Open Access Journal

# The Risks and Safety Practices of Waste Pickers at Selected Dumping Sites in Pretoria, South Africa, During the COVID-19 Pandemic

**L. L. Mugivhisa*†, M. P. Mphitshana* and J. O. Olowoyo****

*Department of Biology and Environmental Sciences, Sefako Makgatho Health Sciences University, Medunsa, 0204, Pretoria, South Africa

**Department of Health Science and The Water School, Florida Gulf Coast University, Fort Myers, USA

†Corresponding author: Liziwe L. Mugivhisa; liziwe.mugivhisa@smu.ac.za

**Nat. Env. & Poll. Tech.**
**Website: www.neptjournal.com**

*Received:* 12-11-2023
*Revised:* 04-01-2024
*Accepted:* 12-01-2024

**Key Words:**
COVID-19 pandemic
Household waste
Waste pickers
Waste handling
Landfill sites
Personal protective equipment

## ABSTRACT

Amid the COVID-19 outbreak, the accumulation of household waste continued to rise as the number of COVID-19 patients increased. COVID-19 can survive and be transmitted from contaminated surfaces, making waste pickers more vulnerable and at risk of contracting and spreading the virus through contact with infected household waste. The study assessed safety practices and risks related to waste picking during the COVID-19 pandemic at two selected dumping sites in the north of Pretoria. Structured questionnaires were used to collect data from 81 waste pickers at these landfill sites. Results showed that 100.0% of waste pickers at Site A and 86.7% at Site B collected plastics; 96.7% at Site A and 90.5% at Site B collected bottles; and 100% at Site B and 95.5% at Site A collected metals. The majority, 92.0% at Site A and 90.0% at Site B, were aware of the dangers and risks associated with waste handling if protective gear was not worn. From sites A and B, 97.0% and 90% of the waste pickers respectively had heard of COVID-19, although 51.9% from both sites believed they could not contract COVID-19 while handling waste. Only 18.0% of waste pickers from Site A and 82.0% from Site B faced challenges with purchasing their own PPE. All waste pickers at Site A wore facial masks, whereas 86.0% at Site B did so. Regarding testing for COVID-19, 22.0% from Site A and 19.0% from Site B were tested, with 2.0% from Site A and none (0.0%) from Site B testing positive. It is recommended that all waste pickers be educated about COVID-19 transmission and provided with PPE during the pandemic.

## INTRODUCTION

Amid the COVID-19 outbreak, the pilling of household waste continued to rise as the number of COVID-19 patients increased daily (Saadat et al. 2020). COVID-19 was asserted as a global pandemic due to the high spreading of the virus. World Health Organization (WHO) defined it as an infectious disease spread through droplets of saliva or mucus when an infected person coughs or sneezes (WHO 2020). The COVID-19 could survive and be transmitted from infected surface materials (WHO 2020). Its sustainability in aerosols, plastic, stainless steel, copper, and cardboard was 3, 72, 48, 4, and 24 hours, respectively (van Doremalen et al. 2020), or could persevere on other nonliving surfaces like glass and metals for as long as 9 days (Kampf et al. 2020). Due to the prolonged relative sustainability of the COVID-19 virus on various surfaces, there was a concern about the potential presence of the virus in discarded waste (van Doremalen et al. 2020). This could lead to transmission through contact with contaminated surfaces or objects if proper safety precautions were not taken. While the general public implemented precautionary measures against COVID-19, daily disposal of items such as masks, gloves, empty hand sanitizer bottles, and used tissues (Saadat et al. 2020) added to the regular waste in dustbins or landfill sites. Used masks, in particular, needed to be handled with care, as they could be infectious, thereby posing a greater risk to waste disposal workers and the broader community (Rhee 2020).

Waste generated by households and businesses that are not associated with healthcare facilities is treated as non-infectious waste that is not required to be managed. According to the Department of Environmental Affairs and Tourism (DEAT) (2005), there are no declared systems for source separation in South Africa, and this leaves waste pickers more vulnerable and at risk of contracting diseases that are transmitted through direct contact with contaminated waste (Lisk 1991, Pleus & Kelly 1996), such as COVID-19.

High population growth rates in most African countries due to industrialization, urbanization, and increased middle-

class society have contributed to increased generation of solid waste (Simelane & Mohee 2015, Chimuka & Ogola 2015, Muzenda et al. 2012). The increased generation of waste, coupled with declining infrastructure for solid waste management, has led to local authorities' inability to manage waste effectively (Dlamini et al. 2019).

In South Africa, as well as in most developing and developed countries, the prime method of waste disposal is the use of landfill systems (Ketlogetswe & Mothudi 2005, Mothiba et al. 2016). Waste pickers handle large quantities of recyclable waste in landfill sites (Komane 2014). Even though some landfill sites are well operated and follow the international best practices in South Africa, only 44.0% of the 1280 landfill areas are authorized to operate through the permits, and there is rare auditing for compliance with the conditions of the permits (Godfrey & Oelofse 2008).

The waste sector has been recognized as an industry capable of contributing to economic growth and job creation for both skilled and unskilled workers (Department of Science & Technology 2013). Municipal waste from households and commercial activities has become an economic resource for others (Kum et al. 2005). Consequently, many South Africans are turning to waste picking, which plays a crucial role in reducing waste and extending the lifespan of landfill sites by preventing them from filling up quickly (Medina 2008). However, waste picking remains inadequately regulated, unsupported, and unrecognized by authorities (Komane 2014).

Waste pickers collect, sort, and sometimes clean recyclable or reusable waste for sale or personal use (Oelofse & Strydom 2010). Approximately 1.0% of the population, or about 15 million people in urban areas, earn a living by salvaging recyclable waste in developing countries (Medina 2008). Around 2004/2005, about 37,000 waste pickers in South Africa were making a living from waste picking (Langenhoven & Dyssel 2007), often under unsafe and hazardous conditions (Oelofse & Strydom 2010). Research indicates that with proper support and organization, waste picking can lead to public investments in poor communities, resulting in poverty reduction, job creation, conservation of natural resources, and environmental protection (Medina 2008).

Waste pickers are exposed to occupational health risks such as diseases because of the direct contact that they make with decomposed materials and potential bio-aerosols that cause the spreading of several different diseases (Coffey & Coad 2010, Pilusa & Muzenda 2013, Mothiba et al. 2016, Ray et al. 2005). The deficiency of proper devices for protection contributes further to undesirable and unhygienic working conditions of the waste pickers (Mothiba et al. 2016).

Since solid waste is a source of income and contributes to job opportunities, waste pickers must be informed and educated about appropriate and safe practices for handling waste. Several studies have looked at facets and problems associated with the management of solid waste in particular related to the recycling of the collected waste (Simatele et al. 2017, Baker & Letsoela 2016). Researchers have been concerned about the minimum attention that is given to the health risks associated with waste pickers (Noel 2010, Chattopadhyay et al. 2009). In South Africa, studies in the Free State Province have looked at landfill waste pickers and street waste pickers in 9 landfill sites with 400 waste pickers (Blaauwet al. 2015).

Even though research has been done on waste pickers who live and work in landfills or dumping sites in South Africa (Schenck & Blaauw 2011), to the best of our knowledge and at the time of doing this study, there had not been any studies done on waste pickers during the COVID-19 pandemic. The waste pickers worked in groups, handled and made direct contact with the waste, which could be contaminated with the COVID-19 virus from the households of infected people. As a result, the waste pickers were vulnerable to being infected with the COVID-19 virus. Hence, the study assessed the safety practices and risks related to waste picking during the COVID-19 pandemic at the selected dumping sites in the north of Pretoria.

## MATERIALS AND METHODS

The study was exploratory, purposive, and based on voluntary participation, relying on the waste pickers' willingness to engage. The purpose of the study was explained to the waste pickers, and consent was sought before data collection. They were informed that participation was purely voluntary, that they could withdraw at any time, and that their unwillingness to participate would not negatively affect or disadvantage them.

The study involved interviewing 81 waste pickers using structured questionnaires developed by the researchers. These questionnaires included both open-ended and close-ended questions. The interviews were conducted orally to assist those waste pickers who could not read or write and to minimize misunderstandings and misinterpretations. This approach also served as a preventive measure against COVID-19 transmission through the exchange of questionnaires between the researcher and the waste pickers.

Sixty waste pickers were from Site A, while twenty-one were from Site B. Sampling had to be abandoned due to the emergence of a new COVID-19 variant. All preventive and safety measures related to COVID-19 were strictly followed

by the researcher during data collection. These measures included wearing full protective gear (mask, boots, long-sleeved clothing, and gloves), frequent sanitizing, social distancing, and hand washing whenever possible.

The general information sought from the waste pickers through the questionnaires included demographic details, safety practices, health status, attitudes and knowledge of COVID-19, and preventive measures against it.

## RESULTS AND DISCUSSION

Table 1 below shows the demographic information and working conditions of the waste pickers at the two dumping sites (sites A and B). From Site A, 87.0% of the waste pickers were above 30 years old, whereas slightly more than half (52.0%) of the waste pickers from Site B were between the ages of 20 and 30 years. These results are not comparable to those in Schenck & Blaauw (2011), where the majority of the street waste pickers were in the age range between 40 and 49 years old. In Samson (2010), the majority of waste pickers were found to be much older than the average age of 28 years old, while in Chvatal (2010), waste pickers included people who were over 60 years old in the Western Cape.

There were slightly more females (53.0%) than males (47.0%) at Site A, whereas at Site B, there were more males (62.0%) than females, who made up 38.0% of the waste pickers. The study conducted on waste pickers in Pretoria by Schenck & Blaauw (2011) found more males (97.2%) practicing waste handling from the streets than females due to males being able to travel long distances searching for recyclables while carrying hefty piles of waste like waste pickers on streets compared to the females (Schenck & Blaauw 2011, Viljoen 2014). Mothiba et al. (2016) also found more females (66.0%) handling waste around Pretoria landfill sites than males, even though this might have changed over the years. According to Viljoen (2014), most of the waste pickers in South Africa are males, while Samson (2010) argues that the variation in gender becomes more prominent when looking at materials that are being collected. In Benson & Vanqa-Mgijima (2010), females were found to make only a small proportion of waste pickers in Cape Town. In China, older women are waste pickers (Schenck & Blaauw 2011).

The uneven distribution of gender at sites A and B in the current study could be due to various factors, such as females at Site A being more willing to take part in the study than males. At Site B, males were more willing to partake in the study. Other waste pickers mentioned that they did not want to participate in the study because there was no compensation or gain for them, while some thought it would waste their time. Others had come across bad experiences from taking part in previous studies where they were promised things and were not given feedback on the results of the studies.

About 69.0% and 76.0% of waste pickers from sites A and B, respectively, had no matric qualification, which is considered to be the lowest level of education a person could have before being considered for employment (Table 1). These results are comparable with those in Blaauw et al. (2015), where more (49.0% and 29.0%) waste pickers at landfill sites had secondary and primary education, respectively, in the Free State Province in 2012. According to Schenck & Blaauw (2011), people who are unskilled and unemployed get a chance to infiltrate the informal economy so that they can earn money through waste picking. According to Theron (2010), it is easier to get into waste picking because there is no requirement for any qualification or permits. Waste picking forms part of the informal economy, as it is unregulated, labor-intensive, and unsystematically pays low wages (Medina 2007, Gill 2007). According to Blaauw et al. (2015), it is an untrained line of work that gives unskilled laborers the prospect of entering the labor market with no entry barriers.

During lockdown level 1, waste pickers from Site A were grouped into two groups, and this resulted in them working during alternate working days per week, with each waste picker working for 2 to 3 days per week (Table 1). This could have resulted in less money being made by the waste pickers from the selling of the waste. However, at Site B, the majority (95.0%) of the waste pickers worked for more than 5 days per week, and some of them even lived on-site throughout the week. Only 5.0% of the waste pickers worked for a period of between 3 and 4 days. This led to the waste

Table 1: The demographic information and working conditions of the respondents at the two dumping sites.

| Demographic Information and Working Conditions | | Number of waste pickers (%) | |
|---|---|---|---|
| | | Site A | Site B |
| Age (years) | 20 – 30 | 13 | 52 |
| | >30 | 87 | 48 |
| Gender | Male | 47 | 62 |
| | Female | 53 | 38 |
| Education | Below matric | 69 | 76 |
| | Matric | 23 | 19 |
| | Tertiary | 8 | 5 |
| Number of days working at the dumping site per week | 1-2 | 100 | 0 |
| | 3-4 | 100 | 5 |
| | >5 | 0 | 95 |

Table 2: Percentage (%) of waste pickers collecting different items at the two dump sites.

| Type of waste collected | Number of waste pickers (%) | |
|---|---|---|
| | Site A (%) | Site B (%) |
| Plastics | 100 | 90.5 |
| Metals | 86.7 | 100 |
| Bottles | 96.7 | 90.5 |
| Paper-products | 100 | 100 |

pickers at Site B being in a better position to generate more income compared to their counterparts in Site A.

Table 2 shows the percentage (%) of waste pickers collecting similar items at the two dumpsites. From the two dumping sites, 100.0% and 90.5% of the waste pickers from Sites A and B, respectively, collected plastics. From Site B, all waste pickers collected metals, whereas 86.7% of the waste pickers from Site A collected plastics. With regards to bottles, 96.7% and 90.5% of waste pickers from sites A and B, respectively, collected bottles from the waste. According to Ali & Alharbi (2020), COVID-19 can survive for an extended period of time on various surfaces from where it can be transmitted. The coronavirus can survive for 3 hours in aerosols, 72 hours in plastic and stainless steel, 4 hours in copper, and 24 h in cardboard (Ali & Alharbi 2020). Most of the waste or recyclables were mainly collected by waste pickers from both landfill sites, resulting in increased chances of COVID-19 transmission and infections amongst waste pickers.

The responses of the waste pickers from each of the dumping sites on the protective measures taken by the waste pickers and the awareness of risks and injuries associated with handling waste are shown in Table 3 below. Ninety-seven percent (97.0%) of waste pickers from Site A and 57.0% from Site B indicated that they used tools such as chisels to break glass. The minority of waste pickers (3.0% from Site A and 43.0% from Site B) did not use any tools when handling waste. From the two sites, 57.0% and 24.0% of the waste pickers from sites A and B, respectively, used safety goggles, whereas 33.0% and 76.0% of the waste pickers from sites A and B, respectively, did not wear any safety goggles when handling waste (Table 3). Most waste pickers who used goggles were those who collected glasses and wore goggles only when they were breaking glass before they could sell it to the buyers.

The majority (92.0% and 90.0% of waste pickers from sites A and B, respectively) reported that they were fully aware of the dangers and risks associated with waste handling (Table 3). The few risks/dangers that waste pickers from Site A landfill mentioned included physical damage to the body, chemical fumes, toxic gases, dust causing diseases, being hit by a dumping truck if not careful, slipping and falling from the slippery floor, especially if it had rained, getting hurt or cut from sharp/broken objects if not wearing protective gear. However, risks/dangers mentioned by waste pickers from Site B were injuries from vehicle accidents and sharp broken objects (e.g., needles), getting sick from medical waste and dirt particles blown by the wind, or being exposed to toxins from chemicals and diseases such as TB, HIV, and COVID-19.

From sites A and B, 2.0% and 29.0% of the waste pickers, respectively, reported injuries while at work, whereas 98.0% and 71.0% of the waste pickers from sites A and B, respectively, had not suffered any injuries while working at the dumping sites. The 2.0% from Site A reported that they had been burnt by acid while at work, whereas the 29.0% from Site B had suffered foot injuries, broken hands, deep cuts on hands due to broken glass, injuries from fights with colleagues, and being hit on the head by offloading trucks. According to Coffey & Coad (2010), there has to be an enforcement of procedures such as reversing trucks at the landfill sites by the supervisors, as this is a common source of accidents. In most cases, the waste pickers usually jump onto trucks to get access to waste that is being offloaded even before the trucks can stop.

Fig. 1 below shows the responses of the waste pickers on the substances they were exposed to while working. Most (97.0% and 92.0%) of the waste pickers from Site A and Site B, respectively, indicated that they had been exposed to dust when handling waste. All the waste pickers (100.0%) from Site B indicated that they were exposed to sharp, broken objects such as metallic nails and broken glasses when handling waste. This could have resulted in the waste pickers being susceptible to injuries while at work. Fewer waste pickers indicated that they were exposed to leachates and pollutants, with 23.0% of waste pickers from Site A and 43.0% from Site B mentioning that they were exposed to toxic gases. Only 48.0% and 8.0% of the waste pickers from

Table 3: Responses of waste pickers on use of tools, awareness of risks associated with waste handling, and injuries at work.

| Protective measures and injuries when handling waste | Number of waste pickers (%) | | | |
|---|---|---|---|---|
| | Site A | | Site B | |
| | Yes | No | Yes | No |
| Use of waste handling tools | 97 | 3 | 57 | 43 |
| Wearing safety goggles | 57 | 33 | 24 | 76 |
| Use of gloves | 100 | 0 | 100 | 0 |
| Wearing of boots | 100 | 0 | 100 | 0 |
| Awareness of risks at work | 92 | 8 | 90 | 10 |
| Injuries sustained at work | 2 | 98 | 29 | 71 |

sites A and B, respectively, revealed that they were exposed to medical waste while handling waste, even though the management had mentioned that they only received general waste. Such exposures, especially to medical waste, could place waste pickers' health at risk of infections, especially now that there is COVID-19.

Fig. 2 shows that 20.0% of those from Site A and 43.0% from Site B had consulted in the past 6 months. Most of those who had consulted in the past 6 months didn't want to disclose their reasons for consultations, with only a few mentioning that they had consulted so that they could collect their diabetes medication or had gone for dentist appointments, for flu, persistent headache, hand injuries, and general check-ups for HIV. According to the Centers for Disease Control and Prevention (CDCP) (2020), people at high risk of COVID-19 infection are those with underlying medical conditions such as asthma, BP, weakened immune system, diabetes, and HIV, which were some of the medical conditions that a few of the waste pickers had mentioned as the reasons for their medical consultations. As a result, some of the waste pickers were at a high risk of being infected with COVID-19.

Fig. 3 below shows the responses of waste pickers on the experiences of certain prevalence symptoms that they had. The majority (60.0%) of the waste pickers from Site A and 76.0% from Site B indicated that they suffered from tiredness, which was normal for people who worked tirelessly for a prolonged period regardless of weather conditions. Only 52.0% and 23.0% reported back pain, whereas 33.0% and 27.0% had joint pain from sites B and A, respectively, which

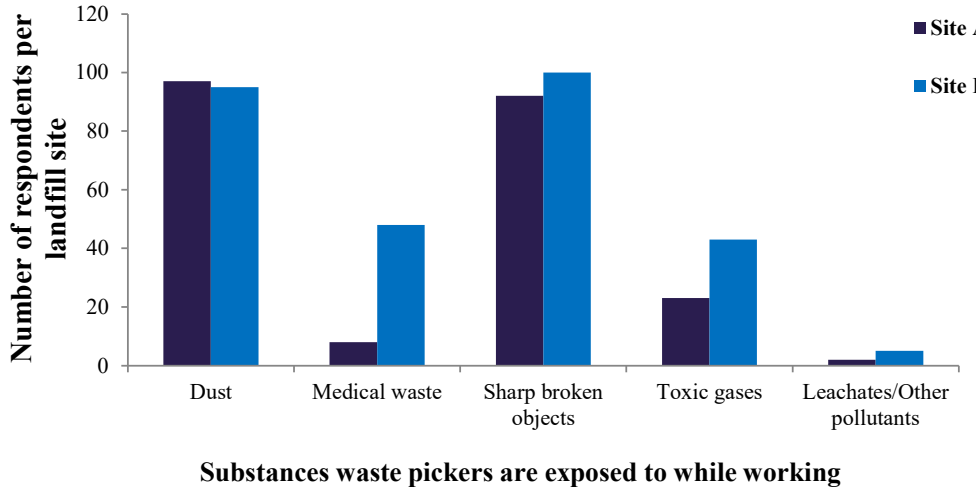


Fig. 1: Responses on the substances that waste pickers are exposed to while handling waste.

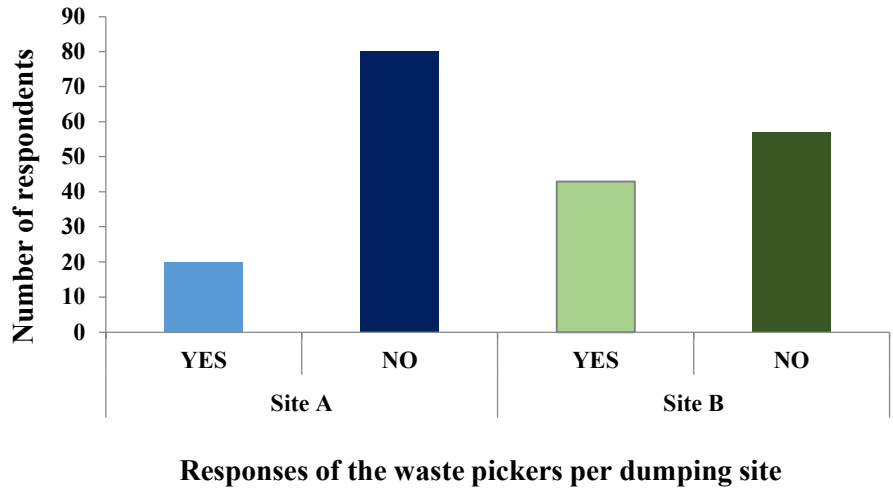


Fig. 2: Responses of waste pickers on having medical consultation in the last 6 months.

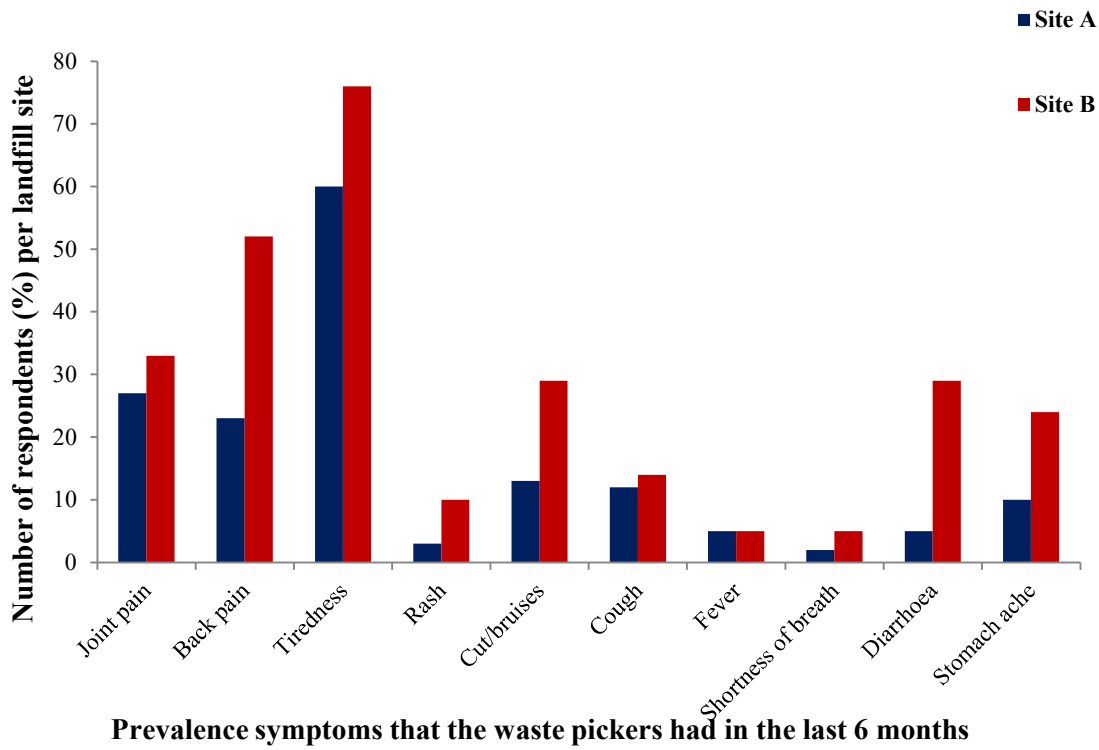


Fig. 3: Responses of waste pickers on the experiences of certain prevalence symptoms.

might be common due to the requirement of their work to bend when collecting waste and carrying heavy waste from one place to another. This hard labour might also explain the reason why the majority of them were suffering from tiredness, time after time. Very few waste pickers from both sites experienced shortness of breath and fever. According to Huang et al. (2019) and Hui et al. (2020), the prevalence symptoms similar to those of COVID-19 include tiredness, muscle pain, sneezing, sore throat, dry cough, high fever, respiratory problems, and kidney failure.

Table 4 below shows the responses of waste pickers from the two dumping sites on the knowledge of COVID-19, accessibility to water, and whether they practiced social distancing while working at the dumping sites. The majority (97.0%) and (90.0%) of waste pickers from sites A and B, respectively, indicated that they had heard of COVID-19.

The few preventative measures against COVID-19 that waste pickers from the two dumping sites mentioned were the use of PPEs such as masks and gloves, practicing social distancing, no handshakes, and frequent hand washing or sanitizing. The majority (75.3%) of all the waste pickers stated that they practiced social distancing, with the remaining 24.7% saying that it was difficult to practice social distancing when they were all handling waste at the same time after the waste had been offloaded from the trucks. The researcher however, observed that while collecting waste, there was no social distancing at all practiced by the waste pickers. These contradicting responses by waste pickers and observations made by the researchers indicated the unreliability of the responses and results in the current study.

The waste pickers mentioned that the strict lockdown regulations, especially during lockdown 5 when they could not work, contributed to a loss of income and buyers of waste. Slightly more than half (51.9%) of the waste pickers from both dumping sites believed that they could not get COVID-19 while handling waste. This could indicate a lack of knowledge on the transmission of COVID-19 from surfaces and materials by the waste pickers.

All (100.0%) waste pickers from Site A and 95% from Site B had access to running water. It was, however, observed that in both dumping sites, there was no running water and that the water was brought daily in tanks even though the tanks seemed inadequate. Fewer (12.0%) waste pickers from Site A compared to the majority (62.0%) of the waste pickers from Site B stated that they found it difficult to practice social distancing when picking waste together at the same time when waste was offloaded from the truck. It was also observed by the researcher that there was no social distancing at the dumping sites even though the majority (88.0%) of the waste pickers from Site A and 38% from

Site B had mentioned that they practiced social distancing while working.

Some waste pickers, as shown in Table 4, had challenges with buying PPE due to lack of money and high expenses of the PPEs. Waste pickers at Site A were provided with PPE such as masks and gloves by the site management after reopening during lockdown level 1, even though some of the waste pickers could have been absent on the days when they were given PPEs and hence had to buy their own PPEs. As a result, only 18.0% of the waste pickers from Site A mentioned that they had challenges with buying their PPEs, while the majority (82.0%) of the waste pickers from Site B had challenges with getting PPEs.

With regards to the two dumping sites, all (100.0%) of the waste pickers from Site A wore facial masks on the days when the interviews were conducted, whereas at Site B, about 86.0% of the waste pickers wore the facial masks, while some of the women waste pickers made use of their head cloths as facial masks. The researcher observed the lack of facial masks at Site B during the interviews, and facial masks were donated to the waste pickers at Site B by the researcher. Nevertheless, 14.0% of waste pickers from Site B disclosed that they did not like wearing masks as they were not comfortable breathing through them, whereas some of those who used masks from both sites mentioned that they were only wearing them due to the COVID-19 regulations and did not use them before the COVID-19 pandemic. This is supported by Mothiba et al. (2016), who stated that waste pickers still found it challenging to make use of PPEs such as masks even though they were exposed to dust and unpleasant odors at their workplace on a daily basis.

Table 4 below shows that from the two sites, 22.0% from Site A and 19.0% from Site B of the waste pickers tested for COVID-19. Of those who had tested, 18.0% and 19% from Sites A and B, respectively, had tested negative, while 2.0% from Site A and none (0.0%) of the waste pickers from Site B had tested positive. Only 2.0% of the waste pickers from Site A were still awaiting the COVID-19 results. Most of the waste pickers thought COVID-19 screening was the same as being tested for COVID-19. At Site A, all waste pickers and everyone who entered the premises were screened for COVID-19, whereas at Site B, there was no COVID-19 screening for whoever entered the site. The suggestions made by waste pickers on how they could be assisted with regards to their protection against COVID-19 and other infections were that they should be supplied with PPE, more water and be given assistance with health issues such as the supply of medication, and be screened for COVID-19 upon entrance at Site B.

Table 4: The responses of the waste pickers regarding the adherence to the COVID-19 safety and regulations.

| Responses to COVID-19 safety protocols and regulations | Number of waste pickers (%) | |
|---|---|---|
| | Site A | Site B |
| Knowledge/awareness of COVID-19 | 97 | 90 |
| Practicing social distancing | 88 | 38 |
| Difficulty in practicing social distancing when handling waste | 12 | 62 |
| Access to water | 100 | 95 |
| Wearing of masks | 100 | 86 |
| Challenge with access to PPE | 18 | 82 |
| Testing for COVID-19 | 22 | 19 |

## CONCLUSIONS

Waste pickers mainly practiced waste picking for economic reasons regardless of the risks associated with the job. The majority of waste pickers were fully aware of the health risks associated with handling waste during the COVID-19 pandemic. Even though most waste pickers used PPEs, such as gloves, boots, masks, and protective glasses, for their protection against injuries and possible diseases such as COVID-19, there were still waste pickers who had challenges with getting PPEs, such as masks. Even though the practices of safe waste handling by the waste pickers and the knowledge they had of COVID-19 measures placed them at a much lower risk of being infected by COVID-19, it was disturbing that half of the waste pickers stated that they did not believe they could be exposed to the COVID-19 while handling waste. It is therefore recommended that there should be education on COVID-19 transmission, provision of free PPEs, sanitizers, more water, and COVID-19 screening to all the waste pickers. More monitoring and checking for adherence to safe waste handling at all dumping sites should be practiced by the dumping site personnel or management.

## ACKNOWLEDGEMENTS

The authors would like to thank all the waste pickers and the management of the two dumping sites in Pretoria North for making time to participate in the study.

## REFERENCES

Ali, I. and Alharbi, O. 2020. COVID-19: Disease, management, treatment, and social impact. Sci. Total Environ., 728: 138861. https://doi.org/10.1016/j.scitotenv.2020.138861.

Baker, M. and Letsoela, N. 2016. Implementation of the Landfill Methane Gas to Electricity Project in the City of Johannesburg: Waste Sector Contribution Low Carbon Economy. Retrieved from https://www.iwmsa.co.za/sites/default/files/downloads/6.%20Baker%2C%20M%20et%20al.pdf. Accessed 28 April 2021.

Benson, K. and Vanqa-Mgijima, N. 2010. Organizing on the streets: A study of Reclaimers in the Streets of Cape Town. Retrieved from http://www.inclusivecities.org/toolbox/Organizing_on_the_Streets_web.pdf. Accessed 05 May 2021.

Blaauw, D., Schenck, R. and Viljoen, K. 2015. Waste Picking in South Africa. Retrieved from https://www.iwmsa.co.za/downloads/UWC%20NWU%20Waste%20pickers%20in%20SA.pdf. Accessed 27 April 2021.

Center for Disease Control and Prevention (CDCP). 2020. People with Certain Medical Conditions. Retrieved from https://www.cdc.gov/coronavirus/2019-ncov/need-extra-precautions/people-with-medical-conditions.html. Accessed 29 April 2021.

Chattopadhyay, S., Dutta, A. and Ray, S. 2009. Clean Development Mechanism Benefits from Municipal Solid Waste Landfill Gas. 7th All India People's Technology Congress, Forum of Scientists, Engineers and Technologists, 06-07 February 2009, Kolkata, India, pp. 350–360.

Chimuka, L. and Ogola, J. 2015. Leading the Way: Directions of Municipal Solid Waste Management in South Africa. Institute of South Africa, South Africa.

Chvatal, J. 2010. A Study of Waste Management Policy Implication for Landfill Waste Salvagers in the Western Cape. Masters Dissertation. University of Cape Town, Cape Town, South Africa.

Coffey, M. and Coad, A. 2010. Collection of Municipal Solid Waste in Developing Countries. Retrieved from https://unhabitat.org/sites/default/files/2021/02/2010_collection-msw-developing-countries_un-habitat.pdf. Accessed 05 March 2021.

Department of Environmental Affairs and Tourism (DEAT). 2005. National Waste Management Strategy Implementation. Department of Environmental Affairs and Tourism. Retrieved from https://www.gov.za/sites/default/files/gcis_document/201409/wastestrategyinceptionrephase0.pdf. Accessed 27 March 2021

Department of Science and Technology. 2013. South African Waste Sector-2012. An Analysis of the Formal Private and Public Waste Sector in South Africa. Retrieved from https://wasteroadmap.co.za/wp-content/uploads/2020/03/waste_sector_survey_2012.pdf. Accessed 03 March 2021.

Dlamini, S., Simatele, M. D. a Kubanza, N. S. 2019. Municipal solid waste management in South Africa: from waste to energy recovery. J. Dev. Stud., 24(3): 249-257. doi: 10.1080/13549839.2018.1561656.

Gill, K. 2007. Interlinked contracts and social power: Patronage and exploitation in India's waste recovery market. J. Dev. Stud., 43(8): 1448-1474. doi: 10.1080/00220380701611519

Godfrey, L. and Oelofse, S. 2008. Systems Approach to Waste Governance-Unpacking the Challenge Facing Local Government. Golder Associates (U.K) Ltd. Managing Organisation for Waste 2008. Proceedings Waste 2008: Waste and Resource Management – A Shared Responsibility, 16-17 September 2008, Avon, Warwickshire, England, pp. 615-646.

Huang, C., Wang, Y., Li, X., Ren, L., Zhao, J., Hu, Y., Zhang, L., Fan, G., Xu, J., Gu, X., Cheng, Z., Yu, T., Xia, J., Wei, Y., Wu, W., Xie, X., Yin, W., Li, H., Liu, M., Xiao, Y., Gao, H., Guo, L., Xie, J., Wang, G., Jiang, R., Gao, Z., Jin, A., Wang, J. and Cao, B. 2019. Clinical features of patients infected with 2019 novel coronavirus in Wuhan, China. Lancet, 395(10223): 497-506. doi: 10.1016/S0140-6736(20)30183-5.

Hui, D. S., Azhar, E., Madani, T. A., Ntoumi, F., Kock, R., Dar, O., Ippolito, G., Mchugh, T. D., Memish, Z. A., Drosten, C., Zumla, A. and Petersen, E. 2020. The continuing 2019-nCoV epidemic threat of novel coronaviruses to global health - The latest 2019 novel coronavirus outbreak in Wuhan, China. Int. J. Inf. Di., 91: 264-266. doi: 10.1016/j.ijid.2020.01.009.

Kampf, G., Todt, D., Pfaender, S. and Stienmann, E. 2020. Persistence of coronaviruses on inanimate surfaces and their inactivation with biocidal agents. J. Hosp. Infect., 104, 246-251. doi: https://doi.org/10.1016/j.jhin.2020.01.022

Ketlogetswe, C. and Mothudi, T. H. 2005. Botswana's environmental policy in recycling. Resour. Conserv. Recycl., 44: 333-342.

Komane, K. A. 2014. Waste Reclaimers and South African Environmental Law. Potchefstroom Campus of the North-West University, South Africa. Retrieved from https://repository.nwu.ac.za/bitstream/handle/10394/11180/Komane_KA.pdf?sequence=1andisAllowed=y. Accessed 05 March 2021.

Kum, V., Sharp, A. and Harnpornchai, V. 2005. Improving the solid waste management in Phnom Penh City: A strategic approach. J. Waste Manag., 25: 626-637.

Langenhoven, B. and Dyssel, M. 2007. The recycling industry and subsistence waste collectors: A case study of Mitchells Plain. Urban Forum, 18(1): 114-132.

Lisk, D. J. 1991. Environmental effects of landfills. Sci. Total Environ., 100: 415-468.

Medina, M. 2007. The World's Scavengers: Salvaging for Sustainable Consumption and Production. Altamira Press, Lanham.

Medina, M. 2008. The Informal Recycling Sector in Developing Countries: Organizing Waste Pickers to Enhance their Impact. World Bank, Washington, DC.

Mothiba, M. P., Loans, C. and Moja, S. J. 2016. A Study on working conditions and health status of waste pickers working at landfill sites in the city of Tshwane Metropolitan Municipality. Environmental Management, University of South Africa.

Muzenda, E., Ntuli, F. and Pilusa, T. J. 2012. Waste management, strategies and situation in South Africa: An overview. WASET, 68: 414.

Noel, C. 2010. Solid waste workers and livelihood strategies in Greater Port-au-Prince, Haiti. Waste Manag., 30: 1138-1148.

Oelofse, S. H. H. and Strydom, W. F. 2010. Picking at waste facilities – scavenging or entrepreneurship. institute of waste management of Southern Africa, CSIR Natural Resources and the Environment, South Africa.

Pilusa, J. and Muzenda, E. 2013. Solid waste management in West Rand District, Gauteng, South Africa. Behav. Sci. Econ., 11: 17-18.

Pleus, R. C. and Kelly, K. E. 1996. Health effects from hazardous waste incineration facilities: Five case studies. Toxicol. Ind. Health, 2(2): 277-87.

Ray, M. R., Roychoudhury, S., Mukherjee, G., Roy, S. and Lahiri, T. 2005. Respiratory and general health impairments of workers employed in municipal solid waste disposal at an open landfill site in Delhi. Int. J. Hyg. Environ. Heal., 208(4): 255-262. doi.10.1016 /j.ijheh.2005.02.00

Rhee, S. 2020. Management of used personal protective equipment and wastes related to COVID-19 in South Korea. Waste Manag. Res., 38(8): 820–824. doi: 10.1177/0734242X20933343.

Saadat, S., Rawtani, D. and Hussain, C. M. 2020. Environmental perspective of COVID-19. Sci. Total Environ., 728: 138870.

Samson, M. 2010. Reclaiming Reusable and Recyclable Materials in Africa: A Critical Review of English Language Literature. Retrieved from https://www.africancentreforcities.net/wp-content/uploads/2013/10/rr6_samson.pdf. Accessed 07 March 2021.

Schenck, C. J. and Blaauw, P. F. 2011. Living on what others throw away: An exploration of the socioeconomic circumstances of people selling recyclable waste. J. Soc. Work Pract. Res., 23: 135-153.

Simatele, D. M., Dlamini, S. and Kubanza, N. S. 2017. From informality to formality: Perspectives on the challenges of integrating solid waste management into the urban development and planning policy in Johannesburg, South Africa. Habitat Int., 63: 122-130.

Simelane, T. and Mohee, R. 2015. Future directions of municipal solid waste management in Africa. Africa. Retrieved from http://www.ai.org.za/wp-content/uploads/downloads/2012/10/No.-81.-Future-Directions-of-Municipal-Solid-waste-Management-in-Africa.pdf. Accessed 07 March 2021.

Theron, J. 2010. Options for organizing waste pickers in South Africa. Retrieved from http://www.wiego.org/publications/Organizing_Waste_Pickers_S_Africa.pdf. Accessed 03 March 2021.

Van Doremalen, N., Bushmaker, T., Morris, D. H., Holbrook, M. G., Gamble, A., Williamson, B. N., Tamin, A., Harcourt, J. L., Thornburg, N. J., Gerber, S. I., Lloyd-Smith, J. O., de Wit, E. and Munster, V. J. 2020. Aerosol and surface stability of SARS-CoV-2 as compared with SARS-CoV-1. N. Engl. J. Med., 382(16): 1564-1567.

Viljoen, J. M. M. 2014. Economic and Social Aspects of Street Waste Pickers in South Africa. Unpublished PhD-Thesis. Faculty of Economic and Financial Sciences, University of Johannesburg, South Africa.

World Health Organization (WHO) 2020. Water, Sanitation, Hygiene, and Waste Management for COVID-19. Retrieved from https://www.who.int/publications-detail/water-sanitation-hygiene-and-waste-management for COVID-19. Accessed 03 March 2021.

S gz|xk J t ~oxut nkt z gt j Uum|zait Yki nt urum¥
An International Quarterly Scientific Journal

p-ISSN: 0972-6268
(Print copies up to 2016)
e-ISSN: 2395-3454

Vol. 23 | No. 3 | pp. 1579-1588 | 2024

Original Research Paper

https://doi.org/10.46488/NEPT.2024.v23i03.027

Open Access Journal

# Effect of Heavy Metal Phytoremediation on Phytochemical Fingerprint and Bioactivity of *Pistia stratiotes*: A Quest for Re-routing Disposal to Commercial Application

**Yashvi Hemani, Trisha Malde, Yashika Puri, Shubhada Walvekar and Sharon D'souza†**
Department of Biotechnology, S.V.K.M's Mithibai College of Arts, Chauhan Institute of Science and Amrutben Jivanlal College of Commerce and Economics, Vile Parle West, Mumbai-400 056, Maharashtra, India
†Corresponding author: Sharon D'souza; sharon.dsouza@mithibai.ac.in

**Nat. Env. & Poll. Tech.**
**Website: www.neptjournal.com**

*Received:* 23-01-2024
*Revised:* 28-02-2024
*Accepted:* 17-03-2024

**Key Words:**
Lead
Iron
Antiurolithic activity
Phytoremediation
Phytochemical fingerprint
Atomic absorption spectrophotometry
Thin layer chromatography

## ABSTRACT

Phytoremediation is one of the non-energy consuming processes of remediating polluted water. However, the disposal of post-remediated plants poses a threat of the re-introduction of pollutants back into the ecosystem. Re-routing remediated pollutants for commercial application could be one way to reduce the re-introduction of pollutants in an ecosystem. Heavy metal pollution in water bodies is one issue, which can be mitigated to an extent with phytoremediation. In the current study, the effect of heavy metal phytoremediation on the phytochemical fingerprint and bioactivity of *Pistia stratiotes* L. was investigated. *Pistia stratiotes* L. was subjected to different concentrations of iron (Fe) and lead (Pb), in the range of 5-20 ppm. Different parameters such as heavy metal estimation (in plants and water post-treatment), thin layer chromatography (TLC), antioxidant activity, and antiurolithic activity were measured. Post remediation, heavy metal concentration was found to be comparatively higher in roots (16.515 ± 0.008 $mg.g^{-1}$ and 5.25 ± 0.086 $mg.g^{-1}$ when treated with 15 ppm iron and lead respectively). TLC revealed differences between the fingerprints of treated and untreated plants. Some bands increased in intensity as the concentration of heavy metal increased, while some bands which were present in untreated, were absent in treated plant samples. Antioxidant activity of treated plants shows lesser $IC_{50}$ values, compared to untreated, in that, treated leaves show better activity ($IC_{50}$ = 1.8 ± 0.5220 $mg.mL^{-1}$ of leaf treated with 2 ppm iron as opposed to $IC_{50}$ > 5 $mg.mL^{-1}$ of untreated leaf extract). The treated plants revealed good antiurolithic activity compared to untreated, in that, the percentage inhibition showed by Iron treated leaves and roots was better (96.87% and 98.95% exhibited by iron-10 ppm treated leaves and roots respectively), while the untreated showed a maximum of only 68.75% inhibition. The results suggest that the bioactivity of the plant extracts increases post-remediation. Potential applications of these extracts can be explored such as nanoparticle synthesis, drug discovery, etc.

## INTRODUCTION

The introduction of heavy metals like lead, iron, mercury, and arsenic to water bodies due to human and natural sources has numerous ill effects because of their inability to degrade and remain until treatment. Lead (Pb) and iron (Fe) are one of the major heavy metal polluters. Many researchers have proposed various chemical methods for the extraction of heavy metals from the ecosystem. Some of these methods are reverse osmosis, electrodialysis, ion exchange, chemical precipitation, and ultrafiltration (Singh et al. 2012). These methods proved to be effective but cost-bearing and produced many non-biodegradable by-products. Green remediation technology uses plants to extract pollutants or transform them into non-toxic forms. *Eichhornia crassipes* L. (Malik et al. 2020), *Lemna minor* L. (Materac & Sobiecka 2017), *Phragmites australis* (Milke et al. 2020), and *Pistia stratiotes* L. (Tripathi et al. 2010) have been majorly used in phytoremediation of wastewater. The heavy metal is effectively extracted from the wastewater and concentrated in the plant; however, the main concern is the disposal of the plants (Farraji et al. 2016). When these plants are disposed of, the extracted heavy metal potentially re-enters the earth.

To break this cycle, we propose the utilization of the whole plant for potential commercial use. Plants under biotic and abiotic stress elicit secondary metabolites for combating the same. We hypothesized that because heavy metals elicit the production of secondary metabolites (Lajayer et al. 2017), the treated *Pistia stratiotes* L. plants can be expected to show a change in their phytochemical fingerprint and bioactive properties. *Pistia stratiotes* L. has already been studied for its wound healing, antifungal, anti-dermatophytic, and antimicrobial properties (Tripathi et al. 2010), so any

enhancement in the production of secondary metabolites or the aforementioned properties can be considered for a commercial application. Although the ill effects of heavy metals on the human body are not fully ruled out, the way they can be safely introduced can be investigated.

Lead and iron have been used in the current study, as heavy metal contaminants. As lead is not known to have any physiological functions in the human body, its concentration in the blood should be very low. The natural sources of lead include volcanic eruptions and forest fires and the artificial sources are batteries, toys, cosmetics, vehicles using leaded petrol or gasoline, lead smelters, burning of coal, and ammunition used in hunting (Iqbal 2012, Zhang et al. 2015). Pratush et al. (2018) mentioned that the lead added to gasoline in vehicles forms chloride, bromide, and oxide salts which exit through the exhaust pipe. The larger particles settle down and enter the soil or groundwater reserves whereas the smaller particles remain suspended in the air. As lead cannot be degraded by natural methods or microbial activity, it remains in the ecosystem for a long time (Zhang et al. 2015). Lead poisoning can cause cardiovascular diseases (Iqbal 2012), dysfunction of the endocrine and reproductive systems, infertility in men, and miscarriages in women (Ara et al. 2015). It can also affect neurological well-being, renal and gastrointestinal health, developmental and immunological issues (Zhang et al. 2015).

On the other hand, iron has many physiological functions in the human body like oxygen transport, DNA synthesis, transport of electrons, etc. Hence, iron is effectively absorbed in the small intestine and is stored in the form of ferritin and hemosiderin in the bone marrow, spleen, and liver (Abbaspour et al. 2014). The presence of iron contamination in water bodies can result from several natural sources including the action of microorganisms and the breaking down of minerals with high iron content. Iron is additionally introduced to water bodies by sewage discharge, corroded water pipes, and other human activities related to the metal industry (Sarkar et al. 2018). Excessive amounts of iron can harm human health by increasing the risk of conditions including diabetes, hepatic cancer, heart ailments, and other illnesses (Kumar et al. 2017). At higher concentrations, iron facilitates the synthesis of reactive oxygen species (ROS) which can damage cellular constituents (Wessling-Resnick 2017).

The presence of heavy metals in water bodies affects marine life adversely. A study conducted in the Mithi River in Mumbai (Kakde & Nagarsekar 2014) discusses the presence of elevated levels of many heavy metals, including lead and iron, and their adverse effects. Lead accumulates in the tissues of fish and causes degenerative diseases and changes in the circulatory and nervous systems (Afshan et al. 2014). In addition, lead pellets used for hunting swans, ducks, and waterfowl are conveyed through the food chain to the higher tropic levels and put bigger carnivores at risk as well (Zhang et al. 2015).

The current paper discusses the effect of increasing concentrations of lead and iron on the phytochemical makeup, antioxidant activity, and anti-urolithic activity of the plants for any potential change. Based on the results, further applications could be proposed for the whole plant utilization and diverting the re-introduction of heavy metals into the earth.

## MATERIALS AND METHODS

### Phytoremediation Studies

**Sample collection, authentication and pre-treatment:** *Pistia stratiotes* L., was collected from a local nursery and authenticated at the Blatter Herbarium in St. Xavier's College. The plants were then divided into equal numbers (10 plants each) and treated with increasing concentrations of lead and iron separately (2 ppm, 5 ppm, 10 ppm, 15 ppm and 20 ppm) in simulated wastewater for 10 days. One batch of plants was not treated with the heavy metals and is referred to as "untreated" in this paper. The leaves and roots of the plants were separated and air-dried for a few days before drying them in the oven at 50°C.

**Lead (Pb) and iron (Fe) estimation in *Pistia stratiotes* L. and water by Atomic Absorption Spectroscopy (AAS):** An amount of 0.1 g of the dried plant parts was taken in a 250 mL conical flask and to these flasks, 10 mL of concentrated nitric acid (69-72%) and 5 mL of perchloric acid (70%) was added. The flasks were then kept on a hot plate until complete acid digestion. The liquid obtained was filtered using Whatman filter paper and diluted to 100 mL with distilled water. The digested plant samples were analyzed for heavy metals by direct air acetylene flame method by using the lead and iron lamps in Atomic absorption spectroscopy (Thermo Scientific). The standards, water, and plant samples (treated & untreated) were measured at wavelengths 217 nm for lead and 246.3 nm for iron.

The bioconcentration factor is the ratio of a chemical's concentration in a living substance to the concentration of that chemical in the surrounding environment, in this case, water (Manahan 2009). It was calculated as follows:

BCF = Metal concentration in roots/leaves ÷ 2

BCF >1 indicates the concentration of metal in the plant is greater than its surroundings. The translocation factor (TF), also known as the shoot-root quotient, describes a plant's

ability to transport metal from its roots to its shoots and leaves, which is principally responsible for phyto-extraction (Nirola et al. 2015).

The translocation factor was also calculated using the formula:

TF = Heavy metal concentration in leaf ÷ Heavy metal concentration in roots

**Phytochemical and Bioactivity Studies**

**Preparation of plant extracts for TLC and bioactivity studies:** The dried plant material was ground and macerated to form a coarse powder. Methanol and ethanol were added to the dried powder in a ratio of 7:3. After 24 hours, the extract was filtered using Whatman filter paper. The extracts were stored in microfuge tubes in the fridge at 4°C.

**Phytochemical fingerprinting by thin layer chromatography:** Using the CAMAG Linomat 5 semi-automatic applicator, 5 microlitres of the plant extracts (Untreated & Treated with 2, 5, 10, 15, 20 ppm Pb and Fe respectively) were applied to a TLC plate of size 10 × 10 cm. The plate was dried and developed in a 10 × 10 twin trough chamber which was saturated with the 20ml mobile phase (toluene: chloroform: ethanol in the proportion 4:4:1) for 10 minutes. The mobile phase was run until 70 mm, after which the plate was dried using a dryer. The plates were first visualized using a TLC visualizer under 256 nm and 366 nm. It was then scanned with the CAMAG TLC scanner at 254 nm, 366 nm, and 540 nm. Further, the plates were derivatized with anisaldehyde reagent and visualized, and scanned again at 366 nm and 540 nm for better visualization. The software used for the entire process was VisionCATS.

**Determination of antioxidant activity by DPPH assay**: The antioxidant activity of treated and untreated leaf and root extracts of *Pistia stratiotes* L. was assessed using the microtiter plate method with 1,1-diphenyl-2-picrylhydrazyl (DPPH). A 0.1 mM DPPH reagent was prepared by dissolving 3.94 mg of DPPH powder in 100 mL of methanol. 100 µL plant methanolic extracts were added to the ELISA plate, followed by 100 µL of DPPH reagent in each well. Ascorbic acid was used as the standard. After an incubation period of 30 minutes, the absorbance was measured using an ELISA plate reader (Erba Mannheim). The percentage inhibition of each sample was calculated by subtracting the absorbance of the sample from the absorbance of the blank and then dividing it by the absorbance of the blank into 100.

**Assessment of antiurolithic activity by methanolic extracts of *Pistia stratiotes* L.:** The antiurolithic activity of the plant *Pisita stratiotes* was investigated using a synthetic urine assay on plants treated with varying doses of lead and iron, respectively. According to Atmani et al. (2000), a synthetic urine assay was used to evaluate the percentage inhibition and development of calcium oxalate monohydrate crystals at varied doses of plant extract.

In the laboratory, artificial urine was created by combining two solutions of the following composition: $Na_2C_2O_4$ (2 mmol.$L^{-1}$) and $CaCl_2.2H_2O$ (10 mmol.$L^{-1}$) (Beghalia et al. 2008). With the addition of NaCl, two solutions were created. To count the number of crystals, a drop of the solution was placed on a hemocytometer slide. To determine the percentage of inhibition, an equal volume of the above-mentioned solution and plant extract were mixed and incubated for 30 minutes. Following incubation, the number of crystals was counted using a hemocytometer slide under a 10X objective lens of a light microscope.

Percentage inhibition = (TSI-TAI) ÷ TSI × 100

TSI = number of Ca-oxalate monohydrate crystals before inhibitor (plant extract)

TAI = number of Ca-oxalate monohydrate crystals after adding inhibitor

## RESULTS AND DISCUSSION

**Heavy Metal Estimation in *Pistia stratiotes* L. and Water by Atomic Absorption Spectroscopy**

From Table 1, it was observed that the treated roots showed a significant increase in iron concentration as compared to the leaves. The lowest concentration of iron in roots was seen at 10 ppm, at which the concentration significantly increased in leaves, which might suggest that at 10 ppm, iron might be translocated efficiently to the leaves from the roots. The concentration of iron in the water samples also significantly decreased with the increase in concentration, thereby indicating that the metal has been taken up by the plant. In this case, the Bioconcentration factor was found to be the highest at 2 ppm. The ratio decreased as the iron concentration increased, which may be because the plant was reaching a saturation level.

From the results obtained in Table 2, we can see that the roots showed a higher accumulation of lead as compared to the leaves. There was also a decrease in the concentration of lead from 15 ppm to 20 ppm in the roots, which could mean that 15 ppm is the saturation point for the uptake of the metal in the plant.

Considering the levels of lead in the water after treatment is also less, there is a possibility of biotransformation of lead within the roots, at 20 ppm. Furthermore, the concentration of lead in leaf

Table 1: Iron concentration in treated and untreated *Pistia stratiotes* L. and water samples. The values for treated samples reported are post-phytoremediation and their corresponding bioconcentration and translocation factors.

| Samples | Roots ($mg.g^{-1}$) | | Leaves ($mg.g^{-1}$) | | Iron concentration of Water ($mg.g^{-1}$)* | Translocation factor (Iron treated) |
|---|---|---|---|---|---|---|
| | Iron concentration | Bioconcentration factor | Iron concentration | Bioconcentration factor | | |
| Untreated | 6.315 ± 0.087 | – | 0.09 | – | 0.000975 | 0.15 |
| Treated 2 ppm | 16.095 ± 0.017 | 8.0475 | 1.26 | 0.63 | 0.00048 | 0.078 |
| Treated 5 ppm | 15.315 ± 0.008 | 3.063 | 1.23 ± 0.008 | 0.246 | 0.00387 | 0.080 |
| Treated 10 ppm | 9.33 | 0.933 | 3.135 ± 0.008 | 0.3135 | 0.005625 | 0.336 |
| Treated 15 ppm | 16.515 ± 0.008 | 1.101 | 1.8 ± 0.008 | 0.12 | 0.00054 | 0.108 |
| Treated 20 ppm | 16.38 ± 0.008 | 0.819 | 2.085 ± 0.017 | 0.10425 | 0.00033 | 0.127 |

*Water analysis post-treatment

Table 2: Lead concentration in treated and untreated *Pistia stratiotes* L. and water samples. The values for treated samples reported are post-phytoremediation and their corresponding bioconcentration and translocation factors.

| Samples | Roots ($mg.g^{-1}$) | | Leaves ($mg.g^{-1}$) | | Lead concentration of Water ($mg.g^{-1}$)* | Translocation factor (Lead treated) |
|---|---|---|---|---|---|---|
| | Lead concentration | Bioconcentration factor | Lead concentration | Bioconcentration factor | | |
| Untreated | 0 | — | 0.15 ± 0.086 | — | 0.00003 | 0.15 |
| Treated 2 ppm | 0.9 ± 0.086 | 0.45 | 0.15 ± 0.086 | 0.075 | 0.00015 | 0.166 |
| Treated 5 ppm | 1.8 ± 0.086 | 0.9 | 0.3 | 0.15 | 0.002745 | 0.166 |
| Treated 10 ppm | 3.6 ± 0.086 | 1.8 | 0.3 ± 0.086 | 0.15 | 0.000555 | 0.083 |
| Treated 15 ppm | 5.25 ± 0.086 | 2.625 | 0.6 | 0.3 | 0.00432 | 0.114 |
| Treated 20 ppm | 1.2 | 0.6 | 1.05 ± 0.086 | 0.525 | 0.000015 | 0.875 |

*Water analysis post-treatment

20 ppm is significantly higher as compared to the other leaves, which also indicates that at 15 ppm lead treatment, the metal could be translocated from roots to leaves.

As can be observed in Tables 1 and 2, the Translocation factor of iron-treated plants increases from 5 ppm to 10 ppm and then decreases from 10 ppm to 15 ppm. The metal is assumed to be translocated efficiently at 10 ppm treatment, following which the plant could be saturated at higher concentrations. However, in the case of lead-treated plants, there is an increase in the translocation factor as the concentration of lead increases in the plant. This is an indication that the metal is translocated from roots to leaves at higher lead concentrations, efficiently. Therefore, *Pistia stratiotes* L.could be an efficient accumulator of lead at higher concentrations.

Heavy metal analysis of iron in *P. stratiotes* L. has been previously studied and it shows a great increase in metal concentration in the treated parts of the plants and the highest concentration was always contained in the roots. The initial concentration was seen as 8.682 $mg.g^{-1}$ and the final was seen as 12.226 $mg.g^{-1}$ in 2 $mg.L^{-1}$ concentration of the Iron (Mishra & Tripathi 2008)**.** Another study reports that the concentration of iron and lead was found to be the highest in roots as compared to the leaves and the translocation factor did not exceed one, indicating that this plant exhibits rhizofiltration (Galal et al. 2018). Studies have also shown *P. stratiotes* L. as a hyperaccumulator of lead and iron and thus can be applied for the remediation of surface waters (Lu et al. 2011). With a clearance percentage of 99.31% at 1 $mg.L^{-1}$, *P. stratiotes* L. had the highest tolerance and removal efficiency for lead. The ability of *P. stratiotes* L. to remove heavy metals, particularly lead, suggested that they could be useful in the treatment of metal-polluted water (Zahari et al. 2021). The result obtained in our study is in alignment with the literature reported.

## Phytochemical Fingerprinting By Thin Layer Chromatography

Heavy metals at a high concentration in the environment act as abiotic stress agents that lead to oxidative damage in plants. Plants growing in such environments respond to the threat with various defense mechanisms. A common defense

mechanism against heavy metals is excessive production of secondary metabolites. These secondary metabolites can precipitate metal ions, act as chelating agents, and help scavenge reactive oxygen species (ROS) (Anjitha et al. 2021). Hence, this suggests that to stimulate the production of excess secondary metabolites, one could treat the plants with heavy metals.

The leaves of *P. stratiotes* L. are said to have many secondary metabolites including alkaloids, phytosterols, triterpenes, flavonoids, and terpenoids (Desai & Aparadh 2014). They also have tannins, saponins, steroids, quinones, and anthraquinones, while the roots of *P. stratiotes* L. harbor flavonoids, quinones, and anthraquinones (Tyagi 2017). When used for phytoremediation of heavy metals, these plants are under abiotic stress which is then expected to produce an enhanced rate of production of some secondary metabolites as seen in the experiments performed by Rao et al. (2021), Zhu et al. (2020), Farrokhzad & Rezaei (2020), Drzewiecka et al. (2018), Kisa et al. (2016), Abnosi et al. (2015), and Kai et al. (2012).

To compare the production of these secondary metabolites in the untreated plants and the plants treated in simulated wastewater containing heavy metal (here, iron or lead), thin-layer chromatography was used. The aim was to compare the phytochemical fingerprints of the untreated plants to the treated ones by chromatography. Visually, many changes in the phytochemical fingerprint of the plant extracts could be observed. Some bands showed an increase in intensity with the increasing concentration of heavy metal in the simulated wastewater. However, some other bands disappeared altogether in the treated samples.

Previous studies such as the one where treatment of plant cell cultures with heavy metals have proven that exposure to heavy metal as an effective way to elicit secondary

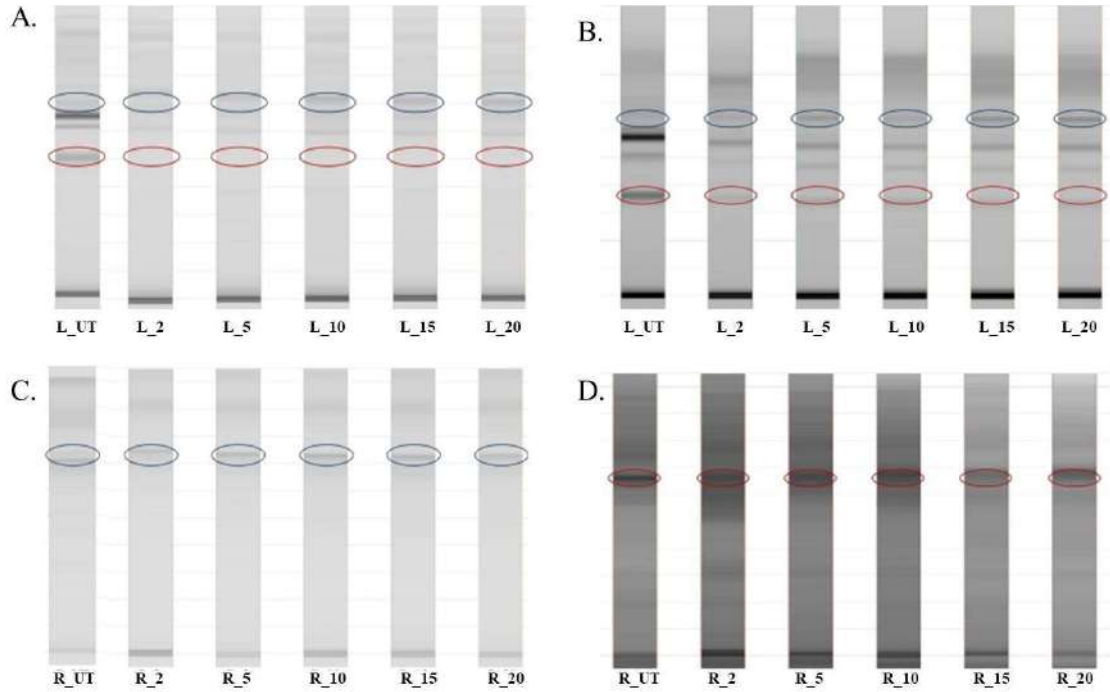


Fig. 1: Densitogram of the developed TLC plates scanned; (A) Methanolic extracts of leaves of *P. stratiotes* L. treated with iron scanned at 366 nm before derivatization with anisaldehyde reagent. The blue circles indicate the increase in the intensity of a band in the samples treated with iron as compared to the untreated. The red circles show a band disappearing after treatment with iron. (B) Leaf methanolic extracts of *P. stratiotes* L. treated with lead scanned at 366 nm before derivatization with anisaldehyde reagent. The bands encircled in blue show an absence of the compound in the untreated sample and an increase in density in the samples treated with lead. The bands encircled in red show a band present in the untreated sample which disappears in the treated samples. (C) Methanolic extracts of roots of *P. stratiotes* L. treated with iron scanned at 254 nm before derivatization with anisaldehyde reagent. The blue circles represent the band that is absent in the untreated sample and is present almost uniformly in the samples treated with iron. (D) Root methanolic extracts of *P. stratiotes* L. treated with lead scanned at 366 nm after derivatization with anisaldehyde reagent The bands encircled in red show the decreasing density of a band in the samples treated with lead as compared to the untreated sample. Key: L_UT – untreated leaves, L_2 – leaves treated at 2 ppm, L_5 – leaves treated at 5 ppm, L_10 – leaves treated at 10 ppm, L_15 – leaves treated at 15 ppm and L_20 – leaves treated at 20 ppm.; R_UT – untreated roots, R_2 – roots treated at 2 ppm, R_5 – roots treated at 5 ppm, R_10 – roots treated at 10 ppm, R_15 – roots treated at 15 ppm and R_20 – roots treated at 20 ppm.

metabolite production. Bota and Deliu noted that $CuSO_4$ can be used to stimulate the production of flavonoids in *Digitalis lanata* suspension cultures (Bota & Deliu 2011). Cultures of *Camellia sinensis* expressed an increase in the production of cinnamic acid in response to the addition of Co ions (Sutini et al. 2019). Resveratrol production can be stimulated in *Vitis vinifera* cell cultures by the presence of $Co^{2+}$, $Ag^{+}$, and $Cd^{2+}$ (Cai et al. 2013). In Fig. 1, we can see a stark difference in the phytochemical fingerprint of untreated and treated plants of *P. stratiotes* L.. This suggests that exposure of plants to heavy metals during phytoremediation has led to a change in the production of secondary metabolites.

The Rf values obtained from the chromatogram of the untreated sample were compared statistically to that of the treated samples at a particular wavelength i.e. 254 nm, 366 nm, and 540 nm using the Kruskal-Wallis test. The null hypothesis of the test (Ho) was considered as "no significant differences between the number and pattern of compounds between untreated and each treated sample", and the alternate hypothesis as "there is a significant difference between the number and pattern of compounds between untreated and each treated sample".

It was seen from Tables 3 and 4, that at all wavelengths, the estimated p-value was greater than 0.05, which means

Table 3: Biostatistical analysis of Rf values obtained from the phytochemical fingerprint of lead-treated *Pistia stratiotes* L. methanolic extracts.

| Sr. No. | Wavelength | Rf between samples | H statistic | P value | Significant difference (P<0.05) |
|---|---|---|---|---|---|
| 1. | 254 nm | UT_L, T_Pb_2_L, T_Pb_5_L, T_Pb_10_L, T_Pb_15_L & T_Pb_20_L | 0.2738 | 0.9981 | No |
| | | UT_R, T_Pb_2_R, T_Pb_5_R, T_Pb_10_R, T_Pb _15_R & T_Pb_20_R | 1.4270 | 0.9213 | No |
| 2. | 366 nm | UT_L, T_Pb_2_L, T_Pb_5_L, T_Pb_10_L, T_Pb_15_L & T_Pb_20_L | 0.2921 | 0.9978 | No |
| | | UT_R, T_Pb_2_R, T_Pb_5_R, T_Pb_10_R, T_Pb_15_R & T_Pb_20_R | 2.6840 | 0.7485 | No |
| 3. | 540 nm | UT_L, T_Pb_2_L, T_Pb_5_L, T_Pb_10_L, T_Pb_15_L & T_Pb_20_L | 0.8141 | 0.9761 | No |
| | | UT_R, T_Pb_2_R, T_Pb_5_R, T_Pb_10_R, T_Pb_15_R & T_Pb_20_R | - | - | - |
| 4. | 366 nm Derivatized | UT_L, T_Pb_2_L, T_Pb_5_L, T_Pb_10_L, T_Pb_15_L & T_Pb_20_L | 2.5032 | 0.7760 | No |
| | | UT_R, T_Pb_2_R, T_Pb_5_R, T_Pb_10_R, T_Pb_15_R & T_Pb_20_R | 1.7225 | 0.8860 | No |
| 5. | 540 nm Derivatized | UT_L, T_Pb_2_L, T_Pb_5_L, T_Pb_10_L, T_Pb_15_L & T_Pb_20_L | 1.6709 | 0.8925 | No |
| | | UT_R, T_Pb_2_R, T_Pb_5_R, T_Pb_10_R, T_Pb_15_R & T_Pb_20_R | 0.5769 | 0.9890 | No |

Key for leaf samples: UT_L: untreated leaves; T_Pb_2_L: leaves treated at 2 ppm Pb; T_Pb_5_L: leaves treated at 5 ppm Pb; T_Pb_10_L:leaves treated at 10 ppm Pb; T_Pb_15_L:leaves treated at 15 ppm Pb & T_Pb_20_L: leaves treated at 20 ppm Pb.

Key for root samples: UT_R: untreated roots; T_Pb_2_R: roots treated at 2 ppm Pb; T_Pb_5_R: roots treated at 5 ppm Pb; T_Pb_10_R:roots treated at 10 ppm Pb; T_Pb_15_R:roots treated at 15 ppm Pb & T_Pb_20_R: roots treated at 20 ppm Pb.

Table 4: Biostatistical analysis of Rf values obtained from the phytochemical fingerprint of iron-treated *Pistia stratiotes* L. methanolic extracts.

| Sr. No. | Wavelength | Rf between samples | H statistic | P value | Significant difference (P<0.05) |
|---|---|---|---|---|---|
| 1. | 254 nm | UT_L, T_Fe_2_L, T_Fe_5_L, T_Fe_10_L, T_Fe_15_L & T_Fe_20_L | 0.9464 | 0.96677 | No |
| | | UT_R, T_Fe_2_R, T_Fe_5_R, T_Fe_10_R, T_Fe_15_R & T_Fe_20_R | 3.7474 | 0.58632 | No |
| 2. | 366 nm | UT_L, T_Fe_2_L, T_Fe_5_L, T_Fe_10_L, T_Fe_15_L & T_Fe_20_L | 1.6557 | 0.89443 | No |
| | | UT_R, T_Fe_2_R, T_Fe_5_R, T_Fe_10_R, T_Fe_15_R & T_Fe_20_R | 0.7780 | 0.97842 | No |
| 3. | 540 nm | UT_L, T_Fe_2_L, T_Fe_5_L, T_Fe_10_L, T_Fe_15_L & T_Fe_20_L | 0.4867 | 0.99260 | No |
| | | UT_R, T_Fe_2_R, T_Fe_5_R, T_Fe_10_R, T_Fe_15_R & T_Fe_20_R | - | - | - |
| 4. | 366 nm Derivatized | UT_L, T_Fe_2_L, T_Fe_5_L, T_Fe_10_L, T_Fe_15_L & T_Fe_20_L | 0.2877 | 0.99787 | No |
| | | UT_R, T_Fe_2_R, T_Fe_5_R, T_Fe_10_R, T_Fe_15_R & T_Fe_20_R | 2.9761 | 0.7037 | No |
| 5. | 540 nm Derivatized | UT_L, T_Fe_2_L, T_Fe_5_L, T_Fe_10_L, T_Fe_15_L & T_Fe_20_L | 1.6826 | 0.89108 | No |
| | | UT_R, T_Fe_2_R, T_Fe_5_R, T_Fe_10_R, T_Fe_15_R & T_Fe_20_R | 1.8428 | 0.87044 | No |

Key for leaf samples: UT_L: untreated leaves; T_Fe_2_L: leaves treated at 2 ppm Fe; T_Fe_5_L: leaves treated at 5 ppm Fe; T_Fe_10_L:leaves treated at 10 ppm Fe; T_Fe_15_L:leaves treated at 15 ppm Fe & T_Fe_20_L: leaves treated at 20 ppm Pb.

Key for root samples: UT_R: untreated roots; T_Fe_2_R: roots treated at 2 ppm Fe; T_Fe_5_R: roots treated at 5 ppm Fe; T_Fe_10_R:roots treated at 10 ppm Fe; T_Fe_15_R:roots treated at 15 ppm Fe & T_Fe_20_R: roots treated at 20 ppm Fe.

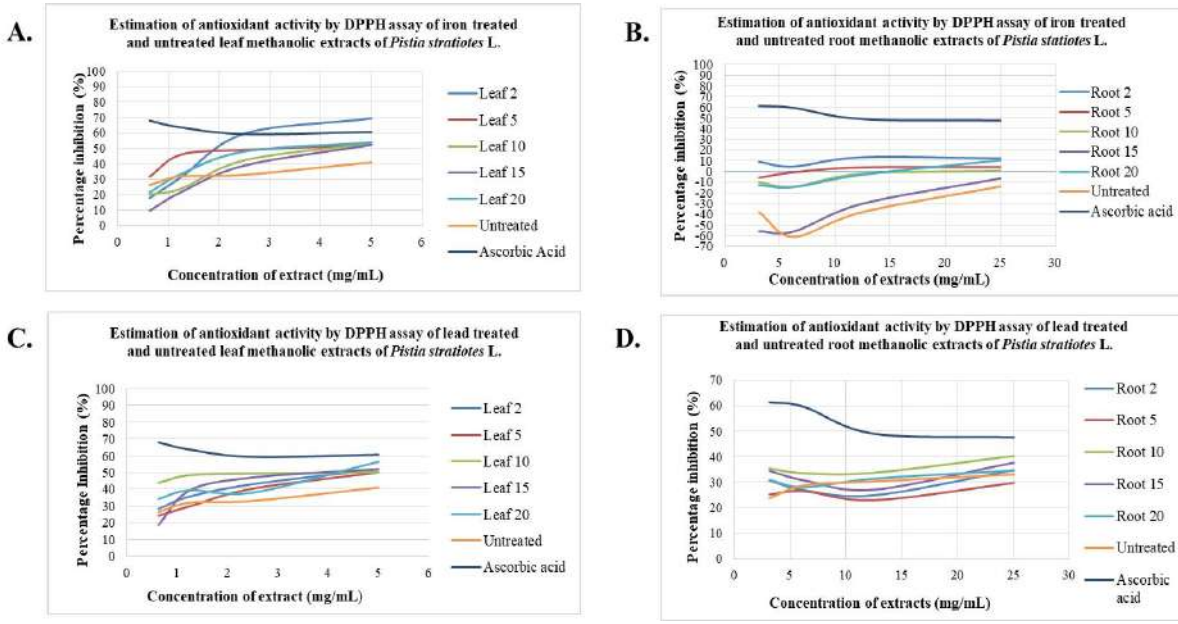


Fig. 2: Percentage inhibition Vs. Concentration of extract graph of: (A) Iron treated and untreated methanolic leaf extracts of *P. stratiotes* L. at different concentrations (0.625 to 5 mg.mL$^{-1}$); (B) Iron treated and untreated methanolic root extracts of *P.stratiotes* L. at different concentrations (3.125 to 25 mg.mL$^{-1}$); (C) Lead treated and untreated methanolic leaf extracts of *P. stratiotes* L. at different concentrations (0.625-5 mg.mL$^{-1}$); (D) Lead treated and untreated methanolic root extracts of *P. stratiotes* L. at different concentrations (3.125 to 25 mg.mL$^{-1}$). Key: Untreated– untreated leaves, leaf 2 – leaves treated at 2 ppm, leaf 5 – leaves treated at 5 ppm, leaf 10– leaves treated at 10 ppm, leaf 15– leaves treated at 15 ppm and leaf 20 – leaves treated at 20 ppm; Untreated– untreated roots, root 2 – roots treated at 2 ppm, root 5 – roots treated at 5 ppm, root 10– roots treated at 10 ppm, root 15 – roots treated at 15 ppm and root 20 – roots treated at 20 ppm.

that the difference in the band patterns of the treated and untreated samples was not statistically significant.

### Determination of Antioxidant Activity of *Pistia stratiotes* L. Heavy Metal Treated and Untreated Samples by DPPH Assay

Antioxidant compounds such as phenolics, flavonoids, and certain enzymes play an important role in protection against cellular damage caused by Reactive Oxygen Species (ROS). Previous studies have shown the presence of antioxidant activity in methanolic extracts of leaves and roots of *Pistia stratiotes* L. (Tyagi & Parashar 2017). A comparative study was done to determine the difference in the antioxidant activity of the plant before and after treatment with heavy metals using the DPPH assay. The results were then plotted on a graph and the $IC_{50}$ value was calculated. Leaf methanolic extracts in the range of 0.625-5 mg.mL$^{-1}$ were used while root methanolic extracts in the range of 3.125 to 25 mg.mL$^{-1}$ were used, since at lower concentrations, $IC_{50}$ values could not be detected in roots.

Table 5: $IC_{50}$ values of lead and iron treated and untreated leaf and root extracts antioxidant activity.

| Samples (Treatment concentration) | $IC_{50}$ values (mg.mL$^{-1}$) for Lead treated plants | | $IC_{50}$ values (mg.mL$^{-1}$) for Iron treated plants | |
|---|---|---|---|---|
| | Leaf methanolic extracts | Root methanolic extracts | Leaf methanolic extracts | Root methanolic extracts |
| Untreated | > 5 | > 25 | >5 | >25 |
| 2 ppm | 4.4 ± 0.0283 | >25 | 1.8 ± 0.5220 | >25 |
| 5 ppm | 4.95 ± 0.1768 | >25 | 3.4 ± 0.3535 | >25 |
| 10 ppm | 4.55 ± 0.4243 | >25 | 4.2 ± 0.0707 | >25 |
| 15 ppm | 3.8 ± 0.2121 | >25 | 4.55 ± 0.1414 | >25 |
| 20 ppm | 4.15 ± 0.5657 | >25 | 3.05 ± 0.03535 | >25 |

Table 6: Study of anti-urolithic activity in Lead and Iron treated and untreated root and leaf samples.

| Concentration of extract ($\mu g.mL^{-1}$) | Lead treated samples | | Iron treated samples | |
|---|---|---|---|---|
| | Leaves (Percent inhibition) | Roots (Percent inhibition) | Leaves (Percent inhibition) | Roots (Percent inhibition) |
| Untreated | 16.66 | 68.75 | 16.66 | 68.75 |
| 2 ppm | 76.04 | 78.12 | 91.79 | 63.54 |
| 5 ppm | 86.98 | 79.16 | 94.87 | 65.12 |
| 10 ppm | 92.7 | 89.58 | 96.87 | 98.95 |
| 15 ppm | 94.79 | 84.37 | 92.3 | 92.3 |
| 20 ppm | 33.33 | 86.97 | 87.17 | 89.58 |

From Fig. 2, it could be observed that the treated leaf extracts showed increased antioxidant activity as compared to the untreated extract. At a concentration of 5 $mg.mL^{-1}$, the untreated leaf extract showed the lowest percentage inhibition (40.98%), whereas a higher percentage inhibition was seen in leaf extract of the plants treated with lead and iron (Fig. 2A and 2C). In iron-treated leaf extracts (Fig. 2A), the highest percentage of inhibition was seen in plants treated with 2 ppm at an extract concentration of 5 $mg.mL^{-1}$ (69.34%). In lead-treated leaf extracts (Fig. 2C), the highest percentage of inhibition was seen in plants treated with 20 ppm at an extract concentration of 5 $mg.mL^{-1}$ (56.33%). However, $IC_{50}$ values of root extracts of the untreated and treated plants (both iron and lead), were not achieved. The same has been reported in Table 5.

The presence of heavy metals is known to induce oxidative stress in plants which may lead to the synthesis of several secondary metabolites (Anjitha et al. 2021). To defend themselves from free radicals, plants may increase the production of bioactive antioxidant compounds (Fryzova et al. 2018). Studies on *Macrotyloma uniflorum* and *Cicer arietinum* L. showed an increase in activity of antioxidative enzymes like superoxidase, dismutase, and catalase on exposure to lead stress (Reddy et al. 2005).

### Assessment of Antiurolithic Activity by Methanolic Extracts of *Pistia stratiotes* L.

The Antiurolithic activity was checked using artificial urine and from the results obtained it was found that the Treated parts of the samples showed a higher percentage of inhibition as compared to the untreated samples as seen in Table 6.

The plants treated with lead comparatively showed a higher percentage of inhibition in treated leaves rather than roots. The plant showed a greater percentage inhibition at 15 ppm as compared to the other concentrations. The highest percentage inhibition difference was seen between 20 ppm roots and leaves. Here, the plant extract acted as an inhibitor. At 2 and 20 ppm, the roots showed a higher percentage of inhibition as compared to the leaves, whereas at 5, 10 and 15 ppm, the leaves showed a higher percentage of inhibition as compared to the roots.

Plants treated with iron showed percentage inhibition was higher in roots as compared to the leaves. It can also be observed that the percent inhibition was seen as the highest in treated samples as compared to the untreated ones.

Previously, antiurolithic activity has been studied in plants like *Tephrosia tinctoria* (Fabaceae) and *Boehmeria macrophylla* (Urticaceae), wherein the methanolic extracts were used to check their ability to prevent the formation of calcium oxalate monohydrate crystals using artificial urine synthesized in the laboratory. Both tropical species inhibited the formation of calcium oxalate crystals in the presence of artificial urine (Bavishi et al. 2019).

Similarly, here methanolic extracts of *Pistia stratiotes* L. showed an inhibition against calcium oxalate crystals in the presence of heavy metals. Further toxicity studies need to be done on the introduction of such metal into the human body.

## CONCLUSION

The results from atomic absorption spectroscopy showed that the *P. stratiotes* exhibit rhizofiltration which is in line with the literature available (Veselý et al. 2011). The highest amount of the metal was found to be stored in roots as compared to the leaves. Hence, *P. stratiotes* could be used in wastewater and industrial waste to reduce the content of heavy metals.

The results of thin layer chromatography show a change in the phytochemical fingerprint of plants treated with heavy metals as compared to the untreated ones. The secondary metabolites that increase in concentration can further be characterized and purified for commercial use. Plant secondary metabolites such as vincristine, paclitaxel, and homoharringtonine are being used in cancer therapy (Seca & Pinto 2018). Nicotine, veratrin, anabasine, anthocyanin

pigments, and tannins have been studied for their insecticidal properties (Rattan 2010). Aristolochic acid, furanoquinoline alkaloids, colchicine, vinblastine, phenylpropanoids, and isothiocyanates are some secondary metabolites that display anti-parasitic properties (Wink 2012). During the green synthesis of nanoparticles from plant extracts, secondary metabolites, especially flavonoids, play an important role in their formation and stabilization (Marslin et al. 2018). Other applications of secondary metabolites include their use as dyes (e.g. indigo), flavoring agents (vanillin), fragrances (essential oils of lavender), painkillers (morphine), and stimulants (caffeine, nicotine) (Rattan 2010).

The antiurolithic activity of the heavy metal-treated plant extracts showed a positive result in inhibiting the formation of calcium oxalate crystals. This can be correlated with the antioxidant activities, where, lead treated leaves at 15 ppm, shows both the highest antioxidant activity ($IC_{50}$ = 3.8 $mg.mL^{-1}$) and antiurolithic activity (Percentage inhibition = 94.79%). Thus, these heavy metal-treated plants can further be analyzed for their use against kidney stones and toxicity studies would also have to be conducted for the introduction of plant extracts containing heavy metals into the human body.

This study paves the way to consider the possibility of using plants subjected to remediation for commercial use since the results strongly emphasize the change in phytochemical and bioactive properties. Being a preliminary study, further investigation of its applications with actual wastewater needs to be reconfirmed.

## ACKNOWLEDGEMENT

We would like to thank our Principal of SVKM's Mithibai college and its management for providing us with a platform to conduct research, and to the Department of Botany, for allowing us to use Atomic Absorption Spectrophotometry.

## REFERENCES

Abbaspour, N., Hurrell, R. and Kelishadi, R. 2014. Review on iron and its importance for human health. Journal of Research in Medical Sciences: The Official Journal of Isfahan University of Medical Sciences, 19(2): 164-174.

Abnosi, M., Amirjani, M., Mahdiyeh, M. and Moradipoor, H. 2015. Biochemical and cellular response of Catharanthus roseus callus cells to cadmium toxicity. Journal of Genetic Resources, 1(2): 101-114. https://doi.org/10.22080/jgr.2015.1169

Afshan, S., Ali, S., Ameen, U., Farid, M., Bharwana, S., Hannan, F. and Ahmad, R. 2014. Effect of different heavy metal pollution on fish. Research Journal of Chemical and Environmental Sciences, 2: 74-79.

Anjitha, K., Sameena, P. and Puthur, J. 2021. Functional aspects of plant secondary metabolites in metal stress tolerance and their importance in pharmacology. Plant Stress, 2. https://doi.org/10.1016/j.stress.2021.100038

Ara, A., Wani, A. and Usmani, J. 2015. Lead toxicity: a review. Interdisciplinary Toxicology, 8(2): 55-64. https://doi.org/10.1515/intox-2015-0009

Atmani, F. and Khan, S. R. 2000. Effects of an extract from Herniaria hirsuta on calcium oxalate crystallization in vitro. Brazilian Journal of Urology, 85: 621-625. https://doi.org/10.1046/j.1464-410x.2000.00485.x

Bavishi, A., Gattani, N. and Walvekar, S. 2019. Study of antiurolithic activity of tropical flora of Western Ghats. Journal of Emerging Technologies and Innovative Research, 6(5): 594-599.

Beghalia, M., Said, G., Allali, H., Belouatek, A. and Marouf, A. 2008. Screening for anti-crystallisation calcium oxalate urolithiasis activity in Algerian plants. Malaysian Journal of Biochemistry and Molecular Biology, 16: 11-15.

Bota, C. and Deliu, C. 2011. The effect of copper sulphate on the production of flavonoids in Digitalis lanata cell cultures. Farmacia, 59(1): 113-118.

Cai, Z., Kastell, A., Speiser, C. and Smetanska, I. 2013. Enhanced resveratrol production in Vitis vinifera cell suspension cultures by heavy metals without loss of cell viability. Applied Biochemistry and Biotechnology, 171(2): 330-340. https://doi.org/10.1007/s12010-013-0354-4

Desai, S. and Aparadh, V. 2014. Screening of bioactive compounds of Sesbania grandiflora and Pistia stratiotes. Indian Journal of Plant Sciences, 1(1): 27-30.

Drzewiecka, K., Gąsecka, M., Rutkowski, P., Magdziak, Z., Golinski, P. and Mleczek, M. 2018. Arsenic forms and their combinations induce differences in phenolic accumulation in Ulmus laevis Pall. Journal of Plant Physiology, 220: 34-42. https://doi.org/10.1016/j.jplph.2017.09.013

Farraji, H., Zaman, N., Tajuddin, R. and Faraji, H. 2016. Advantages and disadvantages of phytoremediation: A concise review. International Journal of Environmental Science and Technology, 2: 69-75.

Farrokhzad, Y. and Rezaei, A. 2020. Aluminum elicitation improves antioxidant potential and taxol production in hazelnut (*Corylus avellana* L.) cell suspension culture. Agriculturae Conspectus Scientificus, 85(3): 229-236.

Fryzova, R., Pohanka, M., Martinkova, P., Cihlarova, H., Brtnicky, M., Hladky, J. and Kynicky, J. 2018. Oxidative stress and heavy metals in plants. Reviews of Environmental Contamination and Toxicology, 245: 129-156. https://doi.org/10.1007/398_2017_7

Galal, T., Eid, E., Dakhil, M. and Hassan, L. 2018. Bioaccumulation and rhizofiltration potential of *Pistia stratiotes* L. for mitigating water pollution in the Egyptian wetlands. International Journal of Phytoremediation, 20(5): 440-447. https://doi.org/10.1080/15226514.2017.1365343

Iqbal, M. 2012. Lead pollution - a risk factor for cardiovascular disease in Asian developing countries. Pakistan Journal of Pharmaceutical Sciences, 25(1): 289-294.

Kai, G., Yang, S., Zhang, Y., Luo, X., Fu, X., Zhang, A. and Xiao, J. 2012. Effects of different elicitors on yield of tropane alkaloids in hairy roots of *Anisodus acutangulus*. Molecular Biology Reports, 39(2): 1721-1729. https://doi.org/10.1007/s11033-011-0912-1

Kakde, U. and Nagarsekar, A. 2014. Studies on heavy metal contamination in Mithi river, Mumbai. International Interdisciplinary Research Journal, 4: 202-216. https://doi.org/10.5923/j.fs.20120203.03

Kisa, D., Elmastas, M., Öztürk, L. and Kayir, O. 2016. Responses of the phenolic compounds of Zea mays under heavy metal stress. Applied Biological Chemistry, 59(6): 813-820. https://doi.org/10.1007/s13765-016-0229-9

Kumar, V., Bharti, P. K., Talwar, M., Tyagi, A. K. and Kumar, P. 2017. Studies on high iron content in water resources of Moradabad district (UP), India. Water Science, 31(1): 44-51. https://doi.org/10.1016/j.wsj.2017.02.003

Lajayer, B., Ghorbanpour, M. and Nikabadi, S. 2017. Heavy metals in contaminated environment: Destiny of secondary metabolite biosynthesis, oxidative status and phytoextraction in medicinal plants.

Ecotoxicology and Environmental Safety, 145: 377-390. https://doi.org/10.1016/j.ecoenv.2017.07.035

Lu, Q., He, Z. L., Graetz, D. A., Stoffella, P. J. and Yang, X. 2011. Uptake and distribution of metals by water lettuce (*Pistia stratiotes* L.). Environmental Science and Pollution Research International, 18(6): 978-986. https://doi.org/10.1007/s11356-011-0453-0

Malik, A., Ali, Q. and Mi, N. 2020. Potential of water hyacinth (*Eichhornia crassipes* L.) for phytoremediation of heavy metals from wastewater. Research Journal of Biological Sciences, 1-6. https://doi.org/10.54112/bcsrj.v2020i1.6

Manahan, S. 2009. Fundamentals of Sustainable Chemical Science. CRC Press, Boca Raton, Florida.

Marslin, G., Siram, K., Maqbool, Q., Selvakesavan, R., Kruszka, D., Kachlicki, P. and Franklin, G. 2018. Secondary metabolites in the green synthesis of metallic nanoparticles. Materials, 11(6). https://doi.org/10.3390/ma11060940

Materac, M. and Sobiecka, E. 2017. The efficiency of macrophytes for heavy metals removal from water. Biotechnology and Food Science, 81(1): 35-40. https://doi.org/10.34658/bfs.2017.81.1.35-40

Milke, J., Gałczyńska, M. and Wróbel, J. 2020. The importance of biological and ecological properties of Phragmites australis (Cav.) Trin. Ex Steud., in phytoremediation of aquatic ecosystems - The review. Water, 12(6). https://doi.org/10.3390/w12061770

Mishra, V. K. and Tripathi, B. D. 2008. Concurrent removal and accumulation of heavy metals by the three aquatic macrophytes. Bioresource Technology, 99(15): 7091-7097. https://doi.org/10.1016/j.biortech.2008.01.007

Nirola, R., Megharaj, M., Palanisami, T., Aryal, R., Venkateswarlu, K. and Naidu, R. 2015. Evaluation of metal uptake factors of native trees colonizing an abandoned copper mine a quest for phytostabilization. Journal of Sustainable Mining, 14(3): 115-123. https://doi.org/10.1016/j.jsm.2015.11.001

Pratush, A., Kumar, A. and Hu, Z. 2018. Adverse effect of heavy metals (As, Pb, Hg and Cr) on health and their bioremediation strategies: a review. International Journal of Microbiology, 21: 97-106. https://doi.org/10.1007/s10123-018-0012-3

Rao, K., Chodisetti, B., Gandi, S., Giri, A. and Kavi Kishor, P. 2021. Cadmium chloride elicitation of Abutilon indicum cell suspension cultures for enhanced stigmasterol production. Plant Biosystems, 156(3): 613-618. https://doi.org/10.1080/11263504.2021.1891151

Rattan, R. 2010. Mechanism of action of insecticidal secondary metabolites of plant origin. Crop Protection, 29(9): 913-920. https://doi.org/10.1016/j.cropro.2010.05.008

Reddy, A. G. K., Kumar, S. S., Jyothsnakumari, G., Thimmanaik, S. and Sudhakar, C. 2005. Lead induced changes in antioxidant metabolism of horsegram (*Macrotyloma uniflorum* (Lam.) Verdc.) and bengalgram (*Cicer arietinum* L.). Chemosphere, 60(1): 97-104. https://doi.org/10.1016/j.chemosphere.2004.11.092

Sarkar, A. and Shekhar, S. 2018. Iron contamination in the waters of upper Yamuna basin. Groundwater for Sustainable Development, 7: 421-429. https://doi.org/10.1016/j.gsd.2017.12.011

Seca, A. and Pinto, D. 2018. Plant Secondary Metabolites as Anticancer Agents: Successes in Clinical Trials and Therapeutic Application. International Journal of Molecular Sciences, 19(1). https://doi.org/10.3390/ijms19010263

Singh, D., Tiwari, A. and Gupta, R. 2012. Phytoremediation of lead from wastewater using aquatic plants. Journal of Agricultural Science and Technology, 8(1): 1-11. https://doi.org/10.7439/ijbr.v2i7.124

Sutini, W., Augustien, N., Purwanto, D. and Muslihatin, W. 2019. The production of cinnamic acid secondary metabolites through in vitro culture of callus *Camellia sinensis* L with the elicitor of cobalt metal ions. AIP Conference Proceedings, 2120(1). https://doi.org/10.1063/1.5115632

Tripathi, P., Kumar, R., Sharma, A., Mishra, A. and Gupta, R. 2010. *Pistia stratiotes* (Jalkumbhi). Pharmacognosy Reviews, 4(8): 153-160. https://doi.org/10.4103/0973-7847.70909

Tyagi, T. and Parashar, P. 2017. Antimicrobial and antioxidant activity of *Pistia stratiotes* L. International Journal of Pharma and Bio Sciences, 8(3). https://doi.org/10.22376/ijpbs.2017.8.3.p391-399

Tyagi, T. 2017. Phytochemical screening of active metabolites present in *Eichhornia crassipes* (mart.) Solms and *Pistia stratiotes* (L.): Role in ethnomedicine. Asian Journal of Pharmaceutical Education and Research, 6(4).

Veselý, T., Tlustos, P. and Száková, J. 2011. The use of water lettuce (*Pistia stratiotes* L.) for rhizofiltration of a highly polluted solution by cadmium and lead. International Journal of Phytoremediation, 13(9): 859-872. https://doi.org/10.1080/15226514.2011.560214

Wessling-Resnick, M. 2017. Excess iron: considerations related to development and early growth. American Journal of Clinical Nutrition, 106(Suppl 6): 1600S-1605S. https://doi.org/10.3945/ajcn.117.155879

Wink, M. 2012. Medicinal Plants: A source of anti-parasitic secondary metabolites. Molecules, 17(11): 12771-12791. https://doi.org/10.3390/molecules171112771

Zahari, N. Z., Fong, N. S., Cleophas, F. N. and Rahim, S. A. 2021. The potential of *Pistia stratiotes* in the phytoremediation of selected heavy metals from simulated wastewater. International Journal of Technology, 12(3): 613-624. https://doi.org/10.14716/ijtech.v12i3.4236

Zhang, R., Wilson, V., Hou, A. and Meng, G. 2015. Source of lead pollution, its influence on public health and the countermeasures. International Journal of Health Animal Science and Food Safety, 2: 18-31. https://doi.org/10.13130/2283-3927/4785

Zhu, Y., Chen, Y., Zhang, X., Xie, G. and Qin, M. 2020. Copper stress-induced changes in biomass accumulation, antioxidant activity and flavonoid contents in *Belamcanda chinensis* Calli. Plant Cell Tissue and Organ Culture, 142: 299-311. https://doi.org/10.1007/s11240-020-01863-w

## ORCID DETAILS OF THE AUTHORS

Shubhada Walvekar: https://orcid.org/0000-0002-7771-8008
Sharon D'souza: https://orcid.org/0009-0004-2020-6038

Nature Environment and Pollution Technology
An International Quarterly Scientific Journal

p-ISSN: 0972-6268
(Print copies up to 2016)
e-ISSN: 2395-3454

Vol. 23 | No. 3 | pp. 1589-1596 | 2024

Original Research Paper

https://doi.org/10.46488/NEPT.2024.v23i03.028

Open Access Journal

# Characteristics, Abundance and Polymer Type of Microplastics in *Anadara granosa* (Blood Clam) from Coastal Area of Palopo City

**Abd. Gafur Rahman*†, Muhammad Farid Samawi* and Shinta Werorilangi****

*Department of Management of the Environment, Graduate School, Hasanuddin University, Makassar (90245), Indonesia
**Department of Marine Science, Faculty of Marine Science and Fishery, Hasanuddin University, Makassar (90245), Indonesia
†Corresponding author: Abd. Gafur Rahman; abd.gafurrahman060998@gmail.com

**Nat. Env. & Poll. Tech.**
**Website: www.neptjournal.com**

*Received:* 05-12-2023
*Revised:* 16-02-2024
*Accepted:* 01-03-2024

**Key Words:**
*Anadara granosa*
Microplastics
Coastal area
Pollution

## ABSTRACT

Plastic waste in marine waters will undergo a degradation process that breaks down large plastic pieces into smaller particles called microplastics. The abundance of microplastics, caused by their small size (<5mm) can be easily indirectly consumed by aquatic animals. *Anadara granosa* is one of the bivalves that is quite vulnerable to microplastic contamination because it has the nature of a filter feeder which means it can sift particles and organic matter around it. The purpose of this study was to determine the characteristics, abundance, and types of microplastic polymers in blood clams (*A. granosa)*. The results of microplastic observations made on 60 blood clams were 153 microplastic particles identified from 47 individuals (78%) of contaminated blood clams with an average microplastic abundance of 0.591 ± 0.083 item/gr. *Fiber*-type microplastics are the most dominant form found and blue is the most dominant color found in the sample. Based on the average abundance of microplastics in *Anadara granosa* in the coastal area of Palopo City, it is lower than several studies that have been conducted previously. Fourier Transform-Infra Red was conducted to determine the type of polymer in microplastics. Three types of polymers were found in the *Anadara granosa* samples polyethylene terephthalate (PET), polystyrene, and polyester. The three types of polymers have effects on human health such as respiratory problems, skin irritation, and genotoxicity. Action is needed to prevent microplastic pollution in Palopo City's rivers before microplastic pollution becomes more severe in the future.

## INTRODUCTION

Plastic pollution has become a global problem today. Anthropogenic activities can increase the amount of plastic waste that will end up in the ocean through rivers (Lebreton et al. 2017, Wicaksono et al. 2021). Exposure to ultraviolet (UV) light, physical abrasion, and temperature helps plastic waste to break down into smaller plastic sizes in the environment (Song et al. 2017). Plastic particles that range in size from 1-5mm are called microplastics (Frias & Nash 2019).

Contaminated microplastics can potentially biomagnify where pollutant transfer occurs in the food chain (Namira et al. 2023). Microplastic biomagnification has been found in aquatic organisms such as fish, bivalves, and gastropods living in contaminated aquatic environments (Caruso 2019). Microplastic biomagnification was also found in human feces (Riba 2021), in river sediment (Wicaksono et al. 2021), and filter feeder aquatic organisms such as blood clam (*Anadara granosa*) found in the Jeneponto river area (Saleh et al. 2023).

Palopo City is one of the cities in South Sulawesi that has considerable potential for marine resources, especially various types of crabs, shellfish, and fish as a source of animal protein. *Anadara granosa* (blood clam) is one type of clam that can be found in Palopo City. These clams can be found in river estuaries that have mangrove vegetation with muddy sediment types and are usually consumed by the local community. Based on the results of the field observation that has been carried out, a lot of plastic waste was found at the sampling location which is thought to come from the waste of people living around the river in Palopo City. Plastic waste is the most dominant type of waste found in the Palopo City River estuary (Sukimin et al. 2023). The correlation between the presence of plastic waste and the abundance of microplastics shows fluctuating values due to several factors such as the activities of residents, the time required for the degradation process of plastic waste into microplastics, and the distribution of microplastics influenced by river flow (Kurniawan et al. 2023). The abundance of microplastics in aquatic organisms can be classified as a potentially hazardous

pollutant to public health and raises concerns about the level of risk to human health.

This study focuses on microplastic pollution in blood clam (*A. granosa*) consumed by the people of Palopo City. This study aims to determine its abundance and characteristics. This study provides new data on microplastic pollution in consumable aquatic organisms in Palopo City. This data can provide new data on microplastic pollution in the coastal environment and can be used to evaluate and improve plastic waste management in Palopo City.

## MATERIALS AND METHODS

**Quality control:** All of the pieces of equipment were pre-cleaned with tap water and rinsed with distilled water. The MPs visual observation workspace was also cleaned using a dust roller before the MP identification process. All of the filter-filled Petri dishes were kept closed to prevent airborne contamination (Wicaksono et al. 2021). Sample blanks and airborne controls were used as the negative control. A total of 3 blood clams blanks were created during this research. The blanks were used to count the amount of contamination during the morphometric measurement process until the sample extraction process by adding 50 mL of 20% KOH solution to an empty sample bottle. 120 Petri dishes (airborne controls) were used to count the amount of contamination during visual observation of microplastics using a stereo microscope by adding distilled water to the Petri dishes and leaving them open during the observation process (Sawalman 2021).

***Anadara granosa* analysis:** Sampling of *Anadara granosa* (blood clams) was conducted by installing 3 × 3 m transects using the Purposive Sampling survey method. There were 8 sampling points determined in this study (Fig. 1). Blood clams were only found in 3 sampling point locations, the number of blood clams collected was 20 individuals per station. The blood clams found were measured morphometrically, including length, width, and weight.

The blood clams were split and the meat was weighed. It was then put into a sample bottle, which contained 20% KOH solution (Wicaksono et al. 2023). The sample bottle is then marked with a label containing sample number information to distinguish the type of sample that has been taken. Extraction of organic matter was carried out with 20% KOH for 1 to 2 weeks, at room temperature. The provision of KOH solution aims to digest organic matter in the sample before observation. Observation of microplastics in the sample was carried out by taking as many as 5 to 10 mL of sample solution was then placed in a petri dish and continued to be observed under a microscope. Through observation, microplastic identification and polymer analysis with FT-IR method were used as primary data.

Visual observations were made using a stereo euromex SB-1902 microscope with zigzag movements on a petri dish. Microplastics found will be placed into an object glass. The shape, color, and size of microplastics were classified according to Frias et al. (2019) and the identification of microplastic shape refers to GESAMP (2019). Image J software (Institute of Health, Bethesda, MD, USA, version

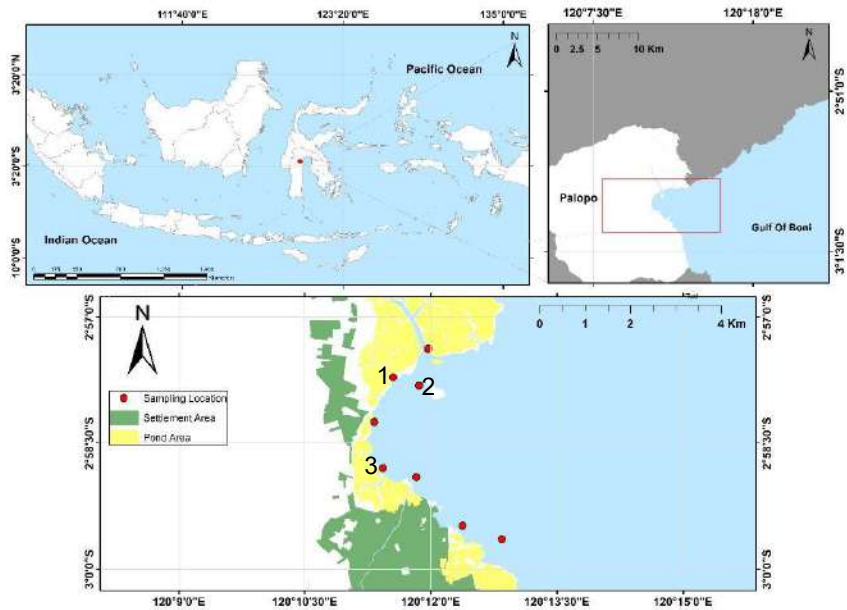


Fig. 1: Sampling locations in Palopo River.

1.54h) was used to measure the length of microplastics. Microplastic sizes were classified in MPs<1mm (small microplastics) and MPS>1-5mm (large microplastics) (Hanke 2013). The abundance of microplastics of MPs in the samples was expressed in items/g for *Anadara granosa* samples. The polymer type of the representative microplastic sample was separately identified using the Fourier-transform Infrared Spectroscopy (FTIR) method. Microplastics were placed on sterile glass and read using FTIR Attenuated Total Reflectance (ATR) machine (model; QATR-S). The wavelength spectra were then matched with the Lab SolutionIR spectrum library to determine the polymer type.

**Data analysis**: Microplastic abundance in *Anadara granosa* was analyzed using the Chi-Square test. The shape, color, size, and polymer of microplastics are described descriptively graphically. Shape, color, size, and polymer are described descriptively. Graphs of abundance, and proportion (size, shape, and color) were displayed using GraphPad software version 8.6.

## RESULTS AND DISCUSSION

### Contamination Control

In the negative airborne control, from 90 Petri dishes used during the microplastic identification process, only 4 microplastics were found (fiber, green and black) with an average microplastic abundance of 0.04 items/petri dish. In research conducted by Sawalman (2021), the negative airborne control abundance was 0.75 items/petri dish. Therefore, microplastic contamination can be ignored. it is assumed that contamination does not affect the identification of microplastics in blood clam samples.

### Microplastic Abundance

A total of 60 individuals were analyzed in this study. There were differences in the level of microplastic contamination (%) and microplastic abundance (mean ± SD) at each blood clam (*A. granosa*) sampling station. The abundance of microplastics found in blood clam (*A. granosa*) samples at Station 1 found 39 microplastic items (0.562 ± 0.128 items/gr) identified from 14 individuals (70%). At station 2, 47 microplastic items (0.622 ± 0.143 items/gr) were identified from 17 individuals (85%). At station 3, 67 microplastic items (0.590 ± 0.087 items/gr) were identified from 16 individuals (80%) (Fig. 2). The mean total abundance of microplastics in Anadara granosa in Palopo City was 0.591 ± 0.083 item/gr.

The abundance of microplastics obtained in this study is lower when compared to research conducted by Goh et al. (2021) on blood clams from fish markets in Thailand with

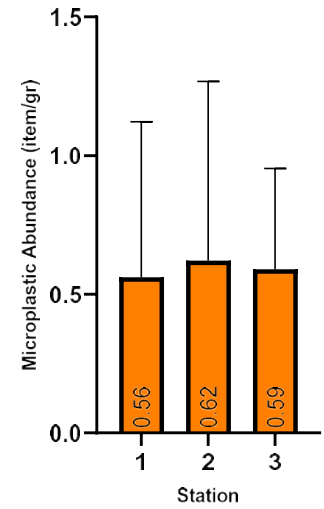


Fig. 2: Microplastic abundance in *Anadara granosa* (n=20).

an abundance of 2.24 ± 1.32 items/gr. In addition, research conducted by Fitri & Patria (2019) on blood clams in Jambi has an abundance value of 4.1 ± 0.43 items/gr is higher compared to the abundance of blood clams found in this study 0.591 ± 0.119 items/gr. The results of research conducted by (Ukhrowi et al. (2021) on blood clams in the Lada-bay area, Banten have a higher microplastic abundance value of 62.67 ± 18.03 items/gr when compared to those obtained in this study. According to Fitri (2017), turtle shells can be contaminated with microplastics because of the location where the shells are already polluted due to anthropogenic activities. Chi-square test results of microplastic abundance (particles/gr) showed that there was no significant difference in the abundance of microplastics in blood clams.

### Microplastic Characterization

Characteristics of microplastics are identified based on shape, color, and size.

### Microplastic Shape

Microplastic *fiber* is the most dominant form found at each station with a percentage at station 2 of 96%, station 3 of 97%, and station 5 of 98%. *Film* form was found at station 2 of 4 %, station 3 of 3%, and station 5 of 2% (Fig. 3).

Among the 153 microplastic particles found in 60 samples of *Anadara granosa*, they were divided into 2 forms of microplastics, namely fibers *of* as many as 152 particles (99.346%) and films *of* as many as one particle (0.654%). no pellet-type plastics were found in this study, which means that all microplastics found were identified as secondary microplastics because pellets or beads are generally included in primary microplastics made with sizes <5mm (Asadi et al. 2019).

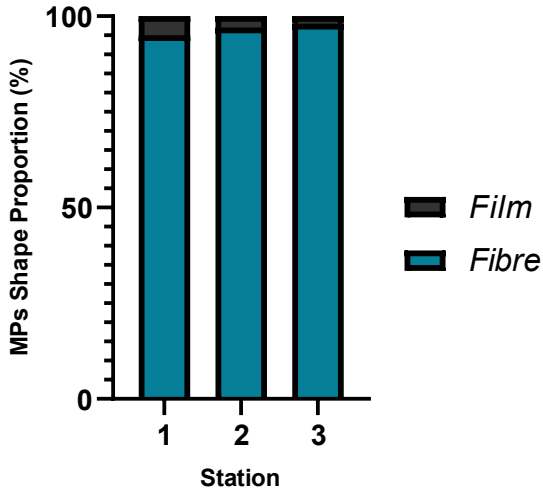


Fig. 3: The proportion of MPs shapes in *Anadara granosa*.

The high level of fiber microplastics in blood clams is thought to be due to the character of the elongated, slender, and smooth fiber shape. (Li et al. 2016) also explained that fiber-shaped microplastics are particles that have a soft and slender texture so that they are easy to clump, this form of microplastic is also easily bound to thread-like organs found in the body of shellfish including the gills, clumping fibers will be easily rejected and involved during the selection process. According to research (Woods et al. 2018) in *Mytilus edulis,* of the 100% of microplastic fibers that enter the mussel's body tissue, 71% will be coagulated and immediately wasted before being swallowed. Browne et al. (2011) explained that microplastic fibers can come from monofilament fragmentation from fishing gear such as ropes and nets, and can even come from clothing fibers through the washing process (polyester) of coastal communities that are carried to the sea.

The presence of fiber and film-shaped microplastics (Fig. 4) indicates a tendency for secondary microplastics to be present in these waters through anthropogenic activities or runoff from land entering the sea (GESAMP 2019). There is no definitive data that fibrous microplastics dominate microplastic pollution in marine waters, but according to Woods et al. (2018), almost 90% of microplastics scattered in marine waters are in the form of *fibers*. This may be related to fishing and aquaculture activities whose equipment is ropes made of plastic materials, as found by (Xue et al. 2020) in Chinese waters. (Qu et al. 2018) conducted a study of microplastics in the water medium and the bodies of blue, *Mytilus edulis* and green, *Perna viridis* living on the North and South coasts of China and they found that microplastic *fibers* dominated in the mussel meat. In bivalve species from the Salish Sea, USA, 96% *fiber* microplastics were found (Martinelli et al. 2020).

**Microplastic Color**

The color composition of microplastics found in *A. granosa is* very varied such as blue, red, and clear. The most dominant color found at each station is blue. The percentage of microplastic color found at station 1 is 91% blue and 9% red. In station 2, the percentage of colors found was blue 92% and red 9%. Station 3 the percentage of colors found was blue 93%, red 6%, and clear 1% (Fig. 5).

A total of 153 microplastic particles were found in 60 samples of *Anadara granosa*, the most dominant colors were blue 92.810%, red 6.538%, and clear or transparent 0.654%. The color source of microplastics originates from the main plastic product, but the color of microplastics can be changed due to the weathering process as well. The color of microplastics can also be used as an initial identification to determine the composition of microplastics (Lambert & Wagner 2018). The blue and red colors identified in the

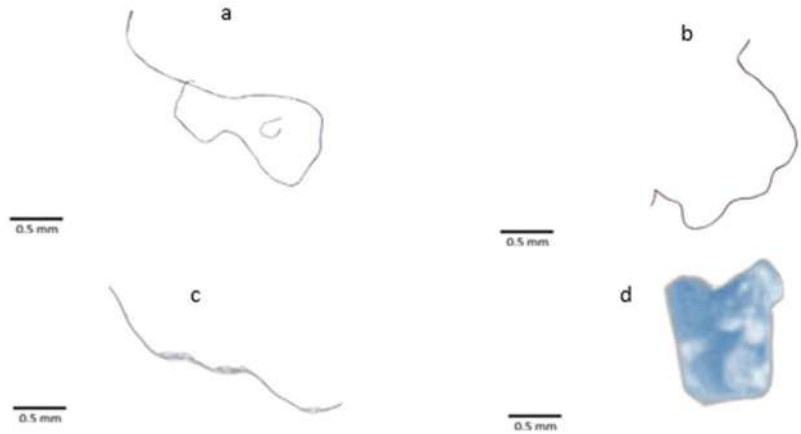


Fig. 4: Visualization of microplastic types in *Anadara granosa*. Blue, red, and transparent fibers (a,b,c) and blue film (d).

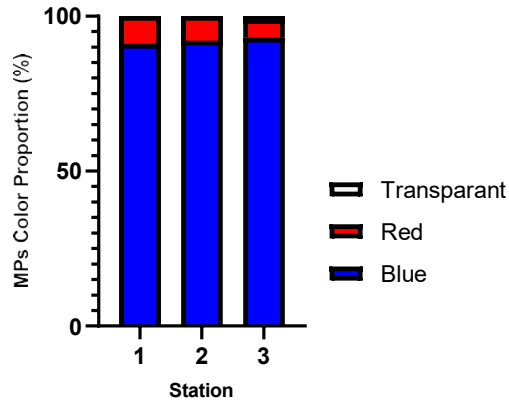


Fig. 5: The proportion of MPs colors in *Anadara granosa*.

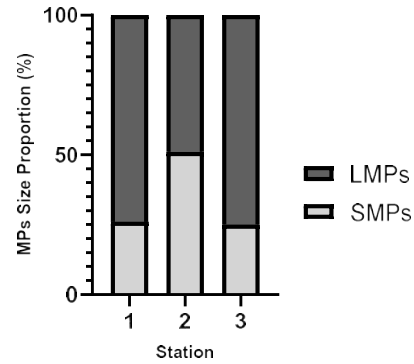


Fig. 6: The proportion of MPs size in *Anadara granosa*.

blood clams may come from fishing activities by fishermen using plastic nets. Seaweed farming activities in waters that use plastic are also suspected to be a source of plastic pollution. Research conducted by (Walkinshaw et al. 2020) also found that blue and red microplastic particles are non-natural organic pigments derived from anthropogenic activities. Clear microplastics can come from microplastics that have undergone a photochemical process that causes the loss of color pigments in the microplastics (Tubagus et al. 2020).

**Microplastic Size**

The microplastic particles found are divided into two size categories, SMPs (<1 mm) and LMPs (1-5mm) (Wicaksono et al. 2021). The dominant size in blood clam samples is LMPs (Fig. 6).

The size of microplastics is an important factor related to the range of effects that affect organisms. According to Widianarko & Hantoro (2018), the large surface area compared to the volume ratio of small particles gives microplastics the potential to release chemicals quickly. Microplastics with smaller sizes will be easy to swallow and enter into tissues, especially in sessile organisms such as shellfish (Browne et al. 2008).

Large microplastics will affect the efficiency of nutrient absorption when stuck in the clam digestive system. This is supported by the statement (Wright et al. 2013) that blockage of digestive tract organs and physical damage to cells in the digestive tissue cause impaired absorption of nutrients and chemical hazards that have been absorbed by microplastic particles from polluted environments. In contrast, microplastics that are small in size tend to pose less of a risk because most of these microplastics can be quickly excreted with the mussel's feces. Even if in the natural environment ingest a certain amount of small microplastics, they will be expelled before they have a detrimental effect on the mussel's body (Kinjo et al. 2019).

**Microplastic Polymer**

Based on the FTIR test, there are 3 types of polymers found in this study (Fig. 7 and Fig 8). Polymer types found in mussel samples are polyester (PES) 60%, polyethylene terephthalate (PET) 23%, and polystyrene (PS) 17%. Polyester and PET polymers were found in the fibre-type microplastics,

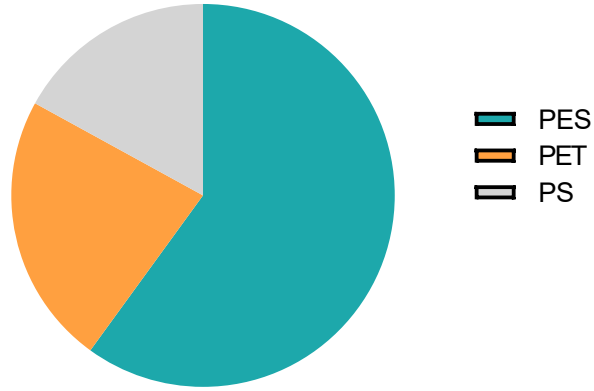


Fig. 7: Microplastics identified in *Anadara granosa*.

while for film-shaped microplastics, polystyrene (PS) was found.

Polyester is the type of polymer that is most commonly found in this study (Fig. 7). Polyester is used as a textile raw material, based on the results of research by Napper & Thompson (2016), in one wash of about 6kg of polyester clothes can release 500,000 polyester fibers in the waste, resulting in a higher abundance of polyester in the environment. Polystyrene is commonly used in household products such as basins, broom combs, buckets,

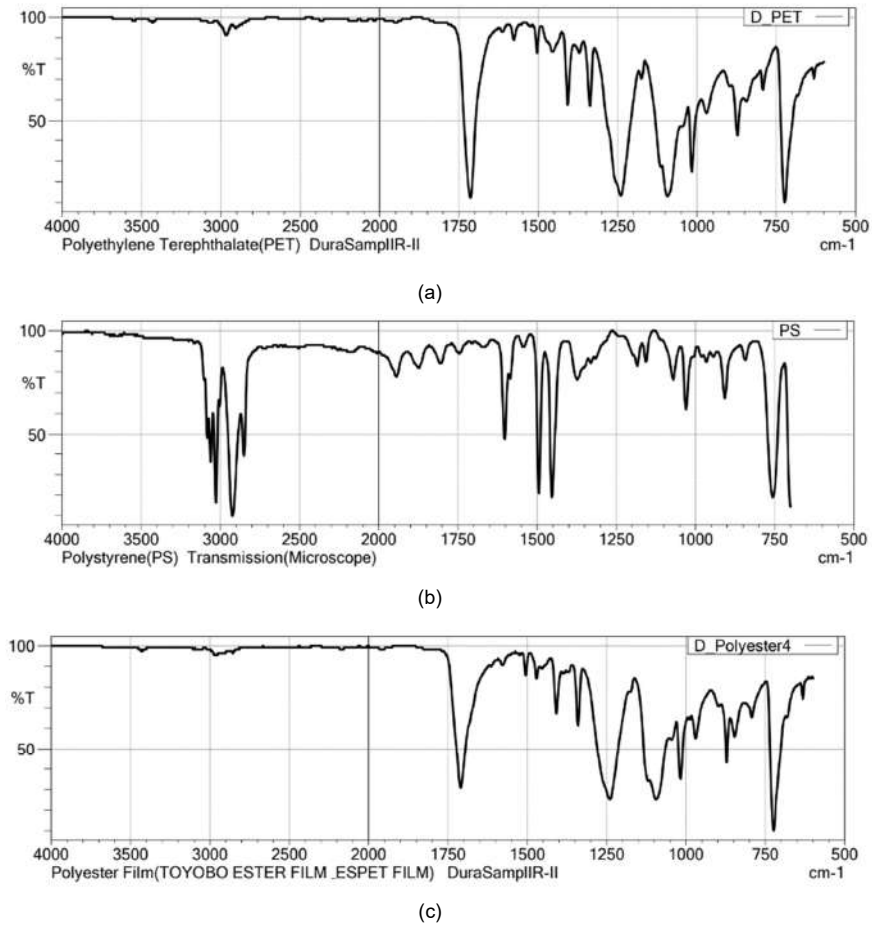


Fig. 8: Result of FTIR analysis of microplastics in blood clam (*Anadara granosa*) (a) polyethylene terephthalate, (b) polystyrene, and (c) polyester.

Table 1: Hazard levels of microplastic polymers identified in blood clam (*Anadara granosa*) coastal estuaries of Palopo City, according to (Lithner et al. 2011).

| No. | Microplastic polymers in blood clams in Palopo City estuary | Hazard level | Hazard Category |
|---|---|---|---|
| 1. | Polyvynil chloride (PVC) | V | *Carcinogenicity, Reproductive toxicity, mutagenicity,* |
| 2. | Polyester (PES) | IV | *Respiratory/skin sensitization* |
| 3. | Polystyrene (PS) | II | *Acute toxicity* |
| 4. | Polyethylene terephthalate (PET) | II | *Acute toxicity* |
| 5. | Polyethylene | II | *Acute toxicity* |

[a] CLP hazard is classified into 5 levels (I-V)

[b] (Not yet categorized/NC)

Table 2: Polymer effect on human health.

| Type of Polymers | Effects on Human Health | Reference |
|---|---|---|
| PET | skin irritation, respiratory problems, and breast cancer | Byrne et al. (2013) |
| PS | congenital disabilities, carcinogen, and gastrointestinal damage | Hahladakis et al. (2018) |
| PES | genotoxicity and apoptosis | Nusair et al. (2019) |

bristle brushes, and hangers (UNEP 2016). The results of research conducted by Namira et al. (2023) show that polystyrene was found in microplastic samples in *Anadara granosa* originating from the degradation of plastic waste of household products disposed of into the river which indirectly passes through the river mouth and then enters marine waters. PET-type bottles are recommended to be "single-use only" if they are used too often to store warm water, which will cause the polymer coating on the bottle to melt and release carcinogenic substances that can cause cancers (Byrne et al. 2013).

Based on research conducted by Rahmatin et al. (2024) on *Anadara granosa* samples referring to Lithner et al. (2011) and European regulations (Classifications, labeling and packaging - CLP). According to Rodrigues et al. (2019), to evaluate the risk assessment of plastics, polymers, their compounds (monomers and additives), and degradation products are classified into five qualitative categories of hazard to human life and the environment (very low to very high hazard), The hazard level of each substance is determined based on the highest negative impact that has been observed.

The presence of microplastics in the human body can come from the food consumed (Table 1 and Table 2). Ingestion of microplastics through food consumption can increase health problems due to the potential for particles from the digestive tract to other tissues or organs containing toxic chemicals (Namira et al. 2023). Microplastics can act as a medium to transport toxic materials that will end up in the bodies of humans who consume them. The absorption and transfer of microplastics contaminated with toxic materials will have an impact on human health in the long term.

## CONCLUSION

Microplastics were found in *Anadara granosa* samples taken at 3 sampling point locations in the coastal area of Palopo City. Based on the results of the research conducted, the fiber form is the most dominant and the blue color is the dominant color found in 60 samples of *Anadara granosa* shells. FTIR test results show that there are 3 types of polymers obtained, namely polyethylene terephthalate (PET), Polystyrene (PS), and polyester. With the discovery of microplastics in *Anadara granosa*, efforts are needed to overcome this such as by properly managing plastic waste and socializing the impact of plastic waste in the environment.

## REFERENCES

Asadi, M.A., Hertika, A.M.S., Iranawati, F. and Yuwandita, A.Y. 2019. Microplastics in the sediment of intertidal areas of Lamongan, Indonesia. Journal of Coastal Research, 12(4): 1065-1073.

Browne, M.A., Crump, P., Niven, S.J., Teuten, E., Tonkin, A., Galloway, T. and Thompson, R. 2011. Accumulation of microplastics on shorelines worldwide: Sources and sinks. Environmental Science and Technology, 45(21): 9175-9179. https://doi.org/10.1021/es201811s

Browne, M.A., Dissanayake, A., Galloway, T.S., Lowe, D.M. and Thompson, R.C. 2008. Ingested microscopic plastic translocates to the circulatory system of the mussel, *Mytilus edulis* (L.). Environmental Science and Technology, 42(13): 5026-5031. https://doi.org/10.1021/es800249a

Byrne, C., Divekar, S.D., Storchan, G.B., Parodi, D.A. and Martin, M.B. 2013. Metals and breast cancer. Journal of Mammary Gland Biology and Neoplasia, 18(1): 63-73. https://doi.org/10.1007/s10911-013-9273-9

Caruso, G. 2019. Microplastics as vectors of contaminants. Marine Pollution Bulletin, 146: 921-924. https://doi.org/10.1016/j.marpolbul.2019.07.052

Fitri, S. and Patria, M.P. 2019. Microplastic contamination on *Anadara granosa* Linnaeus 1758 in Pangkal Babu mangrove forest area, Tanjung Jabung Barat district, Jambi. Journal of Physics: Conference Series, 1282(1). https://doi.org/10.1088/1742-6596/1282/1/012109

Frias, J., Filgueiras, A. and Pedrotti, M.L. 2019. Standardized protocol for monitoring microplastics in seawater. Deliverable 4.1. https://doi.org/10.13140/RG.2.2.14181.45282

Frias, J.P.G.L. and Nash, R. 2019. Microplastics: Finding a consensus on the definition. Marine Pollution Bulletin, 138: 145-147. https://doi.org/10.1016/j.marpolbul.2018.11.022

Goh, P., Pradit, S., Towatana, P., Khokkiatiwong, S., Kongket, B. and Hwei, Z. 2021. Microplastic abundance in blood cockles and shrimps from fishery market, Songkhla Province, Southern Thailand. Sains Malaysiana, 50: 2899-2911. https://doi.org/10.17576/jsm-2021-5010-05

Hahladakis, J.N., Velis, C.A., Weber, R., Iacovidou, E. and Purnell, P. 2018. An overview of chemical additives present in plastics: Migration,

release, fate and environmental impact during their use, disposal and recycling. Journal of Hazardous Materials, 344: 179-199. https://doi.org/10.1016/j.jhazmat.2017.10.014

Hanke, G., Galgani, F., Werner, S., Oosterbaan, L., Nilsson, P., Fleet, D., Kinsey, S., Thompson, R., Palatinus, A., Van Franeker, J. 2013. Guidance on monitoring of marine litter in European Seas. EUR 26113; JRC83985; Publications Office of the European Union: Luxembourg.

Kinjo, A., Mizukawa, K., Takada, H. and Inoue, K. 2019. Size-dependent elimination of ingested microplastics in the Mediterranean mussel *Mytilus galloprovincialis*. Marine Pollution Bulletin, 149. https://doi.org/10.1016/j.marpolbul.2019.110512

Kurniawan, M., Nugroho, S., Adnan, F. and Zulya, F. 2023. Analisis Keterkaitan Kelimpahan Mikroplastik di Sungai Mahakam, Kecamatan Muara Kaman. Jurnal Teknologi Lingkungan UNMUL, 7(1). [Indonesian]

Lambert, S. and Wagner, M. 2018. Microplastics are contaminants of emerging concern in freshwater environments: An overview. In Handbook of Environmental Chemistry, 58: 1-23. Springer Verlag. https://doi.org/10.1007/978-3-319-61615-5_1

Lebreton, L.C.M., Van Der Zwet, J., Damsteeg, J.W., Slat, B., Andrady, A. and Reisser, J. 2017. River plastic emissions to the world's oceans. Nature Communications, *8*(1): 15611. https://doi.org/10.1038/ncomms15611

Li, J., Qu, X., Su, L., Zhang, W., Yang, D., Kolandhasamy, P., Li, D. and Shi, H. 2016. Microplastics in along the coastal waters of China. Environmental Pollution, 214: 177-184. https://doi.org/10.1016/j.envpol.2016.04.012

Martinelli, J.C., Phan, S., Luscombe, C.K. and Padilla-Gamiño, J.L. 2020. Low incidence of microplastic contaminants in Pacific oysters (*Crassostrea gigas* Thunberg) from the Salish Sea, USA. Science of the Total Environment, 715. https://doi.org/10.1016/j.scitotenv.2020.136826

Namira, N., Daud, A., Mallongi, A., Amqam, H., Wahyu, A. and Irwandy 2023. Risk analysis of microplastic exposure through consumption of *Anadara Granosa* in coastal area. Pharmacognosy Journal, 15(4): 558-562. https://doi.org/10.5530/pj.2023.15.119

Napper, I.E. and Thompson, R.C. 2016. Release of synthetic microplastic plastic fibers from domestic washing machines: Effects of fabric type and washing conditions. Marine Pollution Bulletin, 112(1-2): 39-45. https://doi.org/10.1016/j.marpolbul.2016.09.025

Nusair, S.D., Almasaleekh, M.J., Abder-Rahman, H. and Alkhatatbeh, M. 2019. Environmental exposure of humans to bromide in the Dead Sea area: Measurement of genotoxicity and apoptosis biomarkers. Mutation Research - Genetic Toxicology and Environmental Mutagenesis, 837: 34-41. https://doi.org/10.1016/j.mrgentox.2018.09.006

Qu, X., Su, L., Li, H., Liang, M. and Shi, H. 2018. Assessing the relationship between the abundance and properties of microplastics in water and in. Science of the Total Environment, 621: 679-686. https://doi.org/10.1016/j.scitotenv.2017.11.284

Riba', C.S.J. 2021. Identifikasi Keberadaan Mikroplastik Pada Feses Masyarakat di Pesisir Pantai Kabupaten Takalar Provinsi Sulawesi Selatan. Tesis. Univesitas Hasanuddin. Makassar, Indonesia. [Indonesian]

Rahmatin, N.M., Soegianto, A., Irawan, B., Payus, C.M., Indriyasari, K.N., Marchellina, A., Mukholladun, W. and Irnidayanti, Y. 2024. The spatial distribution and physico-chemical characteristic of microplastics in the sediment and cockle (*Anadara granosa*) from the coastal waters of East Java, Indonesia, and the health hazards associated with cockle consumption. Marine Pollution Bulletin, 198: 115906.

Saleh, R., Daud, A., Ishak, H., Amqam, H., Wahyu, A., Birawida, A.B. and Mallongi, A. 2023. Spatial distribution of microplastic contamination in blood clams (*Anadara granosa*) on the Jeneponto coast, South Sulawesi. Pharmacognosy Journal, 15(4).

Sukimin, R., Jenderal Sudirman, J.K., Palopo, K. and Selatan, S. 2023. Identification of inorganic waste in the mangrove ecosystem in Wara Timur and Bara District Palopo City. Journal of Coastal and Ocean Sciences, 4(3): 175-179.

Song, Y.K., Hong, S.H., Jang, M., Han, G.M., Jung, S.W. and Shim, W.J. 2017. Combined effects of UV exposure duration and mechanical abrasion on microplastic fragmentation by polymer type. Environmental Science and Technology, 51: 4368-4376.

Tubagus, W., Sunarto, Ismail, M.R. and Yuliadi, L.P.S. 2020. Identification of microplastic composition on clams (*Gafrarium tumidum*) and sediments in Pari Island, Seribu Islands, Jakarta. Marine Sciences: Indonesian Journal of Marine Sciences, 25(3): 115-120. https://doi.org/10.14710/ik.ijms.25.3.115-120

Ukhrowi, H.R., Wardhana, W. and Patria, M.P. 2021. Microplastic abundance in blood cockle *Anadara granosa* (Linnaeus 1758) at Lada Bay, Pandeglang, Banten. Journal of Physics: Conference Series, 1725(1). https://doi.org/10.1088/1742-6596/1725/1/012053

Walkinshaw, C., Lindeque, P.K., Thompson, R., Tolhurst, T. and Cole, M. 2020. Microplastics and seafood: lower trophic organisms at highest risk of contamination. Ecotoxicology and Environmental Safety, 190. https://doi.org/10.1016/j.ecoenv.2019.110066

Wicaksono, E.A., Werorilangi, S., Afdal, M., Nimzet, R. and Tahir, A. 2023. Microplastic occurrence in the digestive tract of marble goby (*Oxyeleotris marmorata*) from Jeneberang River, Macassar, Indonesia. Journal of Sustainability Science and Management, 18(8): 210-217. https://doi.org/10.46754/jssm.2023.08.014

Wicaksono, E.A., Werorilangi, S., Galloway, T.S. and Tahir, A. 2021. Distribution and seasonal variation of microplastics in Tallo River, Makassar, eastern Indonesia. Toxics, 9(6). https://doi.org/10.3390/toxics9060129

Woods, M.N., Stack, M.E., Fields, D.M., Shaw, S.D. and Matrai, P.A. 2018. Microplastic fiber uptake, ingestion, and egestion rates in the blue mussel (*Mytilus edulis*). Marine Pollution Bulletin, 137: 638-645. https://doi.org/10.1016/j.marpolbul.2018.10.061

Wright, S.L., Thompson, R.C. and Galloway, T.S. 2013. The physical impacts of microplastics on marine organisms: a review. Environmental Pollution, 178: 483-492. https://doi.org/10.1016/j.envpol.2013.02.031

Xue, B., Zhang, L., Li, R., Wang, Y., Guo, J., Yu, K. and Wang, S. 2020. Underestimated microplastics pollution derived from fishery activities and 'hidden' in deep sediment. Environmental Science and Technology, 54(4): 2210-2217. https://doi.org/10.1021/acs.est.9b048

## ORCID DETAILS OF THE AUTHORS

Abd. Gafur Rahman: https://orcid.org/0009-0002-0286-0859

Nature Environment and Pollution Technology
An International Quarterly Scientific Journal

p-ISSN: 0972-6268
(Print copies up to 2016)
e-ISSN: 2395-3454

Vol. 23 | No. 3 | pp. 1597-1604 | 2024

Original Research Paper

https://doi.org/10.46488/NEPT.2024.v23i03.029

Open Access Journal

# Production of Amylase by Solid State Fermentation Using Agricultural Waste

**M. M. Morbia*†, A. A. Pandey*, P. K. Mahla* and S. N. Gohil****

*Microbiology Department, Swarrnim Startup and Innovation University, Bhoyan Rathod, Opp IFCO, near ONGC WSS, Adalaj-Kalol Highway, Gandhinagar, Gujarat, 382420, India

**Vitely Corp LLP, Microbiology laboratory, HO, Commerce House 2, Satya Marg, Opposite Pushparaj Tower, Judges Bungalow Road, Bodakdev, Ahmedabad-380054, Gujarat, India

†Corresponding author: M.M. Morbia; morbiamayur@gmail.com

**Nat. Env. & Poll. Tech.**
**Website: www.neptjournal.com**

*Received:* 28-12-2023
*Revised:* 08-02-2024
*Accepted:* 10-02-2024

**Key Words:**
Amylase
Optimization
Agricultural waste
Solid state fermentation

## ABSTRACT

This study presents a comprehensive investigation into the production of amylase, a crucial enzyme with wide-ranging industrial applications, using locally sourced substrates from Kachchh, Gujarat. The research employed the *Bacillus licheniformis* strain and substrates such as coconut, rice husk, wheat bran, paddy straw, and maize straw. The study found paddy straw to be the most promising substrate for amylase production. The research also systematically optimized various process parameters for amylase production in Solid-State Fermentation (SSF) using the One Variable at a Time (OVAT) method. These parameters included incubation period, temperature, inoculum level, additional carbon sources, starch concentrations, additional nitrogen sources, initial pH, different mineral salt ions, initial moisture level, and surfactants. The results showed that the optimal conditions for maximum amylase yield were an incubation period of 48 hours, an incubation temperature of 35°C, an inoculum level of 10%, starch as the additional carbon source, a starch concentration of 2.5%, yeast extract as the additional nitrogen source, an initial pH of 7, NaCl as the mineral salt, an initial moisture level of 75%, and Tween 80 as the surfactant. This research provides a reliable and sustainable approach to enzyme production, offering valuable insights for the optimization of the solid-state fermentation process for maximum amylase production.

## INTRODUCTION

Enzymes play a pivotal role in numerous industrial applications, catalyzing biochemical reactions with remarkable specificity and efficiency. Among these enzymes, amylase holds a significant position due to its wide-ranging applications in various industries, including food, textiles, and biofuel production. Solid-state fermentation (SSF) has emerged as an environmentally friendly and economically viable approach for amylase production, using agricultural waste as a substrate (Souza & Magalhaes 2010).

Amylase, an enzyme that hydrolyzes starch into simpler sugars, is crucial for many industrial processes. Traditionally, amylase has been produced using submerged fermentation; however, SSF offers distinct advantages, such as reduced water consumption, higher enzyme stability, and the use of solid substrates, particularly agricultural waste. This shift towards SSF aligns with the global efforts to develop sustainable and eco-friendly processes in the biotechnological industry (Saxena & Singh 2011).

Agricultural waste, a substantial byproduct of farming activities, poses environmental challenges when not effectively managed. The utilization of these agricultural residues as substrates for SSF not only addresses the issue of waste disposal but also transforms these residues into valuable resources for enzyme production. The incorporation of agricultural waste into the SSF process adds an extra layer of sustainability to the bioprocess, contributing to the concept of a circular economy (Sadh et al. 2018).

In this context, this research paper aims to investigate the production of amylase through solid-state fermentation, using agricultural waste as a cost-effective and sustainable substrate. The study focuses on optimizing the fermentation conditions to enhance amylase yield and activity, thereby contributing to the development of efficient and environmentally friendly enzymatic processes. The utilization of agricultural waste not only aligns with the principles of sustainable biotechnology but also addresses the dual challenges of enzyme production and waste management in the agricultural sector.

Through a comprehensive exploration of the potential of solid-state fermentation using agricultural waste, this research looks to provide insights into the optimization of amylase production, offering a sustainable alternative to traditional enzyme production methods. The findings

of this study could have far-reaching implications for the biotechnological industry, fostering a greener and more efficient approach to enzyme production.

## MATERIALS AND METHODS

### Selection of Microbial Culture

The research initiative involved the meticulous collection of soil specimens from six distinct Talukas, namely Gandhidham, Rapar, Bhuj, Nakhatrana, Mandvi, and Mundra, situated within the Kachchh District of Gujarat, India. For isolation and screening purposes designated 24-72-h incubation period on the starch agar plates was subjected to meticulous visual examination for growth.

### Selection of Substrate

This study used locally sourced substrates like coconut, rice husk, wheat bran, paddy straw, and maize straw from Kachchh, Gujarat, for amylase production. Their abundant availability ensures a steady supply for enzyme production. Using these agricultural residues promotes sustainability by repurposing waste and economically utilizing local resources.

### Pretreatment of Substrate

The substrate was pretreated through several steps. It was washed with tap water and distilled water, treated with 1% NaOH to remove impurities, and dried at 80°C for two days. After being ground into fine particles, it was autoclaved at 121.6°C for 20 min (Mushtaq et al. 2023).

### Preparation of Bacterial Inoculum

A 500 mL flask was filled with 250 mL of nutrient broth and autoclaved at 121.6°C for 20 min. After cooling, 1 mL of a 24-h-old broth was added and incubated at 37°C with 150 rpm agitation. Post -24hour incubation, 1 mL of the broth culture was added to the dry substrate for enzyme production (Saxena & Singh 2011).

### Effect of Various Substrates on Enzyme Production

Four substrates-coconut, rice husk, wheat bran, paddy straw, and maize straw-were selected based on their starch content. After preparing the substrates, each underwent Solid-State Fermentation as per the below procedure.

### Solid-state Fermentation (SSF)

SSF was conducted in 500 mL flasks, each containing 5 g of substrate. The moisture content was kept at 50%. After autoclaving at 121.6°C for 20 min and cooling, 1 mL of bacterial inoculum was added. The setup was then incubated for 48 h at 37°C (Cerda et al. 2016).

### Purification of Crude Enzyme

Post-incubation, 50 mL of pH 7.4 phosphate buffer was added for crude enzyme extraction. The slurry was strained using a damp cheesecloth and centrifuged at 10000 rpm for 15 min to separate cells and particles. The cell-free supernatant, having the exoenzyme amylase, was used as the crude enzyme (Ramapriya et al. 2018).

### Amylase Activity

Amylase activity was assessed using the 3,5-dinitrosalicylic acid (DNSA) method (Elyasi Far et al. 2020), which measures reducing sugars produced in the enzyme-substrate reaction. This systematic approach, from determining amylase activity to purifying the crude enzyme and conducting detailed assays, provided a reliable method for evaluating the amylase production of bacterial strains.

The amylase assay was conducted using a reaction mixture with 1% soluble starch in a 50 mM phosphate buffer at pH 7.2. The mixture was incubated for 10 minutes at 37°C, and the reaction was stopped by adding 2 mL of DNSA reagent. The mixture was then heat-treated at 100°C for 10 min and cooled. The optical density of each sample was measured at 540 nm using a spectrophotometer. Enzyme activity was quantified in units, with 1 unit.mL$^{-1}$ represents the enzyme amount that releases 1 µ mole of glucose under the assay conditions. The substrate with the highest amylase production was identified for further study.

### Optimization of Amylase Production Using the One Variable at A Time (OVAT) Method

This study systematically optimized various process parameters for amylase production in solid-state fermentation (SSF) (Table 1). Physicochemical parameters like fermentation period, initial pH, moisture level, and inoculum concentration were adjusted to study their effects on α-amylase production. Nutritional parameters like carbon and nitrogen sources, surfactants, and metal ions were also fine-tuned. The goal was to maximize enzyme production in SSF, enhancing the efficiency and yield of α-amylase, which is crucial for practical applications of SSF processes (Dike et al. 2022).

## RESULTS AND DISCUSSION

### Selection of Microbial Culture

Among various pure cultures, the *Bacillus licheniformis* was utilized for the production of amylase enzyme. *Bacillus licheniformis* was screened out as a potent one and identified (16 S rRNA) from a soil sample.

### Effect of Various Substrates on Enzyme Production

Four substrates-coconut, rice husk, wheat bran, paddy straw, and maize straw-were evaluated for amylase production. Paddy straw showed the highest enzyme activity at 1.002 IU.g$^{-1}$, making it a promising substrate for amylase production. Wheat bran also showed good results with an activity of 0.812 IU.g$^{-1}$. Coconut substrates and rice husk had lower activities at 0.513 IU.g$^{-1}$ and 0.612 IU.g$^{-1}$, respectively, while maize straw had a moderate activity of 0.849 IU.g$^{-1}$. (Fig. 1).

### Optimization of Amylase Production Using The One Variable at A Time (OVAT) Method

**Effect of incubation period on enzyme production:** The effect of the incubation period on enzyme production was investigated by varying the duration of fermentation at 24, 48, 72, and 96 h. The enzyme production, measured in IU.g$^{-1}$, varied at different incubation times, as outlined in Fig. 2.

The results show that amylase production varies across different incubation periods. The highest yield was observed at the 48-h mark, reaching 1.40 IU.g$^{-1}$, indicating that this is the optimal duration for enzyme production in this process. The lower yield at 24 hours (0.07 IU.g$^{-1}$) suggests that the fermentation process might not have reached peak efficiency in this short duration. The decline in enzyme production at 72 h (0.36 IU.g$^{-1}$) and 96 h (0.10 IU.g$^{-1}$) could be due to factors like substrate depletion, accumulation of by-products, or other inhibitory factors. Dike et al. (2022) also found a similar kind of pattern during the production of amylase enzyme.

**Effect of incubation temperature on enzyme production**: The study found that incubation temperature significantly affects amylase production. The highest yield was observed at 35°C, with an enzyme production of 0.20 IU.g$^{-1}$, suggesting this is the optimal temperature for this process. At 30°C and 40°C, the production was relatively high (0.18 IU.g$^{-1}$ and 0.15 IU.g$^{-1}$, respectively), indicating these temperatures are also favorable for amylase synthesis. However, a decrease in enzyme production was noted at 45°C (0.10 IU.g$^{-1}$) and

Table 1: Optimization parameters for amylase production.

| Parameter | Levels |
|---|---|
| Incubation Period | 24, 48, 72, 96 h |
| Incubation Temperature | 30, 35, 40, 45, 50, 55°C |
| Inoculum Level *(Bacillus licheniformis)* | 5%, 10%, 15%, 30% |
| Additional Carbon Sources [1%] | Starch, lactose, glucose, and fructose |
| Starch Concentrations | 0.5, 1, 1.5, 2, and 2.5% |
| Additional Nitrogen Sources [1%] | $NH_4Cl$, $(NH_4)_2SO_4$, $NH_4NO_3$, Yeast extract, and peptone |
| Initial pH | 4, 5, 6, 7, and 8 |
| Different Mineral Salts Ions [100 µM] | NaCl, $KH_2PO_4$, $FeCl_2$, $CaCl_2$, and $MgSO_4$ |
| Initial Moisture Level | 25%, 50%, 75%, and 100% |
| Surfactants | Tween 20, Tween 80, SDS, and PEG |

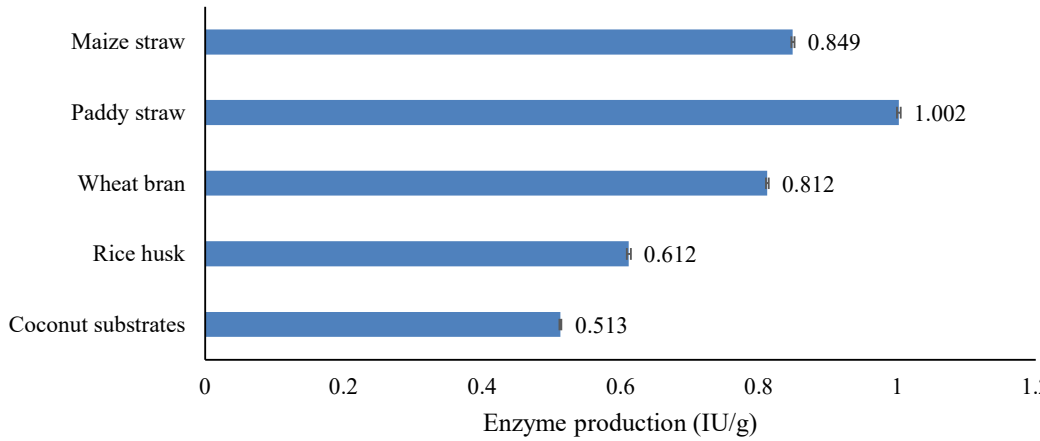


Fig. 1: Amylase production with different substrates.

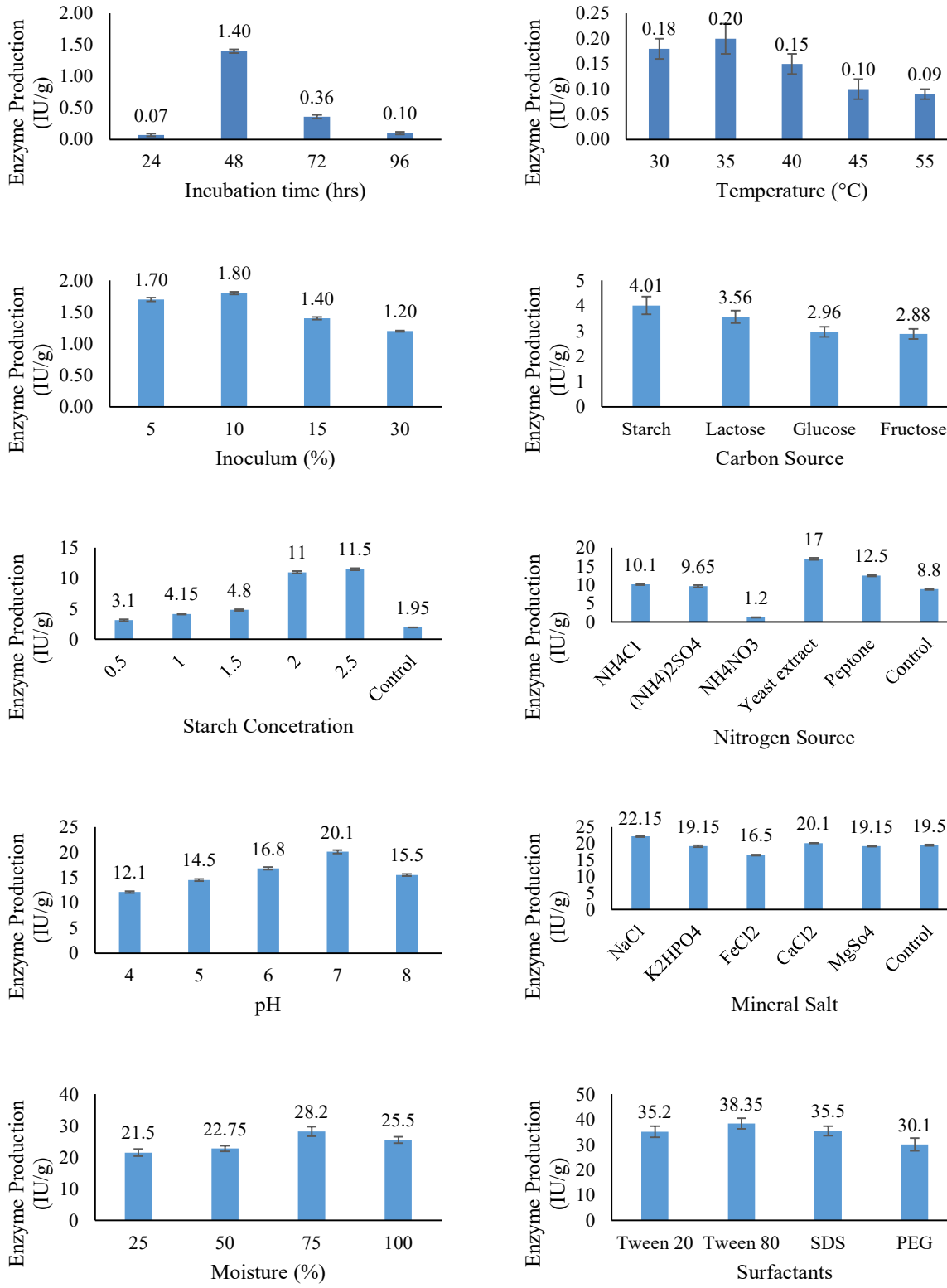


Fig. 2: Results of optimized parameters for amylase production.

55°C (0.09 IU.g$^{-1}$), implying reduced enzymatic activity at higher temperatures. Notably, at 50°C, no measurable amylase production was observed, indicating a temperature beyond the optimal range for enzymatic activity under these conditions (Fig. 2).

In a study on amylase production by *Bacillus subtilis*, it was found that the optimal activity temperature was 40°C. However, the enzyme yield dropped down more quickly with the increase in incubation period at 50°C (Salman et al. 2016). It is important to note that the optimal incubation temperature can vary depending on the specific strain of microorganisms used, the substrate, and the specific conditions of the fermentation process.

**Effect of inoculum level on enzyme production**: The study found that the inoculum level of isolated *Bacillus licheniformis* significantly impacts amylase production. The highest yield was observed with a 10% inoculum, reaching 1.80 IU.g$^{-1}$, suggesting this is the optimal level for this process. At lower inoculum levels of 5% and 15%, the production remained relatively high (1.70 IU.g$^{-1}$ and 1.40 IU.g$^{-1}$, respectively), indicating these levels are also favorable for amylase synthesis. However, a slight decrease in enzyme production was noted at a higher inoculum level of 30% (1.20 IU.g$^{-1}$), implying that an excessively high inoculum may not be conducive to maximum amylase yield (Fig. 2).

Amylase is an enzyme that hydrolyses starch to glucose units. The production of amylase is influenced by several factors, including the inoculum level (Ozdemir et al. 2012).

In a study on amylase production by Aspergillus awamori under solid-state fermentation, an inoculum level of 10% (volume per mass) was found to be optimum for α-amylase production (Kalaiarasi & Parvatham 2015).

**Effect of additional carbon sources on enzyme production**: The investigation into the effect of additional carbon sources on amylase production revealed varying outcomes based on different carbon supplements (Starch, lactose, glucose, and fructose) with paddy straw. The enzyme production, measured in IU.g$^{-1}$, in the presence of different carbon sources, is summarized in Fig. 2.

The study found that the type of carbon source significantly impacts amylase production. Starch was the most effective, yielding the highest enzyme production at 4.01 IU.g$^{-1}$, suggesting that it, along with paddy straw, creates an optimal environment for amylase synthesis. Lactose also showed substantial effectiveness, yielding 3.56 IU.g$^{-1}$ of amylase, indicating its potential as a supplementary carbon source. However, glucose and fructose resulted in lower amylase production (2.96 IU.g$^{-1}$ and 2.88 IU.g$^{-1}$, respectively), suggesting they might not be as conducive to amylase synthesis as starch and lactose under these experimental conditions.

In a study on amylase production by *Trichoderma viride*, it was found that the different commercial carbon substrates significantly affected the concomitant syntheses of amylase (Juwon & Emmanuel 2012).

**Effect of different starch concentrations on enzyme production**: The exploration of different starch concentrations for amylase production revealed varying outcomes, emphasizing the importance of starch concentration in optimizing enzyme yield. The enzyme production, measured in IU.g$^{-1}$ at different starch concentrations, is presented in Fig. 2.

The study found a clear concentration-dependent effect on amylase production. As the starch concentration increased, so did the enzyme yield. Specifically, at starch concentrations of 2% and 2.5%, amylase production significantly increased, reaching 11 IU.g$^{-1}$ and 11.5 IU.g$^{-1}$, respectively, suggesting that higher starch concentrations are favorable for maximizing amylase synthesis.

At lower concentrations (0.5%, 1%, and 1.5%), a progressive increase in enzyme production was also observed, indicating a positive correlation between starch concentration and amylase yield. However, the most substantial enhancement was observed at higher concentrations.

The control experiment with a starch concentration of 0% yielded an amylase production of 1.95 IU.g$^{-1}$, serving as a baseline for comparison. This reinforces the notion that starch is a critical substrate for amylase production and its absence results in significantly lower enzyme yields.

A study on amylase production by *Bacillus licheniformis* ZB-05 under solid-state fermentation found that as additional carbon sources, 2% soluble starch enhanced α-amylase production (Karatas et al. 2013).

**Effect of additional nitrogen sources on enzyme production**: The investigation into the effect of additional nitrogen sources on amylase production revealed distinct outcomes, highlighting the influence of different inorganic nitrogen sources. The enzyme production, measured in IU.g$^{-1}$, with various nitrogen sources at a 1% concentration, is summarized in Fig. 2.

The study found that nitrogen sources significantly impact amylase production. Yeast extract was the most effective, yielding the highest enzyme production at 17 IU.g$^{-1}$, suggesting it provides optimal conditions for amylase synthesis. Peptone also showed substantial effectiveness, producing 12.5 IU.g$^{-1}$ of amylase.

Ammonium chloride and ammonium sulfate resulted in moderate amylase production (10.1 IU.g$^{-1}$ and 9.65 IU.g$^{-1}$, respectively), indicating their suitability as nitrogen sources, albeit with a lower impact compared to yeast extract and peptone.

However, ammonium nitrate led to lower amylase production (1.2 IU.g$^{-1}$), suggesting it might be less conducive to amylase synthesis under these experimental conditions.

The control experiment with no added nitrogen yielded an amylase production of 8.8 IU.g$^{-1}$, serving as a baseline for comparison. This reinforces the notion that the presence of specific nitrogen sources positively influences amylase production.

In a study on amylase production by *Brevibacillus borstelensis* R1, it was found that the addition of different nitrogen sources greatly affected the production of amylase (Suribabu et al. 2014).

**Effect of Initial pH on Enzyme Production**

The investigation into the effect of initial pH on amylase production revealed distinct outcomes, emphasizing the significance of pH in optimizing enzyme yield. The enzyme production, measured in IU.g$^{-1}$ at different pH levels, is summarized in Fig. 2.

The study found that the initial pH significantly impacts amylase production. The optimal pH was found to be 7, yielding the highest enzyme production at 20.1 IU.g$^{-1}$, suggesting a slightly acidic to neutral pH environment is conducive for maximum amylase synthesis.

At pH 6 and 8, substantial amylase production was observed (16.8 IU.g$^{-1}$ and 15.5 IU.g$^{-1}$, respectively), indicating that the enzyme is still active and efficient at these pH levels.

However, lowering the pH to 5 and 4 resulted in decreased amylase production (14.5 IU.g$^{-1}$ and 12.1 IU.g$^{-1}$, respectively), suggesting that excessively acidic conditions may adversely affect amylase synthesis.

A published study emphasized the of pH influence the production of alpha-amylase (Kalaiarasi & Parvatham 2015, Suribabu et al. 2014)

**Effect of different mineral salt ions on enzyme production**: The investigation into the effect of different mineral salts on amylase production provided insights into the influence of specific metal ions on enzyme yield. The enzyme production, measured in IU.g$^{-1}$, with various mineral salts at a concentration of 100 μM is summarized in Fig. 2.

The study found that the addition of specific mineral salts significantly impacts amylase production. Here are the results:

- NaCl (Sodium Chloride): The presence of NaCl resulted in the highest yield at 22.15 IU.g$^{-1}$, suggesting that sodium ions play a positive role in promoting amylase synthesis.
- $K_2HPO_4$ (Potassium Hydrogen Phosphate): The addition of $K_2HPO_4$ yielded 19.15 IU.g$^{-1}$, indicating that potassium ions contribute to the enhancement of amylase synthesis.
- $FeCl_2$ (Iron (II) Chloride): Iron ions resulted in an α-amylase production of 16.5 IU.g$^{-1}$, demonstrating a positive impact on amylase synthesis.
- $CaCl_2$ (Calcium Chloride): Calcium ions positively influenced α-amylase production, yielding 20.1 IU.g$^{-1}$, suggesting that calcium plays a role in enhancing amylase synthesis.
- $MgSO_4$ (Magnesium Sulphate): Magnesium ions resulted in an α-amylase production of 19.15 IU.g$^{-1}$, indicating that, like potassium and calcium, magnesium ions contribute to the positive regulation of amylase synthesis.

The control experiment, without the addition of specific mineral salts, produced α-amylase at 19.5 IU.g$^{-1}$, serving as a baseline for comparison. A Published study shows a significant effect on the production of amylase enzyme (Saxena & Singh 2011).

**Effect of initial moisture level on enzyme production**: The investigation into the effect of different levels of initial moisture on amylase production elucidated the impact of varying substrate moisture content on enzyme yield. The enzyme production, measured in IU.g$^{-1}$ at different moisture levels, is summarized in Fig. 2.

The study found that the initial moisture level of the substrate significantly impacts amylase production. Here are the results:

- 25% Moisture: A moisture level of 25% resulted in an amylase production of 21.5 IU.g$^{-1}$, suggesting that lower moisture levels still support significant amylase synthesis.
- 50% Moisture: Increasing the moisture level to 50% positively impacted amylase production, yielding 22.75 IU.g$^{-1}$, indicating that a moderate increase in substrate moisture enhances enzyme yield.
- 75% Moisture: The highest amylase production was observed at a moisture level of 75%, reaching 28.2 IU.g$^{-1}$, suggesting that the fermentation process

is particularly efficient when the substrate has a higher moisture content.

- 100% Moisture: A further increase to 100% moisture resulted in a slight reduction in amylase production to 25.5 IU.g$^{-1}$, indicating that excessively high moisture levels may not be optimal for enzyme synthesis.

This information is crucial for optimizing the solid-state fermentation process for maximum amylase production. It shows the importance of carefully controlling the moisture level of the substrate to achieve the best results (Gangadharan et al. 2007).

**Effect of various surfactants on enzyme production**: The investigation into the effect of various surfactants on amylase production provided insights into the impact of different surface-active agents on enzyme yield. The enzyme production, measured in IU.g$^{-1}$, with various surfactants is summarized in Fig. 2.

The study found that different surfactants significantly impact amylase production. Here are the results:

- Tween 20: The addition of Tween 20 enhanced amylase production, yielding 35.2 IU.g$^{-1}$, suggesting it positively influences amylase synthesis.
- Tween 80: Tween 80 was the most effective, yielding the highest enzyme production at 38.35 IU.g$^{-1}$, indicating it's particularly effective in promoting amylase production.
- SDS (Sodium Dodecyl Sulphate): The addition of SDS also positively influenced amylase production, yielding 35.5 IU.g$^{-1}$, suggesting it contributes to the enhancement of amylase synthesis.
- PEG (Polyethylene Glycol): PEG resulted in slightly lower amylase production at 30.1 IU.g$^{-1}$ compared to the other surfactants, indicating its impact on amylase synthesis is less pronounced under these experimental conditions.

This information is crucial for optimizing the solid-state fermentation process for maximum amylase production. It shows the importance of carefully selecting the surfactants to achieve the best results (Singh & Kumar Brahman 2013).

## CONCLUSION

The comprehensive study we conducted aimed to optimize amylase production through a systematic exploration of a range of factors and conditions. The final set of media identified to maximize enzyme yield includes:

- Substrate Composition: Paddy straw (5 g) and Starch (3%).
- Mineral Salt and Additives: NaCl (100 µM), Tween-80 (1%), and Yeast Extract (1%).
- Moisture Content: Initial Moisture (75%).
- Incubation Conditions: Incubation Time (48 hours), Temperature (35°C), and pH (7).

This optimal combination ensures significant enzymatic activity and provides insights for process scalability and industrial applications. The established parameters serve as a valuable foundation for further studies and applications in the field of enzyme production. This research offers a systematic and tailored approach to maximize amylase yield, contributing to the advancement of biotechnological processes and applications.

## REFERENCES

Cerda, A., El-Bakry, M., Gea, T. and Sanchez, A. 2016. Long-term enhanced solid-state fermentation: Inoculation strategies for amylase production from soy and bread wastes by Thermomyces sp. in a sequential batch operation. J. Environ. Chem. Eng., 4(2): 2394-2401. DOI:10.1016/j.jece.2016.04.022

Dike, P., Ogugbue, C., Akaranta, O. and Oji, A. 2022. Optimization of B. cereus PW4 alpha-amylase production by OVAT technique. GSC Biol. Pharm. Sci., 20(1): 083-090. DOI:10.30574/gscbps.2022.20.1.0305

Elyasi Far, B., Ahmadi, Y., Yari Khosroshahi, A. and Dilmaghani, A. 2020. Microbial alpha-amylase production: progress, challenges, and perspectives. Adv. Pharm. Bull., 10(3): 350-358. DOI:10.34172/apb.2020.043

Gangadharan, D., Nampoothiri, K. and Pandey, A. 2007. Alpha amylase production by Aspergillus oryzae employing solid-state fermentation. J. Sci. Ind. Res., 66: 621-626.

Juwon, A. D. and Emmanuel, O. F. 2012. Experimental investigations on the effects of carbon and nitrogen sources on concomitant amylase and polygalacturonase production by Trichoderma viride BITRS-1001 in submerged fermentation. Biotechnol. Res. Int., 2: 1-8. DOI:10.1155/2012/904763

Kalaiarasi, K. and Parvatham, R. 2015. Optimization of process parameters for α-amylase production under solid-state fermentation by Aspergillus awamori MTCC 9997. J. Sci. Ind. Res., 74: 286-289.

Karatas, H., Uyar, F., Tolan, V. and Baysal, Z. 2013. Optimization and enhanced production of α-amylase and protease by a newly isolated Bacillus licheniformis ZB-05 under solid-state fermentation. Ann. Microbiol., 63(1): 45-52. DOI:10.1007/s13213-012-0443-6

Mushtaq, Q., Joly, N., Martin, P. and Qazi, J. I. 2023. Optimization of alkali treatment for the production of fermentable sugars and phenolic compounds from potato peel waste using topographical characterization and FTIR spectroscopy. Molecules, 28(21): 7250. DOI:10.3390/molecules28217250

Ozdemir, S., Matpan, F., Okumus, V., Dündar, A., Ulutas, M. S. and Kumru, M. 2012. Isolation of a thermophilic Anoxybacillus flavithermus sp. nov. and production of thermostable α-amylase under solid-state fermentation (SSF). Ann. Microbiol., 62(4): 1367-1375. DOI:10.1007/s13213-011-0385-4

Ramapriya, R., Thirumurugan, A., Sathishkumar, T. and Manimaran, D. R. 2018. Partial purification and characterization of exoinulinase produced from Bacillus sp. J. Genet. Eng. Biotechnol., 16(2): 363-367. DOI:10.1016/j.jgeb.2018.03.001

Sadh, P. K., Duhan, S. and Duhan, J. S. 2018. Agro-industrial wastes and their utilization using solid-state fermentation: a review. Bioresour. Bioprocess., 5(1): 1. DOI:10.1186/s40643-017-0187-z

Salman, T., Kamal, M., Ahmed, M., Siddiqa, S. M., Khan, R. A. and Hassan, A. 2016. Medium optimization for the production of amylase by *Bacillus subtilis* RM16 in shake-flask fermentation. Pak. J. Pharm. Sci., 29(2): 439-444.

Saxena, R. and Singh, R. 2011. Amylase production by solid-state fermentation of agro-industrial wastes using Bacillus sp. Braz. J. Microbiol., 42(4): 1334-1342. DOI:10.1590/S1517-838220110004000014

Singh, P. and Kumar Brahman, L. 2013. Effect of carbon, nitrogen sources, and surfactant on production of α-amylase by *Bacillus subtilis*. J. Kalash Sci., 1(2): 83-86.

Souza, P. M. and Magalhães, P. 2010. Application of microbial α-amylase in industry - A review. Braz. J. Microbiol., 41(4): 850-861. DOI:10.1590/S1517-83822010000400004

Suribabu, K. Govardhan, T. L. and Hemalatha, K. 2014. Optimization of various nitrogen sources for the production of amylase using *Brevibacillus borstelensis* R1 by submerged fermentation. Int. J. Curr. Microbiol. App. Sci., 3(4): 791-800.

## ORCID DETAILS OF THE AUTHORS

M. M. Morbia: https://orcid.org/0000-0001-5339-5868
A. A. Pandey: https://orcid.org/0009-0004-1108-9554
P. K. Mahla: https://orcid.org/0009-0005-8584-9795
S. N. Gohil: https://orcid.org/0000-0001-7446-384X

Nature Environment and Pollution Technology
An International Quarterly Scientific Journal

p-ISSN: 0972-6268
(Print copies up to 2016)
e-ISSN: 2395-3454

Vol. 23 | No. 3 | pp. 1605-1611 | 2024

Original Research Paper

https://doi.org/10.46488/NEPT.2024.v23i03.030

Open Access Journal

# Assessing Heavy Metal Accumulation in Urban Plants: Implications for Environmental Health and Traffic-Related Pollution in Al-Diwaniyah City, Iraq

**Luma Abdalalah Sagban Alabadi*, Wafaa Sahib Abbood Alawsy†** and Dunya A. AL-jibury*****
*Department of Horticulture and Garden Engineering, College of Agriculture, University of Al-Qadisiyah, Iraq
**Department of Soil Science and Water Resources, University of Al-Qadisiyah, Iraq
***Department of Council Affairs/Presidency of the University of Baghdad, Iraq
†Corresponding author: Wafaa Sahib Abbood Alawsy; wafaa.abbood@qu.edu.iq

**Nat. Env. & Poll. Tech.**
**Website: www.neptjournal.com**

*Received:* 06-01-2024
*Revised:* 24-02-2024
*Accepted:* 09-03-2024

**Key Words:**
Pollution
Heavy metals
Bioaccumulation coefficient
Plants
Traffic density

## ABSTRACT

This study aimed to compare the ability of five plant species, including (*Conocarpus erectus, Acacia sensu lato (s.l.), Melaleuca viminalis, Dodonaea viscosa and Lantana camara*) to absorb and accumulate heavy elements in their tissues, which were grown in the central islands in the city of Diwaniyah. This included areas of street in front of the medical college, Umm Al Khail First Street, Umm Al-Khail Street, near Abbas Attiwi Bridge, Al-Adly Street in the Euphrates District, and Clock Field Street, respectively. Results showed that soil samples $S_1$ and $S_3$ were contaminated by Pb, and the rest of the sites were contaminated with nickel only. This indicates through the table findings a rise in these heavy metals' concentrations with a rise in traffic momentum. Thus, the Pb concentrations in the growing plants' shoot parts with respect to this research had surpassed the allowed critical limit of 5.00 $mg.kg^{-1}$ dry matter, in which the highest value was recorded at the site with respect to $S_3$ as well as $S_2$. Meanwhile, the findings indicate that Cd concentrations in S3 and S1 had increased and exceeded the allowable limit of 0.20 mg.kg-1 dry matter. In the meantime, the nickel concentrations were within the permissible limits of 67.90 mg.kg-1 dry matter. The Zn concentration exceeded the permitted limits of 60.00 $mg.kg^{-1}$ dry matter except for plants (*Acacia s.l. and Lantana camara*) in sites $S_5$ and $S_2$. The results confirmed that the values of Heavy Metals Bioaccumulation Coefficient (BAC) for most of the study elements had recorded the highest value in the *Dodonaea* plant for Zn, Cd, and Pb, except for Ni. It was more accumulated in the *Melaleuca viminalis* plant, which indicates the superiority of the *Dodonaea* plant in accumulating Pb, Cd, and Zn over the rest of the study plants, as they took the following order: *Lantana camara* < *Acacia s.l.* < *Conocarpus erectus* < *Melaleuca viminalis* < *Dodonaea viscosa.* The best plants accumulated nickel in the following order: *Acacia s.l.* < *Lantana camara* < *Conocarpus erectus* < *Dodonaea viscosa* < *Melaleuca viminalis.*

## INTRODUCTION

The problem of environmental pollution nowadays is receiving great attention not only at the level of third world countries but also at the level of the whole world, as it has become the biggest threat to the world, whether industrial or non-industrial. This is because pollution affects all countries, and there are no limits to prevent it. Hence, it was necessary to address this danger in parallel with technological progress to obtain a safe and clean environment. Furthermore, it was also necessary to encourage stopping the causes of pollution, creating awareness, and motivating the adoption of methods that are more capable of achieving environmental protection (Alkhafajy 2016). The soil is an important component of an ecosystem and the part in which plants grow and are constantly exposed to pollution, which is increasing daily. There are many sources of contamination with heavy metals, including factory chimneys, sewage waste, vehicle exhaust, and chemicals (Monday et al. 2004). Heavy metals, for example, zinc (Zn), cadmium (Cd), and lead (Pb), are considered one of the most dangerous substances that contaminate soil, water, and air. One of the most important sources of this pollution is vehicle exhaust, factory waste, metal smelting, and coal combustion. Some of these heavy metals remain stable for a long time in a place that is polluted without changing chemically. However, due to chemical changes brought on by humidity, heat, microbes, light reactions, and other environmental conditions, some of them were only stable for a brief time (Singh et al. 2011). In a study by Ali (2010) on the pollution status of some soils in the city of Baghdad, the chemical analysis of soil samples showed that some of the studied areas have high concentrations of

heavy metals, Cd, Pb, and Cd. This increase was attributed to the recent increase in the number of cars and the use of fuel from multiple sources. In addition to the presence of factories, foundry workshops, electrical power stations, and an oil refinery, burning plastic materials as well as throwing waste were all factors that have led to increased pollution in the capital. Other than that, Alfatlawi & Nibras (2013) showed in their research the determination of the percentages of Pb in gasoline available in the local market and its impact on the environment.

Furthermore, the condition of the current gasoline product in gas stations is poor in terms of performance, which does not amount to high-performance gasoline (Hosseinpour et al. 2010). This leads to the damage of vehicle engines and significant economic damage, in addition to the continuous pollution it causes to the environment. Many plants are characterized by their ability to absorb pollutants from soil, water, and air and accumulate them in their tissues in a way that does not cause any harm to them. Thus, plants play a role in addressing environmental pollution in the sites where they grow. The concentration of these elements in plant tissues varies according to the different sources of pollution, the nature and components of the soil and the extent of the readiness of these elements for absorption.

Furthermore, the difference in its ability to absorb and accumulate pollutants within its tissues depends on the plant's genetic ability to remove pollutants. The difference in this ability is due to the difference in the presence of the active groups present in the cell walls, as well as phosphate, hydroxyl, and ammonia groups, which represent ion exchange and bonding sites. These play a role in linking with these pollutants (Al-Hamdani 2010). Plants resist the toxicity of heavy elements in several different ways, including immobilizing these elements in the plant, excluding them from cells, introducing them into chelating compounds, or displaying stress-resistant types by forming ethylene or stress proteins. Hence, some plant species absorb a limited amount of the element, while in others, the element remains in the root system. Only a small amount of it is transferred to the shoot, and this is the phenomenon of repulsion (exclusion), while in other species, the element is found in all parts of the plant, which are tolerant plants (Szalai et al. 2002).

The current study aims to compare the ability of five plant species (*Conocarpus erectus, Acacia sensu lato, Melaleuca viminalis, Dodonaea viscosa, Lantana camara*) to absorb and accumulate heavy elements in their tissues, which were grown in the central islands in the city of Diwaniyah, by adopting the criterion of bioaccumulation coefficient (BAC)

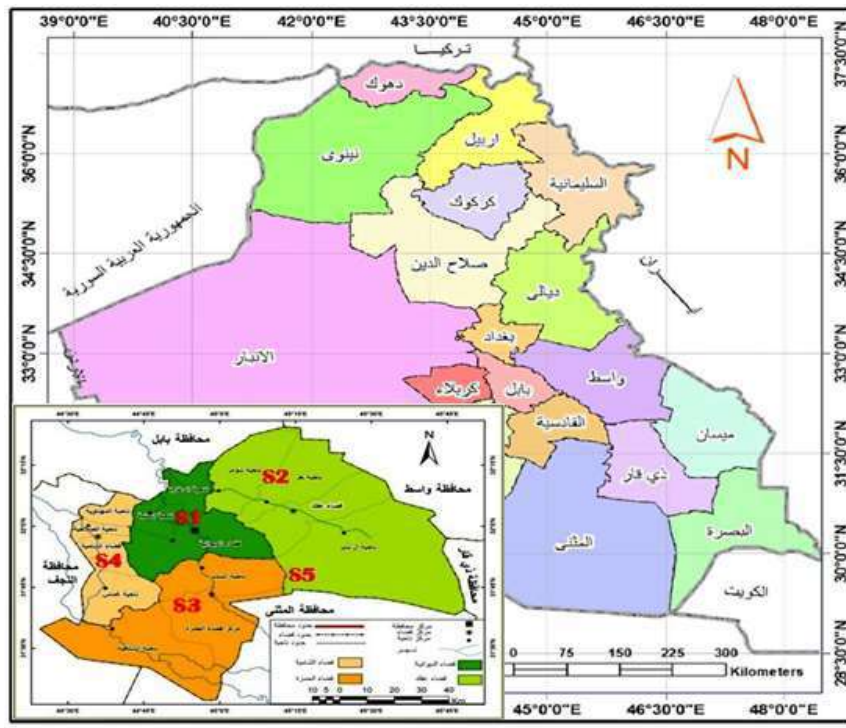


Fig. 1: The distribution of soil and plant sampling areas in the city of Diwaniyah.

in the plant, and the effect of momentum Traffic pollution in the soil and plants growing in it.

## MATERIALS AND METHODS

### Study Area

Five sites were chosen to collect the study samples, Fig. 1, according to the traffic volume and the open central yards planted with plants five, where the study area includes:

1. Street in front of the Medical College with *Conocarpus erectus* plant ($S_1$)
2. Umm Al Khail First Street *with Acacia s.l.* plant ($S_2$)
3. Umm Al-Khail Street, near Abbas Attiwi Bridge with *Melaleuca viminalisp* plant ($S_3$)
4. Al-Adly Street in the Euphrates District with *Dodonaea viscosa* plant ($S_4$)
5. The Clock Field Street with *Lantana camara* plant ($S_5$)

### Collection and Analysis

Several leaves were collected from trees and shrubs growing in the study area (*Conocarpus erectus, Acacia sensu lato, Melaleuca viminalis, Dodonaea viscosa, Lantana camara*). The plant leaves were cleaned in distilled water, dried, and placed at a maximum temperature of 70°C and for 48 h in an oven until the weight was stable and crushed according to the wet digestion method with concentrated acids described by Ryan & Matar (1992).

### Samples Collection and Analysis

Soil samples were collected from the same plant samples collection sites to a depth of 0-15 cm, dried aerobically, and then crushed and sieved with a sieve of 2 mm. The total heavy metals were estimated by treating 1 gm. of dry soil samples with a mixture of two acids ($HNO_3$ and $HClO_4$) according to the method of Jones et al. (2001). Subsequently, total heavy metal concentrations were measured using an Atomic Absorption spectrophotometer (AAS). The efficiency of trees in accumulating heavy elements was calculated by adopting the bioaccumulation criterion for the element in the plant Bioaccumulation Coefficient (BAC), which refers to the concentration of the element in the vegetative total to its total concentration in the soil according to the equation (Li et al. 2007, Cui et al. 2007).

BAC = (Metal) Shoot/(Metal) Soil

BAC = Bioaccumulation factor

(Metal) Shoot = The concentration of the element in the vegetative part ($mg.kg^{-1}$ dry matter)

(Metal) Soil = The total concentration of the element in the soil ($mg.kg^{-1}$)

Table 1: The average traffic density for the study sites ($car.h^{-1}$).

| Samples sites | Averages daily traffic density for 3 days [$car.h^{-1}$] |
|---|---|
| Street in front of the Medical College | 1120 |
| Umm Al Khail First Street | 1000 |
| Umm Al-Khail Street, near Abbas Attiwi Bridge | 1400 |
| Al-Adly Street in the Euphrates District | 852 |
| The Clock Field Street | 800 |

### Traffic Density

The quantification of passing cars in the five designated study sites was conducted with a focus on assessing the prominent source of pollution, the traffic momentum, and emissions emanating from automobile exhaust (refer to Table 1 for detailed statistics). Discrepancies in the number of cars were observed across locations, with continuous traffic prevailing in most areas except for Clock Field Street. Notably, the onset and conclusion of scheduled working hours marked periods of heightened traffic density. To ascertain the impact, the traffic density was systematically calculated by counting the number of automobiles passing through the sampling sites over twelve hours, spanning from 6:00 a.m. to 6:00 p.m., over a three-day duration. This approach aligns with the methodology outlined by (2004).

## RESULTS AND DISCUSSION

### Total Concentration of Heavy Metals in the Study Soils

When compared to the total concentration in sites S1 and S3, Table 2 revealed the heavy metals total concentration in the study soils. With delimiters from the Food and Agriculture Organization (FAO) as well as the World Health Organization (WHO) (WHO/FAO 2007), we find it contaminated with lead (Pb). As for the rest of the sites, they were contaminated with nickel only. It was also evident from the results of Table 2 that with an increase in traffic momentum, there exists a discernible rise in these heavy metal concentrations, and this may be attributed to their exposure to pollution from car exhaust (Warmate et al. 2011, Fadhel & Abdulhussein 2022). These results are consistent with the findings by Joudah (2013). Soil pollution with heavy metals may come from several different sources, most of which are road traffic and the use of Pb gasoline, especially in vehicles, which increases its concentration in the atmosphere (Karam et al. 2019, Essa & Dunya 2017).

### Concentration of Heavy Metals in Study Plant Samples

Table 3 meticulously outlines the concentrations of heavy

Table 2: Total heavy metals concentration in the soils of the middle islands in the road's of city of Al-Diwaniyah (mg.kg$^{-1}$).

| Study sites | Symbol | Heavy metals [mg.kg$^{-1}$] | | | |
|---|---|---|---|---|---|
| | | Pb | Cd | Ni | Zn |
| Street in front of the Medical College | $S_1$ | 106.00 | 2.53 | 122.80 | 125.32 |
| Umm Al Khail First Street | $S_2$ | 88.00 | 2.16 | 85.72 | 109.00 |
| Umm Al-Khail Street, near Abbas Attiwi Bridge | $S_3$ | 125.32 | 2.67 | 131.00 | 139.70 |
| Al-Adly Street in the Euphrates District | $S_4$ | 90.30 | 2.04 | 99.52 | 105.9 |
| The Clock Field Street | $S_5$ | 82.91 | 1.96 | 69.04 | 94.78 |
| WHO/FAO (2007) | | 100.00 | 3.00 | 50.00 | 300.00 |

metals in the shoot parts in the middle islands of the streets of the city of Al-Diwaniyah under study, which ranged between 7.30-14.90, 0.14-0.24, 2.50-3.00, 51.00-87.00 mg.kg$^{-1}$ dry matter for each of the lead (Pb), cadmium (Cd), nickel (Ni) and zinc (Zn) successively. When comparing the concentrations of Pb for the plants under study, which ranged between 7.30-14.90 mg.kg$^{-1}$ dry matter, the determinants of the World Health and Food and Agriculture Organizations (WHO) (WHO/FAO 2007). Apart from that, we find that it has exceeded the permissible critical limit of 5.00 mg.kg$^{-1}$ dry matter, which indicates the plant's ability to absorb heavy metals via the roots and transfer them to the shoot system, or they may be taken directly from the air through the leaves (Kord et al. 2010). The outcomes also indicated a rise in the Pb concentration in the shoot with an increase in the traffic density, as the highest value was recorded at the site of $S_3$ and $S_2$ with values of 14.90 and 12.50 mg.kg$^{-1}$, successively with a traffic momentum (Table 1). These results were similar to those of Rasheed & Hadeel (2013). The traffic momentum due to the combustion of fuel containing Pb results in an Aerosol suspension containing high concentrations of Pb distributed in the surrounding environment, raising pollution levels for soil, air, and plants.

Table 3: Total heavy metals concentrations in plants shoot for study sites (mg.kg$^{-1}$ dry matter).

| Plant species | Heavy metals [mg.kg$^{-1}$ dry matter] | | | |
|---|---|---|---|---|
| | Pb | Cd | Ni | Zn |
| Site one (S1) | | | | |
| *Conocarpus erectus L.* | 12.50 | 0.21 | 4.60 | 76.00 |
| Site two (S2) | | | | |
| Acacia s.l. | 9.80 | 0.17 | 3.00 | 59.00 |
| Site three (S3) | | | | |
| Melaleuca viminalis | 14.90 | 0.24 | 5.20 | 87.00 |
| Site four (S4) | | | | |
| Dodonaea viscosa | 11.00 | 0.20 | 3.80 | 68.00 |
| Site five (S5) | | | | |
| Lantana camara | 7.30 | 0.14 | 2.50 | 51.00 |
| WHO and FAO (2007) | 5.00 | 0.20 | 67.90 | 60.00 |

The result shown in Table 3, Cd concentrations in the shoot parts of plants grown in the soil under study ranged between 0.14-0.24 mg.kg$^{-1}$ dry matter. Here, the highest value can be observed on sites $S_3$ and $S_1$, which reached 0.24 and 0.21 mg.kg$^{-1}$ dry matter sequentially. This was characterized by traffic momentum compared to the rest of the sites (Table 1). When comparing those concentrations with the determinants of the World Health and Food and Agriculture Organizations (WHO) (WHO/FAO 2007), we found that the limit has exceeded 0.20 mg.kg$^{-1}$ dry matter. This demonstrates the traffic density and momentum effect (vehicles staying on the street) on the pollution process of plants growing in the study sites.

The result shown in Table 3, concentrations of nickel in the shoot parts of plants grown in the study soils, which ranged between 2.50-5.20 mg.kg$^{-1}$ dry matter, remained within the allowed limits of 67.90 approved by the World Health and Food and Agriculture Organizations (WHO) (WHO/FAO 2007). This is consistent with what was found by Mohsen & Mohsen (2008). Increasing the concentration of nickel in the soil causes an increase in its concentration in plants growing in it and collects it in its tissues. As for the Zn, the results of Table 3 showed concentrations of Zn for plants grown in the study soils, which ranged between 51.00-87.00 mg.kg$^{-1}$ dry matter. When comparing those concentrations with the determinants of the World Health and Food and Agriculture Organizations (WHO/FAO 2007), we find that they have exceeded the permissible limit of 60.00 mg.kg$^{-1}$ dry matter, except for plants (*Lantana camara* and *Acacia s.l.*) in the $S_5$ and $S_2$ sites, which amounted to 51.00 and 59.00 mg.kg$^{-1}$ dry matter. According to the results of Table 3, it was found that the concentrations of heavy metals increased in plants growing in the middle island with heavy traffic (near Abbas Attiwi Bridge, Faculty of Medicine Street) compared with other sites, Table 1. Results are consistent with the findings of Alsaffawi et al. (2014) and Ammar & Nasr (2017) about the high concentrations of lead in the leaves and branches of growing plants in densely populated and high-traffic areas in the city of Mosul. The results of our current study

were similar to what was obtained by Ammar & Nasr (2017) in their study on the efficiency of some trees and roadside shrubs in the city of Tikrit in accumulating heavy elements, where the highest concentration of lead was in the leaves of growing trees in the annual road of the city of Tikrit, due to its proximity to the industrial neighborhood that prevails It includes the burning of car tires and some types of fuel available from car waste, which confirms the role of gases emitted from vehicles in polluting the soil with heavy elements and their transfer to growing plants.

Moreover, Ali (2010) found some areas of Baghdad soils have high heavy metal concentrations, including Cd, Pb and Zn. This increase has been associated with the recent increase in vehicles and the use of fuels from different sources. As a result, plants growing in soils polluted with heavy metals absorbed these metals from polluted soil and collected them in their tissues compared to plants grown in unpolluted soils (Chojnacha et al. 2005, Saini et al. 2011).

**Bioaccumulation Coefficient (BAC)**

The bioaccumulation factor refers to the plant's ability to store and store heavy metals. It reflects the ability of the plant species to accumulate heavy elements through their absorption from the soil and their accumulation in its tissues (Mahmood et al. 2019, Hassan et al. 2020). The higher values of the bioaccumulation coefficient than one indicate that the plant species is highly efficient in absorbing heavy elements (Hamad et al. 2021)**.** We assessed Figs. 2, 3, and 4 that the bioaccumulation coefficient values with respect to heavy metals for the majority of the study metals observed in the *Dodonaea viscosa* plant reached 0.122, 0.098, and 0.642 for Pb, Cd, and Zn, respectively except for nickel. It

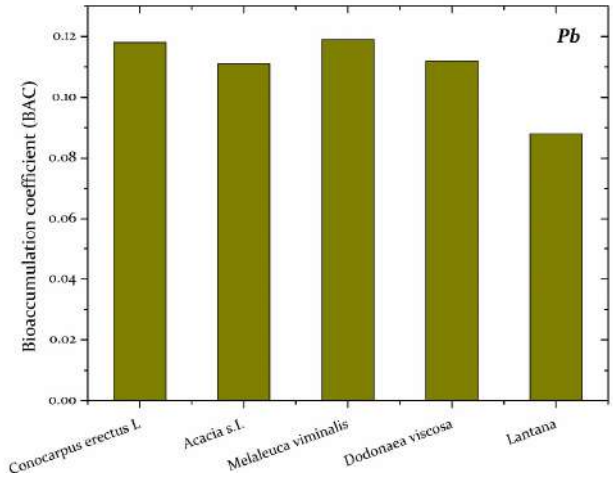


Fig. 2: Bioaccumulation coefficient (BAC) for lead in the study plants.

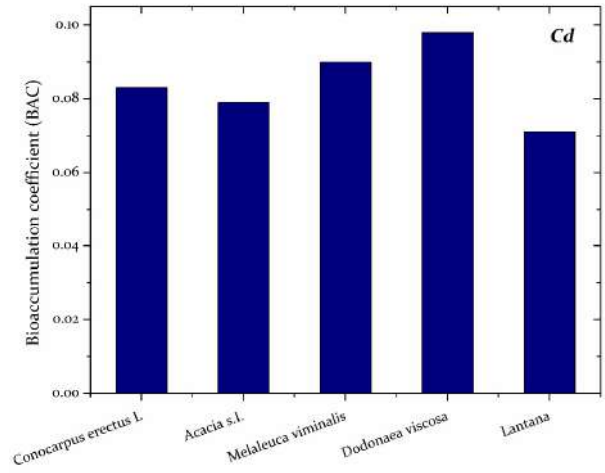


Fig. 3: Bioaccumulation coefficient (BAC) for cadmium in the study plants.

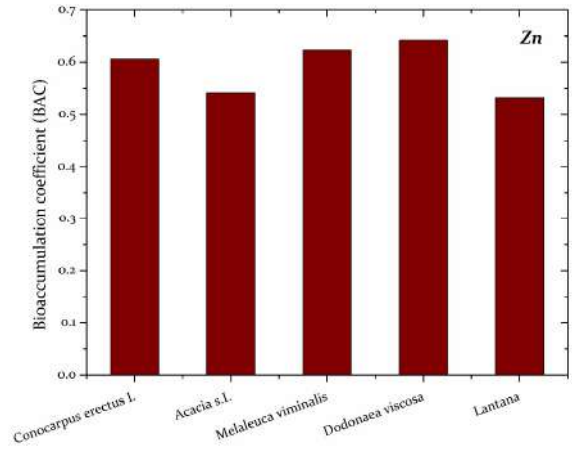


Fig. 4: Bioaccumulation coefficient (BAC) for zinc in the study plants.

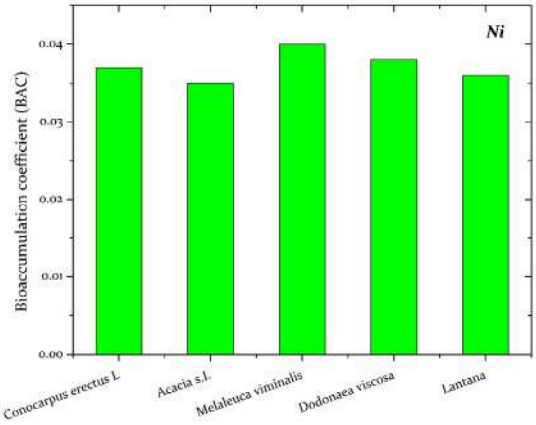


Fig. 5: Bioaccumulation coefficient (BAC) for Nickel in the study plants.

was more accumulated in the *Melaleuca* tree, which had a value of 0.040 (Fig. 5), which indicates the superiority of the *Dodonaea viscosa* plant in accumulating Pb, Cd, and Zn over the rest of the study trees, as they took the following order:

*Melaleuca viminalis* > *Conocarpus erectus* > Acacia s.l. > *Lantana camara* > *Dodonaea viscosa*

The best tree accumulation for nickel is in the following order:

*Melaleuca viminalis* > *Dodonaea viscosa* > *Conocarpus erectus* > *Lantana camara* > *Acacia s.l.*

The reason is attributed to the variation in the ability of plants to absorb and accumulate heavy elements based on the physiological nature of plant species (Azita & Seid 2008). These results were proportional to what was found by Ammar & Nasr (2017). The Dodonaea viscosa plant prefers to accumulate Pb and Zn compared to the rest of the roadside trees and shrubs in Tikrit City.

## CONCLUSION

The investigation yielded significant findings, pinpointing soil contamination with Pb in S1 and S3, while nickel contamination was evident in the remaining sites. The results showed a discernible rise in the concentrations with respect to the study of heavy metals by increasing the traffic momentum.

The lead (Pb) concentrations in the shoot parts with respect to the growing plants under study exceeded the permissible critical limit, as the highest value was recorded at $S_3$ and $S_2$ locations. The results showed an increase in cadmium (Cd) concentrations in $S_3$ and $S_1$ sites, and they exceeded the permissible limit. In comparison, the nickel concentrations were within the permissible limits. The zinc (Zn) exceeded the permissible limits except for the plants (*Lantana camara* and *Acacia s.l.*) in the $S_5$ and $S_2$ sites. The values of the heavy metals Bioaccumulation Coefficient (BAC) for most of the study metals recorded the highest value

in the *Dodonaea viscosa* plant for Pb, Cd, and Zn, except for nickel, which was more accumulated in the *Melaleuca viminalis* tree. This variation is due to the plant's genetic ability to remove pollutants.

## ACKNOWLEDGMENTS

Expansion of the cultivation of *Dodonaea viscosa* and the *Melaleuca viminalis* of the hero in the range of Diwaniyah governorate and similar areas in climatic conditions and its use in the process of air reclamation of soils contaminated with heavy elements due to its ability to absorb and accumulate heavy elements in its tissues.

## REFERENCES

Alfatlawi, A. M. L. and Nibras, M. A. A. A. 2013. Limitation of lead concentration in gasoline that is available in the local market and its effect on the environment. Al-Qadisiyah J. Eng. Sci., 7(4): 90-101.

Al-Hamdani, I. O. S. 2010. An environmental survey of some water sources, sewage discharges, and plant treatment in the city of mosul and its suburbs. PhD thesis. Department of Life Sciences, College of Education, Tikrit University.

Ali, M. O. 2010. Study of pollution by heavy elements in some parts of Baghdad. Baghdad J. Sci., 7(2): 955-962.

Ali, Z. A., Hassan, D. F. and Mohammed, R. J. 2021, April. Effect of irrigation level and nitrogen fertilizer on water consumption and faba bean growth. IOP Conf. Ser. Earth Environ. Sci., 722(1): 012043. https://doi.org/10.1088/1755-1315/722/1/012043

Alkhafajy, A. K. A. B. 2016. Detection of the pollution status of soils and waters of the sawa lake area by using remote sensing techniques. Master thesis, Department of Plant Production, Soil and Water Resources, College of Agriculture, University of Al-Muthanna.

Alsaffawi, A. Y. T., Al-Qathelly, F. A. and Tawfiq, K. S. 2014. Bioaccumulation of lead element in the shoot of some plants in Mosul city, Iraq. Plant Prod., 7: 61-70.

Ammar, F. K. and Nasr, S. A. L. 2017. Testing the efficiency of some roadsides, trees, and bushes to detain dust molecules and accumulation of heavy metals in Tikrit. Agric. Sci., 11: 59-76.

Azita, B. H. and Seid, A. M. 2008. Investigation of heavy metals uptake by vegetable crops from metal-contaminated soil. World Acad. Sci. Eng. Technol., 43(1): 56-58.

Chojnacha, K., Chojnacki, A., Gorecka, H. and Gorecki, H. 2005. Bioavailability of heavy metals from polluted soils to plants. Sci. Total Environ., 337(1-3): 175-182.

Cui, S., Zhou, Q. and Chao, L. 2007. Potential hyper-accumulation of Pb, Zn, Cu, and Cd in endurant plants distributed in an old smeltery in northeast China. Environ. Geol., 51: 1043-1048.

Essa, S. K. and Dunya, A. L. J. 2017. Heavy metals pollution for soils in some of roads and squares of Baghdad city center. Iraqi J. Agric. Sci., 48: 1456-1472. DOI: 10.13140/RG.2.2.23815.04003

Fadhel, M. A. and Abdulhussein, F. M. 2022. Accumulation detection of cadmium in some land-use soil of Baghdad city, Iraq. Iraqi J. Sci., 63(8): 3570-3577. DOI: 10.24996/ijs.2022.63.8.29

Fan, K. C., Hsi, H. C., Chen, C. W., Lee, H. L. and Hseu, Z. Y. 2011. Cadmium accumulation and tolerance of mahogany Swietenia macrophylla seedlings for phytoextraction applications. J. Environ. Manage., 92: 2818-2822.

Grace, N. 2004. Assessment of heavy metal contamination of food crops and vegetables from motor vehicle emissions in Kampala City, Uganda. Technical Report. Department of Botany, Makerere University, Kampala.

Hamad, A. A., Alamer, K. H. and Alrabie, H. S. 2021. The accumulation risk of heavy metals in vegetables that are grown in contaminated soil. Baghdad Sci. J., 18(3): 0471-0479.

Hassan, D., Thamer, T., Mohammed, R., Almaeini, A. and Nassif, N. 2020. Calibration and evaluation of AquaCrop model under different irrigation methods for maize (Zea mays L.) in central region of Iraq. In: Conference of the Arabian Journal of Geosciences (pp. 43-48). Cham: Springer Nature Switzerland. https://doi.org/10.1007/978-3-031-43803-5_10

Hosseinpour, M. A., Ghoreishi, H., Gitipour, S. and Jafarnejad, M. 2010. Investigation of oil inside the wells in the REY area in Tehran oil refining company in Iran. World Acad. Sci. Eng. Technol., 69: 200-206.

Jones, D. L., Eldhuset, T., de Wit, H. A. and Swensen, B. 2001. Aluminum effects on organic acid mineralization in a Norway spruce forest soil. Soil Biol. Biochem., 33(9): 1259-1267.

Joudah, R. A. 2013. Heavy metals pollution in the roadside soil of Bab Al-Muadham city center/Baghdad. Aust. J. Basic Appl. Sci., 7(12): 35-43.

Karam, F. F., Alabadi, L. A. S. and Al-Jibury, D. A. 2019. Levels and distribution of trace metals in surface soils of Al-Diwaniya, Iraq. Asian J. Chem., 31(2): 327-332. DOI: 10.14233/ajchem.2019.21521

Kord, B., Mataji, A. and Babaie, S. 2010. Pine (Pinus eldarica Medw.) needles as an indicator for heavy metals pollution. Int. J. Environ. Sci. Technol., 7(1): 79-84.

Li, M. S., Luo, Y. P. and Su, Z. Y. 2007. Heavy metal concentrations in soils and plant accumulation in a restored manganese mineland in Guangxi, South China. Environ. Pollut., 147(1): 168-175.

Mahmood, M. A., AI-Mashhady, A. A. M. and Ali, A. N. 2019. Heavy metals accumulation in two types of tree leaves from urban areas. Eng. Technol. J., 37(C), (3): 350-355.

Mohsen, B. and Mohsen, S. 2008. Investigation of metals accumulation in some vegetables irrigated with wastewater in share Rwy-loan and toxicological application. Am.-Eurasian J. Agric. Environ. Sci., 4(1): 86-92.

Monday, O., Mbila, M. and Thompson, M. L. 2004. Plant-available zinc and lead in mine spoils and soil at the Mines of Spain. Iowa.

Rasheed, R. T. and Hadeel S. M. 2013. Estimate the proportion of soil contamination at the University of Technology by lead metal. Eng. Technol. J., 31(B), (5).

Ryan, J. and Matar, A. 1992. Fertilizer use efficiency under rain-fed agriculture in West Asia and North Africa. Proc. 4th Reg. Soil Test Calibr. Workshop West Asia-North Africa Reg., Agadir, Morocco, 5-10, 1991. ICARDA, Aleppo, Syria.

Saini, Y., Bhardwaj, N. and Gautam, R. 2011. Effect of marble dust on plants around Vishwakarma Industrial Area (VKIA) in Jaipur, India. J. Environ. Biol., 32: 209-212.

Singh, A., Kumar, C. S. and Agarwal, A. 2011. Phytotoxicity of cadmium and lead in Hydrilla verticillata (I.F). Royle. J. Phytol., 3(8): 1-4.

Szalai, G., Janda, T., Golan-Goldhirsh, A. and Paldi, E. 2002. Effect of Cd treatment on phytochelatin synthesis in maize. Acta Biol. Szeged, 46(3-4): 121-122.

Warmate, A. G., Ideriah, T. J. K., Tamunobereton, I. T., Inyang, A. R. I. and Udonam, U. E. 2011. The concentration of heavy metals in soil and water receiving used engine oil in Port Harcourt, Nigeria. J. Ecol. Nat. Environ., 3(2): 54-57.

WHO/FAO 2007. Joint WHO/FAO. Food standard program codex Alimentarius commission 13th session

## ORCID DETAILS OF THE AUTHORS

Wafaa Sahib Abbood Alawsy: https://orcid.org/0009-0000-6517-5838

Nature Environment and Pollution Technology
An International Quarterly Scientific Journal

p-ISSN: 0972-6268
(Print copies up to 2016)
e-ISSN: 2395-3454

Vol. 23 | No. 3 | pp. 1613-1621 | 2024

Original Research Paper

https://doi.org/10.46488/NEPT.2024.v23i03.031

Open Access Journal

# Stabilization of Dredged Soil by Compensating the Sand Content in the Jhelum River

**Yasir Hamid*, Owais Shafi Malik**, Huma Khan*†, Gauhar Mehmood* and Amina Zakiah*****

*Department of Civil Engineering, Jamia Millia Islamia, New Delhi-110025, India

**Department of Civil Engineering, SSM College of Engineering, Pattan-193121, Jammu & Kashmir, India

***Department of Hydro Science and Engineering, Technische Universitat Dresden, 01062, Germany

†Corresponding author: Huma Khan; huma.engg@gmail.com

**Nat. Env. & Poll. Tech.**
**Website: www.neptjournal.com**

*Received:* 08-01-2024
*Revised:* 26-02-2024
*Accepted:* 16-03-2024

**Key Words:**
Dredged soil
Jhelum river
Sand content
Soil stabilization
Stabilizing agent

## ABSTRACT

River dredging is crucial for mitigating the risk of floods by enhancing the water-carrying capacity of rivers. Nevertheless, the key difficulty lies in the appropriate disposal of dredged material, resulting in escalated costs. Predominantly consisting of silt, the dredged material demonstrates constrained bearing capacity and strength. Nonetheless, there is a prospect to derive value from excavated sediments, with potential applications in diverse public works projects. The processed product derived from dredged material can serve diverse purposes, such as filling railway and highway embankments, as well as the subgrade of pavements. The comprehensive study involved analyzing the fundamental properties of the dredged material collected from the Allochibagh flood channel of the Jhelum River. The analysis focused on determining the basic geotechnical properties of the soil mass. The tests unveiled the fine and cohesive nature of the dredged soil. To enhance its properties, sand was introduced as a stabilizing agent in varying proportions. The investigation revealed an initial augmentation in compressive strength as the proportion of sand increased, attaining an optimal mixture whereafter the strength declined. This study explores the utilization of sand as a stabilizing agent for dredged soil to enhance its strength and optimize its application. The process of stabilizing dredged soil with sand demands a thorough examination of hydrogeological processes, the specific characteristics of the dredged soil, and the intricate transport of contaminants. This formal and multidisciplinary effort seeks to elevate the overall stability of the soil.

## INTRODUCTION

River dredging involves the extraction of sediment and debris from a river's bed and banks to uphold navigability, prevent flooding, and support water infrastructure. One of the elements that exacerbated the flood scenario in Kashmir in September 2014 has been identified as the increased siltation in the river bed of the river Jhelum. As a result, experts have been urging for immediate dredging of the rivers and its spillway to boost its capacity. Two sections of the Dredging have been separated. The Irrigation and Flood Control department is in charge of the first component, which requires dredging of approximately 9,50,000 $m^3$ of material. In the second phase, the Irrigation and Flood Control department contracted with a private company to remove 16 lakh cubic meters of silt by dredging the Jhelum and its spillway. According to estimates, Jhelum's dredging will boost the river's carrying capacity from 34000 to 45000 cusecs and the flood spillway's capacity from 5000 to 10000 cusecs PTI (2016), Amin (2016) However, because poorly graded silt makes up the majority of the dredged material, it has a relatively poor bearing capacity and strength (Mir et al. 2016) and cannot be used directly for different types of building. The disposal of substantial volumes of dredged material in landfills poses significant environmental challenges and hence it must be properly disposed of, which raises the price even more (Nassar et al. 2023). The valorization of excavated sediments and their use in public works, however, offers an option. The processed product can be used for a variety of things, like filling up pavement (subgrade) and railroad and highway embankments. The geotechnical attributes of dredged material make it essential to employ strategies for stabilizing the soil mass, thereby improving its characteristics, particularly its strength, to enable its practical application. This objective can be achieved through diverse techniques, including the introduction of stabilizing agents such as cement, lime, fly ash, and fibers. The selection of a particular additive is contingent upon factors such as the soil type, intended purpose, and prevailing environmental conditions. The primary mechanisms employed by these stabilizers encompass cation exchange, flocculation and agglomeration, pozzolanic reaction, and

carbonate cementation (Croft 1967, Firoozi et al. 2014, Puppala & Musenda 2000, Firoozi et al. 2015, Little 1998, IS 13094 1992). Sand, a naturally occurring granular material, is valuable for its high load-bearing capacity in confined conditions. As a filler material, it can be added in various proportions to cohesive soils, effectively modifying plasticity, compaction, and strength in the mixtures (Kollaros & Athanasopoulou 2016). This versatile use of sand contributes to the overall enhancement of soil properties.

The current study focuses on the valorization of dredged material, specifically through the exploration of stabilization methods. This study delves into the potential enhancement of dredged material by incorporating an inert additive, namely sand. The key aspect under investigation is the engineering characteristics of the soil before and after the additive mix. Through systematic experimentation, varying concentrations of sand were introduced as additives, and a thorough analysis was conducted to assess their influence on the engineering properties of the dredged material. The primary objective of the study is to illustrate the impact of different percentages of sand content on the characteristics of dredged material.

## OBJECTIVE AND SCOPE OF THE STUDY

The primary focus of this study is the geotechnical characterization of dredged material, examining its properties at various locations along the flood-sensitive channel. Through detailed analysis, the study aims to understand the unique geotechnical characteristics of the dredged material. The investigation encompasses aspects such as composition, particle size distribution, moisture content, and other relevant properties. Building on this characterization, the study provides prospective recommendations for the practical application of dredged material based on its distinct properties. These recommendations are designed to guide decisions on the utilization of dredged material, taking into account factors such as its stability, strength, and environmental impact. The overarching goal of this research is to contribute to the effective management of dredged soil along the Jhelum River, ensuring that the handling and application of this material safeguard both human health and the broader ecosystem. By combining geotechnical insights with practical recommendations, the study aims to offer a holistic approach to the responsible use of dredged material in this crucial environmental context.

## MATERIALS AND METHODS

### Methodology

The research commenced with the retrieval of soil samples from the Jhelum flood channel of Allocha Bagh in Srinagar, with the primary objective being the comprehensive assessment of the essential properties inherent in the dredged soil to gain insights into its fundamental characteristics. This involved a systematic series of tests and analyses, commencing with the determination of the specific gravity through a density bottle test. Subsequently, the soil's maximum dry density was established via a proctor compaction test. The particle size distribution was scrutinized using both sieve analysis and hydrometer analysis. The liquid index and plastic index were ascertained utilizing Casagrande's apparatus and the 3mm rolling thick thread rod method, respectively. Following the comprehensive understanding of the soil's intrinsic attributes, the investigation progressed to evaluate its shear strength through the unconfined compression strength (UCS) test. All examinations and sample preparations were carried out in compliance with the established procedures of CE, as cited (Reddy 2022, IS 1498-1970, IS 2720-1980, Punmia 2007). In a subsequent phase, sand was introduced as a stabilizing agent to the dredged soil in varying proportions of 1.5%, 3%, 5%, and 7.5%. Post the sand incorporation, the soil's strength was reevaluated by employing the unconfined compression strength test. The overarching goal of the study was to systematically observe and quantify variations in soil strength corresponding to different proportions of added sand, thereby offering significant insights into the stabilizing effects exerted by sand on the dredged soil.

### Analysis

The specific gravity of a soil sample was determined through the utilization of the density bottle method. Three distinct empty-density bottles denoted as D1, D2, and D3, each initially weighing 32g, were employed in the procedure. Subsequently, 10g of dry soil mass was added to each bottle. The density bottles were then saturated with distilled water, and the resultant masses, encompassing the density bottle, soil, and water, were meticulously recorded for each bottle as 104.31g, 104.5g, and 104.8g respectively. Following this, the density bottles were emptied, and filled solely with distilled water, and the corresponding masses were recorded as 98.12g, 98.3g, and 98.6g respectively. Consequently, the specific gravity values for soil in D1, D2, and D3 were calculated to be 2.62, 2.63, and 2.63, respectively. Upon incorporating temperature corrections, the final average specific gravity of the dredged soil at 27°C was computed as 2.63.

Particle size distribution of soil refers to the relative proportions of sand, silt, and clay particles within a soil sample, determining its texture. With sand particles ranging from 2.0 to 0.05 millimeters, silt between 0.05 and 0.002 millimeters, and clay particles smaller than

0.002 millimeters, the combination of these soil separates influences essential soil properties. This distribution is crucial for soil classification, influencing water retention, drainage, and aeration. It also impacts nutrient availability, with clay particles having a greater surface area for nutrient retention. Engineering properties of soils, such as compressibility and shear strength, are dependent on particle size distribution, making them important in construction. Additionally, understanding soil texture aids in land use planning, agricultural management, and environmental conservation, guiding decisions on crop selection, irrigation practices, and erosion control. Laboratory methods: sieve analysis and hydrometer analysis were employed to assess the particle size distribution, providing valuable insights for a range of applications in soil science.

Sieve analysis serves to ascertain the particle size distribution of granular substances like soil or aggregate. This method entailed passing a sample through a sequence of sieves arranged in decreasing mesh size. After sieving, the material retained on each sieve was weighed, and the percentage within each size range was determined from the total sample. The outcomes offered crucial insights into particle size distribution, facilitating soil classification, evaluating engineering characteristics, and informing decisions in construction, agriculture, and environmental applications. The study involved sieving a dried dredged soil sample of 500g on a sieve set from 4.75mm to 0. 075mm. The results obtained are shown in Table 1.

Table 1: Sieve analysis of the pure dredged soil sample.

| Sieve Size (mm) | Mass of Soil Retained (g) | Percentage Retained | Cumulative Soil Retained | Finer |
|---|---|---|---|---|
| 4.75 | 0 | 0 | 0 | 100 |
| 2 | 0 | 0 | 0 | 100 |
| 1 | 0 | 0 | 0 | 100 |
| 0.6 | 1 | 0.2 | 0.2 | 99.8 |
| 0.3 | 4.5 | 0.9 | 1.1 | 98.9 |
| 0.212 | 9 | 1.8 | 2.9 | 97.1 |
| 0.15 | 13.5 | 2.7 | 5.6 | 94.4 |
| 0.075 | 8 | 1.6 | 7.2 | 92.8 |
| Pan | 0 | 0 | 7.2 | 92.8 |

Hydrometer analysis is employed to assess the particle size distribution of fine-grained soils, particularly those with sizes smaller than those examined through sieve analysis. In this analysis, a mixture of soil and water was created, and a hydrometer was utilized to gauge the settling speed of particles in the suspension. The underlying principle relies on Stokes' Law, connecting particle settling velocity to size and density. By monitoring settling rates over different time intervals, the soil's particle size distribution was determined. This analysis was done to complement sieve analysis, offering valuable insights into soil characteristics, notably soil texture, which holds significance in agricultural and engineering applications. The study involved the analysis of 50g of dredged on a hydrometer, and the analytic data so obtained is shown in Table 2.

Atterberg limits comprise three moisture content points that define soil consistency: the Liquid Limit (LL), indicating the transition from plastic to liquid state; the Plastic Limit (PL), marking the moisture content at which soil can no longer form threads without crumbling; and the Shrinkage Limit (SL), denoting the moisture level at which further loss does not induce additional volume reduction.

The determination of the liquid limit of soil was conducted through the Casagrande method, a standardized

Table 2: Hydrometer analysis of the pure dredged soil sample.

| Time | Hydrometer Reading G (RH') | Water Temperature (°C) | Room Temperature (°C) | Corrected Reading (RH) | Effective Height ($H_e$) | Diameter | % Finer |
|---|---|---|---|---|---|---|---|
| 0.5 min | 29 | 18.5 | 21.3 | 27 | 9.8 | 0.064 | 92.61 |
| 1 min | 28 | 18.4 | 21.3 | 36 | 10.1 | 0.048 | 89.18 |
| 2min | 26 | 18.5 | 21.3 | 24 | 10.7 | 0.035 | 82.32 |
| 4 min | 24 | 18.5 | 21.4 | 22 | 11.4 | 0.025 | 75.46 |
| 8 min | 22 | 18.6 | 21.4 | 20 | 12.1 | 0.018 | 68.6 |
| 15 min | 19 | 18.6 | 21.5 | 17 | 13 | 0.014 | 58.31 |
| 30 min | 16 | 18.7 | 21.5 | 14 | 14.1 | 0.01 | 48.02 |
| 1 hr | 13 | 18.8 | 21.7 | 11 | 15.1 | 0.008 | 37.73 |
| 2 hr | 9 | 18.9 | 21.7 | 7 | 16.4 | 0.006 | 24.01 |
| 4 hr | 5 | 19.2 | 22.5 | 3 | 17.6 | 0.004 | 10.29 |
| 8 hr | 0.996 | 19.8 | 23.6 | 1 | 18.3 | 0.003 | 3.43 |
| 12hr | - | - | - | 0 | 18.7 | 0.002 | 0 |

procedure widely employed in soil mechanics. Initially, a representative soil sample was meticulously prepared, involving air-drying to eliminate excess moisture and subsequent pulverization for homogeneity. The Casagrande cup was then filled with the prepared soil, and a groove was established along its center. Employing a liquid limit device or Casagrande plunger, water was incrementally added to the soil along the groove, and the plunger was dropped at regular intervals. The count of drops required for the soil to close a specified distance against a specific moisture content was noted as shown in Table 3.

The plastic limit (PL) of soil indicates the moisture content at which the soil transitions from a plastic to a crumbly, semi-solid state. The determination of the plastic limit involves initially air-drying a representative soil sample to eliminate excess moisture, followed by pulverizing the soil into a fine powder. Water was then gradually added to the powdered soil, and the mixture was kneaded to form a 3mm thread. This thread was carefully rolled on a flat glass plate until it reached a point of crumbliness. The moisture content at which this crumbliness occurs was identified as the plastic limit (Table 4).

The Atterberg limits calculated provide insights into the soil's characteristics, revealing a plasticity index (PI), which is the difference between the liquid limit (LL) and plastic limit (PL), determined to be 17.172. Additionally, the plastic index (PI) of the A-line, expressed as 0.73(LL-20), was calculated as 14.085. A comparison with the plasticity index of dredged soil indicates that the soil was clayey. The liquid limit of the soil falls within the range of 35-50 at 39.3, suggesting a medium compressibility. Further analysis reveals a flow index, representing the difference in moisture at ten and hundred blows, as 31.37. Moreover, the toughness index, defined as the ratio of the plasticity index to the flow index, was determined to be 0.55. These findings collectively characterize the soil as clayey with medium compressibility, contributing to a comprehensive understanding of its engineering properties.

Table 3: Moisture content of samples at different Casagrande's blows.

| Sample | A | B | C |
|---|---|---|---|
| No. of blows | 39 | 29 | 21 |
| Mass of container + Wet soil | 41.55 | 43.1 | 44.9 |
| Mass of container +Dry soil | 39 | 40 | 41.5 |
| Mass of water | 2.55 | 3.1 | 3.4 |
| Mass of container(g) | 31.5 | 32 | 33 |
| Mass of dry soil(g) | 7.5 | 8 | 8.5 |
| Moisture content | 34 | 38.75 | 40.17 |

Table 4: Plastic limit of pure dredged soil samples.

| Sample | A | B | C |
|---|---|---|---|
| Mass of container + wet soil | 41 | 39 | 38.5 |
| Mass of container + dry soil | 39.5 | 38 | 37 |
| Mass of water | 1.5 | 1 | 1.5 |
| Mass of container | 32.5 | 33 | 31 |
| Mass of dry soil | 7 | 5 | 6 |
| Plastic limit | 21.4 | 20 | 25 |
| Average Plastic limit | 22.13 | | |

Dry density refers to the mass of soil per unit volume when the soil is completely dry. It is a crucial parameter used to characterize the compaction and density of soils. The dry density of soil is maximum at the optimum water content. A curve is drawn between the water content and the dry density to obtain the maximum dry density and the optimum water content. The determination of dry density through light and heavy compaction is a fundamental process in geotechnical engineering. In light compaction, a specified weight was dropped onto a soil sample in a mold, while heavy compaction involves a more significant compaction effort. After compaction, the dry density was calculated by measuring the weight and volume of the compacted soil. The standard proctor test was employed for light compaction, contributing to effective soil compaction control in engineering applications. A soil sample of 100 cc was tested for light compaction and compacted, and the moisture content was varied to identify the maximum dry density. Results obtained to get the optimum moisture content and maximum dry density as shown in Table 5.

Conversely, heavy compaction involving a higher compaction energy on the soil samples was tested using the modified proctor test. To find the maximum dry density, a 100 cc soil sample was compacted and its moisture content was adjusted. Findings that led to the ideal moisture content and highest dry density are displayed in Table 6.

The shear strength of soil is a critical property that influences the stability of slopes, foundations, and other geotechnical structures. The shear strength of soil is typically determined through laboratory tests such as the Triaxial Shear Test and Unconfined Compressive Strength (UCS) test. For the current study, the UCS test was adopted for the determination of the strength of the pure dredged samples and samples mixed with sand in different proportions. The test started with the pure dredged soil specimen's initial length of equal to 7.6cm, initial diameter of 3.8cm, and initial area equal to 11.34 $cm^2$. The specimen under UCS showed a typical strain behavior at various stresses as shown in Table 7.

## RESULTS AND DISCUSSION

In accordance with the analyzed data, Fig. 1 illustrates a particle size distribution curve, depicting the distribution of

Table 5: Dry density of pure dredged soil samples during light compaction.

| Sample | A | B | C | D | E |
|---|---|---|---|---|---|
| Water content | 8 | 11 | 14 | 17 | 20 |
| Mass of empty mold | 4370 | 4370 | 4370 | 4370 | 4370 |
| Mass of mold +compacted soil | 6080 | 6170 | 6350 | 6340 | 6230 |
| Mass of compacted soil | 1710 | 1800 | 1980 | 1970 | 1860 |
| Wet density | 1.71 | 1.8 | 1.98 | 1.97 | 1.86 |
| Crucible no. | C1 | C2 | C3 | C4 | C5 |
| Mass of crucible + wet soil | 52.5 | 48.5 | 77.4 | 48.5 | 74.5 |
| Mass of crucible + dry soil | 50 | 45.5 | 68 | 42.5 | 63 |
| Mass of water | 2.5 | 3 | 9.4 | 6 | 11.5 |
| Mass of crucible | 34.5 | 28 | 26 | 20 | 25.5 |
| Mass of dry soil | 15.5 | 17.5 | 42 | 22.5 | 37.5 |
| Water content | 16.13 | 17.14 | 22.38 | 26.67 | 30.67 |
| Dry density | 1.47 | 1.53 | 1.62 | 1.56 | 1.42 |

Table 6: Dry density of pure dredged soil samples during light compaction.

| Sample | A | B | C | D | E |
|---|---|---|---|---|---|
| Water content | 8 | 11 | 20 | 26 | 20 |
| Mass of empty mold | 4390 | 4390 | 4390 | 4390 | 4370 |
| Mass of mold +compacted soil | 6140 | 6320 | 6380 | 6250 | 6230 |
| Mass of compacted soil | 1750 | 1930 | 1990 | 1860 | 1860 |
| Wet density | 1.75 | 1.93 | 1.99 | 1.86 | 1.86 |
| Crucible no. | H1 | H2 | H3 | H4 | H5 |
| Mass of crucible + wet soil | 62 | 33 | 67.5 | 54 | 74.5 |
| Mass of crucible + dry soil | 58 | 30.5 | 61 | 48.5 | 63 |
| Mass of water | 4 | 2.5 | 6.5 | 5.5 | 11.5 |
| Mass of crucible | 23.5 | 9.5 | 33 | 29 | 25.5 |
| Mass of dry soil | 34.5 | 21 | 28 | 19.5 | 37.5 |
| Water content | 11.59 | 11.9 | 23.21 | 28.2 | 30.67 |
| Dry density | 1.57 | 1.72 | 1.61 | 1.45 | 1.42 |

soil particles across various sizes within a dredged sample. The gradual rise observed at the initial segment of the curve indicates a heightened presence of fine particles (clay and silt) in the soil. Nevertheless, the incline diminishes as one proceeds toward the coarser segment of the curve.

The examination of soil samples using Casagrande's method revealed that when the relationship between moisture content and the number of blows needed to close the groove was graphically represented in Fig. 2. It showed that at 25 blows, the moisture content is 39.3 percent. Consequently, the liquid limit of the dredged soil is determined to be 39.3 percent.

The outcomes of the compaction analysis, as illustrated in Fig. 3, indicate that in the case of light compaction, the dredged soil exhibits an optimal moisture content of 23.2%, resulting in a maximum dry density of 1.6 $g.cc^{-1}$. Conversely, under heavy compaction conditions, the optimal moisture content for the dredged soil is 12%, leading to a maximum dry density of 1.72 $g.cc^{-1}$.

The UCS test of the pure dredged soil sample showed that the Unconfined Compressive Strength ($q_u$) of the sample is 1.077 $kg.cm^{2-}$, indicating the maximum compressive stress the soil can withstand without confinement. The Strain at failure was measured as 6.9%, representing the extent of deformation the soil undergoes at the point of failure. The Failure angle ($\alpha$) was calculated to be to be 84°, while the Angle of internal friction ($\emptyset$) calculated as 20°. Additionally, the Cohesion ($C_u$) computed as half of the unconfined compressive strength, was found to be 1.191 $kg.cm^{2-}$. After the addition of sand in different mixes to the soil (1.5%,

Table 7: Strain at various loads of a pure dredged soil sample.

| S.No. | Deformation | | Strain | Corrected area | | Loa d | Compressive stress |
|---|---|---|---|---|---|---|---|
| | div. | mm | - | $cm^2$ | div. | kg | $kg.cm^{2-}$ |
| 1 | 0 | 0 | 0 | 11.34 | 0 | 0 | 0.000 |
| 2 | 25 | 0.25 | 0.003 | 11.377 | 2 | 1.25 | 0.110 |
| 3 | 50 | 0.5 | 0.007 | 11.415 | 2 | 1.25 | 0.110 |
| 4 | 75 | 0.75 | 0.01 | 11.453 | 5 | 3.125 | 0.273 |
| 5 | 100 | 1 | 0.013 | 11.491 | 7 | 4.375 | 0.381 |
| 6 | 125 | 1.25 | 0.016 | 11.53 | 8 | 5 | 0.434 |
| 7 | 150 | 1.5 | 0.02 | 11.568 | 12 | 7.5 | 0.648 |
| 8 | 175 | 1.75 | 0.023 | 11.607 | 13 | 8.125 | 0.700 |
| 9 | 200 | 2 | 0.026 | 11.646 | 15 | 9.375 | 0.805 |
| 10 | 225 | 2.25 | 0.03 | 11.686 | 16 | 10 | 0.856 |
| 11 | 250 | 2.5 | 0.033 | 11.726 | 17 | 10.625 | 0.906 |
| 12 | 275 | 2.75 | 0.036 | 11.766 | 18 | 11.25 | 0.956 |
| 13 | 300 | 3 | 0.039 | 11.806 | 18 | 11.25 | 0.953 |
| 14 | 325 | 3.25 | 0.043 | 11.847 | 18 | 11.25 | 0.950 |
| 15 | 350 | 3.5 | 0.046 | 11.887 | 19 | 11.875 | 0.999 |
| 16 | 375 | 3.75 | 0.049 | 11.929 | 19 | 11.875 | 0.995 |
| 17 | 400 | 4 | 0.053 | 11.97 | 19 | 11.875 | 0.992 |
| 18 | 425 | 4.25 | 0.056 | 12.012 | 19 | 11.875 | 0.989 |
| 19 | 450 | 4.5 | 0.059 | 12.054 | 19 | 11.875 | 0.985 |
| 20 | 475 | 4.75 | 0.063 | 12.096 | 19 | 11.875 | 0.982 |
| 21 | 500 | 5 | 0.066 | 12.139 | 20 | 12.5 | 1.030 |
| 22 | 525 | 5.25 | 0.069 | 12.181 | 21 | 13.125 | 1.077 |
| 23 | 550 | 5.5 | 0.072 | 12.225 | 21 | 13.125 | 1.074 |
| 24 | 575 | 5.75 | 0.076 | 12.268 | 21 | 13.125 | 1.070 |
| 25 | 600 | 6 | 0.079 | 12.312 | 20 | 12.5 | 1.015 |
| 26 | 625 | 6.25 | 0.082 | 12.356 | 20 | 12.5 | 1.012 |
| 27 | 650 | 6.5 | 0.086 | 12.401 | 20 | 12.5 | 1.008 |
| 28 | 675 | 6.75 | 0.089 | 12.445 | 21 | 13.125 | 1.055 |
| 29 | 700 | 7 | 0.092 | 12.49 | 21 | 13.125 | 1.051 |

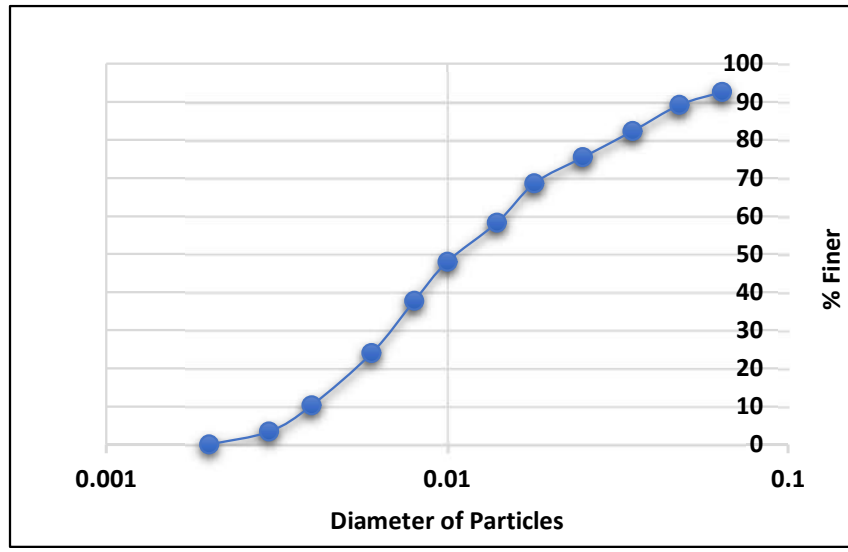


Fig. 1: Particle size distribution curve of pure dredged soil.

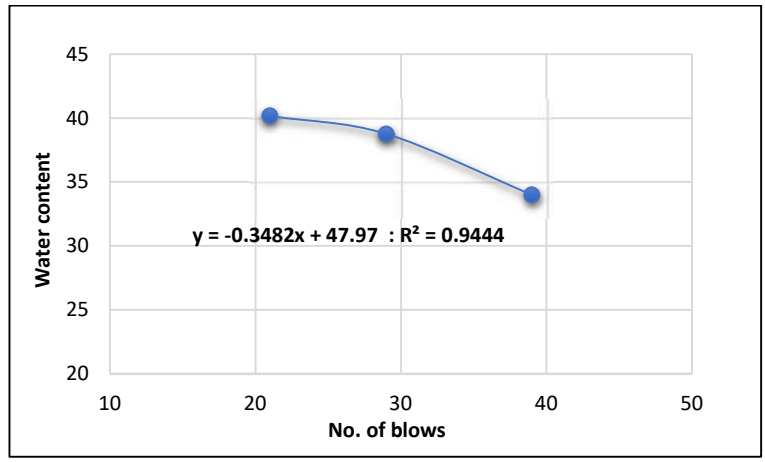


Fig. 2: Liquid limit calibration curve for pure dredged soil.

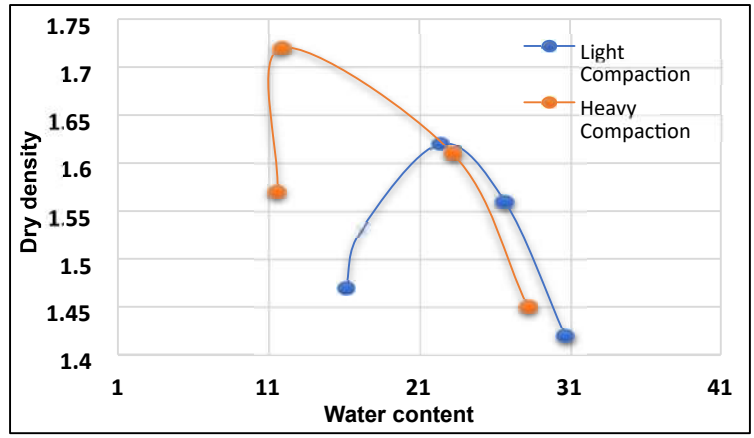


Fig. 3: Optimum dry density of pure dredged soil.

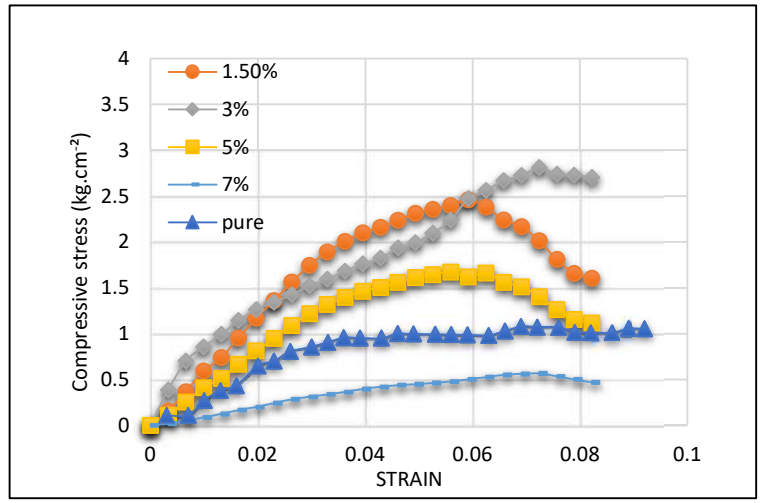


Fig. 4: Stress-strain curve.

3%, 5% & 7%), the unconfined compressive strength was determined in the same way as that done for pure dredged soil. The results obtained when plotted in Fig. 4, showed that for a 1.5% mix of sand to soil Unconfined compressive strength was observed to be 2.4610 kg.cm$^{-2}$ with strain at failure equal to 5.9%. For a 3% mix of sand to the soil, unconfined compressive strength was observed to be 2.8102 kg.cm$^{-2}$ with strain at failure equal to 7.24%. Likewise, a 5% mix of sand to soil unconfined compressive strength was observed to be 1.6595 kg.cm$^{-2}$ with Strain at failure equal to 5.92%. Finally, for a 7% mix of sand to the soil, unconfined compressive strength was observed to be 0.566 kg.cm$^{-2}$ with strain at failure equal to 7.24%.

## CONCLUSION

The properties of the pure dredged material under consideration are crucial indicators for understanding its behavior and suitability for various applications. By considering various tests in the study, it was concluded that the specific gravity of the material was 2.63. The liquid limit was measured to be 39.3, while the plastic limit was found to be 22.133, resulting in a plasticity index of 17.172. The material was classified as medium compressible CM, indicating its cohesive and silty nature. The flow index, representing the material's ability to deform under load, was recorded at 0.55. The toughness index, indicative of its resistance to deformation, was found to be 1.623 g.cc$^{-1}$. The maximum dry density under light compaction was 1.6 g.cc$^{-1}$, with an optimum moisture content (OMC) of 23.2%. For heavy compaction, the maximum dry density was 1.72 g.cc$^{-1}$, with an OMC of 12%. The unconfined compressive strength, a critical parameter for assessing its structural integrity, was measured at 1.077 kg.cm$^{-2}$. The material exhibits a stiff consistency, with a consistency index falling within the range of 75-100%. The detailed properties, when examined collectively, provided a comprehensive understanding of the physical and mechanical characteristics of the dredged material. This information guided decisions to utilize material coarser than the dredged soil for stabilization, with sand being employed for this purpose.

After the determination of the basic engineering properties of the pure dredged soil, the effect of sand addition to dredged material on soil strength was investigated. As shown in Fig. 5, It was observed that the initial soil strength of soil increased to 2.461 kg.cm$^{-2}$ at a 1.5% sand mix. The strength increased to 2.810 kg.cm$^{-2}$ at a 3% sand mix, indicating the stabilization of the soil mass. This increase in the shear strength can be accounted for by several mechanisms occurring due to the mixing. The enhancement of shear strength in very fine clayey soil through the addition of sand involves a multifaceted process. Initially, the incorporation of sand brings about a structural transformation in the soil, fostering a more granular arrangement. This alteration in structure facilitates improved interlocking of particles, consequently diminishing the soil's susceptibility to deformation and elevating its overall shear strength. Notably, clay soils, characterized by their high water-holding capacity, induce heightened pore water pressure and diminished shear strength. The introduction of sand addresses this by enhancing soil permeability and drainage, thereby mitigating excess pore water pressure and fortifying soil stability. Moreover, the augmentation of interparticle friction through added sand contributes to an increased friction angle, ultimately bolstering the soil's shear strength. This augmented resistance to sliding along soil particles culminates in enhanced stability. Furthermore, the inherent cohesion of clay soils, attributed to fine particles, experiences a noteworthy improvement with sand addition, fostering superior particle interaction. The synergistic effect of heightened friction and cohesion collectively fortifies the shear strength of the soil. In summary, the incorporation

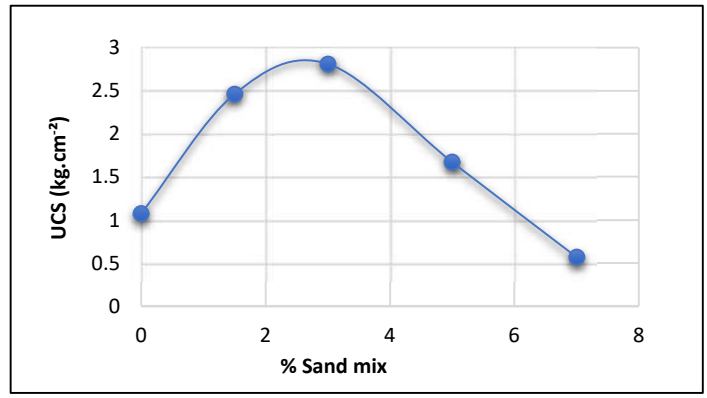


Fig. 5: Unconfined compressive strength at various mixes.

of sand into very fine clayey soil orchestrates a series of interconnected mechanisms that collectively optimize shear strength, encompassing alterations in soil structure, improved drainage, and heightened interparticle interactions. It was observed that further addition of sand beyond 3% resulted in a decline in the soil strength of the mix. The soil strength of the mix was found to be 1.671 kg.cm$^{2-}$ at 5% sand mix which was further reduced to 0.57 kg.cm$^{2-}$ at 7% mix. This may be due to the push of sand to make the soil mix a more granular mass, leading to reduced interlocking making the packing arrangement less favorable, and, consequently, decreased strength. The study concluded by suggesting the utilization of sand as a soil stabilizer, with the highest strength observed at a 3% mixture in this particular scenario.

## REFERENCES

Amin, Z. 2016. Dredging of river Jhelum in J-K to prevent flood situation in future: Govt. The Indian Express. Available at: https://indianexpress.com/article/india/india-news-india/dredging-of-river-jhelum-in-j-k-to-prevent-flood-situation-in-future-govt/

Croft, J. B. 1967. The influence of soil mineralogical composition on cement stabilization. Geotechnique, 17(2): 119-135.

Firoozi, A. A., Taha, M. R. and Firoozi, A. A. 2014. Analysis of the load-bearing capacity of two and three-layered soil. Electron. J. Geotech. Eng., 19: 4683-4692.

Firoozi, A. A., Taha, M. R., Firoozi, A. A. and Khan, T. A. 2015. The influence of freeze-thaw cycles on unconfined compressive strength of clay soils treated with lime. J. Teknologi, 76(1): 107-113.

IS 13094: 1992, Reaffirmed 2011. Selection of ground improvement techniques for foundations in weak soils-guidelines.

IS: 1498-1970. Classification and identification of soils for general engineering purposes. New Delhi: Bureau of Indian Standards.

IS: 2720-part 1 1980. Indian standard code for preparation of soil samples. Bureau of Indian Standards, New Delhi.

IS 13094: Selection of ground improvement techniques for foundations in weak soils-guidelines (1992, Reaffirmed 2011).

IS: 1498 -1970. Classification and identification of soils for general engineering purposes. Bureau of Indian Standards, New Delhi.

IS: 2720-part 1 1980. Indian standard code for preparation of soil samples. Bureau of Indian Standards, New Delhi.

Kollaros, G. and Athanasopoulou, A. 2016. Sand as a soil stabilizer. Bull. Geol. Soc. Greece, 50(2): 770-777.

Little, D. N. 1998. Evaluation of structural properties of lime stabilized soils and aggregates. Arlington: National Lime Association.

Mir, B. A., Amin, F. and Majid, B. 2016. Some studies on physical and mechanical behaviour of dredged soil from flood spill channel of Jhelum river, Srinagar. Acta Ing. Civ., 1(1).

Nassar, S., Saliba, J. and SaiyourI, N. 2023. Investigation of the possible valorization of dredged sediments in compressed earth blocks. Mater. Today: Proc.

PTI 2016. JK Governor to Centre: Release of funds for Jhelum River dredging. Times of India. Available at: https://timesofindia.indiatimes.com/city/jammu/JK-Governor-to-Centre-Release-of-funds-for-Jhelum-river-dredging/articleshow/51251620.cms

Punmia, B. C. 2007. Soil Mechanics & Foundations. Laxmi Publications, New Delhi.

Puppala, A. J. and Musenda, C. 2000. Effects of fibre reinforcement on strength and volume change in expansive soils. Transp. Res. Rec., 1736(1): 134-140.

Reddy, E. S. 2002. Measurement of Engineering Properties of Soils. New Age International, New Delhi.

### ORCID DETAILS OF THE AUTHORS

Yasir Hamid: https://orcid.org/0009-0008-9420-3664
Huma Khan: https://orcid.org/0000-0002-2792-0566
Amina Zakiah: https://orcid.org/0009-0004-2110-8579

Nature Environment and Pollution Technology
An International Quarterly Scientific Journal

p-ISSN: 0972-6268
(Print copies up to 2016)
e-ISSN: 2395-3454

Vol. 23 | No. 3 | pp. 1623-1629 | 2024

Original Research Paper

https://doi.org/10.46488/NEPT.2024.v23i03.032

Open Access Journal

# Waste Generation and Recovery in a Developing Country: A Case Study of Western Province, Sri Lanka

**N. A. Hemali† and A. A. P. De Alwis**
Department of Chemical and Process Engineering, University of Moratuwa, Moratuwa 10400, Sri Lanka
†Corresponding author: N.A. Hemali; arosha.hemali@gmail.com, 188116A@uom.lk

**Nat. Env. & Poll. Tech.**
**Website: www.neptjournal.com**

*Received:* 15-11-2023
*Revised:* 22-01-2024
*Accepted:* 01-02-2024

**Key Words:**
Municipal solid waste management
Waste recycling
Material recovery
Material flow

## ABSTRACT

The study's findings serve as a crucial foundation for policymakers, environmentalists, and stakeholders to take necessary actions and develop sustainable waste management strategies tailored to the specific challenges faced in the Western Province of Sri Lanka, contributing to broader global efforts to mitigate the growing waste crisis. It's a significant concern that the volume of waste is expected to triple by 2050, and the current waste management practices seem insufficient to handle this growth sustainably. The study indicates a per capita waste generation of 0.43 kg in Sri Lanka, with the Western Province at a higher rate of 0.53 kg. This data points to the urgency of addressing waste management practices in this region, especially considering its significance in the country's GDP. The results also show that the total municipal waste generation in the Western Province is 3248 kg per day whereas the recovery is only 25% (803 kg) in terms of recycling and composting. Burning, burying, and open dumping are highlighted as other prevailing practices for managing waste, which have adverse impacts on the environment and public health. Further research is recommended to identify and address these unaccounted waste streams, especially those at the household level.

## INTRODUCTION

Rapid economic growth and urbanization frequently result in heightened resource consumption due to increased demand for goods and services. This surge in consumption generates a significant volume of waste, adversely impacting the environment. The predominant linear resource management model, starting from raw material extraction, through production and consumption, culminating in disposal, has inherent limitations. It prioritizes consumption and disposal over sustainable resource management practices. To mitigate the environmental consequences of resource consumption and waste production, a comprehensive approach is essential, encompassing the entire life cycle of products, from inception to disposal or recycling. This necessitates integrating sustainable practices at each stage of a product's life cycle. Embracing the principles of a circular economy is critical. This approach involves designing products for durability, facilitating reuse, repair, and recycling, thereby minimizing waste and prolonging material life cycles. Urgent policy reforms and systemic changes are imperative to encourage a transition towards a more sustainable and circular resource management approach. This might involve incentivizing eco-friendly product designs, promoting recycling and reuse initiatives, and enforcing regulations governing waste disposal methods.

Developing a holistic approach to managing resources and waste involves a collective effort from various stakeholders, including governments, industries, communities, and consumers. Transitioning to a more sustainable system will require innovative strategies, technological advancements, policy reforms, and behavioral changes to minimize environmental degradation and promote a more circular and responsible approach to resource use.

More than two billion metric tons (Mt) of waste are generated annually. This figure is anticipated to rise to 3.4 billion Mt by 2050, assuming current waste management practices persist (Kaza et al. 2018). By 2050, waste generation in developing nations is expected to triple (Kaza et al. 2018). Notably, the Asia-Pacific region is poised to significantly contribute to the world's waste output, accounting for roughly 23% of the total. In these developing countries, food and green waste collectively constitute over 50% of the overall waste generated. Recyclable materials like paper, cardboard, plastic, metal, and glass form a significant portion of waste streams, ranging from 16% in developing nations to approximately 50% in developed ones (Laurenti et al. 2014).

In Sri Lanka, about 62% of municipal solid waste is composed of biodegradable organic material, while the remaining portion comprises non-biodegradable materials

(Dharmasiri 2019). Reports indicate the absence of proper waste segregation at the household level before disposal (Warunasinghe & Yapa 2016). Bandara (2011) emphasizes the critical necessity of instituting an integrated solid waste management system in the country. Presently, the management of municipal solid waste falls under the jurisdiction of the local government network, comprising 24 Municipal Councils, 41 Urban Councils, and 276 Divisional Councils. However, disparate waste management approaches are adopted by various local government bodies based on their capacities, rather than implementing a unified waste management system nationwide. Hence, conducting a comprehensive assessment of material recovery potential is essential for establishing an integrated waste management system.

Given this context, the primary focus of this study centers on evaluating waste generation volumes, characterizing waste, analyzing waste management practices, and exploring the potential for material recovery in municipal solid waste within Sri Lanka's Western Province. The research endeavors to identify potential recyclable materials present in municipal solid waste. Furthermore, it aims to advocate for the advancement of material recovery options while also contributing to future research directed toward resolving issues associated with mismanaged waste within the household waste material chain.

## MATERIALS AND METHODS

### Study Area

The Western Province of Sri Lanka as shown in Fig. 1, with a population of 5.8 million, accounting for 27% of the nation's total population, was chosen as the focal area for this pilot study. Covering approximately 6% of Sri Lanka's land area, the Western Province accommodates the largest population among all provinces and contributes over 42.6% to the country's overall GDP, playing a vital role in the national economy (C & S 2021), (Dharmasiri 2019). The high population density, coupled with rapid urban development in this region, has significantly escalated the production of municipal solid waste.

The study area encompasses 25 open dumping sites as Fig. 2, where waste is disposed of, and the collected waste is managed through a channel regulated by local authorities. This institutional framework stands as the primary mechanism responsible for waste management in Sri Lanka.

### Data Collection Procedure

The study defined its system boundary to cover the complete waste management process, commencing from household waste generation to its ultimate disposal. Obtaining the essential data for analysis involved identifying various facets such as municipal solid waste generation, waste management practices, different types and quantities of waste, and the methods used for disposal. The waste materials produced within the study area underwent characterization. Furthermore, gathering pertinent information about the waste composition and its management status involved utilizing published surveys, conducting questionnaires and interviews, and eliciting feedback from local authorities in the Western Province as stated in Fig. 3.

### Calculation of Waste Recovery Percentage

This study employs the principles of a circular economy to evaluate the waste material recovery factor. A circular economy is an economic system that aims to eradicate waste while continuously regenerating resources (Tamine 2020). Advancing toward a circular economy necessitates not just responsible natural resource utilization but also facilitating reuse, repurposing, recycling, and reclaiming value from materials conventionally considered waste (Bouton 2016) Additionally, the study employs Material Flow Analysis to delineate the waste material chain from the household level to final disposal in the designated pilot area as shown in

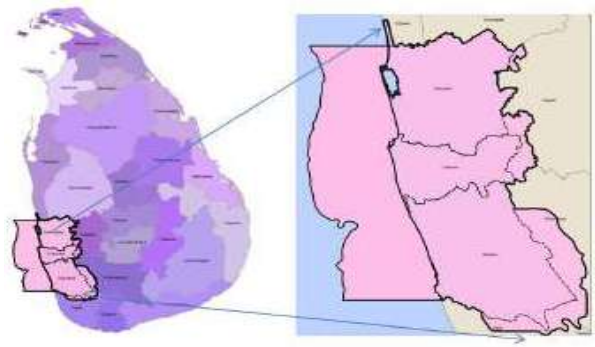

Fig. 1: The Western Province, Sri Lanka.

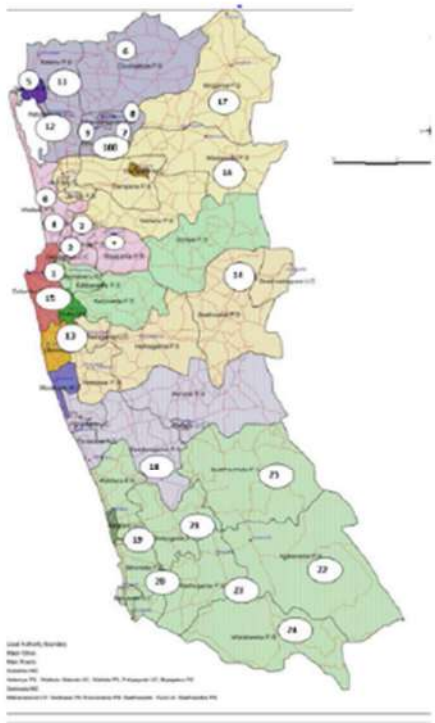

1. Sedewatha dumpsite
2. Manelgamuwa dumpsite
3. Eweriwatta personal land
4. Dikkowita dumpsite
5. Kochchikade dumpsite
6. Dumpsite of Hunumulla
7. Aluthepola coconut land
8. Yatiyana mahayaya coconut land (private land)
9. Walihena rubber cultivation (private land)
10. Niwala coconut cultivation (private land)
11. Low land of welihena and low land of Raddoliwa cemetery (private land)
12. Ambalanmulla dumpsite
13. Karadiyana waste management site
14. Seethawakapura composting plant
15. Maligawatta Government land
16. Dambuwatta dumpsite
17. Meerigama PS dumpsite
18. Bandaragama PS composting plant
19. Kaluthara Pohorawatha compost site
20. Darga town dumpsite
21. Dosat Estate
22. Agalawatta compost plant
23. St. John Estate
24. Walallawita compost plant
25. Bulathsinhala compost plant

Fig. 2: 25 Waste dump sites in the Western Province.

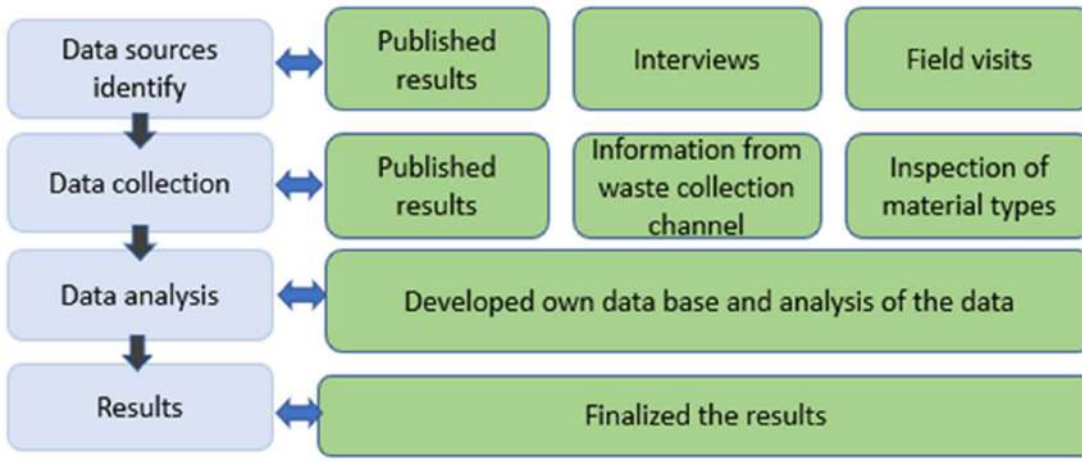


Fig. 3: Methodological framework.

Fig. 4. Material Flow Analysis is an analytical method utilized to quantify the movement and accumulation of materials or substances within a clearly defined system (Hunt et al. 2014). Rooted in the principle of mass conservation, this method finds extensive application in waste material flow analyses across various research fields (Gehrmann et al. 2017, Allesch & Brunner 2015).

Its widespread use in environmental education, particularly in waste management, underscores its significance as an analytical tool for informed decision-making concerning diverse issues related to waste analysis.

The waste recycling factor was developed using the following equation 3, supported by the material flow structure illustrated in Fig. 4.

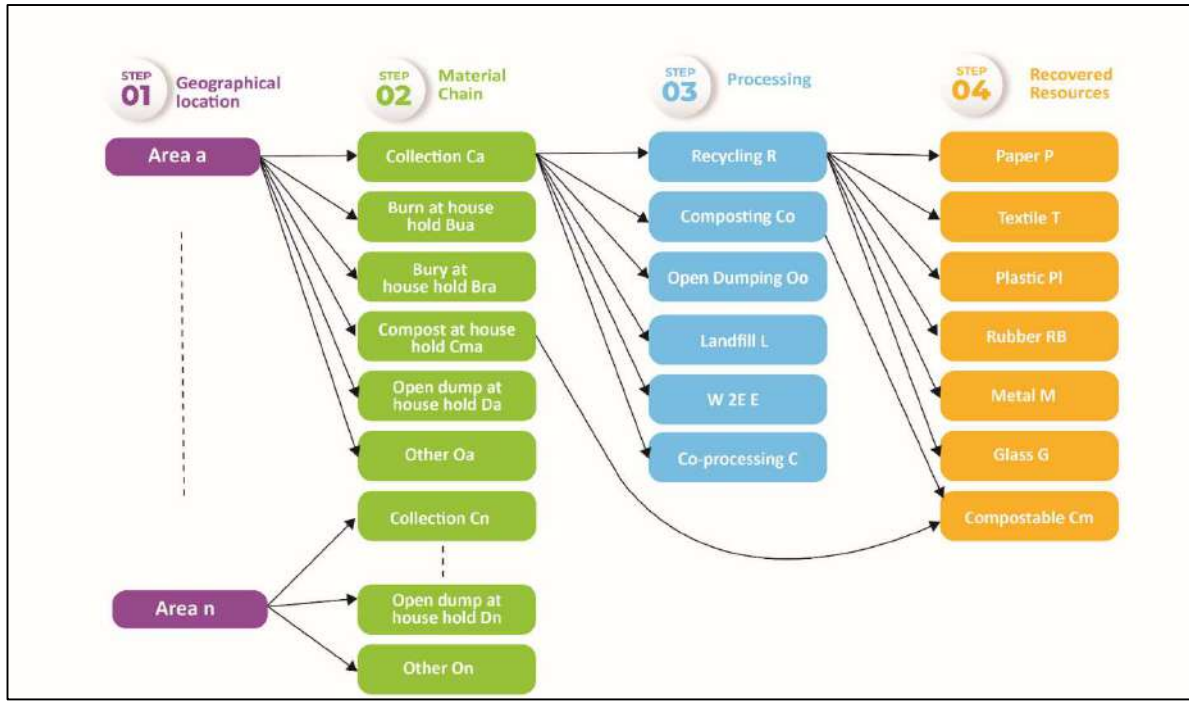


Fig. 4: Material flow structure.

Recycling material is represented in equation 1;

$$\sum_{a}^{n} a\left[\begin{matrix}\mathrm{CaR(P+T+Pl+RB+M+G)+CaCo+}\\ \mathrm{Cm-Bua-Bra-Da-\ Oo-L-E}\end{matrix}\right] \quad ...(1)$$

Where "a" is the MSW generation at area "a" (area can be a GN division etc.) in MT /d.

Ca- MSW collection percentage by local authorities (in GN divisions)

Bua, Bra, Da, Cma, represent the Burn, Bury, and Composting percentages at the household level respectively.

R- MSW recyclable volume percentage out of collection

Co- compostable material percentage out of collected volumes by GN division.

L, E, Oo, and C represent Landfill, Waste to Energy, Open dump, and Co-processing respectively.

P, T, Pl, RB, M, G, and Cm are the percentages of recyclable volumes of Paper, Textile, Plastic, Rubber, Metal, Glass, and compostable material (household and waste collection center point) respectively.

Where total MSW generation is represented in equation 2.

$$\sum_{A}^{n}[a+\cdots+n) \quad ...(2)$$

The total recyclable material percentage out of the whole MSW generation is illustrated by equation 3. equation (1)/ equation (2) …(3)

## RESULTS AND DISCUSSION

### Primary Waste Streams and Treatment Methods

In the results of the study presented in Fig. 5, the primary waste categorization at the household level on a percentage basis indicates the collection of waste by local authorities, burning material at the household level, burying material at the household level, composting waste at the household level, and other disposal mechanisms. Fig. 6 represents the Material Flow Analysis from the household doorstep to the final disposal point through three steps in the Western Province. Step 2 of Fig. 4 and Table 1 represent the basic treatment at the household level, while Table 2 represents the main waste categorization of the material at the collection point. Step 4 of Fig. 4 and Table 3 represent the final disposal solution for municipal solid waste in the Western Province. Previous study shows material flow movements of MSW from household to final disposal (Hemali & Alwis 2022), whereas the present study further elaborates on how MSW in Western Province behave in the context of the semi-urban environment.

### Waste Recycling, Reusing and Repurposing

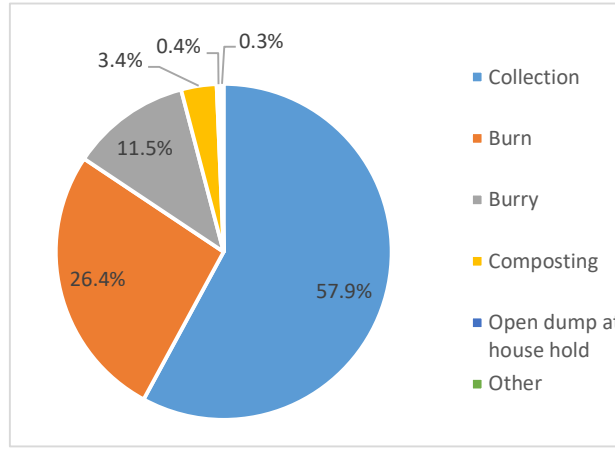


Fig. 5: Primary waste solution percentages at the household level, Western Province.

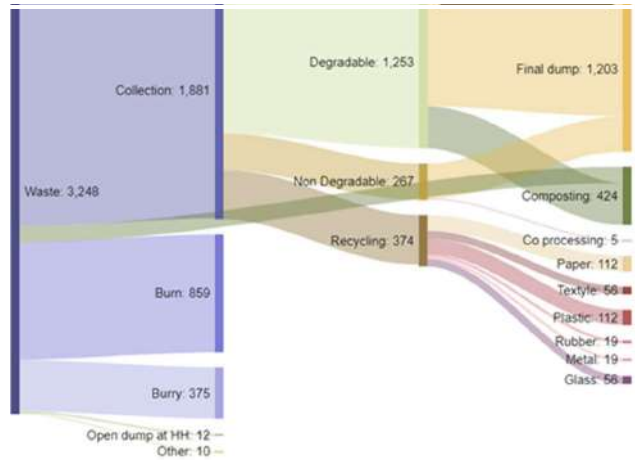


Fig. 6: Waste material flows in tonnes (Mts) from household level to disposal, Western Province, Sri Lanka (Hemal & Alwis 2022).

The study indicates that recycling and composting are the primary recovery methods adopted in the Western Province for proper waste management. However, most of the waste ends up in open dumps, while incineration and landfilling are not considered recovery options. In 2022, a Waste-to-Energy plant with a capacity to process 600 metric tons per day was established in the Western Province, but the plant is still not in full operation. However, waste-to-

Table 1: Types of waste treatment in the Western Province.

| Waste treatment in Western Province step 2 | Volume (tonnes per day) |
|---|---|
| Collection | 1881 |
| Burn | 859 |
| Bury | 375 |
| Composting | 111 |
| Open dump at household | 12 |
| Other | 10 |

Table 2: Waste collection categorization based on primary material types.

| Waste treatment in Western Province step 3 | Volume (tonnes per day) |
|---|---|
| Degradable waste | 1253 |
| Non- degradable waste | 267 |
| Recycling waste | 374 |

Table 3: Waste disposal categorization based on final treatment type.

| Waste Treatment in Western Province Step 4 | Volume (tonnes per day) |
|---|---|
| Open dumping | 1203 |
| Composting | 424 |
| Recycling paper | 112 |
| Recycling plastic | 112 |
| Recycling Textile | 56 |
| Recycling Glass | 56 |
| Recycling Rubber | 19 |
| Recycling Metal | 19 |
| Other | 5 |

Table 4: Waste recycling/repurpose factor for individual waste type in the Western Province.

| Waste Treatment in Western Province Step 4 | Volume (tonnes per day) | Recycling/Repurpose factor for individual waste type |
|---|---|---|
| Composting | 424 | 13.05% |
| Recycling paper | 112 | 3.45% |
| Recycling plastic | 112 | 3.45% |
| Recycling Textile | 56 | 1.72% |
| Recycling Glass | 56 | 1.72% |
| Recycling Rubber | 19 | 0.58% |
| Recycling Metal | 19 | 0.58% |
| Other | 5 | 0.15% |
| Total | 803 | 24.72% |

energy is not considered a material recovery option in this study.

The overall results reveal that per capita waste generation in the Western Province is 0.53 kg, of which open dumping amounts to 0.21 kg while recycling and repurposing stand at 0.14 kg of the waste generated in the Western Province, the total volume of recycling and repurposing is 25%. Furthermore, the waste collection rate is 60% in Western Province, Sri Lanka as shown in Table 4. Further whole country represents the per capita waste generation of 0.43 kg.

### Waste Dumping

As indicated in Table 3, the predominant waste volume is directed towards open dumping. To identify potential recyclable and reusable materials among the waste disposed of in this manner, there is a crucial need for further study on waste composition. Understanding the composition of waste deposited in open dumps is essential to pinpoint valuable materials that could be recycled or repurposed. Analyzing the waste composition allows for the identification of specific materials that could otherwise be salvaged, recycled, or reintroduced into production cycles, consequently reducing the amount of waste ending up in landfills or open dumping sites.

By conducting a detailed analysis of the waste composition in open dumps, the study aims to identify materials that could potentially be diverted from the waste stream for recycling or reusing purposes. This exploration can lead to more effective waste management strategies and contribute significantly to reducing environmental impacts while promoting a more sustainable approach to handling waste. Waste composting of the total waste generation in the Western Province, 13.05% of recovery is reported at waste composting in the Western Provinces as per Table 4. There is a potential to improve compostable volume in the Western Province.

### Waste Burning and Burying at the Household Level

The study, as depicted in Table 1, underscores the necessity for additional research concerning unaccounted and unidentified material flows related to household-level burying and burning practices. These methods of waste disposal often result in significant environmental and human health hazards.

Burning or burying waste at the household level has significant adverse effects on both the environment and human health. These practices, often carried out as a means of waste disposal, contribute to pollution and pose serious risks due to the release of harmful substances into the air and soil. Understanding the materials commonly subjected to these disposal methods is crucial for addressing the associated environmental and health concerns.

There is an urgent need to promote sustainable waste management practices at the household level, such as recycling, composting, and responsible disposal at designated facilities.

Public awareness and education about the environmental and health consequences of improper waste disposal are crucial for encouraging responsible behaviors.

In conclusion, burning or burying waste at the household level has far-reaching and detrimental consequences for the environment and human health. Addressing these issues requires a comprehensive approach that includes proper waste management practices, education, and the development of sustainable alternatives to reduce the negative impact of waste disposal on our surroundings.

Further research in this area is crucial to identify the types of materials commonly disposed of through burning or burying, quantify their impact on environmental degradation, and assess the associated health risks. By shedding light on these unaccounted waste disposal practices, the study aims to provide insights that can drive policy changes, educational campaigns, and improved waste management strategies aimed at minimizing the harmful effects on the environment and human health.

## CONCLUSION

Municipal Solid Waste stands as the primary source of waste generation in the country, constituting the largest volume. Despite being labeled as waste, this material holds immense potential for recycling and reuse. An extensive analysis of scientific literature reveals that a significant portion of municipal solid waste is often incinerated or buried without proper consideration for its recyclable value.

Hence, this study underscores the critical need for research focusing on unaccounted and unidentified material

flows linked to household-level burying and burning practices. Understanding and addressing these inadequately managed waste streams are pivotal, as these methods not only contribute to environmental degradation but also pose risks to human health.

Furthermore, a considerable portion of the collected waste is directed to open dumps. Exploring and evaluating the recycling potential of this particular segment of waste requires further investigation. Uncovering potential recyclable materials within waste deposited in open dumps can lead to the development of effective recycling strategies. This exploration is essential to reduce the burden on landfills, promote sustainable waste management practices, and harness the untapped potential for recycling and reuse within these waste streams.

## REFERENCES

Allesch, A. and Brunner, P.H. 2015. Material flow analysis as a decision support tool for waste management: A literature review. J. Ind. Ecol., 19(5): 753-764.

Bandara, N.J.G.J. 2011. Municipal solid waste management - The Sri Lankan case. Proc. Int. For. Environ. Symp., pp. 12-15.

Bouton, S. 2016. The circular economy: Moving from theory to practice. McKinsey Center for Business and Environment.

Central Bank of Sri Lanka 2021. Annual Report 2021 | Central Bank of Sri Lanka (cbsl.gov.lk), retrieved on 22 Jan 2024. Available at: https://www.cbsl.gov.lk/en/publications/economic-and-financial-reports/annual-reports/annual-report-2021

Dharmasiri, L.M. 2019. Waste management in Sri Lanka: Challenges and opportunities. Sri Lanka Journal of Social Sciences, 9(1). Available at: https://www.researchgate.net/publication/341830497

Gehrmann, H.J., Hiebel, M. and Simon, F.G. 2017. Methods for the evaluation of waste treatment processes. J. Eng., 2017(1): 3567865.

Hemali, N.A. and Alwis, A.A.P.D. 2022. Application of material flow analysis to municipal solid waste in urban areas in developing countries and possible solutions under circular economic framework. Nature Environ. Pollut. Technol., 21(3). DOI: https://doi.org/10.46488/NEPT.2022.v21i03.000

Hunt, D.V., Leach, J.M., Lee, S.E., Bouch, C., Braithwaite, P. and Rogers, C.D. 2014. Material flow analysis (MFA) for liveable cities. In: Proceedings of the 4th World Sustainability Forum, Vienna, Austria, pp. 20-21.

Kaza, S., Lisa, Y., Tata, P.B. and Woerden, F.V. 2018. What a waste 2.0: A global snapshot of solid waste management to 2050. Urban Development Series. Washington, DC: World Bank. DOI: 10.1596/978-1-4648-1329-0

Laurenti, R., Singh, J. and Frostell, B. 2014. Progress and challenges to the global waste management system. Waste Manag., 4: 20-25.

Tamine, I. 2020. The integration of recycling cooperatives in the formal management of municipal solid waste as a strategy for the circular economy. 2(1): 1-22.

Warunasinghe, W.A.A. and Yapa, P.I. 2016. A survey on household solid waste management (SWM) with special reference to a peri-urban area (Kottawa) in Colombo. Procedia Food Sci., 6: 257-260.

Nature Environment and Pollution Technology
An International Quarterly Scientific Journal

p-ISSN: 0972-6268
(Print copies up to 2016)
e-ISSN: 2395-3454

Vol. 23 | No. 3 | pp. 1631-1638 | 2024

Original Research Paper

https://doi.org/10.46488/NEPT.2024.v23i03.033

Open Access Journal

# PM2.5 Concentration Estimation Using Bi-LSTM with Osprey Optimization Method

**S. Saminathan*† and C. Malathy****

*Department of Computing Technologies, SRM Institute of Science and Technology, Kattankulathur-603203, Tamil Nadu, India

**Department of Networking and Communications, SRM Institute of Science and Technology, Kattankulathur-603203, Tamil Nadu, India

†Corresponding author: S. Saminathan; saminats@srmist.edu.in

**Nat. Env. & Poll. Tech.**
**Website: www.neptjournal.com**

*Received:* 07-01-2024
*Revised:* 10-02-2024
*Accepted:* 12-02-2024

**Key Words:**
Air pollution
Air quality
PM2.5 prediction
Bi-LSTM
Osprey optimization algorithm

## ABSTRACT

Outdoor air pollution causes a lot of health problems for humans. Particulate Matter 2.5 (PM2.5), due to its small size, can enter the human respiratory system with ease and cause significant health effects on humans. This makes PM2.5 significant among the various air pollutants. Hence, it is important to measure the value of PM2.5 accurately for better management of air quality. Algorithms for deep learning and machine learning can be used to forecast air quality data. A model that minimizes the prediction error of the PM2.5 forecast is needed. In this paper, a PM2.5 concentration estimation model using Bi-LSTM (Bidirectional Long Short-Term Memory) with meteorological data as predictor variables is proposed. For a better estimation of PM2.5 values, the hyperparameters of the Bi-LSTM model used are tuned using the Osprey Optimization Algorithm (OOA), a recent meta-heuristic algorithm. The model that works with the optimal values of hyperparameters identified by OOA performed better than the other models when they are compared based on evaluation metrics like Mean-Squared Error and $R^2$.

## INTRODUCTION

Air pollution is the process of any material contaminating an interior or outdoor environment and changing the inherent characteristics of the atmosphere. This includes chemical, physical, and biological contaminants (World Health Organization 2023). Recent research by the World Health Organization (World Health Organization 2018) estimates that 4.2 million fatalities globally in 2016 were attributable to outdoor air pollution. The research outlines statistics on the total deaths attributable to ambient air pollution in 2016 under various categories like by region, by disease, and by age and sex. According to WHO data (WHO 2023), nearly all people on the planet (99 %) breathe air that is higher than recommended and contains significant quantities of pollutants. Air Quality Index (AQI) is a measure to identify the level of air pollution in a place. The eight pollutants used in India's AQI computation are particulate matter 10, carbon monoxide, particulate matter 2.5, nitrogen dioxide, ozone, sulphur dioxide, ammonia, and lead (CPCB 2015). There are six AQI categories available (Good to Severe).

Table 1 Displays the AQI breakpoints that relate to each of the eight pollutant characteristics (CPCB 2015).

Air quality is an important issue with broad consequences for both environmental and public health, particularly when it involves PM2.5. Particulate matter (PM10, PM2.5, SPM) is the result of the exhaust of diesel automobiles, building activities, road dust, and domestic wood (Swarna Priya & Sathya 2019). They have a serious health impact on humans. Among other air pollutants, PM2.5 is considered noteworthy because of its detrimental impacts on human health. The following section outlines the main ideas emphasizing the importance of PM2.5.

Based on statistics from the Global Burden of Disease Project WHO, the pollutant PM2.5 is associated with the highest amount of harmful health consequences as a result of air pollution, both nationally and globally (Thangavel et al. 2022).

The incidence and mortality of several diseases, such as lung cancer, stroke, and other breathing disorders, have been related to exposure to ambient PM2.5. Because PM2.5 particles are light and small, they can readily pass through nasal and throat filters in humans and remain in the atmosphere for extended periods (Xing et al. 2016).

Black carbon, polycyclic aromatic hydrocarbons, aryl hydrocarbons, volatile organic hydrocarbons, heavy metals, organic molecules, minerals, inorganic ions, and other hazardous materials are the main constituents of PM2.5. PM2.5 is a typical air quality meter that is frequently released

Table 1: Pollutant parameters and their corresponding AQI breakpoints.

| AQI Category | Range | PM10 24-h | PM2.5 24-h | $NO_2$ 24-h | $O_3$ 8-h | CO 8-h [$mg.m^{-3}$] | $SO_2$ 24-h | $NH_3$ 24-h | Pb 24-h |
|---|---|---|---|---|---|---|---|---|---|
| Good | 0-50 | 0-50 | 0-30 | 0-40 | 0-50 | 0-1.0 | 0-40 | 0-200 | 0-0.5 |
| Satisfactory | 51-100 | 51-100 | 31-60 | 41-80 | 51-100 | 1.1-2.0 | 41-80 | 201-400 | 0.6 - 1.0 |
| Moderate | 101-200 | 101-250 | 61-90 | 81-180 | 101-168 | 2.1-10 | 81-380 | 401-800 | 1.1-2.0 |
| Poor | 201-300 | 251-350 | 91-120 | 181-280 | 169-208 | 10.1-17 | 381-800 | 801-1200 | 2.1-3.0 |
| Very poor | 301-400 | 351-430 | 121-250 | 281-400 | 209-748* | 17.1-34 | 801-1600 | 1201-1800 | 3.1-3.5 |
| Severe | 401-500 | 430 + | 250+ | 400+ | 748+* | 34+ | 1600+ | 1800+ | 3.5+ |

Units are in $mg.m^{-3}$ except if stated otherwise. *One hourly monitoring (exclusively for use in mathematical computations)

from a variety of sources, including home heating, motor vehicles, industrial sources, and the combustion of fuels like gasoline, oil, diesel, or wood (Thangavel et al. 2022).

Because PM2.5 is so tiny, it can irritate and erode the alveolar wall in the lung, causing lung function to be compromised (Xing et al. 2016). For the management of air quality and the preservation of public health, accurate PM2.5 concentration forecasting is essential. Numerous studies have developed original methods for predicting PM2.5, including empirical models (like deep learning models) and physical models like CMAQ4 (Xiao et al. 2020). These models are useful for estimating PM2.5 concentrations for air quality forecasts and for the early diagnosis of air pollution events.

The authors (Ameer et al. 2019, Senthivel & Chidambaranathan 2022, Saminathan & Malathy 2023) have elaborated upon the recent state-of-the-art works carried out in Air quality research using machine learning methods. Besides doing an exhaustive literature survey related to this topic, the authors (Ameer et al. 2019) presented their findings with a prediction method that found Random Forest as the most efficient one among different methods tested on the dataset that includes PM2.5 data along with meteorological data for 5 cities of China.

As the world's population and economy rise, so does its energy consumption, which raises air pollution levels. Many places have had their PM2.5 concentrations predicted using machine learning approaches such as random forests. An example of South African cities has been given in (Morapedi & Obagbuwa 2023).

The key objective of this paper is to develop a model that accurately predicts PM2.5 levels. Precise PM2.5 concentration prediction is essential to human existence and forms the basis of pollution prevention and control. The significance of this research lies in its commitment to developing a model that transcends the limitations of existing approaches. By placing a specific focus on minimizing the prediction error of PM2.5 forecasting, the proposed model seeks to enhance the precision and reliability of air quality predictions. This, in turn, empowers decision-makers with more accurate information for prompt and targeted interventions to mitigate the adverse effects of air pollution.

LSTM and Bi-LSTM have been used in recent PM2.5 prediction systems, and some optimization techniques are also used with them that help in processes like hyperparameter tuning. The following section is an introduction to LSTM, Bi-LSTM, and a recent metaheuristic optimization method called the Osprey optimization technique, along with their applications in recent literature.

LSTM (Long Short-Term Memory) can capture temporal dependencies, making them suitable for sequential data. Input data is organized into sequences with multiple features at each time step, reflecting the multivariate nature of the regression task. Each sequence consists of a series of time steps, and the LSTM processes these steps sequentially to capture temporal patterns.

Bi-LSTMs include two sets of hidden states, forward and backward, concatenated to enhance the model's ability to capture bidirectional dependencies. Like unidirectional LSTMs, input data for Bi-LSTM is organized into sequences with multiple features at each time step. Each sequence comprises a series of time steps, and Bi-LSTMs process these steps bi-directionally, considering information from both earlier and later time steps. The model typically includes one or more Bi-LSTM layers to capture bidirectional temporal dependencies in the sequential input. The final output layer predicts multiple continuous values corresponding to the target variables, integrating information from both forward and backward passes. Mean Squared Error (MSE) is commonly used as the loss function for regression tasks, measuring the difference between predicted and actual values. Training involves adjusting model parameters using backpropagation through time considering bidirectional information flow.

Forecasting PM2.5 concentrations is a crucial issue, and using cutting-edge methods like Bi-LSTM has produced encouraging results. In a study by (Kim et al. 2023), the

authors proposed a method in which a weighted Bi-LSTM model is used to forecast the PM2.5 concentration after input variables are chosen based on the feature importance determined by random forest. In a different study (Zhang et al. 2021), the efficacy of a hybrid model known as CNN-Bi-LSTM-Attention was demonstrated in both short-and long-term forecasts by predicting the PM2.5 concentration over the following two days.

Furthermore, studies (Yang et al. 2021, Masood et al. 2023, Chen et al. 2023) have demonstrated that deep learning models, like LSTM, can efficiently use historical PM2.5 concentrations, air quality indices, and other pertinent data for precise predictions. The promise of Bi-LSTM and other sophisticated models in PM2.5 forecasting is demonstrated by these studies, which also emphasize the models' capacity to manage the intricate and erratic nature of PM2.5 data.

To estimate PM2.5 concentrations, this paper by (Zhang et al. 2023) suggested a weighted complementary ensemble empirical mode decomposition with adaptive noise and an improved long and short-term memory neural network. The adaptive mutation particle swarm optimization technique was established to identify the key hyperparameters of LSTM. This helped to increase the prediction accuracy of PM2.5 values. Correctly setting the hyperparameters of the prediction methods was aided by the application of the AMPSO approach.

Bi-LSTMs are applied in various domains, such as financial forecasting, weather prediction, and healthcare, where capturing bidirectional dependencies in sequential data improves prediction accuracy. Hyperparameters of Bi-LSTM include the following parameters: The number of LSTM units or neurons in each LSTM layer, the number of LSTM layers stacked, dropout that is applied between LSTM layers and after the bidirectional layer to prevent overfitting, learning rate (the rate of update of the weights of the model during training), batch size (the number of samples used in each training iteration), optimizer (the algorithm used during training like Adam), activation functions for LSTM units and output layer, the length of input sequences.

More and more metaheuristic methods are being utilized to optimize hyperparameters for deep neural networks and other machine learning models to improve the accuracy and dependability of predictions. Optimization techniques such as metaheuristics can be applied to find the best hyperparameters in a high-dimensional space. When dealing with complicated optimization issues, where more conventional optimization techniques might not be helpful, these algorithms come in handy. As an example, a study explored the benefits of using metaheuristics in the hyperparameter tuning of deep learning models for energy load forecasting (Bacanin et al. 2023).

A novel metaheuristic algorithm called the Osprey Optimization Algorithm (OOA) mimics the actions of Ospreys. The primary source of inspiration for OOA is the tactic used by Ospreys to catch fish in the ocean. Using this hunting tactic, the osprey locates its prey, hunts it, and then transports it to a suitable location where it will eat it. Osprey's behavior during hunting is simulated to create a mathematical model for the proposed OOA technique, which consists of two phases: exploration and exploitation (Dehghani & Trojovský 2023).

A simplified version of the Osprey Optimization Algorithm is given here. The algorithm is inspired by the hunting behavior of osprey birds and aims to find the best solution to a problem.

| | | |
|---|---|---|
| Initialization | : | Start with a group of potential solutions called the population. |
| Exploration and Hunting | : | For each solution in the population, simulate the hunting behavior of osprey birds. This involves updating the positions of the solutions based on certain calculations. |
| Boundary Checks | : | Make sure the updated positions stay within certain limits (boundaries). |
| Improvement | : | Improve the solutions by adjusting their positions based on a second set of calculations. |
| Boundary Checks Again | : | Ensure the adjusted positions still fall within the specified boundaries. |
| Update Population | : | Keep the best solutions found so far and discard the rest. |
| Repeat | : | Repeat the process for a set number of iterations. |

The overall goal is to guide the solutions through a series of adjustments inspired by osprey hunting behaviors, with the hope that this process leads to finding the best solution to the given problem.

In (Ismaeel et al. 2023), the OOA is used to address one of the primary problems in a power system known as economic load dispatch (ELD). To assess the dependability of the OOA, its performance is contrasted with several methodologies. The OOA is contrasted with various methods found in the literature, including the monarch butterfly optimization (MBO), the chimp optimization algorithm (ChOA), the moth search algorithm (MSA), the sine cosine algorithm (SCA), and artificial bee colonies (ABO). Based on the findings obtained, the OOA is found to be superior to all competing algorithms. Table 2 gives a summary of recent and significant literature on PM2.5 prediction systems.

Table 3 gives a summary of recent and significant literature on metaheuristic algorithms and OOA optimization techniques.

Table 2: Summary of existing literature on PM2.5 prediction systems.

| Sl. No. | Author | Datasets | Pollutants and other factors used | Methodology | Remarks |
|---|---|---|---|---|---|
| 1. | Ameer et al. (2019) | 5 cities, China | PM2.5 data, along with meteorological data | Decision Tree, Random Forest, Multilayer Perceptron, Gradient Boosting | Random Forest was efficient |
| 2. | Kim et al. (2023) | 4 monitoring stations, Republic of Korea | Air pollution data, meteorological data | Weighted Bi-LSTM | It can predict PM2.5 values even when the data in the high-concentration area is not enough |
| 3. | Zhang J. et al. (2021) | Shunyi District, Beijing | PM2.5, Air pollution data, meteorological data | CNN-Bi-LSTM-Attention | Predictions of the next 144 h with this model are superior to those of the next 48 h with other models. |
| 4. | Yang et al. (2021) | Multiple stations, Beijing | PM2.5, Wind Speed | Bi-LSTM | Deep learning outperformed shallow learning models in hourly PM 2.5 prediction. |
| 5. | Masood et al. (2023) | New Delhi | PM2.5 | Extreme Learning Machine - Snake Optimization | This method is a valuable tool for accurately predicting PM2.5 values |
| 6. | Chen et al. (2023) | Kaohsiung, Taiwan | PM2.5 | CNN–RF | The ensemble framework can produce better results compared with the single CNN and RF techniques. |
| 7. | Zhang L. et al. (2023) | Three monitoring stations, Xinyang City | PM2.5 | Weighted complementary ensemble empirical mode decomposition with adaptive noise, an improved LSTM neural network | The experimental results demonstrate the superiority of the proposed model. |

## MATERIALS AND METHODS

In this section, the proposed PM2.5 concentration estimation model using Bi-LSTM (Bidirectional Long Short-Term Memory) with meteorological data as predictor variables is explained. For a better estimation of PM2.5 values, the hyperparameters of the Bi-LSTM model used are tuned using the Osprey Optimization Algorithm (OOA).

The proposed Bi-LSTM+OOA algorithm for PM2.5 prediction is outlined in Fig. 1.

Fig. 2 outlines the Work-Flow Diagram of the PM2.5 Concentration Estimation system with Bi-LSTM+OOA. The steps are explained here. The first step is preprocessing the dataset. This work has made use of data from the Air Quality dataset given in Chen (2019). There are 17 attributes in the data set. The time-related attributes are year, month, day, and hour. The pollution concentration-related ones are PM2.5, $SO_2$, PM10, $NO_2$, CO, and $O_3$. The meteorological attributes are temperature, wind speed, pressure, dew Point, and wind direction. They act as the predictor variables, with PM2.5 being the dependent variable in this study. The dataset includes hourly data on air pollutants collected between March 1, 2013, and February 28, 2017, for 12 air-quality monitoring sites in the People's Republic of China, spanning from Aotizhongxin to Wanshouxigong.

The following factors were considered while choosing the above dataset. There are around 4 lakh records, which is enough to create a machine-learning model that can be built accurately. It incorporates pollutant data and weather-related

Table 3: Summary of existing literature on Metaheuristic OOA optimization techniques.

| Sl. No. | Author | Data used | Methodology | Remarks |
|---|---|---|---|---|
| 1. | Bacanin et al. (2023) | Energy, Weather data, Europe | Six metaheuristics algorithms are used to optimize the LSTM model | Better results are obtained when parameters are tuned with metaheuristics |
| 2. | Dehghani et al. (2023) | CEC 2017 test suite | Implementation of OOA | The proposed OOA has provided superior performance compared to other algorithms by maintaining the balance between exploration and exploitation. |
| 3. | Ismaeel et al. (2023) | Cost of fuel for ELD and the cost of fuel and emissions for CEED | Application of OOA for economic load dispatch | The superiority of the OOA is achieved as per the obtained results compared with other algorithms. |

Step 1: Get the dataset as input.
Step 2: Perform the necessary data preprocessing steps like handling missing values, etc.
Step 3: Apply OOA to find the optimal hyperparameter values for the number of Units drop for the Bi-LSTM model.
Step 4: Apply the LSTM, and Bi-LSTM models on the dataset and build the Bi-LSTM model with the hyperparameter values found in Step 3.
Step 5: Plot the graphs for the chosen metrics for comparing the models used in Step 4.

Fig. 1: PM2.5 prediction using Bi-LSTM+OOA algorithm.

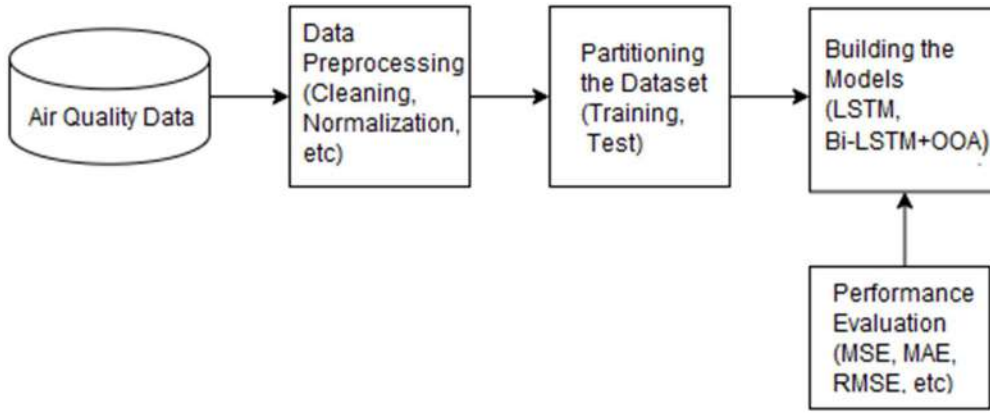


Fig. 2: Work-flow diagram of the PM2.5 concentration estimation system with Bi-LSTM+OOA.

data. In the proposed approach, meteorological data is used as a predictor variable.

The following data preprocessing steps were done:

1. Removal of the Null values.
2. The Wind direction variable is of the type of categorical data. It can be processed with 1-0 encoding or by converting the directions to their equivalent degree values. The second option is followed here.
3. It has been discovered that normalization improves accuracy. Normalization is therefore applied.

Then the dataset is partitioned into training that is used for building the model and test data, which is used for checking the accuracy of the model. The dataset is divided into the 70:30 ratio for training and testing data. The training and testing data size do not change during each iteration.

OOA is applied to find the optimal hyperparameter values for a number of units and the dropout rate for the Bi-LSTM model. hen, LSTM and Bi-LSTM models are applied to the dataset with some arbitrary values for the number of units and dropout. Then Bi-LSTM model is applied with the hyperparameter values found using OOA. Then the graphs are plotted for the chosen metrics for comparing the models.

## RESULTS AND DISCUSSION

The following section discusses the results obtained by running the proposed model. The metrics that can be used for comparing the regression models are MSE, RMSE, MAE, and $R^2$. Table 4 outlines the performance metrics used for the evaluation of the methods used in PM2.5 estimation.

Out of the four metrics here graphs are given for two: RMSE and $R^2$. The reasons are that MSE and RMSE are similar metrics; MSE is a better metric for regression compared to MAE. The OOA gave 74.27 and 0.3394 as the number of units and dropout rate, respectively, as the ideal values for the hyperparameters. Table 5 gives the values of the RMSE values obtained on the dataset for different numbers of units and two dropout rates, 0.5 and 0.33. The values are plotted as a line graph in Fig. 3 and Fig. 4.

In Fig. 3, the RMSE values for Bi-LSTM are always less than the RMSE values for LSTM. In Fig. 4, the same pattern is followed except for the Number of Units=90 and 100. The lowest value for RMSE value obtained, i.e., 68.63 for Number of Units=74 and Dropout rate 0.34, are plotted as a red square with legend Bi-LSTM+OOA. This proves the ability of OOA to identify the optimal values for the hyperparameters: Number of Units and Dropout rate.

Table 4: Performance Metrics for PM2.5 estimation.

| Sl. No. | Metric | Definition | Formula |
|---|---|---|---|
| 1 | Mean Absolute Error (MAE) | The mean absolute difference (MAE) between expected and actual values is calculated. | $MAE = \sum_{i=1}^{N} \lvert Ypred - Yactual \rvert / N$ |
| 2 | Mean Squared Error (MSE) | MSE is commonly used as the loss function for regression tasks, quantifying the difference between predicted and actual values. | $\text{MSE} = \sum_{i=1}^{N} (Ypred - Yactual)^2 / N$ |
| 3 | Root Mean Squared Error (RMSE) | By taking the square root of the mean square error (MSE), the average error magnitude (RMSE) can be determined. | $RMSE = \sqrt{\sum_{i=1}^{N} (Ypred - Yactual)^2 / N}$ |
| 4 | R-squared (R2) | R2 is a statistical measure that indicates the percentage of the dependent variable's variation that can be predicted from the independent variable. | $R^2 = 1 - \frac{\sum_{i=1}^{N} (Yactual - Ypred)^2}{\sum_{i=1}^{N} (Yactual - Ymean)^2}$ |

Table 5: RMSE values for the models used.

| Algorithm | Units/ Dropout Rate | RMSE | | | | | | |
|---|---|---|---|---|---|---|---|---|
| | | 50 | 60 | 70 | **74** | 80 | 90 | 100 |
| LSTM | 0.5 | 70.01 | 69.40 | 69.23 | 69.26 | 69.21 | 69.08 | 69.02 |
| Bi-LSTM | 0.5 | 68.63 | 68.63 | 68.67 | 69.02 | 68.78 | 68.65 | 68.61 |
| LSTM | 0.34 | 69.26 | 69.03 | 68.96 | 68.91 | 68.83 | 68.79 | 68.72 |
| Bi-LSTM | **0.34** | 68.76 | 68.68 | 68.64 | **68.63** | 68.64 | 68.80 | 68.74 |

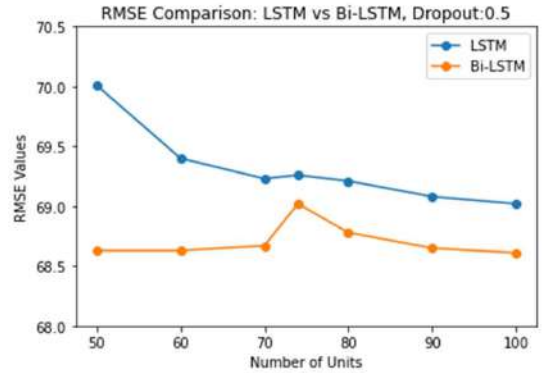


Fig. 3: Root Mean Squared Error comparison chart for different models for Dropout=0.5.

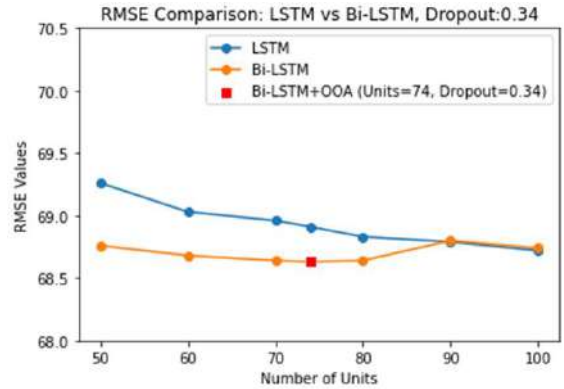


Fig. 4: Root Mean Squared Error comparison chart for different models for dropout = 0.34.

Table 6: $R^2$ values for the models used.

| Algorithm | Units/ Dropout Rate | $R^2$ | | | | | | |
|---|---|---|---|---|---|---|---|---|
| | | 50 | 60 | 70 | 74 | 80 | 90 | 100 |
| LSTM | 0.5 | 0.2626 | 0.2756 | 0.2790 | 0.2784 | 0.2794 | 0.2821 | 0.2835 |
| Bi-LSTM | 0.5 | 0.2834 | 0.2831 | 0.2863 | 0.2834 | 0.2864 | 0.2879 | 0.2873 |
| LSTM | 0.34 | 0.2784 | 0.2832 | 0.2847 | 0.2857 | 0.2874 | 0.2881 | 0.2897 |
| Bi-LSTM | 0.34 | 0.2888 | 0.2905 | 0.2912 | 0.2914 | 0.2913 | 0.2879 | 0.2892 |

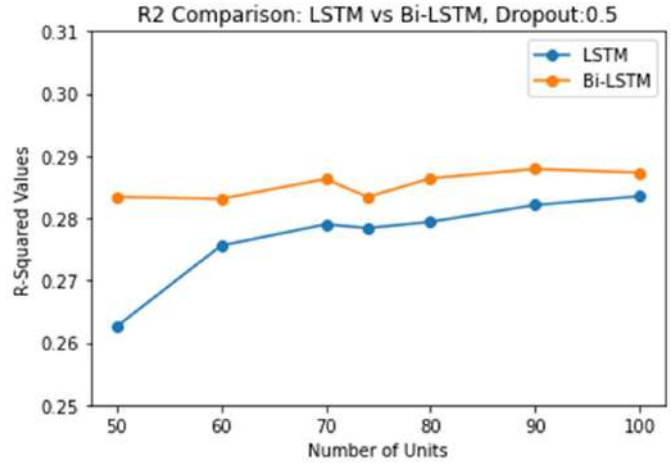


Fig. 5: R-squared error comparison chart for different models for Dropout=0.5.

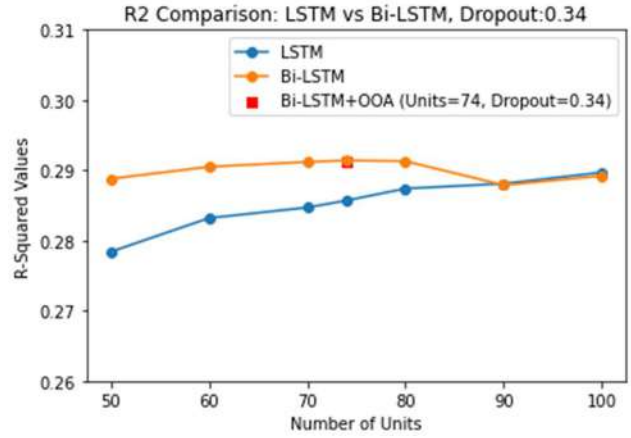


Fig. 6: R-squared error comparison chart for different models for Dropout=0.34.

Table 6 gives the values of the $R^2$ values obtained on the dataset for different numbers of units and two dropout rates, 0.5 and 0.33. The values are plotted as a line graph in Fig. 5 and Fig. 6.

In Fig. 5, the $R^2$ values for Bi-LSTM are always more than the $R^2$ values for LSTM. In Fig. 6, the same pattern is followed except for the Number of Units=90 and 100. The highest value for $R^2$ value obtained i.e., 0.2914 for Number of Units=74 and Dropout rate 0.34, are plotted as a square with legend Bi-LSTM+OOA. This proves the ability of OOA to identify the optimal values for the hyperparameters: Number of Units and Dropout rate.

## CONCLUSION

This work introduces a Bi-LSTM model incorporating meteorological data for accurate PM2.5 concentration estimation. LSTM and Bi-LSTM-based models were used on a dataset involving meteorological data like temperature as a predictor variable. The use of the Osprey Optimization Algorithm for tuning hyperparameters enhances the model's

predictive capabilities. Comparative analysis based on metrics such as Mean-Squared Error and $R^2$ highlights the advantage of the proposed Bi-LSTM+OOA model over the other model. The inclusion of additional relevant data sources to enhance model robustness and reliability can be done as further work. Recommendations for policy interventions include the implementation of the proposed model in air quality monitoring systems and incorporating its insights into decision-making processes. Continuous research and technological advancements in air quality monitoring are crucial for developing effective strategies to control and improve air quality. Research on air pollution, data analysis, model estimation, and machine learning will all be significantly impacted by this work.

## REFERENCES


Ameer, S., Shah, M. A., Khan, A., Song, H., Maple, C., Islam, S. U. and Asghar M. N. 2019. Comparative analysis of machine learning techniques for predicting air quality in smart cities, IEEE Access, 7: 128325-128338. https://doi.org/10.1109/ACCESS.2019.2925082

Bacanin, N., Stoean C., Zivkovic, M., Rakic, M., Strulak-Wójcikiewicz, R. and Stoean, R. 2023. On the benefits of using metaheuristics in the hyperparameter tuning of deep learning models for energy load forecasting. Energies, 16: 1434. https://doi.org/10.3390/en16031434

Central Pollution Control Board (CPCB). 2015. Report on Air Quality Index by Ministry of Environment, Forests and Climate Change, Government of India. Retrieved from http://app.cpcbccr.com/ccr_docs/FINAL-REPORT_AQI_.pdf (access date January 06, 2024).

Chen, S. 2019. Beijing Multi-Site Air Quality. UCI Machine Learning Repository. https://doi.org/10.24432/C5RK5G

Chen, M. H., Chen, Y. C., Chou, T. Y. and Ning, F. S. 2023. PM2.5 Concentration prediction model: A CNN–RF ensemble framework. Int. J. Environ. Res. Public Health, 20: 4077. https://doi.org/10.3390/ijerph20054077

Dehghani, M. and Trojovský, P. 2023. Osprey optimization algorithm: A new bioinspired metaheuristic algorithm for solving engineering optimization problems. Front. Mech. Eng., 8: 1126450. https://doi.org/10.3389/fmech.2022.1126450

Ismaeel, A. A. K., Houssein, E. H., Khafaga, D. S., Aldakheel, E. A., AbdElrazek, A. S. and Said, M. 2023. Performance of osprey optimization algorithm for solving economic load dispatch problem. Mathematics, 11: 4107. https://doi.org/10.3390/math11194107

Kim, B., Kim, E., Jung, S., Kim, M., Kim, J. and Kim, S. 2023. PM2.5 Concentration forecasting using weighted Bi-LSTM and random forest feature importance-based feature selection. Atmosphere, 14: 968. https://doi.org/10.3390/atmos14060968

Masood, A., Hameed, M. M., Srivastava, A., Pham, Q. B., Ahmad, K., Razali, S. F. M. and Baowidan, S. A. 2023. Improving PM2.5 prediction in New Delhi using a hybrid extreme learning machine coupled with the snake optimization algorithm. Sci. Rep., 13: 21057. https://doi.org/10.1038/s41598-023-47492-z

Morapedi, T. D. and Obagbuwa, I. C. 2023. Air pollution particulate matter (PM2.5) prediction in South African cities using machine learning techniques, Frontiers in Artificial Intelligence, 6: 1230087 https://doi.org/10.3389/frai.2023.1230087

Saminathan, S. and Malathy, C. 2023. Ensemble-based classification approach for PM2.5 concentration forecasting using meteorological data. Front. Big Data, 6: 1175259. https://doi.org/10.3389/fdata.2023.1175259

Senthivel, S. and Chidambaranathan M. 2022. Machine learning approaches used for air quality forecast: A review, Revue d'Intelligence Artificielle, 36(1): 73-78. https://doi.org/10.18280/ria.360108

Swarna Priya, R. M. and Sathya, P. 2019. Statistical Analysis of Air Pollutants in Ambient Air, Reality of Sensors and Corrective Measures in India. In Proceedings of the Conference 2019 Innovations in Power and Advanced Computing Technologies (i-PACT), Vellore, India, 1-6. https://doi.org/10.1109/i-PACT44901.2019.8960010.

Thangavel, P., Park, D. and Lee Y. C. 2022. Recent insights into particulate matter (PM2.5)-mediated toxicity in humans: An overview. Int. J. Environ. Res. Public Health, 19: 7511. https://doi.org/10.3390/ijerph19127511

World Health Organization (WHO). 2018. Burden of Disease from Ambient Air Pollution for 2016. Retrieved from https://cdn.who.int/media/docs/default-source/air-pollution-documents/air-quality-and-health/aap_bod_results_may2018_final.pdf (access dated January 06, 2024)

World Health Organization (WHO). 2023. Health Topic on Air Pollution. Retrieved from https://www.who.int/health-topics/air-pollution (accessed date January 06, 2024)

Xiao, F., Yang, M., Fan, H., Fan, G. and Al-qaness M. A. A. 2020. An improved deep learning model for predicting daily PM2.5 concentration. Sci. Rep., 10: 20988. https://doi.org/10.1038/s41598-020-77757-w

Xing, Y. F., Xu, Y. H., Shi, M. H. and Lian, Y. X. 2016. The impact of PM2.5 on the human respiratory system. J. Thoracic Dis., 8(1): E69-74. https://doi.org/10.3978/j.issn.2072-1439.2016.01.19

Yang, J., Yan, R., Nong, M., Liao, J., Li, F. and Sun, W. 2021. PM2.5 concentrations forecasting in Beijing through deep learning with different inputs, model structures, and forecast time, Atmos. Pollut. Res., 12(9): 101168.https://doi.org/10.1016/j.apr.2021.101168.

Zhang, J., Peng, Y., Ren, B. and Li, T. 2021. PM2.5 Concentration prediction based on CNN-BiLSTM and attention mechanism. Algorithms, 14: 208. https://doi.org/10.3390/a14070208

Zhang, L., Liu, J., Feng, Y., Wu, P., and He, P. 2023. PM2.5 concentration prediction using weighted CEEMDAN and improved LSTM neural network. Environ. Sci. Pollut. Res., 30: 75104-75115. https://doi.org/10.1007/s11356-023-27630-w


### ORCID DETAILS OF THE AUTHORS


Saminathan S: https://orcid.org/0000-0001-5344-8958
Malathy C: https://orcid.org/0000-0003-1974-8927

Nature Environment and Pollution Technology
An International Quarterly Scientific Journal

p-ISSN: 0972-6268
(Print copies up to 2016)
e-ISSN: 2395-3454

Vol. 23 | No. 3 | pp. 1639-1645 | 2024

Original Research Paper

https://doi.org/10.46488/NEPT.2024.v23i03.034

Open Access Journal

# Potential Use of *Portulaca* Plant Species in Removing Estradiol Hormone Pollutants in the Surface Water of Bengawan Solo River

**Siti Khoiriyah*†, Suranto**, Prabang Setyono**, Evi Gravitiani*** and Agung Hidayat***

*Department of Environmental Science, Graduate School, Universitas Sebelas Maret. Jl Ir Sutami 36 Surakarta 57126, Indonesia

**The Faculty of Mathematics and Natural Sciences, Universitas Sebelas Maret. Jl Ir Sutami 36 Surakarta 57126, Indonesia

***Department of Development Economic, Faculty of Economic and Business, Universitas Sebelas Maret. Jl Ir Sutami 36 Surakarta 57126, Indonesia

†Corresponding author: Siti Khoiriyah; siti.khoiriyah12@staff.uns.ac.id

**Nat. Env. & Poll. Tech.**
**Website: www.neptjournal.com**

*Received:* 06-11-2023
*Revised:* 20-12-2023
*Accepted:* 11-01-2024

**Key Words:**
Bengawan Solo River
Estradiol hormone pollutants
*Portulaca* plants
Phytoremediation

## ABSTRACT

Bengawan Solo River water is a source of drinking water and raw materials for the government of Surakarta city, but the water has been mixed with domestic, industrial, and agricultural wastes. The waste contains estradiol-17 derived from urine and feces, both from livestock and humans as well as industries around the sub-watershed Bengawan Solo River. The content of estradiol-17 in the Bengawan Solo sub-watershed is quite high. This study is the first conducted in Bengawan Solo River to look at natural estrogens that are very rarely studied in the environment, which are likely could cause several health effects in humans and wildlife due to their relatively strong estrogenic potential and high levels in wastewater and river water. Therefore, research on the elimination of these compounds using effective, energy-efficient, and low-maintenance technologies for water treatment such as phytoremediation is highly expected. The purposes of this study were to identify estradiol, to measure the estradiol levels through HPLC tests as well as to test the effectiveness of phytoremediation with *Portulaca* plant as biological agents. The results show that the water of Bengawan Solo River contained estradiol substances ranging from 3.88 ppm to 5.76 ppm. The *Portulaca* plant species was effective at eliminating estrogenic waste up to 99.89%.

## INTRODUCTION

Estrogenic compounds are micropollutants, that infiltrate the environment and potentially alter human hormone response even in low doses (Maher 2020). The sources of these compounds are animals, human beings, and human estrogenic compounds that have been detected in synthetic and natural human estrogenic compounds in water and wastewater systems (Liu et al. 2015). Synthetic estrogen compounds often called environmental estrogens are persistent in the environment (Shore 2016).

The compound is a hormone that mimics the work of natural estrogens. The artificial estrogenic compound comes from various sources of pollutants namely: 1) agricultural activities (e.g. insecticides DDT, dieldrin, and endrin); 2) factory activities (e.g. dioxins, plastic constituents, and detergents); 3) medications (e.g. diethylstilbestrol (DES), ethinyl estradiol). Synthetic estrogen compounds can mimic or inhibit the activity of the hormone estrogen, so called EDC or Endocrine Disrupting Compound (Jiang et al. 2013). Estrogen is present in both lake water used for drinking and which is used for irrigation at concentrations that can affect the growth of such as alfalfa plants. Estrogen compounds are present in several compartmentalized environments, including soil and groundwater (Shore 2016).

Estradiol in urine is a natural estrogen from wastewater which is grouped in EDC because it can interfere with endocrine function in women during adulthood and causes fertility abnormalities in humans (Rattan 2017). Research with GC-MS analytical methide has been conducted for the identification of natural estrogens in waste and surface water including E1, E2, E3, 2OHE1, 16a-OHE1, 4OHE1, 2-hydroxy estradiol (2OHE2), 4- hydroxy estradiol (4OH E2), 17-epiestriol (17epiE3), 16-epiestriol (16epiE3), and 16 keto-estradiol (16 dan 2OH. Most of them are detected in effluent water and rivers, where their detected concentrations were n.d-14.7 and n.d-51.7 ng.$L^{-1}$ respectively (Tang 2020).

The estradiol compound has two OH groups and 1 benzene ring (Fig. 1). The compound has two hydroxyl groups, one at the C3 position and the other at position 17β, and also three double bonds on the ring. Due to its

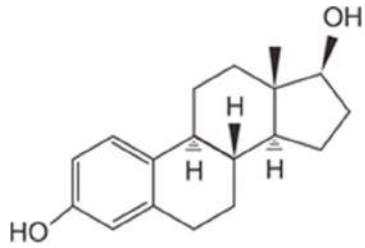


Fig. 1: Chemical structure of estradiol compounds.

two hydroxyl groups, estradiol is often abbreviated as E2. Estradiol (E2) is a steroid, estrogen, and the main female sex hormone. This hormone is functionally important in the regulation of the estrus cycle and menstrual cycle in the female reproductive cycle.

Living creatures exposed to estrogenic waste may experience various hormonal disorders, leading to their classification as Hormone Disrupting Compounds (SPH) or EDC (Endocrine Disrupting Compound). SPH can be detected in environmental media such as water and sediment, as well as in food sources like fish, shellfish, and snails. Furthermore, SPH is found in humans through various biological indicators, including blood, urine, hair, and breast milk. Continuous exposure of humans to pharmaceuticals with estrogenic properties can result in the development of conditions such as testicular dysgenesis syndrome, including testicular cancer in men and breast cancer in women. Additionally, men may experience reduced reproductive capacity, including decreased sperm count and abnormal sperm morphology, as well as an increased risk of testicular carcinoma in situ. The contributor to river water pollution generally comes from municipal wastewater disposal due to the increasing population in urban and suburban areas with a lack of wastewater treatment facilities. In contrast, the investigation of EDC events and distribution in river water is very limited (Khoiriyah 2021). Meanwhile, the condition of rivers in Indonesia is almost the same as other rivers in the world. The water discharge of the Bengawan Solo River watershed comes from domestic wastewater disposal, agriculture, and industry. If this condition is reinforced by the increasing population in urban and suburban areas and with the lack of wastewater treatment facilities, then it should be expected that the endocrine-disrupting chemicals (EDC) in the Bengawan Solo River sub-watershed are considered very important to be examined because it could cause female health problems.

Phytoremediation is a process that involves plants containing chlorophyll to reduce the pollutant content in soil, air and water. Phytoremediation is a technique that uses plants to reduce or reduce pollutant levels in the environment. Phytoremediation is a new green technology that uses plants to eliminate, degrade, or detoxify toxic chemicals (such as heavy metals, radionuclides, organic and inorganic contaminants, xenobiotics, and hydrocarbons) in soil, sediment, groundwater, surface water, and air. Phytoremediation estrogenic waste in this case estradiol compounds in this research used *Portulaca* plants. Phytoremediation is an in-situ remediation technology that utilizes the inherent capabilities of living plants (Wang et al. 2017). Phytoremediation uses plants to clean up pollution in the environment. Plants can help clean up many types of pollution including metals, pesticides, explosives, and oil. Plants also help prevent wind, rain, and groundwater from carrying pollutants from the site to other areas (Antoniadis et al. 2017).

The purposes of this study were to identify the presence of estradiol compound as EDC in the Bengawan Solo River Sub-watershed, to measure estradiol levels as EDC by employing the HPLC method, and to measure the effectiveness of *Portulaca* sp. in eliminating that substance of EDC.

## MATERIALS AND METHODS

### Sample Collection

Samples of estrogenic waste solution in this study were taken from upstream and downstream of the Bengawan Solo River sub-watershed at a distance of 50 meters from the outlets of four tributaries, namely: Premulung River, Pepe River, Pucangsawit River, and Kalianyar. Water samples were taken as much as 2 liters from up-stream and down-stream so that a total number of 8 (eight) samples were collected (Khoiriyah et al. 2019).

### Estradiol Identification Procedure

The method of preservation of the samples was adapted from (Celic 2020, Imai 2007). Each sample was filtered up to 100 mL with nitroacetic filter paper with a pore size of 0.45 μm to remove the solids present in the samples so that very clear samples were obtained. Filtering was assisted by vacuum suctioning to speed up the filtration process. The filtered samples were placed in labeled plastic bottles and stored in the freezer to avoid the sample biodegradation process during storage.

### Standard Estradiol Test, Eluent and HPLC

The standard solution was made by diluting 0.1 g of solid estradiol standard into 1% methanol solution, making the concentration 100 ppm of estradiol standard solution with a concentration of 1-6 $mg.L^{-1}$ made by diluting 0.1 mL to 0.6 mL. Eluent was made from 75% acetone.

### HPLC Grade Eluent Constituent Compounds

Before use, gas content in the eluent was removed or followed up with degassing by stirring with a magnetic stirrer for an hour and followed by vacuum filtration using filter paper with a pore size of 0.45 µm to remove any solids that may be present in the eluent. Estradiol analysis was performed by HPLC with reserve phase and normal delusions. Before being used for the analyte process, the HPLC column was stabilized by draining 100 % methanol for 1 hour at a speed of 1.0 $mL.min^{-1}$. This treatment was also intended to clear the column from the remains of the previous analyte as well as the impactor that may still be left behind in the analytic column. Estradiol was measured at a wavelength of 230 nm in accordance with the results of wavelength optimization that has been done previously.

### Phytoremediation Effectiveness Test

A phytoremediation effectiveness test was conducted by *Portulaca* plants on estrogenic waste (phenol and estradiol). The procedure of effectiveness testing used *Portulaca* plant, as a phytoremediation agent in reducing SPH (Imai 2007). It began with the preparation of *Portulaca* plants, then followed by phytoremediation and HPLC analysis. The first step was the preparation of simplisia, *Portulaca* plants as mature (flowering plants were taken from Pucangsawit, Pepe, Kalianyar and Premulung riversides). The second step was phytoremediation in which two grams of *Portulaca* was taken and incubated in 50 mL liquid SPH. *Portulaca* was then washed and extracted with methanol. Then, it was evaporated and dissolved in ethanol. In the HPLC analysis step, 2 mL of the solution after 96 hours of incubation was taken. Then, 40 µL was taken for the phenol test and HPLC analysis on the C 18 column, and 75% of acetonitrile taken as eluent, meanwhile 400 µL of the solution was taken for the estradiol test, and HPLC analysis on the C 18 column, and 80% methanol was taken as eluent.

Table 1: HPLC test results on 4 pre-phytoremediation river water sample sites.

| No | Site | Estradiol Concentration (ppm) | |
|---|---|---|---|
| | | Upstream | Downstream |
| 1 | Premulung River | 5.76 | 5.19 |
| 2 | Kalianyar River | 5.30 | 3.88 |
| 3 | Pepe River | 4.71 | 4.51 |
| 4 | Pucangsawit River | 5.66 | 4.26 |

Table 2: HPLC test results on pre-phytoremediation river water samples.

| No | Sample code | Estradiol (ppm) | Description |
|---|---|---|---|
| 1. | PW1 | 0.01 | *P. pillosa*, Premulung River Upstream |
| 2. | PW2 | 0.76 | *P. pillosa*, Premulung River Downstream |
| 3. | PK1 | 0.76 | *P. pillosa*, Kalianyar Rive rUpstream |
| 4. | PK2 | 1.05 | *P. pillosa*, Kalianyar River Downstream |
| 5. | PS1 | 1.25 | *P. pillosa*, Pucangsawit River Upstream |
| 6. | PS2 | 1.15 | *P. pillosa*, Pucangsawit River Downstream |
| 7. | PP1 | 2.05 | *P. pillosa*, Pepe River Upstream |
| 8. | PP2 | 2.43 | *P. pillosa*, Pepe River Downstream |
| 9. | GK1 | 3.42 | *P. grandiflora*, Kalianyar River Upstream |
| 10. | GK2 | 3.82 | *P. grandiflora*, Kalianyar River Downstream |
| 11. | GW1 | 3.53 | *P. grandilora*, Premulung River Upstream |
| 12. | GW2 | 3.81 | *P. grandilora*, Premulung River Downstream |
| 13. | GS1 | 5.68 | *P. grandilora*, Pucamgsawit River Upstream |
| 14. | GS2 | 4.52 | *P. grandilora*, Pucangsawit River Downstream |
| 15. | GP1 | 4.89 | *P. grandiflora*, Pepe River Upstream |
| 16. | GP2 | 4.45 | *P. grandiflora*, Pepe River Downstream |
| 17. | OK1 | 4.85 | *P. olleraceae*, Kalianyar River Upstream |
| 18. | OK2 | 4.98 | *P. olleraceae*, Kalianyar River Downstream |
| 19. | OW1 | 6.51 | *P. olleraceae*, Premulung River Upstream |
| 20. | OW2 | 4.98 | *P. olleraceae*, Premulung River Downstream |
| 21. | OP1 | 6.34 | *P. olleracea*, Pepe River Upstream |
| 22. | OP2 | 5.27 | *P. olleracea*, Pepe River Downstream |
| 23. | OS1 | 4.13 | *P. olleraceae*, Pucangsawit River Upstream |
| 24. | OS2 | 5.21 | *P. olleraceae*, Pucangsawit River Downstream |

## RESULTS AND DISCUSSION

### Characteristics of Estradiol in each Sample

The results of estradiol observations with HPLC reserve phase and normal delusions conducted at eight locations of Bengawan Solo River water samples appear as peaks in the chart with different levels. This indicates that all river water samples contained estradiol with varied levels.

Table 1 shows that the highest concentration of estradiol was found in the Premulung River Upstream (5.76 ppm), while the lowest was in Kalianyar River water (3.88 ppm). The average of eight samples was 4.89 ppm. The identification results indicate that the water samples from the Premulung River Upstream had a high estradiol content). Laweyan Village is a batik industrial area so more batik industrial waste flows into the river. EDC in industrial areas is higher than that in other regions. EDC, which is a micro-pollutant, generally exists or comes from various products that are used daily, such as medicines and various pharmaceutical derivative compounds (pharmaceuticals), and personal care products (Jiang et al. 2013).

According to SCHER (Scientific Committee on Health and Environmental Risks) in terms of environmental quality standard-Ethinylestradiol, the quality standard for estradiol in water is 0.035 $ng.L^{-1}$ or 3.5 × 10-8 ppm (2011). Thus, the estradiol found in the four sampling rivers exceeded the quality standard. Meanwhile, according to the Sub-Group on Review of the Priority Substances List, a member of the Common Implementation Strategy for the Water Framework Directive (2011) states that the quality standard for estradiol in water is 0.4 $ng.L^{-1}$. Thus, the sample water from all locations also exceeded the environmental quality standard.

The lowest estradiol content in the water sample of Kalianyar River Downstream was 3.88 ppm. The location of the river leads to the western direction of the city of Surakarta, which is in the area of the Banjarsari sub-district. The river is located in a fairly densely populated urban area. Although found in low amounts, EDC has a strong and irreversible effect. The impact on humans and animals is complex. Micro-pollutant compounds are often associated with EDC or compounds that can interfere with the endocrine system or hormonal organisms (Jiang et al. 2013). The impact of EDC on aquatic animals is mostly a feminizing effect in which it can mimic or change the activity of the hormone estrogen.

The three types of *Portulaca* namely *P.olleraceae, P. grandiflora* and *P. pillosa* give different reactions to the phyto-mediating process of phenols and estradiol in river water from eight sites (Table 2). The phytoremediation process is carried out by incubating water samples with *Portulaca* plants for 96 hours. Incubation was conducted in Erlenmeyer tubes a total of 24 pieces in accordance with the design of testing experiments 3 types of *Portulaca* at 8 sites of river water sampling. After 96 hours of water samples tested HPLC and plant extracts also tested HPLC to find out how estrogenic waste absorption in *Portulaca* plants.

There are three phytoremediation mechanisms that can affect the mass of contaminants in soil, sediment, and water. The first is phytoextraction also called phytoaccumulation, which refers to the uptake and translocation of metal contaminants in the soil by plant roots to above-ground plant parts. The second is rhizofiltration which is mainly used to recover extracted groundwater, surface water, and wastewater with low contaminant concentrations. This research includes a rhizofiltration mechanism because it aims to conserve water exposed to estrogenic waste (estradiol). This method is a method of adsorption or deposition into plant roots or absorption of contaminants in the solution surrounding the root zone (Wang et al. 2017).

Rhizofiltration is usually exploited in groundwater (either in situ or extracted), surface water, or wastewater to remove metals or other inorganic compounds. Plants to be used for cleaning are raised or grown in a greenhouse with their roots in the water, not in the soil. To acclimate to plants and once large root systems are developed, contaminated water is collected from sewage and brought to plants to replace their water source (Gupta et al. 2013). The plant is then planted in a contaminated area where the roots take water and contaminants with them. When the roots become saturated with contaminants, the plant is removed or harvested (Gupta et al. 2013).

In one study, after one hour of treatment, sunflower reduced lead concentrations significantly (Gupta et al. 2013). The highest lead extraction accumulated in the roots of *Portulaca oleracea* L. was 173.39 $mg.kg^{-1}$, and 20.01 $mg.kg^{-1}$ in the shoots, respectively. The translocation factor was obtained from 0.62 to 0.12 for *Portulaca oleracea* L. The translocation factor was obtained to be less than one, indicating poor lead transfer from root to shoot. The ability of *Portulaca oleracea* L. to absorb large amounts of lead from the root zone, high crop yields and the ability to accumulate lead in harvestable organs, makes this plant very effective for remediation (Asadi et al. 2021).

The use of *Portulaca* has several advantages because it can be applied in-situ and ex-situ as well as a faster physiological mechanism. According to Jeevananthama et al. (2019), the advantage of this rhizofiltration method is the ability to use land and water plants for both in-situ and ex-situ applications. Another advantage is that contaminants do not have to be transferred to the shoots. Thus, species

other than hyperaccumulators can be used. Terrestrial plants are preferred because they have a fibrous and longer root system that increases the amount of root area (Gupta et al. 2013). Disadvantages and limitations of this method include the constant need to adjust the pH, the plants may need to be planted first in a greenhouse or nursery; there is periodic harvesting and disposal of crops; tank design must be well engineered; and a good understanding of chemical speciation/ interaction is required. (Gupta et al. 2013).

Extraction of root, stem, and leaf *Portulaca* is done to separate the estradiol component from a material or plant tissue. The initial process of extraction is by smoothing the tissue. This aims to increase the chances of dissolving the components of the desired metabolite components. Before extracting, plant tissue is dried to maintain the content of metabolites in plants that have been cut so that the metabolic process is stopped. One of the extraction stages is the maceration process which is the process of extracting samples using solvents with several times shaking or stirring at room temperature. The result of the extraction process of *Portulaca* samples is liquid, viscous, and dry. Dry extract or powder is a solid preparation obtained by vaporizing solvents based on the content of active ingredients.

The effectiveness of phytoremediation needs to be known from the mass of elements that are expected to be transferred from contaminated soil to plant biomass, taking into account the initial level of contamination and the target value obtained after remediation (Kumar 2015). *Portulaca oleracea* L. commonly called purslane, has a significant phytoremediation ability (Srivastava et al. 2021). *Portulaca* plants have the potential as phytomediators and can lower estradiol levels in polluted water. PW1 treatment (*P. pillosa* to the sample water of Premulung River Upstream) is a treatment that can lower the highest estradiol levels by 5.75 ppm or 99.88%. GW1 treatment (*P grandiflora* to the sample water of Premulung River Upstream was able to lower estradiol levels by 2.34 pp or 40.66%. OW1 treatment (*P. olleraceae* to the sample water of Premulung River Upstream) was able to decrease 0.9 ppm or 15.66% (Table 3).

Table 3: Effectiveness of *Portulaca* phytoremediation against estradiol.

| No. | Species | Location | Before(ppm) | After (ppm) | Difference (ppm) | Effectivness (%) |
|---|---|---|---|---|---|---|
| 1. | *P. pillosa* | Premulung River Upstream | 5.76 | 0.01 | 5.75 | 99.86 |
| | | Premulung River Downstream | 5.19 | 0.76 | 4.43 | 85.31 |
| | | Kalianyar River Upstream | 5.30 | 0.76 | 4.54 | 85.64 |
| | | Pepe River Upstream | 4.71 | 1.05 | 3.67 | 77.78 |
| | | Pucangsawit River Downstream | 4.26 | 1.25 | 3.01 | 70.71 |
| | | Pucangsawit River Upstream | 5.66 | 1.15 | 4.51 | 79.74 |
| | | Pepe River Downstream | 4.51 | 2.05 | 2.45 | 54.45 |
| | | Kalianyar River Downstream | 3.88 | 2.43 | 1.45 | 37.32 |
| 2. | *P. grandiflora* | Premulung River Upstream | 5.76 | 3.42 | 2.34 | 40.66 |
| | | Premulung River Downstream | 5.19 | 3.82 | 1.37 | 26.44 |
| | | Kalianyar River Upstream | 5.30 | 3.53 | 1.77 | 33.35 |
| | | Pepe River Upstream | 4.71 | 3.81 | 0.90 | 19.12 |
| | | Pucangsawit Rive rDownstream | 4.26 | 5.68 | -1.43 | -33.59 |
| | | Pucangsawit River Upstream | 5.66 | 4.52 | 1.14 | 20.19 |
| | | Pepe River Downstream | 4.51 | 4.89 | -0.38 | -8.43 |
| | | Kalianyar River Downstream | 3.88 | 4.45 | -0.56 | -14.49 |
| 3. | *P. olleraceae* | Premulung River Upstream | 5.76 | 4.85 | 0.90 | 15.66 |
| | | Premulung River Downstream | 5.19 | 4.98 | 0.20 | 3.92 |
| | | Kalianyar River Upstream | 5.30 | 6.51 | -1.21 | -22.82 |
| | | Pepe River Upstream | 4.71 | 4.98 | -0.27 | -5.72 |
| | | Pucangsawit River Downstream | 4.26 | 6.34 | -2.09 | -49.08 |
| | | Pucangsawit River Upstream | 5.66 | 5.27 | 0.39 | 6.92 |
| | | Pepe River Downstream | 4.51 | 4.13 | 0.37 | 8.24 |
| | | Kalianyar River Downstream | 3.88 | 5.21 | -1.32 | -34.05 |

*Portulaca* exposed to estrogenic waste requires a special defense mechanism to survive. Plants are often exposed to natural and synthetic toxins such as heavy metals, allelochemicals, organic pollutants, and pesticides. As a result, plants must survive under adverse growth conditions (Zhang et al. 2013). One such mechanism is the ability to metabolize organic compounds derived from abiotic (xenobiotics). Extensive biotransformation is part of a strategy to address the potential negative impact of xenobiotics on plant growth and development. It is specifically proven in its metabolic detoxifying ability of herbicides (Kumar 2015).

The results of estradiol levels in plants in *Portulaca* show that the three types have different levels in samples of roots, stems, and leaves. *P. olleraceae* on the leaves was found to have the highest estradiol levels of 121.42 ppm. *P. grandiflora* on the stem was found at the level of 118.83 ppm, and *P. pillosa* in stem extract was found at the rate of 58.92 ppm estradiol. Estradiol level in the plant extract functions as a hint that the absorption of estradiol by plants was quite high, which is the ability to remove estradiol pollutants by the roots and to translocate them to the leaves and stems. Phytotoxicity by changing cell membrane permeability through reacting with active groups of different enzymes was involved in plant metabolism by reacting with the phosphate groups of adenosine diphosphate (ADP) or adenosine-5′-triphosphate (ATP) (Kumar 2015).

Plants can destroy or break down organic pollutants and absorb as well as stabilize metal pollutants. In this case, the organic pollutants can be cleared by the plant through a value or a combination of phytodegradation, rhizodegradation, and phytovolatilization processes. Organic pollutants such as crude oil, solvents, and polyaromatic hydrocarbons are reversible by this technique. Medium pollutants heavy metals and radioactive elements can be cleaned by plants through the process of phytoextraction/phytoaccumulation, rhizofiltration and/or phytostabilization (Mustafa et al. 2019). Pytofiltration is the process of removing metals from water contaminated by plant roots (Kumar 2015). e. The contaminants are either adsorbed onto the root surface or are absorbed by the plant roots. Plants used for rhizofiltration are not planted directly in situ but are acclimated to the pollutant first (Wuana 2018).

The Cd and Pb reduce the normalized transpiration and growth rate. The greater amount of Cd and Pb accumulate in roots relative to shoots (Lou et al. 2013). Meanwhile, phytostabilization involves the roots absorbing pollutants from the soil, storing them in the rhizosphere, and reducing the spread of pollutants (Gupta et al. 2013). In *Portulaca* there are absorption and translocation of contaminants, causing toxic effects on the metabolic process. Toxic effects resulting in decreased biomass production can be prevented by the induction of various cell mechanisms. Cell mechanisms performed to reduce severe toxic effects of metal are by adsorption to cell walls, vacuole entry compartments, increased active efflux, or higher-level induction of chelated metals such as complex proteins (metallothionein and phytochelatin), organic (citrate), and inorganic complexes (sulfide) (Gupta 2013). Many heavy metals (e.g. Cd, Cu, Fe, etc.) are transition metals and can oxidize as well as reduce different biomolecules (e.g. GSH) and thus can disturb the harmony of the redox status of plant cells. These effects on the redox status of the cell may be further enhanced due to the coupling reaction of these metals with biomolecules or other transition metals that can regenerate their ionic state.

This indicates that the decrease in estradiol concentration in treatment for 96 hours was caused by not only biological decomposition but also synergy between plant root zones, microorganisms, and planting media/river sample water (Maher 2020). Organic substances that can settle are set aside through precipitation and filtration by the media. The absorption process that occurs in the media contributes to the decrease in pollutants. Organic substances filtered by the media become a substrate for microorganisms so that they grow to form a layer on the surface of the media and serve to decompose dissolved organic substances. The process in the media takes place aerobically near the water surface and around rooting (Prajapati et al. 2017). Phytoremediation, in principle, utilizes solar energy and has an extraordinary perspective for abating and assembling heavy metals. The technique of phytoremediation has developed in contemporary times as an efficient method and its success depends on plant species selection. Here in this synthesis, we are presenting a scoping review of phytoremediation, its basic principles, techniques, and potential anticipated prospects (Sabreena et al. 2022).

Microorganisms grown in *Portulaca* rooting also play an important role in absorbing the content of organic pollutants. Plants can absorb pollutants as far as the roots of the plant grow. Microorganisms that grow at the root are more effective in lowering the value of pollutants because the number of microorganisms is increasing and the microorganisms are increasingly able to adapt to the environment (Kumar et al. 2015). The rooting system in *Portulaca* is strong enough, long, and widespread so that it is very effective in expanding the area where microorganisms are attached so as to significantly lower estradiol levels. The effectiveness of the decrease in estradiol concentration is shown in Table 4, PW1 Treatment (*P. pillosa* against the sample water of Premulung River Upstream) is a treatment that is able to

lower the highest estradiol levels by 5.75 ppm or 99.88%. GW1 treatment (*P. grandiflora* to the sample water of Premulung River Upstream was able to lower estradiol levels by 2.34 pp or 40.66%. OW1 treatment (*P. olleraceae* to the sample water of Premulung River Upstream) was able to decrease by 0.9 ppm or 15.66%.

Phytoremediation uses plants to remove pollutants naturally and sustainably. Compared with other methods such as chemical or physical remediation, phytoremediation is more environmentally friendly, more economical, and less invasive. However, phytoremediation may take longer and is not always effective for certain pollutants. Other methods tend to be quicker but can have negative environmental impacts. Phytoremediation offers proprietors and chiefs of toxic polluted locales an imaginative and financially effective choice to address headstrong natural contaminants. As it uses the plant's characteristic capacity to suck the contamination present in the dirt. Numerous plants have this regular capacity to uptake toxic contaminants and natural contaminations from air, soil, and water (Jeevanantham 2019).

## CONCLUSION

The results of the above study indicate that the *Portulaca* plant has the potential as a Phytoremediation agent for water contaminated with estrogenic waste. The ability to reduce the estradiol concentration is effective up to 99.88%. Therefore, this is a very interesting finding and needs to be developed to conserve river water contaminated with estrogenic waste by using the *Portulaca* plant as a phytoremediator agent.

## REFERENCES

Antoniadis, V., Levizou, E., Shaheen, S.M., Ok, Y.S., Sebastian, A., Baum, C., Prasad, M.N., Wenzel, W.W. and Rinklebe, J. 2017. Trace elements in the soil-plant interface: Phytoavailability, translocation, and phytoremediation-A review. Earth-Sci. Rev., 171: 621-645. DOI:10.1016/j.earscirev.2017.06.005

Asadi, S. and Jalali, V. 2021. Phytoremediation and estimation of optimal clean-up time of lead-contaminated soils using Portulaca oleracea L. Environ. Water Eng., DOI: 10.22034/JEWE.2020.248656.1424

Celic, M., Skrbic, B., Sarainsa, J., Ziyancev, J., Gros, M. and Petrovic, M. 2020. Occurrence and assessment of environmental risks of endocrine disrupting compounds in drinking, surface and wastewaters in Serbia. Environ. Pollut., 262: 114344. DOI: 10.1016/j.envpol.2020.114344

Gupta, D.K., Huang, H.G. and Corpa, F.J. 2013. Lead tolerance in plants: strategies for phytoremediation. Environ. Sci. Pollut. Res., 20: 2150-2161. DOI: 10.1007/s11356-013-1485

Imai, S., Shiraishi, A. and Gamo, K. 2007. Removal of phenolic endocrine disruptors by *Portulaca oleraceae*. J. Biosci. Bioeng., 103(5): 420-426. DOI: 10.1263/jbb.103.420

Jeevanantham, S., Saravanan, A., Hemavathy, R.V., Kumar, P.S., Yaashikaa, P.R. and Yuvaraj, D. 2019. Removal of toxic pollutants from water environment by phytoremediation: a survey on application and future prospects. Environ. Technol. Innov., 13: 264-276. DOI: 10.1016/j.eti.2018.12.007

Jiang, J.Q., Zhou, Z. and Sharma, V.K. 2013. Occurrence, transportation, monitoring and treatment of emerging micro-pollutants in wastewater - a review from global views. Microchem. J., 110: 292-300. DOI: 10.1016/j.microc.2013.04.014

Khoiriyah, S., Suranto, Setyono, P. and Gravitiani, E. 2019. Phenol contaminant of Bengawan Solo River and characteristics of Portulaca using flavonoid, saponin and tannin for phytoremediation purposes. Biodiversitas, 20(11): 3269-3274. DOI: 10.13057/biodiv/d201120

Khoiriyah, S. 2021. Konservasi Air Tercemar Limbah Estrogenik Berbasis Agen Hayati Dan Valuasi Ekonomi Di Sub DAS Bengawan Solo. [Dissertation]. Sebelas Maret University, Surakarta [Indonesian].

Kumar, G.H. and Kumari, J.P. 2015. Heavy metal lead influative toxicity and its assessment in phytoremediating plants-A Review. Water Air Soil Pollut., 226: 324. DOI: 10.1007/s11270-015-2547-7

Lou, Y., Luo, H., Hu, T., Li, H., Fu, J. 2013. Toxic effects, uptake, and translocation of Cd and Pb in perennial Ryegrass. Ecotoxicology, 22: 207-214. DOI: 10.1007/s10646-012-1017-x

Liu, Z.H., Lu, G.N., Yin, H., Dang, Z. and Rittmann, B. 2015. Removal of natural estrogens and their conjugates in municipal wastewater treatment plants: A critical review. Environ. Sci. Technol., 49: 5288. DOI: 10.1021/acs.est.5b00399

Maher, E.K., Kassidy, N., O'Malley, M., Dollhopf, M.K., Mayer, B.K. and McNamara, P.J. 2020. Removal of estrogenic compounds from water via energy-efficient sequential electrocoagulation-electrooxidation. Environ. Eng. Sci., 37(2). DOI: 10.1089/ees.2019.0335

Prajapati, M., van Bruggen, J.J.A., Dalu, T. and Malla, R. 2017. Assessing the effectiveness of pollutant removal by macrophytes in a floating wetland for wastewater treatment. Appl. Water Sci., 7(8): 4801-4809. DOI: 10.1007/s13201-017-0625-2

Rattan, S., Zhou, C., Chiang, C., Mahalingam, S., Brehm, E. and Flaws, J.A. 2017. Exposure to endocrine disruptors during adulthood: consequences for female fertility. J. Endocrinol., 233(3): 109-129. DOI: 10.1530/JOE-17-0023

Sabreena, S., Hassan, S., Bhat, S.A., Kumar, V., Ganai, B.A. and Ameen, F. 2022. Phytoremediation of heavy metals: an indispensable contrivance in green remediation technology. Plants, 11(9): 1255. DOI: 10.3390/plants11091255

Shore, L.S. and Shemesh, M. 2016. Estrogen is an environmental pollutant. Bull. Environ. Contam. Toxicol., 97(4). DOI: 10.1007/s00128-016-1873-9

Srivastava, R., Srivastava, V. and Singh, A. 2021. Multipurpose benefits of an underexplored species Purslane (*Portulaca oleracea* L.): A Critical Review. Environ. Manage., *72*(2): 309-320.

Tang, Z., Liu, Z.H., Wang, H., Dang, Z., Yin, H., Zhou, Y. and Liu, Y. 2020. Trace determination of eleven natural estrogens and insights from their occurrence in a municipal wastewater treatment plant and river water. Water Res., 182: 115976. DOI: 10.1016/j.watres.2020.115976

Wang, L., Ji, B., Hu, Y., Liu, R. and Sun, W. 2017. A review on in situ phytoremediation of mine tailings. Chemosphere, 184: 594-600. DOI: 10.1016/j.chemosphere.2017.06.02

Wuana, R.A. and Okieimen, F.E. 2018. Heavy metals in contaminated soils: A review of sources, chemistry, risks and best available strategies for remediation. ISRN Ecol. 2011(1): 402647.

Zhang, J., Deng, H., Wang, D., Chen, Z. and Xu, S. 2013. Toxic heavy metal contamination and risk assessment of street dust in small towns of Shanghai suburban area, China. Environ. Sci. Pollut. Res. Int., 20: 323-332. DOI: 10.1007/s11356-012-0908-y

Nature Environment and Pollution Technology
An International Quarterly Scientific Journal

p-ISSN: 0972-6268
(Print copies up to 2016)
e-ISSN: 2395-3454

Vol. 23 | No. 3 | pp.1647-1654 | 2024

Original Research Paper

https://doi.org/10.46488/NEPT.2024.v23i03.035

Open Access Journal

# Performance Evaluation of Advanced Wastewater Treatment Technologies in Herbal Processing and Extraction Industry

**Avinash Kumar Sharda*, Varinder S. Kanwar*† and Ashok Sharma****
*Department of Civil Engineering, Chitkara University, Himachal Pradesh, India
**Cleantech International Foundation, Chandigarh, India
†Corresponding author: Varinder S. Kanwar; vc@chitkarauniversity.edu.in

**Nat. Env. & Poll. Tech.**
**Website: www.neptjournal.com**

*Received:* 08-03-2023
*Revised:* 03-05-2023
*Accepted:* 29-05-2023

**Key Words:**
Membrane bioreactor
Hydraulic retention time
Pharmaceutical active compounds
Advanced oxidation processes
Mechanical vapor recompression

## ABSTRACT

Due to enormous quantities with hazards and complexity in nature is a big challenge for effective treatment of wastewater from pharmaceutical processes including herbal extraction through conventional methods of distillation. The situation is further aggravated in countries facing high rising population, urbanization, and industrialization resulting in the generation of industrial wastes. The study has been carried out in the herbal extraction industry by conducting stage-wise sampling of ETP based on the conventional method and further coupled with ozonation as an advanced treatment to comply with regulatory standards. Additionally, the same process was studied that implementing the best available technology (BAT) by providing ETP with advanced technology modules such as MBR (membrane bioreactor) + RO + $O_3$ has not only resulted in compliance with standards but also reuse of treated wastewater into the process and utilities has been proved to be techno-economically a viable and sustainable option. Modifying existing aeration tanks and advanced oxidation through ozone injection post-biological treatment has resulted in COD and BOD reduction of 96.42% and 99.0% respectively. Whereas in the case of MBR + RO + $O_3$, the values of pH, BOD, COD, TSS, and sulfide have been observed as 8.32, 2.0 $mg.L^{-1}$, 14.0 $mg.L^{-1}$, 1.0 $mg.L^{-1}$ and 0.0 $mg.L^{-1}$ respectively and 98% recovery of treated effluent, thus saving 44 $KL.day^{-1}$ of freshwater resulting into significant financial benefits of Rupees 12.59 lacs annually, which otherwise was outsourced through tankers.

## INTRODUCTION

The most important food source for human beings is water only and every person has the highest level of consumption in his life cycle thus making its quality a very important issue. Thus, everyone should be concerned about the quality of surface as well as groundwater besides the adverse impacts of effluents entering into it. The removal effect of conventional pollutants such as POPs (Persistent Organic Pollutants has been in the limelight for the last decades and their behavior is well accustomed (Jones et al. 2005, Shahbeig et al. 2013). The wastes from herbal extraction and pharmaceutical processes contain drug residues with high chemical oxygen demand (COD) and Biological Oxygen Demand, pharmaceutically active compounds like hormones, antibodies (PhACs), and toxic organics. The pharmaceutical industries across the world indiscriminately generate huge quantities of residual pharmaceutical ingredients at the outlet of conventional wastewater treatment facilities (Parimal & Ritwik 2013). A big problem frequently encountered in handling wastewater from the conventional methods of herbal extraction and pharmaceutical processes is highly variable due to variations like the composition of raw material widely varying from one class of products to another, many pharmaceutical companies use the pretense of confidentiality of composition to escape from regulations of stringent pollution control norms (Parimal & Ritwik 2013).

Incomplete assessment of the magnitude and nature of toxic substances, the process wastes continue to be released into the environment. The irrelevant empirical relations of pharmaceutical ingredients, wastewater characteristics (COD, BOD, TSS, TP, and oil), operational parameters of flow, hydraulic retention time (HRT), and biodegradability index (BOD: COD) (Santos et al. 2009) makes the treatment process further complicated. Though a very high removal rate (80-100 %) is indicated for pharmaceutical products like ibuprofen, ketoprofen, and mefenamic acid, etc. a sludge retention time of around 10-20 days (Jones et al. 2005) is required. The detection of traces of pharmaceutical and personal care products in the discharges after CETPs (Common Effluent Treatment Plants) indicates the presence of persistent compounds organic and inorganic (Hedgespeth et al. 2012).

The other serious issue in the management of toxic wastewater from different industrial processes is mixing with sewage and further transferring to common effluent treatment plants resulting in very complex wastewater difficult to treat effectively. The recovery of these components from the waste waters is economically unfeasible. Under this distracting situation, evaluating the existing treatment technologies, and effective handling of toxic wastewater is necessary to come out with clear solutions for the implementation of advanced and sustainable technologies. The activated sludge can be compared with other similar processes making use of existing structures and equipment where final effluent quality can be improved in case it is subjected to tertiary treatment such as activated carbon adsorption, residual nutrients removal, etc. The overall reduction of selected pharmaceuticals like 68% of tetracycline, 78% for chloro-tetracycline and 68% of doxycycline (Karthikeyan & Meyer 2006, Yang et al. 2005) have been reported, however, the effectiveness gets weaker due to presence of pharmaceuticals active hormones, antibiotics as a residual component in the wastewaters. Now the research studies have established that Advanced Oxidation Processes (AOP) such as Fenton's treatment, ozonation, and Ultra Violet (UV) radiations, and their recombination can be very effective in the treatment of persistent pollutants generated from herbal extraction processes (Tong et al. 2011, Gupta et al. 2009, Sharma et al. 2013).

These (AOPs)s can be further coupled with the existing conventional activated sludge processes to meet regulatory requirements due to the enforcement of stricter discharge standards besides compliance with the orders of the Hon'ble courts. However, such measures without any resources add to treatment costs. So, the best option in the current situation is implementing a combination of advanced treatment and oxidation processes shall be effective for the removal of toxic residues in the final discharge besides resource recovery through the reuse of treated effluent into the process thus making the treatment sustainable in case these processes are further aided with ultra-filtration. The MBR-Ozone process can achieve the removal of antibiotic acetaminophen up to 98.4%. (Shahbeig et al. 2016)

## MATERIALS AND METHODS

### Background

The existing Effluent Treatment Plant of the unit manufacturing Colchicine (1200 kg per year) and Thiocolchicoside (1200 kg per year) was selected for the study. The unit was not able to comply with discharge standards due to the complex type of toxic chemicals being used in the process. The capacity of the old and new ETP is 30 KLD and 100 KLD respectively comprising physical chemical and biological treatment followed by tertiary treatment. There were numerous public complaints of old ETP regarding the discharge of effluent with inadequate treatment. The unit was under the surveillance radar of regulatory agencies. The treated effluent is being discharged into nearby Nalla having average values of BOD and COD exceeding the discharge standards prescribed as shown in Table 1.

Table 1: Effluent characteristics prior to modification.

| Sl. No. | Parameters | Average Values in $mg.L^{-1}$ except pH | Prescribed limits |
|---|---|---|---|
| 1. | pH | 6.23 | 5.5-9.0 |
| 2. | TSS | 73 | 100 |
| 3. | BOD | 240 | 30 |
| 4. | COD | 420 | 250 |
| 5. | Sulfide | 1.6 | 2.0 |

Accordingly, the unit modified the ETP by replacing the existing perforated pipe with a type diffuser to produce fine bubbles which have further resulted in sufficient oxygenation in the aeration tank along with injection of ozone post-biological treatment. The flow chart of the ETP (Old) is as below.

The performance evaluation of different treatment units was carried out by conducting the stage-wise sampling of the effluent treatment plant. The reduction in values of other parameters after primary treatment has been observed for BOD and COD. The values of TSS have been increased in the aeration tank showing proper growth of MLSS and effective mass oxygen transfer after the replacement of the coarse bubble pipe diffuser with dome type. It has also been observed that the percentage of COD and BOD reduction after biological treatment has been observed as 96.42% and 99.48% respectively. Percentage reduction of sulfide values has been observed as 53.93% indicating low removal rates of sulfide. However, after injection of ozone post-biological treatment, a higher reduction in the values of sulfide levels has been observed with percentage removal reported as 67.66% and complying with discharge standards. The overall reduction in the values has been shown in Table 2 from where it can be inferred that there has been a reduction in all the

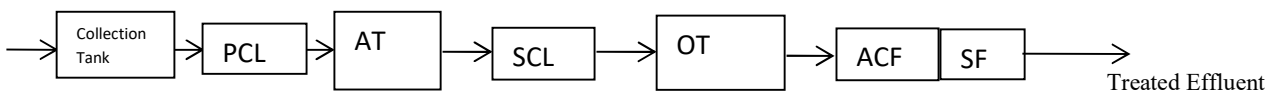


PCL- Primary Clarifier, AT- Aeration Tank, SCL- Secondary Clarifier, OT- Ozonation Tank, ACF- Activated Carbon Filter, SF- Sand Filter

Table 2: Stage-wise reduction (%).

| Parameters | Collection Tank | After Primary Treatment | After Secondary Treatment System (Biological) | Final Outlet after Tertiary treatment |
|---|---|---|---|---|
| TSS ($mg.L^{-1}$) | 430 | 186 | 58 | 58 |
| % Reduction | | 56.74 | 68.81 | 0 |
| COD ($mg.L^{-1}$) | 5930 | 4453 | 159.33 | 181 |
| %Reduction | | 24.90 | 96.42 | 0 |
| BOD ($mg.L^{-1}$) | 4080 | 2541 | 13 | 12.5 |
| % Reduction | | 37.72 | 99.48 | 3.84 |
| Sulfide ($mg.L^{-1}$) | 10.33 | 9.4 | 4.33 | 1.4 |
| % Reduction | | 9.00 | 53.93 | 67.66 |

parameters due to the replacement of coarse bubble diffuser with dome type besides injection of ozone post-biological treatment. The results regarding stage-wise reduction have been shown graphically in Fig.1 to 4.

Before modification of the ETP based on conventional treatment, the unit was not complying with the discharge standards and keeping in view the stage-wise sampling conducted to evaluate performance after the existing conventional ASP treatment was modified by increasing mass oxygen transfer and injection of ozone after secondary treatment has resulted into regulatory compliance. It has also been observed that values of sulfide have been reduced

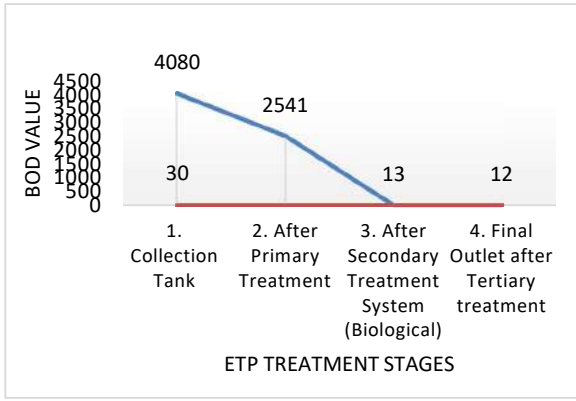


Fig. 1: Stage-wise BOD reduction.

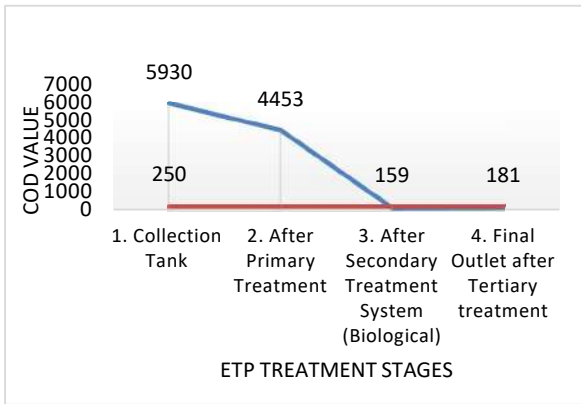


Fig. 2: Stage-wise COD reduction.

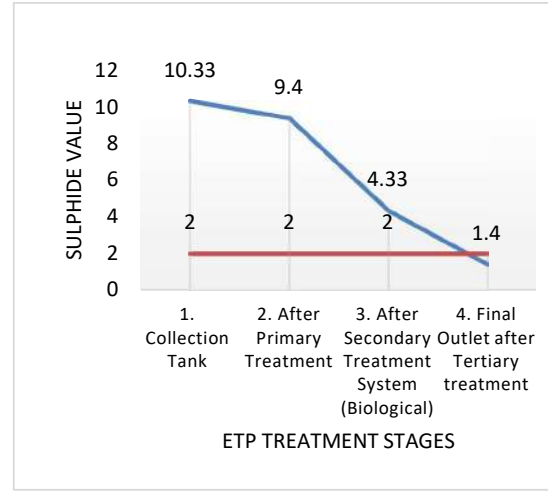


Fig. 3: Stage-wise COD Reduction.

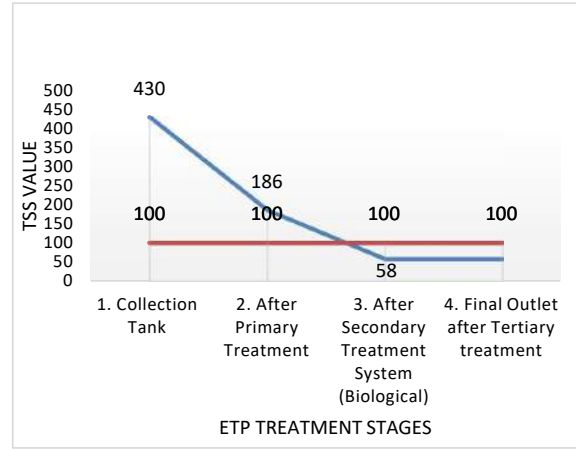


Fig. 4: Stage-wise Sulfide Reduction.

Table 3: Comparative values of results at the final outlet of ETP.

| Sr. No. | Parameters | Pre-modification | Post-Modification | Prescribed limits |
|---|---|---|---|---|
| 1. | pH | 6.23 | 7.56 | 5.5-9.0 |
| 2. | TSS ($mg.L^{-1}$) | 73 | 58 | 100 |
| 3. | BOD ($mg.L^{-1}$) | 240 | 12.5 | 30 |
| 4. | COD ($mg.L^{-1}$) | 420 | 181 | 250 |
| 5. | Sulfide ($mg.L^{-1}$) | 1.6 | 1.4 | 2.0 |

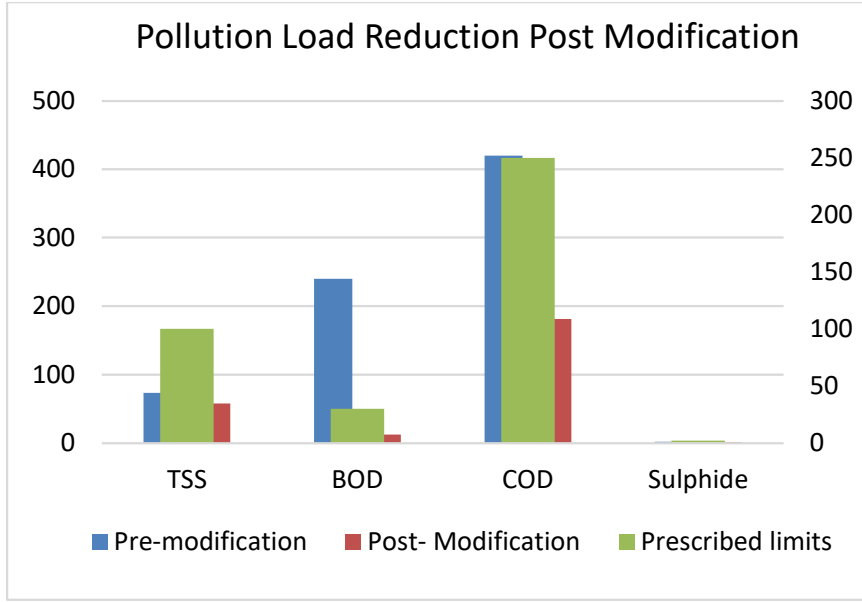


Fig. 5: Pollution load reduction post-modification.

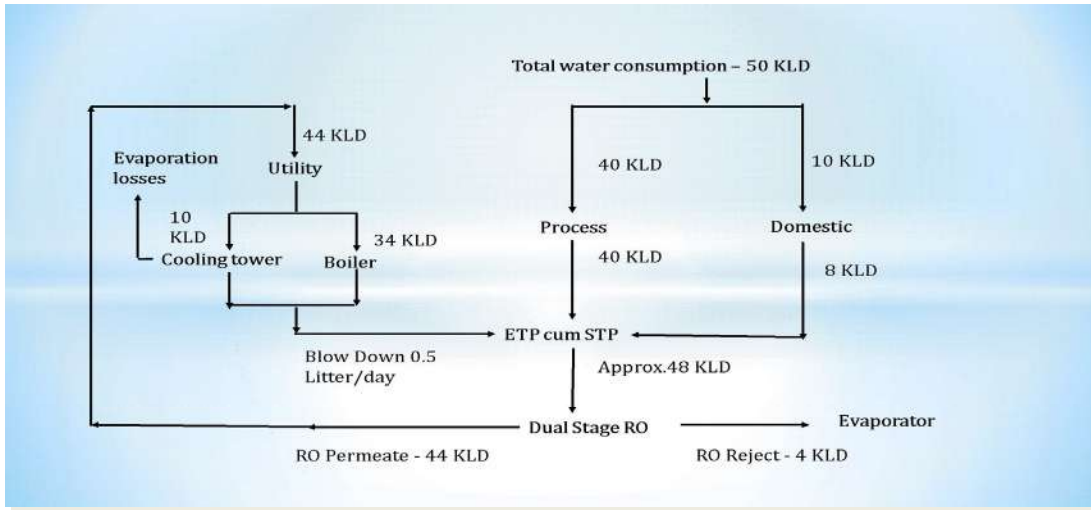


Fig. 6: Water balance after enhancement in production capacity.

considerably after ozone treatment. The analysis results of various parameters pre and post-final out have been shown in Table 3 and graphically represented in Fig. 5. The results shown in Table 3 indicate that post modification the unit is complying with discharge norms; however, it is pertinent to mention that there was no reuse of treated effluent. In the

Table 4: Stage-wise results post implementation of MBR and Advance Technologies.

| Treatment Stage | Parameters | | | | | | | |
|---|---|---|---|---|---|---|---|---|
| | TSS | Removal % | COD (mg.L$^{-1}$) | Removal % | BOD (mg.L$^{-1}$) | Removal % | O&G (mg.L$^{-1}$) | Removal % |
| Collection Tank | 980 | | 10500 | | 3500 | | 16 | |
| Anaerobic (1$^{st}$ Stage) | 294 | 70 | 5250 | 50 | 1225 | 65 | 9.6 | 40 |
| Anaerobic (2nd Stage) | 71 | 76 | 1857 | 65 | 306 | 67 | 4.3 | 55 |
| Aeration + MBR | 7 | 90 | 275 | 85 | 16 | 95 | 3 | 30 |
| RO Outlet + Ozone | 1 | 98 | 14 | 95 | 2 | 95 | 0 | 100 |

meantime, due to increased market demand for products, the unit was in process for further enhancement in the production capacities where the effluent load besides water consumption from the process shall be increased.

The water balance according to enhanced capacity is shown in the Fig. 6.

Keeping in view experience and targeting stricter environmental norms a new ETP of capacity 110 KLD was installed by replacing the old one. However, the management was indecisive about the selection of proper treatment technologies. Accordingly, the management took the decision and implemented a proposal based on advanced technology such as two-stage anaerobic treatment, MBR (Membrane Bio Reactor) further coupled with Ozone and RO treatment to meet ZLD (Zero Liquid Discharge) requirements, keeping in view the following advantages are being foreseen in the new ETP with MBR as main module being implemented by the unit as below.

a) Due to the use of a membrane bioreactor, the life RO membrane is increased from 4 months to about 8 months. In addition to this, there is considerable saving on account of water cost being outsourced.

b) By implementation of MBR coupled with an RO filtration system, the area requirement shall be on the lesser side in comparison to MBBR. ETP with MBR module shall occupy 30% less space.

c) The treated effluent can be reused in the process besides toilet flushing and on land irrigation resulting in the conservation of natural sources besides the removal of inert organics. Without MBR+RO+$O_3$, 50KL of fresh water was being outsourced through tankers costing around Rs. 50/KL (incl. cost of water + transportation). Post implementation of these advanced technologies with the MBR module 85-90% of daily freshwater consumption has been reduced thus saving around Rs. 10-12 lakhs annually

d) The lower power consumption in the case of MBR shall result in savings of around Rs. 2 Lakhs annually in comparison to MBBR.

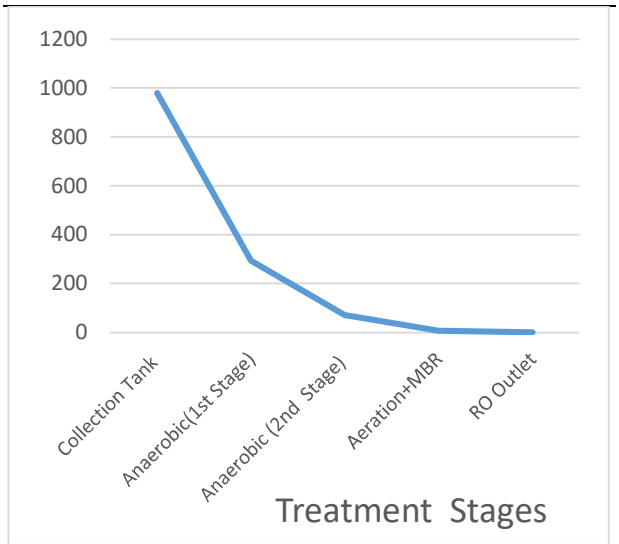


Fig. 7: Stage-wise reduction of TSS.

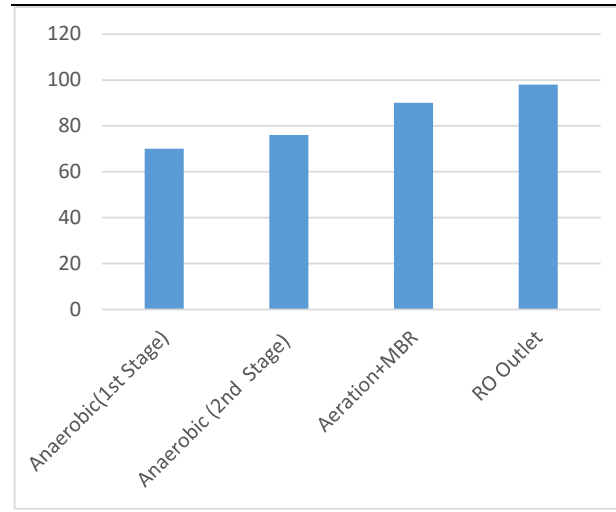


Fig. 8: Percentage of TSS removal stage-wise.

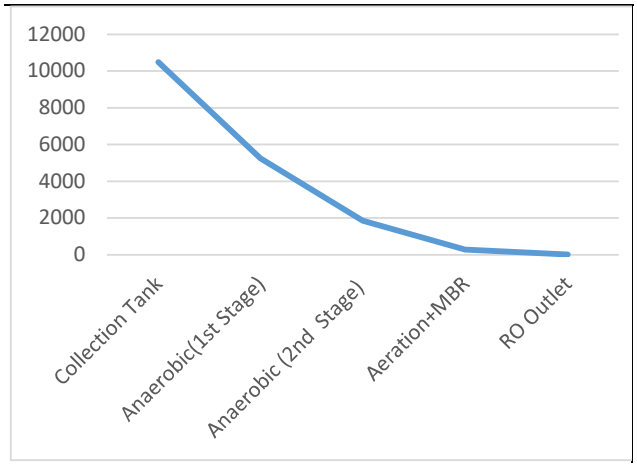


Fig. 9: Stage-wise reduction of COD.

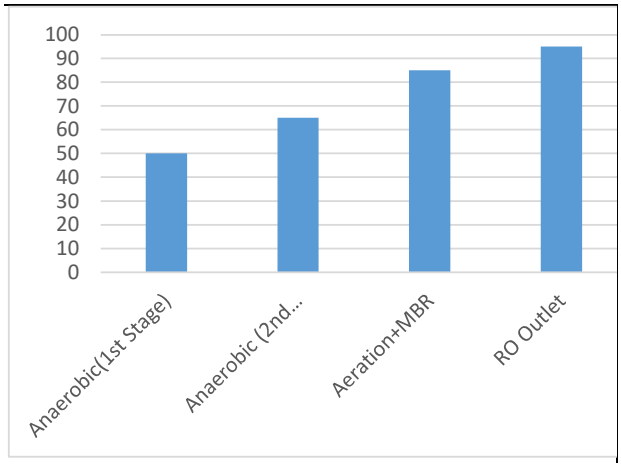


Fig. 10: Percentage COD removal stage-wise.

The stage-wise reduction of parameters such as BOD, COD, TSS, and Oil and Grease have been shown in Table 4 and graphically is represented in Figs. 7 to 12.

It can be inferred from Table 4 and Figs. 7 to 12 that maximum COD removal efficiencies have been observed as 85% and 95% for aeration + MBR + $O_3$ and RO outlet whereas BOD removal efficiencies have been observed as 95% in both situations and the treated wastewater is reused in the process. Due to the use of a membrane bioreactor the life RO membrane is increased.

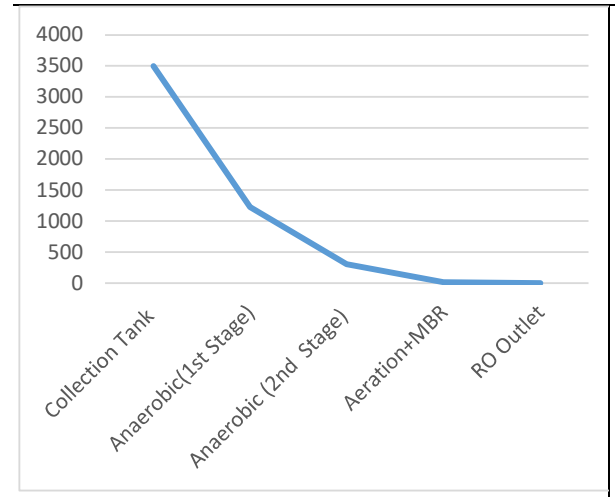


Fig. 11: Stage-wise reduction of BOD.

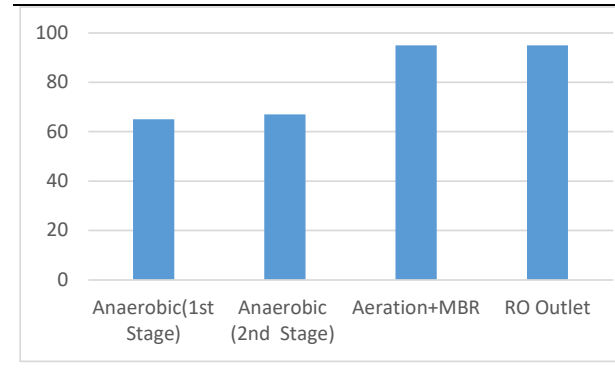


Fig. 12: Percentage BOD removal stage-wise.

The comparative values of various parameters post modifications in the conventional treatment system and the combination of MBR + RO + Ozone are shown in Table 5 and represented graphically in Figs. 13.

Table 5: Comparative values of results at the final outlet of ETP.

| Sl. No. | Parameter | Post-Modification (Conventional + Ozone) | MBR+RO+$O_3$ | Prescribed limits |
|---|---|---|---|---|
| 1. | pH | 7.56 | 8.32 | 7.50 |
| 2. | TSS (mg.$L^{-1}$) | 58 | 1.0 | 100 |
| 3. | BOD (mg.$L^{-1}$) | 12.5 | 2 | 30 |
| 4. | COD (mg.$L^{-1}$) | 181 | 14 | 250 |
| 5. | Sulfide (mg.$L^{-1}$) | 1.4 | 0.0 | 2.0 |

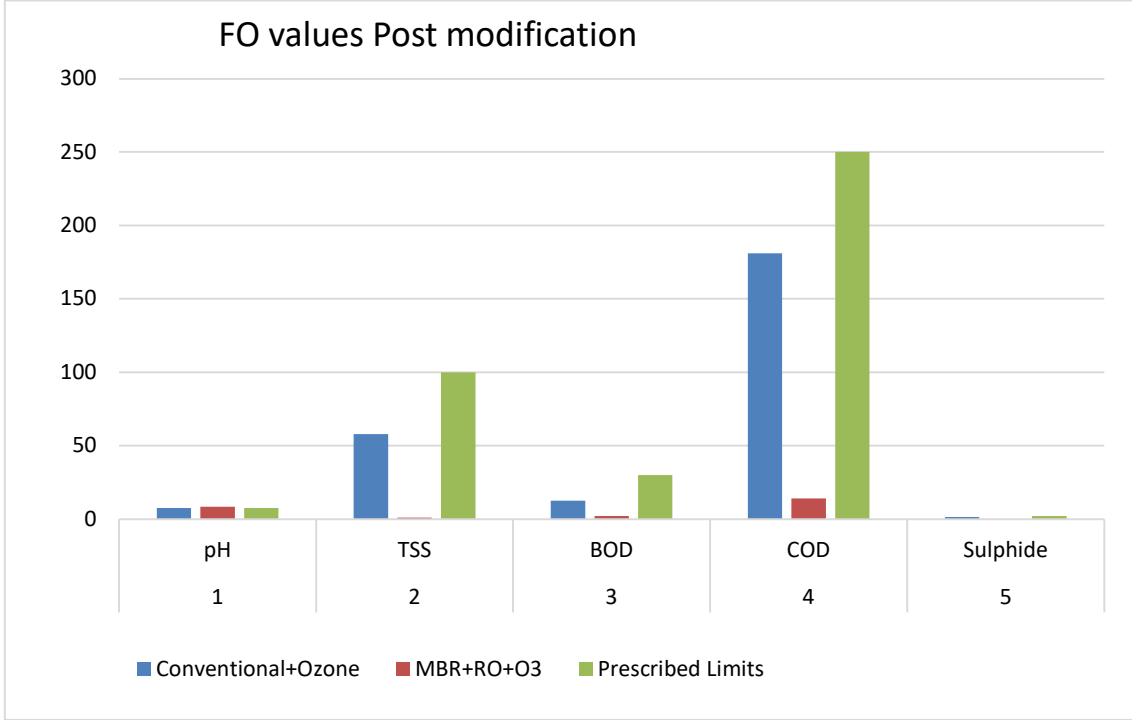


Fig. 13: Final outlet values post-modification.

## CONCLUSION AND RECOMMENDATIONS

The overall reduction of 99.48% in the case of BOD, 96.42% in the case of COD, 68.81% in the case of TSS, and 53.93% has been reported due to an increase in mass oxygen transfer after the replacement of coarse bubble diffuser with fine bubble besides injection of ozone post-biological treatment based on a conventional system. It has been further established that a combination of advanced treatment (MBR) coupled with ozone has resulted in further improvement in the overall treatment by reduction of BOD, COD, TSS, and Sulfide by 99.8%, 99.0%, 93.75%, and 94.80% respectively and shall result into 98% recovery of treated effluent and saving 44 KLD of fresh water and financial benefits of Rs. 12.59 Lakhs annually besides reusing treated wastewater for toilet flushing, irrigation as resource recovery option. In addition to this, the area requirement for secondary clarification is almost negligible. Therefore, the use of advanced treatment technologies comprised of membrane bioreactor further coupled with RO and ozonation is recommended for complex organic wastes generated from herbal extraction and bulk drug manufacturing industries. The management of RO reject is an issue in this situation due to high TDS, accordingly subjecting the same to MVR (Mechanical Vapor Recompression) System can also be recommended.

## REFERENCES

Gupta, V.K., Carrott, P.J.M., Carrott, M.M.L.R. and Suhas, T.L. 2009. Low-cost adsorbents: Growing approach to wastewater treatment. J. Environ. Sci. Technol., 39(10): 783-842.

Hedgespeth, M.L., Sapozhnikova, Y., Pennington, P., Clum, A., Fairy, A. and Wirth, E. 2012. Pharmaceuticals and personal care products (PPCPs) in treated wastewater charges and Charleston Harbor, South Carolina. Sci. J. Total Environ., 437: 1-9.

Jones, O.A., Lester, I.N. and Voulvoulis, N. 2005. A threat to drinking water. J. Trends Biotechnol., 23: 163-167.

Jones, O.A.H., Voulvoulis, N. and Lester, J.N. 2005. Human pharmaceuticals in wastewater treatment processes. Int. J. Environ. Sci. Technol., 35(4): 401-427.

Karthikeyan, K.G. and Meyer, M.T. 2006. Occurrence of antibiotics in wastewater treatment facilities in Wisconsin, USA. Sci. J. Total Environ., 361: 196-207.

Parimal, P. and Ritwik, T. 2017. Pharmaceutical waste treatment and disposal of concentrated rejects: A review. Int. J. Eng. Technol. Sci. Res., *4*(9): 2394-3386.

Santos, J.L., Aparicio, I., Callejón, M. and Alonso, E. 2009. Occurrence of pharmaceutically active compounds during 1-year period in wastewaters from four wastewater treatment plants in Seville (Spain). J. Hazard. Mater., 164(2-3): 1509-1516.

Sharma, S., Mukhopadhaya, M. and Murthy, Z.V.P. 2013. Treatment of chlorophenols from wastewater by advanced oxidation processes. Sep. Purif. Rev., 42(4): 263-295.

Shahbeig, H., Bagheri, N., Ghorbanian, S.A. and Poorkarimi, S. 2013. A new adsorption isotherm model of aqueous solutions on granular activated carbon. J. World Simul., 9: 243-254.

Shahbeig, H., Mehrnia, M.R., Mohammadi, A.R., Moghaddam, P.E. and Rouni, M.R. 2016. Pharmaceutical wastewater

treatment using membrane-bioreactor-ozonation system. 31(1): 57-63.

Tong, A.Y.C., Peake, B.M. and Braund, R. 2011. Disposal practices for unused medications around the world. Int. J. Environ., 37(1): 292-298.

Yang, S., Cha, J. and Carlson, K. 2005. Simultaneous extraction and analysis of 11 tetracycline and sulfonamide antibiotics in influent and effluent domestic wastewater by solid phase extraction and liquid chromatography-electrospray ionization tandem mass spectrometry. J. Chromatogr., 1097(1-2): 40-53.

Nature Environment and Pollution Technology
An International Quarterly Scientific Journal

p-ISSN: 0972-6268
(Print copies up to 2016)
e-ISSN: 2395-3454

Vol. 23 | No. 3 | pp. 1655-1661 | 2024

Original Research Paper

https://doi.org/10.46488/NEPT.2024.v23i03.036

Open Access Journal

# Evaluating the Stages of Environmental Pollution and Vital Indicators in the Qayyarah Refinery Area, Mosul, Iraq

**Juomana Jabbar Saeed***, **Maryam Jasim Hasan***, **Estabraq Mohammed Ati****, **Reyam Naji Ajmi**†**, **Abdalkader Saeed Latif***** and **Hala Ahmed Rasheed***

*College of Science, Mustansiriyah University, Baghdad, Iraq
**Department of Biology Science, Mustansiriyah University, Baghdad, Iraq
***National University of Science and Technology, College of Health and Medical Technology, Nasiriyah, Dhi Qar, Iraq
†Corresponding author: Reyam Naji Ajmi; reyam80a@yahoo.com

**Nat. Env. & Poll. Tech.**
**Website: www.neptjournal.com**

*Received:* 12-12-2023
*Revised:* 19-01-2024
*Accepted:* 01-02-2024

**Key Words:**
Environmental pollution
Qayyarah refinery area
Oil spill
Toxic chemicals

## ABSTRACT

Oil spills can have varying degrees of impact on the aquatic environment depending on factors such as the type of oil spilled, the volume released, and the ecosystem affected because crude oil and refined petroleum contain harmful substances such as hydrocarbons, heavy metals, and toxic chemicals. When released into the water, these substances can have immediate and long-term effects on marine life. This research aims to find the factors affecting the degree of pollution from oil spills on the aquatic environment and the areas adjacent to the Qayyarah refinery in northern Iraq. Combines the fuzzy comprehensive evaluation method and the analytical hierarchy process to evaluate the degree of pollution from oil spill incidents in the areas adjacent to the refinery. The statistical analysis showed that there were statistically significant differences and that the value of the correlation coefficient was positive between exchanged cadmium, residual cadmium, exchanged lead, where the lead exchange rate ranged correlation coefficient at a minimum $R^2$ 0.674 and a clear increase in the number of bacteria indicating contamination the total number of bacteria coli, fecal coliform bacteria, and fecal strep bacteria (where the numbers of coliform bacteria ranged 102 × 102- (cells/011 mL, and fecal coliform bacteria were between 160 × 102 cells/011 mL. These rates are environmental and vital indicators of the presence of significant levels of organic pollution and evidence of the presence of microorganisms dangerous to the health of residents and living organisms.

## INTRODUCTION

The topic of oil pollution emerged due to the swift technological advancements in the oil industry, resulting in heightened production and irregular utilization. However, oil refineries are considered important sources of water pollution because the refineries use water during the process and dispose of it (Cuong & Hong-Xiang 2019).

Oil contaminants stand out as significant water pollutants, known for their swift dispersion, reaching distances up to 110 km from the spill site, manifest in diverse forms originating from various petroleum activities such as extraction, refining, manufacturing, transportation, and more. Hydrocarbons represent the primary components of petroleum pollutants the most important of which are aliphatic compounds, aromatic compounds, aromatic compounds, asphaltenes, and mineral compounds (Jie et al. 2013). These pollutants enter the aquatic environment in several ways, the most important of which are spills as a result of accidents and during the unloading and loading of tankers, which causes cases of pollution (Ajmi et al. 2018).

Pollution of seawater, rivers, and soil with petroleum derivatives is considered one of the most dangerous pollutants in the world, because of its harmful impact on human health, the marine and terrestrial environment, as well as the economy, so companies and entities working in the field of oil, oil wealth, and maritime transport must develop plans to prevent it due to its high toxicity owing to the toxic gases that are released upon evaporation such as hydrogen sulfide and other gases that prevent sunlight to reach plants (Li et al. 2017). Insufficient light for plant organisms causes an imbalance in the food chain, which in turn leads to a sharp decline in fish stocks. Oil flow leads to groundwater pollution, especially when the water formations have high permeability, which facilitates oil leakage. The multiple forms of interaction and diffusion of oil in nature are: diffusion Natural decomposition, Evaporation

and Dispersion, Precipitation, oxidation, dissolution, Biodegradation, and bacterial decomposition (Wang et al. 2020).

The oil refining industry is spread across large parts of Iraq, as large and small refineries are spread over a wide area from north to south, and the waste that is discharged from these refineries varies according to the nature and type of processing units available in the refineries that affect the surrounding environment and throws its waste into the river without a treatment process, and if the treatment processes exist, they are weak and irregular, including the Qayyarah refinery (Do Carmo et al. 2010). This refinery is located in this area, in the southeastern direction of the city of Mosul, 91 km south of the city of Nineveh in northern Iraq. Many special operations are conducted there with the refining of crude oil, which uses large amounts of water; most of this water ends up as waste in the Tigris River, which is one of the most important water resources in the Iraqi environment (Aghajanloo & Pirooz 2011).

The current study aims to evaluate the quality of waste resulting from the Qayyarah refinery treatment station before being treated.

## MATERIALS AND METHODS

Different methods have been to evaluate the degree of pollution due to oil spills in the Qayyarah refinery, the comprehensive evaluation method was adopted in the paper because it takes into account the multiple effects of crude oil, based on the history of the area and accumulative level of pollution resulting from oil spills was based on factors such as oil characteristics, spill location, weather, and hydrological conditions, in addition to emergency measures according to the data source in the refinery to determine pollution factors in the study area and determine standard weights using the subjective method described by (Lang et al. 2011, Han et al. 2018).

The current study was conducted near the Qayyarah refinery located south of the city of Mosul, samples were collected in the period August to September 2023 on the basis of (APHA 2017) to conduct biological and heavy metal tests. Laboratory tests were conducted in the laboratories of the Department of Environment and Quality Control of the Iraqi Ministry of Commerce and were as follows:

### Extraction of Heavy Elements in Water

In the current study, the distribution of heavy metals in the water of the study area was monitored at several levels

### Dissolved Heavy Elements

Water samples were taken from the study sites, and 2 liters of water for each sample was filtered through a type of filter paper and dried at a temperature of 60°C for 12 hours. Add 1.5 mL of concentrated nitric acid for every liter of filtered water samples to preserve the elements in their shape ionic water, and then 1000 mL of filtered water is taken at a temperature of 70°C before drying. The concentrate contains 10 mL of ion-free water, HNO, and 1 mL of acid is added to it. We leave the solution until the dissolution is complete, and then complete the final volume to 25 mL with distilled water. The ions are stored in polyethylene bottles until the concentrations of the element ions are measured using Atomic absorption spectrophotometry, expressed as a result of $\mu g.L^{-1}$ (200).

### Particulate Heavy Elements

The filter papers used to filter the water samples were dried at 20°C for 22 hr and weighed to extract the amount of plankton present in it and then element ions from it with a weight of 0.6 g as for the dry sample, it was placed in special Teflon containers for this purpose and treated with 5 mL of the mixture and heated, concentrated nitric acid, $HNO_3$, and concentrated HCl, heat a plate at a temperature of 20°C and evaporate until almost dry, then add 2 mL of the mixture to it. The two concentrations were mixed in a ratio of 10 to 5. Next, the HF and $HClO_3$ solutions were evaporated. Perchloric acid and leave it until it almost dries, and then the precipitate is dissolved with 30 mL of hydrochloric acid. Ten minutes later, the sample was separated in a centrifuge for 30 min at 2000 rpm, the solution was taken and placed in a 36 mL volumetric bottle, while the precipitate was washed with deionized distilled water. Wash water was added to the volumetric bottle after separating the sediment and the volume was completed to 36 mL, the samples were kept in clean, labeled 36 mL plastic containers to be examined with the flame atomic absorption spectrum, and the result is expressed in $\mu g.g^{-1}$ dry weight according to (Fingas 2011).

### Extraction of Heavy Elements from Sediments

The sediment samples were mixed well after removing the solid and foreign parts, and then dried, it was ground with ceramic mortar and then passed through and stored in special polyethylene containers that are marked exchangeable. The element ions in the exchangeable fraction of the sediment were then extracted as follows: Residual fraction and the remaining fraction according to (Lu & You 2014).

### Extraction of Exchangeable Heavy Elements

Heavy metal ions were extracted from the exchangeable portion of the sediment, and 10 grams of ions were weighed the dried sample was placed in a 60 mL Teflon container

with a tight lid. 30 mL was added to 0.5 mL carefully and carefully, placed in a vibrating device for 50 hr. hours of hydrochloric acid. It was separated by centrifuge at 2000 rpm for 30 min, then the solution was transferred to special plastic bottles were stored until measured using a flame atomic absorption spectrometer according to (Mil'Shtein 2014).

**Extraction of Residual Heavy Elements**

After the exchanged portion of the sediment was extracted, the remaining sediment portion was taken and tested the digestion process to extract the remaining element ions in the sediment was added 20 mL of distilled water free of ions was to the precipitate to eliminate traces of exchanged elements and from used acid was then centrifuged on the samples to quickly get rid of the wash water 2000 rpm for 20 min, then transfer the precipitate quantitatively to a Teflon baker, avoiding any loss of the precipitate. Then the test tube was rinsed several times with deionized distilled water to remove any residue from the sediment stuck to the walls of the tube, and then the washing water was added to the beaker containing the sample evaporated.

The sample was dried until it was nearly dry at 20°C. Then add 5 mL of the mixture to the sediment concentrated nitric and hydrochloric acids in a ratio of (10%) and evaporated at a temperature of 20°C until approximately at the rate of HClO and perchloric acid, 4 HF, then add 2 mL of the hydrofluoric acid mixture, after that, the solution was evaporated until it was almost dry. The precipitate was dissolved with 30 mL of acid 0.5, the solution was left for 10 min, then it was separated by a centrifuge for (N) hydrochloric acid for 30 min at a speed of 2000 rpm, and the solution was placed in a volumetric bottle 36 mL. The sediment was washed. Twice with deionized water, and the rinse water was added to the volumetric bottle after separating the precipitate, then complete the volume to 36 mL and place the solution in clean, marked plastic bottles for examination with Flame atomic absorption spectrum according to (Zhao et al. 2016).

## RESULTS AND DISCUSSION

According to an initial appearance examination by volume and weight, the results of the extraction of elements compounds in the oil residues in the refinery water and sediments including paraffin, naphthenate, precipitated, exchanged, and residual heavy elements, and aromatic hydrocarbons were obtained, this is an indication that the compounds produced during the refining and extraction stage are stable and can remain in water without being decomposed, and this applies to (Sahoo et al. 2016), the greater the intensity and continuity of oil spills, the greater their stability and the longer their retention period increases, with the greater damage to their surroundings. According to (APHA 2017) crude oil levels can be divided into light (>10), medium (10~20), heavy (20~34), and extra thick crude oil (<40).

Compared to our results in Table 1, we note that it is almost dangerous depending on the level of toxicity, persistence, flammability, viscosity, depending on the toxicity and flammability of oil spills resulting from flash depending for the extraction station according to (Zhang & Wang 2015). Through observational evaluation, the flash point level was reached, as the lower the flash point, the greater the risk of oil spillage, through orbital evaluation of the quality of the extracts, petroleum products were divided into lubricating oils and greases (> 125°C), diesel and heavy oil (45~125°C), kerosene (°45~28C), solvent oils and gasoline (< 28°C). The focus was on the level of viscosity, which represents the fluidity of oil spills in the study area, as the higher the viscosity, the greater the value of organic matter assigned to a higher level of oil pollution. This applies to (Wang & Xiao 2010) and this is shown in the distribution form in Fig. 1.

The results of the dissolved, particulate, and residual heavy metals showed that the concentration of dissolved non-sensitized lead and cadmium was 63 $mg.L^{-1}$ in general, and the percentage of cadmium particles ranged from 4.95 to 2.45 ppm in dry weight as a minimum.

The results of the statistical analysis showed that there were no statistically significant differences between the study categories, with a significant positive relationship between dissolved cadmium particles and lead particles,

Table 1: Level sub-indexes of oil properties on site.

| Elements | Dissolved heavy elements in water | Particulate heavy elements in water | Exchangeable heavy elements in water | Residual heavy elements in water |
|---|---|---|---|---|
| Pb | 0.046 | 0.342 | 0.46 | 4.95 |
| Cd | 0.394 | 0.084 | 0.63 | 2.45 |
| Elements | Dissolved heavy elements in Sediments | Particulate heavy elements in Sediments | Exchangeable heavy elements in Sediments | Residual heavy elements in Sediments |
| Pb | 0.901 | 0.984 | 0.054 | 0.122 |
| Cd | 0.999 | 0.768 | 0.074 | 0.046 |

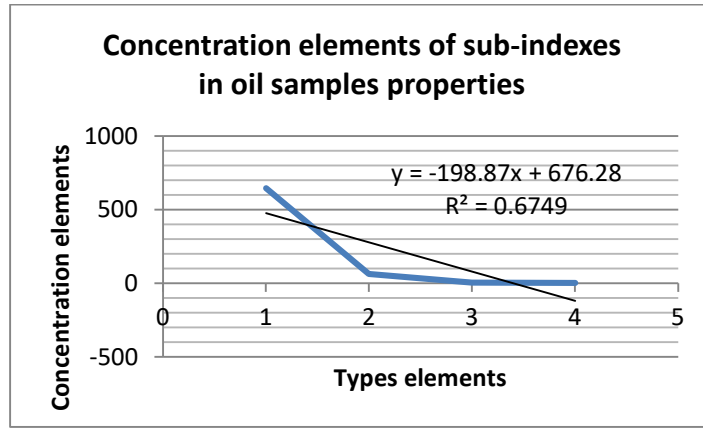


Fig. 1: Concentration elements of sub-indexes of oil properties between elements.

from the water and sediments were also recorded. Given that oil extraction affects the topography and geology of the region and the social conditions and climatic conditions are in their nature, the exploration process and their extraction often leave significant effects that may cause significant damage to it or may cause permanent or temporary changes in it, and it also leaves clear effects on the natural resources and environmental components on the surface of the earth. High concentrations of these two elements were recorded, exceeding the permissible limits internationally and in the Arab world, according to what was mentioned in (Wang & Xiao 2010), that's shown in Fig. 1.

The results of the statistical analysis showed that there were statistically significant differences and that the value of the correlation coefficient was positive between exchanged cadmium, residual cadmium, exchanged lead, and residual lead in Fig. 2, where the lead exchange rate ranged correlation coefficient at a minimum $R^2$ 0.674, and this is consistent with a previous study (Lang et al. 2011). Therefore, studies monitoring oil spill pollution must rely in large part on measuring the concentration of heavy metals in the sediment, especially concerning the remaining quantity, because some factors may affect the re-dissolution of these elements and their return to the water again, and one of the most important of these factors is decomposition during the process. Elements between water and sediments (Lancellotti et al. 2023).

Compared to other studies, the concentration of lead and cadmium was much higher. This may be due to the entry of rainwater laden with clay, silt, and organic materials causing an increase in the concentrations of these elements in the water used to bury oil pollutants, as well as the accumulation of organic biological materials, and this applies according to what he mentioned (Lang et al. 2011).

It was also noted that the concentrations of the remaining elements in the sediments were higher than the exchangeable and short elements in cadmium and lead elements were higher in the exchangeable case. This can be attributed to the introduction of high concentrations resulting from human sources and oxides caused by nearby means of transportation or through wastewater surrounding the area, which contain organic materials that form complexes as a result of dust storms, polluted water and rain, and high concentrations of this element that are carried into river water or any nearby body of water, according to what was mentioned in (Rahmatullah & Ajmi 2022).

This discrepancy in element concentrations between the current studies can be explained by the fact that the final fate of heavy metals in water is their release on plankton or in the form of sediments in water sediments and water sources. Therefore, there are studies on monitoring the pollution of the aquatic environment with heavy metals, and a large part of them must depend on measuring the concentration of heavy metals in sediments, but some factors may influence it. To re-dissolve these elements and return them to the water again, and among these factors is the acidity index and Iraqi studies on different areas of the Euphrates River, relying on sedimentary analytical methods to extract heavy metals from sediments, as well as the degree of sensitivity of the devices used, such as the atomic analysis spectrometer, where they found a variation in the concentrations of the elements. Heavy metals are extracted from soil particles, sediments, dust, and various biological tissues using different mixtures of acids and organic materials (Ajmi et al. 2018).

## Membership Evaluation Indicators

The AHPA references to compare our results are used to

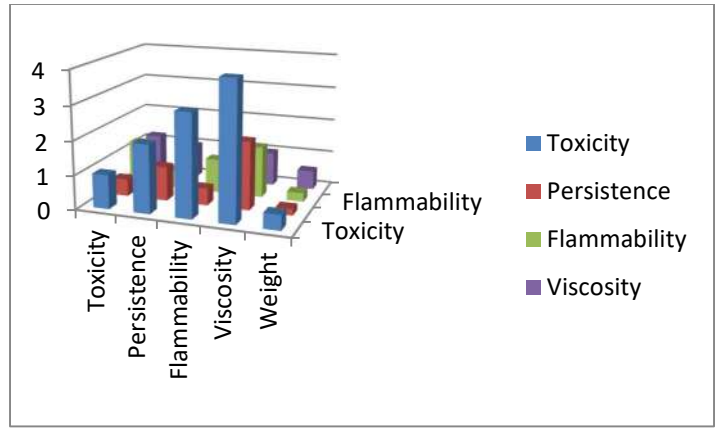


Fig. 2: Membership evaluation indicators elements Level 1.

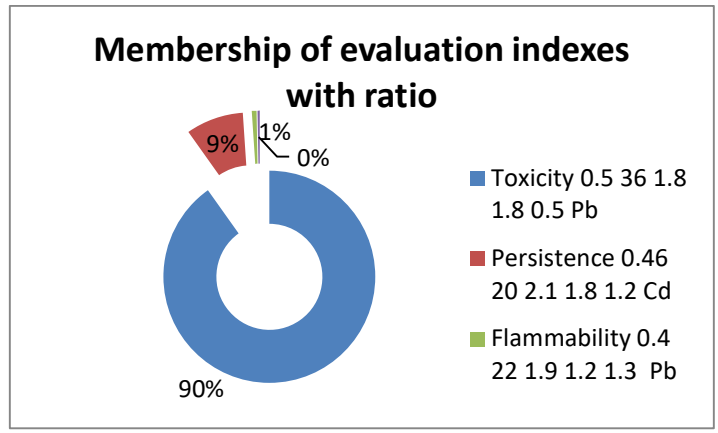


Fig. 3: Membership evaluation indicators elements Level 2.

determine the weight of each indicator and the weights of oil properties and oil spill location respectively in Figs. 2 and 3, levels 1 and 2. It is a level II oil spill pollution classification system, taking oil properties as an example to illustrate the fuzzy comprehensive evaluation process of the first or second level which can be obtained from the membership matrix in the subgroups of toxicity, stability, flammability, and viscosity along with the remaining exchangeable and residual heavy metal concentrations. As an example to illustrate the process level, the overall rating of the membership level R2 can be obtained from the subgroup. Therefore, the overall classification matrix was 90% of toxicity of the study area according to the comprehensive assessment level.

Through the evaluation matrix of pollution levels based on the subgroups of toxicity, stability, flammability, viscosity, and element accumulations, it is considered a second level. Taking the characteristics of the oil as an example to illustrate the level of the process, which amounts to 90 %, which is the result of a comprehensive assessment of the degree of pollution resulting from oil spills on the surface of the sea at the natural level without human influences, according to what was mentioned in (Zhou et al. 2016), to the nature of the bottom, the sediments, the distance it travels, the nature of human activities, and the waste that reaches the river. Therefore, the next step was to detect organic materials, which caused an increase in the evaluation of the level from the first to the second, which is the biological elements, as the presence of coliform bacteria, fecal coliforms, and fecal streptococci that were detected is considered Vital evidence of pollution resulting from drainage water and its ability to persist in areas where petroleum oil is available, as mentioned in (Han et al. 2018).

The actual treatment operations were not carried out in the station except for the process of skimming large oils on the surface of the tanks, and no chemical substance was added to treat the water leaving the refinery. There is no

type of treatment operation on the water leaving the refinery, causing the growth of bacterial colonies that appear in this wastewater is consistent with (Zhao et al. 2016). Therefore, the results of the bacteriological tests were an estimate of the total number of coliform bacteria and fecal coliform bacteria at high levels according to Iraqi specifications and World Health Organization specifications. The presence of this level of bacterial contamination indicates that the Qayyarah refinery environment is vulnerable to organic pollution resulting from water spills, even from conveyor pipes, during pipe leakage incidents, such as corrosion of pipes due to their aging, failure to establish systems to protect against corrosion, and the theft of oil liquids by creating holes in the pipelines.

## CONCLUSION

The process of exploration and extraction often leaves a permanent change in the surrounding environment and is in the form of accumulations resulting from deposition unless preliminary treatment is carried out before discharge. It is in the form of levels according to natural matrices of factors binding to residual and alternative elements and organic materials. The effects related to oil leaks and spills, such as the presence of large quantities of oil ponds and large containers containing crude oil or water with a high percentage of oil spills and leaks lead to significant pollution targeting soil, surface, or groundwater and affect biological and microbiological diversity. Oil is considered one of the most dangerous sources of soil pollution, as it turns it into sterile soil that is unfit for plant and animal life and all living organisms, especially since its accumulations exceed a high level of toxicity, as in our current study, which exceeded 90%, which may lead to complete disruption of the ecosystem. Therefore, it was a process Evaluation of the levels used to set research priorities to determine the permeability of residual and exchangeable elements to learn prevention, response, and mitigation techniques for these organic and microbial contaminants in the future.

## RECOMMENDATIONS

The study can recommend focusing on managing waste resulting from oil pollution and arranging it according to priority, including reducing the amount of oil-contaminated waste, reusing the resources used during the cleaning process, and recycling bulk oil by introducing it into refining streams or stabilizing oil-contaminated materials used in land reclamation projects. or in road construction and restoration, as well as the calorific value of waste materials as fuel for power generation or heating, which is important for getting rid of waste that can only be treated by burning it, burying it in landfills, or converting it into fertilizers to reduce the problems of oil spills.

## ACKNOWLEDGMENT

The authors would like to thank Mustansiriyah University (www.uomustansiriyah.edu.iq) Baghdad-Iraq for its support in the present work and extremely grateful to the National University of Science and Technology / College of Health and Medical Technology for their cooperation and all the people help us to get our data.

## REFERENCES

Aghajanloo, K. and Pirooz, M.D. 2011. The simulation of the oil weathering processes in marine environment. International Conference on Environmental and Computer Science, IPCBEE, 19: 29-34.

Ajmi, R.N., Sultan, M. and Hanno, S.H. 2018. Bioabsorbent of chromium, cadmium and lead from industrial wastewater by waste plant. J. Pharm. Sci. Res., 10(3): 672-674.

Cuong, D.V. and Hong-Xiang, R. 2019. Simulation of Bohai Sea tidal during Penglai 19-3 oil spill accident based on Mike21 model. 2nd Asia Conference on Energy and Environment Engineering (ACEEE), pp. 40-44. DOI: 10.1109/ACEEE.2019.8817047.

Do Carmo, J.A., Pinho, J.L. and Vieira, J.P. 2010. Oil spills in coastal zones: Predicting slick transport and weathering processes. Open Ocean Eng. J., 3(3): 129-142.

Fingas, M., 2011. Weather effects on oil spill countermeasures. In: Oil Spill Science and Technology, pp. 426-339. Gulf Professional Publishing.

Han, Y., Nambi, I.M. and Clement, T.P. 2018. Environmental impacts of the Chennai oil spill accident - A case study. Sci. Total Environ., 626: 795-806.

Jie, G., Xin, L. and Qiang, X. 2013. Characteristics of the Bohai Sea oil spill and its impact on the Bohai Sea ecosystem. Chin Sci Bull., 58(019): 2276-2281.

Lancellotti, B.V., Hensley, D.A. and Stryker, R. 2023. Detection of heavy metals and VOCs in streambed sediment indicates anthropogenic impact on intermittent streams of the U.S. Virgin Islands. Sci Rep., 13(1): 17238. DOI: 10.1038/s41598-023-44455-2.

Lang, Y.H., Cheng, F.F. and Wang, N.N. 2011. Fuzzy comprehensive evaluation of oil spills pollution level for offshore platform. Appl. Mech. Mater., (71-78): 3012-3015.

Li, H., Li, Y. and Li, C. 2017. Bohai and Yellow Sea oil spill prediction system and its application to Huangdao '11.22' Oil Spill Incident. IOP Conf., 81: 012054.

Lu, H. and You, H. 2014. Forecasting the yield of oil field gas with the fuzzy comprehensive evaluation method and the genetic algorithm. Chem. Technol., 9(1): 4-7.

Mil'Shtein, L.M. 2014. Comprehensive evaluation and selection of separators for the oil and gas industry. Chem. Pet. Eng., 49(11-12): 727-735.

Rahmatullah, S.H.A. and Ajmi, R.N. 2022. Anti-pollution caused by genetic variation of plants associated with soil contaminated of petroleum hydrocarbons. Eur. Chem. Bull., 11(7): 33-44.

Sahoo, S., Dhar, A. and Kar, A. 2016. Environmental vulnerability assessment using grey analytic hierarchy process based model. Environ. Impact Assess. Rev., 56: 145-154.

Wang, Y., Lee, K. and Liu, D. 2020. Environmental impact and recovery of the Bohai Sea following the 2011 oil spill. Environ. Pollut., 263(Pt B): 114-343.

Wang, X.L. and Xiao, J.Z. 2010. Multi-objective dynamic programming for the optimal operation of natural gas production and sales. Comput. Commun. Technol. Agric. Eng. Int. Conf., 3: 240-243.

Zhao, J., Jin, J., Zhu, J., Xu, J., Hang, Q., Chen, Y. and Han, D. 2016. Water resources risk assessment model based on the subjective and objective combination weighting methods. Water Resour. Manag., 30(9): 3027-3042.

Zhang, J.Y. and Wang, L.C. 2015. Assessment of water resource security in Chongqing City of China: What has been done and what remains to be done? Nat. Hazards, 75(3): 2751-2772.

## ORCID DETAILS OF THE AUTHORS

Juomana Jabbar Saeed: https://orcid.org/0009-0003-5023-2678
Maryam Jasim Hasan: https://orcid.org/0009-0000-0074-3881
Estabraq Mohammed Ati: https://orcid.org/0000-0002-8411-1060
Reyam Naji Ajmi: https://orcid.org/0000-0003-2623-6671
Abdalkader Saeed Latif: https://orcid.org/0000-0003-1901-9425
Hala Ahmed Rasheed: https://orcid.org/0009-0006-0236-6868

Nature Environment and Pollution Technology
An International Quarterly Scientific Journal

p-ISSN: 0972-6268
(Print copies up to 2016)
e-ISSN: 2395-3454

Vol. 23 | No. 3 | pp. 1663-1669 | 2024

Original Research Paper

https://doi.org/10.46488/NEPT.2024.v23i03.037

Open Access Journal

# Carbon Dioxide Adsorption by Variation in Operating Parameters of Sound Assisted Fluidization Using Coal Based Fine Activated Carbon

**A. P. Ganorkar†** and **A. M. Langde**
Department of Mechanical Engineering, Anjuman College of Engineering and Technology, Nagpur-440001, Maharashtra, India
†Corresponding author: A.P. Ganorkar; apganorkar@rediffmail.com

**Nat. Env. & Poll. Tech.**
**Website: www.neptjournal.com**

*Received:* 12-12-2023
*Revised:* 20-01-2024
*Accepted:* 23-01-2024

**Key Words:**
Activated carbon
Adsorption
Fluidization
Sound assisted fluidization

## ABSTRACT

This research delves into the promising domain of $CO_2$ capture through fine solid activated carbon adsorbent, offering a more energy-efficient alternative to traditional adsorption methods. The central challenge addressed here is the utility of cheaper $CO_2$ adsorbent, fine powder materials whose properties can be precisely tailored via molecular-level fictionalization. Equally vital is selecting an optimal fluidizing column configuration that maximizes $CO_2$ interaction with adsorption particles and enhances adsorption efficiency. The proposed solution is a fluidized bed column uniquely equipped with integrated acoustic vibrations to counteract interparticle forces common in fine powders. For adsorption evaluations, sound-assisted fluidized-bed experimentation on a laboratory size was set up. Adsorbent material activated carbon made up of coal underwent rigorous testing between a range of 20 Hz-200 Hz and 20 dB-135 dB. Results reveal the beneficial effects of acoustic enhancement of fluidization quality and adsorption efficiency, increased adsorption capacity, enhanced bed utilization, and accelerated adsorption rates. Extensive research has been conducted on the detailed effects of major operational variables on adsorption performance, notably frequency, sound intensity, and minimum fluidization velocity. The findings highlight the pivotal role of particle size with mean size 75 microns range as a determinant of adsorption capacity at 100 Hz and 125 dB. At the end of experimentation, the adsorbent considered for the experiment is compared to the study adsorption capacity at operating conditions. The research concludes with a discussion on the effects of influencing parameters for adsorption on employing sound vibrations using fluidization technique adsorption for $CO_2$ capture.

## INTRODUCTION

During the 20th century, there was a surge in energy consumption and global population growth, accompanied by rapid technological progress and material expansion. This transformation resulted in a significant dependence on hydrocarbon fuels and carbon-based electricity production. EPA (Environment Protection Agency) report states that the main source of $CO_2$ is the use of fossil fuels. Indirect human-caused effects on forestry and other land uses, such as deforestation, clearing land for agriculture, and soil degradation, can also release carbon dioxide into the atmosphere. Similarly, land can absorb carbon dioxide from the atmosphere by improving soil, planting new trees, and engaging in other activities. Fossil fuels presently meet more than 80% of the world's energy demands. Still, their combustion generates $CO_2$ emissions, which are responsible for about 75% of human-caused $CO_2$ emissions and have a substantial impact on climate change (Ganorkar & Langde 2023).

The International Energy Agency (IEA) estimates global $CO_2$ emissions from various sources, with power generation responsible for 45% of these emissions (IEA 2022). To address this, carbon capture and storage (CCS) technologies aim to capture $CO_2$ from industrial sources, transport it to storage, and isolate it from the atmosphere for thousands of years. Applications for carbon capture and storage (CCS) have been developed to lower these emissions. Therefore, up to 80% of the global warming potentials released by conventional electricity generation can be avoided by sequestering 96% of the $CO_2$ produced by burning fuels in power plants (Kon & Caner 2024). Successful wide-scale deployment of CCS requires substantial research and development to ensure economic and environmental viability. In light of the information provided, it is evident that post-combustion capture stands out as the most suitable carbon capture and storage (CCS) technology for application in existing power plants. The substantial expense associated with the capture phase, constituting approximately two-thirds

of CCS costs, poses a significant barrier to widespread implementation (Feron & Hendriks 2005). Therefore, the creation of an effective and financially sustainable $CO_2$ adsorption technique is the primary goal. Fighting the anthropogenic emissions of greenhouse gases (GHGs) that cause climate change has become an urgent priority in recent decades (Masson-Delmotte 2021). Chemical absorption using amines, membranes, cryogenic distillation, and selective adsorption on solids is the most developed and most suited technology for removing $CO_2$ from flue gas currently in use (Mathieu 2003). Fluidization is usually difficult with fine powders, which are categorized under Geldart group C because of their small size of particles (<30 μm) and high material density. Fluidization is challenging due to cohesive forces between particles, such as electrostatic, moisture-induced tension on the surface forces, and van der Waals, leading to issues such as plug formation, channeling, and agglomeration (Hakim et al. 2005). Recent tests, however, cast doubt on the predictability of fluidization behavior based on initial particle size and density by indicating that nanoparticles can be fluidized efficiently over a broad range of gas velocities. Because it requires less energy, solid adsorbent-based adsorption is a desirable choice for $CO_2$ capture (Sumida et al. 2012). Regeneration energy and equipment costs are major contributors to capture expenses. Enhancing separation efficiency in capture materials offers significant cost-saving potential. It is crucial to create $CO_2$-specific adsorbents with molecularly tunable physical and chemical characteristics.

A comprehensive 3-D transient heat and mass transfer analysis has been performed to study the adsorption characteristics of carbon dioxide onto highly microporous activated carbon (MaxsorbIII) (Sahoo 2019). A fixed-bed column adsorption system was used to study the adsorption of $CO_2$. This study showed that thermally treated alum sludge at 800°C has a lot of potential as a $CO_2$ adsorbent (Yusuff et al. 2019). Micron-size materials, especially ultra-fine particles, are versatile for customization, allowing improvements in adsorption efficiency. Investigation was carried out of two adsorbates, methanol and acetone, and their adsorption on AC35 activated carbon (Foued & Jemni 2014). When used as an adsorbent for the removal of $CO_2$ and $NO_2$, activated carbon was found to be highly effective at removing $CO_2$(Madiraju et al .2020). Effective modification can involve increasing the surface's $CO_2$ affinity and high adsorption capacity. A variety of raw materials, including coconut shell, wood, peat, and coal, can be used to create activated carbon (AC), which is widely used as an industrial adsorbent and support. Carbon can be chemically modified on the surface to create materials with specific uses (Thakare & Jayaram 2018). Material development must align with practical $CO_2$ separation processes to ensure successful implementation. To achieve efficient fluidization, it is crucial to minimize aggregate size by breaking them apart and overcoming cohesive forces. Externally assisted fluidization, involving forces like acoustics, electricity, magnetism, or mechanical vibrations, can enhance powder dynamics in a fluidized bed. Among these techniques, sound-assisted fluidization is considered a promising option for smoothly fluidizing fine and ultra-fine powders (Raganati et al. 2015). It offers several advantages, including non-intrusiveness, no specific powder requirements, reduction in fine particle elutriation, and cost-effectiveness using readily available equipment like signal generators, audio amplifiers, and loudspeakers.

## MATERIALS AND METHODS

### Experimental Setup

In the pursuit of understanding the intricacies of fluidization behavior and $CO_2$ adsorption capacity, an experimental apparatus on a laboratory scale was employed, illustrated schematically in Fig. 1. The setup features a fluidized bed, a substantial component of which is a transparent PVC column, measuring 50 mm in inner diameter and extending to a height of 800 mm. Situated at the base of this column is a gas distributor with a porous jeans cloth. This apparatus served as the experimental platform, allowing for a detailed exploration of the fluidization phenomena and the adsorption capabilities of $CO_2$ within the bed. The patent office registers this experimental setup design in the name of the authors of this paper (Design No. 366537-001). Through systematic experimentation within this column, crucial insights were gained into the fluid dynamics and adsorption potential of the system, shedding light on its performance and characteristics.

### Apparatus

The experimental setup involved a function generator, amplifier, speaker, sound level meter (RionMake, Japan), and gas analyzer (AVL make). $CO_2$ mass flow controller (Line Take make, Korea). Bed pressure was expertly measured by a U U-tube manometer, whose tapping is situated just 5mm below the gas distributor. To precisely assess the composition of the outlet and inlet gas stream, a gas analyzer was employed. The sonic prowess for enhancing fluidization was achieved via a sound-generation system, a sophisticated arrangement comprising a digital function generator, a sound amplifier for signal amplification, and a capable loudspeaker. The audio system involves a digital function generator producing a specified frequency electric sine wave, amplified by a 40 W audio amplifier and delivered through an 8 W woofer loudspeaker kept above the column in a closed chamber, particularly for high-intensity acoustic fields.

## Physical Characteristics of Coal-Based Activated Carbon

Coal-based Activated carbon purchased from supplier space black adsorbents (Gujarat, India) is used as adsorption material. Morphological characterization of the powder was conducted through SEM analysis, as shown in Fig. 2, in the metallurgy lab of Visvesvaraya National Institute of Technology, Nagpuremploying a Philips XL30 SEM instrument. The resulting powder properties have been meticulously documented and are presented in Table 1, offering a comprehensive overview of their pertinent characteristics.

Table 1: Physical characteristics of coal-based activated carbon.

| | |
|---|---|
| Appearance | Black, Granular |
| Bulk density | 442 $kg.m^{-3}$ |
| Wt. of material loaded in column | 87 g |
| Particle size, MESH(ASTM) | 4%+200 Mesh |

## Conducting Fluidization Experiment

Using $CO_2$ and $N_2$ gas of 99.99% purity, all fluidization tests were conducted under ambient conditions of temperature and pressure. In the trials, the activated carbon materials underwent a meticulous preparation process involving a preheating step, ensuring the complete removal of any residual moisture. Before its utilization for adsorption tests, the activated carbon underwent an extensive fluidization process to evaluate its fluidization behavior under both conventional and sound-assisted conditions. Design Expert Software was used for selecting sound parameters for experimentation, and these conditions encompassed a range of sound intensities (125, 130, 135, and 140 dB) and frequencies (20, 50, 80, 120, and 300 Hz). These sound parameters were in agreement with previously done research

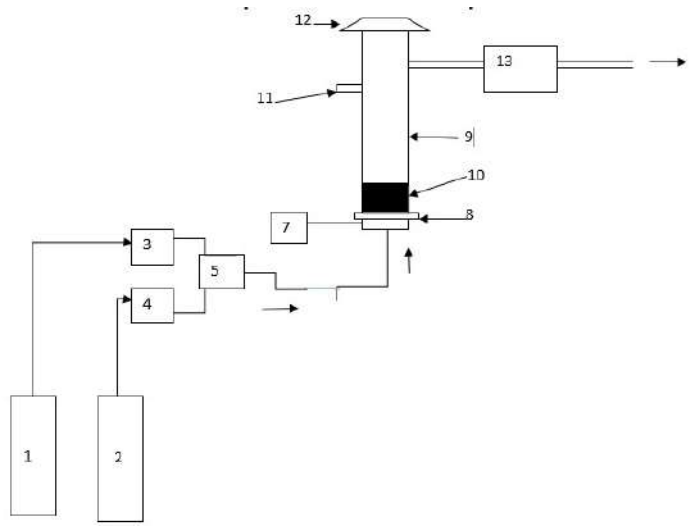


Fig. 1: Experimental setup: (1) $CO_2$ gas cylinder, (2) $N_2$ gas cylinder, (3) $CO_2$ gas mass flow controller, (4) $N_2$ gas rotameter, (5) Gas mixing chamber, (7) Pressure measuring device(U tube manometer), (8) Distributor plate (Jeans cloth), (9) Fluidization column (10) Adsorbent material(Activated carbon powder), (11) Sound level meter,(12) Loudspeaker, (13) Gas analyzer. (14) Microphone

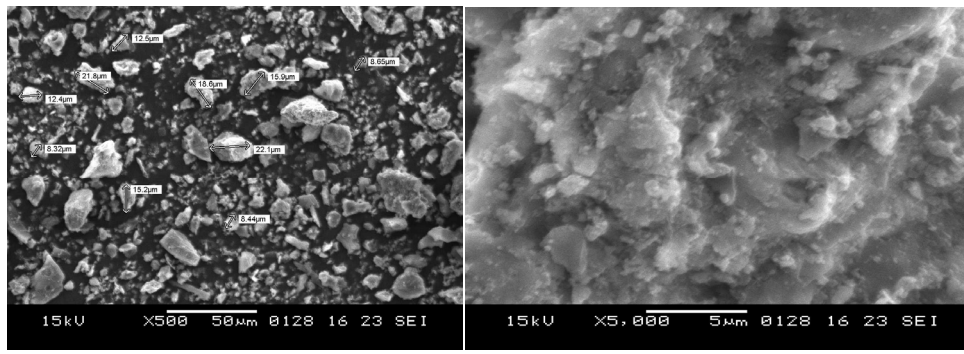


Fig. 2: SEM analysis of coal-based activated carbon.

work (Raganati et al. 2015). It is essential to note that all experiments were meticulously conducted at standard surrounding temperature and pressure, with nitrogen ($N_2$) serving as the fluidizing gas. This choice was made to mitigate the potential increase in powder cohesiveness that can occur due to air moisture. In each experimental run, a precisely measured 87 g (10 cm bed height) of activated carbon was loaded into the fluidization column, ensuring a consistent bed height of approximately 10 cm. Comprehensive data on bed expansion and pressure drop were gathered for each test, including measurements of the superficial gas velocity made both when the $N_2$ flow rate was increasing (UP) and decreasing (DOWN). A graphical process was then used to infer the minimal fluidization velocity ($\mu_{mf}$), as depicted in Fig. 3, from the resulting pressure drop curves (Raganati et al. 2015, Diamantis et al. 2012). Detailed information about the chosen operating conditions and corresponding results for the determining minimum fluidization velocity experiments is discussed in the result section.

### Adsorption Test Procedure

The adsorption tests were executed in standard environmental conditions, and before each test, the activated carbon underwent meticulous heating to eliminate any residual moisture (Raganati & Ammendola 2021). In a typical experiment, precisely 87 g of the activated carbon was loaded into the column, resulting in a consistent bed height of 10 cm. Following this, a pre-conditioning phase lasting approximately 3 min involved the introduction of nitrogen ($N_2$) at a flow rate (around 2.11 pm) that comes from the bottom of the column and corresponds to the minimal fluidization velocity at set values of 100 Hz and 125 dB, ensuring the establishment of stable fluidization conditions. These are the ideal sound parameter values to increase the efficiency of the gas-solid contact and fluidization quality, as concluded from experimentation, which in turn improves the fine-solid materials' capacity to adsorb $CO_2$ without sound characteristics. Subsequently, the core adsorption phase was initiated, introducing controlled flow using a mass flow controller (line tech make, Korea) of a gas mixture of fixed $CO_2$ concentration (15% of $CO_2$ in $N_2$) into the column. The continuous monitoring of $CO_2$ concentration in the outlet gas stream, creating a $CO_2$ outlet concentration profile, was sustained till the gas composition closely matched the initial inlet gas composition (about 90%), indicating that the bed had reached saturation.

Time (t) was noted to establish $CO_2$ concentration profiles, starting from the point at which the gas mixture started to flow through the fluidized column to the gas analyzer. The transit time was accurately recorded from AVL software for a set gas flow rate, a process typically taking around 23 min to reach saturation of activated carbon. This procedure was repeated for 2 test runs using a fresh sample of activated carbon each time for both using sound and without sound parameters. Each adsorption test was performed under both conventional and sound-assisted fluidization conditions, allowing for a comprehensive exploration of the impacts of sound parameters (SPL and frequency), and fluidization velocity, adsorption efficiency.

## RESULTS AND DISCUSSION

### Physical Characteristics

SEM analysis reveals that the powder presents itself in the form of aggregates rather than individual micron-sized particles. On average, the particles have a mean size of approximately 75 microns, following the analysis report provided by the supplier of activated carbon.

### Fluidization Test

The data related to bed expansion were subjected to analysis, facilitating the fluidizing velocity estimation, a process explained in greater detail elsewhere (Raganati et al. 2014, Rashidi & Yusup 2016, Garcia et al. 2011).

In Fig. 4, the provided data illustrates unitless pressure drop and bed expansion curves in standard operating conditions (without sound). To obtain dimensionless pressure drop values, the actual pressure drop (P) was divided by the pressure drop corresponding to the weight of particles per unit area ($P_0$). Likewise, unitless bed expansion values were calculated by dividing the actual bed height (H) by the static bed value ($H_0$), which was set at 10 cm.

It is important to note that under these typical conditions, where no acoustic field is applied, the fluidization quality is notably inadequate and often characterized by channeling (Xu et al. 2022). This is shown by the fact that the approaching pressure ratio value is less than 1. Thus, the introduction of sound is indispensable to establish an appropriate fluidization quality. This transition is closely associated with effectively breaking up the large aggregates formed due to cohesive forces, resulting in smaller, more manageable structures that enhance the fluidization process. A comprehensive examination was conducted, specifically aimed at assessing the most efficient acoustic conditions. This study sought to determine whether it was feasible to identify optimal values for Sound Pressure Level (SPL) and frequency. Results shown in Table 2 indicate that there is no significant effect on fluidization quality over 100 Hz and 125dB operating parameters of sound.

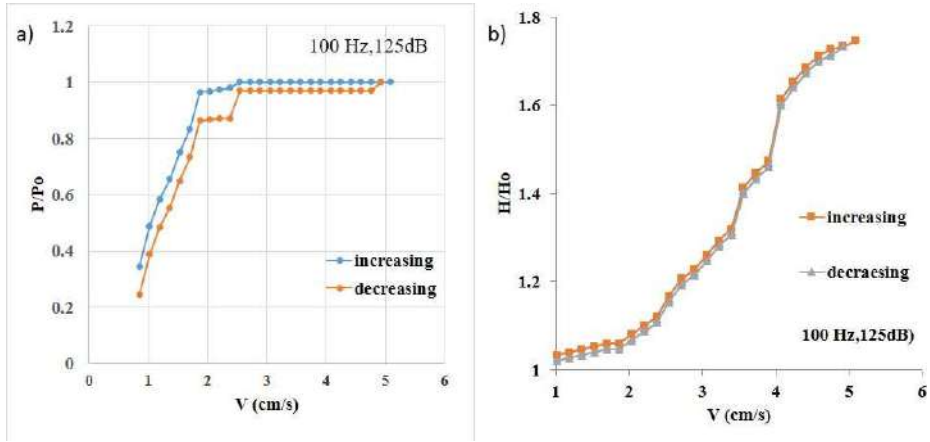


Fig. 3: a) Pressure drop curve Vs velocity of feed gas. b) Bed expansion curve Vs velocity of feed gas at operating sound parameters (100 Hz and 125 dB).

Table 2: Experimental results of minimum fluidization velocities (cm/s) based on the above parameters.

| Frequency | Sound level | | | | | | | |
|---|---|---|---|---|---|---|---|---|
| | 20dB | 50 dB | 80 dB | 100 dB | 120 dB | 125 dB | 130 Db | 135 dB |
| 50Hz | 3.9054 | 3.9054 | 3.7356 | 3.7356 | 3.396 | 3.396 | 3.2262 | 3.2262 |
| 80 Hz | 3.7356 | 3.7356 | 3.5658 | 3.396 | 3.0564 | 3.0564 | 2.8866 | 2.7168 |
| 100 Hz | 3.5658 | 3.396 | 3.0564 | 2.7168 | 2.547 | 2.2074 | 2.2074 | 2.2074 |
| 120 Hz | 3.396 | 3.396 | 3..0564 | 2.7168 | 2.547 | 2.2074 | 2.2074 | 2.2074 |
| 125 Hz | 3.396 | 3.396 | 3..0564 | 2.7168 | 2.547 | 2.2074 | 2.2074 | 2.2074 |
| 150 Hz | 2.3772 | 2.3772 | 2.3772 | 2.3772 | 2.3772 | 2.2074 | 2.2074 | 2.2074 |
| 200 Hz | 2.3772 | 2.3772 | 2.3772 | 2.3772 | 2.3772 | 2.2074 | 2.2074 | 2.2074 |

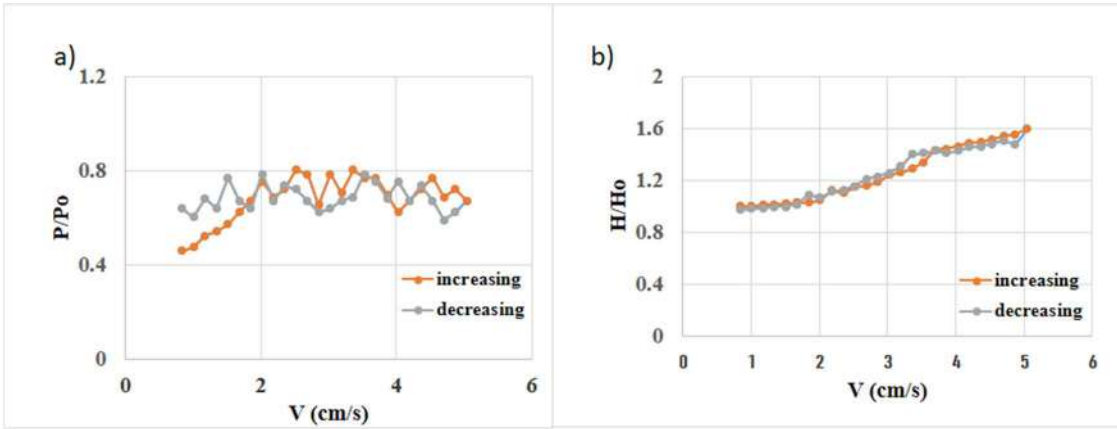


Fig. 4: (a) Pressure drop curves and (b)bed expansion curves acquired during standard tests (without sound).

## Adsorption Capabilities

Every test was run at least twice, and each time, the difference was less than 5% or mostly within the experimental error margin. The typical $CO_2$ outlet concentration curves were found for adsorbent material. After computing these curves, a few more operating parameters were assessed to compare the material's adsorption performance like a. transient time($t_t$), i.e., the time in seconds to reach 90% of inlet $CO_2$ concentration for set sound parameters (100 Hz,125 dB) as shown in Fig. 5

Adsorption time comparison between adsorption capabilities at frequencies lower and higher than 100 Hz at set sound levels of 125 dB and 20 dB (Fig. 6).

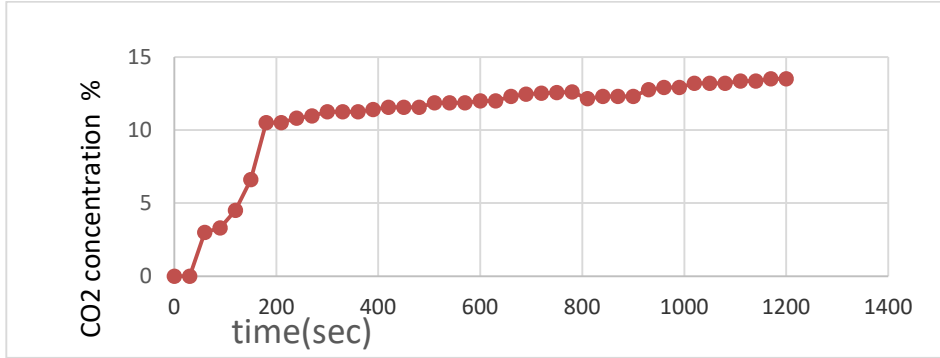


Fig. 5: $CO_2$ Concentration at outlet curve against time ($t_t$) at set sound parameters (100 Hz, 125dB).

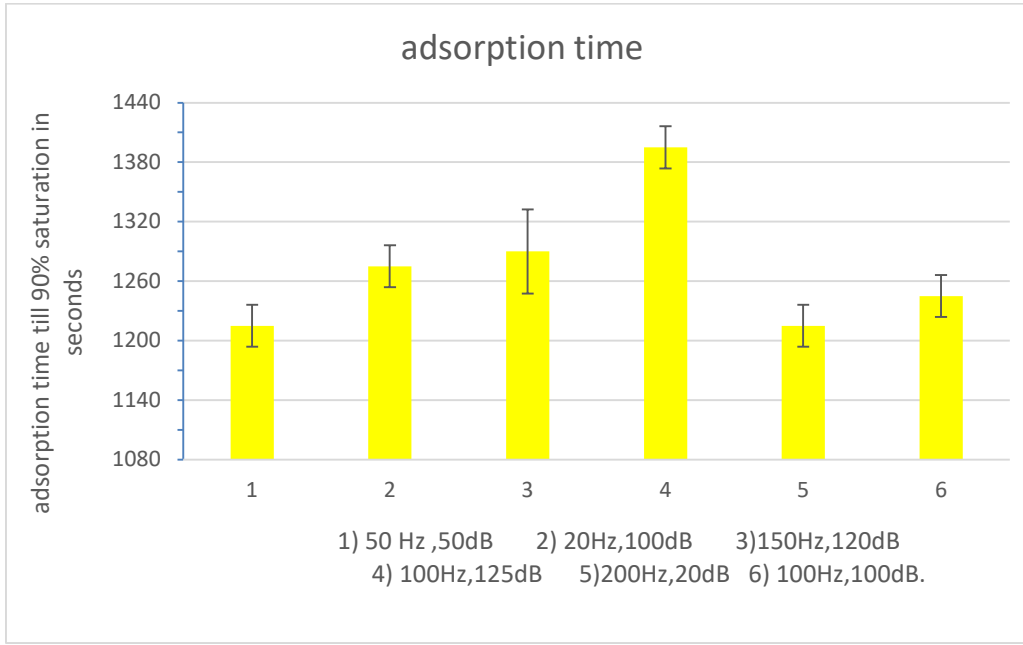


Fig. 6: Comparative analysis of $CO_2$ adsorption time(t) at setsound parameters.

## CONCLUSION

This study compared the $CO_2$ capture capabilities at optimum minimum fluidization velocity of micron-size coal-based activated carbon material. Specifically, audio-assisted fluidization was employed to reduce the limitations on the samples' intrinsic adsorption capacity and boost the gas-solid interaction efficiency. Every adsorption test was carried out using measured $CO_2$ concentrations in a mixture of $CO_2$ and $N_2$ gas at room temperature and pressure. Based on the results, it can be concluded that there is no significant effect on fluidization quality over 100 Hz and 125 dB operating parameters of sound. Moreover, the best $CO_2$ adsorption is found at 100 Hz and 125 dB of sound level parameters in terms of time taken for adsorption. In essence, there is great potential for developing sound-assisted fluidization techniques for CO2 capture to overcome global warming to a greater extent.

## ACKNOWLEDGEMENT

This work is carried out at the research laboratory of Anjuman College of Engineering and Technology, Nagpur. It is financially supported under a research promotion scheme by the All India Council of Technical Education, New Delhi. INDIA. Grant sanction File No 8-130/FDC/RPS (POLICY-1)/2019-20.

## REFERENCES

Diamantis, D.J., Georgiadis, J.G. and Goussis, D.A. 2012. Two-phase modeling of heat and mass transfer in packed bed

absorbers: Implications for process design. J. Porous Media, 15: 5.

Feron, P.H.M. and Hendriks, C.A. 2005. $CO_2$ capture process principles and costs. Oil Gas Sci. Technol., 60: 451-459.

Foued, M. and Jemni, A. 2014. Existence of a characteristic temperature in the case of adsorption on activated carbon. J. Porous Media, 17: 12.

Ganorkar, A.P. and Langde, A. 2023. Experimental investigations of carbon dioxide ($CO_2$) removal through physical adsorption using carbonaceous adsorbents: A review. In AIP Conf. Proc., 2839: 1. AIP Publishing.

Garcia, S., Gil, M.V., Martín, C.F., Pis, J.J., Rubiera, F. and Pevida, C. 2011. Breakthrough adsorption study of a commercial activated carbon for pre-combustion $CO_2$ capture. Chem. Eng. J., 171: 549-556.

Hakim, L.F., Portman, J.L., Casper, M.D. and Weimer, A.W. 2005. Aggregation behavior of nanoparticles in fluidized beds. Powder Technol., 160: 149-160.

IEA. 2022. $CO_2$ Capture at Power Stations and Other Point Sources: Zero Emission Technologies for Fossil Fuels. OECD/IEA, Cedex, France.

Kon, O. and Caner, I. 2024. The social cost of carbon evaluation based on carbon capture and storage technologies for power generation plants. Int. J. Energy Clean Environ., 25: 61.

Masson-Delmotte, V. 2021. Climate Change 2021. The Physical Science Basis. Contrib. Working Group I to the Sixth Assessment Report of the Intergovernmental Panel on Climate Change, p. 2.

Mathieu, P. 2003. Mitigation of $CO_2$ emissions using low and near zero $CO_2$ emission power plants. Int. J. Energy Clean Environ., 4: 1.

Madiraju, S.V.H., Raghunadh, P.V.G. and Kumar, K.R., 2020. Prototype of eco-friendly indoor air purifier to reduce concentrations of $CO_2$, $SO_2$ and $NO_2$. Nat. Environ. Pollut. Technol., 19: 747-753.

Raganati, F. and Ammendola, P. 2021. Sound-assisted fluidization for temperature swing adsorption and calcium looping: A review. Materials, 14: 672.

Raganati, F., Ammendola, P. and Chirone, R. 2015. $CO_2$ capture by adsorption on fine activated carbon in a sound-assisted fluidized bed. Chem. Eng. Trans., 43: 1033-1038.

Raganati, F., Ammendola, P. and Chirone, R., 2014. $CO_2$ capture performances of fine solid sorbents in a sound-assisted fluidized bed. Powder Technol., 268: 347-356.

Rashidi, N.A. and Yusup, S. 2016. An overview of activated carbons utilization for the post-combustion carbon dioxide capture. J. $CO_2$ Util., 13: 1-16.

Sumida, K., Rogow, D.L., Mason, J.A., McDonald, T.M., Bloch, E.D., Herm, Z.R. and Long, J.R. 2012. Carbon dioxide capture in metal-organic frameworks. Chem. Rev., 112: 724-781.

Sahoo, S. 2019. Water as an energy storage medium for $CO_2$ adsorption. In Proc. 25th Natl. 3rd Int. ISHMT-ASTFE Heat Mass Transf. Conf. (IHMTC-2019). Begel House Inc.

Thakare, S.C. and Jayaram, R.V. 2018. Amino-functionalized activated carbon materials in base-catalyzed reactions. Catal. Green Chem. Eng., 1: 2.

Xu, X., Yang, L., Fu, Y., Zhao, Y., Chen, Z., Song, S. and Dong, L. 2022. Enhanced fluidization of solid particles in an oscillating acoustic field. Adv. Powder Technol., 33: 103875.

Yusuff, S.M., Khim, O.K., Yunus, W., Zin, W.M., Ahmad, M., Ibrahim, N.A. and Teoh, C.C. 2019. Isotherms and thermodynamics of $CO_2$ adsorption on thermally treated alum sludge. Nat. Environ. Pollut. Technol., 18: 1.

## ORCID DETAILS OF THE AUTHORS

A. P. Ganorkar : https://orcid.org/0000-0003-1811-9352

Nature Environment and Pollution Technology
An International Quarterly Scientific Journal

p-ISSN: 0972-6268
(Print copies up to 2016)
e-ISSN: 2395-3454

Vol. 23 | No. 3 | pp. 1671-1676 | 2024

Original Research Paper

https://doi.org/10.46488/NEPT.2024.v23i03.038

Open Access Journal

# Assessment of Microplastic Pollution in Fresh Fish and Pindang Fish and its Potential Health Hazards in Coastal Communities of Banyuwangi Regency, Indonesia

**Lilis Sulistyorini*, Novi Dian Arfiani*, Muhammad Addin Rizaldi*, Leka Lutpiatina** and Nurul Izzah Abdul Samad*****

*Department of Environmental Health, Faculty of Public Health, Universitas Airlangga, Surabaya, East Java, 60115, Indonesia

**Medical Laboratory Technology Poltekkes Kemenkes Banjarmasin, Mistar Cokrokusumo Street 4a Banjarbaru, 70714, Indonesia

***Environmental and Occupational Health Programme, School of Health Sciences, Health Campus, Universiti Sains Malaysia, Kubang Kerian, Kelantan, 16150, Malaysia

†Corresponding author: Lilis Sulistyorini; l.sulistyorini@fkm.unair.ac.id

**Nat. Env. & Poll. Tech.**
**Website: www.neptjournal.com**

*Received:* 11-01-2024
*Revised:* 26-02-2024
*Accepted:* 11-03-2024

**Key Words:**
Microplastic pollution
Marine fish
Pindang fish
Public health impacts

## ABSTRACT

This study aimed to analyze the microplastic contamination of fresh and pindang fish and its health impact on the coast of Muncar, Banyuwangi Regency, Indonesia. In this study, a total of 115 respondents participated, providing questionnaire data on their fish consumption habits and health problems. Subsequently, spearman's correlation coefficient, a non-parametric statistical test, was used to analyze the questionnaire data. This study also included 100 samples of marine fish, consisting of 89 fresh fish and 11 pindang fish from various types of marine species. The content of microplastic polymers detected through FTIR (Fourier-Transform Infrared Spectroscopy) was around 3-5 microplastic polymers/fish samples, and the most dominant were Polyethylene, Polyester, Polycaprolactam (Nylon 6) and Polyamide. This study showed that 94 percent of fish samples contained microplastics and only 6 percent of samples did not contain microplastics. The intensity of pindang fish consumption was positively correlated with respondents' health symptoms and problems. Subsequently, implementing effective waste management systems and educational programs in the coastal areas is crucial in reducing the pollution of seawater resulting from inadequate waste disposal practices.

## INTRODUCTION

Plastic is widely used in commercial products and is a significant pollutant in marine environments. According to Jambeck et al. (2015), 192 coastal countries produced 275 million metric tons (MT) of plastic waste in 2010, of which 4.8 to 12.7 million MT entered the sea. Typically, the types of waste found on coasts are made of Polyethylene (PE) materials, such as plastic bags, and polypropylene (PP) materials, for example, packaging products, textiles, and stationery.

Garbage, including plastic waste and microplastics, presents a significant challenge in Indonesia and other regions worldwide. This problem is caused by human activities and inadequate waste management practices. Pollution of marine environments from plastic waste can result from direct and indirect disposal of plastics into the sea, including activities such as oil rigs, fishing, cruises, and land-based activities, especially in densely populated areas where plastic can be transported into the sea by wind, water runoff, or direct discharge (Elizalde-Velázquez et al. 2021). There are two types of microplastics, depending on their source: primary microplastics, which can be associated with plastics produced in microscopic sizes, including scrubbers and pellets (Isobe et al. 2017), and secondary microplastics, resulting from the degradation of microplastics, such as fragments, fibers, or films (Zobkov et al. 2017).

Waste management systems face numerous challenges across different sectors, including Banyuwangi Regency, Indonesia. As the largest district in East Java (5,782.50 $km^2$) with a population growth rate of about 0.44% (BPS 2021), the area has the potential to produce significant

amounts of waste of varying quality. Despite its potential for beach and sea tourism, Banyuwangi Regency experiences environmentally unfriendly dumping of plastic waste into the sea. According to estimates, between 4.8 and 12.7 million tons of plastic waste end up in Indonesian waters (Jambeck et al. 2015).

A study was conducted by Johan et al. on microplastics in the digestive tract of 5 species of fresh fish in Segara Bay, Bengkulu (Johan et al. 2021). While Gunawan et al. studied the meat of 5 types of fresh and pindang fish in northern Bogor (Gunawan et al. 2021). Sawalman et al. conducted a study on the gills, digestive tract, and meat of 3 types of fish at Barranglompo Makassar (Sawalman et al. 2021), and Yona et al. focused on the gills and digestive tract of 12 coral reef fish caught from the waters of small and outer islands of Papua (Liki, Befondi, and Miossu Islands) (Yona et al. 2020). However, there is still limited knowledge on the presence of microplastics in fresh and pindang fish, with a greater number and variety of samples needed, especially along the Banyuwangi coast. Therefore, this study aims to analyze microplastic contamination in fresh and pindang fish and its impact on health on the Muncar coast, Banyuwangi Regency, Indonesia.

## MATERIALS AND METHODS

This observational study examined the presence of microplastic contamination in fresh and pindang fish and their potential health hazards. The study was conducted in the coastal area of Muncar District, Banyuwangi Regency, East Java, Indonesia, from June to December 2022. The study population consisted of people working as fishermen in the coastal village of Tembokrejo, Muncar District, Banyuwangi Regency. A total of 115 respondents participated in the study, providing questionnaire data on their fish consumption habits and health problems. The questionnaires asked respondents about their frequency of consuming fish (1-2 times per week, 2-3 times per week, 3-4 times per week, or every day), the types of fish they consumed in the past week (milkfish, cob, flying fish, semar, or others), and any health symptoms experienced, such as fatigue, cough, shortness of breath, high fever, pain in the mouth area, rashes, abdominal pain, chest pain, indigestion, respiratory problems, dizziness, nausea, and vomiting.

The questionnaire data was then analyzed using simple linear regression to look for the effect of the intensity of fish consumption on health complaints and symptoms. The study also included 100 marine fish samples, consisting of 89 fresh fish and 11 pindang fish from various types of marine fish, including *Heteropriacanthus cruentatus, Sarda orientalis, Euthynnus affinis, Rastrelliger, Caesio erythrogaster, Epinephelus coioides, Sardinella lemuru,* Crustacea, *Helostoma temminckii, Trichiurus lepturus*, and others. The fish samples were tested using the FTIR tool (Thermo Scientific Nicolet iS10) to detect microplastic polymers, in the Laboratory of the Material Institute of Technology Sepuluh Nopember Indonesia. This study has been approved by the ethics committee with certificate number 165/EA/KEPK/2022.

## RESULTS

The research results are presented in Tables 1-4. Table 1 shows that the majority of respondents had a low level of education, with 33% not finishing graduation from elementary school and 31.3% having never attended school. Table 1 also indicates that respondents had low incomes, with about 64.3% earning between 1-1.5 million rupiahs per month.

Table 1: Characteristics of respondents.

| Variable | Category | Frequency | Percentage (%) |
|---|---|---|---|
| Education | No school | 36 | 31,3 |
| | No graduation elementary school | 38 | 33 |
| | Graduation elementary school | 23 | 20 |
| | Graduation junior high school | 12 | 10,4 |
| | Graduation high school | 6 | 5,2 |
| Work | No work | 88 | 76,5 |
| | Work | 27 | 23,5 |
| Income (Rupiah) | < 1 million/month | 6 | 5,2 |
| | 1-1,5 million/month | 74 | 64,3 |
| | 1,5-2 million/month | 33 | 28,7 |
| | 2-2,5 million/month | 2 | 1,7 |

Table 2 shows that five parts were taken as samples, consisting of meat (30 samples), gills (26 samples), skin (26 samples), intestines (18 samples), and stomach (1 sample). The Table reveals that out of 100 fish samples analyzed for microplastics, 94 samples contained microplastics, while only 6 fish samples did not contain microplastics.

Table 3 shows the microplastic polymers detected in fish samples using FTIR. Fresh fish samples contained a variety of polymers, including polyester, polyethylene, polyamide, polyethylene terephthalate, low-density polyethylene, phenol formaldehyde, urea, melamine formaldehyde, and polycaprolactam. meanwhile, pindang fish samples were found to contain polyethylene, polyester, polyamide, and polycaprolactam polymers.

Table 4 shows a linear regression analysis conducted between the intensity of consumption and the type of fresh fish against the complaints and symptoms experienced. Table 4 shows that the value of sig>0.05 which means there is no

Table 2: Microplastics in fish.

| No | Fish Part | Microplastic | | | | | |
|---|---|---|---|---|---|---|---|
| | | Present | % | No Present | % | Total | % |
| 1 | Meat | 29 | 29 | 1 | 1 | 30 | 30 |
| 2 | Gill | 26 | 26 | 0 | 0 | 26 | 26 |
| 3 | Skin | 23 | 23 | 3 | 3 | 26 | 26 |
| 4 | Intestines | 15 | 15 | 2 | 2 | 17 | 17 |
| 5 | Stomach | 1 | 1 | 0 | 0 | 1 | 1 |
| | Sample Total | 94 | 94 | 6 | 6 | 100 | 100 |

Table 3: The content of microplastic polymers in fresh fish and pindang fish.

| | Kind of fish | |
|---|---|---|
| | Fresh fish | Pindang fish |
| Number of samples | 89 samples | 11 samples |
| Examined fish | Meat, gills, skin, intestines, stomach | Meat, skin |
| Found polymers (frequency) | Polyester (63),<br>Polyethylene (55)<br>Polyamide (55)<br>Polycaprolactam (30)<br>Phenol formaldehyde (8)<br>Urea & melamine formaldehyde (5) Polyethyelen Terephtalat (1)<br>Polyethylene Low-Density (1) | Polyester (15)<br>Polyethylene (6)<br>Polyamide (2)<br>Polycaprolactam (3) |

Table 4: Linear regression analysis of fish consumption intensity to health complaints and symptoms.

| Coefficients[a] | | | | | | |
|---|---|---|---|---|---|---|
| Model | | Unstandardized Coefficients | | Standardized Coefficients | t | Sig. |
| | | B | Std. Error | Beta | | |
| 1 | (Constant) | .946 | .206 | | 4.594 | .000 |
| | Intensity of Fish Consumption | .026 | .044 | .056 | .591 | .556 |
| | Types of fish consumed | .017 | .024 | .067 | .709 | .480 |
| a. Dependent Variable: Health Complaints | | | | | | |
| Coefficients[a] | | | | | | |
| Model | | Unstandardized Coefficients | | Standardized Coefficients | t | Sig. |
| | | B | Std. Error | Beta | | |
| 2 | (Constant) | 1.254 | .275 | | 4.562 | .000 |
| | Intensity of Fish Consumption | -.034 | .059 | -.054 | -.571 | .569 |
| | Types of fish consumed | .005 | .032 | .015 | .158 | .875 |
| b. Dependent Variable: Symptoms of the disease | | | | | | |

influence between the intensity of fish consumption and the type of fresh fish consumed on the health problems and symptoms experienced by the community.

## DISCUSSION

The results of the study in Table 1 show that the majority of respondents have a low level of education. The level of education in a community can affect environmental protection measures, such as the use of clean water, energy, and waste management (Wulansari et al. 2020). Education can also influence an individual's mindset; those with higher education are often more involved in planning and implementing waste management activities that can reduce plastic waste pollution in the environment (Ivakdalam et al. 2022). The results in Table 1 also indicate that respondents had low incomes. Community income is a contributing factor to waste management, and other studies have shown that people's income levels affect the management of non-organic waste in the community (Jayanti et al. 2017, Safitri et al. 2019).

The results of this study found 94 samples contained microplastics (Table 2), this research is in line with previous research which found that out of 75 pindang fish samples tested were contaminated with microplastics, while only 11 out of 25 fresh fish samples showed contamination (Gunawan et al. 2021). Other studies have also reported microplastics in various species of fish. For example, microplastics were found in all observed species and were most commonly detected in pelagic skipjack tuna (Neto et al. 2020). On the Colombian Caribbean coast, microplastics were found in the digestive tracts of 9 species of commercial fish (Garcés-Ordóñez et al. 2022). A study along the Finnish coast detected microplastics in the digestive tracts of 38 fish (Sainio et al. 2021), while a study in Japanese waters found microplastics in 39.1% of pelagic fish and 10.3% of demersal fish (Yagi et al. 2022). Wild fish in the Atlantic Ocean were also found to have high levels of microplastic contamination (Guilhermino et al. 2021). Similarly, a study in Guangdong, China, showed that freshwater fish commonly consumed by the public were contaminated with microplastics, with different abundances found in 52 tilapia and 24 mud carp samples from 25 locations (Sun et al. 2021). These findings demonstrate that microplastics have contaminated fresh and pindang fish in marine waters in various parts of the world. The results of the study (Table 2) also showed that as much as 26 percent of microplastics were found in the gills of fish and 15 percent in the intestines, these results were similar to a study by Guilhermino et al. showed that 89% of fish contained microplastics in their gastrointestinal tract and 27% in their gills, indicating high levels of consumption and gill contamination (Guilhermino et al. 2021).

The study results (Table 3) were similar to those reported in other studies, such as one that analyzed 69 microplastic items containing various polymers, including Polyamide, Polyurethane, Polypropylene, Polystyrene, and Polyethylene Terephthalate (Neto et al. 2020). Other studies have identified Polypropylene, Polyethylene, high-density Polyethylene, and Polyethylene as the most abundant microplastic polymers in surface water and sediments (Garcés-Ordóñez et al. 2022), while pelagic and demersal fish were found to contain polyethylene, polyester, polyolefin (PO), polypropylene, poly-perinapthalene (PPN), poly-pentaphenylene (PPP), polystyrene (PS), and polyvinyl chloride (PVC) (Yagi et al. 2022). In the mouth of the Minho River, 36 types of polymers were identified in microplastics found in fish, including polyester, polyethylene, polyacrylate, polypropylene, and cellulose acetate (Guilhermino et al. 2021). Furthermore, several studies have demonstrated the negative effects of polyethylene entering the plankton ecosystem, which can lead to a reduction in heart rate and plankton frequency (Pan et al. 2022).

The results showed that the polymer content of polyester, and polyethylene was the highest in both fresh and pindang fish. The results of this study were similar to a study in freshwater areas in southern Italy showing that Polyethylene, Polyethylene Terephthalate, Polystyrene, and Polypropylene are the most common microplastics Polymers reported in existing fish species, fish containing microplastics are the fish caught in the most polluted waters (Forgione et al. 2023). Other studies have shown that the polymers commonly reported in the digestive tract of fish are hight density polyethylene polymers, polypropylene-polyethylene copolymers, and ethylene vinyl acetate (Parvin et al. 2021). Furthermore, 48% of crustaceans, namely shrimp and crabs, contain microplastics, the most common of which are Polyester and Polyolefin (Ogunola et al. 2022).

Table 3 also shows that the results of microplastic polymer variations in fresh fish are more varied than in pindang fish. Pindang fish has been preserved by adding a lot of salt through a boiling or steaming process so that the microplastics in salted fish come from the raw material of the fish as well as from added salt. Gunawan et al. (2021) research stated that apart from being found in pindang fish, microplastics are also present in salt and boiled fish water. In addition, this study also shows that microplastic levels in pindang fish are higher than in raw fish. The pindang fish microplastic polymer in Table 3 contains more polyester and polyethylene polymers, in accordance with the research of

Gunawan et al which also shows that the dominant polymer in pindang fish is polyethylene (46 percent). So the microplastic polymer of pindang fish with a slight variation in types is probably due to the polymer being derived from the salt content added to the fish.

The consumption intensity and the type of fish chosen do not influence health complaints and symptoms (Table 4). Further research is still needed on health complaints and symptoms caused by microplastic exposure. Still, it does not rule out the possibility that microplastics can enter the human body through fish consumption and potentially cause potential risks to human health. One study showed that there is a strong relationship between the concentration of microplastics in fish, intake rate, frequency of exposure, duration of exposure, and body weight of the respondents (Daud et al. 2021). The amount of microplastics ingested by humans is estimated to be between 0.1-5 g microplastics per week, which is dependent on intake (Senathirajah et al. 2021). The potential contamination of humans by microplastics in fish depends on the amount of fish consumption, and estimates of microplastic intake may vary accordingly (Pan et al. 2022). Another study suggests that microplastics in shellfish pose a more direct threat when the shells are eaten whole, while microplastics in the digestion of fish have a fairly limited effect (Mahu et al. 2022). A research investigation conducted in Ghana revealed that exposure to microplastics in shellfish may be much higher in countries with high levels of consumption (Addo et al. 2022). Furthermore, microplastics and nanoplastics can reach the bloodstream and affect cells of the immune system and their distribution throughout the body (Domenech et al. 2021). A study showed that plastic particles were detected in human blood, with an average of 1.6 µg/mL of plastic particles measurable in blood (Leslie et al. 2022). Microplastics have the potential to carry heavy metals into the human body, which have the potential to cause severe health hazards such as birth defects, formation of Reactive Oxygen Species (ROS), cytotoxicity, severe cardiovascular, respiratory, hematological, gastrointestinal, kidney and liver damage, neurological, neurodegenerative and mental disorders, anemia, hypertension, miscarriage, infertility and carcinogenic effects on breast, liver, kidney, lung (Jadhav et al. 2021).

Exposure to microplastics has the potential to cause toxicity through oxidative stress, inflammatory lesions, and increased absorption or translocation, according to several studies showing the potential for metabolic disorders, neurotoxicity, and increased risk of cancer in humans (Rahman et al. 2021). Other studies have shown that the chemicals reported in microplastics in shellfish are categorized as harmful to human health (Masiá et al. 2022, Saha et al. 2021) and microplastics found in boiled and steamed shellfish products are less than those that are fried (Li et al. 2022).

The limitation of this study is that the health symptoms of the respondents are questionnaire data, so the results are subjective. The strength of the research is the number of samples and the types of fish studied along with an analysis of the differences in the polymer content of fresh fish and salted fish. This study recommends conducting education and a good waste management system in coastal areas so that it can minimize pollution of sea waters, especially due to plastic waste.

The majority of respondents in the coast village of Tembok Rejo, Muncar sub-district had low levels of education and monthly incomes of less than 2.5 million, which may affect waste management in the area and lead to environmental pollution. The results showed that 94 percent of the fish samples contained microplastics and only 6 percent of the fish samples did not contain microplastics. The intensity of pindang fish consumption is positively correlated with health symptoms and health complaints experienced by respondents. To minimize pollution of sea waters due to poor waste management, it is crucial to provide education and implement a proper waste management system in the coastal areas. Further study is necessary to investigate the toxic effects of microplastic exposure and consumption on human health, as well as to develop appropriate processing methods for fish that reduce the intake of microplastics into the human body.

## ACKNOWLEDGMENT

The authors thank all parties involved in this research.

## REFERENCES

Addo, S., Boateng, C. M., Diyie, R. L., Duodu, C. P., Ferni, A. K. and Williams, E. A. 2022. Occurrence of microplastics in wild oysters (Crassostrea Tulipa) from the Gulf of Guinea and their potential human exposure. SSRN Electronic Journal, 8.

BPS 2021. Kabupaten Banyuwangi dalam Angka 2021. Available at: https://banyuwangikab.bps.go.id/publication/2021/02/26/92c9d6985269031f62f278b4/kabupaten-banyuwangi-dalam-angka-2021.html [Accessed 1 March 2023].

Daud, A., Birawida, A. B., Amqam, H., Tahir, A., Hajrah, E. N. and Nurtang, L. 2021. Risk analysis of microplastic in fish (Nemiptus Japonicas & Rastrelliger Sp.) in communities in the coast area of Tamasaju, Galesong Takalar. Medico-Legal Update, 21(2): 196-203.

Domenech, J. and Marcos, R. 2021. Pathways of human exposure to microplastics, and estimation of the total burden. Current Opinion in Food Science, 39: 144-151.

Elizalde-Velázquez, G. A. and Gómez-Oliván, L. M. 2021. Microplastics in aquatic environments: A review on occurrence, distribution, toxic effects, and implications for human health. Science of the Total Environment, 780: 146551.

Forgione, G., Izzo, F., Mercurio, M., Cicchella, D., Dini, L. and Giancane, G. 2023. Microplastics pollution in freshwater fishes in the South of Italy: Characterization, distribution, and correlation with environmental pollutants. Science of the Total Environment, 864: 161032.

Garcés-Ordóñez, O., Saldarriaga-Vélez, J. F., Espinosa-Díaz, L. F., Patiño, A. D., Cusba, J. and Canals, M. 2022. Microplastic pollution in water, sediments and commercial fish species from Ciénaga Grande de Santa Marta lagoon complex, Colombian Caribbean. Science of the Total Environment, 829(2).

Guilhermino, L., Martins, A., Lopes, C., Raimundo, J., Vieira, L. R. and Barboza, L. G. A. 2021. Microplastics in fishes from an estuary (Minho River) ending into the NE Atlantic Ocean. Marine Pollution Bulletin, 173(PA): 113008.

Gunawan, Effendi H. and Warsiki, E. 2021. Cemaran Mikroplastik pada Ikan Pindang dan Potensi Bahayanya terhadap Kesehatan Manusia, Studi Kasus di Bogor. Jurnal Pengelolaan dan Bioteknologi Kelautan dan Perikanan, 16(2): 105-119. [Indonesian]

Isobe, A., Uchiyama-Matsumoto, K., Uchida, K. and Tokai, T. 2017. Microplastics in the Southern Ocean. Marine Pollution Bulletin, 114(1): 623-626.

Ivakdalam, L. M. and Far, R. A. F. 2022. Peningkatan partisipasi masyarakat dalam keberlanjutan pengelolaan sampah melalui bank sampah (Increasing community participation in sustainable waste management through waste banks). Agrikan: Jurnal Agribisnis Perikanan, 15(1): 165-181. [Indonesian]

Jadhav, E. B., Sankhla, M. S., Bhat, R. A. and Bhagat, D. S. 2021. Microplastics from food packaging: An overview of human consumption, health threats, and alternative solutions. Environmental Nanotechnology, Monitoring & Management, 16: 100608.

Jambeck, J. R., Geyer, R., Wilcox, C., Siegler, T. R., Perryman, M., Andrady, A., Narayan, R. and Law, K. L. 2015. Supplementary materials for plastic waste inputs from land into the ocean. Science, 347: 768.

Jayanti, K. R., Christiawan, P. I. and Sarmita, I. M. 2017. Pengaruh Tingkat Pendidikan Dan Tingkat Pendapatan Terhadap Bentuk Pengelolaan Sampah Aorganik Rumah Tangga Di Desa Alasangker. Jurnal Pendidikan Geografi Undiksha, 5(2). [Indonesian]

Johan, Y., Manalu, F., Muqsit, A., Renta, P. P. and Purnama, D. 2021. Analisis mikroplastik pada ikan ekonomis di teluk segara kota Bengkulu. Jurnal Enggano, 2(6): 369-384. [Indonesian]

Leslie, H. A., van Velzen, M. J. M., Brandsma, S. H., Vethaak, A. D., Garcia-Vallejo, J. J. and Lamoree, M. H. 2022. Discovery and quantification of plastic particle pollution in human blood. Environment International, 163: 107199.

Li, J., Zhang, L., Dang, X., Su, L., Jabeen, K. and Wang, H. 2022. Effects of cooking methods on microplastics in dried shellfish. Science of the Total Environment, 837: 155787.

Mahu, E., Datsomor, W. G., Folorunsho, R., Fisayo, J., Crane, R. and Marchant, R. 2022. Human health risk and food safety implications of microplastic consumption by fish from coastal waters of the eastern equatorial Atlantic Ocean. Food Control, 145: 109503.

Masiá, P., Ardura, A. and Garcia-Vazquez, E. 2022. Microplastics in seafood: Relative input of Mytilus galloprovincialis and table salt in mussel dishes. Food Research International, 153.

Neto, J. G. B., Rodrigues, F. L., Ortega, I., Rodrigues, L. dos S., Lacerda, A. L. de F. and Coletto, J. L. 2020. Ingestion of plastic debris by commercially important marine fish in southeast-south Brazil. Environmental Pollution, 267.

Ogunola, S. O., Reis-Santos, P., Wootton, N. and Gillanders, B. M. 2022. Microplastics in decapod crustaceans sourced from Australian seafood markets. Marine Pollution Bulletin, 179: 113706.

Pan, Y., Long, Y., Hui, J., Xiao, W., Yin, J. and Li, Y. 2022. Microplastics can affect the trophic cascade strength and stability of plankton ecosystems via behavior-mediated indirect interactions. Journal of Hazardous Materials, 430: 1-10.

Pan, Z., Liu, Q., Xu, J., Li, W. and Lin, H. 2022. Microplastic contamination in seafood from Dongshan Bay in southeastern China and its health risk implication for human consumption. Environmental Pollution, 303: 119163.

Parvin, F., Jannat, S. and Tareq, S. M. 2021. Abundance, characteristics and variation of microplastics in different freshwater fish species from Bangladesh. Science of the Total Environment, 784.

Rahman, A., Sarkar, A., Yadav, O. P., Achari, G. and Slobodnik, J. 2021. Potential human health risks due to environmental exposure to nano- and microplastics and knowledge gaps: A scoping review. Science of the Total Environment, 757: 143872.

Safitri, M. E. and Rangkuti, A. F. 2019. Hubungan Tingkat Pendidikan, Pengetahuan dan Sikap Dengan Perilaku Pengelolaan Sampah Pada Pedagang Buah dan Sayur Di Pasar Giwangan Yogyakarta. Universitas Ahmad Dahlan, 1-14. [Indonesian]

Saha, M., Naik, A., Desai, A., Nanajkar, M., Rathore, C. and Kumar, M. 2021. Microplastics in seafood as an emerging threat to marine environment: A case study in Goa, west coast of India. Chemosphere, 270: 129359.

Sainio, E., Lehtiniemi, M. and Setälä, O. 2021. Microplastic ingestion by small coastal fish in the northern Baltic Sea, Finland. Marine Pollution Bulletin, 172.

Sawalman, R., Zamani, N. P., Werorilangi, S. and Suaib, E. S. 2021. Kandungan Mikroplastik Pada Ikan Konsumsi Di Pasar Tradisional Kota Palu. Akua: Jurnal Ilmu Perikanan dan Kelautan, 1(2): 1-8. [Indonesian]

Sobandi, R. 2019. Hubungan Tingkat Pendidikan Dan Sikap Siswa Terhadap Lingkungan Dengan Perilaku Siswa dalam Menangani Sampah di Sekolah (Studi Deskriptif Korelasional di SMPN Se-Kecamatan Banjaran Kabupaten Bandung) (Doctoral dissertation, UIN Sunan Gunung Djati Bandung). [Indonesian]

Underwood, A. J., Chapman, M. G. and Browne, M. A. 2017. Some problems and practicalities in design and interpretation of samples of microplastic waste. Analytical Methods, 9: 1332-1345.

Wagner, M. and Lambert, S. 2018. Freshwater microplastics: Emerging environmental contaminants? Springer International Publishing.

Welden, N. A. C. and Lusher, A. L. 2017. Impacts of changing ocean circulation on the distribution of marine microplastic litter. Integrated Environmental Assessment and Management, 13(3): 483-487.

Wright, S. L. and Kelly, F. J. 2017. Plastic and human health: A micro issue?. Environmental Science & Technology, 51(12): 6634-6647.

Zhao, S., Zhu, L. and Li, D. 2016. Microplastic in three urban estuaries, China. Environmental Pollution, 206: 597-604.

## ORCID DETAILS OF THE AUTHORS

Lilis Sulistyorini: https://orcid.org/0000-0002-5005-0677

Nature Environment and Pollution Technology
An International Quarterly Scientific Journal

p-ISSN: 0972-6268
(Print copies up to 2016)
e-ISSN: 2395-3454

Vol. 23 | No. 3 | pp. 1677-1685 | 2024

Original Research Paper

https://doi.org/10.46488/NEPT.2024.v23i03.039

Open Access Journal

# Effects of Rainfall Intensity, Kinetic Energy and Slope Angle to the Upslope, Downslope, and Lateral Slope Components of Splash Erosion in Hillslope Agriculture: A Case in Badiangan, Ajuy, Iloilo

**Shevanee Ruth G. dela Cruz*(**)† and Ricardo L. Fornis****
*College of Engineering, Central Philippine University, Jaro, Iloilo City, 5000, Philippines
**School of Engineering, University of San Carlos, Talamban, Cebu City, 6000, Philippines
†Corresponding author: Shevanee Ruth G. dela Cruz; srdelacruz@cpu.edu.ph

**Nat. Env. & Poll. Tech.**
**Website: www.neptjournal.com**

*Received:* 10-11-2023
*Revised:* 20-12-2023
*Accepted:* 11-01-2024

**Key Words:**
Hillslope agriculture
Kinetic energy
Rainfall intensity
Splash erosion

## ABSTRACT

This study was conducted in Barangay Badiangan, Ajuy, Iloilo City, Philippines (11°10'N, 122°58'E) to determine the effects of rainfall intensity and other rainfall-derived parameters on the directional components of splash erosion in hillslopes. There are five experimental set-ups with slope angles ranging from 0% to 48% were tested under natural rainfall conditions using a modified splash collector. The data collected shows that kinetic energy, slope, and rainfall intensity have shown significant effects on splash erosion. The models obtained using regression analysis are $Q_{det} = 0.0093(KE^{0.80})$ and $Q_{trans} = 0.060(KE^{0.107})(S^{0.700})(I_{20}{}^{0.700})$. The model equation performance has been validated using the Standard Error of Estimates with values of 12 and 9.4 for splash detachment and splash transport, respectively. The constants used for kinetic energy in detachment and slope in transport align with the research by Quansah (1981) for sandy soil, which is similar (the characteristics) to the soil at our research site. Additionally, rainfall intensity, especially with a 20-min duration, generated the best model as it yielded the lowest SEE value for all cases.

## INTRODUCTION

Soil erosion is one of the most serious global and ecological environmental crises in progress today, resulting from the interaction of the soil itself, climate, relief, surface cover, and land use practices (Hoyos & Waylen 2005, Renschler et al. 1999). The problems caused by soil erosion include decreased soil fertility, increased landslide activity, reservoir sedimentation, contaminant diffusion, rocky desertification, and ecosystem disturbances, all of which significantly impact human development (Bai et al. 2013, Jiang et al. 2014, Syvitski et al. 2005).

Splash erosion, which is the first stage of interrill erosion, involves soil detachment and transport resulting from raindrop impact (Kinnell 2005, Morgan 2005), which can destroy soil structure, increase runoff turbulence, and enhance sediment delivery (Dussaillant 2011, Ma et al. 2015). Generally, raindrop kinetic energy (KE) is accepted as the best predictor of rainfall erosivity that can define the ability of raindrops to detach soil particles (Fernández-Raga et al. 2010, Hammad et al. 2006). In splash erosion, to overcome the particle weight and the cohesive force binding the particles together for detachment and transport, some of the important factors to consider are the rainfall intensity-kinetic energy relationship, the slope steepness, and transportability.

Rainfall intensity and the kinetic energy of a rainfall event are important parameters in erosivity (Fornis et al. 2005, van Dijk et al. 2002). The erosive force of rainfall involves the detachment of soil particles by the kinetic energy from falling raindrops and the transport of these soil particles through surface runoff (Vrieling et al. 2014). Rainfall kinetic energy has been known to cause erosion, especially in tilled bare land, since vegetation intercepts the impact of rain and protects the soil surface as well as intercepts runoff (Zuazo & Pleguezuelo 2008).

According to Parsons et al. (1991), although there is some controversy, most authors suggest that the intensity of splash erosion increases with slope. Many studies have been conducted to evaluate the relationship between splash and slope since the influence of slope angle on soil detachment is of importance in soil conservation (Aissa et al. 2014, Bryan 1979, Torri & Poesen 1992). If the soil has no slope, material splashes away from the point of impact randomly in the surrounding area (Kinnell 2005). In a sloped soil surface, material splashed downslope travels further than those upslope, resulting in the net downslope migration of detached material. That downslope migration increases as

the slope gradient increases, but it takes many drop impacts to cause much material to move downslope in most cases (Quansah 1981).

The transport of detached soil particles, according to Kinnell (2005), may occur as a result of raindrops and flow acting either singly or together. He further identified detachment and transport systems; included here is the raindrop detachment with transport by raindrop splash (RD-ST) system. This system is due to the energy from raindrop impact, which causes the breakdown of soil particle bonds that hold them together, resulting in the transportation of particles from the raindrop impact site (Kinnell 2005).

Soil properties and rainfall physical parameters, including rainfall intensity, kinetic energy, and their various interactions, were studied as this research aims to investigate the effects of rainfall parameters at variable slope angles on the directional components (upslope, lateral, and downslope) of splash erosion characteristics. This investigation seeks to help prevent further degradation of the soil. We constructed an experimental setup on hillslopes from the agricultural lands of Badiangan, Ajuy, and Iloilo to develop a model that predicts the net amount of splash erosion downslope as a function of rainfall parameters and the slope of the ground surface. This information can estimate the quantity of splash erosion, which is the initial stage of soil erosion on slopes (Shanshan et al. 2018).

## MATERIALS AND METHODS

### Study Site

Iloilo Province, situated in the center of the Philippine archipelago as shown in Fig. 1, occupies the southern and northeastern portions of Panay Island. The topography of Iloilo Province varies from flat lands and rolling hills to mountain peaks and ranges.

The field experiment was conducted on the hillslope of Ajuy (Fig. 2) in the northeastern part of Iloilo in the Philippines. Ajuy is an agricultural town that produces various crops such as corn, coconut, sugarcane, fruit trees, bananas, coffee, bamboo, root crops, and other minor crops.

Badiangan is a barangay in Ajuy with an estimated elevation of 201.7 meters (661.7 feet) above mean sea level. The barangay's topography is predominantly sloping, making it susceptible to land degradation.

### Experimental Materials

All experiments were carried out from January 2020 until January 2021. The experimental set-ups were placed at slopes of 0%, 5.94% (3.40), 10.17% (5.820), 24.57% (14.01) and 48.92% (27.70). These locations were selected based on the slope variability of the chosen hillslope.

The instrument used is a modified splash collector, which is made up of a soil tray and lateral splash collectors. The splash source was exposed to the natural rain. The soil trays contain soils with more than 50% or more of coarse fractions passing the number 8 sieve and less than 5% passing the number 200 sieve. Therefore, all soils are considered clean sands. More than 50% of soil particles are of sizes between 0.425 mm to 2.00 mm. Therefore, sandy soils are considered medium coarse sands. Based on the grain size distribution curves for all soil samples, it was found that uniformity coefficients (Cu) for all soils are less than 6. Therefore, all

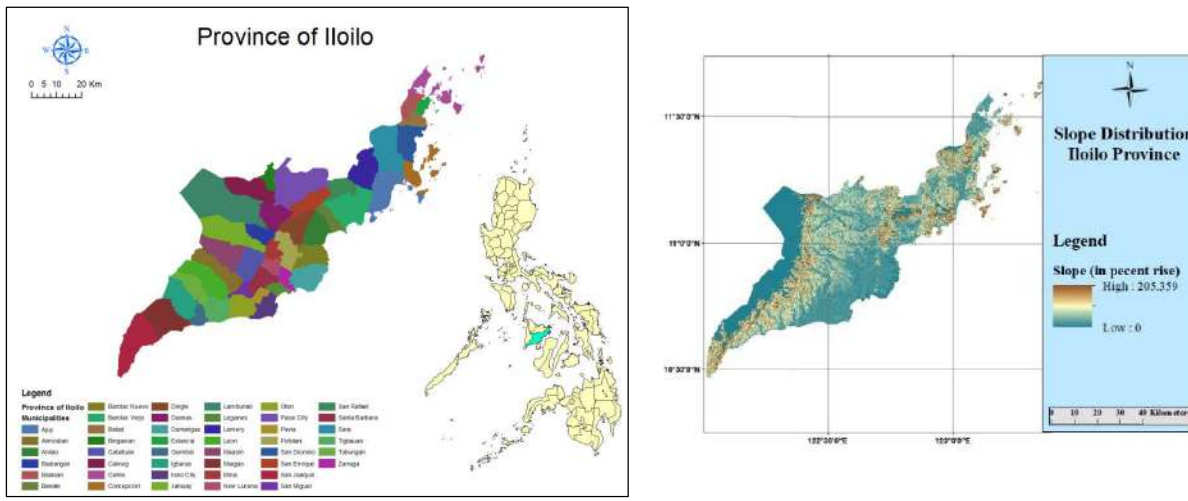


(a) (b)

Fig. 1: Map of the Province of Iloilo and its slope distribution.

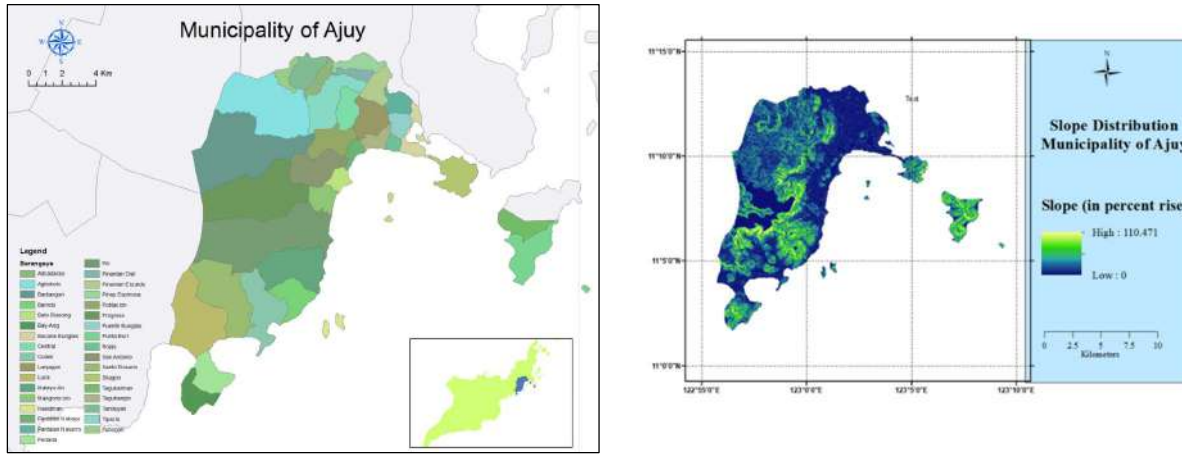


(a) (b)

Fig. 2: Map of the Municipality of Ajuy and its slope distribution.

soil samples in trays 1 to 5 are Poorly Graded Medium Coarse Sand (SP). Samples of the soil particles detached from and thrown outside of the splash source were collected by the splash collectors.

The splashed soil retrieval was done in an irregular schedule due to some difficulty in doing it on steep slopes at times when the soil is still wet because it is slippery. The soil inside the tray was cleaned from stone fragments and roots. The retrieved soil samples are oven-dried and weighed to get the amount of soil splashed after the event.

### Rainfall Measurement

Rainfall intensity was measured using a tipping bucket HOBO Rain Gauge with a Data Logger, that is, the Data Logging Rain Gauge is a battery-powered rainfall data collection and recording system that includes a HOBO® Pendant Event data logger integrated into a tipping-bucket rain gauge. This model automatically records up to 3200 mm of rainfall data that can be used to determine rainfall rates, times, and duration. This data logger operates in an outdoor environment, and in this experiment, the recording was set at a 1-minute time interval.

### Wind Energy

Wind energy affects splash erosion by rolling soil particles along the surface through to a strong wind that lifts a large volume of soil particles into displacements, creating splash erosion. Pedersen & Hasholt (1995) first studied the influence of wind speed on rain splash erosion, where they demonstrated that the rise in kinetic energy of raindrops due to prevalent wind direction during an event can be determined, realizing that wind speed enhances the kinetic energy of rainfall intensity (Pedersen & Hasholt 1995). Because of the varying components of the wind direction, it can cause splash erosion at different directional components.

Wind energy can dislodge surface soil particles and transport them to great distances, with a 5-meter maximum displacement. According to Morgan, the most erodible particles are 0.10–0.15 mm in size; particles between 0.05 and 0.5 mm are generally selectively removed by the wind (Morgan 2005). The soil movement depends upon the grain size of the soil. Clay and sandy soil are more likely to erode than medium-textured soils (Krogman 1983). Resistance to wind erosion increases rapidly when primary particles and aggregates larger than 1 mm predominate (Morgan 2005). In this experiment, the wind direction and velocity were not measured, but its effect was minimized because the perimeter of the set-ups was covered with a tarpaulin (0.8 m high) and, at the same time, the surrounding hills shielded them from direct exposure to the prevailing wind. This analysis can indicate that the wind speed can explain outliers between splash erosion and kinetic energy, especially in those events that are not characterized by other rainfall parameters in splash erosion. However, Pedersen et al. highly noted that it is also important to know the slope aspect of the wind to emphasize how much slope aspects influence energy levels (Pedersen & Hasholt 1995).

### Model Formulation for Splash Detachment and Transport

As raindrops impact the soil, it detaches particles and transports them. This detachment is taken as soil splashed upslope added to the soil splashed downslope, while net

splashed transport is soil splashed downslope less soil splashed upslope (Grosh & Jarrett 1994, Quansah 1981).

$$Q_{det} = Q_{upward} + Q_{downward} \quad \ldots(1)$$

$$Q_{trans} = |Q_{downward} - Q_{upward}| \quad \ldots(2)$$

Quansah noted that downslope splash increased significantly with increasing slope angle and suggested that:

$$Q = a(KE)^b S^c \quad \ldots(3)$$

Where Q is classified into two components – $Q_{det}$ and $Q_{trans}$. The $Q_{det}$ represents the splash detachment while $Q_{trans}$ describes the net splash transport. S is the percent slope, and a, b, and c are empirically determined constants.

Several researchers demonstrated that the power law is the most suitable mathematical function between rainfall kinetic energy and rainfall intensity. However, Quansah (1981) did not include rainfall intensity in their model which was debunked by other researchers. For example, Shin et al. (2016) described the universal power law for a relationship between rainfall kinetic energy and rainfall intensity. They proposed a new model based on the rainfall power theory under an ideal assumption that raindrop is uniformly distributed in constant rainfall intensity. Incorporating rainfall intensity into their model, the accuracy of the model increased by 20% when compared to Quansah (1981). Moreover, using rainfall intensity to splash erosion model has a small average relative difference (0.32%) against the testing data – proving that rainfall intensity increases the predictive capability of the splash erosion model. Therefore, in this study, rainfall intensity is used as one of its explanatory variables.

## Regression Modeling

There are 40 rainfall events gathered and have been considered in the processing. Since the data collected in the experiment consisted of outliers that lie at an abnormal distance from other values in a random sample from a population, multiple options, like the omission of some data from the record, were explored to obtain a higher value for the R-squared.

According to Kinnel (2005), if the soil has no slope, material splashes away from the point of impact randomly in the surrounding area. Still, in the sloping ground, the amount of splashed soil increases as the slope increases (Morgan 2005). Thus, datasets obtained from the slope 0% were discarded.

On a slope receiving rain, the soil particles that are detached by the raindrops may cause more material to travel downward along a hillslope as it travels further than upslope. The downslope transport increased with slope, whereas upslope transport decreased (van Dijk et al. 2003). This downward movement of soil material is caused by the distance of splash along a slope being longer downward than in the upward direction. Splash erosions, therefore, must correspond to this inequality. $Q_{downward} > Q_{upward}$, hence, the discarding values with $Q_{downward} < Q_{upward}$ was also explored.

The amount of rain inducing significant erosion was also studied. Rainfall depth less than 10 mm and maximum rainfall intensities less than 12 mm.h$^{-1}$ ($I_R < 12$) and 25mm.h$^{-1}$ ($I_R < 25$) were discarded to check if there was an improvement in the model to capture the data points. Hudson's study in Zimbabwe emphasized that rainfall intensities less than 25 mm.h$^{-1}$ are not able to yield splash erosion in a significant amount (Hudson 1965). Morgan also used this threshold in his study in Malaysia and values larger than 10 mm.h$^{-1}$ in England (Foot & Morgan 2005, Pedersen & Hasholt 1995).

## Model Simulations

The experimental setup of the study has gathered 40 samples from Badiangan, Ajuy, and Iloilo. Not all of them were used because some samples were discarded, as mentioned in the previous section. Microsoft Excel was used in the regression analysis.

The splash erosion results are evaluated using R-squared and Mean Squared Error (MSE). These performance measures are usually used for model comparison, and it is mathematically expressed as:

$$R^2 = 1 - \frac{\sum(y_i - \hat{y}_i)^2}{\sum(y_i - \bar{y})^2} \quad \ldots(4)$$

where $y$ is the actual splash erosion, while $\hat{y}$ is the predicted splash erosion.

To determine the accuracy made by the regression model, the standard error of estimates (SEE) is used to measure the uncertainty associated with the observed data. It is calculated as:

$$\sigma_{est} = \sqrt{\frac{\sum(Y - Y')^2}{N}} \quad \ldots(5)$$

where $\sigma_{est}$ is the standard error of the estimate, Y is an observed data, Y′ is a predicted data, and N is the number of data pairs. The smaller the value of the SEE, the better the performance of the regression model.

## Data and Processing

The first objective of the study is to relate the amount of the directional splash components to the different rainfall parameters at varying slopes. Linear regression was used in the context of sensitivity analysis to determine which explanatory variables are strong enough to predict splash erosion. Moreover, the impact of uncertainties in the

explanatory variables on the response variable, using the statistical p-value of the regression analysis, was also measured.

The splash erosion collected at the upper slope of the source area results from downward and upward directional components were organized in terms of their corresponding slopes, such that *D(g)* and *U(g)* are the amount of sediments in grams (g) from the downward and upward direction, respectively. The rainfall depth is also included and is measured in millimeters (mm). The study also used the maximum rainfall intensity for the different time durations (5, 10, 15, 20, 25, 30, 45, 60 min) and is measured in millimeters per hour ($mm.h^{-1}$). The instantaneous rainfall intensity is used to calculate the value of the kinetic energy using the equation below recommended by Fornis et al. (2005) as a reference for soil erosion studies. The kinetic energy is in Joules per meter squared ($J.m^{-2}.mm^{-1}$) and expressed as:

$$KE = 30.8\,(1 - 0.55e^{-0.032I}) \quad \ldots(6)$$

## RESULTS AND DISCUSSION

### Sensitivity Analysis for the Directional Splash Components

The statistical significance of the proposed splash erosion model was analyzed to determine the relevant parameters. To assess its significance, normal probability plots and residuals of fitted values were used to determine its probability density function. For the downward splash component, the distribution follows a normal curve. Moreover, using regression analysis, the rainfall intensity is statistically significant with a downward splash component with a p-value of $0.00006767 < \alpha = 0.05$.

Rainfall intensity simulated on an upward splash direction follows a normal distribution. It is also statistically significant to the upward splash component with a p-value of $0.000000539 < \alpha = 0.05$. This significance suggests that the data in the upslope component and rainfall intensity can be used to formulate a splash erosion model.

The relationship of the lateral slope (i.e., right and left) to the rainfall intensity at varying slopes using regression analysis was also evaluated. Results showed that both left and right directional splash components follow normality. This conclusion assumes that a regression model to the lateral directional splash components can also be used. The p-values of the right and left splash components are $1.006 \times 10^{-5}$ and $8.679 \times 10^{-8}$, respectively, suggesting the statistical significance of the rainfall intensity to the lateral directional component. Therefore, rainfall intensity, as an explanatory variable, is a vital component in splash erosion. However, there is still a need to analyze the effect of the impact of raindrops on splash erosion, measured as kinetic energy, to analyze its statistical significance. In the next section, the statistical significance of the kinetic energy in terms of the directional splash component (i.e., upward, downward, right, and left) was also analyzed.

Splash erosion is directly caused by the kinetic energy of raindrops, which is a crucial parameter in erosion prediction models. Simple linear regression was applied to delineate the correlation between splash erosion rate and its directional components with kinetic energy. Table 1 shows the statistical significance of kinetic energy in relation to its directional components.

Results showed that only the downward splash component is statistically significant for the splash erosion model. Other directions have p-values greater than the assumed level of significance. This conclusion correlates with the initial assumption that once raindrops reach the soil surface due to their kinetic energy, they primarily infiltrate and flow downslope along the surface. Moreover, rainfall kinetic energy is often estimated based on measured rainfall intensity due to the lack of direct measurement. A correlation test was used to analyze the relationship between these two parameters. It showed a strong, positive linear relationship, indicating a direct correlation between rainfall intensity and kinetic energy. Because of these findings, the proposed model used only rainfall intensity to simulate splash erosion in the downward component, as other directional components showed no significant effect. Rainfall intensity, soil, and other land use factors affect splash erosion caused by raindrop impact and surface runoff. Specifically, splash erosion depends on the erosivity due to the amount and intensity of rainfall, as well as the resistance of the soil surface or the slope degree, influenced by intrinsic soil properties and the topography of the landscape.

### Downward vs Upward Splash Erosions

Evaluating the results gathered from the experimental setup, descriptive statistics of the independent variables (i.e., rainfall intensity, kinetic energy, slope) and the response variables (i.e., upward and downward slopes) were presented. Some data were omitted to improve the performance of the models, as the dataset contained

Table 1: Statistical Significance of the Kinetic Energy in terms of its Directional Components.

| Direction | Estimate | Standard Error | p-value < 0.05 |
|---|---|---|---|
| Downward | -0.0006257 | 0.9407508 | 0.00989** |
| Upward | 0.0001291 | 0.0001377 | 0.357 |
| Left-lateral | 0.0003661 | 0.0003422 | 0.294 |
| Right-lateral | 0.0003661 | 0.0003422 | 0.172 |

**Significant code: level of significance at 0.05

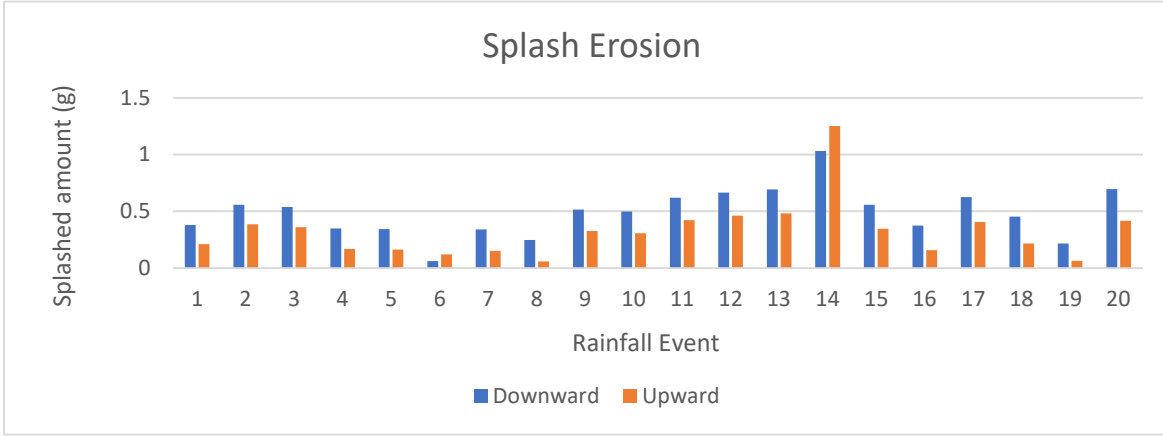


Fig. 3: Downward and upward splash erosions at various rainfall events.

extreme outliers and was compressed from a wide range to a narrower one.

What remains are twenty (20) datasets from the training data for analyzing the statistical setup of downward and upward splash erosion. On a slope receiving rain, soil particles detached by raindrops may cause a net downward movement of soil material along the hillslope. This downward movement occurs because the distance of splash along a slope is longer in the downward direction than in the upward direction. This scenario is validated by the study results, as shown in Fig. 3. Splash erosion in the downward setup is higher than in the upward setup. A positive, linear relationship between the two types of splash erosion was observed, indicating a dependent relationship between the two variables.

### Splash Erosions vs Depth

As hypothesized, rainfall depth plays an important role in splash erosion due to its variation at the spatial and temporal scales from its effects of rainfall intensities. Its effect was also studied against the amount of splash erosion, wherein each treatment included eight groups of rainfall duration (i.e., 5, 10, 15, 20, 25, 30, 45, and 60 mins of rainfall intensity). For the sake of the statistical relationship, the analysis was first done on the relationship between splash erosions and the rainfall depth. The results show that splash erosion is associated with rainfall depth, having a positive linear relationship between the depth and splash erosions for both downward and upward directions.

### Splash Erosions vs Rainfall Intensity

The results indicated that higher intensities of rainfall lead to a higher splash erosion rate on hillslopes. In this study, the experimental setups were surrounded by a corn canopy. The spatial variation of rainfall kinetic energy became relatively complex under the corn canopy, leading to randomness and non-uniformity in the spatial distribution of the splash erosion rate.

### Net Splash Erosion

Evaluation of splash erosion, $Q$ in terms of rainfall intensity $I_{RT}$ as its explanatory variable, such that time $T$ refers to the set $T = \{5, 10, 15, 20, 25, 30, 45, 60\}$. The rainfall intensity and splash erosion rate had a linear relation, using multiple R-squared, R-squared, and adjusted R-squared as the model performance measurement. The splash erosion and the rainfall intensity from different directional components, i.e., downward, upward, left-lateral, and right-lateral, were analyzed. The average rainfall intensity and splash erosion rate increased progressively with higher rainfall intensity, as observed from the experimental setup. Additionally, the significance of each level of rainfall intensity on splash erosion was evaluated using an Analysis of Variance (ANOVA). When classified into four directional components, it was found that downward splash erosion is the most significant, as it has the highest F-score among the directional components.

To validate the effectiveness of the model in terms of its $R^2$, the sensitivity of the rainfall intensity parameters to splash erosion $Q$ was analyzed from the different directional components using standard error, t-test, and ANOVA. It was found that only $I_{RT}$ with $T = \{10, 15, 20, 25, 30, 45, 60\}$ are sensitive to the splash erosion since the p-value $< 0.05$ – making their results consistent with the accuracy as described above. Moreover, only the downward component generated a p-value $< 0.05$.

### Splash Erosion vs Rainfall Kinetic Energy

The relationship of the splash erosion in terms of the rainfall

kinetic energy through simple linear regression models was analyzed using the same model performance methods, i.e., R-squared, adjusted. $R^2$, and multiple $R^2$ such that a higher value suggests the best model performance. In terms of the rainfall kinetic energy, the downward component produced the best regression model with the highest model performance measurement, while the upward directional component generated the poorest model.

### Equation Fitting Between Splash Erosion with Rainfall Physical Parameters

The linear fit of the splash erosion $Q$ for both transport and detachment was evaluated against the significant rainfall physical parameters, i.e., rainfall intensity ($RI$) and kinetic energy ($KE$). The linear fit used two tests – training and validation test to verify the accuracy of the proposed model in terms of splash amount, $Q$, for transport and detachment for the different slope gradients. The training set uses 30 datasets from the results of the experimental setup, while the remaining 10 samples were used for the validation set.

There are six (6) cases considered to evaluate the performance of the model using the standard error of estimate (SEE). SEE was used because it represents each data and, therefore the accuracy of the prediction. Table 2 presents the different cases with the models generated and their respective standard error of estimate (SEE).

After analyzing the results of the different cases, Case 1, which considered all datasets, generated the lowest value for the SEE, which is 26.48 and 18.70 for $Q_{det}$ and $Q_{trans,}$ respectively. This can be associated with the number of datasets considered, as the formula for calculating the Standard Error of Estimate (SEE) includes the number of observations in its denominator. Thus, the higher the number of observations, the lower the SEE value. This finding contrasts with previous research on splash erosion in sloping areas and the tendency of rainfall kinetic energy to detach soil particles, as discussed in the methodology. Additionally, it was noted that a 20-minute rainfall duration consistently yielded the lowest SEE values for both detachment and transport. These results are detailed in the appendices.

The models generated for Case 5 were recommended for both the $Q_{det}$ and $Q_{trans}$. These models omitted datasets, which include the 0% slope, upslope> downslope, rainfall depth < 10 mm, and RI<12 mm.h$^{-1}$. The recommendation was done after it was used in the datasets of Case 6 and found out that it was able to give values for SEE, which are almost the same as that of Case 5.

Table 2: Summary of the Models Obtained with its Respective Standard Error of Estimate.

| Case | | Model | Standard Error of the Estimate | Remarks |
|---|---|---|---|---|
| 1 | $Q_{det}$ | $Q = 0.00000847(KE^{0.8})(S^{0.1158})(I_{20}{}^{1.3419})$ | 26.48104 | All Data Sets were considered. |
| | $Q_{trans}$ | $Q = 0.0051(KE^{0.2486})(S^{0.700})(I_{20}{}^{0.8648})$ | 18.69784 | |
| 2 | $Q_{det}$ | $Q = 0.00000847(KE^{0.8})(S^{0.1158})(I_{20}{}^{1.3419})$ | 29.21948 | Omit: Slope 0 |
| | $Q_{trans}$ | $Q = 0.0051(KE^{0.2486})(S^{0.700})(I_{20}{}^{0.8648})$ | 20.89959 | |
| 3 | $Q_{det}$ | $Q = 0.00000693(KE^{0.8})(S^{0.1160})(I_{20}{}^{1.4095})$ | 29.06314 | Omit: Slope 0, Upslope> Downslope |
| | $Q_{trans}$ | $Q = 0.0046(KE^{0.2521})(S^{0.700})(I_{20}{}^{0.8836})$ | 21.34689 | |
| 4 | $Q_{det}$ | $Q = 0.00000680(KE^{0.8})(S^{0.1161})(I_{20}{}^{1.4125})$ | 33.28780 | Omit: Slope 0, Upslope> Downslope , Depth < 10 mm |
| | $Q_{trans}$ | $Q = 0.00325(KE^{0.2672})(S^{0.700})(I_{20}{}^{0.9288})$ | 25.53425 | |
| 5 | $Q_{det}$ | $Q = 0.0093(KE^{0.8})$ | 33.72979 | Omit: Slope 0, Upslope> Downslope , Depth < 10 mm, RI<12 mm/hr |
| | $Q_{trans}$ | $Q = 0.0598(KE^{0.1072})(S^{0.700})(I_{20}{}^{0.6999})$ | 26.00408 | |
| 6 | $Q_{det}$ | $Q = 0.0139(KE^{0.8})$ | 32.24859 | Omit: Slope 0, Upslope> Downslope , Depth < 10 mm, RI<25 mm/hr |
| | $Q_{trans}$ | $Q = 0.0474(KE^{0.2819})(S^{0.700})(I_{20}{}^{0.3279})$ | 25.80290 | |

Table 3: Validating Datasets Used in the Model with its Respective Standard Error of Estimates.

| Model | SEE |
|---|---|
| $Q_{det} = 0.0093(KE^{0.80})$ | 11.9118 |
| $Q_{trans} = 0.060(KE^{0.107})(S^{0.700})(I_{20}{}^{0.700})$ | 9.3999 |

Utilizing the validating datasets to assess the accuracy of the models in predicting splash erosion, the Case 5 models consistently yielded low SEE values. This result is comparable to the values obtained when using the validating datasets of Case 6. This is presented in Table 3.

## CONCLUSION

In this study, an analysis of the effects of rainfall intensity, kinetic energy, and slope angle on the different directional components of splash erosion in hillslope agriculture was done. Five (5) experimental set-ups were created in the hillslope of Badiangan, Ajuy, and Iloilo, such that its splash source was exposed to the natural rain, with varying degrees of slope. The statistical significance of the directional components was evaluated for the splash erosion, and it was found that the downward component is the most significant among others since the material splash downslope travels further than those in other directional components, resulting in the net downslope migration of the splash materials. Moreover, the downward directional component is directly proportional to the slope gradient since the downward component increases as the slope gradient increases. Because of this, only the samples produced from the downward component were used to investigate the effects of rainfall parameters at variable slope angles. The two models of splash erosion using the rainfall parameters were generated and presented as: $Q_{det} = 0.0093(KE^{0.80})$ and $Q_{trans} = 0.060(KE^{0.107})(S^{0.700})(I_{20}{}^{0.700})$.

The statistical significance of splash components was first evaluated for each rainfall parameter using ANOVA and regression models. It shows that kinetic energy and rainfall intensity are the most sensitive parameters, resulting in a model with sufficient SEE. Kinetic energy is significant in the splash erosion model as it has the ability to detach soil particles from the surface. The values of the constants used for kinetic energy in detachment and slope in transport align with the research conducted by Quansah (1981) on sandy soil, which is characteristic of the research site. Additionally, rainfall intensity, particularly with a duration of 20 minutes, generated the best model among the different cases, as it consistently provided the lowest SEE value across all cases.

## ACKNOWLEDGEMENTS

The authors would like to thank the Engineering Research and Development for Technology (ERDT) and Central Philippine University for their support through scholarship grants. Thank you also to the following institutions for the provision of the required data and equipment needed in this study: University of San Carlos School of Engineering; Center for Geoinformatics and Environmental Solutions; University of the Philippines LiDAR Portal for Archiving and Distribution; Central Philippine University College of Engineering; and Office of the Barangay Captain, Barangay Badiangan, Ajuy.

## REFERENCES

Aissa, H., Mouzai, L. and Bouhadef, M. 2014. The effect of soil surface slope on splash distribution underwater drop impact. Int. J. Agric. Biosyst. Eng., 8(8): 588-591. https://doi.org/10.5281/zenodo.1337411

Bai, X. Y., Wang, S. J. and Xiong, K. N. 2013. Assessing spatial-temporal evolution processes of karst rocky desertification land: Indications for restoration strategies. Land Degrad. Dev., 24(1): 47-56. https://doi.org/10.1002/ldr.1102

Bryan, R. B. 1979. The influence of slope angle on soil entrainment by sheetwash and rain splash. Earth Surf. Process., 4(1): 43-58. https://doi.org/10.1002/esp.3290040105

Dussaillant, A. R. 2011. Estimation of combined splash, interrill, and rill erosion using a hillslope erosion numerical model: An application to dry lands of Chile. J. Soil Water Conserv., 66(2): 142-147. https://doi.org/10.2489/jswc.66.2.142

Fernández-Raga, M., Fraile, R., Keizer, J. J., Varela Teijeiro, M. E., Castro, A., Palencia, C., Calvo, A. I., Koenders, J. and Da Costa Marques, R. L. 2010. The kinetic energy of rain measured with an optical disdrometer: An application to splash erosion. Atmos. Res., 96(2-3): 225-240. https://doi.org/10.1016/j.atmosres.2009.07.013

Foot, K. and Morgan, R. P. C. 2005. The role of leaf inclination, leaf orientation and plant canopy architecture in soil particle detachment by raindrops. Earth Surf. Process. Landforms, 30(12): 1509-1520. https://doi.org/10.1002/esp.1207

Fornis, R. L., Vermeulen, H. R. and Nieuwenhuis, J. D. 2005. Kinetic energy – rainfall intensity relationship for Central Cebu, Philippines for soil erosion studies. J. Hydrol., 300: 20-32. https://doi.org/10.1016/j.jhydrol.2004.04.027

Grosh, J. L. and Jarrett, A. R. 1994. Interrill erosion and runoff on very steep slopes. Trans. ASAE, 37(4): 1127-1133. https://doi.org/10.13031/2013.28186

Hammad, A. H. A., Børresen, T. and Haugen, L. E. 2006. Effects of rain characteristics and terracing on runoff and erosion under the Mediterranean. Soil Tillage Res., 87(1): 39-47. https://doi.org/10.1016/j.still.2005.02.037

Hoyos, N. and Waylen, P. R. 2005. Seasonal and spatial patterns of erosivity in a tropical watershed of the Colombian Andes. J. Hydrol., 314: 177-191. https://doi.org/10.1016/j.jhydrol.2005.03.014

Hudson, N. W. 1965. The Influence of Rainfall on the Mechanics of Soil Erosion: With Particular Reference to Southern Rhodesia. MSc Thesis, University of Cape Town, p. 90.

Jiang, Z., Lian, Y. and Qin, X. 2014. Rocky desertification in Southwest China: Impacts, causes, and restoration. Earth Sci. Rev., 132: 1-12. https://doi.org/10.1016/j.earscirev.2014.01.005

Kinnell, P. I. A. 2005. Raindrop-impact-induced erosion processes and prediction: A review. Hydrol. Process., 19(14): 2815-2844. https://doi.org/10.1002/hyp.5788

Krogman, K. K. 1983. Annotated bibliography on soil erosion by wind applicable to southern Alberta agriculture. Government of Alberta, Alberta, pp. 1-29.

Ma, B., Liu, Y., Liu, X., Ma, F., Wu, F. and Li, Z. 2015. Soil splash detachment and its spatial distribution under corn and soybean cover. Catena, 127: 142-151. https://doi.org/10.1016/j.catena.2014.11.009

Morgan, R. P. C. 2005. Soil erosion and conservation. Third edition. Blackwell Publishing, Oxford, UK

Parsons, A. J., Abrahams, A. D. and Luk, S. H. 1991. Size characteristics of sediment in interrill overland flow on a semiarid hillslope, southern Arizona. Earth Surf. Process. Landforms, 16(2): 143-152. https://doi.org/10.1002/esp.3290160205

Pedersen, H. S. and Hasholt, B. 1995. Influence of wind speed on sage grouse metabolism. Catena, 24: 39-54. https://doi.org/10.1139/z95-088

Quansah, C. 1981. The effect of soil type, slope, rain intensity, and their interactions on splash detachment and transport. Eur. J. Soil Sci., 32(2): 215-224. https://doi.org/10.1111/j.1365-2389.1981.tb01701.x

Renschler, C. S., Mannaerts, C. and Diekkrüger, B. 1999. Evaluating spatial and temporal variability in soil erosion risk: Rainfall erosivity and soil loss ratios in Andalusia, Spain. Catena, 34(3-4): 209-225. https://doi.org/10.1016/S0341-8162(98)00117-9

Shanshan, W., Baoyang, S., Chaodong, L., Zhanbin, L. and Bo, M. 2018. Runoff and soil erosion on slope cropland: A review. J. Resour. Ecol., 9(5): 461-470. https://doi.org/10.5814/j.issn.1674-764x.2018.05.002

Shin, S. S., Park, S. D. and Choi, B. K. 2016. Universal power law for the relationship between rainfall kinetic energy and rainfall intensity. Adv. Meteorol., 1-11. https://doi.org/10.1155/2016/2494681

Syvitski, J.P.M., Kettner, A.J. and Green, P. 2005. Impact of humans on the flux of terrestrial sediment to the global coastal ocean. Science, 6: 376-380. https://doi.org/10.1126/science.1109454

Torri, D. and Poesen, J. 1992. The effect of soil surface slope on raindrop detachment. Catena, 19(6): 561-578. https://doi.org/10.1016/0341-8162(92)90053-E

van Dijk, A. I. J. M., Bruijnzeel, L. A. and Eisma, E. H. 2003. A methodology to study rain splash and wash processes. Hydrol. Process., 167: 153-167. https://doi.org/10.1002/hyp.1154

van Dijk, A. I. J. M., Bruijnzeel, L. A. and Rosewell, C. J. 2002. Rainfall intensity-kinetic energy relationships: A critical literature appraisal. J. Hydrol., 261(1-4): 1-23. https://doi.org/10.1016/S0022-1694(02)00020-3

Vrieling, A., Hoedjes, J. C. B. and van der Velde, M. 2014. Towards large-scale monitoring of soil erosion in Africa: Accounting for the dynamics of rainfall erosivity. Glob. Planet. Change, 115: 33-43. https://doi.org/10.1016/j.gloplacha.2014.01.009

Zuazo, V. H. and Pleguezuelo, C. R. 2008. Soil erosion and runoff prevention by plant covers: A review. Agron. Sustain. Dev., 28(1): 65-86. https://doi.org/10.1051/agro

Nature Environment and Pollution Technology
An International Quarterly Scientific Journal

p-ISSN: 0972-6268
(Print copies up to 2016)
e-ISSN: 2395-3454

Vol. 23 | No. 3 | pp. 1687-1696 | 2024

Original Research Paper

https://doi.org/10.46488/NEPT.2024.v23i03.040

Open Access Journal

# Research Insights into Punjab's Stubble Burning Menace

**Ruchi Kohli***, **Anu Mittal****† and **Amit Mittal*****

*Guru Nanak Dev University College, Narot Jaimal Singh-145026, Punjab, India

**Guru Nanak Dev University College, Patti-143416, Punjab, India

***Department of Pharmaceutical Chemistry, School of Pharmaceutical Sciences, Lovely Professional University, Phagwara-144411, Punjab, India

†Corresponding author: Anu Mittal; anuchem.patti@gndu.ac.in

**Nat. Env. & Poll. Tech.**
**Website: www.neptjournal.com**

*Received:* 21-12-2023
*Revised:* 21-02-2024
*Accepted:* 15-03-2024

**Key Words:**
Crop stubble
Environment
Residue
Stubble burning
Fire counts

## ABSTRACT

The current investigation endeavors to evaluate the prevalence of stubble burning in India, with a special focus on the state of Punjab. The study emphasizes the enormity of stubble burning by examining farm fire incidents, pollutant emissions, its detrimental impacts. It supports the effective management of crop residue along with proposing alternatives to stubble burning. The article conveys the message that stubble burning can result in deleterious effects on the environment, human health, crop growth, natural ecosystems, visibility, and physical infrastructure. The key solutions lie in education, functional literacy, a heightened awareness of environmental laws, rights and duties, stringent governance, and socially responsible public, promoting adherence to the National Green Tribunal's guidelines for managing crop residue and enlightening farmers about the ill effects of stubble burning on animal, soil, human health, crop biodiversity, and climate change. The available data of districts of Punjab indicates the recent waning trend in stubble burning, thus heralding a positive indication of environmental preservation. Decreased stubble burning is the reward of untiring government initiatives, support and subsidies, awareness programs, advanced research and technology, and enforcement of stringent regulations combined with recognition of the deleterious environmental impacts of stubble burning. This research article indicates that there is still a need for efforts to be made to eliminate stubble burning altogether.

## INTRODUCTION

Stubble burning is a human-induced catastrophe and a scorching topic of the present time. The long-standing post-harvest practice prevalent in regions globally is aimed at field waste elimination after harvesting. Farmers burn stubble (Fig. 1) due to time constraints for clearing fields for the next planting cycle, their convenience, cost considerations, scarcity of laborers, lack of awareness about crop residue management, and limited economically viable alternatives, etc. (Gottipati et al. 2021, Chawala et al. 2020). However, farmers often overlook the adverse effects of stubble burning. Burning of biomass is the major contributor to the emission of fine carbon particles and trace gases in the atmosphere. The pressing and contentious issue of Agricultural stubble burning can't be ignored due to its widespread negative impacts on human health, the environment, climate, and the economy. This paper aims to explore the consequences of stubble burning in the Punjab state of India and suggests strategies and solutions for mitigating this practice. The scope of the study lies in conserving the environment by finding sustainable agricultural alternatives safeguarding public health. It can also be utilized to develop policies and regulations to address the issue at regional and national levels.

## MATERIALS AND METHODS

The paper aims to gather insights into the status of stubble burning in India, with a particular focus on Punjab. Relevant literature and secondary data from various sources, including databases such as Google Scholar, Scopus, web of Science, books, national and international journals, and websites, were collected, and results were interpreted in light of the objectives of the study. Specific search items such as crop residue, stubble burning, India, emissions, Punjab, agriculture, fire counts, etc., were utilized. The authors thoroughly reviewed all collected papers.

## RESULTS AND DISCUSSION

Globally, biomass burning has surged in the past decades, with approximately 80% originating from Southeast Asia, Southern Africa, Australia, and South America (Sahu et

Fig. 1: Stubble burning and the huge volume of smoke produced.

al. 2015). Fig. 2 shows the crop residue burning in South Asian countries in the past fifty years. The heightened levels of crop residue burning in India, China, and the United States are particularly concerning. In relative terms, Africa experiences intensive rates per hectare, with notable growth in burning among the top 20 burners, including Mexico and Tanzania. Brazil, Indonesia, Thailand, India, and China have demonstrated significant progress in burning over the past decades.

According to the National Policy for Management of crop residues (NPMCR) report, India tops in crop waste production (500 Mt), followed by Bangladesh (72 Mt), Indonesia (55 Mt), and Myanmar (19 Mt) (Cassou 2018). Alarming statistics from the Intergovernmental Panel on Climate Change (IPCC) reveal that over 25% of crop residue is burnt on farms in India (Jain et al. 2014). The state-wise statistics of crop residue provided by the National Policy for Management of Crop Residues (NPMCR) report the highest crop residue generated in Uttar Pradesh (60 Mt), Punjab (51 Mt), and Maharashtra (46 Mt). The surplus crop residue generated from various crops is exhibited in Fig. 3a & 3b (Jain et al. 2018). In India, cereal crop residues constitute roughly two-thirds of the total 683 million tons of residue generated each year. About 500 million tons of residue is reused in sectors like industry, household and cattle feed. However, there is still an excess of 178 million tons that remain unutilized (MoA & FW. 2019), out of which 87 million tons are incinerated openly.

Globally, crop residue incineration is notably prevalent in Asia, driven primarily by a preference for rice. This trend is particularly pronounced in India, where the practice is 30% more prevalent than in China (mainland) and a striking 93% more common than in Pakistan. (Dutta et al. 2022) (Fig. 4).

## The Magnitude of Stubble Burning in India, with Special Reference to the Punjab

India's economic backbone hinges on agriculture, sustaining nearly 70% of the population depending on agricultural activities for income. India ranks as the world's second-largest producer of vital staple crops such as wheat, rice, and sugarcane. According to reports of the Union Ministry of Agriculture and Farmer's Welfare, the final estimates for food grain output show a remarkable surge in 2022-23, reaching a record 3296.87 lakh tons, which is an impressive 4% increase from than previous year. The recorded estimates for rice are 1357.55 lakh tons, wheat (1105.5 lakh tons), and maize at 380.85 lakh tons. Table 1 shows data on the quantity of agricultural waste produced, used, and burned (by the Indian Ministry of New and Renewable Energy) (NPMCR 2019).

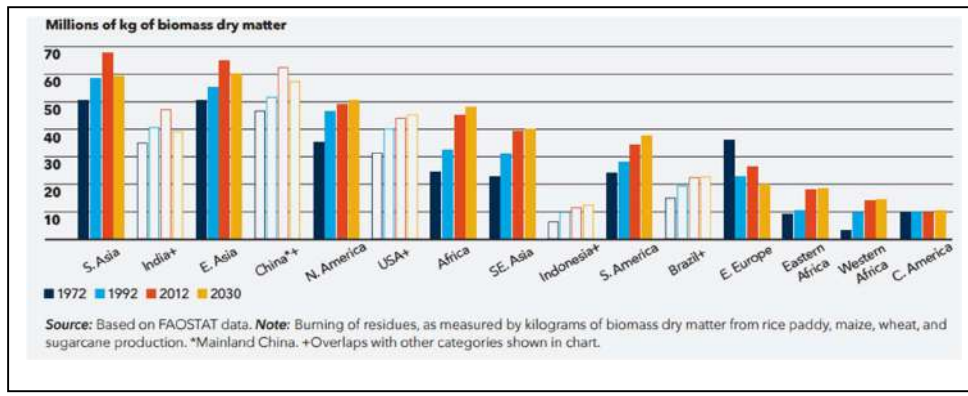


Fig. 2: Burning of crop residues in the past fifty years.

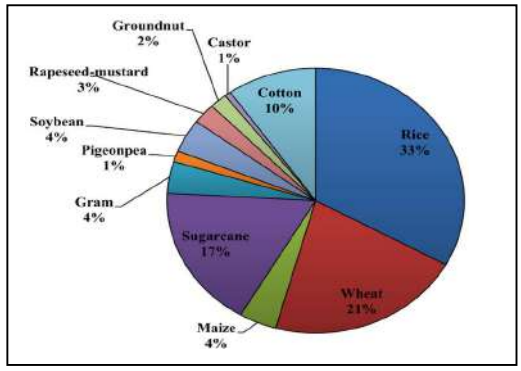


Fig. 3a: % of dry biomass share of different agricultural wastes in India.

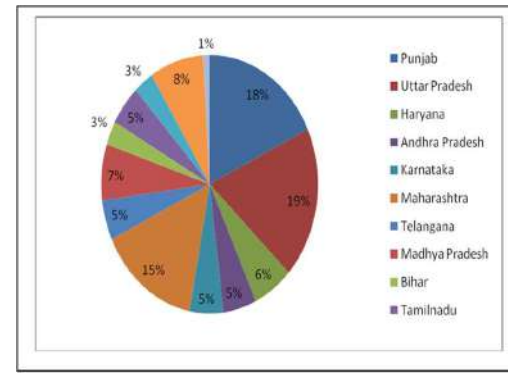


Fig. 3b: % of dry agricultural biomass produced in some states of India.

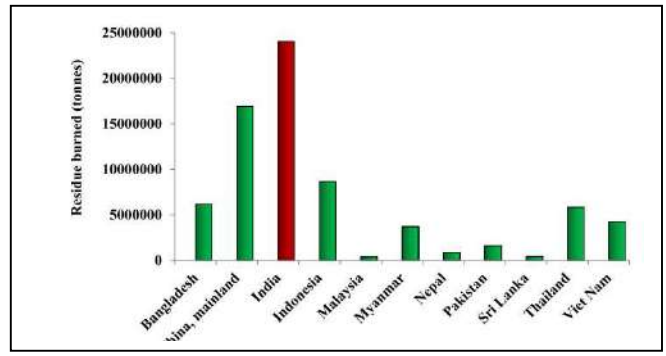


Fig. 4: Incidences of crop residue burning in South East Asian countries.

India's agrarian prowess, notably exemplified by states like Punjab and Haryana, sets a national standard in terms of total food grain production. These states lead, closely followed by Madhya Pradesh, Uttar Pradesh, and certain western and southern counterparts dominating nonfood grain production (Agricultural Statistics at a Glance 2022). Punjab has excelled in agriculture,

Showcasing spectacular performance with substantial wheat and rice surpluses, ensuring food security for India's 140 crore population. This success stems from extensive fertilizer use, pesticide application, large-scale machinery, and adoption of yielding input-intensive varieties alongside efficient irrigation. Despite this productivity, challenges arise with the generation of substantial crop residue called stubble. The shift to mechanized harvesting has intensified this issue, leading to diverse socio-economic, institutional, technological, and commercial constraints. Punjab alone incinerates 9 million tons of paddy residue (Datta et al. 2020, Jain et al. 2018). Post-harvest stubble burning in Punjab's agricultural fields has garnered global attention, underscored by a satellite image from NASA (National Aeronautics and Space Administration) resembling scenes observed in forest fire captures. Fig. 5 shows the total amount of crop produced and residue generated and burnt in various districts of Punjab (estimated using IPCC guidelines, 2019) in the agricultural year 2017-18. Data shows that ~42% of the total residue generated was burnt. The districts of Sangrur, Ludhiana, Patiala, Moga, and Bathinda burnt maximum crop residues (Singh et al. 2020).

Table 1: Data on agricultural waste.

| Quantity of agricultural waste produced | Quantity of agricultural waste utilized for domestic and industrial purposes | Surplus agricultural waste | Crop residue burned |
|---|---|---|---|
| 500 Mt | 360 Mt | 140 Mt | 92 Mt |

**Fire events:** Studying agricultural fire counts while examining stubble burning provides a comprehensive understanding of the practice's scope, environmental consequences, and trends over time. Agricultural fires serve as a catalyst, exacerbating air pollution and diminishing the air quality index (Rambani 2022). Effectively addressing farm fires is a proactive measure to enhance the air quality index (AQI). The detrimental impact of stubble burning on the state's air quality index has persisted for decades. Table 2

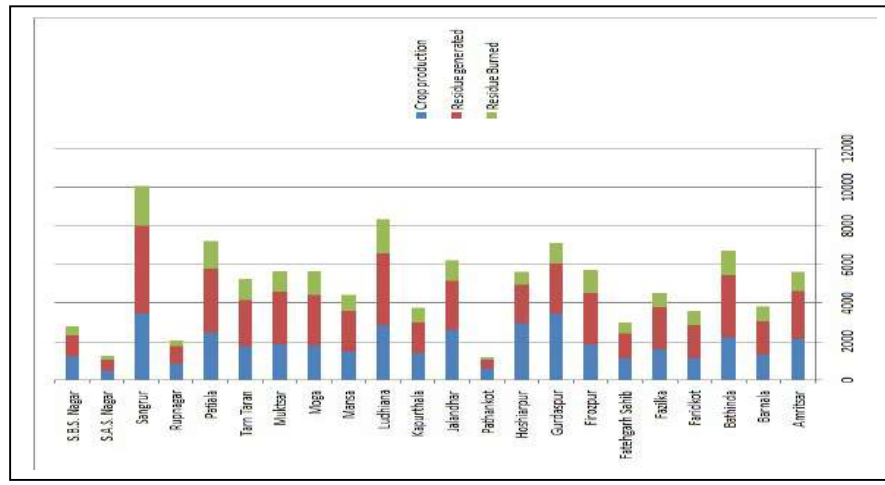


Fig. 5: District-wise distribution of crop produce, residue generated and burnt in Punjab (in kiloton) for the year 2017-18.

Table 2: Total farm fire event counts (Kharif Season) in Punjab, NCR-UP, Haryana, NCR-Rajasthan, and NCT of Delhi during 2021 and 2022.

| Sr. No. | State/UT | 2022 | 2021 | % change |
|---|---|---|---|---|
| 1. | Haryana | 3661 | 6987 | 47.60% |
| 2. | Punjab | 49922 | 71304 | 29.99% |
| 3. | U.P.-NCR+Rajasthan-NCR+NCT of Delhi | 198+1+10=209 | 252+3+4=259 | 21.43, 66.67, and no reduction, respectively. Average reduction=19.3% |
| Total | | 53,792 | 78,550 | 31.51% |

(Source: Ministry of environment, forest and climate change, 30 Nov. 2023)

presents the total number of active fire counts in 2021 and 2022 and the % reduction. Punjab witnessed a decline from 71304 to 49922 incidents in 2022, reflecting a 29.99% drop from the previous year. Additionally, in the U.P.-NCR, Rajasthan-NCR, and Delhi-NCT, stubble burning incidents decreased from 259 in 2021 to 209 in 2022, indicating a 19.30% reduction.

Over the last three years, there has been a noteworthy decline in paddy stubble-burning incidents in Punjab. In contrast to the cumulative 83,002 fire events due to paddy stubble burning in Punjab in 2020, the corresponding count dwindled to 71404 in 2021, further decreasing to 49,922 in 2022 and reaching a mere 36,663 in 2023 (Fig. 6) (Source: Ministry of Environment, forest and climate change, 30 Nov. 2023).

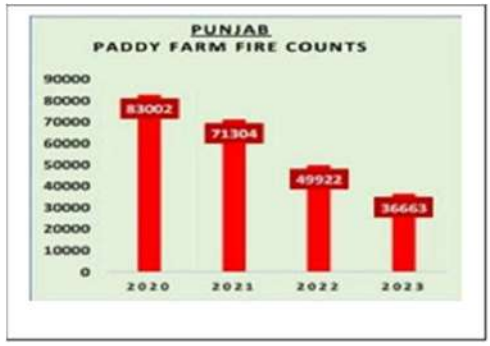


Fig. 6: Paddy farm fires in Punjab in 2020-2023.

## District-Wise Fire Count Percentage in Punjab

The percentage of fire events in each district w.r.t total fire counts for years 2022 and 2023, along with the percentage decrease in stubble fire counts in 2023 w.r.t 2022, are also computed (Table 3). For 2022, Sangrur dominates with> 10% fire events, followed by Bathinda and Ferozepur with ~8.9% and 8.1% respectively. The fire count percentage of Pathankot, S.A.S. Nagar, Rupnagar, and S.B. S. Nagar is found to be <1%. During 2022, the top five hotspot districts for crop burning were Sangrur, Bhatinda, Ferozepur, Muktsar, and Moga. Only Sangrur recorded more than 6000 fire counts in 2022, while in contrast, five districts surpassed 5000 fire counts in 2021. In 2023, the total no. of fire events reported due to crop burning is 43648 as compared with 59166 in 2022. In addition, the total number of fire events in each district shows a decrease. The 2023 data show Rupnagar and Muktsar observed more than 50% reduction in fire events in 2023 as compared to 2022 (source: crop burning. in).

The collaborative endeavors of the central government, Punjab government, NCR State government, and stakeholders,

Table 3: District-wise data of fire events in Punjab (2022 & 2023).

| District | Fire events (2022) | % of fire events (2022) | Fire events (2023) | % of fire events (2023) | %Reduction in number of fire events in 2023 w.r.t 2022 |
|---|---|---|---|---|---|
| Amritsar | 2522 | 4.26 | 2311 | 5.29 | 8.37 |
| Barnala | 2896 | 4.89 | 2502 | 5.73 | 13.60 |
| Bathinda | 5269 | 8.9 | 3736 | 8.56 | 29.09 |
| Faridkot | 2618 | 4.4 | 1978 | 4.53 | 24.45 |
| Fatehgarh Sahib | 1217 | 2.05 | 892 | 2.04 | 26.71 |
| Fazilka | 3163 | 5.3 | 2001 | 4.58 | 36.77 |
| Firozpur | 4806 | 8.1 | 3660 | 8.38 | 23.85 |
| Gurdaspur | 2082 | 3.5 | 1412 | 3.23 | 32.18 |
| Hoshiarpur | 1101 | 1.86 | 684 | 1.57 | 37.87 |
| Jalandhar | 2332 | 3.94 | 1805 | 4.13 | 22.60 |
| Kapurthala | 1941 | 3.28 | 1448 | 3.32 | 25.40 |
| Ludhiana | 3357 | 5.67 | 2676 | 6.13 | 20.28 |
| Mansa | 3062 | 5.17 | 2349 | 5.38 | 23.28 |
| Moga | 4027 | 6.8 | 3262 | 7.47 | 18.99 |
| Muktsar | 4063 | 6.86 | 1890 | 4.33 | 53.48 |
| Pathankot | 236 | 0.4 | 122 | 0.28 | 48.31 |
| Patiala | 3433 | 5.8 | 2039 | 4.67 | 40.60 |
| Rupnagar | 421 | 0.7 | 134 | 0.31 | 68.17 |
| Sahibzada Ajit Singh Nagar | 186 | 0.3 | 143 | 0.33 | 23.12 |
| Sangrur | 6136 | 10.37 | 5904 | 13.53 | 3.78 |
| Shahid Bhagat Singh Nagar | 542 | 0.9 | 469 | 1.07 | 13.47 |
| Tarn Taran | 3756 | 6.35 | 2231 | 5.11 | 40.60 |
| Total | 59166 | | 43648 | | 26.23 |

focusing on improved in situ crop management with crop residue management machinery, PUSA (Indian Agricultural Research Institute is popularly known as PUSA) bio decomposers Utilization, promotion of ex-situ options for paddy straw and conducting extensive awareness campaigns through print, electronic, and social media, have effectively contributed to a notable reduction in fire counts.

## Impacts of Stubble Burning

Stubble burning has severe consequences on both the environment and public health and exhibits unsustainability. Its emissions of greenhouse gases precipitate global warming, elevate particulate matter levels, induce smog with consequential visibility &health complications, and cause loss of biodiversity and soil fertility (Fig. 7). Crop residue burning releases two categories of pollutants: gaseous ($CH_4$, NOx, $N_2O$, $SO_2$, $CO_2$, CO) and particulate matter ($PM_{2.5}$, $PM_{10,}$ VOC) (Singh 2018). The extensive release of gaseous emissions, volatile organic compounds (VOCs), semi-volatile organic compounds (SVOCs), non-methane hydrocarbon (NHMC), and particulate matter during the burning of crop remnants poses a substantial threat to air quality and human well-being. $PM_{2.5}$ and $PM_{10}$ are recognized for their significant health impact. Awasthi et al. (2011) reported 78% and 43% respective increases in the $PM_{2.5}$ concentrations during the paddy and wheat stubble burning duration. Stubble burning and air pollution are inextricably linked both conceptually and contextually. In North India, during winter, particularly in November and December, the air quality deteriorates (Mishra 2019).

In the 5th Air Quality Report (AQR), it was revealed that about 60% of Indian cities documented annual $PM_{2.5}$ levels surpassing WHO guidelines by at least seven times. Particularly, elevated PM levels were observed between November and March. Table 4 shows emissions of various pollutants from the burning of different agricultural residues in India. The annual escalation in air pollution during the rice harvest (October to December) and wheat harvest (March to

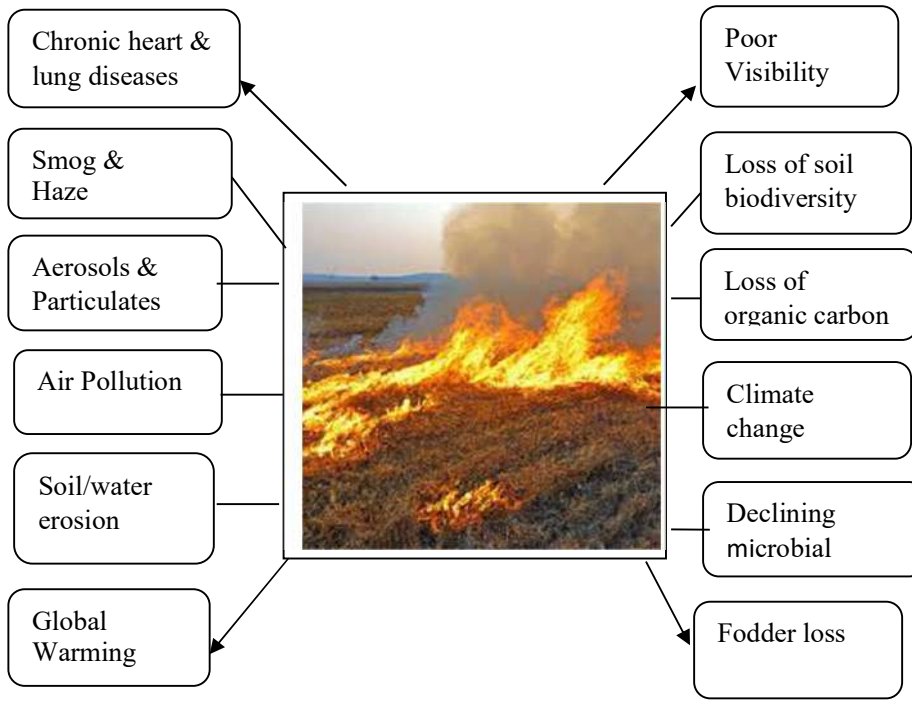


Fig. 7: Impacts of Stubble burning.

Table 4: Emission of different pollutants (Gg.year$^{-1}$*) from various crops in India in 2016-17 (Ravindra et al. 2019).

| Pollutants | Wheat | Rice | Cotton | Sugarcane | All Pulses | 9 oil seeds |
|---|---|---|---|---|---|---|
| Sulfur dioxide ($SO_2$) | 12.31 | 9.07 | 0.63 | 2.33 | 0.87 | 0.71 |
| Carbon monoxide (CO) | 861.38 | 4683.64 | 316.46 | 384.57 | 345.77 | 282.19 |
| Carbon dioxide ($CO_2$) | 54974.27 | 59,275.74 | 4022.31 | 12523.52 | 4527.50 | 3694.99 |
| Nitrous oxides (NOx) | 52.30 | 114.82 | 7.45 | 28.82 | 2.80 | 2.29 |
| Nitrous oxide($N_2O$) | 22.76 | 24.17 | 2.21 | 8.20 | 2.42 | 2.96 |
| Volatile organic compounds (VOC) | 215.34 | 352.53 | 20.93 | 24.38 | 28.05 | 22.89 |
| Polycyclic aromatic hydrocarbon (PAH) | .04 | .026 | .01 | .02 | .01 | .01 |
| Ammonia ($NH_3$) | 39.99 | 206.48 | 3.89 | 11.08 | 5.21 | 4.25 |
| Organic carbon (OC) | 8.92 | 150.58 | 5.47 | 36.57 | 2.80 | 2.29 |
| Elemental carbon (EC) | 4.92 | 25.68 | 2.45 | 7.76 | 1.88 | 1.54 |
| PM2.5 | 264.57 | 418 | 11.66 | 42.11 | 15.63 | 12.75 |
| PM10 | 175.35 | 458.29 | 13.01 | 44.33 | 32.25 | 26.32 |

*1 Gg.year$^{-1}$ = 1000 tonnes.year$^{-1}$

May) is attributed to stubble burning. The stubble-burning practice is primarily pervasive in Punjab, Haryana, and Uttar Pradesh and significantly contributes to the severe winter pollution crisis observed in Delhi and other cities within NCR (Das et al. 2023). In 2015, rice and wheat burning periods in Punjab accounted for 86.7% of $PM_{10}$ and 53.2% of $PM_{2.5}$ (Singh 2015). In 2022, the average $PM_{2.5}$ level was reported to be 53.3 µg.m$^{-3}$ as compared to 58.1 µg.m$^{-3}$ in 2021, and Delhi (NCT) came out as the world's fourth most polluted Metropolitan city with $PM_{2.5}$ levels of 92.6 µg.m$^{-3}$ (source: iqair.com).

Major pollutant emissions on stubble burning, along with their % share, are shown in Fig. 8a & 8b. The highest contribution to emissions came from burning paddy straw, accounting for 40%, followed by wheat at 22% and sugarcane at 20% (Fig. 8b) (Jain et al. 2014).

Table 5 shows district-wise emission data of air pollutants of Punjab 2017-18 according to the IPCCs 2019

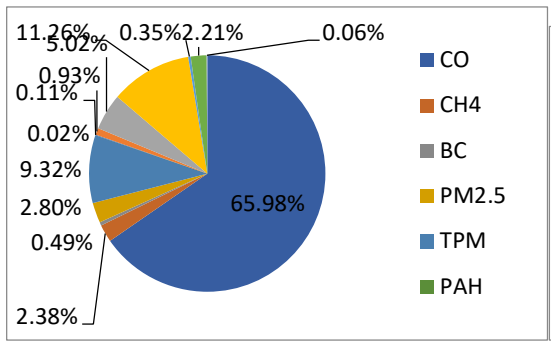


Fig. 8a: Emission of pollutants and GHGs on burning.

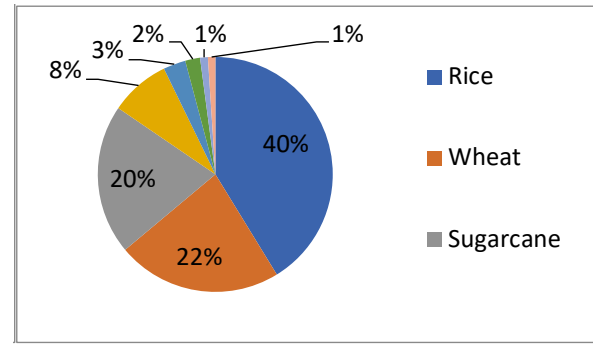


Fig. 8b: Share of different crops in stubble burning.

Table 5: Emission of various pollutants from crop burning in different districts of Punjab (2017-18) (in Gg*).

| | $SO_2$ | $CO_2$ | $CH_4$ | CO | NOx | $N_2O$ | $NH_3$ | NMVOC | EC | OC | PAH | $PM_{2.5}$ | $PM_{10}$ |
|---|---|---|---|---|---|---|---|---|---|---|---|---|---|
| Amritsar | 0.25 | 1386.81 | 7.95 | 75.96 | 2.19 | 0.57 | 3.35 | 7.12 | 0.43 | 2.30 | 0.004 | 6.92 | 8.28 |
| Bathinda | 0.32 | 1745.02 | 9.32 | 90.60 | 2.64 | 0.72 | 3.86 | 8.82 | 0.51 | 2.59 | 0.005 | 8.04 | 9.82 |
| Barnala | 0.19 | 1054.03 | 6.45 | 61.56 | 1.71 | 0.43 | 2.72 | 5.56 | 0.34 | 1.87 | 0.003 | 5.58 | 6.58 |
| Faridkot | 0.18 | 987.35 | 5.91 | 56.13 | 1.57 | 0.40 | 2.48 | 5.17 | 0.31 | 1.69 | 0.003 | 5.10 | 6.06 |
| Fatehgarh Sahib | 0.13 | 759.70 | 4.54 | 43.47 | 1.23 | 0.31 | 1.92 | 3.96 | 0.24 | 1.33 | 0.002 | 3.95 | 4.68 |
| Fazilka | 0.20 | 1064.12 | 4.91 | 47.99 | 1.50 | 0.44 | 2.01 | 5.12 | 0.28 | 1.31 | 0.002 | 4.24 | 5.42 |
| Ferozpur | 0.28 | 1601.31 | 9.69 | 91.99 | 2.56 | 0.66 | 4.07 | 8.42 | 0.51 | 2.77 | 0.005 | 8.36 | 9.90 |
| Gurdaspur | 0.25 | 1374.32 | 7.57 | 73.84 | 2.21 | 0.58 | 3.23 | 6.87 | 0.44 | 2.36 | 0.004 | 6.77 | 8.07 |
| Hoshiarpur | 0.17 | 927.10 | 3.96 | 43.58 | 1.47 | 0.39 | 1.63 | 4.28 | 0.29 | 1.34 | 0.002 | 3.66 | 4.46 |
| Jalandhar | 0.26 | 1436.17 | 8.31 | 80.56 | 2.32 | 0.60 | 3.51 | 7.38 | 0.46 | 2.49 | 0.004 | 7.30 | 8.64 |
| Kapurthala | 0.17 | 956.64 | 5.84 | 56.21 | 1.57 | 0.39 | 2.47 | 5.03 | 0.32 | 1.73 | 0.003 | 5.09 | 5.97 |
| Ludhiana | 0.40 | 2276.46 | 13.96 | 133.31 | 3.70 | 0.94 | 5.88 | 12.01 | 0.74 | 4.06 | 0.007 | 12.09 | 14.23 |
| Mansa | 0.21 | 1152.31 | 6.18 | 59.53 | 1.74 | 0.48 | 2.57 | 5.82 | 0.33 | 1.71 | 0.003 | 5.33 | 6.52 |
| Moga | 0.28 | 1597.03 | 9.89 | 94.07 | 2.59 | 0.65 | 4.16 | 8.47 | 0.52 | 2.85 | 0.005 | 8.54 | 10.04 |
| Pathankot | 0.04 | 225.43 | 1.09 | 11.00 | 0.35 | 0.09 | 0.46 | 1.08 | 0.07 | 0.34 | 0.001 | 0.98 | 1.20 |
| Patiala | 0.35 | 1948.65 | 11.59 | 110.28 | 3.10 | 0.80 | 4.88 | 10.17 | 0.61 | 3.33 | 0.006 | 10.03 | 11.92 |
| Rupnagar | 0.09 | 469.30 | 2.22 | 23.18 | 0.73 | 0.19 | 0.90 | 2.28 | 0.14 | 0.66 | 0.001 | 1.95 | 2.38 |
| Sangrur | 0.48 | 2723.24 | 16.53 | 157.78 | 4.40 | 1.12 | 6.96 | 14.31 | 0.88 | 4.79 | 0.009 | 14.32 | 16.90 |
| S.A.S. Nagar | 0.06 | 295.31 | 1.41 | 13.88 | 0.43 | 0.12 | 0.58 | 1.43 | 0.08 | 0.39 | 0.001 | 1.23 | 1.54 |
| Shri Muktsar Sahib | 0.27 | 1500.77 | 8.32 | 79.39 | 2.30 | 0.62 | 3.47 | 7.65 | 0.44 | 2.32 | 0.004 | 7.17 | 8.70 |
| S.B.S.Nagar | 0.11 | 611.82 | 3.36 | 33.08 | 0.98 | 0.25 | 1.41 | 3.09 | 0.19 | 1.01 | 0.002 | 2.96 | 3.53 |
| Tarn Taran | 0.26 | 1441.65 | 8.72 | 82.93 | 2.31 | 0.59 | 3.67 | 7.57 | 0.46 | 2.51 | 0.005 | 7.54 | 8.92 |
| Total | 4.94 | 27534.53 | 157.74 | 1520.30 | 43.60 | 11.37 | 66.22 | 141.61 | 8.59 | 45.72 | 0.08 | 137.16 | 163.75 |

*1 $Gg.year^{-1}$ = 1000 $tonnes.year^{-1}$

(refinement of 2006) (Singh et al. 2020). The burning of around 20.3 Mt of crop residue in Punjab resulted in the release of $PM_{2.5}$ (137.2 Gg) and $PM_{10}$ (163.7 Gg). Additionally, Punjab witnessed emissions of 8.6 Gg of Elemental Carbon (EC), 45.7 Gg of organic carbon (OC), and 0.08 Gg of polycyclic aromatic hydrocarbons (PAHs). Exposure to particulate matter and gaseous emissions leads to various health problems, such as respiratory and heart diseases, lung cancer, and premature death. Kumar et al. (2015) reported that farmers complained about eye and

lung irritation. Open burning of seed stubble, according to Gadde et al. (2009), emits dioxins such as polychlorinated dibenzo-p-dioxins, polychlorinated dibenzofurans (PCDFs), and polycyclic aromatic hydrocarbons (PAHs), with carcinogenic properties. Stubble burning poses formidable health risks, including chronic obstructive pulmonary diseases, pneumoconiosis, bronchitis, skin ailments, eye irritation, cataracts, corneal opacity, blindness, emphysema, and heightened susceptibility to pulmonary tuberculosis (Kumar et al. 2015, Saggu et al. 2018).

Pollutants from crop stubble burning lead to the death of living organisms, as the elevated levels of CO in the blood convert hemoglobin into carboxyhemoglobin, which is unable to transport oxygen to different parts of the body. This leads to breathlessness, especially for one's with respiratory problems like asthma, bronchitis, and cardiovascular diseases. As per the World Health Organisation (WHO), nearly 7 million deaths per year are attributed to poor ambient air pollution, leading to stroke, heart disease, lung cancer, and chronic respiratory diseases (WHO 2008). Expectant women and young children are especially at risk from the smoke generated by stubble burning. High pollution levels led to a reduction of about 6.4 years in life expectancy for the residents of Delhi (Ghude et al. 2016).

Burning crop residues decreases soil fertility by loss of organic C, N, and other essential nutrients in the soil (Kumar et al. 2015). Soil's natural ability to renew its nutrient levels decreases as helpful microorganisms also get killed during fire. Crop residue isn't mere trash; it stands as a valuable asset. Cereal crops retain 25% N, 50% S, and 75% K from the soil in their residue. Estimates reveal that the burning of paddy straw leads to substantial loss of nutrients, losses viz. 59000 tons of nitrogen, 20000 tons of phosphorus, 34000 tons of potassium, and 3.85 million tons of organic carbon (Saini et al. 2019). Furthermore, crops face challenges from ground-level ozone (Abdurrahman et al. 2020). $SO_2$ and NOx contribute to acid rain, which not only damages plants but also affects soil quality and corrode man-made structures.

Stubble burning disrupts the soil pH, moisture levels, and biotic elements (e.g., bacteria, algae, fungi, protozoa), resulting in significant imbalances. Burning of crop residues leads to the burning of organic carbon into $CO_2$, as well as a shift in nitrogen equilibrium, resulting in the conversion of usable nitrogen in the soil to oxides of nitrogen, which are lost to the atmosphere. Consequently, there is a striking loss of 0.824 million tons of NPK from the soil (Dutta et al. 2022). The elevated soil temperature caused by stubble burning, ranging up to 33.8-42.2 °C, eradicates soil-friendly bacteria, fungi, and other microbes (Gupta et al. 2004). Milk production of livestock plummets by 50% during the stubble-burning period.

**Management of Stubble: Progress Till Now**

1. **Detection and prevention:** to detect and forestall real-time burning, employing a synergy of cutting-edge remote sensing technology, specifically satellite imagery, along with a team of local authorities like SDM, Tehsildar, BDO, Patwaris, and village level workers prove highly productive.
2. **Banning crop residue burning:** Stubble burning has been officially designated as transgression pursuant to the Air Act (1981), the code of criminal procedure, 1973, and other pertinent legislative frameworks. Furthermore, a stringent penalty is levied upon any offending farmer found violating this prohibition. Administrative authorities are currently orchestrating vigorous enforcement measures at both the village and block level.
3. **Establishing a marketplace for stubble:** Intensive endeavors are underway to enhance the diversified utilization of paddy straw and crop residues. Notably, leveraging the substantial calorific content of paddy straw, it serves as a viable fuel source in biomass power plants. Furthermore, its application extends to the production of biofuels and organic fertilizers and contributes to the paper and cardboard industries (Porichha et al. 2021). This comprehensive approach aims to attribute tangible economic and commercial value to agricultural residues, discouraging their incineration as an economic detriment to farmers.
4. **Public awareness campaigns:** Continual endeavors spotlight the health ramifications of crop residue burning, yielding elevated levels of harmful particulates detrimental to well-being. Concurrently, initiatives persist via farmer camps, training sessions, workshops, and televised programs.
5. **Subsidy on agricultural machinery:** The state government, in conjunction with the central government, offers subsidies on mechanized implements facilitating soil tillage to retain crop residue, enhancing soil fertility, or channeling it for commercial purposes. However, the excessive costs render these implements inaccessible to the majority of farmers, limiting current access to a small fraction.
6. **Crop diversification:** Promoting the cultivation of alternative crops with reduced residue production and extended intervals between cropping cycles is underway. Diversification efforts in cropping techniques aim to curb stubble burning.

Table 6: Crop residue management strategies.

| Sr. No. | Crop residue management strategies | |
|---|---|---|
| 1. | Use of Specialized machinery | Happy seeder, zero till seed drill, Baler, Rotavator, Paddy straw chopper, Reaper binder, etc. agricultural machinery should be employed. |
| 2. | Technological interventions | Retention of crop residue by mulching, incorporation, using stubble for composting/ vermicomposting, Mushroom cultivation, promoting agricultural service centres, improvement in combine-harvester, using stubble for cement industry and packaging industry. |
| 3. | Diverse uses of crop residue | Power generation, production of cellulosic ethanol in PPP mode, use for paper/board/panel and packing material, use as fodder, decomposing stubble to turn it into beneficial manure. |

### Alternatives to Stubble Burning

Stubble management is a critical aspect of modern agriculture. Effective stubble management is essential for maintaining soil health and air quality and promoting sustainable agricultural practices. Several concerns associated with stubble burning, such as air pollution, soil degradation, and decreased soil fertility, etc., have led to the need to develop and adopt crop stubble management strategies as listed in Table 6 (Parihar et al. 2023).

### Best Practices

1. The Chhattisgarh Gauthans model is an innovative experiment undertaken by the Chhattisgarh government where stubble (parali) is collected through daan and converted to organic fertilizer. The scheme generates employment for the rural youth.
2. Creating initiatives akin to the Mahatma Gandhi National Rural Employment Guarantee Act (MGNREGA) for harvesting and composting crop residues can greatly enhance sustainable agriculture and environmental conservation efforts.
3. The most efficient current technology to combat stubble burning is the turbo happy seeder.
4. Harnessing straw for electricity generation

### Future Steps

1. Embrace early maturing rice varieties to afford farmers additional time for meticulous field clearance and optimal wheat sowing.
2. To advocate for a transformative shift in Punjab's wheat rice rotation urging a diversified cropping cycle for sustained benefits in the medium and long run.
3. To expedite the decomposition of rice and wheat stubble into compost by developing environment-friendly, user-friendly, and cost-friendly chemicals.
4. Bales of rice straw can serve as effective mulch for reseeding and erosion control purposes.
5. Utilization of rice straw bales as construction material for environment-friendly buildings.
6. Dispel misconceptions among farmers regarding the methodologies and expenses associated with alternative technologies.

## CONCLUSIONS

In terms of annual biomass burned, India and China emerge as the biggest burners of crop residue worldwide. The stubble burning is a major global contributor to atmospheric pollution, releasing gaseous pollutants and particulate matter that adversely impact both human health and the environment. Its effects are dreadful. In 2023, the major stubble-burning districts of Punjab were Sangrur, Bathinda, and Ferozepur. In contrast, the least residue-burning districts include Rupnagar, Sahibzada Ajit Singh Nagar, Shaheed Bhagat Singh Nagar, and Pathankot. The study concludes that the number of stubble-burning cases has recently declined in Punjab. Research promotes the adoption of exemplary agricultural practices, ensuring widespread accessibility of advanced crop residue management technologies such as the happy seeder and super seeder, along with encouraging crop cycle diversification. The government should prioritize subsidizing cutting-edge crop residue technologies and implement compelling behavior change strategies to address the issue collaboratively, leveraging the active participation of farmers. State government can incentivize the farmers to adopt eco-friendly methods and penalize those who don't. There is a strong need for more policies to find a feasible solution and also collaborative efforts by government, NGOs, academicians, researchers, and farmers to eliminate stubble burning altogether.

## REFERENCES

Abdurrahman, M. I., Chaki, S. and Saini, G. 2020. Stubble burning: Effects on health & environment, regulations, and management practices. Environ. Adv., 2: 100011.

Agricultural Statistics at a Glance, 2022. Directorate of Economics and Statistics. Ministry of Agriculture, Govt of India, New Delhi.

Awasthi, A., Singh, N., Mittal, S., Gupta, P. K. and Agarwal, R. 2010. Effects of agriculture crop residue burning on children and

young on PFTs in North West India. Sci. Total Environ., 408: 4440-4445.
Cassou, E. 2018. Field Burning. Agricultural Pollution. World Bank, Washington, DC.
Chawala, P. and Sandhu, H. A. S. 2020. Stubble burn area estimation and its impact on ambient air quality of Patiala & Ludhiana district, Punjab, India. Heliyon, 6: e03095.
Datta, A., Emmaneul, M. A., Ram, N. K. and Dhingra, S. 2020. Crop residue management: Solution to achieve better Air Quality. TERI, New Delhi.
Das, P., Behera, M. and Abhilash, P. 2023. A rapid assessment of stubble burning and air pollutants from satellite observations. Trop. Ecol., 5: 65. https://doi.org/10.1007/s42965-022-00291-5.
Dutta A., Patra A., Hazra K. K., Natha, C. P., Kumar, N. and Rakshit, A. 2022. A state-of-the-art review in crop residue burning in India: Previous knowledge, present circumstances, and future strategies. Environmental Challenges, 8: 100581.
Gadde, B., Menke, C. and Wassmann, R. 2009. Rice straw as a renewable energy source in India, Thailand, and the Philippines: Overall potential and limitations for energy contribution and greenhouse gas mitigation. Biomass Bioenergy, 33: 1532-1546.
Ghude, S. D., Chate, D. M., Jena, C., Beig, G., Kumar, R., Barth, M. C., Pfister, G. G., Fadnavis, S. and Rao, P. 2016. Premature mortality in India due to $PM_{2.5}$ and ozone exposure. Geophys. Res. Lett., 43: 4650-4658. http://dx.doi.org/10.1016/j.envdev.2015.07.009.
Gottipati, R., Burra, M. N. and Pavan, Menon, S. 2021. Stubble burning: Root cause, impacts and its management in Indian scenario. Environ. Conserv. J. 22: 37-45.
Gupta, P. K., Sahai, S., Singh, N., Dixit, C. K., Singh, D. P., Sharma, C. and Garg, S. C. 2004. Residue burning in rice-wheat cropping system: Causes and implications. Curr. Sci., 87: 1713- 1715.
Jain, N., Sehgal, V. K., Singh, S. and Kaushik, N. 2018. Estimation of surplus crop residue in India for biofuel production. Technology Information, Forecasting and Assessment Council (TIFAC), New Delhi.http://krishi.icar.gov.in/jspui/handle/123456789/34455
Jain, N., Bhatia, A. and Pathak, H. 2014. Emission of air pollutants from crop residue burning in India. Aerosol Air Qual. Res. 14: 422-430.
Kumar, P., Kumar S. and Joshi L. 2015. Socioeconomic and Environmental Implications of Agricultural Residue Burning: A Case Study of Punjab, India Springer.
MoA & FW. 2019. Report of the Committee on Review of the Scheme "Promotion of Agricultural Mechanisation for In-Situ Management of Crop Residue in States of Punjab, Haryana, Uttar Pradesh and NCT of Delhi. Department of Agriculture, Cooperation & Farmers Welfare, Ministry of Agriculture and Farmers Welfare, Government of India, New Delhi
Mishra, M. 2019. Poison in the air: Declining air quality in India. Lung India 36: 160.
NPMCR. 2019 Available online: http://agricoop.nic.in/sites/default/files/NPMCR_1.pdf (accessed on 6 March 2023).
Parihar, D. S., Narang, M. K., Dogra, B., Prakash, A. and Mahadik, A. 2023. Rice residue burning in Northern India: an assessment of environmental concerns and potential solutions-a review. Environ. Res. Commun. 5: 062001.
Porichha, G. K., Hu, Y., Venkateswara Rao, K. T. and Xu, C. C. 2021. Crop residue management in India: Stubble Burning vs. Other Utilizations including bioenergy. Energies, 14: 4281.
Rambani, J. K. 2022. Stubble burning and air pollution in Punjab: A sociological exploration. J. Posit. Psychol., 6: 8933-8942.
Ravindra, K., Singh, T. and Mor, S. 2019. Emissions of air pollutants from primary crop residue burning in India and their mitigation strategies for cleaner emissions. J. Clean. Prod., 208: 261-273. doi:10.1016/j.jclepro.2018.10.031.
Saggu, G. S., Mittal, S. K., Agarwal, R. and Beig, G. 2018. Epidemiological study on respiratory health of school children of rural sites of Malwa region (India) during post-harvest stubble burning events. MAPAN, 33: 281-295.
Sahu, L. K., Sheel, V., Pandey, K., Yadav, R., Saxena, P. and Gunthe, S. 2015. Regional biomass burning trends in India: Analysis of satellite fire data, J. Earth Syst. Sci., 124(7): 1377-1387.
Saini, D. K., Singh, V. K. and Kumar A. 2019 Stubble burning: either farmer to be punished or technology needs to be improved? Biomol. Rep., 56: 759.
Singh, R. P., Chanduka, L. and Dhir, A. 2015. Impacts of stubble burning on ambient air quality of a critically polluted area-Mandi-Gobindgarh. J. Pollut. Eff. Cont., 3: 1000135. https://doi. org /10.4172/2375-4397.1000135
Singh, J. 2018. Paddy and wheat stubble blazing in Haryana and Punjab states of India: A menace for environmental health. Environ. Qual. Manag., 28: 47-53.
Singh, T., Biswal, A., Mor, S., Ravindra, K., Singh, V. and Mor, S. 2020. A high-resolution emission inventory of air pollutants from primary crop residue burning over Northern India based on VIIRS thermal anomalies. Environ. Pollut., 266: 115132.
Singh, T., Biswal, A., Mor, S., Ravindra, K., Singh, V. and Mor, S. 2020. A high-resolution emission inventory of air pollutants from primary crop residue burning over Northern India based on VIIRS thermal anomalies. Environmental Pollution, 266: 115132.
World Health Organization (WHO). 2008. Health Risks of Ozone from Long-range Transboundary Air Pollution. Retrieved from https://www.euro.who.int/data/assets/pdf_file/0005/78647/E91843 (Accessed on June 27th, 2020).

## ORCID DETAILS OF THE AUTHORS

Ruchi Kohli: https://orcid.org/0000-0001-5544-036X
Anu Mittal: https://orcid.org/0000-0001-8121-8703
Amit Mittal: https://orcid.org/0000-0001-9689-1642

Nature Environment and Pollution Technology
An International Quarterly Scientific Journal

p-ISSN: 0972-6268
(Print copies up to 2016)
e-ISSN: 2395-3454

Vol. 23 | No. 3 | pp. 1697-1708 | 2024

Original Research Paper

https://doi.org/10.46488/NEPT.2024.v23i03.041

Open Access Journal

# Spatial and Temporal Variation of Air Quality Index in Amman-Zarqa Urban Area

**A. Al-Kraimeen*, S. Hamasha** and M. Abu-Allaban*†**

*Department of Water Management and Environment, Prince El-Hassan bin Talal Faculty for Natural Resources and Environment, The Hashemite University, Zarqa 13133, Jordan

**Department of Physics, Faculty of Science, The Hashemite University, Zarqa 13133, Jordan

†Corresponding author: M. Abu-Allaban; mlaban@hu.edu.jo

**Nat. Env. & Poll. Tech.**
**Website: www.neptjournal.com**

*Received:* 24-12-2023
*Revised:* 20-01-2024
*Accepted:* 02-02-2024

**Key Words:**
Carbon monoxide
$PM_{10}$
$PM_{2.5}$
$NO_2$
Ozone
Amman-Zarqa area

## ABSTRACT

This paper aimed to investigate the Spatial and Temporal Variation of the air quality index (AQI) in the Amman and Zarqa Metropolitan Areas during the period 2016-2022 following the method adopted by the Environmental Protection Agency of the United States of America (EPA). Air quality data for $PM_{10}$, $PM_{2.5}$, $O_3$, $NO_2$, $SO_2$, and CO recorded at five monitoring stations were downloaded from the official website of the Jordanian Ministry of Environment. Calculated AQI values were generally between the Good class (AQI <50) and the Moderate class (AQI 50-100) at all stations, the AQI calculations for $PM_{10}$ demonstrated a noticeable increase during autumnal months, likely due to natural dust. $PM_{2.5}$ demonstrated seasonal variation, with higher values in winter months where residents burn fossil fuel for heating. Stabel air in winter due to the cooled land surface, and the weak natural air mix and ventilation contribute to the deterioration of air quality. Calculated individual AQI for $SO_2$ and $NO_2$ reveals that all extent of the study area falls in the Good AQI class. Similarly, CO and ozone-based AQI values fluctuate within the "Good" class, with occasional episodes of compromised air quality at specific stations.

## INTRODUCTION

Air pollution refers to the presence of harmful substances in the air, such as particulate matter, gases, and pollutants, which can have adverse health effects (Manisalidis et al. 2020). Common sources include vehicle emissions, industrial activities, and natural processes. Its health impacts vary but can include respiratory and cardiovascular problems, increased risk of lung diseases, and other serious health issues. Long-term exposure to high levels of air pollution is associated with a higher risk of developing chronic conditions and can contribute to premature mortality. The World Health Organization estimated that 2.4 people around the world die every year because they are exposed to poor air quality (Sierra et al. 2012). Additionally, air pollution can harm the environment, affecting ecosystems, water bodies, and climate patterns. It is a significant global concern, and efforts to reduce pollution are crucial for public health and environmental sustainability.

Urban areas are particularly susceptible to deteriorated air quality because of anthropogenic activities that release tons of air contaminants. Air quality at a monitoring station depends on meteorological conditions, atmospheric stability, contaminants transported from remote sources, and local natural and anthropogenic sources in addition to the ability of the atmosphere, either to disperse or absorb these pollutants (Jayamurugan et al. 2013).

Environmental impacts of air pollution include acid rain, smog, odors, and global warming. Acid rain adversely affects soil, aquatic life, forest resources, and other environmental features. Smog restricts visibility due to the spread of airborne particles that cause light scattering (Gold & Samet 2013). Air pollution damages property and materials. Antiques are important cultural and economic commodities that are particularly sensitive to air quality as well as microclimates. Hundreds of ancient monuments around the globe have been destroyed because of acid rain and other chemically active airborne agents (Abu-Allaban & El-Khalili 2014).

Global warming is largely blamed on certain air pollutants (carbon dioxide, methane, nitrous oxides, halogens, and sulfur hexafluoride) and their sources (Orru et al. 2017, Singh et al. 2021, Pinho-Gomes et al. 2023). Air pollution can have a significant impact on metals, dies, and stone materials used in buildings, sculptures, and monuments (Ruffolo et al. 2023). Corrosion is mainly caused by wet or dry deposition of airborne acidic pollutants. It is estimated that the annual cost of corrosion worldwide is over 3% of the world's GDP (Rao et al. 2016). Air pollution may also impair visibility by creating a white or brown haze that affects how far we

can see (Majewski et al. 2021). Haze is largely caused by air pollution from human activity including industry, power generation, transportation, and agriculture.

Sources of air pollutants include road traffic, marine vessels, shipping, air traffic, industry, construction, mining, residential heating, wildfires, agricultural activities, dust storms, and volcanic eruptions (Curtis et al. 2006). Common air pollutants in urban areas include tropospheric ozone ($O_3$), sulfur dioxide ($SO_2$), nitrogen dioxide ($NO_2$), carbon monoxide (CO), and airborne particulate matter ($PM_{10}$ and $PM_{2.5}$). Atmospheric abundances of these pollutants are typically higher in urban areas compared to rural areas (UN 2023). Negative impacts of air pollutants become more profound when their concentrations exceed recommended standards (Katsouyanni & Analitis 2009), which identifies limits of air pollutants to reduce exposure risks for people with health problems and sensitive groups (Bachmann 2007).

National ambient air quality standards (NAAQS) are, therefore, legally binding and enforced nationwide. Trained occupation safety and health personnel, site engineers and technicians, environmental inspectors, and researchers are well aware of NAAQS, which is often difficult to convey to the public. Therefore, a simplified air quality indicator, or air quality index (AQI), is used to inform the public about current and forecasted air quality in their domains to take necessary preventive measures. This paper aims to investigate air quality by calculating the Air Quality Index (AQI) as defined by the EPA at the Amman-Zarqa urban area during 2016-2020. This is the most populous metropolitan area in Jordan and most industrial and utility projects are concentrated therein.

## STUDY AREA

The study area is situated at the center of Jordan (Fig. 1) where more than five million persons work and reside (DOS 2023). This region is dominated by rough terrain with elevation ranges between 370 m and 1126 m above the main sea level. It includes two cities: Amman and Zarqa.

Amman is the political and economic capital of Jordan. It enjoys a Mediterranean climate with air temperature rarely exceeding 40ºC on hot summer days and annual precipitation ranges between 150 mm to 580 mm (Dabbour et al. 2021). 80% of industries and vehicles are situated in Amman, where most Jordanians live and work. Local sources of air pollution in Amman include transportation, fugitive dust, industry, brick workshops, rock cutting, and home heating (Alnawaiseh et al. 2015).

Zarqa, to the east of Amman, suffers harsh hot and dry weather conditions with annual precipitation rarely exceeding 150 mm, but because of its proximity to Amman, a good percentage of Zarqa dwellers work in Amman. This leads to heavy trafficking between the two cities. Similar to Amman, the main sources of air pollution sources in Zarqa include motor vehicles, industry, and natural dust from local and regional dust storms (Al-Mashaqbeh et al. 2015), in addition to an oil refinery and a thermal power plant.

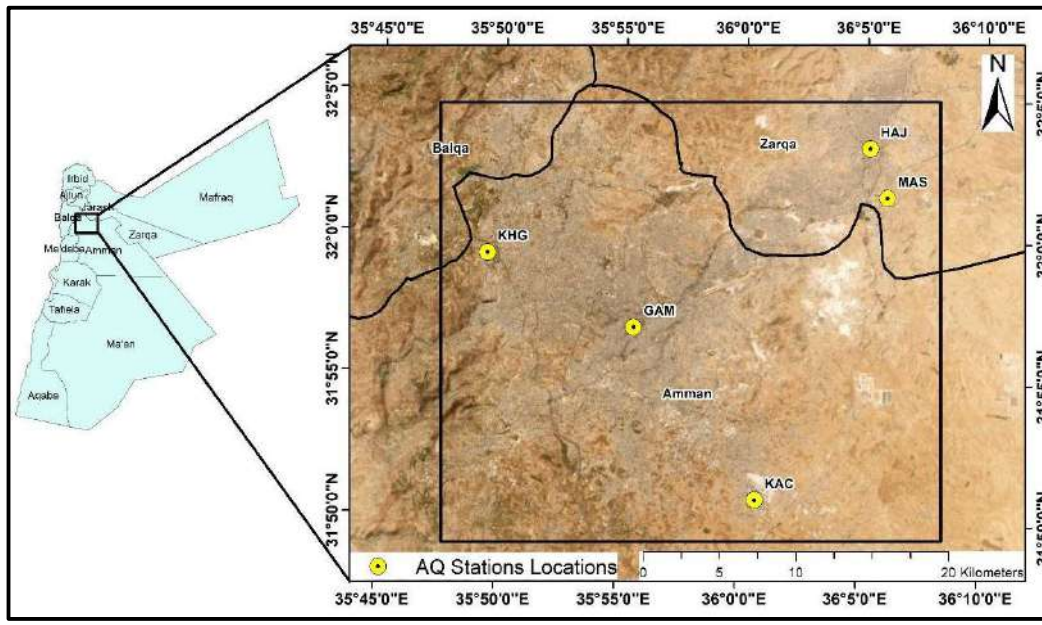


Fig. 1: Location map of the study area with five national air quality monitoring stations.

Natural dust storms, fugitive dust, and frequent stagnation, particularly in autumn and winter, in addition to concentrated anthropogenic activities in the Amman-Zarqa metropolitan area, put air quality under pressure. This situation motivated research groups to investigate and address air quality in this populous area. Saffarini & Odat (2008) examined various time series analyses of the yearly air pollution and reported long-term variations in yearly air pollution at Al-Hashimeya town located at the north-eastern corner of Amman-Zarqa metropolitan area for the years 1992 to 2004 and detected decreasing levels of atmospheric $NO_2$, CO, $H_2S$, NO, and TSP. Al-Mashaqbeh and colleagues reported improved air quality at Al-Hashimeya town after upgrading the Al-Samra wastewater treatment plant, which replaced the outdated sewage facility (Al-Mashaqbeh et al. 2015). Alnawaiseh and colleagues investigated the association between vehicle counts and airborne particulates at four locations in Amman: Downtown, Marka, Shmeisani, and Abu-Nsair. Their findings demonstrated that total elevated concentrations of suspended particulate (TSP) and $PM_{10}$ are associated with large traffic counts and low air temperature (Alnawaiseh et al. 2015). Jaber & Abu-Allaban conducted a study to map the spatial distribution of tropospheric ozone in the northern parts of Jordan, which includes part of the Amman Zarqa metropolitan area, and detected elevated ozone levels on hot days at several parts of the study area due to regional transport of ozone precursors (Jaber & Abu-Allaban 2017). Odat and colleagues conducted a study to assess the influence of Meteorological Parameters on Air Quality at the campus of Hashemite University for two years (1/1/2012 through 30/12/2013) and reported a positive correlation between tropospheric ozone and air temperature, wind speed, and wind direction (Odat et al. 2017).

## MATERIALS AND METHODS

### Data Procurement

Concentrations of airborne $PM_{10}$, $PM_{2.5}$, $O_3$, $NO_2$, $SO_2$, and CO at five monitoring stations were downloaded from the official website of the Jordanian Ministry of Environment (Table 1 & Table 2).

### Data Analysis

After collecting the data, a primary statistical analysis was performed to characterize the data (Table 3)

### Air Quality Index

The AQI is a measure of daily air quality at a particular site used to inform the general public of how clean the air is and stresses the health repercussions that a person may experience in the hours or days following inhaling polluted air. It can be calculated following the method adopted by the U.S. Environmental Protection Agency the following formula (EPA 2018).

Table 1: Air quality stations used in this study and their locations.

| Location | Station Name | Abbreviation | Longitude | Latitude |
|---|---|---|---|---|
| Amman | Greater Amman Municipality | GAM | 35.925921 | 31.945829 |
| | King Abdullah II Industrial City/Sahab | KAC | 36.012713 | 31.846026 |
| | King Hussein Gardens | KHG | 35.823449 | 31.987676 |
| Zarqa | Health Center Wadi Hajar | HAJ | 36.0865 | 32.054607 |
| | Main Slaughterhouse Factories (Masane') Zone | MAS | 36.0992 | 32.025635 |

Table 2: Time periods for the five monitoring stations.

| Parameter | Unit | Data Period | | | | |
|---|---|---|---|---|---|---|
| | | GAM | KAC | KHG | HAJ | MAS |
| $PM_{10}$ (24-hour) | $\mu g.m^{-3}$ | 1/1/2016 to 18/2/2022 | 1/1/2016 to 18/2/2022 | 1/1/2016 to 18/2/2022 | 1/1/2016 to 18/2/2022 | 1/1/2016 to 18/2/2022 |
| $PM_{2.5}$ (24-hour) | $\mu g.m^{-3}$ | 19/2/2022 to 31/12/2022 | 19/2/2022 to 31/12/2022 | 19/2/2022 to 31/12/2022 | 19/2/2022 to 31/12/2022 | 19/2/2022 to 31/12/2022 |
| $O_3$ (8-hour) | Ppm | NA | 1/1/2016 to 31/12/2022 | 1/1/2016 to 31/12/2022 | NA | NA |
| $NO_2$ (1-hour) | Ppb | 1/1/2016 to 31/12/2022 | 1/1/2016 to 31/12/2022 | 1/1/2016 to 31/12/2022 | 1/1/2016 to 31/12/2022 | 1/1/2016 to 31/12/2022 |
| $SO_2$ (1-hour) | Ppb | 1/1/2016 to 31/12/2022 | 1/1/2016 to 31/12/2022 | 1/1/2016 to 31/12/2022 | 1/1/2016 to 31/12/2022 | 1/1/2016 to 31/12/2022 |
| CO (8-hour) | Ppm | 1/1/2016 to 31/12/2022 | NA | NA | 1/1/2016 to 31/12/2022 | NA |

Table 3: Statistical summary of air quality data collected at five monitoring stations in the Amman-Zarqa metropolitan area during the period 2016-2022.

| Parameter | Station | Minimum | Maximum | Average | Standard Deviation |
|---|---|---|---|---|---|
| $NO_2$ (1-hour) ppb | GAM | 0.01 | 267.00 | 28.99 | 15.10 |
| | KAC | 0.49 | 117.00 | 16.60 | 8.78 |
| | KHG | 0.54 | 42.10 | 8.06 | 6.16 |
| | HAJ | 1.80 | 60.70 | 23.19 | 10.60 |
| | MAS | 4.95 | 56.30 | 22.96 | 8.58 |
| $SO_2$ (1-hour) ppb | GAM | 0.15 | 82.00 | 11.99 | 8.61 |
| | KAC | 1.36 | 34.50 | 7.66 | 4.56 |
| | KHG | 0.10 | 204.00 | 4.24 | 4.86 |
| | HAJ | 0.75 | 61.00 | 12.59 | 9.79 |
| | MAS | 1.07 | 41.40 | 6.25 | 3.00 |
| CO (8-hour) ppm | GAM | 0.00 | 6.50 | 2.20 | 1.29 |
| | KAC | NA | NA | NA | NA |
| | KHG | NA | NA | NA | NA |
| | HAJ | 0.00 | 37.55 | 2.15 | 1.65 |
| | MAS | NA | NA | NA | NA |
| $O_3$ (8-hour) ppm | GAM | NA | NA | NA | NA |
| | KAC | 0.00 | 0.05 | 0.01 | 0.01 |
| | KHG | 0.00 | 0.07 | 0.03 | 0.02 |
| | HAJ | NA | NA | NA | NA |
| | MAS | NA | NA | NA | NA |
| $PM_{10}$ (24-hour) $\mu g.m^{-3}$ | GAM | 4.72 | 411.00 | 49.10 | 36.42 |
| | KAC | 4.31 | 306.00 | 46.69 | 31.59 |
| | KHG | 4.08 | 488.00 | 34.39 | 29.20 |
| | HAJ | 7.73 | 419.00 | 58.25 | 37.61 |
| | MAS | 5.08 | 372.00 | 56.52 | 37.98 |
| $PM_{2.5}$ (24-hour) $\mu g.m^{-3}$ | GAM | 7.37 | 498.00 | 29.46 | 32.37 |
| | KAC | 9.22 | 430.00 | 31.70 | 30.88 |
| | KHG | 8.94 | 468.00 | 22.23 | 27.47 |
| | HAJ | 15.30 | 486.00 | 40.38 | 31.97 |
| | MAS | 10.80 | 464.00 | 38.45 | 32.79 |

$$I_p = \frac{I_{Hi} - I_{Low}}{BP_{Hi} - BP_{Low}} \times (c_{P-BP_L}) + I_{Low} \quad \ldots(1)$$

Where:

$I_p$ is the AQI value for pollutant p, Cp is the concentration of pollutant p, $BP_{hi}$ is the concentration breakpoint that is greater than or equal to Cp, $BP_{low}$ is the concentration breakpoint that is less than or equal to Cp, $I_{hi}$ is the AQI value corresponding to $BP_{hi}$, and $I_{low}$ is the AQI value corresponding to $BP_{low}$.

The values of AQI classes and breakpoints for each parameter are found in EPA (2018). After calculating the AQI values for each parameter, the attained values are converted into six colors (codes) to inform the general public in an easy, simple, and understandable way (Table 4).

## RESULTS AND DISCUSSION

### Temporal Variation of $PM_{10}$ and $PM_{2.5}$

$PM_{10}$ and $PM_{2.5}$ can have significant health effects, but

Table 4: Classification of AQI values based on EPA standards (EPA 2018).

| AQI Value | Color | Description |
|---|---|---|
| 0-50 | Green | Good |
| 51-100 | Yellow | Moderate |
| 101-150 | Orange | Unhealthy for sensitive group |
| 151-200 | Red | Unhealthy |
| 201-300 | Purple | Very Unhealthy |
| 301-500 | Maroon | Hazardous |

$PM_{2.5}$ is generally considered to be more harmful to human health due to its smaller particle size. $PM_{2.5}$ particles can penetrate deeper into the respiratory system and even enter the bloodstream, reaching the lungs' alveoli and causing more severe health effects, and ability to enter the bloodstream, $PM_{2.5}$ particles have been linked to a higher risk of cardiovascular diseases, including heart attacks and strokes. That said, both $PM_{2.5}$ and $PM_{10}$ can cause harm to health, and exposure to elevated levels of either type should be minimized. Regulatory measures and air quality standards are often in place to monitor and control levels of both $PM_{2.5}$ and $PM_{10}$ to protect public health.

AQI values calculated for $PM_{10}$ varied between 15 and 85 (Fig. 2). Most AQI values revealed good air quality (AQI <50), with few exceptions where the AQI exceeded 50 but remained below 100, indicating good to moderate air quality at the five stations based on $PM_{10}$ concentrations. Natural dust leads to elevated $PM_{10}$ in autumn and spring leading to higher AQI values at the five monitoring stations. The two stations located at Zarqa City (Health Center at Wadi Hajar and Main Slaughterhouse) experienced the highest $PM_{10}$ concentrations while King Hussein Gardens at Amman enjoyed the lowest $PM_{10}$ levels during the monitoring period. Zarqa is located in a hot and dry area where air temperature frequently approaches 40°C in summer months while receiving low precipitation leading to loose and dry soil particles that can be easily picked up by wind as fugitive dust. Jordan is frequently impacted by dust storms originating in North Africa or the Arabian Peninsula which leads to elevated dust levels at southern and eastern barren territories that lack adequate vegetation to suppress dust emission. Emissions from local sources, including vehicles, light industries, and home heating, also contribute to $PM_{10}$ and $PM_{2.5}$.

The $PM_{2.5}$ data were only available for the period March 2022 to December 2022. Monitoring stations at all stations recorded high $PM_{2.5}$ concentrations in April and December. High $PM_{2.5}$ are attributed to emissions from natural and anthropogenic sources activities including wildfires,

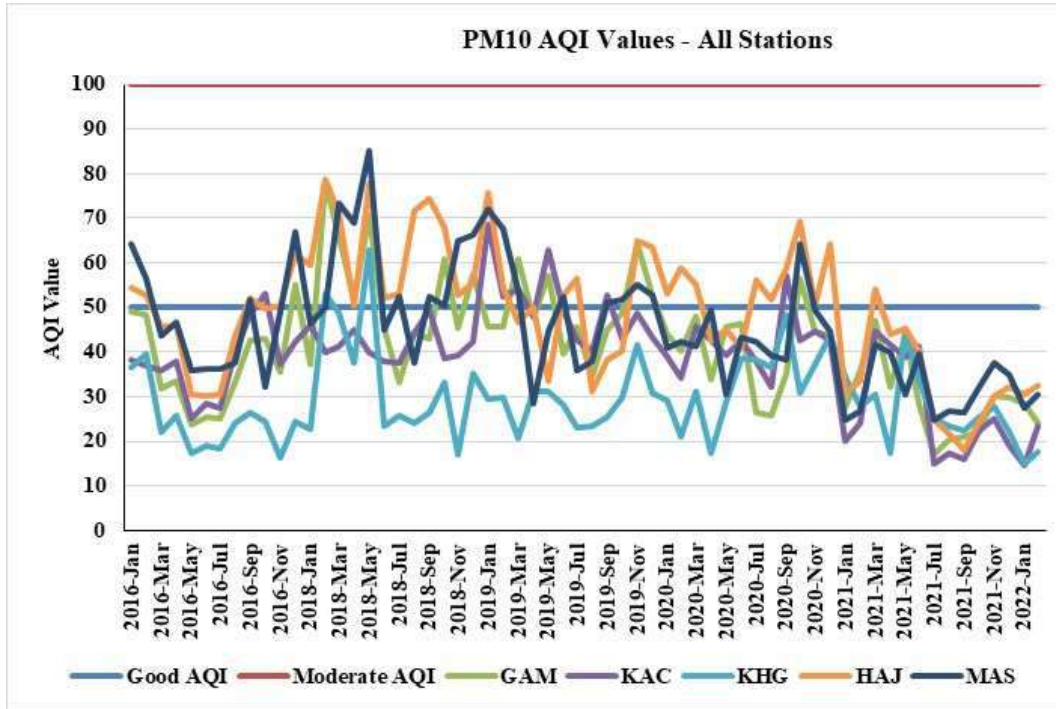


Fig. 2: Mean monthly AQI values for $PM_{10}$ at five air quality monitoring stations in the Amman-Zarqa metropolitan area during the period 2016-2022.

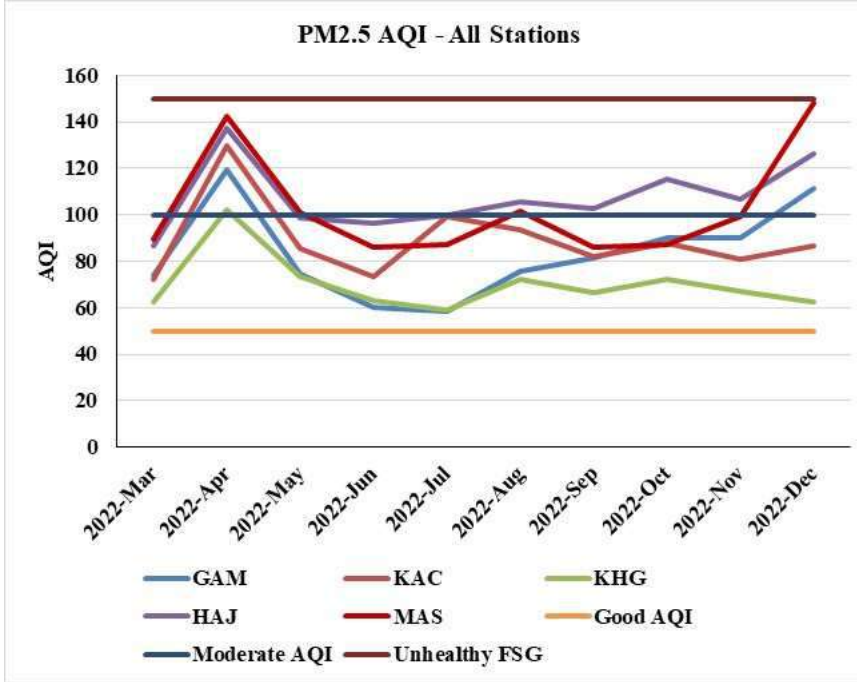


Fig. 3: Mean monthly AQI values for $PM_{2.5}$ at five air quality monitoring stations in the Amman-Zarqa metropolitan area in 2022.

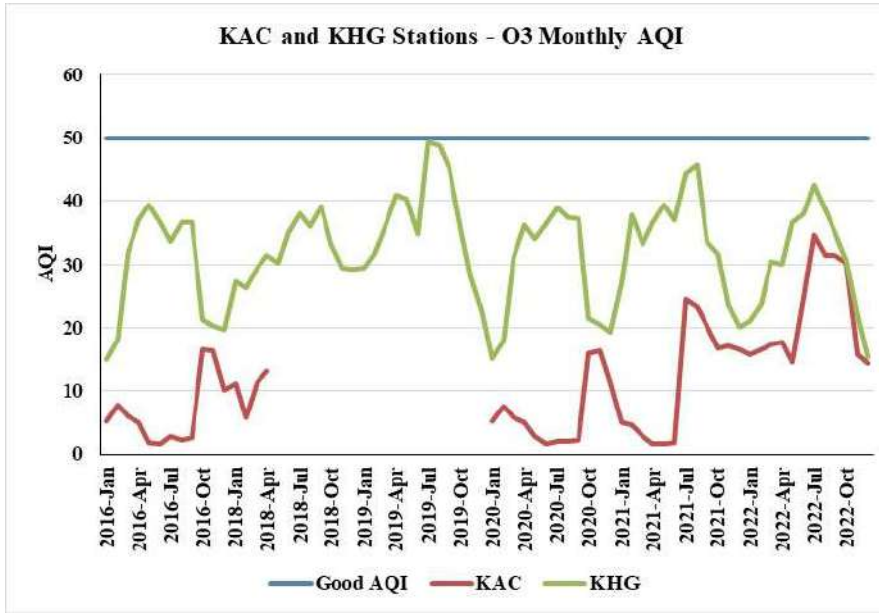


Fig. 4: Mean monthly AQI values for tropospheric ozone at KAC and KHG monitoring stations during the period 2016-2022.

transportation, and burning of fossil fuel for home heating or power generation.

The temporal variation of AQI based on $PM_{2.5}$ fluctuates between good (code green) and unhealthy (code red) air quality (Fig. 3). Highest values were recorded at the Factories Zone in Zarqa during April and December. Cold Earth surface in winter and long nights in spring and autumn promote thermal inversion that halts the mixing of air and constrains dispersing contaminants leading to elevated levels of air pollutants including $PM_{2.5}$.

**Temporal Variation of Tropospheric Ozone**

Readings of tropospheric ozone were available for two monitoring stations only. Therefore, AQI values based on Ozone readings were calculated for King Abdullah II Industrial City (KAC) and King Hussein Gardens (KHG) monitoring stations and found to be below 50 (Fig. 4) indicating good air quality in terms of with respect to tropospheric ozone (code green). Ozone is a secondary photosynthetic gas produced when nitrogen oxides and hydrocarbons transported from regional sources undergo chemical reactions in the air. This implies that ozone created due to activities performed at these stations won't be readily detected at nearby monitoring stations.

**Temporal Variations of Carbon Monoxide**

The monthly air quality index (AQI) based on CO readings collected at the monitoring stations located at the main building of Greater Amman Municipality (GAM) and the Health Center of Wadi Hajar (HAJ) were below 50 (code green) indicating good air quality at both stations (Fig. 5). However, there are notable differences between GAM and HAJ regarding the magnitude and consistency of AQI values. In GAM, the monthly AQI values for CO consistently remained within the good air quality range, ranging from 20.85 to 36.11. This indicates that GAM generally exhibited stable and satisfactory air quality conditions for CO throughout the year. The highest recorded AQI value in GAM was 41.79 in February 2020, which still falls within the moderate air quality range. Despite this temporary increase, GAM's air quality for CO remained relatively consistent, indicating effective control measures and minimal fluctuations in CO emissions.

HAJ experienced a wider range of AQI values compared to GAM. The monthly AQI values for CO in HAJ ranged from 12.75 to 66.47, demonstrating greater variability in air quality levels. In January 2018, HAJ recorded a significantly high AQI value of 63.77, indicating moderate air quality. This suggests that HAJ experienced occasional episodes of compromised air quality for CO, potentially due to local emission sources or meteorological factors.

When comparing GAM and HAJ, it is evident that GAM exhibited slightly more consistent air quality for CO throughout the year. This could be attributed to several factors, including variations in local emission sources, meteorological conditions, and geographic features. GAM's relative stability in air quality may be attributed to effective air pollution control measures, including regulations on vehicle emissions and industrial activities.

In contrast, HAJ's wider range of AQI values indicates greater fluctuations in air quality, which various factors

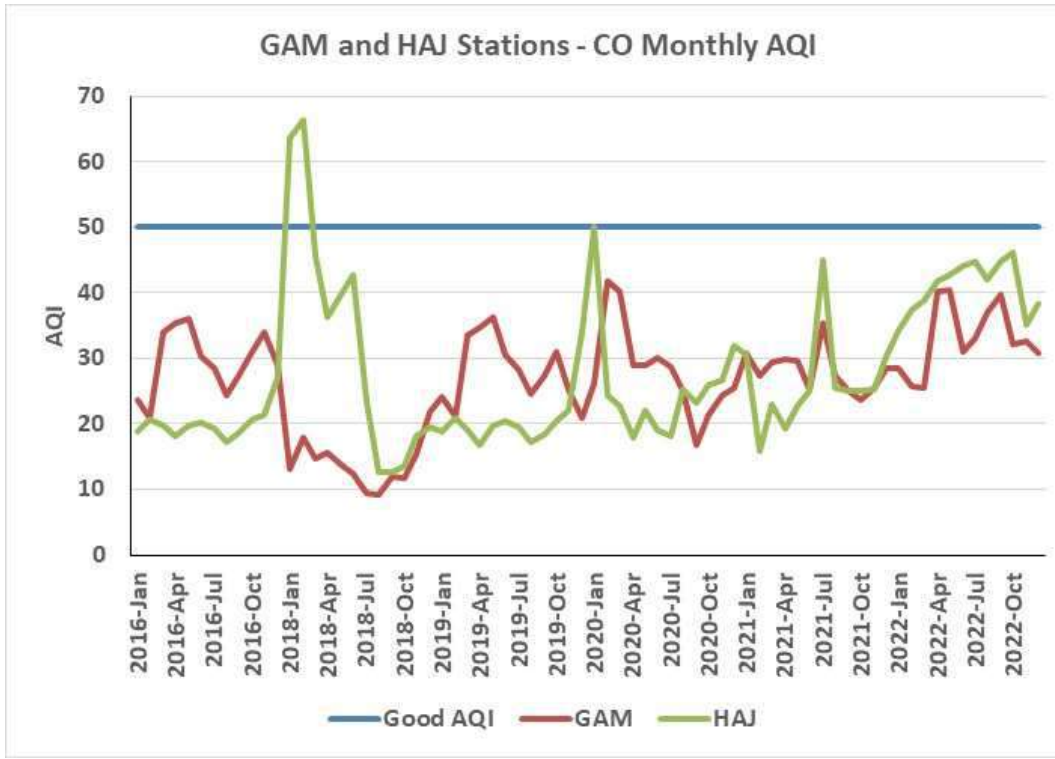


Fig. 5: Mean monthly AQI values for CO readings collected at GAM and HAJ monitoring stations during the period 2016-2022.

could influence. Further analysis is required to identify specific sources contributing to higher AQI values in HAJ. Nonetheless, periodic monitoring, analysis, and implementation of appropriate air quality management measures are crucial for both GAM and HAJ to ensure continuous improvement and maintenance of air quality, particularly for CO.

### Temporal Variations of Sulfur Dioxide

The monthly air quality index (AQI) results for sulfur dioxide ($SO_2$) in the locations of GAM, KAC, KHG, HAJ, and MAS provide valuable insights into the variations in air quality levels throughout the year, comparing them to the good air quality threshold of 50. The data reveals distinct patterns and differences among these locations, indicating variances in $SO_2$ emissions and air quality management practices.

GAM consistently demonstrated monthly AQI values for $SO_2$ below the good air quality threshold of 50, ranging from 3.19 to 29.37. These values consistently indicated good air quality, suggesting the effectiveness of measures implemented in controlling $SO_2$ emissions in GAM throughout the year (Fig. 6).

Similarly, in the station KAC, the AQI values for $SO_2$ varied between 3.19 and 25.94. These values consistently remained below the AQI threshold of 50, indicating that the air quality in KAC was predominantly in the "Good" category throughout the observed months. The low maximum AQI value of 25.94 further demonstrates the area's relatively low levels of $SO_2$ pollution.

In the case of KHG, the monthly AQI values ranged from 2.19 to 9.92. These values signify that the air quality in KHG consistently stayed within the "Good" category, indicating minimal impact from $SO_2$ pollution. The highest AQI value of 9.92 further reinforces the station's good air conditions for $SO_2$.

In contrast, the station HAJ exhibited higher fluctuations in AQI values, ranging from 2.54 to 60.85. Although most recorded months experienced "Good" air quality for $SO_2$, the maximum AQI value of 60.85 indicates an instance where the air quality temporarily exceeded the acceptable threshold. This suggests the possibility of occasional higher concentrations of $SO_2$ in the atmosphere, potentially due to localized emission sources or meteorological factors.

Lastly, the station MAS demonstrated consistent "Good" air quality for $SO_2$, with AQI values ranging from 3.14 to 20.68. The relatively low maximum AQI value of 20.68 indicates that the air quality in MAS remained well below the acceptable threshold, implying favorable air quality conditions for the residents.

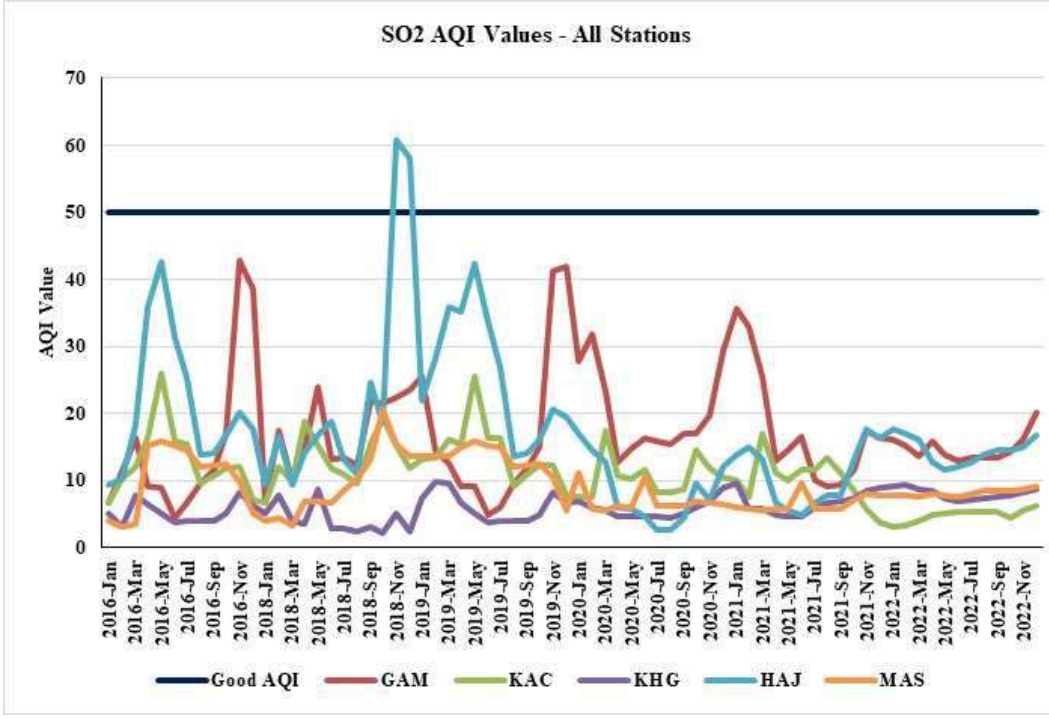


Fig. 6: Mean monthly AQI values for $SO_2$ at five air quality monitoring stations in the Amman-Zarqa metropolitan area during the period 2016-2022.

**Temporal Variations of Nitrogen Dioxide**

In GAM, the monthly average AQI values for $NO_2$ generally remain below the threshold of "good" air quality AQI of 50 throughout the year. However, slight fluctuations can be observed. During the winter months (December to February), the AQI values range from 22.31 to 36.52, indicating a relatively better air quality compared to other seasons. The summer months (June to August) exhibit slightly comparable AQI values, ranging from 26.38 to 26.99. Overall, GAM maintains good air quality with only minor fluctuations (Fig. 7).

KAC also demonstrates relatively good air quality throughout the year, with the monthly average AQI values for $NO_2$ mostly staying below the "good" level of 50. KAC experienced higher AQI values during the winter months (December to February), ranging from 14.25 to 20.81. The summer months (June to August) show slightly lower AQI values, ranging from 11.81 to 17.74. KAC generally maintains good air quality, although there are slight seasonal variations.

At KHG, the monthly average AQI values for $NO_2$ consistently remain below the threshold of "good" air quality level of 50 throughout the year. The winter months (December to February) exhibit slightly higher AQI values, ranging from 13.39 to 19.78, while the summer months (June to August) show lower AQI values, ranging from 3.14 to 5.82. KHG consistently maintains good air quality, with only minimal variations observed.

HAJ demonstrates relatively good air quality, with the monthly average AQI values for $NO_2$ mostly remaining below 50. Similar to the other locations, HAJ experienced higher AQI values during the winter months (December to February), ranging from 17.13 to 18.86. The summer months (June to August) display slightly lower AQI values, ranging from 12.38 to 15.44. HAJ generally maintains good air quality, with seasonal variations within a relatively narrow range.

MAS also enjoyed good air quality, with the monthly average AQI values for $NO_2$ remaining below the "good" level of 50 throughout the year. Similar to the other locations, MAS experienced higher AQI values during the winter months (December to February), ranging from 12.92 to 30.43. The summer months (June to August) exhibit slightly lower AQI values, ranging from 13.62 to 17.26. MAS maintains good air quality with seasonal variations within an acceptable range.

When comparing the locations, it is evident that all five locations generally maintain good air quality with monthly

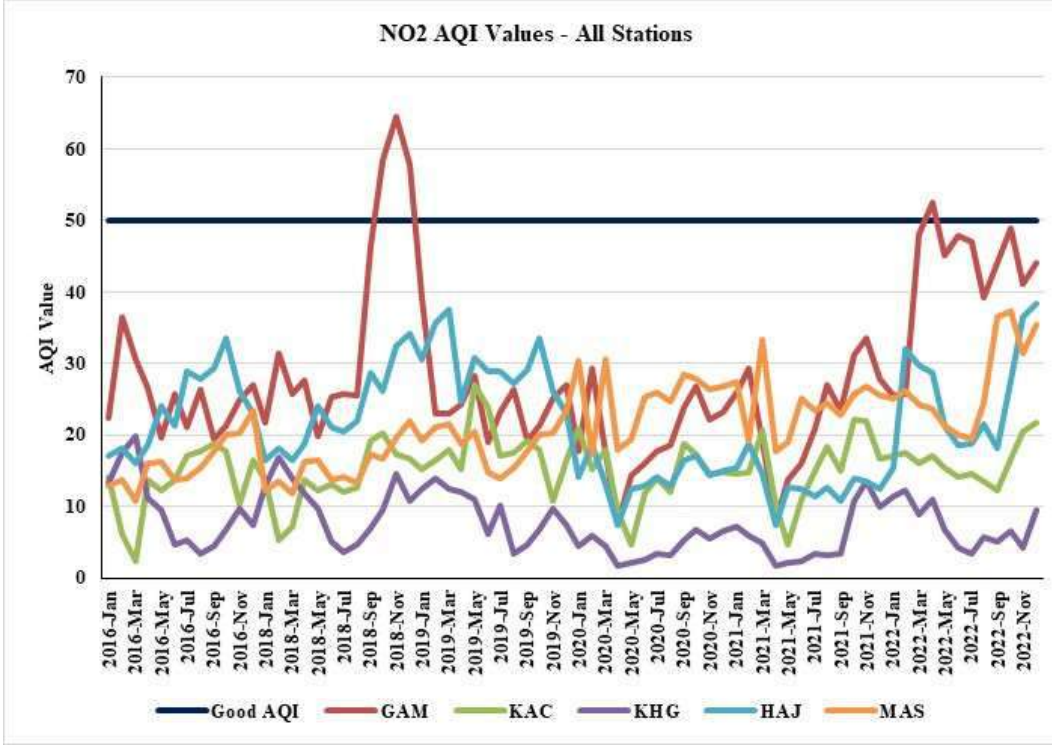


Fig. 7: Mean monthly AQI values for $NO_2$ at five air quality monitoring stations in the Amman-Zarqa metropolitan area during the period 2016-2022.

average AQI values for $NO_2$ below 50. However, slight differences can be observed. For example, KHG consistently exhibits the lowest AQI values among the locations, indicating consistently good air quality. On the other hand, MAS occasionally shows higher AQI values, particularly during the winter months. KAC and HAJ exhibit relatively similar patterns, while GAM consistently maintains good air quality with minimal fluctuations.

The observed seasonal variations in the AQI values can be attributed to several factors. Higher AQI values may occur during the winter months due to increased emissions from heating sources, limited atmospheric dispersion, and potential temperature inversions. Burning fossil fuels in residential and commercial heating systems can release pollutants such as nitrogen dioxide, leading to higher winter AQI values. Limited atmospheric dispersion during this season hinders the dilution and dispersal of pollutants, contributing to higher AQI values. Temperature inversions, where a layer of warm air traps cooler air near the ground, can further exacerbate the accumulation of pollutants.

Conversely, the lower AQI values observed during summer months can be attributed to reduced emissions from heating sources, enhanced atmospheric mixing, and favorable meteorological conditions. Reduced heating-related emissions during summer contribute to lower levels of $NO_2$ in the atmosphere. Enhanced atmospheric mixing, driven by convective processes and increased wind speeds, aids in the dispersion and dilution of pollutants, leading to lower summer AQI values. Furthermore, higher temperatures and increased solar radiation can facilitate the breakdown of pollutants through chemical reactions, further improving air quality.

In conclusion, the monthly average AQI values for $NO_2$ indicate that the five locations generally maintain good air quality. Seasonal variations are observed, with higher AQI values during winter and lower values during summer. These variations can be attributed to increased emissions from heating sources, limited atmospheric dispersion, temperature inversions during winter, reduced emissions, enhanced atmospheric mixing, and favorable meteorological conditions during summer. Understanding these variations and their causes is crucial for implementing effective air quality management strategies in each location.

## CONCLUSIONS

Air pollution is an alarming threat to humanity and ecosystems on Earth with far-reaching consequences impacting climate change, public health, and mortality rates. Immense efforts have been undertaken globally to control emissions of air contaminants, particularly in densely populated urban centers where human activities emit an excessive influx of air pollutants.

This research aimed to calculate the quality index of air pollutants including ground-level ozone, carbon monoxide, sulfur dioxide, particulate matter, and nitrogen dioxide in the mostly populated area in Jordan which spans over Amman-Zarqa metropolitans during the period 2016-2022. A total of five air quality monitoring stations, three located in Amman and two in Zarqa, were selected for this study. Daily air quality data was downloaded from the official website of the Jordanian Ministry of Environment website. The Air Quality Index (AQI) was calculated using the esteemed U.S. Environmental Protection Agency (EPA) method, providing a comprehensive assessment of air quality in the study region. The AQI values were further classified into distinct categories, signifying the varying degrees of air quality, ranging from "Good" to "Hazardous."

Regarding $PM_{10}$, variations in the Air Quality Index (AQI) were observed for each station, with fluctuations occurring predominantly in the "Good" AQI class (0-50), except for several days where it reached the "Moderate" AQI classification (51-100). For $PM_{2.5}$, available data showed AQI values fluctuating between "Moderate" and "Unhealthy for Sensitive Groups" (FSG). Ozone-based AQI values varied within the "Good" class for KAC and KHG stations, while AQI values for CO predominantly remained in the "Good" range at GAM, while HAJ experienced occasional episodes of compromised air quality for CO. Spatially, the GIS interpolation results illustrated areas with higher AQI values, particularly around HAJ and MAS stations, indicating potential hotspots for pollution.

Furthermore, $SO_2$ AQI values were predominantly "Good" for all stations, with GAM, KAC, KHG, and MAS consistently maintaining good air quality throughout the study period. HAJ, however, exhibited higher fluctuations in AQI values, occasionally exceeding the "Good" threshold. When assessing $NO_2$, all five locations demonstrated good air quality, with monthly average AQI values consistently below 50. Seasonal variations were observed, with higher AQI values during winter attributed to increased emissions from heating sources and limited atmospheric dispersion, while lower values during summer were attributed to reduced emissions and enhanced atmospheric mixing.

Based on the study findings, it is suggested that:

1. Develop and enforce strict legislation: Governments should develop and implement strong and stringent legislation to control air pollution. Such legislation should include strict emission standards for industries and transportation and specific laws to prevent waste burning and air pollution from other sources.

2. Encouraging the transition to clean energy sources: The use of renewable and clean energy sources such as solar, wind, and safe nuclear energy should be promoted. Governments should provide encouragement, financial support, and appropriate legislation for companies and individuals to invest in these clean resources.
3. Improving the quality of transportation: Public transportation should be strengthened and improved, and the use of clean transportation such as electric vehicles should be encouraged. This can be achieved by providing adequate infrastructure and encouraging investment in environmental technology for transportation.
4. Awareness and education: Awareness and education should be strengthened about the impact of air pollution on public health and the environment. This can be achieved through information campaigns and the provision of information and educational resources to the public. Efforts should be directed to educate young people and enhance their awareness of the importance of protecting the environment.
5. International cooperation: International cooperation and exchange of knowledge and experience in the field of air quality protection should be strengthened. This can be achieved by forming international and regional organizations that share data and technology and develop joint strategies to improve air quality.
6. Research and development: Research and development in technology to reduce pollution and improve air quality should be supported. This can be done by allocating more funding to scientific research and encouraging cooperation between universities, research institutions and industry.
7. Monitoring and Control: Effective systems for monitoring and controlling air quality must be developed at the global level. Data and information should be exchanged between countries and international organizations to assess the transboundary impact of air pollution and take corrective action based on the assessments.

## LIMITATIONS OF THE STUDY

The air quality index was introduced to inform the public about environmental conditions, which is especially useful for people suffering from illnesses aggravated or caused by air pollution. However, it does have limitations, including a general inability to inform the public regarding health risks occurring at concentrations below regulatory standards and an inability to account for the health effects of exposure to multiple pollutants.

## ACKNOWLEDGMENT

The authors are grateful to the Jordanian Ministry of Environment which made air quality data available free of charge, which greatly helped in undertaking this work.

## REFERENCES

Abu-Allaban, M. and El-Khalili, M.M. 2014. Antiquity impact of air pollution at Gadara, Jordan. Mediterranean Archaeology and Archaeometry, 14(1): 191-199.

Al-Mashaqbeh, A., Abu-Allaban, M. and Al-Malabah, A. 2015. Air quality impact of the upgraded Al-Samra wastewater treatment plant. Jordan Journal of Earth and Environmental Sciences, 7(1): 19-26.

Alnawaiseh, N.A., Hashim, J.H. and Isa, Z. 2015. Relationship between vehicle count and particulate air pollution in Amman, Jordan. Asia Pacific Journal of Public Health, 27(2): NP1742-NP1751.

Bachmann, J. 2007. Will the circle be unbroken: a history of the US National Ambient Air Quality Standards. Journal of the Air and Waste Management Association, 57(6): 652-697.

Curtis, L., Rea, W., Smith-Willis, P., Fenyves, E. and Pan, Y. 2006. Adverse health effects of outdoor air pollutants. Environment International, 32(6): 815-830.

Dabbour, L., Abdelhafez, E. and Hamdan, M. 2021. Effect of climatology parameters on air pollution during COVID-19 pandemic in Jordan. Environmental Research, 202: 111742.

DOS, Department of Statistics. 2023. General Statistics. Amman, Jordan. Available at: http://dosweb.dos.gov.jo/

EPA, U.S. Environmental Protection Agency. 2018. Technical Assistance Document for the Reporting of Daily Air Quality – the Air Quality Index (AQI). Available at: https://www.airnow.gov/sites/default/files/2020-05/aqi-technical-assistancedocument-sept2018.pdf

Gold, D.R. and Samet, J.M. 2013. Air pollution, climate, and heart disease. Circulation, 128(21): 411-414.

Jaber, S.M. and Abu-Allaban, M.M. 2017. Mapping the spatial distribution of tropospheric ozone and exploring its association with elevation and land cover over North Jordan. Journal of Spatial Science, 62(2): 307-322.

Jayamurugan, R., Kumaravel, B., Palanivelraja, S. and Chockalingam, M.P. 2013. Influence of temperature, relative humidity and seasonal variability on ambient air quality in a coastal urban area. International Journal of Atmospheric Sciences, 2013: 264046.

Katsouyanni, K. and Analitis, A. 2009. Investigating the synergistic effects between meteorological variables and air pollutants: Results from the European PHEWE, EUROHEAT and CIRCE projects. Epidemiology, 20(6): S264.

Majewski, G., Szeląg, B., Białek, A., Stachura, M., Wodecka, B., Anioł, E., Wdowiak, T., Brandyk, A., Rogula-Kozłowska, W. and Łagód, G. 2021. Relationship between visibility, air pollution index and annual mortality rate in association with the occurrence of rainfall-A Probabilistic Approach. Energies, 14(24): 8397. https://doi.org/10.3390/en14248397.

Manisalidis, I., Stavropoulou, E., Stavropoulos, A. and Bezirtzoglou, E. 2020. Environmental and health impacts of air pollution: a review. Frontiers in Public Health, 8(14).

Odat, S., Abu-Allaban, M. and Odibat, K. 2017. Influence of meteorological parameters on air quality at Hashemite University, Jordan. Current World Environment, 12(2): 211-221.

Orru, H., Ebi, K.L. and Forsberg, B. 2017. The interplay of climate change and air pollution on health. Curr. Environ. Health Rep., 4: 504-513.

Pinho-Gomes, A.C., Roaf, E., Fuller, G., Fowler, D., Lewis, A., ApSimon, H., Noakes, C., Johnstone, P. and Holgate, S. 2023. Air pollution and climate change. The Lancet, 7(9): 727-728.

Rao, N.V., Rajasekhar, M. and Rao, D.R.G.C. 2016. Detrimental effect of

air pollution, corrosion on building materials and historical structures. American Journal of Engineering Research, 3(3): 359-364.
Ruffolo, S.A., Russa, M.F.L., Rovella, N. and Ricca, M. 2023. The impact of air pollution on stone materials. Environments, 10(7): 119. DOI: 10.3390/environments10070119.
Saffarini, G.A. and Odat, S. 2008. Time series analysis of air pollution in Al-Hashimeya Town Zarqa, Jordan. The Jordan Journal of Earth and Environmental Sciences, 1(2): 63-71.
Sierra-Vargas, M.P. and Teran, L.M. 2012. Air pollution: Impact and prevention. Respirology, 17(7): 1031-1038.
Singh, P., Yadav, D. and Pandian, E.S. 2021. Link between air pollution and global climate change. In: Global Climate Change. Elsevier: 79-108. DOI: 10.1016/B978-0-12-822928-6.00009-5.

## ORCID DETAILS OF THE AUTHORS

M. Abu-Allaban: https://orcid.org/0000-0003-3067-6231

Nature Environment and Pollution Technology
An International Quarterly Scientific Journal

p-ISSN: 0972-6268
(Print copies up to 2016)
e-ISSN: 2395-3454

Vol. 23 | No. 3 | pp. 1709-1716 | 2024

Original Research Paper

https://doi.org/10.46488/NEPT.2024.v23i03.042

Open Access Journal

# Water Treatment: Evaluation of Maleic Acid-Acrylamide Copolymer Inhibitor Efficiency on Calcite Scale by Response Surface Methodology

**Balasubramanian Senthilmurugan*†** and **Jayaprakash Sandhala Radhakrishnan****
*Department of Industrial Chemistry, Alagappa University, Karaikkudi, Tamilnadu 630003, India
**Suez Water Technologies & Solutions, Hoskote Industrial Area, Karnataka 562114, India
†Corresponding author: Balasubramanian Senthilmurugan; dr.senthilmurugan@yahoo.com

**Nat. Env. & Poll. Tech.**
**Website: www.neptjournal.com**

*Received:* 06-11-2023
*Revised:* 18-01-2024
*Accepted:* 22-01-2024

**Key Words:**
Response surface methodology
Calcite scale
Scale inhibitor
Maleic acid
Co-polymer
Flow assurance

## ABSTRACT

Mineral scales of calcite are common in the oil field and pose a serious integrity problem in the wellbore, flow lines, and equipment. It is also a challenge faced by industries such as refineries and power plants. Scale deposition is a complex process depending on various factors such as concentration of scaling species, temperature, pH, and flow rates. Deterministic models are used to predict the scale formation from the level of supersaturation of the scaling species in the water at the operating conditions. However, due to the complexity of the interaction of variables affecting the scaling and inhibition by chemicals, it is suitable to be represented by statistical models. This work focused on applying statistical analysis techniques such as response surface methodology to understand the effect of different operating parameters on the inhibition efficiency of maleic acid-acrylamide copolymer on $CaCO_3$ scales. The copolymer was synthesized, and its inhibition efficiency on the calcite scale was tested using static jar tests at different pH, temperature, and inhibitor concentrations. The effect of the critical parameters on the inhibition efficiency was analyzed using the statistical technique of Response Surface Methodology (RSM). The design of experiments (DoE) was created using a Box–Behnken design with three levels for each factor. The linear and the quadratic effects of the factors were studied and the interaction effects were analyzed using analyses of variance (ANOVA) and RSM. A desirability function was used to optimize the performance for the combination of the variables. The analysis showed that the linear effect of the parameters had the highest impact on the inhibition efficiency. Significant interaction effects were also identified between the operating variables. A transfer function was used to model the experimental data of inhibitor performance.

## INTRODUCTION

Formation of mineral scales in flowlines and equipment is a major challenge faced by industries such as power plants and oil and gas production systems. Carbonates and sulfates of calcium typically deposit as scale in the wells, flowlines, and surface facilities, leading to restricted flow, increased pressure drops, and blockage in the oil field (Olajire 2015, Li et al. 2017). It can also lead to under-deposit corrosion and loss of metal. Scaling is typically controlled by a continuous dosage of scale inhibitors, which hinder the formation of deposits (Fink 2012). Scale formation depends on various parameters such as the water quality, concentration of the scaling ions, suspended solids, pH, temperature, flow rate, etc. Deterministic models have been developed to predict the formation and quantitative severity of scales as a function of the operating parameters (Kan & Tomson 2012, Mackay & Sorbie 1999). These models calculate the extent and amount of scaling from the level of supersaturation and the solubility of the scaling species in the water at the operating conditions. Some of the models also include the mitigating effect of common scale inhibitors. Scaling and the mitigation through chemical action are controlled by the complex interaction between the critical parameters and hence, it is suitable to be modeled using statistical methods. This paper describes the modeling and optimization of the efficiency of a threshold scale inhibitor on a calcium carbonate scale using response surface methodology (RSM).

RSM is a statistical method for analyzing and modeling a process where the outcome depends on several parameters and their interactions. RSM is specifically useful in modeling systems where the effect of the interaction of the independent variables is complex and a deterministic model cannot be developed satisfactorily. RMS is used in the design and development of new products/processes and also in the improvement of existing products and processes. It can be used to identify the critical parameters that affect the process.

The model can also be used to predict what-if scenarios of the process variables (Myers & Montgomery 1995, Martí-Calatayud et al. 2010). The design of experiments and RSM has been used widely in process and manufacturing industries and research laboratories to understand the effect of the operating parameters and optimize the process. It could be used to model the efficiency of chemicals such as corrosion inhibitors (Goh et al. 2008). RSM is applied in the oil industries in areas such as reservoir modeling and production forecasts (Manceau et al. 2002), uncertainty quantification on reserves estimation (Busby & Chugunova 2015), and estimating the wax deposition in the pipeline (Adeyanju & Oyekunle 2015). The use of statistical modeling to predict and optimize scale formation is very limited.

In this paper, the application of RSM for investigating the effect of operating conditions such as pH, temperature, and polymer concentration on scale inhibition efficiency is explained. Low molecular weight copolymers of maleic acid–acrylamide have shown good inhibition of $CaCO_3$ and $CaSO_4$ scales (Senthilmurugan & Ghosh 2009, Senthilmurugan et al. 2010, Senthilmurugan et al. 2019). In this paper, RSM methodology is used to design a new set of experiments for $CaCO_3$ inhibition and analyze the results.

## MATERIALS AND METHODS

### Experimental Methods

Maleic acid (HOOCHC=CHCOOH) and acrylamide ($CH_2$=CHCONH$_2$) were copolymerized in an aqueous medium through free radical polymerization using an initiator in an inert atmosphere. The reaction product was concentrated using vacuum distillation. The scale inhibition efficiency of the synthesized copolymer was tested using static jar tests according to the NACE standard test method TM0374-2016-SG (NACE 2016). Tests were conducted at various levels of pH of 7-8.5 and temperature of 50-70°C with an inhibitor concentration of 1-70 ppm. Cationic ($Ca^{2+}$) and anionic ($CO_3^{2-}$) solutions were prepared separately to maintain a stoichiometric proportion of 300 ppm each. $CO_2$ gas was bubbled through both the brines before mixing. The two solutions were mixed at a ratio of 1:1. Measured quantity of the scale inhibitor was added to the anionic solution before mixing with the cationic solution. The cells were placed in a shaker water bath at constant temperature for 12 h and then allowed to cool for 12 h. The residual calcium ion concentration in the solution was measured using the EDTA titration method before and after precipitation. The tests were performed for various combinations of pH, temperature, and inhibitor concentration, as shown in Table 1. The scale inhibition efficiency of the inhibitor (as a percentage) was calculated using the following equation:

$$\% \text{ Inhibition Efficiency} = 100 \times \frac{C_a - C_b}{C_c - C_b} \quad \ldots(1)$$

Where:

$C_a = Ca^{2+}$ ion concentration in the treated solution after precipitation

$C_b = Ca^{2+}$ concentration ion in the untreated solution after precipitation

$C_c = Ca^{2+}$ ion concentration in the untreated solution before precipitation

### Experimental Design

The experimental conditions need to be selected based on the field conditions to obtain practical inhibition values. Formation of scale, especially of calcite, is a strong function of temperature and pH of the solution. However, it is affected by minor factors such as flow rates, surface metallurgy, the presence of other ions, and suspended impurities. The $CO_2$-$HCO_3$-$CO_3$ equilibrium in water depends on the pH, and the solubility of $CaCO_3$ depends on pH and temperature. Hence pH, temperature, and the inhibitor concentration are selected to be the primary parameters of the study of inhibition efficiency. Based on the experimental constraints and field experience, the following ranges were selected for the operating variables: pH 7-8.5, Temperature 50-70°C, and copolymer concentration 1-70 ppm, as shown in Table 1. This system had three independent variables (pH, temperature, and copolymer concentration, denoted by X) and one dependent response (inhibition efficiency, denoted by Y). The numeric ranges of the dependent variables are coded between -1 (minimum) and 1 (maximum). The design of experiments was formulated according to the Box-Behnken design (Montgomery 2013) with three discrete levels (-1, 0, 1) for each input parameter. The design is composed of 15 runs with three central points (runs 13, 14, and 15 at levels 0,0,0) and 19 error degrees of freedom. The experimental design matrix with the actual and coded values of pH, temperature,

Table 1: Range of parameters used in calcite scale inhibition efficiency measurement experiments.

| Operating Parameters | Code | Levels | | |
|---|---|---|---|---|
| | | -1 | 0 | 1 |
| pH | $X_1$ | 7 | 7.75 | 8.5 |
| Temperature (°C) | $X_2$ | 50 | 60 | 70 |
| Copolymer concentration (ppm) | $X_3$ | 1 | 35.5 | 70 |

concentration, and the measured inhibition efficiency are given in Table 2.

The correlation between the operating variables ($X_1$, $X_2$, $X_3$) and the response variable (Y = Inhibitor Efficiency) was fitted using a quadratic polynomial (Hyder et al. 2009) using the least squares method. This equation captures most of the linear and interaction effects of the parameters. The response model is given by:

$$Y_k = b_0 + \sum_{i=1}^{3} b_i X_i + \sum_{i=1}^{3} b_{ii} X_i^2 + \sum_{i=1}^{2} \sum_{j=1}^{3} b_{ij} X_i X_j + \varepsilon \quad \ldots(2)$$

Where $X_i$ is the dimensionless coded input variable ($X_1$ = pH, $X_2$ = temperature, and $X_3$ = copolymer concentration), $Y_k$ is the response or output variable ($Y_1$ for inhibition efficiency), $b_0$ the intercept or constant, $b_i$ the linear coefficients, $b_{ii}$ the quadratic coefficients, $b_{ij}$ the interaction coefficients and ε the residual (noise or error) term. The coefficients of the equation are determined using the least squares method. The difference between the measured and the predicted value ($\varepsilon = y_i - \hat{y}$) is called the residual or error and denotes the deviation of the model predictions from the actual observations. In the least squares method, the coefficients (b) are selected so that the sum of squares of the residual is minimized. (Baş & Boyaci 2007). Analyses of variance method (ANOVA) were used to determine the linear and quadratic effects of the parameters and the effect of interaction on the response variable. The statistical analyses were performed using the software Design Expert 11 from Stat-Ease (Stat-Ease 2018).

## RESULTS AND DISCUSSION

### Calcite Inhibition Efficiency

The methods of characterization of the synthesized co-polymers and the typical characteristics of maleic acid-acrylamide copolymers are explained in the earlier paper (Senthilmurugan & Ghosh 2009). The average molecular weight of the copolymer was around 2000 g/mol (2000 Da). Lower molecular weight polymeric scale inhibitors are found to be more effective than higher ones. The optimum range of molecular weight of polymers in terms of scale inhibition efficiency is between Mw ~ 1000-4000, and the performance decreases at higher MW ranges (Farooqui et al. 2015).

The results of the static jar tests for calcite scale inhibition are given in Table 2. It is observed that the inhibition efficiency is very high at medium and high concentrations of the inhibitor. The ANOVA of the results is shown in Table 3. The Model F-value of 23.3 implies the model is significant. There is only a 0.02% chance that an F-value this large could occur due to noise. The quadratic polynomial model, as fitted, explains the R-squared of 95.89 of the variability in the percentage of inhibition efficiency. The residual analysis to establish if there is any significant correlation was carried out with the Durbin-Watson (DW) statistic tests, which showed a

Table 2: Design of experiments and results of $CaCO_3$ inhibition tests.

| Runs | Actual Values | | | Coded Values | | | Inhibition efficiency [%] $Y_1$ |
|---|---|---|---|---|---|---|---|
| | pH [-] $x_1$ | Temperature [°C)] $x_2$ | Copolymer concentration [ppm] $x_3$ | pH $X_1$ | Temperature $X_2$ | Copolymer concentration $X_3$ | |
| 1 | 7 | 50 | 35.5 | -1 | -1 | 0 | 100 |
| 2 | 8.5 | 50 | 35.5 | 1 | -1 | 0 | 100 |
| 3 | 7 | 70 | 35.5 | -1 | 1 | 0 | 100 |
| 4 | 8.5 | 70 | 35.5 | 1 | 1 | 0 | 84 |
| 5 | 7 | 60 | 1 | -1 | 0 | -1 | 89 |
| 6 | 8.5 | 60 | 1 | 1 | 0 | -1 | 66 |
| 7 | 7 | 60 | 70 | -1 | 0 | 1 | 100 |
| 8 | 8.5 | 60 | 70 | 1 | 0 | 1 | 92 |
| 9 | 7.75 | 50 | 1 | 0 | -1 | -1 | 90 |
| 10 | 7.75 | 70 | 1 | 0 | 1 | -1 | 76 |
| 11 | 7.75 | 50 | 70 | 0 | -1 | 1 | 100 |
| 12 | 7.75 | 70 | 70 | 0 | 1 | 1 | 100 |
| 13 | 7.75 | 60 | 35.5 | 0 | 0 | 0 | 97 |
| 14 | 7.75 | 60 | 35.5 | 0 | 0 | 0 | 100 |
| 15 | 7.75 | 60 | 35.5 | 0 | 0 | 0 | 100 |

value greater than 5.0% (P=0.9599). There is no indication of serial autocorrelation in the residuals at the 5.0% significance level. The value of variance inflation factor (VIF) was used to prove if this design is orthogonal. The value of VIF was 1 for all the factors included in the analysis, and then the model is adequate for the observed data at a 95% confidence level. The model coefficients were selected based on the p-value. For a 95% confidence level, a factor significantly affects the result if the p-value is less than 0.05. Anova was performed step by step by eliminating the insignificant terms that have a p-value greater than 0.05 to improve the accuracy of the model. The final p-value of the model is 0.0002, which indicates that the fitted model is statistically significant. The model results and the coefficients of the transfer function are shown in Table 3.

Fig. 1 shows a Pareto chart of the linear, quadratic, and interaction coefficients to compare the effect of parameters on the inhibition efficiency. The linear coefficients of copolymer concentration ($b_3$) show the most significant effect ($p<0.0001$, F-ratio 64.22) to increase the inhibition efficiency. In addition, the interaction factors pH - temperature ($b_{12}$) and pH - copolymer concentration ($b_{13}$) also showed a significant effect ($p \leq 0.05$) to increase the inhibition efficiency. On the other hand, the quadratic effect of copolymer concentration ($b_{33}$), the linear coefficients of pH ($b_1$), and temperature ($b_2$) showed a significant effect ($p \leq 0.05$) to decrease the inhibition efficiency. The interaction factor $b_{23}$, which represents the product of temperature and concentration, and the quadratic term of temperature ($b_{22}$), did not produce a significant effect ($P \geq 0.05$) on the inhibition efficiency; therefore, these factors are not included in the regression model equation of the inhibition efficiency.

The resulting transfer function is given by:

$$Y_1 = 100 - 5.88X_1 - 4.13X_2 + 8.5X_3 - 4.0X_1X_2 + 3.75X_1X_3 - 4.0X_1^2 - 9.25X_3^2 \quad \ldots(3)$$

where $Y_1$ is the predicted calcium carbonate inhibition percentage. $X_1$, $X_2$ and $X_3$ are the dimensionless coded input

Table 3: ANOVA for a quadratic model for calcite scale inhibition efficiency of the copolymer.

| Source | Sum of Squares | DF | Mean Square | F-value | p-value | Coefficient (Coded) |
|---|---|---|---|---|---|---|
| Model | 1469.93 | 7 | 209.99 | 23.33 | 0.000242 | |
| Intercept | | | | | | 100 |
| A-pH | 276.13 | 1 | 276.13 | 30.68 | 0.00087 | -5.875 |
| B-Temp | 136.13 | 1 | 136.13 | 15.13 | 0.00598 | -4.125 |
| C-Conc | 578 | 1 | 578 | 64.22 | 9.01E-05 | 8.5 |
| AB | 64 | 1 | 64 | 7.11 | 0.0321 | -4.0 |
| AC | 56.25 | 1 | 56.25 | 6.25 | 0.0410 | 3.75 |
| $A^2$ | 59.43 | 1 | 59.43 | 6.60 | 0.037 | -4.0 |
| $C^2$ | 317.80 | 1 | 317.80 | 35.31 | 0.000574 | -9.25 |
| Residual | 63 | 7 | 9 | | | |
| Lack of Fit | 63 | 5 | 12.6 | | | |
| Pure Error | 0 | 2 | 0 | | | |
| Cor Total | 1532.93 | 14 | | | | |

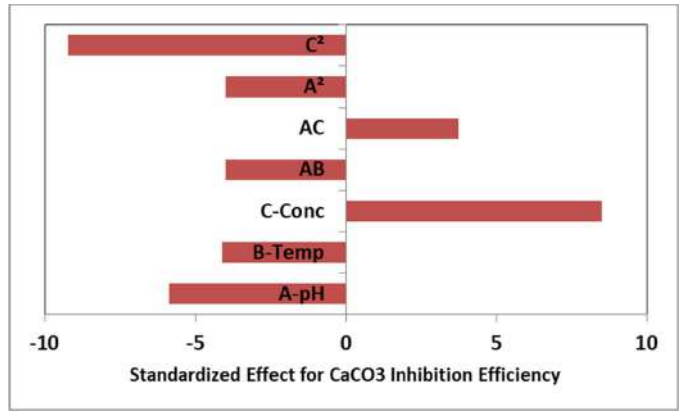


Fig. 1: Standardized Pareto chart for $CaCO_3$ inhibition efficiency.

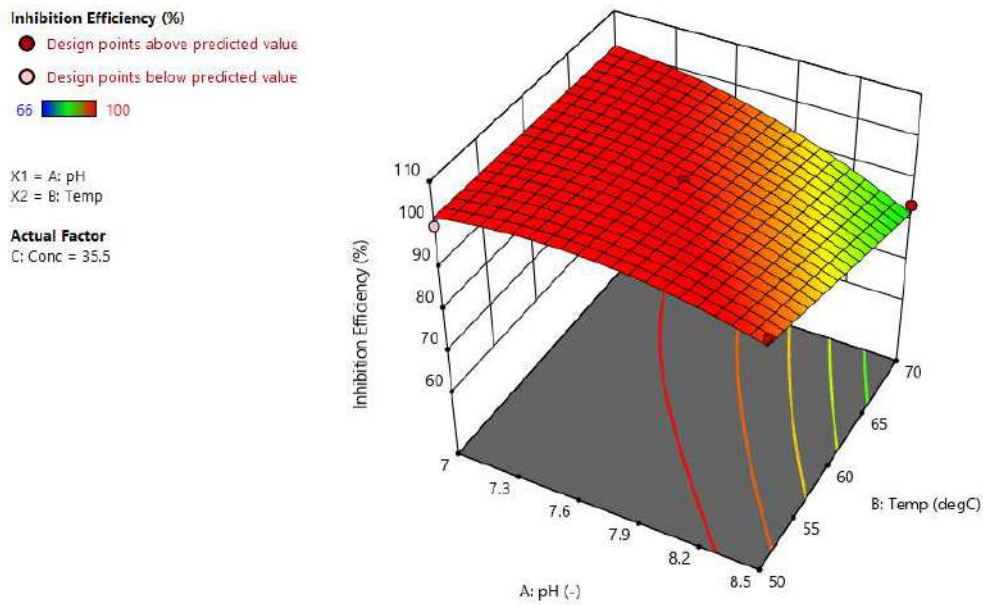


Fig. 2: 3D response surface with contour plot for the effect of pH and temperature on calcite scale inhibition efficiency.

parameters ($X_1$ = pH, $X_2$ = Temperature, $X_3$ = Inhibitor Concentration). A positive coefficient indicates that the parameter has a direct effect on the inhibition efficiency, and a negative coefficient indicates that the parameter has an inverse effect. The equation indicates that the inhibition efficiency increases with an increase in copolymer concentration. In contrast, it decreases with an increase in either pH or temperature, which is also observed from the data (Table 2). In linear terms, the effect of the various parameters on the efficiency is in the order of Concentration > pH > Temperature.

The response surface of the inhibition efficiency is plotted against two input parameters, while the third parameter is kept constant (at level 0 in Table 1). The 3D plot (Fig. 2) generated using equation (3) shows the effect of temperature and pH on the inhibition efficiency. Temperature has a linear effect in the range studied (50-70°C), where the inhibition efficiency decreases when the temperature increases (denoted by the absence of quadratic term of temperature in equation 3). The effect of pH is non-linear due to the presence of a quadratic term of pH in the equation. The data shows that at the maximum inhibitor concentration, the inhibition efficiency is always higher irrespective of the values of pH or temperature. This indicates that the calcite scale can be controlled by MA-AD copolymer even in adverse conditions by increasing the dosage.

Change in the pH affects the precipitation of calcium carbonate by altering the carbonate – bicarbonate - carbon dioxide balance in water. The solubility of calcium carbonate increases with a decrease in pH due to the conversion of carbonate ions into soluble bicarbonate ions and carbon dioxide gas. This aids in the increased efficiency of the scale inhibitor at lower pH. A similar effect is observed for the temperature, where an increase in temperature produces a decrease in the inhibition efficiency. At higher temperatures, the liquid layer adjacent to the hot surface acts as a super-saturation zone, leading to the precipitation of the compounds. However, these compounds may be soluble in the bulk liquid. This will lead to reduced inhibition efficiency at higher temperatures. Another factor affecting the efficiency at higher temperatures is the thermal stability of the inhibitors. The activity and stability of the inhibitors decrease with increasing temperature, leading to a reduction in efficiency.

Fig. 3 shows the combined effect of pH and copolymer concentration on the inhibition efficiency. The curvature in this 3D plot arises due to the quadratic effect of copolymer concentration. The inhibition efficiency decreases while the pH value increases from 7 to 8.5. The copolymer concentration effect is the opposite because the inhibition efficiency increases while the copolymer concentration is increasing.

The effect of temperature and copolymer concentration is shown in Fig. 4, where it is evident that an increase in the temperature produces a decrease in the inhibition efficiency in the range investigated (50-70°C). On the other hand, the copolymer concentration shows a quadratic dependence with an increase in the inhibition efficiency when the copolymer

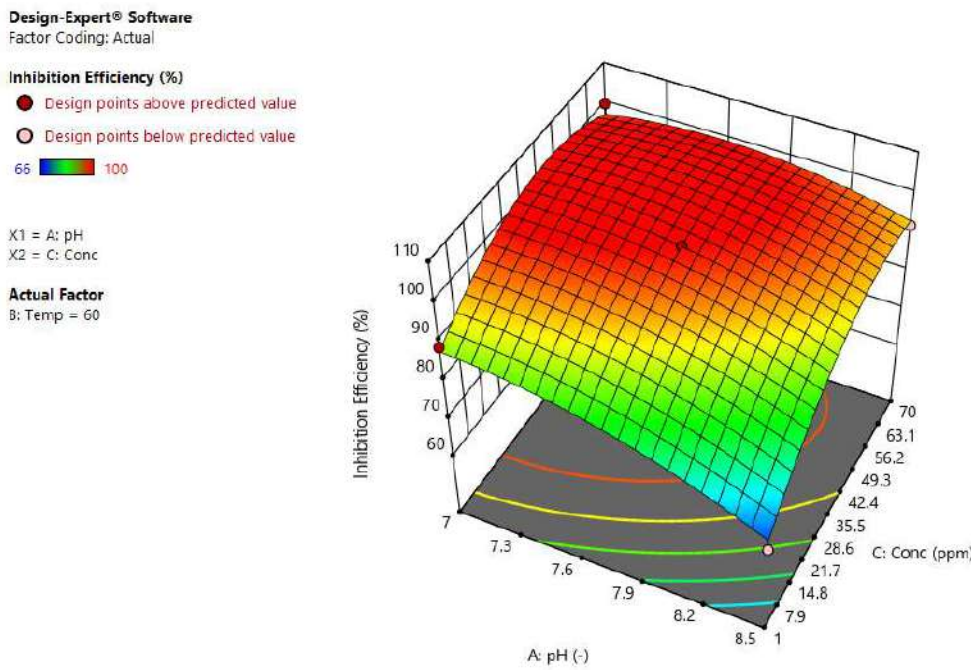


Fig. 3: 3D response surface with contour plot for the effect of pH and copolymer concentration on calcite scale inhibition efficiency.

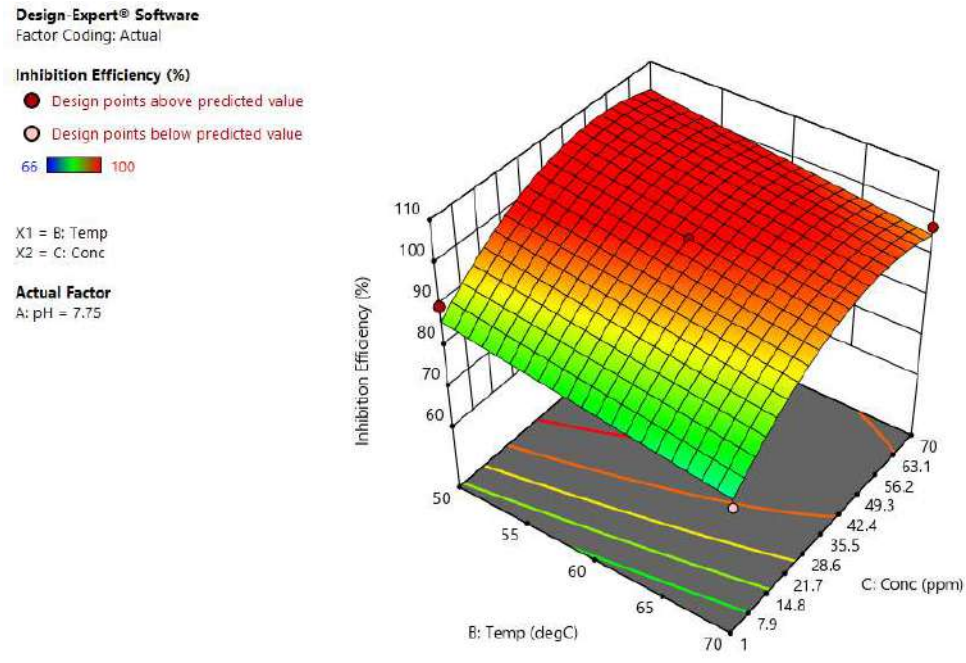


Fig. 4: 3D response surface with contour plot for the effect of temperature and copolymer concentration on calcite scale inhibition efficiency.

concentration is increased. The tested inhibitor (MA-AD) is a threshold or kinetic scale inhibitor that affects the kinetics of the nucleation and crystal growth of scaling species, thus allowing supersaturation without scale formation. Hence, threshold scale inhibitors can be dosed at low concentrations, far below the stoichiometric amounts required for inhibition through chelation.

## Optimization of Responses

The desirability function (DF) is widely used in RSM to

determine the combination of input variables to optimize multiple responses (Kalil et al. 2000, Harrington, 1965). If y(x) denotes the response as a function of the input parameters (x), the desirability function is denoted by DF = $d_k(y_k)$ with a range in values between 0 and 1. A value of 0 for DF represents a completely undesirable or unfavorable value of y, and DF = 1 represents a completely desirable value of y. The desirability function is used to find the operating conditions ($x_k$) which result in the most desirable responses. This is done by maximizing the overall desirability as a function of input parameters. Depending on whether a particular response $y_i$ has to be maximized, minimized, or assigned to a target value, Different desirability functions can be used depending on whether the observed response (y) need to be minimized, maximized, or set to a target value (Del Castillo 1996).

Optimization was done to obtain the operating conditions resulting in the maximum inhibition efficiency equal to 100%. In this case, the operating conditions should be 7.75, 60°C, and 35.5 ppm for pH, temperature, and copolymer concentration, respectively, to attain maximum calcium carbonate inhibition. With sufficient data sets, this model could be improved and used for determining minimum inhibitor concentration (MIC) for the given operating conditions. This approach can also be extended for other scale inhibitors and could be used to select the appropriate scale inhibitor for a given set of conditions.

## CONCLUSIONS

This work focused on applying statistical analysis techniques such as response surface methodology to understand the effect of different operating parameters on the inhibition efficiency of maleic acid - acrylamide copolymer scale inhibitor on $CaCO_3$ scales. The copolymer was synthesized, and its inhibition efficiency on the calcite scale was tested using static jar tests at various levels of temperature, pH, and inhibitor concentration. The design of experiments was formulated using Box-Behnken design with three levels for each factor. The results were analyzed using ANOVA and response surfaces. The analysis showed that the linear effect of the variables had the highest impact on inhibition efficiency. The order of influence of the parameters for the calcite scale was copolymer concentration > pH > temperature. There was also a significant effect of the interaction between pH – concentration, and temperature-concentration factors, indicating that scale inhibition involves a complex interaction of operating parameters. The linear factors had the highest influence, followed by the quadratic term of temperature and the interaction effects. A quadratic transfer function was fitted to the data by selecting the significant factors using backward elimination regression. This model can be used to predict the performance of the scale inhibitor for different operating conditions. Statistical methods could be used to model and optimize complex phenomena such as scale inhibition and aid in optimum mitigation of inorganic scaling in industrial systems.

## REFERENCES

Adeyanju, O.A. and Oyekunle, L.O. 2015. Optimization of wax deposition in a sub-cooled pipeline using response surface methodology. Proceedings of SPE Nigeria Annual International Conference and Exhibition, Lagos, Nigeria, SPE-178275-MS.

Baş, D. and Boyaci, I.H.J. 2007. Modeling and optimization I: Usability of response surface methodology. Food Eng., 78: 836-845.

Busby, D. and Chugunova, T. 2015. Embedded response surfaces approach for uncertainty quantification. Proceedings of International Petroleum Technology Conference, Doha, Qatar, Paper IPTC-18441-MS.

Del Castillo, E., Montgomery, D.C. and McCarville, D.R. 1996. Modified desirability function for multiple response optimization. J. Qual. Technol., 28: 337-345.

Farooqui, N.M., Sorbie, K.S. and Boak, L.S. 2015. Molecular weight effects in polymeric scale inhibitor precipitation squeeze treatments. Proceedings of SPE European Formation Damage Conference and Exhibition, Budapest, Hungary, Paper SPE-174214-MS

Fink, J. K. 2012. Petroleum Engineer's Guide to Oil Field Chemicals and Fluids. Elsevier, Amsterdam, The Netherlands, pp 253-274.

Goh, K.H., Lim, T.T. and Chui, P.C. 2008. Evaluation of the effect of dosage, pH, and contact time on high-dose phosphate inhibition for copper corrosion control using response surface methodology (RSM). Corrosion Sci., 50: 918-927.

Harrington, E.C. 1965. The desirability function. Ind. Qual. Contr., 21: 494-498.

Hyder, M.N., Huang, R.Y.M. and Chen, P.J. 2009. Pervaporation dehydration of alcohol-water mixtures: optimization for permeate flux and selectivity by central composite rotatable design. Membr. Sci., 326: 343-353.

Kalil, S.J., Maugeri, F. and Rodrigues, M.I. 2000. Response surface analysis and simulation as a tool for bioprocess design and optimization. Process Biochem., 35: 539-550.

Kan, A.T. and Tomson, M.B. 2012. Scale prediction for oil and gas production. SPE J., 17(2): 364-378.

Li, J., Tang, M., Ye, Z., Chen, L. and Zhou, Y. 2017. Scale formation and control in oil and gas fields: A review. J. Dispersion Sci. Tech., 38(5): 661-670.

Mackay, E.J. and Sorbie, K.S. 1999. An evaluation of simulation techniques for modeling squeeze treatments, Proceed. Ann. SPE Tech. Conf., 111: 373-387.

Manceau, E., Zabalza-Mezghani, I. and Roggero, F. 2002. Use of experimental design methodology to make decisions in an uncertain reservoir environment from reservoir uncertainties to economic risk analysis. World Petrol. Congr., 32: 161.

Martí-Calatayud, M.C., Vincent-Vela, M.C., Álvarez-Blanco, S., Lora-García, J. and Bergantiños-Rodríguez, E. 2010. Analysis and optimization of the influence of operating conditions in the ultrafiltration of macromolecules using a response surface methodological approach. Chem. Eng. J., 156: 337-346.

Montgomery, D.C. 2013. Design and Analysis of Experiments. Eighth edition. John Wiley & Sons, Hoboken, USA.

Myers, R.H. and Montgomery, D.C. 1995. Response Surface Methodology: Process and Product Optimization Using Designed Experiments. John Wiley Sons, Hoboken, USA.

NACE 2016. NACE Standard Test Method, TM0374-2016-SG, 2016. Laboratory screening tests to determine the ability of scale inhibitors to prevent the precipitation of calcium sulfate and calcium carbonate from solution (for oil and gas production systems), Product Number: 21208-SG, ISBN: 1-57590-124-2, NACE International, Houston, USA.

Olajire, A.A. 2015. A review of oilfield mineral scale deposits management technology for oil and gas production. J. Pet. Sci. Eng., 135: 723-737.

Senthilmurugan, B. and Ghosh, B. 2009. Low molecular weight co-polymer for calcium scale inhibition at high temperature. Proceedings of SPE International Symposium on Oilfield Chemistry, The Woodlands, TX, USA, pp 217-284.

Senthilmurugan, B., Ghosh, B., Kundu, S.S., Haroun, M. and Kameshwari, B. 2010. Maleic acid-based scale inhibitors for calcium sulfate scale inhibition in high-temperature application. J. Petrol. Sci. Eng., 75: 189-195.

Senthilmurugan, B., Radhakrishnan, J.S., Arana, V. and Al-Foudari, M. 2019. High-temperature kinetic scale inhibitor for flow assurance application. Int. J. Petrol. Sci. Technol., 13(1): 21-38.

Stat-Ease Inc. 2018. Design-Expert User Manual (version 11.1). Minneapolis, USA.

## ORCID DETAILS OF THE AUTHORS

B. Senthilmurugan: https://orcid.org/0000-0002-2859-8708
J. S. Radhakrishnan: https://orcid.org/0000-0002-5530-7363

Nature Environment and Pollution Technology
An International Quarterly Scientific Journal

p-ISSN: 0972-6268
(Print copies up to 2016)
e-ISSN: 2395-3454

Vol. 23 | No. 3 | pp. 1717-1722 | 2024

Original Research Paper

https://doi.org/10.46488/NEPT.2024.v23i03.043

Open Access Journal

# Microbes Breaking Down Plastic: Insights for Sustainable Waste Management

**C. J. Patel†, R. H. Kansagara, D. V. Modi, N. J. Dudhat, K. H. Sojitra and D. M. Babaria**
Department of Biological Sciences, P.D. Patel Institute of Applied Science, Charotar University of Science and Technology (CHARUSAT), Changa-388 421, Anand, Gujarat, India
†Corresponding author: Chitra Patel; chitrapatel1987@gmail.com

**Nat. Env. & Poll. Tech.**
**Website: www.neptjournal.com**

*Received:* 01-12-2023
*Revised:* 02-02-2024
*Accepted:* 12-03-2024

**Key Words:**
Microbial degradation
Plastic pollution
Waste management
LDPE
HDPE

## ABSTRACT

This research investigates the microbial degradation of low-density polyethylene (LDPE) and high-density polyethylene (HDPE) plastics by *Bacillus* sp., *Proteus* sp., *Pseudomonas* sp., and *Salmonella* sp. The study employs a systematic approach, isolating microorganisms from plastic-contaminated soil and subjecting them to a series of biochemical tests for identification. The research evaluates the weight loss of LDPE and HDPE over two months, revealing varying degrees of degradation among the bacterial strains. Results suggest a potential greater susceptibility of HDPE to microbial degradation. Scanning Electron Microscopy (SEM) analysis provides high-resolution images of the plastic surface, indicating structural changes and biofilm formation during degradation. The findings highlight the unique enzymatic capabilities of each strain and underscore the significance of SEM in elucidating microbial interactions with plastics. The study prompts discussions on optimization, synergistic effects, and the identification of key enzymes in plastic degradation, emphasizing the importance of microbial strategies for waste management. Overall, this research contributes valuable insights into the potential of bacterial strains for addressing plastic pollution challenges.

## INTRODUCTION

Plastic is a synthetic polymer derived from petrochemicals, widely used for its durability and versatility. Its persistence in the environment leads to long-lasting pollution, as it does not easily biodegrade. Improper disposal and accumulation in oceans harm marine life, disrupt ecosystems, and contribute to global environmental challenges. Addressing plastic pollution requires sustainable alternatives and responsible waste management (Banerjee & Bhattacharya 2022, Ghatge et al. 2020, Kotova et al. 2021, Montazer et al. 2020). Here are a few examples illustrating the severe consequences of plastic pollution worldwide. The Great Pacific Garbage Patch, an extensive accumulation of plastic debris primarily consisting of microplastics, has formed in the Pacific Ocean, posing a significant threat to marine life through ingestion and entanglement (Ghatge et al. 2020).

Additionally, on Midway Atoll, albatross chicks often meet tragic fates as a result of ingesting plastic fed to them by their parents, mistakenly taken for food (Auman et al. 1997, Sileo et al. 1990). These instances highlight the pervasive and impactful nature of plastic pollution, reaching even the most remote locations and adversely affecting isolated wildlife populations. Efforts to mitigate plastic pollution encompass multidisciplinary strategies rooted in scientific research and environmental conservation. Initiatives focus on the development of biodegradable polymers, employing advanced microbial degradation processes, and implementing eco-friendly substitutes for traditional plastics (Babaremu et al. 2023, Liu et al. 2020, Song et al. 2009). Technological innovations in waste management, such as advanced sorting and recycling techniques, aim to enhance the efficiency of plastic recovery and reduce reliance on landfill disposal (Byrne et al. 2022, Mohanan et al. 2020, Montazer et al. 2020). Additionally, scientific endeavors emphasize public awareness campaigns, advocating for behavioral shifts to minimize plastic consumption, coupled with policy interventions to regulate the production and disposal of plastics. Collaborative research endeavors are crucial for advancing our understanding of the environmental impact of plastics and developing sustainable solutions that harmonize with ecological systems.

Microbial degradation of plastic involves the enzymatic breakdown of polymer chains by microorganisms, offering a promising avenue for plastic waste remediation (Gajendiran et al. 2016, Kopecká et al. 2022, Kotova et al. 2021, Mohanan et al. 2020). One notable success story involves the discovery of Ideonella sakaiensis, a bacterium capable of depolymerizing polyethylene terephthalate (PET), a common

plastic used in beverage bottles. The enzyme PETase, produced by this bacterium, catalyzes the hydrolysis of PET into its monomeric components (Banerjee & Bhattacharya 2022, Kotova et al. 2021, Mohanan et al. 2020, Ojha et al. 2017). Another breakthrough centers on the isolation of a microbial consortium from a plastic-contaminated environment, exhibiting the ability to degrade diverse plastic types. These microbial-driven advancements underscore the potential for harnessing natural processes to address plastic pollution, with ongoing research exploring ways to optimize and scale microbial degradation techniques for practical waste management applications (Gajendiran et al. 2016, Kopecká et al. 2022, Mohanan et al. 2020, Montazer et al. 2020). Here a study is designed to isolate the potential microorganisms capable of degradation of HDPE and PDPE type of plastics. The entire study was planned in a very simple yet effective way, where isolated microorganisms were allowed to degrade the plastic for two months, and the rate of degradation was calculated by measuring the weight loss.

## MATERIALS AND METHODS

### Sample Collection

The plastic samples were meticulously gathered from the plastic-laden soil of Valetva, Anand, employing a non-invasive collection method to preserve the integrity of the specimens. A comprehensive survey of the area ensured the representation of various plastic types within the collected samples.

### Isolation

The isolation process commenced with a systematic serial dilution technique. In this method, 0.5 g of the plastic soil sample was precisely weighed and introduced into 5 mm of sterile water, initiating a 1:10 dilution. Sequential dilutions followed, with 0.5 mm of each preceding dilution being added to 5 milliliters of sterile water to achieve subsequent dilution factors (e.g., 1:100, 1:1000, and so forth). The last three dilutions underwent plating on Nutrient Agar (NA) medium, enriched with 2% Polyethylene Glycol (PEG), employing the pour plate method (Alshehrei 2017, Nademo et al. 2023). This specific medium was selected for its ability to mimic environments containing crucial sources of plastic. The inoculated plates were then meticulously incubated at 37°C for 48 h, fostering optimal conditions for microbial growth and allowing for the subsequent assessment of microbial colonization and adaptation to plastic-rich environments. The resulting colonies were subjected to further analyses to identify and characterize potential plastic-degrading microorganisms.

### Identification

In the microbial identification and characterization process, isolates obtained from plastic-contaminated soil underwent a rigorous set of procedures for thorough analysis. Gram staining involved applying a smear of the bacterial culture onto a clean slide, followed by drying, fixing, and staining with crystal violet, Gram's iodine, Gram's decolorizer, and Safranin. The resulting slides were air-dried, and cell morphologies were meticulously examined under a microscope with an oil immersion objective (100X). Simultaneously, spore staining procedures included preparation of a boiling water bath, staining with malachite green, steaming, counterstaining with Safranin, and microscopic examination of the dried slides. Additionally, colony morphology, encompassing shape, edge, color, and surface characteristics, was assessed for each colony post-purification. The subsequent biochemical tests utilized the Hibacillus identification kit (HIMEDIA) and manual methods for catalase, oxidase, mannitol utilization, malonate utilization, nitrate reduction, citrate utilization, motility, gas production from glucose, carbohydrate utilization, urease, indole, MacConkey agar, and spirit blue agar tests. These tests aimed to unravel key metabolic activities, contributing to a comprehensive identification and characterization of the isolated strains based on their biochemical profiles (Franco-Duarte 2019, Rave et al. 2019).

### Determination of Weight Loss

In a controlled experiment, 100 mL of a pre-poured liquid mineral salt medium was dispensed into a 250 mL Erlenmeyer flask, and high-density polyethylene (HDPE) and low-density polyethylene (LDPE) plastics were introduced. The mixture was then subjected to sterilization in an autoclave. Each treatment, including controls on plastic plates in a sterile environment, was contained in separate bottles and placed in a shaker at 150 rpm and room temperature for 2 months. Following one month of continuous shaking, the plastic sheets were carefully collected, thoroughly washed with distilled water, shadow-dried, and subsequently weighed to determine their final weight (Ru et al. 2020, Zeenat et al. 2021). The weight loss data of the plastics were calculated using the dry loss percentage formula

$$\text{Percentage of losses of dry weight} = \frac{\text{Wi - Wf}}{\text{Wi}}$$

Where: Wi represents the initial dry weight before degradation (g), and Wf represents the dry weight after degradation (g). This methodology ensures a systematic approach to quantifying the impact of environmental

conditions on the degradation of HDPE and LDPE plastics.

### Scanning Electron Microscope

In the analysis of plastic degradation by microorganisms using a scanning electron microscope (SEM), the process begins with the collection of plastic samples representing various degradation stages, followed by thorough cleaning and fixation with a suitable fixative. Subsequent steps involve dehydration through a series of ethanol concentrations, critical point drying to preserve sample structure, and mounting onto SEM stubs using conductive adhesive or carbon tabs. Optionally, a thin conductive coating may be applied. Once prepared, the samples are placed in the SEM chamber, and imaging parameters are set to capture high-resolution images of the plastic surface, highlighting features such as cracks, pits, and attached microorganisms. Analysis of SEM images allows for the identification of surface alterations indicative of microbial degradation. Additionally, quantitative analysis using image processing tools can be employed for more detailed measurements. The entire process is meticulously documented, including SEM settings, sample preparation details, and observed surface features, providing a comprehensive record for further interpretation and refinement of the analytical approach based on specific sample characteristics and research objectives.

## RESULTS AND DISCUSSION

Based on the results of primary isolation, four different colonies were identified for further study. These Four bacterial isolates (Isolate 1, Isolate 2, Isolate 3, and Isolate 4) were subjected to a series of biochemical tests to characterize their metabolic activities. All isolates exhibited positive results for the catalase and oxidase tests, indicating the presence of catalase enzyme and cytochrome c oxidase, respectively. In terms of motility, Isolate 3 and Isolate 4 demonstrated motility, while Isolate 1 and Isolate 2 were non-motile. The nitrate reduction test revealed positive results for Isolate 1, Isolate 2, and Isolate 4 but negative for Isolate 3. Isolate 3 was the only one to utilize citrate, as indicated by a positive citrate utilization test. Malonate utilization was not observed in any of the isolates. Isolate 2 and Isolate 4 exhibited positive results for the phenylalanine agar test, while Isolate 1 and Isolate 3 were negative. All isolates showed positive results for starch hydrolysis. The indole test yielded negative results for all isolates, and only Isolate 2 and Isolate 4 were positive for the urease test. Lysine decarboxylation was not observed in any isolate. Isolate 2 and Isolate 3 showed positive results in the triple sugar iron test, while Isolate 1 and Isolate 4 were negative. Isolate 2 and Isolate 4 tested positive for the methyl red test. The MacConkey agar test indicated positive results only for Isolate 1. None of the isolates demonstrated lipase activity, as observed in the negative results for the spirit blue agar test. The carbohydrate utilization profiles of four bacterial isolates (Isolate 1, Isolate 2, Isolate 3, and Isolate 4) were determined through a series of tests for different sugars. All isolates exhibited positive reactions for the utilization of Dextrose, Sucrose, Mannitol, Fructose, and Maltose. Isolate 2, Isolate 3, and Isolate 4 displayed positive results for Galactose and Lactose, while Isolate 1 did not utilize these sugars. Based on the results of the biochemical assay, the isolates were identified as Isolate 1 in *Bacillus* sp., Isolate 2 in *Proteus* sp., Isolate 3 in *Pseudomonas* sp., and Isolate 4 in *Salmonella* sp.

### Results of Degradation of LDPE and HDPE by isolates

In the investigation of plastic degradation by bacterial strains, namely *Bacillus* sp., *Proteus* sp., *Pseudomonas* sp., and *Salmonella* sp., on low-density polyethylene (LDPE) and high-density polyethylene (HDPE), the initial and final weights of each plastic sample were meticulously recorded to assess the extent of degradation. *Bacillus* sp. exhibited a 20% weight loss for LDPE, with a difference of 0.004 grams, and a 22.36% weight loss for HDPE, with a difference of 0.1154 grams, indicating its notable capability to degrade both plastic types. *Proteus* sp. demonstrated a 15% weight loss for LDPE, with a difference of 0.003 grams, and a 17.28% weight loss for HDPE, with a difference of 0.0864 grams, showcasing its efficiency in plastic degradation as well. *Pseudomonas* sp. exhibited a 20% weight loss for LDPE, with a difference of 0.004 grams, suggesting a comparable performance to *Bacillus* sp., while demonstrating a remarkable 23.08% weight loss for HDPE, with a difference of 0.1118 grams. *Salmonella* sp. displayed a substantial 22.5% weight loss for LDPE, with a difference of 0.0045 grams, and an even more significant 24.36% weight loss for HDPE, with a difference of 0.1218 grams, indicating its effectiveness in degrading both plastic types (Table 1 & Fig. 1).

The varying degrees of plastic degradation observed among the bacterial strains underscore their unique enzymatic capabilities and metabolic pathways involved in plastic biodegradation. The higher weight loss percentages for HDPE compared to LDPE in most cases suggest a potentially greater susceptibility of HDPE to microbial degradation. These findings contribute to the ongoing exploration of microbial strategies for plastic waste management, emphasizing the importance of understanding the specific bacterial strains that can effectively degrade different types of plastics (Gajendiran et al. 2016, Islami et

al. 2019, Kyaw et al. 2012, Midhun et al. 2015, Nademo et al. 2023, Ojha et al. 2017, Sanniyasi et al. 2021).

The results prompt further discussions on the optimization of conditions for enhanced plastic degradation, potential synergistic effects when combining different bacterial strains, and the identification of key enzymes involved in the degradation process (Cai et al. 2023, Crystal Thew et al. 2023, Pischedda et al. 2019, Rani et al. 2021). Additionally, exploring the genetic and biochemical mechanisms underlying the observed variations among the bacterial strains can provide valuable insights for the development of targeted approaches to address plastic pollution challenges (Gilani et al. 2023, Kumari et al. 2021, Purohit et al. 2020, Urbanek et al. 2021).

The research findings provide a fascinating insight into the potential of bacterial strains in degrading plastic materials, particularly LDPE and HDPE. The varying degrees of degradation observed among *Bacillus* sp., *Proteus* sp., *Pseudomonas* sp., and *Salmonella* sp. highlight the unique enzymatic capabilities of each strain. Interestingly, the higher weight loss percentages for HDPE compared to LDPE suggest that HDPE might be more susceptible to microbial degradation. This could be due to the structural differences between LDPE and HDPE. HDPE has a more crystalline structure which might make it easier for the bacteria to access and degrade the polymer chains (Kyaw et al. 2012, Midhun et al. 2015, Ojha et al. 2017). The results also open up several avenues for further research. For instance, it would be interesting to explore the optimization of conditions for enhanced plastic degradation. Factors such as temperature, pH, and nutrient availability could potentially influence the efficiency of plastic degradation. Another intriguing aspect is the potential synergistic effects when combining different bacterial strains (Ojha et al. 2017, Rani et al. 2021).

Furthermore, identifying the key enzymes involved in the degradation process could provide valuable insights. Understanding the biochemical mechanisms underlying the observed variations among the bacterial strains can lead to the development of targeted approaches to address plastic pollution challenges. Overall, this research underscores the importance of exploring microbial strategies for plastic waste management. It emphasizes the need for a deeper

Table 1: Result of degradation of plastic LDPE and HDPE by Bacteria.

| Bacterial strain | Type of plastic | Initial weight [g] | Final weight [g] | Difference | Weight loss [%] |
|---|---|---|---|---|---|
| *Bacillus* sp. | LDPE | 0.02 | 0.016±0.010 | 0.004 | 20% |
| *Bacillus* sp. | HDPE | 0.5 | 0.3846±0.08 | 0.1154 | 22.36% |
| *Proteus* sp. | LDPE | 0.02 | 0.017±0.007 | 0.003 | 15% |
| *Proteus* sp. | HDPE | 0.5 | 0.4136±0.07 | 0.0864 | 17.28% |
| *Pseudomonas* sp. | LDPE | 0.02 | 0.016±0.0011 | 0.004 | 20% |
| *Pseudomonas* sp. | HDPE | 0.5 | 0.3882±0.08 | 0.1118 | 23.08% |
| *Salmonella* sp. | LDPE | 0.02 | 0.0155±0.007 | 0.0045 | 22.5% |
| *Salmonella* sp. | HDPE | 0.5 | 0.3782±0.06 | 0.1218 | 24.36% |

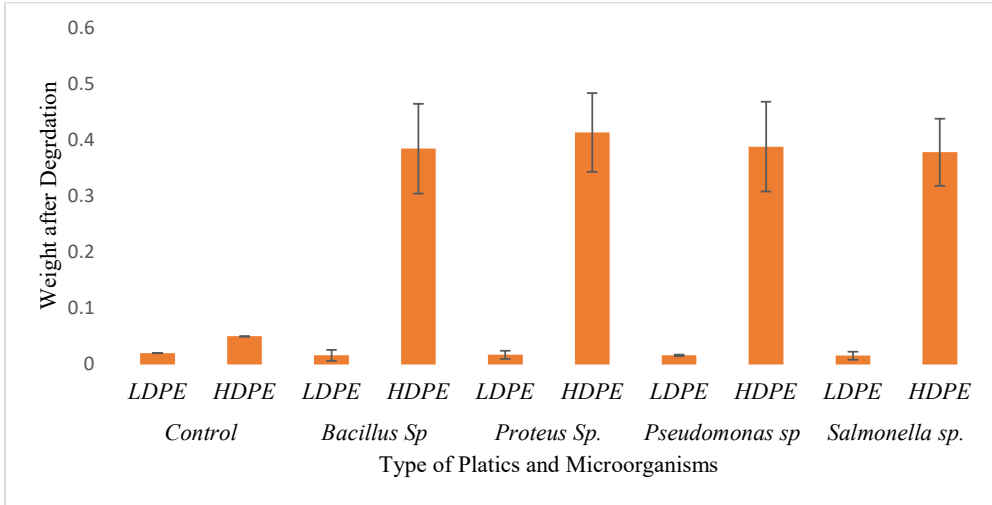


Fig. 1: Result of degradation of plastic LDPE and HDPE by Selected Microorganisms.

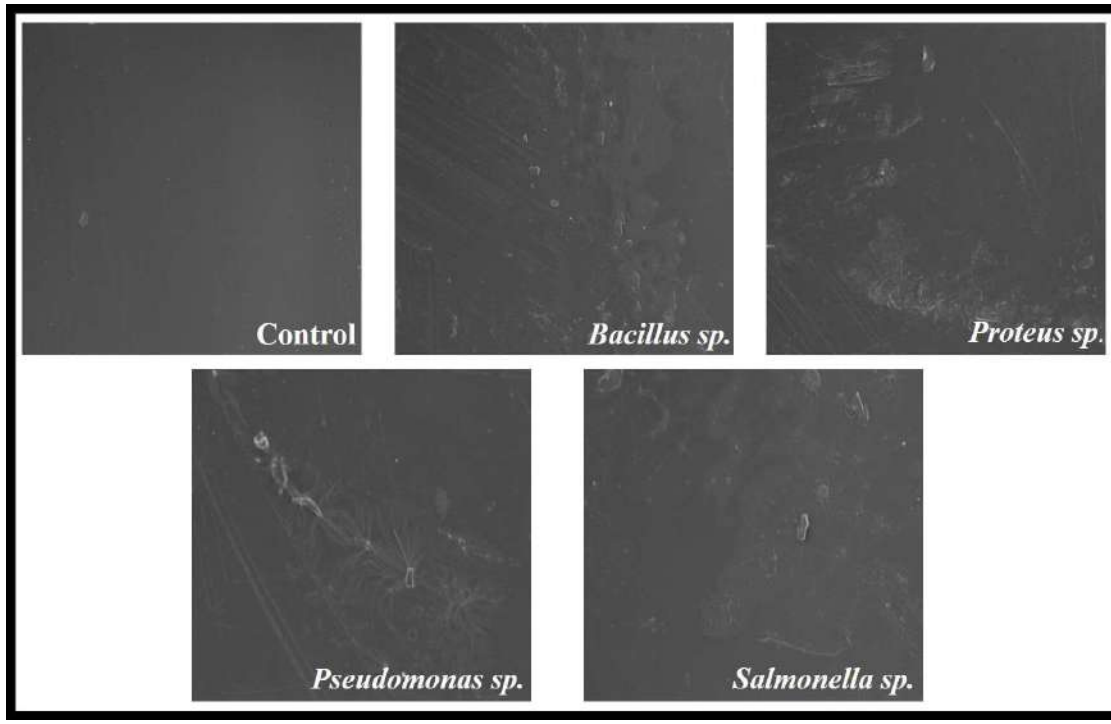


Fig. 2: SEM analysis of LDPE by selected microorganisms.

understanding of the specific bacterial strains that can effectively degrade different types of plastics. This could potentially lead to innovative solutions to tackle the global issue of plastic pollution.

**SEM Analysis**

The Scanning Electron Microscopy (SEM) analysis plays a significant role in the study of microbial degradation of plastics. It provides high-resolution imaging of the surface morphology, which allows for the observation of microbial attachment, biofilm formation, and structural modifications on the plastic surface. In this study, SEM analysis revealed that the surface of LDPE became rough upon exposure to microorganisms, indicating the action of microbial enzymes on the plastic (Fig. 2). This observation suggests that LDPE can be efficiently digested by microbial enzymes, leading to its degradation. SEM analysis not only facilitates the identification of the microorganisms involved in the degradation process but also enables quantitative analysis of surface features and the evaluation of degradation quality. This is crucial for monitoring time-course studies and understanding degradation kinetics, which can inform the development of biodegradable plastics (Cai et al. 2023, Crystal Thew et al. 2023, Gilani et al. 2023). The findings from this study underscore the importance of SEM analysis in plastic degradation research. It provides valuable insights into the interactions between microorganisms and plastics and the subsequent changes in the plastic's surface morphology. These insights can guide future research and development efforts in the field of plastic waste management, particularly in the design of biodegradable plastics and the optimization of microbial degradation processes.

## CONCLUSION

In conclusion, this study elucidates the diverse enzymatic capabilities of *Bacillus* sp., *Proteus* sp., *Pseudomonas* sp., and *Salmonella* sp. in the degradation of HDPE and LDPE plastics. The observed variations in plastic degradation underscore the significance of considering polymer-specific characteristics in microbial waste management. Additionally, SEM analysis provides crucial visual insights into structural modifications on LDPE surfaces during microbial action, informing our understanding of degradation kinetics. The findings emphasize the need for further research on optimization conditions, potential synergistic effects, and the identification of key enzymes involved in the degradation process. Overall, this study contributes valuable knowledge to the multidisciplinary efforts addressing plastic pollution, highlighting the potential of microbial strategies in sustainable plastic waste management.

## REFERENCES


Alshehrei, F. 2017. Biodegradation of Low-Density polyethylene by fungi isolated from Red Sea water. Int. J. Curr. Microbiol. Appl. Sci., 6(9): 1703-1709.

Auman, H.J., Ludwig, J.P., Giesy, J.P. and Theo, Colborn. 1997. Plastic ingestion by Laysan Albatross chicks on Sand Island, Midway Atoll, in 1994 and 1995. Albatross Biol. Conserv., 11: 239-244.

Babaremu, K., Oladijo, O.P. and Akinlabi, E. 2023. Biopolymers: A suitable replacement for plastics in product packaging. Adv. Ind. Eng. Polym. Res., 6: 333-340.

Banerjee, R. and Bhattacharya, T. 2022. Degradation of synthetic polymers: Microbial approach. Indian J. Microbiol. Res., 9(1): 9-13.

Byrne, E., Schaerer, L.G., Kulas, D.G., Ankathi, S.K., Putman, L.I., Codere, K.R., Schum, S.K., Shonnard, D.R. and Techtmann, S.M. 2022. Pyrolysis-aided microbial biodegradation of high-density polyethylene plastic by environmental inocula enrichment cultures. ACS Sustain. Chem, Eng., 10: 2022-2033.

Cai, Z., Li, M., Zhu, Z., Wang, X., Huang, Y., Li, T., Gong, H. and Yan, M. 2023. Biological Degradation of Plastics and Microplastics: A Recent Perspective on Associated Mechanisms and Influencing Factors. Microorganisms, 11(8): 1661.

Crystal Thew, X.E., Lo, S.C., Ramanan, R.N., Tey, B.T., Huy, N.D. and Chien Wei, O. 2023. Enhancing plastic biodegradation process: strategies and opportunities. Crit. Rev. Biotechnol., 1-18.

Franco-Duarte, R. 2019. Advances in chemical and biological methods to identify microorganisms: From past to present. Microorganisms, 7(5): 130.

Gajendiran, A., Krishnamoorthy, S. and Abraham, J. 2016. Microbial degradation of low-density polyethylene (LDPE) by *Aspergillus clavatus* strain JASK1 isolated from landfill soil. 3 Biotech, 6: 85.

Ghatge, S., Yang, Y., Ahn, J.H. and Hur, H.G. 2020. Biodegradation of polyethylene: a brief review. Appl. Biol. Chem., 63: 135.

Gilani, I.E., Sayadi, S., Zouari, N. and Al-Ghouti, M.A. 2023. Plastic waste impact and biotechnology: Exploring polymer degradation, microbial role, and sustainable development implications. Bioresour. Technol. Rep., 24: 101606.

Islami, A.N., Tazkiaturrizki, T. and Rinanti, A. 2019. The effect of pH-temperature on plastic allowance for Low-Density Polyethylene (LDPE) by *Thiobacillus* sp. and *Clostridium* sp. J. Phys. Conf. Ser., 1402: 033003.

Kopecká, R., Kubínová, I., Sovová, K., Mravcová, L., Vítěz, T. and Vítězová, M. 2022. Microbial degradation of virgin polyethylene by bacteria isolated from a landfill site. SN Appl. Sci., 4: 161.

Kotova, I.B., Taktarova, Y.V., Tsavkelova, E.A., Egorova, M.A., Bubnov, I.A., Malakhova, D.V., Shirinkina, L.I., Sokolova, T.G. and Bonch-Osmolovskaya, E.A. 2021. Microbial degradation of plastics and approaches to make it more efficient. Microbiology, 90(6): 671-701.

Kumari, A., Bano, N., Bag, S.K., Chaudhary, D.R. and Jha, B. 2021. Transcriptome-guided insights into plastic degradation by the marine bacterium. Front. Microbiol., 12: 688526.

Kyaw, B.M., Champakalakshmi, R., Sakharkar, M.K., Lim, C.S. and Sakharkar, K.R. 2012. Biodegradation of low-density polyethylene (LDPE) by pseudomonas species. Indian J. Microbiol., 52(3): 411-419.

Liu, W., Liu, H., Liu, K., Du, H., Liu, Y. and Si, C. 2020. Paper-based products as promising substitutes for plastics in the context of bans on non-biodegradables. BioResources, 15(4): 7309-7312.

Midhun, K.D., Kalyani, L.T., Girijasankar, G. and Dandu, S.D. 2015. Biodegradation of low density polyethylene (LDPE) by a new biosurfactant-producing thermophilic *Streptomyces coelicoflavus* NBRC 15399T. African Journal of Biotechnology, 14(4), pp.327-340.

Mohanan, N., Montazer, Z., Sharma, P.K. and Levin, D.B. 2020. Microbial and enzymatic degradation of synthetic plastics. Front. Microbiol., 11: 624709.

Montazer, Z., Habibi Najafi, M.B. and Levin, D.B. 2020. Challenges with verifying microbial degradation of polyethylene. Polymers, 12(1): 123.

Nademo, Z.M., Shibeshi, N.T. and Gemeda, M.T. 2023. Isolation and screening of low-density polyethylene (LDPE) bags degrading bacteria from Addis Ababa municipal solid waste disposal site "Koshe". Ann. Microbiol., 73: 8.

Ojha, N., Pradhan, N., Singh, S., Barla, A., Shrivastava, A., Khatua, P., Rai, V. and Bose, S. 2017. Evaluation of HDPE and LDPE degradation by fungus, implemented by statistical optimization. Sci. Rep., 7: 39715.

Pischedda, A., Tosin, M. and Degli-Innocenti, F. 2019. Biodegradation of plastics in soil: The effect of temperature. Polym. Degrad. Stab., 170: 109017.

Purohit, J., Chattopadhyay, A. and Teli, B. 2020. Metagenomic exploration of plastic degrading microbes for biotechnological application. Curr. Genomics, 21(4): 253-270.

Rani, R., Jitender, Singh, N.P. and Santal, A.R. 2021. Isolation, characterization and optimization of bacterial isolate SARR1 for biodegradation of pretreated low density polyethylene. J. Appl. Nat. Sci., 13(3): 561-570.

Rave, A.F.G., Kuss, A.V., Peil, G.H.S., Ladeira, S.R., Villarreal, J.P.V. and Nascente, P.S. 2019. Biochemical identification techniques and antibiotic susceptibility profile of lipolytic ambiental bacteria from effluents. Braz. J. Biol., 79(4): 555-565.

Ru, J., Huo, Y. and Yang, Y. 2020. Microbial degradation and valorization of plastic wastes. Front. Microbiol., 11: 442.

Sanniyasi, E., Gopal, R.K., Gunasekar, D.K. and Raj, P.P. 2021. Biodegradation of low-density polyethylene (LDPE) sheet by microalga, *Uronema africanum* Borge. Sci. Rep., 11: 13694.

Sileo, L., Sievert, P.R. and Sameul, M.D. 1990. Causes of mortality of albatross chicks at Midway Atoll. J. Wildl. Dis., 26(3): 329-338.

Song, J.H., Murphy, R.J., Narayan, R. and Davies, G.B.H. 2009. Biodegradable and compostable alternatives to conventional plastics. Philos. Trans. R Soc. B, 364(1526): 2127-2139.

Urbanek, A.K., Kosiorowska, K.E. and Mirończuk, A.M. 2021. Current knowledge on polyethylene terephthalate degradation by genetically modified microorganisms. Front. Bioeng. Biotechnol., 9: 688178.

Zeenat, E.A., Bukhari, D.A., Shamim, S. and Rehman, A. 2021. Plastics degradation by microbes: A sustainable approach. J. King Saud Univ. Sci., 33(2): 101538.


### ORCID DETAILS OF THE AUTHORS

C. J. Patel: https://orcid.org/0000-0002-8294-2848

Nature Environment and Pollution Technology
An International Quarterly Scientific Journal

p-ISSN: 0972-6268
(Print copies up to 2016)
e-ISSN: 2395-3454

Vol. 23 | No. 3 | pp. 1723-1727 | 2024

Original Research Paper

https://doi.org/10.46488/NEPT.2024.v23i03.044

Open Access Journal

# Investigation of Rosemary Oil as Environmentally Friendly Corrosion Inhibitor of Aluminum Alloy

**K. V. Kamarska**

Department of Mathematics, Physics and Chemistry, Technical University of Sofia, Branch Plovdiv, 4000, Plovdiv, Bulgaria

†Corresponding author: K. Kamarska; kamarska@tu-plovdiv.bg

**Nat. Env. & Poll. Tech.**
**Website: www.neptjournal.com**

*Received:* 18-05-2023
*Revised:* 03-07-2023
*Accepted:* 05-07-2023

**Key Words:**
Rosemary oil
Corrosion inhibitor
Aluminum alloy

## ABSTRACT

The inhibitory effect of Rosemary oil on the corrosion of aluminum alloy EN AW-2011 in 1M $H_2SO_4$ solution was studied by weight loss and electrochemical methods such as open circuit potential (OCP), linear sweep voltammetry (LSV) and linear polarization resistance (LPR). The inhibition efficiency increases with increasing the concentration and shows maximum inhibition efficiency (70.7 %) at optimum concentration (0.05 $g.L^{-1}$). The linear polarization resistance measurements show that the presence of Rosemary oil in 1M $H_2SO_4$ solution influences polarization resistance increasing and corrosion current decreasing. The voltammetric curve shows that Rosemary oil reduces the anodic process. Open circuit potential results confirmed that organic compounds present in Rosemary oil can form a protective layer on aluminum surfaces. The inhibitive effect was probably caused by the adsorption of organic compounds such as 1,8-cineole, α-pinene, borneol, limonene, and myrcene on aluminum surfaces which are non-toxic and environmentally friendly. This study showed that the essential oil of Rosemary could be used as an environmentally friendly inhibitor of the corrosion of alloy EN AW-2011 in an acidic medium.

## INTRODUCTION

Aluminum alloy EN AW 2011 is among the most preferred in machine building and the automotive industry due to the fact, that it is easy to process, has high mechanical strength, and allows coloring in various colors. There are various methods for protecting metals against corrosion, one of which is the addition of inorganic or organic corrosion inhibitors. In practice, organic corrosion inhibitors frequently are used in natural products – plant extracts from roots, leaves, and oils. Some plant extracts and essential oils can be used as organic ecological inhibitors. This is possible thanks to their molecules, containing heteroatoms such as O in polar groups or heterocyclic compounds with π-bonds (Khadraoui et al. 2013, Prabhu & Padmalatha 2013). The use of natural plant products to protect metals from corrosion is important because they show a high inhibitory efficiency of up to 98% and at the same time, they are environmentally friendly, non-toxic, and much more effective than the inorganic inhibitors (Sangeetha et al. 2013).

The plant extract and essential oil from *Mentha spicata* (Bensabah et al. 2013), *Terminalia ivorensis* extract (Wisdom et al. 2018), gum exudates from *Pachylobus edulis* in sodium chloride (Umoren et al. 2007), *Asparagus racemosus* extract (Bashir et al. 2019), *Ricinus communis* (Onukwuli et al. 2020), ethanolic extract of *Cordia dichotoma* seeds (Sharma & Sharma 2019) and *Glycine max* extract (El-Azaly 2019) in hydrochloric acid solution have a great importance in their use as environmental anti-corrosion products.

The literature review shows that the information about the essential oil of Rosemary (*Rosmarinus officinalis*) is limited but the investigation of the plant has great potential. The essential oil of Rosemary contains bicyclic monoterpene (α-pinene, -1,8cineol, borneol) and cyclic monoterpene (limonene) which are non-toxic and innocuous in the environment and biodegradable (Gonzalez-Minero et al. 2020).

Thanks to the adsorption of these organic compounds on the metal surface, a protective layer is formed, which reduces the corrosion.

This paper studies the inhibitory effect of Rosemary oil, used as an environmentally friendly inhibitor on the destruction of aluminum alloy EN AW-2011 in an acidic medium.

## MATERIALS AND METHODS

Aluminum alloy EN AW-2011 was used for all corrosion measurements. As an aggressive medium, 1M $H_2SO_4$, Pure

100% Rosmarinus officinalis essential oil was provided by "Rivana" (LLC, Bulgaria).

### Weight Loss Measurement

Before carrying out the weight loss experiments the samples were polished with abrasive papers with different grades (400-800), rinsed with acetone then with water, and dried. The samples were weighed and then placed in a test solution of 1M $H_2SO_4$ for 4 hours without the inhibitor and with Rosemary essential oil (0.01-0.05 $g.L^{-1}$) in the role of an inhibitor. 4 hours later, the samples were rinsed with distilled water, dried, and reweighed. The corrosion rate (W, $g.m^{-2}.h$) and the inhibition efficiency ($\eta_w$, %) of the alloy were determined by the equations:

$$W = \frac{\Delta m}{S.t} \quad \ldots(1)$$

$$\eta_w \% = \frac{W_{blank} - W_{inh}}{W_{blank}} \text{ x } 100 \quad \ldots(2)$$

where $\Delta m$ is the average weight loss of the sample (g); $S$ is the total area of the specimen ($m^2$); $t$ is immersion time (h), $W_{blank}$ is the corrosion rate values in the absence of inhibitor, and $W_{inh}$ in the presence of inhibitor.

### Electrochemical Measurements

The open circuit potential and linear sweep voltammetry were performed using the electrochemical workstation PalmSens and potentiostat/galvanostat (PAR model 263A) for linear polarization resistance. The obtained data were processed by the Power Suite program. All measurements were carried out in a three-electrode cell. A platinum wire as the auxiliary electrode, a Sat. Ag/AgCl electrode as a reference and aluminum alloy EN AW-2011 as a working electrode with an area of 1 $cm^2$.

The OCP was measured for 600 s. Linear sweep voltammetry measurement was performed at a scan rate of 0.010 V/s. The LPR measurements were performed from -0.020 V to +0.020 V vs. $E_{corr}$ at a scan rate of 0.10 mV $s^{-1}$.

Equation (3) was used to determine the inhibition efficiency ($\eta_p$ %) from linear polarization method data:

$$\eta_p \% = \frac{I_{corr} - I'_{corr}}{I_{corr}} \text{x}100 \quad \ldots(3)$$

where $I_{corr}$ is the corrosion current value in the absence of an inhibitor and $I'_{corr}$ in the presence of an inhibitor.

### Surface Analysis

The surface of aluminum alloy specimens was examined by immersing them in various test solutions before and after exposure to 1M $H_2SO_4$ (blank) and with and without inhibitor of 0.05 $g.L^{-1}$ for 4 hours. A digital microscope (Digi Micro Scope 2,0M Pixels) was used to obtain the images of the specimen surface.

## RESULTS AND DISCUSSION

### Weight Loss Measurement

The values of percentage inhibition efficiency and corrosion rate obtained from weight loss measurement for aluminum alloy EN AW-2011 in 1M $H_2SO_4$ in the absence (blank) and presence of different concentrations of essential oil of Rosemary are summarized in Table 1. Inspection of the data in the table reveals that the addition of Rosemary oil decreases the corrosion rate of aluminum alloy EN AW 2011. This result indicates the inhibitive effect of the added essential oil of Rosemary on aluminum alloy corrosion in the acidic solution.

The inhibition efficiency increases as the concentration of added essential oil of Rosemary is increased. The optimal value of $\eta_w$ of 70.7% was received for 0.05 $g.L^{-1}$ of Rosemary oil.

### Electrochemical Measurements

**Open circuit potential:** The experiment with the OCP was conducted to investigate the effect of the Rosemary oil on the behavior of the aluminum alloy EN AW-2011 in 1M solution of $H_2SO_4$. Fig. 1 shows the current curves of the open circuit for the electrodes, made of Al 2011 and placed in 1M $H_2SO_4$ (a), and 0.01 $g.L^{-1}$ (b), 0.03 $g.L^{-1}$ (c), 0.05 $g.L^{-1}$ (d), placed in Rosemary oil.

During the first one or two minutes after the immersion into 1M $H_2SO_4$, the potential of the studied aluminum alloy quickly deviates in the negative direction and continues to deviate in the negative direction over time, i.e., the alloy breaks down in the 1M $H_2SO_4$.

After the addition of 0.01 $g.L^{-1}$ Rosemary oil to 1M $H_2SO_4$, the alloy potential initially deviates in the negative direction; but after the first minute it starts deviating in the positive direction and increases over the time of conducting the study. With the addition of 0.03 and 0.05 $g.L^{-1}$ Rosemary oil, the OCP value initially moves in the negative direction but then increases rapidly in the positive direction and

Table 1: Corrosion parameters of Al alloy EN AW 2011 in 1M $H_2SO_4$ and the presence of Rosemary oil (0.01-0.05 $g.L^{-1}$) determined by weight loss method.

| Concentration, $g.L^{-1}$ | W, $g/m^2.h$ | $\eta_w$, % | θ |
|---|---|---|---|
| blank | 0.0041 | - | - |
| 0.01 | 0.0018 | 56.1 | 0.561 |
| 0.03 | 0.0015 | 63.4 | 0.634 |
| 0.05 | 0.0012 | 70.7 | 0.707 |

remains approximately constant over time. It can be noted that with the increase in the oil concentration from 0.03 to 0.05 $g.L^{-1}$, the OCP value is shifted in the positive direction, i.e., the risk of corrosion decreases.

The deviation of the OCP in the negative direction at the beginning of the study period is probably due to the adsorption of the inhibitor molecules on the active side of the aluminum alloy (Radošević et al. 2001).

**Linear sweep voltammetry:** On the voltammetric curve, recorded for 1M $H_2SO_4$, a peak at a potential of 0 V (vs Ag/AgCl) (Fig. 2) is observed, which is associated with the oxidative reaction of intermetallic inclusions in the studied alloy, dissolving in an acidic medium (*Mrad* et al. 2017).

The presence of Rosemary oil reduces the anodic process, associated with the electrochemical oxidation of the aluminum alloy. The interaction between the organic substances in the Rosemary oil and the surface of the alloy affects the value of the potential and there is a slight shift in the positive direction. It is observed that the current value decreases almost in proportion to the concentration of the oil. Assuming that the current at this potential is associated with the destruction of the oxide layer, then it is evident that the presence of Rosemary oil decreases the current value almost proportionally with respect to the concentration of the oil. In addition, after the addition of Rosemary oil, a new peak appears at about 0.16 V (vs Ag/AgCl), which is associated with the oxidation of the monoterpene.

**Linear polarization resistance:** The linear polarization resistance experiment was conducted to establish the inhibitory effect of Rosemary oil on the corrosion of

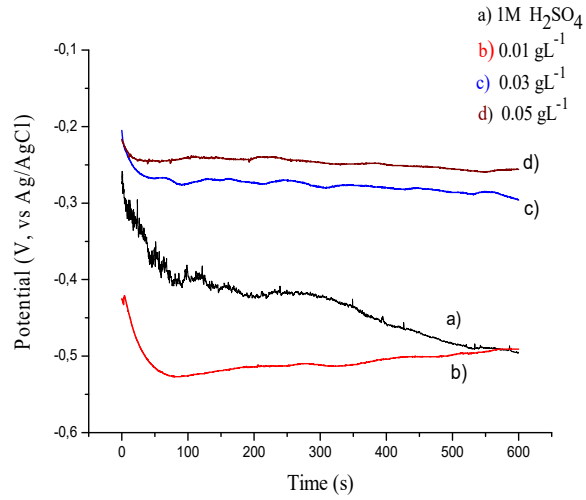


Fig. 1: OCP of Al alloy EN AW 2011 in 1M $H_2SO_4$ without and with Rosemary oil.

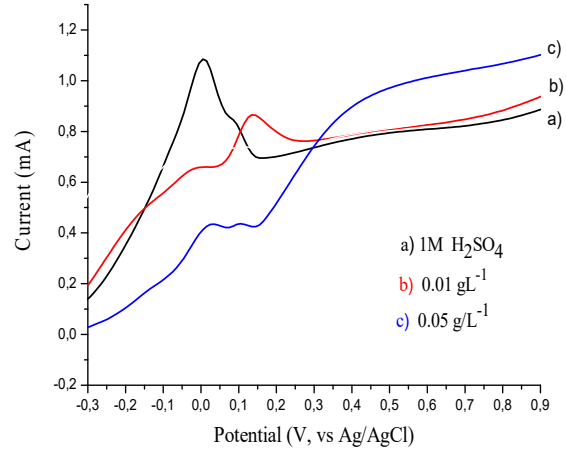


Fig. 2: Linear sweep voltammetry of aluminum alloy EN AW-2011 in 1 M $H_2SO_4$ without and with Rosemary oil.

Table 2: Electrochemical parameters of Al alloy EN AW 2011 in 1M $H_2SO_4$ and the presence of Rosemary oil (0.01-0.05 $g.L^{-1}$) determined by the LPR.

| concentration, $g.L^{-1}$ | $I_{corr}$ (μA) | CR (mpy) | Rp (kΩ $cm^{-2}$) | $\eta_p$, % |
|---|---|---|---|---|
| blank | 9.319 | 1.226 | 2.333 | - |
| 0.01 | 4.899 | 0.644 | 4.437 | 47.42 |
| 0.03 | 3.088 | 0.406 | 7.041 | 66.86 |
| 0.05 | 1.771 | 0.233 | 12.30 | 80.99 |

aluminum alloy 2011 in a 1 M $H_2SO_4$ and to determine the mechanism of inhibition. Table 2 presents the value of the corrosion current ($I_{corr}$), corrosion rate (CR), polarization resistance ($R_P$), and inhibition efficiency ($\eta_p$ %) for aluminum alloy 2011 in a 1 M solution of $H_2SO_4$ without and with Rosemary oil.

It can be observed that the values of Rp constantly increase with increasing Rosemary oil concentration, while the corrosion current and corrosion rate values decrease. The polarization resistance value is the highest at a concentration of 0.05 $g.L^{-1}$ Rosemary oil, while a higher Rp value indicates a lower corrosion rate.

According to data from Rivana, LLC, Bulgaria, the main components of Rosemary essential oil are 1,8-cineole, α-pinene, borneol, limonene, and myrcene.

Most of these components are monoterpene (bicyclic or cyclic monoterpene), having heteroatoms in their aromatic rings and they can be used as ecological corrosion inhibitors. These organic molecules can be adsorbed on the metal surface by the sharing electrons of an oxygen atom (such as a 1,8-cineole) or interactions between π-electrons of double bonds in the aromatic ring in monoterpene and vacant d-orbitals of aluminum (such as limonene) (Juergens et al. 2004, Bourazmi et al. 2018). As a result of these reactions is formed protective layer and thus reduces corrosion.

To understand the process of adsorption of the Rosemary oil on the surface of the aluminum alloy, the surface coverage values were fitted in the Langmuir adsorption isotherm and the values of the correlation coefficient ($R^2$) were used to determine the best fit.

A comparison of the obtained data from the weight loss and polarization method shows a good correlation between the two methods (Fig. 3). A correlation coefficient ($R^2$) from weight loss data is 0.998 and 0.995 from polarization data. In both methods a slope close to 1.

## Surface Analysis

The aluminum alloy coupons were immersed for 4 hours at room temperature in 1M $H_2SO_4$ with 0.05 $g.L^{-1}$ Rosemary oil in the role of an inhibitor. The surface morphologies of the aluminum alloy EN AW-2011 in 1M $H_2SO_4$ without and with the presence of an optimum concentration of inhibitor are recorded and shown in Fig. 4.

Many differences occur in both images. The aluminum alloy coupon, which was immersed in 1M $H_2SO_4$ without inhibitor (Fig. 4A), appeared to be heavily corroded when compared to the surface of aluminum alloy in the presence of Rosemary oil (Fig. 4B) due to the protective layer on the aluminum alloy surface. Microscopic pictures of the studied aluminum show that the presence of Rosemary oil in the solution changes the structure of the pores of the metal surface. Therefore, the corrosion rate decreases, since the adsorption of the inhibitor changes the mechanism of

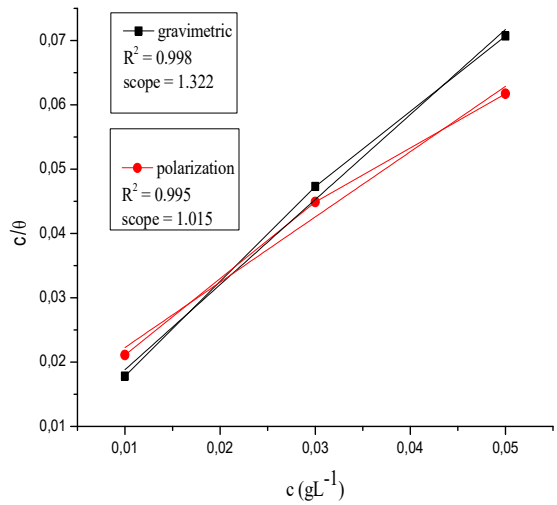


Fig. 3: Curve fitting of weight loss and polarization data obtained for aluminum alloy EN AW 2011 in 1M $H_2SO_4$ with Rosemary oil to Langmuir adsorption isotherm.

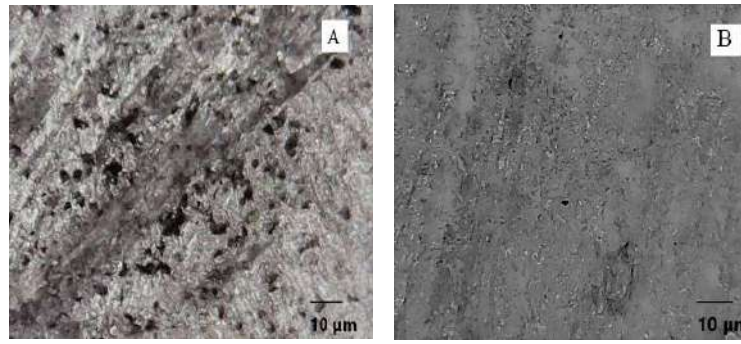


Fig. 4: Micrography of aluminum alloy EN AW-2011 surface A) in 1M $H_2SO_4$ and B) inhibited aluminum alloy (1M $H_2SO_4$ + 0.05 $g.L^{-1}$ Rosemary oil).

anodic dissolution and aluminum passivation during its stay in sulfuric acid.

## CONCLUSIONS

The essential oil of Rosemary (*Rosmarinus officinalis*) is organic in nature and can be used in the production of environmentally friendly inhibitors and it is one of the natural inhibitors which has an inhibitive action on the corrosion of metals. It contains various active organic compounds such as α-pinene, -1,8cineol, borneol, and limonene which are non-toxic and have no ecological hazards.

Weight loss measurements confirm that the Rosemary essential oil successfully inhibits the corrosion of aluminum alloy EN AW-2011 and the inhibition efficiency goes up with the increase in the concentration of the oil. Electrochemical measurements give reasons to conclude that the investigated Rosemary oil can be successfully used as a corrosion inhibitor for aluminum alloys in 1M $H_2SO_4$. The inhibition efficiency of the investigated essential oil depends on its concentration in the solution. This study proves that the essential oil of Rosemary (Rosmarinus officinalis) has a good ability to inhibit the corrosion of aluminum alloy EN AW 2011 in 1M $H_2SO_4$ and can used as an environmentally friendly inhibitor in this medium.

## ACKNOWLEDGEMENT

The author would like to thank the Research and Development Sector at the Technical University of Sofia for the financial support.

## REFERENCES

Bashir, S., Singh, G. and Kumar, A. 2019. Shatavari (Asparagus racemosus) as green corrosion inhibitor of aluminum in an acidic medium. Port. Electrochim. Acta., 38(2): 83-91.

Bensabah, F., Houbairi, S., Essahli, M., Lamiri, A. and Naja, J. 2013. Chemical composition and inhibitory effect of the essential oil from Mentha spicata irrigated by wastewater on the corrosion of aluminum in 1 molar hydrochloric acid. Port. Electrochim. Acta., 31(4): 195-206.

El-Azaly, A. 2019. Influence of Soybean (Glycine max) plant extract on corrosion of aluminum in 1M HCl. Int. J Electrochem. Sci., 14: 2714-2731.

González-Minero, J., Bravo-Díaz, L. and Ayala-Gómez, A. 2020. Rosmarinus officinalis L. (Rosemary): An ancient plant with uses in personal healthcare and cosmetics. Cosmetics., 7(4): 77.

Juergens, U., Engelen, T., Racké, K., Stöber, M., Gillissen, A. and Vetter, H. 2004. Inhibitory activity of 1,8-cineol (eucalyptol) on cytokine production in cultured human lymphocytes and monocytes. Pulmon. Pharmacol. Therap., 17: 281-287.

Khadraoui, A., Khelifa, A., Touafri, L., Hamitouche, H. and Mehdaoui, R. 2013. Acid extract of Mentha pulegium as a potential inhibitor for corrosion of 2024 aluminum alloy in 1 M HCl solution. J. Mater. Environ. Sci., 4(5): 663-670.

*Mrad*, M., Ben amor, Y., Dhouibi, I. and Montemor, F. 2017. Electrochemical study of polyaniline coating electropolymerized onto AA2024-T3 aluminum alloy: Physical properties and anticorrosion Performance. Synth. Met., 234: 145-153.

Onukwuli, O., Omotioma, M. and Obiora-Okafo, I. 2020. Thermometric and gravimetric analyses of aluminum corrosion control in an HCl medium, using Ricinus communis extract. Port. Electrochim. Acta., 38(1): 19-28.

Prabhu, D. and Padmalatha, R. 2013. Studies of corrosion of aluminum and 6063 aluminum alloy in phosphoric acid medium. Int. J. ChemTech. Res., 5(6): 2690-2702.

Radošević, J., Kliškić, M. and Višekruna, A. 2001. Inhibition of corrosion of the Al-2.5Mg alloy by means of the third acidic phenolic subfraction of aqueous extract of rosemary. Kem Ind., 50(10): 537-542.

Sangeetha, M., Rajendran, S., Sathiyabama, J. and Krishnaveni, A. 2013. Inhibition of corrosion of aluminum and its alloys by extracts of green inhibitors. Port. Electrochim. Acta., 31(1): 41-52.

Sharma, S. and Sharma, Y. 2019. Cordia dichotoma as corrosion inhibitor for aluminum alloy (AA6063) in hydrochloric acid. Port. Electrochim. Acta., 37(1): 1-22.

Umoren, S., Obot, I., Ebenso, E. and Okafor, P. 2007. Eco-friendly Inhibitors from naturally occurring exudate gums for aluminum corrosion inhibition in an acidic medium. Port. Electrochim. Acta., 26(3): 267-282.

Wisdom, J., Kelechi, D. and Ugochukwu, J. 2018. Green inhibitor for corrosion of aluminum alloy AA 8011A in an acidic environment. Int. Res. J. Eng. Tech., 5(2): 121-124.

Nature Environment and Pollution Technology
An International Quarterly Scientific Journal

p-ISSN: 0972-6268
(Print copies up to 2016)
e-ISSN: 2395-3454

Vol. 23 | No. 3 | pp. 1729-1734 | 2024

Original Research Paper

https://doi.org/10.46488/NEPT.2024.v23i03.045

Open Access Journal

# Decolorization of Textile Dyes by Extracellular Enzymes Produced from *Trametes sanguinea* and *Perenniporia taephropora* Immobilized on Natural Media

**Siriorn Boonyawanich, Nipon Pisutpaisal and Saowaluck Haosagul†**
Department of Agro-Industrial, Food and Environment Technology, Faculty of Applied Science, King Mongkut's University of Technology, North Bangkok, Bangkok, Thailand
†Corresponding author: Saowaluck Haosagul; h_saowaluck@hotmail.com

**Nat. Env. & Poll. Tech.**
**Website: www.neptjournal.com**

*Received:* 29-08-2023
*Revised:* 14-10-2023
*Accepted:* 15-10-2023

**Key Words:**
Textile wastewater
White rot fungi
Decolorization
Immobilized fungi
Ligninolytic enzyme

## ABSTRACT

The color of textile wastewater is still a main problem in wastewater treatment by biological processes. The colored effluents from textile factories usually exceed effluent standards. Therefore, various innovations were developed to treat textile wastewater for decolorization in the effluents. This research aims to decolorize textile wastewater by immobilizing white rot fungi degradation. At first, the 11 fungal stains were tested to find the decolorized efficiency then the high decolorized efficiency fungal stains were immobilized on four material media, namely water hyacinth stalks, coconut husk, corn cob, and loofah. After that, the immobilized fungi were cultivated in the culture media at 30, 60, and 120 C/N ratios, respectively. The results showed that *Trametes sanguinea* and *Perenniporia tephropora* were two stains with a high decolorized efficiency of 68.8% and 67.5% respectively, and the decolorized efficiency was increased when immobilized on loofahs and fed with 120 C/N ratio medium. In a comparison of two fungal stains, *P. tephropora* was found more suitable for the decolorization of textile wastewater than *T. sanguinea* because *T. sanguinea* could produce red-orange pigments that induced the colored enhancement in wastewater over time. Finally, immobilized *P. tephropora* was cultivated in a 120 C/N ratio medium within a 10 L continuous stirred tank reactor (8 L working volume) to investigate the decolorized efficiency, enzymatic activity, and repeated batch. It was found that three repeated cycles were carried out by reusing the immobilized *P. tephropora* and the highest decolorized efficiency was 63.4%. The enzymatic activity of laccase, manganese peroxidase, and lignin peroxidase was 15.5 U/L, 85.9 U/L, and 0 U/L, respectively

## INTRODUCTION

The textile dyeing industry is important to the economic development of Thailand. Currently, there are 159 textile dyeing factories in Thailand (Department of Industrial Works 2022), and they have continuously exported garments that generate income for the country. During the production process, high volumes of water are used in various steps such as de-sizing, scouring, bleaching, and dyeing, while chemicals and dyes are applied to improve the properties of the fabric. As a result, a huge quantity of wastewater is discharged and dark color. Characteristics of these wastewaters are high suspended solids and BOD values (Pollution Control Department 2022) which are caused by organic substances from the dyeing process (starch, fiber, dye, and solvents) and containing heavy metal inorganic compounds (copper, lead, chromium, cobalt and zinc) from dyes, so the effluent has a color and high pH value (The Bureau of Science and Technology Information Service 2022). It is necessary to have decolorization and wastewater treatment processes in accordance with the wastewater standards of the Department of Industrial Works before releasing it into natural water sources. Synthetic organic dyes such as azo dyes and disperse dyes are now widely used in the textile dyeing industry. It was found that about 10-15% of dye components were leaked from the dyeing process into the effluent (Naghizadeh & Nabizadeh 2016).

The active methods for textile wastewater decolorization can be treated in many ways, both physical and chemical treatments, including chemical sedimentation, ozone oxidation, adsorption by activated carbon, and membrane technology (Sachidhanandham & Periyasamy 2021). These methods are costly and leave chemical residues in the environment. Consequently, it's not popular nowadays. Decolorization with the biological process by using white rot fungi is the best choice to be suitable and highly effective for decoloring wastewater from the textile dyeing industry (Zainith et al. 2020). White rot fungi can produce extracellular enzymes such as laccase, lignin peroxidase,

and manganese peroxidase to decompose derivatives of ethanolamine in azo dyes and anthraquinone dyes which can decolorize the industrial wastewater.

In addition, a lot of research studied ligninolytic enzyme production by white rot fungi and its decolorization efficiency. Patel et al. (2014) found that *Pleurotus ostreatus* HP-1 can excellently produce laccase enzyme and is stable at 70°C. Cheng et al. (2007) studied manganese peroxidase produced from *Schizophyllum* sp. F17, which is stable under pH 4-7 at 25°C. Kong et al. (2016) investigated manganese peroxidase from *Echinodontium taxodii* 2538 for lignin degradation, it has the highest enzyme activity at pH 3.5 and 55°C. Lignin peroxidase enzyme was produced in the white rot fungi, *Trametes versicolor* (Manavalan et al. 2015) and *Phanerochaete chrysosporium* (Bilal & Iqbat 2020). Moreover, white rot fungi have also been used in the decolorization treatment of industrial wastewater such as *Daedaleopsis* sp. and *P. chrysosporium* (Prasongsuk et al. 2009), *Phanerochaete chrysosporium*, *Trametes versicolor* (Costa et al. 2017); *Pleurotus ostreatus* (Haider 2019); *Trametes hirsuta* PW17-41 (Tampropaporn et al. 2022), It was found that the efficiency of color removal was in the range of 70-90%.

Therefore, this research aims to select white rot fungi strains that have high efficiency in removing color in real dyeing industrial wastewater by immobilizing cells on supporting media (corn cob, coconut husk, loofah, water hyacinth stalk) coupled with varying C/N ratios in the culture medium inside the continuous stirred tank reactor (CSTR) with a working volume of 8 L to increase filament forming capacity and obtain high decolorized efficiency and enzymes.

## MATERIALS AND METHODS

### Microorganisms

Nine isolates of white-rot fungi were obtained from the Department of Microbiology, Faculty of Science, Srinakharinwirot University, Thailand. These fungi were *Coriolopsis retropicta* (MK589270), *Ganoderma* sp. (MK589271), *Ganoderma* sp. (MK589274), *Ganoderma* sp. (MK589275), *Microporus* sp. (MK589280), *Microporus* sp. (MK589281), *Trametes elegans* (MK589285), *Trametes sanguinea* (MK589287) and *Pseudolagarobasidium* sp. (MK589289). Two isolates of white rot fungi (*Perenniporia tephropora* (OP358037) and *Pleurotus* sp. (OP358038) were derived from the Department of Agro-Industrial, Food and Environmental Technology, Faculty of Applied Science, King Mongkut's University of Technology North Bangkok. The GenBank accession numbers of internal transcribed spacer sequences were represented in parentheses.

### Textile Wastewater and Chemicals

Textile wastewater (containing azo and anthraquinone dyes) was obtained from the aeration tank of the activated sludge process in the textile factory located in Bang Khun Thian District, Bangkok, Thailand. Other chemicals and media were purchased from Sigma-Aldrich (Missouri, USA) Himedia (Mumbai, India), and Ajax Finechem (New South Wales, Australia).

### Decolorized Screening by White Rot Fungi

Eleven isolates of white rot fungi were grown on a Potato Dextrose Agar (PDA) plate at 30°C for 7 days. Five plugs, 8 mm in diameter from the growing edge of mycelia in the PDA plate were inoculated in 250 mL Erlenmeyer flasks containing 50 mL of basal medium (pH 5). The basal medium was consisted of 10 $g.L^{-1}$ glucose, 1 $g.L^{-1}$ peptone, 1 $g.L^{-1}$ $KH_2PO_4$, 0.5 $g.L^{-1}$ $MgSO_4 \cdot 7H_2O$, 0.05 $g.L^{-1}$ $Na_2HPO_4$, 0.01 $g.L^{-1}$ $CaCl_2$, 0.01 $g.L^{-1}$ $FeSO_4 \cdot 7H_2O$, 0.001 $g.L^{-1}$ $MnSO_4 \cdot 4H_2O$, 0.001 $g.L^{-1}$ $ZnSO_4 \cdot 4H_2O$, 0.002 $g.L^{-1}$ $CuSO_4 \cdot 5H_2O$ and textile wastewater 100%v/v. Culture media were incubated at 30°C, 100 rpm for 5 days. The experiment was performed in triplicate. Ligninolytic enzyme activities (laccase, MnP and LiP) and color in ADMI color units were assayed.

### Fungal Immobilization on Different Media

Four types of media (water hyacinth stalks, coconut husk, corn cob, and loofah) were used for fungal mycelium immobilization. These media were washed with distilled water, dried at 50 °C for 24 hours, and cut into 1 $cm^3$ cubes. Then, five plugs (8 mm in diameter) of the selected isolate from the growing edge of mycelia were inoculated in 250 mL Erlenmeyer flasks containing 100 mL of Potato Dextrose Broth (PDB) and 5 pieces of media (3 replicates). The culture was shaken at 100 rpm, 30°C for 7 days. The immobilized fungal mycelia on media were taken out, washed with sterile distilled water, and dried at 50°C for 48 hours. The dry weight of mycelia adhered to the four types of media was measured.

### Effect of Carbon on Nitrogen Ratios

The effect of carbon-to-nitrogen ratios on wastewater decolorization was observed. Five immobilized fungal mycelia on the selected media were inoculated in 500 mL Erlenmeyer flasks that contained 200 mL modified basal medium (pH 5) which used sucrose and ammonium tartrate as carbon and nitrogen sources, respectively (Tampropaporn et al. 2022, Huang et al. 2020). The C/N ratio in the modified basal medium was varied to 30, 60, and 120. The control treatment was a basal medium used for the decolorized screening. The experiment was tested in triplicate. Culture media were incubated in agitated conditions (100 rpm) at

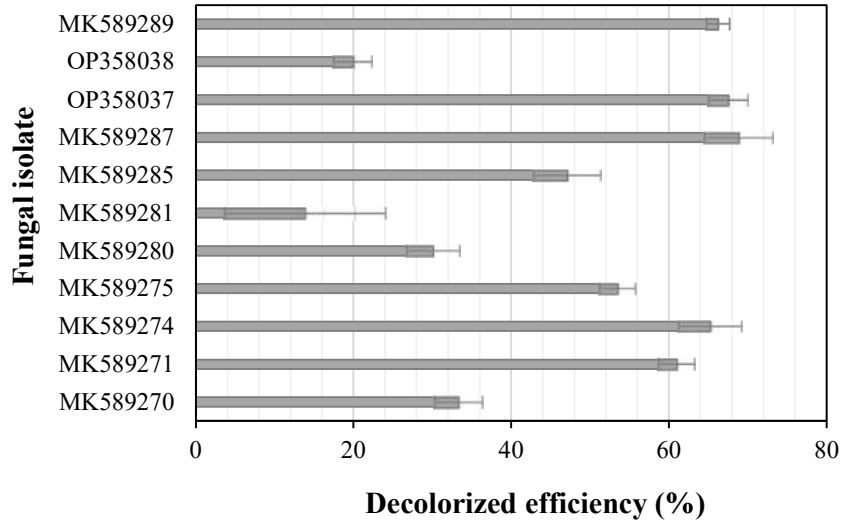


Fig. 1: The highest decolorized efficiency of eleven fungal isolates.

30°C for 6 days. Enzyme activity (laccase, MnP and LiP) and color in ADMI color units were assayed.

### Decolorization of Wastewater in Bioreactor

Eighty immobilized fungal mycelia on the selected media were cultured in a 10 L continuous stirred tank reactor (CSTR) containing 8 L modified basal medium with the optimal C/N ratio. The aeration was continuously supplied, and the reactor was kept at 30°C. After the color value dropped below 300 ADMI, the old modified basal medium was replaced by a new modified basal medium, and the replacement was repeated until the decolorization was inefficient. Enzyme activities (laccase, MnP and LiP), the number of replacements, and color in ADMI color units were analyzed.

### Analytical Determinations

Ligninolytic enzyme activities (laccase, MnP and LiP) were analyzed following the method of Kietkwanboot et al. (2020). They were expressed as units per liter, in which one unit of enzyme activity was defined as the amount of enzyme oxidizing 1 μmol of substrate per liter per minute. The decolorized efficiency (DE) was calculated from the following equation:

$$DE = (ADMI_0\text{-}ADMI_1)/ADMI_0 \times 100$$

Where, $ADMI_0$ = initial color in ADMI color units

$ADMI_1$ = final color in ADMI color units

## RESULTS AND DISCUSSION

### Decolorized Screening by White Rot Fungi

Numerous researchers indicate that white rot fungi could break down synthetic dyes because of the production of non-specific extracellular ligninolytic enzymes (Anastasi et al. 2010, Teerapatsakul & Chitadon 2016, Tampropaporn et al. 2022). As a result, eleven isolates of white rot fungi were screened for textile wastewater treatment. *Trametes sanguinea* (MK589287) showed the highest decolorized efficiency (68.8%) followed by *Perenniporia tephropora* (OP358037) (67.5%) (Fig. 1). The highest ligninolytic enzyme activity of 11 isolates white rot fungi was presented in Table 1.

*T. sanguinea* and *P. tephropora* were reported for application in dye and wastewater decolorization such as anthraquinone dye (Lu et al. 2007), phenolic dye (Ling et al. 2015), acid dye (Younes et al. 2006) and pulp mill effluent (Teerapatsakul & Chitradon 2016). It was not surprising that both isolates showed high decolorization, therefore, they were tested in further experiments.

Table 1: The highest ligninolytic enzyme activity (U/L) of eleven fungal isolates.

| Accession number | Ligninolytic enzyme activity (U/L) | | |
|---|---|---|---|
| | Laccase | Manganese peroxidase | Lignin peroxidase |
| MK 589270 | 120.08 | 172.97 | 3.76 |
| MK 589271 | 10.52 | 22.12 | 10.22 |
| MK 589274 | 52.11 | 237.21 | 2.15 |
| MK 589275 | 8.59 | 32.00 | 9.86 |
| MK 589280 | 0.06 | 1.46 | 8.24 |
| MK 589281 | 0.00 | 1.88 | 11.29 |
| MK 589285 | 0.34 | 1.70 | 2.69 |
| MK 589287 | 273.15 | 2432.12 | 2.15 |
| MK 589289 | 41.35 | 86.73 | 1.25 |
| OP 358037 | 47.16 | 121.09 | 11.47 |
| OP 358038 | 47.10 | 64.73 | 1.97 |

Table 2: Dry weights of *T. sanguinea* and *P. tephropora* on four types of media.

| Type of media | Fungal isolate | |
|---|---|---|
| | T. sanguinea | P. tephropora |
| Corn cob | 0.000±0.000 | 0.000±0.000 |
| Water hyacinth stalks | 0.000±0.000 | 0.081±0.010 |
| Coconut husk | 0.033±0.013 | 0.149±0.021 |
| Loofah | 0.049±0.007 | 0.372±0.018 |

## Fungal Immobilization on Different Media

Four different media were observed for fungal immobilization. Dry weights of *T. sanguinea* and *P. tephropora* mycelia on four types of media were displayed in Table 2. The result revealed that loofah was the most suitable media for fungal immobilization while corn cob was so decayed that the fungal mycelium could not adhere to it. The immobilized mycelium dry weight of *P. tephropora* was higher than *T. sanguinea* because the mycelium of *P. tephropora* could grow rapidly and intertwined very tightly. Loofah was the suitable media due to a lot of pores and rough surfaces which the fungal mycelium could insert in the pores and adhere to the rough surface (Tampropaporn et al. 2022). Thus, the fungal mycelium could grow to cover the surface of the loofah.

## Effect of Carbon to Nitrogen Ratios

Effects of C/N ratios on decolorized wastewater were examined. The optimal C/N ratio for decolorized efficiency by *T. sanguinea* and *P. tephropora* was 120 at 52.7% and 60.2%, respectively (Fig. 2). For ligninolytic enzyme activity, the highest activity was found in 120 C/N ratio medium and lignin peroxidase was the lowest activity enzyme while manganese peroxidase was the highest activity enzyme (Fig. 3). Anastasi et al. (2010) reported that the decolorized efficiency of most fungi was increased when cultured in high C/N ratio medium because the lack of nitrogen stimulated the production of ligninolytic enzyme such as laccase, manganese peroxidase and lignin peroxidase.

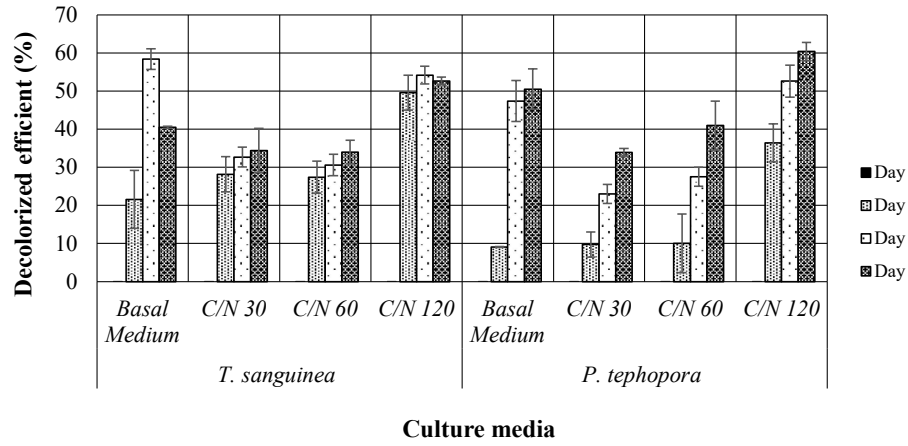


Fig. 2: Decolorized efficiency of *T. sanguinea* and *P. tephropora* in various C/N ratios media.

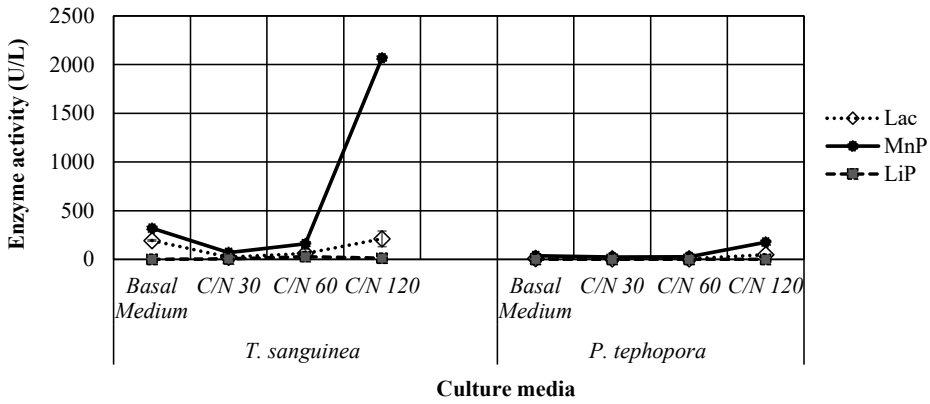


Fig. 3: Ligninolytic enzyme activity of *T. sanguinea* and *P. tephropora* in various C/N ratios media.

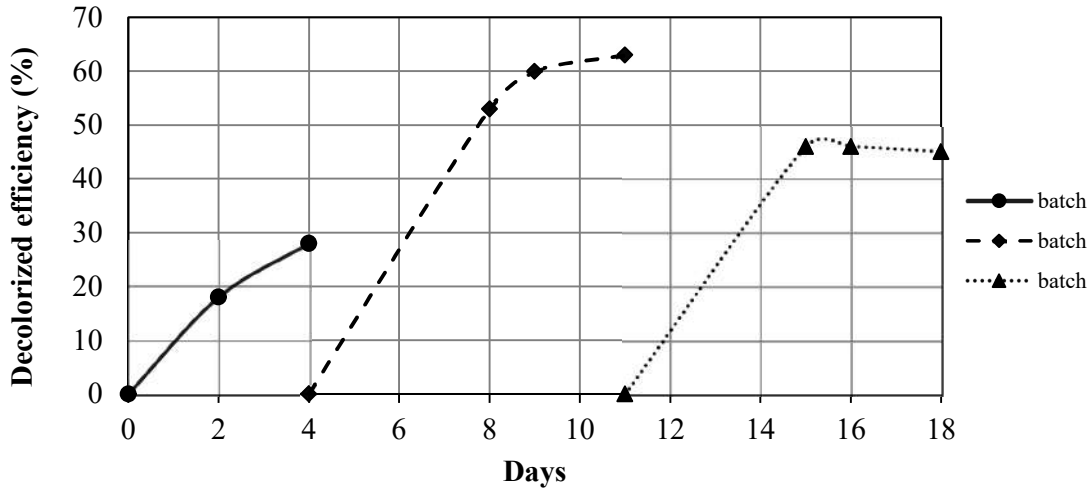


Fig. 4: Decolorized efficiency of immobilized *P. tephropora* in bioreactor.

However, the decolorized efficiency of *T. sanguinea* was decreased after 6 days because the color of textile wastewater was darkened. Téllez-Téllez et al. (2016) reported that *T. sanguinea* could synthesize a salmon red color pigment, cinnabarin, cinnabarinic acid, tramesanguin, and it led to the darker color, thus, the final experiment (decolorization of wastewater in bioreactor) was only tested by *P. tephropora*.

**Decolorization of Wastewater in Bioreactor**

The decolorized efficiency and repeated batch of textile wastewater treatment in the bioreactor were observed. The result showed that three repeated batches were carried out by the immobilized *P. tephropora*. In the first batch (initial color as 361 ADMI), the decolorized efficiency was 27.8% with a color of 260 ADMI (Fig. 4). In the second batch (initial color as 457 ADMI), the decolorized efficiency was 63.4% with a color of 167 ADMI. In the third batch, (initial color as 417 ADMI), the decolorized efficiency was 46.2% with a color of 224 ADMI. It was notable that the decolorized efficiency in the third batch slightly decreased, and it indicated that the decolorization of immobilized *P. tephropora* began inefficiently. For ligninolytic enzyme activities, laccase and MnP activities were increased but LiP activity was not detected (Table 3).

The relationship between the decolorized efficiency and ligninolytic activities was considered. It appeared that the decolorized efficiency did not correspond to the enzyme activity. The highest decolorized efficiency was received in the second batch and decreased in the third batch, the highest laccase and MnP activities happened in the third batch. The explanations of this inconsistency were (1) the production of enzyme isoforms with different affinity to dyes and substrates used in the reaction assays, (2) the restricted distribution of enzymes in the culture medium, and (3) other enzymes (such as cytochrome P450) occurred in the degradation process was not measured (Anastasi et al. 2010).

Table 3: Ligninolytic enzyme activity in bioreactor.

| No. of batch | Ligninolytic enzyme activity (U/L) | | |
|---|---|---|---|
| | Laccase | MnP | LiP |
| 1st batch | 11.5 | 25.6 | 0.0 |
| 2nd batch | 15.5 | 85.9 | 0.0 |
| 3rd batch | 113.0 | 445.1 | 0.0 |

## CONCLUSIONS

A total of 11 isolates of white rot fungi were examined for the decolorized textile wastewater. Both *T. sanguinea* and *P. tephropora* were the fungal isolates with the highest potential for decolorization at 68.6% and 67.5%, respectively. Loofah was the best media for fungal immobilization and 120 C/N ratio was the optimal ratio for the decolorization. For the decolorized textile wastewater in a bioreactor, three repeated batches were carried out by the immobilized *P. tephropora*, and the highest decolorized efficiency was received in the second batch at 63.4%.

## ACKNOWLEDGEMENTS

This research was funded by the National Science, Research and Innovation Fund (NSRF), and King Mongkut's University of Technology North Bangkok with Contract no. KMUTNB-FF-65-68.

## REFERENCES

Anastasi, A., Spina, F., Prigione, V., Tigini, V. and Giansanti, P. 2010. Scale-up of a bioprocess for textile wastewater treatment using *Bjerkandera adusta*. Bioresour. Technol., 101: 3067-3075.

Bilal, M. and Iqbal, H. 2020. Ligninolytic enzymes mediated ligninolysis: an untapped biocatalytic potential to deconstruct lignocellulosic molecules in a sustainable manner. Catal. Lett., 150: 524-543.

Cheng, X. B., Jia, R., Li, P. S., Tu, S. Q., Zhu, Q., Tang, W. Z. and Li, X. D. 2007. Purification of a new manganese peroxidase of the white-rot fungus *Schizophyllum sp*. F17, and decolorization of azo dyes by the enzyme. Enzyme Microb. Technol., 41: 258-264.

Costa, S., Dedola, D. G., Pellizzari, S., Blo, R., Rugiero, I., Pedrini, P. and Tamburini, E. 2017. Lignin biodegradation in pulp-and-paper mill wastewater by selected white rot fungi. Water, 9: 935.

Department of Industrial Works. 2022. Guidelines for color wastewater management in textile factory. [Online] Available at: http://www.diw.go.th/hawk/job/1_8.pdf

Haider, A. and Zulfiqar, M. 2019. Optimization of cultural conditions for the treatment of pulp and paper industrial effluent by *Pleurotus ostreatus* (L.). Pak. J. Agri. Res., 32: 507-513.

Huang, S., Huang, D., Wu, Q. T., Hou, M. F., Tang, X. Y. and Zhou, J. 2020. Effect of environmental C/N ratio on activities of lignin-degrading enzymes produced by *Phanerochaete chrysosporium*. Pedosphere, 30: 285-292.

Kietkwanboot, A., Chaiprapat, S., Muller, R. and Suttinun, O. 2020. Biodegradation of phenolic compounds present in palm oil mill effluent as single and mixed substrates by *Trametes hirsuta* AK04. J. Environ. Sci. Health A, 55: 989-1002.

Kong, W., Chen, H., Lyu, S., Ma, F. Y., Yu, H. Y. and Zhang, X. Y. 2016. Characterization of a novel manganese peroxidase from white-rot fungus *Echinodontium taxodii* 2538, and its use for the degradation of lignin-related compounds. Process Biochem., 5: 1776-1783.

Ling, Z. R., Wang, S. S., Zhu, M. J., Ning, Y. J., Wang, S. N., Li, B., Yang, A. Z., Zhang, G. Q. and Zhao, X. M. 2015. An extracellular laccase with potent dye decolorizing ability from white rot fungus *Trametes sp*. LAC-01. Int. J. Biol. Macromol., 81: 785-793.

Lu, L., Zhao, M., Zhang, B. B., Yu, S. Y., Bian, X. J., Wang, W. and Wang, Y. 2007. Purification and characterization of laccase from *Pycnoporus sanguineus* and decolorization of an anthraquinone dye by the enzyme. Appl. Microbiol. Biotechnol., 74: 1232-9.

Manavalan, T., Manavalan, A. and Heese, K. 2015. Characterization of lignocellulolytic enzymes from white-rot fungi. Curr. Microbiol., 70: 485-498.

Naghizadeh, A. and Nabizadeh, R. 2016. Removal of reactive blue 29 dye by adsorption on modified chitosan in the presence of hydrogen peroxide. Environ. Prot. Eng., 42.

Patel, H., Gupte, S., Gahlout, M. and Gupte, A. 2014. Purification and characterization of an extracellular laccase from solid-state culture of *Pleurotus ostreatus* HP-1. 3 Biotech, 4: 77-87.

Pollution Control Department 2022. The practice for prevention and reduction of pollution in the dying industrial. [Online] Available at: http://infofile.pcd.go.th/water/water_fokyom.pdf.

Prasongsuk, S., Lotrakul, P., Imai, T. and Punnapayak, H. 2009. Decolourization of pulp mill wastewater using thermotolerant white rot fungi. Science Asia, 35: 37-41.

Sachidhanandham, A. and Periyasamy, A. P. 2021. Environmentally friendly wastewater treatment methods for the textile industry. In: Handbook of Nanomaterials and Nanocomposites for Energy and Environmental Applications. Springer, p. 2269-2307.

Tampropaporn, B., Phosri, C., Pisutpaisal, N., Thamvithayakorn, P., Chotelersak, K., Sarp, S. and Suwannasai, N. 2022. High potential decolorization of textile dyes from wastewater by manganese peroxidase production of newly immobilized *Trametes hirsute* PW17-44 and FTIR analysis. Microorganisms, 10: 992.

Teerapatsakul, C. and Chitradon, L. 2016. Physiological regulation of an alkaline-resistant laccase produced by *Perenniporia tephropora* and efficiency in biotreatment of pulp mill effluent. Mycobiology, 44: 260-268.

Téllez-Téllez, M., Villegas, E., Rodríguez, A., Acosta-Urdapilleta, M.L. and Díaz-Godínez, G. 2016. Mycosphere Essay 11: Fungi of Pycnoporus genus: morphological and molecular identification, worldwide distribution and biotechnological potential. Mycosphere, 7: 1500-1525.

The Bureau of Science and Technology Information Service. 2022. Textile and garment factory in Thailand, January-June 2022. [Online] Available at: https://www.thaitextile.org/th/insign/detail.3147.1.0.html.

Younes, S.B., Mechichi, T. and Sayadi, S. 2006. Purification and characterization of the laccase secreted by the white rot fungus *Perenniporia tephropora* and its role in the decolorization of synthetic dyes. J. Appl. Microbiol., 102: 1033-1042.

Zainith, S., Chowdhary, P., Mani, S. and Mishra, S. 2020. Microbial ligninolytic enzymes and their role in bioremediation. In: Microorganisms for Sustainable Environment and Health. Elsevier, p. 179-203.l

Nature Environment and Pollution Technology
An International Quarterly Scientific Journal

p-ISSN: 0972-6268
(Print copies up to 2016)
e-ISSN: 2395-3454

Vol. 23 | No. 3 | pp. 1735-1742 | 2024

Original Research Paper

https://doi.org/10.46488/NEPT.2024.v23i03.046

Open Access Journal

# Effect of Fly Ash in Pyrolysis of HDPE, LDPE and PP Plastic Waste

**Y. B. Sonawane*†, M. R. Shindikar** and M. Y. Khaladkar*****

*Environmental Studies, Department of Applied Science and Humanities, COEP Technological University, Pune, Maharashtra, India

**Environment and Biology, Department of Applied Science and Humanities, COEP Technological University, Pune, Maharashtra, India

***Department of Chemistry, Government College of Engineering & Research, Avasari Khurd, Pune, Maharashtra, India

†Corresponding Author: Y. B. Sonawane; yogitabs@gmail.com

**Nat. Env. & Poll. Tech.**
**Website: www.neptjournal.com**

*Received:* 28-12-2023
*Revised:* 23-02-2024
*Accepted:* 15-03-2024

**Key Words:**
Catalytic pyrolysis
Fly ash
Petroleum products
Calorific value
GC-MS

## ABSTRACT

Fly ash is generally obtained as a by-product from the combustion of coal and other waste materials. It is used for making bricks, but it has few limitations. The fly ash consists of Silica, Alumina, and other metal oxide components in minor quantities. Fly ash particles are observed in the range of nanometers to micrometers and can act as a catalyst in various reactions. The use of low-cost catalysts in the pyrolysis of thermoplastic waste would achieve a high percentage of low molecular weight fractions in liquid form which increases its applicability in commercial sectors. Hence, there is a need to enhance these fractions to achieve a sustainable approach in the catalytic pyrolysis process. fly ash, being a side product, is very cheap, so its effect on the plastic waste pyrolysis process has been studied. In the present research paper, Physical & chemical characterization of fly ash has been carried out. As fly ash consists of different metal oxides in proportion, its applicability in the process of pyrolysis of HDPE, LDPE, and PP waste has been studied. The different weight percent of fly ash (i.e., 5, 10, 15, 20) have been tried in all pyrolysis experiments. It has been observed that 5 wt % fly ash is effective for enhancing the yield of liquid fuel as compared to that without a catalyst. Liquid fuel obtained from catalytic pyrolysis of HDPE, LDPE, and PP waste with Fly ash consists of a high percent of low molecular weight fractions as compared to that of liquid fuel without catalyst, which has been concluded by calorific values & GC-MS result.

## INTRODUCTION

Fly ash is generally obtained as a by-product from the combustion of coal and other waste materials. In recent years, intensive research has been on fly ash due to the increasing demand for recycling industrial by-products to improve sustainability in manufacturing and infrastructure (Sarker et al. 2013, Hong et al. 2023, Joseph et al. 2020, Sonawane et al. 2017, 2015). Fly ash is generally used in making bricks and in construction activities with cement. It is also used as a fertilizer in agriculture. It consists of Silica and alumina as major components and some minor components like ferrous, calcium, etc. It has been used as a catalyst for biodiesel production by some researchers (Omotola et al. 2010), and fly ash-derived zeolite has also been used as a catalyst in catalytic cracking of crude oil from refineries (Ojha & Pradhan 2001) and for the production of carbon nanotubes (Oskar et al. 2009). Production of fatty acid methyl esters (FAME) from waste frying oil (WFO) was studied using fly ash as a heterogeneous catalyst by researchers (Robinson Muñoz et al. 2020). Researchers also focused on synthesizing modified catalysts by using fly ash with other catalysts (Zhang et al. 2020). In the present research, after the chemical characterization of fly ash, its effect as a catalyst on enhancing the yield in the pyrolysis of thermoplastic waste, including HDPE, LDPE, and PP, has been studied.

## MATERIALS AND METHODS

The pyrolysis glass reactor has been designed and developed for treating plastic waste of 100 grams. The reactor consisted heating mantle of high quality insulation jacket and temperature controlling system with an energy regulator, Borosilicate glass reactor, Thermocouple and Temperature indicator (Nickel-Chromium), Condenser and Collection flask, etc.

Pyrolysis experiments on HDPE, LDPE and PP waste were carried out separately without catalyst and by using Fly ash as a catalyst. 100 grams of waste material was used for each experiment. The catalyst-to-feed ratios (1:5, 1:10,

1:20), i.e., 5, 10, 15 and 20 wt % of Fly ash were used. Experiments were carried out at a temperature range of 400-470$^{o}$C, depending on the type of plastic waste material. The Plastic waste material (100g) was fed into a reactor flask of 500 mL capacity and attached with a connector consisting of a nitrogen inlet, thermocouple, temperature indicator, and outlet connected to the condenser. The mouth of the flask was then tightened with its lid and sealed with the help of Teflon tape to avoid any leakage of vapors.

Firstly, the nitrogen gas with a flow rate of 50 mL.min$^{-1}$ for 2-3 min and with pressure slightly above atm. The pressure was purged into the flask to make an inert atmosphere and then started heating waste plastic. Heating was supplied with the rise of temperature 20$^{o}$C.min$^{-1}$. The melting temperature of each type of plastic was recorded. After melting and boiling of plastic waste, condensation of generated vapors produced liquid fuel in major quantities with wax and gases in minor quantities. The process required around 20-30 min to obtain liquid fuel in the collection flask and 1-2.5 hrs to complete the reaction. The quantity of liquid fuel was measured in milliliters, and wax was measured in grams. The generated gas was measured by using material balance. The required amount of energy was recorded with the help of an energy meter. All performed experiments were replicated twice to obtain statistically significant results.

## RESULTS AND DISCUSSION

### Characterization of Fly Ash

Fly ash (FA) (on dry basis) generally consists of $SiO_2$ 50.91%, $Al_2O_3$ 30.91%, $Na_2O$ 0.10%, CaO 6.2%, $Fe_2O_3$ 3.46%, MgO 1.48%, $TiO_2$ 1.65%, MnO 0.02%, $K_2O$ 0.60%, $P_2O_5$ 0.56%. The average $SiO_2/Al_2O_3$ ratio of Fly ash was found to be 1.65 (Omotola et al. 2010). Grey-colored, amorphous fly ash was obtained for the study from the cement industry located near Pune and was ground to a fine powder before use.

Characterization of Fly ash has been done for SEM, XRD, XRF, and TGA-DTA to know the suitability as a catalyst for enhancing the yield and quality of liquid fuel in the pyrolysis process.

Scanning electron microscopic images of raw Fly ash at different magnifications of 5 and 40 KX are shown in Fig. 1. From the SEM image, the particle size of Fly ash was found to be 1.5 µm to 5 µm. Given Fly ash sample possesses a glossy and smooth surface, but due to spherical particles, the available surface area for the reaction was observed more.

From energy dispersion spectroscopy, it was observed that Fly ash consisted of $SiO_2$ $Al_2O_3$, CaO, $Fe_2O_3$, MgO, $TiO_2$, MnO, $K_2O$, $P_2O_5$, etc.

### X-Ray Diffraction Study of Fly Ash

The XRD graph of Fly ash is shown in Fig. 2. Graph is plotted by considering 2Θ values on the X-axis and intensity on the Y-axis.

Fly ash has a major peak at 2Θ value of 26 with smaller peaks at 22.02, 30.94, 41.12, 50.52, 52.33, 61.23, 69.01 etc. The structure of Fly ash was observed to be monoclinic from 2Θ values and JCPDS reference. XRD pattern of Fly ash showed multiple numbers of small peaks, which represent the amorphous nature of Fly ash.

### X-Ray Fluorescence Study of Fly Ash

From the XRF spectrum, the composition of Fly ash was found to be 66.50% $SiO_2$, 28.54% $Al_2O_3$, 1.64% CaO, 0.56% MgO, 4.081% $Fe_2O_3$, 2.36% $TiO_2$, 1.16% $K_2O$ and 0.504% $P_2O_5$. The percentage of silica was found to be the highest. Alumina and iron were also found in

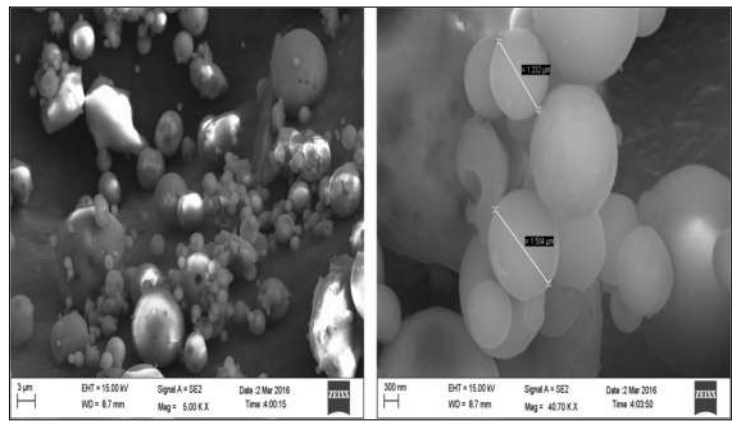

Fig. 1: SEM images of fly ash at different magnifications.

significant concentration with minor concentration of other elements.

### Thermo Gravimetric Study of Fly Ash

A graphical representation of the TG and DTA of fly ash is shown in Fig. 3. The x-axis represents temperature in degrees Celsius, the Y-axis on the left side gives percent weight loss, and the Y-axis on the right side gives potential difference values. The black line represents the TG graph, and the blue line represents the DTA graph. Thermo gravimetric and differential thermal analysis study of Fly ash was done at the temperature range of 30 to 800°C.

From the graph, weight loss of Fly ash was observed around 0.9% at 450°C, which shows the thermal stability of fly ash at higher temperatures in pyrolysis.

### The Percent Yield of Liquid Fuel

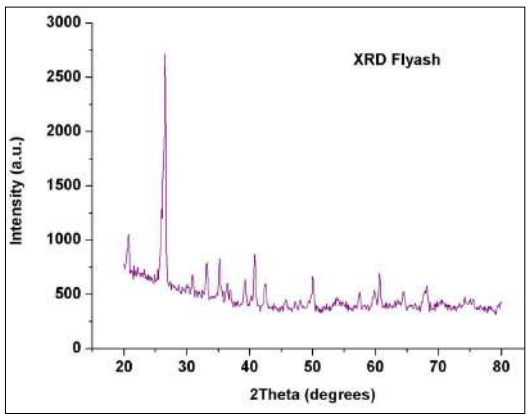


Fig. 2: XRD pattern of fly ash.

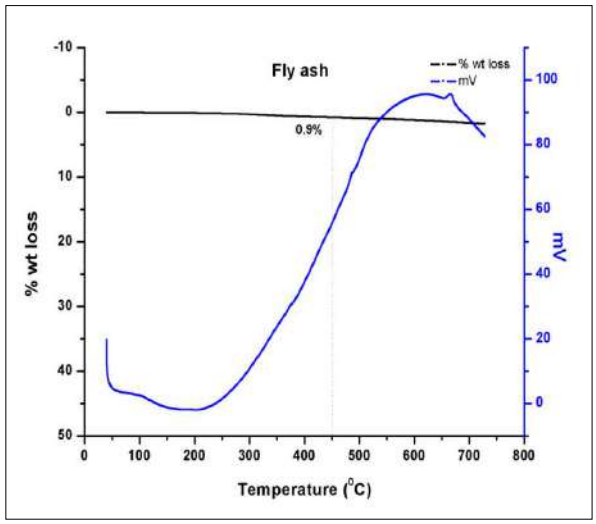


Fig. 3: TG-DTA graph of Fly ash.

The effect of Fly ash was studied in pyrolysis of HDPE, LDPE, PP, and mixed waste by conducting pyrolysis experiments at 450°C by using 5, 10 and 20% fly ash, and the yield of liquid fuel obtained was compared with that without catalyst, and displayed in Fig. 4.

The use of 5% fly ash enhanced the yield of liquid fuel in HDPE, LDPE while the use of 10% Fly ash enhanced the yield of liquid fuel for PP waste. The use of 20% fly ash reduced the yield of liquid fuel for all types of plastic wastes used as compared to that without catalysts.

### FTIR Analysis of Liquid Fuel Obtained in Plastic Waste Pyrolysis Without Catalyst and By Using Fly ash Catalyst

Fourier Transform Infrared Spectroscopic (FTIR) analyses of liquid fuel samples obtained from HDPE, LDPE, PP, and mixed waste without catalysts and with fly ash were done to know functional groups or hydrocarbons and to detect the type of vibration in liquid fuel. Wave number range, type of vibrations, name of functional group observed in different liquid fuel samples

Fig. 5 represents FTIR spectra for liquid fuel samples obtained from pyrolysis of HDPE, LDPE, PP, and mixed waste without a catalyst and by using Fly ash as a catalyst. C-H bending vibrations were observed at wave numbers 721, 991, and 1080 $cm^{-1,}$ which proved the presence of alkenes, while peaks with wave numbers 1373 and 1462 $cm^{-1}$ indicated C-H scissoring and bending vibrations which represent the presence of alkanes. C=C stretching was observed at wave number 1648 $cm^{-1,}$ which showed the presence of alkenes. The peak with carbonyl groups was found at 1736 $cm^{-1}$ in liquid fuel samples obtained from pyrolysis of HDPE waste with fly ash.

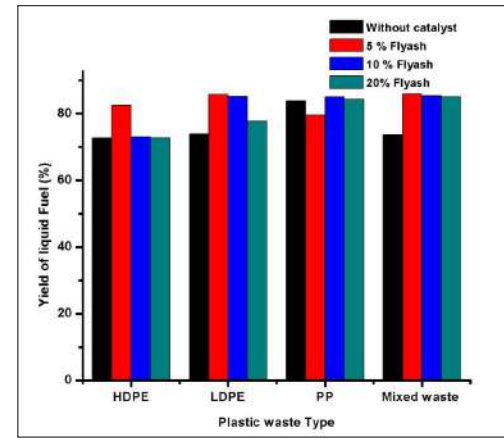


Fig. 4: Effect of fly ash on yield of liquid fuel in pyrolysis of plastic waste.

**GC-MS Results of Liquid Fuel Obtained from Pyrolysis of HDPE Waste Without Catalyst and By Using Fly Ash**

Fig. 6 & 7 show a gas chromatograph and mass spectrograph of liquid fuel obtained by using HDPE waste without a catalyst and by using a fly ash catalyst.

Liquid fuel obtained from HDPE waste consisted of hydrocarbons in the range of C-10 to C-27. From the GC-MS data, it was observed that the concentration of alcohol named 2 hexyl, 1-decanol was highest in liquid fuel obtained from HDPE waste as the total area percent of it was found to be maximum (44.07%). Low molecular weight fractions like Decene, Hexadecane, and Nonadecane were found in the sample but in lower concentrations. The area percent for Heptacosane was observed at about (20.56%) which represented a high percentage of it in the liquid fuel sample. As Heptacosane represents a high molecular weight fraction, its presence was found to be undesirable.

Gas chromatography of Pyrofuel (liquid fuel obtained from plastic waste pyrolysis) obtained with Fly ash consisted of C-9 to C-27 hydrocarbon fractions. The presence of low molecular weight alkenes and alcohols was found in significant amounts. The area percent of peaks for C-8 to C-15 fractions was observed to be around 78%, while the area percent for C-16 to C-19 fractions was around 15%. The peak area percent of Tetradecene was found highest i.e., 39%. A negligible amount of high molecular weight fraction of Heptacosane was observed in the fuel sample.

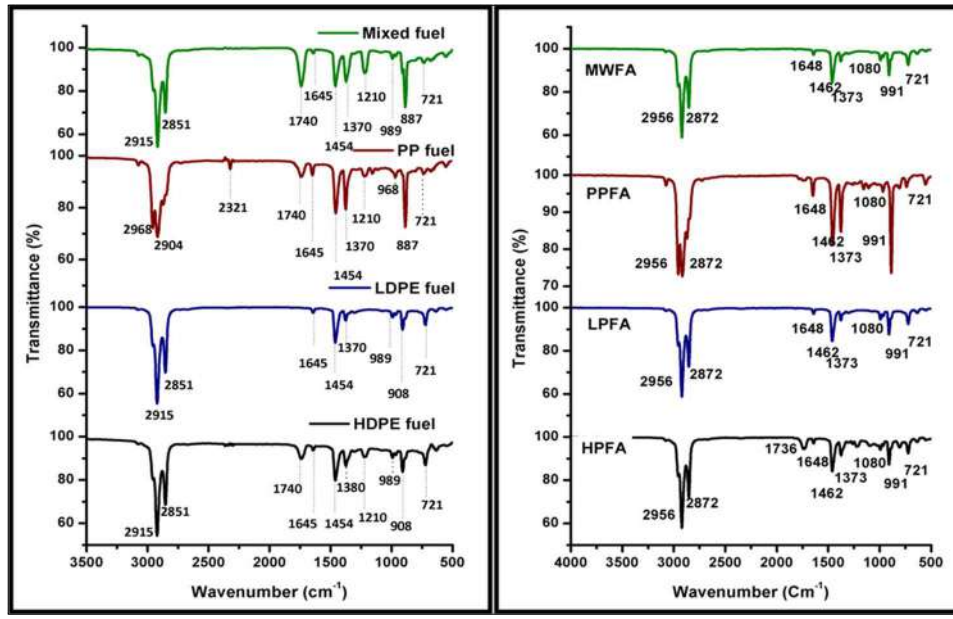


Fig. 5 (a & b): FTIR spectra for liquid fuel obtained without catalyst (a) and by using fly ash (b) in pyrolysis of HDPE, LDPE, PP, and mixed waste.

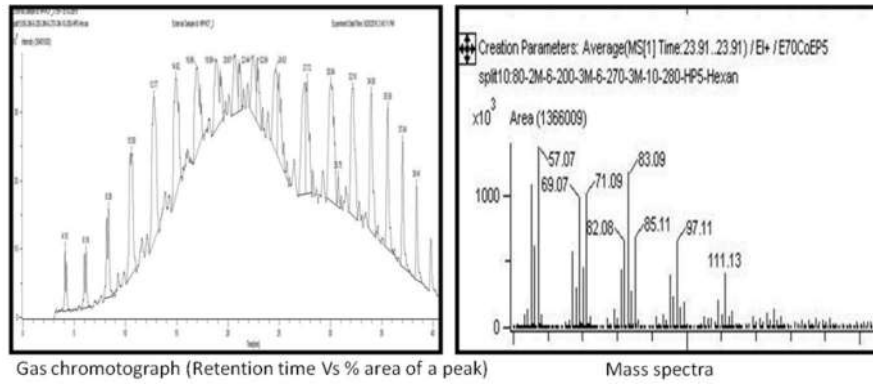


Fig. 6 (a & b): Gas chromatograph and mass spectrograph of liquid fuel sample-HPWC.

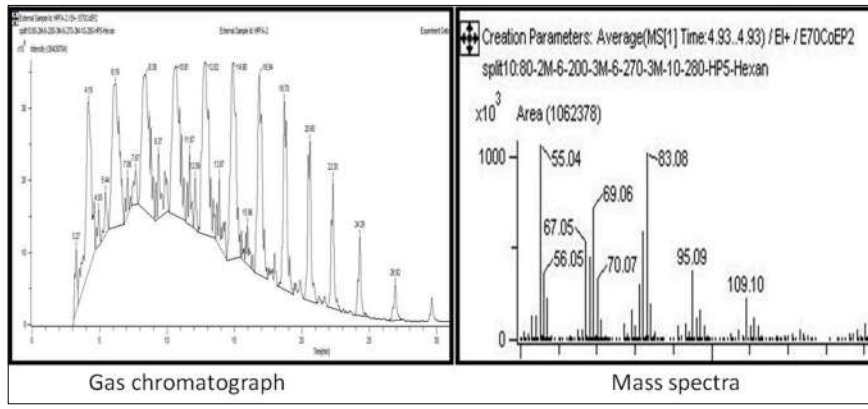


Fig. 7 (a & b): Gas chromatograph and mass spectrograph of liquid fuel sample-HPFA.

**GC-MS Results of Liquid Fuel Obtained From Pyrolysis of LDPE Waste Without Catalyst & By Using Fly Ash**

Fig. 8a & b show the gas chromatograph and mass spectra of liquid fuel obtained by using LDPE waste without a catalyst. From the chemical composition of liquid fuel obtained from pyrolysis of LDPE waste without a catalyst, it was observed that liquid fuel obtained from LDPE waste has hydrocarbons in the range of C-7 to C-44.

The area percent for the C-7 to C-15 hydrocarbons was observed to be around 55.3%. No significant amounts

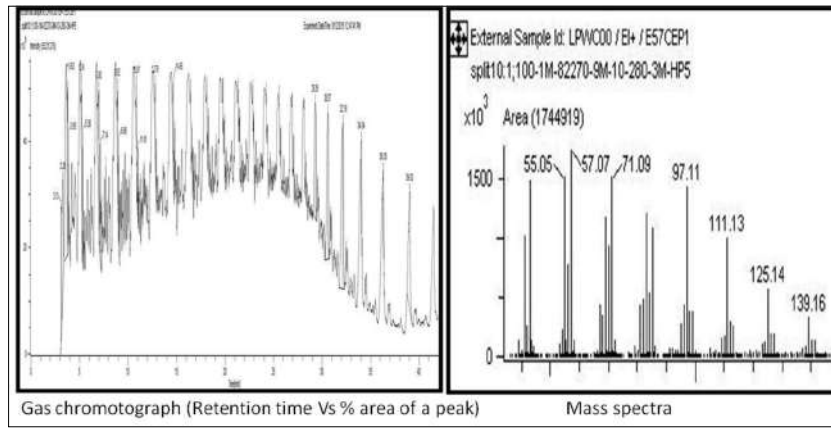


Fig. 8 (a & b): Gas chromatograph of liquid fuel sample-LPWC mass spectrograph of liquid fuel sample-LPWC.

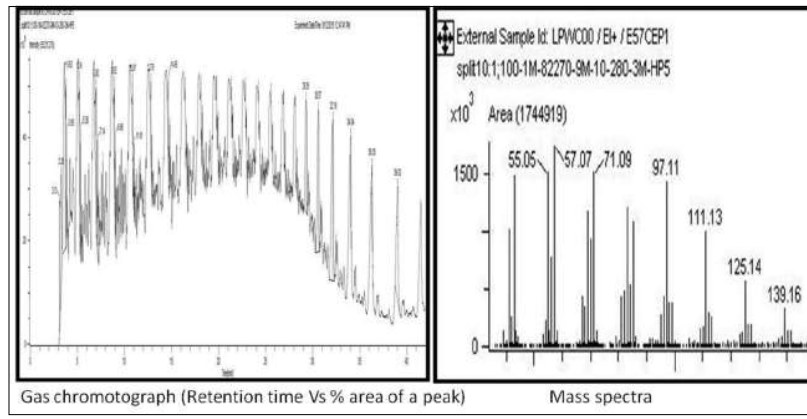


Fig. 9 (a & b): Gas chromatograph of liquid fuel sample-LPFA, mass spectrograph of liquid fuel sample-LPFA.

of hydrocarbons were observed from C-15 to C-25 in the liquid fuel. However, the presence of high molecular weight fractions like Nonacosane and Tetratetracontane with an area of peak of around 22% was found undesirable.

Fig. 9a and 9b show GC and mass spectrograph of liquid fuel obtained by using LDPE waste with fly ash catalyst. It was observed that liquid fuel obtained from LDPE waste with Fly ash has hydrocarbons in the range of C-9 to C-19. Various low molecular weight alkenes, Undecene, Dodecene, Tridecene, Tetradecene, Pentadecene, and alkanes butyl -Cyclopentane and Undecane were observed. Overall results showed high concentrations of low molecular weight hydrocarbons ranging from C-11 to C-15. The alcohol fraction Z-10-Pentadecenol was observed with a peak area of around 3.67%.

**GC-MS Results of Liquid Fuel Obtained from Pyrolysis of PP Waste Without Catalyst and by Using Fly Ash**

Fig. 10 shows the gas chromatograph and mass spectra of liquid fuel obtained by using PP waste without a catalyst.

GC-MS results obtained for liquid fuel with PP waste showed the presence of hydrocarbons from C-7 to C-29. Low molecular weight hydrocarbon fractions like 3-methyl-2 Hexene, Nonane, and 3-ethyl Heptane were observed. The total area of peaks in the hydrocarbon range C-7 to C-15 was found to be around 50.6%. The peak area for alcohol fractions, tridecanol and hexadecanol, was observed to be around 10.7%. The heavy oil fractions, nonacosane and heptacosane were also observed with a high peak area, i.e., 34.35%.

Fig. 11a and 11b show the GC and mass spectrograph of liquid fuel obtained by using PP waste with a fly ash catalyst. From the results, it was observed that fuel consisted of C-10 to C-22 hydrocarbon fractions. Significant amounts of various alcohol fractions like 2,7-dimethyl Octanol, 2-isopropyl, 5-methyl 1-Heptanol, 2-butyl 1-Octanol, 1-cyclopropanol, 2 hexyls, 1 Octanol, 2 hexyls, 1-Decanol,

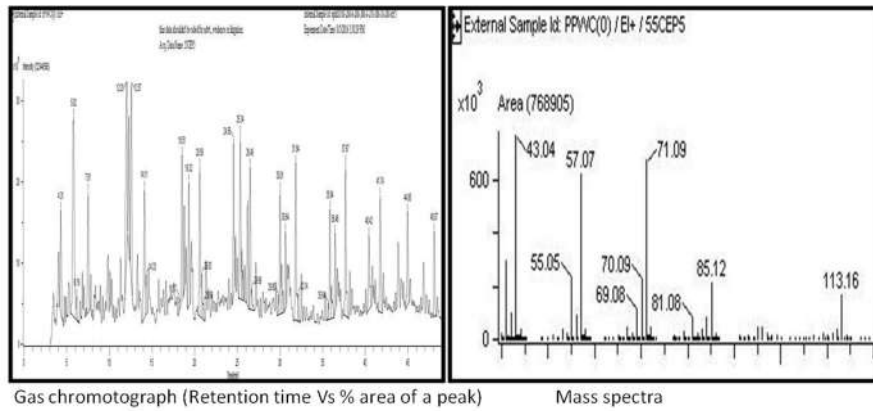


Fig. 10 (a & b): gas chromatograph and mass spectrograph of liquid fuel sample-PPWC.

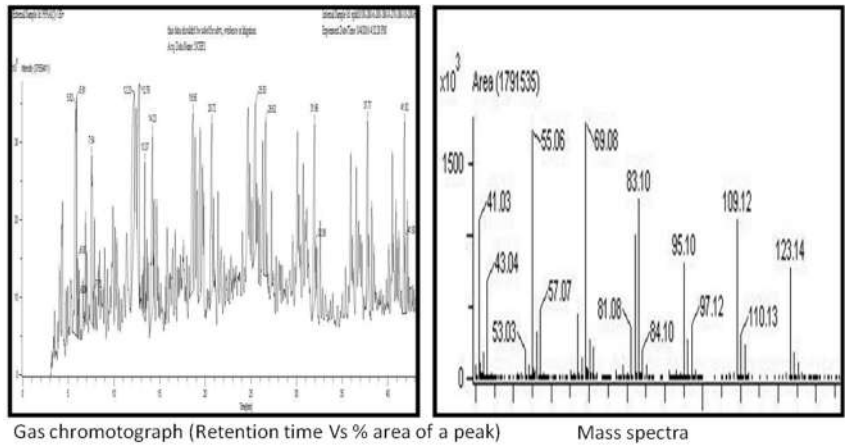


Fig. 11 (a & b): Gas chromatograph and Mass spectrograph of liquid fuel sample-PPFA.

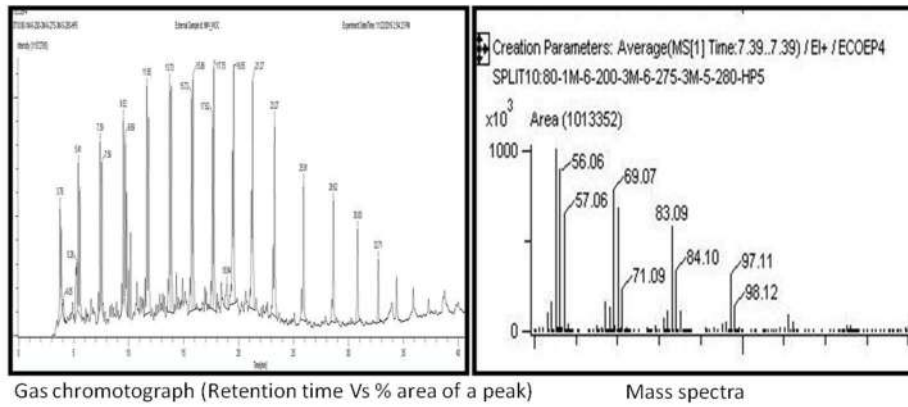


Fig. 12 (a & b): Gas chromatograph of liquid fuel sample-MWWC & Mass spectrograph of liquid fuel sample-MWWC.

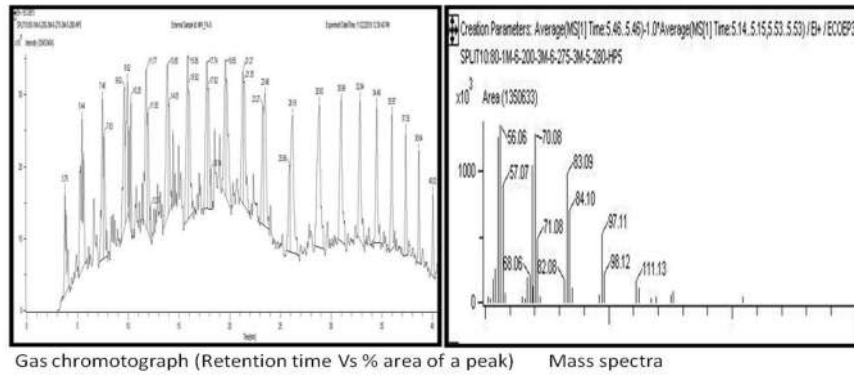


Fig. 13 (a & b): Gas chromatograph of liquid fuel sample-MWFA and mass spectrograph of liquid fuel sample-MWFA.

etc. were observed in the fuel. The area percent of alcohol peaks was found to be around 42%. Alkane fractions like Undecane, Dodecane, tetra isopropyl Cyclohexane, and alkenes like- Undecene and Dodecene were observed in the GC-MS graph. The presence of heavy oil fractions like Cyclotetradecane and 1-Docosene were also observed, with peak areas around 11.5% and 6.23%, respectively.

### GC-MS Results of Liquid Fuel Obtained From Pyrolysis of Mixed Waste Without Catalyst & By Using Fly Ash

Fig. 12a and b show the gas chromatograph and mass spectra of liquid fuel obtained by using mixed waste without catalyst and with fly ash catalyst.

From the above data, it was found that liquid fuel obtained from the mixture of HDPE, LDPE, and PP waste without catalysts has hydrocarbons in the range of C-10 to C-27. Low molecular weight fractions like Decene,1-heptyl, 2 methyl cyclopropane, tridecene, tetradecane, and hexadecane were observed and found desirable. The highest area percent (i.e., 30.56%) was observed for 1-nonadecane fraction ($C_{19}H_{40}$), which showed that the concentration of 1-nonadecane is maximum in liquid fuel obtained from the mixture of HDPE, LDPE, and PP waste without catalyst. High molecular weight fractions like docosene and heptacosane were also observed in less concentration, but their presence was found to be undesirable in terms of quality.

Fig. 13b shows a mass spectrograph of liquid fuel obtained by using mixed waste with a fly ash catalyst. It was observed that fuel consisted of hydrocarbons ranging from C-11 to C-21. The presence of Hexadecane with a peak area of around 34% showed the maximum diesel component in the liquid fuel. The presence of high concentrations of low molecular weight alkanes, alkenes, and alcohols in the fuel was observed.

### Calorific Values of Liquid Fuel Obtained From Pyrolysis of Plastic Waste by Using Fly Ash

Table 1. displays calorific values of liquid fuel obtained from pyrolysis of plastic waste with 5, 10, and 20% fly ash.

By using 5% fly ash in HDPE and LDPE, PP, and mixed waste pyrolysis, the calorific values of liquid fuel were significantly enhanced. In comparison, the use of 10 and

Table 1: Calorific values of liquid fuel obtained from plastic waste by using 5, 10, and 20 % fly ash.

| Liquid fuel from Plastic waste | Calorific values [KJ.Kg$^{-1}$] | | | |
|---|---|---|---|---|
| | Without catalyst | 5 % FA | 10 % FA | 20 % FA |
| Liquid fuel from HDPE waste | 40614 | 49622 | 43034 | 43897 |
| Liquid fuel from LDPE waste | 41220 | 47858 | 42587 | 44811 |
| Liquid fuel from PP waste | 42200 | 49392 | 41675 | 44027 |
| Liquid fuel from Mixed waste | 44558 | 47578 | 42157 | 39857 |

20% fly ash reduced calorific values of liquid fuel for all plastic wastes used as compared to that without catalysts. The highest increase in calorific value was observed for liquid fuel obtained from HDPE waste with 5% Fly ash.

## CONCLUSION

After a comparative study of liquid fuel yield and fuel characteristics without a catalyst and by using a fly ash catalyst, it was found that the use of fly ash enhanced the yield of liquid fuel in pyrolysis of HDPE, PP, and mixed plastic waste. The use of 5% fly ash showed enhanced calorific values of liquid fuel for HDPE, LDPE, PP, and mixed waste as compared to that of without catalysts due to the presence of low molecular weight fractions and alcohol in them. So, from all results obtained by using fly ash as a catalyst in the pyrolysis, it was concluded that fly ash enhanced the yield and low molecular weight fractions in liquid fuel in the pyrolysis of all plastic wastes used. GC-MS results and calorific values of the liquid fuel samples obtained in pyrolysis of HDPE, LDPE and PP waste give justification for improvement in the quality of liquid fuel. From the surface morphology, XRD, chemical composition, and thermal analysis of fly ash, it is proved that the Silica alumina ratio, surface morphology and nanoparticle size, and thermal stability of Fly ash can prove it as a better and cost-effective catalyst in catalytic pyrolysis of thermoplastic waste.

## ACKNOWLEDGEMENT

The authors would like to thank the Vice-Chancellor, Directors, Deans, and HODs of COEP Technological University, Pune, for their constant support and motivation during the research work, the Department of Metallurgy for SEM analysis, the Department of Physics, SAIF, SPPU for FTIR and XRD analysis and SAIF, IIT Bombay for GC-MS analysis of liquid fuel samples.

## REFERENCES

Hong, H. T., Nguyen, S. F. A., Natarajan, R., Yusuf, M., Sharma, A., Arunkumar, P., Balakrishnan, D. and Tran, D. V. N. 2023. Emerging waste-to-wealth applications of fly ash for environmental remediation: A review. Environ. Res., 227: 115800. ISSN 0013-9351.

Joseph, I. V., Lubomira, T. and Aidan, M. D. 2020. Simultaneous removal of Cd(II), Co(II), Cu(II), Pb(II), and Zn(II) ions from aqueous solutions via adsorption on FAU-type zeolites prepared from coal fly ash. J. Environ. Chem. Eng., 8(4): 103895.

Ojha, K. and Pradhan, N. C. 2001. Treated fly ash: A potential catalyst for catalytic cracking. Indian J. Eng. Mater. Sci., 8: 100-103.

Omotola, K., Petrik, L., Onaneye, B., Leslie, M., Musyoka, N., Bamikole, A. and Amigun, F., Ameer. 2010. Use of coal fly ash as a catalyst in the production of biodiesel. Pet. Coal, 52.

Oscar, M. D., Kieran, J. M. and Andrew, T. H. 2009. Synthesis of multi-walled carbon nanotubes on fly ash-derived catalysts. Environ. Sci. Technol., 43(20): 7889-7894. DOI: 10.1021/es901779c

Robinson Muñoz, A., González, F., Valdebenito, G., Ciudad, G., Navia, R., Pecchi, G. and Azócar, L. 2020. Fly ash is a new versatile acid-base catalyst for biodiesel production. Renew. Energy, 162: 1931-1939.

Sarker, P. B., Rashedul, R. and Karamchand. 2013. Fracture behavior of heat-cured fly ash-based geopolymer concrete. Mater. Des., 44: 580-586. DOI: 10.1016/j.matdes.2012.08.005.

Sonawane, Y. B., Khaladkar, M. Y. and Shindikar, M. R. 2017. High calorific value fuel from household plastic waste by catalytic pyrolysis. Nat. Environ. Pollut. Technol., 16(3): 879.

Sonawane, Y. B., Shindikar, M. R. and Khaladkar, M. Y. 2015. Use of catalyst in pyrolysis of polypropylene waste into liquid fuel. Int. Res. J. Environ. Sci., 4(7): 24-28.

Zhang, L., Qi, L., Shu, H., Jia, Y., Zhang, L., Yang, C., Bai, F. and Sun, Z. 2020. Formation of fly ash catalysts and selection of a matrix binder and its application in denitration. ACS Omega, 5(49): 31567-31574.

Nature Environment and Pollution Technology
An International Quarterly Scientific Journal

p-ISSN: 0972-6268
(Print copies up to 2016)
e-ISSN: 2395-3454

Vol. 23 | No. 3 | pp. 1743-1749 | 2024

Original Research Paper

https://doi.org/10.46488/NEPT.2024.v23i03.047

Open Access Journal

# Exploring the Adsorption Efficiency of Local Apricot Seed Shell as a Sustainable Sorbent for Nitrate Ion

**Mohd Ishaq*†, R. C. Chhipa*, Anupama Sharma*, Gh. Ali** and Riyaz-ul Hussain****

*Department of Chemistry, Suresh Gayan Vihar University, Jaipur, Rajasthan, India

**Department of Chemistry, Kargil Campus, University of Ladakh, India

†Corresponding author: Mohd Ishaq; isackar440@gmail.com

**Nat. Env. & Poll. Tech.**
**Website: www.neptjournal.com**

*Received:* 27-12-2023
*Revised:* 10-02-2024
*Accepted:* 12-02-2024

**Key Words:**
Agro-waste
Biochar
Sorbent
Apricot
Activated carbon

## ABSTRACT

Locally available apricot seed shell as agro-waste was used for the preparation of adsorbents. The biochar was prepared at 370°C via pyrolysis and 80 mesh particle sizes were modified by 1N HCl. Nitrate adsorption and effect of co-ions from aqueous solution were studied under batch model using apricot seed shell powder (ASSP), apricot seed shell biochar (ASSB), and activated apricot seed shell biochar (AASSB). FTIR and $pH_{PZC}$ measurements were used to characterize the adsorbents. Based on the experimental findings, the optimum conditions follow pH 2, 0.3g dosage, initial concentration of 50 $mg.L^{-1}$, and contact time of 90 min. The three forms of adsorbent exhibited good adsorption for nitrate. However, the maximum percentage removal of nitrate ions from the aqueous solution followed the order AASSB>ASSB>ASSP. The adsorption kinetic of nitrate ion was best fitted by pseudo $2^{nd}$ order, and the parameters of adsorption isotherms elucidated favorable and improved sorption. This agro-waste could be used to develop sustainable adsorbents in water and wastewater treatment methods and has great potential to replace commercially available sorbents.

## INTRODUCTION

Worldwide, nitrate is a common pollutant of surface and groundwater. Water nitrate pollution is a serious problem, especially in arid and semi-arid areas (Shukla & Saxena 2020). Nitrate is a polyatomic ion, stable, and highly soluble in water. It is frequently caused by runoff from farms, poorly maintained residential and commercial sewage systems, massive trash dumps, atmospheric fixation, and lightning (Shukla & Saxena 2020, Zhou 2015). In 1945, nitrate toxicity was identified for the first time (Zhou 2015). Nitrate poisoning in humans can occur through two different routes, including oral exposure and cutaneous contact. However, oral exposure is more common than dermal contact in the general population (Rahman et al. 2021). World Health Organization (WHO) has set a recommended threshold value of 50 $mg.L^{-1}$ for nitrate in drinking water, considering the health hazards, likely the possibility of methemoglobinemia or "blue baby syndrome" in young children linked to elevated levels of nitrate in the water (Shukla & Saxena 2020c, Zhou 2015c). This disorder arises from the body's conversion of nitrates found in water to nitrites, which can disrupt hemoglobin's ability to deliver oxygen throughout the blood. Thus, in order to address this issue, appropriate management and mitigation techniques are essential. There are numerous ways and strategies available to remove different types of contaminants from water (Dai et al. 2018, Khatoon & Rai 2016, Sardar et al. 2021). The adsorption approach is regarded as the most effective treatment method owing to its affordability, simplicity, high absorption capabilities, and diversity among all other techniques (Dai et al. 2018, Das et al. 2020, Mitra et al. 2019).

A large volume of agricultural waste is produced during harvesting, post-harvesting, and processing, which can be converted into various useful products (Tiwari & Pal 2021). The agricultural biomasses, such as the shell or peel from fruits and vegetables, sugarcane bagasse, rice husks, peanut shells, jackfruit, chestnut shells, coconuts, and hazelnuts, were used to remove a range of contaminants (Khatoon & Rai 2016). According to published research works, the underlying chemical structure and composition of raw agricultural biomasses have been shown to have a somewhat lower capacity for the adsorption of pollutants (Liu et al. 2022). As a result, surface alterations were suggested for improved adsorption capacities. Nitrate was reduced by using powdered banana peel (Reddy et al. 2015). While banana peel biochar was used for the reduction of nitrate (Zoungranan et al. 2021). Nitrate was eliminated using barley straw (Ansari et al. 2017). Biochar is a promising material

Fig. 1: Systematic presentation of biochar preparation.

for treating water. It is made by pyrolyzing, gasifying, and hydrothermally carbonizing at high temperatures (between 300-900°C) in an inert atmosphere (Janković et al. 2019).

Worldwide, approximately 3.72 million tonnes of apricots are produced. The main producers of apricots are Turkey, Uzbekistan, Iran, Italy, and Algeria. Ladakh is the largest apricot-producing state in India. Himachal Pradesh and Jammu and Kashmir also produce it. Every year, Ladakh produces 15000 metric tons of apricots. According to the Horticulture Department, Kargil UT Ladakh, an estimated 1655 hectares of land is under apricot production in district Kargil of UT Ladakh, with an annual production of 11,067.46 Metric tons. During the winter, the seed shell is typically burned in the local heating system to warm the rooms in this region. The shell is hard, and agro-waste is produced during the kernel separation process.

Moreover, a substantial amount of apricot seed shells is produced as agro-waste during the processing of fruits worldwide, which are disposed of either as agro-waste or used to improve soil fertility (Hashem et al. 2022, Challab et al. 2020, Zhang et al. 2022a). The different forms of apricot seed shell including powder, biochar, and activated carbons, were utilized by different researchers for the removal of pollutants. The powder form of apricot seed shell was used to remove acid blue 193 dye (Hashem et al. 2022), activated carbon was used for the removal of metals like $Mn^{2+}$ and $Zn^{2+}$, and similarly, biochar of this material was used for the removal of pesticides like atrazine (Zhang et al. 2022b). In this work, biochar and activated biochar from locally available apricot seed shells were prepared, and nitrate sorption behavior was assessed.

## MATERIALS AND METHODS

### Chemicals and Materials

Apricot seed shell was collected from the oil processing unit at Hardas, Kargil of UT Ladakh. All the chemicals of analytical grade, such as potassium nitrate ($KNO_3$), hydrochloric acid (HCl), sodium hydroxide (NaOH), and other reagents were used. Deionized water was used for preparing the solution, and synthetic water was used.

### Preparation of Adsorbents and Synthetic Water

Apricot seed shells were washed with water and deionized water to remove dirt. The dry seed shells were then crushed to a fine powder and sieved using 80 mesh sieves. The apricot seed shell powder (ASSP) was then preserved in an airtight container for further application. 300g of crushed apricot seed shells were placed in the electric furnace reactor and heated for 5 h with a continuous flow of nitrogen gas at temperatures of 300°C, 330°C, 350°C, and 370°C. The resulting apricot seed shell biochar (ASSB) is then passed through an 80-mesh sieve. The biochar was then washed with deionized water until neutral pH was reached and then left to dry at 50°C. Fig. 1 systematically shows the biochar preparation process.

The impact of temperature on the biochar yield during pyrolysis is summarized in Table 1. Synthetic water of 100 ppm, 70 ppm, 50 ppm, 30 ppm, and 10 ppm was prepared by dissolving potassium nitrate ($KNO_3$) in deionized water. Synthetic water containing nitrate and other ions like fluoride, chloride, Phosphate, and sulfate was also prepared to investigate the interfering ions on the adsorption efficiency of nitrate ions.

**Modification of adsorbent:** The apricot seed shell biochar (ASSB) was modified by using a 1N HCl solution. The 10g of ASSB was soaked in 1 N HCl solution for 5 h and then separated the biochar. The biochar was washed with water till the pH of the filtrate became 7. The biochar was allowed to dry in the oven at 60°C, and acid-modified apricot seed shell biochar (AMASSB) was preserved for further use.

**Characterization of biochar:** The surface functional groups and surface charge of ASSP, ASSB, and AASSB were investigated by using a Fourier transform infrared (FTIR) spectrometer and zero point charge (pHpzc).

Table 1: Effect of working temperature on yield of Biochar.

| Temperature [°C] | Yield [g] |
|---|---|
| 330 | 210.14 |
| 330 | 222.67 |
| 350 | 258.64 |
| 370 | 209.337 |

**Determination of pH at zero point ($pH_{pzc}$):** The $pH_{pzc}$ is the pH at which the net surface charge of a given sorbent is zero. It is an important parameter to determine the extent of uptake capacity of charged ions by the sorbent. The pH of the solution greater than $pH_{zpc}$ favors the adsorption of cationic ions, while pH less than $pH_{pzc}$ favors the adsorption of anionic ions (Hashem et al. 2022). Ten samples of varying pH (2-10) were prepared by using 0.01 M NaCl as a base electrolyte in a volumetric flask, and the pH of the solution was adjusted by using 0.1N HCl and 0.1N NaOH solution. 1g of the biochar is added in 50 mL of each flask and kept in the shaker for 6h and recorded pH using a pH meter as $pH_{final}$. A plot of change in pH ($pH_{final}$- $pH_{initial}$) against $pH_{initial}$ was generated. The $pH_{zpc}$ of the adsorbents was recorded where ΔpH was zero.

**Batch adsorption analysis:** A stock solution of 100 ppm nitrate solution was prepared and diluted to form 70 ppm, 50 ppm, 30 ppm, and 10 ppm nitrate solutions. 10 mL of each solution was taken in a beaker and evaporated to dryness on a hot plate. Added to each 2 mL of phenoldisulphonic acid (PDA) and then added 10mL ammonia solution. A yellow solution was obtained due to rearrangement in the structure of the nitro derivative. Absorbances of the series of solutions were recorded at 410 nm wavelength using a UV-visible spectrophotometer, and the calibration curve between absorbance and concentration was plotted. To investigate the adsorption, 0.3g of biochar was placed in a centrifuge tube, and 50 mL nitrate solution was added. After centrifugation at 200 rpm, the supernatant was taken at the contact time of 10, 30, 50, 70, 90, 120,140, and 160 min. After filtration through Whatman grade 1 filter paper, the same procedures were applied, and determined the concentrations were from the calibration curve.

### Influencing Variables on Adsorption

**Effect of pH:** The effect of solution pH on the adsorption of nitrate was investigated by taking 50 mL of nitrate solution and 0.3g of adsorbents. The pH of the solutions was adjusted to 2, 4, 6, 8, and 10 with 0.1 N solutions of HCl and NaOH. The content of nitrate ion after 90 min of contact time was determined in the supernatant.

**Effect of contact time:** The effect of contact time on the adsorption of nitrate ion on the adsorbents was determined by taking a 50 $mg.L^{-1}$ initial concentration of nitrate at 2 pH by using 0.3 g of adsorbents. The nitrate concentrations were determined at the interval of 10, 30, 50, 70, 90, 120, 140 and 160 min.

**Effect of dosage:** The effect of the dosage of adsorbent was investigated by using 50 $mg.L^{-1}$ of nitrate solution by using dosages of 100, 200, 300, 500, and 700 mg of adsorbents at the contact time of 90 min and 2 pH.

**Effect of initial concentration:** The effect of the initial concentration of nitrate solution on the adsorption was determined by taking 10, 30, 50, 70, and 100 $mg.L^{-1}$ of nitrate solutions by using the dosage of 300 mg.

**Effect of co-ions:** To determine the effect of co-ions on the adsorption of nitrate, 10 $mg.L^{-1}$ of fluoride, chloride, phosphate, and sulphate were used. 10 mL of each co-ion solution was added one by one to the nitrate solutions, and the concentration before and after the addition of co-ion was determined.

### Data Processing

MS Excel was used to calculate the various parameters involved in adsorption kinetics and isotherms. MS Excel 2010 was used to analyze the experimental data and to draw the figures.

**Calculation of adsorption capacity and removal percentage:** The amount of nitrate ion adsorbed ($mg.g^{-1}$) by the sorbents was calculated by using the following formula

$$Qe = (C_i - C_e)\ V/m \quad \ldots(1)$$

$$Qt = (C_i - C_t)\ V/m \quad \ldots(2)$$

The percentage removals of nitrate by the sorbents were calculated by the following formula.

$$\%\ \text{Removal} = (C_i - C_e) / Ci \times 100 \quad \ldots(3)$$

Where $Q_e$ is the adsorption capacity at equilibrium ($mg.g^{-1}$), $Q_t$ is the adsorption capacity at time t. The initial concentration ($C_i$) of adsorbate ($mg.L^{-1}$) and $C_e$ is the concentration after time t. V is the Volume (50 mL), and m is the mass of the adsorbent (g).

**Adsorption kinetics:** The adsorptions of nitrate ion on the sorbents were fitted to pseudo 1st order and pseudo 2nd order kinetic models.

The equation for Pseudo first-order kinetic model:

$$Ln\ (Qe - Qt) = Ln\ Qe - K_1 t \quad \ldots(4)$$

The equation for Pseudo first-order kinetic model:

$$t / Qe = 1 / K_2 Qe^2 + 1 / Qe \quad \ldots(5)$$

Where Qt and Qe are the adsorption capacity at time t and equilibrium, $K_1$ and $K_2$ are the rate constant for pseudo 1st order and pseudo 2nd order models.

**Adsorption isotherm:** The adsorption of nitrate ion onto the various forms of adsorbents of apricot seed shell was fitted to the Langmuir and Freundlich model.

Langmuir model:

$$1 / Qe = 1 / K_L\ Qmax\ .1 / Ce + 1 / Qmax \quad \ldots(6)$$

Freundlich model:

$$Log\ Qe = log\ K_f + 1/n\ log\ Ce \quad \ldots(7)$$

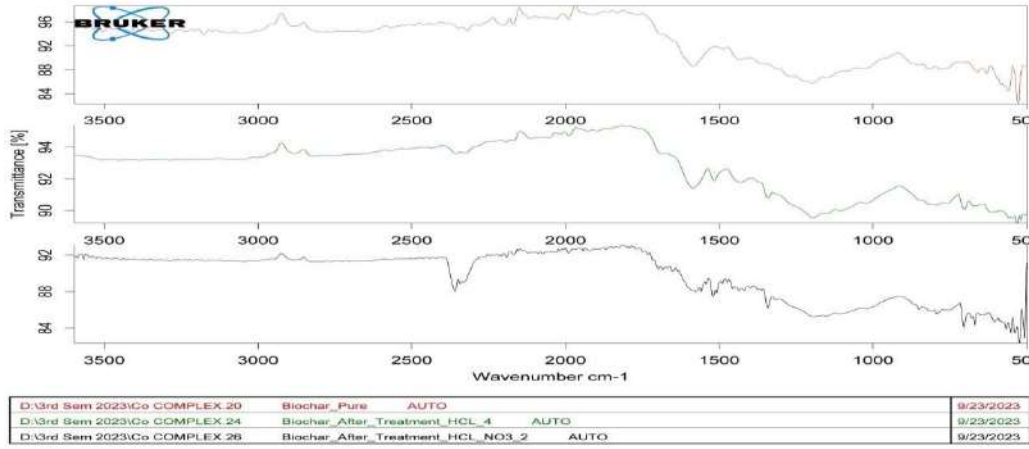


Fig. 2: FTIR Spectra.

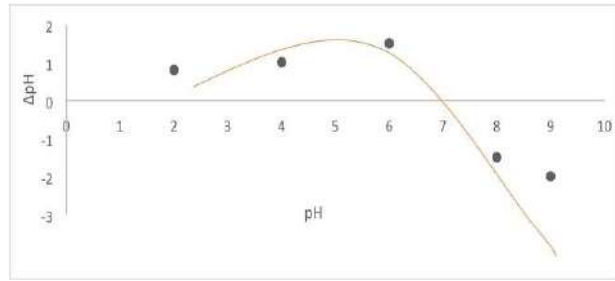


Fig. 3: Point of Zero charge (biochar).

Where Qe is the adsorption capacity of the adsorbent at equilibrium, $K_L$ and $K_f$ are the Langmuir and Freundlich isotherm constant, Qmax is the maximum adsorption capacity ($mg.g^{-1}$), and Ce is the equilibrium concentration ($mg.L^{-1}$).

## RESULTS AND DISCUSSION

### Characterization of Adsorbents

**Fourier transmission infrared spectrometric analysis (FTIR):** The IR spectra of Apricot seed shell biochar (ASSB), acid treated, and nitrate loaded is shown in Fig. 2. A prominent peak around 1650-1700 $cm^{-1}$ indicated the presence of an unsaturated carbonyl (C=O) group. There are no prominent changes in the spectra on treatment with acid. However, loading with nitrate, a shift in the spectra was seen around 2400 $cm^{-1,}$ which is probably due to the O=C=O bond, and a band around 1550 $cm^{-1}$ probably due to the N-O bond. These bands revealed that there is the formation of a bond between the surface functional group and $NO_3$.

**The pH point of zero charge ($pH_{PZC}$) analysis:** The adsorption capacity of the adsorbent depends on the point of zero charge (Hashem et al. 2022). The pH point of zero charge ($pH_{PZC}$) of the adsorbent was determined and found to be around pH 7.9, 7.4, and 8.9 for ASSP, ASSB, and AASSB. The plot is shown in Fig. 3.

### Effect of Variables on Adsorption

**Effect of pH:** Solution pH is an important factor that controls the adsorption process. The powder and biochar form of apricot seed shell showed very low absorption capacity at higher pH (pH > 7). This indicates negatively charged surface functional groups that can cause anionic repulsion. In this study, the effect of solution pH on adsorption capacity was investigated in the range of pH 2-10 using a constant concentration of 50 ppm nitrate and 0.3 g of adsorbents. The experimental results are shown in Fig. 4(a). The results showed that a decrease in solution pH favors the adsorption, and removal percentages become maximizing at a solution with pH 2. At lower pH, the biochar surface gets positively charged, and the interaction between biochar and adsorbent is purely electrostatic (Hashen et al. 2022d, Das & Goud 2020). As the pH increases, the adsorbent surface becomes negatively charged, and the adsorption capacity decreases due to repulsion. Moreover, the pH of the solution does not have much effect on the activated biochar, and even

at neutral pH, modified biochar (AASSB) showed good removal efficiency.

**Effect of contact time and initial adsorbate concentration:** The effect of contact time at a range of 0-160 min and initial concentration of nitrate in the range of 10-100 mg.L$^{-1}$ were investigated, and the results were presented in Fig. 4(c, d). The equilibrium adsorption was attained around a contact time of 90 min. The slope of the initial adsorptions within the range of 90 min is larger, indicating a faster sorption rate than after the 90 min in the initial stage, the nitrate molecules quickly occupying the active sites of the adsorbents. Moreover, the adsorption process is relatively faster in the case of AASSB owing to its protonated surface.

**Effect of adsorbent dosage:** The effect of dosage on the adsorption capacity was investigated by taking 50 mg.L$^{-1}$ initial concentration of Nitrate at pH 2 by varying the dosage (100-700 mg). The result is shown in Fig. 4(b). The uptake percentage removals were maximum at the dosage of 300 mg and minimum at the dosage of 100 mg. With the increase in dosage, the active site will increase, but also, there is the possibility of agglomeration and clogging of active sites, which decrease the adsorption capacity of the adsorbent.

**Effect of co-ions:** To assess the adsorbents in the real sense, the effect of co-ions, which are mostly common in water, was also investigated. Fluoride and chloride ions do not have much effect on the sorption capacity of nitrate. Still, phosphate and sulfate caused an appreciable decrease in the nitrate sorption with the increase in concentration of co-ions. Being a high negative charge on sulfate, the adsorption of nitrate is much affected due to dominant competition. The effect of co-ions on the adsorption of nitrate by the apricot seed shell biochar (ASSB) is shown in Fig. 5 (a, b).

The removal percentage of adsorbents at varying pH and initial concentration was calculated to obtain the optimum

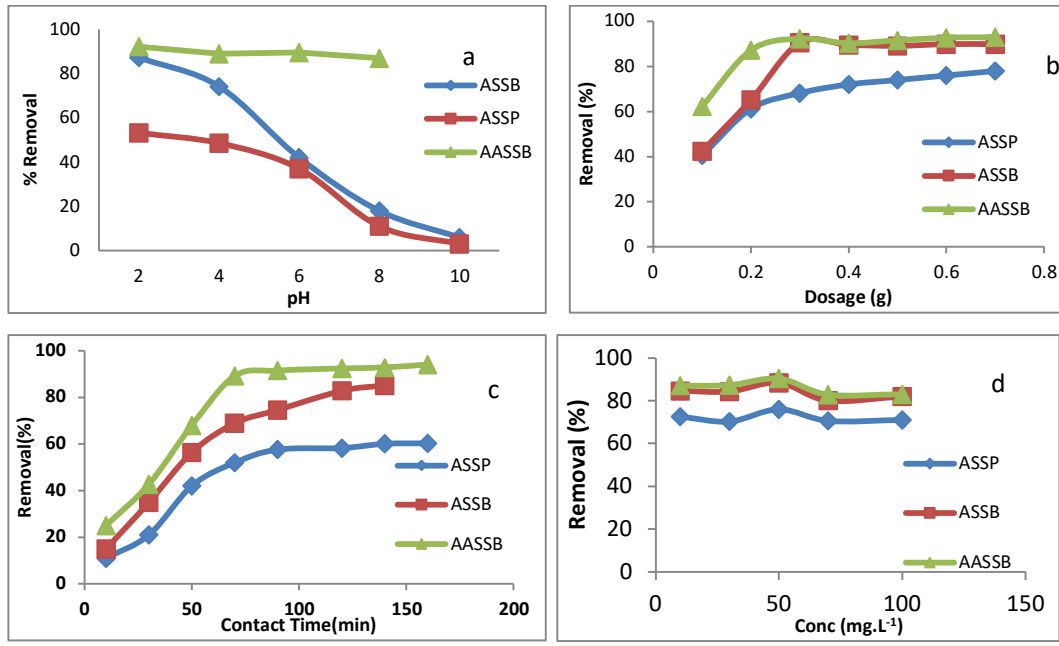


Fig. 4: Effect of variables on adsorption.

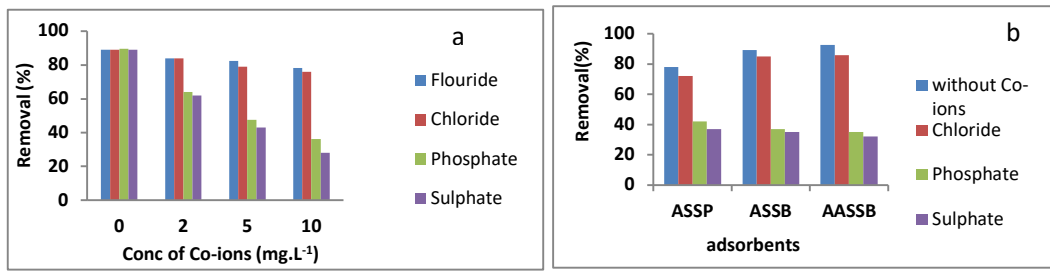


Fig. 5: Effect of co-ions.

condition. The result indicated that the maximum percentage removals was achieved at the optimum condition of 50 $mg.L^{-1}$ initial concentration and 0.3 g of dosage at pH 2. The higher adsorption capacity of ASSB and AASSB than the ASSP is due to greater porosity and specific surface area. The acid activation of adsorbent further enhanced the adsorption due to the protonation of functional groups on the surface of the biochar, which serves as the enhanced interaction with the negatively charged ions (Nitrate). The percentage removal of nitrate by the adsorbents of apricot seed shell followed the order- AASSB > ASSB > ASSP (Fig. 4).

### Adsorption Modeling

**Adsorption kinetics:** The kinetic modeling is an important parameter to evaluate the rate of solute-mass transfer and the mechanism of the adsorption. In this study, pseudo, $1^{st,}$ and $2^{nd}$ order kinetic models were applied to the adsorption of nitrate ions onto ASSP, ASSB, and AASSB. The fitting to kinetic models were evaluated and calculations of relevant parameters in Table 2 were done by using Excel 2010. The fitting parameter ($R^2$) for the adsorption of nitrate by ASSP, ASSB, and AASSB to pseudo $1^{st}$ order and pseudo $2^{nd}$ order is 0.4567, 0.5894, 0.4858 and 0.9144, 0.9796, 0.9690, respectively. The adsorptions of nitrate by adsorbents were more closely fitted to pseudo $2^{nd}$ order.

**Adsorption isotherms:** The Langmuir and Freundlich isotherm model were applied to fit the adsorption isotherm of nitrate on the adsorbents, including apricot seed shell powder (ASSP), apricot seed shell biochar (ASSB) and activated apricot seed shell biochar (AASSB). The relevant isotherm parameters are shown in Table 3. The parameters of the Langmuir isotherm model with $R_L$ values $0< R_L <1$ and $K_L$ values less than 1 favor improved adsorption (Hashem et al. 2022). The present sorption studies of nitrate on the adsorbents are efficient as the $K_L$ and $R_L$ values indicated favorable and improved sorption, which are attested by the larger value of $Q_{max}$. The values of n can elucidate the favourability and sorption affinity in terms of Freundlich isotherm- $(1< n<10)$ and $K_f$ - $(K_f>1)$values (Hashem et al. 2022). The n and $K_f$ values of the present sorption favor favorable processes.

## CONCLUSION

The pollution of nitrate in water is abundant throughout the world, and research is focusing on developing strategies and technologies to prevent and reduce nitrate ions in water ecosystems. In this study, apricot seed shell powder, biochar, and acid-activated biochar have been utilized for investigating nitrate ion sorption through batch adsorption procedures. The analysis showed that the adsorption of nitrate ions onto the ASSP, ASSB, and AASSB was affected by the pH of the solution, contact time, dosage, and ion concentration. The adsorptions of nitrate ions were fitted to the Langmuir and Freundlich isotherm model, and the equilibrium parameters indicated a favorable and improved efficiency. Likewise, the adsorption of nitrate ions onto the adsorbents was simulated to pseudo $1^{st}$ order and $2^{nd}$ order kinetic model, and the data were analyzed using MS Excel 2010 software. The pseudo-2nd-order kinetics model well describes the coefficient of determination ($R^2$). The equilibrium and kinetic data suggest an involvement of surface adsorption, diffusion, electrostatic, and ion exchange interaction. The adsorption efficiency of the adsorbents was greatly affected by the presence of co-ions in the solution. The percentage removal of nitrate decreases with highly negative ions like phosphate and sulfate. The apricot seed shell could be utilized for the development of effective adsorbents in water and wastewater treatment.

Table 2: Kinetic model and relevant parameters.

| Adsorbents | Pseudo $1^{st}$ Order | | | Pseudo $2^{nd}$ Order | | |
|---|---|---|---|---|---|---|
| | Qe [$mg.g^{-1}$] | K1 | $R^2$ | Qe [$mg.g^{-1}$] | K2 | $R^2$ |
| ASSP | 7.821 | 0.0096 | 0.4567 | 7.734 | 0.00178 | 0.914 |
| ASSB | 13.117 | 0.0206 | 0.5894 | 10.6383 | 0.0013 | 0.979 |
| AASSB | 13.908 | 0.0327 | 0.4858 | 9.478 | 0.0030 | 0.969 |

Table 3: Adsorption isotherms and relevant parameters.

| Adsorbents | | Langmuir isotherm | | | Freundlich isotherm | | |
|---|---|---|---|---|---|---|---|
| | Qmax [$mg.g^{-1}$] | KL | RL | $R^2$ | n | Kf | $R^2$ |
| ASSP | 224.7 | 0.00197 | 0.911 | 0.9948 | 1.030291 | 0.9996 | 0.9828 |
| ASSB | 384.6 | 0.00242 | 0.892 | 0.9865 | 1.1399 | 1.0443 | 0.9429 |
| AASSB | 400 | 0.00284 | 0.875 | 0.9845 | 1.1941 | 1.1546 | 0.9354 |

## ACKNOWLEDGEMENTS

We are thankful to the Department of Chemistry, the Kargil Campus University of Ladakh, for providing laboratory facilities for conducting the experimental works. The author is highly thankful to Prof. RC Chippa for his consistent support and guidance.

## REFERENCES

Ansari, S., Heidarpour, M. and Mousavi, S. F. 2017. Application of barley straw to remove nitrate from drainage water. Iran agric. Res., 36(1): 105-110.

Challab, M. and Alhameedawi, F. and Al-Alaq, S. 2020. Use apricot seed peels as adsorbents to remove mn2+ and zn2+ ions from aqueous solutions. J. Clean. Prod., 41: 786

Dai, Y., Sun, Q., Wang, W., Lu, L., Liu, M., Li, J., Yang, S., Sun, Y., Zhang, K., Xu, J., Zheng, Z., Hu, Z., Yang, Y., Gao, Y., Chen, Y., Zhang, X., Gao, F. and Zhang, Y. 2018. Utilizations of agricultural waste as adsorbent for the removal of contaminants: a review. Chemosphere, 253-235 :211. Https://doi.org/10.1016/j.chemosphere.2018.06.1793.

Das, S. and Goud, V. V. 2020. Characterization of a low-cost adsorbent derived from agro-waste for ranitidine removal. Mater Sci. Energy Technol., 3: 879-888.

Hashem, A., Aniagor, C. O., Morsy, O. M., Abou-Okeil, A. and Aly, A.A. 2022. Apricot seed shell: An agro-waste biosorbent for acid blue193 dye adsorption. Biomass Convers. Biorefin., 17: 1-4. Https://doi.org/10.1007/s13399-022-03272-9

Janković, B., Manić, N., Dodevski, V., Radović, I., Pijović, M., Katnić, D. and Tasić, G. 2019. Physico-chemical Characterization of carbonized apricot kernel shell as a precursor for activated carbon preparation in clean technology utilization. J. Clean. Prod., 236: 117614. Https://doi.org/10.1016/j.jclepro.2019.117614

Khatoon, H. and Rai, J. P. N. 2016. Agricultural waste materials as biosorbents for the removal of heavy metals and synthetic dyes: A review. Octa J. Environ. Res., 4(3): 208-229.

Liu, G., Dai, Z., Liu, X., Dahlgren, R. A. and Xu, J. 2022.Modification of agricultural wastes to improve sorption capacities for pollutant removal from water: A review. Carbon Res., 1(1): 24.https://doi.org/10.1007/s44246-022-00025-1

Mitra, T., Bar, N., and Das, S. K. 2019. Rice husk: Green adsorbent for Pb (II) and Cr (VI) removal from aqueous solution-column study and GA–NN Modelling. SN Appl. Sci., 1: 1-5. Https://doi.org/10.1007/s42452-019-0513-5

Rahman, A., Mondal, N. C. and Tiwari, K. K. 2021.Anthropogenic nitrate in groundwater and its health risks in the view of background concentration in a semi-arid area of Rajasthan, India. Sci. Rep., 11(1): 9279. Https://doi.org/10.1038/s41598-021-88600-1

Reddy, C. A., Prashanthi, N., Babu, P. H. and Mahale, J. S. 2015. Banana peel as a biosorbent in the removal of nitrate from water. Int. J. Adv. Res. Sci. Eng. Technol., 2(10): 94-98. http://doi.org/10.17148/iarjset.2015.21020

Sardar, M., Manna, M., Maharana, M. and Sen, S. 2021. Remediation of dyes from industrial wastewater using low-cost adsorbents: green adsorbents to remove metals, dyes, and boron from polluted water. Springer, Cham, pp. 377-403. http://doi.org/10.1007/978-3-030-47400-3_15

Shukla, S. and Saxena, A. 2020. Sources and leaching of nitrate contamination in groundwater. Curr. Sci., 118(6): 25.

Tiwari, A. K. and Pal, D. B. 2021. Bio-Processing: biomass to commercial alcohol. bioenergy research: biomass waste to energy, Springer, Cham, pp. 149-68. Https://doi.org/10.1007/978-981-16-1862-8_6

Zhang, Z., Zhou, C., Yang, J., Yan, B., Liu, J., Wang, S., Li, Q. and Zhou, M. 2022. Preparation and characterization of apricot kernel shell biochar and its adsorption mechanism for atrazine. Sustainability, 14(7): 4082. Https://doi.org/10.3390/su14074082.

Zhou, Z. A. 2015. Global Assessment of Nitrate Contamination In Groundwater. International Ground Water Assessment Centre. Retrieved from https://www.un-igrac.org.

Zoungranan, Y., Dobi-Brice, K. K., Eric, K. D. O., Stanislas, S.A., Tchirioua, E. and Lynda, E. 2021. Reduction of nitrate content in water by the use of banana peel biochar. Am. J. Phys. Chem., 10(4): 59-66. Http://dx.doi.org/10.11648/j.ajpc.20211004.13

### ORCID DETAILS OF THE AUTHORS

Mohd Ishaq: https://orcid.org/0000-0002-6134-4750

Nature Environment and Pollution Technology
An International Quarterly Scientific Journal

p-ISSN: 0972-6268
(Print copies up to 2016)
e-ISSN: 2395-3454

Vol. 23 | No. 3 | pp. 1751-1760 | 2024

Original Research Paper

https://doi.org/10.46488/NEPT.2024.v23i03.048

Open Access Journal

# Novel Bacterial Consortium for Mitigation of Odor and Enhance Compost Maturation Rate of Municipal Solid Waste: A Step Toward a Greener Economy

**P.A.K.C. Wijerathna*, K.P.P. Udayagee**, F.S. Idroos* and Pathmalal M. Manage*†**

*Centre for Water Quality and Algae Research, Department of Zoology, Faculty of Graduate Studies, University of Sri Jayewardenepura, Gangodawila, Nugegoda, 10250, Sri Lanka

**Department of Bio-systems Technology, Faculty of Technology, University of Sri Jayewardenepura, Dampe-Pitipana Road, Homagama, Nugegoda, 10250, Sri Lanka

†Corresponding author: Pathmalal M. Manage; pathmalal@sjp.ac.lk

**Nat. Env. & Poll. Tech.**
**Website: www.neptjournal.com**

*Received:* 20-11-2023
*Revised:* 05-01-2024
*Accepted:* 14-01-2024

**Key Words:**
Odor reduction
Bacterial consortia
Composting
Municipal solid waste
Greener economy

## ABSTRACT

Composting is an integral component of sustainable Municipal Solid Waste (MSW) management within the circular bio-economy platform. However, it faces challenges due to malodorous emissions that impact environmental and societal equilibrium. The present study aims to minimize odorous emissions and expedite compost maturation using a novel, efficient microbial consortium. Bacteria sourced from open dump sites in Sri Lanka were carefully screened based on concurrent enzyme production. Five developed consortia were tested for their performance in reducing malodors during the composting process of MSW. Consortium No. 5 (C5), comprised of Bacillus haynesii, Bacillus amyloliquefaciens, and Bacillus safensis, demonstrated outstanding performance with a significant ($p < 0.05$) reduction in odorous emissions. Additionally, consortium C5 exhibited impressive control over gas emissions, maintaining VOC, $CH_4$, $NH_3$, and $H_2S$ concentrations within ranges of 0.5-6 ppm, 0.5-0.8 ppm, 0.3-0.5 ppm, and 0.5-0.6 ppm, respectively, compared to control concentrations of 4.5-10.2 ppm, 0.5-5.5 ppm, 0.3-5.5 ppm, and 0.5-6.4 ppm, respectively. Additionally, comprehensive Electronic nose (E-nose) analysis substantiated C5's efficiency in attenuating Methane-Aliphatic compounds, Sulfur and Aromatic compounds, along with low-polarity aromatic and alkane compounds, all with statistical significance ($p < 0.05$). Further, the developed consortium could reduce the composting time from 110 ± 10 days to 17 ± 3 days, offering a sustainable solution for global MSW management.

## INTRODUCTION

The relentless advance of rapid industrialization and urbanization has resulted in a mounting tide of Municipal Solid Waste (MSW) globally, leading to severe environmental conditions of unprecedented scale. A detailed analysis of waste footprints reveals that annual MSW production exceeds an astounding 2 billion tons, with a projected increase of 70% by 2050 (Gautam & Agrawal 2021, Golroudbary 2019, Zhao et al. 2022). In this troubling scenario, the average individual contributes 0.74 kg of waste daily, with a staggering 70% destined for landfills and dumpsites (Golroudbary 2019, Pal & Tiwari 2023). Given this escalating crisis, composting has emerged as an eco-friendly solution, providing a sustainable approach to solid waste management within the circular bio-economy. Composting involves controlled, aerobic processes that transform organic materials into a nutrient-rich soil amendment or mulch through natural decomposition (Ayilara et al. 2020, Wijerathna et al. 2023).

The introduction of bacterial consortia adds a dynamic element to the rapid degradation of various organic materials within a greener framework. This approach has proven integral to novel composting technologies (Behera et al. 2021, Wijerathna et al. 2022). The heterogeneous nature of bacterial consortia can synergistically enhance both mesophilic and thermophilic composting phases, leading to an accelerated transformation driven by their combined metabolic and co-metabolic mechanisms (Ali et al. 2021).

Particularly, the emission of greenhouse gases (GHGs), including ammonia and methane, results in significant environmental consequences. Methane has a global warming potential 28 times greater than carbon dioxide (Silva et al. 2017) and is primarily emitted from the anaerobic fermentation of wastes (Costa et al. 2021). Additionally, odorous compounds such as hydrogen sulfide ($H_2S$), methyl mercaptan, dimethyl sulfide, ammonia, and Volatile Organic Compounds (VOCs) are generated during the composting process (Jiang et al. 2017). Ammonia emission is especially

problematic in sewage sludge composting, as it can cause odor issues and lead to nitrogen loss in the mature compost (Shou et al. 2019). Therefore, mitigating odor during the composting process is a major concern.

Different techniques have manifested through a variety of physicochemical symphonies, where bio-filters, odor neutralizers, sorbent materials, compost covers, and bulking agents have all played their part in the grand stage of odor control (Wysocka et al. 2019). Yet, most of these physico-chemical methods are not economically feasible and have limited accessibility. Thus, the exploration of the serenading potential of microbial consortia targeting odor reduction and enhancing the composting process is noted as a greener approach to meeting sustainability in solid waste management.

The synergistic collaborations within microbial consortia may reduce the generation of odor-causing compounds while improving the composting efficiency, fostering an environment of mutual nourishment (Bajpai Bajpai 2018, Kumar et al. 2022, Zhang & Dong 2022, Pacheco et al. 2019). Thus, this study focuses on the analysis of the performances of microbial consortia for their capacity to transmute malodorous compounds and accelerate compost maturation.

## MATERIALS AND METHODS

### Isolation and Screening of Potential Bacteria

The potential bacteria for effective solid waste degradation was isolated from soil/solid waste and leachate samples collected from MSW dump sites in Sri Lanka. The bacteria were isolated following the standard pour plate method on a nutrient agar medium, and morphologically different pure cultures were obtained following the streak plate method. The isolated microorganisms were subjected to the primary screening following plate assays for Cellulase, Amylase, lipase, and Proteinase enzymes on Congo Red Agar, Carboxyl Methyl Cellulose (CMC) agar starch-agar and skimmed milk agar medium (Sarkar & Chourasia 2017). The secondary screening for cellulase, amylase, lipase, and proteinase enzymes was performed using the method described by Sarkar & Chourasia (2017). The best potential isolates used for the consortia preparation are based on their concomitant enzyme production in an artificial broth media containing Cellulose, Starch, Lipids, and protein substrates.

### Experimental Design for Comparative Study

Based on the enzyme production potential, five bacterial consortia (C1-C5) were prepared (Table 2) using the most potential bacterial species. They were inoculated to the compost bins to evaluate their efficiency on compost maturation and odor reduction potential. The composting experiment was conducted employing eighteen regular compost bins (each measuring 150 cm in height and 45 cm in diameter) as triplicates for both control groups and five distinct bacterial consortia setups. Ninety-five kg of a mixed organic portion of municipal solid waste was added into each bin. Nutrient broth 1% bacterial inoculum (v/w) was added into every bin except for the control group. Throughout the study, different composting indicators, pH, electrical conductivity, moisture content, total organic carbon, and total Kjeldahl nitrogen were monitored daily to observe and analyze the dynamic changes occurring within each compost bin.

### Sampling and Odor Analysis

Gaseous odor emissions from various compost setups were assessed using both portable gas analyzers and Electronic Nose (E-Nose) devices. The odorous gases, including $NH_3$, $CH_4$, $H_2S$, and Total Volatile Compounds (TOC), were quantified in the cap space of the compost bins. The probes of gas analyzers (Aeroqual HH S500L analyzer with a range of 0–10,000 ppm and 5 IR multi-gas detector with a range of 0–50,000 ppm) were directly exposed to the cap space of the compost bins at intervals of every 3 days.

### Odor Characterization Using E-Nose

Gas samples were collected from the cap space of the compost bins employing syringes and subsequently transferred to GCMS vials to facilitate Electronic Nose (E-Nose) analysis. Weekly characterization of the gaseous composition was carried out using an automated E-Nose comprising ten distinct sensors. For the instrumental sensory analysis, an E-Nose system (Model - PEN3 Airsense Analytics GmbH, Schwerin, Germany) equipped with an automated sampling device was employed. This E-Nose system featured ten thermo-regulated (ranging from 150°C to 500°C) metal oxide semiconductor sensors, each demonstrating slight sensitivity to different classes of chemical compounds, as noted by Jonca et al. (2022) and Eusebio et al. (2016).

These ten sensors, adept at discriminating compounds within samples, are outlined in Table 1. The measurement process was orchestrated through a computer program, and each measurement phase spanned 50 seconds, a duration sufficient for the sensors to attain stable readings. Data collection was carried out at 1-second intervals. A flush time of 3 min was interposed between successive samplings, and the flow rate was maintained at 300 $mL.min^{-1}$. To ensure signal stability and encompass sample variability, the procedure was iterated three times for each sample, as

Table 1: The list of sensors used to discriminate compounds in samples.

| Sensor Number | Sensitive compounds |
|---|---|
| R1 | Aromatic |
| R2 | Broad range Polar and NOx |
| R3 | Aromatic compounds, ketones, and aldehydes |
| R4 | Hydrogen |
| R5 | Low polarity aromatic and alkane |
| R6 | Broad-methane |
| R7 | Sulphur organic |
| R8 | Broad alcohols, ketones, and partially aromatic |
| R9 | Sulfur and aromatic |
| R10 | Methane-aliphatic |

corroborated by Cipriano & Capelli (2019). At operating conditions, relationships with volatiles from the headspace and the sensing device's surface caused alterations in the conductivity of the semiconductor. Thus, the ratio G/G0 (in which G and G0 represent the resistance of a sensor when detecting a gas and when inhaling clean air, respectively) was recorded by the e-nose dedicated software (Ottoboni et al. 2018).

## RESULTS AND DISCUSSION

### Isolation and Screening of Potential Bacterial Species

After 24-h incubation at 30°C, 226 morphologically different bacterial colonies were isolated from the soil, leachate, and solid waste sample. Out of all isolates, 15 bacterial isolates were positive for cellulase, 15 for amylase, 15 for proteinase, and four were positive for lipase. According to the secondary screening results, Cellulase-positive bacterial isolates *Bacillus haynesii* exhibited the highest cellulase activity at 6.2 ± 0.2 $U.mL^{-1}.min^{-1}$ and the highest amylase activity at *Bacillus haynes* and *Bacillus velezensis* with values of 6.5 ± 0.1 $U.mL.min^{-1}$ and 6.2 ± 0.3 $U.mL.^{-1}min^{-1}$, respectively. Similarly, the most significant proteinase activity was found in bacteria *Bacillus amyloliquefaciens* and *Bacillus velezensis*, with 7.2 ± 0.2 $U.mL.min^{-1}$ and 6.5 ± 0.1 $U.mL^{-1}.min^{-1}$ enzyme activities, respectively. Further, Bacteria *Bacillus velezensis* and *Bacillus safensis* exhibited the highest lipase activity, with enzyme activity values of 4.2 ± 0.2 $U.mL^{-1}.min^{-1}$ and 3.8 ± 0.2 $U.mL.min^{-1}$, respectively. The bacterial isolates with the highest extracellular enzyme activities were subjected to the consortia preparation. Table 2 demonstrates the prepared five consortia for evaluating odor reduction and compost maturity potential. The odor reduction potential of prepared five consortia was evaluated following the standard methods.

Table 2: Different bacterial consortia used for the experimental setup.

| Set up name | Bacterial combination in the prepared consortium |
|---|---|
| C1 | *Bacillus haynesii, Bacillus hisashii, Bacillus licheniformis* |
| C2 | *Bacillus haynesii , Bacillus licheniformis , Bacillus subtilis,* |
| C3 | *Bacillus haynesii, Bacillus safensis, Bacillus velezensis* |
| C4 | *Bacillus haynesii, Bacillus amyloliquefaciens, Bacillus subtilis,* |
| C5 | *Bacillus haynesii, Bacillus amyloliquefaciens, Bacillus safensis* |
| Control | Not Applicable |

### Odor Reduction of Prepared Bacterial Consortia

Fig. 1 illustrates the spectrum of odor-inducing gases produced throughout the composting process, with Fig. 1(a) specifically highlighting the dynamic changes in Volatile Organic Compounds (VOCs). As shown in Fig. 1(a), the control sample exhibited a pronounced and statistically significant increase in VOC production compared to all treatment samples. Notably, the experimental setup with the C5 consortium inoculation resulted in the lowest VOC production during composting. This reduction is likely due to the efficient bioconversion of solid waste facilitated by the bacterial consortia, leading to lower VOC emissions (Rastogi et al. 2020). Additionally, setups C4, C3, and C2 each demonstrated a statistically significant reduction ($p < 0.05$) in VOC levels compared to the control, confirming the effectiveness of the inoculated microbial consortia.

VOCs contain a diverse array of chemical constituents, including alkanes (such as Butane, Pentane, Cyclopentane, Heptane, Octane, and Decane), Terpenes (including Propylene and Limonene), aromatic compounds (encompassing Benzene, Toluene, Ethylbenzene, p-xylene, and o-xylene), halogenated compounds (like Chloromethane, Methylene chloride, Chloroform, Carbon tetrachloride, Ethyl chloride, Styrene, and Chlorobenzene), oxygenated compounds (Ethanol, Acetone, Ethyl acetate, and 2-Hexanone), and Sulfur-containing compounds (such as Carbon disulfide, Methanethiol, Dimethyl Sulfide, and Dimethyl disulfide) which can harm the environment and social well-being through air pollution, smog and its contribution to global warming (Halios et al. 2022, Saraga et al. 2023). According to Hu et al. (2016), a specific bacteria consortium consisting of *Zoogloea resiniphila* HJ1 *Methylobacterium rhodesianum* found similar results: lowered release of volatile organic compounds during composting. In addition, Awasthi et al. (2020) have studied the effect of biochar and bacterial inoculum additions on cow dung composting for the reduction of VOC emission and have achieved a successful reduction of VOC generation. Preferred species of organic-

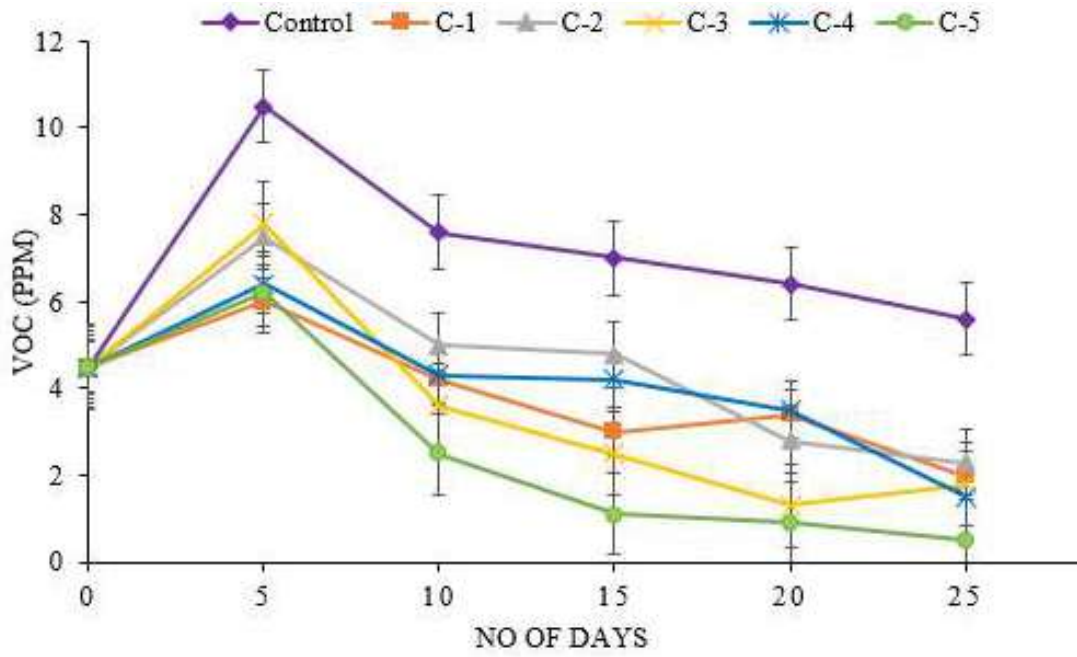


(a)

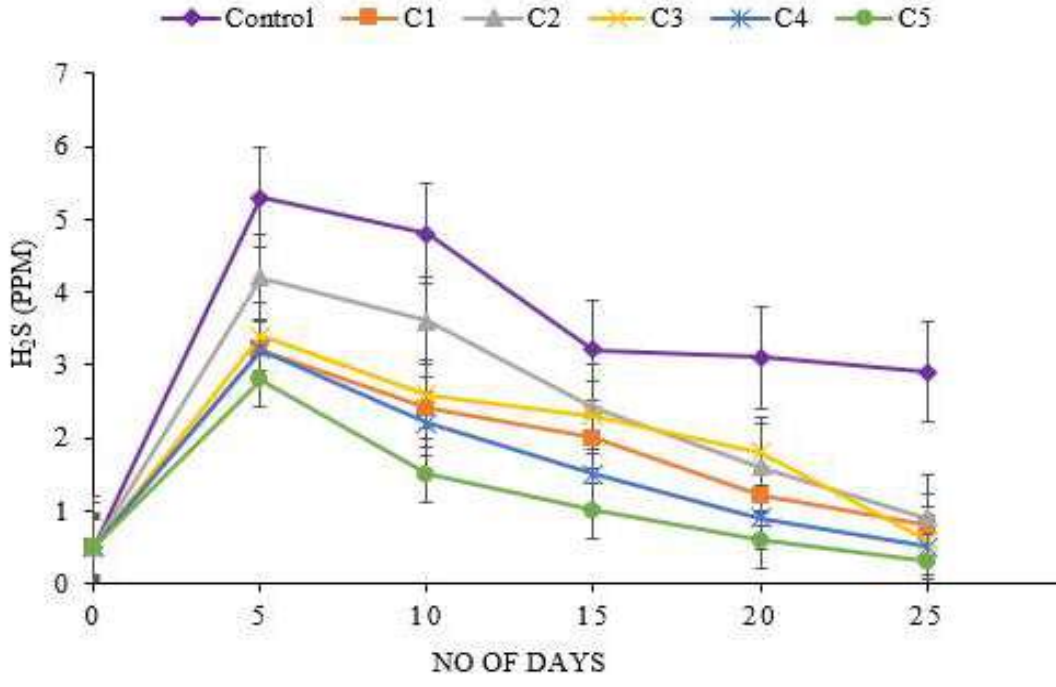


(b)

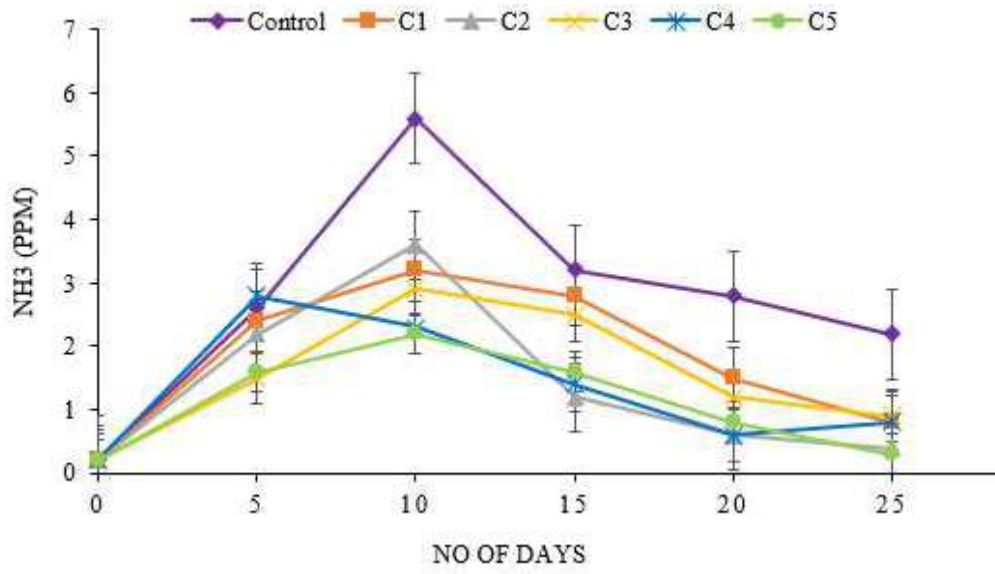


(c)

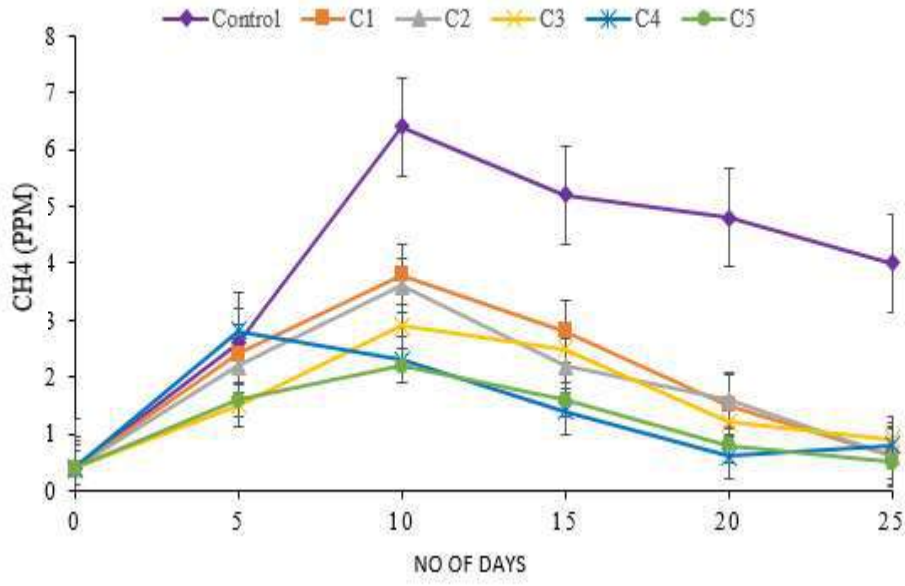


(d)

Fig. 1: VOC (a), $H_2S$ (b), $NH_3$ (c), and $CH_4$ (d) concentrations of different treatments.

digesting microorganisms include bacteria of *Bacillus*, *Clostridium*, and *Deinococcus*, particularly *Bacillus subtilus*, *Bacillus licheniformis*, and VFAs. Additionally, these microorganisms produce lytic enzymes such as urease, phytase, lipases, proteases, cellulases, xylanase, hemicellulases, and amylases that degrade organic matter and reduce odor. Further, some bacteria can eliminate odors and reduce gaseous pollutants via their biochemical digestive reaction processes (Barbusinski et al. 2021).

Hydrogen sulphide ($H_2S$), another odorous gas released during composting, arises from the microbial transformation of protein substrates rich in Sulphur (Yao et al. 2022).

The dynamics of $H_2S$ are shown in Fig. 1(b) throughout composting. Parallel to the VOCs, a distinct pattern took place, with the control sample exhibiting a significant surge in $H_2S$ production, while the C5 sample exhibited the most lowered $H_2S$ emissions. Among the compost bins, the peak of $H_2S$ concentration was noticed as 5.5 ± 0.4 ppm within the cap space of the control setup on the fifth day of composting, followed by a gradual decline. This behavior could be attributed to the gradual reduction of Sulphur-containing protein compounds during the mesophilic phase of composting. Fig. 1(c) presents the dynamic evolution of Ammonia ($NH_3$) levels throughout the composting process. Ammonia emerges as a primary odorant compound, predominantly generated through the ammonification process during the transformative conversion of nitrogen-rich organic materials (Ahmad et al. 2021). As the figure depicts, the control sample exhibited the highest $NH_3$ production, notably peaking on the 10th day of composting.

Furthermore, the C5 treatment displayed comparatively lower $NH_3$ emissions during the entirety of the composting period. This alignment highlights the potential of these setups in mitigating $NH_3$ production. The genesis of ammonia during composting is influenced by factors including moisture content, aeration, temperature, pH of composting materials, and the carbon-to-nitrogen (C/N) ratio of the waste substrate. Lowered ammonia synthesis may result in higher nitrogen content in the compost, leading to delayed breakdown and a buildup of nitrogenous molecules (Anas et al. 2020). Kim et al. (2014) showed that the bacterium release of bacteriocins, which prevent the establishment of many bacteria that are responsible for odor generation, may be connected to the lowering of $NH_3$. As an alternative, a variety of extracellular enzymes may be responsible for the reduction of ammonia (Leite et al. 2022). Further, the bacterial genus *Bacillus* can help keep the slurry's pH levels stable by producing acidic substances, which might reduce the rate of hydrolysis of urea and other nitrogen molecules being delaminated, resulting in the emission of $NH_3$ (Nowocień & Sokołowska 2022).

Methane ($CH_4$) is a key contributor to the odor released during composting, as shown in Fig. 1(d), which displays the changing $CH_4$ concentrations in the composting bins' cap space. The control setup had notably higher $CH_4$ production compared to the bins with consortia, indicating that the consortia might help with composting while reducing gaseous $CH_4$ emissions. After the 10th day of composting, $CH_4$ levels gradually decreased in all samples. The production of methane in composting primarily occurs through a microbial process called methanogenesis. Archaea, which are primarily methanogenic microbes, can decompose organic matter in anaerobic environments and flourish in low-oxygen circumstances. The sequence of events in this process includes hydrolysis, acidogenesis, acetogenesis, and, finally, methanogenesis (Koniuszewska et al. 2020, Rath et al. 2022). Some bacterial groups utilize methane as their sole carbon and energy source via the enzyme methane monooxygenase, which is capable of the co-metabolism of some persistent compounds concurrently (Wang et al. 2022). These bacteria serve as biofilters for the oxidation of methane produced in anaerobic environments, and when oxygen is present in soils, atmospheric methane is oxidized (Ray et al. 2023, Qiu et al. 2022). Therefore, the bacterial species (*Bacillus haynesii, Bacillus amyloliquefaciens,* and *Bacillus safensis*) in the C5 treatment may contain methanotroph enzymes or synergistic interaction to oxidize methane by mitigating $CH_4$ emissions.

## Electronic Nose (E-nose) Odor Profile for the Compost Samples during Composting Period

Fig. 2 shows the fluctuation patterns of major gas types detected by ten distinct sensors of the E-Nose throughout the composting duration. Analysis of gas levels during the first week of composting revealed a noticeable increase in odorous emissions from the control sample. The $G/G_0$ ratio for a wide range of polar compounds and NOx, as measured by the R2 sensor, was 4 for the control sample, while the ratios for the C1, C2, C3, C4, and C5 samples were distinctly lower at 0.6, 0.6, 0.7, 0.6, and 0.5, respectively. Additionally, the ratio of low-polarity aromatic and alkane compounds showed a significant increase ($p < 0.05$) in the control sample, with a value of 5. In contrast, the ratios for the C1, C2, C3, C4, and C5 samples were 0.7, 0.6, 0.7, 0.7, and 0.5, respectively.

Sulfur-containing organic compounds, as detected by the R7 sensor, showed a higher $G/G_0$ ratio in the control samples (4), compared to lower values of 2.3, 2.2, 2.3, 1.3, and 1.8 for the C1, C2, C3, C4, and C5 samples, respectively. Similarly, odor-forming sulfur and aromatic compounds, as detected by the R9 sensor, were more prevalent in the control sample, with a $G/G_0$ ratio of 6. In contrast, the ratios for the C1, C2, C3, C4, and C5 samples were 2, 2, 2, 1.5, and 1.3, respectively. Sulfide derivatives can result from both biological (decomposition of proteins) and non-biological reactions. Certain microbial groups decompose compost material to produce $SO_2$ as incomplete oxidation products. $H_2S$ is produced under anaerobic conditions and is often detectable during the initial stages of composting (Kacprzak et al. 2023). The latest study suggests that *Bacillus* species can lower substances, including $NH_3$, $H_2S$, and $SO_2$. Kim et al. (2014) looked at how well *Bacillus amyloliquefaciens* reduced odor emissions from swine manure in anaerobic environments and observed a noticeable odor reduction during the process of anaerobic fermentation.

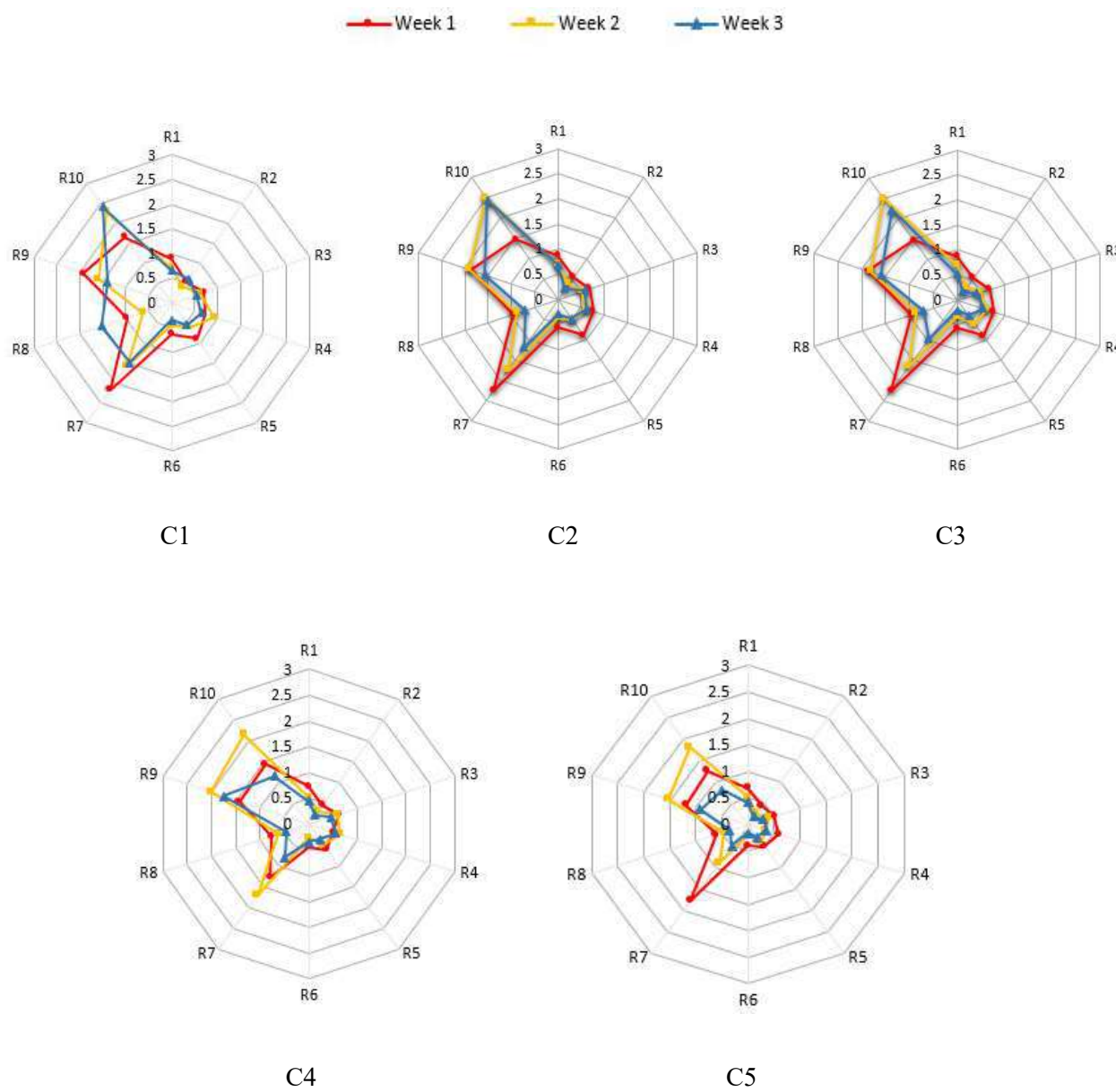


Fig. 2: E-nose odor profile in the compost treatments for three weeks.

In the present study, the second week of composting brought some changes in the gases released; the main gases detected were sulfur and aromatic compounds, along with methane-aliphatic compounds. This change might be because there was less oxygen in the composting bins and the progressed performance of the anaerobic microbes that break down the waste in the low-oxygen microenvironment (Nowocień & Sokołowska 2022). The G/Go ratio of methane-aliphatic compounds, which is detected by sensor 10, the control sample showed the highest ratio at 10.2, while for the C1, C2, C3, C4, and C5 samples, the ratios were lower, indicating less odor. Notably, among these, the C5 sample had the least odor (Mahapatra et al. 2022).

The results of the 3rd week of composting indicate that the overall odor profile of all the samples has been reduced compared to the 2$^{nd}$ week. This may be governed by the continuous odor emission and the conversion of the protein-based complex substrates into simple monomers, which reduce the microbial metabolism in the compost. However, in the control sample odor profile, it was recorded a significant ($P < 0.05$) greater methane-aliphatic (R10) concentration and broad methane (R6) concentration which was which

were 6.6 and 6, G/Go ratio, respectively. Importantly, all the consortia inoculated samples recorded much lower odor values compared to the control, ranging from 0.4 -0.5 broad methane and 0.8 2.5 methane-aliphatic concentration, respectively. Out of all the consortia inoculated samples C5 sample showed a clear overall odor reduction compared to all other treatments.

The bacterial strains in the C5 consortium-*Bacillus haynesii*, *Bacillus amyloliquefaciens*, and *Bacillus safensis*, each bring unique biological attributes that collectively contribute to the promising results observed in the composting process. *Bacillus haynesii* is known for its ability to produce extracellular enzymes that degrade complex organic compounds into simpler forms, facilitating the breakdown of odor-causing substances. *Bacillus amyloliquefaciens* enhances this process through its robust metabolic activity and production of antimicrobial peptides, which suppresses unwanted microbial growth and reduces the overall microbial load responsible for odor production. *Bacillus safensis* adds value with its resilience in varying environmental conditions and its ability to metabolize a wide range of organic compounds, including those that are typically resistant to decomposition. The combined metabolic pathways and enzymatic activities of these strains effectively target and reduce volatile organic compounds (VOCs) and other odorous substances, leading to improved compost quality and reduced emissions.

## Statistical Analysis of the Odor Parameters

The loading plot for the odor values detected by different sensors reveals that the odor components measured by R1, R7, R8, and R9 are positively correlated. Similarly, the components detected by R2, R3, R4, and R5 also show positive correlation. R6, however, appears to have minimal correlation with the other sensors, and no parameters were found to be negatively correlated. Additionally, the score plot indicates that the control sample released the majority of the odorant compounds, in contrast to the samples inoculated with bacterial consortia.

## Changes in Composting Parameters

Solid waste composting is a process associated with both physico-chemical and microbial process mechanisms. Therefore, the maturity and stability of compost are vital to using compost as an agricultural supplement. The compost maturity and stability can be measured by monitoring the parameters including the compost pH, Temperature, Electrical conductivity, Bulk density, and mesophilic and thermophilic viable microbial cell counts. Based on the pH changing pattern, the pH ranged between 6.6 ± 0.1 – and 9.5 ± 0.1. All the consortia inoculated samples were shown a significant difference ($P < 0.05$) compared to the control samples. Importantly, C5 samples were shown an exceptionally faster rate of composting while rapidly moving to the acidification and stabilizing phases.

Temperature is another crucial factor that reflects microbial metabolism during composting, which affects the rate of microbial enzymatic reactions (Ge et al. 2020). In the study, a significant difference ($P < 0.05$) was observed

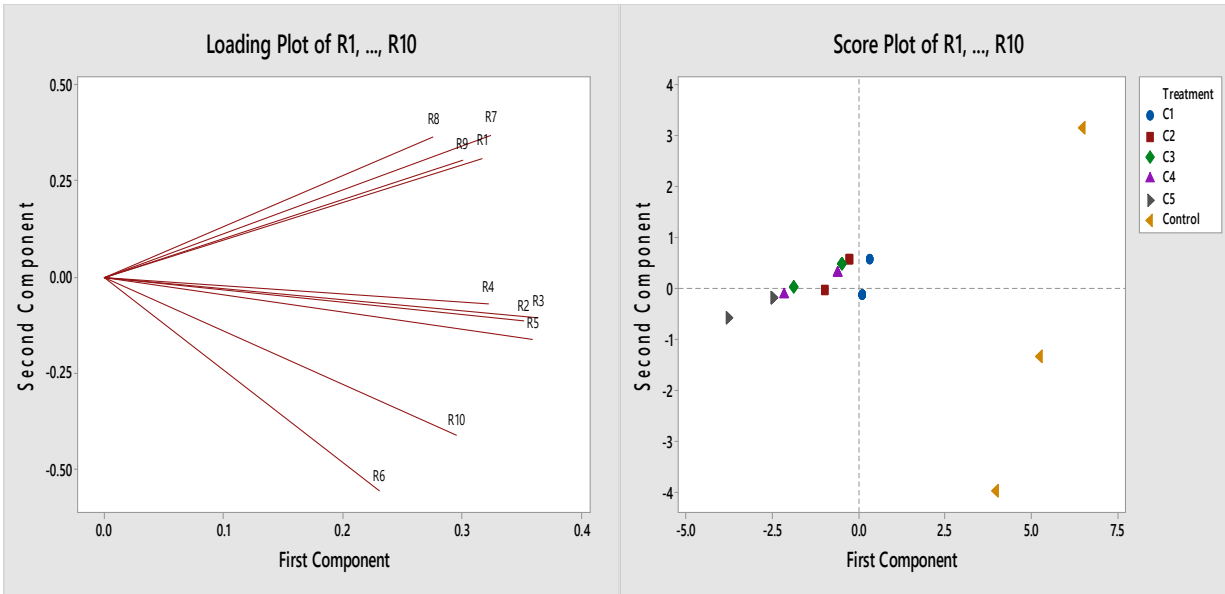


Fig. 3: Loading plot and Score plot for the PCA analysis of the odor parameters.

between the five inoculated samples and the control sample in terms of compost temperature, and it ranged between 30.1 ± 0.3°C and 65.5 ± 0.2°C. Interestingly, the added sample rapidly entered the thermophilic phase within two days, while the other consortia-inoculated samples showed a slower transition. Further, the Electric conductivity (EC) reflects the level of salinity in the final compost product, which impacts nutrient availability for plant growth (Asquer et al. 2019). The results showed that all the consortium-inoculated samples had a significantly higher EC ($P < 0.05$) compared to the control sample.

Further, the microbial dynamics of viable cell counts during the composting period also provide valuable information about the phase alteration of the composting period. In terms of the mesophilic bacterial count, a significant difference ($P < 0.05$) was observed between all the consortium-added samples and the control sample. Further, the thermophilic bacterial count of all the consortium-added samples demonstrated a significant increase ($P < 0.05$) compared to the control sample. In contrast, all analyzed compost parameters indicated that the inoculated bacterial consortia accelerated the overall composting process, and out of all inoculated consortia, the C5 consortia showed an exceptionally faster composting rate by producing mature compost within 17 ± 3 days.

## CONCLUSIONS

The bacterial consortium (C5), comprising *Bacillus haynesii*, *Bacillus amyloliquefaciens*, and *Bacillus safensis*, exhibited significant odor reduction ($p < 0.05$) and an accelerated compost maturation rate in MSW composting. Specifically, the emission of malodorous VOCs, $H_2S$, $NH_3$, and $CH_4$ was significantly reduced ($p < 0.05$) by the inoculated bacterial consortium. Additionally, changes in pH, temperature, and bulk density were significant in the C5 consortium compared to the control and other bacterial consortia. These changes demonstrate the rapid degradation of MSW by the inoculated bacterial consortium through the acceleration of both mesophilic and thermophilic phases.

## ACKNOWLEDGMENTS

The authors wish to thank for University of Sri Jayewardenepura, Nugegoda, Sri Lanka, for financial assistance for this research under the university grant, Grant No: ASC/1/RE/SCI/2021/28.

## REFERENCES

Ahmad, Z., Mosa, A., Zhan, L. and Gao, B. 2021. Biochar modulates mineral nitrogen dynamics in soil and terrestrial ecosystems: A critical review. Chemosphere, 278: 130378. doi:10.1016/j.chemosphere.2021.130378.

Ali, S. S., Elsamahy, T., Al-Tohamy, R., Zhu, D., Mahmoud, Y. A. G., Koutra, E., Metwally, M. A., Kornaros, M. and Sun, J. 2021. Plastic wastes biodegradation: Mechanisms, challenges, and future prospects. Sci. Total Environ., 780: 146590. doi:10.1016/j.scitotenv.2021.146590.

Anas, M., Liao, F., Verma, K. K., Sarwar, M. A., Mahmood, A., Chen, Z. L., Li, Q., Zeng, X. P., Liu, Y. and Li, Y. R. 2020. Fate of nitrogen in agriculture and environment: agronomic, eco-physiological and molecular approaches to improve nitrogen use efficiency. Biol. Res., 53(1): 1-20. doi:10.1186/s40659-020-00287-0.

Asquer, C., Cappai, G., Carucci, A., De Gioannis, G., Muntoni, A., Piredda, M. and Spiga, D. 2019. Biomass ash characterization for reuse as an additive in the composting process. Biomass Bioenergy, 123: 186-194. doi:10.1016/j.biombioe.2019.02.008.

Awasthi, M. K., Duan, Y., Awasthi, S. K., Liu, T. and Zhang, Z. 2020. Effect of biochar and bacterial inoculum additions on cow dung composting. Bioresour. Technol., 297: 122407. doi:10.1016/j.biortech.2019.122407.

Ayilara, M. S., Olanrewaju, O. S., Babalola, O. O. and Odeyemi, O. 2020. Waste management through composting: Challenges and potentials. Sustainability, 12(11): 4456. doi:10.3390/su12114456.

Bajpai, P. and Bajpai, P. 2018. Biofiltration of odorous gases. Biotechnol. Pulp Paper Process, 10: 453-480. doi:10.1016/B978-0-12-409508-3.10921-6.

Barbusiński, K., Parzentna-Gabor, A. and Kasperczyk, D. 2021. Removal of odors (mainly H2S and NH3) using biological treatment methods. Clean Technol., 3(1): 138-155. doi:10.3390/cleantechnol3010011.

Behera, B., Das, T. K., Raj, R., Ghosh, S., Raza, M. B. and Sen, S. 2021. Microbial consortia for sustaining productivity of non-legume crops: prospects and challenges. Agric. Res., 10: 1-14. doi:10.1007/s40003-020-00522-8.

Cipriano, D. and Capelli, L. 2019. Evolution of electronic noses from research objects to engineered environmental odor monitoring systems: A review of standardization approaches. Biosensors, 9(2): 75. doi:10.3390/bios9020075.

Costa, C., Wironen, M., Racette, K. and Wollenberg, E. K. 2021. Global Warming Potential (GWP): Understanding the implications for mitigating methane emissions in agriculture.

Duan, Y., Awasthi, S. K., Liu, T., Zhang, Z. and Awasthi, M. K. 2019. Evaluation of integrated biochar with bacterial consortium on gaseous emissions mitigation and nutrients sequestration during pig manure composting. Bioresour. Technol., 291: 121880. doi:10.1016/j.biortech.2019.121880.

Eusebio, L., Capelli, L. and Sironi, S. 2016. Electronic nose testing procedure for the definition of minimum performance requirements for environmental odor monitoring. Sensors, 16(9): 1548. doi:10.3390/s16091548.

Fan, F., Xu, R., Wang, D. and Meng, F. 2020. Application of activated sludge for odor control in wastewater treatment plants: Approaches, advances, and outlooks. Water Res., 181: 115915. doi:10.1016/j.watres.2020.115915.

Gautam, M. and Agrawal, M. 2021. Greenhouse gas emissions from municipal solid waste management: A review of the global scenario. Carbon, 11: 123-160. doi:10.1016/B978-0-12-822549-3.00006-4.

Ge, M., Zhou, H., Shen, Y., Meng, H., Li, R., Zhou, J., Cheng, H., Zhang, X., Ding, J., Wang, J. and Wang, J. 2020. Effect of aeration rates on enzymatic activity and bacterial community succession during cattle manure composting. Bioresour. Technol., 304: 122928. doi:10.1016/j.biortech.2020.122928.

Golroudbary, S. R., El Wali, M. and Kraslawski, A. 2019. Environmental sustainability of phosphorus recycling from wastewater, manure, and solid wastes. Sci. Total Environ., 672: 515-524. doi:10.1016/j.scitotenv.2019.03.489.

Halios, C. H., Landeg-Cox, C., Lowther, S. D., Middleton, A., Marczylo, T. and Dimitroulopoulou, S. 2022. Chemicals in European residences–Part I: A review of emissions, concentrations, and health effects of

volatile organic compounds (VOCs). Sci. Total Environ., 839: 156201. doi:10.1016/j.scitotenv.2021.156201.

Hallsworth, J. E. 2022. Water is a preservative of microbes. Microb. Biotechnol., 15(1): 191-214. doi:10.1111/1751-7915.13932.

Hu, J., Zhang, L., Chen, J., Luo, Y., Sun, B. and Chu, G. 2016. Performance and microbial analysis of a biotrickling filter inoculated by a specific bacteria consortium for removal of a simulated mixture of pharmaceutical volatile organic compounds. Chem. Eng. J., 304: 757-765. doi:10.1016/j.cej.2016.06.120.

Jiang, G., Melder, D., Keller, J. and Yuan, Z. 2017. Odor emissions from domestic wastewater: A review. Crit. Rev. Environ. Sci. Technol., 47(17): 1581-1611.

Jonca, J., Pawnuk, M., Arsen, A. and Sówka, I. 2022. Electronic noses and their applications for sensory and analytical measurements in the waste management plants: A review. Sensors, 22(4): 1510.

Kacprzak, M., Malińska, K., Grosser, A., Sobik-Szołtysek, J., Wystalska, K., Dróżdż, D., Jasińska, A. and Meers, E. 2023. Cycles of carbon, nitrogen and phosphorus in poultry manure management technologies–environmental aspects. Crit. Rev. Environ. Sci. Technol., 53(8): 914-938.

Kim, Y. J., Ahmed, S. T. and Islam, M. 2014. Evaluation of Bacillus amyloliquefaciens as manure additive for control of odorous gas emission from pig slurry. Afr. J. Microbiol. Res., 8: 2540-2546. doi:10.5897/AJMR2014.6742

Koniuszewska, I., Korzeniewska, E., Harnisz, M. and Czatzkowska, M. 2020. Intensification of biogas production using various technologies: A review. Int. J. Energy Res., 44(8): 6240-6258.

Kumar, M. A., Sinha, D. and Basheer, S. M. 2022. Biological Treatment of Volatile Organic Compounds (VOCs) and Odorous Compounds. In Biotechnol. Environ. Prot., pp. 131-164.

Leite, A. H. P., da Silva, I. H. A., Pastrana, L., Nascimento, T. P., da Silva Telles, A. M. and Porto, A. L. F. 2022. Purification, biochemical characterization and fibrinolytic potential of proteases produced by bacteria of the genus *Bacillus*: A systematic literature review. Arch. Microbiol., 204(8): 503.

Mahapatra, S., Ali, M. H. and Samal, K. 2022. Assessment of compost maturity-stability indices and recent development of composting bin. Energy Nexus, 6: 100062.

Nowocień, K. and Sokołowska, B. 2022. Bacillus spp. as a new direction in biocontrol and deodorization of organic fertilizers. AIMS Environ. Sci., 9(2).

Ottoboni, M., Pinotti, L., Tretola, M., Giromini, C., Fusi, E., Rebucci, R., Grillo, M., Tassoni, L., Foresta, S., Gastaldello, S., Furlan, V., Maran, C., Dell'Orto, V. and Cheli, F. 2018. Combining E-nose and lateral flow immunoassays (LFIAs) for rapid occurrence/co-occurrence of aflatoxin and fumonisin detection in maize. Toxins (Basel), 10(10): 416. doi:10.3390/toxins10100416

Pacheco, A. R., Moel, M. and Segrè, D. 2019. Costless metabolic secretions as drivers of interspecies interactions in microbial ecosystems. Nat. Commun., 10(1): 103.

Pal, D. B. and Tiwari, A. K. (Eds.). 2023. Sustainable Valorization of Agriculture & Food Waste Biomass: Application in Bioenergy & Useful Chemicals. Springer Nature, Singapore.

Qiu, L., Lok, K. S., Lu, Q., Zhong, H., Guo, X. and Shim, H. 2022. Zinc and copper supplements enhance trichloroethylene removal by *Pseudomonas plecoglossicida* in water. Environ. Technol., 24: 1-12.

Rastogi, M., Nandal, M. and Khosla, B. 2020. Microbes as vital additives for solid waste composting. Heliyon, 6(2): 484.

Rath, P. P., Das, K. and Pattanaik, S. 2022. Microbial activity during composting and plant growth impact: A review. J. Pure Appl. Microbiol., 16(1): 63-73.

Ray, S., Jin, J. O., Choi, I. and Kim, M. 2023. Recent trends of biotechnological production of polyhydroxyalkanoates from C1 carbon sources. Front. Bioeng. Biotechnol., 10: 907500.

Saraga, D. E., Querol, X., Duarte, R. M., Aquilina, N. J., Canha, N., Alvarez, E. G., Jovasevic-Stojanovic, M., Bekö, G., Bycenkienė, S., Kovacevic, R. and Plauškaitė, K. 2023. Source apportionment for indoor air pollution: Current challenges and future directions. Sci. Total Environ., 16: 5744.

Sarkar, P. and Chourasia, R. 2017. Bioconversion of organic solid wastes into biofortified compost using a microbial consortium. Int. J. Recy. Org. Waste Agri., 6: 321-334.

Shou, Z., Zhu, N., Yuan, H., Dai, X. and Shen, Y. 2019. Buffering phosphate mitigates ammonia emission in sewage sludge composting: Enhanced organics removal coupled with microbial ammonium assimilation. J. Clean. Prod., 227: 189-198.

Silva, S., Rodrigues, A. C., Ferraz, A. and Alonso, J. 2017. An integrated approach for efficient energy recovery production from livestock and agro-industrial wastes. Waste Biomass, 16: 339-366.

Wang, J., Zhang, C., Poursat, B. A., de Ridder, D., Smidt, H., van der Wal, A. and Sutton, N. B. 2022. Unraveling the contribution of nitrifying and methanotrophic bacteria to micropollutant co-metabolism in rapid sand filters. J. Hazard. Mater., 424: 127760.

Wijerathna, P. A. K. C., Ekanayake, M. S., Idroos, S. F. and Manage, P. M. 2022. Biological Wastewater Treatment Technology. In Karn, S.K. and Bhambri, A. (Eds.), Microbial Technology and Their Applications, Nova Science Publishers, Y, pp. 293-321. doi:10.52305/JUTX4763

Wijerathna, P. A. K. C., Udayagee, K. P. P., Idroos, F. S. and Manage, P. M. 2023. Waste Biomass Valorization and Its Application in the Environment. In Pal, D.B. and Tiwari, A.K. (Eds.), Sustainable Valorization of Agriculture & Food Waste Biomass Application in Bioenergy & Useful Chemicals, Springer Nature, Singapore, pp. 1-28. doi:10.1007/978-981-99-0526-3_1

Wysocka, I., Gębicki, J. and Namieśnik, J. 2019. Technologies for deodorization of malodorous gases. Environ. Sci. Pollut. Res., 26: 9409-9434.

Yao, X., Shi, Y., Wang, K., Wang, C., He, L., Li, C. and Yao, Z. 2022. Highly efficient degradation of hydrogen sulfide, styrene, and m-xylene in a bio-trickling filter. Sci. Total Environ., 808: 152130.

Zhang, G. and Dong, Y. 2022. Design and application of an efficient cellulose-degrading microbial consortium and carboxymethyl cellulase production optimization. Front. Microbiol., 13: 957444.

Zhao, C., Tian, Z., Yi, J., Shi, Y., Zhu, J., Ji, Z., Chen, S., Kang, Q. and Lu, J. 2022. Characterization and correlation of bacterial community and volatile flavor compounds in Xinjiang, a Chinese traditional fermented condiment. Food Res. Int., 162: 111904.

Nature Environment and Pollution Technology
An International Quarterly Scientific Journal

p-ISSN: 0972-6268
(Print copies up to 2016)
e-ISSN: 2395-3454

Vol. 23 | No. 3 | pp. 1761-1773 | 2024

Original Research Paper

https://doi.org/10.46488/NEPT.2024.v23i03.049

Open Access Journal

# Nephrotoxicity of Cylindrospermopsin (CYN) and Microcystin-LR (MC-LR) on Mammalian Kidney: Wistar Rat as a Model Assessment

**H.A.S.N. Abeysiri*(**), J.K.P. Wanigasuriya***, T.S. Suresh****, D.H. Beneragama***** and P.M. Manage*†**

*Centre for Water Quality and Algae Research, Department of Zoology, University of Sri Jayewardenepura, Sri Lanka
**Faculty of Graduate Studies, University of Sri Jayewardenepura, Sri Lanka
***Centre for Kidney Research, Department of Medicine, Faculty of Medical Sciences, University of Sri Jayewardenepura, Sri Lanka
****Department of Biochemistry, Faculty of Medical Sciences, University of Sri Jayewardenepura, Sri Lanka
*****Department of Pathology, Faculty of Medical Sciences, University of Sri Jayewardenepura, Sri Lanka
†Corresponding author: Pathmalal M. Manage; pathmalal@sjp.ac.lk

**Nat. Env. & Poll. Tech.**
**Website: www.neptjournal.com**

*Received:* 17-11-2023
*Revised:* 12-01-2024
*Accepted:* 15-01-2024

**Key Words:**
Cylindrospermopsin
Microcystin-LR
Kidney injury molecule-1
Serum and urine creatinine
Wistar rats

## ABSTRACT

Naturally derived cyanotoxins, cylindrospermopsin (CYN), and microcystin-LR (MC-LR) have shown hepatotoxic and nephrotoxic effects in several studies. The present study aimed to determine the possible nephrotoxicity of MC-LR and CYN on mammalian kidneys using male Wistar rats as an animal model. Potential nephrotoxicity was evaluated at different doses of CYN (0.175 $\mu g.kg^{-1}$, 0.140 $\mu g.kg^{-1}$, 0.105 $\mu g.kg^{-1}$) and MC-LR (0.105 $\mu g.kg^{-1}$, 0.070 $\mu g.kg^{-1}$, 0.035 $\mu g.kg^{-1}$) was observed. Water samples from dug wells contaminated with CYN (0.161 $\mu g.kg^{-1}$) and MC-LR (0.091 $\mu g.kg^{-1}$) from the Padaviya area in Anuradhapura, Sri Lanka were used as environmental samples. The control groups were treated with distilled water. The exposure time of rats to the toxin was 90 days. Evaluation of urinary creatinine, serum creatinine, and Kidney Injury Molecule-1 (KIM-1) were estimated using standard protocols. A significant increase in serum creatinine levels was observed in all CYN and MC-LR treated groups ($p<0.05$) after 7 and 42 days of exposure, respectively, compared to control. It was found a decrease of urine creatinine when rats were treated with different concentrations of CYN and MC-LR ($p<0.05$) after 7 days compared to the control. The highest KIM-1 concentrations were recorded at 0.175 $\mu g.kg^{-1}$ of CYN and 0.105 $\mu g.kg^{-1}$ of MC-LR. The concentrations of KIM-1 in the control groups for CYN-treated and MC-LR-treated were not detected. Luminal protein, nuclear pyknosis, mild tubular epithelial swelling, vascular congestion, and interstitial inflammation in CYN and MC-LR treated groups were common. No predominant changes were observed in the control groups treated with CYN and MC-LR. The results of the present study confirm that the consumption of CYN and MC-LR-contaminated water may lead to kidney injury in Wistar rats.

## INTRODUCTION

Cyanotoxins can accumulate in aquatic wildlife and enter the food chain (Lance et al. 2007), resulting in the risk of human and livestock poisoning. Among different cyanotoxins, cylindrospermopsin (CYN) and Microcystins (MCs) are the most dominant and toxic in the aquatic environment (Sethunga & Manage 2010, Wijewickrama & Manage 2019). MCs and CYN have heat-stable chemical structures and cannot be removed even when heated at 100°C (Lawton et al. 2011, Manage 2019). MC-LR is the most dominant and toxic MC variant among over 100 MC congeners: MC-LR, -RR, -LW, -YR, -LA, etc. (Du et al. 2019). The endotoxin CYN is another commonly found hydrophilic alkaloid with a stable chemical structure. Colonial cyanobacteria produce MC-LR; *Microcystis* spp., *Planktothrix*, and the filamentous *Anabaena, Gloeotrichia, Nodularia, Oscillatoria,* and *Nostoc* sp. whereas CYN is produced by non-bloom-forming cyanobacteria *Cylindrospemospis raciborskii*, *Raphidiopsis curvata, Lyngbya whole, Umezakia natans, Anabaena bergii, Aphanizomenon flos-aquae, Aphanizomenon ovalisporum, Anabaena lapponica* (Foss & Aubel 2013). Considering the toxic nature and the influence of toxicity on human health, the World Health Organization (WHO) established a provisional limit of 1 $\mu g.L^{-1}$ for MC-LR and 2 $\mu g.L^{-1}$ for CYN in drinking water (WHO 2003). Further Tolerable Daily Intake (TDI) for humans was established as 0.04 $\mu g.kg^{-1}$ of body weight/day for MC-LR (Do Carmo Bittencourt-Oliveira et al. 2016) and 0.02 $\mu g.kg^{-1}$ of body weight/day for CYN (Guzmán-Guillén et al. 2014).

MCs are generally considered hepatotoxins. Several studies have shown MC-LR convinced hepatotoxicity by inhibiting protein phosphatase 1 and 2A (PP1 and PP2A) and inducing the production of reactive oxygen species (ROS), followed by destroying the cell cytoskeleton, which eventually leads to liver cell necrosis and apoptosis (Clark et al. 2007). In recent times, MCs have been shown to penetrate renal cells in organic anion-transporting polypeptides (OATPs) dependent manner, subsequently promoting the accumulation of MC-LR (Jia et al. 2014). Therefore, exposure to MCs may cause toxicity in the kidney (Menezes et al. 2013). Exposure to MC-LR could induce apoptosis in both human embryonic kidney (HEK-293) and human kidney adenocarcinoma (ACHN) cell lines by decreasing the G2/M phase population (Piyathilaka et al. 2015).

CYN has become a public health concern following reports of "mysterious disease" events on Palm Island, Australia (Chernoff et al. 2018). CYN is a 415 Da alkaloid, stable over large ranges of pH and temperatures. Single-dose intraperitoneal administration of 0.2 mg CYN.kg$^{-1}$ bw revealed that the renal excretory pathway plays a major role and is responsible for 65.2% of the dose excretion (Moraes & Magalhães 2018). Chernoff et al. (2018) revealed that intraperitoneal administered CYN in mice affects intense membrane proliferation in convoluted proximal tubule cells. Necrotic cells and cytoplasmic fat droplets have been reported in both the proximal and distal tubules. Renal toxicity was well-defined following the treatment of male Swiss mice with toxic cellular extracts following both single oral dose and intraperitoneal administrations; the effects contained large cytoplasmic vacuoles and proximal apical vesicles and the distal tubule clog with proteinaceous material (Moraes & Magalhães 2018). Other studies used single oral dose exposure of toxic cellular extracts to confirm intense cytoplasmic vacuolization and increased lumen and protein contents in the proximal tubular cells (Chernoff et al. 2018).

MCs (MC-LR) and CYN are being hypothesized as one of the risk factors for Chronic Kidney Disease of unknown etiology (CKDu) in Sri Lanka (Abeysiri et al. 2018a, Abeysiri et al. 2018b, Manage, 2019, Piyathilaka et al. 2015). The highest prevalence of CKDu is reported in the North Central Province of Sri Lanka and emerging in the Uva, Eastern, and North Western Provinces (Chandrajith et al. 2011). The disease is unrelated to conventional risk factors of chronic kidney disease (CKD), and the pathology is consistent with tubule-interstitial nephritis (Wijethunga et al. 2015). The impact of cyanotoxins on kidneys has become a research interest as cyanobacteria were found in 75% of freshwater bodies tested in CKDu highly prevalent areas (Manage 2019). Studies have further demonstrated that surface and dug well water in CKDu endemic areas used for drinking and irrigation has a significant relationship between the cell density of cyanobacteria and cyanotoxins (Abeysiri et al. 2018a). These findings favor the hypothesis that cyanotoxin-induced nephrotoxicity is one of the possible explanations for CKDu prevalence (Abeysiri et al. 2018a, 2019b, 2019a, Manage 2019). The objective of this study was to determine the possible effects of CYN and MC-LR on mammalian kidneys using male Wistar rats as the animal model.

## MATERIALS AND METHODS

### Animals

Eight-week-old male Wistar rats were purchased from the Medical Research Institute (MRI), Sri Lanka. Animals were acclimatized for one week and maintained in the Animal House, Faculty of Medical Sciences, the University of Sri Jayewardenepura, on a 12h: 12h light-dark cycle at 28 ± 2°C. Food and water were available ad libitum. Ethics approval was obtained from the Ethics Review Committee of the Faculty of Medical Sciences (No.17/18, ERC, FMS, USJ), University of Sri Jayewardenepura.

### Experimental Design for CYN and MC-LR Chronic Exposure Study

In the present study, two experiments were conducted to evaluate the nephrotoxicity of the cyanotoxins CYN and MC-LR. For each experiment, thirty-five rats were divided into five experimental groups. One set of groups was for CYN, with the following dosages: HW-0.175 μg.kg$^{-1}$, W-0.140 μg.kg$^{-1}$, LW-0.105 μg.kg$^{-1}$, EN-0.161 μg.kg$^{-1}$, and a control group. Another set of thirty-five rats was divided into five experimental groups for MC-LR, with dosages of HW-0.105 μg.kg$^{-1}$, W-0.070 μg.kg$^{-1}$, LW-0.035 μg.kg$^{-1}$, EN-0.091 μg.kg$^{-1}$, and a control group and each group comprised seven rats. In the CYN exposure study, rats were treated at 0.175 μg.kg$^{-1}$, 0.140 μg.kg$^{-1}$, and 0.105 μg.kg$^{-1}$, respectively. CYN-contaminated water was orally administered to individual rats for oral feeding using a Sondi needle during the study period of 90 days. The environmental exposure (EN) group received environmental water samples contaminated with CYN (0.161 μg.kg$^{-1}$) obtained from a randomly selected well in Padaviya.

For the MC-LR exposure study, rats received the toxin as 0.105 μg.kg$^{-1}$, 0.070 μg.kg$^{-1}$, and 0.035 μg.kg$^{-1}$. MC-LR contaminated water was orally administered to individual rats for oral feeding using a Sondi needle during the study period of 90 days. The Environmental exposure (EN) group received an environmental water sample contaminated with MC-LR (0.091 μg.kg$^{-1}$) obtained from a randomly selected well in Padaviya.

Finally, the absolute and relative weights of the left and right kidneys were calculated. Relative weight was calculated using the following equation.

Relative weight (%) = (Organ weight/Body weight) × 100

### Blood Collection

The venous blood samples were collected from the lateral tail veins of each rat at 0, 7, 14, 28, 42, and 60 days. Blood was transferred to 1.5 mL Eppendorf tubes and centrifuged at 13,000 rpm for 10 min. to separate the serum. The serum was stored at -80°C. At the end of the experiment (90 days), rats were anesthetized, and blood was collected by direct heart puncture for both chemical analyses (Karp et al. 2023).

### Urine Collection and Analysis

Urine was collected from each rat at 0, 7, 14, 28, 42, 60, and 90 days using the metabolic cages and stored at -80°C (Wajda et al. 2020). Kidney Injury Molecule-1 (KIM-1) in urine was analyzed weekly using Elabscience diagnostic kits. This kit recognized Rat KIM-1 in samples. No significant cross-reactivity or interference between Rat KIM-1 and analogs was observed (Sensitivity: 18.75 $pg.mL^{-1}$, Detection range: 31.25-2000 $pg.mL^{-1}$, Repeatability: Coefficient of variation is < 10%).

Serum creatinine and urine creatinine were analyzed using Bialabo diagnostic kits (France) and a fully automated analyzer (Thermo Fisher Scientific, INDIKO, Finland).

### Histopathological Evaluation

Each rat was sacrificed after 90 days, and both kidneys of each rat were bi-valved and then placed in 10% formalin for fixation. The fixed kidneys were paraffin-embedded, sectioned at 5 µm, and stained with hematoxylin and eosin. The prepared sections were examined under the light microscope (Olympus CX31, magnification ×40 ×100 and ×400) for any histological changes. After an initial review, selected tissues were re-evaluated.

### Statistical Evaluation

The data was expressed as the mean ± standard deviation (SD). All statistical analyses were carried out via MINITAB version 17 statistical software (MINITAB, State College, PA, USA). One-way ANOVA was used to analyze the difference between groups, and differences were considered significant if $p < 0.05$.

## RESULTS AND DISCUSSION

### Clinical Findings

The physical appearance of CYN-treated and MC-LR-treated animals did not differ from controls, and no signs of toxic effects were observed throughout the study.

Increment of mean body weight in CYN treated and a control group of animals was recorded until the fourteenth week; afterward, body weight was comparable to the control group with an increment of weight (Fig. 1a). A decrease in body weights of rats treated with 0.175 $\mu g.kg^{-1}$, 0.140 $\mu g.kg^{-1}$, and 0.161 $\mu g.kg^{-1}$ concentrations of CYN, compared to the control group, was found at 12, 13, and 14 weeks ($p > 0.05$). The mean body weight of MC-LR treated and control groups increased until the twelfth week and after that decreased (Fig. 1b). A decreasing trend in body weight across doses was recorded when rats received 0.105 $\mu g.kg^{-1}$ and 0.091 $\mu g.kg^{-1}$ concentrations of MC-LR which were lower than controls at 13 and 14 weeks of exposure (Fig. 1b). Increment of body weight with low CYN doses (30 and 60 $\mu g.kg^{-1}.day^{-1}$) and decrease of body weight at high CYN (432 and 657 $\mu g.kg^{-1}.day^{-1}$) in mice study was recorded by Humpage and Falconer (2003). The gradual increase of mean body weights of the Wister rat model with oral administration of toxic *M. aeruginosa* (PCC 7820) was recorded up to the $10^{th}$ week treatment, and after that decline of body weight was recorded by Manage et al. (2009) as well. A significant reduction of mean body weight following the MC-LR treated rat group ($p<0.05$) was recorded by Milutinović et al. (2003). The hardening of the glomeruli is often a feature of CKDu, which leads to a reduction in kidney size as the disease progresses. CYN is known to affect both hepatic and renal systems (Bazin et al. 2012), and some studies have confirmed hepatotoxicity (Lone et al. 2015), gastrointestinal toxicity (Wu et al. 2018), neurotoxicity (Wu et al. 2018), and reproductive toxicity (Lone et al. 2015) of MC-LR. However, the studies on nephrotoxicity induced by prolonged oral exposure to MC-LR and CYN are limited.

The absolute and relative weights of the right and left kidneys of CYN and MC-LR-treated rats were less than the control, and the difference was statistically significant ($p < 0.05$) in 0.175 $\mu g.kg^{-1}$ and 0.161 $\mu g.kg^{-1}$ of CYN-treated rats. The reduction of relative weight differed significantly in 0.105 $\mu g.kg^{-1}$ and 0.091 $\mu g.kg^{-1}$ of MC-LR treated rats, and the reduction of absolute weight significantly differed from only the 0.091 $\mu g.kg^{-1}$ MC-LR treated group ($p < 0.05$) (Table 1).

Chernoff et al. (2018) showed significant dose-related increases ($p < 0.05$) in absolute and relative weights of kidneys in male mice, and Manage et al. (2009) reported the mean absolute weight of kidneys among MC-LR treated animals was not statistically significant ($p < 0.33$) and relative weights of kidneys did not differ significantly. The weight loss of kidneys is a common cause of acute kidney

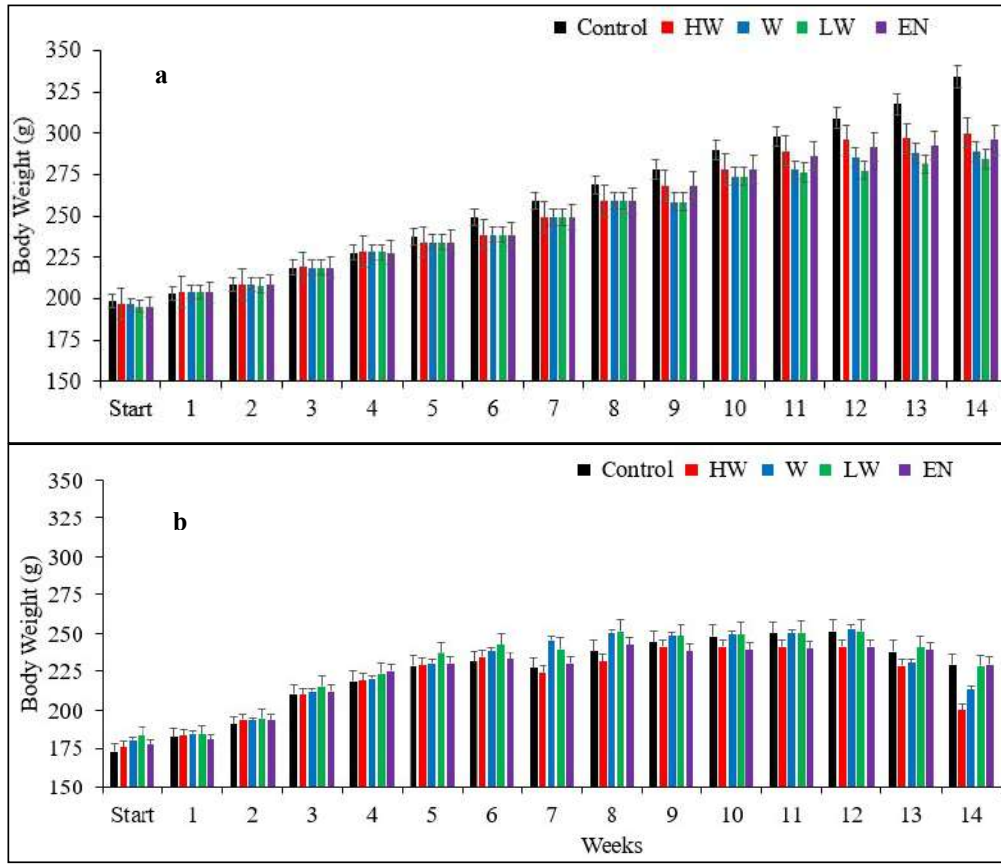


Fig. 1: Mean body weight changes of Wistar rats in different CYN doses (a) (HW; 0.175 µg.kg$^{-1}$, W; 0.140 µg.kg$^{-1}$, LW; 0.105 µg.kg$^{-1}$, EN; 0.161 µg.kg$^{-1}$ and MC-LR treatments) (b) (HW; 0.105 µg.kg$^{-1}$, W; 0.070 µg.kg$^{-1}$, LW; 0.035 µg.kg$^{-1}$, EN; 0.091 µg.kg$^{-1}$).

Table 1: Absolute weight (g) and relative percentage of right and left kidneys of male Wistar rats exposed to oral administration of different doses of CYN and MC-LR for 90 days.

| Body/Kidney weight [g]/% | CYN Exposure | | | | | MC-LR Exposure | | | | |
|---|---|---|---|---|---|---|---|---|---|---|
| | Control | Pure CYN Dose [ µg.kg$^{-1}$] | | | CYN Environmental dose [ µg.kg$^{-1}$] | Control | Pure MC-LR Dose [ µg.kg$^{-1}$] | | | MC-LR Environmental dose [ µg.kg$^{-1}$] |
| | 0 | 0.105 | 0.140 | 0.175 | 0.161 | 0 | 0.035 | 0.070 | 0.105 | 0.091 |
| Absolute weight (g) of Right Kidney | 0.84 ± 0.08 | 0.76 ± 0.03 | 0.75 ±0.06 | 0.73 * ±0.04 | 0.74 * ±0.04 | 0.63 ±0.08 | 0.51 ±0.04 | 0.54 ±0.06 | 0.52 ±0.03 | 0.46 * ±0.03 |
| Absolute weight (g) of Left Kidney | 0.81 ± 0.09 | 0.79 ± 0.06 | 0.77 ±0.06 | 0.72 * ±0.04 | 0.72 * ±0.05 | 0.59 ±0.07 | 0.51 ±0.04 | 0.54 ±0.04 | 0.53 ±0.03 | 0.47 * ±0.04 |
| % Right Kidney | 0.25 ± 0.01 | 0.23 ± 0.03 | 0.21 ±0.06 | 0.20 * ±0.04 | 0.18 * ±0.04 | 0.29 ±0.01 | 0.23 ±0.03 | 0.21 ±0.06 | 0.20* ±0.04 | 0.18 * ±0.04 |
| % Left Kidney | 0.24 ± 0.02 | 0.22 ± 0.06 | 0.21 ±0.06 | 0.19 * ±0.04 | 0.1 8* ±0.05 | 0.24 ±0.02 | 0.22 ±0.06 | 0.21 ±0.06 | 0.19* ±0.04 | 0.1 8* ±0.05 |

* $p < 0.05$

injury and is often reversible. It can be caused by severe nephrotoxic drugs or contrast agents used in imaging. The serum creatinine values showed a significant increment after 7 days of exposure in all CYN-treated groups: 0.175 µg.kg$^{-1}$, 0.140 µg.kg$^{-1}$, and 0.161 µg.kg$^{-1}$ compared to the control ($p < 0.05$) (Fig. 2a).

In MC-LR treated groups, a significant increase of serum creatinine was not found until 42 days of exposure,

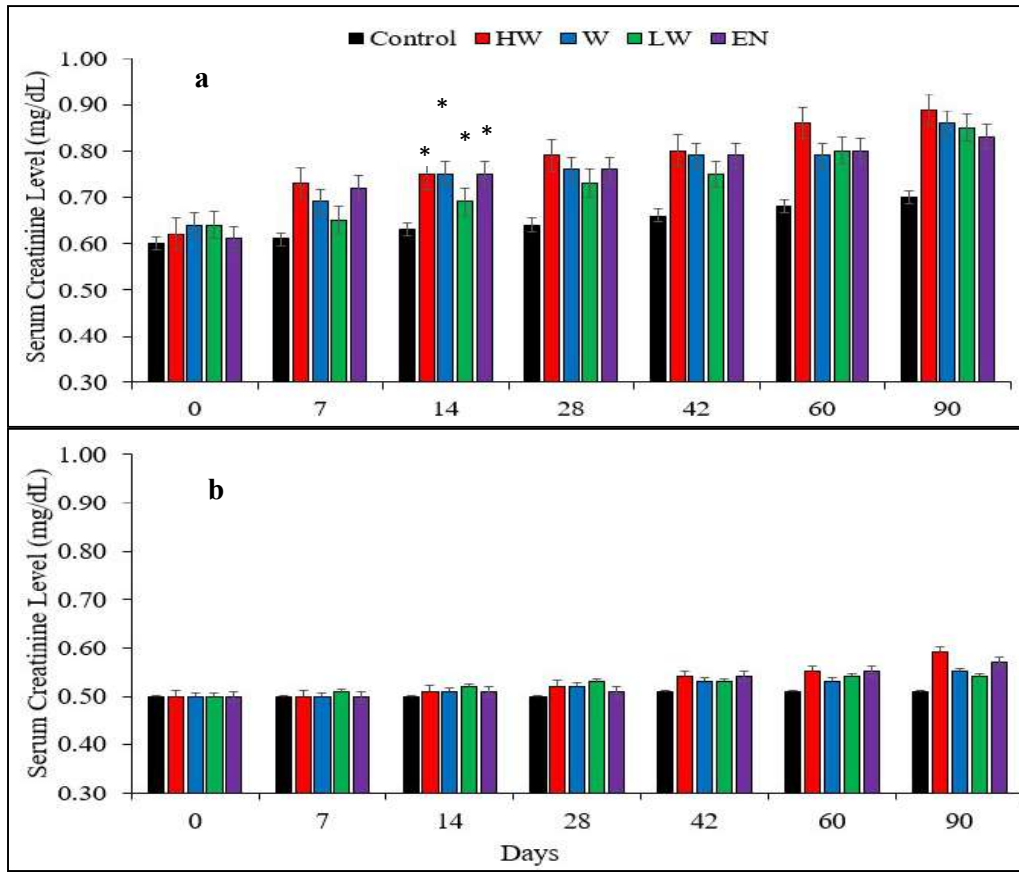


Fig. 2: Mean serum creatinine levels of Wistar rat groups treated with different CYN (a) (HW; 0.175 μg.kg$^{-1}$, W; 0.140 μg.kg$^{-1}$, LW; 0.105 μg.kg$^{-1}$, EN; 0.161 μg.kg$^{-1}$) and MC-LR (b) (HW; 0.105 μg.kg$^{-1}$, W; 0.070 μg.kg$^{-1}$, LW; 0.035 μg.kg$^{-1}$, EN; 0.091 μg.kg$^{-1}$) concentrations.

and after that significant increment of the serum creatinine was detected for different MC-LR concentrations ($p < 0.05$) compared to the control group (Fig. 2b).

The present data specified a significant decrease of urine-creatinine in rats after 7 days of exposure to all concentrations of CYN compared to the control ($p < 0.05$; Fig. 3a). Also, was found a decrease in urine creatinine when rats were treated with different concentrations of MC-LR (0.105 μg.kg$^{-1}$, 0.070 μg.kg$^{-1}$, 0.035 μg.kg$^{-1,}$ and 0.091 μg.kg$^{-1}$ (Fig. 3b).

The highest serum-creatinine in rats treated with CYN concentration 0.175 μg.kg$^{-1}$ ($p < 0.05$), following 0.140 μg.kg$^{-1}$ ($p < 0.05$) and 0.105 μg.kg$^{-1}$ was found. Rats exposed to the 0.161 μg.kg$^{-1}$ showed a significant increment of serum-creatinine ($p<0.05$), lower than the rats that received the high dose of CYN in the study. Decrease in urine creatinine levels in the 0.175 μg.kg$^{-1}$, 0.140 μg.kg$^{-1}$, and 0.105 μg.kg$^{-1}$ were found, and the rats exposed to 0.161 μg.kg$^{-1}$ concentration of CYN in the experiment compared to the control. Significant increment of the serum creatinine levels in rats treated with different concentrations of MC-LR was found following the descending order from 0.105 μg.kg$^{-1}$ ($p<0.05$), 0.070 μg.kg$^{-1}$ ($p<0.05$), and 0.035 μg.kg$^{-1}$ ($p<0.05$), respectively. Similar to the CYN exposure, the second-highest serum creatinine was recorded in rats exposed to 0.161 μg.kg$^{-1}$ ($p < 0.05$). Decreases in urine creatinine levels in the MC-LR treated rat groups were followed by 0.105 μg.kg$^{-1}$, 0.091 μg.kg$^{-1}$, 0.070 μg.kg$^{-1}$, and 0.035 μg.kg$^{-1}$, respectively to the control was detected.

In general, an increase in serum creatinine and a decrease in urine creatinine indicate renal damage (Hsu et al. 2020). Rises of the serum creatinine are a significant marker of renal function, which correlated to renal dysfunction (Do Amaral et al. 2008). Yi et al. (2019) recorded no significant changes in the serum creatinine levels in mice treated with MC-LR at different concentrations (1, 30, 60, 90, and 120 μg.L$^{-1}$) from 3 and 6 months and Chernoff et al. (2018) recorded no significant alterations in the serum creatinine levels in the mice given CYN at 3 months at different dose levels 0, 75, 150 and 300 μg.kg$^{-1}$.d$^{-1}$. However, in the present study, the mean serum creatinine level was raised with a reduction

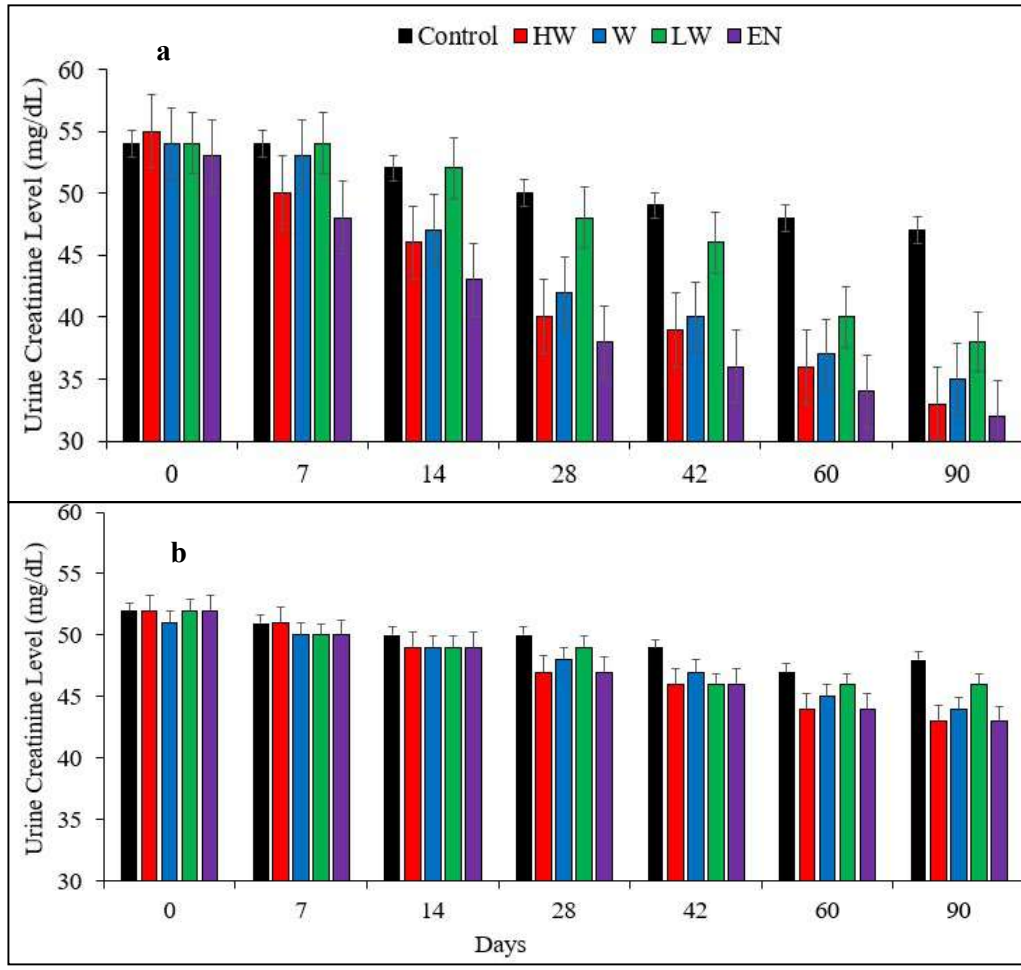


Fig. 3: Mean Urine creatinine levels of Wistar rat groups treated with different CYN (**a**) (HW; 0.175 µg.kg$^{-1}$, W; 0.140 µg.kg$^{-1}$, LW; 0.105 µg.kg$^{-1}$, EN; 0.161 µg.kg$^{-1}$) and MC-LR (b) (HW; 0.105 µg.kg$^{-1}$, W; 0.070 µg.kg$^{-1}$, LW; 0.035 µg.kg$^{-1}$, EN; 0.091 µg.kg$^{-1}$) concentrations.

of urine creatinine levels in the different CYN and MC-LR exposure groups of rats, indicating nephrotoxic injury. When the renal function ~~is~~ normal, these small creatinine molecules are filtered from the glomerulus. However, when the filtering ability of the glomerulus decreases, the concentration of serum creatinine increases. This rise in serum creatinine levels could often be used as an indicator of kidney dysfunction (Chernoff et al. 2011). Reduction of urine creatinine was found in the present study also noted in CYN and MC-LR exposure groups of rats, indicating possible renal injury.

Increment of urinary KIM-1 level was found in CYN-treated rats following descending order from 0.175 µg.kg$^{-1}$ (35.4 ± 2.3-1328.4 ± 32.1 Pg.mL$^{-1}$), 0.140 µg.kg$^{-1}$ (34.5 ± 2.3-985.3 ± 14.1 Pg.mL$^{-1}$) and 0.105 µg.kg$^{-1}$ (35.2 ± 1.6-456.3 ± 11.6 Pg.mL$^{-1}$) respectively. Further, it was found 0.161 µg.kg$^{-1}$ exposure rat group reported higher KIM-1 level (36.3±0.9-1134.2±11.4 Pg.mL$^{-1}$) than the W and LW dose exposures comparable to the control from weeks 2 to 8 (Fig. 4a). A similar descending pattern of the urinary KIM-1 level was found in MC-LR treated rat groups 0.105 µg.kg$^{-1}$ (275.1±21.2-1562.1±22.4 Pg.mL$^{-1}$), 0.070 µg.kg$^{-1}$ (164.2±12.3-987.1±15.4 Pg.mL$^{-1}$), 0.035 µg.kg$^{-1}$ (117.2±9.6-993.7±16.3 Pg.mL$^{-1}$) and high KIM-1 level recorded for 0.091 µg.kg$^{-1}$ (217.1±16.8-1328.2±18.3 Pg.mL$^{-1}$) than the 0.070 µg.kg$^{-1}$ and 0.035 µg.kg$^{-1}$ dose exposures compare to control from 4 to 8 weeks of exposure (Fig. 4b).

CYN-treated groups at two weeks and MC-LR-treated groups at four weeks showed an increasing level of KIM-1. This was found during 2-8 weeks with the treatment of 0.175 **µg**.kg$^{-1}$ and 0.161 µg.kg$^{-1}$, and the delayed effect was found during 3-8 weeks when animal exposure to 0.140 µg.kg$^{-1}$ and 0.105 µg.kg$^{-1}$ of CYN in drinking water. For the MC-LR study, descending order of KIM-1 was found following

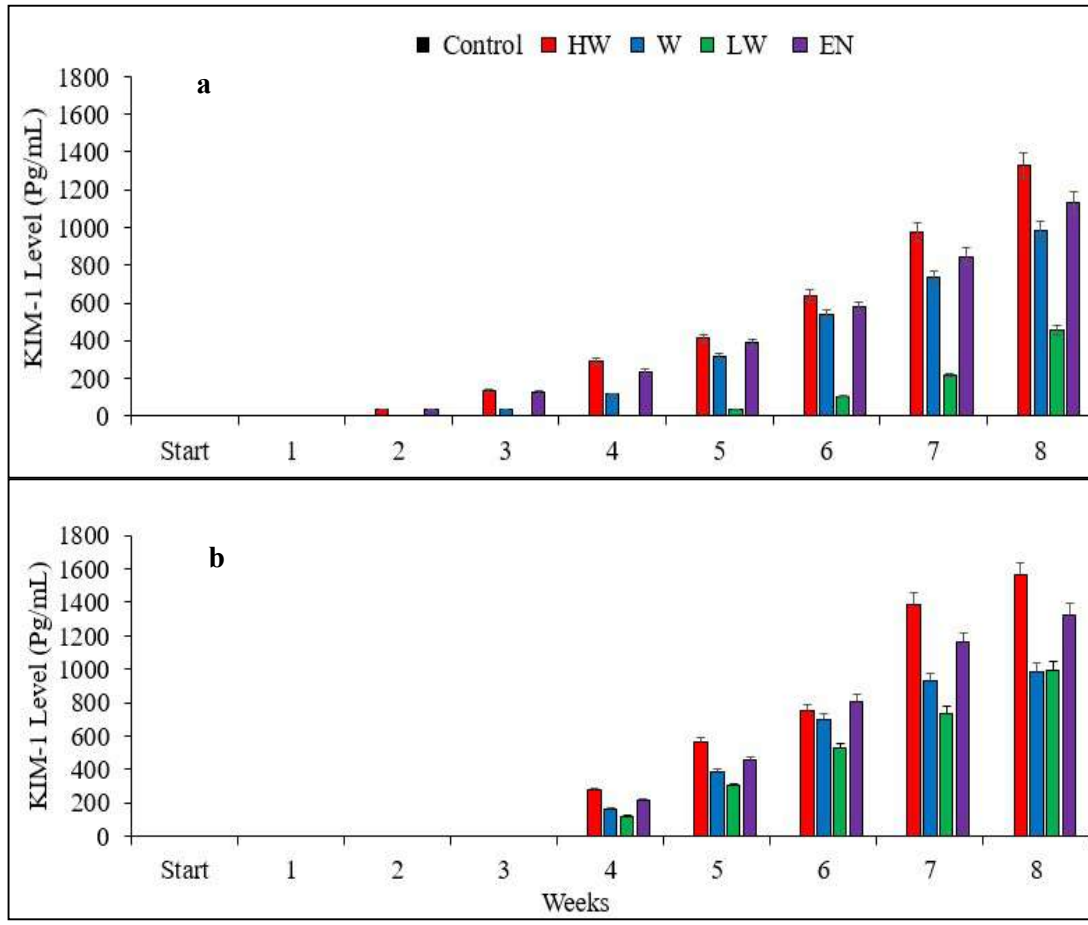


Fig. 4: Mean KIM-1 levels of Wistar rats treated with different concentrations of CYN (a) (HW; 0.175 µg.kg$^{-1}$, W; 0.140 µg.kg$^{-1}$, LW; 0.105 µg.kg$^{-1}$, EN; 0.161 µg.kg$^{-1}$ and MC-LR (b) (HW; 0.105 µg.kg$^{-1}$, W; 0.070 µg.kg$^{-1}$, LW; 0.035 µg.kg$^{-1}$, EN; 0.091 µg.kg$^{-1}$).

exposure of 0.105 µg.kg$^{-1}$, 0.091 µg.kg$^{-1}$, 0.070 µg.kg$^{-1}$, and 0.035 µg.kg$^{-1}$ during 4-8 weeks.

High concentrations of urinary KIM-1, which is an indication of proximal convoluted tubular damage were reported from individuals with early stages of CKDu (De Silva et al. 2016). Our study showed increased levels of KIM-1 in the second week of CYN treatment and the fourth week of the MC-LR treatment compared to the control group, indicating early renal tubular damage. Up-regulation of KIM-1 is well-known to occur in proximal tubule damage of the nephron. Increased levels of KIM-1 may also signify its involvement in phagocytosis of damage to the proximal tubule epithelial cells by converting epithelial cells into semi-professional phagocytes (Bonventre et al. 2010, Ichimura et al. 2008). KIM-1 up-regulation may be responsible for restoring the functional and morphological integrity of kidneys as well (Waanders et al. 2010).

## Histopathology

Significant histopathological changes in the 0.175 µg.kg$^{-1}$ group included mild nuclear pyknosis (Fig. 5b), moderate pigmentation (Fig. 5c), severe cellular swelling and moderate luminal protein (Fig. 5d), and severe glomerular collapse (Fig. 5e). Severe cellular swelling and inflammation (Fig. 6b), severe tubular epithelial swelling and moderate vascular congestion (Fig. 6c) were significant in 0.161 µg.kg$^{-1}$ group. Further, it was observed that mild cellular swelling of renal tubules (Fig. 7b, Fig. 8b) in rats exposed to the WHO-recommended dose of CYN and lowered to 0.140 **µg**.kg$^{-1}$ of CYN well.

The predominant lesions were observed in the outer medulla, and cortical tubular changes in rat groups exposed to different concentrations of MC-LR: 0.105 µg.kg$^{-1}$, 0.070 µg.kg$^{-1}$, 0.035 µg.kg$^{-1}$, 0.091 µg.kg$^{-1}$. Significant renal changes in the 0.105 µg.kg$^{-1}$ exposure group included

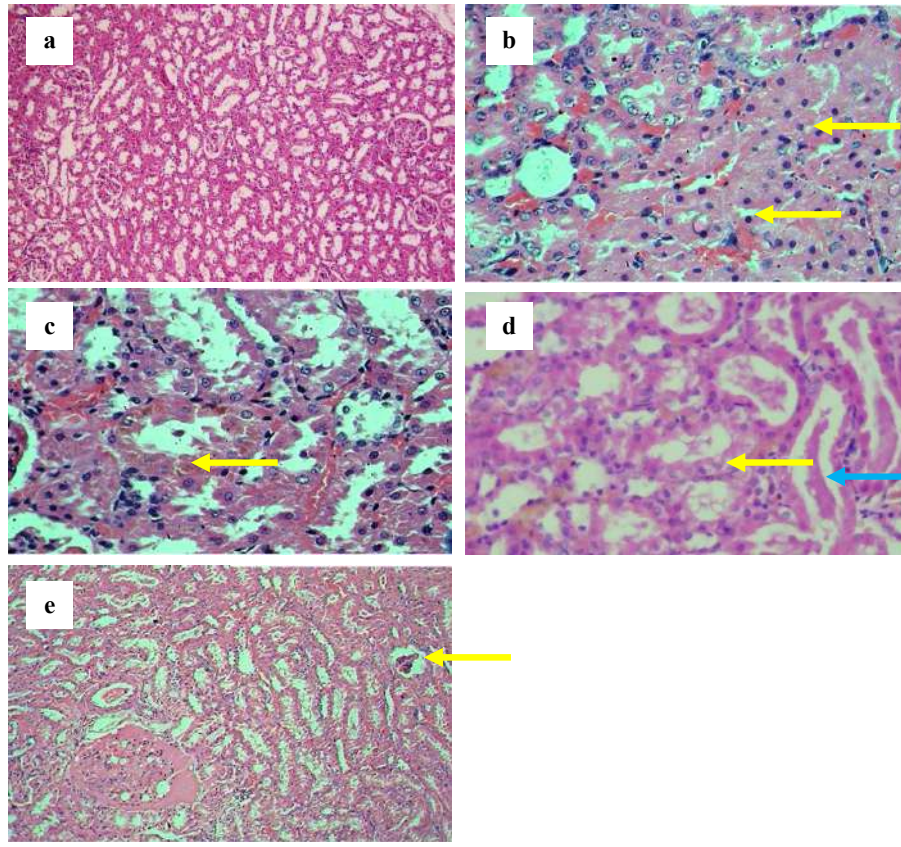


Fig. 5: Haematoxylin and eosin stain of Histopathological features in kidney sections after 90 days of exposure to 0.175 µg.kg-1 of CYN Fig. 5a Control ×100, Fig. 5b 0.175 µg.kg-1 of CYN – Nuclear pyknosis (yellow arrows) ×400, Fig. 5c Pigmentation – Tubular cells (yellow arrow) ×400, Fig. 5d Cellular swelling (yellow arrow) with luminal protein (blue arrow) ×400, Fig. 5e Glomerular collapse (yellow arrow) ×100 .

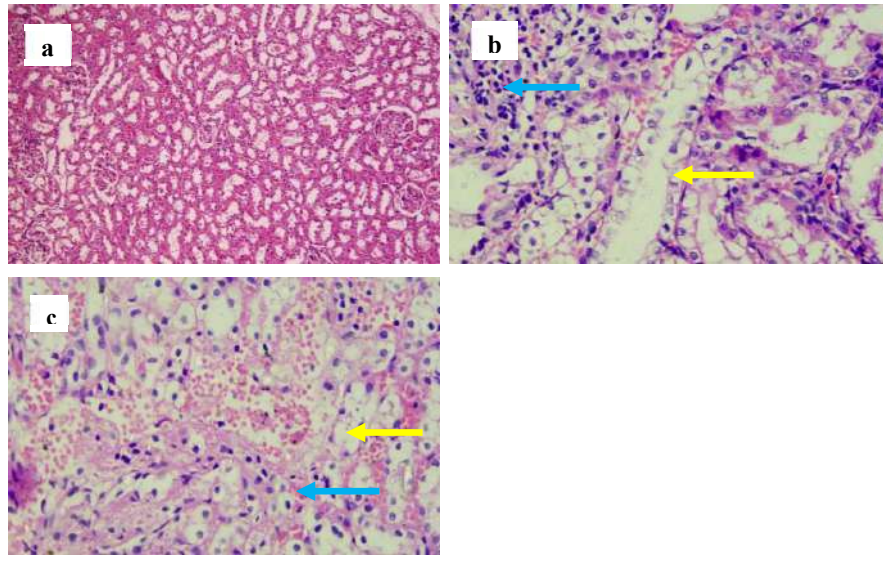


Fig. 6: Haematoxylin and eosin stains of Histopathological features in kidney sections after 90 days of exposure to CYN at 0.161 µg.kg$^{-1}$**.** Fig. 6a Control ×100, Fig. 6b 0.161 µg.kg$^{-1}$ – Cellular swelling (yellow arrow) and inflammation (blue arrow) ×400, Fig. 6c CYN at 0.161 µg.kg$^{-1}$ - Tubular epithelial swelling (yellow arrow) and vascular congestion (blue arrow) ×400.

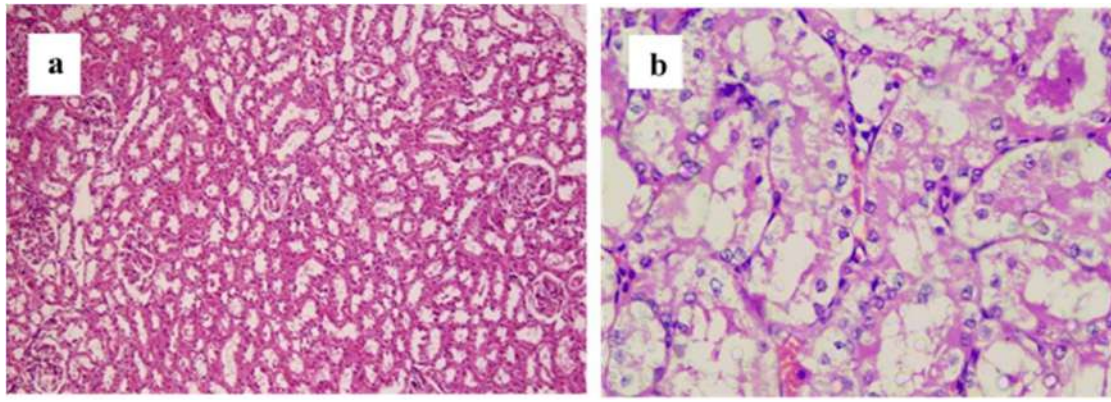


Fig. 7: Haematoxylin and eosin stains of histopathological features in kidney sections after 90 days of exposure to the CYN at 0.140 μg.kg$^{-1}$. Fig. 7a Control ×100, Fig. 7b CYN at 0.140 μg.kg$^{-1}$ – Cellular swelling of renal tubules (yellow arrow) ×400.

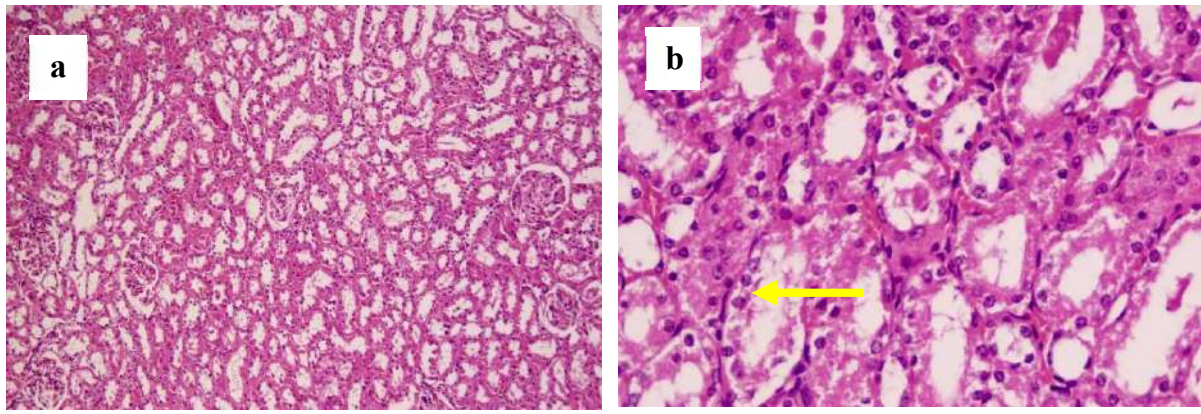


Fig. 8: Haematoxylin and eosin stains of histopathological features in kidney sections after 90 days of exposure to CYN at 0.105 μg.kg$^{-1}$. Fig. 8a Control ×100, Fig. 8b CYN at 0.105 μg.kg$^{-1}$ – Cellular swelling of renal tubules (yellow arrow) ×400.

luminal protein (Fig. 9b), tubular epithelial swelling (Fig. 9c), vascular congestion (Fig. 9e), and mild interstitial inflammation (Fig. 9d). Mild tubular epithelial swelling (Fig. 10b) and luminal proteins (Fig. 10c) were observed to be significant in 0.091 μg.kg$^{-1}$ exposure group. Mild cellular swelling (Fig. 11b) and luminal proteins (Fig. 11c) were significant in the 0.070 μg.kg$^{-1}$ exposure group. Mild epithelial swelling (Fig. 12b) was significant in the 0.035 μg.kg$^{-1}$ exposure group.

The predominant changes observed histologically were confined to the renal tubules in both CYN and MC-LR exposed groups. Luminal proteins, nuclear pyknosis, cellular swelling, luminal protein, pigmentation, vascular congestion, and interstitial inflammation were mild to severe records in 0.175 μg.kg$^{-1}$ and 0.161 μg.kg$^{-1}$ doses of CYN-treated groups. Since the tubular epithelium plays a critical role in homeostasis, damage to tubules is expected to impair renal functions (Liu et al. 2018). Further, the mild pyknotic nuclei that occurred in cortex tubules may indicate an early stage of renal damage in 0.175 μg.kg$^{-1}$ doses of CYN-treated groups. The histological changes in the current study confirm cyanotoxin-induced renal damage due to tubular pathology, and the changes were most marked in the group fed with a higher dose than the 0.140 μg.kg$^{-1}$ and 0.161 μg.kg$^{-1}$ group.

Although CYN is often defined as a hepato-toxin, Chernoff et al. (2018) described that the kidney was the most sensitive organ for CYN exposure in male mice. Chernoff et al. (2018) investigated CYN-initiated dose-dependent renal toxicity in both cortex and medulla. An increase in lesions in cortical tubules with increasing concentration of CYN was recorded in the study. In the renal cortex, microscopic changes in this region consisted of epithelial cytoplasmic alterations, including epithelia swelling and intraluminal protein. Thus, the results of the present study support the findings and agreement presented by Humpage & Falconer (2003).

The presence of mild luminal protein, tubular epithelial swelling, vascular congestion and interstitial inflammation

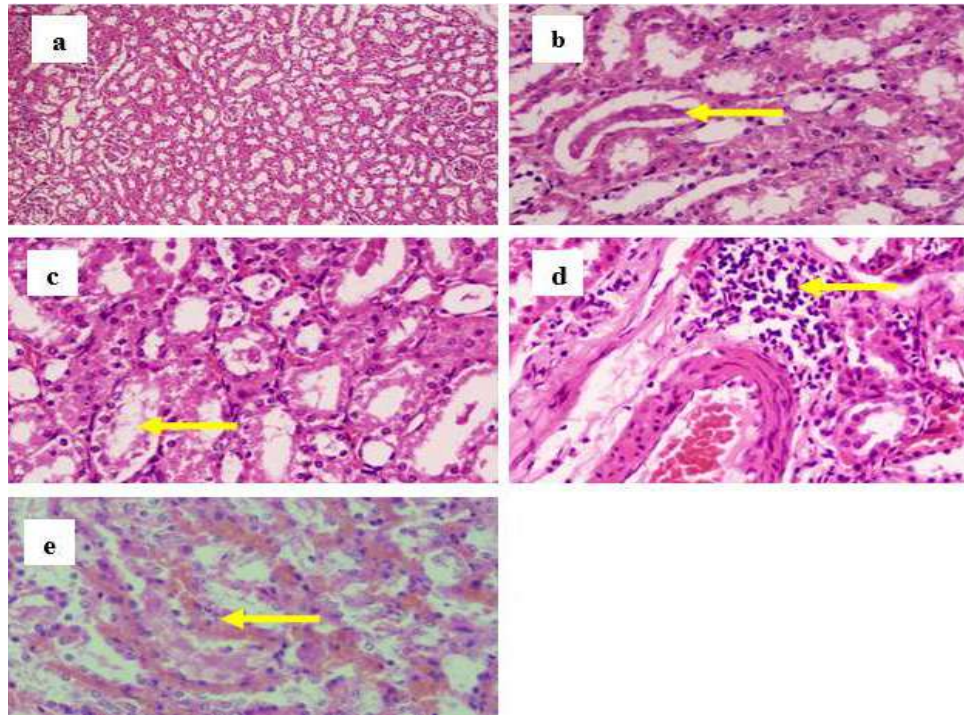


Fig. 9: Haematoxylin and eosin stain of Histopathological features in kidney sections at 90 days of exposure to 0.105 µg.kg$^{-1}$ of MC-LR. Fig. 9a Control ×100, Fig. 9b 0.105 µg.kg$^{-1}$ of MC-LR – Luminal protein (yellow arrow) ×400, Fig. 9c 0.105 µg.kg$^{-1}$ of MC-LR - Tubular epithelial swelling (yellow arrow) ×400, Fig. 9d 0.105 µg.kg$^{-1}$ of MC-LR - Mild interstitial inflammation (yellow arrow) ×400, Fig. 9e 0.105 µg.kg$^{-1}$ of MC-LR - Vascular congestion (yellow arrow) ×400.

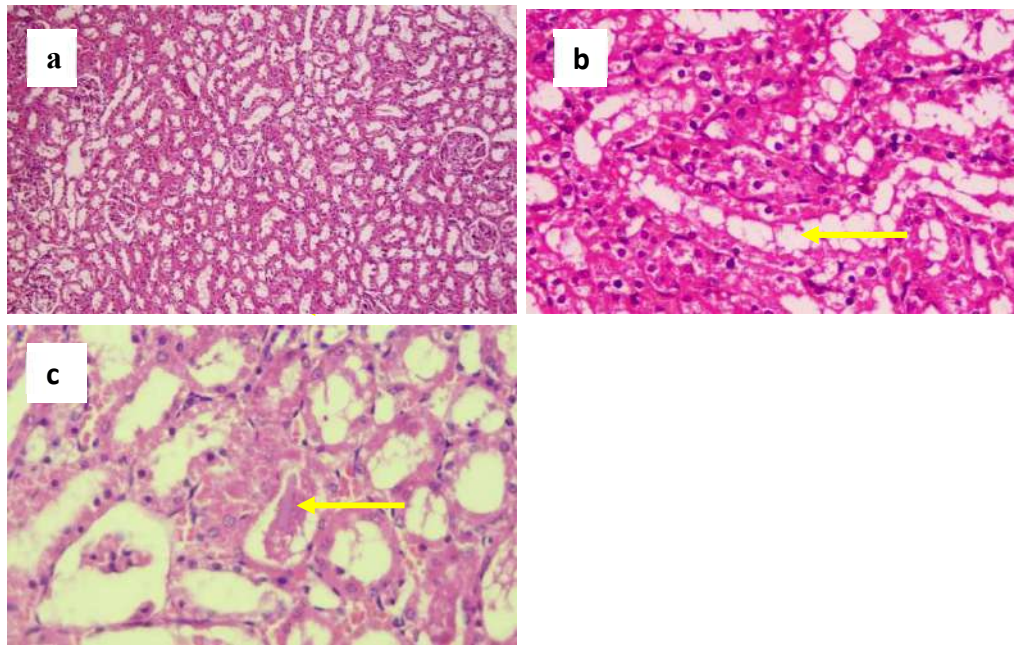


Fig. 10: Haematoxylin and eosin stains of histopathological features in kidney sections at 90 days of exposure to MC-LR at 0.091 µg.kg$^{-1}$. Fig. 10a Control ×100, Fig. 10b MC-LR at 0.091 µg.kg$^{-1}$ –Tubular epithelial swelling (yellow arrow) ×400, Fig. 10c MC-LR at 0.091 µg.kg$^{-1}$ – Intraluminal protein (yellow arrow) ×400.

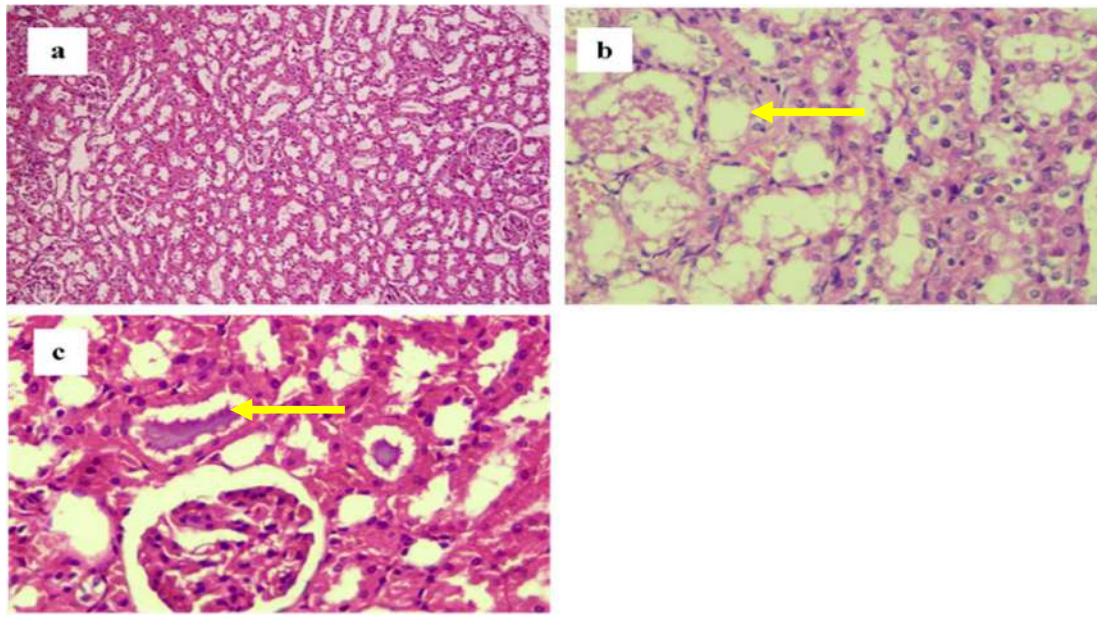


Fig. 11: Haematoxylin and eosin stains of Histopathological features in kidney sections after 90 days of exposure to MC-LR at 0.070 μg.kg$^{-1}$. Fig. 11a Control ×100, Fig. 11b MC-LR at 0.070 μg.kg$^{-1}$ – Tubular epithelial swelling (yellow arrow) ×400, Fig. 11c MC-LR at 0.070 μg.kg$^{-1}$ – Intraluminal protein (yellow arrow) ×400.

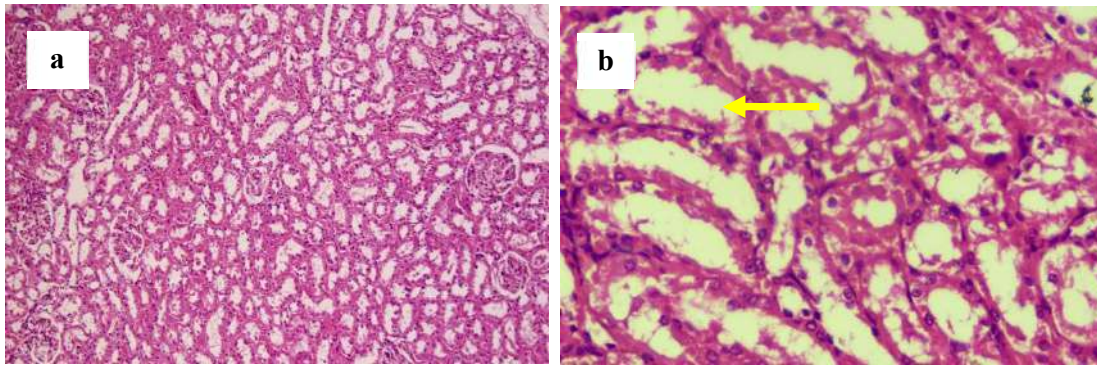


Fig. 12: Haematoxylin and eosin stains of Histopathological features in kidney sections at 90 days of exposure to MC-LR at 0.035 μg.kg$^{-1}$. Fig. 12a Control ×100, Fig. 12b MC-LR at 0.035 μg.kg$^{-1}$ – Tubular epithelial swelling (yellow arrow) × 400.

was recorded in MC-LR exposed rats in this study. No significant structural changes in the kidney in mice exposed to 1 μg.L$^{-1}$ and 30 μg.L$^{-1}$ MC-LR were observed (Yi et al. 2019). In the present study, intraluminal proteins and mild epithelial swelling were significant in cortex tubules in rats' exposure to 1μg.L$^{-1}$ of MC-LR (0.070 μg.kg$^{-1}$). Nevertheless, it was reported that exposure to 60 μg.L$^{-1}$ MC-LR for 3 months enlarged renal corpuscles with compressed Bowman's space (Yi et al. 2019). In all MC-LR exposure groups, no significant lesions were observed in the glomeruli of rat kidneys in the present study. Exposure to MC-LR for 6 months, obvious lymphocyte infiltrate in interstitial tissue was significant in mice treated with 60 μg.L$^{-1}$ MC-LR, with dilated renal tubule. Moreover, exposure to 90 μg.L$^{-1}$ and 120 μg.L$^{-1}$ MC-LR, numerous renal corpuscles enlarged with compressed Bowman's space in the kidney cortex, and renal tubules were enlarged and filled with eosinophilic material recorded (Yi et al. 2019).

Further, with the increase in exposure concentration of MC-LR in mice, an increase in lymphocyte infiltration in the renal pelvis has been recorded (Yi et al. 2019). The mice that were exposed to MC-LR for 6 months displayed more lymphocytes than the 3-month groups (Yi et al. 2019). The results of the present study indicate the possibility that chronic exposure to CYN and MC-LR is associated with nephrotoxicity. We demonstrated that chronic oral exposure

to CYN and MC-LR leads to nephrotoxicity in Wistar rats, as evidenced by changes in concentrations of serum creatinine, urine creatinine, and urinary biomarker KIM-1. Most importantly, the rats exposed to the environmental samples contaminated with CYN and MC-LR exhibited renal toxicity. Therefore, it could be debated that prolonged exposure to CYN and MC-LR may lead to chronic kidney disease.

## CONCLUSION

The concentrations of CYN and MC-LR at and above the recommended WHO levels and environmental samples used in this study induced signs of mild to moderate renal injury in Wistar rats as evidenced by elevated serum creatinine values, urinary KIM-1, and mild to moderate renal pathological changes consistent with tubular interstitial involvement. These results provide significant evidence that consumption of CYN and MC-LR-contaminated drinking water could lead to kidney injury, possibly leading to CKD.

## ACKNOWLEDGMENTS

We want to acknowledge the support of Staff Technical Officer Mrs. M.D.S.S. Jayathilake and Mr. M.S.E. Premalal in the Pathology Department, Faculty of Medical Sciences, and University of Sri Jayewardenepura on slide preparation for histopathology and Ms. K.T. Dilrukshi for support on animal study.

## REFERENCES

Abeysiri, H. A. S. N., Wanigasuriya, K. and Manage, P. M. 2018b. Detection of cylindrospermopsin and microcystin-LR in the well water of CKDu prevalence Medirigiriya, Sri Lanka. Pure Appl. Sci., 17: 656.

Abeysiri, H. A. S. N. and Manage, P. M. 2018a. Detection of cylindrospermopsin from well water in CKDu endemic Padaviya, Medawachciya, and Kebithigollewa area in Anuradhapura district, Sri Lanka. Water Qual. Human Health, 32: 53-66.

Abeysiri, H. A. S. N., Dilrukshi, K. T., Abinaiyan I., Manage S. P., Wanigasuriya K., Suresh T. S. and Manage P. M. 2019b. In-vivo toxicity study of cylindrospermopsin on Wistar rats. Forest. Environ. Symp., 55: 112-121.

Abeysiri, H. A. S. N., Wanigasuriya, K. and Manage, P. M. 2019a. Detection of microcystin-LR from well water in CKDu high prevalence Padaviya, Medawachchiya, and spring water in Kebithigollewa in Anuradhapura district, Sri Lanka. Water Air Pollut. Res. Trends Res., 20: 486.

Bazin, E., Huet, S., Jarry, G., Hégarat, L. L., Munday, J. S., Humpage, A. R. and Fessard, V. 2012. Cytotoxic and genotoxic effects of cylindrospermopsin in mice treated by gavage or intraperitoneal injection. Environ. Toxicol., 27(5): 277-284. https://doi.org/10.1002/tox.20640

Bonventre, J. V., Vaidya, V. S., Schmouder, R., Feig, P. and Dieterle, F. 2010. Next-generation biomarkers for detecting kidney toxicity. Nat. Biotechnol., 28(5): 436-440. https://doi.org/10.1038/nbt0510-436

Chandrajith, R., Nanayakkara, S., Itai, K., Aturaliya, T. N. C., Dissanayake, C. B., Abeysekera, T., Harada, K., Watanabe, T. and Koizumi, A. 2011. Chronic kidney diseases of uncertain etiology (CKDue) in Sri Lanka: geographic distribution and environmental implications. Environ. Geochem. Health, 33(3): 267-278. https://doi.org/10.1007/s10653-010-9339-1

Chernoff, N., Hill, D. J., Chorus, I., Diggs, D. L., Huang, H., King, D., Lang, J. R., Le, T. T., Schmid, J. E., Travlos, G. S. and Whitley, E. M. 2018. Cylindrospermopsin toxicity in mice following a 90-d oral exposure. J. Toxicol. Environ. Health Part A, 81(13): 549-566. https://doi.org/10.1080/15287394.2018.1460787

Chernoff, N., Rogers, E. H., Zehr, R. D., Gage, M. I., Malarkey, D. E., Bradfield, C. A., Liu, Y., Schmid, J. E., Jaskot, R. H., Richards, J. H. and Wood, C. R. 2011. Toxicity and recovery in the pregnant mouse after gestational exposure to the cyanobacterial toxin, cylindrospermopsin. J. Appl. Toxicol., 31(3): 242-254. https://doi.org/10.1002/jat.1586

Clark, S. P., Davis, M. A., Ryan, T. P., Searfoss, G. H. and Hooser, S. B. 2007. Hepatic gene expression changes in mice associated with prolonged sublethal microcystin exposure. Toxicol. Pathol., 35(4): 594-605. https://doi.org/10.1080/01926230701383210

De Silva, P. M. C., Abdul, K. S. M., Eakanayake, E. M., Jayasinghe, S. S., Jayasumana, C., Asanthi, H. B., Perera, H. S., Chaminda, G. G. T., Chandana, E. P. and Siribaddana, S. H. 2016. Urinary biomarkers KIM-1 and NGAL for detection of chronic kidney disease of uncertain etiology (CKDu) among agricultural communities in Sri Lanka. PLoS Negl. Trop. Dis., 10(9): e0004979. https://doi.org/10.1371/journal.pntd.0004979

Do Amaral, C. L., Francescato, H. D. C., Coimbra, T. M., Costa, R. S., Darin, J. D. A. C., Antunes, L. M. G. and Bianchi, M. D. L. P. 2008. Resveratrol attenuates cisplatin-induced nephrotoxicity in rats. Arch. Toxicol., 82(6): 363-370. https://doi.org/10.1007/s00204-007-0262-x

Do Carmo Bittencourt-Oliveira, M., Cordeiro-Araújo, M. K., Chia, M. A., De Toledo Arruda-Neto, J. D., De Oliveira, Ê. T. and Dos Santos, F. 2016. Lettuce irrigated with contaminated water: photosynthetic effects, antioxidative response and bioaccumulation of microcystin congeners. Ecotoxicol. Environ. Saf., 128: 83-90. https://doi.org/10.1016/j.ecoenv.2016.02.014

Du, X., Liu, H., Yuan, L., Wang, Y., Ma, Y., Wang, R., Chen, X., Losiewicz, M. D., Guo, H. and Zhang, H. 2019. The diversity of cyanobacterial toxins on structural characterization, distribution, and identification: A systematic review. Toxins, 11(9): 530. https://doi.org/10.3390/toxins11090530

Foss, A. J. and Aubel, M. T. 2013. The extraction and analysis of cylindrospermopsin from human serum and urine. Toxicon, 70: 54-61. https://doi.org/10.1016/j.toxicon.2013.04.007

Guzmán-Guillén, R., Prieto, A. I., Moreno, I., Rios, V., Vasconcelos, V. M. and Cameán, A. M. 2014. Effects of depuration on oxidative biomarkers in tilapia (Oreochromis niloticus) after Subchronic Exposure to Cyanobacterium Producing Cylindrospermopsin. Aquat. Toxicol., 149: 40-49. https://doi.org/10.1016/j.aquatox.2014.01.026

Hsu, R. K., Hsu, C. Y., McCulloch, C. E., Yang, J. anderson, A. H., Chen, J., Feldman, H. I., He, J., Liu, K. D., Navaneethan, S. D. and Porter, A. C. 2020. Research-based versus clinical serum creatinine measurements and the association of acute kidney injury with subsequent kidney function: findings from the Chronic Renal Insufficiency Cohort study. Clin. Kidney J., 13(1): 55-62. https://doi.org/10.1093/ckj/sfz057

Humpage, A. R. and Falconer, I. R. 2003. Oral toxicity of the cyanobacterial toxin cylindrospermopsin in male Swiss Albino mice: Determination of no observed adverse effect level for deriving a drinking water guideline value. Environ. Toxicol., 18(2): 94-103. https://doi.org/10.1002/tox.10104

Ichimura, T., Asseldonk, E. J., Humphreys, B. D., Gunaratnam, L., Duffield, J. S. and Bonventre, J. V. 2008. Kidney injury molecule–1 is a phosphatidylserine receptor that confers a phagocytic phenotype on epithelial cells. J. Clin. Invest., 118(5): 1657-1668. https://doi.org/10.1172/JCI34487

Jia, J., Luo, W., Lu, Y. and Giesy, J. P. 2014. Bioaccumulation of microcystins (MCs) in four fish species from Lake Taihu, China:

Assessment of risks to humans. Sci. Total Environ., 487: 224-232. https://doi.org/10.1016/j.scitotenv.2014.04.037

Karp, N. A., Coleman, L., Cotton, P., Powles-Glover, N. and Wilson, A. 2023. Impact of repeated micro and macro blood sampling on clinical chemistry and hematology in rats for toxicokinetic studies. Regul. Toxicol. Pharmacol., 141: 105386. https://doi.org/10.1016/j.yrtph.2023.105386

Lance, E., Paty, C., Bormans, M., Brient, L. and Gerard, C. 2007. Interactions between cyanobacteria and gastropods II. Impact of toxic *Planktothrix agardhii* on the life-history traits of *Lymnaea stagnalis*. Aquat. Toxicol., 81: 389-396. https://doi.org/10.1016/j.aquatox.2006.12.019

Lawton, L. A., Welgamage, A., Manage, P. M. and Edwards, C. 2011. Novel bacterial strains for the removal of microcystins from drinking water. Water Sci. Technol., 63(6): 1137-1142. https://doi.org/10.2166/wst.2011.352

Liu, B. C., Tang, T. T., Lv, L. L. and Lan, H. Y. 2018. Renal tubule injury: A driving force toward chronic kidney disease. Kidney Int., 93(3): 568-579. https://doi.org/10.1016/j.kint.2017.09.033

Lone, Y., Koiri, R. K. and Bhide, M. 2015. An overview of the toxic effect of potential human carcinogen microcystin-LR on the testis. Toxicol. Rep., 2: 289-296. https://doi.org/10.1016/j.toxrep.2015.01.008

Manage, P. 2019. Cyanotoxins: A hidden cause of chronic kidney disease of unknown etiology (CKDu) in Sri Lanka- A Review. Sri Lanka J. Aquat. Sci., 24: 1-10.

Manage, P. M., Yasawardna, S. G. and Wedage, W. S. 2009. Hepatotoxic effects of microcystis aeruginosa (PCC7820) on Wistar Rats. Vidyodaya J., 23-26.

Menezes, C., Valério, E. and Dias, E. 2013. The kidney Vero-E6 cell line: A suitable model to study the toxicity of microcystins. New Insights Toxicol. Drug Test., 29-48.

Milutinović, A., Živin, M., Zorc-Plesković, R., Sedmak, B. and Šuput, D. 2003. Nephrotoxic effects of chronic administration of microcystins-LR and-YR. Toxicon., 42(3): 281-288. https://doi.org/10.1016/S0041-0101(03)00143-0

Moraes, A. C. N. and Magalhães, V. F. 2018. Renal tubular damage caused by cylindrospermopsin (cyanotoxin) in mice. Toxicol. Lett., 286: 89-95. https://doi.org/10.1016/j.toxlet.2017.12.028

Piyathilaka, M. A. P. C., Pathmalal, M. M., Tennekoon, K. H., De Silva, B. G. D. N. K., Samarakoon, S. R. and Chanthirika, S. 2015. Microcystin-LR-induced cytotoxicity and apoptosis in human embryonic kidney and human kidney adenocarcinoma cell lines. Microbiology, 161(4): 819-828. https://doi.org/10.1099/mic.0.000046

Sethunge, S. and Manage, P. M. 2010. Nuisance algae in water supply projects in Sri Lanka. Proc. Symp. Sustain. Built Environ. (ICSBE-2010).

Waanders, F., van Timmeren, M. M., Stegeman, C. A., Bakker, S. J. and van Goor, H. 2010. Kidney injury molecule□1 in renal disease. J. Pathol., 220(1): 7-16. https://doi.org/10.1002/path.2642

Wajda, J., Dumnicka, P., Kolber, W., Sporek, M., Maziarz, B., Ceranowicz, P., Kuźniewski, M. and Kuśnierz-Cabala, B. 2020. The marker of tubular injury, kidney injury molecule-1 (KIM-1), in acute kidney injury complicating acute pancreatitis: a preliminary study. J. Clin. Med., 9(5):1463. https://doi.org/10.3390/jcm9051463

Wijewickrama, M. M. and Manage, P. M. 2019. Accumulation of microcystin-LR in grains of two rice varieties (*Oryza sativa* L.) and a leafy vegetable, *Ipomoea aquatica*. Toxins, 11(8):432. https://doi.org/10.3390/toxins11080432

Wijethunga, S., Ratnatunga, N. V. I., Abeysekera, T. D. J., Wazil, A. W. M. and Selvarajah, M. 2015. Endemic chronic kidney disease of unknown etiology in Sri Lanka: Correlation of pathology with clinical stages. Indian J. Nephrol., 25(5): 274-280. doi: 10.4103/0971-4065.145095

World Health Organization (WHO). 2003 Cyanobacterial Toxins: Microcystin-LR in Drinking Water. World Health Organization: Geneva, Switzerland

Wu, J. X., Huang, H., Yang, L., Zhang, X. F., Zhang, S. S., Liu, H. H., Wang, Y. Q., Yuan, L., Cheng, X. M., Zhuang, D. G. and Zhang, H. Z. 2018. Gastrointestinal toxicity induced by microcystins. World J. Clin. Cases, 6(10): 344. doi: 10.

Yi, X., Xu, S., Huang, F., Wen, C., Zheng, S., Feng, H., Gu, J., Chen, J., Feng, X. and Yang, F. 2019. Effects of chronic exposure to microcystin-LR on kidney in mice. Int. J. Environ. Res. Publ. Health, 16(24): 5030. https://doi.org/10.3390/ijerph16245030

Nature Environment and Pollution Technology
An International Quarterly Scientific Journal

p-ISSN: 0972-6268
(Print copies up to 2016)
e-ISSN: 2395-3454

Vol. 23 | No. 3 | pp. 1775-1782 | 2024

Original Research Paper

https://doi.org/10.46488/NEPT.2024.v23i03.050

Open Access Journal

# Fuzzy Logic Harmony in Water: Mamdani Inference System Applied to Evaluate Pristine Pond Water Quality

**M. Priya* and R. Kumaravel**†**

*Department of Mathematics, College of Engineering and Technology, SRM Institute of Science and Technology, Kattankulathur-603203, Tamil Nadu, India

**Department of Career Development Centre, College of Engineering and Technology, SRM Institute of Science and Technology, Kattankulathur-603203, Tamil Nadu, India

†Corresponding author: R. Kumaravel; kumaravr@srmist.edu.in

**Nat. Env. & Poll. Tech.**
**Website: www.neptjournal.com**

*Received:* 12-01-2024
*Revised:* 26-02-2024
*Accepted:* 17-03-2024

**Key Words:**
Water quality
Fuzzy logic harmony
Fuzzy inference system
MATLAB

## ABSTRACT

Aquatic ecosystems that are subject to urbanization and environmental changes, such as the Kapaleeswarar and Chitrakulam tanks, depend on evaluating water quality. Their complicated data present challenges for conventional approaches. The usefulness of the Mamdani fuzzy inference system in determining the water quality in these tanks is investigated in this work. It creates a comprehensive assessment based on subject-matter expertise by handling ambiguous descriptors with linguistic variables and fuzzy sets. The system's procedures for implementation are described in detail, with an emphasis on how well they can manage interrelated variables. The study shows how well the system measures the water quality in tanks and suggests ways to improve it. Tank evaluation that incorporates the Mamdani system encourages comprehensive resource management and cultural preservation.

## INTRODUCTION

The well-being of humans and ecosystems are both profoundly impacted by water quality. In surface water and underground aquifers, a complex interplay of physical, chemical, biological, and microbial variables regulates fundamental biological and industrial processes (Ammar 2018). To characterize the quality of a water sample, the word "composition" is frequently used. However, it can be difficult and time-consuming to analyze data to determine the quality of the water. For efficient water resource management, planning, and assessment enhancement, accurate estimation of water quality indicators is essential (Asgari et al. 2021).

A crucial component of water quality modeling is the mathematical prediction of water pollution. The concentrations of important elements like dissolved oxygen (DO), biological oxygen demand (BOD), pH, and turbidity in a sample must be taken into account when evaluating water quality indicators (WQIs). Best-fit models are frequently used to predict WQIs once these properties have been evaluated in the lab. Many mathematical models, however, are complex and difficult to incorporate into real-time systems (Balamurugan et al. 2020).

The vast and diverse nature of water quality makes accurate data assessment challenging. Due to the inherent uncertainties (Bawoke et al. 2020), seeing water quality data as a fuzzy set with terms like "Good, Moderate, Poor, and Very Poor" provides a more useful framework. The effectiveness of fuzzy-based approaches in resolving subjectivity and ambiguity in environmental concerns has been established (Chauhan et al. 2023).

Fuzzy logic helps to categorize and quantify the subjective environmental effects by formalizing the evaluation of hidden data and water quality. The quality of both surface and groundwater has been predicted using fuzzy logic (Dewanti et al. 2019, Ellina et al. 2020, Gupta et al. 2019). Although multivariate analysis and artificial neural networks are effective in detecting water quality, the shortcomings of deterministic and WQI methods highlight the necessity for sophisticated classification systems that can handle ambiguous and fuzzy data (Jang et al. 2005).

Recent methods, which go beyond the conventional WQI 0-100 scale, generate acceptable fuzzy sets that reflect the inherent uncertainty in water quality evaluation by using fuzzy membership values ranging from 0 to 1. This change improves forecast accuracy while lowering

computing expenses (Jha et al. 2020, Kalaivanan et al. 2017, Karunathilake et al. 2019).

Set theory is expanded by fuzzy logic, a mathematical representation of ambiguity. It has replaced conventional techniques in many scientific and engineering fieldswhere it has found applications (Kaushal et al. 2018). Even so, there hasn't been much study on WQI prediction utilizing soft computing techniques, notably fuzzy logic systems. This points to a viable area for additional research in the field of assessing water quality (Kumaravel & Vallinayagam 2016).

## STUDY AREA

Two noteworthy bodies of water with important cultural and historical value in Chennai, India, are the Chitrakulam tank and the Kapaleeswarar tank. These tanks have played a significant role in research, providing insightful information on the area's history and enduring customs. In addition to having religious significance, the Kapaleeswarar tank is a vital water source for the neighborhood and is located next to the Kapaleeswarar Temple. The Chitrakulam tank, which is close to the Parthasarathy Temple, has also been important to the local community's religious and cultural practices. These two tanks provide a singular chance to investigate the connections between religion, tradition, and environmental sustainability, making them interesting topics for academic research and study.

### Kapaleeswarar Tank

One of the most venerated and historic holy sites in Chennai is thought to be the Kapaleeswarar Temple (Fig. 1). In Mylapore, a Chennai suburb, is the temple dedicated to Lord Shiva, Kapaleeswarar. The inscriptionsfound on the temple grounds date around 1250 AD. The temple was reportedly constructed by the governing Pallava Dynasty in the eighth century AD, but it is possible that the Portuguese damaged it. The Vijayanagar Kings of the Tuluva dynasty (1491-1570 CE) then reconstructed it.

The sacred tank is situated on the west side of the temple, enhancing the picture view of the temple from the three Mada streets. The brilliant lights from the stores, which are constantly crowded with locals shopping, make the four Mada (east, west, north, and south) streets look incredibly attractive at night. Another noticeable aspect of the tank's water is the way the light reflects off of it. In the center of the tank is a Neerazhi mandapam, which enhances its attractiveness. Kapali Theertham, or holy water, is the name of the liquid in the tank. Sakthi Gangai and Mukthi Theertham are two names used by many followers. The tank is also known as Thamarai thadagam because, in its early years, it was covered in a profusion of lotus creepers that were blossoming and multicolored lotus. 629 feet long and 475 feet wide, the tank is a large structure. On the west side of the tank is a mandapam that is 40 square meters.

### Chitrakulam Tank

In Chennai, Tamil Nadu, the Chitrakulam tank (90607 m) (Fig. 2) is around two km northeastof Royapettah. In terms of latitude and longitude, it is located close to $13^{o}$ 1'52" N and $80^{o}$ 16'14" E. The Kapaleeswarar temple tank is in Chennai, Tamil Nadu, about 7 km southeast of Mylapore. Geographically, it is located close to $13^{o}$ 27'71" Nlatitude and $80^{o}$ 16'5" E longitude. Both of the above tanks are multipurpose tanksused for a variety of summertime activities such as gardening and residential use.

## MATERIALS AND METHODS

The assessment contents are chosen based on the results of

Fig. 1: Kapaleeswarar tank.

Fig. 2: Chitrakulam tank.

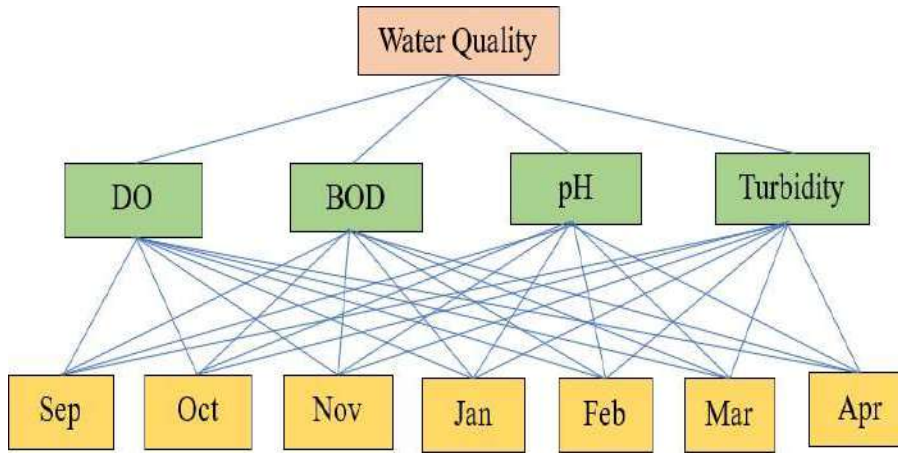


Fig. 3: Hierarchy of water quality assessment.

the field investigations and the monitoring data for water quality at the two tanks. For the parameters Dissolved Oxygen (DO), Biological Oxygen Demand (BOD), pH, and Turbidity (Fig. 3).

## Introduction to the Water Quality Index

Water quality index ranges from 1 to 100; a higher number is indicative of better water quality. WQI rating scale is as follows: 91-100: excellent water quality, 71-90: good water quality, 51-70: medium water quality, 26-50: fair water quality, 0-25: poor water quality (11). The parameters used in defining WQI are pH, Biological Oxygen Demand (BOD), Dissolved Oxygen (DO), and Turbidity. The criteria are given in Table 1 to determine how healthy the water is on a given day (Kumaravel et al. 2020).

Table 1: Water Quality Criteria.

| S. No. | Parameter | Good Quality | Moderate | Poor Quality |
|---|---|---|---|---|
| (a) | pH | 7.5-9.0 | 6.5-7.5 | 5-6.5 |
| (b) | DO | 2-4.5 | 4.5-7 | 7-10 |
| (c) | BOD | Below 2 | 2-3 | 3-6 |
| (c) | Turbidity | 5-10 | 10-25 | - |

## Fuzzy Inference System

In this study, we used an FIS model, a mathematical method that uses fuzzy logic to translate an input into an output. Three essential steps make up the fuzzy inference process: fuzzification, if-then rules, and defuzzification (40). A fuzzy inference approach may be useful for resolving ambiguity and assessing water quality because the data on water quality are ambiguous and unclear (Nayak et al. 2020). The Mamdani method is the most used fuzzy inference approach. In 1965, Zadeh presented the fuzzy logic model (Oladipo et al. 2021).

## Operation of Fuzzy Inference System

Fuzzification of variables, rule evaluation, rule aggregation,

and defuzzification are the four key components of the robust Mamdani fuzzy inference system. The fundamental design of the FIS is shown in Fig. 4.

**Step 1. Fuzzification**

Fuzzification is the first stage of the FIS. Through a variety of membership functions, crisp inputs are converted in this stage into fuzzy inputs known as linguistic variables. A membership function is a visual representation that quantitatively expresses linguistic concepts and visually depicts a fuzzy collection (Palanichamy et al. 2022). To relate the numerical input values to membership grades in fuzzy sets provided with text, fuzzification is used. In this investigation, the input and output parameters were both subjected to a trapezoidal membership function. The trapezoidal membership function, one of the most extensively used membership functions (MF) in fuzzy controller design, has the advantage of simplicity (Ram et al. 2021, Ramirez et al. 2007, Ren et al. 2021 & Rustum et al. 2020).

**Step 2. Inference Engine**

The fuzzy output is produced by the inference engine using the fuzzy rules from the knowledge base. An expression with if-then conditions is known as a fuzzy rule. The following is the ambiguous rule: Y must be B if X is A. In this fuzzy rule, A and B are fuzzy sets, while X and Y are linguistic variables. The aggregation method is used to merge all of the If-then rules into a single fuzzy set after all of the rules have been defined.

**Step 3. Defuzzification**

An expert system's defuzzifier is a crucial part. The processing of fuzzy inference systems ends with defuzzification (Sajan & Christoper 2023). It involves turning a hazy input into a clear output (Shitong et al. 2005). The mean of maximum method (MOM), the centroid of area (COA), the biggest of maximum (LOM), the bisector of area (BOA), and the smallest of maximum (SOM) are some of the different types of defuzzifiers. The most popular defuzzification technique, known as the center of area (CoA) defuzzification method, is also known as the center of gravity (CoG) defuzzification technique. The fuzzy controller in this defuzzification method (CoA) calculates the area under the scaled membership functions and within the output variable's range first.

## RESULTS

**Step 1. Input and Output Variables**

The identification of the variables that make up the system, sometimes referred to as the input and output variables, is the first step in the system modeling process. The factors that have a substantial impact on the result have been selected as inputs. The complexity increases as the number of rules required to manage the inputs increases. Depending on the physical nature of the issue, the conversation may go further or shorter.

**Step 2. Membership Function**

Fuzzy sets are used to express linguistic values. Typically, a fuzzy set's membership functions are used to define it. The employment of the trapezoidal membership function to normalize the acute inputs is made possible by its computational efficiency and simplicity. The membership functions for the inputs and outputs are depicted in Fig. 5 and 6.

**Step 3. Establishing a Linguistic Rule Base**

The relationship between the input and the output was

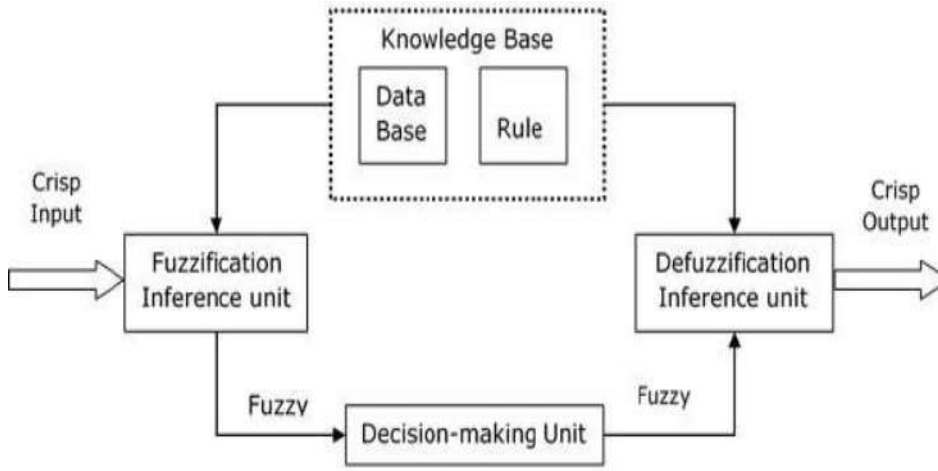


Fig. 4: Structure of fuzzy inference system.

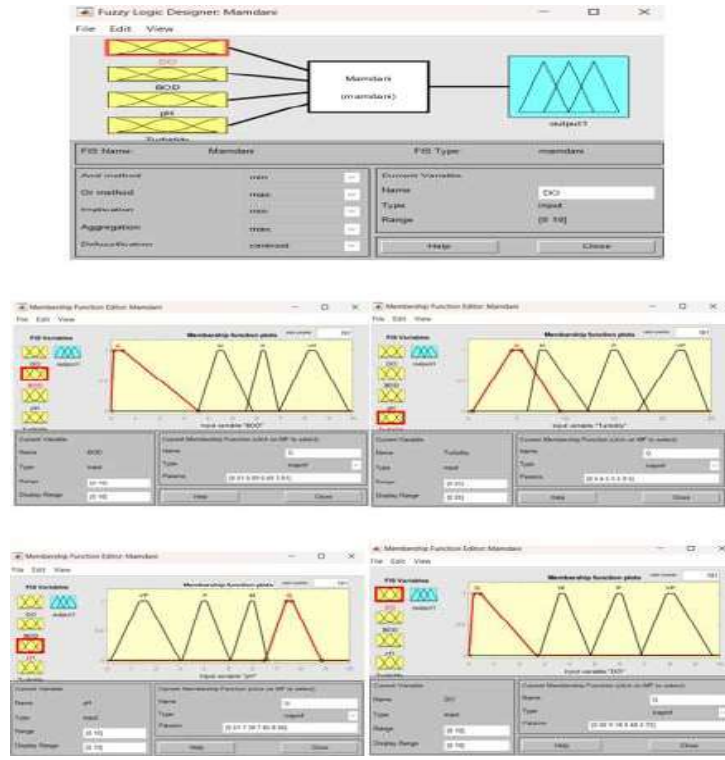


Fig. 5: Input membership function.

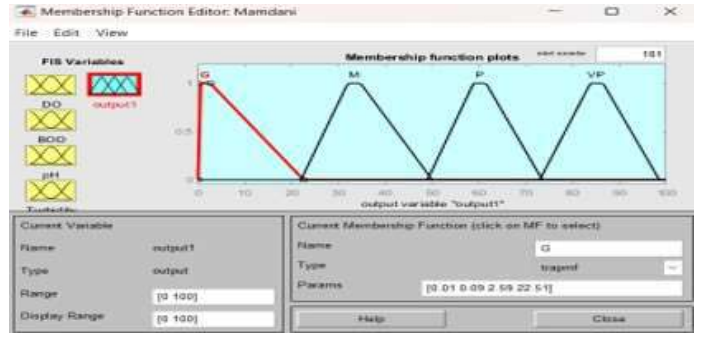


Fig. 6: Output membership function.

demonstrated using IF-THEN rules. As $X_1$, $X_2$, $X_3$, and $X_4$ respectively, the inputs DO, BOD, pH, and turbidity are employed. The values y1 indicate the output of the system (Wu 2019). The model that is suggested in this paper has two fuzzy systems. In this setup, the inputs for $X_1$, $X_2$, $X_3$, and $X_4$ each have four MF. The very first fuzzy system consists of 256 rules. The proposed fuzzy model is built on the architecture of the Mamdani fuzzy model and employs Max-Min inference. The Mamdani fuzzy system's rules are created with the following techniques (Figs. 7 and 8):

### Step 4. Defuzzification

The recommended model employs the Centroid of Area (COA) method of defuzzification to arrive at the answer.

## DISCUSSION

The main objective of this study is the thorough evaluation of water quality indicators for two different ponds, and this evaluation is done in accordance with the recognized Indian water quality standards. Kapaleeswarar Pond receives a 50% weighting in the evaluation procedure, whereas Chitrakulam

Pond receives a 70% weighting, representing the different levels of significance and value that these two aquatic ecosystemshave in relation to the study's objectives.

The study's findings are: (1) The FIS method is appropriate for addressing ambiguous and uncertain environmental issues, particularly assessing water quality to get a clear output and overcome the uncertainty of water quality; (2) The FIS method can be used to evaluate the quality of various types of water; and (3) The Mamdani fuzzy inference system is easier to understand because it is rule-based, and (4) The FIS can apply various defuzzification techniques and, additionally, it is possible to apply various

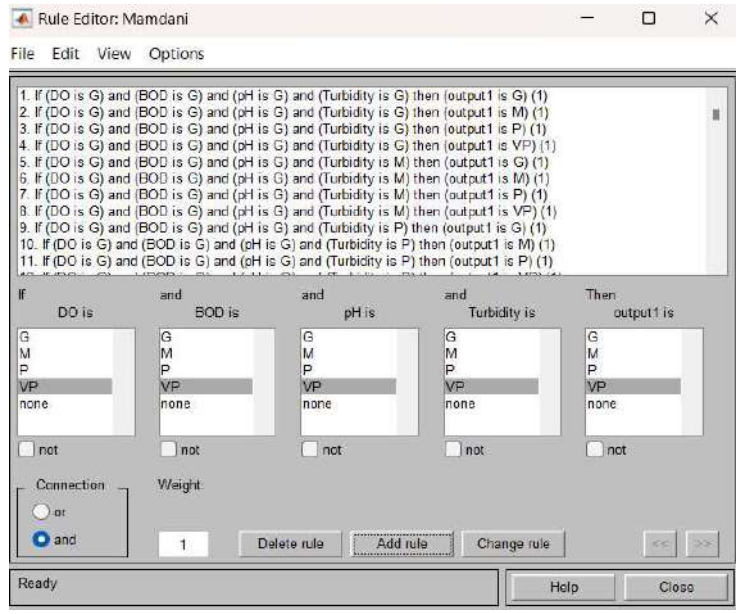


Fig. 7: Rules.

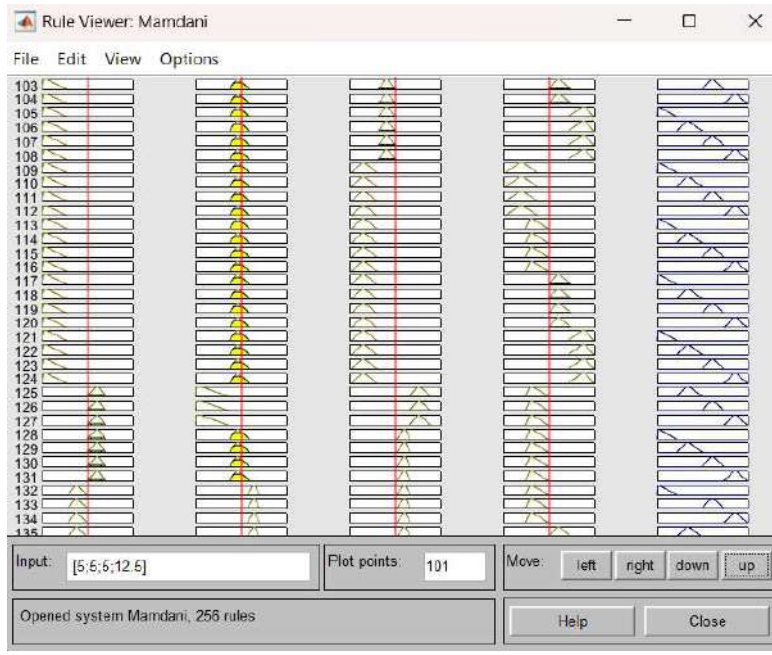


Fig. 8: Rule viewer.

types of membership functions. The FIS can also be used to understand and evaluate the impact of each input parameter on the final water quality.

The outcomes from the proposed Fuzzy Inference System (FIS) model are brought into sharp focus after completing a thorough examination. Comparing these data to the established water quality guidelines reveals an incredibly high degree of similarity. In essence, the predictions and analyses produced by the FIS model show a startlingcongruence with the exact water quality standards set by Indian regulatory bodies.

This extraordinary agreement between the FIS model's predictions and the legally required water quality criteria highlights the model's accuracy in determining the water quality of Kapaleeswarar Pond and Chitrakulam Pond. It highlights the FIS model's potential as a reliable instrument for continued monitoring, management, and conservation efforts targeted at preserving and enhancing the water quality in these essential aquatic ecosystems. Furthermore, it demonstrates the crucial role that cutting-edge modeling and simulation methods may play in improving our comprehension and management of important natural resources.

## CONCLUSION

This article represents an extension of a fuzzy inference system for pond water quality using MATLAB research endeavors, where our primary objective was to developa comprehensive fuzzy model for water quality evaluation. In our ongoing pursuit of enhancing environmental assessment methodologies, we have delved deeper into the intricacies of this model, refining and expanding its capabilities to provide even more valuable insights into the assessment of water quality. Our approach continues to rely on the Mamdani fuzzy inference system, a powerful tool known for its ability to handlecomplex and uncertain environmental data. Within this framework, we meticulously consider four crucial input parameters and an extensive network of 256 fuzzy rules forms the foundation of each fuzzy model. This intricate structure enablesus to address the complexities inherent in assessing water quality in diverse contexts. This article represents a continuation of our commitment to advancing the field of water quality assessment. We recognize that there is always room for improvement, and our model is designed to evolve continually. Future directions include the incorporation of additional input parameters and the exploration of different membership functions, such as sigmoid and Gaussian, to enhance accuracy and comprehensiveness. In essence, this extended article builds upon the foundation established in our earlier research, offering a deeper and more nuanced exploration of our hierarchical fuzzy model's capabilities. It is a testament to our ongoing dedication to refining and expanding our methodologies for assessing and managing water quality, ultimately contributing to a more sustainable and environmentally conscious future.

## REFERENCES

Ammar, T., Lazhar, B. and Lotfi, M. 2018. Evaluation of surface water quality for drinking purposes using fuzzy inference system. Groundw. Sustain. Dev., 6: 235-244.

Asgari, G., Komijani, E., Seid-Mohammadi, A. and Khazaei, M. 2021. Assessment of the quality of bottled drinking water through mamdani fuzzy water quality index. Water Resour. Manag., 35: 5431-5452.

Balamurugan, P., Kumar, P. S., Shankar, K., Nagavinothini, R. and Vijayasurya, K. 2020. Non-carcinogenic risk assessment of groundwater in southern part of Salem District in Tamilnadu, India. J. Chil. Chem. Soc., 65(1): 4697-4707.

Bawoke, G. T. and Anteneh, Z. L. 2020. Spatial assessment and appraisal of groundwater suitability for drinking consumption in Andasa watershed using water quality index (WQI) and GIS techniques: Blue Nile Basin, Northwestern Ethiopia. Cogent Eng., 7(1): 1748950.

Chauhan, S. S. and Trivedi, M. K. 2023. Assessment of surface water quality index of Gwalior-Chambal region using fuzzy-based approach. J. Inst. Eng. India Ser., 104: 1-17.

Dewanti, N. A. and Abadi, A. M. 2019. Fuzzy logic application as a tool for classifying water quality status in Gajahwong River, Yogyakarta, Indonesia. In: IOP Conf. Ser.: Mater. Sci. Eng., 546(3): 032005.

Ellina, G., Papaschinopoulos, G. and Papadopoulos, B. K. 2020. Research of fuzzy implications via fuzzy linear regression in data analysis for a fuzzy model. J. Comput. Methods Sci. Eng., 20(3): 879-888.

Gupta, R., Singh, A. N. and Singhal, A. 2019. Application of ANN for water quality index. Int. J. Mach. Learn. Comput., 9(5): 688-693.

Jang, J. S. R., Sun, C. T. and Mizutan, E. 2005. Neuro-fuzzy and soft computing. New Delhi: Prentice Hall of India Private Limited.

Jha, M. K., Shekhar, A. and Jenifer, M. A. 2020. Assessing groundwater quality for drinking water supply using hybrid fuzzy-GIS-based water quality index. Water Res., 179: 115867.

Kalaivanan, K., Gurugnanam, B., Pourghasemi, H. R., Suresh, M. and Kumaravel, S. 2017. Spatial assessment of groundwater quality using water quality index and hydrochemical indices in the Kodavanar sub-basin, Tamil Nadu, India. Sustain. Water Resour. Manag., 4(3).

Karunathilake, H., Hewage, K., Merida, W. and Sadiq, R. 2019. Renewable energy selection for net zero energy communities: lifecycle-based decision making under uncertainty. Renew. Energy, 130: 558-573.

Kaushal, J. and Basak, P. 2018. A novel approach for determination of power quality monitoring index of an AC microgrid using fuzzy inference system. Iran J. Sci. Technol. Trans. Electr. Eng., 42: 429-450.

Kumaravel, R. and Vallinayagam, V. 2016. A fuzzy inference system for pond water quality using MATLAB. J. Ultra Sci. Phys. Sci., 24(1).

Kumaravel, R., Sudarsan, J. S., Jyothirmai, V. K. and Arun, S. 2020. Water quality index estimation using fuzzy optimization technique. In: AIP Conf. Proc., 2277(1).

Nayak, J. G., Patil, L. G. and Patki, V. K. 2020. Development of water quality index for Godavari River (India) based on fuzzy inference system. Groundw. Sustain. Dev., 10: 100350.

Oladipo, J. O., Akinwumiju, A. S., Aboyeji, O. S. and Adelodun, A. A. 2021. Comparison between fuzzy logic and water quality index methods: A case of water quality assessment in Ikare community, Southwestern Nigeria. Environ. Chall., 3: 100038.

Palanichamy, J., Palani, S., Hebsiba, G. A., Viola, J., Tungsrimvong, A. and Babu, B. 2022. Simulation and prediction of groundwater quality of a semi-arid region using fuzzy inference system and neural network techniques. J. Soft Comput. Civ. Eng., 6(1): 110-126.

Ram, A., Tiwari, S. K. and Pandey, H. K. 2021. Groundwater quality assessment using water quality index (WQI) under GIS framework. Appl. Water Sci., 11: 46.

Ramirez, E. M. and Mayorga, R. V. 2007. A cascaded fuzzy inference system for dynamic online portals customization. Int. J. Intell. Syst. Technol., 2: 7-20.

Ren, J., Man, Y., Lin, R. and Liu, Y. 2021. Multicriteria decision making for the selection of the best renewable energy scenario based on fuzzy inference system. Renew. Energy Driven Future, pp.491-507.

Rustum, R., Kurichiyanil, A. M. J., Forrest, S., Sommariva, C., Adeloye, A. J. and Zounemat Kermani, M. 2020. Sustainability ranking of desalination plants using mamdani fuzzy logic inference systems. Sustainability, 12(2): 631.

Sajan, R. I. and Christopher, V. B. 2023. A fuzzy inference system for enhanced groundwater quality assessment and index determination. Water Qual. Res. J., 58(3): 230-246.

Shitong, W., Chungb, F. L., Bina, S. H. and Dewenc, H. 2005. Cascaded centralized TSK fuzzy system universal approximator and high interpretation. Appl. Soft Comput., 5: 131-45.

Wu, H. C. 2019. Fuzzification of real-valued functions based on the form of decomposition theorem: applications to the differentiation and integrals of fuzzy-number-valued functions. Soft Comput., 23(16): 6755-6775.

## ORCID DETAILS OF THE AUTHORS

M. Priya: https://orcid.org/0000-0003-4505-489X
R. Kumaravel: https://orcid.org/0000-0003-0873-4757

Nature Environment and Pollution Technology
An International Quarterly Scientific Journal

p-ISSN: 0972-6268
(Print copies up to 2016)
e-ISSN: 2395-3454

Vol. 23 | No. 3 | pp. 1775-1782 | 2024

Original Research Paper

https://doi.org/10.46488/NEPT.2024.v23i03.050

Open Access Journal

# Fuzzy Logic Harmony in Water: Mamdani Inference System Applied to Evaluate Pristine Pond Water Quality

**M. Priya* and R. Kumaravel**†**

*Department of Mathematics, College of Engineering and Technology, SRM Institute of Science and Technology, Kattankulathur-603203, Tamil Nadu, India

**Department of Career Development Centre, College of Engineering and Technology, SRM Institute of Science and Technology, Kattankulathur-603203, Tamil Nadu, India

†Corresponding author: R. Kumaravel; kumaravr@srmist.edu.in

**Nat. Env. & Poll. Tech.**
**Website: www.neptjournal.com**

*Received:* 12-01-2024
*Revised:* 26-02-2024
*Accepted:* 17-03-2024

**Key Words:**
Water quality
Fuzzy logic harmony
Fuzzy inference system
MATLAB

## ABSTRACT

Aquatic ecosystems that are subject to urbanization and environmental changes, such as the Kapaleeswarar and Chitrakulam tanks, depend on evaluating water quality. Their complicated data present challenges for conventional approaches. The usefulness of the Mamdani fuzzy inference system in determining the water quality in these tanks is investigated in this work. It creates a comprehensive assessment based on subject-matter expertise by handling ambiguous descriptors with linguistic variables and fuzzy sets. The system's procedures for implementation are described in detail, with an emphasis on how well they can manage interrelated variables. The study shows how well the system measures the water quality in tanks and suggests ways to improve it. Tank evaluation that incorporates the Mamdani system encourages comprehensive resource management and cultural preservation.

## INTRODUCTION

The well-being of humans and ecosystems are both profoundly impacted by water quality. In surface water and underground aquifers, a complex interplay of physical, chemical, biological, and microbial variables regulates fundamental biological and industrial processes (Ammar 2018). To characterize the quality of a water sample, the word "composition" is frequently used. However, it can be difficult and time-consuming to analyze data to determine the quality of the water. For efficient water resource management, planning, and assessment enhancement, accurate estimation of water quality indicators is essential (Asgari et al. 2021).

A crucial component of water quality modeling is the mathematical prediction of water pollution. The concentrations of important elements like dissolved oxygen (DO), biological oxygen demand (BOD), pH, and turbidity in a sample must be taken into account when evaluating water quality indicators (WQIs). Best-fit models are frequently used to predict WQIs once these properties have been evaluated in the lab. Many mathematical models, however, are complex and difficult to incorporate into real-time systems (Balamurugan et al. 2020).

The vast and diverse nature of water quality makes accurate data assessment challenging. Due to the inherent uncertainties (Bawoke et al. 2020), seeing water quality data as a fuzzy set with terms like "Good, Moderate, Poor, and Very Poor" provides a more useful framework. The effectiveness of fuzzy-based approaches in resolving subjectivity and ambiguity in environmental concerns has been established (Chauhan et al. 2023).

Fuzzy logic helps to categorize and quantify the subjective environmental effects by formalizing the evaluation of hidden data and water quality. The quality of both surface and groundwater has been predicted using fuzzy logic (Dewanti et al. 2019, Ellina et al. 2020, Gupta et al. 2019). Although multivariate analysis and artificial neural networks are effective in detecting water quality, the shortcomings of deterministic and WQI methods highlight the necessity for sophisticated classification systems that can handle ambiguous and fuzzy data (Jang et al. 2005).

Recent methods, which go beyond the conventional WQI 0-100 scale, generate acceptable fuzzy sets that reflect the inherent uncertainty in water quality evaluation by using fuzzy membership values ranging from 0 to 1. This change improves forecast accuracy while lowering

computing expenses (Jha et al. 2020, Kalaivanan et al. 2017, Karunathilake et al. 2019).

Set theory is expanded by fuzzy logic, a mathematical representation of ambiguity. It has replaced conventional techniques in many scientific and engineering fieldswhere it has found applications (Kaushal et al. 2018). Even so, there hasn't been much study on WQI prediction utilizing soft computing techniques, notably fuzzy logic systems. This points to a viable area for additional research in the field of assessing water quality (Kumaravel & Vallinayagam 2016).

## STUDY AREA

Two noteworthy bodies of water with important cultural and historical value in Chennai, India, are the Chitrakulam tank and the Kapaleeswarar tank. These tanks have played a significant role in research, providing insightful information on the area's history and enduring customs. In addition to having religious significance, the Kapaleeswarar tank is a vital water source for the neighborhood and is located next to the Kapaleeswarar Temple. The Chitrakulam tank, which is close to the Parthasarathy Temple, has also been important to the local community's religious and cultural practices. These two tanks provide a singular chance to investigate the connections between religion, tradition, and environmental sustainability, making them interesting topics for academic research and study.

### Kapaleeswarar Tank

One of the most venerated and historic holy sites in Chennai is thought to be the Kapaleeswarar Temple (Fig. 1). In Mylapore, a Chennai suburb, is the temple dedicated to Lord Shiva, Kapaleeswarar. The inscriptionsfound on the temple grounds date around 1250 AD. The temple was reportedly constructed by the governing Pallava Dynasty in the eighth century AD, but it is possible that the Portuguese damaged it. The Vijayanagar Kings of the Tuluva dynasty (1491-1570 CE) then reconstructed it.

The sacred tank is situated on the west side of the temple, enhancing the picture view of the temple from the three Mada streets. The brilliant lights from the stores, which are constantly crowded with locals shopping, make the four Mada (east, west, north, and south) streets look incredibly attractive at night. Another noticeable aspect of the tank's water is the way the light reflects off of it. In the center of the tank is a Neerazhi mandapam, which enhances its attractiveness. Kapali Theertham, or holy water, is the name of the liquid in the tank. Sakthi Gangai and Mukthi Theertham are two names used by many followers. The tank is also known as Thamarai thadagam because, in its early years, it was covered in a profusion of lotus creepers that were blossoming and multicolored lotus. 629 feet long and 475 feet wide, the tank is a large structure. On the west side of the tank is a mandapam that is 40 square meters.

### Chitrakulam Tank

In Chennai, Tamil Nadu, the Chitrakulam tank (90607 m) (Fig. 2) is around two km northeastof Royapettah. In terms of latitude and longitude, it is located close to $13^{o}$ 1'52" N and $80^{o}$ 16'14" E. The Kapaleeswarar temple tank is in Chennai, Tamil Nadu, about 7 km southeast of Mylapore. Geographically, it is located close to $13^{o}$ 27'71" Nlatitude and $80^{o}$ 16'5" E longitude. Both of the above tanks are multipurpose tanksused for a variety of summertime activities such as gardening and residential use.

## MATERIALS AND METHODS

The assessment contents are chosen based on the results of

Fig. 1: Kapaleeswarar tank.

Fig. 2: Chitrakulam tank.

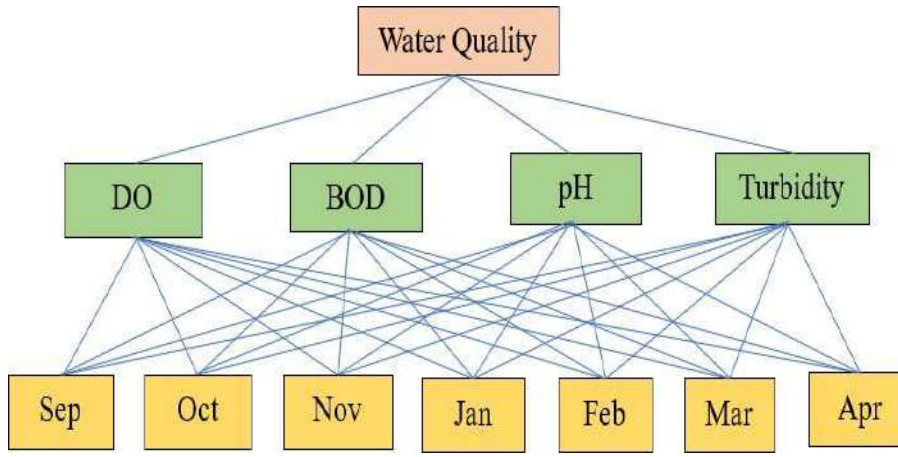


Fig. 3: Hierarchy of water quality assessment.

the field investigations and the monitoring data for water quality at the two tanks. For the parameters Dissolved Oxygen (DO), Biological Oxygen Demand (BOD), pH, and Turbidity (Fig. 3).

## Introduction to the Water Quality Index

Water quality index ranges from 1 to 100; a higher number is indicative of better water quality. WQI rating scale is as follows: 91-100: excellent water quality, 71-90: good water quality, 51-70: medium water quality, 26-50: fair water quality, 0-25: poor water quality (11). The parameters used in defining WQI are pH, Biological Oxygen Demand (BOD), Dissolved Oxygen (DO), and Turbidity. The criteria are given in Table 1 to determine how healthy the water is on a given day (Kumaravel et al. 2020).

Table 1: Water Quality Criteria.

| S. No. | Parameter | Good Quality | Moderate | Poor Quality |
|---|---|---|---|---|
| (a) | pH | 7.5-9.0 | 6.5-7.5 | 5-6.5 |
| (b) | DO | 2-4.5 | 4.5-7 | 7-10 |
| (c) | BOD | Below 2 | 2-3 | 3-6 |
| (c) | Turbidity | 5-10 | 10-25 | - |

## Fuzzy Inference System

In this study, we used an FIS model, a mathematical method that uses fuzzy logic to translate an input into an output. Three essential steps make up the fuzzy inference process: fuzzification, if-then rules, and defuzzification (40). A fuzzy inference approach may be useful for resolving ambiguity and assessing water quality because the data on water quality are ambiguous and unclear (Nayak et al. 2020). The Mamdani method is the most used fuzzy inference approach. In 1965, Zadeh presented the fuzzy logic model (Oladipo et al. 2021).

## Operation of Fuzzy Inference System

Fuzzification of variables, rule evaluation, rule aggregation,

and defuzzification are the four key components of the robust Mamdani fuzzy inference system. The fundamental design of the FIS is shown in Fig. 4.

**Step 1. Fuzzification**

Fuzzification is the first stage of the FIS. Through a variety of membership functions, crisp inputs are converted in this stage into fuzzy inputs known as linguistic variables. A membership function is a visual representation that quantitatively expresses linguistic concepts and visually depicts a fuzzy collection (Palanichamy et al. 2022). To relate the numerical input values to membership grades in fuzzy sets provided with text, fuzzification is used. In this investigation, the input and output parameters were both subjected to a trapezoidal membership function. The trapezoidal membership function, one of the most extensively used membership functions (MF) in fuzzy controller design, has the advantage of simplicity (Ram et al. 2021, Ramirez et al. 2007, Ren et al. 2021 & Rustum et al. 2020).

**Step 2. Inference Engine**

The fuzzy output is produced by the inference engine using the fuzzy rules from the knowledge base. An expression with if-then conditions is known as a fuzzy rule. The following is the ambiguous rule: Y must be B if X is A. In this fuzzy rule, A and B are fuzzy sets, while X and Y are linguistic variables. The aggregation method is used to merge all of the If-then rules into a single fuzzy set after all of the rules have been defined.

**Step 3. Defuzzification**

An expert system's defuzzifier is a crucial part. The processing of fuzzy inference systems ends with defuzzification (Sajan & Christoper 2023). It involves turning a hazy input into a clear output (Shitong et al. 2005). The mean of maximum method (MOM), the centroid of area (COA), the biggest of maximum (LOM), the bisector of area (BOA), and the smallest of maximum (SOM) are some of the different types of defuzzifiers. The most popular defuzzification technique, known as the center of area (CoA) defuzzification method, is also known as the center of gravity (CoG) defuzzification technique. The fuzzy controller in this defuzzification method (CoA) calculates the area under the scaled membership functions and within the output variable's range first.

## RESULTS

**Step 1. Input and Output Variables**

The identification of the variables that make up the system, sometimes referred to as the input and output variables, is the first step in the system modeling process. The factors that have a substantial impact on the result have been selected as inputs. The complexity increases as the number of rules required to manage the inputs increases. Depending on the physical nature of the issue, the conversation may go further or shorter.

**Step 2. Membership Function**

Fuzzy sets are used to express linguistic values. Typically, a fuzzy set's membership functions are used to define it. The employment of the trapezoidal membership function to normalize the acute inputs is made possible by its computational efficiency and simplicity. The membership functions for the inputs and outputs are depicted in Fig. 5 and 6.

**Step 3. Establishing a Linguistic Rule Base**

The relationship between the input and the output was

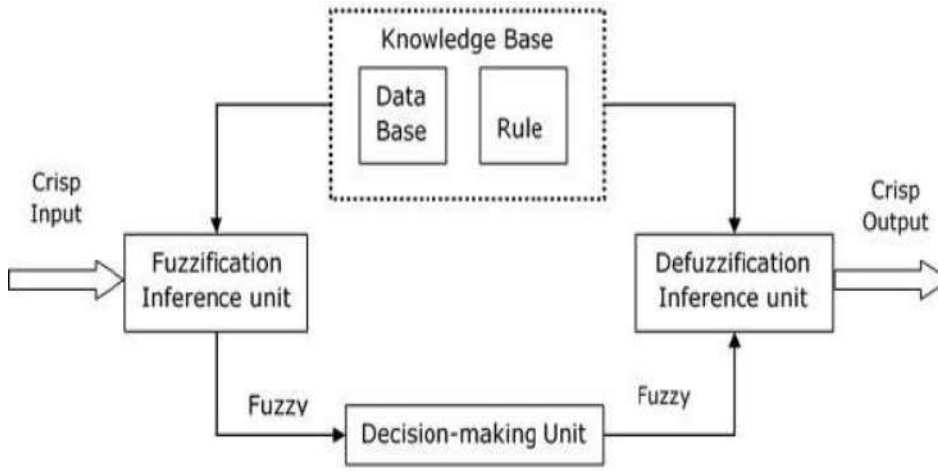


Fig. 4: Structure of fuzzy inference system.

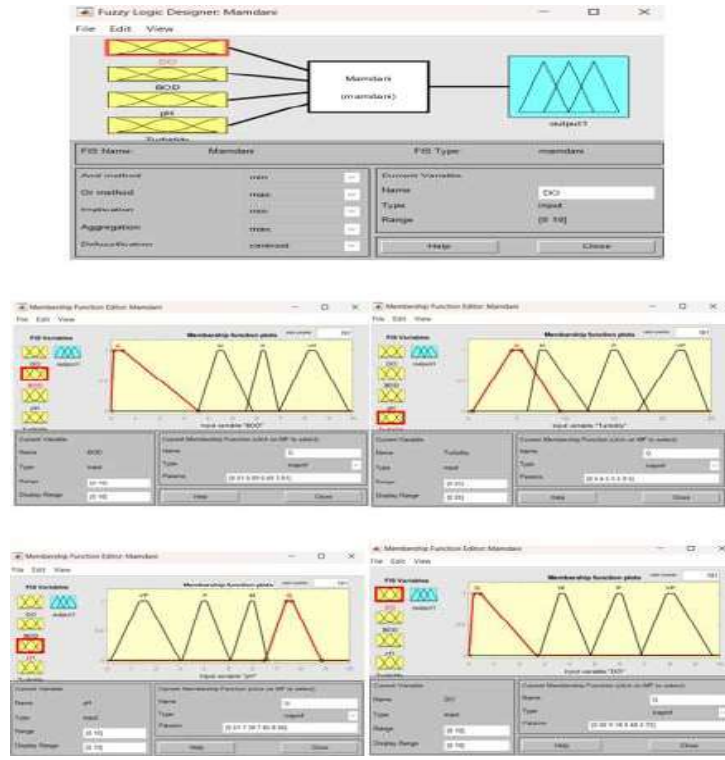


Fig. 5: Input membership function.

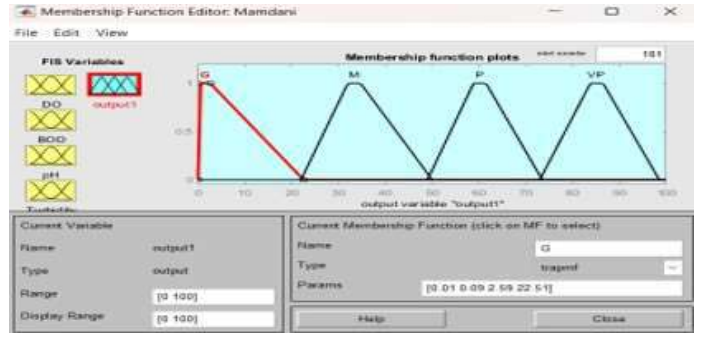


Fig. 6: Output membership function.

demonstrated using IF-THEN rules. As $X_1$, $X_2$, $X_3$, and $X_4$ respectively, the inputs DO, BOD, pH, and turbidity are employed. The values y1 indicate the output of the system (Wu 2019). The model that is suggested in this paper has two fuzzy systems. In this setup, the inputs for $X_1$, $X_2$, $X_3$, and $X_4$ each have four MF. The very first fuzzy system consists of 256 rules. The proposed fuzzy model is built on the architecture of the Mamdani fuzzy model and employs Max-Min inference. The Mamdani fuzzy system's rules are created with the following techniques (Figs. 7 and 8):

### Step 4. Defuzzification

The recommended model employs the Centroid of Area (COA) method of defuzzification to arrive at the answer.

## DISCUSSION

The main objective of this study is the thorough evaluation of water quality indicators for two different ponds, and this evaluation is done in accordance with the recognized Indian water quality standards. Kapaleeswarar Pond receives a 50% weighting in the evaluation procedure, whereas Chitrakulam

Pond receives a 70% weighting, representing the different levels of significance and value that these two aquatic ecosystemshave in relation to the study's objectives.

The study's findings are: (1) The FIS method is appropriate for addressing ambiguous and uncertain environmental issues, particularly assessing water quality to get a clear output and overcome the uncertainty of water quality; (2) The FIS method can be used to evaluate the quality of various types of water; and (3) The Mamdani fuzzy inference system is easier to understand because it is rule-based, and (4) The FIS can apply various defuzzification techniques and, additionally, it is possible to apply various

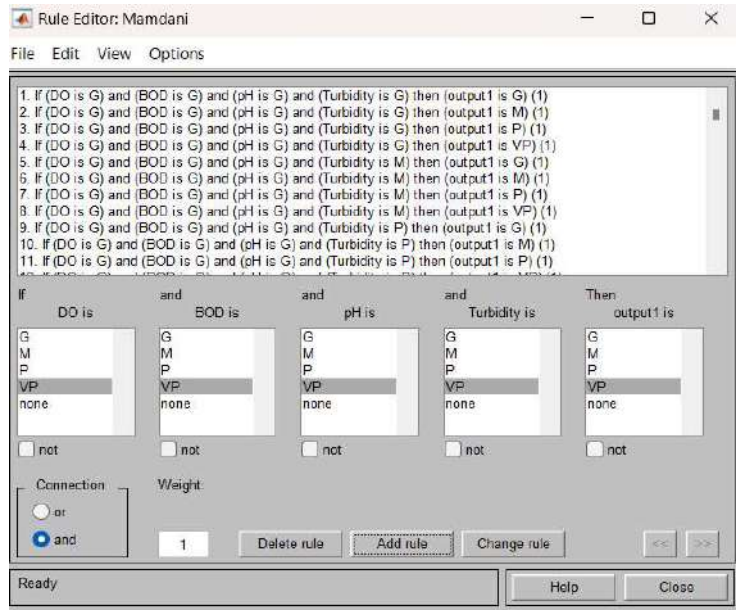


Fig. 7: Rules.

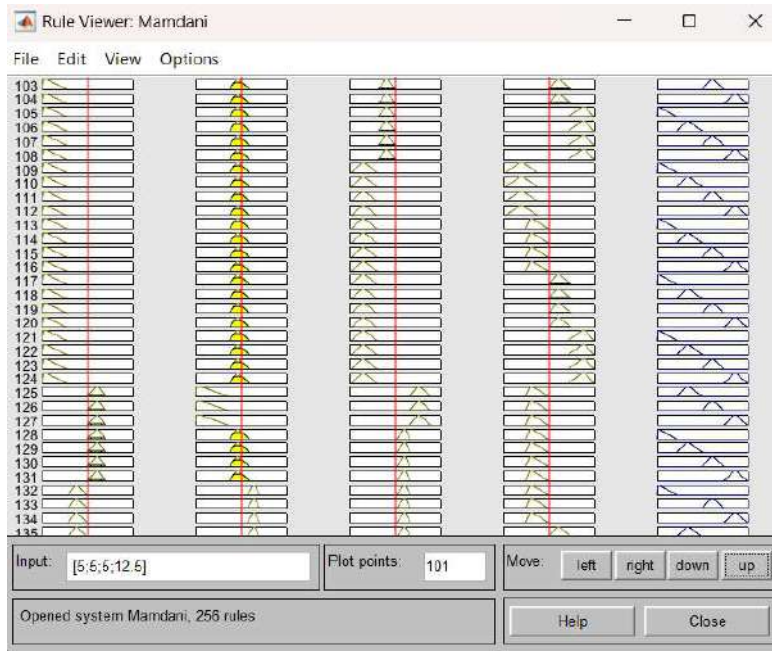


Fig. 8: Rule viewer.

types of membership functions. The FIS can also be used to understand and evaluate the impact of each input parameter on the final water quality.

The outcomes from the proposed Fuzzy Inference System (FIS) model are brought into sharp focus after completing a thorough examination. Comparing these data to the established water quality guidelines reveals an incredibly high degree of similarity. In essence, the predictions and analyses produced by the FIS model show a startlingcongruence with the exact water quality standards set by Indian regulatory bodies.

This extraordinary agreement between the FIS model's predictions and the legally required water quality criteria highlights the model's accuracy in determining the water quality of Kapaleeswarar Pond and Chitrakulam Pond. It highlights the FIS model's potential as a reliable instrument for continued monitoring, management, and conservation efforts targeted at preserving and enhancing the water quality in these essential aquatic ecosystems. Furthermore, it demonstrates the crucial role that cutting-edge modeling and simulation methods may play in improving our comprehension and management of important natural resources.

## CONCLUSION

This article represents an extension of a fuzzy inference system for pond water quality using MATLAB research endeavors, where our primary objective was to developa comprehensive fuzzy model for water quality evaluation. In our ongoing pursuit of enhancing environmental assessment methodologies, we have delved deeper into the intricacies of this model, refining and expanding its capabilities to provide even more valuable insights into the assessment of water quality. Our approach continues to rely on the Mamdani fuzzy inference system, a powerful tool known for its ability to handlecomplex and uncertain environmental data. Within this framework, we meticulously consider four crucial input parameters and an extensive network of 256 fuzzy rules forms the foundation of each fuzzy model. This intricate structure enablesus to address the complexities inherent in assessing water quality in diverse contexts. This article represents a continuation of our commitment to advancing the field of water quality assessment. We recognize that there is always room for improvement, and our model is designed to evolve continually. Future directions include the incorporation of additional input parameters and the exploration of different membership functions, such as sigmoid and Gaussian, to enhance accuracy and comprehensiveness. In essence, this extended article builds upon the foundation established in our earlier research, offering a deeper and more nuanced exploration of our hierarchical fuzzy model's capabilities. It is a testament to our ongoing dedication to refining and expanding our methodologies for assessing and managing water quality, ultimately contributing to a more sustainable and environmentally conscious future.

## REFERENCES

Ammar, T., Lazhar, B. and Lotfi, M. 2018. Evaluation of surface water quality for drinking purposes using fuzzy inference system. Groundw. Sustain. Dev., 6: 235-244.

Asgari, G., Komijani, E., Seid-Mohammadi, A. and Khazaei, M. 2021. Assessment of the quality of bottled drinking water through mamdani fuzzy water quality index. Water Resour. Manag., 35: 5431-5452.

Balamurugan, P., Kumar, P. S., Shankar, K., Nagavinothini, R. and Vijayasurya, K. 2020. Non-carcinogenic risk assessment of groundwater in southern part of Salem District in Tamilnadu, India. J. Chil. Chem. Soc., 65(1): 4697-4707.

Bawoke, G. T. and Anteneh, Z. L. 2020. Spatial assessment and appraisal of groundwater suitability for drinking consumption in Andasa watershed using water quality index (WQI) and GIS techniques: Blue Nile Basin, Northwestern Ethiopia. Cogent Eng., 7(1): 1748950.

Chauhan, S. S. and Trivedi, M. K. 2023. Assessment of surface water quality index of Gwalior-Chambal region using fuzzy-based approach. J. Inst. Eng. India Ser., 104: 1-17.

Dewanti, N. A. and Abadi, A. M. 2019. Fuzzy logic application as a tool for classifying water quality status in Gajahwong River, Yogyakarta, Indonesia. In: IOP Conf. Ser.: Mater. Sci. Eng., 546(3): 032005.

Ellina, G., Papaschinopoulos, G. and Papadopoulos, B. K. 2020. Research of fuzzy implications via fuzzy linear regression in data analysis for a fuzzy model. J. Comput. Methods Sci. Eng., 20(3): 879-888.

Gupta, R., Singh, A. N. and Singhal, A. 2019. Application of ANN for water quality index. Int. J. Mach. Learn. Comput., 9(5): 688-693.

Jang, J. S. R., Sun, C. T. and Mizutan, E. 2005. Neuro-fuzzy and soft computing. New Delhi: Prentice Hall of India Private Limited.

Jha, M. K., Shekhar, A. and Jenifer, M. A. 2020. Assessing groundwater quality for drinking water supply using hybrid fuzzy-GIS-based water quality index. Water Res., 179: 115867.

Kalaivanan, K., Gurugnanam, B., Pourghasemi, H. R., Suresh, M. and Kumaravel, S. 2017. Spatial assessment of groundwater quality using water quality index and hydrochemical indices in the Kodavanar sub-basin, Tamil Nadu, India. Sustain. Water Resour. Manag., 4(3).

Karunathilake, H., Hewage, K., Merida, W. and Sadiq, R. 2019. Renewable energy selection for net zero energy communities: lifecycle-based decision making under uncertainty. Renew. Energy, 130: 558-573.

Kaushal, J. and Basak, P. 2018. A novel approach for determination of power quality monitoring index of an AC microgrid using fuzzy inference system. Iran J. Sci. Technol. Trans. Electr. Eng., 42: 429-450.

Kumaravel, R. and Vallinayagam, V. 2016. A fuzzy inference system for pond water quality using MATLAB. J. Ultra Sci. Phys. Sci., 24(1).

Kumaravel, R., Sudarsan, J. S., Jyothirmai, V. K. and Arun, S. 2020. Water quality index estimation using fuzzy optimization technique. In: AIP Conf. Proc., 2277(1).

Nayak, J. G., Patil, L. G. and Patki, V. K. 2020. Development of water quality index for Godavari River (India) based on fuzzy inference system. Groundw. Sustain. Dev., 10: 100350.

Oladipo, J. O., Akinwumiju, A. S., Aboyeji, O. S. and Adelodun, A. A. 2021. Comparison between fuzzy logic and water quality index methods: A case of water quality assessment in Ikare community, Southwestern Nigeria. Environ. Chall., 3: 100038.

Palanichamy, J., Palani, S., Hebsiba, G. A., Viola, J., Tungsrimvong, A. and Babu, B. 2022. Simulation and prediction of groundwater quality of a semi-arid region using fuzzy inference system and neural network techniques. J. Soft Comput. Civ. Eng., 6(1): 110-126.

Ram, A., Tiwari, S. K. and Pandey, H. K. 2021. Groundwater quality assessment using water quality index (WQI) under GIS framework. Appl. Water Sci., 11: 46.

Ramirez, E. M. and Mayorga, R. V. 2007. A cascaded fuzzy inference system for dynamic online portals customization. Int. J. Intell. Syst. Technol., 2: 7-20.

Ren, J., Man, Y., Lin, R. and Liu, Y. 2021. Multicriteria decision making for the selection of the best renewable energy scenario based on fuzzy inference system. Renew. Energy Driven Future, pp.491-507.

Rustum, R., Kurichiyanil, A. M. J., Forrest, S., Sommariva, C., Adeloye, A. J. and Zounemat Kermani, M. 2020. Sustainability ranking of desalination plants using mamdani fuzzy logic inference systems. Sustainability, 12(2): 631.

Sajan, R. I. and Christopher, V. B. 2023. A fuzzy inference system for enhanced groundwater quality assessment and index determination. Water Qual. Res. J., 58(3): 230-246.

Shitong, W., Chungb, F. L., Bina, S. H. and Dewenc, H. 2005. Cascaded centralized TSK fuzzy system universal approximator and high interpretation. Appl. Soft Comput., 5: 131-45.

Wu, H. C. 2019. Fuzzification of real-valued functions based on the form of decomposition theorem: applications to the differentiation and integrals of fuzzy-number-valued functions. Soft Comput., 23(16): 6755-6775.

## ORCID DETAILS OF THE AUTHORS

M. Priya: https://orcid.org/0000-0003-4505-489X
R. Kumaravel: https://orcid.org/0000-0003-0873-4757

Nature Environment and Pollution Technology
An International Quarterly Scientific Journal

p-ISSN: 0972-6268
(Print copies up to 2016)
e-ISSN: 2395-3454

Vol. 23 | No. 3 | pp. 1783-1794 | 2024

Review Research Paper

https://doi.org/10.46488/NEPT.2024.v23i03.051

Open Access Journal

# Green Nanotech: A Review of Carbon-Based Nanomaterials for Tackling Environmental Pollution Challenges

**Rameeja Shaik, Buddhadev Ghosh, Harish Chandra Barman, Arijit Rout and Pratap Kumar Padhy†**
Department of Environmental Studies, Siksha Bhavana (Institute of Science), Visva-Bharati, Santiniketan-731235, West Bengal, India
†Corresponding author: Pratap Kumar Padhy; pkpadhy@visva-bharati.ac.in

**Nat. Env. & Poll. Tech.**
**Website: www.neptjournal.com**

*Received:* 07-01-2024
*Revised:* 08-03-2024
*Accepted:* 17-03-2024

**Key Words:**
Carbon-based nanomaterials
Environmental sustainability
Nanotechnology
Environmental pollutants

## ABSTRACT

In recent times, nanotechnology has experienced widespread acclaim across diverse sectors, including but not limited to tissue engineering, drug delivery systems, biosensors, and the mitigation and monitoring of environmental pollutants. The unique arrangement of carbon atoms in sp3 configurations within carbon nanomaterials endows them with exceptional physical, mechanical, and chemical characteristics, driving them to the forefront of materials research. Their appeal lies in their efficacy as superior adsorbents and their exceptional thermal resistance, making them versatile in various applications. The present review extensively explores a range of carbon-based nanomaterials, delving into their synthesis methods and examining their multifaceted applications in addressing environmental pollutants. It is crucial to emphasize that the popularity of carbon-based nanomaterials arises from their potential to serve as superior adsorbents, coupled with their outstanding thermal resistance properties. These attributes contribute to their applicability in diverse environmental contexts. Looking ahead, carbon-based nanomaterials are poised to emerge as environmentally friendly and cost-effective materials, representing promising and potential avenues for the advancement of sustainable technology.

## INTRODUCTION

Nanotechnology, a convergence of science, engineering, and technology dedicated to manipulating materials at the nanoscale, where structures or devices range from 1 to 100 nanometers in size (Guldi & Prato 2000), is a transformative domain that employs nanotechnological methods to manipulate the molecular structure of materials. This manipulation serves to alter their intrinsic properties, unlocking a plethora of revolutionary applications (Ghorbani et al. 2020). The broad scope of nanotechnology extends to environmental applications, contributing to environmental protection by comprehending and regulating emissions from diverse sources. It acts as a catalyst for the development of green technologies, minimizing the generation of undesirable by-products. Moreover, nanotechnology not only offers solutions for addressing current waste and polluted sites but also demonstrates remarkable capabilities in the targeted elimination of minute contaminants from the soil, water, and air ecosystems (Lucky et al. 2015, Qin et al. 2021).

The historical deployment of nanoscale materials traces back millions of years (Aris et al. 2020). In contemporary times, nanotechnology stands as an emerging applied technology in the developing world, addressing challenges in environmental and human health mitigation (Hao et al. 2021). Present-day scientists and engineers are exploring diverse avenues to create novel materials at the nanoscale, aiming to enhance properties such as strength and chemical activities. A prominent example of materials at the nanoscale is found in carbon-based nanomaterials, also referred to as organic nanomaterials. This category includes fullerene, carbon dots, graphene, carbon nanoparticles (CNP), and carbon nanotubes, among others. These structured nanomaterials are distinguished by the presence of sp2-bonded carbon atoms, further classified based on their dimensions (Testa et al. 2019). The unique properties of carbonaceous- nanomaterials and their application in the environment are listed in Table 1.

This comprehensive review synthesizes various applications and fields where modern carbon-based nanoscience technology can be harnessed for environmental pollution mitigation. Its applications span the removal of dyes, heavy metals, pesticides, hydrocarbons, and radioactive compounds, showcasing the diverse potential of this cutting-edge technology in contributing to environmental sustainability.

Table 1: The unique properties of carbonaceous- nanomaterials and their application in the environment (Meagan et al. 2008).

| The unique properties | Pollution prevention | Absorbents | Composite filters | Sensors | Energy Storage |
|---|---|---|---|---|---|
| Size | - | √ | √ | √ | - |
| Surface Area | √ | √ | √ | | |
| Molecular Specificity | - | √ | - | √ | √ |
| Hydrophobicity | - | √ | √ | - | - |
| Thermal Conductivity | √ | - | - | - | √ |
| Electrical Conductivity | - | - | - | √ | √ |
| Optical Activity | - | √ | - | - | - |

## SYNTHETIC STRATEGIES FOR CARBON-BASED NANOMATERIALS

Carbon-based nanomaterials showcase distinctive characteristics stemming from their nanoscale dimensions, extensive surface area, and quantum effects. Carbon is the building block of choice for a wide variety of carbon-based nanomaterials at this scale. Notable examples of these nanomaterials are carbon nanotubes, graphene, fullerenes, and carbon nanodots, all of which will be discussed in more detail next.

### Carbon Nanotubes

A novel class of nanomaterials known as carbon nanotubes (CNTs) are made of concentric graphite carbons arranged in one or more tubular forms. Within the CNT classification, both single-walled nanotubes (SWNT) and multiple-walled nanotubes (MWNT) demonstrate extraordinary three-dimensional and thermally stable features along with unique chemical activities (Derakhshi et al. 2022). These nanomaterials hold significant potential for the remediation of various hydrocarbons, including chemical pesticides. The presence of a wide range of surface-accessible functional groups and the pore structure of CNTs are closely related to their adsorption capacity for contaminants. Enhancing the performance of CNTs for specific applications requires the customization of functional groups through chemical or thermal methodologies.

The synthesis of CNTs can be achieved through diverse methods, with three noteworthy approaches, including:

### Arc Discharge

An arc voltage is applied in this technique between two graphite electrodes that are placed across from one another. As temperatures rise to about 6000ºC, carbon directly transitions from a solid to a gaseous form without passing through a liquid phase. Nanotube formation occurs on the cathode as atoms migrate toward colder regions within the chamber (Karimi et al. 2015). The electric arc discharge method is also called as Plasma Arcing method. The electrodes are made to strike each other under these conditions, it produces an electric arc.

The energy produced in the arc is transferred to the anode, which ionizes the carbon atoms of a pure graphite anode, produces $C^+$ ions, and forms plasma (Plasma is atoms or molecules in a vapor state at high temperature). These positively charged carbon ions move towards the cathode, get reduced and deposited, and grow as CNTs on the cathode.

### Chemical Vapor Deposition

Chemical vapor deposition is a technique in which the vaporized reactants react chemically and form a nanomaterial product that is deposited on the substrate. Substrates are materials on which the carbon nanotube is grown. Zeolite, silica, and silicon plates coated with iron particles are commonly used substrates in chemical vapor deposition.

Hydrocarbons play a pivotal role in this method, serving as both a carbon source and a catalyst (utilizing iron, nickel, or cobalt nanoparticles) for nanotube growth on its surface (Okai et al. 2000).

### Laser Ablation

The laser ablation method is also called as physical vapor deposition method. In this technique, graphite is vaporized with a laser in the presence of Ni or Co catalysts. When the laser interacts with a graphite surface, the vaporized carbon atoms coalesce to form soot, which is then collected by a cooled copper collector (Bota et al. 2014).

The graphite target is vaporized by either a continuous laser source or a pulsed laser source. The vaporized target atoms (carbon) are swept toward the cooled copper collector by the flow of argon gas. The carbon atoms are deposited and grown as CNTs on a cooled copper collector. By this method, multi-walled carbon nanotubes are synthesized, and to synthesize single-walled carbon nanotubes, catalyst nanoparticles of Fe, Co, and Ni are used. At last, the obtained carbon nanotubes are further purified to get the pure form of carbon nanotubes.

## Graphene Nanomaterials

With its unique two-dimensional atomic crystal structure, graphene is a breakthrough in the field of carbon-based nanomaterials. It is essential for the removal of heavy metals from wastewater. When it comes to the removal of heavy metals from contaminated water and wastewater, graphene oxide (GO) and reduced graphene oxide (RGO) are both very useful (Okai et al. 2000). A variety of oxygen-based functional groups, including hydroxyls, carboxyls, epoxides, and carbonyl functionalities, are included in graphene oxide, an oxidative derivative of graphene. Its capacity to extract heavy metals from tainted wastewater is enhanced by these functional groups (Derakhshi et al. 2022). The fundamental process by which they are effective in removing heavy metals can be attributed to their large specific surface area and diverse functional groups. Synthesis techniques like Scotch tape, Chemical Vapor Deposition (CVD), laser-assisted methods, or exfoliation are employed to produce graphene sheets, with the oxidation of GO contributing to chemical exfoliation (Ye & Tour 2019).

The utilization of graphene-based materials, such as GO/RGO, for the removal of heavy metals from wastewater has been extensively studied. Variables like temperature, ion coexistence, adsorbent dosage, contact time, and pH have all been examined. According to earlier research, the adsorption process closely resembles the second pseudo-second-order kinetics and Langmuir isothermal models. GO was proven to be a highly effective adsorbent for zinc [II], with a maximum adsorption capacity of 246 $mg.g^{-1}$. The present research trajectory emphasizes the application of nanomaterials based on graphene for the removal of heavy metals from wastewater and water. To remove heavy metals, for example, calcium alginate (CA) beads embedded in graphene oxide and further decreased by polyethyleneimine significantly increase the adsorption capacity. The nanocomposite is superior in eliminating Pb [II], Hg [II], and Cd [II] ions, as evidenced by the Langmuir isotherm, which shows that it reaches high adsorption capacities for these ions at 602 $mg.g^{-1}$, 374 $mg.g^{-1}$, and 181 $mg.g^{-1}$, respectively. Functionalized beads, often reduced by polyethyleneimine, exhibit even higher adsorption abilities due to a synergistic effect.

Beyond the realm of heavy metal removal, graphene nanomaterials find diverse applications in gene/drug delivery, tissue engineering, and photodynamic therapies, leveraging their exceptional Surface Enhanced Raman Scattering (SERS), mechanical and electrical compatibility, aqueous processability, among other attributes (Ghosal & Sarkar 2018).

## Carbon Dots

Carbon dots (CDs) represent carbon-based nanomaterials synthesized through advanced methods such as chemical oxidation, electrochemical processes, microwave treatment, microplasma techniques, and solvothermal/hydrothermal methods. Carbon Dots (CDs) are classified into discrete categories, including Carbonized Polymer Dots (CPDs), Graphene Quantum Dots (GQDs), and Carbon Quantum Dots (CQDs), every one of which has a different structure and set of properties due to the different synthesis techniques used. Because CDs have a large surface area, stability, and a variety of functional groups, they are very desirable for managing environmental pollution because of their exceptional sorption capacity for contaminants. CDs have found practical applications as nano-photocatalytic and nano-organocatalytic platforms, showcasing their versatility and effectiveness in addressing environmental challenges (Rosso et al. 2020).

## Carbon Fibers

During the 1960s, carbon fibers (CNFs) emerged as a significant focus in industrial applications and scientific research, primarily synthesized through the melt-spinning of carbon precursors, as detailed by Rodriguez in 1993. An essential precursor was polyacrylonitrile (PAN), which underwent several changes, such as low-temperature oxidation stabilization, addition of additives, stretching during stabilization, and carbonization after that. A key factor in the creation of vapor-grown carbon fibers (VGCFs) was the catalytic chemical vapor deposition (CVD) technique. Two predominant methods for CNF synthesis, as outlined by Ruiz-Cornejo et al. (2020), involve:

a) Carbonization and electrospinning of polymers.

b) Catalytic decomposition of carbon precursors.

In carbon nanofibers (CNFs) synthesis by using catalytic chemical vapor deposition (CVD), carbon-containing gas undergoes decomposition, and it is catalyzed by metal particles. The most commonly employed metal catalysts for the development of CNF include Ni, Co, and Fe, with additional investigations into the catalytic capabilities of metals such as V, Ni, Cr, and Mo (Ashok et al. 2010). In groundbreaking research led by Zhou et al. (2016), an environmentally friendly approach was adopted for carbon fiber manufacturing.

Traditionally, carbon fibers are derived from fossil fuels as starting materials. However, waste cotton linter was used in this experiment as a raw material, enabling the cost-effective production of crude Cellulose Carbamate (CC) fibers through the innovative Carba Cell technology, incorporating carbonization and wet-spinning methods. This sustainable and resource-efficient method signifies a departure from the conventional reliance on fossil fuels for carbon fiber production, as testified by Zhou et al. (2015) in their study.

### Fullerenes

Discovered in 1985, Buckminsterfullerene (C60) has gained widespread acknowledgment for its unique photochemical and photophysical attributes, extensively elucidated by Arbogast et al. (1991). As a representative of spherical fullerenes, C60 exhibits a distinctive propensity to serve as a sensitizer in the photo-induced generation of singlet oxygen (1O2) reactive oxygen species (ROS), as discussed by Sharma et al. (2011). This specific property of fullerenes has been strategically applied in practical domains such as photodynamic cancer therapy and blood sterilization, as emphasized by the research works of Arbogast et al. (1991), Sharma et al. (2011), and Accorsi et al. (2010).

Initially, the synthesis of fullerenes involved a controlled environment utilizing laser vaporization of carbon. However, methodologies for C60 fullerene production have advanced, encompassing techniques like arc heating of graphite as a carbonization source and laser irradiation of polyaromatic hydrocarbons, as meticulously detailed by Nimibofa et al. (2018). Sinitsa et al. (2017) conducted an exhaustive exploration into the formation of fullerenes from amorphous carbon clusters, delineating a two-step process. The initial phase involves rapid reactions leading to the transformation of the amorphous structure into hollow sp2 structures. Subsequently, the remaining carbon chains are concurrently integrated into the sp2 structure during the formation of the fullerene shell.

### Carbon Nanodiamond [NDs]

Nanodiamonds, belonging to the nanocarbon family, are carbon nanoparticles characterized by truncated octahedral structures with a diameter ranging from 2 to 8 nm. This structural feature facilitates the effective delivery of proteins, nucleic acids, and small molecules, as demonstrated by Chen et al. (2008) and Zhang et al. (2009). The distinctive optical, chemical, and biological properties, in conjunction with their non-toxic nature and expansive surface area attributes, render diamond nanoparticles a subject of significant interest, especially in the fields of drug and gene delivery, as expounded by Mengesha in 2013.

The production of Nanodiamonds (NDs) involves various methodologies, including hot filament chemical vapor deposition, laser ablation, high-energy ball millings, microwave plasma-enhanced chemical vapor deposition, irradiation of graphite with high-energy ions at room temperature, low-temperature neutral beam-enhanced chemical vapor deposition, and electrical irradiation of carbon ions, as comprehensively detailed by Pandey et al. (2021).

### Activated Carbons (ACs)

AC is a carbonic substance distinguished by well-defined micropores, presenting a substantial internal surface area, pore volume, and notable adsorption capabilities (Galvão et al. 2021). Its versatile applicability is evident across diverse domains, particularly in water treatment, purification processes, organic dye removal, and gas adsorption, spanning industries such as petroleum, cosmetics, textiles, and automobiles (Lima et al. 2016, Tadda et al. 2016). The predominant commercially available forms of AC include powdered activated carbons (PACs) and granular activated carbons (GACs) (Deng et al. 2015).

PACs typically exhibit superior adsorption capacities compared to GACs, attributed to their increased specific surface area and microporosity (Alslaibi et al. 2013). GAC can result from rigid biomass materials like palm kernel shells and coconut shells, undergoing activation through physical or chemical methods of producing GAC (Jjagwe et al. 2021). Alternatively, GAC can be synthesized from soft biomass waste materials, utilizing low-density granulation or PAC granulation with binders to create pellets or granules with enhanced adsorption capacity (Deshannavar et al. 2018).

Various granulation processes, such as vibration dropping, spray coating, extrusion, or manual application on raw precursors, contribute to the synthesis of GAC (Mustafa & Asmatulu, 2020), PAC (Nagalakshmi et al. 2019), and/or carbonized precursors (Aransiola et al. 2019). Moreover, activated carbon can be produced from diverse waste materials, including agricultural, fruits, vegetables, plastic, and electronic waste (e-waste). E-waste, encompassing discarded electronic gadgets such as mobile phones, CPUs, and refrigerators, especially non-metallic segments like printed circuit boards (PCBs), serves as a valuable resource for nano-activated carbon production. Activated carbon generated from e-waste demonstrates significant potential as an adsorbent for the removal of $Cu^{+2}$, $Zn^{+2}$, $Cd^{+2}$, and $Pb^{+2}$ metals from wastewater (Hadi et al. 2014).

## APPLICATIONS FOR CARBON-BASED NANOMATERIALS

Using carbon-based nanomaterials for ecological remediation is a useful way to promote sustainable development and reduce pollution, and it provides a workable alternative to current approaches. Fig. 1 explains the various uses of carbon-based nano-materials.

### Removal of Synthetic Dyes

Dyes are widely used in a variety of industries, including textiles, leather, cosmetics, and pigments. However, when

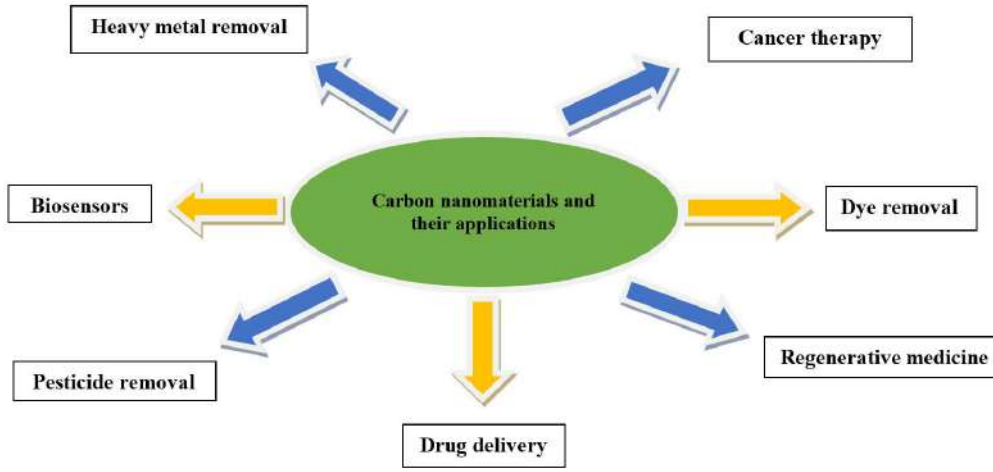


Fig. 1: Various applications of carbon nano-materials.

they are disposed of into wastewater, they provide serious health and environmental hazards. Mitigating these risks necessitates careful consideration due to their potential hazards. Recent years have witnessed significant efforts devoted to addressing this issue through the implementation of conventional biological, chemical, and physical methods for the elimination of colorants from water. Amid these methods, adsorption, acknowledged for its efficiency and cost-effectiveness in dye removal (Wang et al. 2012a), has gained prominence, particularly with the emergence of Carbon Nanotechnology as a rapidly advancing field. As thoroughly covered in a review offering a wealth of literature information on diverse dye removal techniques, including dyes, classification, toxicity, and the use of carbon-based nanomaterials, the use of carbon-based nanomaterials for dye removal has proven beneficial (Ghaedi et al. 2012).

Azo dyes, constituting a significant group of organic compounds extensively used in textiles, leather, and various industries, present a considerable environmental challenge, with an estimated global production of one million tonnes annually. These synthetic compounds, characterized by azo groups (-N = N-) as chromophores, contribute to substantial wastewater discharge during dyeing, accounting for 10-15% of the applied dye. This discharge poses severe problems globally, as the inefficiency of immobilizing dyes to substrates, dependent on the immobilization method or affinity, results in the formation of colored water, thereby deteriorating water quality (Rajabia et al. 2017). Azo dyes, being water-soluble, enter the environment through runoff, exhibiting mutagenic and carcinogenic effects on various living organisms and impacting the photosynthetic activity of plants by limiting sunlight penetration. Furthermore, the toxic effects of these dyes lead to tumors, cancers, and allergies in humans, inhibiting the growth of algae, bacteria, protozoa, plants, and various animals (Ghaedi et al. 2012).

A wide range of methodologies, including physical, chemical, and biological approaches, have been utilized in the elimination of azo dyes. Microbial degradation, especially bacterial degradation, is a highly effective way to remove pollutants from the environment (Kaizar & Ismail 2015, Kaizar et al. 2016). While molds and algae primarily discolor contaminated dyes in wastewater through adsorption rather than decomposition, bacteria can destroy the dye under specific conditions, producing intermediate by-products such as aromatic amines with the help of hydroxylase and oxygenase enzymes. Carbon-based nanomaterials, notably carbon nanotubes, have garnered attention for their efficacy in removing dyes and treating wastewater through adsorption (Mashkoor & Nasar 2020). Noteworthy studies involve low-cost graphene-based nano adsorbers, such as sulfonated magnetic graphene oxide (SGMO), demonstrating efficacy in eradicating methylene blue from aqueous solutions. After seven cycles of eliminating cationic pollutants, numerous reuse and regeneration analyses revealed that SGMO's efficacy was consistently maintained above 80%, making it a viable option for wastewater treatment (Kumari et al. 2023). Table 2 in various studies underscores the potential of carbon nanotubes as adsorbents, showcasing their capacity to effectively remove synthetic dyes from waste, providing a promising avenue for sustainable and efficient dye removal processes.

## Removal of Heavy Metals

Nowadays, the burgeoning challenge of metal pollution has emerged as a formidable concern within environmental ecosystems, necessitating immediate and concerted efforts to mitigate severe threats. The urgency for proficient heavy metal processing emanates from the potential enduring

Table 2: Types of carbon adsorbents and their adsorption capacity.

| Adsorbent | Dye | Adsorption capacity [mg.g$^{-1}$] | Reference |
|---|---|---|---|
| MWCNT | Methyl Blue | 57.6 | Wang et al. (2012) |
| MWCNT | Reactive Blue 4 | 309.2 | Machado et al. (2012) |
| Carbon nanotubes | Methylene blue | 188.68 | Royer et al. (2009) |
| SWCNT-COOH | Basic red 46 | 49.45 | Rajabia et al. (2017) |
| $HNO_3$/NaClO/MWCNTs | Bromothymol blue | 55.25 | Ghaedi et al. (2012) |

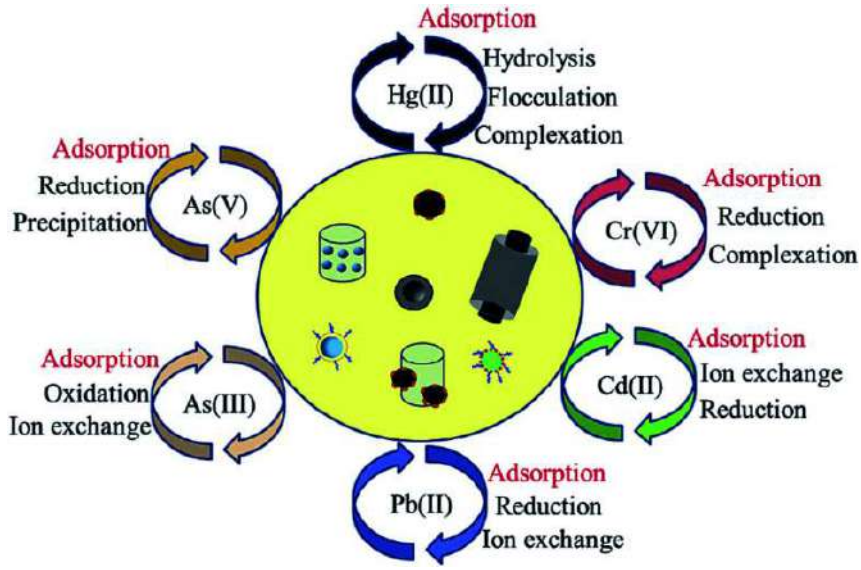


(Source from Xu et al. 2018)

Fig. 2: The Pathways for removal of heavy metal ions by functionalized nanomaterials in aqueous solution.

consequences on sustainability and environmental resilience (Tanveer et al. 2018). A variety of approaches to the removal of heavy metals from wastewater have been thoroughly examined. Conventional procedures include flotation, coagulation-coagulation, adsorption, membrane filtration, ion exchange, chemical precipitation, and electrochemical processes. (Lihua et al. 2018). The comprehensive analysis of the literature highlights the critical role that nanoscale materials play in the treatment of wastewater contaminated with heavy metals, with a focus on ion exchange, adsorption, and membrane filtration (Tanveer et al. 2018).

While nanomaterials have demonstrated efficacy in water treatment, challenges pertaining to stability, toxicity, and recovery have spurred innovative solutions. In the realm of heavy metal removal, this review provides an updated panorama of key technologies and materials, with specific emphasis on nanoscale materials and processes. Surprisingly, certain carbon-based nanomaterials, such as graphene and its derivatives, activated carbon, and carbon nanotubes (SWCNTs and MCWNTs), have gotten a lot of interest because of their outstanding characteristics and efficacy in heavy metal removal (Alekseeva et al. 2016, Dehghani et al. 2015).

In recent decades, a great deal of research has been conducted on carbon-based nanomaterials, which have demonstrated high adsorption properties, especially for heavy metal ions like arsenic, chromium, zinc, lead, nickel, and mercury. Due to these metals' lack of biodegradability, there are significant dangers to both human health and the food chain. (Farghali et al. 2017). Table 3 summarizes a comprehensive summary of the adsorption capacities of various carbon nanomaterials for eliminating heavy metal ions from wastewater. The intricate relationship between surface functional groups and heavy metal ions is intimately linked to the surface properties of the nanomaterials. Carbon nanomaterials can absorb metal ions primarily through physical adsorption, precipitation, reduction/sorption, ion exchange, and electrostatic interactions. (Fig. 2). A complete understanding of these mechanisms is crucial to designing and implementing carbon-based nanomaterials to remove heavy metals from wastewater as effectively as possible.

## Removal of Pesticides

Globally, pesticides play a pivotal role in safeguarding agricultural crops against the detrimental impact of pests,

Table 3: Metal ion adsorption capacity of carbon nanomaterials.

| Adsorbent | Metal ions | Adsorption capacity [$mg.g^{-1}$]/efficiency % | Reference |
|---|---|---|---|
| Fullerene [C6] | $Cu^{+2}$ | 14.6 $mmol.g^{-1}$ | Alekseeva et al. (2016) |
| Porous graphene | $As^{+3}$ | 90% | Tanveer et al. (2018) |
| SWCNTs | $Cr^{+6}$ | 2.35 $mg.g^{-1}$ | Dehghani et al. (2015) |
| Functionalized MWCNTs | $Pb^{+2}$<br>$Ni^{+2}$<br>$Cd^{+2}$<br>$Cu^{+2}$ | 93%<br>83%<br>15%<br>78% | Farghali et al. (2017) |
| Spent activated carbon | $Pb^{+2}$<br>$Cd^{+2}$ | 95% | Lihua et al. (2018) |

Table 4: The adsorbent capacity of graphene-based materials of pesticides.

| Adsorbent | Pesticide | Adsorption capacity [$mg.g^{-1}$] | Reference |
|---|---|---|---|
| Cellulose/Graphene composite | Triazine pesticides, Prometryn, Simeton, Cyprazine, Altrazine, Ametryn | 30 | Zhou and Fang (2015) |
| Graphene quantum dots [GQD] | Carbamate pesticide oxamyl | 0.6 | Aris et al. (2020) |
| Graphene oxide [GO] and iron oxide magnetic nanoparticles [MNPs] | Dieldrin and Endrin | Dieldrin-28 $mg.L^{-1}$<br>En<br>drin-99 $mg.L^{-1}$ | Suo et al. (2018) |
| Reduced graphene oxide-silver nanocomposite [rGO@Ag] | Endosulfan, Dichlorodiphenyl dichloroethylene, Chloropyrifos | 1534 | Sen Gupta et al. (2015) |
| Sieve-like cellulose/ Graphene oxide composites [ACCE/G] | Chloropyrifos | 152.5 | Wanjeri et al. (2018) |

weeds, and fungi, thereby significantly contributing to enhanced agricultural productivity (Suo et al. 2018). Nevertheless, the extensive utilization of pesticides has resulted in the widespread dispersion of their residues in critical environmental reservoirs, including drinking water, groundwater, and soil. The pervasive environmental pollution caused by pesticides is attributed to multiple pathways, including dust, agricultural runoff, direct spraying, and industrial waste streams. This omnipresent presence poses substantial environmental threats to aquatic ecosystems and diverse life forms (Aris et al. 2020).

Acknowledging the environmental repercussions of pesticide residues, regulatory agencies have implemented stringent limits to mitigate their impact. For instance, the drinking water directive establishes a threshold of 0.1 $\mu g.L^{-1}$ for individual drugs and pesticides and 0.5 $\mu g.L^{-1}$ for all pesticides detected during follow-ups (Sen Gupta et al. 2015). Regulatory mandates necessitate the identification of pesticides in soil and water, prompting swift actions to eradicate them from contaminated sites. Various technologies, including adsorption, photocatalysis, membrane separation, and biodegradation, are deployed for pesticide removal, with their effectiveness contingent on the material properties and chemistry of the contaminants. Advanced water and wastewater treatment methods, particularly those leveraging nanotechnology and nanomaterials, have gained prominence, bolstering the overall efficiency of the system (Wanjeri et al. 2018).

Operating at the molecular scale, ranging from 1 nm to approximately 100 nm, nanotechnology introduces novel physical properties, chemistry, and biology distinct from their bulk counterparts. Nanomaterials, characterized by their microscopic size, high surface area-to-volume ratio, surface-modifying capabilities, and exceptional magnetic properties, prove more effective and efficient in pesticide removal.

The physicochemical attributes of nanomaterials, coupled with their specific targeting capabilities and environmental friendliness, position them as ideal candidates for pesticide removal. Functionalization with diverse chemical groups is a common strategy to enhance nanomaterials' efficiency in removing targeted compounds. This paper aims to provide a comprehensive overview of recent advances in nanotechnology applied to pesticide removal, spanning adsorption, filtration, and decomposition (Zhou & Fang 2015).

A groundbreaking method introduced by Xu et al. (2019) involves the preparation of Magnetic Porous Carbon Materials (MPMs) comprising porous carbon and iron nanoparticles, showcasing exemplary pesticide removal efficacy in rice fields. Adsorption emerges as a predominant application in pesticide removal, offering advantages such as low initial cost, flexibility, design simplicity, ease of use, and

insensitivity to toxic pollutants. Importantly, the adsorption process does not generate additional toxic by-products post-treatment. This surface phenomenon hinges on factors like porosity, the availability of adsorption sites, diverse interactions, and the specific surface area of the adsorbent.

Shifting focus to India, a region extensively employing pesticides like lindane and malathion, the utilization of low-cost adsorbents such as graphene and its derivatives (graphene oxide, graphene quantum dots, and reduced graphene oxide) presents a promising avenue for reducing pesticide levels in water. Table 4 provides a detailed insight into the adsorption capacity of graphene-based materials for removing pesticides.

Various physicochemical factors, including initial concentration level ($mg.L^{-1}$), average time of contact (min), pH value, operating temperature (°C), and efficiency of removal (%), undergo variation to attain their optimal values in the interaction between sorbate and sorbent. This optimization is crucial for achieving the maximum efficiency of adsorption of carbon-based nanomaterials in the reduction of pesticides, and the pertinent details are consolidated in Table 5.

## Removal of Hydrocarbons

Hydrocarbon pollutants represent a substantial environmental hazard, predominantly emanating from sources such as crude oil, petroleum-based derivatives, pesticides, and the discharge of diverse hazardous organic compounds into aquatic ecosystems via sewage channels (Fasfous et al. 2010). In the concerted effort to confront the challenges posed by environmental contamination, nanotechnology emerges as a propitious solution, capitalizing on technological advancements and ongoing progress (Tóth et al. 2012). Carbon-based nanomaterials (CNM) assume significance in this domain, comprising a category of materials distinguished by distinctive physical and chemical attributes, including expansive surface areas, elevated mechanical strength, conductivity, and stability (Yao et al. 2014). Noteworthy examples of carbon-based nanomaterials encompass fullerenes, carbon nanotubes, graphene, and graphene derivatives, each characterized by a specific array of properties. To provide a comprehensive elucidation of their capabilities, Table 6 furnishes an overview of the hydrocarbon removal capacities exhibited by various carbon adsorbents.

## Removal of Radioactive Waste

Radioactive waste, predominantly originating from domestic and industrial activities, represents a significant concern for environmental integrity and human well-being (Mubarak et al. 2016, Zhang et al. 2013, Tan et al. 2016, Yılmaz et al. 2020). Effective management of radioactive waste is imperative due to the inherent risks associated with radioactive materials. The ionizing nature of these materials leads to the generation of free radicals, instigating oxidative stress that detrimentally impacts proteins, membranes, and nucleic acids. The interaction between free radicals and DNA plays a pivotal role in cancer development, disrupting molecular processes and fostering mutations that may result in malignant tumors.

Table 5: Optimized physiochemical parameters of different pesticides for adsorption during removal of Pesticides using carbon-based nanocomposite materials.

| Carbon-Based Nanocomposite Materials | Name of pesticide | Initial concentration level [$mg.L^{-1}$] | Average time of contact [min] | pH value | Operating temperature [°C] | Efficiency of removal [%] | Reference |
|---|---|---|---|---|---|---|---|
| Graphene-coated | Bifenthrin, Cyhalothrin, Permethrin, Cypermethrin, Phenvalerate & Deltamethrin | 0.01 | 90 | - | 270 | - | Chen et al. (2010) |
| Graphene-based | Thiamethoxam | $5 \times 10^{-7}$ | 10 | 6 | 30 ± 2 | 55 | Wang et al. (2012) |
| | Imidacloprid | $5 \times 10^{-7}$ | 10 | 6 | 30 ± 2 | 78 | |
| | Acetamiprid | $5 \times 10^{-7}$ | 10 | 6 | 30 ± 2 | 72 | |
| Graphene-based magnetic nanocomposite | Atrazine | 0.01 | 30 | 6–7 | 25 ± 2 | 84-96.4 | Wu et al. (2011) |
| | Prometon | 0.01 | 30 | 6–7 | 25 ± 2 | 84-96.4 | |
| | Ametryn | 0.01 | 30 | 6–7 | 25 ± 2 | 84-96.4 | |
| | Prometryn | 0.01 | 30 | 6–7 | 25 ± 2 | 84-96.4 | |
| Graphene-coated silica | Thiacloprid | 10–7 | 10 | 6 | 30 ± 2 5 | 70 | Liu et al. (2013) |
| cellulose/graphene composite | Atrazine | 1 | 0 | 9 | 25-45 | 98 | Zhang et al. (2013), (2015) |

Table 6: Hydrocarbon removal capacity of carbon adsorbents.

| Adsorbent | Hydrocarbon | Removal capacity [%] | Reference |
|---|---|---|---|
| MWCNTs | Tetrabromobisphenol [TBBPA] | 90 | Fasfous et al. (2010) |
| Oxidized SWNTs | p-Nitrophenol | 97.9 | Yao et al. (2014) |
| MWCNT-COOH | 3-chlorophenol | 95% | Tóth et al. (2012) |
| $HNO_3$ and $KMnO_4$ functionalized MWCNTs | Phenol | 88% | Mubarak et al. (2016) |
| Graphene oxide[GO] | TBBPA | 70 - 90% | Zhang et al. (2013) |

Table 7: The adsorptive capability of carbon nanomaterials for radioactive compounds.

| Adsorbent | Radioactive material | Adsorption capacity [$mg.g^{-1}$]/Removal efficiency % | Reference |
|---|---|---|---|
| Graphene oxide | $^{137}Cs$ | 55% | Nagalakshmi et al. (2019), Yin et al. (2016), Tan et al. (2016) |
| Graphene | Iodine-131 | 0.878 $mg.g^{-1}$ | Yılmaz and Gürol (2020) |
| SWCNTs | Iodine-131 | 1.356 $g.g^{-1}$ | Yılmaz and Gürol (2020) |
| MWCNTs | $^{137}Cs$ | 45 % | Delgado et al. (2014), Yavari et al. (2011) |
| Pristine graphene | $^{137}Cs$ | 41 % | Kaewmee et al. (2017) |

Primarily generated as a byproduct of nuclear power plants and various nuclear applications, including research and medical treatments, radioactive waste presents formidable challenges (Yılmaz et al. 2020). In therapeutic applications, specific radionuclides are pre-diluted before administration. The domain of nanotechnology, particularly the utilization of nanostructured materials, emerges as a promising avenue for effectively mitigating the oxidative damage associated with radioactive waste (Yavari et al. 2011). Diverse carbon nanomaterials, such as single-walled carbon nanotubes (SWCNTs), carboxyl-functionalized SWCNTs (SWCNT-COOH), graphene, and graphene oxide, find application in the removal of radioactive compounds such as iodine-131 and cesium.

Cesium, a radioactive byproduct resulting from nuclear power plant fission, contains highly toxic isotopes like 137Cs and 134Cs, capable of contaminating water, air, and soil. The half-life of 134Cs is approximately two years, 137Cs is 30.4 years, and Iodine-131 has a half-life of eight days (Rauwel & Rauwel 2019, Kaewmee et al. 2017). Table 7 provides a comprehensive overview of the adsorption capacity of various carbon adsorbents for radioactive materials.

### Carbon-Based Nano-remediation of Air Pollutants

The most common and harmful outdoor air pollutants are particle matter ($PM_{10}$ and $PM_{2.5}$), carbon monoxide, lead, nitrogen oxides, sulfur dioxide, and ground-level ozone, i.e., forming by chemical reactions between nitrogen oxides and volatile organic compounds (VOCs). To mitigate this problem, few researchers have investigated and got good results that include the use of graphene oxides (GOs), graphite oxides, and CNTs with highly reactive surface sites and surface area, large pore volume, mesoporous silica materials with ordered and tunable porous structure and thermal stability. More oxygen-containing functional groups are there on the surface of graphite oxide, which can be controlled by changing the reaction temperature with the addition of water (Yeh et al. 2010). These nanomaterials can be used for ammonia gas sensors operating at different temperatures. The graphene oxides and zirconium hydroxide/graphene composites have been applied for the adsorption of $SO_2$ (Luo et al. 2018)

Graphene oxide was also used as a photocatalyst to degrade VOCs under ultraviolet light irradiation through photoreduction. Continuous pore structure and large specific surface area Graphene oxide membrane were used to capture PM2.5. These properties help to enhance the adsorption capacity when it's used on CNTs (Weiwu et al. 2019)

## CONCLUSION

In conclusion, nanotechnology emerges as a potent tool, providing inventive solutions to a range of environmental challenges. The current landscape witnesses the rise of novel toxic substances, evolving alongside the changing toxicology of e-waste due to advancements in electronics. The distinct properties of artificial nanomaterials position them as pivotal facilitators of sustainable environmental solutions, encompassing pollution reduction, water treatment, environmental monitoring, remediation, and cost-effective alternative energy sources. This review extensively explores the ecological applications of engineered carbon nanomaterials, emphasizing their integral role in sustainable practices. It also underscores the future potential of these materials within natural environmental systems. A notable observation from the comprehensive review is the

relatively limited quantity of research dedicated to toxin removal from the environment within the broader field of nanotechnology. While the emphasis on the sustainability of carbon nanotechnology is frequent, it is essential to address any unwarranted expectations associated with its potential. Carbon-based nanotechnology significantly contributes to enhancing environmental quality sustainably, particularly in mitigating pollutants like dyes, e-waste, and pesticides, among others. The widespread adoption of carbon-based nanomaterials in diverse industries underscores their popularity, attributed to their non-toxic nature, expansive surface area, and cost-effectiveness. As these materials have become integral to numerous sectors, their enduring popularity is expected to persist in the years to come. Proceeding forward, the conclusion recognizes the wide range of uses for carbon-based nanomaterials and emphasizes their great potential for further studies. This ongoing research aims to establish carbon-based nanomaterials as a key component in the field of environmental pollution remediation and to play a pivotal role in attaining environmental sustainability.

## ACKNOWLEDGEMENT

The authors are grateful to Visva-Bharati (Central University) Santiniketan, Birbhum, West Bengal 731235, India for their continuous support.

## REFERENCES

Accorsi, G. and Armaroli, N. 2010. Taking Advantage of the Electronic Excited States of [60]-Fullerenes. J. Phys. Chem. C, 114: 1385-1403.

Alekseeva, O. V., Bagrovskaya, N. A. and Noskov, A. V. 2016. Sorption of heavy metal ions by fullerene and polystyrene/fullerene film compositions. Prot. Met. Phys. Chem. Surf., 52: 443-447.

Alslaibi, T. M., Abustan, I., Ahmad, M. A. and Foul, A. A. 2013. A review: production of activated carbon from agricultural byproducts via conventional and microwave heating. J. Chem. Technol. Biotechnol., 88: 1183-1190. doi: 10.1002/jctb.4028.

Aransiola, E. F., Oyewusi, T. F., Osunbitan, J. A. and Ogunjimi, L. A. O. 2019. Effect of binder type, binder concentration, and compacting pressure on some physical properties of carbonized corncob briquette. Energy Rep., 5: 909-918.

Arbogast, J. W., Darmanyan, A. P., Foote, C. S., Diederich, F. N., Whetten, R. L., Rubin, Y., Alvarez, M. M. and Anz, S. J. 1991. Photophysical properties of sixty-atom carbon molecule (C60). J. Phys. Chem., 95: 11-12.

Aris, N. I. F., Rahman, N. A., Wahid, M. H., Yahaya, N., Keyon, A. S. A. and Kamaruzaman, S. 2020. Superhydrophilic graphene oxide/electrospun cellulose nanofibre for efficient adsorption of organophosphorus pesticides from environmental samples. R. Soc. Open Sci., 19: 500.

Ashok, J., Reema, S., Anjaneyulu, C. and Subrahmanyam, Venugopal, A. 2010. Methane decomposition catalysts for COx-free hydrogen production. Rev. Chem. Eng., 26: 29-39.

Bota, P. M., Dorobantu, D., Boerasu, I., Bojin, D. and Enachescu, M. 2014. Synthesis of single-wall carbon nanotubes by excimer laser ablation. Surf. Eng. Appl. Electrochem., 50: 294-299.

Chen, J., Zou, J., Zeng, J. and Song, X. 2010. Preparation and evaluation of graphene-coated solid-phase micro-extraction fiber. Anal. Chim. Acta, 678: 44-49. https://doi.org/10.1016/j.aca.2010.08.008

Chen, M., Pierstorff, E. D., Lam, R., Xu, X. and Dean Ho, E. O. 2008. Nanodiamond-mediated delivery of water-insoluble therapeutics. Acs Nano, 3: 2016-2022.

Dehghani, M. H., Taher, M. M., Bajpai, A. K., Heibati, B., Tyagi, I., Asif, M., Agarwal, S. and Gupta, V. K. 2015. Removal of noxious Cr (VI) ions using single-walled carbon nanotubes and multi-walled carbon nanotubes. Chem. Eng. J., 279: 344-352. doi:10.1016/j.cej.2015.04.151

Delgado, J. L., Filippone, S., Giacalone, F., Herranz, M. A., Illescas, B., Pérez, E. M. and Martín, N. 2014. Buckyballs. Springer-Verlag Berlin Heidelberg, Germany, pp. 1-64.

Deng, S. B., Nie, Y., Du, Z. W., Huang, Q., Meng, P. P., Wang, B., Huang, J. and Yu, G. 2015. Enhanced adsorption of perfluorooctane sulfonate and perfluorooctanoate by bamboo-derived granular activated carbon. J. Hazard. Mater., 282: 150-157.

Derakhshi, M., Daemi, S., Shahini, P., Habibzadeh, A., Mostafavi, E. and Ashkarran, A. A. 2022. Two-dimensional nanomaterials beyond graphene for biomedical applications. J. Funct. Biomater., 13: 27.

Deshannavar, U. B., Hegde, P. G., Dhalayat, Z., Patil, V. and Gavas, S. 2018. Production and characterization of agro-based briquettes and estimation of calorific value by regression analysis: an energy application. Mater. Sci. Energy Technol., 1: 175-181.

Farghali, A. A., Abdel Tawab, H. A., Abdel Moaty, S. A. and Rehab, K. 2017. Functionalization of acidified multi-walled carbon nanotubes for removal of heavy metals in aqueous solutions. J. Nanostructure Chem., 7: 101-111.

Fasfous, I. I., Radwan, E. S. and Dawoud, J. N. 2010. Kinetics, equilibrium, and thermodynamics of the sorption of tetrabromobisphenol A on multiwalled carbon nanotubes. Appl. Surf. Sci., 256: 7246-7252. doi:10.1016/j.apsusc.2010.05.059

Galvão, R. B., Moretti, da Silva., Fernandes, A. A. and Kuroda, F. E. K. 2021. Post-treatment of stabilized landfill leachate by upflow gravel filtration and granular activated carbon adsorption. Environ. Technol., 42: 4179-4188.

Ghaedi, M., Khajehsharif, H. and Yadkuri, A. H. 2012. Oxidized multiwalled carbon nanotubes as efficient adsorbent for bromothymol blue. Toxicol. Environ. Chem., 94: 873-883. https://doi.org/10.1080/02772248.2012.678999.

Ghorbani, F., Kamari, S., Zamani, S., Akbari, S. and Salehi, M. 2020. Optimization and modeling of aqueous Cr(VI) adsorption onto activated carbon prepared from sugar beet bagasse agricultural waste by application of response surface methodology. Surf. Interf., 18: 100444.

Ghosal, K. and Sarkar, K. 2018. Biomedical Applications of graphene nanomaterials and beyond. ACS Biomater. Sci. Eng., 4(8): 2653-2703. doi:10.1021/acsbiomaterials.8b00

Guldi, D. M. and Prato, M. 2000. Excited-state properties of C(60) fullerene derivatives. Acc. Chem. Res., 33: 695-703.

Hadi, P., Barford, J. and McKay, G. 2014. Selective toxic metal uptake using an e-waste based novel sorbent-single, binary and ternary systems. J. Environ. Chem. Eng., 2: 332-339. https://doi.org/10.1016/j.jece.2014.01.004

Hao, M., Qiu, M., Yang, H., Hu, B. and Wang, X. 2021. Recent advances in preparation and environmental applications of MOF-derived carbons in catalysis. Sci. Total Environ., 760: 143333.

Jjagwe, J., Olupot, P. W., Menya, E. and Herbert Kalibbala, M. 2021. Synthesis and application of granular activated carbon from biomass waste materials for water treatment: A review. J. Bioresour. Bioprod., 6: 292-322. doi:10.1016/j.jobab.2021.03.003.

Kaewmee, P., Manyam, J., Opaprakasit, P., Truc Le, G. T., Chanlek, N. and Sreearunothai, P. 2017. Effective removal of cesium by pristine graphene oxide: performance, characterizations and mechanisms. RSC Adv., 7(61): 38747-38756. doi:10.1039/c7ra04868h

Kaizar, H. and Ismail, N. 2015. Bioremediation and detoxification of pulp

and paper mill effluent: A review. Res. J. Environ. Toxicol., 9(3): 113-134.

Kaizar, H., Quaik, S., Ismail, N., Rafatullah, M., Maruthi, A. and Rameeja, S. 2016. Bioremediation of textile wastewater with membrane bioreactor using the white-rot fungus and reuse of wastewater. Iran. J. Biotechnol., 14(3): e124-16: DOI:10.15171/ijb.1216.

Karimi, M., Solati, N., Amiri, M., Mirshekari, H., Mohamed, E., Taheri, M., Hashemkhani, M., Saeidi, A., Estiar, M. A., Kiani, P. and Ghasemi, A. 2015. Carbon nanotubes part I: preparation of a novel and versatile drug-delivery vehicle. Expert Opin. Drug Deliv., 12**:** 1071-1087.

Kumari, P., Nayak, M. K., Dhruwe, D., Patel, M. K. and Mishra, S. 2023. Synthesis and characterization of sulfonated magnetic graphene-based cation exchangers for the removal of methylene blue from aqueous solutions. Ind. Eng. Chem. Res., 62(3): 1245-1256. DOI: 10.1021/acs.iecr.2c04432

Lihua, D., Li'an, H., Zhansheng, W., Ping, G., Guanyi, C. and Renfu, J. 2018. A new function of spent activated carbon in BAC process: removing heavy metals by ion exchange mechanism. J. Hazard. Mater., 359: 76-86.

Lima, L., Baêta, B. E., Lima, D. R., Afonso, R. J., De Aquino, S. F. and Libânio, M. 2016. Comparison between two forms of granular activated carbon for the removal of pharmaceuticals from different waters. Environ. Technol., 37: 1334-1345.

Liming, L., Tongjiang, P., Mingliang, Y., Hongjuan, S., Shichan, D. and Long, W. 2018. Preparation of graphite oxide containing different oxygen-containing functional groups and the study of ammonia gas sensitivity. Sensors, 18: 3745, doi:10.3390/s18113745

Liu, X., Zhang, H., Ma, Y. and Wu, X. 2013. Graphene-coated silica is a highly efficient sorbent for residual organophosphorus pesticides in water. J. Mater. Chem. A, 1(1): 1875-1884. https://doi.org/10.1039/c2ta00173j

Lucky, S. S., Soo, K. C. and Zhang, Y. 2015. Nanoparticles in photodynamic therapy. Chem. Rev., 115(4): 1990-2042.

Machado, F. M., Bergmann, C. P., Lima, E. C., Royer, B., de Souza, F. E. and Jauris, I. M. 2012. Adsorption of Reactive Blue 4 dye from water solutions by carbon nanotubes: Experiment and theory. Phys. Chem., 14(31): 11139. doi:10.1039/c2cp41475a

Mashkoor, F. and Nasar, A. 2020. Magsorbents: Potential candidates in wastewater treatment technology- A review on the removal of methylene blue dye. J. Magn. Magn. Mater., 500: 166408. https://doi.org/10.1016/j.jmmm.2020.166408

Mauter, S. M. and Elimelech, M. 2008. Environmental applications of carbon-based nanomaterials. Environ. Sci. Technol., 42(16): 5843-5849.

Mengesha, A. E. 2013. Diamond-Based Materials for Biomedical Applications. In N. I. Khan (Ed.), Nanodiamonds for Drug Delivery Systems, Woodhead Publishing Limited, Sawston, UK, pp. 186-205. doi:10.1533/9780857093516.2.186

Mubarak, N. M., Sahu, J. N., Abdullah, E. C. and Jaykuamr, N. S. 2016. Radioadsorption of toxic Pb(II) ions from aqueous solution using multiwall carbon nanotubes synthesized by microwave chemical vapor deposition technique. J. Environ. Sci., 45: 143-155. https://doi.org/10.1016/j.jes.2015.12.025

Mustafa, R. and Asmatulu, E. 2020. Preparation of activated carbon using fruit, paper, and clothing wastes for wastewater treatment. J. Water Process Eng., 35: 101239.

Nagalakshmi, T. V., Emmanuel, K. A. and Bhavani, P. 2019. Adsorption of dispersed blue 14 onto activated carbon prepared from Jackfruit-PPI-I waste. Mater. Today: Proc., 8: 2036-2051.

Nimibofa, A., Newton, E. A., Cyprain, A. Y. and Donbebe, W. 2018. Fullerenes: synthesis and applications. J. Mater. Sci., 7: 22-33.

Okai, M., Muneyoshi, T., Yaguchi, T. and Sasaki, S. 2000. Structure of carbon nanotubes grown by microwave-plasma-enhanced chemical vapor deposition. Appl. Phys. Lett., 77: 3468-3470.

Pandey, P. C., Shukla, S., Pandey, G. and Narayan, R. J. 2021. Nanostructured diamond for biomedical applications. Nanotechnology, 32: 132001.

Qin, J. X., Yang, X. G., Lv, C. F., Li, Y. Z., Liu, K. K., Zang, J. H. and Shan, C. X. 2021. Nanodiamonds: Synthesis, properties, and applications in nanomedicine. Mater. Des., 10: 110091.

Rajabia, M., Mahanpoora, K. and Moradi, O. 2017. Removal of dye molecules from aqueous solution by carbon nanotubes and carbon nanotube functional groups: critical review. RSC Adv., 7: 47083-47090. https://doi.org/10.1039/c7ra05569b

Rauwel, P. and Rauwel, E. 2019. Towards the extraction of radioactive cesium-137 from water via graphene/CNT and nanostructured Prussian Blue hybrid nanocomposites: A review. Nanomaterials, 9: 682. doi:10.3390/nano9050682

Rodriguez, N. M. 1993. A review of catalytically grown carbon nanofibers. J. Mater. Res., 8: 3233-3250.

Rosso, C., Filippini, G. and Prato, M. 2020. Carbon dots as nano-organocatalysts for synthetic applications. ACS Catal., 18: 989. doi:10.1021/acscatal.0c01989

Royer, B., Cardoso, N. F., Lima, E. C., Vaghetti, J. C., Simon, N. M., Calvete, T. and Veses, R. C. 2009. Applications of Brazilian pine-fruit shell in natural and carbonized forms as adsorbents to the removal of methylene blue from aqueous solutions--kinetic and equilibrium study. J. Hazard. Mater., 164(2-3): 1213-1222. https://doi.org/10.1016/j.jhazmat.2008.09.028

Ruiz-Cornejo, J. C., Sebastian, D. and Lazaro, M. J. 2020. Synthesis and applications of carbon nanofibers: A review. Rev. Chem. Eng., 36: 493-511.

Sen Gupta, S., Chakraborty, I., Maliyekkal, S. M., Adit Mark, T., Pandey, D. K., Das, S. K. and Pradeep, T. 2015. Simultaneous dehalogenation and removal of persistent halocarbon pesticides from water using graphene nanocomposites: A case study of Lindane. ACS Sustain. Chem. Eng., 3: 1155-1163. https://doi.org/10.1021/acssuschemeng.5b00080

Sharma, S. K., Chiang, L. Y. and Hamblin, M. R. 2011. Photodynamic therapy with fullerenes in vivo: Reality or a dream? Nanomedicine (London, England), 6(10): 1813-1825. https://doi.org/10.2217/nnm.11.144

Sinitsa, A. S., Lebedeva, I. V., Popov, A. M. and Knizhnik, A. A. 2017. Transformation of amorphous carbon clusters to fullerenes. J. Phys. Chem. C, 121(24): 13396-13404. doi:10.1021/acs.jpcc.7b04030

Suo, F., Xie, G., Zhang, J., Li, J., Li, C., Liu, X. and Ji, M. A. 2018. Carbonized sieve-like corn straw cellulose-graphene oxide composite for organophosphorus pesticide removal. RSC Adv., 8: 7735-7743. https://doi.org/10.1039/C7RA12898C

Tadda, M. A., Ahsan, A., Shitu, A., ElSergany, M., Arunkumar, T., Jose, B. and Daud, N. N. 2016. A review on activated carbon: Process, application, and prospects. J. Adv. Civil Eng. Pract. Res., 2: 7.

Tan, L., Wang, S., Du, W. and Hu, T. 2016. Effect of water chemistries on adsorption of Cs(I) onto graphene oxide investigated by batch and modeling techniques. Chem. Eng. J., 292: 92-97.

Tanveer, A. T., Fayyaz, A. M., Diego, E. G., David, W. H. and Shaowei, Zhang 2018. A facile synthesis of porous graphene for efficient water and wastewater treatment. Sci Rep., 8: 1817.

Testa, C., Zammataro, A., Pappalardo, A. and Sfrazzetto, G. T. 2019. Catalysis with carbon nanoparticles. RSC Adv., 9: 27659-27664. doi:10.1039/c9ra05689kTóth, A., Tör˝ocsik, A., Tombácz, E., László, K. 2012. Competitive adsorption of phenol and 3-chlorophenol on purified MWCNTs. J. Colloid Interface Sci., 387: 244-249.

Wang, S., Ng, C. W. and Wang, W. 2012. Synergistic and competitive adsorption of organic dyes on multi-walled carbon nanotubes. Chem. Eng. J., 197: 34-40. https://doi.org/10.1016/j. cej.2012.05.008

Wanjeri, V. W. O., Sheppard, C. J., Prinsloo, A. R. E., Ngila, J. C. and Ndungu, P. G. 2018. Isotherm and kinetic investigations on the adsorption of organophosphorus pesticides on graphene oxide-

based silica-coated magnetic nanoparticles functionalized with 2-phenylethylamine. J. Environ. Chem. Eng., 6: 1333-1346. https://doi.org/10.1016/j.jece.2018.01.064

Weiwu, Z., Baoshan, G., Shiqing, S., Shidong, W., Xin, L., Haoqi, Z. and Peiyan, Y. 2019. Preparation of a graphene oxide membrane for air purification. Mater. Res. Exp., 6(10). DOI 10.1088/2053-1591/ab3eec

Wu, Q., Zhao, G., Feng, C., Wang, C. and Wang, Z. 2011. Preparation of a graphene-based magnetic nanocomposite for the extraction of carbamate pesticides from environmental water samples. J. Chromatogr. A, 1218: 7936-7942. https://doi.org/10.1016/j.chroma.2011.09.027

Xu, J. Cao, Z., Zhang, Y., Yuan, Z., Lou, Z., Xu, X. and Wang, X. 2018. A review of functionalized carbon nanotubes and graphene for heavy metal adsorption from water: Preparation, application, and mechanism. Chemosphere, 195: 351-364.

Xu, J., Chen, J., Ahmad, M., Zhang, Q. and Zhang, B. 2019. Novel synthetic method for magnetic porous carbon materials for efficient adsorption of organic pollutants from aqueous solution. J. Chem. Eng. Data, 64: 12: 5974-5984. doi:10.1021/acs.jced.9b00830

Yao, Y. X., Li, H. B., Liu, J. Y., Tan, X. L., Yu, J. G. and Peng, Z. G. 2014. Removal and adsorption of p-nitrophenol from aqueous solutions using carbon nanotubes and their composites. J. Nanomater., 84: 1-9.

Yavari, R., Huang, Y. D. and Ahmadi, S. J. 2011. Adsorption of cesium (I) from aqueous solution using oxidized multiwall carbon nanotubes. J. Radioanal. Nucl. Chem., 287, 393-401.

Ye, R. and Tour, J. M. 2019. Graphene at fifteen. ACS Nano, 13:10872-10878. 180057267864

Yeh, T. F., Syu, J. M., Cheng, C., Chang, T. H. and Teng, H. 2010. Graphite oxide as a photocatalyst for hydrogen production from water. Adv. Funct. Mater., 20: 2255-2262.

Yılmaz, D. and Gürol, A. 2020. Efficient removal of iodine-131 from radioactive waste by nanomaterials, Instrument. Sci. Technol., 49(1): 54-45. DOI: 10.1080/10739149.2020.1775094

Yin, L., Zhou, H., Lian, L., Yan, S. and Song, W. 2016. Effects of $C_{60}$ on the photochemical formation of reactive oxygen species from natural organic matter. Environ. Sci. Technol., 50: 11742-11751.

Zhang, C., Zhang, R. Z., Ma, Y. Q., Guan, W. B., Wu, X. L., Liu, X., Li, H., Du, Y. L. and Pan, C. P. 2015. Preparation of cellulose/graphene composite and its applications for triazine pesticide adsorption from water. Sustain. Chem. Eng., 3: 396-405.

Zhang, X. Q., Chen, M., Lam, R., Xu, X. and Dean Ho, E. O. 2009. Polymer-functionalized nanodiamond platforms as vehicles for gene delivery. ACS Nano, 3: 2609-2616.

Zhang, Y., Tang, Y., Li, S. and Yu, S. 2013. Sorption and removal of tetrabromobisphenol A from solution by graphene oxide. Chem. Eng. J., 222: 94-100. doi:10.1016/j.cej.2013.02.027.

Zhou, Q. and Fang, Z. 2015. Graphene-modified TiO2 nanotube arrays as an adsorbent in micro-solid phase extraction for determination of carbamate pesticides in water samples. Anal. Chim. Acta, 869: 43-49. https://doi.org/10.1016/j.aca.2015.02.019

Zhou, X., Wang, P., Zhang, Y., Zhang, X. and Jiang, Y. 2016. From waste cotton linter: a renewable environment-friendly biomass-based carbon fibers preparation. ACS Sustain. Chem. Eng., 4(10): 5585-5593. doi:10.1021/acssuschemeng.6b01408

## ORCID DETAILS OF THE AUTHORS

Rameeja Shaik: https://orcid.org/0000-0002-3525-6853

Nature Environment and Pollution Technology
An International Quarterly Scientific Journal

p-ISSN: 0972-6268
(Print copies up to 2016)
e-ISSN: 2395-3454

Vol. 23 | No. 3 | pp. 1795-1799 | 2024

Original Research Paper

https://doi.org/10.46488/NEPT.2024.v23i03.052

Open Access Journal

# Alternate Chemical Compounds as a Condensation Nucleus in Cloud Seeding

**Hasan M. Azeez†, Nagham T. Ibraheem and Hazim H. Hussain**
Atmospheric Science Department, Collage of Science, Mustansiriyah University, Baghdad, Iraq
†Corresponding author: Hasan M. Azeez; hassan.m.a7878@uomustansiriyah.edu.iq

**Nat. Env. & Poll. Tech.**
**Website: www.neptjournal.com**

*Received:* 24-12-2023
*Revised:* 09-01-2024
*Accepted:* 31-01-2024

**Key Words:**
Condensation nuclei
Cloud seeding
Precipitation
Refrigerated helfa

## ABSTRACT

Cloud seeding involves boosting precipitation by releasing substances into the air that act as cloud condensation or ice nuclei. These substances encourage the development of clouds and precipitation. It's like giving Mother Nature a gentle push to assist with rainfall in specific areas. The current work aimed to suggest $Al_2O_3$ as an alternate compound in cloud seeding rather than silver iodide. In this research, a unique approach is used to identify condensation nuclei, which play a crucial role in cloud formation and droplet growth. Various samples and four sources were included in the current study; refrigerated helfa powder, Himalayan salt, generator powder, and pollen, were analyzed using different physicochemical instruments. The proportions of chemical compounds in the samples show that there is 1.392% of $Al_2O_3$ in Refrigerated helfa which is the highest than in the other 3 sources, while the proportions of elements in the samples indicate that refrigerated helfa contains the lowest toxic compound, and although $Al_2O_3$ is insoluble in water, it is hygroscopic and can absorb 6.4% of humidity within 24 hours. As for the surface tension, refrigerated helfa shows lower density and surface tension than the other three sources with values of 0.9480 and 47.89 respectively. $Al_2O_3$ shows high humid absorptivity and refrigerated helfa can be used as a main source for $Al_2O_3$ which has a low effect on biota and is recommended for use in cloud seeding. However further work is recommended to be carried out in using $Al_2O_3$ as an alternative compound to silver iodide in cloud seeding.

## INTRODUCTION

Clouds consist of small droplets of water or ice crystals that form when water vapor cools in the atmosphere layers and condense around particles known as condensation nuclei which usually are dust, sodium and magnesium salts, silicates, and carbon (AL-Saleem et al. 2019), the presence of these particles participate in the formation of raindrops or snowflakes.

Artificial cloud seeding stands to act as a crucial method for modifying the atmosphere. Its objective is to regulate nature through a certain quantity of precipitation by releasing these substances into the air. These materials serve as condensation nuclei, increasing the possibility of rain or snow, and targeting it to specific locations at specific times (Mielke Jr et al. 1971).

Cloud seeding is a technique used to modify weather by altering the precipitation that falls from clouds. This is achieved by dispersing substances into the air, which act as cloud condensation or ice nuclei, thus influencing the microphysical processes within the cloud. Ground-based generators or aircraft can be employed for cloud seeding, with commonly used chemicals including silver iodide, potassium iodide, dry ice, and liquid propane. Silver iodide, for instance, is often employed to facilitate the formation of ice crystals, providing a foundation for the development of snowflakes. Despite being utilized for decades, the effectiveness of cloud seeding is still a subject of debate, and its success can be different (Wondie 2023, Sadeghi & Yaghoubi 2024).

In 2018, French and his colleagues conducted an experiment related to cloud seeding. Their aim in glaciogenic seeding of orographic clouds was to introduce aerosols into the clouds, thereby influencing the natural progression of cloud particles and boosting winter precipitation in a specific area. They suggested a sequence of events ie., injection of silver iodide aerosol into cloud areas with supercooled liquid water. This triggers the formation of ice crystals, which then grow into sizable particles, eventually causing snowfall (French et al. 2018). However, when exposed to 0.43 µM of AgI, a notable reduction in photosynthetic activity occurred, primarily linked to respiration (with an 80% inhibition) and, to a lesser degree, net photosynthesis (with a 40% inhibition) in both strains of phytoplankton. Additionally, there was a moderate decline in the viability of soil bacteria. These findings indicate that the impact of AgI from cloud seeding on terrestrial and aquatic ecosystems may be moderate when cloud seeding is regularly practiced in a particular region, leading to the accumulation of substantial amounts

of seeding materials in the environment (Fajardo et al. 2016).

In 2006, Gou and his coworkers did a project to use $CO_2$ as an alternate substance to silver, the research project examined the dynamic and microphysical impacts of cloud seeding through liquid carbon dioxide (liquid $CO_2$) and compared it with AgI, the investigation utilized a 3D cloud model that incorporated seeding processes, the finding was that when liquid $CO_2$ is introduced into the area of maximum supercooled water, with temperatures ranging from 0 to -5°C, it can generate a significantly more potent dynamic effect and precipitation Gou et al. 2006).

In 2022, Dr. Ghassan published a review study about cloud seeding, in his review, he mentioned that cloud seeding can be executed through various methods, with the most commonly utilized chemicals being dry ice and potassium iodide (Ghassan 2022).

Each droplet of liquid water in a cloud without ice originally began as a minuscule aerosol particle in the atmosphere. These particles belong to the category known as cloud condensation nuclei (CCN), characterized by favorable physical and chemical attributes. These CCN can rapidly expand through the condensation of water vapor when the air's relative humidity exceeds 100% (referred to as water supersaturation). However, to enhance comprehension of the CCN activation process, an investigation delved into the impact of various controlling factors. These factors encompass the formation rate, growth rate, background particle distribution, hygroscopicity, and surface tension of the particles (Ovadnevaite et al. 2017, Cai et al. 2021).

The primary goal of this study was to identify Aluminum oxide as an alternative material serving as condensation nuclei in cloud seeding.

## MATERIALS AND METHODS

This study employs a novel method for identifying condensation nuclei, a crucial factor in cloud formation and droplet growth. Three powder variants-Refrigerated helfa powder, Himalayan salt, and generator powder-along with pollen were utilized as samples and analyzed using different physicochemical apparatuses.

Tables 1 show the compounds that are present in the three sources, while Table 2 shows the toxic element concentrations in the three salt sources in ppm. Yet, all the samples must be dried in an oven for one and to ensure precise data collection, the samples underwent desiccation in a desiccator before analysis.

Physical and chemical tests were carried out using different physicochemical instruments; Table 3 shows the solubility of the isolated inorganic salts from the four sources, while Table 4 shows the hygroscopicity of the alternative compounds that could be used in cloud seeding.

Table 1: The proportions of chemical compounds in the samples.

| No. | Sample | $SiO_2$ % | $Al_2O_3$ % | $Fe_2O_3$ % | CaO % | $Na_2O$ % | $K_2CO_3$ % | MgO % | MnO % | $TiO_2$ % | $P_2O_5$ % |
|---|---|---|---|---|---|---|---|---|---|---|---|
| 1. | Refrigerated helfa | 4.761 | **1.392** | 1.128 | 26 | 4.722 | 0.131 | 2.152 | 0.008 | 0.072 | 0.33 |
| 2. | Carbon generators | 0.67 | 0.249 | 0.792 | **0.891** | 0 | 0 | 0 | 0.011 | 0.06 | 0.197 |
| 3. | Himalayan salt | 0.387 | 0.217 | 0 | 0.071 | **38.5** | 0.067 | 0.819 | 0 | 0.017 | 0.028 |
| 4. | Pollen grains | 0.685 | 0.214 | 0.357 | 3.658 | 0.032 | **4.296** | 0.38 | 0.031 | 0.061 | 4.866 |

Table 2: The proportions of elements in the samples.

| No | S ppm | Cl ppm | Ba ppm | Co ppm | Cr ppm | Cu ppm | Mo ppm | Nb ppm | Ni ppm | Pb ppm | Rb ppm | Sr ppm | V ppm | Y ppm | Zn Ppm | Zr ppm | As ppm |
|---|---|---|---|---|---|---|---|---|---|---|---|---|---|---|---|---|---|
| 1. | 37 | 23306 | 2133 | N | N | 45 | 644 | 299 | 44 | 116 | 291 | 1612 | 25 | 718 | 1031 | 660 | 12 |
| 2. | 42890 | 107 | 5837 | 17 | N | 129 | 839 | 375 | 182 | 223 | 444 | 1302 | 28 | 1064 | 479 | 841 | 25 |
| 3. | **2802** | **59.50%** | **512** | **N** | **N** | **5** | **544** | **272** | **N** | **79** | **241** | **670** | **10** | **603** | **94** | **536** | **6** |
| 4. | 6911 | 3080 | 5285 | 14 | N | 127 | 842 | 375 | 175 | 219 | 422 | 1301 | 27 | 1056 | 434 | 840 | 26 |

1 = Refrigerated helfa , 2 = Carbon generators , 3 = Himalayan salt , 4 = pollen grains

Table 3: The solubility rates of some chemical compounds.

| Chemical compounds | $SiO_2$ | $Al_2O_3$ | $Fe_2O_3$ | CaO | $Na_2O$ | $K_2CO_3$ | MgO | MnO | $TiO_2$ | $P_2O_5$ |
|---|---|---|---|---|---|---|---|---|---|---|
| solubility rates in water | 0.012g.100 $mL^{-1}$ | Insoluble | Insoluble | React | react | 112g.100 $mL^{-1}$ | Acid | Insoluble | Insoluble | hydrolysis |

One gram of each compound, and they were tested in laboratory conditions at a relative humidity of (95%) and a temperature of (21°C), $Al_2O_3$ was heated at a temperature of (115°C) in the oven for an hour, and then the sample was placed in the desiccator to monitor its weight. Table 5 shows the values of surface tension of each salt source and its density.

## RESULTS AND DISCUSSION

Table 1 shows the proportions of chemical compounds in the samples in the four sources, and it appears that $Al_2O_3$ is the main compound in Refrigerated helfa while Table 2 shows the percent of toxic compounds in the four sources by which Himalayan salt is contained in the highest percentage. Despite Table 3 showing that $Al_2O_3$ is insoluble in water, Table 4 shows the high hygroscopicity of the $Al_2O_3$ (0.94 g) compound that could be used in cloud seeding.

Table 5 indicates the data of surface tension measured in Newton meter ($mN.m^{-1}$), refrigerated helfa shows the lower surface tension (0.9480). The correlation between surface tension and cloud seeding is related to the role of surface tension in the formation of cloud droplets.

A study carried out by Facchini et al. 2000, found that a reduction in surface tension compared to that of pure water was noted in wet aerosol and cloud/fog samples. The observed decrease in surface tension is directly linked to the concentration of total soluble organic compounds present in the samples.

Another study carried out by Davies et al. 2019 has shown that the evolving surface tension, particularly due to the presence of organic compounds, plays a significant role in the activation of aerosol particles into cloud droplets. Hence, the examination of surface tension, particularly its changes influenced by different factors, plays a crucial role in comprehending the mechanism of cloud droplet formation,

Table 4: Hygroscopicity of certain compounds.

| No. | Compound | Wt. Before Heating | Wt. After Heating | Wt. (after 24hr) | Recommendation | Solubility in water |
|---|---|---|---|---|---|---|
| 1. | $Al_2O_3$ | 1 | 0.94 | 1 | Hygroscopic | Insoluble |
| 2. | MgO | 1 | 0.90 | 0.90 | Hygroscopic | |
| 3. | TiO | 1 | 1 | 1 | Non-Hygroscopic | Insoluble |
| 4. | $K_2CO_3$ | 1 | 0.70 | 1 | Hygroscopic | Soluble |
| 5. | $Fe_2O_3$ | 1 | 1 | 1 | Non-Hygroscopic | Insoluble |
| 6. | CaO | 1 | 1 | 1 | Non-Hygroscopic | |
| 7. | $Na_2O$ | 1 | 1 | 1 | Non-Hygroscopic | |
| 8. | MnO | 1 | 0.90 | 0.90 | Hygroscopic | Insoluble |
| 9. | $SiO_2$ | --- | --- | --- | Hygroscopic | Soluble |
| 10. | CaO | --- | --- | --- | Hygroscopic | |

Table 5: Value surface tension in Newton meter ($mN.m^{-1}$) unit.

| Samples | Wight.$g^{-1}$ | Density ($kg.L^{-1}$) | Surface tension ($mN.m^{-1}$) |
|---|---|---|---|
| Pollen grains | 0.5 | 0.9811 | 51.67 |
| Pollen grains | 1 | 0.9790 | 43.95 |
| Pollen grains | 1.5 | 0.9794 | 46.27 |
| Pollen grains | 2 | 0.9811 | 42.03 |
| Refrigerated helfa | 0.5 | 0.9692 | 55.35 |
| Refrigerated helfa | 1 | 0.9807 | 52.49 |
| Refrigerated helfa | 1.5 | 0.9475 | 49.40 |
| Refrigerated helfa | 2 | 0.9480 | 47.89 |
| Carbon generators | 0.5 | 0.9459 | 67.17 |
| Carbon generators | 1 | 0.9465 | 70.08 |
| Himalayan salt | 0.5 | 0.9476 | 68.30 |
| Himalayan salt | 1 | 0.9942 | 62.11 |
| Himalayan salt | 1.5 | 0.9856 | 56.42 |
| Himalayan salt | 2 | 0.9772 | 49.44 |

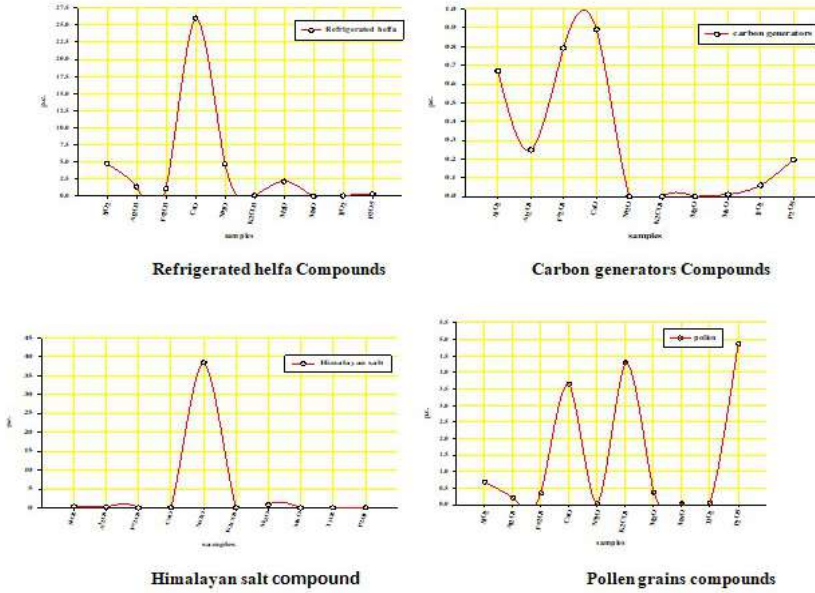


Fig. 1: The main compounds in the four compounds.

a key aspect in the realm of cloud seeding techniques. Nevertheless, establishing a precise connection between surface tension and the practices of cloud seeding may necessitate additional focused research and analysis.

Fig. 1 supports the data in Table 1 and shows the main compounds in each source, and it is clear from the figure that the main compound in Refrigerated helfa is $Al_2O_3$, while in Carbon generators are CaO, however, in Himalayan salt is NaO, and Pollen grains is $K_2CO_3$.

The possibility of utilizing aluminum oxide in cloud seeding involves dispersing fine particles of this compound into clouds to encourage precipitation. The aluminum oxide particles can serve as nucleation sites, promoting the coalescence of water droplets and enhancing the likelihood of rainfall. This technique is employed in weather modification efforts to potentially increase precipitation in targeted areas, although its effectiveness and environmental impact remain subjects of ongoing research and discussion.

Repeated application of cloud seeding with AgI may have a moderate impact on the biota residing in terrestrial and aquatic ecosystems, particularly when substantial amounts of seeding materials accumulate in the environment (Fajardo et al. 2016), this expectation of the hard effect of silver iodide on the biota of soil in addition to its toxicity

In 2021, Li and his coworkers (Li et al. 2021) studied the effect of silver ions on human lungs; the research indicates that silver ions released from nanoparticles caused cell necrosis by facilitating the influx of $Na^+$ and $Ca^{2+}$ ions, leading to pulmonary inflammation through the elevation of mitochondrial-related contents released from these necrotic cells.

Hill et al. (2012) mentioned that it is possible to use aluminum oxide in cloud seeding. Cloud seeding is a weather modification technique that involves spraying microscopic particles into clouds to encourage the formation of ice crystals, which can lead to precipitation. Aluminum oxide, along with other substances such as silver iodide and dry ice, has been used as a seeding agent in various cloud seeding efforts

In 2015, the National Research Council confirmed that the use of aluminum oxide for cloud seeding is mentioned as a part of experiments and operations to modify weather, such as increasing snowfall or suppressing lightning

In 2020, an article published in SBS Indonesian (Source: Australian Geographic) stated that Aluminum Oxide is a substance capable of serving as the essential nuclei where moisture gathers to create precipitation.

Godlee (2022) declared that aluminum oxide is a potential substance for cloud seeding to induce rain and its effectiveness and environmental impact of using aluminum oxide for cloud seeding are subjects of ongoing research and debate.

## CONCLUSIONS

- Four sources were investigated in the current study; refrigerated helfa powder, Himalayan salt, generator powder, and pollen.

- The hygroscopicity and solubility of compounds were measured in the four sources.
- Refrigerated helfa can be used as a main source for $Al_2O_3$.
- $Al_2O_3$ shows high humid absorptivity.
- Due to the specifications of $Al_2O_3$, it is recommended to be used in cloud seeding due to its low effect on biota.

## ACKNOWLEDGMENT

The authors would like to introduce their thanks and gratefulness to Al-Mustansiriyah University (https://www.uomustansiriyah.edu.iq/) for the support and help to achieve this article.

## REFERENCES

Al-Saleem, H.H.H., Azeez, H.M. and Ibraheem, N.T. 2019. Study the size and type of condensation nuclei of raindrop over Baghdad city in (2018). J. Phys. Conf. Ser., 1294(7): 072004. DOI: 10.1088/1742-6596/1294/7/072004.

Cai, M., Liang, B., Sun, Q., Liu, L., Yuan, B., Shao, M., Huang, S., Peng, Y., Wang, Z., Tan, H., Li, F., Xu, H., Chen, D. and Zhao, J. 2021. The important roles of surface tension and growth rate in the contribution of new particle formation (NPF) to cloud condensation nuclei (CCN) number concentration: Evidence from field measurements in southern China. Atmos. Chem. Phys., 21: 8575-8592. https://doi.org/10.5194/acp-21-8575-2021.

Davies, J.F., Zuend, A. and Wilson, K.R. 2019. Technical note: The role of evolving surface tension in the formation of cloud droplets. Atmos. Chem. Phys., 19: 2933-2946. https://doi.org/10.5194/acp-19-2933-2019.

Facchini, M.C., Decesari, S., Mircea, M., Fuzzi, S. and Loglio, G. 2000. Surface tension of atmospheric wet aerosol and cloud/fog droplets in relation to their organic carbon content and chemical composition. Atmospheric Environment, 34(28): 4853-4857. https://doi.org/10.1016/S1352-2310(00)00237-5.

Fajardo, C., Costa, G., Ortiz, L.T., Nande, M., Rodríguez-Membibre, M.L., Martín, M. and Sánchez-Fortún, S. 2016. Potential risk of acute toxicity induced by AgI cloud seeding on soil and freshwater biota. Ecotoxicol. Environ. Saf., 133: 433-441. DOI: 10.1016/j.ecoenv.2016.06.028.

French, J.R., Friedrich, K., Tessendorf, S.A., Rauber, R.M., Geerts, B., Rasmussen, R.M., Xue, L., Kunkel, M.L. and Blestrud, D.R. 2018. Precipitation formation from orographic cloud seeding. Proc. Natl. Acad. Sci. U.S.A., 115(6): 1168-1173. DOI: 10.1073/pnas.1716995115.

Ghassan, S. 2022. Cloud Seeding - A Review. Al-Bayan Center Studies Series. Available at: https://www.bayancenter.org/en/wp-content/uploads/2022/07/ugyh.pdf

Godlee, F. 2022. Who cares about climate change? BMJ, 377: 01150. DOI: 10.1136/bmj.o1150.

Gou, X., Zheng, G. and Jin, D. 2006. A numerical comparison study of cloud seeding by silver iodide and liquid carbon dioxide. Atmos. Res., 79: 183-226. DOI: 10.1016/j.atmosres.2005.04.005.

Hill, S.A. and Yi, M. 2012. Nonlinear climate response to regional brightening of tropical marine stratocumulus. Geophys. Res. Lett., 39(15): L15707. https://doi.org/10.1029/2012GL052064.

Leon, A., Borrahero, I. and Martinez, D. 2020. Study of the dispersion of AgI emitted from ground-based generators using the WRF-Chem model. Atmósfera, 33(4): 385-400. https://doi.org/10.20937/atm.52624.

Li, L., Bi, Z., Hu, Y., Sun, L., Song, Y., Chen, S., Mo, F., Yang, J., Wei, Y. and Wei, X. 2021. Silver nanoparticles and silver ions cause inflammatory response through induction of cell necrosis and the release of mitochondria in vivo and in vitro. Cell Biol. Toxicol., 37(2): 177-191. DOI: 10.1007/s10565-020-09526-4.

Mielke, J.R., Grant, P.W. and Chappell, C.F. 1971. An independent replication of the Climax wintertime orographic cloud seeding experiment. J. Appl. Meteorol., 10: 1198-1212.

National Research Council. 2015. Climate Intervention: Reflecting Sunlight to Cool Earth. Washington, DC: The National Academies Press. https://doi.org/10.17226/18988.

Ovadnevaite, J., Zuend, A., Laaksonen, A., Sanchez, K.J., Roberts, G., Ceburnis, D., Decesari, S., Rinaldi, M., Hodas, N., Facchini, M.C., Seinfeld, J.H. and O'Dowd, C. 2017. Surface tension prevails over solute effect in organic-influenced cloud droplet activation. Nature, 546: 637-641. DOI: 10.1038/nature22806.

Sadeghi, M. and Yaghoub, S. 2024. Optimization models for cloud seeding network design and operations. Eur. J. Oper. Res., 312(3): 1146-1167. https://doi.org/10.1016/j.ejor.2023.07.041.

Wondie, M. 2023. Modeling cloud seeding technology for rain enhancement over the arid and semiarid areas of Ethiopia. Heliyon, 9(4): e14974. https://doi.org/10.1016/j.heliyon.2023.e14974.

### ORCID DETAILS OF THE AUTHORS

Hasan M. Azeez: https://orcid.org/0000-0003-4509-5966
Nagham T. Ibraheem: https://orcid.org/0000-0003-0906-9752
Hazim H. Hussain: https://orcid.org/0000-0002-5588-8030

Nature Environment and Pollution Technology
An International Quarterly Scientific Journal

p-ISSN: 0972-6268
(Print copies up to 2016)
e-ISSN: 2395-3454

Vol. 23 | No. 3 | pp. 1801-1816 | 2024

Original Research Paper

https://doi.org/10.46488/NEPT.2024.v23i03.053

Open Access Journal

# Sewage Treatment by Kolkata's Natural Wetland System

**I. Khan†, D. Das Gupta and A. Gupta**
Department of Civil Engineering, Indian Institute of Engineering, Science and Technology, Shibpur, P.O. Botanic Garden, Howrah-711 103, West Bengal, India
†Corresponding author: I. Khan; indrani.env.rs2015@civil.iiests.ac.in

**Nat. Env. & Poll. Tech.**
**Website: www.neptjournal.com**

*Received:* 03-12-2023
*Revised:* 23-01-2024
*Accepted:* 25-01-2024

**Key Words:**
Nature-based sewage treatment
East Kolkata wetlands
Resource recovery
Sewage-fed fishery

## ABSTRACT

The metropolis of Kolkata stands uniquely positioned to implement a natural sewage treatment paradigm through the utilization of waste stabilization ponds, specifically within the East Kolkata Wetlands (EKW). These shallow oxidation ponds harness solar irradiation and algae bacteria symbiotic processes to effectively treat incoming sewage. Concurrently, nutrient-rich effluents are assimilated through fish production, converting available nutrients into protein—a hallmark of nature-based treatment. A portion of raw sewage is used to cultivate a chunk of vegetables before treatment in fish ponds, and the reclaimed water after treatment is used for vegetable and paddy cultivation downstream. This investigation explains the delineation of a sewage flow system to EKW, a Ramsar-designated site. Substantively, it offers quantitative insights into the sewage volumes and quality undergoing treatment. The sewage flow is higher in the winter months (909.07 MLD) compared to the summer months (709.34 MLD). In general, the sewage from the Kolkata city flowing to the EKW is moderately polluted. Extensive scrutiny of sewage from pond inlets and outlets serves as a quantitative metric for evaluating treatment efficacy. EKW efficiently treats the sewage, demonstrating 59.1% Biological Oxygen Demand (BOD) removal and a 99.28% reduction in fecal coliform. The natural treatment system excels in removing ammoniacal nitrogen (80.38%) and phosphate (90%). The treated water's quality along the EKW boundary, culminating at the Kulti Gong River discharge point, was systematically assessed. Analytical findings indicate that all measured concentrations in the treated water adhere to prescribed inland surface water discharge standards prescribed by the Central Pollution Control Board, India, barring a marginal elevation in BOD during winter. Evidently, the EKW system adeptly manages substantial sewage volumes, fostering efficient treatment while concurrently facilitating resource recovery through fish production, yielding economic dividends. Despite its substantial land footprint, preserving this inherently sustainable wastewater management paradigm is imperative.

## INTRODUCTION

India's wastewater is predominantly composed of domestic and municipal effluents, accounting for approximately 75% of the total volume. Globally, only about 20% of wastewater produced receives proper treatment (UN-Water 2012, WWAP 2017). In developing countries, sewage treatment plants have varying levels of compliance. Urban wastewater in India has been estimated as 72,368 MLD and only 28% (20,236 MLD) is treated (Niti Aayog 2022). Consequently, a significant portion of the wastewater, approximately 72%, is left untreated and could potentially be discharged into rivers, lakes, or groundwater sources. According to the Central Pollution Control Board (CPCB), an entity operating under the Ministry of Environment, Forests & Climate Change (MoEFCC) of the Government of India, approximately 39% of sewage treatment plants fail to meet the overall standards outlined in the Environmental (Protection) Rules for releasing effluents into water bodies (CPCB 2021).

The city of Kolkata (206.08 sq. km) generates a huge volume of sewage as it has a population of more than 4.5 million (Census of India 2011) along with a floating population of 6 million per day (KMC 2022). The sewage of this city is treated in the wetlands in an eco-friendly manner, along with the cultivation of fish in the sewage-fed ponds. A portion of the sewage, before entering the fish pond area of EKW, is also used for irrigation in the vegetable fields. In addition to this, the treated water is reused for cultivating edibles like paddy and vegetables for the city. Reusing treated wastewater is an important approach to water conservation. The utilization of sewage for irrigating vegetables and other short-term crops has been documented in developing nations across Africa and southern Asia (Vymazal 2010). The city

of Kolkata also has five municipal sewage treatment plants (STPs), namely, Baghajatin, Bangur, Gardenr Reach, Hatisur and Keorapukur. However, their treatment capacity is much less than the sewage generated every day from the city. The total installed capacity of these STPs is 179 MLD. The treated water from these STPs partially complies with the standards.

Wetland systems are recognized as a practical and economical method for treating wastewater on-site. These systems are known for their low energy consumption and environmentally friendly nature (Cui et al. 2020). Many researchers have studied the biogeochemical, hydrological, biological, and cultural services of wetlands in various countries (Chen et al. 2009, Geber & Bjorklund 2002, Moreno et al. 2007). Along with these services, wetlands have been used for wastewater treatment for a long time (Stainbridge 1976). Shallow wetlands, which work as oxidation ponds, are used to treat water, specifically in warm climatic areas (Butler et al. 2017). Wetlands, despite their mechanical simplicity, exhibit a profound biological complexity that empowers them to accomplish significant levels of treatment (Kadlec & Wallace 2009). By effectively reducing suspended solids, toxic organic substances, nutrients, heavy metals, and bacteria, wetlands play a pivotal role in enhancing the quality of wastewater.

Moreover, these systems hold great potential for addressing climate change and reducing greenhouse gas emissions (Gude et al. 2013). It has been proven that Constructed wetlands can efficiently decrease micro-pollutants in municipal sewage (Breitholtz et al. 2012). Constructed wetlands are highly efficient in treating concentrated livestock wastewaters, exhibiting an average removal rate of 65% for $BOD_5$, 53% for TSS, 48% for $NH_4^+$-N, 42% for Total Nitrogen, and 42% for Total Phosphate (Knight et al. 2000). The reduction of pollutants levels is achieved mainly due to algae bacteria symbiosis. The shallow wetlands (30-45 cm depth) have a high algal growth rate, which maintains dissolved oxygen levels throughout the pond (USEPA 2011). The photosynthetic activity occurring during the day ensures a steady supply of oxygen, while the gentle wind that enters the area facilitates the aeration of the shallow pond water (Davis & Cornwell 2008). These shallow aerobic ponds, characterized by their low depth, offer an excellent solution for sewage treatment as they possess a high capacity for removing organic substances (BOD). Operating within a detention time of 2–6 days and a BOD loading rate ranging from 112 to 225 kg.1000 $m^{-3}$ per day, these ponds achieve an impressive 95% efficiency in BOD removal (USEPA 2011). The utilization of algae primarily facilitates the treatment process in maturation ponds. These ponds remove fecal coliform, pathogens, and nutrients along with the BOD (Varon & Mara 2004). Considered one of the most productive ecosystems worldwide, wetlands offer vital support to a wide variety of aquatic and semiaquatic organisms (Cherry 2011, Dalu et al. 2017, Bai et al. 2019, Bird et al. 2019).

The utilization of wastewater for aquaculture has been acknowledged for a considerable time in Asia, with a history spanning several centuries. Subsequently, the utilization of municipal wastewater has experienced significant growth since the 1950s. Since the late 19$^{th}$ Century, wastewater-fed aquaculture has been extensively researched by scientists in Germany (Prein 1990). Whereas, in India, it commenced much earlier, in 1879, by a local landlord and fish farm proprietor, Bhabanath Sen, who let Kolkata's sewage into his fishponds (Bunting et al. 2010). The Kolkata waste water fish pond system offers the benefit of not only fish production but also the enhancement of the quality and the mitigation of pathogens in the sewage. However, a detailed study on how the sewage of Kolkata is entering the EKW and the quantity of sewage was hardly assayed.

Along with this, literature on the comparison of sewage quality at the incoming channels with the treated water coming out from the ponds is scanty. The treatment capacity of ponds of EKW has become crucial to keep the wetlands working as a natural sewage treatment system. The objectives of the study were to measure the volume and quality of incoming sewage received by the EKW and to estimate the treatment efficacy of the system.

## STUDY AREA

The investigated site EKW is located between 22°25' to 22°40' North and 88°20' to 88°35' East (Ramsar convention 1971) within the districts of South 24 Parganas. North 24 Parganas, West Bengal, India (Fig. 1). It covers rural/panchayat areas and also peri-urban areas lying within Kolkata and Bidhannagar Municipal Corporations of West Bengal. The total area of the wetlands is 12,500 hectares. Among the total area, a substantial water body-oriented area (fish farming) is 5852.14 hectares, along with an agricultural area (paddy and floriculture) of 4718.56 ha, a productive farming area (vegetable farming) of 602.78 ha, and an urban/rural settlement area of 1326.52 ha (Ghosh 2005). The EKW, selected as a Ramsar site in 2002, comprises sewage-carrying channels and an ensemble of interconnected oxidation ponds.

The unique hydraulic nature of these ponds is they are neither lotic nor lentic. The inflow of sewage into the ponds occurs through inlet channels in batches, and the outflow is likewise regulated. In the large ponds (40-45 hectares), the sewage enters continuously, and the pond acts as a lotic

system (Ray Chaudhuri & Thakur 2006). The ponds of EKW are shallow with a depth of about 45-60 cm so that the sunlight can reach up to the bottom. This allows algal growth, which increases the dissolved oxygen (DO) level in the water (USEPA 2011). Bacteria thrive there by taking up the DO and breaking down the organics. The degradation of sewage occurs in the ponds of EKW as they act as waste stabilization ponds (Ghosh 2005).

In 7-8 days of retention time, the sewage is purified (Sarkar et al. 2016) because it takes only 3-4 days for the anoxic water to become clear and oxic (Sarkar et al. 2014). This form of treatment is very effective for the removal of pathogens, including viruses, from wastewater. The prudent usage of the water to cultivate fish in the sewage ponds was discovered by the fishermen of this area as they have gathered experience about the particular timing of the introduction of sewage into these ponds. Fish cultivated in the ponds help in resource recovery by utilizing the available nutrients and converting them into protein for human consumption. The problem of eutrophication due to high algal growth is controlled by cultivating fish in the ponds. Water quality in wastewater-fed ponds is evaluated by examining the color of the water, the extent to which light can penetrate it, and the behavior of fish surfacing after dawn when the concentration of DO in the pond is at its lowest point during the night. The presence of green coloration and limited light penetration indicate good water quality, as they suggest the presence of an adequate number of protein-rich plankton for fish to consume. Feeding of sewage is done at regular intervals to maintain the organic load of the water. The treated water is removed from the pond through the outlets, which fall into various interconnecting canals. These canals carry the treated water to the SWF canal. A part of the treated water is also utilized for other non-potable purposes, viz., growing vegetables and paddy (Ghosh 2005, Ghosh & Sen 1987, Bose 1944).

Treatment of sewage is a continuous process in the ponds of EKW. However, ponds must be preserved and managed for efficiency. At the time when the pond bottom is filled with excess sludge/sediment, it is cleaned following different management practices depending on the size of the pond. For small to medium-sized ponds (up to 4 acres), the first step is to remove the water, which is done mostly during

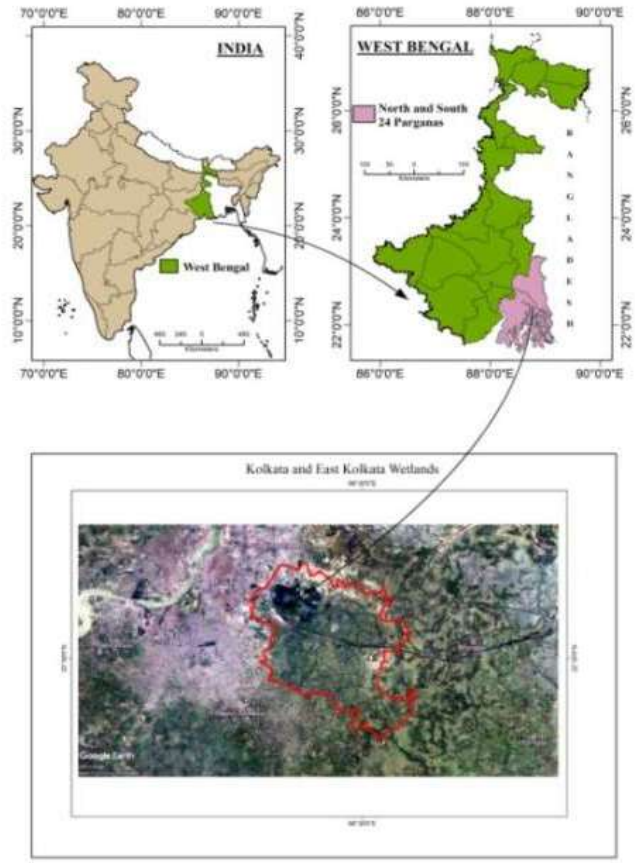


Fig. 1: Geographical location of the study area.

winter months (November to March). The sediment is then thoroughly dried, turned over, and further dried. Then, lime (calcium hydroxide) and Mahua oil cake, a natural fertilizer rich in macro and micronutrients, are added. The utilization of lime in the pond preparation process leads to a substantial decline of 96-99% in fecal coliform levels (Pradhan et al. 2008). After that, the sewage is let into the pond for about 30-45 cm depth or more, depending on the size of the pond. After that, a sedimentation time of 15-21 days is allowed and the water changes its color from blackish to greenish due to the growth of algae, and the water turns clearer as the DO level rises substantially. The entire pond preparation process takes 30-45 days. From India, only EKW managed and maintained by fishermen and farmers, was identified among one of the 17 tutorial wetland ecosystems in the world by the Ramsar Convention in 1993, as reported in their wise use project.

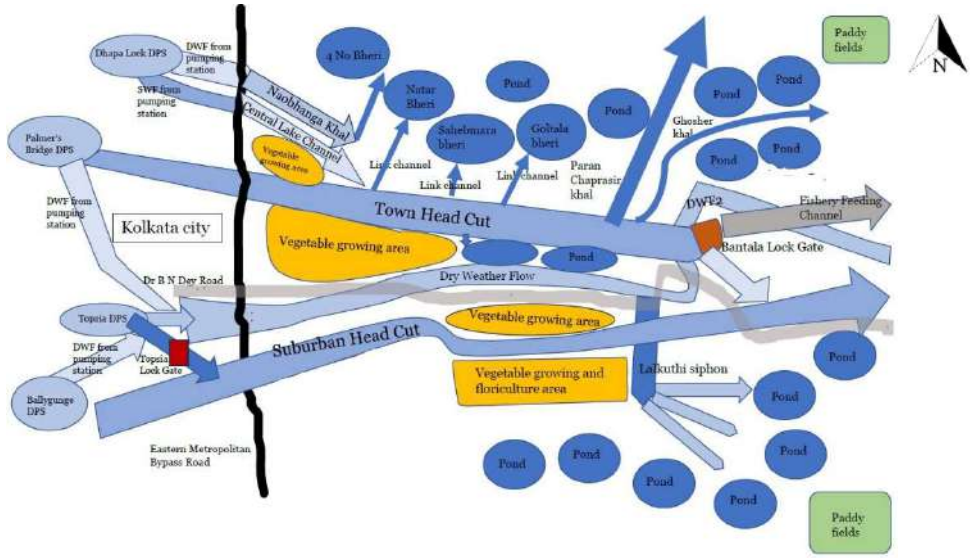


Fig. 2: Sewage flow pattern from Kolkata into EKW.

Table 1: Details about sewage-carrying channels connected to EKW from the city of Kolkata.

| Name of main sewage channel | Origin of sewage carried | Name of distributary sewage canals | Location of ponds served by the channel |
|---|---|---|---|
| Naobhanga *Khal* (NBK) | Sewage from Dhapa Lock DPS | | Upstream of Bantala Lock Gate |
| Central Lake Channel (CLC) | Sewage from Dhapa Lock DPS | | Upstream of Bantala Lock Gate |
| Town Head Cut (THC) | Sewage originating from Dhapa Lock and Palmer's Bridge DPS | 1. Natar bheri link *Khal*<br>2. Sahebmara link *Khal* 1<br>3. Sahebmara link *Khal* 2<br>4. Goltala link *Khal*<br>5. Khanaberia *Khal*<br>6. Paran Chaprashir *Khal*<br>7. Ghosher *Khal* | Upstream and downstream of Bantala Lock Gate |
| DWF | Sewage from Palmer's Bridge, Topsia, and Ballygunge DPS | 1. Bidyadhari 1 *Khal*<br>2. Bidyadhari 2 *Khal*<br>3. Bidyadhari 3 *Khal* | The right side of Dr. B.N. Dey road via Lalkuthi siphon; southern part of EKW |
| Suburban Head Cut and SWF | Stormwater flow of Ballygunge DPS with link channel from Topsia as a tributary | | |
| Fishery Feeding Canal (FFC) | Sewage of THC from Bantala Lock Gate | | The left side of Dr. B.N. Dey Road, up to the central point of the EKW boundary |


Fig. 3: Location of volume flow measurements in incoming sewage channels (marked red).

## SEWAGE FLOW TO EKW

Few reconnaissance surveys were conducted, and it was found that the sewage generated from the city was carried by a network of sewage-carrying channels that were initiated from four sewerage and drainage pumping stations (DPS), namely Dhapa Lock (DPS 1), Palmer's Bridge (DPS 2), Topsia (DPS 3), and Ballygunge (DPS 4) (Fig. 2 and 3). From the pumping stations, the sewage was pumped out with great force through outfall channels that carry the sewage to the wetlands for distribution. Each of the four DPS has two channels: dry weather flow (received sewage uniformly throughout the year) and stormwater flow (received sewage more heavily during the monsoon). These drainage-pumping stations pump the sewage to the dry weather flow and stormwater flow channels according to the sewage availability throughout the year.

The two channels that start from Dhapa Lock DPS are called Central Lake Channel (CLC) and Naobhanga *Khal* (NBK; canals are known as *khal* in the local language). NBK and CLC provide water to the ponds located on the northern side of the EKW area. The surplus water of CLC joins the stormwater flow channel of Palmer's Bridge DPS, which is known as Town Head Cut (THC). The ponds at the left side of THC receive sewage from it through seven distributary *khals*. The left-over sewage reaches the end of the THC channel at Bantala, Kolkata. It is distributed down the Southern side through a set of ten regulator gates at Bantala, known as Bantala Lock Gate, located on the left side of Dr. B. N. Dey Road. From the lock gate, the Fishery Feeding Canal (FFC) begins, which serves the northern EKW ponds downstream of the Bantala lock gate. The sewage of THC is channeled by gravity flow into the FFC.

The dry weather flow channel of Palmer's Bridge DPS meets the dry weather flow channels of Topsia DPS and Ballygunge DPS, and combined, these channelize their sewage into the main Dry Weather Flow (DWF) channel. The DWF canal, while traveling downstream, provides sewage to the ponds located on the southern part of EKW (right side of Dr. B. N. Dey Road) through a siphon called the Lalkuthi siphon. The stormwater flow of Ballygunge DPS is known as Suburban Head Cut (SHC), and a short connecting channel (stormwater flow channel of Topsia DPS) acts as a tributary of SHC. This channel is named the Storm Weather Flow (SWF) after the Bantala lock gate. The FFC, DWF, and SWF travel parallelly. The DWF and SWF fall into the river Kulti Gong, which is about 27 km away from the Bantala Lock Gate (Drainage Enquiry Committee 1945). It has also been observed that sewage water is utilized for watering the rice and vegetable fields situated in the eastern region of the EKW area. Table 1 and Fig. 2 show the details of the channels carrying sewage to EKW.

The flow of sewage to the EKW was estimated at NBK (near 19-bigha field), CLC (near Tapuriaghata Boy's Sporting Club), $THC_{TB}$ (under CESC Truss Bridge at Metropolitan bus stop), and $DWF_{AP}$ (located at Auropota) as these four are the incoming sewage channels for all the ponds of EKW (Fig. 3). Samples were collected from each channel during winter and summer spanning January 2023 to October 2023 with the aid of the Acoustic Doppler Current Profiler (ADCP) along the cross-section of the channels

Fig. 4: A sewage channel to EKW.

(Fig. 4). The ADCP measures the instantaneous volume flow in $m^3 \cdot s^{-1}$. So, flow was measured multiple times in each canal to get the average volume flow.

It was observed that there were seasonal variations in the combined flow from the four main canals - during winter, it reached 909.07 million liters per day (MLD), whereas during summer, it was 709.34 MLD. After calculating the total average flow of the sewage-carrying channels, the percentage distribution of sewage by each channel was determined.

Table 2: Volume of sewage carried by the channels.

| Sewage channels | Winter | | Summer | |
|---|---|---|---|---|
| | MLD | Percentage | MLD | Percentage |
| NBK | 110.59 | 12 | 72.00 | 10 |
| CLC | 191.19 | 21 | 130.72 | 18 |
| $THC_{TB}$ | 316.29 | 35 | 41.59 | 6 |
| $DWF_{AP}$ | 291.00 | 32 | 465.03 | 66 |
| Total Flow | 909.07 | 100 | 709.34 | 100 |

Table 2 provides the average daily flow of the four sewage channels and also as percentage. Notably, $THC_{TB}$ exhibits the highest average flow in winter (316.29 MLD; 35%; Fig. 5a), and $DWF_{AP}$ shows the highest average flow in summer (465.03 MLD; 66%; Fig. 5b).

## Physicochemical and Microbiological Quality of Incoming Sewage

Sterile containers were used for bacteriological tests and clean polyethylene terephthalate (PET) bottles were used (with and without preservatives) for other tests. The bottles were rinsed three times taking water from the sampling site before being utilized for sample collection. Subsequently, water samples from each site (collected at various times on the same day) were combined to create composite samples. These collected samples were then placed in an icebox and transported to the laboratory for analysis.

pH and turbidity were measured on-site using portable meters. Alkalinity, chloride, Total Solids (TS), Total

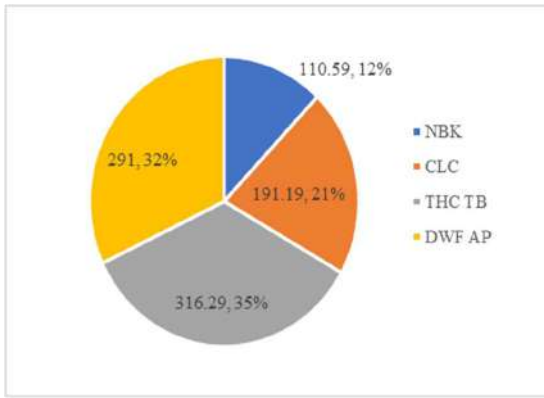


Fig. 5a: Percentage of sewage flow in winter.

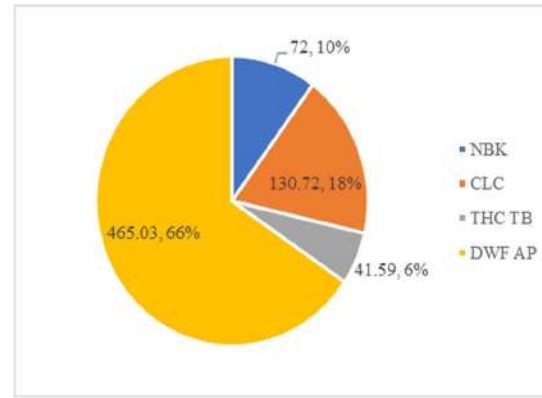


Fig. 5b: Percentage of sewage flow in summer.

Suspended Solids (TSS), Total Dissolved Solids (TDS), Total Volatile solids (TVS), Volatile Suspended Solids (VSS), phosphate, Biochemical Oxygen Demand (BOD), Chemical Oxygen Demand (COD), Total Kjeldahl Nitrogen (TKN), total coliform and *E. coli* were measured following standard methods as outlined by APHA (2017). Ammoniacal nitrogen ($NH_4^+$-N) and nitrate were measured using an ion-selective electrode, and Total Organic Carbon (TOC) was measured using a TOC analyzer. All the reagents and chemicals utilized in the current investigation were of analytical quality. Deionized water was employed for all the procedures of preparation and dilution during the study.

Nine locations were chosen to estimate the physico-chemical and microbiological parameters present in the sewage throughout the canals, namely NBK, CLC, $THC_{TB}$, and $DWF_{AP}$. THC at Khanaberia ($THC_{KB}$; as it is near the Dhapa solid waste dumping site, to investigate potential contamination from the leachate), starting point of $FFC_B$ (at Bantala lock gate) and Lalkuthi siphon (LKTS), $FFC_{KT}$ (FFC at Kantatala; located at the edge of the EKW border) and $DWF_{KT}$ (DWF at Kantatala) (Fig. 6). Samplings were done in winter (Jan-Feb 2023) and in summer (May-June 2023).

The first four locations were before sewage entered into any production activity (near the western boundary of the EKW area), the subsequent three locations are inside the EKW area (near the Bantala lock gate), and the remaining two are located at the EKW eastern boundary (towards the Kulti river). The reduction percentage was calculated by taking into account the average value found at the initial four locations and the average value of the final two locations, including both seasons.

The pH values ranged from 7.05 to 7.56 in all channels, including both seasons. The measured pH values were within the discharge limit of 6.5 to 9.0 laid by CPCB (1993) ( Fig. 7). The pH levels were a little higher in summer than in winter, though there were no significant differences across all the channels that were measured. During winter, the levels of Total Solid (TS) and Total Suspended Solid (TSS) tend to be higher due to the reduced volume of water in the channels, except for $THC_{KB}$ and $FFC_B$ (Fig. 8). The range of TSS concentration in all the nine locations was between 170 to 766 $mg.L^{-1}$ in the winter. In contrast, in the summer, the range was found in between 126 to 687 $mg.L^{-1}$. The average value of TS in the first four locations (NBK, CLC, $THC_{TB}$, and $DWF_{AP}$ before delivering sewage to the ponds) was 600 $mg.L^{-1}$, taking into account both seasonal values. The average seasonal value (considering both seasons) of TS was reduced to 457.5 $mg.L^{-1}$ in $THC_{KB}$, $FFC_B$, and LKTS. The $FFC_{KT}$ and $DWF_{KT}$, at the final point of EKW, had 177.5 $mg.L^{-1}$ of TS on an average value covering both seasons. This shows that the settleable portion of the TS accumulates at the bottom of the channels and ponds, necessitating periodic cleaning to ensure proper function. Meanwhile, the range of TSS was found to be between 28 to 68 $mg.L^{-1}$ in winter and 21 to 52 mg.Lv in summer in the first four locations. The average value of TSS in these four channels was 40.86 $mg.L^{-1}$ and the TSS is much lower than the prescribed limit (100 $mg.L^{-1}$) of discharge in inland surface water (CPCB 1993). However, the average TSS concentration in the $THC_{KB}$, $FFC_B$, and LKTS was 42.75 $mg.L^{-1}$, and the average TSS of $FFC_{KT}$ and $DWF_{KT}$ was 32 $mg.L^{-1}$ (including both seasons), which was within the discharge limit. The reduction percentages for TS and TSS were 70.4 and 21.7, respectively. In the winter season, the average concentration of COD in the first four locations (NBK, CLC, $THC_{TB}$, and $DWF_{AP}$ before delivering sewage to the ponds) was recorded at 158.75 $mg.L^{-1}$, while in the summer season, the average concentration dropped to 88.25 $mg.L^{-1}$ with a range of 76 to 248 $mg.L^{-1}$ in winter and 74 to 110 $mg.L^{-1}$ in summer. The $THC_{KB}$, $FFC_B$, and LKTS had a range of 213 to 266 $mg.L^{-1}$ of COD in winter and 38 to 88 $mg.L^{-1}$ in summer. The final sampling locations (downstream of EKW) of $FFC_{KT}$ and $DWF_{KT}$ had a COD between 26 to 165 $mg.L^{-1}$, covering both seasons. The average COD in all the locations in both seasons was 123.22 $mg.L^{-1}$. Despite these variations, the concentration of COD at the final locations remained within the discharge limit (250 $mg.L^{-1}$ for inland surface water as laid by CPCB 1993) during both seasons. COD shows much lower levels in summer in all the channels (Fig. 9). The reduction percentage is 34 from the initial point to the final point. Similarly, the average BOD concentration in the winter season was measured at 43 $mg.L^{-1}$. In contrast, in the summer season, it decreased to 22.75 $mg.L^{-1}$ across the first four locations, with a range of 19 to 66 $mg.L^{-1}$ in winter and 20 to 28 $mg.L^{-1}$ in summer. However, the concentration of BOD at the middle portion of the channels, i.e., $THC_{KB,}$ $FFC_B$, and LKTS, lies between 9.4 to 70 $mg.L^{-1}$, including both seasons, with an average of 38.4 $mg.L^{-1}$. The $FFC_{KT}$ and $DWF_{KT}$ (the final locations downstream of EKW) have an average of 35 $mg.L^{-1}$ of BOD in winter and 15 $mg.L^{-1}$ in summer. This observation confirms that microbes function more efficiently in summer (concentration is within the discharge standards; CPCB 1993), and sewage treatment is carried out partially throughout the entire stretch of the sewage channels. However, it is worth noting that most of the BOD values measured in winter slightly exceeded the discharge limit of 30 $mg.L^{-1}$ (CPCB 1993; Fig. 9) due to the less activity of microbes at lower temperatures. In the first four channels, the average concentrations of phosphate and nitrate were 0.89 $mg.L^{-1}$ and 0.53 $mg.L^{-1}$, respectively, when considering both seasons. The range was between 0.65 -1.17 and 0.41-0.65 $mg.L^{-1}$ for phosphate and nitrate,

respectively, in the first four sites. In the mid-section, at $THC_{KB}$, $FFC_B$, and LKTS, the average concentration of phosphate and nitrate were 0.75 and 0.83 $mg.L^{-1}$, considering both seasons. At the final locations (downstream of EKW) at $DWF_{KT}$ and $FFC_{KT,}$ the average seasonal concentrations were 0.47 and 0.30 $mg.L^{-1}$. These concentrations were found to be far below the discharge limit (CPCB 1993) for both phosphate (5 $mg.L^{-1}$) and nitrate (10 $mg.L^{-1}$) in all the nine samples measured (Fig. 10). The reduction percentages were 47.31 and 43.01 for phosphate and nitrate, respectively. On the other hand, the average concentration of TKN was significantly higher in the winter compared to the summer in all the locations. The average TKN of the first four locations was 18.36 (range 4.3 -37.8) $mg.L^{-1}$, including both seasons (Fig. 11). The $THC_{KB}$, $FFC_B$, and LKTS had an average of 12.6 (range 3.6-21.5) $mg.L^{-1}$ and the average of $FFC_{KB}$, and $DWF_{KB}$ was 9.45 $mg.L^{-1}$ including winter and summer. The measured values of TKN in all the samples were found to be much lower than the discharge limit of 100 $mg.L^{-1}$ (CPCB 1993). The reduction percentage was 48.39.

During the summer season, it has been observed that the levels of E. coli are significantly higher in all the measured channels. The average count of E. coli during summer at the first four channels was much greater compared to winter, reaching 1190 on an average (range 920-1500) MPN.100 $mL^{-1}$, as microbial growth tends to accelerate in warmer temperatures (Fig. 12). The average count of E. coli at the first four channels in the winter was 598 on an average (range 430-920) MPN.100 $mL^{-1}$. The $THC_{KB}$, $FFC_B$, and LKTS have a count of 757 and 380 MPN.100 $mL^{-1}$ in the summer and winter seasons, respectively, at an average. Furthermore, the concentration of E. coli in $FFC_{KT}$ and $DWF_{KT}$ were 49 and 705 MPN.100 $mL^{-1}$ at an average considering both seasons. It has been observed that the E. coli count was within the discharge limit for STP of CPCB (2017; 1000 MPN.100 $mL^{-1}$) at $FFC_{KT}$ and $DWF_{KT}$ in both winter and summer.

It has been observed that except BOD (in winter) all other values of $FFC_{KT}$ and $DWF_{KT}$ were within the discharge limit. Taking into account the fact that the water from these channels may be lowered further while traveling downstream to the final discharge point, which is approximately 27 Km away at the Kulti Gong River, the microbes will persistently break down the organic matter along the entire pathway. In general, the sewage from the Kolkata city flowing to the EKW is moderately polluted (Fig. 7-12). EKW is providing a natural system of treatment of sewage in the city, protecting the health of the receiving river Kulti Gong.

## SEWAGE TREATMENT IN EKW PONDS

To determine the extent of sewage treatment by the ponds located in the EKW area (Fig. 13), four representative ponds were selected according to size and location, covering three seasons (pre-winter, winter, and pre-summer of 2022; Table 3). Among the four, two are situated on the left side of the DWF canal and receive sewage from THC (via a sewage distributing canal named Ghosher *Khal*), and the other two are located on the right side of the DWF canal and obtain water from Lalkuthi siphon by a connected sewage distribution canal. Dakshin Gorumara Bheri (pond 4) is the largest among the four ponds and Bantala 2 no. Bheri (pond

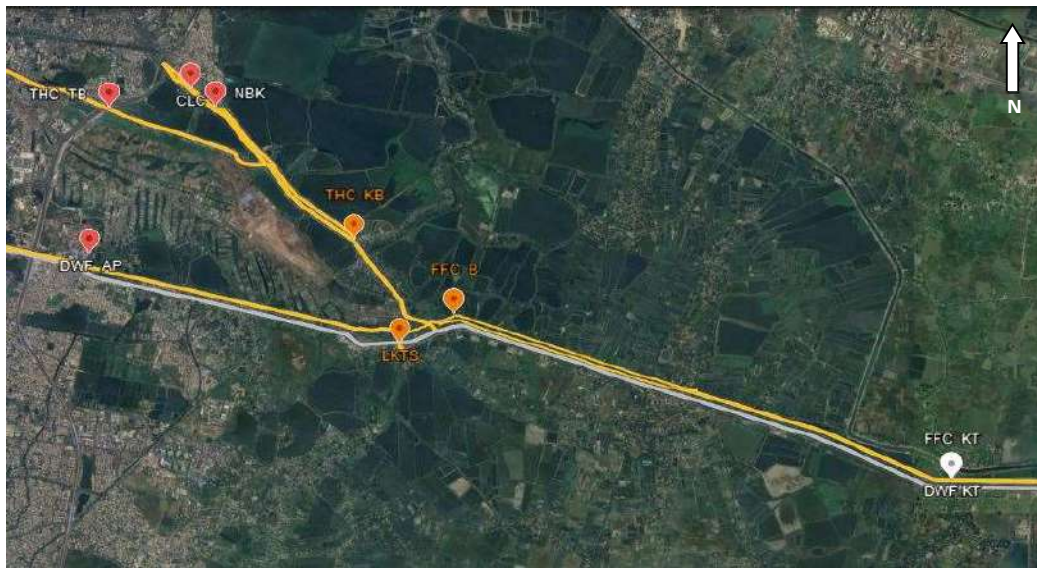


Fig. 6: Location of sampling sites for physicochemical and microbiological analysis throughout the sewage channels.

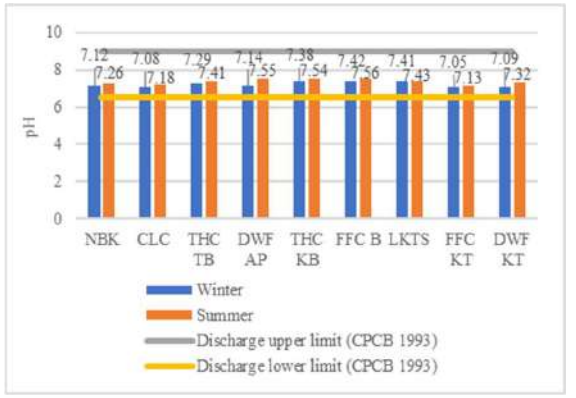


Fig. 7: pH at the sewage samples.

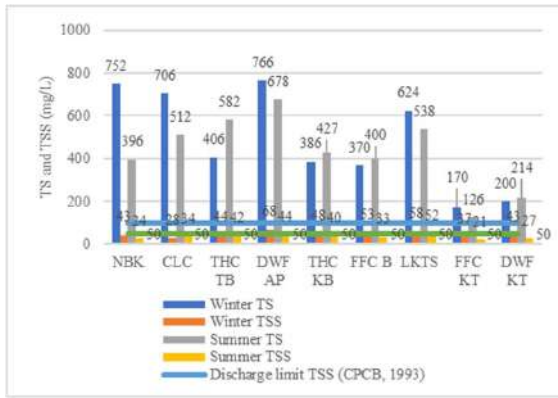


Fig. 8: TS and TSS at the sewage samples.

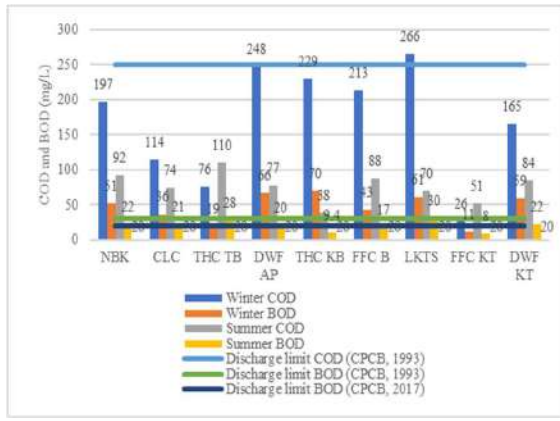


Fig. 9: COD and BOD at the sewage samples.

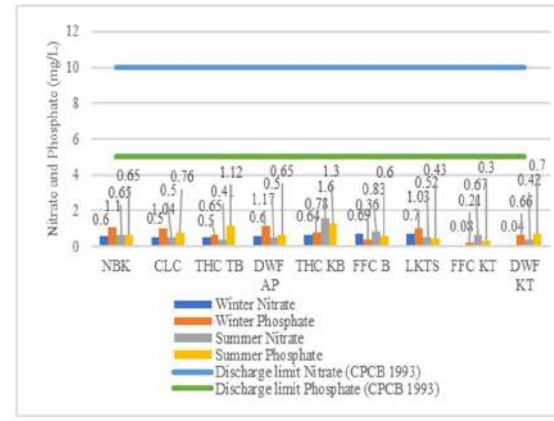


Fig. 10: Nitrate and Phosphate at the sewage samples.

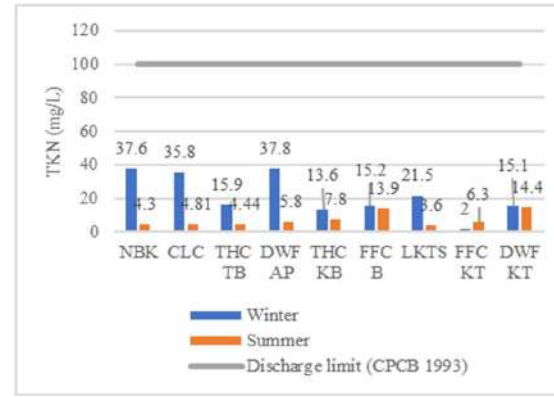


Fig. 11: TKN at the sewage samples.

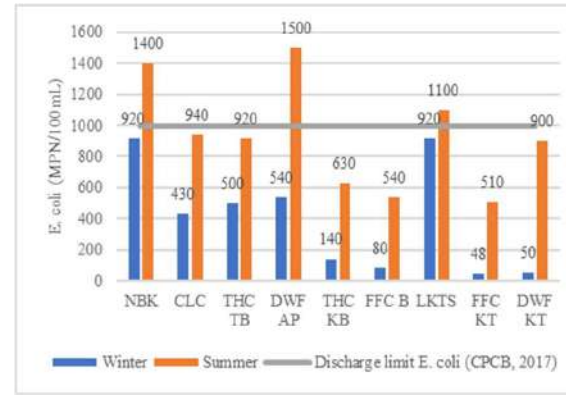


Fig. 12: E. coli at the sewage samples.

3) is the smallest (Fig. 14). To explore further and compare the mean of one group with the mean of another, a one-way analysis of variance (ANOVA) was followed. Fisher's Least Significant Difference (LSD) test was evaluated among the concentrations of inlets and outlets of the four ponds by Minitab 18 software.

The average seasonal value of each parameter of the inlets and outlets of the four selected ponds was estimated.

The pH in the outlets of the ponds was higher than the inlets but within the discharge limit (Fig. 15). The average increase in pH is 7.2 percent in the ponds ($F_{1,22}$=12.98;

Fig. 13: A pond of EKW area.

Table 3: Location and details of the four selected ponds.

| Name of the pond | Referred as | Location | Receive sewage from | Area of the pond (Hectare) |
|---|---|---|---|---|
| Harhare Bheri | Pond 1 | 22.531823; 88.446096 | THC via Ghosher *Khal*; | 2.9551 |
| Sujit Mondal's Bheri | Pond 2 | 22.530119; 88.443782 | THC via Ghosher *Khal*; diluted | 1.1298 |
| Bantala 2 No. Bheri | Pond 3 | 22.525048; 88.442679 | DWF via Lalkuthi siphon; raw | 0.4037 |
| Dakshin Gorumara Bheri | Pond 4 | 22.524334; 88.445838 | DWF via Lalkuthi siphon; raw | 5.3804 |


Fig. 14: Location of four selected ponds in EKW area.

$p$=0.002). At moderate alkalinity, the removal of carbon dioxide by algae by the process of photosynthesis shifts the forms of alkalinity existing from bicarbonate to carbonate and from carbonate to hydroxide (Sawyer & McCarty 1978), as shown in the equation below:

$$2HCO_3^- \leftrightarrow CO_3^{2-} + H_2O + CO_2$$

$$CO_3^{2-} + H_2O \leftrightarrow 2OH^- + CO_2$$

As the pond receives an ample amount of sunlight, the algae remove $CO_2$ from the solution more rapidly than the $CO_2$ generated by the organisms present in the water. This would cause an increase in pH. However, the pH of the pond water was suitable for discharging this water into inland surface water bodies as they were within the discharge limit (CPCB 1993). This pH range is also suitable for pisciculture as the ideal pH levels for fish production are in the range of 6.5 to 9.0 (Kaoud 1999).

Alkalinity is the capacity of water to buffer pH. The buffering capacity of water should be at least 20 mg.L$^{-1}$ as $CaCO_3$ for protecting the aquatic organisms (Wurts & Durburrow1992). However, the alkalinity found in the four ponds was higher than the required buffering capacity.

The alkalinity was reduced slightly by the four ponds (Fig. 16). The average removal percent was 29.04 for alkalinity ($F_{1,22}$=13.88; $p$=0.001); however, CPCB does not prescribe any discharge standard regarding Alkalinity. As compared to the inlets, alkalinity was reduced as nitrification of 1 mg.L$^{-1}$ of ammoniacal nitrogen ($NH_3$-N) decreased alkalinity by 7.14 mg.L$^{-1}$ (Boyd 2016). The nutrients that are dissolved in the water are absorbed by aquatic plants. To maintain charge balance in the water, other positive ions (usually $H^+$) replace the ammonium ions ($NH_4^+$) used up by the plants. Therefore, the release of hydrogen ions lowers alkalinity. Materials such as silt, fine organic and inorganic matter, mineral dissolution (iron), phytoplankton (algae), and other microscopic organisms (bacteria, viruses, etc.) cause turbidity in water, making it murkier. These particles can be both colloidal and suspended. The turbidity is decreased in the outlets compared to the inlets. As the water is treated, the solids settle down, and turbidity should decrease a lot, but the population of algae that grow in the ponds contributes to turbidity. The turbidity was reduced in the four ponds with an average of 54% in the outlets as compared to inlets ($F_{1,22}$=41.03; $p$=0.0). (Fig. 17). The ponds were not very effective in reducing the chloride concentration ($F_{1,22}$=6.11; $p$=0.022). The average removal was noticed to be 34% in all the ponds (Fig. 18). The removal of TS was highest in the first pond, and the average removal percentage by all the ponds was 40 ($F_{1,22}$=87.88; $p$=0.0). The concentration of TSS in the outlets of the first, second, and fourth ponds was slightly higher than the discharge limit (Fig. 19), which was possibly contributed by algal biomass.

In all the four ponds, COD and BOD decreased significantly. The ponds worked efficiently in the removal of the COD and BOD with an average of 50.5% ($F_{1,22}$=39.55; $p$=0.0) and 59.1 % ($F_{1,22}$=79.98; $p$=0.0), respectively. The bacteria fed on the organic matter to build their biomass using the dissolved oxygen and brought down the BOD level. The average concentration of COD at the outlets of all the ponds was 66.76 mg.L$^{-1}$, which is far lower than the discharge limit (250 mg.L$^{-1}$) of CPCB 1993. The average concentration of BOD at the outlets of all the ponds was 23.3, which is also within the discharge limit of 30 mg.L$^{-1}$ (CPCB 1993; for inland surface water); however, compared with the discharge limit for STP (20 mg.L$^{-1}$; CPCB 2017), the concentration is marginally higher (Fig. 20). These ponds are far from the river Kulti Gong, the final discharge point for Kolkata sewage. Downstream of the ponds, other ponds will take up this water at their intake, and it will be further treated in those oxidation ponds as EKW consists of a series of ponds. All four ponds reduced TOC ($F_{1,22}$=10.68; $p$=0.004) at an average rate of 36.64%, and the highest removal rate was noticed at the first pond (Fig. 21). The concentration of dissolved phosphate was 4.09, 5.89, 5.23, and 5.45 mg.L$^{-1}$ in the inlets of four ponds, respectively (Fig. 22) indicating that the ponds are ideal for eutrophication as the threshold value of phosphorus is greater than 0.1 mg.L$^{-1}$ for a pond to be hypereutrophic (Nemery 2019). However, the ponds were not covered with an algal bloom, indicating that the growth of phytoplankton was restricted due to the fishes grazing on them. Thus, the problem of eutrophication is mitigated. Ammonium is produced when the nitrogenous organic wastes decompose. It is a by-product of protein breakdown. All four ponds were very efficient in removing ammonium ($F_{1,22}$=41.04; $p$=0.00). The third and fourth ponds reduced ammonium by over 90%. The average removal rate of ammonium in the four ponds was 80.38% (Fig. 23), and phosphate removal was by over 90% ($F_{1,22}$=208.42; $p$=0.00) at the first, second, and third ponds. The reduction in these nutrients indicated that the aquatic plants took up the nutrients for their growth. Some amount of phosphate also got adsorbed on the surface of soil minerals, porous oxides of Fe and Al (Nichols 1983). The concentration of phosphate and ammonium was within the discharge standards of CPCB (1993). As per Sinton et al. (2007), oxidation ponds are capable of reducing *E. coli,* and the removal of *E. coli* depends on pH, DO, and sunlight (Maiga et al. 2009). The ponds of EKW worked wonderfully in reducing the indicator organism *E. coli* ($F_{1,22}$=350.17; $p$=0.00) with an average of 97.76% (Fig. 24), and the effluent fecal coliform content was far below the prescribed discharge limit of CPCB (2017). In the beginning, untreated sewage contains a significant amount of organic matter, which can act as a source of nutrients for various microorganisms, resulting in a high level of functional diversity. However, as the purification process continues, the organic matter in the wastewater decreases, leading to a reduction in nutrient availability for microbial growth and subsequently causing a decrease in functional diversity (Sarkar et al. 2017). The oxidation pond system efficiently serves to remove fecal coliform from the sewage (Tiley et al. 2014, Von Sperling 2007, Pescod 1992, Arthur 1983), and in the case of the four ponds studied in the EKW, the total coliform levels decreased by 99.28% on an average (Fig. 25). Sarkar et al. 2016 studied the potential of microbes to purify the sewage. They have also found that the maximum number of microbes decreases as the sewage purifies.

## IMPORTANCE OF EKW

Kolkata, being an 'ecologically subsidized city' (Ghosh 2004), is blessed with unique geography: one river (Hooghly, the final stretch of the river Ganga) for drinking water abstraction on the west and another (Kulti river) for treated sewage disposal and a wetland system between the city and Kuti rivers that treats the municipal sewage by a natural

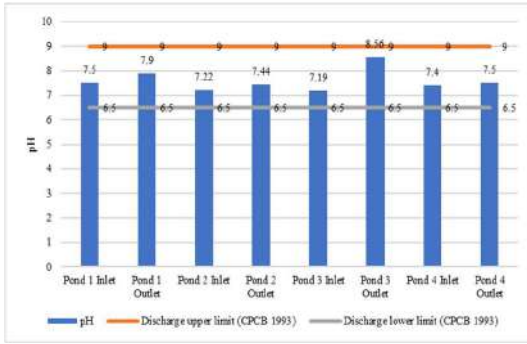


Fig. 15: pH in the inlets and outlets of ponds.

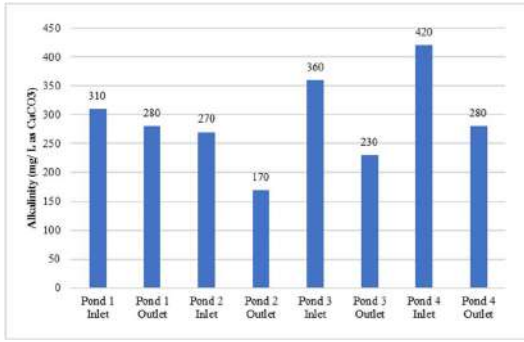


Fig. 16: Alkalinity in the inlets and outlets of ponds.

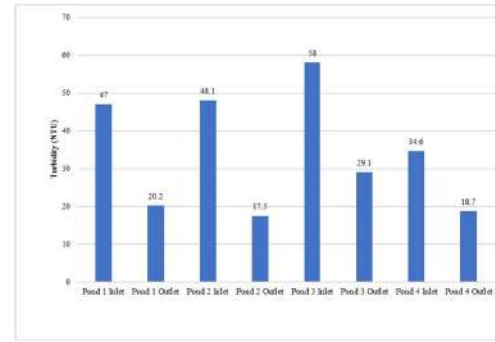


Fig. 17: Turbidity in the inlets and outlets of ponds.

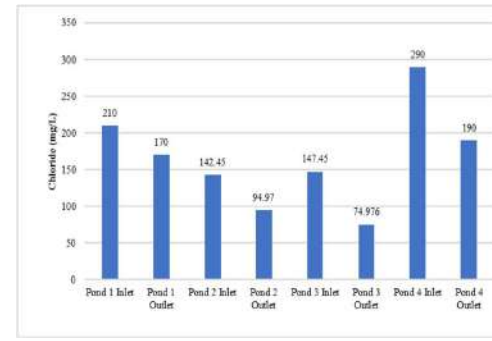


Fig. 18: Chloride in the inlets and outlets of Ponds.

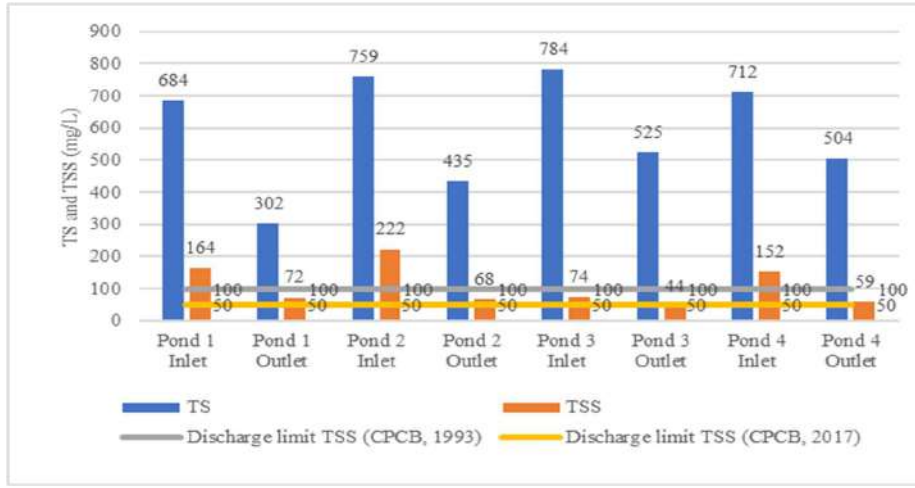


Fig. 19: TS and TDS in the inlets and outlets of ponds.

biological treatment method. The EKW stands as a unique testament to the successful integration of environmental protection and development management. The delicate balance achieved in this ecosystem, where local farmers have mastered resource recovery activities, is exemplified by the intricate interplay of aquaculture, horticulture, and agriculture (Bhattacharya et al. 2012).

At the heart of EKW's importance is its ingenious use of sewage for aquaculture and agriculture. This practice not only showcases environmental innovation but also yields substantial benefits. The sewage-fed fisheries in EKW contribute significantly to the region's annual fish production. The treated water discharged from these fish ponds is channeled into irrigating paddy fields and

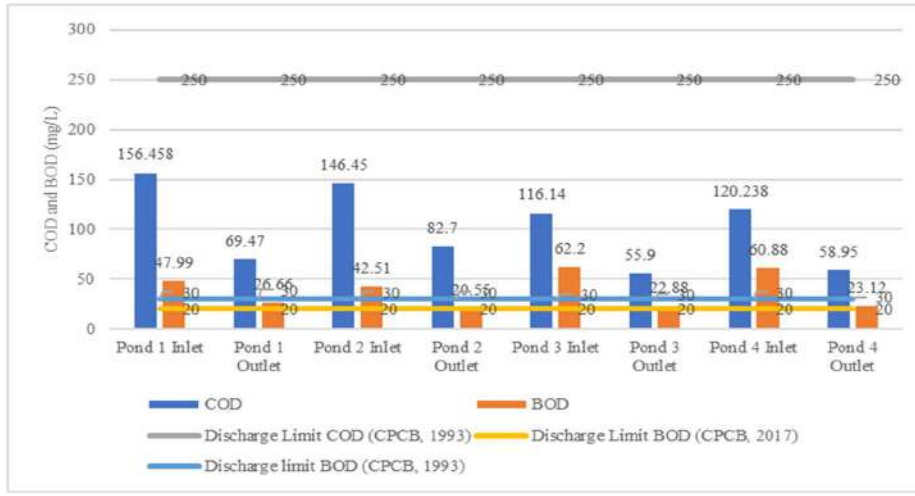


Fig. 20: COD and BOD in the inlets and outlets of ponds.

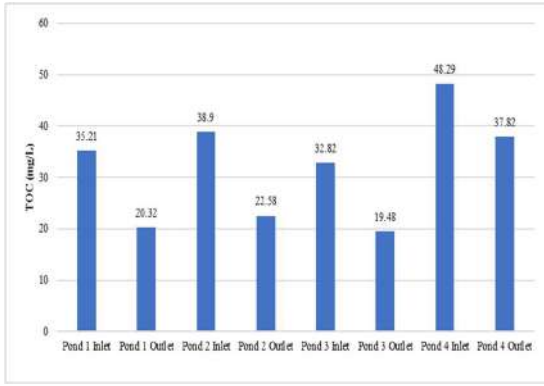


Fig. 21: TOC in the inlets and outlets of ponds.

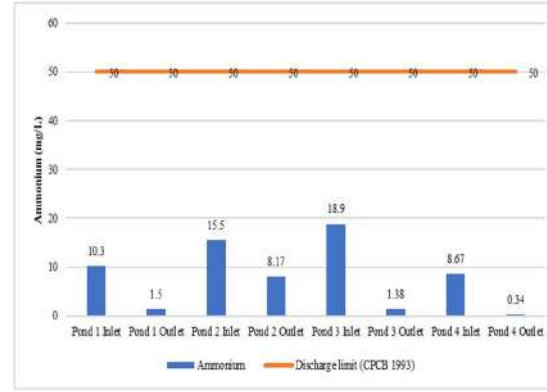


Fig. 23: Ammonium in the inlets and outlets of ponds.

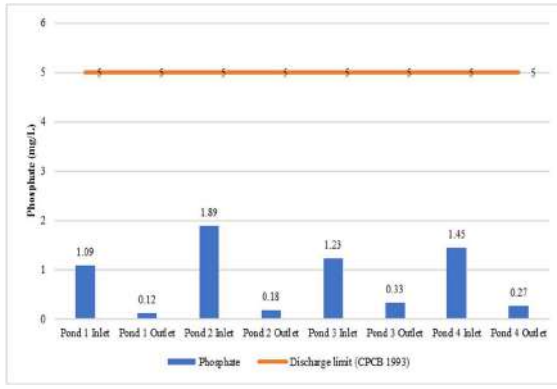


Fig. 22: Phosphate in the inlets and outlets of ponds.

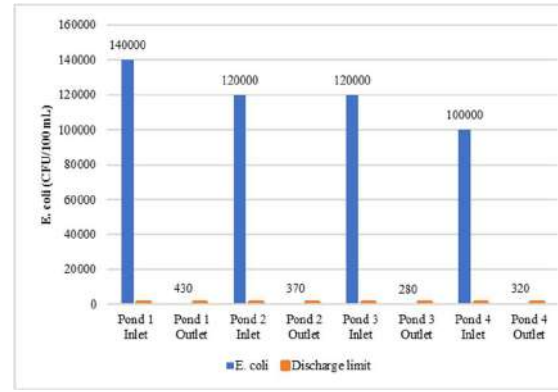


Fig. 24: *E. coli* in the inlets and outlets of ponds.

agriculture farms, creating a closed-loop system of resource utilization.

The organic wastewater discharged by the city of Kolkata finds a purpose in EKW as they are utilized as valuable manure for cultivating fresh vegetables. This not only serves as an effective waste management strategy but also economically benefits the local farmers. By repurposing organic waste, the system minimizes the need for external

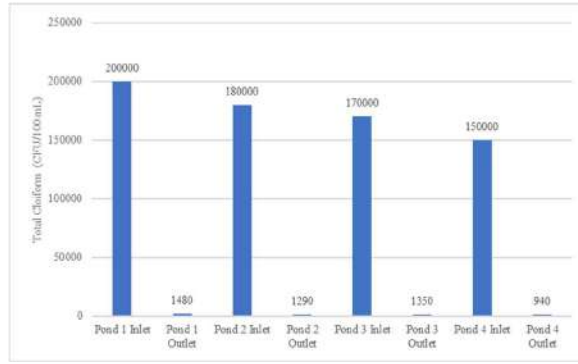


Fig. 25: Total coliform in the inlets and outlets of ponds.

fertilizers, thus reducing costs and increasing overall profitability.

Resource recovery systems from the EKW are a revenue earner. EKW produces about 11,000 metric tonnes of fish per year (Government of West Bengal 1997). Regularly, the garbage farms generate an average of 152.41 metric tons of freshly harvested vegetables and an annual output of 16,000 tonnes of paddy (EKWMAP 2021). Mukherjee (2018) calculated the cost of sewage treatment per million liters for STPs as 1246 INR. The sewage cleaning cost by EKW was calculated by subtracting the cost of fish production from the profit earned by selling the fish. The cost of fish production was calculated by summing the rent paid by the fishermen for using the ponds. It is about -10302.00 INR per million liters (the value is negative as the profit from selling fish was higher than the cost of production).

Being next to the city, EKW faces constant threats from rapid urbanization, leading to a 26% shrinkage in wetlands from 1973 to 2010 (Parihar et al. 2013) and 57% land acquisition from 1991 to 2018 (Mandal et al. 2019). The treatment system also depends on the continuous supply of sewage from the city. So, it is of utmost importance to protect the EKW area from land use change and maintain an unremitting supply of sewage on a daily basis.

## CONCLUSION

The current study on East Kolkata Wetlands revealed a complex sewage drainage system delivering an average of 909.07 MLD in winter and 709.34 MLD in summer. EKW efficiently treats the sewage, demonstrating 59.1% BOD removal and a 99.28% reduction in fecal coliform. The natural treatment system excels in removing ammoniacal nitrogen (80.38%) and phosphate (90%). Local management practices showcase waste-to-wealth recycling, offering a self-sustaining model that can be replicated as a low-cost sanitation option for smaller cities with ample sunshine. The Ramsar Convention recognizes EKW as one of the 17 tutorial wetland ecosystems in the world and the only such from India. The symbiotic relationship between environmental protection and economic prosperity in EKW serves as a model for sustainable development, emphasizing the need for preservation amid looming threats.

## ACKNOWLEDGMENT

The authors of this article are highly thankful to the local people of the study area for the help during sampling and the WBPCB of India for providing the funds for the study.

## REFERENCES

APHA 2017. Standard Methods for the Examination of Water and Wastewater. 23rd Edition, American Public Health Association/American Water Works Association/Water Environment Federation, Washington DC.

Arthur, J. P. 1983. Notes on the design and operation of waste stabilization ponds in warm climates of developing countries. World Bank Technical Paper No 7. World Bank: Washington, DC.

Bai, J., Zhao, Q., Wang, W., Wang, X., Jia, J., Cui, B. and Liu, X. 2019. Arsenic and heavy metals pollution along a salinity gradient in drained coastal wetland soils: Depth distributions, sources, and toxic risks. Ecol. Indic., 96: 91-98.

Bhattacharya, S., Ganguli, A., Bose, S. and Mukhopadhyay A. 2012. Biodiversity, traditional practices and sustainability issues of East Kolkata Wetlands: A significance Ramsar site of West Bengal, (India). Res. Rev. Biosci., 6(11): 340-347.

Bird, M. S., Mlambo, M. C., Wasserman, R. J. Dalu, T. Holland, A. J., Day, J. A., Villet, M. H., Bilton, D. T., Barber-James, H. M. and Brendonck, L. 2019. Deeper knowledge of shallow waters: Reviewing the invertebrate fauna of southern African temporary wetlands. Hydrobiologia, 827: 89-121.

Bose, P. C. 1944. Calcutta sewage and fish culture. Proceed. Nat. Instit. Sci. India, 10(4): 443-454.

Boyd, C. 2016. What causes alkalinity changes in aquaculture waters? Global Seafood Alliance https://www.aquaculturealliance.org/advocate/what-causes-alkalinity-changes-in-aquaculture-waters/, accessed on June 15, 2022.

Breitholtz, M., Näslund, M., Stråe, D., Borg, H., Grabic, R. and Fick, J. 2012. An evaluation of free water surface wetlands as tertiary sewage water treatment of micro-pollutants. Ecotoxicology and environmental safety, 78: 63-71. https://doi.org/10.1016/j.ecoenv.2011.11.014.

Bunting, S. W., Pretty, J. and Edwards, P. 2010. Wastewater-fed aquaculture in the East Kolkata Wetlands, India: anachronism or archetype for resilient ecocultures? Revi. Aquacult., 2: 138-153. doi: 10.1111/j.1753-5131.2010.01031.x

Butler, E., Hung, Y. T., Ahmad, M. S. A., Yeh, R. Y. L., Liu, R. L. H. and Fu, Y. P. 2017. Oxidation pond for municipal wastewater treatment. Appl. Water Sci., 7(31): 31-51.

Census of India. 2011. https://www.census2011.co.in/census/city/215-kolkata.html, accessed on 26 July 2022.

Chen, Z. M., Chen, G. Q., Chen, B., Zhou, J. B., Yang, Z. F. and Zhou, Y. 2009. Net ecosystem services value of wetlands: environmental economic account. Commun Nonlinear Sci Numer Simul., 14: 2837-2843.

Cherry, J. A. 2011. Ecology of Wetland Ecosystems: Water, Substrate, and Life. Nat. Educ. Know., 3(16).

CPCB 1993. The Environment (Protection) Amendment Rules, 1993, Schedule VI. The Gazette of India, New Delhi.

CPCB 2017. The Environment (Protection) Amendment Rules, 2017. The Gazette of India, New Delhi.

CPCB 2021. Status of Sewage Treatment in India. The Gazette of India, New Delhi

Cui, S., Yu, T., Zhang, F., Fu, Q., Hough, R., An, L., Gao, S., Zhang, Z., Hu, P., Zhu, Q. and Pei Z. 2020. Understanding the risks from diffuse pollution on wetland ecosystems: the effectiveness of water quality classification schemes. Ecol. Eng., 155 Article 105929.

Dalu, T. Wasserman, R. J. and Dalu, M. T. B. 2017. Agricultural intensification and drought frequency increases may have landscape-level consequences for ephemeral ecosystems. Glob. Chang. Biol., 23: 983-985.

Davis, M. L. and Cornwell, D. A. 2008. Introduction to Environmental Engineering. Fourth edition. McGraw-Hill, New York.

Drainage Enquiry Committee. 1945. Report of the Committee to Enquire into the Drainage Condition of Calcutta and Adjoining Areas. Government of Bengal, Calcutta, India pp. 56-59.

EKWMA, 2021. East Kolkata Wetlands: Management Action Plan 2021-2026. East Kolkata Wetlands Management Authority and Wetlands. Department of Environment. Government of West Bengal. International South Asia. Report ID: EKW-2021-01.

Geber, U. and Björklund, J. 2002. The relationship between ecosystem services and purchased input in Swedish wastewater treatment systems: A case study. Ecol. Eng., 19: 97-117.

Ghosh, D. 2004. Kolkata: An Ecologically Subsidised City. Down to Earth magazine. https://www.downtoearth.org.in/coverage/economy/ecologically-subsidised-city-11722

Ghosh, D. 2005. Ecology and Traditional Wetland Practice: Lessons from Wastewater Utilisation in the East Kolkata Wetlands. Kolkata, India. Worldview.

Ghosh, D. and Sen, S. 1987. Ecological History of Calcutta's Wetland Conversion. Environmental Conservation, 14(3): 219-226.

Government of West Bengal. 1997. Baseline document for management action plan, East Calcutta Wetlands and Waste Recycling Region, Calcutta Metropolitan Water and Sanitation Authority, Kolkata.

Gude, V., Magbanua, B. and Truax, D. 2013. Natural treatment and onsite processes. Water Environment Research, 86. https://doi.org/10.2175/106143014X14031280667615.

Kadlec, R.H. and Wallace, S.D. 2009. Treatment Wetlands. Taylor and Francis Group, Boca Raton.

Kaoud, H. A. 1999. Aquaculture Hygiene. ISBN 977-17-6281-8.

KMC. 2022. Kolkata Municipal Corporation. https://www.kmcgov.in/KMCPortal/jsp/BasicStatistics.jsp, accessed on 27 July 2022.

Knight, R., Payne, V., Borer, R., Clarke, R. and Pries, J. 2000. Constructed wetlands for livestock wastewater management. Ecological Engineering, 15: 41-55. https://doi.org/10.1016/S0925-8574(99)00034-8.

Maiga, Y., Wethe, J., Denyigba. K. and Ouattara, A. S. 2009. The impact of pond depth and environmental conditions on sunlight inactivation of Escherichia coli and enterococci in wastewater in a warm climate. Can J Microbiol, 55: 1364-1374.

Mandal J., Ghosh N. and Mukhopadhyay A. 2019. Urban growth dynamics and changing land-Use land-cover of megacity Kolkata and its environs. J. Indians Soc. Remote Sens., 47: 1707-1725.

MoEFCC. 2017. The Gazette of India Extraordinary, Part II-Section 3(i). MoEFCC, New Delhi. https://cpcb.nic.in/uploads/Industry-Specific-Standards/Effluent/105-sewage_treatment_plants.pdf

Moreno, D., Pedrocchi, C., Comín, F. A., García, M. and Cabezas, A. 2007. Creating wetlands for the improvement of water quality and landscape restoration in semi-arid zones degraded by intensive agricultural use. Ecol Eng., 30: 103-111.

Mukherjee, S. 2018. An Indigenous Aquaculture Based Sewage Purification Process Versus the Conventional Sewage Treatment Plant A Case Study of the East Kolkata Wetlands West Bengal India. Doctoral Thesis. IIEST, Shibpur. https://shodhganga.inflibnet.ac.in/handle/10603/466365#

Nemery, J. 2019. Phosphorus and Eutrophication: Encyclopaedia of the Environmenthttps://www.encyclopedie-environnement.org/en/water/phosphorus-and-eutrophication/. Accessed on 5 December 022.

Nichols, D.S. 1983. The capacity of natural wetlands to remove nutrients from wastewater. Water Pollut. Contr. Fed., 55(5): 495-505. http://www.jstor.org/stable/25041910

Niti Aayog 2022. Urban Wastewater Scenario in India 2022. Published by the Niti Aayog and Atal, Innovation Mission. Available online: https://www.niti.gov.in/sites/default/files/2022-09/Waste-Water-A4_20092022.pdf

Parihar, S. M., Sarkar, S., Dutta, A., Sharma, S. and Dutta, T. 2013. Characterizing wetland dynamics: A post-classification change detection analysis of the East Kolkata Wetlands using open-source satellite data. Geo. Int., 28(3): 273-287.

Pescod, M. B. 1992. Wastewater Treatment and Use in Agriculture. FAO Irrigation and Drainage Paper 47. FAO, Rome, Italy

Prein, M. 1990. Wastewater-fed fish culture in Germany. In Edwards, P. and Pullin, R.S.V. (eds.) Wastewater-Fed Aquaculture. Calcutta, India. pp. 13-47.

Ramsar Convention 1971. Ramsar Convention on Wetlands on International Importance Especially as Waterflow Habitat. As amended by the Paris Protocol of 3.12.1982, certified copy, UNESCO.

Ray Chaudhuri, S. and Thakur, A.R. 2006. Microbial genetics mapping of East Kolkata Wetland. Curr. Sci., 2: 212-217.

Sarkar, S., Ghosh, P., Sil, A.K. and Saha, T. 2014. Suspended particulate matter dynamics act as a driving force for a single-pond sewage stabilization system. Ecol. Eng., 69: 206-212.

Sarkar, S., Tribedi, P., Das Gupta, A., Saha, T. and Sil, A. K. 2017. Microbial functional diversity decreases with sewage purification in stabilization ponds. Waste Biomass Valor., 8(2): 417-423. DOI 10.1007/s12649-016-9571-8

Sarkar, S., Tribedi, P., Ghosh, P., Saha, T. and Sil, A.K. 2016. Sequential changes of microbial community composition during biological wastewater treatment in single unit waste stabilization system. Waste Biomass Valor., 7(3): 483-493. DOI 10.1007/s12649-015-9471-3

Sawyer, C. N. and McCarty, P. L. 1978. Chemistry for Environmental Engineering. Third Edition. McGraw-Hill Book Company, NY.

Sinton, L., Hall, C. and Braithwaite, R. 2007. Sunlight inactivation of *Campylobacter jejuni* and *Salmonella enterica*, compared with Escherichia coli, in seawater and river water. J Water Health, 5: 357-365.

Stainbridge, H. H. 1976. History of Sewage Treatment in Britain: Land Treatment. Institute of Water Pollution Control, Maidstone.

Tiley, E., Ulrich, L., Luthi, C. Reymond, P. and Zurbrugg, C. 2014. Compendium of Sanitation Systems and Technologies. Second edition. Swiss Federal Institute of Aquatic Science and Technology (Eawag). Dübendorf, Switzerland.

United States Environmental Protection Agency (USEPA). 2011. Principles of Design and Operations of Wastewater Treatment Pond Systems for Plant Operators, Engineers, and Managers. USEPA, Office of Research and Development, Cincinnati.

UN-Water. 2012. UN-water Global Annual Assessment of Sanitation and Drinking Water (GlAAS) 2012 report: the challenge of extending and sustaining service. Switzerland: World Health Organisation.

Varon, M.P. and Mara, D. 2004. Waste Stabilization ponds. Universidad del Valle, Instituto Cinara. Cali, Colombia and Duncan Mara School of Civil Engineering, University of Leeds. Leeds, UK. IRC, International Water and Sanitation Centre, Netherlands.

Von Sperling, M. 2007. Wastewater Characteristics, Treatment, and Disposal. IWA Publishing, London, UK.

Vymazal, J. 2010. Constructed wetlands for wastewater treatment. Water, 2(3): 530-549. https://doi.org/10.3390/w2030530.

World Water Assessment Programme (WWAP). 2017. Wastewater: The Untapped Resource. The United Nations World Water Development Report 2017. UNESCO, Paris.

Wurts, W. A. and Durborow, R. M. 1992. Interactions of pH, Carbon Dioxide, Alkalinity, and Hardness in Fish Ponds. Publication No. 464. Southern Regional Aquaculture Center, Stoneville, MS.

## ORCID DETAILS OF THE AUTHORS

I. Khan: https://orcid.org/0000-0001-8486-4591
D. Das Gupta: https://orcid.org/0009-0004-0413-5719
A. Gupta: https://orcid.org/0000-0002-5557-2423

Nature Environment and Pollution Technology
An International Quarterly Scientific Journal

p-ISSN: 0972-6268
(Print copies up to 2016)
e-ISSN: 2395-3454

Vol. 23 | No. 3 | pp. 1817-1827 | 2024

Original Research Paper

https://doi.org/10.46488/NEPT.2024.v23i03.054

Open Access Journal

# Effects of Carbon Dioxide and Nitrogen Oxides on Climate Change in Afghanistan

**Mairaj Khan**
Faculty of Curative Medicine, Ahmad Shah Abdali Institute of Higher Education, Khost, Afghanistan
†Corresponding author: Mairaj Khan; mairajszu@gmail.com

**Nat. Env. & Poll. Tech.**
**Website: www.neptjournal.com**

*Received:* 18-01-2024
*Revised:* 26-02-2024
*Accepted:* 10-03-2024

**Key Words:**
Climate change
Carbon dioxide
Nitrogen oxides
Greenhouse effect
Afghanistan

## ABSTRACT

Climate change is a global threat to the environment and human health. Two of the main greenhouse gases that cause the greenhouse effect and raise global temperatures are carbon dioxide and nitrogen oxides. In this review paper, we investigated the effects of carbon dioxide and nitrogen oxides on climate change and the effects of climate change on Afghanistan. We found that high concentrations of carbon dioxide, which is now $CO_2$ levels, have increased by 50% than before the Industrial Revolution, contributing to a rise in global temperature and precipitation. At the same time, Nitrous oxide is an important greenhouse gas, with 310-fold higher potential for global warming than $CO_2$ and leads to the depletion of stratospheric Ozone and other Nitrogen oxides, has a significant impact on plant health, including effects on chlorophyll levels, oxidative stress, and antioxidant responses. Afghanistan's climate change is predicted to increase the country's prevalence of illnesses linked to dust storms and poor air quality, especially in Kabul, the nation's capital. In addition, air pollution in Kabul is also likely to increase as a result of climate change. The alarming impacts of air pollution, with more than 3,000 deaths attributed to air pollution annually. Additionally, at least 700,000 individuals in Kabul have experienced various respiratory diseases. Due to climate change, Afghanistan's total glacier area has shrunk by 13.8%. In 2023, Afghanistan experienced early snow melt and below-average precipitation, causing second-season and irrigated crops to have less access to water. Reducing emissions and coping with the changing climate are essential steps towards tackling the complex issues these gases present and their wider effects on the environment and human health.

## INTRODUCTION

The change in temperature, rainfall, wind, and other elements with time is known as climate change (MacCracken 2019). Many gases pass the incoming sunlight through them and heat the land and oceans. This heat is released by the Earth in the Infrared region of radiation to space. These gases absorb the Infrared radiation and do not allow the infrared radiation to pass to space and radiate it back to the Earth, and the temperature of the Earth rises. This effect is called the Greenhouse effect (Doll et al. 2011). The Earth is heated by the greenhouse effect, which causes it to be warmer than it would be if sunlight were straight overhead. The proof for the greenhouse effect is the 33°C difference between the actual average temperature of 14°C and the effective temperature with sunlight, which is -19°C. The major gases that impart the Greenhouse effect are $CO_2$, $N_2O$, $CH_4$, Water vapors, and CFC. These gases have more than two atoms, joined together loosely, and can vibrate by absorbing the heat (Kweku et al. 2018). The Greenhouse Effect is shown in Fig. 1.

Earth's average temperature has increased by 1°C since 1900. Since 1850, the previous four decades have continuously been warmer than any other, despite trend variations, as shown in the instrumental record Fig. 2. Other evidence like reduction in Arctic sea content, elevation in ocean heat content, and evidence from the natural world show strong proof of the Earth's warming (National Academy of Sciences 2020).

Since about 1750, human activity has increased the concentration of greenhouse gases. Both the atmospheric $CO_2$ and $N_2O$ concentrations in 2019 were higher than they had been in at least 2 million years and 800,000 years, respectively. Climate extremes such as heat waves, intense precipitation, droughts, and tropical cyclones are being impacted by climate change brought on by human activity. Human health is impacted by climate change in both direct and indirect ways. Direct effects include injury and even death from hurricanes and heat waves. In contrast, indirect effects include changes in temperature and precipitation that can disrupt the life cycles of insects that spread the West Nile virus and Lyme disease, resulting in a variety of new outbreaks. Climate change frequently coexists with additional health stressors such as poverty, social hardship, and linguistic impairment, causing heightened susceptibility

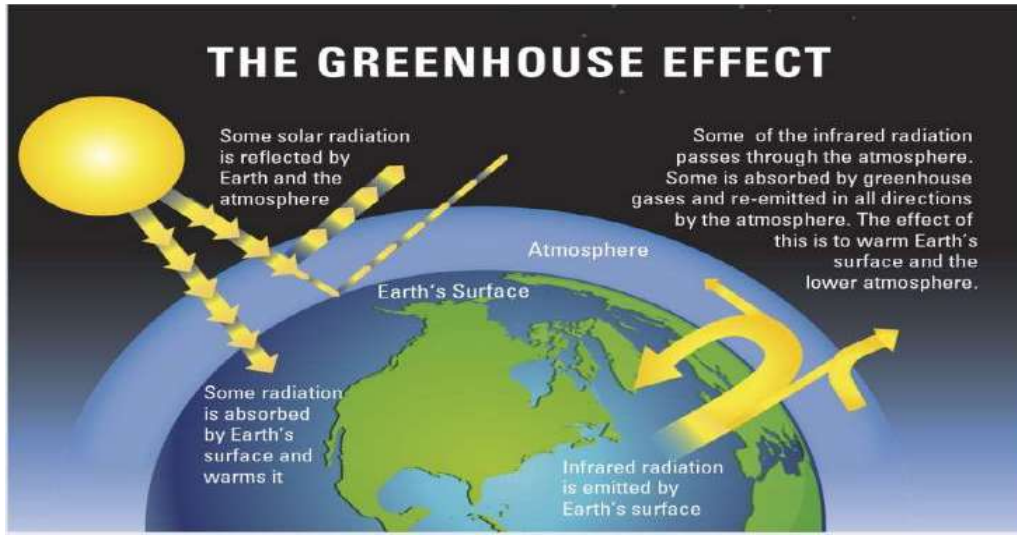


Fig. 1: The greenhouse effect.

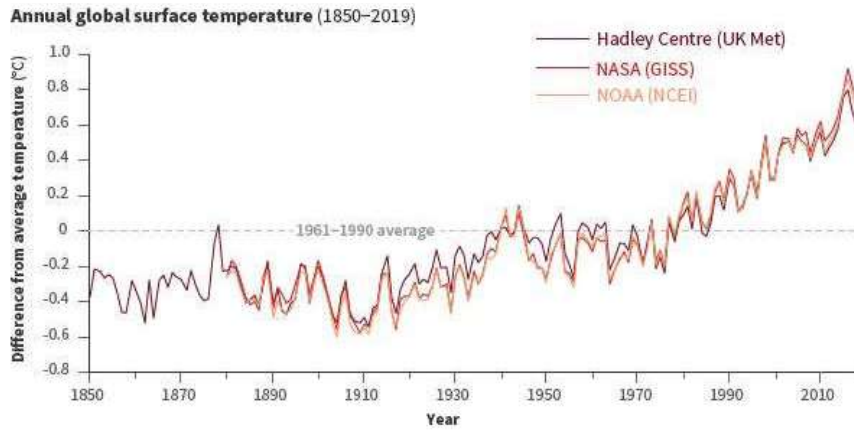


Fig. 2: Annual global surface temperature (1850-2019).

(McMichael & Woodruff 2005). The consequences of climate change on water resources have been well-documented, and it is expected that these resources will be seriously threatened in the future on a regional and worldwide scale. (Shokory et al. 2023).

The expected effects of climate change in Afghanistan are concerning. Raising temperatures are predicted to have a major effect on the country's ecosystems, agriculture, economy, biodiversity, and food security. Even with limited greenhouse gas emissions, Afghanistan will face significant challenges in adapting to these changes. However, if GHG emissions are not curbed, the effects of global warming are probably going to be considerably more extreme and unpredictable, exacerbating the existing adaptation deficit in the country areas (Aich & Khoshbeen 2016). According to the World Health Organization (WHO), in Afghanistan, 26% of total mortality is attributed to environmental risks and pollution (Masood et al. 2022). Based on the INFORM 2019 Index, Afghanistan is ranked as the fifth most at-risk country globally, meaning it faces the highest levels of natural disaster hazards. (Climate Risk Country Profile Afghanistan 2021). Climate models suggest that Afghanistan will experience an array of novel and amplified climate-related risks. In Afghanistan, drought is the most likely negative effect of climate change. By 2030, drought will no longer be considered an isolated or cyclical occurrence but rather the standard. (Savage et al. 2009).

In this review paper, we investigated the effects of $CO_2$ and nitrogen oxides on climate change and the effects of climate change on Afghanistan. We reviewed most of the reports, research articles, authenticated web pages, and books section for this purpose.

## EFFECTS OF CARBON DIOXIDE ON CLIMATE CHANGE

Without $CO_2$, the Earth's natural greenhouse effect would be insufficient to keep the global average temperature above freezing. As individuals release more $CO_2$ into the atmosphere, the global temperature rises (Lindsey 2023). For the previous 800,000 years up until the 20th century, the atmospheric $CO_2$ content varied between 170 and 300 ppm (National Academy of Sciences 2020). According to the NOAA Monitoring Lab annual report, the global average $CO_2$ was 417.06 ppm in 2022, setting a new high record. Compared to before the Industrial Revolution, atmospheric $CO_2$ is currently 50% greater (Lindsey 2023). $CO_2$ is the largest contributor to global warming, emitted from various sources to the environment like, the combustion of fuels, transportation, and industrialization processes (Thiruvenkatachari et al. 2009). The major sources of $CO_2$ have been given in Table 1 (Yoro & Daramola 2020).

To keep atmospheric $CO_2$ levels in equilibrium, the Earth's natural mechanisms for absorbing and storing $CO_2$ are crucial. These procedures, including photosynthesis in plants and absorption by the ocean, have been a component of the carbon cycle for millions of years, which regulates $CO_2$ levels. However, human activities like Deforestation and the burning of fossil fuels have disrupted these processes, resulting in a persistent increase in atmospheric $CO_2$ concentration. This increase in $CO_2$ has led to global warming and climate change (Nunes 2023). For the next 1000 years, climate change caused by a rise in $CO_2$ concentration is largely irreversible (Solomon et al. 2009). $CO_2$ acts like a blanket in the air, trapping the heat, warming up the Earth, and preventing the Earth from cooling (Ali et al. 2020). Even if global average temperatures stabilize at some point, rising $CO_2$ concentrations have a direct impact on the climate system and may have an ongoing impact on Earth (Harvey 2018). Destructive storms intensify and increase in frequency throughout various regions as temperatures rise. Due rise in temperature, more water evaporates, which exacerbates heavy rainfall and flooding. By warming the ocean, the extent and frequency of the tropical storm are also affected. Warm water at the ocean's surface provides fuel to hurricanes, typhoons, and cyclones (UN n.d.). Many researchers have shown the inhibitory effects of different heat stresses in crop plants. It is an essential environmental pressure that restrains plant growth and development and disturbs its several metabolic and physiological activities, hence rendering yield production at the global level (Javadmohammadi et al. 2013). Due to human activities, 30% to 40% of $CO_2$ emitted into the atmosphere dissolves into the oceans (Millero 1995), where $CO_2$ reacts with seawater and has increased its acidity to 0.1 pH since the pre-industrial era. The terrestrial biosphere absorbs about 20% of the $CO_2$ emissions caused by human activity. Here, it combines with soil moisture to modify soil acidity, meaning that $CO_2$ can make the air, soil, and ocean more acidic (Mitchell et al. 2010). Numerous ocean species are already being impacted by ocean acidification, particularly those that combine calcium and carbonates from seawater to form hard shells and skeletons.

Ocean acidification reduces the amount of carbonate ions available for calcifying organisms to form their shells, skeletons, and other calcium carbonate structures by increasing the carbonate ions' link with excess hydrogen (NOAA 2020). The lower pH also affects the senses of reef fishes and reduces their survival, and might target most of the commercial fishes that produce seafood for humans (Branch et al. 2013). The start and end of growing seasons have changed due to warmer temperatures and shifting precipitation patterns. There is a high degree of confidence that this has decreased regional crop yield, freshwater availability, and biodiversity. There is a medium degree of confidence that the increase in atmospheric $CO_2$ has contributed to the observed increase in plant development and woody plant cover in grasslands and savannahs (Shukla et al. 2019). However, studies have found that this accelerated

Table 1: Major sources of $CO_2$.

| Anthropogenic Sources | | Non anthropogenic Sources | |
|---|---|---|---|
| Sources | $CO_2$ emission [Billion Mt] | Sources | $CO_2$ emission [Billion Mt] |
| Fossil fuel combustion engines | 392 | Plant, animal, and human respiration | 7 |
| Cement Production Plants | 113 | Ocean-atmosphere exchange | 7 |
| Power generation (coal-fired power plants) | 279 | Soil respiration and decomposition | 1.54 |
| Transportation | 191 | Volcanic eruptions | 0.15 |
| Industrial manufacturing | 178 | | |
| Land use changes | 13 | | |

Adapted from Yoro & Daramola (2020)

growth under elevated $CO_2$ can lead to a dilution of essential nutrients in crops. When plants grow faster, they allocate more carbon to structural components like stems and leaves rather than to nutrients such as protein, vitamins, and minerals. As a result, the concentration of these vital nutrients in staple crops can decrease. For example, research has shown that elevated $CO_2$ levels can reduce the protein content of wheat and barley, making them less nutritious.

Similarly, increased $CO_2$ can lower the iron and zinc content in rice, which are important micronutrients for human health. Potatoes, another staple crop, may experience reduced vitamin C content when exposed to higher $CO_2$ concentrations (Ebi & Ziska 2018). Rising atmospheric $CO_2$ levels, rising temperatures, and shifting precipitation patterns cause significant effects on agriculture and agricultural insect pests. Climate change has the potential to increase the risk of invasion by migratory pests, increase the incidence of insect-transmitted plant diseases, increase the number of generations, increase the geographic distribution, increase survival during overwintering, change plant-pest synchrony, and alter interspecific interaction. It can also decrease the efficacy of biological control of agricultural pests. As a result, there is a significant chance that the crop will suffer financial losses, which poses a threat to global food security for humans (Skendžić et al. 2021). $CO_2$ also causes acidic rain, which physically harms the trees and builds the environment (Ali et al. 2020).

Along the glacial to interglacial cycles when humans first appeared, $CO_2$ concentrations in the atmosphere ranged between 135 and 280 ppm. Human blood's pH during this time narrowly varied between 7.35 and 7.45 for arterial and venous blood, respectively. Humans are now exposed to atmospheric $CO_2$ concentrations that have never before been experienced by mammals or humans due to the recent increase in $CO_2$ concentration, which is currently over 400 ppm. Similar to the pH drop in the ocean that happened during the Industrial Revolution, this suggests a minor drop in blood pH below the 7.35-7.45 typical performance range for the human proteome. (Duarte et al. 2020). High $CO_2$ concentrations may have negative effects on human health that are more frequent and persistent due to higher indoor air concentrations and longer indoor exposure times (Jacobson et al. 2019). There were noticeable immediate physiological alterations in the circulatory and autonomic systems with exposure to $CO_2$ at concentrations between 500 and 5000 ppm. (Azuma et al. 2018). People's decreased lung gas transport in response to $CO_2$ retention is strongly suggested to be the cause of the decline in cognitive function. (Shriram et al. 2019). It is unclear if $CO_2$ by itself is a pollutant and whether it can be harmful to health at low concentrations ($\leq$ 5000 ppm). However, according to current criteria, $CO_2$ levels can be used to measure the quality of indoor air; values below 1000 ppm are deemed good, while levels above 1500 ppm are deemed poor. High $CO_2$ levels can cause discomfort and reduced cognitive function and can also indicate poor ventilation and the accumulation of other pollutants. Therefore, it is important to monitor and control $CO_2$ levels to ensure healthy indoor environments (Lowther et al. 2021).

## EFFECTS OF NITROGEN OXIDES ON CLIMATE CHANGE

Nitrogen, a chemical element, can exist as a diatomic molecular ($N_2$) nitrogen gas, which is mostly inert and makes up 80% of the air we breathe. However, as a single atom, nitrogen can be reactive and have several valence states from +1 to +5, resulting in the formation of multiple oxides of nitrogen ( $NO_x$ ), including $N_2O$, NO, $N_2O_2$, $N_2O_3$, $NO_2$, $N_2O_4$, and $N_2O_5$ (Cox 1999). Climate, air quality, and atmospheric chemistry are all significantly influenced by Nitrogen oxides. Both human activities and natural processes emit them into the atmosphere. Naturally occurring wildfires, microbial activity in soil, and lightning are among the natural sources of Nitrogen oxide emissions. Fossil fuel combustion, home heating, cooking, industry, and the energy sector are the primary producers of $NO_x$. (Lange et al. 2022). In the air, the most abundant nitrogen oxides are $N_2O$, NO, and $NO_2$ (Cox 1999).

It is considered that $NO_x$ is an indirect greenhouse gas, while $N_2O$ is a direct greenhouse gas (Lasek & Lajnert 2022). Nitrous oxide is a significant greenhouse gas with a global warming potential 310 times larger than $CO_2$ (Aryal et al. 2022). The use of nitrogen fertilizers and manures in agricultural soils has raised the concentration of $N_2O$ over the past century, and these activities are the primary human sources of $N_2O$ (Skiba & Rees 2014). Over time, the amount of $N_2O$ in the atmosphere keeps rising. Furthermore, it has increased annually during the past decade, averaging 1.1 $ppb.yr^{-1}$. The $N_2O$ values for 2020, 2021, and 2022 represent some of the fastest annual rises yet noted. Between 1990 and now, $N_2O$ has increased radiative forcing by 0.086 to 0.81 $Watts.m^{-2}$, or almost 7.5% (NOAA 2022). In the troposphere, $N_2O$ is an inert gas with no substantial sinks near the Earth's surface. However, $N_2O$ is carried into the stratosphere where it is primarily broken down by short-wavelength photolysis to produce atomic Oxygen (O) and molecular Nitrogen ($N_2$). The primary source of nitrogen oxides in the stratosphere is the dissociation of $N_2O$ to a lesser extent into nitric oxide (NO), yet the proportion is less than 10%. (Müller 2021). In the stratosphere, NO reacts with Ozone ($O_3$) and forms

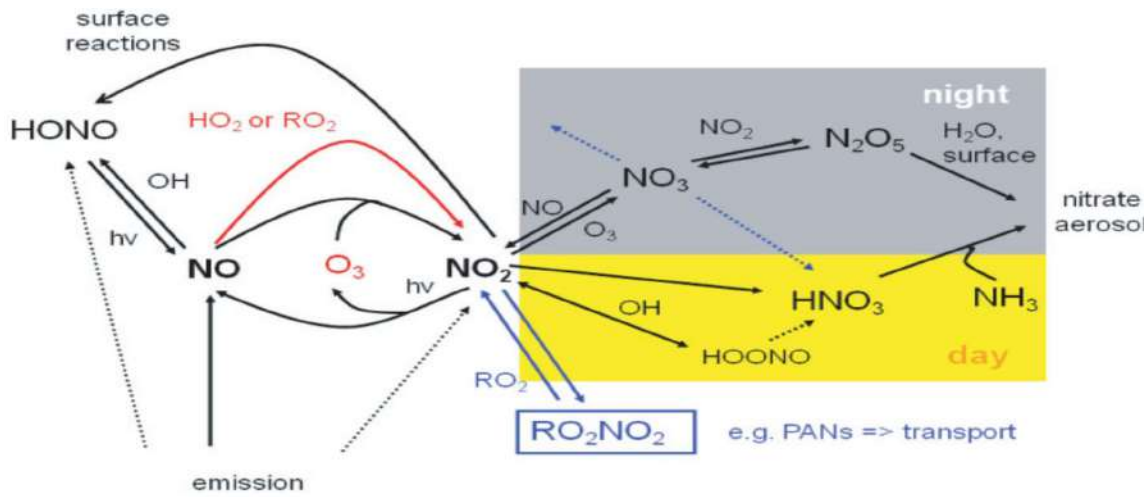


Fig. 3: Chemistry of $NO_x$ in the troposphere (Richter 2009).

nitrogen dioxide ($NO_2$) and ($O_2$). $NO_2$ is photolyzed and forms NO and an oxygen atom (O) again (Lange et al. 2022). A greater concentration of $N_2O$ leads to an increased concentration of $NO_x$, which destroys the stratospheric ozone layer. Due to this ozone depletion, UV radiation enhances and photolyzed more $N_2O$ (Ehhalt & Prather 2001). The Ozone layer acts as a natural filter, collecting UV radiation from the Sun and keeping it from reaching the surface of the Earth. However, alterations to the ozone layer have led to a rise in the percentage of UV-B radiation that reaches the surface. This increase can have negative effects on biological life and processes, as well as on non-living things like building materials made of polymers. (Umar & Tasduq 2022). Additionally, the release of nitrogen oxides into the atmosphere leads to a rise in tropospheric Ozone ($O_3$) and Particulate Matter (PM). The emissions of $NO_x$ play a significant influence in the generation of ($O_3$), one of the most important air pollutants impacting human health. Since 1900 the increase in $O_3$ is 60% due to an increase emission of $NO_x$ (de Vries 2021). PM precursors include $NO_x$, $NH_3$, and $SO_2$ pollutants that have a direct impact on human health and are partially converted into pollutant particles in the atmosphere by photochemical processes (Lovarelli et al. 2020).

Nitric acid ($HNO_3$) is produced when $NO_2$ combines with hydroxyl ions ($OH^-$); aerosols and droplets can readily absorb this compound. $HNO_3$ is a strong acid and can readily dissociate in water to release $H^+$ ions, contributing to the acidity of aerosols and cloud droplets. Through this pathway, these acidic particles are deposited on land or water surfaces. They can disrupt the pH balance and harm sensitive ecosystems through the formation of acid rain. The reduction in $SO_2$ emissions has led to a decrease in sulfate aerosols, which were previously the dominant contributor to acid rain, so the relative importance of $HNO_3$ has increased in most industrialized countries. A simplified picture of the chemistry of $NO_x$ in the troposphere is shown in Fig. 3.

Plant species diversity often begins to decline when nitrogen deposition levels rise over 5-10 $kgN.ha^{-1}.yr^{-1}$. The dominance of nitrophilic species, which outcompete species adapted to nitrogen deprivation in oligotrophic settings, is blamed for this decline. Indirect soil-mediated effects, such as soil enrichment, eutrophication, and acidification, primarily cause the loss of plant species diversity due to increased nitrogen inputs. These effects can alter soil microbial communities and nutrient cycling processes (Environmental Protection Agency (EPA) 2018). There are many ways in which nitrogen oxides ($NO_x$) can affect plant health, both directly and indirectly. NO and $NO_2$ are phytotoxins that can cause direct damage to plant growth and yield reduction. Indirectly, NOx may aid in the production of Particulate Matter (PM) aerosols and Ozone ($O_3$), both of which may be harmful to crops. $NO_x$ is a crucial precursor to the generation of Ozone in the troposphere. Elevated quantities of $O_3$ can harm plant tissues, hinder photosynthesis, and lower agricultural output. In addition, $N_{Ox}$ can take part in atmospheric reactions that result in the production of (PM) aerosols. Ammonium nitrate aerosols ($NH_4NO_3$) and ammonium sulfate aerosol [$(NH_4)_2SO_4$] can be more concentrated when $NO_x$ is present in the presence of ammonia, which is frequently found in agricultural regions due to the usage of nitrogenous fertilizers. By reflecting and dispersing incoming sunlight, these aerosols can lower the quantity of photosynthetically active radiation that reaches crops, thus hindering photosynthesis (Lobell et

al. 2022). Exposure to nitrogen dioxide ($NO_2$) can indeed have significant impacts on plant health, including effects on chlorophyll levels, oxidative stress, and antioxidant responses. $NO_2$ exposure can also induce oxidative stress in plants, leading to lipid peroxidation and protein dissolution. In response to $NO_2$-induced oxidative stress, plants often increase the activity of enzymes such as peroxidase (POD), which helps to detoxify reactive oxygen species. Despite the negative impacts of $NO_2$ exposure, plants can recover and resume normal growth after the removal of the pollutant. This recovery process can involve the repair of damaged cellular components and the restoration of normal physiological functions (Sheng & Zhu 2019).

The 1-Hour Standard and the Annual Standard are the two main standards for Nitrogen oxides. The 2010 establishment of the 1-Hour Standard established a limit of 100 parts per billion (ppb). Its foundation is the 98th percentile of the daily maximum 1-hour $NO_2$ concentrations' annual distribution. To determine compliance with this requirement, the maximum per day's 1-hour $NO_2$ values are taken as an average over three years. The Annual Standard was first established in 1971 and is now maintained at 53 parts per billion. It is based on the average annual concentrations of $NO_2$. Compliance with this standard is determined by calculating the average $NO_2$ concentration over a full year (Environmental Protection Agency (EPA) 2018). The majority of the public's exposure to nitrogen oxides comes from breathing in air. Individuals who live close to sources of combustion, such as power plants powered by coal, or in places with a lot of traffic may be more exposed to nitrogen oxides. Within homes where wood is burned extensively or kerosene heaters and gas stoves are used, nitrogen oxide levels tend to be higher compared to homes without these appliances.

Additionally, tobacco smoke contains nitric oxide and nitrogen dioxide. Thus, individuals who smoke or come into contact with secondhand smoke could potentially be exposed to nitrogen oxides (ATSD 2014). Depending on the concentration and length of exposure, nitrogen dioxide ($NO_2$) exposure can have both short-term and long-term health impacts. Prolonged exposure to low $NO_2$ concentrations can aggravate respiratory disorders, including asthma and chronic obstructive lung disease, and cause respiratory problems like sneezing, coughing, and shortness of breath (COPD). Severe exposure to elevated $NO_2$ levels, which is rare but can occur during industrial events or in heavily polluted areas, can cause severe damage to the respiratory system, leading to respiratory distress, lung inflammation, and even respiratory failure. Even individuals without pre-existing conditions can experience respiratory symptoms and decreased lung efficiency in the presence of elevated $NO_2$ levels. Even at low doses, those with respiratory disorders are more susceptible to the effects of $NO_2$. It is important to reduce $NO_2$ emissions and limit exposure to protect public health, especially for those with respiratory conditions. This can be achieved through regulations, emission control technologies, and sustainable practices in transportation and industry (Javadmohammadi et al. 2013).

## Effects of Climate Change on Afghanistan

Afghanistan is a mountainous nation that lies in the subtropical zone and stretches from 29°21′ to 38°30′N latitude and from 60°31′ to 75°E longitude. Its climate is primarily dry and semi-arid, with traits of steppe, highlands, and deserts with regard to precipitation and temperature patterns (Shokory et al. 2023). With a population of over 4.6 million people, Kabul stands as the most populous city in Afghanistan. The city has experienced rapid urbanization, making it the fifth fastest-growing city globally. At present, its population is growing at a pace of 2.71% annually, and by 2035, it is expected to surpass 6.7 million (Masood et al. 2022). While conflict-related deaths in Afghanistan have significantly decreased in 2022, the country still faces challenges due to climate and environmental stressors. These stressors not only hinder development but also have a negative impact on community resilience and worsen social divisions (Jiayi & Seyuba 2023).

Table 2: Afghanistan's $CO_2$ emissions from 2015 to 2019.

| Sector | 2015 $CO_2$ emission [Mt] | 2016 $CO_2$ emission [Mt] | 2017 $CO_2$ emission [Mt] | 2018 $CO_2$ emission [Mt] | 2019 $CO_2$ emission [Mt] |
|---|---|---|---|---|---|
| Agriculture | 15.53682 | 15.2975 | 15.20713 | 14.83939 | 14.48123 |
| Energy | 12.19827 | 11.41276 | 12.18425 | 13.13404 | 13.43123 |
| Waste | 3.28 | 3.365385 | 3.448441 | 3.531498 | 3.614555 |
| Industrial Processes | 0.60166 | 0.789337 | 0.910724 | 1.07556 | 1.209746 |
| Land-Use Change and Forestry | - 0.24622 | 0.154657 | 0.154657 | 0.154657 | 0.154657 |
| Total | 31.3637 | 31.01964 | 31.90521 | 27.84 | 32.89143 |

Note: Adapted from Climate Watch Historical GHG Emissions (2022).

In Afghanistan and other countries, the fundamental cause of climate change is the release of greenhouse gases, especially $CO_2$. Table 2 presents the yearly $CO_2$ emissions in Afghanistan and the associated sectors from 2015 to 2019.

Table 2 gives the $CO_2$ emissions in a million tons in Afghanistan from 2015 to 2019, attributing these emissions to sectors such as agriculture, energy, waste, industrial processes, changing land uses, and forestry. In 2019, Afghanistan's emissions totaled 28.79 million tons of $CO_2$ equivalent, representing only 0.06% of global emissions and ranking the country as the 116th largest producer of greenhouse gases worldwide (Zaki & Lederer 2023). In Afghanistan, climate change is primarily characterized by increasing temperatures. The country has observed a significant temperature rise, surpassing the global average, with an increase of 1.8℃ between 1951 and 2010. This upward trend in temperatures is expected to continue from 2006 to 2050, with a projected rise of 1.7- 2.3℃. Subsequently, temperatures are anticipated to increase further, ranging from 2.7-6.4 until 2099 across the entire country (Přívara & Přívarová 2019). Afghanistan's water supplies have been impacted by climate change, especially in the Kabul River watershed. Due to the changing climate, there has been a noticeable impact on the glaciers and snowmelt that feed the river, increasing their melting trend. Additionally, this trend has been further supported by a change in the seasonal monsoons in the river basin (Qutbudin et al. 2019). In the twenty-five years between 1990 and 2015, Afghanistan's total glacier area shrank by 13.8%, and the country's projected ice reserves shrank by 14.4%. Moreover, there have been 3.1% fewer glaciers in the 25 years between 1990 and 2015 and 1.7% fewer between 1990 and 2010. Most likely, the consequences of climate change are to blame for this decrease in glacier area and ice storage. The reduction and retreat of glaciers, which act as vital freshwater reservoirs, will negatively affect the future availability of freshwater downstream and the coordinated management of water resources (Maharjan et al. 2021). The majority of models indicate a notable reduction in precipitation in the spring, which is essential for agricultural production that depends on rainfall. These anticipated precipitation declines are between around -30% and almost -40% in the relevant East, North, and Central Highlands regions relative to historical levels. This decrease in precipitation poses a significant challenge for agricultural activities in these areas (Aich & Khoshbeen 2016). Over two-thirds of Afghanistan's provinces were directly impacted by the country's catastrophic drought in 2018, which affected about 10.5 million people. 2018's drought emphasizes how urgently the nation must solve issues related to food security, climate change, and development that is sustainable (FAO 2020). In 2022, Afghanistan's agricultural sector, which contributes around 36 percent to the GDP, experienced a contraction of 6.6 percent. This decline was primarily caused by widespread drought conditions and below-average precipitation, leading to a significant reduction in the wheat crop. Moreover, certain regions of the country faced inadequate rainfall, negatively impacting the livelihoods of pastoralists who were already struggling due to limited pasture availability in the previous years (Muhammad et al. 2023). In 2023, Afghanistan experienced early snow melt and below-average precipitation, which means that there is now less water available for irrigated and second-season crops. As a consequence, the prospects for the second-season harvest are expected to be below normal. Rice and maize are particularly major second-season crops in the country's northern and eastern areas. Additionally, fruits like melons and oilseed crops are also cultivated during this season, primarily in the Northern provinces. Many farmers extensively rely on deep boreholes to obtain water for farming crops like rice, sesame, and maize in order to deal with the restricted supply of water. The recurrent drought in Kabul Province is causing a severe impact on surface water sources and groundwater levels. This is evidenced by the fact that almost half of the boreholes assessed in the province are dry, and the remaining ones are operating at significantly reduced efficiency (OCHA 2023). It is anticipated that the lower yields from the 2022 crops and the shortages in 2023 will significantly affect food security in 2024. As of 2023, an estimated four million individuals who are considered vulnerable are suffering from acute malnutrition. This comprises about 2.3 million children with moderate acute malnutrition (MAM), 840,000 pregnant and lactating women (PLW) with acute malnutrition, and about 875,000 children with severe acute malnutrition (SAM) (UNICEF 2023). Afghanistan, a nation plagued by prolonged conflict, is also susceptible to natural calamities. Earthquakes, droughts, floods, and heavy snowfall have a significant influence on many Afghans' lives. In 2005 and 2006, severe flooding left thousands homeless and destroyed agricultural land, livestock, and infrastructure (Hagen 2009). In Afghanistan, there are two primary types of floods: those resulting from intense rainfall over a brief period, leading to river overflow and heavy surface runoff in surrounding areas, as well as those brought on by the swift melting of snow and ice in highland regions in the spring, which overflows downstream rivers and stream. Afghanistan saw severe flash flooding in its central, eastern, and southern regions in August 2022. Approximately 15,875 people were affected by the floods, which destroyed or damaged over 5,600 homes in provinces including Kunar, Laghman, Logar, Maidan Wardak, Nangarhar, Nuristan, Paktiya, Kandahar, Zabul, Uruzgan,

and Parwan (UNICEF 2022). Heavy rains continued in July 2023, resulting in flash flooding that harmed around 6,193 people across eight provinces in Afghanistan, including Kabul, Kunar, Laghaman, Maidan Wardak, Nangarhar, Nuristan, Parwan, and Zabul. This event tragically led to the loss of 40 lives, with 30 others sustaining injuries. Furthermore, the flooding caused damage to 551 houses and the destruction of 121 others (UNICEF 2023).

Afghanistan's impoverished population is especially susceptible to the effects of climate change. It is anticipated that climate change will make the problems with food security worse and have a big effect on people who depend on agriculture for their livelihoods. The adverse effects are likely to disproportionately affect women, children, and individuals engaged in subsistence agriculture or pastoralism. Changes in the climate have the potential to drive a sizable fraction of the Afghan people into poverty, as a sizable portion currently lives barely over the poverty line (Savage et al. 2009). Poverty and food insecurity are widespread issues in Afghanistan, particularly in rural areas. Events like the 2011 drought, which caused over 100,000 children to go malnourished, and the 2018 and 2019 drought, which forced over 400,000 people to relocate, demonstrate the dangers that climate change poses. These risks also have a big impact on the economy. For example, the 2018 drought reduced wheat production by more than 60%, necessitating a deficit of $550 million to feed the country's livestock. The drought crisis in Afghanistan in 2019 was aggravated by severe floods, exacerbating the humanitarian situation. The flooding resulted in the displacement of 42,000 people and tragically led to at least 63 deaths. There is growing evidence to suggest that human-induced climate change has made natural hazards, such as droughts and floods, more likely and more intense in Afghanistan (Climate Risk Country Profile Afghanistan 2021). The complex humanitarian crisis in Afghanistan is becoming more severe due to a combination of factors, including the contraction of the economy, environmental pressures, and climate change. Nearly three-quarters of the predicted total population, or around 28.3 million people, are expected to need direct humanitarian aid in 2023. According to a May 2022 food security assessment, by the end of 2022, 47% of the population will be experiencing emergency or crisis shortages of food (Jiayi & Seyuba 2023).

Evidence from various regions globally indicates that climate change and global warming are having negative impacts on essential elements of life, including water, air, food, and human habitats, leading to health security risks. Malnutrition, diarrhea, and malaria are particularly sensitive to climate change and are currently significant contributors to the global burden of disease. Estimates suggest that malnutrition causes 3.5 million deaths annually, while diarrhea and malaria cause 1.8 million and 0.9 million deaths, respectively (World Health Organization 2008). In developing nations, the issue is exacerbated by rapid population growth, unregulated urban expansion, and the growth of industrialization. This results in inadequate air quality, particularly in countries with social inequality and a lack of information regarding long-term environmental management. People who depend on inexpensive fuels like wood or solid fuel for domestic needs due to financial constraints are at risk of breathing in tainted indoor air. It's important to note that almost three billion people worldwide depend on these sources of energy to meet their everyday heating and cooking needs (Manisalidis et al. 2020). Conditions brought on by climate change, such as more frequent droughts, intense rainfall, floods, and elevated temperatures, are influencing the environment and aiding in the development of vector-borne and water-borne illnesses. Children in Afghanistan are particularly vulnerable to the health risks associated with diarrheal disease; according to UNICEF estimates, in 2016, 7,300 deaths in this age range occurred in Afghanistan due to diarrheal disease, which makes up around 9% of all disease deaths in this group. The incidence of diseases linked to dust storms and air quality in Afghanistan is predicted to increase due to climate change. During an extended drought in the early 2000s, dusty storms were especially common around Lake Hamun on the Iran-Afghanistan border, and they were associated with a rise in hospital admissions for asthma and chronic obstructive pulmonary disease in that region. Usually, when the lake beds dry out, these dust storms happen. Consequently, because of the anticipated rise in the frequency of droughts in Afghanistan, climate change may make dusty storms more likely in this western border region in the ensuing decades. Moreover, the situation could worsen in the long run if the predicted decline in glacier mass in the Hindu Kush limits the amount of snowmelt that replenishes Lake Hamun (Climate Risk Country Profile Afghanistan 2021). In the near to medium future, there will be a heightened risk of malaria and dengue fever due to the anticipated rise in temperature and precipitation brought on by climate change. This will include an extended transmission season and the expansion of mosquito habitats into highland areas. Furthermore, temperature fluctuations due to climate change may increase the prevalence of neglected tropical diseases like Leishmaniasis. Eastern Afghanistan bears the highest burden of Malaria cases, but roughly 76% of the country's population is exposed to Malaria-causing mosquitoes. The increase in temperature resulting from climate change may lead to higher transmission of Malaria due to faster vector development (Aditi et al. 2021). The study discovered that

measles appeared in late spring, pneumonia occurred in the winter, and diarrhea and typhoid fever peaked in the summer. Acute viral hepatitis and meningitis, however, did not exhibit any discernible seasonal trends. While rates of pneumonia and diarrhea remained consistent over the years, the incidence of Typhoid fever, acute viral hepatitis, and meningitis declined. (Wagner et al. 2017). The results show that Afghanistan's incidence of diarrhea is positively correlated with both mean daily temperature and aridity. Specifically, the risk of diarrhea increased by 0.70% and 4.79% for every 1°C increase in the mean daily temperature and 0.01 units in the aridity index, respectively. In contrast, there was a negative correlation found for the average annual temperature, with a 3.7% reduction in risk for each degree Celsius that the average annual temperature increased. It was also observed that, except for the eastern region, where variations in climatic patterns and population density may be linked to high rates of diarrhea all year round, most districts showed comparable seasonal tendencies, with the frequency of diarrhea peaking in the summer. These findings highlight the important influence of climate on Afghanistan's diarrheal patterns (Anwar et al. 2019). Kabul's polluted air condition has certainly deteriorated dramatically over time. In autumn and winter, the World Health Organization's (WHO) recommended levels of sulfur dioxide ($SO_2$), Nitrogen dioxide ($NO_2$), and Particulate Matter ($PM_{2.5}$ and $PM_{10}$) are frequently exceeded. The average $PM_{2.5}$ concentration in Kabul was measured at 92.2 $\mu g.m^{-3}$ over 24 h, exceeding the World Health Organization's (WHO) recommended limit of 25 $\mu g.m^{-3}$ for the same duration. Additionally, the average $PM_{10}$ concentration in Kabul was recorded at 120.6 $\mu g.m^{-3}$ over 24 h, surpassing the WHO's recommended limit of 50 $\mu g.m^{-3}$ for the same duration. The average $NO_2$ concentration in Kabul was recorded at 305.4 $\mu g.m^{-3}$, which indeed exceeds the World Health Organization's (WHO) recommended limit of 200 $\mu g.m^{-3}$ for a 1-hour measurement. The average $SO_2$ concentration in Kabul was measured at 63.7 $\mu g.m^{-3}$ over a 24-hour period, which is indeed higher than the World Health Organization's (WHO) recommended limit of 20 $\mu g/m^3$ for the same duration (Mehrad 2020). One major concern in Afghanistan is the effect of air pollution on public health, especially in Kabul, the country's main city. The Ministry of Public Health's spokesperson claims that the effects of air pollution are alarming, with more than 3,000 deaths attributed to air pollution annually. Additionally, at least 700,000 individuals in Kabul have experienced various respiratory diseases, with this figure reflecting only those who sought treatment at government hospitals. It's important to note that many others may have sought treatment at other medical facilities, indicating that the actual number of people affected by respiratory issues due to air pollution could be even higher (Jahed & Fang 2023).

## CONCLUSION

In conclusion, the impact of carbon dioxide and nitrogen oxides on climate change is undeniable, with these gases contributing to rising global temperatures through the greenhouse effect. This has led to a range of consequences, including the melting of glaciers, rising sea levels, shifts in precipitation patterns, and disruptions to plant yields. Furthermore, the resulting air pollution from these gases has had detrimental effects on human health, potentially leading to various diseases. Afghanistan has experienced severe repercussions from climate change, including alterations in precipitation patterns, drought, food insecurity, floods, and a rise in serious human health issues. In Afghanistan and elsewhere, it is essential to address the underlying causes of these environmental issues and put policies in place to lessen the effects of climate change. In order to address the complex issues these gases present and their wider ramifications for the environment and human well-being, efforts must be made to reduce emissions and adapt to the changing climate.

## REFERENCES

Aditi, K., Tilly, A. and Tesse de Boer, K. G. 2021. Climate change impacts on health and livelihoods: Afghanistan Assessment. Climate Center, Afghanistan.

Aich, V. and Khoshbeen, A. J. 2016. Afghanistan: Climate Change Science Perspectives. National Environmental Protection Agency and UN Environment, Kabul. Available at https://www.acbar.org/upload/1493192115761.pdf

Ali, K. A., Ahmad, M. I. and Yusup, Y. 2020. Issues, impacts, and mitigations of carbon dioxide emissions in the building sector. Sustainability (Switzerland), 12(18): 10412. https://doi.org/10.3390/SU12187427

Anwar, M. Y., Warren, J. L. and Pitzer, V. E. 2019. Diarrhea patterns and climate: A spatiotemporal Bayesian hierarchical analysis of diarrheal disease in Afghanistan. Am. J. Trop. Med. Hyg., 101(3): 525-533. https://doi.org/10.4269/ajtmh.18-0735

Aryal, B., Gurung, R., Camargo, A.F., Fongaro, G., Treichel, H., Mainali, B., Angove, M. J., Ngo, H. H., Guo, W. and Puadel, S. R. 2022. Nitrous oxide emission in altered nitrogen cycle and implications for climate change. Environ. Polluti., 314: 120272. https://doi.org/10.1016/j.envpol.2022.120272

Azuma, K., Kagi, N., Yanagi, U. and Osawa, H. 2018. Effects of low-level inhalation exposure to carbon dioxide in indoor environments: A short review on human health and psychomotor performance. Environ. Int., 121: 51-56. Elsevier Ltd. https://doi.org/10.1016/j.envint.2018.08.059

Branch, T. A., DeJoseph, B. M., Ray, L. J. and Wagner, C. A. 2013. Impacts of ocean acidification on marine seafood. Trends Ecol. Evol., 28(3): 178-186. https://doi.org/10.1016/j.tree.2012.10.001

Climate Risk Country Profile Afghanistan. 2021. Asian Development Bank, Tokyo. Available at https://www.adb.org/sites/default/files/publication/660566/climate-risk-country-profile-afghanistan.pdf

Climate Watch Historical GHG Emissions, 2022. World Resources Institute. Washington, DC. Available at https://www.climatewatchdata.org/ghg-emissions

Cox, L. 1999. Nitrogen oxides (NOx) why and how they are controlled. Diane Publishing.

de Vries, W. 2021. Impacts of nitrogen emissions on ecosystems and human

health: A mini-review. Curr. Opin. Environ. Sci. Health, 21: 100249. https://doi.org/10.1016/j.coesh.2021.100249

Doll, J. E. and Barański, M. 2011. Greenhouse Gas basics. Michigan State University, US, pp. 6-7.

Duarte, C. M., Jaremko, L. and Jaremko, M. 2020. Hypothesis: Potentially systemic impacts of elevated CO2 on the human proteome and health. Front. Public Health, 8(11): 1-9. https://doi.org/10.3389/fpubh.2020.543322

Ebi, K. L. and Ziska, L. H. 2018. Increases in atmospheric carbon dioxide: Anticipated negative effects on food quality. PLoS Med., 15(7): 2-4. https://doi.org/10.1371/journal.pmed.1002600

Ehhalt, D. and Prather, M. 2001. Atmospheric Chemistry and Greenhouse Gases. IPCC, US

Environmental Protection Agency (EPA). 2018. Review of the primary national ambient air quality standards for oxides of nitrogen. EPA, Washington DC

FAO 2020. Afghanistan Drought Risk Management Strategy 2019-2030. Available at http://www.fao.org/fileadmin/user_upload/emergencies/docs/Afghanistan_Drought-Risk-Managment_Strategy9Feb2020.pdf

Hagen, E. 2009. Flooding in Afghanistan: A Crisis. Springer, Cham, pp. 179-180. https://doi.org/10.1007/978-90-481-2344-5_19

Harvey, C. 2018. $CO_2$ Can directly impact extreme weather, research suggests. Sci. Am., 15: 25-36.

Jacobson, T. A., Kler, J. S., Hernke, M. T., Braun, R. K., Meyer, K. C. and Funk, W. E. 2019. Direct human health risks of increased atmospheric carbon dioxide. Nat. Sustain., 2(8): 691-701. https://doi.org/10.1038/s41893-019-0323-1

Jahed, J. and Fang, P. 2023. Impact of air pollution on human health in Kabul City. Int. J. Sci. Res. Publ., 13(7): 264-278. https://doi.org/10.29322/ijsrp.13.07.2023.p13929

Javadmohammadi, M., Neisi, A. K., Saki, H., Babaei, A. A. and Rad, H. D. 2013. Estimation of health effects attributed to $NO_2$ exposure from the use of AirQ model in Ahvaz. Apadana J. Clin. Res., 1: 5-12.

Jiayi, Z. and Seyuba, K. T. 2023. Climate, Peace, and Security Fact Sheet Afghanistan. Stockholm International Peace Research Institute, Afghanistan.

Kweku, D., Bismark, O., Maxwell, A., Desmond, K., Danso, K., Oti-Mensah, E., Quachie, A. and Adormaa, B. 2018. Greenhouse effect: Greenhouse gases and their impact on global warming. J. Sci. Res. Rep. 17(6): 1-9. https://doi.org/10.9734/jsrr/2017/39630

Lange, K., Richter, A. and Burrows, J.P. 2022. Variability of nitrogen oxide emission fluxes and lifetimes estimated from Sentinel-5P TROPOMI observations. Atmos. Chem. Phys., 22(4): 2745-2767. https://doi.org/10.5194/acp-22-2745-2022

Lasek, J. A. and Lajnert, R. 2022. On the issues of $NO_x$ as greenhouse gases: An ongoing discussion. Appl. Sci., 12(20): 429. https://doi.org/10.3390/app122010429

Lindsey, R. 2023, May 12. Climate Change: Atmospheric Carbon Dioxide. NOAA Climate, US Commerce Department, US.

Lobell, D. B., Tommaso, S. D. and Burney, J. A. 2022. Globally ubiquitous negative effects of nitrogen dioxide on crop growth. Sci. Adv., 8(22): 1-10. https://doi.org/10.1126/sciadv.abm9909

Lovarelli, D., Conti, C., Finzi, A., Bacenetti, J. and Guarino, M. 2020. Describing the trend of ammonia, particulate matter and nitrogen oxides: The role of livestock activities in northern Italy during Covid-19 quarantine. Environ. Res., 191: 110048. https://doi.org/10.1016/j.envres.2020.110048

Lowther, S. D., Dimitroulopoulou, S., Foxall, K., Shrubsole, C., Cheek, E., Gadeberg, B. and Sepai, O. 2021. Low level carbon dioxide indoors-a pollution indicator or a pollutant? A health-based perspective. Environment, 8(11): 10125. . https://doi.org/10.3390/environments8110125

Maccracken, M. C. 2019. What is climate change? Biodiversity and Climate Change: Transforming the Biosphere, 12-22. Available at www.un.org/sites/un2.un.org/files/fastfacts-what-is-climate-change.pdf

Maharjan, S. B., Joya, E., Rahimi, M. M., Azizi, F., Muzafari, K. A., Bariz, M., Bromand, M. T., Shrestha, F., Shokory, A. G., A., A., Sherpa, T.C. and Bajracharya, S. R. 2021. Glaciers in Afghanistan: Status and changes from 1990 to 2015. International Centre for Integrated Mountain Development (ICIMOD): Patan, Nepal. Available at https://lib.icimod.org/record/35341

Manisalidis, I., Stavropoulou, E., Stavropoulos, A. and Bezirtzoglou, E. 2020. Environmental and Health Impacts of Air Pollution: A Review. Front. Public Health, 8(2): 1-13. https://doi.org/10.3389/fpubh.2020.00014

Masood, W., Aquil, S., Ullah, H., Nadeem, A., Mehmood, H., Islam, Z., Essar, M. Y. and Ahmad, S. 2022. Impact of climate change on health in Afghanistan amidst a humanitarian crisis. J. Clim. Change Health, 6: 100139. https://doi.org/10.1016/j.joclim.2022.100139

McMichael, A. J. and Woodruff, R. E. 2005. Climate change and human health. Encycl. Earth Sci. Ser., 22: 209-213. https://doi.org/10.1007/1-4020-3266-8_41

Mehrad, A. T. 2020. Causes of air pollution in Kabul and its effects on health. Indian J. Ecol., 47(4): 997-1002.

Millero, F. J. 1995. Thermodynamics of the carbon dioxide system in the oceans. Science, 59(4): 661-677.

Mitchell, M. J., Jensen, O. E., Cliffe, K. A. and Maroto-Valer, M. M. 2010. A model of carbon dioxide dissolution and mineral carbonation kinetics. Phys. Eng. Sci., 466(2117): 1265-1290. https://doi.org/10.1098/rspa.2009.0349

Muhammad, W., Silvia, R., Wasim, S. and Shahid Malik, A. S. 2023. Afghanistan Development Update: Uncertainty After Fleeting Stability. World Bank, Washington DC

Müller, R. 2021. The impact of the rise in atmospheric nitrous oxide on stratospheric ozone: This article belongs to Ambio's 50th Anniversary Collection. Ambio, 50(1): 35-39. https://doi.org/10.1007/s13280-020-01428-3

National Academy of Sciences 2020. Climate Change: Evidence and Causes: Update 2020. Washington, DC: The National Academies Press. https://doi.org/10.17226/25733.

NOAA 2020. Ocean acidification. National Oceanic and Atmospheric Administration. Accessed on September 19, 2023, available at https://www.noaa.gov/education/resource-collections/ocean-coasts/ocean-acidification

NOAA 2022. The NOAA annual greenhouse gas index (AGGI). Available at https://gml.noaa.gov/aggi/aggi.html

Nunes, L. J. R. 2023. The rising threat of atmospheric $CO_2$: A review on the causes, impacts, and mitigation strategies. Environment, 10(4): 4006. https://doi.org/10.3390/environments10040066

OCHA 2023. Afghanistan: The alarming effects of climate change. Avialable at https://www.unocha.org/news/afghanistan-alarming-effects-climate-change

Přívara, A. and Přívarová, M. 2019. Nexus between climate change, displacement and conflict: Afghanistan case. Sustainability (Switzerland), 11(20): 5586. https://doi.org/10.3390/su11205586

Qutbudin, I., Shiru, M. S., Sharafati, A., Ahmed, K., Al-Ansari, N., Yaseen, Z. M., Shahid, S. and Wang, X. 2019. Seasonal drought pattern changes due to climate variability: Case study in Afghanistan. Water (Switzerland), 11(5): 1096. https://doi.org/10.3390/w11051096

Richter, A. 2009. Nitrogen oxides in the troposphere- What have we learned from satellite measurements? EPJ Web Conf., 1: 149-156. https://doi.org/10.1140/epjconf/e2009-00916-9

Savage, M., Dougherty, B., Hamza, M., Butterfield, R. and Bharwani, S. 2009. Socio-economic impacts of climate change in Afghanistan. Stockholm Environment Institute: Oxford, UK.

Sheng, Q. and Zhu, Z. 2019. Effects of nitrogen dioxide on biochemical responses in 41 garden plants. Plants, 8(2): 45. https://doi.org/10.3390/

plants8020045
Shokory, J. A. N., Schaefli, B. and Lane, S. N. 2023. Water resources of Afghanistan and related hazards under rapid climate warming: a review. Hydrol. Sci. J., 68(3): 507-525. https://doi.org/10.1080/02626667.2022.2159411
Shriram, S., Ramamurthy, K. and Ramakrishnan, S. 2019. Effect of occupant-induced indoor $CO_2$ concentration and bioeffluents on human physiology using a spirometric test. Build. Environ., 149: 58-67. https://doi.org/10.1016/j.buildenv.2018.12.015
Shukla, J., Skea, E., Calvo Buendia, V. and Masson-Delmotte, S. 2019. Framing and Context. Springer, Cham.
Skendžić, S., Zovko, M., Živković, I. P., Lešić, V. and Lemić, D. 2021. The impact of climate change on agricultural insect pests. Insects, 12(5): 440. https://doi.org/10.3390/insects12050440
Skiba, U. M. and Rees, R. M., 2014. Nitrous oxide, climate change and agriculture. CABI Reviews, pp.1-7. https://doi.org/10.1079/PAVSNNR20149010
Solomon, S., Plattner, G. K., Knutti, R. and Friedlingstein, P. 2009. Irreversible climate change due to carbon dioxide emissions. Science, 106(6): 1704-1709. https://doi.org/10.1073/pnas.0812721106
Thiruvenkatachari, R., Su, S., An, H. and Yu, X. X. 2009. Post combustion $CO_2$ capture by carbon fibre monolithic adsorbents. Prog. Energy Combust. Sci. 35(5): 438-455. https://doi.org/10.1016/J.PECS.2009.05.003
Umar, S. A. and Tasduq, S. A. 2022. Ozone Layer Depletion and Emerging Public Health Concerns - An Update on Epidemiological Perspective of the Ambivalent Effects of Ultraviolet Radiation Exposure. Front. Oncol. 12. https://doi.org/10.3389/FONC.2022.866733
UN n.d. Causes and Effects of Climate Change. United Nations. Accessed on September 18, 2023. Available at https://www.un.org/en/climatechange/science/causes-effects-climate-change
UNICEF 2022. Afghanistan Humanitarian Situation Report (August). Available at https://www.unicef.org/afghanistan/documents/afghanistan-humanitarian-situation-report-1-31-august-2022
UNICEF. 2023. Afghanistan Humanitarian Situation Report 1 - 31 July 2023 Report (July). Avialable at https://www.unicef.org/afghanistan/documents/unicef-afghanistan-humanitarian-situation-report-1-31-july-2023
Wagner, A. L., Mubarak, M. Y., Johnson, L. E., Porth, J. M., Yousif, J. E. and Boulton, M. L. 2017. Trends of vaccine-preventable diseases in Afghanistan from the disease early warning system. PLoS ONE, 12(6): e0178677. https://doi.org/10.1371/journal.pone.0178677
World Health Organization 2008. Technical discussion on Climate change and health security (No. EM/RC55/Tech. Disc. 1). Avialable at https://applications.emro.who.int/docs/EM_RC55_tech_disc_1_en.pdf
Yoro, K. O. and Daramola, M. O. 2020. $CO_2$ emission sources, greenhouse gases, and the global warming effect. In: Advances in Carbon Capture: Methods, Technologies and Applications. Elsevier Inc., Netherlands, p. 3. https://doi.org/10.1016/B978-0-12-819657-1.00001-3
Zaki, N. and Lederer, M. 2023. An Overview of Climate Change in Afghanistan: Causes, Consequences, Challenges and Policies (January). Available at https://www.politikwissenschaft.tu-darmstadt.de/media/politikwissenschaft/ifp_dokumente/arbeitsbereiche_dokumente/ib/Zaki_13.02.2023_An_overview_of_climate_change_in_Afghanistan-2.pdf

## ORCID DETAILS OF THE AUTHORS

Mairaj Khan: https://orcid.org/0000-0003-3067-6231

Nature Environment and Pollution Technology
An International Quarterly Scientific Journal

p-ISSN: 0972-6268
(Print copies up to 2016)
e-ISSN: 2395-3454

Vol. 23 | No. 3 | pp. 1829-1837 | 2024

Original Research Paper

https://doi.org/10.46488/NEPT.2024.v23i03.055

Open Access Journal

# Quantification of the Few Parameters and Metallic Elements in the Quaternary Sediments of "Baie Du Repos" and their Interrelation

**M. T. Moulaye Taher*†, A. M. El Mokhtar**, E. C. S'Id*** and A. Mahfoudh***

*Unité de recherche: Changement Climatique/FST – Université de Nouakchott, Mauritania

**L'office National d'inspection sanitaire des produits de la pêche et l'aquaculture, Mauritania

***Unité de recherche: Membrane, Matériaux, Environnement et Milieux Aquatiques (2MEMA), FST - Université de Nouakchott, Mauritanie

†Corresponding author: M. T. Moulaye Taher; taher.moulay1@gmail.com

**Nat. Env. & Poll. Tech.**
**Website: www.neptjournal.com**

*Received:* 29-10-2023
*Revised:* 13-12-2023
*Accepted:* 31-12-2023

**Key Words:**
Baie du Repos
Metallic elements
Cadmium
Lead
Quaternary sediments

## ABSTRACT

Mauritania is a fishing country. However, the Mauritanian coast is increasingly exposed to environmental issues mainly due to anthropogenic activities such as the mining, gas, oil, and fishing industries, as well as new agricultural practices that unreasonably use inputs. Environmental monitoring of the Mauritanian coast faces several challenges; thus, improving the fisheries sector begins with enhancing the state of marine ecosystems and implementing environmental monitoring adapted to climatic conditions and local needs. This study aims to evaluate the quality of the sediments of the "Baie du Repos" in the town of Nouadhibou, Mauritania, through the study of organic matter and the quantification of trace metallic elements in the Quaternary sediments of the Bay. Six samples deemed representative of this Bay were taken and transported to the laboratory. The physicochemical analysis of these samples shows that the superficial horizons of 30 cm depth have overall organic matter contents higher than the average threshold value proposed by the literature for 4 out of 6 of the points studied. The contents recorded for the different metallic trace elements indicate that point 1 is the most exposed to contamination, with the highest concentrations of cadmium, lead, copper, iron, and zinc. The ACP (Principal Component Analysis) showed that the metallic trace elements Pb, Cu, Fe, Cd, and Zn are closely related and evolve positively in the same direction. Additionally, it was found that the points studied are divided into three groups: Group 1 contains only point 1, which is the most exposed to contamination by these toxic elements (Pb, Cu, Zn, Fe, and Cd). Group 2 contains points 3, 5, and 6, which are moderately contaminated by metallic elements with a significant dominance of organic matter (OM). Finally, Group 3 is the least contaminated, with a very high content of organic matter (OM).

## INTRODUCTION

Seawater is considered an essential resource for life and, therefore, deserves preservation and particular attention, as it is exposed to various sources of anthropogenic contamination. Indeed, human activities have significantly impacted the marine ecosystem (Tornero & Hanke 2016). This includes acid mine drainage, fallout from atmospheric pollutants, gas and oil exploration activities, and effluent from industrial discharges, agriculture, and fisheries. The harmful effects caused by these organic and inorganic contaminants are consistently reported in the scientific literature and continue to be the subject of research (Nriagu & Pacyna 1988, Shirahata et al. 1980).

The physicochemical and metallic quality of the marine environment plays a crucial role in determining its biological quality and degree of contamination (Cebu & Orale 2017, Echapare et al. 2019). In this context, the "Baie du Repos" in Nouadhibou is exposed to discharges from the fishing and mining industries, which significantly contribute to the physicochemical and metallic contamination of the bay's waters.

This study aims to evaluate the degree of contamination in the "Baie du Repos." It proposes an analytical investigation to determine the content of metallic trace elements and organic carbon, as well as their correlation. The study focuses on metallic trace elements such as Cd, Pb, Zn, Cu, Al, Fe, and organic matter in the Quaternary sediments of the "Baie du Repos." To achieve this, six samples deemed representative of the bay were collected using a specialized sample collector. These samples were analyzed at the Chemistry Laboratory of the National Office for Health

Inspection of Fisheries and Aquaculture Products (ONISPA) in Nouadhibou, Mauritania.

## MATERIALS AND METHODS

### Sampling

Six samples considered representative of the "Baie du Repos" (Nouadhibou, Mauritania) were taken for this study. A portable GPS was used to determine the in-situ geographic coordinates of the sampling points. These Universal Transverse Mercator (UTM) coordinates were used with Google Earth Pro and ArcGIS 10.2.2 to produce a geographic map and perform spatial geo-referencing (Fig. 1). The sediment samples were taken from superficial horizons approximately 30 cm deep using a sediment grab, with each 500 g glass tube filled to the top. Fig. 1 shows the spatial location of the samples taken. All samples were conditioned in situ and then transported to the laboratory for analysis.

However, to avoid any contamination, the sample tubes were washed carefully with a solution of 1:1 HCl and 1:1 HNO3 and stored at 4°C in the refrigerator until their use (Abdallah & Adel 2015, Abdallah 2007, ASTM 1991)

### Chemical Analysis

Each sample was analyzed in duplicate. The surface layer of the sediment, potentially oxidized by oxygen, was removed. Part of the sample was freeze-dried to analyze trace metal elements, while another part was air-dried. The dried sediment clods were then broken up using a plastic mortar and pestle, and the sediments were sieved to 2 mm to measure the organic matter.

Organic carbon ($C_{org}$) was determined according to the protocol of Walkley and Black (Centre d'expertise en analyse environnementale du Québec et ministère de l'agriculture et QUÉBEC 2003) to deduce the level of organic matter (OM). Metallic trace elements (MTE) (Cu, Fe, Zn, Pb, Al, and Cd) were determined after acid mineralization by atomic absorption spectrophotometry (ISO 15586 2003).

The analysis was carried out at the Chemistry Laboratory of the National Office of Sanitary Inspection of Fishing and Aquaculture Products (ONISPA) in Mauritania, in collaboration with the Laboratory of Marine Geosciences and Soil Sciences of the Faculty of Sciences at Chouaib Doukkali University (Morocco).

The analysis results were statistically processed using Xlstat software. Descriptive statistical analysis, linear regression, and principal component analysis (PCA) were performed to better describe the characteristics of the sediments in the studied Bay. The correlation between metallic elements and organic matter was also assessed using the Pearson method (Ling et al. 2023).

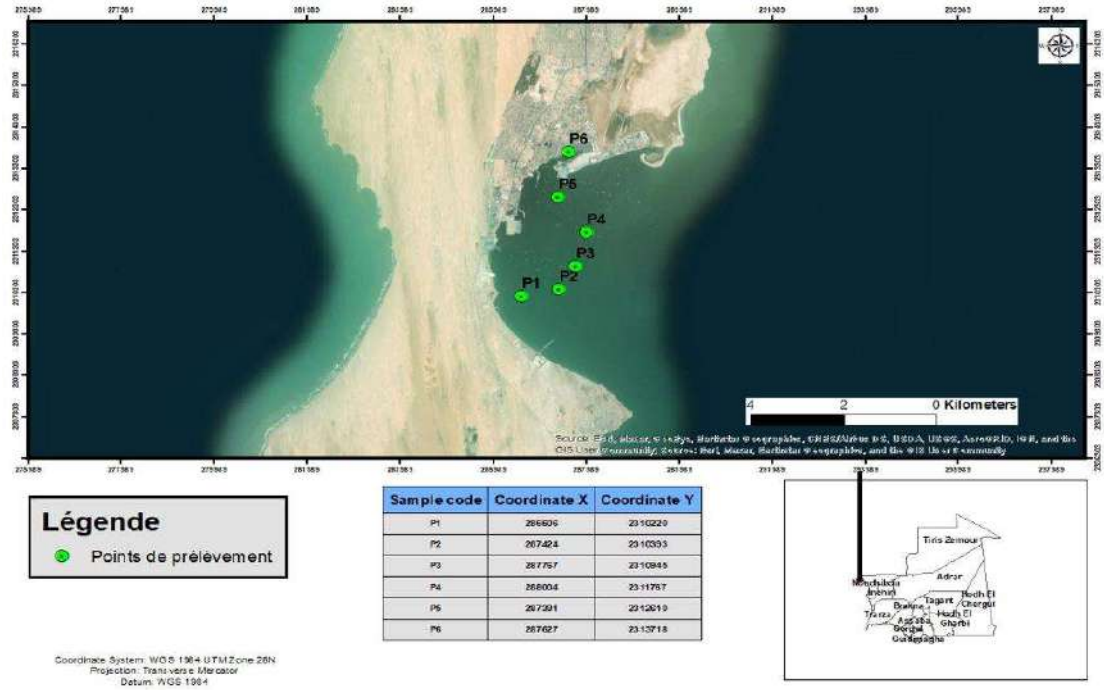


Fig. 1: Geographic location of the study area and sample location (sat image from Google Earth Pro).

Table 1: Content of metallic elements and organic matter.

| Samples code | CO in % | | | OM in % | | | Cd in mg.kg$^{-1}$ | | | Pb in mg.kg$^{-1}$ | | |
|---|---|---|---|---|---|---|---|---|---|---|---|---|
| | Trial 1 | Test 2 | Average | Trial 1 | Test 2 | Average | Trial 1 | Test 2 | Average | Trial 1 | Test 2 | Average |
| P1 | 5,274 | 5,178 | 5,226 | 9,093 | 8,927 | 9,010 | 0.922 | 0.905 | 0.914 | 17,545 | 18,785 | 18,165 |
| P2 | 0.036 | 0.038 | 0.037 | 0.062 | 0.066 | 0.064 | 0.834 | 0.840 | 0.837 | 2,649 | 2,567 | 2,608 |
| P3 | 4,629 | 4,611 | 4,620 | 7,980 | 7,949 | 7,964 | 0.089 | 0.093 | 0.091 | 0.635 | 0.629 | 0.632 |
| P4 | 0.906 | 0.909 | 0.907 | 1,562 | 1,567 | 1,565 | 0.337 | 0.326 | 0.331 | 2,889 | 2,833 | 2,861 |
| P5 | 6,010 | 6,080 | 6,045 | 10,361 | 10,482 | 10,421 | 0.143 | 0.150 | 0.146 | 0.681 | 0.722 | 0.702 |
| P6 | 7,050 | 7,090 | 7,070 | 12,155 | 12,223 | 12,189 | 0.425 | 0.431 | 0.428 | 3,108 | 2,981 | 3,045 |
| Samples code | Cu in mg.kg$^{-1}$ | | | Fe in mg.kg$^{-1}$ | | | Zn in mg.kg$^{-1}$ | | | Al in mg.kg$^{-1}$ | | |
| | Trial 1 | Test 2 | Average | Trial 1 | Test 2 | Average | Trial 1 | Test 2 | Average | Trial 1 | Test 2 | Average |
| P1 | 1,964 | 1,989 | 1,976 | 21207,386 | 22289,519 | 21748,453 | 2800.15 | 2791.36 | 2795,754 | 5574,802 | 5667,649 | 5621,225 |
| P2 | 0.593 | 0.582 | 0.587 | 14928,624 | 14593,489 | 14761.056 | 990.81 | 991.40 | 991,106 | 6854,563 | 7008,354 | 6931,459 |
| P3 | 0.210 | 0.206 | 0.208 | 2496,887 | 2357,139 | 2427.013 | 48.56 | 47.62 | 48,086 | 4871.016 | 4945,839 | 4908,428 |
| P4 | 0.198 | 0.200 | 0.199 | 13351,792 | 12949,629 | 13150.711 | 282.48 | 280.66 | 281,571 | 5746,640 | 5505,935 | 5626,287 |
| P5 | 0.126 | 0.130 | 0.128 | 3399.079 | 3297,534 | 3348,306 | 133.13 | 134.14 | 133,635 | 6318,815 | 6238,190 | 6278.503 |
| P6 | 0.314 | 0.314 | 0.314 | 12578.980 | 12811.009 | 12694,995 | 406.72 | 406.31 | 406,514 | 4997,512 | 4992,545 | 4995.029 |

## RESULTS AND DISCUSSION

The results, presented in Table 1, show the concentrations obtained for the samples taken from six points considered representative of the Bay.

### Organic Materials

The results presented in Table 1 show that the percentages of the parameters and metal concentrations vary slightly at different points. Notably, 4 out of 6 of the sediment samples have organic matter (OM) contents greater than 2% (Fig. 2). The high levels of OM in the Bay are primarily due to discharges from the fishing industries (Bouyer & Dabin 1963).

### The Metallic Trace Elements Cd, Pb and Cu

For cadmium, the highest values were obtained in the sediments of points 1 and 2, which are respectively of the order of 0.914 mg.kg$^{-1}$ and 0.837 mg.kg$^{-1}$, while the lowest concentrations, which were identified are 0.146 mg.kg$^{-1}$ and 0.091 mg.kg$^{-1}$, respectively for points 3 and 5. Generally, there does not seem to be a significant difference between the six points sampled. For lead, the sediments have high levels, particularly in point 1 (18.165 mg.kg$^{-1}$), which is notable in the histogram as shown in Fig. 3. This is essentially due to the presence of factories and thermal centers in the vicinity of point 1. These factories dispose of their industrial waste directly into the Bay. Regarding copper, its content in the sediments is higher in point 1 (1.9764 mg.kg$^{-1}$) than in the other points, 0.587; 0.314; 0.208; 0.199, and 0.128 mg.kg$^{-1}$, respectively, for points 2, 6, 3, 4 and 5 (Ouaty et al. 2022, Wang et al. 2022).

### Contents of Metallic Elements Fe, Zn and Al

For the three metallic elements Fe, Zn, and Al, we see that their maximum concentrations are identified at point 1. These contents are 21748, 453, 2795.754, and 5621.225 mg.kg$^{-1}$, respectively, which denotes the effect of these factories on the environment of Rest Bay, especially at points 1 and 2 (Fig. 4). This proves the presence of iron and aluminum in the marine environment at very high concentrations (Abdallah & Adel 2015, Armstrong-Altrin et al. 2015, Lopes-Rocha et al. 2017).

This heterogeneity in the distribution of these parameters is primarily due to the locations of the points, with those closest to the shore being more exposed to contamination.

The results found in the sediments of Rest Bay (Table 2) were compared with results from several bays located on different continents to evaluate the results found in the sediments of Rest Bay (Table 3). The concentrations of

Pb and Cu were observed to be lower than all the comparison results. However, the average Cd content recorded in 'Baie du Repos' is lower than all comparison concentrations except for Beibu Bay in China. For Zn, the comparison shows that 4 out of 6 concentrations are lower than the average Zn value obtained in the sediments of the bay studied, while 2 out of 6 are higher.

Fig. 5 illustrates the significant correlation curves observed in the correlation matrix, highlighting significant correlations between zinc and the following elements: cadmium (Cd), copper (Cu), iron (Fe), and lead (Pb). Additionally, significant correlations are observed between iron (Fe) and cadmium (Cd), as well as between copper (Cu) and lead (Pb). Therefore, the correlation curves indicate that 4 out of the 6 elements studied exhibit significant correlations with zinc.

## Correlation Between Metallic Elements and Organic Matter

Principal component analysis (PCA) established a correlation between several elements studied in the sediments from the Bay, with a correlation coefficient of R = 0.80 at the 5% significance level. This provides a better understanding of the possible results and sources affecting the studied system (Alves et al. 2018, Garcia et al. 2023, Tripathi & Singal 2019) (Table 4).

According to the correlation matrix, we can make the following observations: Zinc is well correlated with all metallic

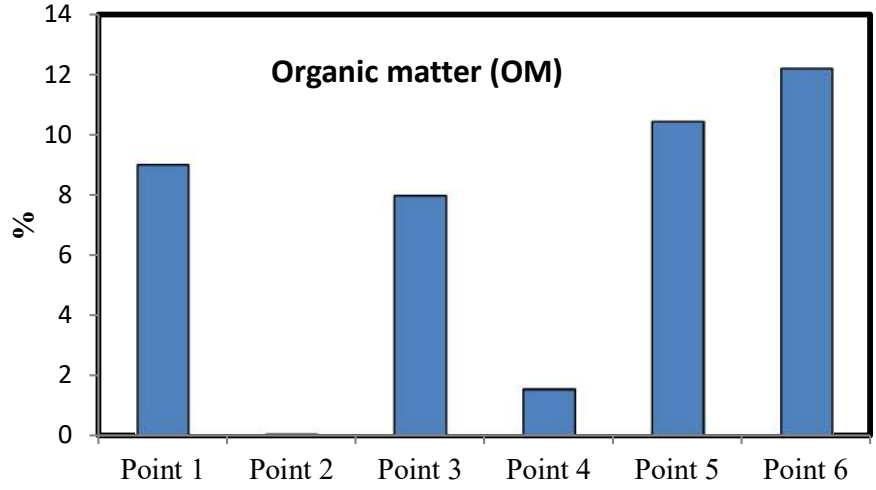


Fig. 2: Percentage of organic matter.

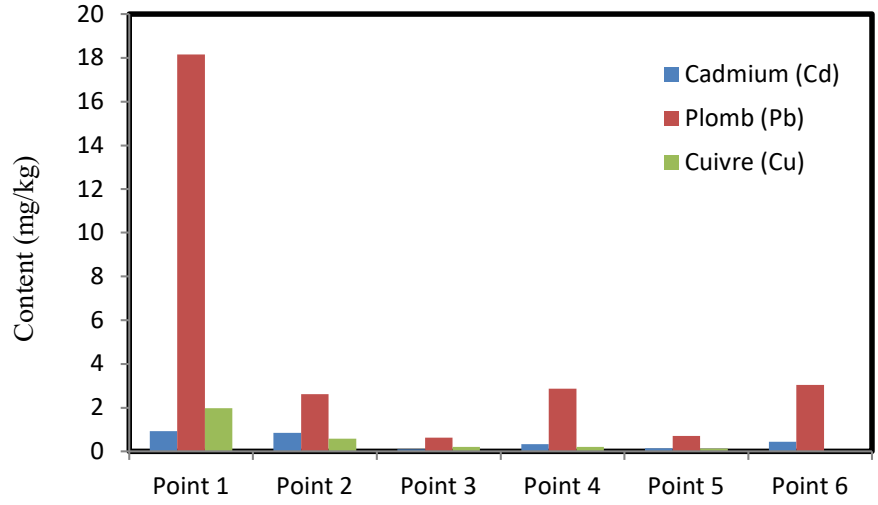


Fig. 3: Content of trace metal elements.

elements except aluminum. This could be explained by the fact that zinc likely shares the same source as cadmium (Cd), copper (Cu), iron (Fe), and lead (Pb). On the other hand, aluminum (Al) shows a very low correlation with all the elements.

As for cadmium (Cd), the correlation matrix indicates that it is strongly correlated with iron and moderately correlated with zinc (Zn), copper (Cu), and lead (Pb). Conversely, it is only slightly correlated with aluminum (Al). The latter elements are considered lithological (natural) elements, unlike the others, which originate from contaminating industrial sources.

### Principal Component Analysis (PCA)

For a relevant graphical visualization of the correlations and to ensure access to all interactions between the variables, a PCA was performed. Fig. 6 displays the observations in a new coordinate system, with component 1 as the abscissa and component 2 as the ordinate. The PCA results reveal groupings, oppositions, and directional trends. The F1 axis accounts for 56.42% of the variance and contrasts MO with aluminum (Al). Meanwhile, the other metallic trace elements Cu and Zn are closely linked, evolving positively in the same direction and differentiating along the F1 axis.

Axes F1 and F2, therefore, present, respectively, 56.42% and 32.47% affinity between the elements studied from different points. The variables Pb, Cu, Zn, Fe, and Cd are well represented and positively correlated in the correlation circle and approach the axis F1 of positive coordinate. The aluminum variable Al is very close to the axis F2.

Fig. 7 illustrates the distribution of the different points studied in relation to the PCA axes. The points are divided into three groups: Group 1 contains only point 1, which is the most exposed to contamination by toxic elements (Pb, Cu, Zn, Fe, and Cd). Group 2 includes points 3, 5, and 6 and is characterized by moderate contamination with a significant presence of organic matter (OM). Finally, Group 3 is the least contaminated but has a very high content of organic matter (OM). The results reveal a slight correlation between organic matter and these metallic trace elements (Elmokhtar et al. 2021, Tiquio et al. 2017).

## CONCLUSION

The values of the parameters obtained in 'Baie du Repos'

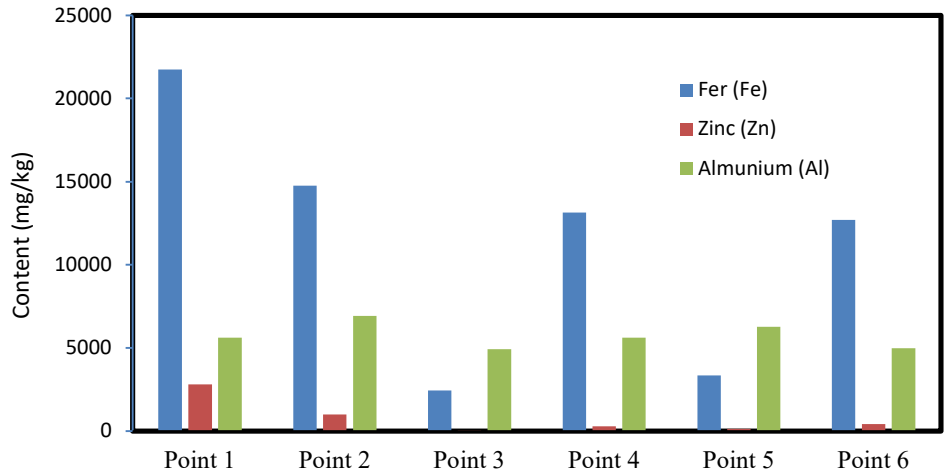


Fig. 4: Content of metallic elements.

Table 2: Descriptive statistics.

| Statistical | Cd in mg.kg$^{-1}$ | Pb in mg.kg$^{-1}$ | Cu in mg.kg$^{-1}$ | Fe in mg.kg$^{-1}$ | Zn in mg.kg$^{-1}$ | Al in mg.kg$^{-1}$ | CO in % | MO in % |
|---|---|---|---|---|---|---|---|---|
| Minimum | 0.091 | 0.632 | 0.128 | 2427.013 | 48,086 | 4908,428 | 0.037 | 0.064 |
| Maximum | 0.914 | 18,165 | 1,976 | 21748,453 | 2795,754 | 6931,459 | 7,070 | 12,189 |
| Average | **0.458** | **4,669** | **0.569** | **11355.089** | **776,111** | **5726,822** | **3,984** | **6,869** |
| Standard deviation (n) | 0.317 | 6,115 | 0.646 | 6689.063 | 952,991 | 704,988 | 2,607 | 4,493 |
| Asymmetry (Pearson) | 0.356 | 1,685 | 1,597 | -0.030 | 1,430 | 0.463 | -0.474 | -0.474 |
| Flattening (Pearson) | -1.476 | 1,021 | 0.820 | -1.145 | 0.469 | -1.020 | -1,398 | -1,398 |

Table 3: Comparison of heavy metal concentrations in "Baie du Repos" with values from other studies (mg.kg$^{-1}$).

| Continent | Region | CD | Pb | Cu | Zn | Year | References |
|---|---|---|---|---|---|---|---|
| Africa | Eastern harbor (Egypt) | 0.79 | 82.50 | 53.44 | 1588.59 | 2007 | (Abdallah 2007) |
| Africa | Western Harbor (Egypt) | 8.09 | 53.59 | - | 305.38 | 2007 | (Abdallah et al. 2007) |
| Europe | Thermaikos Gulf (Greece) | - | 77.0 | 80.1 | 184.1 | 2009 | (Christophoridis et al. 2009) |
| Asia | Coastal Bohai Bay (China) | - | 34.7 | 38.5 | 131.1 | 2012 | (Gao & Chen 2012) |
| Asia | Beibu Bay (China) | 0.16 | 27.99 | 58.26 | 67.28 | 2013 | (Dou et al. 2013) |
| Africa | AbuQir Bay (Egypt ) | 17.21 | 56.05 | 12.07 | 8532 | 2014 | (Abdallah & Mohamed 2015) |
| Africa | Baie du Repos (Mauritania) | **0.458** | **4,669** | **0.569** | **776,111** | **2022** | **Current study** |

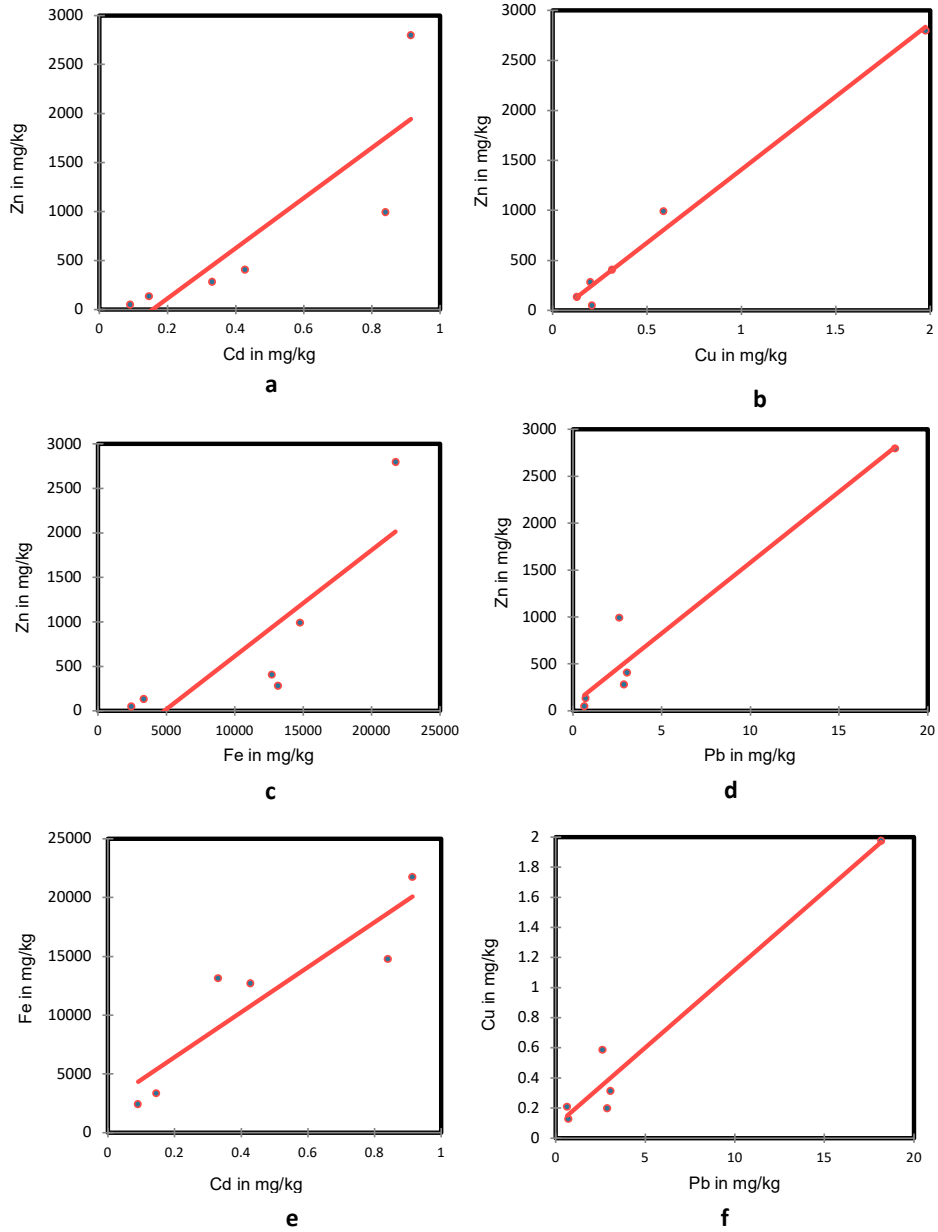


Fig. 5: Curves of significant correlations observed in the correlation matrix.

for the six points covered by this study allow us to make the following observations: significant levels of organic matter were found at the different sampled points. Additionally, observations were made regarding the metallic elements.

For cadmium, the highest value was obtained in the sediments of point 1, which is of the order of 0.914 mg.kg$^{-1}$. However, for lead, the sediments studied have high levels, particularly in point 1 (18.165 mg.kg$^{-1}$). And also, it is the same for copper, which is of the order of 1.9764 mg.kg$^{-1}$ in point 1. As for the two metallic elements, Iron and Zinc, we also see that their maximum concentrations have been identified in point 1. These contents are respectively 21748, 453, and 2795.754 mg.kg$^{-1}$. On the other hand, the highest Aluminum content was identified in point 2.

The results show that point 1 is the most exposed to sources of pollution. In contrast, point 3 contains the lowest levels of metallic elements, likely due to its geographical position, which benefits from natural aeration. This factor is more significant here than at other points, leading to continuous dilution of the metallic elements' concentrations. According to the correlation matrix, all elements except aluminum are well correlated with zinc. Aluminum (Al), however, shows a very low correlation with all other elements due to its natural (lithological) origin. For cadmium (Cd), the correlation matrix indicates a strong correlation with

Table 4: Correlation matrix of physicochemical parameters of the sediments studied.

| Variables | Cd in mg.kg$^{-1}$ | Pb mg.kg$^{-1}$ | Cu in mg.kg$^{-1}$ | Fe in mg.kg$^{-1}$ | Zn in mg.kg$^{-1}$ | Al in mg.kg$^{-1}$ | CO in % | MO in % |
|---|---|---|---|---|---|---|---|---|
| Cd in mg.kg$^{-1}$ | **1** | | | | | | | |
| Pb in mg.kg$^{-1}$ | 0.719 | **1** | | | | | | |
| Cu in mg.kg$^{-1}$ | 0.792 | **0.980** | **1** | **1** | | | | |
| Fe in mg.kg$^{-1}$ | **0.908** | 0.797 | 0.788 | | | | | |
| Zn in mg.kg$^{-1}$ | 0.852 | 0.967 | 0.993 | 0.836 | 1 | | | |
| Al in mg.kg$^{-1}$ | 0.429 | -0.055 | 0.055 | 0.167 | 0.151 | **1** | | |
| CO in % | -0.307 | 0.154 | 0.088 | -0.230 | 0.017 | -0.564 | **1** | |
| MO in % | -0.306 | 0.154 | 0.088 | -0.230 | 0.017 | -0.564 | **1,000** | **1** |

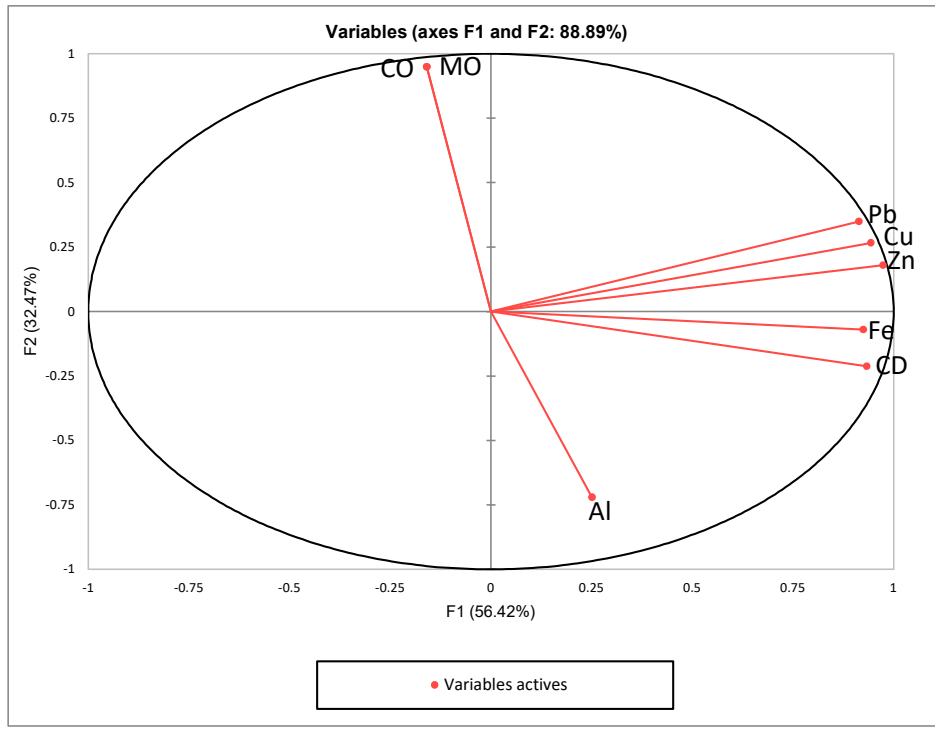


Fig. 6: Analysis of the principal components of the physicochemical variables of the sediments.

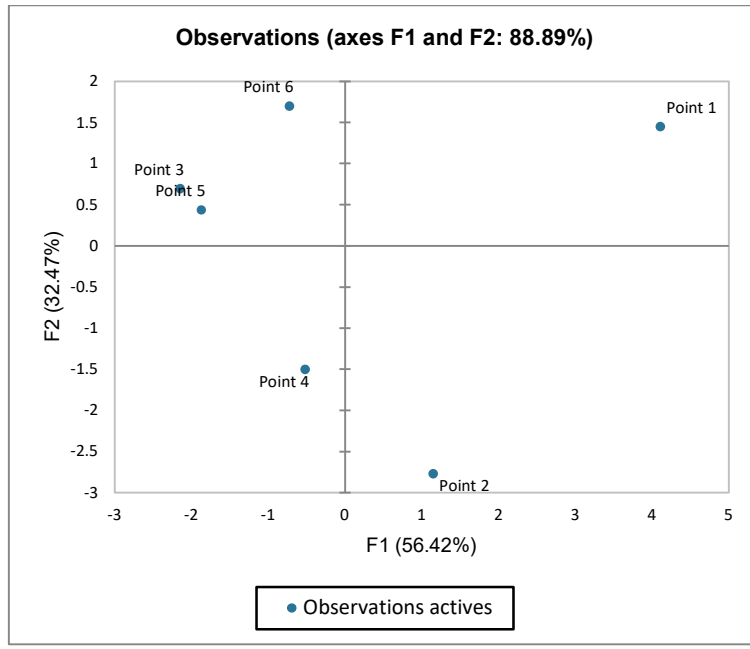


Fig. 7: Plots of scores based on mean values for each principal component analysis (PCA).

iron and a moderate correlation with copper (Cu), lead (Pb), and zinc (Zn).

To enhance this investigation, it should be complemented by a study focusing on the hydrochemical characteristics of the Bay to determine both the degree of anthropogenic activity and the main constraints affecting the ecosystem of "Baie du Repos."

## REFERENCES

Abdallah, M. A. M. and Adel, A. M. 2015. Assessment of heavy metals by sediment quality guideline in surficial sediments of Abu Qir Bay southeastern Mediterranean Sea, Egypt. Environ. Earth Sci., 73(7): 3603-3609.

Abdallah, M. A. M. 2007. Accumulation and distribution of heavy metals in surface sediments of a semi-enclosed basin in the southeastern Mediterranean Sea, Egypt. Mediterr. Mar. Sci., 8(1): 31-40.

Abdallah, M. A. M., El Sayed, N. B. and Saad, M. A. 2007. Distribution and enrichment evaluation of heavy metals in El-Mex Bay using normalization models. Fresen. Environ. Bull., 16(7): 719.

Alves, J. P. H., Fonseca, L. C., Chielle, R. S. A. and Macedo, L. C. B. 2018. Monitoring water quality of the Sergipe River Basin: An evaluation using multivariate data analysis. Rev. Bras. Rec. Hidr., 23: 1-12.

Bouyer, S. and Dabin, B. 1963. Etudes pédologiques du Delta Central du Niger. Agron. Trop., 12: 1300-1304.

Armstrong-Altrin, J. S., Machain-Castillo, M. L., Rosales-Hoz, L., Carranza-Edwards, A., Sanchez-Cabeza, J. A. and Ruíz-Fernández, A. C. 2015. Provenance and depositional history of continental slope sediments in the Southwestern Gulf of Mexico unraveled by geochemical analysis. Cont. Shelf Res., 95: 15-26.

ASTM. 1991. American Society for Testing and Materials (ASTM) Guide for conducting 10-day static sediment toxicity tests with marine and estuarine amphipods. ASTM Standard Methods, 11.04, Method Number E-1367-90.

Cebu, E. H. and Orale, R. L. 2017. Seawater physicochemical parameters in the green mussel belts in Samar Philippines. J. Acad. Res., 2: 1-15.

Christophoridis, C., Dedepsidis, D. and Fytianos, K. 2009. Occurrence and distribution of selected heavy metals in the surface sediments of Thermaikos Gulf, N. Greece. Assessment using pollution indicators. J. Hazard. Mater., 168: 1082-1091.

Dou, Y., Li, J., Zhao, J., Hu, B. and Yang, S. 2013. Distribution, enrichment, and source of heavy metals in surface sediments of the eastern Beibu Bay, South China Sea. Mar. Pollut. Bull., 67: 137-145.

Echapare, E. O., Pacala, F. A. A., Mendaño, R. V. and Araza, J. B. 2019. Physico-chemical and microbial analysis of water in Samar mussel farms. Egypt. J. Aquat. Res., 45(3): 225-230.

Elmokhtar, A. M., Saleck, A., Aajjane, A., Zamel, M. and Tounkara, H. 2021. Pedo-agronomic and environmental analysis of some agricultural soils of Keur-Macene South of Mauritania. Int. J. Adv. Res. Eng. Tech., 12(3): 298-310.

Gao, X. and Chen, C. T. A. 2012. Heavy metal pollution status in surface sediments of the coastal Bohai Bay. Water Res., 46: 1901-1911.

Garcia, C. A. B., Monteiro, A. S. C., Costa, S. S. L., Arguelho, M. L. P. M., Araújo, R. G. O., Carneiro, M. E. R. and Alves, J. P. H. 2023. Geochemistry of trace metals in surface sediments from the continental slope of the states of Sergipe and Alagoas, Northeastern Brazil. Mar. Pollut. Bull., 186(May 2022).

Ling, S. Y., Asis, J. and Musta, B. 2023. Distribution of metals in coastal sediment from northwest Sabah, Malaysia. Heliyon, 9(2): e13271. doi:10.1016/j.heliyon.2023.e13271.

Lopes-Rocha, M., Langone, L., Miserocchi, S., Giordano, P. and Guerra, R. 2017. Spatial patterns and temporal trends of trace metal mass budgets in the western Adriatic sediments (Mediterranean Sea). Sci. Total Environ., 599-600: 1022-1033.

Nriagu, J. O. and Pacyna, J. M. 1988. Quantitative assessment of worldwide contamination of air, water, and soils by trace metals. Nature, 333: 134-139.

Ouaty, O. E., El M'rini, A., Nachite, D., Marrocchino, E., Marin, E. and Rodella, I. 2022. Assessment of the heavy metal sources and

concentrations in the Nador Lagoon sediment, Northeast-Morocco. Ocean Coast. Manag., 216: 105900.

Shirahata, H., Elias, R. W. and Patterson, C. C. 1980. Chronological variations in concentrations and isotopic compositions of anthropogenic lead in sediments of remote subalpine pond. Geochim. Cosmochim. Acta, 44: 49-162.

Tiquio, M. G. J., Hurel, C., Marmier, N., Taneez, M. andral, B., Jordan, N. and Francour, P. 2017. Sediment-bound trace metals in Golfe-Juan Bay, Northwestern Mediterranean: Distribution, availability and toxicity. Mar. Pollut. Bull., 118(1-2): 427-436.

Tornero, V. and Hanke, G. 2016. Chemical contaminants entering the marine environment from sea-based sources: A review with a focus on European seas. Mar. Pollut. Bull., 112(1-2): 17-38.

Tripathi, M. and Singal, S. 2019. Use of principal component analysis for parameter selection for development of a novel water quality index: A case study of River Ganga, India. Ecol. Indic., 96: 430-436.

Wang, W., Lin, C., Wang, L., Liu, Y., Sun, X., Chen, J. and Lin, H. 2022. Potentially hazardous metals in the sediment of a subtropical bay in South China: Spatial variability, contamination assessment, and source apportionment. Mar. Pollut. Bull., 184: 114185.

## ORCID DETAILS OF THE AUTHORS

M. T. Moulaye Taher: https://orcid.org/0009-0006-9446-7921
E. C. S'Id: https://orcid.org/0000-0002-5887-1840

Nature Environment and Pollution Technology
An International Quarterly Scientific Journal

p-ISSN: 0972-6268
(Print copies up to 2016)
e-ISSN: 2395-3454

Vol. 23 | No. 3 | pp. 1839-1848 | 2024

Original Research Paper

https://doi.org/10.46488/NEPT.2024.v23i03.056

Open Access Journal

# Effect of Rice Biochar on Typical Cadmium, Lead and Zinc Form in Contaminated Soil in Northwest Guizhou Province, China

**Ji Wang*, Die Xu**, Xiongfei Cai*† and Shuai Zhao*****

*School of Geographic and Environmental Sciences, Guizhou Normal University, Guiyang, 550025, China
**School of Education Science, Qiannan Normal University for Nationalities, Duyun, 558000, China
***School of Environmental Science and Engineering, Dalian Maritime University, Dalian, 116000, China
†Corresponding author: Xiongfei Cai; ddwll5201@163.com

**Nat. Env. & Poll. Tech.**
**Website: www.neptjournal.com**

*Received:* 14-11-2023
*Revised:* 13-12-2023
*Accepted:* 11-01-2024

**Key Words:**
Rice biochar
Historical pollution soil
Heavy metals
Passivation repair

## ABSTRACT

This study was conducted in Hezhang County, Bijie City, Guizhou Province. The soil in the zinc smelting area has been contaminated with cadmium, lead, and zinc. Therefore, these elements are the focus of this research. Rice husk biochar was used as the passivation material. The Fourier infrared spectrum was utilized to study the biochar's morphology, element content, mineral composition, structure, and surface functional groups. Moreover, the physical and chemical properties of the biochar were analyzed to explore its passivation effect. Biochar is beneficial in the cleaning of cadmium, lead, and zinc minerals and can be used for the passivation of heavy metals in contaminated soil. This study aims to understand the detailed mechanism behind this process and provide experimental data and ideas for pollution control. The results indicate that the biochar contains many functional groups, including -OH, C-H, C-O, C=O, C=C, and C-O-C. It also consists of a significant quantity of potassium salt, calcite, and quartz. Biochar has a noticeable pore structure, and as the pyrolysis temperature increases, the pore structure becomes more developed and thinner, with a smooth surface. The main minerals in the soil are quartz, mica, zeolite, illite, and chlorite. The aromatic degree of biochar increased with pyrolysis temperature. In contrast, the aromatic degree and polarity first increased and then decreased. The 0.2-0.45 mm biochar exhibited the best passivation effect on cadmium, lead, and zinc.

## INTRODUCTION

Soil is an important part of the human living environment. However, due to the rapid expansion of modern society, many heavy metal pollutants released during mining have contaminated the soil, resulting in severe soil heavy metal pollution. According to the 2014 National Soil Pollution Survey Bulletin, the soil is predominantly polluted by inorganic pollutants. Of all the sites with pollutant levels exceeding the limit, 82.8% are affected by inorganic pollutants. Among these, cadmium (Cd) is the primary heavy metal contaminant in China's soil, with an over-limit rate of 7%. The over-limit rates of lead (Pb) and zinc (Zn) are 1.5% and 0.9%, respectively (MEP & MLR 2014).

The zinc smelting industry in northwestern Guizhou Province has a history of more than 300 years. Historically, there was a greater focus on development than on environmental protection. This outdated smelting technique contributed to economic growth but at a significant environmental cost. Inadequate waste treatment led to the release of large quantities of toxic exhaust gases, soot, and heavy metal pollutants such as Cd, Pb, and Zn. These pollutants were discharged during smelting, causing serious soil contamination. As a result, over 20 million tons of waste and 1200 hectares of soil remain untreated (Lin 2009). To remediate and treat these contaminated areas, it is urgent to find appropriate methods.

At present, studies on heavy metal-contaminated soils in the historical legacy of zinc refining in northwest Qianxi primarily focus on investigating the current state of soils in the contaminated area. These studies analyze the distribution of heavy metal morphology and geochemical transport characteristics and evaluate the biological effectiveness of heavy metals in soils within the historically contaminated area using relevant methods and predictive models. They also explore the soil-crop system in the legacy contaminated area by heavy metals. However, there are few studies on the use of chemical passivation agents to remediate soil in the historical legacy of zinc refining in northwest Qianxi (Yang et al. 2003, Lin et al. 2009, Ao et al. 2009, Gao et al. 2017, Zhang et al. 2017a, Sun et al. 2013, Liu et al. 2020, Sun et al. 2006, Kang et al. 2015)

Soil remediation methods for heavy metal contamination can be divided into physical remediation, chemical remediation, and bioremediation (Derakhshan et al. 2017). Among chemical methods, in situ passivation remediation has received wide attention due to its high operability, cost-effectiveness, and suitability for large-scale applications. In recent years, it has become a research hotspot for remediating soil polluted by heavy metals (Li et al. 2019).

Passivators used for treating soil with heavy metals are often categorized into inorganic passivators (such as lime, phosphate, metals and their oxides, and clay minerals) and organic passivators (including organic waste, organic acids, and biochar) (Zhao et al. 2021). Biochar, a highly carbon-containing aromatized solid material prepared by pyrolysis under anoxic and relatively low-temperature conditions, is particularly effective. It has a complex pore structure, a large specific surface area, and abundant surface functional groups, making it excellent at absorbing and immobilizing heavy metal pollutants. Consequently, biochar has become a research hotspot in the environmental field in recent years (Shi et al. 2019).

According to the Ministry of Agriculture and Rural Affairs of China, current agricultural straw resources in China mainly include rice, corn, and wheat, which together account for 83.51% of the total straw resources. In 2021, China produced 900 million tons of straw, ranking first in the world.

Moreover, the production is increasing at an annual rate of 3%, providing sufficient raw material for biochar. Therefore, biochar is a green and reasonable solution for recycling agricultural straw resources (Wei et al. 2019, Xie et al. 2010, Meng et al. 2018). Currently, many studies have analyzed biochar's passivation effects on the remediation of soil polluted by heavy metals. However, most of them regard biochar as a homogeneous body and do not consider the influence of different sizes of biochar particles. Therefore, it is necessary to investigate biochar's passivation effects on the remediation of polluted soil with different particle sizes. In the soil of the historical legacy of zinc refining in northwestern Qianxi, this investigation has practical application significance and aligns with the current development trend of national environmental ecology.

This paper focuses on the historical Zn refining area in northwest Guizhou province, where heavy metals, including Cd, Pb, and Zn, have contaminated the soil. The rice husk biochar was used as the test material for passivation remediation. We analyzed the biochar and the test soil samples using characterization techniques such as scanning electron microscopy, Fourier infrared spectroscopy, X-ray diffraction, specific surface area measurement, and organic elemental analysis. The study investigated the differences in the morphological structure, elemental content composition, and surface functional groups of the biochar. This paper aims to provide basic experimental data and pollution prevention ideas by investigating the rice husk biochar's passivation effects on soil contaminated by heavy metals.

## MATERIALS AND METHODS

### Test Materials

The test soil was obtained from a 0-20 cm soil layer of a vegetable field in a soil refining area of Hezhang County, Bijie City, Guizhou Province. The collected soil samples were mixed well in a sealed bag, brought back to the laboratory, and laid flat on kraft paper. A rubber hammer was used to break up the lumpy soil to prevent clumping. After removing impurities, the samples were dried naturally at room temperature. The dried samples were then filtered through a 2 mm nylon sieve and sealed in bags for use. The basic physical and chemical properties are as follows: the soil type was loam, the moisture content after air-drying was 4.75%, the pH was 7.51, indicating weak alkalinity and the conductivity was 155.11 $\mu s.cm^{-1}$, cation exchange was 8.78 $cmol(+).kg^{-1}$, soil organic matter content was 36.89 $g.kg^{-1}$, total N and total P are 0.05 and 1.00 $g.kg^{-1}$, respectively. The total amounts of Cd, Pb, and Zn were 14.07, 4518.15, and 71,786.83 $mg.kg^{-1}$, respectively. The rice husk biochar products, which were prepared by pyrolysis at 300°C, 400°C, and 500°C, are noted as W300, W400, and W500, respectively. They were purchased from Henan Lize Environmental Protection Technology Co, with sizes of 0.075-0.2mm, 2: 0.2-0.45mm, and 3: $0.45^{-1}$mm. Their basic physicochemical properties are shown in Table 1.

The aromaticity, hydrophilicity, and polarity magnitudes of biochar can be expressed by the ratios of the organic

Table 1: Physical and chemical properties of biochar.

| Biochar type | Water content | pH | EC [$\mu s.cm^{-1}$] | Ash | Specific surface area[$m^2.g^{-1}$] | Total pore volume [$cm^3.g^{-1}$] | Average pore size[nm] | C[%] | H[%] | N[%] | O[%] | S[%] |
|---|---|---|---|---|---|---|---|---|---|---|---|---|
| W300 | 3.67% | 11.56 | 8475 | 53.51% | 61.89 | 0.166 | 4.39 | 28.24 | 2.77 | 0.43 | 8.36 | 0.58 |
| W400 | 3.88% | 10.44 | 5335 | 51.88% | 67.53 | 0.165 | 4.25 | 34.80 | 1.07 | 0.54 | 9.62 | 0.73 |
| W500 | 0.67% | 12.28 | 14500 | 50.21% | 130.28 | 0.309 | 4.90 | 42.59 | 1.34 | 0.75 | 12.37 | 1.05 |

components' H/C, O/C, and (O+N)/C. The ratio of H/C atoms is negatively correlated with the degree of biochar aromaticity (Lin et al. 2017). Conversely, the ratios of O/C and (O+N)/C are positively correlated with the aromaticity and polarity of biochar (Chen et al. 2013, Wu et al. 2015, Hseu 2006). Based on the analysis of organic elements in rice husk biochar, the aromaticity of rice husk biochar in this study increased with temperature. The aromaticity and polarity showed an increasing trend before experiencing a downturn.

### Material Characterization Analysis

Soil mineral types were analyzed using an X-ray diffractometer (XRD) (BrukerD8advance, Bruker, Germany). The surface morphology of biochar was determined using a scanning electron microscope (SEM) (ZEISSGemini300, Carl Zeiss AG, Germany). The organic elemental composition of biochar was analyzed with an organic elemental analyzer (EA) (ElementarvarioEl III, Erimenta, Germany). A fully automatic specific surface and porosity analyzer (BET) (McASAP2460, McMurritic Instruments Co., Ltd., USA) was used to determine the specific surface area, pore size, and pore volume of the biochar. A Fourier infrared spectrometer (FTIR) (FTIR-850 Ltd.) was used to qualitatively analyze the surface functional groups of biochar.

### Design of Experiments

The experiment was conducted on January 14, 2021, at the Key Laboratory of Karst Mountain Ecology and Environment of Guizhou Normal University. It aimed to analyze the soil's static passivation. The soil in the pots was mixed with biochar. First, an appropriate amount of ultra-pure water was added to the pots to moisten the soil to 60% of the field water-holding capacity. During incubation, lost water was replenished using the weighing method. After 100 days of incubation, the soil samples were removed, air-dried, ground, and sieved for analysis and testing.

### Analytical Methods and Instruments

Using the potentiometric method (water-soil ratio 2.5:1), the soil's pH was determined by the pH meter (PHS-320, Shanghai Yidian Scientific Instruments Co., Ltd.). Soil electrical conductivity refers to the electrical conductivity of a solution within a unit distance. Using the electrode method, the soil's electrical conductivity (EC) was determined by the electrical conductivity meter (DDSJ-308F, Shanghai Yidian Scientific Instruments Co., Ltd.). Cation exchange capacity (CEC) is a measure of the total negative charges within the soil that adsorb plant nutrient cations. The leaching-spectrophotometric method, adopting hexamine-cobalt trichloride, was used to determine the soil's cation exchange capacity (CEC). The automatic interrupted chemical analyzer (CleverChem200+, DeChem-Tech GmbH, Germany) was used to determine the total nitrogen (TN) and total phosphorus (TP), using sulfuric acid boiling sodium salicylate and sulfuric acid boiling-molybdenum antimony resistance, respectively. The ultraviolet-visible spectrophotometer (UV-5500, Shanghai Yuananalysis Instruments Co., Ltd.) was used to determine the content of soil organic matter (SOM) using the hydrated thermal potassium dichromate oxidation-colorimetric method. The total amount of soil Cd, Pb, and Zn was evaluated using tetraacid digestion (HCl-HNO3-HF-HClO4), the plant active Cd, Pb, and Zn (DTPA-Cd, DTPA-Pb, and DTPA-Zn) were extracted using diethylenetriaminepentaacetic acid (DTPA) leaching. The toxic leached Cd, Pb, and Zn (TCLP-Cd, TCLP-Pb, and TCLP-Zn) were extracted by acetic acid (CH3COOH). The total amount and the other two forms were determined by the flame atomic absorption spectrometer (GGX-800, Beijing Haiguang Instruments Co., Ltd.).

### Data Processing

Excel 2019 was used for data processing and calculation, and Origin 2019 b was used for the plotting.

## RESULTS AND DISCUSSION

### Effect of Biochar on Soil Physicochemical Properties

Biochar W3 (300), W2 (400), W2 (500), and W3 (500) treatments have clear effects of pH reduction. However, biochar of different particle sizes generates different results of soil CEC. The CEC in soil treated by rice husk biochar at 300°C increased first and then decreased as the biochar's particle size grew. While at 400°C, the CEC showed a descending trend along with the increase of the biochar's particle size. At 500°C, the CEC trend was opposite to that at 400°C. The W3 (500) treatment resulted in the highest CEC of 9.16 $cmol^{+}.kg^{-1}$, followed by the W2 (300) treatment. At 400°C, the maximum CEC of the rice husk biochar treatment was 8.92 $cmol^{+}.kg^{-1}$. At 300°C and 400°C, the EC of soil treated with rice husk biochar tended to decrease as the biochar particle size decreased. At 300°C and 400°C, the CEC of soil treated with rice husk biochar decreased as biochar particle size reduced. However, the EC of soil in the W2(500) treatment was the largest and could reach 466.21 $\mu s.cm^{-1}$ (Table 2).

### Effect of Biochar on the Effective State Cd, Pb, and Zn Content

The total content of heavy metals in soil indicates their potential hazard. The DTPA-extracted state of heavy metals is closely related to the plant-available fraction. It can be used

Table 2: Physical and chemical properties of soil under different treatments.

| Processing Category | pH | CEC [$cmol^+.kg^{-1}$] | EC [$\mu s.cm^{-1}$] | TN [$mg.kg^{-1}$] | TP [$g.kg^{-1}$] |
|---|---|---|---|---|---|
| CK | 7.51 | 8.78 | 155.11 | 46.67 | 1.00 |
| WF(300) | 7.38 | 8.39 | 355.71 | 2.00 | 0.61 |
| W1(300) | 7.41 | 8.15 | 318.71 | 87.23 | 0.23 |
| W2(300) | 7.46 | 8.93 | 302.21 | 19.19 | 0.23 |
| W3(300) | 7.19 | 7.19 | 262.71 | 8.91 | 0.72 |
| WF(400) | 7.38 | 8.92 | 334.21 | 52.54 | 0.59 |
| W1(400) | 7.35 | 8.52 | 375.71 | 18.07 | 0.38 |
| W2(400) | 7.25 | 8.07 | 266.21 | 10.16 | 0.53 |
| W3(400) | 7.30 | 6.96 | 167.81 | 5.72 | 0.48 |
| WF(500) | 7.44 | 7.65 | 446.71 | 15.41 | 0.24 |
| W1(500) | 7.46 | 7.74 | 367.71 | 26.55 | 0.22 |
| W2(500) | 7.17 | 6.68 | 466.21 | 26.97 | 0.26 |
| W3(500) | 7.22 | 9.16 | 346.71 | - | 0.71 |

Note: "-" means not detected.

to measure the content of heavy metal elements in soil that are effective for plants (Cao et al. 2009). Effective state Cd, Pb, and Zn in soil accounted for 28.57%, 24.47%, and 7.51% of the total, respectively. Biochar has the most significant effect on the content of DTPA-Pb in soil (Fig. 1). Under the W1 (400) treatment, the content of DTPA-Cd is reduced by 15.85%. Under the W2 (300) treatment, the reduced percentages of DTPA-Pb and DTPA-Zn were 40.92% and 23.94%, respectively. Overall, biochar with a size of 0.2-0.45 mm had the most significant effect on all three heavy metals in their effective states. Pb is less mobile in soil and has a strong affinity for the soil's mucilage and organic matter. Even under acidic conditions, Pb is easily precipitated with phosphoryl chloride (Sauve et al. 2000). Previous studies have shown that different factors can account for the solid phase-solution partitioning of heavy metals in soil (Buchter et al. 1989, Gao et al. 2018).

## Effect of Biochar Addition on the Content of TCLP-Cd, Pb, and Zn

The TCLP method (Toxicity Characteristic Leaching Procedure) can easily, quickly, and effectively evaluate the ecological risk of heavy metals in solids and is often used to assess soil heavy metal pollution and remediation effects (Wu et al. 2017). TCLP-Cd, Pb, and Zn accounted for 17.27%, 35.77%, and 24.8% of the total, respectively (Fig. 2). The passivation effect of different particle size biochar treatments on toxic leaching state heavy metals was similar to that of the effective state. The passivation effect on Pb and Zn was better than that on Cd. The W2(400) treatment showed the

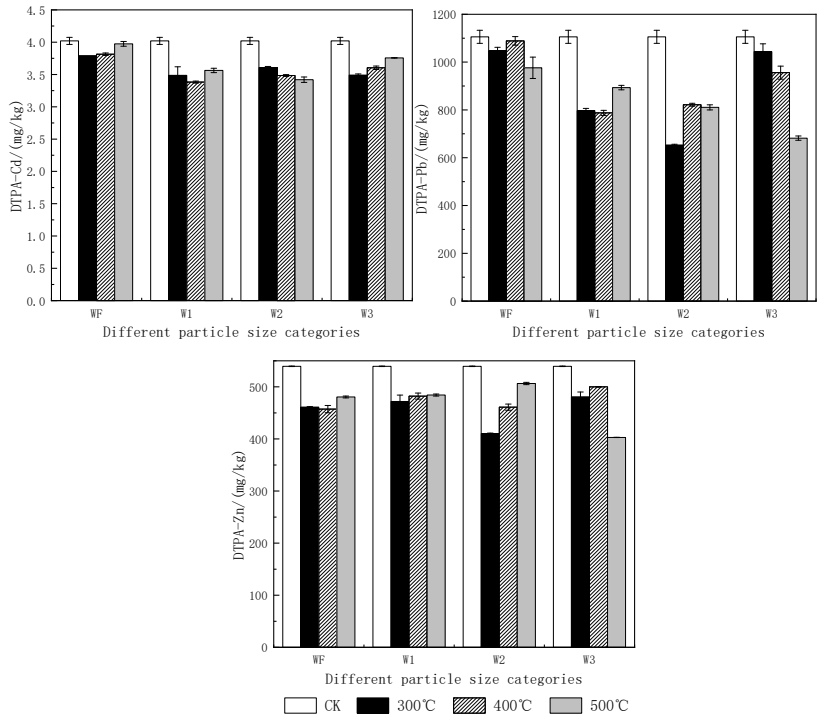


Fig. 1: Changes of DTPA-Cd, Pb, and Zn contents after different rice biochar treatments.

best passivation effect on Cd and Zn, reducing TCLP-Cd and TCLP-Zn by 25.81% and 36.13%, respectively. The W2(300) treatment demonstrated the best passivation effect on TCLP-Pb, with a reduction rate of 51.62%. Overall, biochar with a size of 0.2-0.45 mm had the most significant passivation effect, significantly reducing the two effective forms of the three heavy metals.

## Characterization and Analysis of Biochar and Soil Samples

**X-ray diffraction analysis:** According to the X-ray diffraction analysis, the minerals contained in the test soil mainly included quartz, feldspar, mica, zeolite, illite, and chlorite (Fig. 3). The surface of some minerals in the soil could adsorb and immobilize heavy metals, thereby reducing their mobility and impact on the environment (Miguel et al. 2002, Li et al. 2007). In this study, the rice husk biochar primarily contained potassium salt (KCl), calcite ($CaCO_3$), and quartz ($SiO_2$). This finding is consistent with the research of Liu et al. (2017) and Zhong et al. (2019). The sharp diffraction peaks in the plots mainly represented inorganic crystals $SiO_2$ (Zhong et al. 2019), $CaCO_3$, and KCl. $SiO_2$ corresponded to the highest diffraction peak, indicating that its content was greater than that of the other inorganic compounds. As the pyrolysis temperature increased, inorganic ions such as $SiO_2$, Ca, K, and Mg sintered and fused into inorganic minerals and alkali metals. At higher temperatures, the presence of K converts some Ca elements into silicates, which may lead to a decrease in $CaCO_3$ (Zhang et al. 2017b). The characteristic peaks of cellulose and hemicellulose appeared at $2\theta$ = 15-20° (Feng et al. 2009). During the charring of biochar, these characteristic peaks gradually widened, and their intensity decreased as the temperature increased. The charring process destroyed the microcrystalline structure of cellulose, and the volatile components continued to escape. At lower temperatures, the biochar made from rice straw lacked characteristic peaks of cellulose and was amorphous. The characteristic peaks at 26° and around 43° correspond to the (002) and (100) crystalline surfaces of graphite, reflecting the degree of graphitization.

After charring, as the temperature increased, the diffraction peaks of the rice husk biochar shifted toward

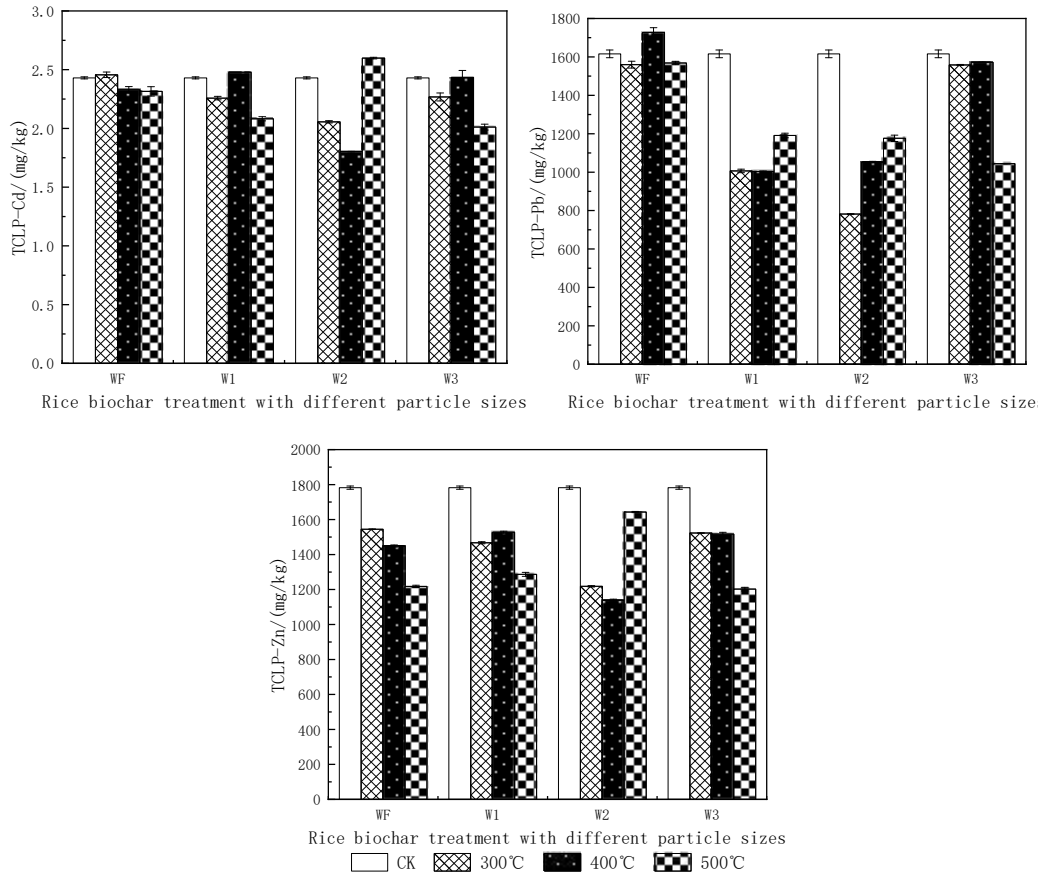


Fig. 2: Changes of TCLP-Cd, Pb, and Zn contents after different rice biochar treatments.

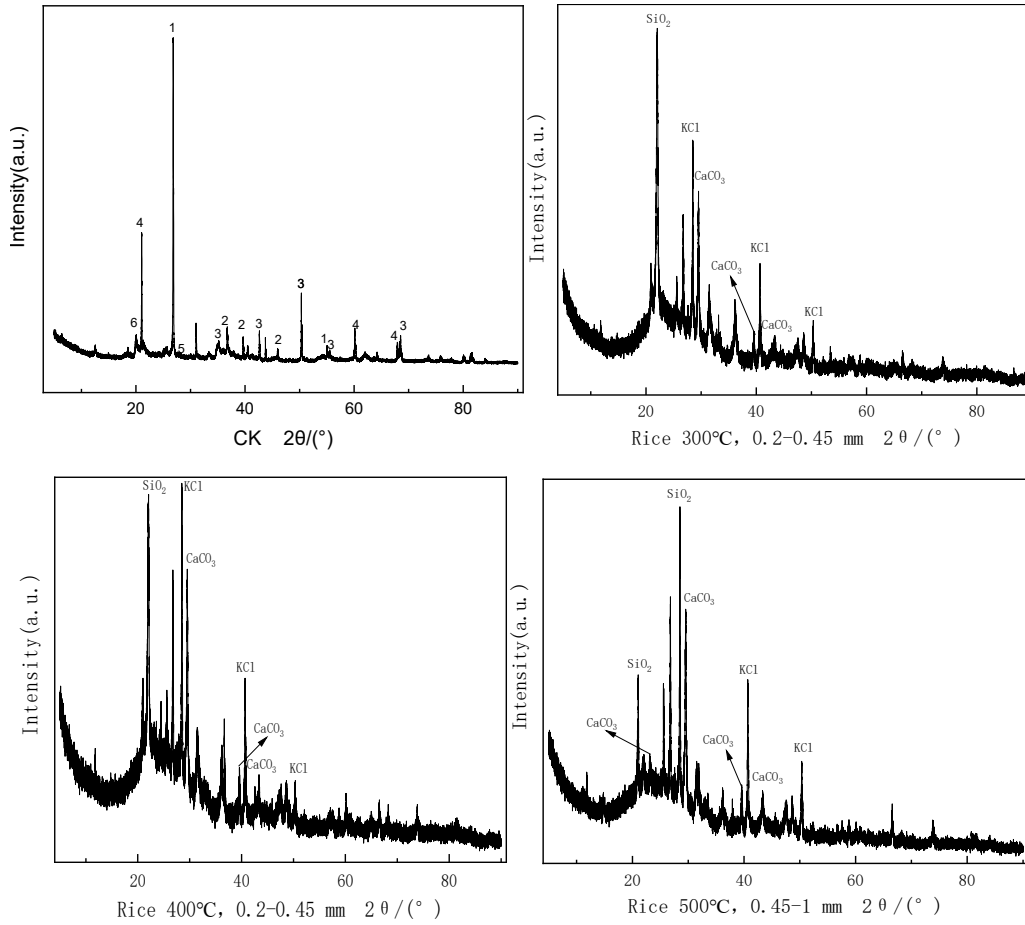


1: Quartz ($SiO_2$), 2: Feldspar ($SiO_2$, $Al_2O_3$, $K_2O$, $Fe_2O_3$, $Na_2O$, CaO), 3: Mica ($KAl_2(AlSi_3O_{10})(OH)_2$), 4: Zeolite ($Na(AlSi_2O_6)\cdot H_2O$, $Ca(Al_2Si_3O_{10})\cdot 3H_2O$), 5: Illite ($KAl_2[(SiAl)_4O_{10}]\cdot(OH)_2\cdot NH_2O$), 6: Chlorite ($Y_3[Z_4O_{10}](OH)_2\cdot Y_3(OH)_6$) (Y: mainly represents Mg, Fe & Al; Z: mainly Si and Al)

Fig. 3: XRD patterns of CK and three kinds of biochar.

higher theta angles. Due to further charring of the biomass, the aromaticity of carbon increased, and the stacking mode between aromatic lamellae tended to become more ordered. Therefore, biochar prepared at high temperatures had less volatile organic carbon and more aromatized carbon. The functional groups remaining on the carbon structure were more stable, enhancing the chemical stability of the biochar. This explains why biochar is suitable for the passivation of heavy metals in contaminated soil and benefits remediation (Lin et al. 2016, Ma 2019). Rice prefers Si and absorbs a large amount of Si during its life cycle. Therefore, rice husk is rich in Si, consistent with previous research (Liang et al. 2006, Wu & Gong 2010, Xiao et al. 2014). The broad half-peak of the diffraction indicated that the prepared biochar particles were small and rich in irregular pores, which helped increase the specific surface area of the material (Yu et al. 2019).

**Swept surface electron microscopy analysis:** The scanning electron microscope showed the images of rice husk biochar (Fig. 4). At different pyrolysis temperatures, all the images of biochar exhibited obvious pore structures. However, the degree of porosity varied. When the pyrolysis temperature was 300°C, the rice husk biochar was flaky without well-developed pores. Instead, the pores were few and irregular, and the surface of the biochar was covered with granular material. When the temperature was raised to 400 or 500°C, the rice husk biochar had a more developed pore structure. The structure was evenly distributed with stable sized round pores with a smooth and flat surface. The biochar became lighter and thinner, which was good for the passivation and fixation of heavy metal pollutants.

**Fourier infrared spectral analysis:** The preparation of biochar by pyrolysis had four steps: water evaporation, transition, decomposition of organic matter, and charring. In this study, the rice biochar consisted of hemicellulose, cellulose, and lignin. The cracking temperature of different components varied. Hemicellulose could be cracked at low

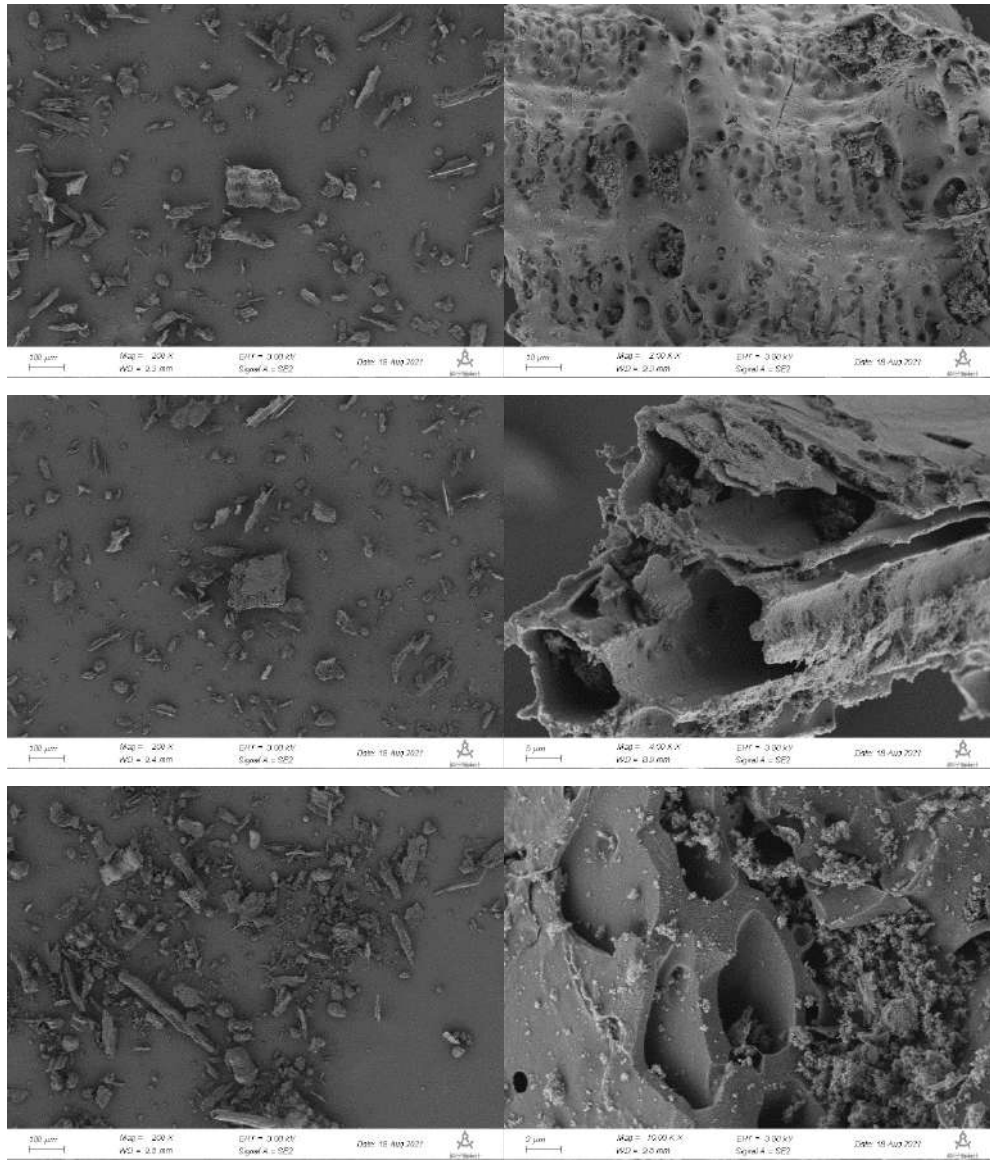

Fig. 4: SEM image of W2(300), W2(400) and W3(500).

temperatures, and cellulose and lignin gradually started to decompose as the pyrolysis temperature increased (Jian et al. 2015). From the analysis of IR spectra (Fig. 5), the surface of rice husk biochar contained functional groups such as carbonyl, hydroxyl, methylene, and aromatic rings (Zhu et al. 2021). At 3440 $cm^{-1}$, there was a broad and strong absorption peak. The absorption peak in this band can be explained by the hydrogen-bonded phenolic hydroxyl-OH stretching vibration. The effect of pyrolysis' temperature effect on this absorption peak was not significantly obvious. At 2939 $cm^{-1}$, there was an absorption peak with lower intensity. This was caused by the asymmetric C-H stretching vibration of the aliphatic methylene CH2. The source of this functional group included aliphatic compounds, alicyclic compounds, and carbohydrates in organic matter. The weakening of the peak intensity of rice husk biochar at 400 and 500°C might be related to the decomposition of aliphatic-CH2 (Chun et al. 2004). The functional groups at 1644 $cm^{-1}$ were polycyclic aromatic hydrocarbons C =C and C=O (Que et al. 2018). The absorption peak functional group at 1428 $cm^{-1}$ was methylene-CH2. The absorption peak functional group at 1104 $cm^{-1}$ was caused by cellulose or hemicellulose C-O-C (Keiluweit et al. 2010). In this study, the functional groups C=C, C=O, and C-H were higher in rice husk biochar at

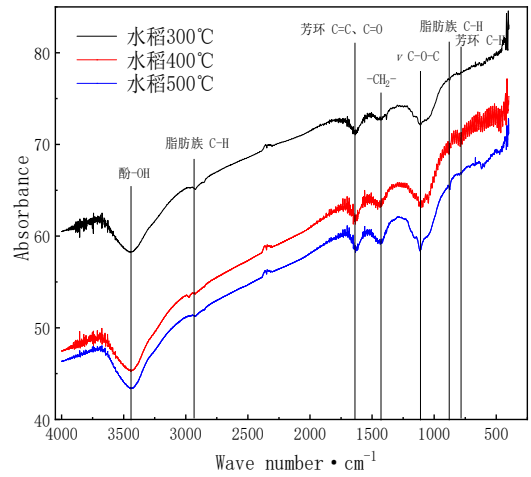


Fig. 5: FTIR spectra of the biochars.

300 °C and 400 °C. However, the original composition and structure in rice husk biochar were gradually decomposed at 500 °C. High temperatures significantly reduced the number of functional groups. The oxygen-containing functional groups -OH and C=O could react with heavy metal ions (Chen et al. 2008, Torri & Fabbri 2014). The absorption peaks at 888 and 788 $cm^{-1}$ were caused by the bending vibrations of the aromatic ring C-H. The absorption peaks of rice husk biochar increased with pyrolysis temperature, indicating that the aromatic rings were formed and the aromatization increased during the pyrolysis. This was consistent with the results of organic elemental analysis.

## CONCLUSION

1. Biochar had little effect on soil pH. Biochar with different particle sizes had variable effects on the soil's CEC. Under W3(400) treatment, the CEC of soil became as high as 9.16 $cmol.kg^{-1}$. W2(500) treatment achieved the best effect on the soil's EC, which increased by 466.21 $\mu s.cm^{-1}$.
2. Rice husk biochar had a better passivation effect on DTPA-Pb compared to others. Under the W2(300) treatment, the content of DTPA-Pb was reduced by 40.92%. When heavy metals were in a toxic leaching state, the biochar's passivation effects were better for Pb and Zn than for Cd. The W2(400) treatment reduced the TCLP-Cd and TCLP-Zn contents by 25.81% and 36.13%, respectively. The W2(300) treatment was the most effective for TCLP-Pb, reducing it by 51.62%. The medium-sized rice husk biochar, which was 0.2-0.45 mm, had the best passivation effect on all three heavy metals.
3. According to the characterization analysis, the minerals in the test soil included quartz, feldspar, mica, zeolite, illite, and chlorite. The rice husk biochar contained KCl, $CaCO_3$, and $SiO_2$, with $SiO_2$ being more prevalent than the other inorganic compounds. Scanning electron microscope images showed that rice husk biochar at 300°C was flaky, with an underdeveloped pore structure. As the pyrolysis temperature increased, the biochar became lighter and thinner, with more developed pores and smoother surfaces. The functional groups in the rice husk biochar included carbonyl, hydroxyl, methylene, and aromatic rings.

Future research should focus more on natural environment experiments to investigate the in situ remediation effects of biochar on polluted sites. The duration of passivation should be adjusted to measure the content of different forms of heavy metals at various time points. The dynamic changes in heavy metals over different time ranges should be explored. It is also recommended to study the relationship between biochar aging and its passivation effect.

## ACKNOWLEDGEMENTS

This work was supported by the Technology Foundation, Guizhou Province (Qian Sci. Co., [2019], NO.1231).

## REFERENCES

Ao, Z. Q., Lin, W. J., Yan, C. L., Qu, L. Y., Xiao, T. F. and Lin, K. 2009. Speciation and transformation of heavy metals in the indigenous zinc smelting area. J. Ecol. Environ. Sci., 18(3): 899-903.

Buchter, B., Davidoff, B. and Amacher, M. C. 1989. Correlation of Freundlich Kd and n retention parameters with soils and elements. J. Soil Sci., 148(5): 370-379.

Cao, X. D., Wahbi, A. and Ma, L. 2009. Immobilization of Zn, Cu, and

Pb in contaminated soils using phosphate rock and phosphoric acid. J. Hazard. Mater., 164(2): 555-564.

Chen, B. L., Zhou, D. D., Zhu, L. Z. and Shen, X. Y. 2008. The adsorption effect of biochar adsorbent on organic pollutants in water mechanism. Sci. Sin. Chim., (6): 530-537.

Chen, Z. M., Chen, B. L. and Zhou, D. D. 2013. Composition and sorption properties of rice-straw derived biochars. Acta Sci. Circumst., 33(1): 9-19.

Chun, Y., Sheng, G. Y. and Chiou, C. T. 2004. Compositions and sorptive properties of crop residue-derived chars. Environ. Sci. Technol., 38(17): 4649-4655.

Derakhshan, N. Z., Jung, M. C. and Kim, K. H. 2017. Remediation of soils contaminated with heavy metals with an emphasis on immobilization technology. Environ. Geochem. Health, 40: 927-953.

Feng, X. and Ju, C. H. H. 2009. Comparison of biosorbents with inorganic sorbents for removing copper(Ⅱ) from aqueous solutions. J. Environ. Manage., 90(10): 3105-3109.

Gao, H., Song, J., Lv, M. C., Zhang, X., Zhang, Q., Liu, L. F. and Log, J. 2017. Evaluation of cadmium phytoavailability in soils from a zinc smelting area in Hezhang County, Guizhou Province, using diffusive gradients in thin films and conventional chemical extractions. J. Agro-Environ. Sci., 36(10): 1992-1999.

Gao, P., Chen, Y. and Liang, Y. 2018. Study of the aging effect on the stability of biochar initially adsorbed Cd(II). Acta Sci. Circumst., 38(5): 1877-1884.

Hseu, Z. Y. 2006. Extractability and bioavailability of zinc over time in three tropical soils incubated with biosolids. Chemosphere, 63: 762-771.

Jian, M. F., Gao, K. F., Yu, H. P. and Yang, Y. 2015. Comparison of surface characteristics and cadmium solution adsorption capacity of un-acidified or acidified bio-chars prepared from rice straw under different temperatures. J. Ecol. Environ. Sci., 24(8): 1375-1380.

Keiluweit, M., Nico, P. S. and Johnson, M. G. 2010. Dynamic molecular structure of plant biomass-derived black carbon (biochar). Environ. Sci. Technol., 44(4): 1247-1253.

Kang, H. J., Lin, J., Zhang, N. M., Bao, L. and Liu, B. S. 2015. Passivation effect of different passive materials on heavy metal polluted soil. Chin. Agric. Sci. Bull., 31(35): 176-180.

Li, K. W., Wu, Y. X., Huang, Z. M., Fan, R. and Li, J. F. 2007. Measurement results comparison between laser particle analyzer and sieving method in particle size distribution. China Powder Sci. Technol., (5): 10-13.

Li, Y., Zhu, S. H., Shang, J. Y. and Huang, Y. Z. 2019. Immobilization materials for cadmium and arsenic-contaminated soil remediation and their scientific metrology.

Liang, Y. C., Hua, H. X. and Zhu, Y. G. 2006. Importance of plant species and external silicon concentration to active silicon uptake and transport. New Phytol., 172(1): 63-72.

Lin, J. Y., Zhang, Y., Liu, Y., Xia, J. J. and Tong, Sh.T. 2016. Structure and properties of biochar under different materials and carbonization temperatures. Chin. J. Environ. Eng., 10(6): 3200-3206.

Lin, Q. Y., Jiang, C. C. and Zhang, M. Y. 2017. Characterization of the physical and chemical structures of biochar under simulated aging conditions. Environ. Chem., 36(10): 2107-2114.

Lin, W. J. 2009. Ecological degeneration and heavy metals pollution in zinc smelting areas. Ecol. Environ. Sci., 18(1): 149-153.

Lin, W. J., Xiao, T. F., Zhou, W. C., Ao, Z. Q. and Zhang, J. F. 2009. Environmental concerns on geochemical mobility of lead, zinc, and cadmium from zinc smelting areas: Western Guizhou, China. Environ. Sci., 30(7): 2065-2070.

Liu, Y. X., Yang, S. and Wang, Y. Y. 2017. Bio-and hydrochars from rice straw and pig manure: Inter-comparison. Bioresour. Technol., 235: 332-337.

Liu, H., Wu, Y. G., Luo, Y. F. and Wu, P. 2020. Effects of different organic acid-phosphate rock powder composites on the immobilization of heavy metals in waste slags of indigenous smelting zinc. Earth Environ., 48(2): 258-267.

Ma, S. 2019. Physicochemical properties of rice straw biochar under the same temperature treatment and its impact on soil heavy metals the impact of genus bioavailability. Yangzhou: Yangzhou University.

Meng, Q. J., Liu, Y., Li, P. F., Liang, S. C. and Zhang, Y. 2018. Study on adsorption characteristics and mechanism of biochar on trichloroethylene. J. Environ. Sci., 49(12): 36-43.

Miguel, A. M., Marti and Montero, S. 2002. Laser diffraction and multifractal analysis for the characterization of dry soil volume-size distributions. Soil Tillage Res., 64(1-2): 113-123.

MEP and MLR 2014. Announcement on national soil pollution survey. Available at https://english.www.gov.cn/policies/latest_releases/2014/08/23/content_281474983026954.htm

Que, W., Zhou, Y. H. and Liu, Y. G. 2018. Appraising the effect of in-situ remediation of heavy metal contaminated sediment by biochar and activated carbon on Cu immobilization and microbial community. Ecol. Eng., 127: 519-526.

Sauve, S., Hendershot, W. and Allen, H. E. 2000. Solid-solution partitioning of metals in contaminated soils: Dependence on pH, total metal burden, and organic matter. Environ. Sci. Technol., 34(7): 1125-1131.

Shi, Z. L., Wang, F., Wang, J. C., Li, X., Sun, R. H. and Song, C. J. 2019. Utilization characteristics, technical model, and development suggestion on crop straw in China. J. Agric. Sci. Technol., 21(5): 8-16.

Sun, L., Yang, Y. G., Bai, W. Y., Bi, X. Y. and Jin, Z. S. 2006. Heavy metal accumulation in natural plants in the zinc smelting area in northwestern Guizhou Province. Earth Environ., (2): 61-66.

Sun, L., Zhao, L., Zhang, L. J., Shi, C. M., Zhu, X. W. and Wang, K. Y. 2013. Cadmium pollution caused by artisanal zinc-smelting in Hezhang County. Chin. J. Public Health., 29(4): 541-543.

Torri, C. and Fabbri, D. 2014. Biochar enables anaerobic digestion of aqueous phase from intermediate pyrolysis of biomass. Bioresour. Technol., 172: 335-341.

Wei, H. J., Yang, Q., Li, J. S., Yang, H. P. and Chen, H. P. 2019. Analysis of spatiotemporal and density changes of crop straws resources in China. Renew. Energy Resour., 37(9): 1265-1273.

Wu, J. R. and Gong, J. Y. 2010. Research progress on silicon nutrition in rice. China Rice, 16(3): 5-8.

Wu, S. X., Wang, X., Chen, C., Peng, B., Tan, C. Y., Zhang, F., Xu, Y. Q. and Zhang, Y. J. 2015. Characterization of biochar derived from water hyacinth, rice straw, and sewage sludge and their environmental implications. Environ. Chem., 35(12): 4021-4032.

Wu, T., Li, X. P., Cai, Y., Ai, Y. W., Sun, X. M. and Yu, H. T. 2017. Geochemical behavior and risk of heavy metals in different size lead-polluted soil particles. China Environ. Sci., 37(11): 4212-4221.

Xiao, X., Chen, B. L. and Zhu, L. Z. 2014. Transformation, morphology, and dissolution of silicon and carbon in rice straw-derived biochars under different pyrolytic temperatures. Environ. Sci. Technol., 48(6): 3411-3419.

Xie, G. H., Wang, X. Y. and Ren, L. T. 2010. China's crop residue resources evaluation. Chin. J. Biotechnol., 26(7): 855-863.

Yang, Y. G., Liu, C. Q., Wu, P., Zhang, G. P. and Zhu, W. H. 2003. Zinc smelting is an important factor leading to heavy metal accumulation in soils and sediments in Hezhang County, Guizhou Province. Acta Mineral. Sin., (3): 255-262.

Yu, X. H., Luo, Q. L., Pan, J., Han, Y. Q. and Zhang, Q. F. 2019. Preparation and properties of flexible supercapacitor based on biochar and solid gel-electrolyte. CIESC J., 70(9): 3590-3600.

Zhang, X. Q., Hou, G. J., Zhang, Y. H. and Zhao, Y. 2017a. Structural and physico-chemical properties of biochars prepared from different rice straws. Environ. Eng., 35(9): 122-126.

Zhang, X., Song, J., Gao, H., Zhang, Q., and Liu, G. 2017b. Assessment and modeling of Cd and Pb availability in contaminated arable soils in the mining area of Guizhou. Soils, 49(2): 328-336.

Zhao, S., Cai, X. F., Wang, J., Li, X. Y., Li, D., Zhao, S. J., Yu, X. J. and Xu, D. 2021. Research progress on the effects of raw and modified biochar on soil heavy metal pollutants. Sci. Soil Water Conserv., 19(2): 135-150.

Zhong, X., Jian, X. M., Jiang, E.CH., Sun, Y. and Wang, M. F. 2019. Structure and properties of rice husk biochar/acetate starch-urea starch composite films. Acta Mater. Compos. Sin., 36(7): 1746-1752.

Zhu, Q. L., Cao, M., Zhang, X. B., Tao, K., Ke, Y. C. and Meng, L. 2021. Physicochemical and infrared spectroscopic properties of gramineae plants biochar at different pyrolysis temperatures. Biomass Chem. Eng., 55(4): 21-28.

Nature Environment and Pollution Technology
An International Quarterly Scientific Journal

p-ISSN: 0972-6268
(Print copies up to 2016)
e-ISSN: 2395-3454

Vol. 23 | No. 3 | pp. 1849-1856 | 2024

Original Research Paper

https://doi.org/10.46488/NEPT.2024.v23i03.057

Open Access Journal

# Navigating the Global Environmental Agenda: A Comprehensive Analysis of COP Conferences, with a Spotlight on COP28 and Key Environmental Challenges

**Sabina Akhtar*†, S. Shaima*, G. Rita*, A. Rashid* and A. J. Rashed***
*College of Education, American University in the Emirates, Academic City, Dubai, U.A.E
†Corresponding author: Sabina Akhtar; akhtar.sabinaskuast@gmail.com

**Nat. Env. & Poll. Tech.**
**Website: www.neptjournal.com**

*Received:* 29-11-2023
*Revised:* 19-01-2024
*Accepted:* 02-02-2024

**Key Words:**
Biochar
Historical pollution soil
Heavy metals form
Passivation repair

## ABSTRACT

The purpose of the research work is to explore the objective and competence of COP (Conference of Parties) in the context of environmental issues and climate change management and this is performed by evaluating respective articles published in the context of the subject. COP is found efficient in empowering global nations to be aligned with the objective of sustainable growth by making corrective negotiations and agreements as per the current and future environmental issues like the greenhouse effect and air pollution. COP helps ensure environmental issues are fixed by conducting benchmark index-based performance reviews and analyses. It has been observed that the agenda significantly contributes to the green economy, as it promotes sustainable change and development in the environment, society, and economy. A significant innovative strategy was developed at the conference to reduce global temperatures and emissions. In this context, the development of the EV sector plays a crucial role in mitigating environmental impact. The COP28 conference is addressing the climate and nature crisis, considering it a global health emergency. Methodology states that the literature search is conducted from peer-reviewed journal articles from authentic sources like Wiley's Online Library and Science Direct Pages. Only the journals that were published after the year 2019 have been used in the study. Also, it is seen that COP28 (2023) conventions focused on global warming, climate change, and the production of a green economy, which is continuously being considered, and also, the implications and steps that are required to be taken are discussed.

## INTRODUCTION

In the contemporary global business environment, the concern of sustainable development has increased substantially as the degree of adverse impact on the surrounding environment in terms of the greenhouse effect, carbon emission, and pollution surged by more than 13 % in 2022 in comparison to the previous decade (Our World Data 2023). Sustainable development refers to the approach in which the authority belonging to a company or region follows a sustainable approach for conducting defined kinds of industrial or commercial practices so that the degree of adverse influence on surroundings might be minimized (Dey et al. 2022). To assist nations like the UAE and other countries of the world in having sustainable growth from the perspective of both economic and non-economic metrics, the provision for COP (Conference of Parties) is made by the authorities of the United Nations. The first and foremost objective of the COP meeting is to assist the governments of countries belonging to the world in making corrective decisions regarding commercial and non-commercial practices so that the degree of adverse influence on the surrounding environment and community might be minimized (UNFCCC 2023). In the COP meeting, representatives of different countries take part in the conference to present their opinions regarding the competitive ways following which the rising risk of climate change in terms of carbon emission, resource shortage, and greenhouse effect might be identified and mitigated substantially.

The foundation of the COP meeting was made in 1992 with the strategic multilateral treaty adopted by the management and members of UNFCCC (United Nations Framework Convention on Climate Change) for understanding and monitoring the progress in the context of climate change management. To provide a competitive kind of future to the global population without facing any severe climate change effects, two types of landmark agreements are made by the members and authorities of UNFCCC and these are the Kyoto Protocol and the Paris Agreement. The Kyoto Protocol-related agreement was made by the authority and group members of UNFCCC in 1997 to ensure sustainable business and non-commercial practices within every field so that a higher degree of sustainable growth might be achieved

without any adverse impact (Saseendran 2023). On the other hand, the Paris Agreement was made in 2015 between all the group members of UNFCCC so that they might use innovative and creative techniques in their industrial and commercial practices to maximize sustainability across the globe without facing any resource shortage-related issues.

With the support of the article, the contribution made by the COP meetings related provision of UNFCCC is critically evaluated in the context of climate change and environmental issue management, and this is performed by analyzing peer-reviewed 5 competitive articles. The research work highlights the methodology, which is efficient for validating the insights derived from qualitative analysis or quantitative evaluation, and this is eventually used to find valuable inferences for addressing the problem of the artifact.

## PAST STUDIES

### Overview of COP, COP28, and its Goal

COP (Conference of Parties) is a kind of meeting that is held by the authority and group members of UNFCCC every year to bring all representatives of global countries on a single platform to make a competitive decision on the identification and management of climate change (UNFCCC 2023). The management of COP holds a meeting every year, and the respective collaborative decision is marked as COPFY (Financial Year), where FY is replaced with the name of the year in which the meeting is held. The meeting titled COP27 was held by the group countries and members of UNFCCC between 6$^{th}$ November 2022 and 18$^{th}$ November 2022 in Egypt. On the other hand, the next meeting of UNFCCC with the name of COP28 is to be held in 2023 in Dubai to empower global countries to consider the rising concern of environmental issues and climate change so that corrective decisions might be taken to mitigate respective adverse impacts on the global population. The Key objectives and goals of the COP meeting are detailed below in the context of short-term and long-term vision regarding global environment management-

- To develop a competitive agreement among group countries regarding the decision of the global climate change agreement so that the possibility of any deviation in terms of the usage of innovative and collaborative decisions in environmental sustainability might be curbed (Di Simone et al. 2022).
- To monitor the progress of the agreement and initiative taken by the group members of UNFCCC regarding the effective implementation of climate change management-related strategy
- To evaluate the financial need of each group member country regarding the effective implementation of climate change management-related strategy
- To develop and implement a pledge for balanced usage of financial and natural resources to augment the collaborative nature within group members regarding competitive action against climate change management (Dyer & Dyer 2017)
- To facilitate the effective kind of technology and platforms to the group countries to empower them to develop competitive kind of infrastructure across the regions for -managing and mitigating climate change-related risk precisely (Saseendran 2023)

### Analysis of Different Environmental Issues and Their Short-term and Long-Term Impact

Environmental issue refers to the availability of adverse influences on the surrounding environment in terms of factors like pollution, greenhouse effect, carbon emission, and fertility rate, and this plays a significant role in determining the sustainability of the population belonging the world (Fig. 1). As per the principle of sustainable development, the understanding of key environmental issues associated with a region plays a significant role in determining corrective approaches in terms of the usage of financial and non-financial resources, and this eventually helps in meeting sustainable growth objectives (Gazi et al. 2022). The key environmental issues that the group members of COP authority significantly identify and UNFCCC are detailed below, along with highlighting respective influence in the surrounding ecosystem in the context of both short-term and long-term-

### Air Pollution

An environmental issue is marked as air pollution when the ratio of $CO_2$ level and other pollutants like ozone gas is increased by more than the permissible limit. This plays a significant role in augmenting breathing and liveability-related issues for the surrounding population. If UNFCCC and its group members do not take corrective action on time regarding curbing the continuation of commercial and non-commercial activities responsible for air pollution, then the possibility of critical diseases related to respiration, heart, and lungs might increase, and this might prove deadly in critical condition (Kempeneer et al. 2021). Apart from this, the availability of extensive amounts of air pollution level in the atmosphere might create the possibility of acid rain in the long run and this might eventually damage the fertility of soil, which might surge acute hunger across the globe.

### Climate Change

Climate change is one of the significant environmental issues which occur due to a substantial amount of variation in the composition of elements available in the air and this eventually leaves an adverse impact on the purity level of air and water.

If the management of UNFCCC and its group members do not take corrective action on time, then the possibility of heatwaves and hurricanes might surge across the nation, and this might eventually destroy farming systems. With the availability of destruction in the ecosystem of agriculture, the possibility of crop failure might surge and this might eventually create a food shortage-related situation in the long run. The availability of uncontrolled heatwaves and hurricanes might increase the level of the sea, and this might eventually create threats related to flood and water security (Lewandowski 2016).

### Deforestation

In the contemporary global environment, deforestation is one of the most critical environmental issues as the availability of the situation creates flood, carbon emission, and air pollution-related situations substantially and this might eventually surge the risk of sustainability-related risk in the long run. In the case of deforestation, the frequency of cutting trees is comparatively higher in comparison to normal situations and this eventually reduces the availability of plants efficient in controlling the ratio of carbon dioxide in the atmosphere. With the reduction in the number of plants in the surrounding environment, the possibility of flood and greenhouse effect-related situations surges, and this might eventually maximize the probability of severe weather scenarios like the disrupted cycle of weather and reduced level of oxygen in the environment (Lin et al. 2022).

### Critical Analysis of the Competitiveness of COP in Environmental Issues and Climate Change Management

According to Oghazi & Mostaghel (2018), the availability of a central monitoring committee for strategy development in the context of sustainability management plays a significant role in ensuring the level of quality and accuracy of the implemented action, and this eventually helps in meeting objectives precisely. On the evaluation of the functionalities of COP, it is found that it plays a significant role in creating and managing a competitive kind of negotiation between the group members on an international level. This eventually helps in ensuring the implementation of a competitive kind of climate change management approach. For example, with the strategic and periodic negotiation management-related practice, the administration and authority of COP have been successful in getting the Paris Agreement executed and finalized precisely in 2015 without any internal conflict, and this eventually helped in deciding a competitive approach to managing climate change (UNFCCC 2023).

The availability of collaborative and precise kinds of international agreements like the Paris Agreement has played a significant role in the management of COP to bring all group members on a single platform to understand the critical situation of different environmental issues. This has eventually assisted in mitigating respective impacts. With the availability of a collaborative decision-making culture within the operational framework of COP, it has been feasible to include the opinions of different group members regarding the pros and cons of different environmental issues. This has eventually helped in taking corrective and innovative

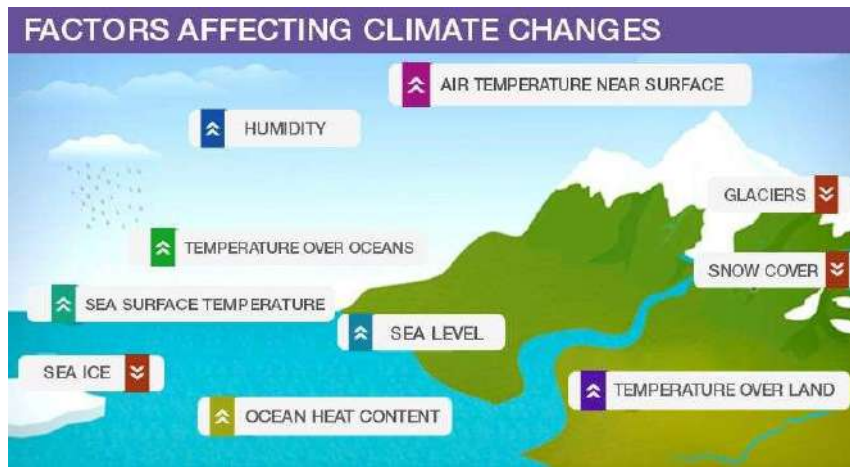


Source: (Di Simone, Petracci, & Piva, 2022).

Fig. 1: Climate change.

action on time. It means that the strategic agreement and negotiation kind of culture available within the operational framework of COP has significantly helped in finding the root cause of potential kind of environmental issues using collaborative decision-related traits and this has eventually assisted in meeting concerned objectives precisely.

On the contrary, Reim et al. (2019) stated the availability of COP meeting culture on an international level has played a significant role in measuring and evaluating the performance of each deployed climate change management strategy, and this has been possible by implementing a competitive kind of benchmark. On the evaluation of the strategic practices of COP, it is identified that it has implemented the culture for the usage of benchmark index for each environmental issue and climate change management-related strategy. This has eventually helped in reviewing respective performance periodically. For example, as per the strategic report of COP published in 2022, the respective authority has implemented a benchmark regarding the reduction in carbon emission to 1.5 degrees Celsius, and this has been eventually used to measure whether all group countries are on the way to achieving the metric or not (UNFCCC 2023). The outcome of the availability of benchmark index-based performance review techniques within the operational framework of COP is that its authority has been efficient in ensuring integrity and alignment between the actions of each country, and this has eventually assisted in taking corrective action on time. In short, the availability of periodic reviews and benchmark-based performance comparison related approach of COP has significantly helped in managing and improving the approaches of each group member country to manage environmental issues.

**Overview of Green Economy and its Importance**

Green economy refers to the economic system in which emphasis on promoting practices in all the commercial and non-commercial fields is made so that a progressive growth trend might be achieved without leaving any adverse impact on the surrounding environment, society, and community (Rodríguez-Olalla & Avilés-Palacios 2017). In other words, a green economy plays a significant role in the authority of a nation or region to shift its traditional economy to a sustainable system in which dependency on natural resources is limited in order to optimize any adverse harm to the surrounding environment (Fig. 2).

The inclusion of the green economy concept in the strategic practices of a nation plays a significant role in finding a competitive technique following the extensive usage of natural resources that might be optimized and minimized with the usage of alternative resources like solar panels. It means that the implementation of a green economy within the strategic practices of a country plays a pivotal role in curbing the possibility of resource shortage-related situations by diversifying dependency on environment-friendly resources, and this eventually reduces the amount of environmental and societal costs (Rodríguez-Olalla & Avilés-Palacios 2017). With the adoption of green economy-related concepts, it becomes easy for the authority of a nation like the UAE to find a competitive technique to reuse the limited natural resources to meet current and upcoming needs. This eventually assists in minimizing industrial costs and maximizing their GDP contribution.


Source: (Lewandowski 2016)

Fig. 2: Green Economy.

### Contribution of COP Meetings to Green Economy Achievement

The significance of COP meetings related to green economy achievement is to bring world leaders together and address the impact of climate change. The meeting is referred to as a formal conference where the government acts as parties. It delivers the global effort related to the limitation of global warming, which can be close to the pre-industrial level. COP ("conference of the parties") reviews the legal instruments that promote the implementation of the convention regarding administration and institutional arrangement. The contribution of parties which are involved with the COP conference mainly resolves the issues related to the "global average temperature" regarding 1.5°C to avoid the impact of climate change-related problems.

This action has an effective contribution to the economy and society, regarding "High-Level Champions" had launched to involve with global climate action to mitigate the environmental crisis. This global climate action needs to involve climate resilience which has a higher moral imperative that supports future generations to get prosperous and healthy future. Related to "The Marrakech Partnership at COP 27", collaboration with stakeholder influence to take transformative action related to climate change has been catalyzed by regional and local circumstances related to well-being and health. In this conference, partners are brought together to take successful climate action related to adaptation efforts and climate mitigation related to global climate policy and science processes.

Considering the green economy, climate change is responsible for creating problems and results suffered by farmers related to agriculture. It also affects tourism and the fishing industry as "Red Sea coral reef ecosystems" have been hampered. However, due to the introduction of the EV industry, it is not harmful to the climate. Related to the landmark agreement regarding climate losses, the negotiation among different developed nations like the US and EU support to solve issues related to the burning of fossil fuels and emissions reduction to meet the 1.5C target. However, due to the damage and loss of funds, climate disasters have also been observed due to lower triggering options in developing countries. One of the effective contributions of COP is related to transitioning to clean energy and developing targets to slash emissions before 2030. In COP28, it occurs to adapt to the changes related to vulnerable communities. The contribution of COP28 is to set new formwork to deal with finance that will be related to accessible, available, and affordable in the case of developing countries. Additionally, it ensures the collaboration of the local community and Indigenous Peoples.

## MATERIALS AND METHODS

The COP conferences are mainly designed by the United Nations to enhance the goal of environmental sustainability and create a green economy throughout the globe (COP28 2023). It is a collaboration among several countries, and the present study focuses on reviewing the statements made at the latest conference called COP28 and its objectives (The Nature Conservancy 2023). To find out the environmental issues and how such instances are resolved, the present methodology that is adopted in this particular time is a descriptive-analytical method, which focuses on the peer-reviewed journals in the literature on COP28 of the economy.

The methodology is completely based on the present literature that is related to the green economy, which is mainly from the year 2019. Five peer-reviewed journals focus on the COP28 agenda, and objectives pertaining to the system are considered. One of the primary factors that is associated with the methodology constitutes the literature collection, and its process of screening, which is mentioned.

### Literature Collection

The main focus of the COP28 conference is a complete focus on the parameters connected with global warming, and climate change, and also the factors that ensure the creation of a green economy. To understand these factors, and how it is required to be improved, such keywords are used in finding out specifically 7 articles, out of which 5 articles are shortlisted. The authentic sources are being used for finding out the articles that are mainly required, which constitutes the Science Direct Pages, Elsevier journals, and also, Wiley's Online Library in order to find the information.

### Screening of Specific Literature Articles

While doing the screening of the articles, the latest articles, which are from the year 2019 are considered. Also, it is seen that only peer-reviewed articles are considered to ensure that the details of the COP28 conference in the UN are understood in the connected processes, which mainly creates an understanding pertaining to the study.

## RESULTS AND DISCUSSION

The clarification of the articles by determining the country and considering the key findings. The articles are evaluated for analyzing the journals and considering COP28 in terms of tackling the climate challenges. The analysis of the five articles is determined based on representing authors, journal name, and country of publishing the articles and the key findings (Table 1).

Table 1: Analysis of Five Articles, including information on Authors, Journal, Country of publication, and Key Findings.

| Author | Journal Name | Country | Key findings |
|---|---|---|---|
| Roberts et al. (2023) | UCL Open: Environment Preprint | United Kingdom | The article represents the annual conference of the parties (COP) for determining the collective actions towards tackling the climate challenge. UCL's carbon footprint calculator is determined to compare diverse modes of transport from the UK to COP28 in Dubai. |
| Leiter (2022) | Carbon and Climate Law Review | United Kingdom | The article determines that climate adaptation is an existing challenge and its impacts on the global economy. The increasingly diverse climate-related impacts evaluate the understanding of the COP28 climate conference. |
| Abbasi et al. (2023) | African Journal of Clinical and Experimental Microbiology | Africa | The journal ensures the understanding of the COP28 climate change conference in terms of determining the treatment towards the climate and nature crisis considering the invisible global health emergency. |
| Michaelowa (2022) | Handbook of International Climate Finance | UAE | The journal represents the understanding that ensures the international climate finance directed from advanced to developing countries through public interventions for mitigation and adaptation. |
| Evangelista-Vale et al. (2021) | Biological Conservation | Brazil | It is found from the article that the financial global climate change governance is the overall understanding in terms of considering the COP28 conferences. The article ensures the understudying of the issues related to climate and the policy, which determine the policy requirements. |

Table 2: Articles Used in the Investigation.

| Year | Number of Articles | Articles |
|---|---|---|
| 2021 | 1 | Evangelista-Vale et al. (2021) |
| 2022 | 2 | Michaelowa (2022) Leiter (2022) |
| 2023 | 2 | Roberts et al. (2023) Abbasi et al. (2023) |

The overall content represents the analysis that evaluates the main aims of the research that investigate the values towards determining the feasibility in terms of clarifying the journal name, authors, years, and findings. The clarification of the articles represents the use of the articles based on considering the topic and the analysis on considering the insight. The analysis of the articles represents an overall understanding of the COP28 and the conference regarding environmental issues. It is found from the analysis that fossil fuel use must be reduced to increase the potential of a green economy, like the use of electric vehicles, even in public transport, as much as possible. Also, it is observed in the study that there are techniques that ensure the right kind of measures for climate change and global warming by reducing the carbon footprint and making the policies stricter.

The clarification of the articles by considering the years is also determined, which represents the utilization of the journals (Table 2).

The articles are selected researching the topic that determines the overall analysis of the workings investigating

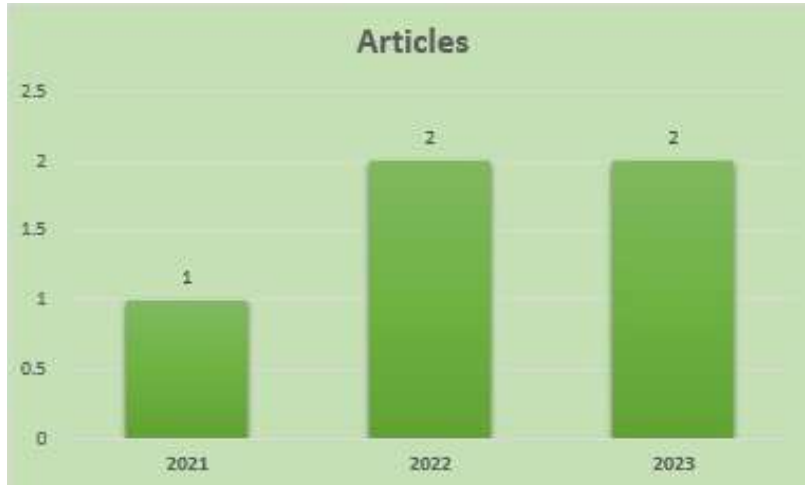


Source: Author.

Fig. 3: Articles by years;

the possible years. It is seen that the literature is conducted based on determining the climate challenges and the aspect of COP28 that considers the research insights. The article selection is based on the last 3 years that determine overall determination. The analysis investigates the utilization of the content and its overall clarification that determines the utilization. The overall understanding illustrates that there are 2 articles from 2023, 2 from 2022, and 1 from 2021(Fig. 3). The authors and the journal also evaluated towards considering the factors that evaluate the changes in the market situation for facing the challenges related to climate and COP28 concept determination.

**Literature Review Analysis and Results**

Based on the findings of secondary results in the literature review, it is seen that the green economy is involved with sustainable development, these are economy, environment, and social. Related to climate change action, the green economy has involved inclusive and sustainable growth, green jobs, and green transition. Sustainable climate change is interlinked with the green economy as it emits lower production of greenhouse gases by minimizing the eliminated waste and using effective resources. In the case of economic growth, this has been related to the income and employment that drive private and public investment. The green economy is responsible for creating people and social resilience through the effective transition. Investment in sustainable solutions turns on the end use of fossil fuel that is beneficial for controlling pollution. Discussion of this green economy refers to the combination of environmental responsibility and economic growth that led to social development.

COP has contributed to the launch of a number of initiatives that are related to a green economy. These are "Sustainable Urban Resilience for the Next Generation (SURGe)" and "Low Carbon Transport for Urban Sustainability ($L^cO_2TUS$)," which have been related to sustainable transport and the use of renewable and affordable energy. Considering land management, a plan regarding climate action has also been taken in COP. The key fact in COP28 has seen are limitations of global warming by reducing temperature which has lower harmful effects on climate change. By demonstrating the collaboration of different cities, the goal related to climate change has been planning related to the transition of clean energy, centering lives, people, and nature, mobilizing inclusivity, and delivering on finance.

The thematic program of COP28 has been set by dramatically protecting livelihoods and lives and reducing emissions that support the green transition actress society. In this climate meeting, digital action has been taken hold in UAE related to preparing a plan for future climate change. The international climate change meeting delivers effective global efforts to meet global warming that decrease the possible chances of reduction of temperature. It has been seen that "global climate change governance" ensures understanding the issues that are related to the policy and climate change regarding the mitigation of environmental problems. This milestone involved a stock of progress which provided solutions on time for global change. It has also been evaluated that, in this global conference, nature and climate crises are being discussed, which solve invisible global health emergencies. In determining the carbon footprint, a discussion of the different diverse modes of transport has been calculated. By aligning and updating the climate plan, negotiating with foreign leaders, and government support to build resilience regarding society, reduce emissions, and invest in adaptation efforts and mitigation. This conference has also been aligned with digital action related to renewable energy transition and the application of natural climate solutions that assist synch countries related to climate change. It also ensures the voice of the local and Indigenous communities as they also suffer in this natural calamity.

## CONCLUSION

It is concluded from the study that most of the factors that are linked with the COP28 conference in the UN are focused on the factors pertaining to global warming, climate change, and the green economy. It is seen that the global warming program plans to reduce the temperature by 1.5 degrees globally, and also, for the sake of climate change, the campaign for planting trees is considered, and also, the reduction of greenhouse gases is mainly important. Also, it is observed from the study that the peer-review-based research conducted, which focused on the green economy, found that the reduction of fossil fuels and the creation of sustainable energy are equally important.

## RECOMMENDATION

Based on the analysis, it is seen that COP28 has also been focused on clean energy transition, protecting lives, and delivering finance. However, the recommendation is that in this international conference, leaders need to focus on policy development related to maintaining healthy water in the ocean, as it also harms biodiversity. Additionally, the research also needs to critically analyze in compare different COP program and their success, which would be effective for further planning related to climate change action.

## REFERENCES

Abbasi, K., Ali, P., Barbour, V., Benfield, T., Bibbins-Domingo, K., Hancocks, S. and Shehab, A. 2023. COP28: Time to treat the climate and nature crisis as one indivisible global health emergency. Int. J. Health Policy Manag.,12(1): 1-3.

COP28. 2023. What is COP? Retrieved from https://www.cop28.com/what-is-cop (accessed November 08, 2023)

Dey, P. K., Yang, G. L., Malesios, C., De, D. and Evangelinos, K. 2021. Performance management of supply chain sustainability in small and medium-sized enterprises using a combined structural equation modelling and data envelopment analysis. Comput. Econ., 58(3): 573-613.

Di Simone, L., Petracci, B. and Piva, M. 2022. Economic sustainability, innovation, and the ESG factors: An empirical investigation. Sustainability, 14(4): 22-70.

Dyer, G. and Dyer, M. 2017. Strategic leadership for sustainability by higher education: the American College and University Presidents' Climate Commitment. J. Clean. Prod., 140: 111-116.

Evangelista-Vale, J. C., Weihs, M., José-Silva, L., Arruda, R., Sander, N. L., Gomides, S. C., Machado, T. M., Pires-Oliveira, J. C., Barros-Rosa, L., Castuera-Oliveira, L., Matias, R. A. M., Martins-Oliveira, A. T., São Bernardo, C. S., Silva-Pereira, I., Carnicer, C., Carpanedo, R. S. and Eisenlohr, P. V. 2021. Climate change may affect the future of extractivism in the Brazilian Amazon. Biol. Conserv., 257: 109093.

Gazi, F., Atan, T. and Kılıc, M. 2022. The assessment of internal indicators on the balanced scorecard measures of sustainability. Sustainability, 14(14): 8595.

Kempeneer, S., Peeters, M. and Compernolle, T. 2021. Bringing the user back in the building: An analysis of ESG in real estate and a behavioral framework to guide future research. Sustainability, 13: 3239.

Leiter, T. 2022. Too little, too slow? Climate adaptation at the United Nations Climate Change Negotiations since the adoption of the Paris Agreement. CCLR, 16(4): 243-258.

Lewandowski, M. 2016. Designing the business models for the circular economy: Towards the conceptual framework. Sustainability, 8: 43.

Lin, M., Effendi, A. A. and Iqbal, Q. 2022. The mechanism underlying the sustainable performance of transformational leadership: organizational identification as moderator. Sustainability, 14: 15568.

Michaelowa, A. 2022 A vision for International Climate Finance after 2025: Handbook of International Climate Finance. Edward Elgar Publishing, Cheltenham UK, 476-486.

Reim, W., Sjödin, D.R. and Parida, V. 2019. Servitization of global service network actors–A contingency framework for matching challenges and strategies in service transition. Journal of Business Research, 104: 461-471.

Roberts, C., Chin-Yee, S., Taylor, R., Maslin, M., Vanhala, L., Yaguma, P., McGlade, J. and

Rodríguez-Olalla, A. and Aviles-Palacios, C. 2017. Integrating sustainability in organisations: An activity-based sustainability model. Sustainability, 9(6): 10-72.

Saseendran, S. 2023. COP28 in UAE to Seek Global Pledge for Tripling Renewable Energy by 2030.Gulf News. Retrieved from https://gulfnews.com/uae/environment/cop28-in-uae-to-seek-global-pledge-for-tripling-renewable-energy-by-2030-1.99083235 (access date Nov 08, 2023)

The Nature Conservancy 2023. COP Climate Change Conference. Retrieved from https://www.nature.org/en-us/what-we-do/our-priorities/tackle-climate-change/climate-change-stories/cop-climate-change-conference/ (access date Nov 08, 2023)

Our World in Data 2023. Air Pollution. Retrieved from https://ourworldindata.org/air-pollution (access date Nov 08, 2023)

UNFCCC 2023. Conference of the Parties (COP). Retrieved from https://unfccc.int/process/bodies/supreme-bodies/conference-of-the-parties-cop (access date Nov 08, 2023)

## ORCID DETAILS OF THE AUTHORS

Sabina Akhtar: https://orcid.org/0000-0002-6848-7738

... Continued from inner front cover

- The text of the manuscript should run into Abstract, Introduction, Materials & Methods, Results, Discussion, Acknowledgement (if any) and References or other suitable headings in case of reviews and theoretically oriented papers. However, short communication can be submitted in running with Abstract and References. The references should be in full with the title of the paper.
- The figures should preferably be made on a computer with high resolution and should be capable of withstanding a reasonable reduction with the legends provided separately outside the figures. Photographs may be black and white or colour.
- Tables should be typed separately bearing a short title, preferably in vertical form. They should be of a size, which could easily be accommodated in the page of the Journal.
- References in the text should be cited by the authors' surname and year. In case of more than one reference of the same author in the same year, add suffix a,b,c,.... to the year. For example: (Thomas 1969, Mass 1973a, 1973b, Madony et al. 1990, Abasi & Soni 1991).

## List of References

The references cited in the text should be arranged alphabetically by authors' surname in the following manner: (Note: The titles of the papers should be in running 'sentence case', while the titles of the books, reports, theses, journals, etc. should be in 'title case' with all words starting with CAPITAL letter). The references should be given in the **"Harvard Pattern"** as exemplified below.

- Dutta, A. and Chaudhury, M., 1991. Removal of arsenic from groundwater by lime softening with powdered coal additive. *Journal of Water Supply: Research and Technology—Aqua*, 40(1), pp.25-29. **(For Papers Published in Journals)**
- Goel, P.K., 2006. *Water pollution: Causes, Effects and Control*. New age international, New Delhi. **(For Authored Books)**
- Environmental Protection Agency (EPA), 2023. Air Quality and Pollution Data. Retrieved June 25, 2024, from https://www.epa.gov/air-quality-and-pollution-data **(For Data Retrieved from a Website)**
- Hammer, D.A. (ed.), 1989. *Constructed Wetlands for Wastewater Treatment-Municipal, Industrial and Agricultural*. Lewis Publishers Inc., pp.831. **(For Edited Book)**
- Haynes, R.J., 1986. Surface mining and wetland reclamation. In: J. Harper and B. Plass (eds.) *New Horizons for Mined Land Reclamation*. Proceedings of a National Meeting of the American Society for Surface Reclamation, Princeton, W.V. **(For Papers published in Edited Books)**

## Submission of Papers

- The paper has to be submitted online in a single WORD file through the online submission portal of journal's website: **www.neptjournal.com**

## Attention

1. Any change in the authors' affiliation may please be notified at the earliest.
2. Please make all the correspondence by e-mail, and authors should always quote the manuscript number.

**Note:** In order to speed up the publication, authors are requested to correct the galley proof immediately after receipt. The galley proof must be checked with utmost care, as publishers owe no responsibility for mistakes. The papers will be put on priority for publication only after receiving the processing and publication charges.

# Nature Environment and Pollution Technology

## (Abbreviation: Nat. Env. Poll. Tech.)

**(An International Quarterly Scientific Journal)**

Published by

**Technoscience Publications**
A-504, Bliss Avenue, Opp. SKP Campus
Balewadi, Pune-411 045, Maharashtra, India

In association with

**Technoscience Knowledge Communications**
Mira Road, Mumbai, India

For further details of the Journal, please visit the website. All the papers published on a particular subject/topic or by any particular author in the journal can be searched and accessed by typing a keyword or name of the author in the 'Search' option on the Home page of the website. All the papers containing that keyword or author will be shown on the home page from where they can be directly downloaded.

**www.neptjournal.com**



Published for Proprietor, Printer and Publisher: Mrs. T. P. Goel, A-504, Bliss Avenue, Balewadi, Pune, Maharashtra, India; Editors: Dr. P. K. Goel (Chief Editor) and Prof. K. P. Sharma (Honorary Editor)